

# Evaporation, Evapotranspiration, and Irrigation Water Requirements

Second Edition



Task Committee on  
Revision of Manual 70

**EDITED BY**  
Marvin E. Jensen, Ph.D., NAE  
Richard G. Allen, Ph.D., P.E.

**ASCE**



ENVIRONMENTAL &  
WATER RESOURCES  
INSTITUTE

# Evaporation, Evapotranspiration, and Irrigation Water Requirements

## Second Edition

Prepared by the  
Task Committee on Revision of Manual 70

Edited by  
Marvin E. Jensen, Ph.D., NAE  
Richard G. Allen, Ph.D., P.E.

Sponsored by the  
Committee on Evapotranspiration in Irrigation  
and Hydrology of the Irrigation and Drainage Council of the  
Environmental and Water Resources Institute of the  
American Society of Civil Engineers



Published by the American Society of Civil Engineers

### Library of Congress Cataloging-in-Publication Data

Names: Jensen, Marvin Eli, 1926- editor. | Allen, R. G. (Rick G.), editor. | American Society of Civil Engineers. Task Committee on Revision of Manual 70. | Environmental and Water Resources Institute (U.S.). Committee on Evapotranspiration in Irrigation and Hydrology

Title: Evaporation, evapotranspiration, and irrigation water requirements / prepared by the Task Committee on Revision of Manual 70 ; edited by Marvin E. Jensen, Ph.D., NAE, Richard G. Allen, Ph.D., P.E. ; sponsored by the Committee on Evapotranspiration in Irrigation and Hydrology of the Irrigation and Drainage Council of the Environmental and Water Resources Institute of the American Society of Civil Engineers.

Other titles: Evapotranspiration and irrigation water requirements.

Description: Second edition. | Reston, Virginia : American Society of Civil Engineers, [2016] | Series: ASCE manuals and reports on engineering practice ; No. 70 | Includes bibliographical references and index.

Identifiers: LCCN 2015011931 | ISBN 9780784414057 (print : alk. paper) | ISBN 9780784479209 (ebook)

Subjects: LCSH: Evapotranspiration—Handbooks, manuals, etc. | Crops—Water requirements—Handbooks, manuals, etc. | Irrigation water—Handbooks, manuals, etc. | Irrigation farming—Handbooks, manuals, etc.

Classification: LCC S600.7.E93 E93 2016 | DDC 631.5/87—dc23 LC record available at <http://lccn.loc.gov/2015011931>

2015011931

Published by American Society of Civil Engineers

1801 Alexander Bell Drive

Reston, Virginia, 20191-4382

[www.asce.org/bookstore](http://www.asce.org/bookstore) | [ascelibrary.org](http://ascelibrary.org)

Any statements expressed in these materials are those of the individual authors and do not necessarily represent the views of ASCE, which takes no responsibility for any statement made herein. No reference made in this publication to any specific method, product, process, or service constitutes or implies an endorsement, recommendation, or warranty thereof by ASCE. The materials are for general information only and do not represent a standard of ASCE, nor are they intended as a reference in purchase specifications, contracts, regulations, statutes, or any other legal document. ASCE makes no representation or warranty of any kind, whether express or implied, concerning the accuracy, completeness, suitability, or utility of any information, apparatus, product, or process discussed in this publication, and assumes no liability therefor. The information contained in these materials should not be used without first securing competent advice with respect to its suitability for any general or specific application. Anyone utilizing such information assumes all liability arising from such use, including but not limited to infringement of any patent or patents.

ASCE and American Society of Civil Engineers—Registered in U.S. Patent and Trademark Office.

*Photocopies and permissions.* Permission to photocopy or reproduce material from ASCE publications can be requested by sending an e-mail to [permissions@asce.org](mailto:permissions@asce.org) or by locating a title in ASCE's Civil Engineering Database (<http://cedb.asce.org>) or ASCE Library (<http://ascelibrary.org>) and using the "Permissions" link.

*Errata:* Errata, if any, can be found at <http://dx.doi.org/10.1061/9780784414057>.

Copyright © 2016 by the American Society of Civil Engineers.

All Rights Reserved.

ISBN 978-0-7844-1405-7 (print)

ISBN 978-0-7844-7920-9 (PDF)

Manufactured in the United States of America.

# **MANUALS AND REPORTS ON ENGINEERING PRACTICE**

(As developed by the ASCE Technical Procedures Committee, July 1930, and revised March 1935, February 1962, and April 1982)

A manual or report in this series consists of an orderly presentation of facts on a particular subject, supplemented by an analysis of limitations and applications of these facts. It contains information useful to the average engineer in his or her everyday work, rather than findings that may be useful only occasionally or rarely. It is not in any sense a "standard," however; nor is it so elementary or so conclusive as to provide a "rule of thumb" for nonengineers.

Furthermore, material in this series, in distinction from a paper (which expresses only one person's observations or opinions), is the work of a committee or group selected to assemble and express information on a specific topic. As often as practicable the committee is under the direction of one or more of the Technical Divisions and Councils, and the product evolved has been subjected to review by the Executive Committee of the Division or Council. As a step in the process of this review, proposed manuscripts are often brought before the members of the Technical Divisions and Councils for comment, which may serve as the basis for improvement. When published, each work shows the names of the committees by which it was compiled and indicates clearly the several processes through which it has passed in review, so that its merit may be definitely understood.

In February 1962 (and revised in April 1982), the Board of Direction voted to establish a series titled "Manuals and Reports on Engineering Practice," to include the Manuals published and authorized to date, future Manuals of Professional Practice, and Reports on Engineering Practice. All such Manual or Report material of the Society would have been refereed in a manner approved by the Board Committee on Publications and would be bound, with applicable discussion, in books similar to past Manuals. Numbering would be consecutive and would be a continuation of present Manual numbers. In some cases of joint committee reports, bypassing of journal publications may be authorized.

A list of available Manuals of Practice can be found at <http://www.asce.org/bookstore>.

This page intentionally left blank

## **TASK COMMITTEE ON REVISION OF MOP 70**

### **Task Committee**

Marvin E. Jensen, Editor	Consultant, Fort Collins, Colorado (formerly Director, Colorado Institute for Irrigation Management, and National Program Leader for Water Management, Agricultural Research Service, USDA)
Richard G. Allen, Editor	Water Resources Engineering Professor, Kimberly Research and Extension Center, University of Idaho, Kimberly
Terry A. Howell	Laboratory Director (retired), Conservation and Research Leader, Conservation and Production Laboratory, Agricultural Research Service, USDA, Bushland, TX
Derrel L. Martin	Professor, Department of Biological Systems, Engineering, University of Nebraska, Lincoln
Richard Snyder	Biometeorologist Specialist, Department of Land, Air, and Water Resources, University of California, Davis
Ivan A. Walter	Principal, Ivan's Engineering, Centennial, CO

### **BLUE RIBBON REVIEW PANEL**

Paul W. Brown	University of Arizona, Tucson
Ronald L. Elliott	University of Oklahoma (retired), Stillwater
Thomas W. Ley	formerly with Colorado Division of Water Resources, Pueblo, now with Natural Resources Consulting Engineers, Fort Collins, CO
Thomas Trout	Agricultural Research Service (retired), USDA, Fort Collins, CO

This page intentionally left blank

## DEDICATION

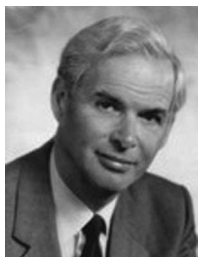


In loving memory of Doris Jensen, 1929–2009, lifelong spouse, supporter, encourager, and traveling companion of Marvin Jensen.



In fond memory of William Oregon Pruitt, 1922–2009, Irrigation Engineer at the University of California-Davis, who was a primary leader in developing and advancing the concept of reference crop evapotranspiration (ET) and transferable crop coefficients, in trusting the use of energy balance equations to estimate ET, in advocating data and research quality and integrity, and in promoting education in experimental methods. Bill Pruitt, along with Dr. James L. Wright of the USDA-ARS (retired), Kimberly, Idaho, mentored many present-day practitioners on the physics of ET estimation and the requirements for accurate ET measurement. Pruitt and Wright were both longtime members of and contributors to the ASCE Technical Committee on Evapotranspiration in Irrigation and Hydrology.

## DEDICATION



In fond memory of John Lennox Monteith, 1929–2012, who influenced many Americans in the application of physical principles to describe how plants interact with their immediate environment and microclimate, with his own work leading to the evolution of the Penman combination equation into the Penman-Monteith equation, which has become a primary basis for estimating irrigation water requirements.

## CONTENTS

PREFACE .....	xiii
ACKNOWLEDGMENTS .....	xv
NOTATION .....	xvii
<b>PART 1: BASIC CONCEPTS .....</b>	<b>1</b>
<b>1. INTRODUCTION AND HISTORY .....</b>	<b>3</b>
1.1 Introduction to Second Edition .....	3
1.2 Development of ET and CU Studies in the United States ....	7
1.3 Revised Edition.....	16
<b>2. EVAPORATION AND EVAPOTRANSPIRATION PROCESSES .....</b>	<b>19</b>
2.1 Introduction .....	19
2.2 The Water Budget .....	20
2.3 The Energy Budget .....	21
2.4 Controlling Factors.....	21
2.5 Estimating Concepts .....	27
2.6 Measurement Methods.....	29
<b>3. SOIL-PLANT-ATMOSPHERE SYSTEM.....</b>	<b>35</b>
3.1 Introduction .....	35
3.2 Physical Properties of Water, Water Vapor, and Air .....	35
3.3 Soil Properties .....	44
3.4 Soil-Water System .....	44
3.5 Vegetative (Crop) Properties .....	54
<b>4. ENERGY BALANCE.....</b>	<b>59</b>
4.1 Introduction .....	59
4.2 Energy Balance .....	59

4.3	Net Radiation.....	61
4.4	Soil Heat Flux Density.....	80
5.	<b>SURFACE-ENERGY AND AIR-MASS INTERACTIONS AND THE CONCEPT OF REFERENCE ET .....</b>	87
5.1	Introduction .....	87
5.2	Weather and Surface Effects on Conversion of Energy to Latent Heat Flux.....	90
5.3	Standardization of the Vegetative Cover .....	93
6.	<b>EVAPORATION FROM WATER SURFACES .....</b>	99
6.1	Introduction .....	99
6.2	Methods of Estimating Water Surface Evaporation .....	100
6.3	Example Applications of Evaporation Estimation Methods and Measurements .....	126
6.4	Summary of Methods for Estimating Evaporation from Water Bodies .....	135
<b>PART 2: EVAPOTRANSPIRATION FROM LAND SURFACES .....</b>		139
7.	<b>WATER AND ENERGY BALANCE COMPONENTS FOR MEASUREMENT AND ESTIMATION .....</b>	141
7.1	Introduction to Chapters 7–12.....	141
7.2	Volumetric Measurements for Estimating Land Surface ET.....	142
7.3	Mass Balance Methods .....	149
7.4	Energy Balance Methods—Bowen Ratio .....	162
7.5	Mass Transfer Method Using Eddy Covariance .....	168
7.6	Fetch Requirements for Boundary Layer Measurement ...	172
7.7	Advantages and Disadvantages of ET Measurement Methods .....	175
7.8	Combined Energy Balance and Mass Transfer Methods ...	176
8.	<b>REFERENCE CROP ET .....</b>	189
8.1	Introduction .....	189
8.2	The Penman-Monteith Equation .....	190
8.3	Aerodynamic and Surface Parameters for the PM Equation .....	192
8.4	Reference $ET_{ref} K_c$ Approach .....	195
8.5	Missing or Bad Weather Data .....	206
8.6	Reference ET by Analogy or Association .....	214
9.	<b>EVAPORATION FROM SOIL .....</b>	221
9.1	Introduction .....	221
9.2	The Evaporation Process.....	221
9.3	Diurnal Effects and Redistribution of Soil Water.....	222
9.4	Stage 1 Evaporation .....	223

9.5	Stage 2 Evaporation .....	225
9.6	Evaporation Models.....	227
9.7	Relationships between Evaporation and Transpiration ....	240
9.8	Water Balance of the Evaporation Layer.....	243
9.9	Example Estimates of Evaporation.....	245
9.10	Summary .....	258
<b>10.</b>	<b>CROP COEFFICIENT METHOD .....</b>	<b>261</b>
10.1	Introduction .....	261
10.2	The Crop Coefficient.....	261
10.3	Crop (Vegetation Cover) Coefficients .....	265
10.4	FAO Grass-Based Crop Coefficients .....	273
10.5	Alfalfa-Based Crop Coefficients .....	285
10.6	Estimates of $K_c$ Curves for Natural and Agricultural Vegetation.....	287
10.7	Landscape Coefficients .....	294
10.8	Estimates of $K_c$ during Wintertime and Nongrowing Seasons .....	313
10.9	Summary .....	321
<b>11.</b>	<b>DIRECT PENMAN-MONTEITH AND AERODYNAMIC ENERGY BALANCE EQUATIONS .....</b>	<b>323</b>
11.1	Introduction .....	323
11.2	Common Forms of Resistance-Based Equations .....	325
11.3	Challenges with Types of Resistance-Based Models .....	340
11.4	Parameters for the Penman-Monteith for Equivalency with More Complicated Models .....	342
11.5	Comparative Model Performance.....	343
11.6	Roughness Length and Zero Plane Displacement .....	345
11.7	Bulk Surface (Stomatal) Resistance.....	355
11.8	Evaporation from Soil and Surface Resistance .....	379
11.9	Weather Measurements for Direct Application of the Penman-Monteith and AFIB Methods and Reference ET Calculation .....	387
11.10	Example Applications of the Single-Layer Penman-Monteith.....	396
11.11	Applications of Evapotranspiration Models Using Remote Sensing Inputs .....	408
11.12	Measurement and Estimation of ET on Sloping Lands .....	409
11.13	Evaporation of Intercepted Rainfall .....	410
<b>12.</b>	<b>REGIONAL ESTIMATES OF EVAPOTRANSPIRATION .....</b>	<b>415</b>
12.1	Introduction .....	415
12.2	Theory .....	416
12.3	Applications .....	418

<b>PART 3: WATER REQUIREMENT ESTIMATES .....</b>	<b>425</b>
<b>13. SELECTION OF APPROPRIATE ESTIMATING METHOD ....</b>	<b>427</b>
13.1 Introduction .....	427
13.2 Time Frame and Required Accuracy .....	427
13.3 Input Data Collection, Screening, and Processing .....	428
13.4 Crop Coefficient Method vs. Direct Methods.....	430
13.5 Evaporation and Evapotranspiration Calculations .....	431
13.6 Summary .....	433
<b>14. ESTIMATES OF IRRIGATION WATER REQUIREMENTS AND STREAMFLOW DEPLETION .....</b>	<b>435</b>
14.1 Introduction .....	435
14.2 Net Irrigation Water Requirement and Effective Precipitation .....	435
14.3 Leaching Requirement.....	439
14.4 Miscellaneous Water Requirements .....	443
14.5 System Losses .....	445
14.6 Precipitation Runoff .....	451
14.7 Improvements in Estimating Water Requirements .....	454
14.8 Depletions to the Water Resource .....	455
<b>APPENDIXES</b>	
A. Conversion and Meteorological Tables .....	457
B. Mean Crop Coefficients in Subhumid Climates .....	471
C. Lengths of Crop Development Stages.....	487
D. Basal Crop Coefficients in Subhumid Climates .....	499
E. Mean and Basal Crop Coefficients for Crops Common to Temperate and Continental Climates.....	513
F. Basal Crop Coefficients for Crops Common to Temperate and Continental Climates with Thermal Basis.....	523
G. Documentation for Crop Coefficient and ET Data Reporting and Determination of ET from Remote Sensing .....	543
H. Weather Data Integrity .....	569
I. Contribution of Capillary Flow from a Shallow Water Table to Evaporation and Evapotranspiration.....	609
J. Derivation of the Penman-Monteith Equation.....	619
K. Regional Estimating Methods and Methods Not Commonly Used in the United States .....	627
L. Comparison and Ranking of Methods for Estimating ET .....	637
M. Glossary .....	661
<b>REFERENCES .....</b>	<b>669</b>
<b>INDEX .....</b>	<b>733</b>

## PREFACE

This Manual of Practice provides information on evaporation and evapotranspiration that practicing engineers, hydrologists, and others need to evaluate data received from various sources. It also provides background information to enable practicing engineers, educators, and researchers to improve procedures for estimating evapotranspiration (ET) to achieve the accuracy needed for specific purposes.

This manual updates and expands the scope of the first edition, *Evapotranspiration and Irrigation Water Requirements*, published in 1990. The manual is intended for use by consulting engineers working on water issues and instructors in agricultural and civil engineering, environmental sciences, and agronomy. It is intended to serve as a primary reference for agricultural, environmental, and engineering students, and professionals in water-related agencies. This revised edition incorporates many years of user experience with the previous manual and recent advances in the physics of evaporation from plant and soil surfaces. It also incorporates extensive material from the ASCE *Hydrology Handbook* (1996). The first edition of this manual required many years of planning, and its organization evolved through a series of revisions starting with the report "Consumptive Use and Irrigation Water Requirements" (Jensen 1973). Manual 70 followed the same organization as Jensen (1973), with several new sections added. This revised edition has been restructured based on the experience gained by users of Manual 70. The scope now includes a chapter on evaporation from water surfaces and expanded and more detailed information on estimating evaporation from land surfaces using the crop coefficient method. The manual includes chapters on applying the direct Penman-Monteith and other resistance-based ET estimating methods, producing regional ET and stream depletion estimates, and irrigation requirement estimates. Appendixes A-L have been expanded to include more details on the crop coefficient method, weather data integrity, and derivation of the Penman-Monteith equation and to

include a section summarizing estimating methods not commonly used in the United States.

Data sets used for evaluations have been revised based on new data and information from test sites. In this edition, evaluations focused on accuracy of estimates rather than on comparing various estimating methods, as was done in the first edition. Some comparative statistics among ET methods from the first edition are repeated in Appendix L of this edition.

International System of Units (SI) units are used throughout the manual, as in the first edition. The SI unit used for daily total energy, megajoules per square meter ( $\text{MJ}/\text{m}^2$ ), was retained even though some users may prefer to work with average daily or hourly energy units of watts per square meter ( $\text{W}/\text{m}^2$ ).

Background information on consumptive use in Chapter 1 of the first edition was originally prepared by early experts such as H. F. Blaney Sr. Part of this information was retained in the second edition for historical purposes. The editors, Jensen and Allen, updated chapters from the first edition and functioned as the principal authors of new chapters and sections. Drafts of updated and new chapters were reviewed by the Task Committee, and the final manuscript was reviewed and accepted by the Blue Ribbon Review Committee.

Marvin E. Jensen

Richard G. Allen

## ACKNOWLEDGMENTS

The following organizations and individuals contributed valuable assistance in the research and preparation of the second edition of this manual:

- University of Idaho Research and Extension Center and Idaho Agricultural Experiment Station, Kimberly, ID;
- Agricultural Research Service, U.S. Department of Agriculture, Bushland, TX;
- Agricultural Research Service, U.S. Department of Agriculture, Kimberly, ID;
- Department of Land, Air and Water Resources, University of California, Davis, CA;
- Department of Biological Systems Engineering, University of Nebraska, Lincoln, NE;
- Ivan's Engineering, Inc., Centennial, CO;
- Dr. Frank H. Quinn, Great Lakes Environmental Research Laboratory, NOAA, Ann Arbor, MI; Dr. Richard Allen, University of Idaho; and Prof. Emeritus William O. Pruitt, University of California, Davis, CA, were primary contributors to Chapter 4, "Evaporation and Evapotranspiration" of the ASCE *Hydrology Handbook* (1996 2nd Ed.), which served as a major source of material for evaporation from open water used in this revised version of Manual 70;
- The meticulous and long-term collection of accurate and representative agricultural ET data from weighing lysimeter systems by W. O. Pruitt of the University of California, Davis, and Dr. James L. Wright of the USDA-ARS, Kimberly, ID (ret.), contributed substantially to the foundation of crop coefficient tables summarized in this edition; lysimeter measurement of grass reference ET by Pruitt and alfalfa reference ET by Wright provided much of the basis for the form and calibration of the ASCE standardized Penman-Monteith equation;
- The ASCE-EWRI Task Committee on Standardized Calculation of Reference Evapotranspiration Calculation (ASCE 2005) recommended

- definitions and calculation procedures for reference ET and supporting equations;
- United Nations Food and Agriculture Organization and the International Commission on Irrigation and Drainage (ICID) supported development of international standardization of ET and associated crop coefficients and helped organize data and methods for ET estimation in FAO-24 (Doorenbos and Pruitt 1977) and FAO-56 (Allen et al. 1998); crop coefficient material from these publications is included in Appendixes **B-F**;
  - Blue Ribbon Panel Reviewers Thomas W. Ley, Colorado Division of Water Resources, Pueblo; Ronald L. Elliott, University of Oklahoma, Stillwater (retired); Thomas Trout, ARS, USDA, Fort Collins, CO (ret.); and Paul W. Brown, University of Arizona, Tucson, contributed substantially to the completeness and accuracy of the manuscript;
  - Professor Luis Santos-Pereira and students of the University of Lisbon, Portugal, provided long-term review, testing, and validation of many concepts and methodologies described in this manual;
  - Professor Ayse Kilic and students of the University of Nebraska-Lincoln, provided substantial review, testing, and validation of concepts and calculation methodologies;
  - Thanks are due to the Northern Colorado Water Conservancy District for hosting the task committee and providing facilities for the task committee to meet in November 2004; and
  - Co-editor Marvin Jensen, who has retired and donated his books, greatly appreciates the tremendous input to the revised manual provided by Rick Allen; Rick has kept abreast of recent developments on measurement and methods for measuring and estimating ET.

## NOTATION

Abbreviations, symbols, and common subscripts and superscripts are listed, along with a chart of units used in the International System. Only the most frequently used symbols are included with their common units. Less frequently used symbols and empirical expressions are defined in the text. Some abbreviations and symbols have other dimensions, which are specified in the text. In a few cases, the same symbol is used for different variables; the use will be specified in the text. Symbols for empirical equations are defined in the text.

### Abbreviations

AW	Available soil water
BREB	Bowen ratio energy balance
CU	Consumptive use
E	Evaporation
ET	Evapotranspiration
FWS	Free-water surface
LAI	Leaf-area index
MAD	Management allowed depletion
PM	Penman-Monteith
RAW	Readily available water
TAW	Total available water
VPD	Vapor pressure deficit
YTD	Year to date

## Symbols

Symbol	Definition	Common units
$A$	Area	$\text{m}^2$
$C_d$	Denominator coefficient for the ASCE Standardized PM equation	—
$C_n$	Numerator coefficient for the ASCE Standardized PM equation	—
$E$	Evaporation, depth rate	$\text{mm d}^{-1}$ , $\text{mm h}^{-1}$
$E_{eq}$	Equilibrium evaporation	$\text{mm d}^{-1}$ , $\text{mm h}^{-1}$
$E_o$	Evaporation rate from free water as latent heat flux density, $\lambda E$	$\text{mm d}^{-1}$ , $\text{mm h}^{-1}$ $\text{MJ m}^{-2} \text{d}^{-1}$ , $\text{MJ m}^{-2} \text{h}^{-1}$ , $\text{W m}^{-2}$
$E_{pan}$	Evaporation rate from Class A pan	$\text{mm d}^{-1}$
$EC_e$	Electrical conductivity of the saturated soil extract ( $1 \text{ mmho cm}^{-1} = 1 \text{ dS m}^{-1}$ )	$\text{dS m}^{-1}$
$ET$	Evapotranspiration rate	$\text{mm d}^{-1}$ , $\text{mm h}^{-1}$
$ET_c$	ET from a particular crop	$\text{mm d}^{-1}$ , $\text{mm h}^{-1}$
$ET_o$	ET from a well-watered grass reference crop as latent heat flux density, $\lambda ET_o$	$\text{mm d}^{-1}$ , $\text{mm h}^{-1}$
$ET_r$	ET from a well-watered alfalfa reference crop as latent heat flux density, $\lambda ET_r$	$\text{mm d}^{-1}$ , $\text{mm h}^{-1}$
$ET_{ref}$	Reference evapotranspiration, general	$\text{mm d}^{-1}$ , $\text{mm h}^{-1}$
$G$	Heat flux density to the ground	$\text{MJ m}^{-2} \text{d}^{-1}$ , $\text{MJ m}^{-2} \text{h}^{-1}$ , $\text{W m}^{-2}$
$G_{sc}$	Solar constant	$\text{MJ m}^{-2} \text{h}^{-1}$ , $\text{W m}^{-2}$
$H$	Heat flux density to the air	$\text{MJ m}^{-2} \text{d}^{-1}$ , $\text{MJ m}^{-2} \text{h}^{-1}$ , $\text{W m}^{-2}$
$J$	Day of the year	
$K_A$	Clearness index for solar radiation	

(Continued)

Symbol	Definition	Common units
$K_B$	Clearness index for direct beam solar radiation	
$K_c$	Crop coefficient general (not the same as the Blaney-Criddle $K$ )	
$K_{cb}$	Crop coefficient (basal), soil water not limiting transpiration, but the soil surface is visually dry	
$K_{cm}$	Mean, or single, crop coefficient	
$K_e$	Coefficient to adjust for increased evaporation from the soil	
$K_L$	Landscape coefficient	
$K_s$	Adjustment coefficient for water stress	
$K_t$	Turbidity coefficient	
$LAI$	Leaf-area index	
$LF$	Leaching fraction	
$LR$	Leaching requirement	
$P$	Atmospheric pressure	kPa
$P$	Precipitation	mm
$Q_i$	Inflow rate	$\text{m}^3 \text{d}^{-1}$
$Q_o$	Outflow rate	$\text{m}^3 \text{d}^{-1}$
$R$	Universal gas constant	$\text{kJ kg}^{-1} \text{K}^{-1}$
$R$	Radiation, general	$\text{MJ m}^{-2} \text{d}^{-1}$ , $\text{MJ m}^{-2} \text{h}^{-1}$ , $\text{W m}^{-2}$
$R_a$	Exoatmospheric (extraterrestrial) solar radiation on a horizontal surface	$\text{MJ m}^{-2} \text{d}^{-1}$ , $\text{MJ m}^{-2} \text{h}^{-1}$ , $\text{W m}^{-2}$
$R_b$	Net outgoing long-wave radiation	$\text{MJ m}^{-2} \text{d}^{-1}$ , $\text{MJ m}^{-2} \text{h}^{-1}$ , $\text{W m}^{-2}$
$R_{bo}$	Net outgoing long-wave radiation on a cloudless day	$\text{MJ m}^{-2} \text{d}^{-1}$ , $\text{MJ m}^{-2} \text{h}^{-1}$ , $\text{W m}^{-2}$
$R_n$	Net incoming radiation	$\text{MJ m}^{-2} \text{d}^{-1}$ , $\text{MJ m}^{-2} \text{h}^{-1}$ , $\text{W m}^{-2}$
$R_{nl}$	Net outgoing long-wave radiation	$\text{MJ m}^{-2} \text{d}^{-1}$ , $\text{MJ m}^{-2} \text{h}^{-1}$ , $\text{W m}^{-2}$

(Continued)

(Continued)

Symbol	Definition	Common units
$R_{ns}$	Net solar radiation	$\text{MJ m}^{-2} \text{d}^{-1}$ , $\text{MJ m}^{-2} \text{h}^{-1}$ , $\text{W m}^{-2}$
$R_s$	Solar radiation at the surface on a horizontal plane	$\text{MJ m}^{-2} \text{d}^{-1}$ , $\text{MJ m}^{-2} \text{h}^{-1}$ , $\text{W m}^{-2}$
$R_{so}$	Solar radiation on a cloudless day	$\text{MJ m}^{-2} \text{d}^{-1}$ , $\text{MJ m}^{-2} \text{h}^{-1}$ , $\text{W m}^{-2}$
$RH$	Relative humidity	%
$RH_{max}$	Daily maximum relative humidity	%
$RH_{min}$	Daily minimum relative humidity	%
$T$	Temperature	$^{\circ}\text{C}$ , K, $^{\circ}\text{F}$
$T_d$	Dew point temperature of the air	$^{\circ}\text{C}$ , K
$T_{max}$	Maximum daily air temperature	$^{\circ}\text{C}$ , K
$T_{min}$	Minimum daily temperature	$^{\circ}\text{C}$ , K
$T_o$	Surface temperature	$^{\circ}\text{C}$ , K
$T_w$	Wet bulb temperature of the air	$^{\circ}\text{C}$ , K
$VPD$	Vapor pressure deficit	kPa
$W_f$	Wind function, linear $W_f = a_w + b_w u_2$	
$Z$	Elevation	cm, m
$a, b$	Constants	See usage
$c_p$	Specific heat at constant pressure	$\text{kJ kg}^{-1} ^{\circ}\text{C}^{-1}$
$d$	Zero plane displacement of wind profile	cm, m
$e$	Water vapor pressure in air	kPa
$e_a$	Actual vapor pressure	kPa
$e_d^o$	Saturation vapor pressure at dew point temperature of air	kPa
$e_s$	Saturation vapor pressure	kPa
$e_w^o$	Saturation vapor pressure at wet bulb temperature	kPa
$e_z^o$	Saturation vapor pressure of air at height $z$	kPa
$g$	Acceleration of gravity	$\text{m s}^{-2}$
$g_s$	Surface conductance	$\text{m s}^{-1}$
$h$	Height of vegetation	cm, m
$k$	von Kármán's constant	

(Continued)

Symbol	Definition	Common units
$k_p$	Evaporation pan coefficient	
$m$	Mass, $m_v$ for water vapor, $m_a$ for dry air, $m_s$ for soil	$\text{kg m}^{-3}$
$q$	Specific humidity = $m_v(m_v + m_d)^{-1}$	—
$r_a$	Diffusion resistance of air layer (aerodynamic resistance)	$\text{s m}^{-1}$
	$r_{ah}$ for sensible heat flux	$\text{s m}^{-1}$
	$r_{av}$ for vapor flux	$\text{s m}^{-1}$
$r_i$	Internal leaf diffusion resistance	$\text{s m}^{-1}$
$r_l$	Single leaf stomatal resistance	$\text{s m}^{-1}$
$r_s$	Surface resistance (generally a bulk canopy resistance)	$\text{s m}^{-1}$
$t$	Time	$\text{s, h, d}$
$u_z$	Horizontal wind speed at height $z$	$\text{m s}^{-1}, \text{km d}^{-1}$
$z_{om}$	Roughness length, momentum	cm, m
$z_{ov}$	Roughness length, heat and water vapor	cm, m
$\alpha$	Shortwave reflectance coefficient or albedo	
$\beta$	Bowen ratio, $=H/\lambda E$	
$\Gamma$	Adiabatic lapse rate	$^{\circ}\text{C m}^{-1}$ and $\text{K m}^{-1}$
$\gamma$	Psychrometric constant, $\gamma = c_p P / (0.622\lambda)$	$\text{kPa } ^{\circ}\text{C}^{-1}$
$\gamma^*$	Psychrometric constant modified by the ratio of surface resistance to atmospheric resistance, $\gamma^* = \gamma(1 + r_s/r_a)$	$\text{kPa } ^{\circ}\text{C}^{-1}$
$\Delta$	Slope of the saturation vapor pressure-temperature curve, $de/dT$	$\text{kPa } ^{\circ}\text{C}^{-1}$
$\Delta$	Difference	See usage
$\varepsilon$	Emissivity, $\varepsilon' = \text{net emissivity}$ , $\varepsilon_a = \text{atmospheric emissivity}$ , and $\varepsilon_{vs} = \text{vegetative and soil emissivity}$	

(Continued)

(Continued)

Symbol	Definition	Common units
$\lambda E$	Latent heat flux density	$\text{MJ m}^{-2} \text{d}^{-1}$ , $\text{MJ m}^{-2} \text{h}^{-1}$ , $\text{W m}^{-2}$
$\Theta$	Volumetric soil water content	
$\lambda$	Latent heat of vaporization	$\text{MJ kg}^{-1}$
$\pi$	$\pi = 3.14159$	
$\rho_a$	Air density, $\rho_w$ for water vapor, $\rho_b$ for bulk soil, and $\rho_y$ for absolute humidity	$\text{kg m}^{-3}$
$\sigma$	Stefan-Boltzmann constant	$\text{kJ m}^{-2} \text{s}^{-1} \text{K}^{-4}$ , $\text{MJ m}^{-2} \text{d}^{-1} \text{K}^{-4}$ , $\text{W m}^{-2} \text{K}^{-4}$
$\omega_s$	Sunset hour angle	radians

### Subscripts

$a$	Property of air
$o$	Property at the atmosphere-surface interface, or reference value
$s$	Property of soil or the surface
$v$	Property of vegetation or vapor
$w$	Property of water
$z$	Property at height $z$
1, 2	Reference times

### Superscript

$o$	Saturation
-----	------------

### International System (SI) of Units

Quantity	Unit	Symbol	Formula
<b>Base Units</b>			
Length	meter	m	
Mass	kilogram	kg	
Time	second	s	
Electric current	ampere	A	

(Continued)

Quantity	Unit	Symbol	Formula
Thermodynamic temperature	kelvin	K	
Amount of substance	mole	mol	
<b>Derived Units</b>			
Force	newton	N	$\text{kg m s}^{-2}$
Pressure	pascal	Pa	$\text{N m}^{-2}$
energy, work, quantity of heat	joule	J	$\text{N m}$
Radiant flux	watt	W	$\text{J s}^{-1}$
Electric potential	volt	V	$\text{W A}^{-1}$
Conductance	siemens	S	$\text{A V}^{-1}$
<b>Additional Units</b>			
Time	minute	min	$1 \text{ min} = 60 \text{ s}$
	hour	h	$1 \text{ h} = 60 \text{ min} = 3,600 \text{ s}$
	day	d	$1 \text{ d} = 24 \text{ h} = 86,400 \text{ s}$
Temperature	degree Celsius	°C	$^{\circ}\text{C} = \text{K} - 273.15$
Volume	liter	L	$1 \text{ L} = 1 \text{ dm}^3 = 10^{-3} \text{ m}^3$
Mass	metric ton	t	$1 \text{ t} = 10^3 \text{ kg}$

**Prefixes**

Multiplication factor	Prefix	Symbol
$1,000,000,000 = 10^9$	giga	G
$1,000,000 = 10^6$	mega	M
$1,000 = 10^3$	kilo	K
$0.1 = 10^{-1}$	deci	D
$0.01 = 10^{-2}$	centi	C
$0.001 = 10^{-3}$	milli	m
$0.000001 = 10^{-6}$	micro	:
$0.000000001 = 10^{-9}$	nano	H

Sources: ASTM 380-76 (1976); Wandmacher and Johnson (1995).

This page intentionally left blank

# **PART 1**

## **BASIC CONCEPTS**

This page intentionally left blank

# CHAPTER 1

## INTRODUCTION AND HISTORY

### 1.1 INTRODUCTION TO SECOND EDITION

In 1990, the American Society of Civil Engineers (ASCE) published the first edition of *Manuals and Reports on Engineering Practice No. 70*, which was prepared by the Irrigation Water Requirements Committee of the Irrigation and Drainage Division. In 1995, the Committee was renamed the “Evapotranspiration in Irrigation and Hydrology Technical Committee” to include evapotranspiration on nonirrigated lands. The mission of the committee is to advance the science and practice of measuring and estimating evapotranspiration with emphasis on developing and evaluating procedures and tools for integrated water management needed in planning, design, and management of irrigation projects, hydrologic units, and water resources systems. In 2000, when the stock of printed copies had been sold, the Committee appointed a Task Committee to prepare an updated revised edition of the manual.

Since its publication, *Manual 70* has served as a valuable reference for specialists working in agrometeorology, hydrology, and irrigation planning and management. The first edition contained equations for estimating evapotranspiration, both theoretical and empirical, and equations to calculate parameters in the ET equations and for various components of the energy balance. Because the general knowledge base of users has improved greatly over the past two decades, the manual has been restructured for greater ease in applying new technology and standardized calculations, and new information has been included. The manual’s current focus is on state-of-the-art technology with less emphasis on older empirical equations and comparisons among various methods of estimating evapotranspiration (ET).

This revised edition includes extensive material from the ASCE *Hydrology Handbook* (Allen et al. 1996), which was a product of the previously noted ET technical committee. Additional material on the standardization of reference ET calculation and clarification of its application developed by a task committee of the ET committee from 1999 through 2004 (ASCE 2005) has been brought into this edition. Because integrated water management often involves estimating evaporation from water bodies such as storage and regulating reservoirs, new material on estimating evaporation (E) from water surfaces has been added.

The revised edition presents various methods for estimating ET and example calculations as a guide to users in applying the new technology. Graduate students preparing to enter one of these fields should find this manual to be useful as a source of basic information. Tables of basic air and water properties, conversion factors, and meteorological tables are retained for reference purposes.

## Objectives

Objectives of the first edition were

1. To define and interpret ET, or consumptive use, terminology;
2. To provide practicing engineers, hydrologists, educators, and researchers with a concise summary of factors controlling ET;
3. To describe modern methods for measuring and estimating ET;
4. To describe the major factors to consider in determining irrigation water requirements for fields, farms, projects, and river basins;
5. To summarize representative measured ET from irrigated crops;
6. To evaluate the accuracy of various estimating procedures under various climatic regimes;
7. To present improvements in methods for estimating ET; and
8. To present a selected bibliography for additional information.

The large volume of recent literature on ET makes it impractical for the engineer who does not specialize in this field to review and evaluate available ET data and methodology best suited for solving a particular hydrology, irrigation, or water supply problem. The first edition of this manual was intended to meet this continuing need. Many of these objectives are still current; however, recent improvements and acceptance of standardized methods for estimating ET make review of historic, or empirical, methods less relevant. The new objectives include more focus on the latest technology for estimating ET and E during the growing and the nongrowing seasons and E from water bodies that may be associated with irrigation projects. These technologies include numerical models and the use of remotely sensed variables for estimating ET over large areas.

## Chapter Content

This chapter briefly summarizes the history of activities leading to the development of the first edition and preparation of the revised edition. As competition for available water resources continues to increase, transfers of water rights and associated litigation require background on historical water use measurements and the methods previously used to estimate crop water requirements. Summaries of older ET-estimating procedures have been retained in the appendixes for reference purposes along with a summary of comparisons of estimating methods that were presented in the first edition.

Chapter 2 summarizes evaporation (E) and evapotranspiration (ET) processes and controlling factors such as water and energy budgets and vegetation, soil, and management factors. Concepts for estimating evaporation from soils and water surfaces and estimating ET are summarized in Chapter 2 and presented in detail in Chapters 4–6. E and ET measurement methods from land surfaces, including measuring changes in soil water content over time, lysimetry, Bowen ratio energy balance, eddy covariance, and water balance, are introduced in Chapter 2 and discussed in detail in Chapters 7–11.

Chapter 3 describes the soil-plant-atmosphere system beginning with a summary of the physical properties of water, water vapor, and air. Equations relating the various variables are presented. Soil properties are summarized along with equations relating the energy state of soil water. Equations describing the soil water characteristics along with basic equations of water flow through soil are presented. A summary of soil-plant characteristics follows a summary of soil water properties as influenced by soil texture. Vegetative, or crop, properties and plant root characteristics are described.

Chapter 4 presents the surface energy balance with descriptions of the components of net radiation. The chapter also summarizes surface properties affecting the absorption and reflection of solar radiation and presents equations presented for calculating components of net radiation. The surface energy balance is emphasized throughout the revised edition because of its importance in establishing upper limits on the transformation of liquid water to vapor and consequently ET. The surface energy balance forms the basis of the most complete and accurate ET equations, including the Penman and Penman-Monteith methods.

Chapter 5 describes surface-atmosphere interactions that affect net radiation and the ET process. The chapter emphasizes the use of a standardized surface to isolate the evaporative demand due to weather effects. Two surfaces are described. These are a short crop such as clipped grass and a tall crop such as alfalfa having about 0.5-m plant height.

Chapter 6 describes typical methods of estimating evaporation from water surfaces. These include use of an evaporation pan with appropriate

coefficients, water balance, and aerodynamic and energy balance procedures along with the use of combination methods. The chapter presents several examples of estimating evaporation using a combination method and important precautions.

Chapter 7 describes methods of estimating ET from land surfaces using various methods. These methods include a detailed discussion of volumetric measurement of soil water depletion and the use of lysimeters and evaporimeters. Procedures based on energy balance and aerodynamic methods are described, including the Bowen ratio energy balance and eddy covariance methods along with fetch requirements for these methods. The chapter describes the methods in detail along with example calculations and recommendations for collection of accurate data.

Chapter 8 describes the procedures for estimating ET from land surfaces using the Penman-Monteith (PM) equation together with guidelines for characterizing the surface parameters that determine the bulk aerodynamic resistance. The chapter emphasizes the development of the standardized equation for estimating ET from a reference crop surface and the use of vegetative coefficients to estimate ET.

Chapter 9 describes the development of typical soil water profiles during evaporation from soils, stage 1 and stage 2 evaporation, evaporation models for estimating evaporation and evaporation-transpiration relations, and example estimates of evaporation compared with measured evaporation.

Chapter 10 describes the crop coefficient (and landscape coefficient) method for estimating evaporation from land surfaces. It summarizes the development of coefficients to characterize ET as a function of the amount of natural or landscape vegetation or the development of annual or perennial crops. These coefficients are used in conjunction with an estimate of evaporative demand or reference ET such as short-clipped grass or 0.5-m tall alfalfa. An example of generalized mean crop coefficient illustrates the effects of increasing leaf area and surface wetness and decreasing available soil water. The chapter describes basal crop coefficients, representing conditions when the soil surface is visually dry. With basal coefficients, adjustments are made when the surface is wetted by rainfall or irrigation. The chapter also describes characteristics of evaporation from bare soils along with typical soil water profiles in the upper layers of soil. The effects of leaf area on the rate of evaporation are explained along with several methods for estimating the amount of evaporation. Finally, the chapter presents the typical linear Food and Agriculture Organisation (FAO)-style crop coefficient curve along with procedures for estimating the magnitude of the various growth stages and durations including several example calculations.

Chapter 11 describes procedures for estimating evaporation from land surfaces using the direct Penman-Monteith (PM) equation and full energy balance equations. Procedures include estimating surface roughness, zero

plane displacement, relationships between surface roughness and plant height, example roughness length scalars, determination of roughness and zero plane displacement from wind profile measurements, leaf area estimates and leaf resistances, bulk surface resistance for various types of green vegetation cover, and stomatal conductance. The chapter also presents procedures for estimating evaporation from soil using the direct PM method and evaporation from intercepted rainfall. Required weather measurements for using the direct PM are described along with procedures for adjusting noncharacteristic data. The chapter presents several calculation examples, including estimates for sloping lands.

Chapter 12 covers several methods for regional estimates of evaporation from land surfaces. These include the complementary approach and the use of energy balance models for forests and grasslands and for cultivated lands. The chapter briefly describes approximating monthly streamflow for ungauged watersheds and data sources for cultivated areas and natural vegetation.

Chapter 13 summarizes the factors to consider in selecting a method for estimating ET, including the available timeframe, required accuracy, and the screening of input climate data. The various methods available for ET calculations are presented.

Chapter 14 summarizes methodology for estimating irrigation water requirements and refers to various chapters and sections in the manual for specific details. It includes procedures for estimating soil leaching requirements, miscellaneous water requirements, and effective precipitation. The chapter also provides brief descriptions of storage and distribution system losses and methods to account for nonuniform water applications.

The appendixes include several appendixes from the first edition such as a saturation vapor pressure-temperature table, conversion factors, thermodynamic constants, air density equations, and an updated glossary. New appendixes include several sets of crop coefficients, a listing of recent publications that include crop coefficients, weather data assessment, contribution of capillary flow to E and ET, a summary of estimating methods no longer commonly used in the United States, a derivation of the Penman-Monteith equation, and a summary of comparisons of estimating methods that were presented in the first edition.

## 1.2 DEVELOPMENT OF ET AND CU STUDIES IN THE UNITED STATES

### Consumptive Use and Evapotranspiration

Consumptive use (CU) of water, or evapotranspiration, is one of the most basic components of the hydrologic cycle. It affects the water

balance from the time water falls upon the land as precipitation until the residual reaches the ocean. Consumptive use, which includes evaporation of water from land and water surfaces, transpiration by vegetation, and the generally small volume of water contained in harvested vegetation, continues to be of foremost importance in water resources planning and management and in irrigation management. Consumptive use has been particularly important in arid and semiarid irrigated areas of the world. It will become more important as available water resources are reallocated to meet various needs of growing populations. Its importance in humid areas has been increasing with the expansion of supplemental irrigation and inadequate water storage.

The term *evapotranspiration* (ET) has become more common than the term consumptive use. ET is the same as consumptive use, except the latter includes water retained in the plant tissue that is minor relative to the total ET. This edition uses primarily the term ET.

Knowledge of ET is necessary in planning and operating water resource projects. ET is involved in problems of water supply, both surface and underground, and water management, and in the economics of multipurpose water projects for irrigation, power, water transportation, flood control, municipal and industrial water uses, and wastewater reuse systems.

ET is important in negotiating water compacts and treaties and in the litigation and adjudication of water rights in major river systems in which the welfare of people in urban centers, states, and even nations is involved. ET data are essential for estimating irrigation water requirements. They also are useful for estimating municipal and industrial water needs, sizing wastewater reuse systems, and estimating water yield from watersheds, recharge to and safe yields from ground water basins, and streamflow depletions in river basins.

Numerous formulas have been developed that relate ET and climatological data based on physical theory and experimental data collected by engineers and scientists. These formulas are used to transpose observed ET data from one area to other areas where few or no data, except climatological records, are available.

The standardization of methodology and availability of data for estimating ET have improved greatly since the 1950s, and they are still evolving. Engineers, agronomists, soil scientists, and water planners need to adapt relationships that are based on sound physical laws and principles. Future estimates of ET will need to be more accurate than in the past as competition for water increases and its value increases. The legal system involved in water rights transfer can no longer justify "simple" estimating procedures if more accurate methods are available.

## Historical Background (United States)

The first edition contained a brief summary of developments of methodology for estimating consumptive use, or ET. Evaporation and transpiration have been studied for centuries (Brutsaert 1982), but the term “consumptive use” probably was not applied to water consumption prior to 1900 in the United States. The first edition also briefly summarized extensive early plot and field studies of ET using soil-sampling techniques.

In 1938, the National Resources Committee (Blaney et al. 1938) published definitions of consumptive use (ET). The ASCE *Hydrology Handbook* (ASCE 1949) stated, “...the terms ‘evapotranspiration’ and ‘consumptive use’ have received general acceptance, these terms denote the quantity of water transpired by plants during their growth or retained in the plant tissue, plus the moisture evaporated from the surface of the soil and the vegetation, expressed in feet or inches depth of water lost or used in a specified time.”

Definitions of some other terms such as *duty of water* sometimes have been confused with consumptive use. In this manual, the terms “consumptive use” and “evapotranspiration” are considered synonymous because the amount of water contained within plant tissue is very small compared with that evaporated from soil and plant surfaces.

An excellent summary of seasonal consumptive use of water was prepared by the Duty of Water Committee of the Irrigation Division of ASCE and presented in 1927 and later published (ASCE 1930). Major changes made by engineers and scientists during the second half of the last century are summarized in several publications such as the proceedings of a meeting of physicists in 1955 (Penman 1956b), various conferences on ET (Jensen 1966; ASAE 1985; Camp et al. 1996), and publications such as FAO-56 (Allen et al. 1998). Jensen and Allen (2000) summarized historic events and methods for estimating ET at the ASAE 2000 National Irrigation Symposium. The ASCE Consumptive Use Committee made an early, major compilation of energy balance theory, current methods, and comparisons (Jensen 1973). That publication served as the basis for the first edition of *Manual 70*.

Studies of irrigation water requirements can be traced back many centuries to when irrigation was first practiced as civilization began to rely on agriculture as a way of life. The first edition presented a brief summary of irrigation water requirement studies to show that many recent investigations have only refined general concepts that have been known for decades. Other studies have advanced the science of ET and form the foundation of current and future irrigation management technology.

Problems of nonrepresentative environmental conditions plaguing studies that measured ET using pots and containers and biases caused by unsaturated drainage between sampling dates were recognized in the

1920s. The energy balance concept, which was applied to evaporation from water surfaces in the 1920s and 1930s, was applied to cropped surfaces by Penman (1948) and Budyko (1948). Penman combined energy balance and aerodynamic equations into what is commonly known as the “combination equation.” The Penman equation is well known, and improved versions of the combination equation have been and are used extensively throughout the world. Monteith (1987) presented the background and history of Penman’s career and equation developments.

With modern and continually evolving electronic instrumentation, investigations of evaporation and transpiration mushroomed during the 1960s, 1970s, and 1980s. Special studies have now been conducted in many countries. Unfortunately, increased sophistication and reduced costs of measurement methods have not necessarily improved the accuracy of data collection and, in fact, have frequently facilitated measurement by individuals having too little experience, care, or understanding of the physics and methodology, resulting in data having relatively poor accuracy. Allen et al. (2011c) summarized errors common to modern ET measurement methods. Much of that material is repeated in Chapter 2. Because water resources management has played an increasingly dominant role in regional, national, and international affairs, crop water requirements and irrigation water management have received more attention at all levels of planning.

The Food and Agriculture Organization (FAO) of the United Nations produced a landmark publication on crop water requirements in 1975 (Doorenbos and Pruitt 1975) that was revised in 1977 (Doorenbos and Pruitt 1977). This publication, referred to as FAO-24, almost singly converted ET estimation practices worldwide to the use of reference ET and reference ET-based crop coefficients. The International Commission on Irrigation and Drainage (ICID) Work Group on Crop Water Requirements sponsored a round table conference on evapotranspiration in Budapest, Hungary, in May 1977 (Perrier and Jensen 1979). Definitions originating with the 1977 conference were published in 1985 (Perrier 1985). The Work Group organized an international conference on crop water requirements in Paris in September 1984 (Perrier 1985).

A workshop on evapotranspiration from plant communities was held in Bunbury, West Australia, in May 1982. A selection of papers presented at that workshop was later published (Sharma 1984). The American Society of Agricultural Engineers (ASAE) sponsored a symposium on advances in evapotranspiration in December 1985 that involved several international speakers (ASAE 1985). This symposium summarized advancements in evapotranspiration theory, measurement, and application methods. In 1990, the FAO organized an experts’ conference to discuss updating FAO-24 (Smith et al. 1991). The results of that conference were incorporated into an expanded and refined version of FAO-24 that was published as

FAO-56 ([Allen et al. 1998](#)), where a single equation for reference ET in the form of the standardized Penman-Monteith equation was recommended. The ASCE Committee behind this manual organized an international symposium on lysimetry for evapotranspiration and environmental measurements in 1991 ([Allen et al. 1991a](#)). In 1993, the Working Group on Crops and Water Use of the International Commission on Irrigation and Drainage organized a second workshop on crop-water models ([Pereira 1995](#)). In 1996, ASAE sponsored an international conference on evapotranspiration and irrigation scheduling ([Camp et al. 1996](#)).

These references, along with many other references cited in the first edition of this manual, provide detailed coverage of extensive studies of evapotranspiration and crop water requirements. Readers interested in more detailed aspects of evapotranspiration will find these references to be useful starting points. In addition, many books on hydrology and climatology include sections on evapotranspiration. Some books focus on the principles of the evaporation process such as those of Monteith ([1973](#)), Brutsaert ([1982](#)), Rosenberg et al. ([1983](#)), Monteith and Unsworth ([1990](#)), and Campbell and Norman ([1998](#)). Other books summarize the results of recent conferences. For example, the publication by the Netherlands Committee on Hydrologic Research contains a series of papers that were presented at Technical Meeting 44 at Ede, the Netherlands on 25 March 1987. These papers summarized progress that had been made on this subject in Europe ([Hooghart 1987](#)).

## Evolution of ET Estimating Methods

The need to improve accuracy or efficiency of application motivates development of new technology. Current methodology based on energy balance and mass transfer evolved rapidly during the second half of the twentieth century as competition for available water resources increased and development of new electronics and instrumentation technology enabled measuring variables controlling the ET process.

Jensen and [Allen \(2000\)](#) traced the evolution of practical ET estimating methods over the past century. In the United States, engineers, the main users of ET estimating methods, did not begin with rigorous theories in developing new ET estimating methods, but generally sought empirically based relationships that reproduced measurements. Also, agrometeorological theory and methodology were not well developed until after the 1960s. Most early estimating methods were based on mean air temperature as an index of evaporative demand, or as an indicator of solar radiation. Few early estimating methods involved air humidity, and none involved wind speed directly.

Between 1896 and 1939, many irrigation investigations involving plot and field studies were conducted to determine the relation between

quantity of water used by crops and crop yields. Similar studies were conducted to determine the loss of water by evaporation from soils. For example, Sleight (1917) studied evaporation near Denver in 1916. He reviewed early work starting with Dalton in 1802 and cited Livingston's bibliography on evaporation (Livingston 1908). The need for estimating evaporation from reservoirs was the driving force for many evaporation studies. Houk (1927) summarized investigations of evaporation by the U.S. Bureau of Reclamation (USBR). This paper included discussions by 13 other engineers and specialists. Rohwer (1931) conducted a comprehensive study of evaporation from pans of various sizes and exposures at Fort Collins, Colorado, in cooperation with the Colorado Agricultural Experiment Station. Penman (1948) cited the work of Rohwer as classic and compared his own empirically derived aerodynamic equation with that obtained by Rohwer. Later studies and reports on evaporation included measurements made on Lake Hefner (USGS 1954), on pans and lakes (Kohler et al. 1955), and on Lake Mead (Harbeck et al. 1958).

Many measurements of annual or seasonal ET (or consumptive use, CU) were made from 1890 through 1925. The Duty of Water Committee of the Irrigation Division, ASCE, summarized seasonal CU data in a progress report presented by O.W. Israelsen in 1927 and later published (Duty of Water Committee 1930).

Interest in understanding the daily rate of transpiration ( $T$ ) produced studies of the impact of climate on transpiration by plants in containers beginning in the latter part of the 19th century. L. J. Briggs of the Bureau of Plant Industry in the USDA conducted many transpiration studies early in the twentieth century. Briggs toured the Great Plains states in the fall of 1905 and arranged cooperative work at six stations in the area. In 1910, Briggs and Shantz initiated their classic studies at Akron, CO, on relative water requirements of plants. In 1916, they summarized their 1912–1914 work and recognized that solar radiation was the primary cause of cyclic change of environmental factors. They corrected measured solar radiation for the area of the plants exposed to direct sunlight and probably were the first to recognize and measure the significance of advected energy in the balance of transpiration. They stated that even on bright days, other sources of energy, such as indirect radiation from the sky and from surrounding objects and heat energy received directly from the air, contributed materially to energy dissipated through transpiration. The concepts of the substantial impact of effective area of vegetation in intercepting and absorbing solar radiation and impact of microscale advection of convected and radiated thermal energy, although recognized by Briggs and Shantz (1916) more than a century ago, have been frequently missed by practitioners today, for example in the operation of lysimeters (Allen et al. 2011c). Briggs and Shantz also evaluated the hourly loss of water from atmometers and evaporation pans in comparison with hourly transpiration

and developed prediction equations for hourly transpiration using the vertical component of solar radiation and temperature rise and solar radiation and vapor saturation deficit. This important relationship laid the foundation for energy-based ET estimating methods that remained dormant for 30 years until Penman (1948) developed the combination equation.

From 1920 to 1940, researchers placed much emphasis on estimating evaporation and seasonal ET. Engineers began studying the CU of irrigation water relative to general climatic conditions. Several empirical equations were developed, many of which were used for various engineering and water rights purposes until the latter part of the twentieth century. Mean air temperature was the primary climatic parameter used in these equations. The USBR began studying temperature and CU relationships in 1920. Hedke (1924) submitted a proposed procedure to the ASCE Duty of Water Committee. His method was based on the assumption that heat (energy) consumed in ET was determined by the energy available. He assumed that the influences of wind, humidity, and vapor pressure on CU were small compared with the influence of heat based on air temperature. The general theory was sound except that radiant energy was not considered.

In the 1920s, Blaney measured ET by alfalfa in California using soil sampling methods. He developed procedures for estimating CU using mean air temperature, percent of annual daytime hours, and average humidity (Blaney and Morin 1942). This approach was later modified by Blaney and Criddle (1945b, 1950). Lowry and Johnson with the USBR developed a procedure for estimating seasonal CU using maximum temperature above 0°C (32°F) during the growing season based on inflow-outflow data from irrigation projects (Lowry and Johnson 1942). Both of these methods involved developing empirical relationships between measured ET and commonly measured weather parameters such as air temperature or parameters available from standard tables such as potential hours of sunshine. Unfortunately, exoatmospheric solar radiation data, which were available in tables, were not used by these authors rather than potential hours of sunshine. Later, Olivier in England developed an estimating method based on a radiation-latitude factor derived from cloudless day solar radiation for latitudes of 5 to 55° and wet bulb depression (Olivier 1961).

In 1939, Thornthwaite and Holzman (1939, 1942) applied aerodynamic and gradient transport theory to ET estimation. They proposed a method that required measuring wind speed and humidity at two heights above the surface. Although theoretically correct, the method was difficult to apply due to difficulty and expense in accurately making the measurements. Thornthwaite later correlated mean air temperature with ET as determined by water balance in valleys with adequate soil water so as not to limit ET (Thornthwaite 1948). He defined this latter empirical and widely

applied equation as an estimate of potential evapotranspiration. The 1948 Thornthwaite method has been shown to estimate best in humid climates and to substantially underestimate in drier climates (Jensen et al. 1990). Pelton et al. (1960) thoroughly evaluated temperature-based methods for estimating potential ET. Tanner and Pelton (1960) developed potential evapotranspiration estimates based on the energy balance method of Penman.

Jensen and Haise (1963) developed a simple equation based on solar radiation and mean air temperature for estimating ET for well-watered crops at full cover. Their intent was to acquaint engineers with the concept of applying energy balance to obtain ET estimates. At that time, the Penman equation was thought to be too complicated to use, given the status of computational tools, weather data commonly collected during this period, and the training of engineers.

Christiansen and Hargreaves, working in California and Utah, developed a string of regression-based equations for predicting monthly grass ET based on pan evaporation, air temperature, and humidity data (Christiansen 1968; Christiansen and Hargreaves 1969). They later reduced weather data requirements to only air temperature, including calculated exoatmospheric radiation, to predict potential available energy and used the difference between maximum and minimum air temperatures to estimate the effect of relative humidity and cloudiness. A culmination of these efforts was the widely accepted 1985 Hargreaves equation for grass reference ET (Hargreaves et al. 1985; Hargreaves and Samani 1985).

Substantial errors or biases in electronic and mechanical measurements of weather parameters or in-field measurements of ET based on lysimeters often plagued by “non-one-dimensionality” hampered much of the early development in ET methods. In many applications, water consumption measured from the lysimeter did not concur, energy-balance wise, to ET from vegetation in a large agricultural field environment. This was due to differences in vegetation growth such as density and height, management practices, watering regime, inner-outer tank gap, and sparseness of vegetation surrounding the lysimeter (Allen et al. 1991b, 2011c). The science of using lysimeters for measuring ET was well documented in a series of 49 papers published in Allen et al. (1991a).

In Europe, engineers and scientists also developed empirical equations for estimating ET. Makkink (1957) published a formula in the Netherlands for estimating potential ET based on solar radiation and air temperature, and Turc (1961) developed a formula in France for potential ET also based on mean air temperature and solar radiation. Makkink’s equation utilized the energy weighting term of the Penman equation, solar radiation, and a small negative constant, and its use is still popular in the Netherlands today.

Today's methods for estimating ET using standard weather measurements of air temperature, humidity, wind, and solar radiation are based on the Penman equation ([Penman 1948, 1956a, 1963](#)). The Penman equation was developed by Howard Penman during World War II in support of the war effort. His objective was to predict soil surface wetness in Western Europe to determine whether Allied tanks and trucks could advance without bogging down ([Penman and Schofield 1951](#)). Penman, a British physicist, deviated from the traditional American engineering approach to estimating ET, which was largely based on empiricism and commonly available data. He began with physics and a theoretical combination of weather parameters in the form of the energy balance equation where the components of evaporation, sensible heat flux, and soil heat flux sum to available net radiation energy. Penman also formulated evaporation in terms of an empirical aerodynamic expression that was supported by measurements of Rohwer ([1931](#)). He then combined the energy balance and aerodynamic expressions by using the Bowen ratio concept to eliminate all terms that relate to measurements at the evaporating surface. The result was the Penman "combination" equation, which required only measurements of air temperature, humidity, and wind speed at some height above the surface, along with solar radiation that was estimated initially from observations of cloud cover. Penman's comprehensive understanding of the physical processes involved in ET and the influence of plants was clearly evident in the introductory paper he presented at the informal meeting on physics held in the Netherlands in September 1955 ([Penman 1956b](#)), where he suggested that both biology and soil science should complement physics in evolving ET estimation methodology.

Application of the Penman equation for routine ET predictions did not become widespread in the United States until the 1970s and 1980s, when two activities occurred: (1) computerized irrigation scheduling models were developed ([Jensen et al. 1970](#)) that required more accurate estimates of ET on a daily time-step basis, and (2) advancements in silicon-based and miniaturized computers made battery-based electronic data loggers available at relatively low cost. These data loggers automated the collection of weather data required for the Penman equation, reducing expense and improving consistency of data collection.

Following the development of the Penman equation, another U.K. researcher, John Monteith, based partly on his research work in California, reformulated the combination equation in 1965 using a more theoretical equation for the aerodynamic transport component of the Penman equation. This new combination equation, commonly termed the Penman-Monteith (PM) equation, included the new parameters of aerodynamic resistance and surface resistance. The resistance parameters provided flexibility to the PM equation for application to a wide range of surfaces and vegetation types. Monteith's efforts ([Monteith 1965](#)) were mirrored by

the development of a similar resistance-based combination equation in the Netherlands by Rijtema (1965). The Meteorological Office Rainfall and Evapotranspiration Calculation System (MORECS) that applied the PM equation to all of the British Isles (Hough and Jones 1997) was the first notable effort at widespread operational application of the PM method beginning in 1981. Ambiguity in predicting roughness and stomatal parameters for these terms impeded widespread application of the method. In 1989, standardized procedures were developed for estimating aerodynamic and surface resistance parameters for reference crops of grass and alfalfa (Allen et al. 1989). This effort was part of the revision of the 1973 ASCE "Consumptive Use of Water and Irrigation Water Requirements" report (Jensen 1973) that was published in 1990 as *ASCE Manual 70* (Jensen et al. 1990).

Throughout recent history, the development of new technology has been influenced by the need for better ET estimates than existed previously. The development of the current standardized reference ET equation (ASCE 2005) was stimulated by the Irrigation Association's 1999 request to the ASCE's ET Committee to help establish a benchmark reference ET equation. The resulting standardized equation represents the current state of the art in estimating ET.

### 1.3 REVISED EDITION

When the first edition was started in the 1960s, the main methods for estimating ET used by engineers were empirical equations in which daily mean air temperature was the primary variable. The edition's objectives and organization were prepared to provide practicing engineers with basic background on the physics and results of research conducted since the 1950s showing that the ET process was largely controlled by net radiation when soil water was not limiting and full plant cover existed. The older edition compared numerous empirical equations developed since about 1940 and more recent energy-based methods and included example calculations using most of these methods.

The revised edition contains substantial material from the first edition, but focuses more narrowly on the recent improvements and standardizations in estimating and measuring ET and their application. Many details of these developments can be found in other publications such as Chapter 4 of the updated ASCE *Hydrology Handbook* (Allen et al. 1996), the updated FAO publication on crop water requirements (Allen et al. 1998), and *The ASCE Standardized Reference Evapotranspiration Equation* (ASCE 2005). As with the first edition, the revised edition emphasizes the need for users of the various methodologies to fully understand the physical foundations that govern and support the methods. Foremost is the law of conservation of

energy that essentially fixes an upper limit on the rate of ET from a large expanse of vegetation. This law serves as a universal guide for assessing the quality and accuracy of ET measurements and as an upper bound on ET at both the field and regional scales. A knowledge of the physics describing thermal (long-wave) radiation emission from both the surface and atmosphere, short-wave transmission through the atmosphere, and turbulent convection processes is paramount to understanding the behavior of methods and in discerning when adjustments to the method application or data handling are warranted. Allen et al. (2011c) summarizes the physical processes associated with modern ET measurement and estimation processes, and Allen et al. (2011d) recommends documentation of ET measurements and calculations to be reported with data and method applications.

In 2000, a task committee of the ASCE Committee on Evapotranspiration in Irrigation and Hydrology organized a special session focused on the development of a single equation for estimating reference crop ET. The session was part of the 4th Decennial National Irrigation Symposium (Evans et al. 2000). The standardized equation is a reduced form of the ASCE Penman-Monteith equation. The development of the standardization was partly due to requests from the Irrigation Association and landscape industry for a single procedure for estimating reference ET. The objective of the request was to help standardize the basis for the myriad landscape (i.e., crop) coefficients that have developed since the late 1980s across the United States. The reduced form equation has been standardized for both a tall reference crop like alfalfa and a short reference crop like clipped grass to support usage in both agricultural and landscape industries. Sets of equations and coefficients were developed for estimating daily or hourly reference ET for the short and tall references. The various forms and applications of the PM and Penman equations and commonly used empirical equations have been implemented in various software including REF-ET (Allen 2012) and spreadsheets (Snyder 2004).

This edition contains a detailed summary of a reduced form, standardized Penman-Monteith equation for estimating reference ET. Details of that equation and its development were presented in separate papers at the 2000 ASAE conference (Allen et al. 2000; Itenfisu et al. 2000), in Itenfisu et al. (2003), and in the task committee report *The ASCE Standardized Reference Evapotranspiration Equation* (ASCE 2005).

This page intentionally left blank

## CHAPTER 2

# EVAPORATION AND EVAPOTRANSPIRATION PROCESSES

### 2.1 INTRODUCTION

Evaporation ( $E$ ) in the natural environment is a basic component of the hydrologic cycle. Evaporation is the physical process by which liquid water is transferred to the gaseous state of water vapor. Sublimation is the physical process of conversion of ice or snow directly to water vapor. Transpiration is the physical process by which water within plant cells evaporates and is transferred as water vapor to the air through plant surfaces, primarily via stomata. Minor amounts of transpiration occur by guttation, a process in which water is expelled from the tips of leaves in small quantities, usually at night following complete rehydration. Evapotranspiration ( $ET$ ) is the sum of vaporization by the combined processes of evaporation and transpiration.

Potential evaporation ( $E_p$ ) is the rate of evaporation from a surface where all surface-atmosphere interfaces are wet or from a free water surface, so that no surface restriction on the rate occurs. Potential evapotranspiration ( $ET_p$ ) is the rate of  $ET$  that can occur when all soil and plant surfaces are wet; therefore, its rate depends on atmospheric conditions and surface characteristics such as its albedo and roughness. Because all soil and plant surfaces do not remain wet for long periods of time,  $ET_p$ , a term once used to describe the maximum rate of  $ET$ , has limited applications. Potential crop  $ET$ ,  $ET_{cp}$ , is a term generally used to represent the maximum value of  $ET$  from a specific crop type having specific properties under conditions of full soil water supply, but not necessarily having a saturated surface, as is the case for  $E_p$  and  $ET_p$ . Under the same weather conditions,  $ET_{cp}$  values can vary according to the wetness of the soil surface and associated evaporation component.

Reference crop  $ET$ , or reference evapotranspiration ( $ET_{ref}$ ), is a concept suggested by Jensen (1968), Wright and Jensen (1972), and Doorenbos and Pruitt (1975, 1977) to address some of the ambiguities associated with definitions for potential  $ET$  and to serve as a consistent climatic index for  $ET$ .  $ET_{ref}$  is the rate at which soil water, if readily available, would be converted to water vapor for a specific type and characteristics of the reference surface under given atmospheric conditions. The leaf surfaces of the well-watered reference crop typically are not wet, so that some minimum surface resistance occurs. The term  $ET_{ref}$  has become the standard to characterize climatic effects on the  $ET$  rate. When estimating  $ET$ , the effects of crop cover, such as leaf area, and stage of growth, such as maturation, are related to  $ET_{ref}$  by a factor that varies with crop development. This factor is typically referred to as the crop coefficient, or the crop coefficient curve.

## 2.2 THE WATER BUDGET

When accounting for water evaporated from the soil-plant system, the conservation of mass for a hydrologic unit is called the water budget, or the water balance. Major components of the water budget for a given period of time are

$$P + I - E + Q_i - Q_o - \Delta S = 0 \quad (2-1)$$

where  $P$  is the precipitation volume;  $I$  is the irrigation volume (if irrigation is applied);  $E$  is the evaporation (or evapotranspiration,  $ET$ ) volume;  $Q_i$  is inflow volume besides that from  $P$  and  $I$ , including lateral inflow and upward flow from a water table;  $Q_o$  is the outflow volume besides  $E$ , including surface runoff, subsurface lateral outflow, and vertical drainage; and  $\Delta S$  is the change in water storage volume within the unit. For some hydrologic units, the rate of  $E$ , or  $ET$ , can be determined by measuring the components  $P$ ,  $Q_i$ ,  $Q_o$ , and  $\Delta S$  expressed on a unit area basis per unit time. When a large soil mass is isolated from its surrounding soil mass and weighed as in a lysimeter, the  $E$  or  $ET$  rate can be measured as the change in mass over short time periods. This is the procedure by which many estimating methods are verified or calibrated. For unit land areas, and for most engineering applications, measuring  $E$  or  $ET$ ,  $Q_i$ ,  $Q_o$ , and  $\Delta S$  is not practical. Therefore, the rate of  $E$  or  $ET$  is usually estimated using climate data and, in some cases, augmented with remotely sensed data. In controlled research and special investigations, if  $Q_i$  and  $Q_o$  are negligible, then  $E$  or  $ET$  can be determined by measuring the change in soil water content,  $\Delta S$ , along with  $P$  over a period of time such as five days or more.

## 2.3 THE ENERGY BUDGET

The process of converting water to water vapor requires a large amount of energy—about 600 times that required to raise the temperature of an equal quantity of water by 1 degree Celsius (C). Therefore, the most common method for estimating  $E$  or  $ET$  is to estimate the energy that is available for  $E$  or  $ET$ . The energy consumed in evaporating water is represented by the latent heat flux density,  $\lambda E$ , so called because the energy flux is “hidden” in the water vapor. That energy becomes “visible” later on, in the form of sensible heating of the atmosphere when the vapor recondenses to liquid during cloud formation. The energy budget for a unit land area comprises a balance among net radiation,  $R_n$ ; latent heat flux density,  $\lambda E$ ; soil heat flux density by conduction,  $G$ ; and sensible heat flux density to or from air by convection,  $H$ . Net radiation is the net amount of radiant energy exchange at a land or water surface considering incoming and reflected solar (i.e., short-wave) radiation and incoming, reflected, and emitted long-wave radiation. Net radiation is the primary energy source for evaporation and evapotranspiration. The main component of net radiation is incoming short-wave solar radiation. Long-wave (i.e., terrestrial) radiation, however, is also an important component of net radiation. When estimating  $E$  or  $ET$  using the energy balance equation, minor components such as energy used in metabolism or stored within the canopy are generally neglected.  $\lambda E$  is converted to  $ET$  depth by dividing  $\lambda E$  by  $\lambda \rho_w$ , where  $\lambda$  is the latent heat of vaporization and  $\rho_w$  is the density of water. Dividing by  $\lambda$  yields  $E$  (or  $ET$ ) in units of  $\text{kg m}^{-2} \text{ time}^{-1}$ , and further division by  $\rho_w$  in  $\text{kg m}^{-3}$  yields  $ET$  depth in units of  $\text{m time}^{-1}$ , which are commonly converted to  $\text{mm time}^{-1}$ .

In semiarid and arid areas, the temperature of well-watered plant leaves can be lower than air temperature during afternoon hours. When this occurs, sensible energy is transferred from the air to the plants and  $H$  becomes negative. As a result, daily latent heat flux can be greater than net radiation, as illustrated in Figure 2-1, where 24-hour  $\lambda E$  from alfalfa in southern Idaho exceeded 24-hour  $R_n$  by 50% on many days, due to advection (i.e., transfer) of sensible heat. Procedures for estimating net radiation and other terms of the energy balance equation are provided in Chapter 4.

## 2.4 CONTROLLING FACTORS

The most accurate means to estimate evapotranspiration is by applying methods, such as the Penman-Monteith equation, that consider all primary factors impacting the evapotranspiration rate. Those factors include weather, which supplies both the energy to evaporate water and the means to

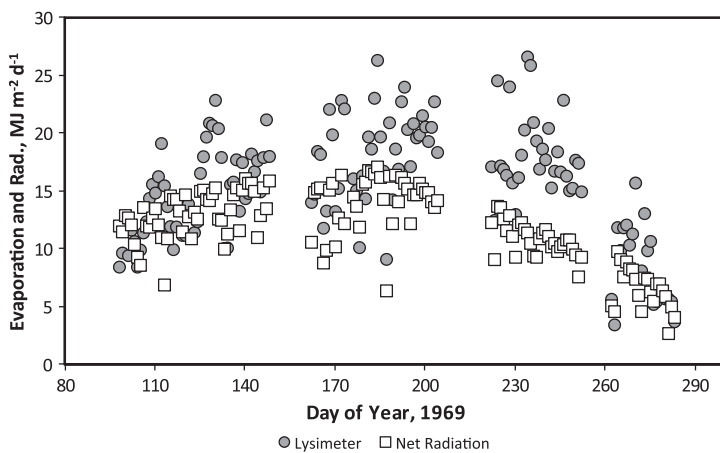


*Fig. 2-1. Daily  $ET$  from full cover alfalfa (height  $> 0.3$  m) collected during 1969 near Kimberly, ID, by weighing lysimeter and expressed as  $\lambda E$  in  $\text{MJ m}^{-2} \text{d}^{-1}$ , along with 24-hour  $R_n$  in  $\text{MJ m}^{-2} \text{d}^{-1}$*

Source: Data from Dr. J. L. Wright, USDA-ARS (ret.)

transport water vapor from the surface. The factors include vegetation characteristics that govern energy interception and controls on transpiration rates, the characteristics of the soil, and the availability of water to supply the evaporation and transpiration processes.

### Weather

The primary weather factor controlling  $E$  and  $ET$  is solar radiation. Solar radiation is the ultimate source of almost all energy required to vaporize water. Other important weather factors are humidity and wind speed. Air temperature also affects the  $E$  or  $ET$  rate, but it has a minor direct impact, although it is highly correlated with both solar radiation and  $ET$ . Because average daily temperatures of plant leaves, shallow water bodies, and soil surfaces are near air temperatures, water vapor pressure at the evaporating surface is generally exponentially related to mean air temperature. The saturation vapor pressure of water is the pressure exerted by its vapor when the liquid and vapor are in dynamic equilibrium at any given temperature. In meteorology, the term vapor pressure means the partial pressure of water vapor in the atmosphere. The water vapor gradient from the plant and soil surfaces to the air depends on surface vapor pressure and vapor pressure of the air, or air humidity. Drier air generally leads to a greater vapor pressure gradient. In addition to the vapor pressure gradient, wind speed affects the potential rate of vapor transfer from the evaporating surfaces to the air.

## Vegetation

**Agricultural Crops** Agricultural crops are the main vegetation for which estimates of ET are needed. For annual crops, the soil remains essentially bare after planting until new plants emerge. The rate of ET from planting until about 10% plant cover is governed by the factors controlling the rate of evaporation from the soil. From about 10% until about 75% plant cover, or a leaf-area index (LAI), of about 3.0, the rate of ET is influenced by increasing LAI. LAI is defined as the area of one side of plant leaves per land area including areas between plants and rows. The rate of ET increases in proportion to leaf-area development under given climatic conditions until the plant canopy reaches about 75%. After 75% cover, the relative ET rate (relative to  $ET_{ref}$ ) remains essentially constant ([Ritchie 1972](#); [Tanner and Jury 1976](#); [Wright 1982](#)) until plants begin to mature, or senesce, after which the relative rate begins to decrease.

For well-watered perennial crops that are dormant during the winter period, the relative rate of ET begins to increase when plants green up in the spring. The increase in relative ET rate is similar to that for annual crops. The relative rate remains essentially constant at full cover until the crop is harvested, such as the cutting of a forage crop. For a short period after harvest, the relative rate of ET will be near that of bare soil if the forage is cut very short. The relative rate of ET increases during regrowth as the LAI again increases ([Ritchie 1972](#); [Tanner and Jury 1976](#); [Wright 1982](#)).

The maximum rate of ET for most common farm crops is nearly the same after the LAI exceeds about 3.0, or the fraction of ground covered exceeds about 0.75 to 0.80, for given climatic conditions ([Ritchie 1972](#); [Tanner and Jury 1976](#); [Wright 1982](#)). The characteristics of the plants, such as aerodynamic roughness and stomatal resistance, also influence the maximum rate.

**Natural Vegetation** As water supplies become limited, greater attention is given to water consumption by natural vegetation, both for water conservation and for sustaining important natural systems. During the growing season, natural vegetation areas include wetland vegetation such as tules and cattails that may be associated with leaking water conveyance systems. During the nongrowing season, estimates of evaporation from dormant vegetation and areas with varying amounts of organic residue are becoming more important in managing water supplies. Surface conditions such as bare soil and snow cover will be different from those of a reference crop, and refined estimates of net radiation are required to account for surface conditions such as crop residue and snow ([Allen and Robison 2007](#)).

For deciduous plants that lose their leaves in the fall, the ratio of ET to reference ET increases rapidly as new leaves emerge in the spring.

After reaching about 70% to 80% cover, the ratio of ET from well-watered natural vegetation to reference ET will generally remain nearly constant until leaves are shed in the fall. The maximum rate of ET is influenced by the height of the vegetation, which is generally greater for trees than for most agricultural crops, and the control of transpiration by leaf stomates. Trees and shrubs generally have more stomatal control than do agricultural crops. Typically, the stomatal control by evergreen trees is greater than that of deciduous trees.

**Landscape Vegetation** Estimates of water requirements and ET for landscape vegetation are not as well established as they are for agricultural crops or large areas of uniform turfgrass such as golf courses. One of the problems associated with estimating landscape ET is that the areas involved are small, edge effects can be large, areas may be shaded part of the day by buildings, and parts of the grass areas and shrubs may be shaded by trees. Many landscape plantings are mixtures of ground cover and shrub and tree plants. Trees are often subjected to harsh environments such as those within or surrounded by paved parking lots. Performance of landscape vegetation is usually based on appearance and function rather than optimal growth. Many species maintain their aesthetical and functional value when irrigated within a range of 20% to 80% of grass reference ET depending on the species and local conditions (Pittenger and Shaw 2004). Plant physiology research has shown that water use by some woody plants does not increase in proportion to reference ET throughout the day under harsh site conditions. Some species may actually use less water because their stomates close. Pittenger and Shaw (2004) recommend that for many landscape species with unknown water requirements, initial irrigation schedules should be set at 50% of grass reference ET. Plant performance must then be evaluated, and irrigation increased or decreased incrementally as needed.

Field research on water requirements of non-turf landscape plants is limited to several commonly used ground cover, tree, and shrub species (Pittenger and Shaw 2004). More information is available for turfgrass. For example, monthly crop coefficients for use with grass reference ET have been developed for cool-season and warm-season turfgrass in California (Pittenger and Shaw 2004). Cool-season species include tall fescue, ryegrass, bentgrass, and Kentucky bluegrass. Warm-season species include Bermuda grass, zoysia grass, and St. Augustine grass. Chapter 10 describes a method for estimating landscape coefficients that is traceable to Pittenger and Shaw (2004), Pittenger and Henry (2005), and other research in California. Landscape coefficients for local areas with conditions different from those described in Chapter 10 can usually be found in publications such as that by Brown et al. (2001).

## Soil Factors

The main soil factors that influence the rate of evaporation from bare soil include the soil's water content and its water characteristic curve, which describes the ability of a soil to hold water and the soil's hydraulic and thermal conductivities. The hydraulic conductivity is largest at saturation and decreases as the soil water content decreases, and therefore influences the rate at which water moves to the surface. The hydraulic gradient toward the surface increases as the surface begins to dry, but the hydraulic conductivity decreases. An additional factor controlling both rate and amount of evaporation from soil is the influence of organic or man-made residue on the soil surface. Residue acts both as a reflective cover and as a thermal insulator, thereby reducing the amount of energy at the soil surface for evaporation. The main soil factor that may influence ET, depending on the frequency of irrigation or rainfall events, is the water-holding capacity of the soil. Chapter 3 gives a summary of soil water-holding characteristics for various soil textures.

## Water Bodies

Estimates of evaporation from water bodies can be obtained by using a relationship between reference ET and pan evaporation, by estimating net radiation and the rate of change in energy storage for the water body and applying the Penman or Penman-Monteith equation, or by applying aerodynamically based equations. The albedo for a water surface is much smaller than for a land area with a green crop, i.e., about 0.06 compared with 0.20–0.25. Albedo is defined as the reflectance of incoming solar radiation from the surface, integrated across the entire solar radiation spectrum. Surface water temperatures are needed, but mean daily surface water temperatures may be relatively close to mean air temperatures for shallow water bodies. An important component in the energy available for evaporation is the advection of energy in the inflow and outflow volumes to or from the water body, e.g., inflow and outflow such as occurs in reservoirs located within river systems.

When the temperatures are low enough that ice forms on the water body and remains over the winter period, estimates of net radiation for ice and snow-covered water becomes more complicated. Winter loss involves estimates of sublimation from ice and snow-covered ice.

Estimates of evaporation from deepwater bodies are more complex compared with shallow water bodies. During the increasing period of the annual cycle of solar radiation, for a somewhat clear water profile, a significant portion of the net solar radiation penetrates below the surface where it is absorbed, warming the water body. Because evaporation is a surface phenomenon, a time lag occurs before stored energy is transported to the surface where it contributes to evaporation or loss by sensible heat

transfer to the atmosphere. During the energy storage period, a thermal profile extending to a depth of 20 m or more may develop in clear water, and the rate of evaporation will be less than the rate of E from shallow water bodies. During periods of decreasing daily solar radiation, transfer of the stored energy to the surface can increase the rate of evaporation to rates above that from a shallow water body. Part of the stored energy may be lost to the atmosphere by convection of sensible heat during cool periods, often making deep, cold lakes and reservoirs efficient storage devices as compared with shallow systems.

### Management Factors

**Available Soil Water** The major management factor affecting the ET rate for agricultural crops and landscapes is the level at which the soil water content is maintained. For high-value crops and those with adequate water supplies, managers endeavor to irrigate to maintain a consistently high soil water level so that plant growth and ET rate are not constrained. As competition for water increases and as supplies become limiting, irrigation of low-value crops such as forages may be reduced. Allowing the soil water to be depleted to lower levels reduces the rate of ET compared with that of a well-watered crop. For some crops like cotton, irrigation may be limited for a period during the vegetative growth period to limit plant size, encourage flowering, and enhance the production of fiber. Limiting irrigation during the vegetative stage may decrease seasonal ET somewhat with little or no loss in crop yield. Regulated deficit irrigation, irrigating less than that for maximum growth, is practiced with some types of orchard and vineyard production systems to reduce total seasonal ET.

**Other Management Factors** Other factors that can affect the rate of crop ET include spacing of rows and plant population density, salinity level in the soil affected by irrigation practices and water management, and the effects of plant pests and diseases. Crop yields are not a good indicator of ET unless soil water limits plant growth. For example, new plant cultivars and hybrids are more efficient in converting dry matter into marketable crop yields with similar ET than older cultivars. Yields of corn hybrids, for example, have increased greatly over the past half-century. Jensen (1994) found that when hybrids were grown under similar nonirrigated or irrigated conditions, yields varied only with the date the hybrid was released. Side-by-side comparison of winter wheat varieties near Bushland, Texas, made in the 1980s showed that the grain yield of the more recent cultivars was about twice that of the 1950s cultivars with no statistically significant difference in ET (Musick et al. 1984). Likewise, fertilizers may influence crop yields greatly when the soil is deficient in

a plant nutrient. Such large increases in crop yields are usually accompanied by small increases in seasonal ET rate due to more prolonged stomatal opening from healthier plants and generally greater leaf area ([Howell 1990](#)).

The type of irrigation system can affect the evaporation component of ET, especially in orchards and vineyards where plants are widely spaced. If the bare soil area is not wetted by the irrigation system, the overall ET rate for a mature vineyard, citrus grove, or deciduous orchard will be less than for a comparable field with an irrigation system that wets the entire soil surface.

## 2.5 ESTIMATING CONCEPTS

Most current estimates of E and ET are based on some form of the energy balance equation or a combination equation containing energy balance and aerodynamic components. Estimates of evaporation from shallow water bodies are often based on measured evaporation in evaporation pans. Estimates for deepwater bodies may also be based on pan evaporation, but pan coefficients require adjustment for energy storage effects.

### Evaporation from Water Surfaces

In the past, the evaporation pan was the most common method for estimating evaporation from small and shallow water bodies. The most commonly used pan in the United States and in many countries is the USA Class A pan. Numerous studies have been made relating pan evaporation to lake evaporation and evaluating pan evaporation as affected by type and size of pan and impact of the local pan environment. Examples of significant early papers are those of Rohwer ([1931, 1934](#)), Young ([1947](#)), Hounam ([1958](#)), Kohler et al. ([1955](#)), Pruitt ([1960](#)), and a review by Hounam ([1973](#)). The literature provides ample evidence of the extreme care that must be exercised in interpreting pan evaporation data, due to the substantial differences in energy balance between pans and many water bodies, to obtain reliable estimates of open water evaporation. Detailed procedures for estimating evaporation are presented in Chapter 6.

### Evaporation from Soils

**Bare Soils** The evaporation rate from bare soil occurs in several stages. During the first stage, which may last for only one to three days in midsummer, the rate of evaporation is controlled by energy input and can be greater than grass ET<sub>ref</sub>. The duration of the first stage is influenced by the rate of evaporation, soil depth, and hydraulic properties of the soil ([Gardner and Hillel 1962](#)). The higher the rate of evaporation, the shorter

the duration of the first stage ([Bond and Willis 1970](#)). The rate of first-stage evaporation is also influenced by the amount of crop residue on the surface. The transition from the first to second stage of drying is variable and depends on climate and soil conditions. Visually, the transition begins when dry places appear on the soil surface. The transition can sometimes be identified by a measured change in albedo or color ([Jackson et al. 1976](#)).

During the second or falling stage, the surface has begun to dry and the source of water for evaporation is largely below the soil surface. Water vapor from evaporation beneath the surface reaches the surface by molecular diffusion and mass flow that is influenced by fluctuating air pressure and vapor gradients. A dry surface soil greatly increases the effective surface resistance to evaporation. After the dry surface mulch has formed, the evaporation rate from the soil,  $E_s$ , will be substantially less than  $ET_{ref}$ , and the rate is controlled mainly by soil characteristics, especially the hydraulic properties and the depth and extent of the original wetting of the soil profile. During the second stage the cumulative evaporation tends to increase with the square root of time for a given soil and somewhat constant evaporation potential. Detailed estimating procedures are given in Chapters [9](#) and [10](#).

**Soils with Partial or Full Vegetative Cover** During the initial stages of annual crop development, the rate of ET is essentially the rate of evaporation until about 10% plant cover has been established. As leaf area develops, the fraction of total ET that is evaporation decreases and the transpiration fraction increases. As leaf area and light interception increase, the energy reaching the soil and resulting evaporation decrease. This principle is commonly used in models of soil evaporation ([Boote and Loomis 1991](#); [Villalobos and Fereres 1990](#); [Bonachela et al. 1999](#)). Procedures for estimating the proportions of  $E$  and transpiration ( $T$ ) are provided in Chapters [9–11](#).

## Reference Evapotranspiration

The concept of reference ET was developed to characterize weather effects on ET as independently as possible from specific crop and natural vegetation effects. This approach also enables comparing climate effects on ET rates in different regions and environments. Estimated reference ET is based on an assumed standard set of surface conditions, including surface albedo, type of well-watered uniform vegetation with a fixed surface resistance, and standardized coefficients for the aerodynamic component of a combination equation. The standardized surface, especially for grass and alfalfa reference ET, can be approximated using lysimeters and the rate of ET determined by measuring the change in weight of the lysimeter or by careful micrometeorologically based (i.e., aerodynamic) measurements.

## Crop Factors (Coefficients)

Crop factors, or crop coefficients, represent the rate of ET from various crops relative to a reference ET and vary within growth stages. Current crop coefficients are based mainly on measurements of ET from sensitive weighing lysimeters or micrometeorological methods that have been related to calculated or measured reference ET. The objective of crop coefficients is to increase the transferability of costly ET measurements by normalizing them with reference ET. More detail on crop coefficients and application is provided in Chapter 10.

## 2.6 MEASUREMENT METHODS

Conferences and workshops over the past 30 years have addressed various methods of measuring ET. One such workshop on ET from plant communities was held in Bunbury, Australia, in May 1982 and included a series of papers on measurement of ET by various methods. A summary of this workshop was presented by Rose and Sharma (1984). Various methods of estimating ET were discussed at the 1993 ASCE National Conference on Irrigation and Drainage Engineering (Allen 1993), including a series of papers on calibration of the neutron probe used to measure changes in soil water and ET. Textbooks or monographs that describe measurement of ET via micrometeorology include Lee et al. (2004) and Hatfield et al. (2005). Brief descriptions of the main methods for measuring ET are summarized in the following sections, with more detailed descriptions given in Chapter 7.

### Change in Soil Water

Determining ET under field conditions by measuring the change in soil water over a period of time is a method that has been used in the United States for nearly a century. Up until the early 1960s, the primary method was by soil sampling and gravimetric analyses to determine the soil water content. Beginning in the 1960s, the neutron soil water probe largely replaced the gravimetric procedure except for evaluating soil water content in the surface 0 to 0.2, or 0 to 0.3-m layer and for calibrating the neutron probe. Since the 1980s, new types of electromagnetic devices based on dielectric and capacitance properties have been used to measure soil water content. Some electromagnetic systems can have a small zone of influence and therefore may not be capable of sampling a large and representative volume of depleted water for determining ET.

Drainage from the zone sampled or the upward movement of water from a lower saturated zone into the zone sampled is a major potential source of error in ET determined by the soil water balance method.

These errors are difficult to detect, but they can be minimized with proper precautions. The soil is usually sampled two to four days after irrigation and again seven to 15 days later or just before the next irrigation. Because the change in soil water over the time interval is desired, most investigators fill the holes from which the soil cores were removed (gravimetric procedure) with soil, mark the site, and then take the next sample 0.3 to 0.4 m from the first core to minimize error due to soil variability.

With the neutron probe and some electromagnetic devices, access tubes are used and the water content at the same site is measured periodically. One of the problems encountered is damage to the plants around the access tube by technicians making the readings. Data obtained from sites with damaged plants will not be representative of field conditions. The average rate of ET in  $\text{mm d}^{-1}$  between sampling dates is then calculated as the change in total soil water plus effective rainfall minus any known drainage that may have occurred.

Determining reliable ET rates by soil sampling requires adequate precautions such as

1. Using a sufficient number of sampling sites to produce ET estimates that are representative of the soil-vegetation complex; for example, six or more for general field conditions ([Allen et al. 2011](#)) and a minimum of four when using neutron techniques ([Kamgar et al. 1993](#) describes the number of neutron probe sites needed relative to plot size);
2. Selecting sites where the depth to the water table is much greater than the root zone depth;
3. Using only those sampling periods when rainfall is light as values for periods of high rainfall is questionable because runoff or drainage may occur; and
4. Minimizing error caused by drainage by
  - a. Applying heavy preplant irrigation at least 10 days before planting,
  - b. Applying less water at each irrigation than the amount that can be retained in the root zone,
  - c. Waiting at least two days after a normal light irrigation before taking the first sample and longer with heavier irrigations or when the ET rate is small, and
  - d. Using only the active root zone depth for ET computations.

Detailed discussions of the problems encountered in determining ET by soil sampling have been presented by Robins et al. ([1954](#)), Jensen ([1967](#)), Jensen and Wright ([1978](#)), and Hignett and Evett ([2002](#)). General problems associated with soil sampling were discussed by Taylor ([1955](#)), Staple and Lehane ([1962](#)), Pratt et al. ([1976](#)), and Evett and Steiner ([1995](#)). More information is given in Chapter 7.

## Lysimetry

Weighing lysimeters (evapotranspirometers) are isolated blocks of soil or tanks filled with soil suspended on a weighing mechanism in which crops are grown. The amount of water lost by evaporation and transpiration is based on the change in weight of the lysimeter. This method provides a direct measurement of ET and is frequently used to study climatic effects on ET and to evaluate estimating procedures and develop crop coefficients. However, lysimeter data may not be representative of field conditions. Soil conditions inside the lysimeters must be essentially the same as those outside. The lysimeter must be surrounded by the same crop that is growing in the lysimeter to ensure one-dimensionality of the measurement (Allen et al. 1991b). Otherwise, errors as large as 200% can occur. Preferably, the lysimeter should be located within an open field of the same crop. Studies of advection at the edges of fields suggest that the lysimeter should be located at least 100 m from the edge of the field.

Lysimeters surrounded by sidewalks or gravel will not provide reliable data, nor will lysimeters planted to a crop surrounded by shorter or taller vegetation. Differences in growth and maturity between the lysimeter plants and surrounding plants and resulting ET measured in the lysimeter relative to ET measured in the surrounding field can be significant (Pruitt and Lourence 1985). High crop coefficients reported in the literature may have resulted from such differences in plant growth between the lysimeter and the surrounding field. The lysimeter-rim-area-to-lysimeter-area ratio should be less than 0.1 (Allen et al. 1991b). For example, with a 10-mm gap and 5-mm inner and outer walls of weighing lysimeter tanks, this ratio would be 0.08 for a lysimeter with an inside dimension of  $1 \times 1$  m [ $4(0.02)(1.02)/1.0$ ].

Lysimeters can be grouped into three categories: (1) nonweighing constant water-table type, which provides reliable data for weekly or longer time periods in areas where a high water table exists and where the water table level is maintained essentially at the same level inside and outside the lysimeter; (2) nonweighing percolation type, in which changes in water stored in the soil are determined by sampling or neutron methods and the rainfall and irrigation percolate are measured (often used in areas of high precipitation); and (3) weighing types, in which changes in soil water are determined either by weighing the entire unit with a mechanical scale or by counterbalanced scale and load cell, by directly suspending by load cells, or by supporting the lysimeter hydraulically. Weighing lysimeters, if well managed, can provide the most accurate data for short time periods. However, mismanagement of the vegetation and vegetation area inside and outside the lysimeter can cause large error, regardless of the precision of the measurement (Allen et al. 1991b, 2011c). ET can be determined

accurately over periods as short as 30 minutes with a mechanical scale, load cell system, or floating lysimeter. Hydraulically weighed lysimeters generally are not accurate for periods less than 24 hours. A detailed summary of the use of lysimeters for ET can be found in publications by Harrold (1966), Aboukhaled et al. (1982), Howell et al. (1985), Marek et al. (1988), and Pruitt and Lourence (1985). The proceedings of an international symposium on lysimetry organized by ASCE provide many examples of poor lysimeter systems along with guidelines for the operation of lysimeters to ensure high-quality data for ET and related environmental purposes (Allen et al. 1991a).

### Bowen Ratio Energy Balance (BREB)

The Bowen ratio energy balance (BREB) method is a practical and generally reliable micrometeorological method. Use of the BREB concept (Bowen 1926) has enabled solving the energy balance equation by measuring the ratio of air-temperature gradient to water vapor gradient over the land or water area being studied. Numerous special studies have been conducted over various land surfaces using this methodology. The methodology enables measurement of latent heat flux for periods of an hour or less. The method works best when soil water is not limiting ET. As water becomes less readily available and the Bowen ratio (BR) increases, the relative error in  $\lambda E$  increases due to errors as BR becomes larger (Angus and Watts 1984). Details and equations for the BREB method are given in Section 7.4.

Todd et al. (1998) and Devitt et al. (1998) reviewed prior studies in which investigators used the BREB methodology. They also compared measurements of alfalfa ET using BREB with ET measured with precision-weighing lysimeters in the semiarid area of west Texas during a two-year period. The BREB overestimated ET when ET rates were greater than  $6 \text{ mm d}^{-1}$ . Overestimation occurred whether sensible heat flux was positive or negative. BREB error tended to be positive in the morning hours and negative in the afternoon. The accuracy of the BREB method is directly proportional to the accuracy of the net radiation and soil heat flux measurements, which nonuniformity of vegetation and soil and sensor calibration, placement, and care can strongly affect. Details and equations for the BREB method are given in Section 7.4.

### Eddy Covariance

With the improvement in instrumentation technology, current technology has enabled direct measurement of water vapor flux using principles set forth a half century ago by Swinbank (1951). Early examples of eddy instrumentation were described by Tanner (1988) and Tanner et al. (1993). Since then, many advances in instrumentation have been made and more

use of this method is now being made, as illustrated by Baldocchi (2003) and Shaw and Snyder (2003). The eddy covariance method tends to suffer from what is referred to as lack of closure on the energy balance, where the sum of measured  $\lambda E + H$  does not equal measured  $R_n - G$  (Baldocchi et al. 1988; Twine et al. 2000; Wilson et al. 2002). Possible reasons for the lack of closure are storage of heat in canopies; horizontal advection; change in storage of heat in the developing boundary layer below the instrumentation (causing flux divergence); frequency response of sensors relative to frequency spectrum of eddies; and regional scale heterogeneity of vegetation and ET that can cause large-scale eddies that are effective in transport of  $\lambda E$  and  $H$ , but are not readily sensed by eddy covariance systems usually placed within 20 m of the surface (Foken et al. 2006). Many users “close” the energy balance by scaling  $H$  and  $\lambda E$  in the same proportion (Twine et al. 2000) until the sum equals  $R_n - G$ . Details and equations for the eddy covariance method are given in Section 7.5.

## Water Balance

For integrated areas of land and water, the water balance, i.e., the inflow-outflow method has generally been used. Examples of ET by water balance are large areas such as valleys in which the inflow and outflow are determined from streamflow and precipitation measurements and where the basin is confined to eliminate other significant sources of inflow or outflow. An early example of a water balance study used for determining the average ET for an area is that reported by Lowry and Johnson (1942). In that study, annual inflow-outflow data for irrigation projects were used to obtain an empirical relationship between the annual ET for an “equivalent valley area” of cropped, irrigated land and degree days using maximum temperatures above 0°C. Such studies generally provide only gross seasonal estimates of the average water evaporated and transpired from cropped and noncropped areas within a project. The results represent a combination of the crops grown and generally apply only to climatic, cropping, and irrigation conditions similar to those existing in the study area. Thornthwaite (1948) correlated mean monthly air temperatures with ET as determined by water balance studies in the east central part of the United States. Hydrological methods of estimating ET in catchments were described by Morton (1971) and Holmes (1984). An evaluation of large-scale models of an experimental catchment (watershed) and a river basin in Australia indicated satisfactory agreement in monthly values between the computed and measured ET. At the river basin level, acceptable estimates of ET were inferred on the basis of the monthly computed and measured runoff (Dunin and Aston 1984). A summary of water balance methodology is presented in Section 2.2.

## Remote Sensing Energy Balance

New techniques using satellite imagery have been developed since about 1990 to determine E and ET from large areas using energy balance (Bastiaanssen et al. 1998a, b, 2005; Anderson et al. 1997, 2005; Kustas and Norman 1999; Kustas et al. 2003; Li et al. 2005; Norman et al. 2000, 2003; Allen et al. 2007a, b). The emerging technology of energy balance by satellite is showing substantial promise and has been used to quantify and illustrate the population variance in ET that can be associated with the same crop type and to refine crop coefficient curves (Tasumi et al. 2005a; Allen et al. 2007a, b; Singh and Irmak 2009). Remotely sensed energy balance techniques are also useful for identifying areas experiencing water stress and corresponding reductions in ET. Anderson et al. (2011, 2012) reviewed the use of thermal imagery from satellite systems for estimating stress-limited ET and the ability to view the signatures of evaporation from wet soil. That review discussed the constraints caused by resolution of satellite imagery and derived ET images. Currently the Landsat system provides the highest resolution imagery (30 m pixel size) with repeatable coverage and thermal imager, having a 16-day return coverage required to follow the evolution of vegetation development and to follow increases or decreases in water stress. Satellite-based estimates of ET and, in particular, those based on Landsat imagery will increasingly find their way into court proceedings, water transfers, and hydrologic studies because of the high value of spatial coverage over an extended time period. For example, the thermal Landsat archive extends over a more than 30-year period beginning in 1982.

## CHAPTER 3

# SOIL-PLANT-ATMOSPHERE SYSTEM

### 3.1 INTRODUCTION

This chapter describes the soil-plant-atmosphere (SPA) system to support the development and calculation of ET methods presented in later chapters. The SPA system involves absorption and storage of energy in the soil; the storage of water in the soil; evaporation from the soil and plant surfaces; transpiration from leaves of plants; and transfer of water vapor, sensible heat, and radiation from the soil and plants to the atmosphere. Liquid phase continuity exists in all actively growing plants from the water in the soil through the plant to the liquid-gas interface at evaporation sites in the leaves. The proliferation of roots in the soil provides an extensive absorbing surface across which most of the water and mineral nutrients utilized by plants pass.

Additional information about the SPA system can be found in various sources such as Slatyer (1967), Pierre et al. (1966), Kozlowski (1968a, 1968b, 1972, 1976), Sharma (1984), Monteith and Unsworth (1990), Campbell and Norman (1998), *Encyclopedia of Soils in the Environment* (2004), *Encyclopedia of Hydrological Sciences* (2002), and Stewart and Howell (2003). This chapter focuses on those items of concern to engineers in solving problems involving evaporation (E) and evapotranspiration (ET) from plant and soil communities, conducting research in E and ET, and managing water supplies and delivery systems. More detailed information is presented in Chapters 4–7 dealing with estimates of E and ET.

### 3.2 PHYSICAL PROPERTIES OF WATER, WATER VAPOR, AND AIR

The physical basis of the evaporation process requires a thorough understanding and employment of physical properties of liquid water,

vapor, and air. These properties are integrated into the physical equations for ET such as the Penman-Monteith equation. The following section describes these properties and sources for information.

### Liquid Water

Important physical properties of liquid water are summarized in Table 3-1. All properties in Table 3-1 change as temperature departs from 0°C. The maximum density of pure water is at 4°C.

### Water Vapor

Vapor pressure is used as an indicator of the water vapor content of air and to describe mean humidity gradients in air that drive the evaporation process. Vapor pressure is the partial pressure in air caused by molecular-scale collisions of water molecules against a surface. At the water-air interface, molecules flow continuously from the water surface to the air and then return to the liquid surface. When equilibrium with pure water exists, the two flows are equal and the air is saturated with water vapor,  $e^o$ . The partial pressure exerted by the water vapor at this time is called the saturation vapor pressure. The vapor pressure at equilibrium depends on the liquid water pressure, temperature, and its chemical content (solutes). Typical values of saturation vapor pressure and density of water vapor over a plane surface of pure water at the same temperature and pressure are summarized in Table 3-2. At the boiling point,  $e^o$  equals air pressure.

Saturation vapor pressure in kPa can be calculated based on equations by Tetens (1930) and Murray (1967) for  $T$  in °C as

$$e^o = 0.6108 \exp\left(\frac{17.27T}{T + 237.3}\right) \quad (3-1)$$

This expression provides values within 0.1% of those in the *Smithsonian Meteorological Tables* for temperatures in the range of 0 to 50°C (Allen et al. 1989). In some later chapters,  $e^o$  is expressed as  $e^o(T)$  indicating that  $e^o$  is solved at temperature  $T$ . The slope of the saturation vapor pressure curve,  $\Delta$ , kPa °C<sup>-1</sup>, is obtained by differentiating Eq. (3-1) (Allen et al. 1998):

$$\Delta = \frac{2503 \exp\left(\frac{17.27T}{T + 237.3}\right)}{(T + 237.3)^2} \quad (3-2)$$

Absolute humidity,  $\rho_v$ , is the water vapor density, i.e., the mass of water vapor per unit volume of air. It can be calculated from the ideal gas law:

Table 3-1. Physical Properties of Liquid Water

Temperature (°C)	Density (kgm <sup>-3</sup> )	Surface Tension (N m <sup>-1</sup> )	Dynamic Viscosity (10 <sup>-3</sup> Pas)	Latent Heat of Vaporization (MJ kg <sup>-1</sup> )	Specific Heat (kJ kg <sup>-1</sup> °C <sup>-1</sup> )	Thermal Conductivity (J m <sup>-1</sup> s <sup>-1</sup> °C <sup>-1</sup> )
-10	997.94	—	—	2.525	4.271	—
-5	999.18	0.0764	—	—	—	—
0	999.87	0.0756	1.792	2.501	4.218	0.561
4	1,000.00	0.0750	—	2.492	4.205	0.596
5	999.99	0.0748	1.519	2.489	4.202	0.574
10	999.73	0.0742	1.308	2.477	4.192	0.586
15	999.13	0.0734	1.140	2.466	4.186	0.595
20	998.23	0.0727	1.005	2.453	4.182	0.603
25	997.08	0.0719	0.894	2.442	4.180	0.611
30	995.68	0.0711	0.801	2.430	4.178	0.620
35	994.06	0.0703	0.723	2.418	4.178	0.628
40	992.25	0.0695	0.656	2.406	4.178	0.632
45	990.24	0.0687	0.599	2.394	4.179	0.641
50	988.07	0.0679	0.549	2.382	4.181	0.645

Source: Data from Van Wijk and de Vries (1963)

Table 3-2. Physical Properties of Water Vapor

Temperature (°C)	Saturation Vapor Pressure over Water (kPa)	Saturation Vapor Density over Water ( $10^{-3}$ kg m $^{-3}$ )	Diffusion Coefficient at $P = 100$ kPa ( $10^{-5}$ m $^2$ s $^{-1}$ )
0	0.61	4.85	2.26
5	0.87	6.80	—
10	1.23	9.40	2.41
15	1.70	12.83	—
20	2.34	17.30	2.57
25	3.17	23.05	—
30	4.24	30.38	2.73
35	5.62	39.63	—
40	7.38	51.19	2.89
45	9.59	65.50	—
50	12.34	83.06	—

Note: 1 kPa = 10 mb = 7.501 mmHg;  $10^{-3}$  kg m $^{-3}$  =  $10^{-6}$  g cm $^{-3}$

Source: Data from List (1984) and ASTM (1976)

$$\rho_v = \frac{1,000e}{R_v T} \quad (3-3)$$

where  $\rho_v$  is the absolute humidity, kg m $^{-3}$ ;  $e$  is the vapor pressure, kPa (1 Pa = 1 Nm $^{-2}$ );  $R_v$  is the gas constant for water vapor (461.5 J kg $^{-1}$  K $^{-1}$ ); and  $T$  is the absolute temperature in K. For  $e$  in kPa the density of water vapor in kg m $^{-3}$  is

$$\rho_v = \frac{2.167e}{T} \quad (3-4)$$

Specific humidity,  $q$ , is the relative density of water vapor, i.e., the mass of water vapor per unit mass of moist air:

$$q = \frac{\rho_v}{\rho_a} = \frac{m_v}{m_v + m_a} = \frac{0.622e}{P - 0.378e} \quad (3-5)$$

where  $q$  is the specific humidity, kg kg $^{-1}$ ;  $\rho_a$  is the density of moist air;  $m_v$  is the mass of water vapor;  $m_a$  is the mass of dry air;  $P$  is the total atmospheric pressure in kPa;  $e$  is the vapor pressure in kPa; 0.622 is the ratio of the molecular mass of water (18.016) to the apparent molecular mass of dry air (28.966); and  $(1 - 0.622) = 0.378$ .

Vapor pressure deficit,  $VPD$ , of the air is a term used in the Penman and Penman-Monteith equations for ET:

$$VPD = e^o - e \quad (3-6)$$

Relative humidity,  $RH$ , is the dimensionless ratio of actual vapor pressure to saturation vapor pressure, usually expressed in percent.  $RH$  is defined as

$$RH = 100 \frac{e}{e^o} \quad (3-7)$$

and  $VPD$  can be calculated as

$$VPD = e^o \left( \frac{100 - RH}{100} \right) \quad (3-8)$$

Because of the very strong and nonlinear dependence of  $e^o$  on  $T$ , relative humidity by itself has limited utility in E and ET calculations unless air temperature or one of the vapor terms, which corresponds to the same timescale and interval as  $RH$ , is given.

Dew point temperature,  $T_d$ , is the temperature to which a parcel of air must be cooled at constant pressure and constant vapor content until saturation occurs, or the temperature at which saturation vapor pressure is equal to the actual vapor pressure of the contained vapor. At the dew point temperature, condensation will normally occur on a flat surface. Dew point temperature can be calculated from vapor pressure by inverting Eq. (3-1):

$$T_d = \frac{116.91 + 237.3 \ln(e)}{16.78 - \ln(e)} \quad (3-9)$$

The thermodynamic wet bulb temperature is the temperature that is achieved in an adiabatic process in which water evaporates into the air until vapor pressure equals the saturation vapor pressure at the air-water interface. Energy for wet bulb evaporation comes from the air, so the air temperature drops as the vapor pressure increases. Wet bulb temperature,  $T_w$ , is the temperature that a moist evaporating surface may approach when the radiation energy balance is zero. In practice, the wet bulb temperature represents the equilibrium temperature of a thermometer covered with a cloth that has been wetted with pure water in air moving between 4 and  $10\text{ ms}^{-1}$  (List 1984). The wet bulb thermometer cools as sensible heat transfers to the wet surface and vaporizes water, leading to water vapor flux from the surface and an increase in latent heat content of the contacted air. With sufficient ventilation ( $>4\text{ ms}^{-1}$ ) so that effects of

radiation transfer are small, the vapor pressure of the ambient air can be computed using the standard psychrometric constant,  $\gamma$ :

$$e = e_w^o - \gamma(T - T_w) \quad (3-10)$$

where  $e_w^o$  is saturation vapor pressure at  $T_w$  and  $T$  is ambient air temperature (i.e., dry bulb temperature). The psychrometric constant,  $\gamma$ , is computed as

$$\gamma = \frac{c_p P}{\lambda \epsilon} \quad (3-11a)$$

Where  $P$  is atmospheric pressure,  $c_p$  is the specific heat of the air at constant pressure,  $\lambda$  is the latent heat of vaporization, and  $\epsilon$  is the ratio of the molecular mass of water to that of dry air (0.622). At sea level,  $P = 101.3 \text{ kPa} = 1.0 \text{ atm}$ . A recommended value for  $c_p$  is  $1.013 \text{ kJ kg}^{-1} \text{ K}^{-1}$  (Brutsaert 1982), representing air with relatively low humidity ( $RH \sim 60\%$  at  $T = 10^\circ\text{C}$ ,  $RH \sim 30\%$  at  $T = 20^\circ\text{C}$ ,  $RH \sim 20\%$  at  $T = 30^\circ\text{C}$ , and  $RH \sim 10\%$  at  $T = 40^\circ\text{C}$ ). For  $P$  in kPa,  $\lambda$  is in  $\text{kJ kg}^{-1}$ , and  $\gamma$  has units of  $\text{kPa} \text{ }^\circ\text{C}^{-1}$ . Thus a good estimate of the psychrometric constant, as used in the standardized calculation of the Penman-Monteith equation for  $ET_{ref}$ , assuming  $\lambda = 2,450 \text{ kJ kg}^{-1}$  is the simplification:

$$\gamma = 0.000665P \quad (3-11b)$$

where  $P$  is atmospheric pressure in kPa and  $\gamma$  has units of  $\text{kPa} \text{ }^\circ\text{C}^{-1}$ .

The psychrometric constant used in Eq. (3-10) to convert wet and dry bulb data from a psychrometer is commonly given by

$$\gamma_{psy} = a_{psy} P \quad (3-12)$$

where  $a_{psy}$  is a coefficient depending on the type of ventilation of the wet bulb ( $^\circ\text{C}^{-1}$ ), and  $P$  is mean atmospheric pressure (kPa). The coefficient  $a_{psy}$  depends primarily on the design of the psychrometer and on the rate of ventilation around the wet bulb and is essentially the same as the standard constant from Eq. (3-11b) under high-ventilation conditions. When ventilation of the psychrometer drops below  $4 \text{ ms}^{-1}$ , the wet bulb temperature can be influenced by the long-wave radiation balance of the psychrometer. The following values are often used (ASCE 2005):

- $a_{psy} = 0.000662$  for ventilated (Asmann type) psychrometers, with air movement of approximately  $5 \text{ ms}^{-1}$ ;
- $= 0.000800$  for naturally ventilated psychrometers with air movement of about  $1 \text{ ms}^{-1}$ ; and
- $= 0.001200$  for nonventilated psychrometers installed in glass or plastic greenhouses (List 1984).

Using these values, the values for  $\gamma$  in Eq. (3-10) become about 1.2 times the standard psychrometric constant for naturally ventilated psychrometers having air movement of about  $1\text{ ms}^{-1}$ , and about 1.8 times the standard constant for nonventilated psychrometers installed in glass or plastic greenhouses.

## Air

Mean atmospheric air pressure,  $P$ , can be computed using the ideal gas law ([List 1984](#); [Burman et al. 1987](#)) as follows:

$$P = P_o \left[ \frac{T_o - \Gamma(z - z_o)}{T_o} \right]^{\frac{g}{\Gamma R}} \quad (3-13)$$

where  $P_o$  and  $T_o$  are standardized atmospheric pressure in kPa, and absolute temperature in K at elevation  $z_o$  in m and  $z$  is the elevation of the location or instrument in m above mean sea level. The assumed constant adiabatic lapse rate,  $\Gamma$ , is normally taken as  $0.0065\text{ Km}^{-1}$  for saturated air or  $0.010\text{ Km}^{-1}$  for nonsaturated air;  $g$  is gravitational acceleration,  $9.807\text{ ms}^{-2}$  and  $R$  is the specific universal gas constant for dry air,  $287.0\text{ J kg}^{-1}\text{ K}^{-1}$ . Values for  $P_o$ ,  $T_o$ , and  $z_o$  for the standard atmosphere ([List 1984](#)) are 101.3 kPa, 288 K, and 0 m. The base value  $T_o$  is generally set to 293 K ([Smith et al. 1991](#); [Allen et al. 1998](#)) during calculation of  $ET_{ref}$  to better represent common field environments. Eq. (3-13) is somewhat insensitive to the value of  $\Gamma$  for elevations up to 3,000 m. In the ASCE-EWRI report on standardization of  $ET_{ref}$  ([ASCE 2005](#)), Eq. (3-13) was simplified to

$$P = 101.3 \left( \frac{293 - 0.0065z}{293} \right)^{5.26} \quad (3-14)$$

where the base temperature is set at 293 K. Air density,  $\rho_a$ , can be computed as

$$\rho_a = \frac{1,000P}{T_v R} \quad (3-15)$$

where  $P$  is the barometric pressure in kPa,  $R$  is  $287.0\text{ J kg}^{-1}\text{ K}^{-1}$ , and  $T_v$  is virtual temperature in K. Barometric pressure is so called because barometers are used to measure it. It is the pressure exerted on the earth's surface by the weight of the air above the point where it is being measured. Virtual temperature is the temperature at which dry air possesses the same density as moist air at the same pressure  $P$  and temperature  $T$ .  $T_v$  in Eq. (3-15) enables the use of  $R$  for dry air.  $T_v$  can be computed as ([Jensen et al. 1990](#))

$$T_v = \frac{T}{1 - 0.378 \frac{e}{P}} \quad (3-16)$$

where  $T$  is air temperature, K, and  $e$  is mean vapor pressure of the air, kPa. Substitution of Eq. (3-16) into (3-15) produces

$$\rho_a = \frac{1,000(P - 0.378e)}{TR} \quad (3-17)$$

where  $(P - 0.378e)$  represents the partial pressure of dry air, and  $R$  is the universal gas constant for dry air.

Latent heat of vaporization,  $\lambda$ , in  $\text{MJ kg}^{-1}$ , can be computed following Harrison (1963) as

$$\lambda = 2.501 - 2.361 \times 10^{-3}T \quad (3-18)$$

where  $T$  is mean air temperature in  $^{\circ}\text{C}$ . If available, mean surface temperature or wet bulb temperature can be used to compute the value of  $\lambda$ , which better represents conditions at the evaporating surface.  $\lambda$  has a value of  $2.45 \text{ MJ kg}^{-1}$  at  $21.6^{\circ}\text{C}$ , a value that was used during the standardization of the  $\text{ET}_{\text{ref}}$  calculation (ASCE 2005).

### Standard Atmosphere (Lower Atmosphere)

Characteristics of a standard atmosphere (average conditions for the United States at latitude  $40^{\circ}\text{N}$ ) are given in Table 3-3 at a base temperature of  $15^{\circ}\text{C}$ . Characteristics of standard atmospheres at other latitudes are summarized by Burman et al. (1987). Characteristics of the lower atmosphere using a base temperature of  $20^{\circ}\text{C}$  are given in Table 3-4.

Table 3-3. Standard Lower Atmosphere

Altitude (m)	Temperature ( $^{\circ}\text{C}$ )	Barometric Pressure		Density ( $\text{kg m}^{-3}$ )
		(kPa)	(mb)	
0	15.0	101.3	1,013	1.226
500	11.75	95.5	955	1.168
1,000	8.50	89.9	899	1.112
1,500	5.25	84.6	846	1.058
2,000	2.00	79.5	795	1.007
3,000	-4.50	70.1	701	0.909

Source: Data from Table 63 (List 1984) based on the assumption by List of dry air and an adiabatic lapse rate of  $0.0065^{\circ}\text{C m}^{-1}$

Table 3-4. Characteristics of the Lower Atmosphere Using 20°C Base Temperature at Sea Level Instead of 15°C

Altitude (m)	Temperature (°C)	Barometric Pressure (kPa)	Density Dry Air ( $\text{kg m}^{-3}$ )	Saturation Vapor Press. at Sat. (kPa)	Virtual Saturated Air Temp. (K)	Density ( $\text{kg m}^{-3}$ )
0	20.00	101.3	1.204	2.34	295.7	1.193
500	16.75	95.5	1.148	1.91	292.1	1.139
1,000	13.50	90.0	1.094	1.55	288.5	1.087
1,500	10.25	84.8	1.042	1.25	285.0	1.037
2,000	7.00	79.8	0.992	1.00	281.5	0.988
3,000	0.50	70.5	0.898	0.63	274.6	0.895

Note: Calculated using Eqs. (3.13)–(3.15) and an adiabatic lapse rate of  $0.0065^{\circ}\text{C m}^{-1}$

### 3.3 SOIL PROPERTIES

A unit volume of soil,  $V$  contains solids,  $V_s$ ; water,  $V_w$ ; and air and water vapor,  $V_{av}$ , and can be expressed as

$$V = V_s + V_w + V_{av} \quad (3-19)$$

The soil water content is commonly expressed on a volume basis as  $\text{m}^3 \text{m}^{-3}$ ,  $\theta$ , or on a mass basis,  $\text{kg kg}^{-3}$ ,  $\theta_m$ :

$$\theta = \frac{V_w}{V} \quad (3-20)$$

$$\theta_m = \frac{m_w}{m_s} \quad (3-21)$$

where  $m_w$  and  $m_s$  are the masses of water and dry soil, respectively. In practice, the soil water content is determined by drying at 105°C.

Conversion of soil water content on a mass to a volumetric basis requires knowing the bulk density of the dry soil matrix,  $\rho_b$ , where  $\rho_b = m_s/V$ , from which

$$\theta = \frac{\rho_b}{\rho_w} \theta_m \quad (3-22)$$

where  $\rho_w$  is the density of liquid water, and units cancel.

The volumetric water content represents the equivalent depth of water per unit soil depth. Prior to the use of the neutron moisture probe and electromagnetic devices, which are calibrated to indicate  $\theta$ , most field studies involved gravimetric determination of the water content per unit mass of dry soil,  $\theta_m$ . To determine the volumes of water involved, Eq. (3-22) was used and in most cases,  $\rho_b$ , once determined during a study, was considered to remain constant at a given depth throughout the season or study. This assumption is reasonable below the tillage depth, but can result in substantial measurement error in the total soil water in the tilled layer. The error is not great for determining changes in soil water content over 5- to 15-day periods. However,  $\rho_b$  should be adjusted for water content changes in swelling and cracking soils.

### 3.4 SOIL-WATER SYSTEM

The availability of water in soil and its energy state can control the rates of evaporation and transpiration. As soil dries, its energy state decreases,

and the energy gradients between soil and atmosphere that control evaporation fluxes decrease.

### Energy State of Soil Water

Because the movement of water in soil is slow, its kinetic energy can be neglected. The major energy components that affect mass flow in soils are the gravitational and pressure potentials. These variables, when combined, are commonly expressed as hydraulic head,  $H$ , which is the sum of pressure and gravitational potentials.

$$H = \frac{1,000P_w}{\rho_w g} + z = h + z \quad (3-23)$$

where  $P_w$  is the pressure of water (kPa or  $\text{kJ m}^{-3}$ ),  $\rho_w$  is the density of liquid water ( $\text{kg m}^{-3}$ ),  $g$  is the gravitational acceleration ( $\text{m s}^{-2}$ ),  $h$  is the fluid pressure head (m), and  $z$  is the gravitational potential (m) or the vertical distance from the reference datum. The water pressure datum is normally taken as the free water surface or land surface under atmospheric conditions. A tensiometer can be used to directly measure  $h$  ranging from small positive values to about  $-0.8$  m.

Most soils literature use the terms capillary potential, matric potential, and soil water suction or tension when referring to the pressure potential of water in soils. Soil water energy terms and other commonly used units are presented in Table 3-5. A pressure potential of  $-153$  m water or a suction of 15 bars approximates the wilting point.

When considering the impact of total suction on water extraction by roots, soil scientists refer to the sum of the matric potential and osmotic potential caused by solutes in the soil water. Solutes may have little effect on mass flow, but become important in flow across membranes, including those in plant roots, in vapor diffusion, and in soil water potential measurement using vapor pressure techniques. Soil physics texts such as Jury et al. (1991) provide more information on the energy status of water in soils.

### Soil-Water Characteristic Curve

The soil-water characteristic curve describes soil water-holding characteristics as a function of the energy level of the soil water. An example of such a curve is illustrated in Figure 3-1. When a parcel of soil is saturated, the fluid pressure may be positive or zero. As the water pressure decreases below atmospheric pressure, little change in water content occurs until the air-entry pressure is reached (the air-entry region). Air-entry pressure is the pressure at which the largest pore begins to empty. Decreasing the water pressure below the air-entry point results in a decrease in water content as

Table 3-5. Methods and Units of Soil-Water Energy

Soil Water Suction or Tension		Soil-Water Potential Energy			
Head, $H$ , of Water		Per Unit Mass		Per Unit Volume	
(m)	(kPa)	(bar)	(MPa)	( $\text{kg}^{-1}$ )	(kPa)
0.01	0.1	0.001	0.0001	-0.1	-0.1
0.10	1.0	0.010	0.0010	-1.0	-1.0
1.02	10.0	0.100	0.0100	-10.0	-10.0
152.952	1,500.0	15.000	1.5000	-1,500.0	-1,500.0

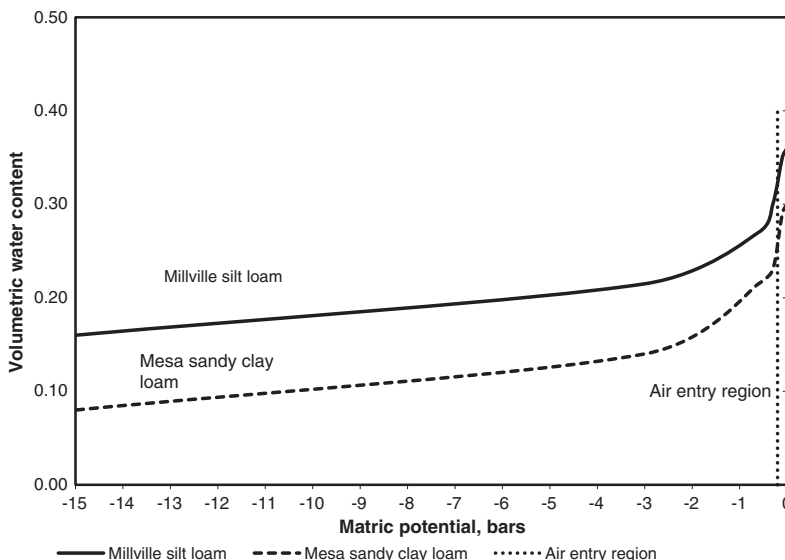


Fig. 3-1. Water content related to matric potential for two soils. The volumetric water content at -15 bars is commonly considered the permanent wilting point (shown along the left vertical axis). Values shown are for Millville silt loam and Mesa sandy clay loam

Source: Data from James et al. (1982)

illustrated Figure 3-1. The water content at a specific energy level is not unique. The curve shape depends on whether it was derived during a wetting or drying phase. The difference in curve shape due to wetting or drying is often referred to as hysteresis.

### Flow of Water in Soils

The flow of water in soils is important in many applications such as when determining irrigation water requirements, determining average ET rates by measuring the change in soil water content over time, and performing water balance studies. These flows are vertical unsaturated drainage from the root zone; upward flow from a shallow, saturated zone; and radial flow to plant roots. Darcy's law is often used to describe one-dimensional flow through soil.

$$v = -K \frac{\Delta H}{\Delta S} = -K \frac{\partial H}{\partial S} \quad (3-24)$$

where  $v$  is the bulk or average flow with units of discharge per unit cross-sectional area in the direction of increasing distance  $S$ ,  $K$  is the

hydraulic conductivity that varies with  $\theta$ , and  $H$  is the hydraulic head. Because  $H = h + z$ , vertical one-dimensional flow can be expressed as

$$v = -K \left( \frac{\partial h}{\partial z} + 1 \right) \quad (3-25)$$

where  $z$  is positive upward, and  $h$  is the water pressure head relative to atmospheric pressure (negative for unsaturated conditions). If  $v$  becomes negative, flow is downward and always in the direction of decreasing  $H$ . For  $v = 0$ , or static conditions,  $\partial h / \partial z$  must equal  $-1.0$ . When the water table is several meters below the effective root zone in irrigated fields, and excess water has been applied, finding  $\partial h / \partial z = 0$  is not uncommon, and the downward hydraulic gradient is unity. Under these conditions, drainage occurs at a velocity  $v = K$ . The rate of drainage is normally not constant, but changes slowly with time. Therefore,  $\theta$  and  $h$  may change only slightly along with a corresponding change in  $K$ .

For nonsteady flow,  $\partial\theta/\partial t \neq 0$ , Darcy's law, and the continuity equation are combined and for the one-dimensional vertical case reduces to

$$\frac{\partial\theta}{\partial t} = \frac{\partial}{\partial z} \left( K \frac{\partial H}{\partial z} \right) = \frac{\partial}{\partial z} \left( K \frac{\partial h}{\partial z} \right) + \frac{\partial K}{\partial z} \quad (3-26)$$

Eq. (3-26) is generally solved for soil systems by numerical techniques using computers, for example, with the HYDRUS model ([Šimůnek et al. 2005](#)). Challenges in applying Eq. (3-26) for practical problems include obtaining accurate soils information ( $K$  vs.  $\theta$  and  $h$ ).

## General Soil Water Properties

Soils vary greatly in their ability to retain water. Estimates of the capacity of soils to retain irrigation water and precipitation and to release the water to plants are primary variables involved in scheduling irrigation depths and frequencies. Given adequate time, water at a point within a homogeneous soil profile will decrease, due to drainage caused by gravity, to a level on the characteristic curve that is at an energy level equivalent to the elevation of the point above the water table. For soils overlying deep-water tables, drainage may continue for many days at a decreasing rate. The rate of decrease in water content in a given zone typically follows the function  $d\theta/dt = at^{-b}$  where  $a$  and  $b$  are constants for a given zone of soil, and  $t$  is time in days after complete wetting and evaporation is prevented ([Richards et al. 1956](#)). As the water content of an initially saturated zone of soil depth decreases, it approaches a near equilibrium level called *field capacity* ([Ratliff et al. 1983](#)). This limit may not be reached until two to 12 days after a heavy irrigation or precipitation if ET rates are near zero.

Field capacity has also been referred to as the “drained upper limit” (Ratliff et al. 1983) and is primarily a function of soil texture. Other factors also affect the shape of the characteristic curve. Generally, the water content at field capacity occurs at soil water potentials near  $-10\text{ kPa}$  ( $-0.1\text{ bar}$ ) in coarse-textured soils and at potentials near  $-30\text{ kPa}$  ( $-0.3\text{ bar}$ ) in medium to fine-textured soils. Average values and ranges of field capacities of general soil classes are presented in Table 3-6. These values and ranges were summarized from similar data presented by McDole et al. (1974), Evans (1980), Ratliff et al. (1983), and Keller (1986).

As root extraction or evaporation withdraws water from soil, withdrawing additional water becomes increasingly difficult because the soil matric and osmotic potentials become more negative. In addition, as soil water content decreases, the hydraulic conductivity decreases, reducing the flow of water to roots. Because of the decrease in the “availability” of water to plant roots, a lower limit of available water is often set that has historically been termed the *permanent wilting point*. Water below this limit is

Table 3-6. General Soil Water Classes for Agricultural Soils (Water Content, Volume Basis)

Texture Class	Field Capacity		Permanent Wilting Point		Available Water	
	Average Range	(%)	Average Range	(%)	Average Range	(%)
<b>Coarse</b>						
Sand	12	7–17	4	2–7	8	5–11
Loamy sand	14	11–19	6	3–10	8	6–12
<b>Moderately coarse</b>						
Sandy loam	23	18–28	10	6–16	13	11–15
<b>Medium</b>						
Loam	26	20–30	12	7–16	15	11–18
Silt loam	30	22–36	15	9–21	15	11–19
Silt	32	29–35	15	12–18	17	12–20
<b>Moderately fine</b>						
Silty clay loam	34	30–37	19	17–24	15	12–18
<b>Fine</b>						
Silty clay	36	29–42	21	14–29	15	11–19
Clay	36	32–39	21	19–24	15	10–20

Source: Data from McDole et al. (1974), Evans (1980), Ratliff et al. (1983), and Keller (1986)

considered to be unavailable to plants, with plants experiencing severe water stress with corresponding wilting and eventually plant death.

Other terms for the permanent wilting point include “lower limit of crop-extractable water” and “lower limit of available water” (Ratliff et al. 1983). Traditionally, the permanent wilting point has been related to soil water at a matric potential of approximately  $-1,500\text{ kPa}$  ( $-15\text{ bars}$ ). However, the water potential equivalent to the permanent wilting point is a function of other factors in addition to the shape of the soil characteristic curve. These other factors include the ability of the plant to survive under stressed conditions, root densities, and the magnitude of evaporative demand. Typical values and ranges of the lower limit of extractable water of general soil textural classes are presented in Table 3-6.

This manual defines available water as the quantity of soil water between field capacity and permanent wilting point. It is the amount of stored soil water that can be extracted by plant roots. A portion of this amount is not “readily” available to the plant, i.e., the rate of uptake by the roots may be less than potential transpiration, and plant growth may begin to decrease as water is extracted beyond a certain water content. Average values and ranges of available water are presented in Table 3-6. In addition to the ultimate extraction of total available water, plants may extract some additional water temporarily stored at water contents above field capacity or the drained upper limit during the two- to five-day period required for soil water to approach field capacity after irrigation or heavy rain.

## Soil-Plant Interactions

**General Plant Rooting Depths** Root growth occurs as new cells form and expand. Many factors affect root growth (Taylor 1983). These factors include such variables as transpiration rate and water stress, aluminum content and salinity of soils, soil strength, aeration, temperature, nutrient supply, and soil water content. Root systems are generally of two main types: taproot and fibrous. Grass-type plants have fibrous roots and dicotyledonous plants have a taproot and fibrous roots. Shoot and root growth are coordinated so that in water management the depth of rooting often relates to the development of shoots, or crop canopy.

Effective rooting depth is usually less than the maximum rooting depth of a mature plant due to decreased rooting density near the lower portions of the root zone. A general rule of thumb is that about 80% to 90% of a plant's feeder roots are contained in the upper 60% to 75% of the effective root zone (Hansen et al. 1979; Keller 1986). Typical maximum effective rooting depths for agricultural crops are presented in Table 3-7. These represent rooting depths for healthy plants in soils under typical irrigated conditions with no soil or water-induced restrictions such as hard layers or nearly saturated profiles. Similar values for maximum effective

Table 3-7. General Maximum Effective Rooting Depths of Fully Grown Crops and Management-Allowed Depletion (MAD) Levels in Percent of Available Water

Crop	Rooting Depth Range (m)	MAD (%)	Crop	Rooting Depth Range (m)	MAD (%)
Alfalfa	1.0–2.0	55	Maize, grain	1.0–1.7	60
Artichoke	0.6–0.9	45	Melons	1.0–1.5	35
Asparagus	1.2–1.8	45	Mint	0.4–0.8	40
Avocado	0.6–0.9	40	Olives	1.2–1.7	65
Banana	0.5–0.8	40	Onions	0.3–0.5	25
Barley	1.0–1.5	55	Palm trees	0.7–1.0	65
Beans (dry)	0.6–0.9	45	Parsnip	0.6–0.9	40
Beans (green)	0.5–0.7	45	Passion fruit	0.3–0.5	35
Beets	0.6–1.0	50	Peas	0.6–1.0	40
Berries	0.6–1.2	50	Peppers	0.5–1.0	25
Broccoli	0.6	40	Pineapple	0.3–0.6	50
Brussels sprouts	0.6	40	Potatoes	0.4–0.6	35
Cabbage	0.4–0.5	45	Pumpkin	0.9–1.2	40
Cantaloupe	0.6–1.2	40	Radish	0.3	30
Carrots	0.5–1.0	35	Safflower	1.0–2.0	60
Celery	0.3–0.5	20	Sisal	0.5–1.0	80
Citrus	1.2–1.5	50	Sorghum	1.0–2.0	55
Clover	0.6–0.9	50	Soybeans	0.6–1.3	55
Cotton	0.8–1.7	60	Spinach	0.3–0.5	20
Cucumber	0.7–1.2	50	Squash	0.6–0.9	50
Dates	1.5–2.5	50	Strawberries	0.2–0.3	15
Deciduous orch.	1.0–2.0	50	Sugar beets	0.7–1.2	55
Eggplant	0.8	45	Sugarcane	0.8–1.8	65
Fig	0.9	50	Sunflower	0.8–1.5	45
Flax	1.0–1.5	50	Sweet potatoes	1.0–1.5	65
Grains, small	0.9–1.5	60	Tobacco	0.5–1.0	55
Grains, sm. win.	1.5–2.0	60	Tomatoes	0.4–0.8	40
Grapes	1.0–2.0	35–45	Turnip (white)	0.5–0.8	40
Grass	0.5–1.5	50	Walnuts	1.7–2.4	50
Groundnuts	0.5–1.0	50	Watermelon	1.0–1.5	45
Hops	1.0–1.2	50	Wheat, spring	1.0–1.5	55
Lettuce	0.3–0.5	30	Wheat, winter	1.5–1.8	55

Source: Data from Doorenbos and Pruitt (1977) and Keller (1986). Additional values are given in Appendix B

rooting depth are contained in Appendix B based on FAO-56 (Allen et al. 1998).

Annual crops typically attain maximum rooting depths shortly after developing a complete crop canopy. Borg and Grimes (1986) listed maximum rooting depths for several annual crops. They also described a sine-based function for estimating the increase in root depth,  $R_z$ , over time for annual crops in temperate climates having a nongrowing period:

$$R_z = R_{z \max} \left[ 0.5 + 0.5 \sin \left( 3.03 \frac{D - D_p}{D_m - D_p} - 1.47 \right) \right] \quad (3-27)$$

where  $R_{z \max}$  is the maximum effective rooting depth for a mature crop,  $D$  is the day of the year in the Northern Hemisphere,  $D_p$  is the planting date, and  $D_m$  is the date of crop maturity (near maximum root extent and based on local observation).  $D$  is constrained to  $D_p \leq D \leq D_m$  and  $R_z = R_{z \max}$  when  $D > D_m$ . Parameters  $D$ ,  $D_p$ , and  $D_m$  can be added to 180 in the Southern Hemisphere. Borg and Grimes (1986) showed good agreement between Eq. (3-27) and field observations for soybean, cotton, wheat, and oats. Martin et al. (1990) and Allen et al. (1998) described the growth in  $R_z$  as a linear function of time:

$$R_z = R_{z \text{ini}} + \frac{D - D_p}{D_x - D_p} (R_{z \max} - R_{z \text{ini}}) \quad \text{for } D < D_x \quad (3-28)$$

$$R_z = R_{z \max} \quad \text{for } D \geq D_x \quad (3-29)$$

where  $R_{z \text{ini}}$  is the initial effective rooting depth at planting (or plant emergence), and  $D_x$  is the date of maximum effective root depth (often taken as the date of effective full cover for many annual crops). The value for  $R_{z \text{ini}}$  is generally assumed to range from 0.05 to 0.15 m because of upward flow of soil water and rapid expansion of the root system following germination.

For annual crops, especially row crops, the increase in effective rooting depth and density relates to the increase in crop canopy. The basal crop coefficient ( $K_{cb}$ ), which is defined in Chapter 10, increases with the relative amount of actively transpiring crop canopy. Therefore, the increase in rooting depth for many annual crops before effective full cover can be estimated in proportion to the basal crop coefficient (Martin et al. 1990; Allen et al. 1998):

$$R_z = R_{z \text{ini}} + \frac{K_{cb} - K_{cb \text{ini}}}{K_{cbc} - K_{cb \text{ini}}} (R_{z \max} - R_{z \text{ini}}) \quad \text{for } D < D_x \quad (3-30)$$

$$R_z = R_{z \max} \quad \text{for } D \geq D_x \quad (3-31)$$

where  $K_{cb}$  is the basal crop coefficient on the current day  $D$ ,  $K_{cbini}$  is the initial basal crop coefficient (at planting or emergence), and  $K_{cbc}$  is the basal crop coefficient at effective cover (on day  $D_x$ ). Crop coefficients are described in Chapter 10, and values for various crops are presented in the appendixes. Martin et al. (1990) presented a graphic comparison of the crop coefficient model, the linear model, and the Borg-Grimes sine function model showing the general similarity of these models.

**Soil Water Depletion Levels** Only a portion of the available soil water between field capacity and the lower limit of extractable water is “readily” available to the plant. Because of decreases in hydraulic conductivity and soil water potential as soil water content decreases, the rate of extraction of soil water by plant roots may be less than the evaporative demand, thus causing plant water stress. The soil water content at which the supply to the roots is less than the evaporative demand relates to the magnitude of evaporative demand, the density of roots in the soil, the osmotic pressures in the soil, and the hydraulic properties of the soil. The concept of “management-allowed depletion” or “management-allowed deficiency” (Merriam and Keller 1978) is one approach that is used in scheduling irrigations to avoid plant water stress. Management-allowed depletion (MAD) is defined as the management-planned percentage of the available soil water (between field capacity and the lower limit of extractable water) that is depleted between irrigations. MAD contrasts with the yield threshold depletion, YTD, which is the fraction of available soil water that can be depleted before adversely affecting crop production. Another parameter,  $p$ , is the fraction of available water that can be depleted before sufficient stress is experienced to decrease transpiration (Doorenbos and Pruitt 1977; Allen et al. 1998). Generally,  $MAD < YTD$ ; however, MAD can exceed YTD in management systems where crop water stress is implemented to improve fruit quality or to optimize economics. The parameter MAD is used in irrigation scheduling, whereas  $p$  is used to estimate reduction in ET caused by crop water stress.

Typical values for MAD for irrigated crops are included in Table 3-7, and values for  $p$  are included in Appendix B. Values of MAD are typically about 25 to 40% for high-value, shallow, or sparsely rooted crops; 50% for deep-rooted crops; and 60 to 65% for low-value, deep-rooted crops. In addition to maintaining available soil water to meet the evaporative demand, adjustments in the value of MAD may be required to compensate for uncertainties in the estimated total available soil water, effective rooting depth and lateral distribution, soil water depletion, net irrigation depths, and ET rates. Thus, MAD also can provide a safety factor against plant water stress. Some crops require greater soil water depletions directly

before harvest to enhance the quality of the fruit or grain. Greater depletion at harvest also enables storing a higher proportion of overwinter precipitation. The values for MAD in Table 3-7 represent average conditions for ET rates of about 5 to 6  $\text{mm d}^{-1}$ . Values may be decreased by 5 to 10% during periods with ET rates greater than 6  $\text{mm d}^{-1}$  to maintain a higher soil hydraulic conductivity. The values for MAD and rooting depths listed in Table 3-7 may need to be adjusted by the user to fit local conditions or varietal differences among crops.

The net maximum depth of soil water that should be depleted between irrigations to avoid significant plant water stress—sometimes referred to as readily available water, RAW—can be estimated as

$$\text{RAW} = \frac{p}{100} R_z \text{AW} \quad (3-32)$$

where AW is the average value of total available water (field capacity less the lower limit of extractable water) in the root zone of the soil profile. In many evaluations of impacts of water stress on ET, values for  $p$  are set equal to values for MAD as listed in Table 3-7.

### 3.5 VEGETATIVE (CROP) PROPERTIES

#### Foliage Factors

**Leaf Area and Leaf-Area Index (LAI)** As emerging seedlings develop leaves and their root systems permeate the soil, the plants increase their effectiveness in transferring water from the soil to the atmosphere. The crop foliage factors that affect ET are the leaf-area index, LAI, and the ground cover. LAI is defined as the area of one side of plant leaves per land area including areas between plants and rows. LAI is expressed as  $\text{m}^2 \text{m}^{-2}$ . Ground cover is the fraction of the total surface that is covered by foliage (i.e., shaded when the sun is directly overhead) and is expressed as a fraction or percentage. For many common agricultural crops, the rate of ET under given environmental conditions increases with LAI until LAI reaches a value of about 2.7–3.0 or with ground cover up to 70 to 80%. Most of the energy available for evaporation is absorbed by a canopy with  $\text{LAI} = 3.0$ , so further leaf production does not usually increase energy absorption (Ritchie 1972; Wright 1982). The relationship between LAI and crop factors affecting ET rates is discussed in detail in Chapter 10.

**Stomatal Resistance (Conductance)** Water moves in the liquid phase from the soil through the plants to the evaporation sites in cell walls. It then moves to the atmosphere in the vapor phase through the stomates. The stomates are openings in the plant leaves shielded by guard cells that

enable plants to absorb carbon dioxide from the air. When plant leaves are turgid, the stomates are generally fully open in bright sunlight and the resistance to the flow of water vapor and carbon dioxide is at a minimum, or the conductance is at a maximum. As soil water begins to limit the rate at which water can be transferred to the atmosphere, the stomates begin to close, increasing the stomatal resistance. The concept of resistance to vapor transfer at the leaf surface was introduced by Penman and Schofield (1951). Slatyer (1967) described the resistance to water vapor transfer for a whole leaf as

$$\frac{1}{r_l} = \frac{1}{r_{cu}} + \frac{1}{r_{st}} \quad (3-33)$$

where  $r_l$  is the total internal resistance of the whole leaf, and  $r_{cu}$  and  $r_{st}$  are the resistances in the cuticular and stomatal pathways in units of  $\text{sm}^{-1}$ .

**Bulk Surface Resistance** Bulk surface (stomatal) resistance of plant leaves is a dynamic property that changes with sunlight, vapor pressure deficit, leaf temperature, and soil water potential, or available soil water. For a single-layer model of ET, such as the PM equation, the bulk surface resistance represents the integrated resistance of vapor flow through the stomates, vapor diffusion from the soil, and vapor transport within a dense plant canopy. Detailed discussion of bulk surface resistance, the factors affecting it, and its magnitude are discussed in Chapter 11.

## Root Factors

**Root Type and Density** The primary pattern of root system development depends on the plant species. Root system patterns comprise three basic types: diffuse or fibrous, which is characteristic of most monocotyledonous crops, and taprooted and modified taprooted, which is characteristic of most dicotyledonous plants. Root systems generally grow downward, whereas individual roots can grow in any direction. Taproots of dicotyledonous plants and the main seminal axes of cereal crops grow vertically downward while lateral roots grow perpendicular to the parent root and may even grow upward. Stone et al. (2001) present an example of measured changes in root density and root penetration over time for grain sorghum and sunflower based on soil core analyses. The soil was a silt loam with moderate permeability and high-availability water capacity. The root density results for grain sorghum, a fibrous root plant, shown in Figure 3-2, indicated that downward growth of the root system was nearly linear in the days after planting to a depth of 2 m. As depth of rooting increased, the relative distribution of roots also changed as illustrated in Figure 3-3. The downward growth of sunflower roots, a monocotyledon plant, was essentially linear for the first 80 days as it approached

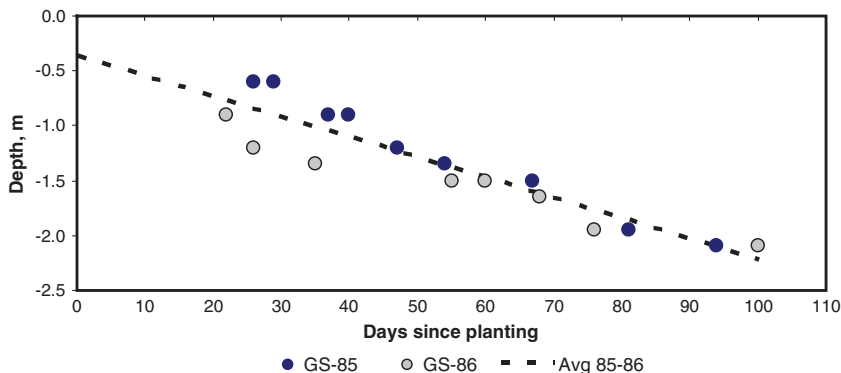


Fig. 3-2. Change in maximum depth of rooting by grain sorghum (GS) during two years, 1985 and 1986, at Manhattan, KS, in days after planting  
Source: Data from Stone et al. (2001)

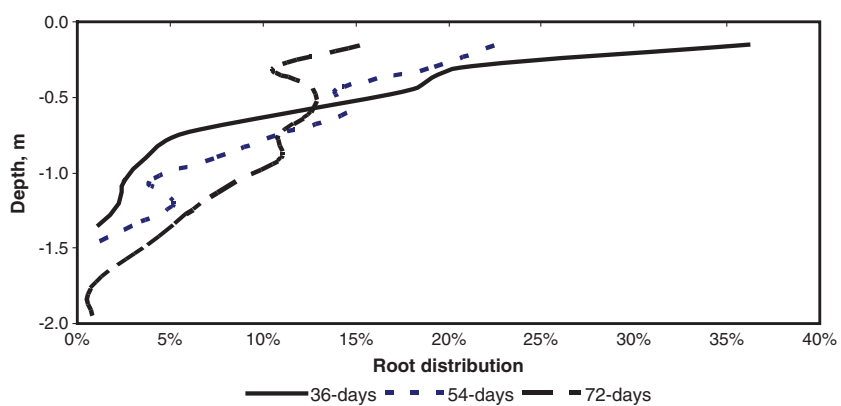


Fig. 3-3. Average percentage distribution of grain sorghum roots with depth at 36, 54, and 72 days after planting. Percentage values are approximate root lengths per 0.3 m  
Source: Data from Stone et al. (2001)

the maximum depth of 3 m. The root distribution for sunflowers was similar to that of grain sorghum except for having a greater percentage of roots at the 0.15-m depth. Klepper (1990) presents a similar pattern of cotton root distribution, and Jones et al. (1991) show similar patterns of modeled maize root densities.

**Root-Soil Interactions** Many studies of plant root systems have been conducted since the 1960s, and a vast amount of literature is available on

root growth and root-soil interactions. Two excellent sources of information with extensive bibliographies are those by Taylor (1983) and Klepper (1990). Taylor presents an overview of soil environmental effects on root growth and function. Klepper summarizes growth and water extraction by field crops, including concepts for modeling water uptake by plant roots, and indicates that numerous soil and cultural factors influence root distributions in field soils. Environmental factors can also affect the ratio of leaf area to root length. Unfavorable soil conditions can reduce the rate of vertical and lateral root elongation. Details on modifying the root environment can be found in a monograph by Arkin and Taylor (1981).

Roots grow as new cells form and then expand in volume. Elongation of both main roots and branches occurs as a result of cell enlargement immediately behind the root tip. Somewhat distinct characteristic development patterns exist between monocotyledonous and dicotyledonous species.

For high rates of cell elongation, roots need energy, which requires oxygen for oxidative phosphorylation. If oxygen levels fall below 3% in the soil atmosphere, which can occur in the presence of a shallow water table, root elongation will slow and eventually cease. Reduced oxygen also causes roots to be thicker. Large amounts of oxygen are required for biosynthesis of new cell materials such as membranes and wall materials. Another energy-requiring process is the active and selective accumulation of ions from the surrounding soil solution. To sustain rapid root elongation in soils, rapid radial influx of water from the surrounding soil solution must occur. Soil factors including soil structure, strength, water content, temperature, porosity, gaseous diffusivity, pH, toxicity, and fertility greatly influence root growth. Traffic pans, plow pans, and other adverse subsoil conditions that limit pore space and cause excessive soil strength often limit the space required for new root material. Large pores provide channels for easy root penetration and can affect the shape of the root system. Two factors that influence soil resistance to penetration are soil density and soil water content. Poor aeration is often a confounding factor when compaction decreases available pore space and when soil water content increases to a point where pore space is filled with water (Klepper 1990).

Root and shoot development are interdependent, and limitations on one affect the other (Klepper 1990). In normal soils and with adequate soil water, roots develop to their full potential. Irrigation schedules are generally based on normal root-shoot development, weather, allowable plant water stress, and the available water-holding capacity of soils. When physical or chemical soil conditions impede root development, adjustments in normal irrigation scheduling practices may be required.

This page intentionally left blank

## CHAPTER 4

# ENERGY BALANCE

### 4.1 INTRODUCTION

Historical and recent studies of evaporation (E) and evapotranspiration (ET) clearly show that, where soil water is not limiting, the primary variable controlling the rate of E and ET is solar radiation impinging on the evaporating surfaces (irradiance). Part of the solar radiation is reflected back to the atmosphere, and part of that which is absorbed at the surface changes to another energy state and may be reradiated back as long-wave radiation or convected to the air as sensible heat. Part of the loss of energy by the emitted long-wave radiation is compensated by the long-wave radiation emitted from the sky. The radiation balance determines the net radiant energy available at the evaporating surfaces. The most accurate methods of estimating E and ET require determining the radiation balance, or net radiation, for the surface. During daytime, E and ET are closely linked to changes in solar and net radiation, even over periods as short as five minutes. However, examples that follow reveal that the actual fraction of net radiation converted into E or ET can vary markedly depending upon air mass conditions above the surface and on the availability of water at the surface.

### 4.2 ENERGY BALANCE

The surface energy balance relates to the various ways in which net radiation,  $R_n$ , is balanced by the inputs or outputs of energy from non-radiative parameters. The vertical energy balance at the soil or water surface, or at the “effective surface” of a crop, is the sum of sensible heat

flux to or from the air and soil (or water), latent heat, net radiation, and other miscellaneous fluxes. The energy balance of land and water surfaces and the sign convention used in this manual is expressed as follows and illustrated in Figure 4-1:

$$R_n = \lambda E + H + G \quad (4-1)$$

where  $R_n$  is net radiation to the surface,  $\lambda E$  is latent heat flux from the surface,  $H$  is sensible heat flux from the surface, and  $G$  is soil heat flux into the ground ( $Q_t$  is used in place of  $G$  for heat flux into water). The miscellaneous energy flux terms such as energy storage within the foliage, photosynthesis, and respiration are generally less than a few percent and are neglected in Eq. (4-1). The common energy units used in this manual are for cumulative fluxes over specific time periods such as  $\text{MJ m}^{-2} \text{h}^{-1}$  for hourly periods and  $\text{MJ m}^{-2} \text{d}^{-1}$  for daily values. Net radiation is defined as positive to the surface, and values of the variables on the right side of Eq. (4-1) are positive when the flux is away from the surface. By rearranging Eq. (4-1), latent heat flux is computed as

$$\lambda E = R_n - G - H \quad (4-2)$$

In cold, humid climates, or in cold winter months of temperate, semiarid zones, only 50 to 60% of the net radiation,  $R_n$ , may be converted to latent heat, even under high water availability. In hot, arid climates, latent heat may exceed net radiation by 10 to 50%, as shown in Figure 2-1, because sensible heat derived from the air is converted to latent heat via the process

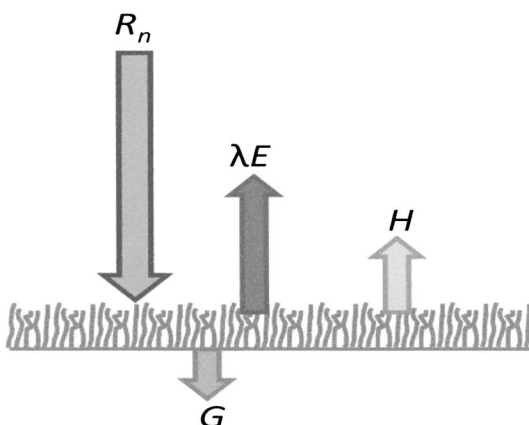


*Fig. 4-1. Schematic showing the four primary components of the surface energy balance and directions of energy flow from the surface*

of sensible heat advection. Because of these variations, the surface energy balance approach to determining or estimating E and ET is recognized as a reliable and conservative method. A thorough understanding of the factors controlling the energy balance of a water body or land area enables making accurate estimates or predictions of E and ET. The purpose of this chapter is to provide sufficient material and understanding of underlying principles to enable users to estimate hourly and daily net radiation and soil heat flux as needed to solve E and ET problems.

### 4.3 NET RADIATION

Net radiant energy absorbed by the land or water surface is the primary energy source for evaporation and evapotranspiration. The main component of net radiation is shortwave radiation, or solar radiation. Net radiation also has a long-wave radiation component. The following sections describe these two components along with methods for measuring or estimating their magnitudes.

#### Solar Radiation

The principal source of energy for E and ET and the major component of  $R_n$  is solar radiation,  $R_s$ . Although minor fluctuations exist in the intensity of solar radiation, they are insignificant for practical purposes, and the intensity of the source at the mean distance of the earth from the sun is commonly referred to as the *solar constant*. Measurements of solar radiation received on a surface normal to the incident radiation outside the earth's atmosphere indicate the constant to be  $1,367 \text{ J m}^{-2} \text{ s}^{-1}$ , or  $1,367 \text{ W m}^{-2}$  ([London and Fröhlich 1982](#); [Lean 1989](#)). Total solar irradiance describes the radiant energy emitted by the sun over all wavelengths that falls each second on  $1 \text{ m}^2$  outside the earth's atmosphere. In this manual, solar irradiance is generally referred to as solar radiation, which has common usage. The total daily solar radiation in the absence of an atmosphere, termed exoatmospheric radiation or extraterrestrial radiation,  $R_a$ , varies with the solar angle, or elevation, which changes as the earth revolves about the sun and on the declination of the earth's axis. The annual variation in  $R_a$  for northern latitudes is shown in Figure 4-2.

When measured at the earth's surface,  $R_s$  includes both direct and diffuse shortwave radiation and may be called "global radiation." The energy per unit area received at the earth's surface is called "total global irradiance" or "irradiance" and is commonly expressed in  $\text{W m}^{-2}$ , which is equivalent to  $\text{J m}^{-2} \text{ s}^{-1}$ . The distribution of solar radiation energy by wavelength is illustrated in Figure 4-3. Solar radiation, or shortwave

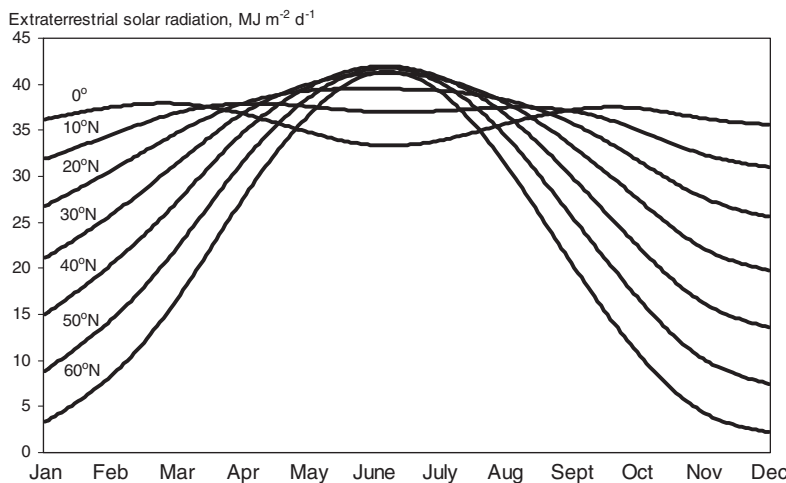
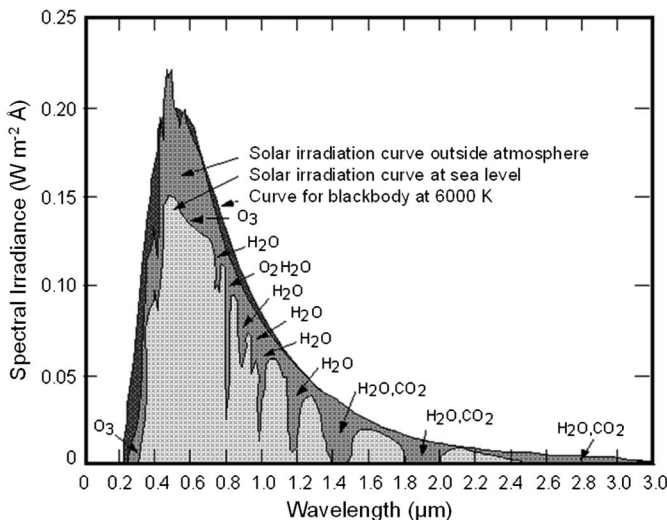


Fig. 4-2. Total daily undepleted (exoatmospheric) solar radiation for various latitudes in the Northern Hemisphere

radiation, consists of radiation in wavelengths up to about 3  $\mu\text{m}$ . Diffuse radiation is due to absorption and forward and backward scattering of some of the direct (beam) radiation that occurs in the earth's atmosphere. Solar radiation can be measured directly with instruments ranging in complexity from bimetallic sensors to complex sensors such as black sensor surfaces equipped with glass filters and thermopiles or solar-radiation-sensitive photovoltaic detectors, both of which are used with automated data-logging systems. The latter two sensor systems are generally referred to as pyranometers.

**Cloudless Day Solar Radiation,  $R_{so}$**  Radiation in the absence of the earth's atmosphere is called *extraterrestrial* or *exoatmospheric* radiation,  $R_a$ . On cloudless days, the atmosphere is more transparent to solar or short-wave radiation. About 70 to 80% of the exoatmospheric radiation reaches the earth's surface in semiarid areas as shown in Figure 4-3. The balance is reflected from dust particles or is absorbed by various gases in the atmosphere. Techniques for estimating atmospheric transmittance are presented by Idso (1981), Hatfield et al. (1983), Monteith and Unsworth (1990), Allen (1996a), and ASCE (2005).

Estimates of daily cloudless day, or clear sky, solar radiation received at the earth's surface,  $R_{so}$ , can be made using the theoretical radiation received in the absence of the earth's atmosphere and atmospheric transmittance. The magnitude of  $R_{so}$  can be approximated under most conditions as



*Fig. 4-3. Exoatmospheric solar radiation and solar radiation flux at the earth's surface compared with a 6,000 K blackbody radiation curve. Arrows from  $O_3$ ,  $H_2O$ , and  $CO_2$  point to regions of substantial absorption of radiation by those molecules. The Angstrom unit,  $\text{\AA}$ , for the vertical axis is equivalent to  $10^{-10} \text{ m}$*

$$R_{so} = k_a R_a \quad (4-3)$$

where  $k_a$  is a clearness index that is largely a function of station elevation, sun angle (atmospheric thickness), atmospheric water content, and atmospheric turbidity. For conditions of low turbidity,  $k_a$  can be approximated as a function of station elevation for locations less than 6,000 m using a relationship developed by Allen et al. (1994b):

$$k_a = 0.75 + 0.00002E \quad (4-4)$$

where  $E$  is elevation in m. Eq. (4-4) was derived by integrating Eq. (3-15) (air density) with respect to elevation, assuming constant turbidity with elevation and absorption and scattering of solar radiation in proportion to air density. Atmospheric pressure in Eq. (3-15) was computed using Eq. (3-14). Eq. (4-4) produces  $k_a = 0.75$  at sea level, which agrees with Eq. (4-24) for  $n/N = 1$ . For areas of high turbidity due to pollution or airborne dust, the  $k_a$  may need to be reduced as much as 10% depending on the relative amount of turbidity.

When needed, more accurate estimates of  $R_{so}$  can be obtained by considering the effects of sun angle and water vapor on absorption of shortwave radiation and by separating the components of beam and diffuse radiation, so that

$$R_{so} = (K_B + K_D)R_a \quad (4-5)$$

where  $K_B$  is the clearness index for direct beam radiation,  $K_D$  is the corresponding index for diffuse radiation, and  $R_{so}$  and  $R_a$  are in  $\text{MJ m}^{-2} \text{d}^{-1}$ ,  $\text{MJ m}^{-2} \text{h}^{-1}$ , or  $\text{W m}^{-2}$ .

The following equation for  $K_B$  was extended from Majumdar et al. (1972) by Allen (1996a) and is applied here with coefficients improved by ASCE (2005) over those recommended in Allen (1996a) and Allen et al. (1998):

$$K_B = 0.98 \exp \left[ \frac{-0.00146P}{K_t \sin \beta} - 0.075 \left( \frac{W}{\sin \beta} \right)^{0.4} \right] \quad (4-6)$$

where  $K_t$  is a clearness coefficient that is affected by turbidity and haze ( $0 < K_t \leq 1.0$ ;  $K_t = 1.0$  for clean air; and  $K_t \approx 0.5$  for turbid, dusty, or polluted air);  $P$  is atmospheric pressure in kPa;  $\beta$  is the angle of the sun above the horizon in radians; and  $W$  is the precipitable water in the atmosphere in mm. The improved coefficients are based on comparisons of  $R_{so}$  from Eq. (4-5) with observations measured at 42 locations across the United States as summarized by ASCE (2005).

The value for  $K_t$  may vary with time of year and with cleansing of the atmosphere by precipitation. General values for  $K_t$  for a region can be determined using a pristine pyranometer that has a calibration traceable to the national or international solar standard. In general, for routine prediction of  $R_n$  and  $R_{so}$  envelopes, using  $K_t = 1.0$  is sufficient, especially for agricultural areas where the air is generally free of dust. An exception might be during the premonsoon season on the Indian subcontinent, when substantial haze can exist. The ratio  $P/K_t \sin \beta$  in Eq. (4-6) represents the effective air mass along the solar beam. Aerosols and dust can substantially increase haziness of the atmosphere, especially when coupled with high humidity levels. Haze reduces the beam component of solar radiation, but may increase the diffuse component through increased scattering of radiation. Under hazy conditions, a value  $K_t = 0.5$  essentially doubles the effective thickness of the atmosphere, and a value  $K_t = 0.25$  quadruples the effective thickness.

Precipitable water is estimated from Garrison and Adler (1990) as

$$W = 0.14e_a P + 2.1 \quad (4-7)$$

where  $W$  is the precipitable water in the atmosphere in mm,  $e_a$  is the actual vapor pressure of the air (at approximately a height of 2 m) in kPa, and  $P$  is mean atmospheric pressure in kPa. Tasumi et al. (2008) show that  $W$  from Eq. (4-7) agrees well with  $W$  determined from profiling imagers onboard the MODIS satellite during tests in Idaho, New Mexico, and Florida. The values for MODIS  $W$  were determined from atmospheric humidity profiles based on specific infrared soundings.

The diffuse radiation index is estimated from  $K_B$  (ASCE 2005):

$$\begin{aligned} K_D &= 0.35 - 0.36K_B, \quad \text{for } K_B \geq 0.15 \\ K_D &= 0.18 + 0.82K_B, \quad \text{for } K_B < 0.15 \end{aligned} \quad (4-8)$$

The diffusive component increases as the direct beam component decreases when  $K_B > 0.15$  due to the increased amount of scatter of the direct beam component. For clear sky conditions,  $K_B$  is always  $>0.15$  for daily data and is nearly always  $>0.15$  for hourly periods. Even for hours close to sunrise and sunset, generally  $K_D$  can be computed as  $K_D = 0.35 - 0.36K_B$  for clear sky conditions, ignoring the second conditional.

For daily (24-hour) time periods, the mean daily sun angle, weighted according to  $R_a$ , can be approximated as (Allen 1996a)

$$\sin \beta_{24} = \sin \left[ 0.85 + 0.3\phi \sin \left( \frac{2\pi}{365}J - 1.39 \right) - 0.42\phi^2 \right] \quad (4-9)$$

where  $\beta_{24}$  is the average  $\beta$  during the daylight period, weighted according to  $R_a$ , in radians;  $\phi$  is the latitude in radians; and  $J$  is the day of the year (1–366). The  $\sin \beta_{24}$  variable is to be used in place of  $\sin \beta$  in Eq. (4-6) and represents the average sun angle during daylight hours. The value for  $\beta_{24}$  should be limited to positive values. Eq. (4-9) compares well to a theoretical but more complicated solution for  $\sin \beta_{24}$  by Allen et al. (2006c).

For hourly or shorter periods, the sun angle  $\beta$  is calculated as

$$\sin \beta = \sin \phi \sin \delta + \cos \phi \cos \delta \cos \omega \quad (4-10)$$

where  $\phi$  is the latitude in radians,  $\delta$  is the solar declination in radians, and  $\omega$  is solar time angle at the midpoint of the hourly or shorter period in radians. The user is cautioned that Eqs. (4-3)–(4-8) produce only estimates for  $R_{so}$  and that reasons may exist for measured  $R_s$  on cloud-free days to deviate from the theoretical  $R_{so}$  curve. These reasons include air turbidity and haziness caused by dust and aerosols that are not reflected by the equations, effects of nearly invisible clouds high overhead, and late afternoon clouding.

Estimates of  $R_{so}$  for a given area can also be developed from an envelope curve plotted through measured radiation data on cloudless days. Ordinarily,  $R_{so}$  should plot as an upper envelope of measured  $R_s$  as shown in Figure 4-4, where  $R_{so}$  values calculated using  $k_a$  from Eq. (4-4) and the more complicated Eqs. (4-5)–(4-9) are plotted with measured  $R_s$  for daily time steps. The inclusion of precipitable water in Eq. (4-6) causes the  $R_{so}$  envelope to increase on dry days, which corresponds to increases in

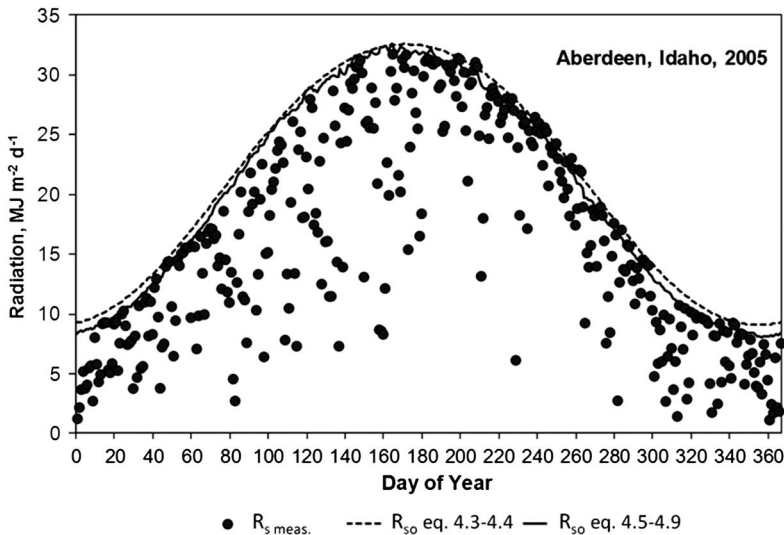


*Fig. 4-4. Daily measured solar radiation and calculated cloudless day solar radiation, Eqs. (4-3)–(4-4) (smooth curve) and Eqs. (4-5)–(4-9) for Aberdeen, ID, during 2005*

*Source: Measured data are from the U.S. Bureau of Reclamation Agrimet network*

measured  $R_s$  on the same dry, cloud-free days. Reflection of solar radiation by adjacent clouds can occasionally increase measured  $R_s$  to levels that are above  $R_{so}$ . Meek (1997) described a detailed procedure for estimating  $R_{so}$  for specific locations using measured data and considering aerosol optical depth. The relationships  $R_{so} = k_a R_a$  and/or  $R_{so} = (K_B + K_D) R_a$  are useful for verifying correct operation of pyranometers.

**Exoatmospheric Solar Radiation,  $R_a$**  Exoatmospheric radiation,  $R_a$ , can be computed for a location using integrated trigonometric relationships as a function of latitude and day of the year from Duffie and Beckman (1991) for 24-h time steps:

$$R_a = \frac{24}{\pi} G_{sc} d_r [\omega_s \sin(\phi) \sin(\delta) + \cos(\phi) \cos(\delta) \sin(\omega_s)] \quad (4-11a)$$

and for hourly or shorter time steps:

$$R_a = \frac{12}{\pi} G_{sc} d_r \{ (\omega_2 - \omega_1) \sin(\phi) \sin(\delta) + \cos(\phi) \cos(\delta) [\sin(\omega_2) - \sin(\omega_1)] \} \quad (4-11b)$$

where  $R_a$  is exoatmospheric radiation in  $\text{MJ m}^{-2} \text{d}^{-1}$  [Eq. (4-11a)] or  $\text{MJ m}^{-2} \text{h}^{-1}$  [Eq. (4-11b)];  $G_{sc}$  is the solar constant of  $4.92 \text{ MJ m}^{-2} \text{h}^{-1}$  (equivalent to  $1,367 \text{ W m}^{-2}$ ) as recommended by the International Association of Meteorology and Atmospheric Physics ([London and Fröhlich 1982](#));  $d_r$  is an eccentricity factor to account for the effect of the variation in the relative distance of the earth from the sun;  $\omega_s$  is the sunset hour angle;  $\omega_1$  and  $\omega_2$  are sun hour angles at the beginning and end of an hourly period, all in radians; and  $\phi$  is latitude of the station in radians (negative for southern latitudes). The declination,  $\delta$ , in radians, can be estimated from Duffie and Beckman ([1991](#)) as

$$\delta = 0.4093 \sin \left[ 2\pi \frac{(284 + J)}{365} \right] \quad (4-12)$$

where  $J$  is the day of the year (January 1 = 1). The term  $d_r$  is calculated as

$$d_r = 1 + 0.033 \cos \left( \frac{2\pi J}{365} \right) \quad (4-13)$$

The sunset hour angle,  $\omega_s$ , in radians, can be calculated using Eq. (4-14) or (4-15):

$$\omega_s = \arccos[-\tan(\phi) \tan(\delta)] \quad (4-14)$$

or if the  $\arccos$  function is unavailable,

$$\omega_s = \frac{\pi}{2} - \arctan \left\{ \frac{-\tan(\phi) \tan(\delta)}{[1 - \tan^2(\phi) \tan^2(\delta)]^{1/2}} \right\} \quad (4-15)$$

The argument in Eq. (4-14) must be limited to less than or equal to 2.0 in extreme latitudes ( $>55^\circ$ ) during winter months. If the argument is less than  $-1.0$  in extreme latitudes ( $>55^\circ$ ) during summer months, then the argument should be set equal to  $[\tan(\phi) \tan(\delta) - 2.0]$ . The maximum value for  $\omega_s$  is  $\pi$  radians, indicating no nighttime, and the minimum value is  $0$ , indicating no daytime.

For hourly or shorter periods, the solar time angles at the beginning and end of each period are given by

$$\omega_1 = \omega - \frac{\pi t_1}{24} \quad (4-16)$$

$$\omega_2 = \omega + \frac{\pi t_1}{24} \quad (4-17)$$

where  $\omega$  is the solar time angle at the midpoint of the period in radians, and  $t_1$  is the length of the calculation period in hours ( $t_1$  is 1 for hourly periods

and 0.5 for 30-minute periods). The solar time angle at the midpoint of an hourly or shorter period is

$$\omega = \frac{\pi}{12} \{ [t + 0.06667(L_z - L_m) + S_c] - 12 \} \quad (4-18)$$

where  $t$  is standard clock time at the midpoint of the period (hour, after correcting time for any daylight savings shift). For example, for a period between 1400 and 1500 hours,  $t = 14.5$  hours. Parameter  $L_z$  is the longitude of the center of the local time zone, expressed as positive degrees west of Greenwich, England. In the United States,  $L_z = 75, 90, 105$ , and  $120^\circ$  for the Eastern, Central, Rocky Mountain, and Pacific time zones, respectively, and  $L_z = 0^\circ$  for Greenwich;  $345^\circ$  for Paris, France; and  $255^\circ$  for Bangkok, Thailand. Parameter  $L_m$  is the longitude of the solar radiation measurement site, expressed as positive degrees west of Greenwich, England, and  $S_c$  is seasonal correction for solar time in hours.

Because  $\omega_s$  is the sunset hour angle and  $-\omega_s$  is the sunrise hour angle (noon has  $\omega = 0$ ), values of  $\omega < -\omega_s$  or  $\omega > \omega_s$  from Eq. (4-18) indicate that the center of the solar disk is below the horizon so that, by definition,  $R_a$  is zero and its calculation has no meaning. Therefore, when the values for  $\omega_1$  and  $\omega_2$  span or exceed the value for  $-\omega_s$  or for  $\omega_s$ , sunrise or sunset occurs within the hourly (or shorter) period, and the integration limits in Eq. (4-11b) should be adjusted using the following conditionals:

$$\begin{aligned} &\text{If } \omega_1 < -\omega_s \text{ then } \omega_1 = -\omega_s \\ &\text{If } \omega_2 < -\omega_s \text{ then } \omega_2 = -\omega_s \\ &\text{If } \omega_1 > \omega_s \text{ then } \omega_1 = \omega_s \\ &\text{If } \omega_2 > \omega_s \text{ then } \omega_2 = \omega_s \\ &\text{If } \omega_1 > \omega_2 \text{ then } \omega_1 = \omega_v \end{aligned} \quad (4-19)$$

Eqs. (4-13), (4-14), and (4-18) are from Duffie and Beckman (1991).

The aforementioned conditionals ensure numerical stability of the application of Eq. (4-11b) for all time steps. Eqs. (4-16)–(4-18) presume an extensive, flat ground surface and are based on a vector to the center of the sun's disk. Where hills or mountains impede a view of the horizon, the hour angle when the sun first appears or disappears may increase for sunrise or decrease for sunset.

The seasonal correction for solar time from Duffie and Beckman (1991) is

$$S_c = 0.1645 \sin(2b) - 0.1255 \cos(b) - 0.025 \sin(b) \quad (4-20)$$

$$b = \frac{2\pi(J - 81)}{364} \quad (4-21)$$

where  $J$  is the number of the day in the year and  $b$  has units of radians.

### Solar Radiation Estimation

Solar radiation,  $R_s$ , data are not always available and are frequently estimated. On a given day  $R_s$  is affected mainly by cloud cover. Therefore, if not measured,  $R_s$  can be estimated using  $R_{so}$  and either the degree of cloud cover or the percent of sunshine. More reliable  $R_s$  estimates are obtained using recorded percent sunshine as compared with observed cloud cover data because observed cloud cover data are qualitative. Pyranometers provide the most accurate measurements of  $R_s$ . Where local orographic features do not strongly influence cloud cover, measurement of daily  $R_s$  at a single station may be used for estimates over large areas (100–200 km in diameter) without significant error over five- or 10-day periods. Constants developed for a linear equation for the United States are similar to those obtained in Canada and Australia ([Fritz and MacDonald 1949](#)):

$$R_s = (0.35 + 0.61S)R_{so} \quad (4-22)$$

where  $S$  represents the ratio of actual to possible sunshine. Eq. (4-22) suggests that recording instruments tend not to measure a full record of sunshine on cloudless days because 0.35 and 0.61 sum to 0.96.

Solar radiation also can be estimated from exoatmospheric radiation,  $R_a$ . Black et al. ([1954](#)) correlate exoatmospheric solar radiation and duration of sunshine as recorded by Marvin and Campbell-Stokes sunshine recorders. The resulting equation of Black et al. ([1954](#)), based on 32 stations, is

$$R_s = \left( 0.23 + 0.48 \frac{n}{N} \right) R_a \quad (4-23)$$

Doorenbos and Pruitt ([1977](#)) recommended a generalized form of the  $R_s$  equation:

$$R_s = \left( 0.25 + 0.5 \frac{n}{N} \right) R_a \quad (4-24)$$

Doorenbos and Pruitt ([1977](#), p. 10) define the quantity  $n/N$  as “the ratio between actual measured bright sunshine hours and maximum possible sunshine hours.” In practice  $n/N$  and  $S/100$  are usually assumed to be the same quantity. Doorenbos and Pruitt ([1977](#)) present a table to convert cloudiness expressed in eighths (octas) or in tenths to  $n/N$  values and constants for Eq. (4-24) in an appendix table for several

specific locations.  $N$  in Eq. (4-24) can be calculated from the sunset hour angle as

$$N = \omega_s \left( \frac{24}{\pi} \right) \quad (4-25)$$

where  $\omega_s$  is sunset hour angle in radians, calculated using Eq. (4-14) or (4-15).

Average  $R_s$  over 10-day to monthly periods can be approximated from the range in daily air temperature using an empirical equation derived by Hargreaves and Samani (1982):

$$R_s = K_{RS} (T_{\max} - T_{\min})^{0.5} R_a \quad (4-26)$$

where  $T_{\max}$  and  $T_{\min}$  are maximum and minimum daily air temperature in °C.  $K_{RS}$  is an empirical coefficient equal to about 0.16 for interior regions (Hargreaves and Samani 1982) and about 0.19 for coastal regions (G. H. Hargreaves, 1994, personal communication).  $R_s$  and  $R_a$  have the same units. Eq. (4-26) performs best using mean monthly data. When applied to daily data, Eq. (4-26) tends to overestimate for cloudy days.  $R_s$  predicted by Eq. (4-26) should be limited to  $\leq R_{so}$ . Allen (1997) applies Eq. (4-26) to autocalibrate  $K_{RS}$  using the  $R_{so}$  clear sky envelope for seven locations in the western United States. Amatya et al. (2000) find the Allen autocalibration technique to provide good estimates of daily solar radiation at three locations in North Carolina.

Bristow and Campbell (1984) develop an equation similar to Eq. (4-26). However, their formulation requires regional calibration and has similar accuracy as Eq. (4-26) (Ball et al. 2004). Thornton and Running (1999) improve on the Bristow and Campbell equations and introduce a general calibration based on solar radiation data from across the United States. Their method, rearranged and simplified, is

$$R_s = R_{so} \{ 1 - 0.9 \exp[-B(T_{\max} - T_{\min})^{1.5}] \} \quad (4-27)$$

where  $R_{so}$  is clear sky solar radiation having the same units as  $R_s$ , and  $B$  is an empirical coefficient.  $T_{\max}$  and  $T_{\min}$  are maximum and minimum daily air temperature in °C. The equation for  $B$  by Thornton and Running for general application is

$$B = 0.031 + 0.201 \exp[-0.185(T_{\max} - T_{\min})_{\text{monthly}}] \quad (4-28)$$

where  $(T_{\max} - T_{\min})_{\text{monthly}}$  is the average difference between  $T_{\max}$  and  $T_{\min}$  over the one-month period of interest. Allen and Robison (2007) derive an equation for  $B$  based on data for two western U.S. stations (Portland and

Eugene, Oregon) from Thornton and Running that produced more accurate estimates for  $R_s$  across southern Idaho:

$$B = 0.023 + 0.1 \exp[-0.2(T_{\max} - T_{\min})_{\text{monthly}}] \quad (4-29)$$

Eq. (4-27) has advantages over Eq. (4-26) in that it is self-limiting to  $R_{so}$  as an upper bound and tends to estimate more representative ranges for  $R_s$  under cloudy conditions.

**Solar Radiation Database, United States** The National Renewable Energy Laboratory has compiled a mean monthly solar radiation database for hourly and daily data from 30 years (1961–1990) for 239 stations and from 15 years (1991–2005) for 1,020 stations in the United States ([NREL 1992](#)). The data include measured and modeled solar radiation and meteorological data. They are available on digital media from the National Climate Data Center in Asheville, North Carolina, and via the Internet ([http://rredc.nrel.gov/solar/old\\_data/nsrdb/](http://rredc.nrel.gov/solar/old_data/nsrdb/)).

**Solar Radiation Estimated from GOES Satellite Images of Cloud Cover** Advancements have been made in estimating solar radiation from the Geostationary Operational Environmental Satellite (GOES) system, where nearly continuous observations of cloud cover can be translated into estimated solar radiation at the earth's surface. Applications for estimating  $R_s$  and in some cases ET have included Pinker and Lazlo ([1992](#)), Rossow and Gardner ([1993](#)), Whitlock et al. ([1995](#)), Stewart et al. ([1999](#)), Garatuza-Payan et al. ([2001a,b](#)), and Jacobs et al. ([2004](#)). These satellite-based estimates provide spatial information on solar radiation that may be useful for developing solar radiation and ET maps.

Other sources of daily  $R_s$  and other weather data include gridded time series data from the U.S. National Weather Service's National Centers for Environmental Prediction (NCEP). NCEP runs a series of computer analyses and forecasts operationally, including the Global Land Data Assimilation System (GLDAS). Since 2001, the National Oceanic and Atmospheric Administration's GLDAS has been producing six-hourly climate parameter data sets for the globe at 1-degree spatial resolution that go back to about 1950. GLDAS data are complemented by North American Land Data Assimilation System (NLDAS) and North American Regional Reanalysis (NARR) gridded data sets, which are based on similar modeling efforts. Information on these data can be found on the NCEP website (<http://ldas.gsfc.nasa.gov/gldas/> and <http://www.emc.ncep.noaa.gov/mmb/rreanal/>). Senay et al. ([2008](#)) use the NCEP GLDAS data to calculate reference ET with the ASCE standardized Penman-Monteith equation for gridded areas and make comparisons against reference ET obtained from California Irrigation Management Information System (CIMIS) stations. Caution is needed,

however, in using air temperature and humidity from the NLDAS and NARR gridded data sets without verifying their conditioning to reflect evaporating environments associated with reference ET. More discussion on the impact of aridity characteristics of the station environment or of the gridded weather data set on net radiation calculation is given in the section of this chapter called Net Radiation Measurement and Estimation, and the impact on reference ET calculation is given in Chapters 8 and 11. Agricultural weather data from the CIMIS network have been interpolated into a 2-km gridded surface for the state of California (Hart et al. 2009). Readers are encouraged to consult the most recent literature on estimating solar radiation from satellite data and on gridded weather products because these areas and products are evolving rapidly.

### Long-Wave Radiation

Net long-wave radiation is a component of net radiation. The atmosphere is less transparent to long-wave radiation as compared with shortwave radiation. Water vapor, carbon dioxide, and ozone are good absorbers and emitters at some far infrared wavelengths as shown in Figure 4-5. Radiant energy absorbed by these various gases is emitted in all directions according to the radiation law:

$$R_L = \varepsilon_a \sigma T^4 \quad (4-30)$$

where  $\varepsilon_a$  is broadband emissivity of the atmosphere,  $\sigma$  is the Stefan-Boltzmann constant, and  $T$  is the effective absolute temperature, K, ( $K = 273.15 + ^\circ C$ ) of the atmosphere. Values of the Stefan-Boltzmann constant are

$$\sigma = 5.675 \times 10^{-8} \text{ J m}^{-2} \text{ K}^{-4} \text{ s}^{-1} \quad \text{for } R_L \text{ in W m}^{-2},$$

$$\sigma = 4.901 \times 10^{-9} \text{ MJ m}^{-2} \text{ K}^{-4} \text{ d}^{-1} \quad \text{for } R_L \text{ in MJ m}^{-2} \text{ d}^{-1}, \quad \text{and}$$

$$\sigma = 2.042 \times 10^{-10} \text{ MJ m}^{-2} \text{ K}^{-4} \text{ h}^{-1} \quad \text{for } R_L \text{ in MJ m}^{-2} \text{ h}^{-1}.$$

Because of high transparency of the atmosphere to the 8 to 13  $\mu\text{m}$  wavelengths, a net loss of radiant energy to space occurs within this range during cloudless and partly cloudy 24-hour periods. For practical purposes, only the long-wave radiation components are important between sunset and sunrise. A small amount of diffuse shortwave sky radiation is usually present just after sunset and prior to sunrise, respectively.

### Net Radiation Measurement and Estimation

Net radiation flux can be measured directly using hemispherical net radiometers, or estimated from net shortwave and net long-wave components:

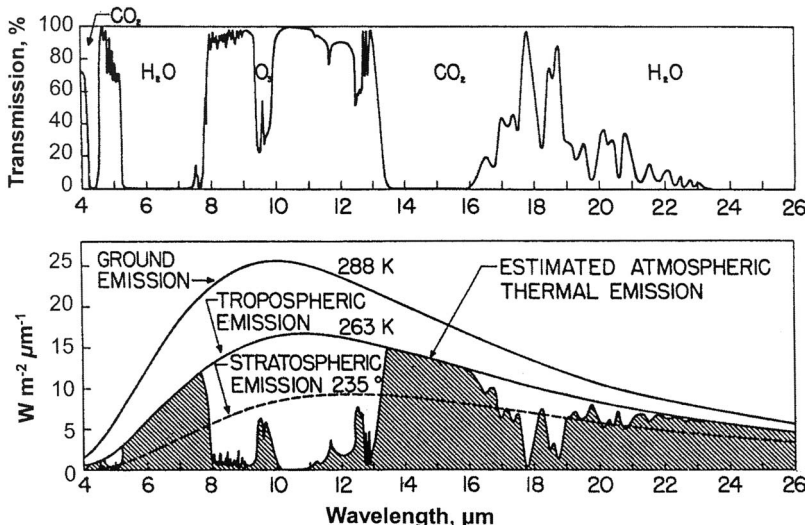


*Fig. 4-5. Infrared (long-wave) transmission following absorption by atmospheric gases  $H_2O$ ,  $CO_2$ ,  $O_3$ , and  $O_2$  (top) and the thermal emission from the ground (bottom) as a function of the wavelength. The cross-sectioned area is the estimated emission from the atmosphere at 263 K. The area between the 288 K curve and the cross-sectioned area represents the net loss of long-wave radiation from the surface at 288 K to a cloudless atmosphere having a uniform temperature at 263 K*

Source: Gates (1963). Reprinted with permission of Am. Scientist, magazine of Sigma Xi, the Scientific Research Society

$$R_n = R_s \downarrow - \alpha R_s \uparrow + R_L \downarrow - R_L \uparrow = (1 - \alpha)R_s - R_{nl} = R_{ns} - R_{nl} \quad (4-31)$$

where  $R_s$  is shortwave radiation or solar radiation,  $R_L$  is long-wave radiation,  $R_{ns}$  is net solar radiation, and  $R_{nl}$  is net long-wave radiation. The arrows indicate direction;  $(1 - \alpha)R_s$  represents the net shortwave radiation received by a water, soil, or vegetated surface; and  $\alpha$  is the shortwave broad-spectrum reflectance or albedo.

Rather than estimating net radiation for each vegetated surface, or for each crop and growth stage, net radiation, used in estimating  $ET_{ref}$ , is commonly measured or estimated for a well-watered reference crop like grass or alfalfa. Mean daily reflectance coefficients (albedo) for most greenfield crops with a full cover range from 0.20 to 0.25. A value of 0.23 for  $\alpha$  is commonly used for vegetated surfaces with a full cover. This value (0.23) is used in the standardized definitions for alfalfa and clipped grass reference ET (ASCE 2005). Full cover generally exists when the leaf-area index, which is the leaf area per unit land area, is 3 or greater (Ritchie 1972; Wright 1982).

Wright (1982) presents an equation for estimating net radiation received by alfalfa in Kimberly, Idaho, in which the daily average albedo varies during the growing season (Jensen et al. 1990, Eq. (6-67), p. 137). Dong et al. (1992) develop an equation for hourly albedo that varies with sun angle (i.e., time of day). Martin and Gilley (1993) integrate the Dong equation to obtain a daily albedo equation for grass. Brutsaert (1982) summarizes albedo values as reported by previous researchers (Table 4-1). The albedo values for inland water bodies range from 0.04 to 0.09. Bolsenga and Vanderploeg (1992) suggest a range from 0.07 to 0.15 depending upon water-surface conditions.

Long-wave radiation emitted by a surface can be estimated using Eq. (4-32) if the surface temperature is known. The broadband emissivity of a mixture of vegetation and soil surfaces,  $\epsilon_{vs}$ , is about 0.98. Table 4-2 lists reported broadband emissivity,  $\epsilon_s$ , values for several surfaces. The emissivity of water surfaces is about 0.97. The Moderate Resolution Imaging Spectroradiometer University of California Santa Barbara (MODIS UCSB) Emissivity Library (<http://www.icesc.ucsb.edu/modis/EMIS/html/em.html>) contains  $\epsilon_s$  for a wide range of soils, vegetation, and metals. Data at the site show  $\epsilon_s$  to vary widely with thermal wavelength. Generally, the  $\epsilon$  used in Eq. (4-30) is the integrated broadband emissivity covering the 8–13  $\mu\text{m}$  band. The incoming long-wave radiation is more difficult to estimate because it must be an integrated value based on variations in

Table 4-1. Approximate Mean Albedo Values for Various Natural Surfaces

Nature of Surface	Albedo Values
Deep water	0.04–0.08
Moist dark soils, plowed fields	0.05–0.15
Gray soils, bare fields	0.15–0.25
Dry soils, desert	0.20–0.35
White sand, lime	0.30–0.40
Green grass and other short vegetation (e.g., alfalfa, potatoes, beets)	0.15–0.25
Dry grass, stubble	0.15–0.20
Dry prairie and savannah	0.20–0.30
Coniferous forest	0.10–0.15
Deciduous forest	0.15–0.25
Forest with melting snow	0.20–0.30
Old and dirty snow cover	0.35–0.65
Clean, stable snow cover	0.60–0.75
Fresh dry snow	0.80–0.90

Source: Data from Brutsaert (1982)

Table 4-2. Values of the Broad-Band Thermal Emissivities,  $\varepsilon$ , of Some Natural Surfaces

Nature of Surface	Emissivity
Bare soil (mineral)	0.95–0.97
Bare soil (organic)	0.97–0.98
Grassy vegetation	0.97–0.98
Tree vegetation	0.96–0.97
Water	0.97
Snow (old)	0.97
Snow (fresh)	0.99

water vapor and temperature with elevation above the ground surface, degree of cloud cover, and temperature of the clouds. It can be directly measured during dark hours with a total hemispheric radiometer (upward facing), or indirectly computed during daylight hours by subtracting  $R_s$  from the radiometer readings. Dense clouds act as a blackbody, essentially blocking the long-wave window (8 to 13  $\mu\text{m}$ ) to outer space, and they emit long-wave radiation to the ground. The temperature at the cloud base is required to accurately calculate this component of incoming thermal radiation.

Calculation of net thermal radiation is complex for partly cloudy conditions. A detailed analysis of the factors affecting net radiation involves both the atmospheric and surface emittances and cloud cover. Partly cloudy conditions have less effect under humid conditions because much of the long-wave radiation emitted from the surface is absorbed by water vapor in the near-surface layer of the atmosphere (Anderson 1954). Allen et al. (2006c) describe calculation of  $R_n$  on sloping terrain.

Kimball et al. (1982) derive a complex model involving the areas of cloud cover and cloud temperature and transmittance in the 8 to 13  $\mu\text{m}$  wavelength window. For a more complete discussion, see Davies and Idso (1979) and Dong et al. (1992).

In theory, outgoing long-wave radiation integrated over the entire thermal spectrum is proportional to the fourth power of surface temperature:

$$R_L \uparrow = \varepsilon_{vs} \sigma T_s^4 \quad (4-32)$$

where  $\varepsilon_{vs}$  is vegetative and soil emittance, and  $T_s$  is surface temperature in K. Incoming long-wave radiation is proportional to the fourth power of effective atmospheric temperature:

$$R_L \downarrow = \varepsilon_{sky} \sigma T_{sky}^4 \quad (4-33)$$

where  $\epsilon_{\text{sky}}$  is the effective emissivity of the atmosphere, and  $T_{\text{sky}}$  is the effective sky temperature, integrated over the hemisphere, K. Generally,  $T_{\text{sky}}$  is tens of degrees cooler than near-surface air temperature ( $T$ ) at screen height, i.e., 1 to 5 m above the surface. However,  $T_{\text{sky}}$  is generally closely coupled with  $T_s$  and  $T$ , due to the large values for  $R_L \uparrow$  and  $R_L \downarrow$  that often average 300 to 400 W m<sup>-2</sup> (25 to 40 MJ m<sup>-2</sup> d<sup>-1</sup>). These large values tend to keep surface and lower atmospheric temperature in a close equilibrium.

Recognizing that surface temperature can easily vary by 30°C between a wet, evaporating surface (including the reference condition for  $ET_{\text{ref}}$ ) and a dry surface, such as hot, bare soil, is absolutely essential. Differences in  $R_L \uparrow$  between the two surface conditions can therefore be as much as 200 W m<sup>-2</sup>, which has enormous impact on the value for  $R_n$  and calculation of ET. For example, given common surface temperatures of 25°C for a wet surface and 45°C for a corresponding dry surface (20°C difference in temperature),  $R_L \uparrow$  fluxes would be (assuming emissivity of 0.97 for both surfaces)  $0.97 (5.675E-8) (298.15)^4 = 434 \text{ W m}^{-2}$  and  $0.97 (5.675E-8) (318.15)^4 = 563 \text{ W m}^{-2}$ , for a difference of 129 W m<sup>-2</sup> or 30% error in  $R_L \uparrow$  for the reference condition. The impact of surface temperature on  $R_L \uparrow$  and subsequently on  $R_n$  is one reason why practitioners are encouraged to estimate  $R_n$  using standard equations when calculating reference ET, rather than attempting to measure  $R_n$ , because of the difficulty of maintaining a cooled, evaporating surface beneath the radiometer. As discussed in a later section, when under reference conditions where the surface is evaporating and transpiring at rates of  $ET_{\text{ref}}$ , air temperature at 2 m is often within a few degrees of surface temperature (Allen et al. 2006a), so that one can make somewhat consistent and accurate estimates of  $R_n$  based on air temperature alone. This is not the case for nonreference conditions.

Because measurements of incoming long-wave radiation data or effective sky temperature are generally not available, incoming long-wave radiation is usually estimated based on near-surface air temperature,  $T$ , and vapor pressure at near-surface measurement height. The effects of cloud cover on long-wave atmospheric radiation and simple empirical equations to estimate net long-wave radiation are presented in the following.

Early work by Brunt (1932, 1952) related an “apparent” clear sky atmospheric emittance,  $\epsilon_a$ , to vapor pressure at near-surface humidity measurement height,  $e_a$ , which took the following general form:

$$\epsilon_a = a_b + b_b \sqrt{e_a} \quad (4-34)$$

where  $a_b$  and  $b_b$  are empirical coefficients. The value for  $\epsilon_a$  does not represent true  $\epsilon_{\text{sky}}$ , but is biased to work with near-surface  $T$ :

$$R_L \downarrow = \epsilon_a \sigma T^4 \quad (4-35)$$

For cloudy conditions, the net long-wave or thermal radiation loss,  $R_{nl}$ , is influenced by the degree of cloud cover and its elevation and temperature:

$$R_{nl} = R_L \uparrow - R_L \downarrow = R_{vs} - R_b = R_{vs} - (R_{bo} + R_c) \quad (4-36)$$

where  $R_{nl}$  is net long-wave radiation from the surface,  $R_{vs}$  is long-wave radiation emitted by the vegetation or soil surface,  $R_b$  is integrated long-wave radiation emitted by the sky (including clouds),  $R_{bo}$  is full-spectrum long-wave radiation emitted by a cloudless sky, and  $R_c$  is additional long-wave radiation emitted by clouds and transmitted to the earth's surface, over the entire 8–13  $\mu\text{m}$  wave band. In practice, because outgoing and incoming long-wave radiation terms in Eq. (4-36) are usually calculated using only instrument height data, then

$$R_{nl} = f_{cd} (\epsilon_{vs} - \epsilon_a) \sigma T^4 \quad (4-37)$$

where  $\epsilon_a$  is apparent atmospheric emittance for clear sky,  $\epsilon_{vs}$  is combined vegetation and soil emittance,  $T$  is near-surface air temperature in K, and  $f_{cd}$  is a factor to adjust for cloud cover. Eq. (4-37) assumes that the surface temperature and air temperature at instrument height are equal. This is a reasonable assumption for the reference ET surface (only), where the near-surface temperature profile is nearly isothermal. This is a poor assumption when the surface is dry, with low relative ET flux.

The two emittances may be combined into a single term known as the net apparent emittance,  $\epsilon'$ , which represents the difference between the combined vegetation and soil emittance and apparent atmospheric emittance when a single temperature is used. Values for  $\epsilon_{vs}$  for common, fully developed crops range from 0.94 to 0.995. A canopy value of 0.98 is recommended for most radiation balance calculations over vegetated surfaces. A value of 0.97 is recommended for water.

The Brunt expression for the net apparent emittance  $\epsilon'$  is

$$\epsilon' = \epsilon_{vs} - \epsilon_a = a_1 + b_1 \sqrt{e_a} \quad (4-38)$$

where  $e_a$  is the actual vapor pressure, kPa, which equals the saturation vapor pressure at dew point temperature. When  $\epsilon_{vs}$  and  $\epsilon_a$  are combined, as in Eq. (4-38), some loss in accuracy of the  $R_{nl}$  estimate occurs because the cloud-cover factor,  $f_{cd}$ , is effectively multiplied by both the atmospheric and surface emissions, rather than by the atmospheric emission alone.

Combining Eqs. (4-37) and (4-38) results in a general equation for net outgoing long-wave radiation:

$$R_{nl} = f_{cd}(a_1 + b_1 \sqrt{e_a})\sigma T^4 \quad (4-39)$$

For 24-hour or longer time steps,  $T^4$  in Eq. (4-39) should be replaced by  $(T_{\max}^4 + T_{\min}^4)/2$  for greater accuracy, due to strong nonlinearity caused by the exponent on  $T$ , where  $T_{\max}$  and  $T_{\min}$  are daily maximum and minimum air temperatures in K at screen or shelter height. Experimental values of the coefficients for use in Eq. (4-39) are presented in Table 4-3. The Stefan-Boltzmann constant,  $\sigma$ , is  $4.901 \times 10^{-9} \text{ MJ m}^{-2} \text{ d}^{-1} \text{ K}^{-4}$  for daily calculations with  $R_{nl}$  in  $\text{MJ m}^{-2} \text{ d}^{-1}$  and  $T_{\max}$  and  $T_{\min}$  in K. For hourly calculations,  $\sigma = 2.042 \times 10^{-10} \text{ MJ m}^2 \text{ h}^{-1} \text{ K}^{-4}$ ,  $R_{nl}$  is in  $\text{MJ m}^{-2} \text{ h}^{-1}$ , and  $T$  is in K.

Wright and Jensen (1972) developed an expression for  $f_{cd}$  in Eq. (4-39) that uses the ratio of observed solar radiation,  $R_s$ , to solar radiation under clear sky conditions,  $R_{so}$ , to represent the amount of cloudiness:

$$f_{cd} = a \frac{R_s}{R_{so}} + b \quad (4-40a)$$

where  $a$  and  $b$  are empirical coefficients. For hourly or shorter periods during nighttime, no  $R_s$  or  $R_{so}$  is available to estimate cloudiness effects. Therefore, for hourly or shorter time-step calculations where the sun angle

Table 4-3. Experimental Coefficients for Net Long-Wave Radiation, Eqs. (4-39) and (4-40)

Region	$(a, b)$	$(a_1, b_1)$
Davis, California	(1.35, -0.35) <sup>a</sup>	(0.35, -0.145) <sup>b</sup>
Southern Idaho	(1.22, -0.18) <sup>c</sup>	(0.325, -0.139) <sup>c</sup>
England	Not available	(0.47, -0.206) <sup>d</sup>
England	Not available	(0.44, -0.253) <sup>e</sup>
Australia	Not available	(0.35, -0.133) <sup>f</sup>
Denmark	(1.0, 0.0) <sup>g</sup>	
General	(1.3, -0.3) <sup>h</sup>	(0.39, -0.158) <sup>i</sup>

Note: For  $e$  in mb, divide  $b_1$  values by  $\sqrt{10}$ .

<sup>a</sup>Pruitt, W. O. (1973, personal communication).

<sup>b</sup>Goss and Brooks (1956)

<sup>c</sup>Wright and Jensen (1972)

<sup>d</sup>Monteith and Szeicz (1962)

<sup>e</sup>Penman (1948)

<sup>f</sup>Fitzpatrick and Stern (1965)

<sup>g</sup>Kjaersgaard et al. (2007), Jensen (1973), and Jensen et al. (1990) for humid climates

<sup>h</sup>Suggested for arid areas

<sup>i</sup>Budyko (1956)

Source: Data from Jensen et al. (1990)

above the horizon,  $\beta$ , at the midpoint of the period is less than 0.3 radians ( $\approx 17^\circ$ ), a substitution is made so that

$$f_{cd} = f_{cd\beta>0.3} \quad (4-40b)$$

where  $f_{cd\beta>0.3}$  is the cloud-cover function for the time period prior to when the sun angle  $\beta$  falls below 0.3 radians in the afternoon or evening (ASCE 2005).

Because single-level temperature measurements are used, Eq. (4-38) represents  $\epsilon'$ , or the difference between the emittance for the reference crop surface and the effective apparent emittance for the atmosphere under cloudless conditions. The dew point temperature does not change greatly during the day, and a single-level dew point temperature observation during the day may be adequate for most daily estimates of  $R_{nl}$  for eventual calculation of E or ET. Where humidity measurements are not available, minimum air temperatures may be taken as the dew point temperature in subhumid and humid areas. In arid areas, the dew point temperature may be several degrees Celsius lower than the minimum air temperature. Simple calibration relationships can be developed to enable using minimum air temperature as a substitute for dew point temperature as discussed in Chapter 8.

The coefficients  $a$  and  $b$  are derived empirically, and  $a + b = 1.0$ . Smith et al. (1991), Allen et al. (1994b, 1998), and ASCE (2005) have recommended using  $a = 1.35$ ,  $b = -0.35$ ,  $a_1 = 0.34$ , and  $b_1 = -0.14$  at most locations for consistency in standardized reference ET calculations. Kjaersgaard et al. (2007) find Eq. (4-40) to best fit a long time series of  $R_{nl}$  measurements in Denmark when  $a = 1.0$  and  $b = 0$ . The  $a = 1.35$  and  $b = -0.35$  coefficients underestimated  $R_{nl}$ . The 1.0 and 0.0 coefficients consider the colder cloud temperatures and less downward thermal emission in Denmark ( $\sim 55^\circ$  north latitude), given the same  $R_s/R_{so}$  ratio. The  $a = 1.0$  and  $b = 0$  coefficients were also suggested by Jensen (1973) and Jensen et al. (1990) for use in humid regions.

Allen and DeBruin (2008) demonstrate that net outgoing long-wave radiation,  $R_{nl}$ , can be estimated for well-watered, vegetated surfaces (e.g., for reference conditions) using a simple function of atmospheric transmissivity for shortwave radiation,  $\tau_{sw}$ , represented, for clear sky conditions, by the sum of the indices  $K_B$  and  $K_D$  for beam and diffuse shortwave radiation as calculated for clear conditions using Eq. (4-5) (i.e.,  $\tau_{sw} = K_B + K_D$ ):

$$R_{nl} = (170 - 33\sqrt{e_a})\tau_{sw} \quad (4-41)$$

where  $e_a$  is vapor pressure of the air in kPa, and units for  $R_{nl}$  are  $\text{W m}^{-2}$ . In the absence of data for vapor pressure, Allen and DeBruin recommend the simplification:

$$R_{nl} = 140\tau_{sw} \quad (4-42)$$

which represents  $e_a$  of about 0.83 kPa. In practice,  $\tau_{sw}$  is equal to the ratio of  $R_s/R_a$  where  $R_s$  is the measured solar radiation, which will be less than  $R_{so}$  under cloudy conditions, and  $R_a$  is exoatmospheric solar radiation. Allen and DeBruin (2008) find Eqs. (4-41) and (4-42) to estimate well at locations in Germany, the Netherlands, Idaho, and Oklahoma for hourly or shorter and for daily calculation time steps. The use of  $\tau_{sw}$  in the equations automatically accounts for effects of cloud cover on incoming thermal radiation, and thus  $R_{nl}$ , and for effects of sun angle on  $R_{nl}$ . For low sun angles and during nighttime, where the ratio  $R_s/R_a$  does not apply due to zero or near zero  $R_a$ , the following estimates for  $\tau_{sw}$  are made:

$$\begin{aligned} \text{if } \sin \beta \geq 0.09 & \text{ then } \tau_{sw} = \frac{R_s}{R_a} \\ \text{if } 0.09 > \sin \beta > -0.36 & \text{ then } \tau_{sw} = \min \left[ \tau_{sw_{i-1}}, 0.6 - 0.2 \left( \frac{\sin \beta - 0.09}{-0.36 - 0.09} \right) \right] \\ \text{if } \sin \beta \leq -0.36 & \text{ then } \tau_{sw} = \min(\tau_{sw_{i-1}}, 0.4) \end{aligned} \quad (4-43)$$

where  $\sin \beta$  is the sine of the angle of the sun above the horizon from Eq. (4-10). Values 0.09 and  $-0.36$  are in radians and correspond to angles of  $5^\circ$  and  $-20^\circ$ . Variable  $\tau_{sw_{i-1}}$  is the  $\tau_{sw}$  from the previous time step.

The relationships are valid for use in calculating  $ET_{ref}$  only, particularly Eqs. (4-37), (4-39), (4-41), and (4-42). None of the relationships for  $R_n$ ,  $R_{nl}$ , and  $R_L \uparrow$  given in this section apply for ambient conditions when ET from the surface is significantly less than  $ET_{ref}$ . Under those conditions, partitioning of net radiation into surface heating will cause an increase in  $R_L \uparrow$ , an increase in  $R_{nl}$ , and a decrease in  $R_n$ .

#### 4.4 SOIL HEAT FLUX DENSITY

For daily or longer periods, soil heat flux density,  $G$ , can be ignored, although with large variation in  $R_n$  and/or air mass conditions from one day to the next,  $G$  over a 24-h period can be as large as 5% of  $R_n$ . For shorter periods, e.g., hourly,  $G$  must be taken into account. Some of the minor terms such as changes in energy storage in a canopy may also need to be considered, especially in forest canopies.

The magnitude of soil energy storage or release can be significant over a few hours, but is usually small from day to day because much of the energy stored early in the day as the soil warms is lost late in the day or at night as the soil cools. The rate of energy flux at any depth  $z$  can be expressed by

$$G = K_{Ts} \frac{\partial T_{sl}}{\partial z} \quad (4-44)$$

where  $T_{sl}$  is the temperature of the soil and  $K_{Ts}$  is the thermal conductivity of the soil in  $\text{J m}^{-1} \text{s}^{-1} \text{K}^{-1}$ . Therefore  $G$  in Eq. (4-44) has units of  $\text{J m}^{-2} \text{s}^{-1}$  ( $\text{W m}^{-2}$ ) for  $T_{sl}$  in K and  $z$  in m.  $K_{Ts}$  varies widely with soil water content. Soil water provides thermal continuity between soil particles, thereby increasing bulk  $K_{Ts}$ . Brutsaert (1982, Figure 6-9) presents curves of thermal conductivity as a function of volumetric water content for four widely different soils. These values range from 0.1 to  $2.5 \text{ J m}^{-1} \text{s}^{-1} \text{K}^{-1}$ .

Soil heat flux density can also be estimated by monitoring the change in temperature of a soil or water profile over time:

$$G = C_s \int_0^{z_s} \frac{\partial T_{sl}}{\partial t} dz \quad (4-45)$$

where  $C_s$  is the heat capacity per unit volume of soil in  $\text{MJ m}^{-3} \text{K}^{-1}$ ,  $t$  is time with the same units as used in  $G$ , and  $z_s$  is the depth of soil that responds to increased or decreased temperature change.  $C_s$  can be estimated from the following equation by de Vries (1963):

$$C_s = 1.93V_m + 2.51V_{om} + 4.190 \quad (4-46)$$

where  $V_m$ ,  $V_{om}$ , and  $\theta$  represent the volume of minerals, organic matter, and water per unit volume of soil, respectively. For example, if a soil has 50% solids, negligible organic matter, and a volumetric water content of 0.27, its estimated heat capacity will be  $2.1 \text{ MJ m}^{-3} \text{K}^{-1}$  and  $G$  from Eq. (4-45), for  $z_s$  in m, will have units of  $\text{MJ m}^{-2} \text{t}^{-1}$ . Approximate values of thermal properties for soils and soil components are given in Table 4-4. Eq. (4-45) is often used in combination with soil heat flux plates to estimate heat flux absorbed or contributed by the soil layer above a buried plate when calculating total soil heat flux at the soil surface as described in the following section.

### **Soil Heat Flux Density Measurement**

For application to short periods, e.g., when hourly data for  $G$  are required, measuring  $G$  is customary, especially in research settings or when employing a surface energy balance, such as with the Bowen ratio ET measurement method. One method commonly used to measure  $G$  is to use heat flux plates installed near the soil surface, generally at 0.04 to 0.15 m depth with correction for heat storage above the plates using Eq. (4-45). For full cover vegetation situations where temperature gradients near the surface are minor, heat flux plates can give reasonably accurate data for  $G$ . Strong temperature gradients exist near bare soil surfaces, and

Table 4-4. Thermal Properties of Soil Constituents at 20°C and Standard Atmospheric Pressure

Soil Material	Density $\rho$ ( $Mg m^{-3}$ ; $kJ kg^{-1} K^{-1}$ )	Specific Heat ( $MJ m^{-3} K^{-1}$ )	Volumetric Capacity $C_s$ ( $J m^{-1} s^{-1} K^{-1}$ )	Thermal Conductivity $\lambda$ ( $10^{-6} m^2 s^{-1}$ )	Thermal Diffusivity $\alpha$
Quartz	2.65	0.733	1.93	8.37	4.3
Minerals*	2.65	0.733	1.93	2.93	1.5
Organic matter*	1.3	1.926	2.51	0.25	0.1
Water	1.00	4.187	4.19	0.59	0.142
Air	0.0012	1.005	0.0012	0.026	0.021

\* Approximate average values:  $1,000 \text{ kg m}^{-3} = 1 \text{ g cm}^{-3}$ ;  $4,186.8 \text{ J kg}^{-1} K^{-1} = 1 \text{ cal g}^{-1} C^{-1}$ ;  $4,186.8 \text{ MJ m}^{-3} K^{-1} = 1 \text{ cal cm}^{-3} C^{-1}$ ;  $0.41868 \text{ J m}^{-1} s^{-1} K^{-1} = 0.41868 \text{ W m}^{-1} K^{-1} = 10^{-3} \text{ cal cm}^{-1} s^{-1} C^{-1}$ ;  $10^{-6} \text{ m}^2 s^{-1} = 10^{-2} \text{ cm}^2 s^{-1}$

Source: Data from van Wijk and de Vries (1963)

differences in thermal conductivities of the plate and of the soil can produce large errors in estimating  $G$  if heat flux plates are placed too near the surface. Also, with the strong thermal gradients during day and night, condensation and evaporation near the upper or lower surface of the flux plate can be a significant problem. In addition, heat flux plates function as "umbrellas" to infiltration of precipitation or irrigation water, so that more shallow placement depths impede water flow to greater degrees, causing a localized buildup of moisture above the plate and a dry area beneath the plate. These localized aberrations in moisture can seriously affect the thermal conductivity and heat storage near the plate, invalidating measurements. Soil heat flux plates should be placed below depths of evaporation in soil (generally 0.08 to 0.15 m) to avoid errors associated with  $H$  to  $\lambda E$  conversion at depths below the plate. Ham (2001) recommends 0.12 m depth for plate installation to avoid energy balance errors associated with shallower placement. The measurement by the plate is corrected to the ground surface by measuring soil temperature at a minimum of two depths in the soil layer above the plate and averaged over several locations to decrease impacts of spatial variation. The equation is

$$G = G_{\text{plate}} + C_s \frac{T_{s2} - T_{s1}}{t_2 - t_1} z_{\text{plate}} \quad (4-47)$$

where  $G_{\text{plate}}$  is the measurement by the soil heat flux plate at depth  $z_{\text{plate}}$  beneath the soil surface,  $T_{s2}$  is average soil temperature of the surface to the  $z_{\text{plate}}$  layer at time  $t_2$ , and  $T_{s1}$  is soil temperature at time  $t_1$ . Generally  $C_s$  is calculated using Eq. (4-46), with soil water content  $\theta$  measured to account for effects of variation in water content over time. For  $z_{\text{plate}}$  in m,  $G$  and  $G_{\text{plate}}$  will have units of  $\text{MJ m}^{-2} \text{t}^{-1}$ . Because of the strong thermal gradients near the soil surface during late morning and early evening, more than two temperature depths are generally recommended, with vertical depth increments of as small as 0.01 to 0.02 m near the surface. Zhao and Allen (2012) routinely placed heat flux plates at two depths (0.04 and 0.08 m) for rigorous energy balance study and generally obtained similar values for  $G$  between the two depth systems based on Eq. (4-47). They used four depths for temperature measurement and explored the use of second- and third-degree polynomial equations to extrapolate the nonlinear temperature profiles to the surface to better account for large amounts of heat storage change within a few cm of the surface. The use of two depths for plate placement provided independent computation of  $G$  at the surface with different weighting of heat storage change and measured fluxes at depth. In applications where soil is saturated or is very dry, the user should check with the manufacturer to ascertain whether the standard plate calibration applies.

## Soil Heat Flux Density Estimation

**For Hourly or Shorter Periods** In situations where measuring soil heat flux density is not possible, or where  $G$  is part of a standardized definition for ET, such as with the standardized reference ET conditions presented in Chapter 8,  $G$  can be approximated for soil covered by vegetation using a universal relationship proposed by Choudhury et al. (1987) and Choudhury (1989) that is generally valid for daylight periods:

$$G = 0.4 \exp(-0.5\text{LAI})R_n \quad (4-48)$$

where LAI is the leaf-area index, and  $G$  has the same units as  $R_n$ . Eq. (4-48) estimates  $G = 0.1R_n$  for  $\text{LAI} = 2.8$ , which is a typical LAI for the clipped-grass reference ET definition described in Chapter 8. Eq. (4-48) estimates  $G = 0.04R_n$  for  $\text{LAI} = 4.5$ , which is typical for the alfalfa reference ET definition described in Chapter 8. Verma et al. (1986) uses a very low value for  $G/R_n$  (0.036) during daylight for a deciduous forest. For bare soil, where  $\text{LAI} = 0$ , Eq. (4-48) estimates  $G/R_n$  as 0.4, which has been observed by Choudhury et al. (1987) and Kustas and Daughtry (1990). Tasumi (2003), using data from J. L. Wright of the USDA in Kimberly, Idaho, observed  $G/R_n$  for bare soils to range from about 0.45 when wind speed at 2 m was less than  $1 \text{ ms}^{-1}$  to 0.25 when wind speed exceeded  $5 \text{ ms}^{-1}$ . He also found the  $G/R_n$  ratio to increase with increased surface temperature. Some textbooks, for example Stull (1988) and Brutzaert (1982), suggest estimating  $G$  as a function or ratio of sensible heat flux density,  $H$ , for bare soil conditions. The principle behind a  $G:H$  relationship is that both are strong functions of surface temperature, with high correlation between them. Allen et al. (2011b) utilizes the  $G:H$  concept in a surface energy balance-based ET method for processing thermal satellite data.

For nighttime conditions under grass forage, Allen et al. (1994b) observe  $G = 0.5R_n$ . At Davis, California, Pruitt observed  $G = 0.3R_n$  at night beneath clipped grass (William Pruitt 1995, personal communication). In computerized evapotranspiration models where soil surface temperatures are calculated from surface heat exchange equations,  $G$  can be estimated using a “force-restore” method (Lin 1980). A thin surface layer simulates surface temperature for use in estimating long-wave radiation and in “forcing” turbulent heat transfer to the air. A deeper second layer “restores” the surface layer temperature.

**For 24-h Periods** Under a crop canopy, daily soil heat flux is small due to cancellation of daytime and nighttime fluxes and normally can be neglected for most practical estimates involving energy balance, in particular, for the reference surfaces of grass and alfalfa. The total value of  $G$  over a multiday period, however, may be significant, especially for 30 days or longer where the soil profile is warming or cooling.

**For Monthly Periods** An approximation of the soil heat flux over long periods of time ( $\geq 30$  days) can be obtained by assuming that the soil temperature to a depth of 2 m changes approximately with average air temperature and that the average volumetric heat capacity for the soil is  $2.1 \text{ MJ m}^{-3} \text{ K}^{-1}$ ,

$$G = -4.2 \frac{T_{i-1} - T_{i+1}}{\Delta t} = 4.2 \frac{T_{i+1} - T_{i-1}}{\Delta t} \quad (4-49a)$$

where  $G$  is the average daily soil heat flux in  $\text{MJ m}^{-2} \text{ d}^{-1}$ ,  $T$  equals the mean air temperature in  $^{\circ}\text{C}$  or  $\text{K}$  for time period  $i$ , and  $\Delta t$  equals the time in days between the midpoints of the two periods. In real time predictions, where  $T_{i+1}$  is unknown,  $G$  for monthly or longer time periods can be estimated as

$$G = 4.2 \frac{T_i - T_{i-1}}{\Delta t} \quad (4-49b)$$

Additional information can be found in publications by van Wijk and de Vries (1963), de Vries (1963), and Brutsaert (1982).

This page intentionally left blank

# CHAPTER 5

## SURFACE-ENERGY AND AIR-MASS INTERACTIONS AND THE CONCEPT OF REFERENCE ET

### 5.1 INTRODUCTION

The conservation of energy at the evaporating surface controls the close linkage between solar or net radiation, the primary energy source, sensible heat flux ( $H$ ) to and from the air and to and from the soil ( $G$ ), and the resulting conversion of energy into latent heat flux ( $\lambda E$ ). An example of the partitioning of energy at the surface over a 24-hour period in a hot arid environment is illustrated in Figure 5-1 from an early energy balance study by van Bavel and Ehrler (1968). The figure shows energy components from an irrigated grain sorghum crop with complete cover and a leaf-area index of 4.2 on June 15 following irrigation on June 1 so that some soil water depletion had occurred. The figure shows that during the daytime hours, the interactions are very dynamic, while at night changes occur slowly. Figure 5-1 shows negative values for  $H$ , indicating a downward flow of sensible heat from the air to the surface, thereby contributing additional energy to the ET process so that  $\lambda E$  exceeded net radiation ( $R_n$ ). Negative  $H$  is common for well-watered surfaces in arid and semiarid climates where irrigated agriculture is surrounded by dry lands that generate  $H$  that is then transferred to irrigated areas. This process is often referred to as advection. When estimating evapotranspiration (ET) both the nighttime effects and daytime variables must be considered.

With annual crops, the soil-plant-atmosphere system changes as plants emerge and develop from bare soil at planting to full cover. With partial plant cover, the effect of a wet soil surface following rain or irrigation is large, but the effect decreases as leaf area approaches full plant cover and most of the solar energy is absorbed by the plant canopy. An example of the daily dynamic changes that occur during the period from planting to

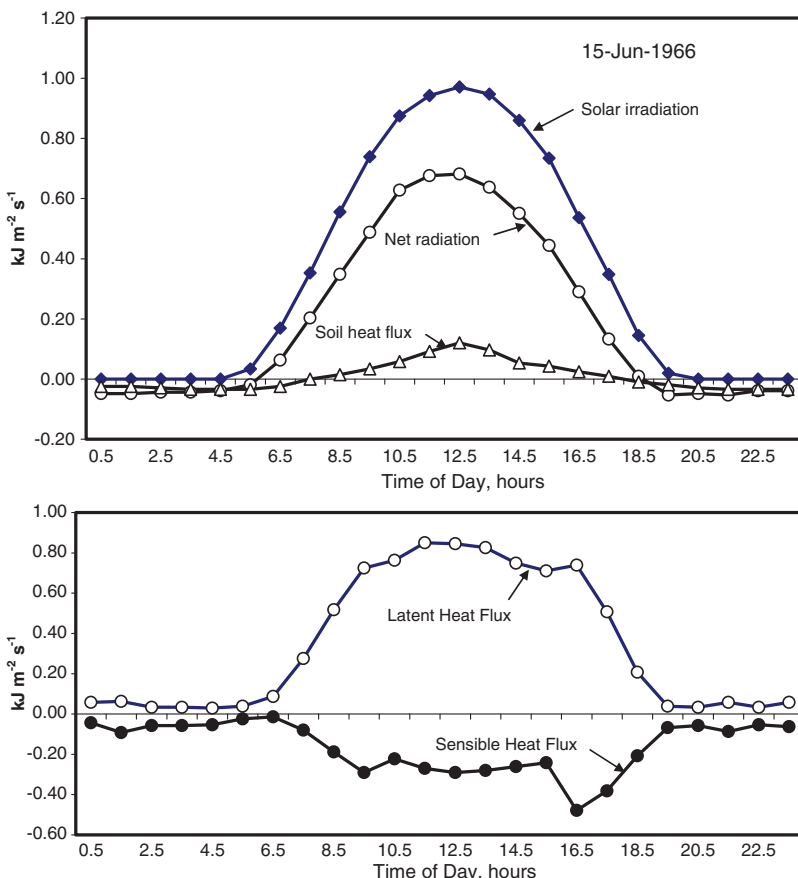
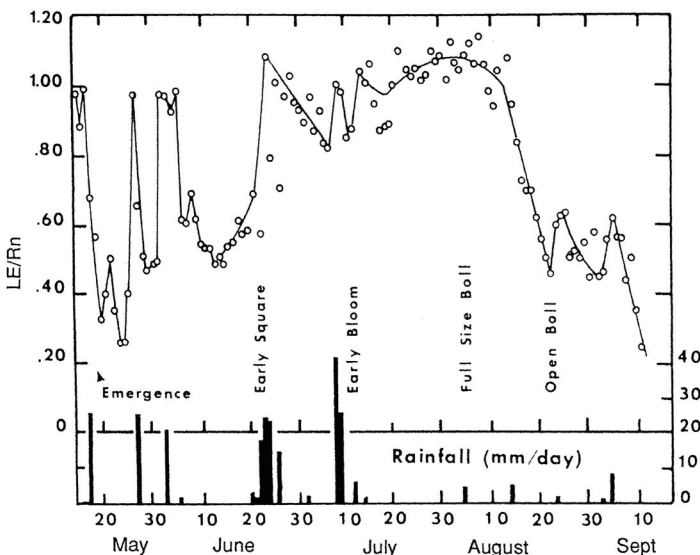


Fig. 5-1. Example energy balance components and resulting conversion of net radiation and advected (negative) sensible heat to latent heat and soil heat flux for a grain sorghum crop in central Arizona. Wind speed generally ranged from  $1 \text{ ms}^{-1}$  to  $2.5 \text{ ms}^{-1}$ . Grain sorghum leaf temperatures were consistently lower than air temperatures throughout the day

Source: Figure redrawn from van Bavel and Ehrlер (1968); reproduced with permission from ACSESS

maturity of cotton is illustrated in Figure 5-2 for a subhumid area of Texas. When plant cover was limited, the daily ratio of latent heat to net radiation,  $\lambda E/R_n$ , varied greatly as a function of rainfall events. The ratio generally increased to about 1.0 as leaf area developed and then decreased as the cotton crop began to mature. In contrast to the drier condition illustrated in Figure 5-1, little or no  $H$  was converted to latent heat, reflected by the ratio



*Fig. 5-2. Daily ratios of  $\lambda E/R_n$  for a field of cotton in Texas. Rainfall is shown in the lower part of the graph. The solid line represents the averaged time-based trend in  $\lambda E/R_n$  when the soil surface was dry and actual day-to-day changes in  $\lambda E/R_n$  when the soil surface was wet or drying*

Source: Ritchie (1971); reproduced with permission from ACS/ESS

$\lambda E/R_n$  not exceeding about 1.1. The effects of  $G$  are not included in Figure 5-2. Just after planting cotton, when the bare soil surface was wet following rainfall,  $\lambda E/R_n$  increased to nearly 1.0, but decreased rapidly as the soil dried. Typically, as soil dries, the soil water content decreases logarithmically with depth as illustrated in Figure 5-3. The dry soil near the surface greatly increases the resistance to vapor transfer to the atmosphere.

The factors illustrated in Figures 5-1–5-3 must be considered when estimating ET from annual crops. For deciduous tree crops and other perennial natural vegetation, a large change in canopy resistance occurs as trees green up in the spring and as leaves mature during late summer and fall. For citrus groves that retain leaves all year, the area of leaves exposed to direct solar radiation increases as the elevation of the sun decreases during winter months.

Engineers and water managers routinely estimate ET for irrigation planning and scheduling, water balance computations, and various other purposes. This chapter describes the general interactions of the available surface energy and air mass along with the common approaches that are used to obtain ET estimates.

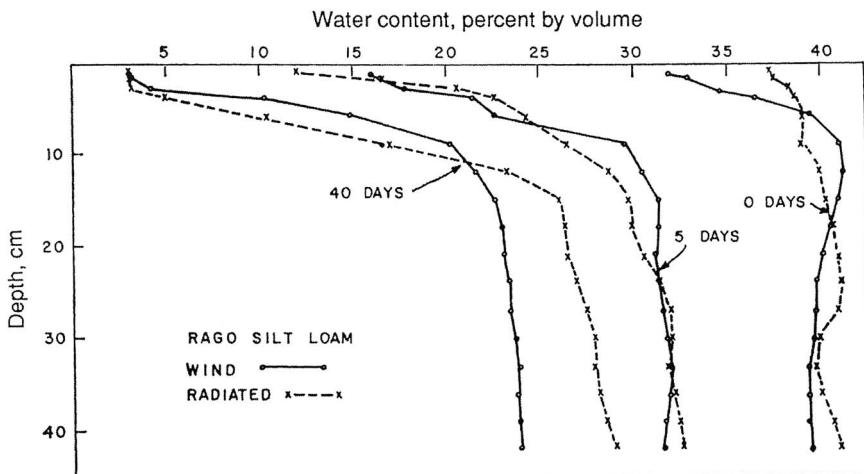


*Fig. 5-3. Soil water profiles as a function of time and type of drying (energy supplied primarily by wind or radiation) for a silt loam soil*

Source: Hanks et al. (1967); reproduced with permission from ACSESS

## 5.2 WEATHER AND SURFACE EFFECTS ON CONVERSION OF ENERGY TO LATENT HEAT FLUX

The combination energy balance-aerodynamic equations, such as those proposed by Penman (1948) or Slatyer and McIlroy (1961), are excellent models for illustrating how various weather parameters interact to affect energy partitioning at evaporating surfaces. These models are based on empirically determined aerodynamic wind functions, while the more theoretically based Penman-Monteith (Monteith 1965) equation has a wind function term based on the log-law wind profile and includes a canopy resistance term.

The PM equation will be used later in examples that describe the effects of air mass conditions and surface resistance on partitioning of net radiation at the surface into the various energy balance components. At this point, the simpler Slatyer-McIlroy equation is used to illustrate some aspects of weather-surface interactions and to introduce a widely used method for estimating ET for nonadvection conditions (Priestley and Taylor 1972):

$$\lambda E = \left( \frac{\Delta}{\Delta + \gamma} \right) (R_n - G) + h(D_z - D_s) \quad (5-1)$$

where  $\lambda E$  is the latent heat flux density,  $\gamma$  is the psychrometric constant, and  $\Delta$  is the slope of the saturation vapor pressure vs. air temperature relationship

calculated by Slatyer and McIlroy (1961) at the average of wet-bulb temperature of the air at the top of the canopy and the air temperature at height  $z$ . Units for  $\lambda E$ ,  $R_n$ , and  $G$  are the same.  $D_z$  is the wet-bulb depression at height  $z$ ;  $D_s$  is the wet-bulb depression for air in equilibrium with the surface, °C; and  $h$  is a wind-speed-dependent heat-transfer coefficient that varies with canopy resistance, crop roughness, and stability conditions of the air mass above the surface. For units for  $\lambda E$ ,  $R_n$ , and  $G$  in  $\text{W m}^{-2}$  or  $\text{MJ m}^{-2} \text{t}^{-1}$ ,  $h$  will have units of  $\text{W m}^{-2} \text{°C}^{-1}$  or  $\text{MJ m}^{-2} \text{t}^{-1} \text{°C}^{-1}$ . For a hypothetical effectively wet surface,  $D_s$  drops out of Eq. (5-1) and, except for the empiricism of the wind-function term normally determined under nonwet surface conditions, Eq. (5-1) becomes a predictor of potential evaporation,  $E_o$ , defined later.

Considering the effects of temperature alone on the energy balance, the term  $\Delta/(\Delta + \gamma)$  in Eq. (5-1) varies with temperature, e.g., at a barometric pressure of 101.3 kPa, it varies from 0.4 at 0°C to 0.85 at 40°C. Hence, under very humid conditions, where the second term of the equation has little significance, the equation indicates that the fraction of  $R_n$  converted to  $\lambda E$  will be greater during warm fall months as compared with cooler spring months, or greater in warm afternoon periods as compared with cold or cool morning periods. In more arid climates, warmer fall temperatures (or afternoon periods) will result in greater wet-bulb depressions,  $D_z$ , producing even higher fall or afternoon ratios of  $\lambda E/R_n$ . In locations well away from the equator, Pruitt (1964) showed that well-defined seasonal effects can be expected in the relationships of  $\lambda E$  vs.  $R_n$  (or  $R_s$ ) on an annual basis (Figure 5-4).

A case to consider, and one that provides a realistic estimate of the lowest  $\lambda E/R_n$  to be expected for potential evaporation cases, is the use of the first term of Eq. (5-1). This portion of the equation provides an estimate of so-called *equilibrium evaporation*, a condition described by Slatyer and McIlroy (1961) for cases where air in the lower meter is saturated, or nearly so. The modeled effects of wind become zero (except as it affects temperature), and the ratio of  $\lambda E/R_n$  is defined by  $[\Delta/(\Delta + \gamma)]$ , a function of only temperature for any given barometric pressure. Such conditions would seldom exist on a daily or longer period. On a diurnal basis, however, relative humidity (RH) is nearly 100% for the first hour or so of sunlight in many climates.

The well-known Priestley-Taylor (1972) equation provides an estimate of *equilibrium evaporation* without the requirement of including the effects of aerodynamic transport shown in Eq. (5-1). The Priestley-Taylor equation is expressed as

$$\lambda E = \alpha \left( \frac{\Delta}{\Delta + \gamma} \right) (R_n - G) \quad (5-2)$$

where  $\Delta$  is the slope of the saturation vapor pressure vs. air temperature relationship, and  $\alpha$  is a multiplier that essentially compensates for the lack

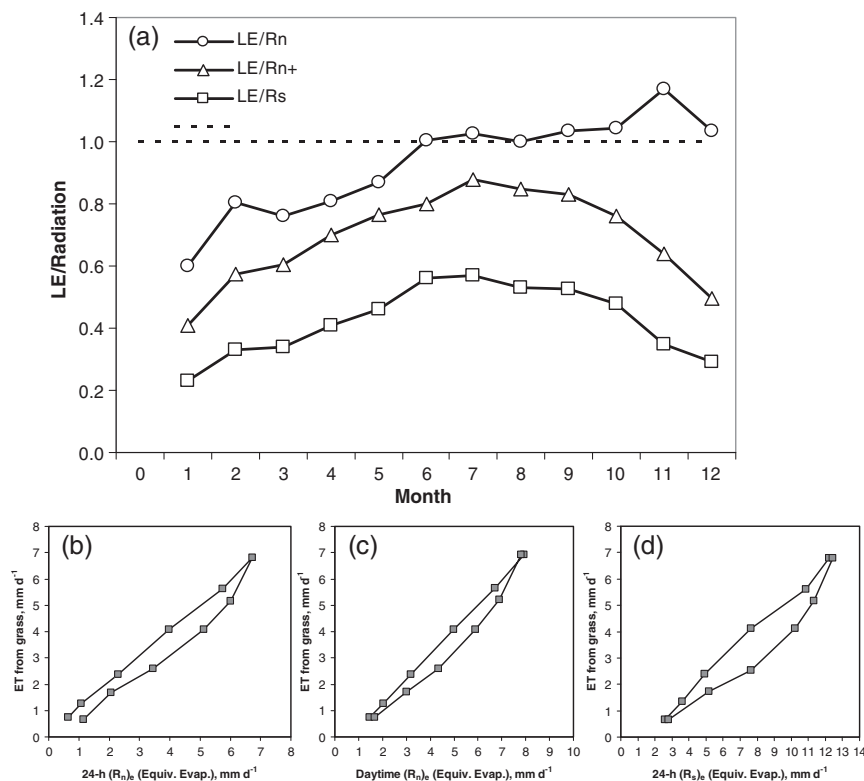


Fig. 5-4. (a) Mean monthly fractions of solar and net radiation used as  $\lambda E$  (denoted at LE) by perennial ryegrass, and (b–d) the seasonal, cyclic relationships of ET vs.  $(R_n)_e$ ,  $(R_{n+})_e$ , and  $(R_s)_e$  (equiv. mm evap.), Jan.–June 1960–63, Davis, CA.  $R_{n+}$  indicates daytime net radiation

Source: Data from Pruitt and Angus (1960); Pruitt (1971)

of an aerodynamic term typical of combination aerodynamic–energy balance equations.

Priestley and Taylor analyzed data obtained in earlier studies conducted over both land and ocean surfaces and found that a value for  $\alpha$  of 1.26 in Eq. (5-2) provided estimates of ET for the land studies in good agreement with measured ET. However, this was the case only when data from land-based studies were restricted to include the first few days immediately following rainfall over an extensive upwind area and/or when sufficiently long-term rainfall had supplied potential ET and associated vegetation cover. Jensen et al. (1990) provide a comprehensive analysis of this and

other methods using worldwide data. Steiner et al. (1991) review values for  $\alpha$  in arid environments.

The equilibrium evaporation estimated by Eq. (5-2) can only occur when a large region (on the scale of 1,000 km) is fully supplied with water to support the equilibrium evaporation rate and to humidify and cool the air mass to equilibrium conditions. This is an example of the strong negative feedback between evaporation rate and evaporation demand. The equilibrium condition rarely exists. Semiarid and arid climates occur because the actual ET of a large region is less than the equilibrium rate, and consequently air masses are drier and warmer than for the equilibrium condition. Advection of dry, warm air to smaller irrigated or riparian systems (smaller relative to the size of the region) can substantially increase the ET from those smaller systems to rates that substantially exceed the equilibrium rate. This is the basis of the complementary theory (Brutsaert 1982) and is why methods that include a humidity and aerodynamic term, such as the Penman and Penman-Monteith equations, are essential to estimate ET from irrigated systems in dry climates.

### 5.3 STANDARDIZATION OF THE VEGETATIVE COVER

This section discusses reasons why the term *potential evaporation* has been replaced with the term *reference evapotranspiration* in irrigation design, planning, and management. Potential evaporation, when used as a climatic index, is, in the strictest and most correct usage, impossible to sustain in equilibrium with the near-surface boundary layer and is difficult to measure. Reference ET is a more visual and practical means to establish a near maximum index of climatic demand for water and is straightforward to measure.

#### Potential Evaporation

The Working Group on Water Requirements of the International Commission on Irrigation and Drainage defined potential evaporation as "the evaporation from a given surface when all surface-atmospheric interfaces are wet (saturated) so that there is no restriction due to either biological control or soil water content on the water vapor loss from the surface area" (ICID 1985, p. 11). The working group pointed out that the magnitude of evaporation will depend primarily on atmospheric conditions and surface albedo, but will also vary with geometric characteristics of the surface. In terms of hydrology, potential evaporation would apply only following precipitation, condensation (dew), fog interception, or irrigation by sprinkling. Allen (2005) provides additional distinction between potential evaporation and reference evapotranspiration. In this manual, potential evaporation is identified as  $E_o$  and relates to the aforementioned definition.

## Reference Evapotranspiration

Because of ambiguities in the definition of potential evaporation and difficulties in sustaining measurable rates of potential evaporation, the term *reference crop evapotranspiration* ( $ET_{ref}$ ) is preferred for operational calculation of evaporative demand from vegetation. Two primary “types” of reference crops have been and continue to be in use around the globe. These are clipped, cool-season grass and tall, full cover alfalfa (ASCE 2005).

**Grass and Alfalfa References** The magnitude of energy-balance and air-mass interactions can be more routinely quantified by eliminating, or minimizing, the effects of changes in plant characteristics and soil water content during the growing season. Penman (1956b, p. 20) defined potential transpiration (evapotranspiration) as “the amount of water transpired in unit time by a short green crop, completely shading the ground, of uniform height and never short of water,” with the intention of using potential transpiration as a climatic evaporative index. Others, such as Monteith (1981), defined potential transpiration or potential ET as evapotranspiration from vegetation having a saturated surface (surface resistance,  $r_s = 0$ ). This latter definition, although correct, has proven to be difficult to measure in the field and to apply, especially in the absence of weather data that are measured over a wet surface to preserve the requirement of equilibrium and feedback between surface and air, in this case reflecting a potential ET environment. Therefore, use of the term *potential ET* has been discouraged as a climatic index and for estimating ET from various surfaces. The term potential ET is, however, commonly used to represent the rate of ET expected from any vegetated surface when soil water content of the root zone is sufficient to support full transpiration so that the bulk canopy resistance of the vegetation is at a minimum, but nonzero value, for example,  $r_s = 30 \text{ sm}^{-1}$  specified for the alfalfa reference described in the following paragraphs. In that usage, this condition can exist in the presence or absence of a wet soil surface and is in essence the rate of ET to expect under “fully watered” or “nonstressed” conditions for a specific crop. In that context, the potential ET can vary for each crop or vegetation type.

Jensen (1968) suggests that ET from a well-watered crop of alfalfa (*Medicago sativa*) of a height of 0.3 to 0.5 m may approximate maximum ET (as constrained by available energy) for nonsaturated surface conditions. Jensen et al. (1971) and Wright and Jensen (1972) recommend the use of the term *reference crop ET*. Doorenbos and Pruitt (1975, 1977, p. 136) describe reference crop evapotranspiration ( $ET_o$ ) as “the rate of evapotranspiration from an extended surface of 8- to 15-cm tall, green grass cover of uniform

height, actively growing, completely shading the ground and not short of water." Subsequently, this definition specified the grass cover as comprising one of the cool-season grasses with roughness, density, leaf area, and canopy resistance characteristics similar to perennial ryegrass (*Lolium perenne*) or fescue (*Festuca arundinacea* Schreb. "Alta"), because warm-season grass varieties, such as Bermuda (*Cynodon dactylon*), can exercise considerable control over transpiration.

Grass has served as a standard reference crop largely due to the preponderance of grass used in lysimeter studies around the world (Doorenbos and Pruitt 1977; Jensen et al. 1990; Allen et al. 1994d; Pereira et al. 1999a). Also, in much of the world, several species of cool-season grasses remain green throughout the year. With grass, maintaining a near-constant canopy with a leaf-area index (LAI) of ~3 is possible, and with weekly or so mowing frequency growth differences within and outside of a lysimeter, whether due to fertility or soil moisture differences, can be minimized.

However, using cool-season, clipped grass as a reference has some disadvantages. Because grass is short and aerodynamically quite smooth, the ET can be considerably lower than that which can occur with many other common crops and types of vegetation with taller, aerodynamically rougher canopies, particularly in hot, dry, and windy conditions. Also, cool-season grass varieties are not well adapted to warm tropical environments. Therefore, well-irrigated alfalfa, some 0.3 to 0.7 m in height, has been the other major crop used as a reference, with the symbol  $ET_r$  (Jensen 1968; Jensen and Haise 1963; Jensen et al. 1990). Few vegetative canopies have higher ET rates than 0.3- to 0.7-m tall alfalfa. Thus, in a two-step procedure (using  $ET_r$  and a crop coefficient  $K_c$ ), for full cover conditions, a narrower range in  $K_c$  values and a more predictable upper limit for  $K_c$  should occur when using the alfalfa reference  $ET_r$ , than when using  $ET_o$  (grass) as a reference. This is especially the case when a wide range of climates and crops are involved.

Using measured ET from alfalfa as a reference has some disadvantages if field validation is required. Cuttings remove most of the canopy, and actual ET is drastically reduced for about a week following each cutting. Trampling of the crop in the vicinity of the ET measurement such as surrounding a neutron meter tube, or extension of the alfalfa canopy beyond the boundaries of a lysimeter, thereby increasing the ET measurement, can present much more of a problem than with a grass turf. Alfalfa can be difficult to grow in some tropical climates and at high altitudes. In addition, varieties of alfalfa may exhibit different amounts of erectness of stems and stomatal control. These variations may create differences in ET among varieties that are as large as 10% (Wright 1988). Similar variations in ET can occur among different varieties of cool-season grass.

ICID (1985) provides an updated terminology listing for evapotranspiration and water requirements. It defines reference crop evapotranspiration as

The evapotranspiration from a given well-adapted crop selected for comparative purposes under given weather conditions and with adequate fetch (sufficient to make edge effects relatively unimportant) and for a standardized watering regime appropriate for this crop and the region concerned. (p. 7)

**ASCE Standardized References** In 2000, a task committee (TC) of the Evapotranspiration in Irrigation and Hydrology Committee of the Environmental and Water Resources Institute of the American Society of Civil Engineers (abbreviated ASCE-ET) and the Irrigation Association (IA) Water Management Committee addressed the need for uniform reference crop ET methodology. The TC concluded that two  $ET_{ref}$  surfaces with *standardized* computational procedures were needed to support applications across agricultural, horticultural, and landscape applications and to support current cultural practices (Walter et al. 2000; ASCE 2005). The two adopted  $ET_{ref}$  surfaces were (1) a standardized short crop (similar to clipped grass) and (2) a standardized tall crop (similar to full cover alfalfa). Additionally, the TC recognized that an equation capable of calculating both hourly and daily  $ET_{ref}$  was needed. The TC concluded that  $ET_{ref}$  from each of the two surfaces could be modeled using a single standardized reference evapotranspiration ( $ET_{sz}$ ) equation with appropriate constants and standardized computational procedures. The surfaces were defined in (ASCE 2005) as

*Standardized Reference Evapotranspiration for Short Reference  $ET_{os}$ :* Reference ET calculated for a short crop having height of 0.12 m (similar to grass), albedo of 0.23, surface resistance of  $70 \text{ sm}^{-1}$  for 24-h calculation time steps, and  $50 \text{ sm}^{-1}$  for hourly or shorter periods during daytime and  $200 \text{ sm}^{-1}$  during nighttime with daytime  $G/R_n = 0.1$  and nighttime  $G/R_n = 0.5$ .

*Standardized Reference Evapotranspiration for Tall Reference  $ET_{rs}$ :* Reference ET calculated for a tall crop having height of 0.50 m (similar to alfalfa), albedo of 0.23, surface resistance of  $45 \text{ sm}^{-1}$  for 24-h calculation time steps, and  $30 \text{ sm}^{-1}$  for hourly or shorter periods during daytime and  $200 \text{ sm}^{-1}$  during nighttime with daytime  $G/R_n = 0.04$  and nighttime  $G/R_n = 0.2$ .

The ASCE-ET Committee adopted the PM equation as parameterized by Allen et al. (1989) and Jensen et al. (1990) and simplified the terms to implement these definitions (ASCE 2005). The two standardized surfaces are similar to known full cover crops of grass and alfalfa that have been in widespread use as  $ET_{ref}$  across the United States. Each reference has unique

advantages for specific applications and times of the year. The short ( $ET_{os}$ ) standardized reference is essentially the same as the  $ET_o$  of FAO-56 (Allen et al. 1998) for 24-h calculation time steps. In addition, a recommendation by Allen et al. (2006a) to use the same  $50\text{ sm}^{-1}$  surface resistance for hourly or shorter periods during daytime and  $200\text{ sm}^{-1}$  during nighttime with the FAO-56 Penman-Monteith method has made the FAO  $ET_o$  and  $ET_{os}$  references equivalent for hourly time steps and for 24-h periods. The form of the Penman-Monteith equation adapted to the aforementioned reference standardizations is introduced in Chapter 8. In Chapter 7, data are presented and equations are used to illustrate some basic general interactions that occur between plants and the atmosphere.

## Summary

Air and surface interactions; temperature and humidity levels; and the degree of plant cover, stage of maturity, and soil water status can significantly affect actual ET by crops. The most accurate methods for estimating ET consider net radiation and the basic interactions between plants and the atmosphere that affect ET. This chapter describes the basic surface-energy basis for estimating ET and the premise for using reference ET concepts associated with standardized surfaces to promote consistency and reproducibility in estimating near-maximum values for ET.

This page intentionally left blank

# CHAPTER 6

## EVAPORATION FROM WATER SURFACES

### 6.1 INTRODUCTION

Evaporation from water surfaces is a major component of the hydrologic cycle and must be considered in hydrologic and water resource studies. Because of its nature, evaporation from water surfaces is rarely measured directly, except over relatively small spatial and temporal scales ([Jones 1992](#)). Evaporation from a water surface is most commonly computed indirectly by one or more techniques. The techniques described here are applicable to many engineering and hydrologic studies. They include pan coefficients, measured pan evaporation, water balance, energy balance, mass transfer procedures, and combined techniques. The selection of the “best” technique to use for a particular computation is largely a function of the data availability, depth and turbidity of the water body, and the required accuracy of the computed evaporation.

Theories of evaporation from water surfaces go back to at least the eighth century B.C., but measurement and experimentation go back to the seventeenth and eighteenth centuries ([Brutsaert 1982](#)). Brutsaert credits [Dalton's 1802](#) paper on aerodynamics of evaporation as a major event in the development of evaporation theory. One of the earliest detailed evaporation studies in the United States was that by Sleight ([1917](#)). Bowen ([1926](#)) develops what is now known as the Bowen ratio, which has had a major impact on evaporation measurement technologies. McEwen ([1930](#)) describes evaporation as a transformation of energy based on the earlier work of Bowen ([1926](#)) and Cummings and Richardson ([1927](#)).

Many states have tabulated evaporation data measured with various types of evaporation pans. Some states have computed statewide estimates of evaporation from shallow ponds and reservoirs ([Borrelli et al. 1998](#)).

Many early studies and reports have also addressed pan evaporation relative to large water bodies. More recently, studies have incorporated energy balance concepts. This chapter describes some earlier and more recent U.S. research-oriented studies on estimating evaporation from water bodies. Particular emphasis will be on practical procedures and techniques that professionals can use to estimate evaporation from water surfaces using pan evaporation, available weather data, or new data collected specifically for estimating daily evaporation. A portion of material in this chapter was originally assembled by F. H. Quinn of the Great Lakes Environmental Research Laboratory of the National Oceanic and Atmospheric Administration as part of Chapter 4 of the *ASCE Hydrology Handbook* ([Allen et al. 1996](#)).

## 6.2 METHODS OF ESTIMATING WATER SURFACE EVAPORATION

Several methods are commonly used to estimate evaporation from water surfaces. These methods are described in this section, with discussions on strengths, weaknesses, data requirements, and relative accuracies.

### Pan Evaporation

There has been a more than century-long endeavor to develop accurate, universal, and repeatable methods to estimate evaporation from open water using evaporation measured from some type of pan-like container. The purpose has been to reduce costs for monitoring and estimating evaporation losses and to promote consistency in estimates. However, the endeavor has been less than completely successful due to differences in radiative and aerodynamic effects of pans from large water bodies caused by differences in water depth, water turbidity, and pan shapes and measuring environments between pan and open water. These factors and history of developments are described this section.

**Traditional Pan Methods** Traditional methods for estimating evaporation from water bodies were based on evaporation measured from a network of evaporation pans. The standard evaporation pan in the United States is the Class A pan, which is 1.21 m in diameter and 0.254 m deep placed 0.15 m above ground level on an open timber framework. Two other internationally used evaporation pans rarely used in the United States are the Soviet GGI-3000 (0.3 m<sup>2</sup>) pan and the GGI-20 m<sup>2</sup> tank, both placed in the soil with only 0.075 to 0.1 m of rim above the soil surface. Details can be found in World Meteorological Organization ([1970](#)). Daily evaporation is computed from the water balance of the pan, which is the difference

between the change in storage in the pan and inputs of precipitation and water added to maintain an adequate supply in the pan for evaporation. Due to differing thermal characteristics between the pan and large water bodies, evaporation from most surface pans exceeds the total amount of evaporation from large water bodies and distorts the seasonal distribution. For example, on a seasonal basis, pan evaporation usually peaks several months before peak evaporation from deep lakes. Estimates based on pan evaporation are questionable during late fall and early winter periods when ice may form in the pan but not on large water bodies.

**Early U.S. Studies** L. G. Carpenter at Fort Collins, Colorado, carried out one of the earliest studies of pan and lake evaporation in the late 1800s ([Carpenter 1898](#)). He observed that water temperatures were higher in the shallow areas of lakes than in the deep areas and that pan evaporation at night is almost the same as during the day. He reported 11 years of evaporation data measured in Colorado's  $3 \times 3$  ft ( $0.91 \times 0.91$  m) sunken pan where the rim of the pan was within 5 cm of the ground surface. The Colorado pan was originally 2 ft deep and since 1889, 3 ft deep. That pan was considered to be a superior design relative to the elevated Class A pan due to reduced heat transfer through the walls ([Kohler et al. 1955](#)). A significant observation was that during the day, the surface water warmed rapidly and the lower layers slowly. Differential absorption of solar radiation with depth caused this thermal profile, where absorption depth varies by solar wavelength, as illustrated in Figures [6-6](#) and [6-7](#). When cooling at night, the whole mass of water cooled as cooler, denser surface water settled.

During the early 1920s in the United States, a major concern for engineers was estimating the evaporation losses from U.S. Bureau of Reclamation reservoirs. The principal method used was to estimate evaporation by multiplying a factor, or coefficient, by measured pan evaporation. No consensus existed on which of several pan designs would provide the best estimates. Houk ([1927](#)) presents a comprehensive summary of monthly pan evaporation, mean temperature, and, when available, wind speed from 50 sites near Reclamation's projects in the western United States. Many of the discussants of his paper reported additional pan evaporation data and estimated reservoir evaporation. Houk, in his closing discussion, commented on each of the statements presented by the discussants.

In 1931, Rohwer ([1931](#)) published the results of a series of indoor studies of evaporation from water surfaces conducted from 1923 to 1925 and from ice in 1928 and 1929. Several outdoor studies were conducted in 1927–1928 that included evaluating elevation effects on evaporation. He reviewed several Dalton-type equations expressing evaporation as a function of wind speed and the vapor pressure deficit (VPD). The most notable

outdoor study involved an 85-ft diameter (25.9 m) copper-lined reservoir 6.75 ft (2.06 m) deep along with several types of evaporation pans. Daily measurements reported for the periods of Oct.–Nov., 1926; Apr.–Nov., 1927; and Apr.–Nov., 1928, included surface water and air temperatures, VPD, wind speed, and evaporation. The other pans or tanks included the Geologic Survey floating tank, Colorado-type land tank, and the Weather Bureau (WB) Class A “land tank.” The floating tank was set in the middle of the reservoir. Rohwer contended that evaporation from a lake or reservoir is substantially the same as that from a circular tank 12 ft (3.66 m) in diameter and 3 ft (0.91 m) deep, whereas, the standard National Weather Service (NWS) Class A pan is 4 ft (1.21 m) in diameter and 0.254 m deep. He derived several evaporation formulas from indoor controlled wind evaporation measurements using a  $3 \times 3$  ft square tank 10 in. deep ( $0.91 \times 0.91 \times 0.25$  m), including his formula 6 of  $E = (0.44 + 0.118W)(e_s - e_d)$  where  $W$  is “water-surface” wind speed in mi/h and vapor pressures of the air and the water surface are in in. of mercury. Penman (1948) extrapolated Rohwer’s evaporation equation made at 5,000 ft (1,524 m) elevation to sea level and to wind speed at a height of 2 m to obtain his Eq. (3). Penman then showed in Figure 4 that Rohwer’s equation was similar to what he had derived in England, although Penman perceived that a power wind function [ $E = (aW^b)(e_s - e_d)$ ] was more theoretical.

During a symposium addressing evaporation from water surfaces in 1933, two papers were added to the ASCE Final Report of the Special Committee on Irrigation Hydraulics (Anonymous 1930). In this symposium, Rohwer (1934) presented a detailed discussion of evaporation from different pans including a section by R. Follansbee, who summarized national and international records of reservoir evaporation as related to pan evaporation. The papers were followed by nine discussions. Rohwer, in summarizing the nine discussions, noted that the works of I. S. Bowen, N. W. Cummings, G. F. McEwen, B. Richardson, and C. Montgomery, who succeeded in placing the physics of evaporation on a firm basis, should be noted as being significant in their contribution to the literature.

Hardy et al. (1939) summarized precipitation and evaporation data from locations throughout New Mexico as measured in 4-ft diameter standard pans and floating pans at two locations. Using suggested pan coefficients, they estimated annual evaporation from Elephant Butte reservoir to be about 72 in. (1,830 mm). Meyer’s (1942) comprehensive document summarizes estimated evaporation from lakes and reservoirs based on 50 years of U.S. Weather Bureau records. Hickox (1946) conducted a study of evaporation from a pan 1 ft (0.305 m) in diameter and 6 in. (0.15 m) deep in still air under controlled conditions of  $71.0^\circ\text{F}$  ( $21.7^\circ\text{C}$ ) and 53.1% relative humidity. The pan was insulated with a 4-in. layer of hair felt. The paper presented a detailed discussion of his results compared with others,

including a list of 65 references on evaporation. Based on his analysis, evaporation should vary with the 0.75 power of wind speed.

Young (1947) summarizes pan records and coefficients in California, including pan coefficients for the WB Class A pan and a screened pan for Lake Elsinore. Lake Elsinore is a small lake near Los Angeles with an area of about 2,220 ha and a maximum depth of about 6 m. The annual WB pan-to-lake ratio is 0.77 for Lake Elsinore. The screened pan was designed at Fullerton to approximate the evaporation from a 12-ft diameter ground pan. The screened ground pan is 2 ft (0.61 m) in diameter and 3 ft (0.91 m) deep and is covered with a quarter-inch mesh galvanized hardware screen midway between the rim and the water surface. The annual screened pan-to-lake ratio is 0.98 for Lake Elsinore. The coefficient averaged 0.89 for February–June and 1.11 for September–November due to energy storage early in the year and release later in the year. Monthly Class A pan coefficients for evaporation from Lake Elsinore, with evaporation showing the effects of energy storage and release, are shown in Figure 6-1. Also shown are pan coefficients for Lake Okeechobee, Florida, a shallow lake in a warm, humid climate with an average depth of about 3 m. Blaney and Muckel (1959) expand on Young (1947) with the addition of estimated evaporation for the San Francisco Bay and Sacramento-San Joaquin delta areas.

Kohler (1954) used the results of the detailed USGS Lake Hefner evaporation study combined with pan evaporation to estimate lake evaporation. One of his objectives was to derive a more reliable procedure for estimating lake evaporation from pan evaporation and related meteorological data normally collected by the Weather Bureau. To that end, the paper presents a summary of pan coefficients derived from previous

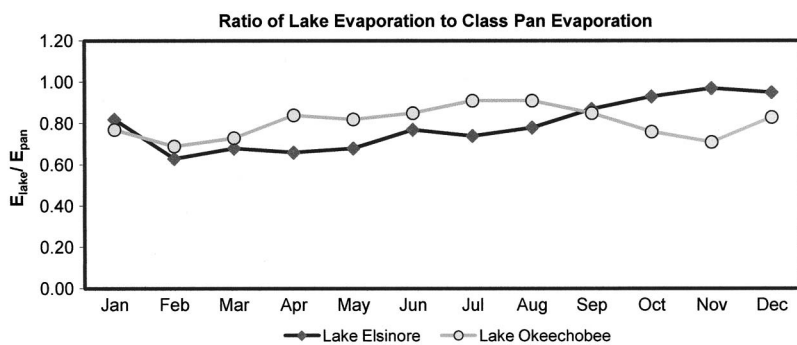


Fig. 6-1. Ratios of lake evaporation to Class A pan evaporation (Lake evap divided by  $E_{pan}$ )

Source: Lake Elsinore, CA, data from Young (1947) and Lake Okeechobee, FL, data from Kohler (1954)

studies. In some cases, evaporation from the 12-ft (3.66-m) sunken pan is assumed to be equivalent to lake evaporation. A summary of pan-to-pan ratios was also presented. The annual Class A pan coefficient derived for Lake Hefner was 0.69. Monthly coefficients vary because of the temperature lag in the lake due to differences in energy storage capacities of the two water bodies. Pan coefficients tend to be lower in spring months. Kohler concluded that annual lake evaporation could be estimated within 10–15% by applying the annual coefficient to pan evaporation. His analysis also substantiates the conclusions of Rohwer (1931) that the area of the water surface in the range considered does not greatly influence the rate of evaporation.

Kohler et al. (1955, 1958) develop an empirical equation for estimating annual lake evaporation based on pan evaporation and weather data. Variables include pan evaporation, atmospheric pressure, an advective factor related to pan wind movement, pan water temperature, and air temperature. The authors conclude that better results are obtained with monthly data than with annual data and that further improvement might be expected if daily values were used.

Kohler et al. (1959) presents a series of maps of average Class A pan evaporation, average annual lake evaporation in in., average annual Class A pan coefficients in percent, and average annual May–October evaporation in percent of annual values. These maps still serve as a useful guide to expected annual evaporation in the United States, although they have been replaced with free water surface evaporation estimates (Farnsworth et al. 1982).

These early studies using pan evaporation to estimate evaporation from water bodies clearly show that in deepwater bodies the rate of evaporation lags pan evaporation rates because of energy storage in the water body. The energy storage effects were illustrated by the parallel studies of evaporation from Pyramid Lake (a deep lake) and Lake Winnemucca (a shallow lake) (Harding 1962).

**Environmental Factors** Annual lake evaporation estimates are often obtained by multiplying the annual pan data by an appropriate coefficient applied to a U.S. National Weather Service (NWS) Class A pan. These coefficients have been computed for several water bodies and tend to range in value from 0.65 to 0.85 (World Meteorological Organization 1973; U.S. Department of Commerce 1968). The coefficient is higher under humid conditions and lower under arid or dry conditions. A coefficient of 0.70 is applicable when water and air temperatures are approximately equal.

Early U.S. studies in semiarid to arid climates reveal a significant response in pan evaporation to pan size, but now it is clear that this was primarily the result of a decreasing effect of local advection with increasing size of the water surface area. Pruitt and Doorenbos (1977) report almost no

difference (4%) between evaporation from a 0.62-m diameter Soviet pan and a 5-m diameter Soviet pan when both are located in a 5-ha irrigated grass field. However, at a dry site in Nevada, evaporation from the smaller Soviet pan averaged some 1.6 times that of the larger pan, although when corrected for the net energy transfer from soil to the pans, a factor of 1.45 resulted (Hounam 1973).

Young (1947) discusses the problem of local pan environment in relation to estimating lake evaporation. Soon thereafter, studies in India by Ramdas (1957) and studies at Prosser, Washington, and in California (Pruitt 1960, 1966; State of California 1975) provided clear evidence that unless the local environment of the pan was taken into account, the estimation of lake evaporation was subject to errors of up to 35%. Figure 6-2 presents some early results, which illustrate the problem (even for a given sized pan) associated with the environment just upwind of the pan. These results came from a study involving four Class A pans located within a large fallow field, with three of them placed within various-sized circular areas, flood irrigated frequently and planted to grass. The fifth pan located within a 5-ha irrigated grass field had a minimum upwind fetch of grass or irrigated pastureland of some 200 m. Data from the one pan in the fallow field, which had no surrounding grass, were plotted as if having a 0.3-m fetch of grass to use a log-linear plot. From this and similar studies (e.g., Ramdas 1957; Pruitt 1960; Stanhill 1962a), Pruitt developed recommended pan coefficients ( $K_p$ ) for estimating  $ET_o$  and in turn evaporation from shallow water bodies, accounting for the effects of upwind fetch (both

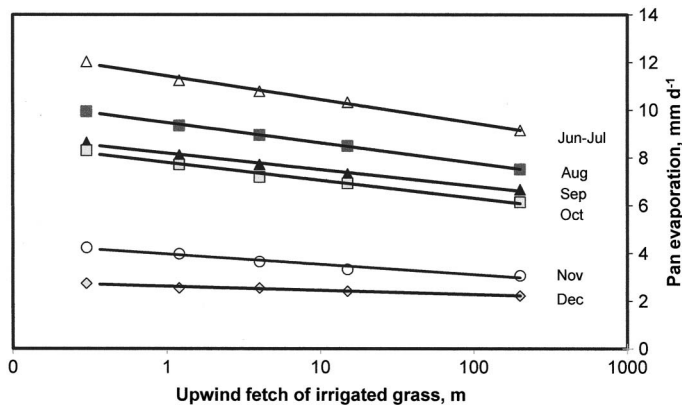


*Fig. 6-2. Evaporation from NWS Class A pans vs. upwind fetch of irrigated grass 0.07- to 0.15-m tall, Davis, California, 1959. The upwind fetch effect decreases from June to December*

Source: Data from Pruitt (1966)

dry and moist), mean relative humidity, and total daily wind on  $K_p$  (Jensen 1973; Doorenbos and Pruitt 1975, 1977; Jensen et al. 1990).

Mean monthly, seasonal, and annual Class A pan evaporation for individual stations throughout the United States have been tabulated by Farnsworth and Thompson (1982) and Farnsworth et al. (1982). The second reference, "Evaporation Atlas for the Contiguous 48 United States," contains maps with isolines of pan coefficients recommended for use with the evaporation maps in estimating so-called free water surface evaporation (FWS) from shallow water bodies. Figure 6-3 presents a portion of the annual FWS evaporation map for the 48 states (Farnsworth et al. 1982). Seasonal maps for the periods May–October and November–April are included in this NWS report. Farnsworth et al. (1982, p. 4) defined FWS as evaporation from a thin film of water having no appreciable energy storage. They state, "Only when the change in heat storage is negligibly small will FWS be a good estimation of the evaporation from the lake." Farnsworth did not address the problem of solar radiation that penetrates beneath the "thin film." Therefore, estimation of evaporation from lakes and reservoirs should not be based on the FWS data without adjustment. In nontropical climates in the spring, energy is stored in the water, and actual lake evaporation can be much less than the computed FWS. During the fall, stored energy is released and the actual lake evaporation can be much greater than the FWS evaporation. The most reliable map in Farnsworth et al. (1982) is Map 2 covering the period May–October, the warmer period when pan evaporation data were available. A map for November–April, not published, was developed, and the two seasonal maps were graphically added to obtain annual values (Map 3). In the northern part of the United States and especially in higher elevation western areas, a minimum value of 178 mm (7 in.) was estimated for the November–April FWS evaporation.

Many reservoirs are operated using estimated evaporation based on measured pan evaporation from the U.S. Weather Service Class A pan. The guidelines for siting and maintenance of evaporation pans, however, are not always followed closely. Some pans have had screens placed on them to keep birds and animals from drinking the water. Heating devices have been used to keep ice from forming on the pan in the spring and fall to facilitate observations, some pan sites have been moved to new locations that do not meet the criteria for a representative pan evaporation site, and some sites are poorly maintained. The remainder of this chapter focuses on estimating evaporation using potentially more accurate energy balance and aerodynamic approaches that have become feasible with the availability of daily and hourly weather data and the wide use of automated weather stations by various agencies and other entities.

**Behavior of Evaporation from Large Midlatitude Lakes** Estimation of evaporation from deep and/or clear water bodies from pan evaporation

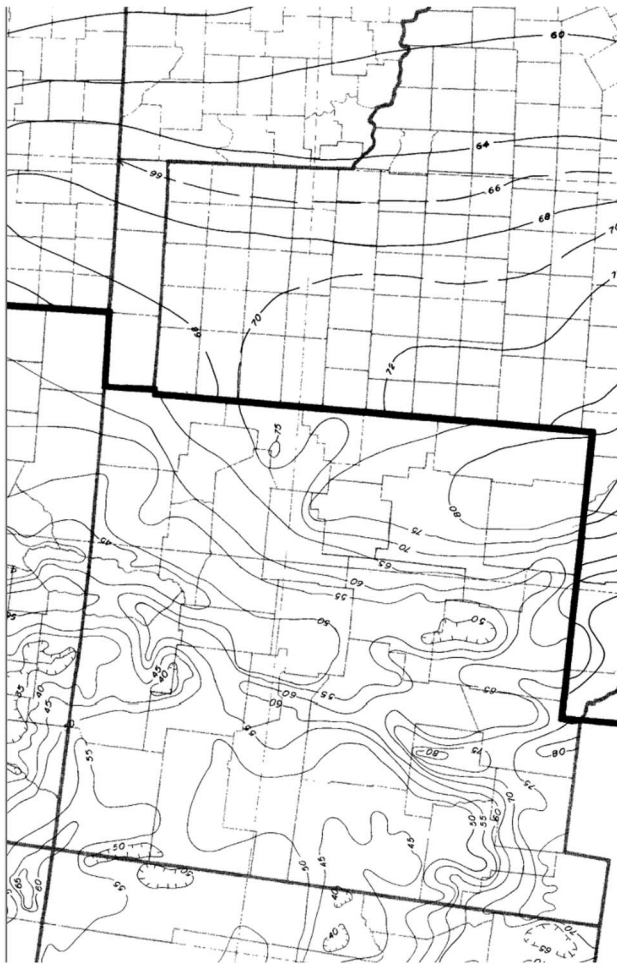


Fig. 6-3. A portion (south-central United States) of a map of estimated free water surface (FWS) annual evaporation for the 48 states showing somewhat strong east-west gradients caused by decreasing humidity from east to west  
Source: Fig. from Farnsworth et al. (1982), <http://www.weather.gov/oh/hdisc/studies/pmp.html>

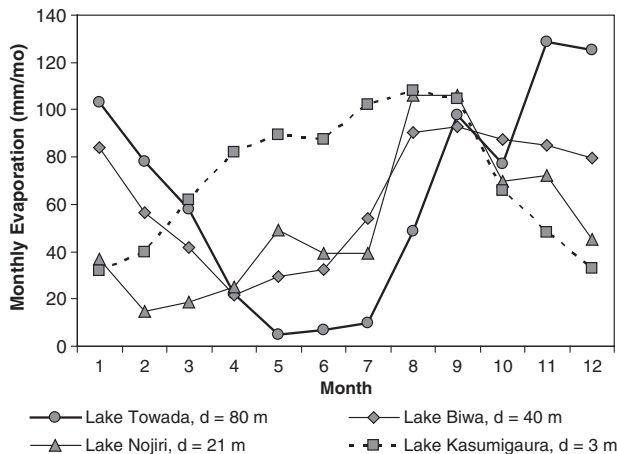


Fig. 6-4. Seasonal change of lake evaporation in Japan for water bodies of different depths

Source: Data from Kondo (1994)

can be speculative due to potentially large differences in heat storage between water body and pan. Figures 6-4 and 6-5 present data from Kondo (1994) and Croley et al. (1996) (NOAA Great Lakes Environmental Research Laboratory) that show the extreme lags possible between solar radiation and evaporation for large, cold lakes lying north of 40° latitude or south of -40° latitude. Evaporation can be low during summer when short-wave radiative energy is absorbed by the cold water bodies and when vapor pressure gradients above the water are small due to high humidity of air caused by regional ET. Evaporation is high during winter as dry air

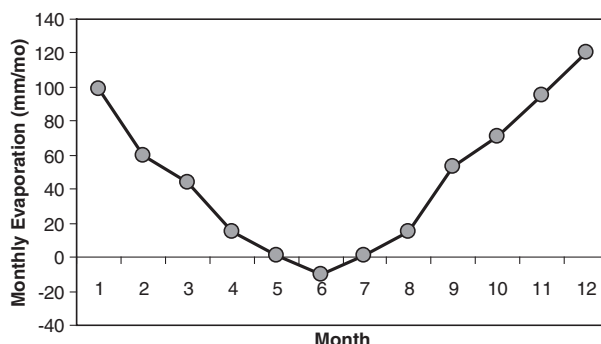


Fig. 6-5. Simulated values of evaporation for Lake Superior

Source: Data from Croley et al. (1996)

from nontranspiring frozen regions is coupled with saturation vapor pressure at the water surface that may be much higher than the air. The energy to evaporate the water during winter comes from stored energy. The pattern from Lake Towada of Japan, an 80-m deep lake, is similar to that of Lake Superior. The data from Kondo (1994) show that as mean depth of a water body decreases, the annual evaporation pattern approaches that of solar radiation. The trends of Figures 6-4 and 6-5 illustrate the inability to estimate evaporation from deepwater bodies using pan evaporation records. The annual peaks and lows can be as much as 180 days out of synch due to the large changes in energy storage ( $Q_t$ ) as discussed in a later section.

### Water Budget Procedure

The water budget procedure is a simple method for computing evaporation for monthly, seasonal, or annual time periods. All of the terms in the water balance, except for evaporation, are either measured or estimated with the evaporation computed as a residual. The water balance procedure is based upon the hydrologic equation,

$$\text{Inflow} = \text{Outflow} + \Delta\text{Storage} \quad (6-1)$$

Inflow terms consist of precipitation on the water surface, runoff from the land basin, major channel inflow from outside the immediate drainage basin, groundwater inflow, and diversions from outside the basin into a free water body (lake, reservoir, pond, etc.). Outflow terms consist of evaporation from the water surface, major channel flow out of the water body, diversions out of the water body, and groundwater flow from the water body. The water balance equation can be expressed in terms of depth or volume of water evaporated from the surface per unit time:

$$E = P_r + R + Q_i + G_{gw} + D_i - Q_o - D_o - \Delta S \quad (6-2)$$

where  $E$  is the amount of water evaporated;  $P_r$  is the precipitation on the water surface;  $R$  is the runoff inflow from the drainage basin;  $Q_i$  and  $Q_o$  are major channel flows into and out of the water body, respectively;  $G_{gw}$  is the net groundwater flow into the water body;  $D_i$  and  $D_o$  are net diversions into and out of the water body, respectively; and  $\Delta S$  is the change in water body storage, where a positive value indicates an increase. Units for all parameters in Eq. (6-2) are the same and can be expressed in terms of volume or in units of depth (i.e., in mm) over the water body surface for a specified time interval. The computations are most accurate when the evaporation is of the same order of magnitude or larger than the other terms of the water balance. The groundwater component is usually the most difficult term to estimate due to its diffusive nature. For most lakes,

the volume in storage and surface area is required to extrapolate volumes to depths.

Water balance data sources for the United States are the National Climatic Data Center, NOAA regional data centers, and state climatologists for precipitation data, and USGS, state water agencies, and flood and conservation districts for runoff, major channel flows, and diversion data.

### Aerodynamic Method (Mass Transfer)

Aerodynamic methods are among the most widely applied to determine evaporation from lakes and large reservoirs. The basic equations were tested on Lake Hefner in Oklahoma and Lake Mead in southern Nevada in the 1950s ([USGS 1954, 1958; Harbeck 1962](#)). The basic Lake Hefner form of the mass transfer equation is

$$E = M(e_s - e_z)u_z \quad (6-3)$$

where  $E$  is the evaporation in  $\text{mm t}^{-1}$ ;  $M$  is the mass transfer coefficient in  $\text{mm s}^{-1} (\text{kPa m})^{-1} \text{t}^{-1}$  and includes conversion units for depth and time;  $e_s$  is the saturation vapor pressure in kPa at the surface water temperature,  $T_s$ ;  $e_z$  is the vapor pressure of the air in kPa at level  $z$  in kPa; and  $u_z$  is the wind speed in  $\text{m s}^{-1}$  at level  $z$ . The vapor pressure of the air  $e_z$  is equivalent to the saturation vapor pressure of the air at the dew point temperature and can be computed with

$$e_z = 0.01RH(e_z^0) \quad (6-4)$$

where  $e_z^0$  is saturation vapor pressure in kPa at air temperature  $T_z$  at level  $z$ , and  $RH$  is the relative humidity in %. Saturation vapor pressure at the surface can be estimated using Eq. (3-1), and a measurement or estimate of water surface temperature, when  $T_s$  has values close to  $T_z$ , which is typical.  $T_s$  must represent the “skin” temperature of the water body because of potentially strong thermal gradients within the first few cm of water during periods of strong solar radiation, which are caused by absorption of infrared radiation near the surface and during nighttime during strong radiative cooling. Measurements made using thermal sensors such as thermocouples even 1 cm below the surface may err by several degrees. This error can cause substantial error in the estimation of  $e_s$  and in emitted long-wave radiation. Generally, in modern systems, infrared transducer-type sensors (IRTs) are used to measure skin temperature.

The mass transfer coefficient,  $M$  in Eq. (6-3), is a function of the height of the meteorological measurements, the atmospheric stability and barometric pressure, roughness of the water surface, size of water body, and the density and viscosity of the air. For the Lake Hefner study ([USGS 1954](#)),  $M$  was 0.097 for mean daily wind, temperature, and humidity measurements at the 8-m level, with vapor pressure expressed in kPa and  $E$  in  $\text{mm d}^{-1}$ .

The basic mass transfer equation requires measurement of surface water temperature, air temperature, humidity or vapor pressure, and wind speed. A more complete and decomposed method is to use a bulk transfer coefficient as in Eq. (6-7), rather than a mass transfer coefficient, where the bulk transfer coefficient can be related to aerodynamic roughness. The wind speed can be adjusted from one level to another level over the same surface by the logarithmic law (Oke 1978; Allen et al. 1989; Jensen et al. 1990), provided that the effect of stability is negligible:

$$u_2 = u_1 \frac{\ln(\frac{z_2-d}{z_{om}})}{\ln(\frac{z_1-d}{z_{om}})} \quad (6-5)$$

where  $z_1$  and  $z_2$  are the measurement heights in m for level 1 and level 2, respectively;  $z_{om}$  is the roughness height in m for momentum transfer for water; and  $d$  is the zero plane displacement in m. Literature values for  $z_{om}$  vary from 0.00001 m to more than 0.001 m, depending on wind speed and wave type, with a value of 0.0001 m as a typical average. Brutsaert (1982) listed  $z_{om}$  of 0.0001 to 0.0006 m for large water bodies.  $d$  is generally 0 for water. The wind level adjustments over water are somewhat insensitive to the value of  $z_{om}$ . The difference between using 0.0001 m and 0.001 m is approximately 5%, which is well within the required application accuracy. Adjustment of wind speed to account for difference in roughness of the weather station measurement surface from the roughness of a water surface is done with Eq. (11-60). That equation can also be used to adjust for wind measurement height differences among locations. Stull (1988) and Lofgren (2004) recommend the Charnock (1955) relation to describe  $z_{om}$  as a function of wind speed effects on wave height. The parameters suggested by Lofgren (2004) yield the equation

$$z_{om} = 4.5 \times 10^{-7} u_{10}^{2.55} \quad (6-6)$$

where  $u_{10}$  is wind speed at 10 m height over water in  $\text{ms}^{-1}$ . A lower limit of 0.00005 m for the  $z_{om}$  estimate from Eq. (6-6) is recommended, occurring at  $u_{10}$  of  $6.5 \text{ ms}^{-1}$ .

Most mass transfer research over the past several decades has been directed toward the bulk aerodynamic equation. The bulk equations consider the effect of atmospheric stability and air mass characteristics on the evaporation rate. This equation can be written as

$$E = \frac{1,000 k_t C_E \rho_a (q_s - q_z) u_z}{\rho_w} \quad (6-7)$$

where  $E$  is the evaporation in  $\text{mm t}^{-1}$ ;  $C_E$  is the bulk evaporation coefficient for level  $z$  (dimensionless);  $\rho_a$  is the density of air in  $\text{kg m}^{-3}$ ;  $q_s$  is the saturation-specific humidity at the water surface temperature in  $\text{kg}_w \text{ kg}_a^{-1}$

(subscripts *w* and *a* signify water and air);  $q_z$  is the specific humidity of the air at level  $z$  in  $\text{kg}_w \text{kg}_a^{-1}$ ;  $u_z$  is the wind velocity at level  $z$  in  $\text{ms}^{-1}$ ;  $\rho_w$  is the density of water in  $\text{kgm}^{-3}$ ; 1,000 converts from m to mm; and  $k_t$  is a conversion for time ( $k_t = 86,400$  for  $E$  in  $\text{mm d}^{-1}$  and  $k_t = 3,600$  for  $E$  in  $\text{mm h}^{-1}$ ). The specific humidity is defined in Eq. (3-5), where units of  $e$  and  $P$  are the same. In saline water bodies, salinity of the water will reduce the surface saturation vapor pressure and hence the surface specific humidity (List 1984).  $C_E$  is equivalent to the classical aerodynamic expression

$$C_E = \frac{k^2}{\ln(z/z_{om}) \ln(z/z_{ov})} = \frac{1}{u \times r_{av}} \quad (6-8)$$

for near-neutral stability conditions where  $z_{om}$  and  $z_{ov}$  are roughness lengths for momentum and vapor transfer,  $k$  is the von Kármán constant (0.41), and  $r_{av}$  is bulk aerodynamic resistance for vapor transfer between the surface and height  $z$ . The roughness height  $z_{ov}$  is generally considered to be similar in value to  $z_{om}$ , or even exceeding the value for  $z_{om}$  when applied to water (Brutsaert 1982). For detailed, theoretical aspects of relationships between  $z_{ov}$  and  $z_{om}$  for water, the reader is referred to Brutsaert (1982).

Eqs. (6-3) and (6-7) are nearly equivalent as shown by expressing Eq. (6-7) in a form using vapor pressure:

$$E = k_t 1,000 C_E \frac{\rho_a 0.622}{\rho_w} \frac{(e_s - Ke_z)}{(P - 0.378e_z)} u_z \quad (6-9)$$

where  $E$  has units of  $\text{mm t}^{-1}$  and  $K = (P - 0.378e_s)/(P - 0.378e_z)$ . For typical values of  $P$ ,  $e_z$ , and  $e_s$ ,  $K$  over water tends to approach 1.0. The pressure correction term  $0.378e_s$  in the denominator is generally small in relation to  $P$  and can be neglected with little error in  $E$ . The combined error of the two assumptions, on the order of 1 % or less, is well within data precision. Thus, the mass transfer coefficient  $M$  can be expressed in terms of the bulk evaporation coefficient  $C_E$  as

$$M = 0.622(k_t 1,000) \frac{\rho_a}{\rho_w} \frac{C_E}{P} \quad (6-10)$$

which shows a dependence of  $M$  on the air density,  $\rho_a$ , which varies with air temperature and barometric pressure; the barometric pressure,  $P$ , itself, which varies with elevation; and on the bulk evaporation coefficient  $C_E$ .

The solution of Eqs. (6-3) and (6-10) depends upon the selection of the bulk evaporation coefficient,  $C_E$ , or the mass transfer coefficient  $M$ . Extensive research conducted during the International Field Year for the Great Lakes (IFYGL) (Aubert and Richards 1981) indicated an average value for  $C_E$  of 0.00125 for the 8-m level. The IFYGL Atmospheric Boundary Layer Panel (Aubert and Richards 1981) recommends  $C_E = (1.5 \pm 0.3) \times 10^{-3}$  for

the 3-m level, with all values in this range being equally possible. Kondo (1975) recommends  $C_E = 0.0012$  for neutral conditions. Donelan et al. (1974), using a wind profile procedure, determined the following values of  $C_E$  at the 4-m level based on atmospheric stability:  $C_E = 0.00131$  for neutral conditions,  $C_E = 0.00159$  for unstable conditions, and  $C_E = 0.00135$  as the best overall estimate. Converting coefficients to the 8-m level yields values for  $C_E$  of 0.00115, 0.00140, and 0.00119 for neutral, unstable, and overall conditions, respectively. Parameters to which evaporation is most sensitive are wind speed, followed by the water surface and dew point temperatures and humidity.

For detailed studies on large lakes, using ratios of overlake to overland wind speed and humidity and considering atmospheric stability (Phillips and Irbe 1978) may be desirable. Quinn (1979) and Liu and Schwab (1987) discuss the estimation of  $C_E$  using wind speed and air-sea temperature differences. More discussion is provided later in the applications section.

### Energy Balance Method

The energy balance procedure as applied to water bodies is based upon the principle of conservation of energy. As with the water balance procedure, the evaporation is computed as a residual. This procedure is the most data intensive of the standard evaporation procedures, but it has wide applicability to many differing water bodies for time periods of minutes to years. Evaporation determined by energy balance for a water body may be expressed as

$$E = \frac{1,000}{\rho_w \lambda} (R_n - Q_t - H + Q_v - Q_w) \quad (6-11)$$

where  $E$  is the evaporation rate in  $\text{mm t}^{-1}$ ,  $R_n$  is net radiative energy to the water body in  $\text{MJ m}^{-2} \text{t}^{-1}$ ,  $Q_t$  is the change in energy stored in the water body in  $\text{MJ m}^{-2} \text{t}^{-1}$ ,  $H$  is the energy convected from the water body as sensible heat in  $\text{MJ m}^{-2} \text{t}^{-1}$ ,  $Q_v$  is the net energy advected into the water body by streamflow or groundwater in  $\text{MJ m}^{-2} \text{t}^{-1}$ ,  $Q_w$  is the energy advected by the evaporated water in  $\text{MJ m}^{-2} \text{t}^{-1}$ ,  $\rho_w$  is density of liquid water in  $\text{kg m}^{-3}$ , and  $\lambda$  is the latent heat of vaporization in  $\text{MJ kg}^{-1}$ . The product  $\lambda \rho_w E / 1,000$  is the energy utilized by evaporation in  $\text{MJ m}^{-2} \text{t}^{-1}$ .

**Net Radiation for Water** The net radiative energy flux at a surface was introduced in Eq. (4-31). A more specific method for calculating  $R_n$  for water is

$$R_n = (1 - \alpha) R_s \downarrow + (1 - \alpha_1) R_L \downarrow - \epsilon \sigma (T_s)^4 \uparrow \quad (6-12)$$

for  $R_n$ ,  $R_s$ , and  $R_L$  in  $\text{MJ m}^{-2} \text{t}^{-1}$ , where  $\alpha$  is the solar albedo for water (0.04–0.15) dependent upon surface conditions (Brutsaert 1982; Bolsenga and Vanderploeg 1992);  $\alpha_1$  is the long-wave albedo, equivalent to  $(1 - \epsilon)$  or

approximately 0.03 ([World Meteorological Organization 1970](#));  $\sigma$  is the Stefan-Boltzmann constant ( $4.901 \times 10^{-9} \text{ MJ m}^{-2} \text{ K}^{-4} \text{ d}^{-1}$  for daily time steps and  $2.042 \times 10^{-10} \text{ MJ m}^{-2} \text{ K}^{-4} \text{ h}^{-1}$  for hourly time steps);  $\epsilon$  is the long-wave emissivity (0.92 – 0.97, with  $\epsilon = 0.97$  typically used) ([Anderson 1954](#)); and  $T_s$  is the water surface temperature in K. Estimation of emitted long-wave radiation must be based on  $T_s$  for the water surface because water surface temperature can deviate substantially from air temperature, especially in small to medium-sized water bodies surrounded by warmer or cooler land surfaces. In applying Eq. (6-12), shortwave and long-wave radiation may be measured or estimated with several empirical equations ([Croley 1989](#); [Derecki 1976](#); [Gray 1970](#); [Sellers 1965](#)).

Albedo varies with water turbidity, wave height, and the ratio of diffuse to total solar radiation. Cogley ([1979](#)) presents a table of albedo for water surface as a function of latitude based on an accurate weighting for radiation received at different elevation angles. These were based on the Fresnel equation for a plane surface of pure water under direct radiation and modified by measurements made by Grishchenko ([1959](#)) for wave heights of 0.1 to 0.7 m and cloud cover of 0 to 25%. Table 6-1 summarizes these values.

**Factors Governing Heat Storage,  $Q_t$ , of Water Bodies** An important distinction between  $R_n$  for a water body and  $R_n$  for vegetation or soil is that with soil and vegetation, essentially all of the  $R_n$  quantity is captured at the “opaque” surface and is immediately available for conversion to  $\lambda E$  or  $H$  or conduction into the surface as  $G$ . With water, however, much of the solar radiation,  $R_s$ , penetrates to some depth in the water body, depending on the turbidity of the water, where it is converted to  $Q_t$ . Therefore, with water bodies,  $R_n$  is the net radiation captured by the water body, but is not necessarily available at the surface for immediate conversion to  $\lambda E$  or  $H$ . This is why the energy storage change,  $Q_t$ , is used in the energy balance for water rather than the ground energy flux density term,  $G$ , that is used for soil. The term  $G$  for soil is governed only by thermal conduction into the surface, whereas  $Q_t$  for water is governed by both conduction and by penetration of solar radiation. The value for  $Q_t$  can be very large, as shown later in Figure 6-12 for American Falls Reservoir, Idaho.

Absorption of solar irradiance in pure water varies widely with the wavelength of spectral irradiance (Figure 6-6). The mean absorption depth is very shallow for wavelengths shorter than 0.4  $\mu\text{m}$ , but it is relatively deep for wavelengths between 0.4 and 0.6  $\mu\text{m}$ , which is primarily blue and green visible radiation. Most of the energy in solar irradiance occurs in the 0.2–1.0  $\mu\text{m}$  wavelength band. Figure 6-7 shows absorption of total solar radiation in pure (clear) water, indicating that most warming of clear water will occur more than several m below the surface. However, some warming of the top 1 m of even clear water will always occur due to the ready

Table 6-1. Monthly Mean Grishchenko (1959) Albedo (Percent) of Open Water for Latitudes 0° to 70° N

$\theta$ (deg)	Jan	Feb	Mar	Apr	May	Jun	Jul	Aug	Sep	Oct	Nov	Dec	Year
70	30.1	33.8	22.9	14.8	11.6	11.2	11.4	13.4	20.2	31.3	30.1	—	14.1
60	33.9	24.0	15.5	10.5	8.8	8.4	8.6	9.8	13.6	21.6	32.1	35.5	12.0
50	22.0	16.1	10.8	8.4	7.5	7.3	7.4	8.0	9.9	14.4	21.0	24.1	10.2
40	14.5	11.1	8.5	7.3	6.8	6.7	6.8	7.1	8.0	10.3	13.8	16.1	8.6
30	10.3	8.6	7.3	6.7	6.5	6.4	6.4	6.6	7.1	8.2	10.0	11.1	7.6
20	8.3	7.4	6.7	6.4	6.3	6.3	6.3	6.4	6.6	7.2	8.1	8.7	6.9
10	7.2	6.7	6.4	6.3	6.4	6.4	6.4	6.3	6.3	6.6	7.1	7.4	6.6
0	6.6	6.4	6.3	6.4	6.6	6.8	6.7	6.4	6.3	6.4	6.6	6.8	6.5

Source: Data from Cogley (1979), Table 5

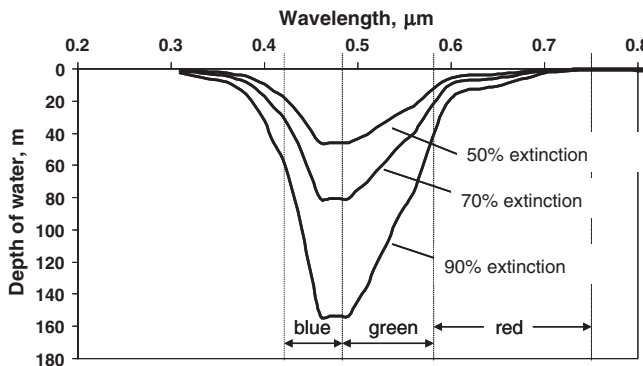


*Fig. 6-6. Relative extinction depths for solar radiation in pure water as a function of wavelength*

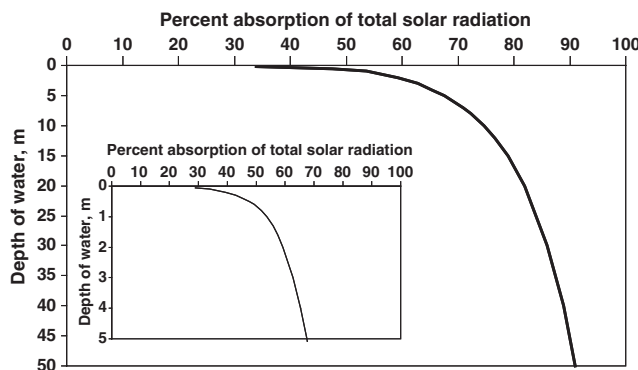


*Fig. 6-7. Percent absorption of total solar radiation as a function of water depth for pure water. The inset provides detail over the first 5 m*

absorption of the near- and mid-infrared wavelengths. In addition, penetration of blue and green wavelengths is reduced with increasing turbidity of the water.

When inflow and outflow rates are significant, or when deep reservoirs are involved, estimating the change in energy storage over periods of time can become complex. The advection of energy and the energy stored as a thermal profile develops below the water surface of the reservoirs must be considered. Rosenberry et al. (1993) and Sturrock et al. (1992) report measured energy storage in Williams Lake in north-central Minnesota. Measurements made over five seasons indicated that substitution of energy storage measured at one location in the lake from a raft placed in the center of the lake rather than at 16 locations distributed over the lake resulted in

estimates within 2% of the best estimates. Williams Lake, a somewhat bowl-shaped basin, has an area of 36 ha and a maximum depth of about 10 m. Average annual evaporation was 670 mm. During May–June, solar energy storage input,  $Q_t$ , averaged  $4\text{--}5 \text{ MJ m}^{-2} \text{ d}^{-1}$  or about 20% of  $R_n$ . Amayreh (1995) measured large values of  $Q_t$  of  $9\text{--}10 \text{ MJ m}^{-2} \text{ d}^{-1}$  during June and July on Bear Lake in Idaho and Utah. Bear Lake is a clear, cold, and deep high desert lake with a maximum depth of 60 m. Other studies (Anderson 1954; Harbeck et al. 1958; Hughes 1967; Ficke 1972; Keijman 1974) apply a range of methods for measuring energy storage in water.

**Energy Storage to Water Bodies from Thermal Profiles** One of the more difficult problems in applying the energy balance or the combination approach to estimating evaporation is that of estimating energy stored or released from the water body. The data shown in Figures 6-8 and 6-9 illustrate typical thermal profiles encountered as solar radiation increases during the year and after solar radiation begins to decrease. Figure 6-8 shows the thermal profile that has developed as a result of solar radiation penetrating the water body and some conduction of energy downward. As shown in Figure 6-6, about 50% of total solar radiation penetrates to a depth of 1 m and 20% to a depth of 10 m in pure water. The thermal conductivity of water is not high, and most of the increase in temperature is due to absorbed solar radiation that decreases exponentially with depth. At the end of October, as solar radiation has decreased and with the loss of energy due to evaporation, long-wave radiation emitted from the water surface and the transfer of sensible heat to the air, the surface of the water cools (Figure 6-9). Then, because of the increasing density of water near the

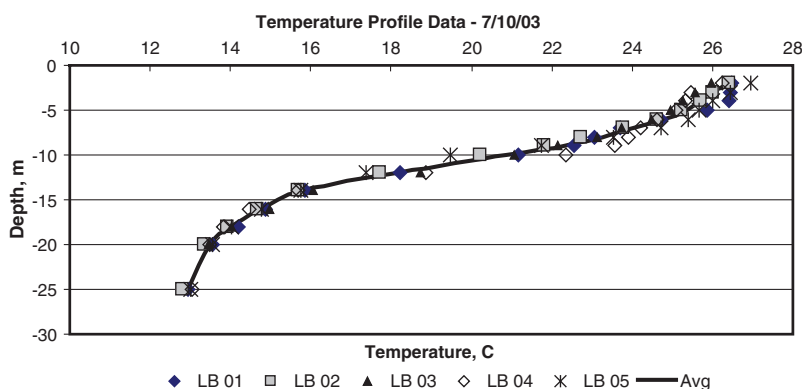


Fig. 6-8. Thermal profile data for Lake Berryessa, California, on July 10, 2003. The various symbols refer to locations within the reservoir  
Source: Jensen et al. (2005); copyright ASCE

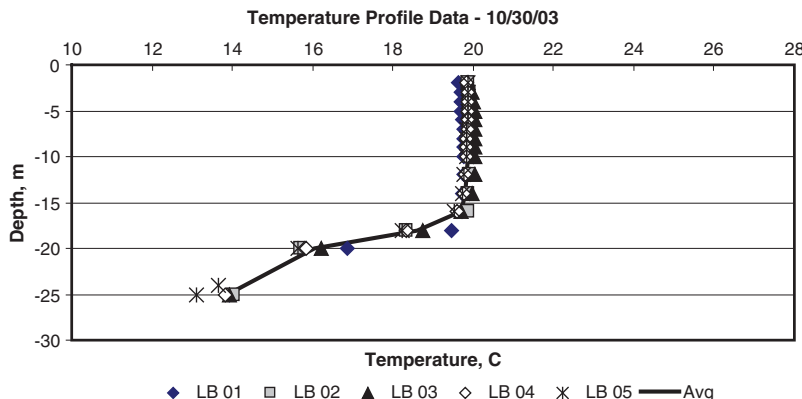


Fig. 6-9. Thermal profile data for Lake Berryessa, California, on October 30, 2003. The various symbols refer to locations within the reservoir  
Source: Jensen et al. (2005); copyright ASCE

surface as it cools, upper water layers settle until they reach the same temperature as water lower in the profile. The astute observation made in 1898 by Carpenter that the water in evaporation tanks is nearly uniform in the morning, while a thermal gradient exists during the day, illustrates this physical phenomenon of cooled water settling and mixing with deeper water in a container.

For shallow lakes and reservoirs less than 3–5 m deep, measuring water temperature near the surface in the mornings will likely produce a good estimate of daily changes in energy storage. Daily measurements of near-surface temperature in the morning can enable calculating average rates of energy storage. The trend in average daily change in energy storage measured in Pretty Lake, Indiana, and Williams Lake in Minnesota illustrates the magnitude of energy storage and release rates that can be expected for deepwater bodies >5–10 m (Figure 6-10). The values for  $Q_t$  shown in Figure 6-10, especially during early spring, late summer, and fall are relatively large, averaging about  $\pm 5 \text{ MJ m}^{-2} \text{ d}^{-1}$ , when  $R_n$  during these periods averaged only 5 to 20  $\text{MJ m}^{-2} \text{ d}^{-1}$ .

Energy storage in shallow to moderately deepwater bodies (<5–30-m depth) can use measurements of water temperature over various time periods and calculations of the change in energy storage.  $Q_t$  is estimated by differencing water temperature profiles over time and multiplying by the specific heat of water,  $C_w$ :

$$Q_t = \rho_w C_w \frac{\left[ \left( \int_{z_s}^{z_e} T(z) dz \right)_{t_2} - \left( \int_{z_s}^{z_e} T(z) dz \right)_{t_1} \right]}{t_2 - t_1} \quad (6-13)$$

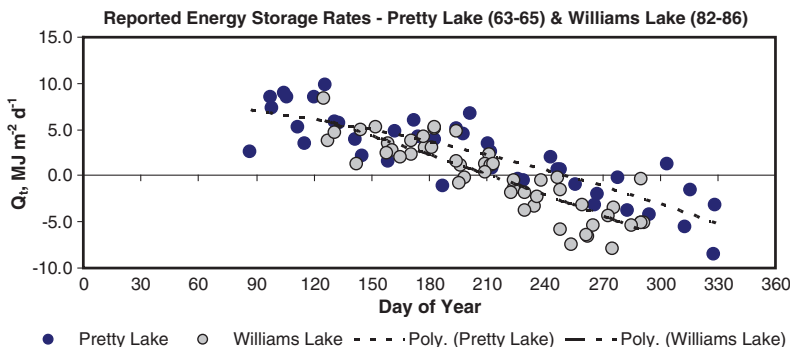


Fig. 6-10. Reported energy storage rates in Pretty Lake, Indiana, 1963–1965, and Williams Lake, Minnesota, 1982–1986

Source: Jensen et al. (2005); copyright ASCE

where  $\rho_w$  is the density of liquid water in  $\text{kg m}^{-3}$ ;  $C_w$  is the specific heat of water in  $\text{MJ kg}^{-1} \text{ K}^{-1}$ ; and  $T(z)$  is the temperature of water in K at depth  $z$ , evaluated at times  $t_1$  and  $t_2$ . Depth  $z_s$  is generally at the water surface ( $z_s = 0$ ), and  $z_e$  is a depth below the surface in m where temperature change over time is small. Units for  $t$  in seconds will produce  $Q_t$  in  $\text{MW m}^{-2}$ , and  $t$  in h or d will produce  $\text{MJ m}^{-2} \text{ h}^{-1}$  and  $\text{MJ m}^{-2} \text{ d}^{-1}$ . Positive values for  $Q_t$  from Eq. (6-13) indicate energy entering the water body system. For practical problems, the water density can be assumed to be  $1,000 \text{ kg m}^{-3}$  and  $C_w = 4.1868 \text{ MJ m}^{-3} \text{ K}^{-1}$ . Because of the decrease in density with an increase in temperature, the average  $C_w$  over the range of 10 to  $25^\circ\text{C}$  is  $4.18 \text{ MJ m}^{-3} \text{ K}^{-1}$ .

**Energy Storage to Water Bodies Based on Meteorological Measurements** Estimates for  $Q_t$  can also be related to radiation received by a water body because radiation is the primary source for heating water. Jensen et al. (2005) estimated daily energy storage in Pretty Lake, Indiana; Williams Lake, Minnesota; and Lake Berryessa, California, based on net shortwave and long-wave radiation:

$$Q_t = 0.5R_{sn} - 0.8R_{nl}, \quad \text{for day of year } < 180 \quad (6-14a)$$

and

$$Q_t = 0.5R_{sn} - 1.3R_{nl}, \quad \text{for day of year } > 180 \quad (6-14b)$$

where  $Q_t$  is average daily energy storage in the water body in  $\text{MJ m}^{-2} \text{ d}^{-1}$ ,  $R_{sn}$  is net solar radiation  $(1 - \alpha)R_s$ , and  $R_{nl}$  is net outgoing long-wave radiation [ $R_{nl} = R_1 \uparrow - (1 - \alpha_1)R_1 \downarrow$ ]. Williams Lake is a small lake (36 ha)

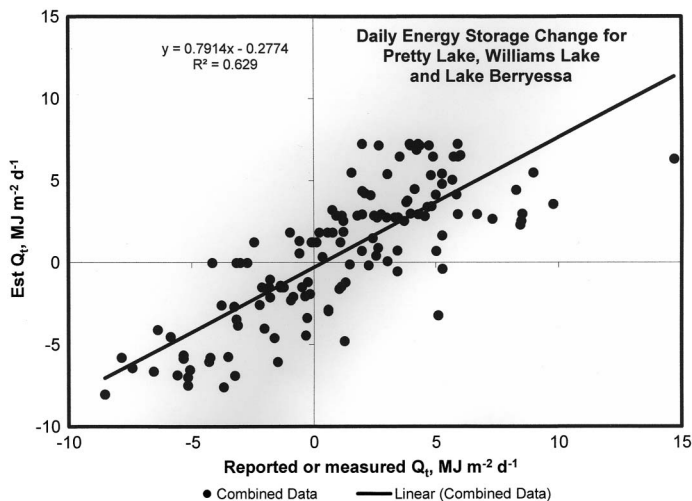


*Fig. 6-11. Estimated daily  $Q_t$  from Eq. (6-14) vs. reported or measured  $Q_t$  for Pretty Lake, Indiana (1963–1965); Williams Lake, Minnesota (1982–1986); and Lake Berryessa, California (2003–2004)*

*Source: Data from Jensen (2006), personal communication*

with a maximum depth of about 10 m. Pretty Lake has an area of about 75 ha, a maximum depth of about 25 m, and an average depth of about 8 m because of large shallow areas. Lake Berryessa has an area of 8,320 ha when full, a maximum depth of 58 m near the dam, and an average depth of about 40 m. The  $r^2$  for both equations combined was 0.63. A comparison of estimated  $Q_t$  from Eq. (6-14) vs. reported or measured  $Q_t$  is shown in Figure 6-11.

Data required to apply the energy balance method can be obtained from the National Climatic Data Center for radiation components and from satellite analysis for surface water temperature, and in situ measurements can be obtained from thermistor or thermocouple strings or water intakes for the changes in energy storage. A detailed energy budget for Lake Ontario is given by Aubert and Richards (1981). This includes an evaluation of all energy terms.

**$Q_t$  and Evaporation by Indirect Measurements** Figure 6-12 shows average hourly patterns of  $R_n$ ,  $\lambda E$ ,  $H$ , and  $Q_t$  during two months of 2004 for American Falls Reservoir, Idaho, where mean water depth was 9 m (Allen and Tasumi 2005). The figures show the substantial addition of energy to the reservoir (positive  $Q_t$ ) during daytime via the penetration of solar radiation. The rate of  $Q_t$  was lower in July due to the increased transfer of

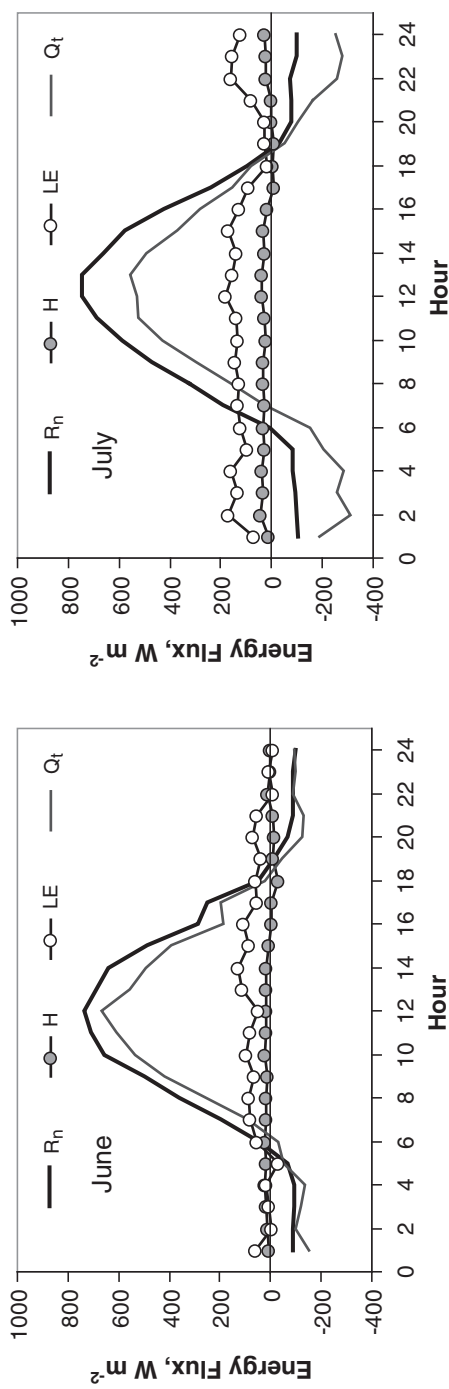


Fig. 6-12. Average hourly  $R_n$ ,  $\lambda E$ , sensible heat ( $H$ ), and energy storage flux density ( $Q_t$ ) during two months of 2004 for American Falls Reservoir, Idaho  
Source: Data from Allen and Tasumi (2005)

energy to the water surface and consequent higher rates of  $\lambda E$ . Negative  $Q_t$  during nighttime and nighttime evaporation in July coincided with the negative  $R_n$  from the surface. Evaporation rates were somewhat constant throughout the day and night due to close coupling between water surface temperature and air temperature.

Allen and Tasumi (2005) estimate  $Q_t$  as a residual of the energy balance by inverting Eq. (6-11), assuming that the  $Q_v$  and  $Q_w$  terms are zero, and retaining  $\lambda E$  in energy units:

$$Q_t = R_n - H - \lambda E \quad (6-15)$$

Evaporation and  $Q_t$  use a combination of eddy covariance and Bowen ratio to determine  $\lambda E$  and  $H$ , where the Bowen ratio (see also Eq. 7-8) is expressed as

$$\beta = \frac{H}{\lambda E} = \gamma \frac{(T_s - T_z)}{(e_s^o - e_z)} = \gamma \frac{(T_1 - T_2)}{(e_1 - e_2)} \quad (6-16)$$

where  $\beta$  is the Bowen ratio,  $T_s$  is the water surface temperature,  $T_z$  is the air temperature at level  $z$  in  $^{\circ}\text{C}$ ,  $e_s^o$  is the saturation vapor pressure in kPa at  $T_s$ ,  $e_z$  is the vapor pressure in kPa at level  $z$ , and  $\gamma$  is the psychrometric constant  $\text{kPa}^{\circ}\text{C}^{-1}$  [Eq. (3-11a)]. Parameter  $\beta$  is dimensionless. The last set of terms in Eq. (6-16) presents an alternative means for measurement of  $\beta$ , where paired measurements of air temperature ( $T_1$  and  $T_2$ ) and vapor pressure ( $e_1$  and  $e_2$ ) are observed at two heights  $z_1$  and  $z_2$  above the water surface. Precision and bias correction or bias elimination are required in the measurement of the differences  $T_1 - T_2$  and  $e_1 - e_2$  due to their potentially small values under near-neutral conditions or low evaporation rates.

Allen and Tasumi (2005) compute the latent heat flux using the measured Bowen ratio coupled with  $H$  measured by eddy covariance and inversion of the Bowen ratio relationship:

$$\lambda E = \frac{H_{EC}}{\beta} \quad (6-17)$$

where  $H_{EC}$  is sensible heat flux determined by eddy covariance and  $\beta$  is determined by measuring humidity and temperature between two interchanging arms suspended over the water via Eq. (6-16). Determination of  $\lambda E$  from this approach cannot be used when the air temperature profile above the water surface is close to neutral, so that the determination of  $\beta$  via Eq. (6-16) becomes close to zero. The minimum value for the absolute value of  $\beta$  for employment of Eq. (6-17) should be about 0.05 to 0.10 to retain sufficient precision and management of residual measurement biases. Allen and Tasumi (2005) also estimate evaporation rates using

aerodynamic transfer methods based on Eq. (6-7) using the humidity and  $T$  measurements from 1.0 and 3.0 m heights above the water surface via the Bowen ratio arms and, as a second means, using  $T$  and  $H$  from the 1.0 m height with surface temperature measured using an infrared sensor. Those evaporation estimates were used as an independent check on  $\lambda E$  derived from Eq. (6-17).

**Other Components of the Energy Balance for Water** The energy advected by the evaporating water,  $Q_w$ , i.e., by the removal of water from the system, although typically less than 1% of  $\lambda E$ , can be accounted for with

$$Q_w = \rho_w C_w \frac{E}{1,000} (T_s - T_b) \quad (6-18)$$

where  $\rho_w$  is the density of liquid water in  $\text{kg m}^{-3}$ ,  $C_w$  is the specific heat of water in  $\text{MJ kg}^{-1} \text{K}^{-1}$ ,  $T_s$  is the temperature of the evaporated water in K (i.e., surface temperature),  $T_b$  is a base temperature, and  $E$  is the evaporation rate in  $\text{mm t}^{-1}$ . Eq. (6-18) accounts for the warming of water from the base temperature to the water-surface evaporating temperature. Because the change in energy storage is used in calculating evaporation, the choice of base temperature is largely immaterial (Harbeck et al. 1958). The base temperature can be set equal to the mean annual temperature of the water body, or to  $0^\circ\text{C}$  (273 K) for convenience.

The net energy advected into a water body,  $Q_v$ , is composed of the energy transported into the water body by runoff, precipitation, and out-of-basin inflows. The energy advected out of a water body is composed of any outflows from the water body and the melting of solid precipitation at the lake surface. This quantity, when expressed as energy per unit area per time-step basis for a base operating temperature equal to  $0^\circ\text{C}$  in Eq. (6-18), is

$$Q_v = (V_r T_r + V_p T_p + V_i T_i - V_o T_o) \frac{\rho_w C_w}{A} - \frac{V_{sp} \rho_w \lambda_f}{A} \quad (6-19)$$

where  $V_r$  is the volume of diffuse runoff to the water body in  $\text{m}^3 \text{t}^{-1}$ ,  $T_r$  is the temperature of the runoff in  $^\circ\text{C}$ ,  $V_p$  is the volume of precipitation in  $\text{m}^3 \text{t}^{-1}$ ,  $T_p$  is the temperature of the precipitation in  $^\circ\text{C}$ ,  $V_i$  is the volume of basin inflow in  $\text{m}^3 \text{t}^{-1}$ ,  $T_i$  is the temperature of the inflow in  $^\circ\text{C}$ ,  $V_o$  is the volume of outflow in  $\text{m}^3 \text{t}^{-1}$ ,  $T_o$  is the temperature of the outflow in  $^\circ\text{C}$ ,  $A$  is the surface area of the water body in  $\text{m}^2$ ,  $V_{sp}$  is the volume of solid precipitation in  $\text{m}^3 \text{t}^{-1}$ ,  $\rho_w$  is the water density in  $\text{kg m}^{-3}$ , and  $\lambda_f$  is the latent heat of fusion in  $\text{MJ kg}^{-1}$ . The energy advected into a lake is usually relatively small compared with other energy terms and may be neglected in many studies. The energy advected into or out of reservoirs, however, may be significant because outflow temperatures below dams are usually very cool and

relatively stable because the depth of the normal outflow is near the bottom of the reservoir. The temperature of spills or overflows can be near the surface water temperature, depending on the geometry of the discharge structure. In reservoirs where water contents warm over time,  $T_o$  can exceed  $T_i$ . In some high-elevation reservoirs,  $T_i$  is low because melted snow is the primary water source.

Once estimates for all energy balance terms are collected, evaporation can be estimated from the relationship

$$E = 1,000 \frac{R_n - Q_t + Q_v}{\rho_w [(1 + \beta \frac{1,000}{\rho_w}) \lambda + C_w (T_s - T_b)]} \quad (6-20)$$

where  $E$  is the evaporation rate in  $\text{mm t}^{-1}$ ,  $R_n$  is net radiation in  $\text{MJ m}^{-2} \text{t}^{-1}$ ,  $Q_t$  is the rate of change in lake energy storage in  $\text{MJ m}^{-2} \text{t}^{-1}$ ,  $Q_v$  is the net energy advected into the water body per unit area in  $\text{MJ m}^{-2} \text{t}^{-1}$ ,  $\rho_w$  is the density of water in  $\text{kg m}^{-3}$ ,  $\lambda$  is the latent heat of vaporization in  $\text{MJ kg}^{-1}$ ,  $\beta$  is the Bowen ratio, and  $C_w$  is the specific heat of water in  $\text{MJ kg}^{-1} \text{C}^{-1}$ . The latent heat of vaporization can be found in standard meteorological tables ([List 1963, 1984](#)) or computed by Eq. (3-18). Note that the computation of  $E$  via Eq. (6.20) becomes unstable as the Bowen ratio approaches  $-1$ . Eq. (6-20) requires the measurement of  $\beta$ , which involves measurement of air temperature and vapor pressure at two heights above the water surface or at one height with measurement of  $T_s$  via Eq. (6-16), and it requires the measurement or estimation of  $Q_t$ , which can be large and uncertain.

## Combination Methods

For many applications a combination of the aerodynamic and energy balance procedures is desirable. The first combined equation was derived by Penman ([1948, 1956b](#)), which in its general form is written as

$$\lambda E = \frac{\Delta (R_n - Q_t) + \gamma E_a}{\Delta + \gamma} \quad (6-21)$$

where  $\lambda E$  is the latent heat of evaporation in  $\text{MJ m}^{-2} \text{t}^{-1}$ ,  $\gamma$  is the psychrometric constant in  $\text{kPa}^\circ\text{C}^{-1}$  [Eq. (3-11)],  $\Delta$  is the slope of the saturation vapor pressure curve at temperature  $T_a$  in  $\text{kPa}^\circ\text{C}^{-1}$  [Eq. (3-2)],  $(R_n - Q_t)$  is the net radiation minus the change in energy storage in  $\text{MJ m}^{-2} \text{t}^{-1}$ , and  $E_a$  is a bulk aerodynamic expression in  $\text{MJ m}^{-2} \text{t}^{-1}$  containing an empirical wind function:

$$E_a = 6.43(a_w + b_w u_z)(e_z^0 - e_z) \quad (6-22)$$

where  $a_w$  and  $b_w$  are empirical wind function coefficients, and  $u_z$  is wind speed at  $z$  height in  $\text{m s}^{-1}$ . Variable  $e_z^0$  is the saturation vapor pressure, and  $e_z$

is the actual vapor pressure at height  $z$ . The value 6.43 is for  $\lambda E$  in  $\text{MJ m}^{-2} \text{d}^{-1}$ . For  $\lambda E$  in  $\text{MJ m}^{-2} \text{h}^{-1}$ , the factor becomes 0.268. Various values for the empirical coefficients  $a_w$  and  $b_w$  have been proposed (Penman 1948; Cuenca and Nicholson 1982). Penman (1948) initially proposed  $a_w = 1.0$ , but later revised it to 0.5 for open water (Penman 1956a, 1963), and  $b_w = 0.54 \text{ s m}^{-1}$  for open water for  $z = 2 \text{ m}$  and for  $e_z^o$  computed using mean daily air temperature.

An equation similar to Eq. (6-21) results from application of the PM equation [introduced as Eq. (8-2) in Chapter 8] to water, where bulk surface resistance,  $r_s$ , in the PM equation is set equal to 0. Generally the  $z_{oh}$  roughness length parameter in the PM equation is similar in value to  $z_{om}$  or even exceeds the value for  $z_{om}$  when applied to water (Brutsaert 1982).

An important consideration in the use of combination equations (and others as well) is that the use of weather data collected at a typical weather station on land cannot be expected to give as reliable values as computations using data collected over the water surface (de Bruin 1982). For one, the wind at a height  $z$  over aerodynamically smooth water may be significantly greater than wind at height  $z$  over a typical weather station site. Temperature and humidity may also be quite different over the two sites. Further discussion of effects of surfaces on weather data is included in Chapter 11. That chapter includes suggestions for adjusting noncharacteristic humidity, temperature, and wind data according to the evaporating surface. Eq. (11-60) can be used to translate wind data measured over land to corresponding wind data representing conditions over water.

An important impediment to the use of combination equations is that the estimation of  $Q_t$  shown in Figures 6-10–6-12 and later in Figure 6-15 is a potentially large component in the calculation of available energy in the combination equation (i.e.,  $R_n - G$ ). The estimation of  $Q_t$  can have large uncertainties and should not be ignored in calculating evaporation. Many previous evaporation studies and applications have ignored this requirement, causing substantial overestimation in most cases.

## Simulation Studies

For many complex studies such as determining the effects of potential climate change or variability on lake evaporation, combining the energy balance and mass transfer procedures is necessary (Croley 1989; Hostetler and Bartlein 1990). In this type of approach, the mass or bulk transfer equations are substituted for  $\lambda E$  and  $H$  in the energy balance and solved for the water temperature  $T_s$  and the resulting energy stored in the lake  $Q_t$ . The evaporation is determined using the computed  $T_s$  in the bulk transfer equation. Depending upon the accuracy desired and the overlying assumptions, many simplifications may be employed in the procedure. Many water resource and climate-change studies apply this type of technique (Henderson-Sellers 1986; Henderson-Sellers and Davis 1989).

Because of the complexity in accounting for changes in energy storage when inflow and outflow to the water body are significant, such as reservoirs within river systems, computer models for calculating the reservoir thermal structure may be used. One such model, CE-THERM, was developed by the U.S. Army Corps of Engineers ([USACE 1995](#)). Johnson et al. ([2004](#)) describes use of the CE-THERM model to evaluate the effects of large flow releases in 1995 on the physiological rates of organisms in the Blue Mesa Reservoir located in southwest Colorado. The model was calibrated based on several daily time steps by adjusting radiation and mixing parameters during the calibration period. Turbidity, or Secchi depths, and temperature profiles were measured biweekly between May 24 and September 16 in 1994. (A Secchi disk is divided into black and white quarters to gauge water clarity by measuring the depth at which it is no longer visible from the surface.) Temperature measurements at three stations showed only minor differences in the surface layer of the stratified water body in 1995. Temperature profile measurements in front of the dam and at a midlake location in 1995 were nearly indistinguishable. Data from 1987 were used to estimate total dissolved solids (TDS). Meteorological data from the Gunnison Airport, about 25 km upstream, were used. Based on daily wind speed measurements at the airport and reservoir in 1996, wind speeds were increased by a factor of 1.7 to account for local topographic conditions.

### **6.3 EXAMPLE APPLICATIONS OF EVAPORATION ESTIMATION METHODS AND MEASUREMENTS**

In this section, results of example applications of the combination method, aerodynamic, and Bowen ratio methods are presented for a shallow lake, a deep lake, a river-reservoir system, and from a reservoir where advection of energy is small. The examples illustrate some of the techniques and considerations employed in estimating evaporation and various means for independent checks and assessment.

#### **Evaporation from a Shallow Lake**

Using daily climate data for 1996, estimates of May–October evaporation from Home Lake near Alamosa, Colorado, were made using the PM equation (M. E. Jensen, personal communication, 2006; based on data from L. Salazar as summarized in a memo from Jensen to Salazar, January 21, 1999). During that time, the depth of Home Lake varied from 0.3 to 3 m and averaged about 1.5 m. Twice-daily temperature measurements were made at the 0.05-m, 0.3-m, and 0.6-m depths at about 0800 and 1630 hours. The near-surface temperatures increased 4 to 8°C during the eight-hour

daytime period because much of the solar radiation was absorbed near the surface. Some solar radiation likely penetrated to the bottom of the shallow lake. As surface water cooled at night due to evaporation and positive net outgoing long-wave radiation, the heavier cold water settled (Carpenter 1898), thereby mixing the water in the lake. Using a regression of the 0.3-m depth temperature and air temperature, the estimated daily average temperature at 0.3 m plus 3°C was used to represent daily average surface temperature and to estimate the change in daily energy storage. The lake surface was frozen by October 29.

The estimated albedo varied from 0.06 to 0.08. Net long-wave radiation was estimated using estimated surface water temperature and Brutsaert's Eq. 6-18 (Brutsaert 1982). The variation in estimated daily energy storage change is shown in Figure 6-13 and was used to estimate  $(R_n - Q_t)$ . These values for  $Q_t$  are substantially smaller than those shown in Figure 6-10 because of the shallowness of Home Lake and somewhat rapid transfer of stored energy to the surface caused by thermally induced mixing. The resulting estimated average monthly evaporation is shown in Figure 6-14. The estimated total evaporation from May through October 1996 was 890 mm (35 in.), essentially the same as in NWS 33 (Farnsworth et al. 1982). Estimated evaporation using FAO-56  $ET_o \times 1.05$  for shallow water systems was about 5% lower than estimates based on the PM equation with specific  $(R_n - Q_t)$  for April–October with the majority of underestimation occurring during July–September.

Evaporation from shallow water bodies can be approximated by multiplying reference  $ET_o$  for short grass by a coefficient of 1.05 (Allen et al. 1998). Monthly multiplication coefficients based on  $ET_o$  from the PM

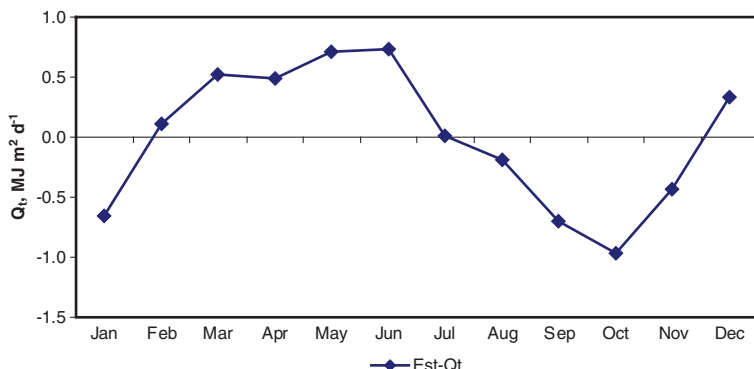


Fig. 6-13. Estimated energy storage rate for Home Lake assuming an average depth of 1.5 m

Source: Data from Jensen, personal communication, 2006

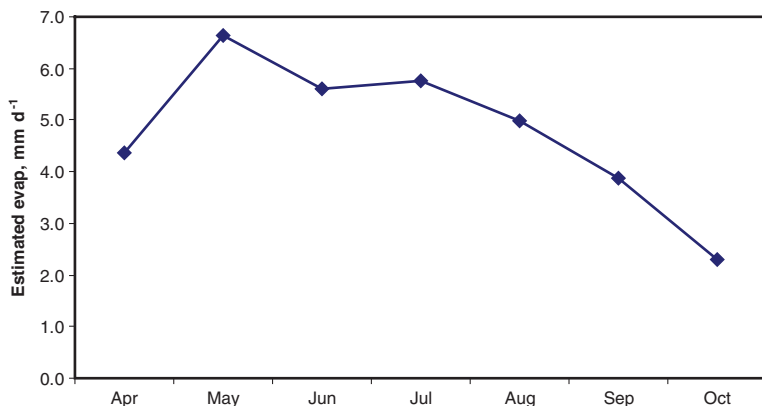


Fig. 6-14. Estimated evaporation from Home Lake near Alamosa, Colorado, in 1996

Source: Data from Jensen, personal communication, 2006

Table 6-2. Evaporation Values by Different Methods

Estimating Method	PM	Penman	NWS 33	$ET_o \times 1.05$
Estimated evaporation, mm	894	906	889	852
Estimate, percentage of PM	100	101	99	95

equation increased linearly from 1.1 in May to 1.15 in October for the high-elevation shallow lake example presented earlier in this chapter. For this example, the total May–October evaporation values by different methods were similar, indicating that any or a combination of methods would have provided reasonable values (see Table 6-2).

### Evaporation from Deep Lakes

Allander et al. (2009) estimated evaporation from Walker Lake, a somewhat deep (23-m) terminal lake in western Nevada, using a Bowen ratio energy balance approach. Results of this study highlight the large amount of energy storage that can occur in deepwater bodies. Figure 6-15 summarizes the monthly average estimated energy storage ( $Q_t$ ) and measured net radiation ( $R_n$ ) from 2005 and 2006, clearly showing that 25% to more than 40% of  $R_n$  was stored as energy during the spring and summer months due to penetrating solar radiation beneath the water surface. Figure 6-16 shows the Bowen ratio energy balance-determined mean monthly lake evaporation by Allander et al. (2009) compared with

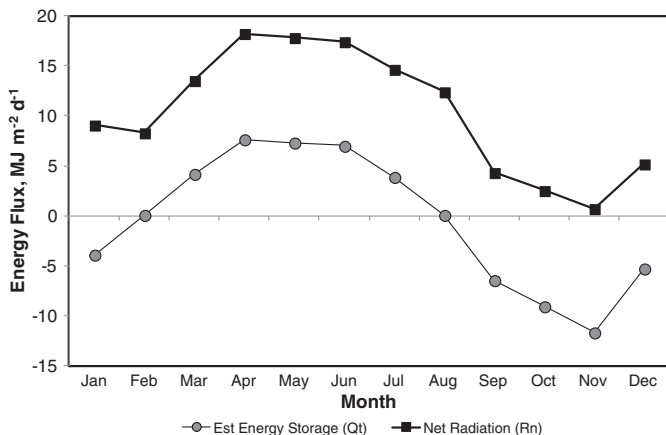


Fig. 6-15. Average monthly measured net radiation ( $R_n$ ) and estimated energy storage ( $Q_t$ ) for Walker Lake, Nevada, during 2005 and 2006  
Source: Data from Allander et al. (2009)

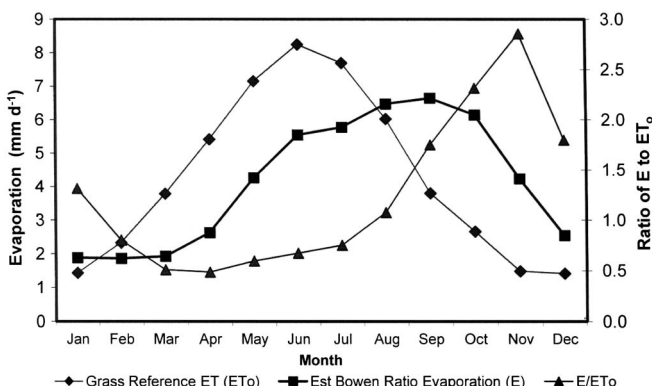


Fig. 6-16. Average monthly  $ET_o$ , estimated Bowen ratio energy balance evaporation (E), and the ratio of E to  $ET_o$  for Walker Lake, Nevada, during 2005 and 2006  
Source: Data from Allander et al. (2009); Huntington and Allen (2010)

the standardized  $ET_o$  computed using weather variables measured at the Bowen ratio station that was located on a floating platform in the center of Walker Lake. The effect of lake energy storage is evident in causing lake evaporation from the relatively deep lake to be significantly lower than the ASCE standardized grass reference ET ( $ET_o$ ) during spring and early summer and higher than the  $ET_o$  in fall and winter. The mean monthly

ratio of  $E$  to  $ET_0$  varied from less than 0.5 in the spring to more than 2.5 in the late fall due to the effect of energy storage in reducing the available energy in spring and summer when  $Q_t$  was positive and increasing available energy in the fall and winter when  $Q_t$  was negative (Huntington and Allen 2010).

Trask (2007) applied three Dalton mass transfer formulations using measured air temperature, lake surface temperature, and regional atmospheric Mesoscale Model (MM5) simulated monthly dew point temperature and wind speed to estimate monthly evaporation from Lake Tahoe, California and Nevada, over the period 1968–2000. The three methods included the Harbeck, Ryan, and Adams methods (Harbeck 1962; Ryan et al. 1974; Adams et al. 1990). Results indicate that energy storage in Lake Tahoe, which occurs primarily from penetrating solar radiation, significantly affects the timing of evaporation such that the peak evaporation occurs during August through November (Figure 6-17), unlike pan evaporation measurements made in Tahoe City, which report peak rates occurring from June through August. Lake Tahoe is known for its clarity (ranging from 20–30 m) and its depth (maximum of 500 m). Even though Lake Tahoe is significantly deeper than Walker Lake, seasonal evaporation results for Lake Tahoe are similar to Walker Lake due to thermal stratification that occurs in Lake Tahoe, where a strong thermocline develops in

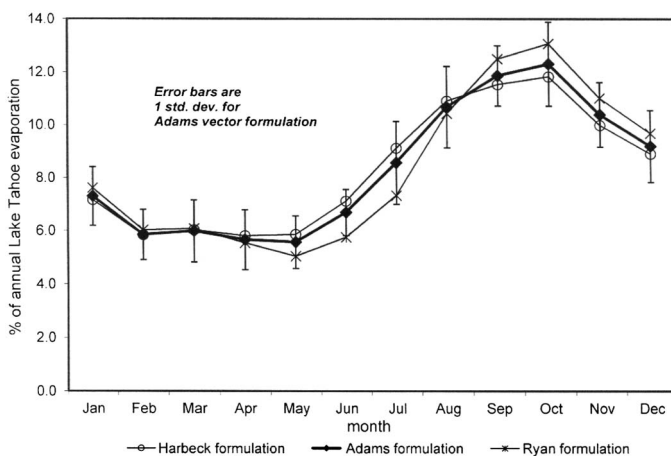


Fig. 6-17. Percent of average monthly annual evaporation from Lake Tahoe of 0.9 m, 0.97 m, and 1.24 m per year computed using three Dalton mass transfer formulations of Harbeck, Adams, and Ryan, respectively. See Trask (2007) for details on mass transfer applications and uncertainty estimates for Lake Tahoe. Source: Data from Trask (2007)

June that ranges from 21 to 32 m deep from August to October, respectively (Coats et al. 2006).

### Evaporation from a River-Reservoir System

There are four subbreaches of the Colorado River from Hoover Dam to Morelos Dam at the United States-Mexico border. The first is from Hoover Dam to Davis Dam, the second from Davis Dam to Parker Dam, the third from Parker Dam to Imperial Dam, and the fourth from Imperial Dam to Morelos Dam. Because of the immense size of Lake Mead, water is released from Hoover Dam at a nearly constant temperature of about 12–15°C. The average rates of flow vary greatly during the year from about  $180 \text{ m}^3 \text{s}^{-1}$  in January and February to about  $470 \text{ m}^3 \text{s}^{-1}$  in May. Water is exported to Arizona and Los Angeles from above Parker Dam and to the Imperial Valley from above Imperial Dam.

There are two reservoirs in this section of the river, Mohave Reservoir above Davis Dam and Lake Havasu above Parker Dam. Below Davis Dam the water temperature varies from about 11°C in January to about 19°C in July and August. Below Parker Dam the water temperature varies from about 11°C in December–January to about 25°C in August. Above Morelos Dam, the water temperature varies from about 13°C in December to about 31°C in August. The increases in water temperature in each subreach represent the net radiation absorbed by water surfaces and is energy that is not immediately available for evaporation. The increase in water temperature leaving a subreach compared with inflow temperature represents the advection of energy out of each subreach.

In addition to estimating surface water temperature in a reservoir from limnology data, advected energy must be considered. The resulting estimated average depth of evaporation (calculated using several automated weather stations along the river and the PM equation) increased from the Davis-Parker subreach to the Imperial-Morelos subreach as shown in Figure 6-18. The average annual evaporation for 1999–2001 was estimated to be 1,640; 1,750; and 1,920 mm (64.4, 69.0, and 75.4 in.) for the Davis-Parker, Parker-Imperial, and Imperial-Morelos subreaches, respectively. Limited weather data were available for the Hoover-Davis subreach. Limnology studies show that a thermal profile exists in the reservoirs for much of the summer season even with the relatively large river flows. Mixing during the summer appears to occur only near the entry points to the reservoirs, as the cold, higher density water inflows appear to plunge below the thermal layer. Complete mixing within the reservoirs does not occur until October–November. The changes in thermal profiles represent a significant component of the total change in energy storage in addition to very large changes due to horizontal advection because of the large flows. Therefore the value for  $Q_v$  for the reservoirs is negative.

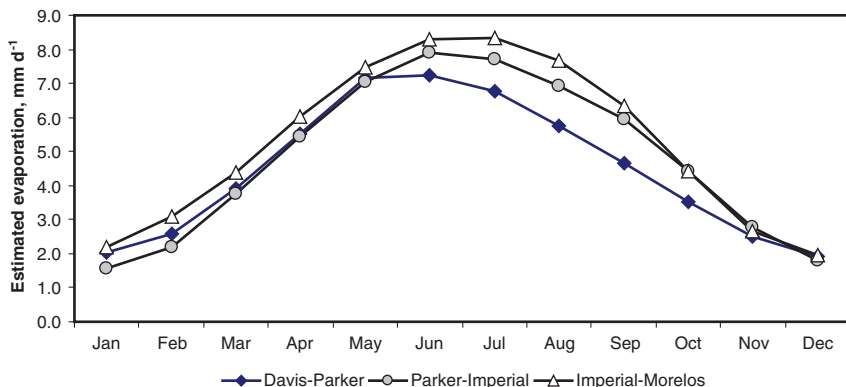


Fig. 6-18. Estimated evaporation from river and water surfaces of the Colorado River from Davis Dam to Morelos Dam for the period 1999–2001  
Source: Data from Jensen (2003)

### Evaporation from Reservoirs

Estimates of evaporation from a reservoir or lake where advection of energy is relatively small require estimates of surface water temperature, the rate of energy flow into the body of water in the form of solar radiation, and the water temperature increase as illustrated in Figures 6-8 and 6-9. In an example application to Lake Berryessa Reservoir by Jensen et al. (2005), the change in daily energy storage was estimated using a slight modification of Eq. (6-14a, b), calibrated by measured changes in energy storage between several temperature profile determinations to a depth of 25 m and changes recorded by thermographs located near the dam with sensors at several depths. The equations for  $Q_t$  were  $Q_t = 0.55 R_{sn} - 1.20 R_{nl}$  for day of year <180 and  $Q_t = 0.50 R_{sn} - 1.50 R_{nl}$  for day of year  $\geq 180$ . These relationships differ somewhat from Eq. (6-14a, b) and are specific to Lake Berryessa. The reservoir surface area is 8,320 ha when full at an elevation of 137 m and 4,060 ha at an elevation of 110 m. Surface water temperature was estimated using measurements by a thermograph sensor at the 0.15-m depth. Those measurements were lower than skin temperature during daytime and higher during night. However, 24-hour averages were probably within 1°C. Surface temperature was used only to estimate  $R_{nl}$ . Inflow to the reservoir occurs during the November–February rainy period. Water release temperature at the dam was essentially constant at about 9°C all year, resulting in a small advection of energy during the summer months (Jensen et al. 2005).

Estimated annual depths of evaporation in mm using the PM, Priestley-Taylor (P-T), and Penman equations are compared in the following with estimates by reservoir operations using an evaporation pan and pan

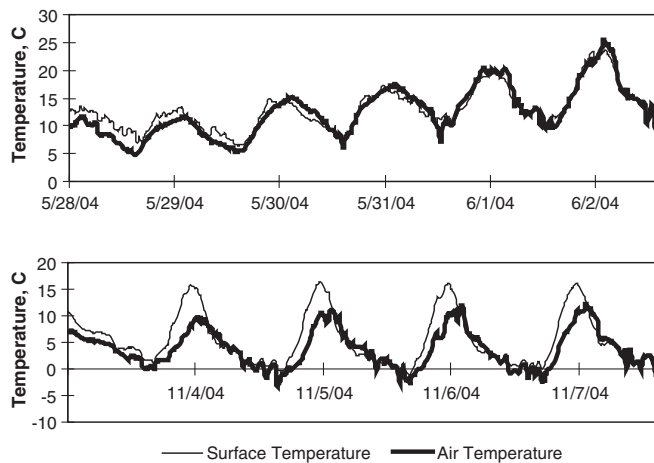
coefficients developed shortly after the reservoir was completed. The PM estimates were reduced by 5% because of the uncertainty associated with humidity and wind speed measurements made over land at a site adjacent to the reservoir and some shading of the water surface in several narrow segments of the reservoir. The results indicate that estimates based on pan evaporation data from an improper pan site and original pan coefficients are about 72% of those of PM. The same energy storage estimates were used for PM, P-T, and Penman equations. The average estimates from 2003 to 2005 were 1,326 mm (PM); 1,278 mm (P-T); 1,424 mm (Penman); and 955 mm (pan evaporation  $\times$  pan coefficient).

The main reason for the lower pan  $\times$  coefficient – based estimates was the use of pan evaporation measured by reservoir operators in an area that was shaded part of the day by topography and surrounded by equipment and trees that obstructed wind movement. The measured pan evaporation was much lower than pan evaporation measured in a similar Class A pan located in an open area downwind from the reservoir. This outcome emphasizes the importance of evaporation pan location in providing consistent and standardized measurements. Penman equation estimates were higher than PM estimates mainly because the wind speed coefficient is the same as Penman (1956) derives for a rougher grass surface and not for a water surface.

Pan evaporation at the original pan site was about 70% of that at the new pan site downwind from the reservoir. Using pan evaporation at the new site and the recommended monthly pan coefficients for this site, the average 2003–2005 estimated annual evaporation for the reservoir was 1,420 mm. The new recommended monthly pan coefficients were based on PM estimates of evaporation.

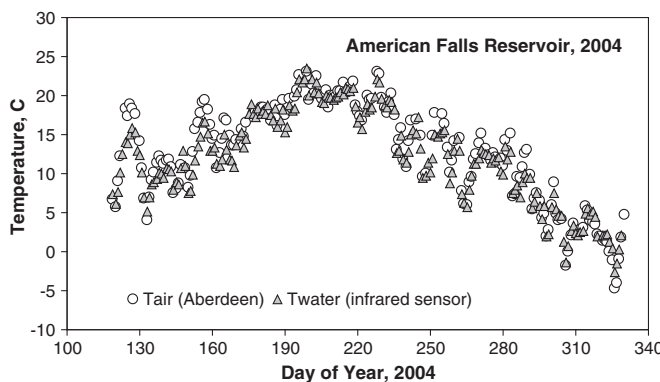
The close coupling of surface temperature of many water bodies to the atmosphere provides the possibility for applying the direct aerodynamic method [Eq. (6-7)] using only measured air temperature. Figure 6-19 shows 15-min averages of water surface temperature and corresponding air temperature at 3 m for American Falls Reservoir in southern Idaho during 2004. The two temperatures were closely coupled with regard to time and magnitude during the late May–early June period shown in the top of the figure when the water body was warming. Air temperature lagged  $T_s$  in both time and magnitude in early November when the water body was cooling. The close coupling is primarily caused by the strong relationship between outgoing and incoming thermal radiation terms. These two long-wave radiation components have magnitudes of 300 to 450  $\text{W m}^{-2}$  (25 to 40  $\text{MJ m}^{-2} \text{d}^{-1}$ ) as compared with  $\lambda E$  and  $H$ , which averaged only about 20 to 100  $\text{W m}^{-2}$  (2 to 10  $\text{MJ m}^{-2} \text{d}^{-1}$ ) over 24-h periods. Hence, the water surface and atmosphere become closely coupled via radiation exchange.

Figure 6-20 shows daily mean surface and air temperature on the same water body. The close coupling permitted the estimation of daily mean  $T_s$



*Fig. 6-19. Fifteen-min water surface temperature of American Falls Reservoir measured by infrared thermometer and air temperature at 3 m during two periods in 2004*

Source: Data from Allen and Tasumi (2005)



*Fig. 6-20. Daily average water surface temperature of American Falls Reservoir measured by infrared thermometer and mean daily air temperature at 3 m during 2004*

Source: Data from Allen and Tasumi (2005)

from  $T$  for application of the direct aerodynamic method [Eq. (6-7)] on a daily time step, where saturation specific humidity at the surface  $q_s$  was estimated using estimated  $T_s$ , and specific humidity of the air at 3 m,  $q_z$ , was calculated from measured actual vapor pressure. The value for  $q_z$  was

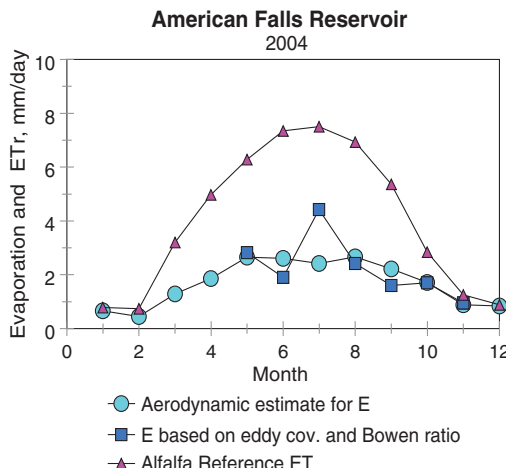


Fig. 6-21. Estimated monthly evaporation from American Falls Reservoir using the direct aerodynamic method [Eq. (6-7)] and an eddy covariance–Bowen ratio combination method by Allen and Tasumi (2005). Also plotted is alfalfa reference  $ET_r$

approximately  $q_z = (RH/100) (q_s)$ . The value for  $T_s$  was approximated as  $T_s = T - b_t$  where  $b_t$  was an offset varied by month. Values for  $b_t$  varied from 0°C during spring and summer to 4°C during winter. A value for  $C_E = 0.0015$ , equivalent to  $z_{ov} \sim z_{om} = 0.00005$  m, was found to best fit evaporation measured by a combination of eddy covariance and Bowen ratio methods. Average monthly estimates for  $E$  are shown in Figure 6-21 where they are compared against the eddy covariance–Bowen ratio-based estimates described previously. Also shown in the figure is mean monthly reference evapotranspiration for the standardized alfalfa reference method. The estimated evaporation from the approximately 9-m deep reservoir was substantially less than the alfalfa reference due to the large positive value for  $Q_f$ . The river temperature entering American Falls Reservoir (not measured) is relatively cold, especially during spring and early summer due to mountain snowmelt. The reservoir outflow is remarkably similar to surface temperature and air temperature all season long.

#### 6.4 SUMMARY OF METHODS FOR ESTIMATING EVAPORATION FROM WATER BODIES

Evaporation is rarely measured directly, even for small water bodies. It is usually estimated by association with measured evaporation from evaporation pans or calculated by water balance, energy balance, mass

transfer, or a combination of energy balance and aerodynamic techniques. The method selected depends on the depth of the water body and the availability of weather data or micrometeorological equipment.

### Small Water Bodies

For small water bodies such as shallow lakes, the most widely used method is to multiply monthly coefficients by measured pan evaporation. The most commonly used pan in the United States is the Weather Service Class A pan. The accuracy of this method relates to the environment surrounding the pan, as illustrated in Figure 6-2, and the pan coefficient. Monthly pan coefficients can be obtained from Map 4 for May–October in Farnsworth et al. (1982) or estimated using procedures outlined by Kohler et al. (1955). However, estimates based on Class A pans can be uncertain and biased. Evaporation estimates for some states may be available, such as that by Borrelli et al. (1998) for Texas. Local or regional calibration or verification of the coefficients used is recommended, and caution is needed to account for poor pan siting.

Evaporation from a shallow water body can be estimated using a combination method following procedures similar to those described for a shallow lake or the Penman equation (Penman 1956b, 1963) with wind speed coefficients of  $a_w = 0.5$  and  $b_w = 0.54$  for wind speed in  $\text{m s}^{-1}$  measured at about 2 m above the water surface and saturation vapor pressure based on mean air temperature. Attention must be given to the estimation of energy storage,  $Q_t$ , although heat storage is relatively smaller for shallow water bodies than for deep bodies.

Consideration should be given to employment of aerodynamic (mass transfer) methods, especially in situations where relationships between land-based air temperature and water surface temperature can be established.

### Large Water Bodies

For water bodies greater than 2–3 m in depth, the increase in energy storage early in the season and release later in the season must be considered. If pan evaporation methodology is used, pan coefficients at latitudes of about 35° N can be expected to vary similarly to those for Lake Elsinore as shown in Figure 6-1. A check of estimated average rate of energy storage can be conducted using periodic temperature profile measurements made from the surface to the bottom of the lake or reservoir or at least to a depth of about 30 m for clear water. Several profile measurements, beginning when daily solar radiation begins to increase or when ice on frozen water bodies has melted, should be made at 2–3 week intervals near the center of the lake or reservoir to calculate the average daily change in energy storage. Commercial equipment can be

obtained by simultaneously measuring depth and temperature. More measurements should be made at shallow depths where more rapid temperature change occurs. Profile measurements can cease when complete mixing occurs late in the season.

Other techniques such as a combination of eddy covariance and Bowen ratio methodology can be used to periodically measure changes in energy storage as illustrated in Figure 6-12 (Allen and Tasumi 2005). Periodic measurements of the rate of change in energy storage during the year can be used to estimate the average rates for a given lake or reservoir.

In some cases where inflow and outflow components can be measured and net advection is small, water budget procedures can be used to estimate mean monthly evaporation [Eq. (6-2)]. For large water bodies, mass transfer procedures can be used [Eqs. (6-7) and (6-9)]. This usually requires measurement of wind speed and air humidity over the water and surface water temperature. Mean air temperature may act as a surrogate for surface water temperature.

For instream reservoirs, net advected energy must be considered when using an energy budget or combination method to estimate evaporation [Eq. (6-21)]. Energy advected by evaporating water [Eqs. (6-18) and (6-19)] is usually small and may generally be neglected. The net energy advected can be large if inflows to a reservoir are warm and the outflow temperatures are low, which is common because release locations through the dam are usually near the bottom of the reservoir. The temperature of reservoir overflows or spills may be at the average water temperature near the surface.

This page intentionally left blank

## **PART 2**

# **EVAPOTRANSPIRATION FROM LAND SURFACES**

This page intentionally left blank

# CHAPTER 7

## WATER AND ENERGY BALANCE COMPONENTS FOR MEASUREMENT AND ESTIMATION

### 7.1 INTRODUCTION TO CHAPTERS 7–12

Chapters 7–12 describe estimation and measurement methods for vegetation and soil surfaces that are somewhat uniform and, in the case of vegetation, have an adequate supply of soil water. Extensions are made to natural vegetation and to vegetation that may be short of water. The methods are summarized and extended from FAO 24 ([Doorenbos and Pruitt 1977](#)), FAO-56 ([Allen et al. 1998](#)), the ASCE *Hydrology Handbook* ([Wootton et al. 1996](#)), the ASCE-EWRI report on standardization of reference ET calculation ([ASCE 2005](#)), and from ASCE 70 ([Jensen et al. 1990](#)). These chapters describe procedures for measuring ET and methods for estimating ET using aerodynamic and energy balance procedures, the combination equation, and association or inference methods. The combination equation is presented in Chapters [8](#) and [11](#) and is applied both directly and as part of the reference ET-crop coefficient approach.

When estimating ET in areas where precipitation is greater than the potential ET rate for vegetative cover ( $ET_c$ ), or where full irrigation is practiced, ET can be estimated using the reference ET concept and crop coefficients, or by direct application of the Penman-Monteith (PM) or some other resistance-based method using well-watered surface resistances ( $r_s$ ). However, when precipitation is less than  $ET_c$  for extended time periods, actual evapotranspiration ( $ET_a$ ) usually falls below the potential ET for the particular surface and  $ET_c$  becomes more difficult to estimate accurately.

Incorporating soil water balance is usually required to estimate ET when precipitation and irrigation are less than  $ET_c$ . Two methods are discussed in Chapters [8](#) and [11](#) that can be used to reduce the ET estimate

according to available soil water. One method applies the  $K_c \times ET_{ref}$  or crop coefficient approach. The other applies the direct application of the PM method or a combined set of energy balance and aerodynamic equations.

Other approaches to estimating ET from land surfaces during water shortage include making direct measurements of ET. This chapter describes various ET measurement approaches. The challenge with these approaches is in extrapolating point or localized measurements to large spatial scales and in extrapolating measurements to other time periods. ET measurement can be difficult and time consuming and is therefore generally used to develop and calibrate weather-based ET estimation methods that are then applied to larger scales and to different time periods. In addition to point measurements, methods employing energy balance based on satellite imagery can be applied successfully to estimate actual ET over large areas. This is a relatively new area of practice that is under substantial development.

## 7.2 VOLUMETRIC MEASUREMENTS FOR ESTIMATING LAND SURFACE ET

All ET-estimating methods provide only estimates of the average actual ET from a field, watershed, or region under consideration. As might be expected, the larger and more diverse the area, the more uncertain the estimate.

Fortunately, the evaporation process is largely controlled by solar radiation (or more directly, net radiation). Therefore, the variation of ET within areas of uniform vegetation and uniform access to water will be rather minor except for advective edge effects. Spatially uniform ET is normally the case for some time following extensive precipitation in an area with uniform vegetation or following irrigation of a farm field. Under limited water supply, variability will increase as soil water depletes in areas receiving less than the average water stored in a region. The uniformity of precipitation or water applied by irrigation is also a factor. The problem becomes difficult when the areas under consideration, e.g., watersheds or regions, involve a wide variety of vegetation species, vegetation heights, aerodynamic roughness, leaf development, rooting depth, soil type, and differing responses to soil water levels and weather conditions.

### Soil Water Balance

Chapter 3 describes the soil-plant-atmosphere (SPA) system. Soil water balance as applied to watersheds usually involves estimating water runoff

where one of the components estimated independently is the ET. For small watersheds where interbasin groundwater flow is highly restricted and runoff can be measured, ET can be determined from the hydrologic balance if watershed precipitation is known. In recent years this approach has been vital in developing water and salt balance data for large basins, especially in relation to irrigation projects. An example is the water balance evaluation of the large Imperial Valley in California (Oster et al. 1984; Allen et al. 2005a).

The basic soil water balance equation for a study volume (i.e., a defined area having depth  $z_s$ , thus constituting a volume) for a specific time period,  $\Delta t$ , can be written as

$$\Delta\theta z_s = P - Q_r + I - ET_a - DP + GW \quad (7-1)$$

where  $\Delta\theta$  is the change in mean water content of the soil profile ( $m^3 m^{-3}$ ),  $z_s$  is the depth of the soil profile monitored (mm),  $P$  is total depth of precipitation plus any surface inflow from outside the study volume (mm),  $Q_r$  is the depth of surface runoff leaving the study area (mm),  $I$  is gross irrigation depth infiltrated over the area (mm),  $ET_a$  is actual evapotranspiration (mm),  $DP$  is the depth of percolation below depth  $z_s$  (mm), and  $GW$  is depth of groundwater that has moved upward or a net depth that has entered horizontally into the profile (mm). Generally, the depth of soil profile of interest ( $z_s$ ) is the plant root zone, which, by definition, is the upper portion of the soil where water extraction by plant roots occurs. In this case,  $GW$  and  $DP$  in Eq. (7-1) are the sum of flux densities into and out of the bottom or sides of the root zone for the specific time period.

$\Delta\theta$  can be defined as

$$\Delta\theta = -\frac{\int_0^{z_s} \theta_{1(z)} dz - \int_0^{z_s} \theta_{2(z)} dz}{z_s} \quad (7-2)$$

where  $\theta_{1(z)}$  is volumetric water content at depth  $z(m^3 m^{-3})$  at time  $t=1$ ,  $\theta_{2(z)}$  is volumetric water content at depth  $z(m^3 m^{-3})$  at time  $t=2$ , and  $z_s$  is the effective depth of the root zone (mm). Eq. (7-1) can be rearranged in terms of Eq. (7-2) to estimate total soil water in the root zone or at greater depths, if of interest, as

$$\int_0^{z_r} \theta_{2(z)} dz = \int_0^{z_r} \theta_{1(z)} dz + \Delta\theta z_r = \int_0^{z_r} \theta_{1(z)} dz + P - Q_r - ET_a - DP + GW \quad (7-3)$$

Reduction of  $ET_a$  below potential levels due to soil water deficiency is discussed later.

Generally, deep percolation flux density is estimated based on the field capacity ( $\theta_{fc}$ ) of the soil (also known as the drained upper limit).

$\theta_{fc}$  represents the water content to which the soil will drain under a unit hydraulic gradient (gravity) two to three days after wetting.  $\theta_{fc}$  represents the upper limit of the soil's ability to retain water after initial rapid drainage. Average values and ranges of  $\theta_{fc}$  are given in Table 3-6 for general soil texture classes along with values for the permanent wilting point ( $\theta_{wp}$ ) for the soil (also known as the lower limit of extractable water) and total retained water available for plant extraction (available water, AW). Available water is calculated as  $AW = \theta_{fc} - \theta_{wp}$ . One item to note from the data in Table 3-6 is that even though values for  $\theta_{fc}$  and  $\theta_{wp}$  vary widely with soil texture, values for available water vary less, especially for moderately coarse to fine-textured soils. When possible, specific values for  $\theta_{fc}$  and  $\theta_{wp}$  should be determined from field studies (Ratliff et al. 1983).

When the calculation time step for Eq. (7-3) is one day,  $DP$  is often assumed to occur if total  $\theta$  of the root zone is greater than  $\theta_{fc}$  on any day. In this case,

$$\text{If } \int_0^{z_s} \theta_{2(z)} dz > \theta_{fc} z_s$$

$$\text{then } DP = \int_0^{z_s} \theta_{2(z)} dz - \theta_{fc} z_s \quad (7-4)$$

and  $\theta_{2(z)} = \theta_{fc}$  over 0 to  $z_s$   
otherwise,  $DP = 0$

One may wish to delay application of Eq. (7-4) until two days after a major precipitation or irrigation event to account for some ET extracted from water above  $\theta_{fc}$  during the first two days while the soil profile is draining to field capacity. In application of Eq. (7-4) to layered soils with different water-holding characteristics, the  $\theta_{fc} z_s$  term can be replaced with an integral that integrates  $\theta_{fc}$  over the 0 to  $z_s$  depth, where  $\theta_{fc}$  may vary with  $z$ .

Generally, when solving the soil water balance equation for ET, one should sample  $\theta$  to depths well below the root zone and attempt to schedule irrigation to avoid the occurrence of  $DP$ . If no change occurs in soil water at lower depths between sampling dates, this does not ensure that drainage is not occurring because drainage can take place under a unit hydraulic gradient with no apparent change in soil water content. Generally, periods with little or no precipitation are selected for evaluation. Occasionally sharp changes in soil texture, such as a sand or gravel layer below the root zone, or the presence of bedrock, can reduce the rate of deep percolation and improve measurement accuracy.

One should avoid situations where saturated conditions (i.e., a water table) exist near the root zone. In the absence of a shallow water table ( $GW = 0$ ) and with adequate sampling depth, a record of soil water change over a period of 7–10 days or more can yield reliable measurements of ET at the measurement site.

The careful use of a neutron moisture meter (also referred to as a neutron probe) can, in some cases, provide relatively accurate data. When calibrated with gravimetric sampling, it can provide data of adequate accuracy for ET studies or for irrigation scheduling programs. The difficulty with either of these procedures (neutron moisture meter and gravimetric sampling) is in estimating the water flux density ( $DP$  or  $GW$ ) at the bottom of the measured profile. Often this difficulty limits the usefulness of applying the soil water balance equation to determine ET. Information on applying the neutron probe technique and relative error associated with the method is provided by Evett and Steiner (1995), Hignett and Evett (2002), and Evett et al. (2003, 2005). In addition, a suite of eight papers on accuracy of neutron probe operation and calibration is included in Allen (1993).

Usually soil water measurements are made at discrete depth increments, e.g., every 0.15 m. Total soil water in the profile can be estimated from discrete measurements as

$$\int_0^{z_s} \theta_z dz = \sum_{i=1}^n d_i \theta_i \quad (7-5)$$

where  $\theta_i$  is the volumetric soil water content representing layer  $i$  ( $m^3 m^{-3}$ ),  $d_i$  is the thickness of layer  $i$  (mm), and  $n$  is the total number of layers measured between 0 and  $z_s$ . Water content for the surface soil layer usually requires use of gravimetric or electronic measurement such as time domain reflectometry (TDR) due to problems of escaping neutrons from the surface when using the neutron probe method within 0.2 m or possibly 0.3 m of the surface (Evett and Steiner 1995). Using smaller depth increments for measurement within the top 0.15 to 0.20 m from the surface may provide more accurate estimation of total soil water content of the root zone due to the frequently rapidly changing  $\theta_z$  with depth in that zone.

General practices to reduce the variability encountered with periodic soil water measurements for determining ET include

1. Use a minimum time step of about seven days for estimating ET with the soil water balance equation so that the magnitude of estimated ET is significantly greater than random errors associated with measurements of water content.
2. For gravimetric sampling, mark the site of the first samples taken after an irrigation or heavy rain and take the next set of samples

within a 0.3-m radius to minimize variability caused by spatial differences in soil characteristics, root distribution, and water infiltration.

3. Obtaining soil samples or taking sensor readings and installing sensors or access tubes without significantly altering the plant cover condition at the sampling site are essential. ET from trampled plants can be drastically reduced as compared with ET by plants in pristine condition. Figure 7-1 illustrates means to suspend the observer over vegetation while taking neutron probe readings to avoid any foot traffic within 1 m of the access tube. Besides damaging vegetation, foot traffic can alter density, aeration, and infiltration characteristics of the surface soil, thereby affecting plant growth and ET.
4. Calculate ET for each set of measurements made for time periods between irrigations to screen for errors and to gain an understanding of measurement error and uncertainty.
5. Avoid periods following heavy rain, as deep percolation may continue to occur following the initial sampling date for the period. This can introduce error with shallow-rooted crops in particular.

**Example Gravimetric Data** Table 7-1 gives an example of results from Pruitt (1955) for a 6.5-day period when  $ET_a$  for a dense crop of ladino clover was estimated from a well-replicated (18 sites within a 0.2-ha plot) gravimetric soil sampling study. Even with near ideal soil and underlying conditions (sampling was from the surface to bedrock), the standard deviation (based on the 18 sampling sites) of estimated ET determined



*Fig. 7-1. Taking a neutron probe reading using a light, above-crop platform to avoid trampling of vegetation and compaction of soil near the access tube site*  
Source: Photo from R. G. Allen, personal communication, 1992

Table 7-1. An Example of a Gravimetric Soil Sampling Program  
to Determine ET, Washington State University Irrigation  
Experiment Station, Prosser, WA

Sampling Site	Sampling Depth, $z_s$ (m)	June 4		June 10		Difference 6/4–6/10
		$\theta$ (%)	$\theta z_s$ (mm)	$\theta$ (%)	$\theta z_s$ (mm)	
1	1.16	12.9	205	8.5	135	70
2	1.18	15.8	256	12.2	198	58
3	1.31	15.2	274	12.1	218	56
4	1.18	15.3	248	11.0	178	70
5	1.19	14.6	237	11.0	179	58
6	1.20	15.5	255	11.6	191	64
7	1.15	14.8	233	11.1	175	58
8	1.19	16.7	272	12.5	203	68
9	1.22	16.2	270	12.3	205	65
10	1.08	17.0	250	12.3	181	69
11	1.09	17.9	268	11.8	177	91
12	1.11	17.0	259	12.7	194	66
13	1.03	17.3	243	12.6	177	66
14	1.02	18.7	262	12.8	179	83
15	1.02	19.8	276	15.2	212	64
16	0.99	14.1	191	9.2	124	67
17	1.00	15.1	208	9.4	129	78
18	1.01	16.3	226	11.9	165	61
Avg.			246		179	67
				Std. Dev.	8.75	
				100 × (8.75)/67) =		13.0%

Source: Data from Pruitt (1955)

from each single measurement point was 13% of the mean ET determined by averaging depletions over all 18 sites over the 6.5-day period. In contrast, the standard error of the mean ET resulting from utilizing all 18 sites was only 3.1% of the mean ( $13/18^{0.5} = 3.1\%$ ). This demonstrates the substantial value of multiple sample locations when estimating ET from soil water depletion measurements. The range in estimated ET between the high and low measurement sites was more than 50%. One might expect a lower standard deviation using a neutron probe at the same number of neutron access sites. However, at this particular site, the variation in the depth of this relatively shallow soil (0.99–1.31 m) and the problem of

interpreting both the uppermost and lowest layer readings might have presented more of a problem with overall accuracy than that experienced with the gravimetric technique.

**Other Soil Water Measurement Methods** Tensiometers, soil water electrical resistance blocks, and heat dissipation electronic sensors can be valuable tools in computing a soil water balance. These devices measure matrix potential (or soil water tension) and can provide a means of following volumetric water content changes when soil water characteristic curves are available. Campbell and Campbell (1982), Evett and Parkin (2005), and Evett et al. (2006) provide in-depth discussions of some of these methods. Bertuzzi et al. (1994) present a detailed analysis of various sampling strategies for estimating ET.

Time domain reflectometry (TDR), time domain transmission (TDT), and capacitance-based sensors and probes are commonly used for measuring soil water content indirectly. Advantages of these electronic sensors are in situ measurements with nearly continuous measurement. Disadvantages and challenges with capacitance-based sensors include the typically small volumes of soil sampled (on the order of 1 cm extent from the sensor as compared with 10 cm for neutron probes) and the possible need to calibrate sensors for soil type. The small volume of soil sampled makes the influence of air gaps around the sensor and lack of contact between sensor and soil problematic (Evett and Steiner 1995; Evett and Parkin 2005; Evett et al. 2006).

**Precipitation Measurement** Other biases in estimating ET from soil water balances stem from inaccuracies in measuring precipitation and irrigation additions or using data that are not representative for the sites. Precipitation gauges should be located within a few hundred meters of the sampled area because precipitation can vary widely even over a few km. In addition to biases in spatial variation, precipitation amounts are often undermeasured by gauges for both rain and snow amounts due to Venturi effects, blowout, splash-out, and evaporation. Data should be corrected using wind functions such as those recommended by the World Meteorological Organization (Yang et al. 1998b). That publication recommends a correction to liquid precipitation catch by a standard U.S. National Weather Service 8-in. (203-mm) gauge of

$$P_{\text{corrected}} = P_{\text{gauge}} [\exp(0.062 u_g^{0.58})] \quad (7-6)$$

where  $u_g$  is wind speed at gauge height in  $\text{ms}^{-1}$ ,  $P_{\text{corrected}}$  is the corrected precipitation, and  $P_{\text{gauge}}$  is the original measurement, in the same units. The correction increases the estimated capture of  $P$  by 8% for wind speed of  $2 \text{ ms}^{-1}$  and by 13% when wind speed is  $4 \text{ ms}^{-1}$ . A stronger correction was

recommended by Yang et al. (1998b) for snow. Yang et al. (1998a, 1999) found needed corrections to U.S. National Weather Service (NWS) 203-mm standard gauges at 10 NWS climate stations in Alaska and to Hellmann gauge-measured precipitation at 12 stations in Greenland to range from 30 to 400 mm per year in Alaska and from 8 to 70 mm per year in Greenland for low rainfall areas. The German-style Hellmann gauge is similar to the NWS standard gauge. Of the biases, wind-induced undercatch was the source of greatest error, followed by gauge wetting loss, and nonrecording of trace amounts of precipitation. Monthly correction factors differed by station and by type of precipitation (liquid vs. solid). The value for  $u_g$  in Eq. (7-6) can be estimated from wind speed measured at a reference height above the surface using a logarithmic transformation, for example as given in Eqs. (6-5) or (11-60).

In addition to wind-induced effects, all tipping bucket rain gauges can lose, on average, one-half tip equivalent of rain between wetting events through evaporation from the untipped bucket. Also, tipping gauges do not record precipitation received during part of the time interval in which the tip occurs. This error is fairly insignificant except during high precipitation rates.

Typical problems associated with estimating ET by soil water sampling and advantages, disadvantages, and requirements are summarized in Table 7-2.

### 7.3 MASS BALANCE METHODS

Mass balance involves measuring the change in mass caused by evaporation or evapotranspiration and determining the E or ET rate or volume as a residual of a balance. This method can be extremely accurate if all components other than E or ET are measured accurately. However, often some components cannot be measured due to their diffusive or distributed nature.

#### Tanks and Lysimeters

Highly sensitive weighing or floating lysimeters are the best absolute method for accurately measuring water loss from soil and crop canopy surfaces. The use of lysimeters has been very important in the development and testing of the more theoretical micrometeorological methods for estimating ET. The water evaporated from even very simple lysimeters may be accurately determined over 24-hour or longer periods. Weighing lysimeters have played an important role in providing accurate half-hourly or hourly ET data. An example of a 2-m weighing lysimeter during installation is shown in Figure 7-2. Weighing lysimeter designs

Table 7-2. Summary of Advantages, Disadvantages, and Requirements Associated with Estimating ET Using Soil Water Balance, Lysimetry, Bowen Ratio, and Eddy Covariance Methods

Method	Characteristics
<b>Soil Water Sampling and Balances</b>	<p><b>Advantages</b></p> <ul style="list-style-type: none"> <li>• Ability to obtain samples from multiple sites;</li> <li>• Potentially low costs, depending on equipment and labor; and</li> <li>• Direct measurement of depletions.</li> </ul> <p><b>Potential Problems</b></p> <ul style="list-style-type: none"> <li>• Horizontal and vertical variability of bulk density and water-holding characteristics of the soil;</li> <li>• Inaccuracies in measuring precipitation and irrigation additions or unrepresentative data;</li> <li>• Possible deep percolation losses or gains by capillary rise;</li> <li>• Potential need for calibration of sensors for soil type;</li> <li>• For some vegetation types, difficulty in obtaining samples or taking readings (or installing access tubes or sensors) without significantly altering the plant cover and soil surface conditions at the sampling site; ET from trampled plants can be drastically reduced as compared with ET by plants in pristine condition (see Fig. 7-1);</li> <li>• Potential for foot or equipment traffic to alter the density, aeration, and infiltration characteristics of the surface soil; if water intake and/or aeration at and near the sampling site differs from general field areas, then plant growth is likely affected, thus reducing soil water extraction and leading to estimated ET unrepresentative of the field ET;</li> <li>• Nonuniformity of irrigation systems (e.g., differential spatial wetting of soil due to spatial variation in irrigation applications, for example, with drip or microsprinkler systems or even with some furrow systems) making accurate measurement of changes in soil water content difficult and laborious; and</li> <li>• Differential spatial extraction of soil water due to spatial variation in root systems, for example, with orchard and vine crops.</li> </ul>

Table 7-2. Summary of Advantages, Disadvantages, and Requirements Associated with Estimating ET Using Soil Water Balance, Lysimetry, Bowen Ratio, and Eddy Covariance Methods (*Continued*)

Method	Characteristics
Lysimetry	<p><b>Advantages</b></p> <ul style="list-style-type: none"> <li>• Short timescale,</li> <li>• Direct measurement of depletions,</li> <li>• Conceptual simplicity,</li> <li>• Mechanically validated calibration,</li> <li>• Smaller fetch requirement than for micrometeorological methods,</li> <li>• Ability to fully automate lysimeters, and</li> <li>• Nearly full visibility for inspection.</li> </ul> <p><b>Disadvantages</b></p> <ul style="list-style-type: none"> <li>• Reduced measurement accuracy due to lysimeter area often representing a small sample relative to a field area;</li> <li>• Difficulty in maintaining or reconstructing original soil profile characteristics, including density, layering, and structure during and following construction;</li> <li>• Difficulty in reducing any edge effects in vegetation;</li> <li>• Difficulty in measuring trees and plants with large spacing;</li> <li>• Difficulty in maintaining exact field conditions for vegetation and soil water;</li> <li>• Difficulty in reproducing rooting characteristics of the surrounding field;</li> <li>• Difficulty in detecting the presence of low levels of water stress due to subtle visual effects; and</li> <li>• Difficulty in accurately reproducing ET from nonpotential (stressed) vegetation due to inability to match soil water profile and thermal profile conditions to those of the surrounding field.</li> </ul> <p><b>Potential Problems with the Lysimeter Environment</b></p> <ul style="list-style-type: none"> <li>• Two-dimensionality of lysimeter boundaries;</li> <li>• Vegetation height and density differences between inside and outside;</li> <li>• Different vegetation characteristics between immediate and local fetch around the lysimeter and around the weather station;</li> </ul>

(Continued)

Table 7-2. Summary of Advantages, Disadvantages, and Requirements Associated with Estimating ET Using Soil Water Balance, Lysimetry, Bowen Ratio, and Eddy Covariance Methods (*Continued*)

Method	Characteristics
	<ul style="list-style-type: none"> <li>• Thermal conditions of the lysimeter soil block differing from the surrounding soil profile;</li> <li>• Thermal conditions and advective effects due to a high, exposed rim; and</li> <li>• Bulk density and lysimeter depth effects on root development and effects of the specific moisture profile or water table within the lysimeter on evaporation and moisture extraction.</li> </ul> <p>Requirements</p> <ul style="list-style-type: none"> <li>• Adequate fetch around the lysimeter, a minimum of 50 m recommended;</li> <li>• Requirement that vegetation inside and immediately outside the lysimeter be very similar in <ul style="list-style-type: none"> <li>◦ Height,</li> <li>◦ Density and ground coverage, and</li> <li>◦ Leaf area;</li> </ul> </li> <li>• Need to carefully document vegetation inside and outside lysimeter via photography and description;</li> <li>• Accurate calculation of effective area of the lysimeter vegetation;</li> <li>• Requirement that water management of the lysimeter be precise and similar to outside conditions;</li> <li>• Management of salinity via drainage;</li> <li>• Requirement that thermal characteristics of the lysimeter soil be similar to that outside; and</li> <li>• Minimized foot traffic.</li> </ul>
Bowen ratio	<p>Advantages</p> <ul style="list-style-type: none"> <li>• Nondestructive, direct sampling of the turbulent boundary layer;</li> <li>• No requirement for aerodynamic data;</li> <li>• Simple measurement of air temperature and vapor pressure at two heights;</li> <li>• Ability to measure ET over both potential and nonpotential surfaces;</li> <li>• Averaging of fluxes over a medium-sized area (3,000 to 100,000 m<sup>2</sup>); and</li> <li>• Automation.</li> </ul>

Table 7-2. Summary of Advantages, Disadvantages, and Requirements Associated with Estimating ET Using Soil Water Balance, Lysimetry, Bowen Ratio, and Eddy Covariance Methods (*Continued*)

Method	Characteristics
Disadvantages	<ul style="list-style-type: none"> <li>• Requires accurate and representative <math>R_n</math> and <math>G</math>;</li> <li>• Assumes that transfer coefficients <math>K_h</math> and <math>K_v</math> for <math>H</math> and <math>\lambda E</math> are equal (therefore assumes that sources for heat and vapor are horizontally and vertically similar);</li> <li>• Is numerically unstable when <math>H</math> is near zero (however, this usually causes only minor problems);</li> <li>• Requires that measurements of <math>T</math> and <math>e</math> be unbiased because <math>\Delta T</math> and <math>\Delta e</math> can be small;</li> <li>• Requires medium to large fetch; and</li> <li>• Has limitation that small stands of similar vegetation may be too small to use Bowen ratio energy balance (BREB), for example, narrow riparian systems, so that the Bowen ratio system samples <math>T</math> and <math>e</math> gradient artifacts created by areas upwind of the vegetation of interest (for example, from upwind areas of pasture, desert, or agriculture) due to an underdeveloped equilibrium boundary layer.</li> </ul>
Requirements	<ul style="list-style-type: none"> <li>• Uniform fetch of sufficient distance to establish an equilibrium boundary layer (EBL) deeper than the <math>z_2</math> height (this is often violated),</li> <li>• Sufficient sensor elevation above the canopy to avoid the roughness sublayer,</li> <li>• Accurate and representative measurement of <math>R_n</math> and <math>G</math>, and</li> <li>• Heterogeneous or sparse vegetation common to riparian systems generally require multiple net radiometers and soil heat flux stations.</li> </ul>
Recommendations for Deployment of Net Radiometers	<ul style="list-style-type: none"> <li>• Mount sensors over representative vegetation away from any obstructions including <ul style="list-style-type: none"> <li>◦ Towers;</li> <li>◦ Other instruments below or above the radiometer, especially bright, white instruments; and</li> <li>◦ Solar panels that are dark and often hot;</li> </ul> </li> </ul>

(Continued)

Table 7-2. Summary of Advantages, Disadvantages, and Requirements Associated with Estimating ET Using Soil Water Balance, Lysimetry, Bowen Ratio, and Eddy Covariance Methods (*Continued*)

Method	Characteristics
	<ul style="list-style-type: none"> <li>• When over complex or sparse canopies, deploy a minimum of three radiometers in separate locations:           <ul style="list-style-type: none"> <li>◦ Mount to view the true proportion of sunlit vegetation, shaded vegetation, sunlit soil, and shaded soil;</li> <li>◦ Recognize that multiple towers for <math>R_n</math> may be needed;</li> <li>◦ Consider deploying four-component radiometers for separate measurement of incoming and outgoing shortwave and long-wave components for improved quality assessment and control and for improved understanding of each component; and</li> <li>◦ Deploy a minimum of six soil heat flux measurement systems under the same conditions; and</li> </ul> </li> <li>• Use some independent means for testing <math>R_n</math> measurements, for example, compare against remote sensing-based <math>R_n</math> estimates, infrared thermometers, modeling <math>R_n</math> with standardized solar radiation-based algorithms, etc.</li> </ul>
Eddy Covariance	<p>Advantages</p> <ul style="list-style-type: none"> <li>• Nondestructive, continuous direct sampling of the turbulent boundary layer;</li> <li>• Ability to measure ET over both potential and nonpotential surfaces;</li> <li>• Ability to average fluxes over medium-sized (5,000 to 100,000 m<sup>2</sup>) areas; and</li> <li>• Automated systems.</li> </ul> <p>Disadvantages</p> <ul style="list-style-type: none"> <li>• A number of “corrections” are needed; these are often not well defined and are often empirical.</li> <li>• Method may miss transport by very small and very large eddies.</li> <li>• Energy balance closure error (<math>R_n - G = \lambda E + H</math>) can be 10–30%.</li> <li>• Method requires substantial fetch, generally 100 times the height of the instrument above the zero plane displacement height.</li> </ul>

Table 7-2. Summary of Advantages, Disadvantages, and Requirements Associated with Estimating ET Using Soil Water Balance, Lysimetry, Bowen Ratio, and Eddy Covariance Methods (*Continued*)

Method	Characteristics
	<ul style="list-style-type: none"> <li>• Narrow vegetation systems may cause the EC (or Bowen ratio) system to sample ET from areas upwind of the vegetation area (for example, with a narrow riparian system, from pasture, desert, or agriculture that is beyond the riparian system).</li> <li>• Method requires consistently nearly horizontal flow lines.</li> <li>• Change in vertical direction of flow lines during an averaging period causes large errors (portions of the streamline can be misinterpreted as <math>w'</math> (relative to mean vertical wind speed) so that <math>w'T'</math> or <math>w'q'</math> are overstated). This occurs when <ul style="list-style-type: none"> <li>• Sensors are too close to roughness elements such as tree limbs;</li> <li>• The surface of vegetation is irregular, for example, a convex-shaped riparian system where the shape and vertical components of streamlines change with respect to wind direction; and</li> <li>• Vertical components of streamlines can easily change with wind direction as wind direction changes.</li> </ul> </li> <li>• It is difficult to know the effects of wind direction changes on any change in vertical components of flow lines.</li> <li>• Problems in eddy formation may occur if sensors are too close to the surface or are too close to individual roughness elements.</li> <li>• Results may be questionable when used for understory measurements because of a changing horizontal plane orientation during an averaging period.</li> <li>• Mounting of net radiometers and location of soil heat flux plates for energy balance closure assessment are difficult for representative sampling.</li> <li>• Mounting arm and other nearby equipment, including the hygrometer, can impede and distort flow lines and eddy shapes for some wind directions.</li> </ul>

(Continued)

Table 7-2. Summary of Advantages, Disadvantages, and Requirements Associated with Estimating ET Using Soil Water Balance, Lysimetry, Bowen Ratio, and Eddy Covariance Methods (*Continued*)

Method	Characteristics
	<ul style="list-style-type: none"> <li>• Tower or scaffolding may bend and distort flow lines.</li> <li>• Instrumentation is somewhat fragile and expensive.</li> <li>• The method requires personnel who are well trained in electronics, turbulence theory, and biophysics.</li> </ul> <p>Requirements</p> <ul style="list-style-type: none"> <li>• Uniform fetch of sufficient distance to establish an equilibrium boundary layer (EBL) deeper than the instrument height (this is often violated);</li> <li>• Sufficient elevation of instruments above the canopy to reduce roughness sublayer impacts and to increase mean eddy size to match the sensor path length;</li> <li>• Required “corrections” to maximize accuracy; and</li> <li>• Accurate, high-frequency instrumentation and knowledge of physics of turbulence.</li> </ul>

Source: Data from Allen et al. (2011c)

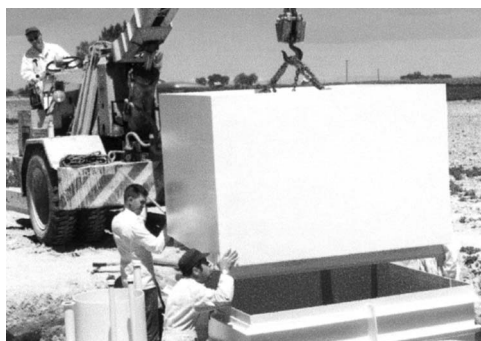


Fig. 7-2. A 2-m weighing lysimeter system being installed near Kimberly, Idaho  
Source: Photo courtesy of J. L. Wright (USDA-ARS), personal communication, 1990

include those by Ritchie and Burnett (1971), Wright (1982), Schneider and Howell (1991), and Allen and Fisher (1990). For detailed coverage of lysimeter types and designs, the following references are recommended reading: World Meteorological Organization (1966), Aboukhaled et al. (1982), Howell et al. (1985), Marek et al. (1988), Schneider and Howell (1991), and Allen et al. (1991a,b). Allen et al. (1991a) is the proceedings of an international symposium on lysimeters and contains descriptions of many lysimeter types in use around the world, results of research involving many of them, and cautionary information in lysimeter management and data interpretation.

### Typical Problems

Table 7-2 summarizes advantages, disadvantages, problems, and recommendations with lysimeters. Any lysimeter, no matter how precise a measuring system, provides a measure of ET from a very limited plant sample size. Therefore, one can only expect to obtain accurate estimates of actual field ET from lysimeters when plant density, height, and leaf area of vegetation inside the lysimeter are similar to those of the surrounding field. When plant density or leaf area differs significantly, then even though the results may be valuable in plant physiology or other studies, the actual ET obtained will generally not represent actual field ET. Wind disturbance of mass readings can also produce significant errors for short time periods.

Differences between conditions inside the lysimeter and outside in the field (soil characteristics, water availability, fertility, soil temperature, and rooting characteristics) can cause differences in crop growth, plant cover, leaf temperature, and maturation, and thus produce differences in ET between the field and lysimeter. Differences in plant height in particular can produce erroneous data with the errors related significantly to the lysimeter area; the smaller the lysimeter size, the larger the possible error. Differences in maturation are typical in fairly shallow lysimeters unless irrigations are continued to near the season's end. An illustration of a well-managed weighing lysimeter system (Figure 7-2) is shown in Figure 7-3, where vegetation inside the lysimeter has similar density and size as that immediately outside and no gaps in vegetation are visible at the lysimeter boundaries. One concern with the lysimeter management in Figure 7-3 is that the entire soil surface was inadvertently wetted by irrigation inside the lysimeter, whereas only about 50% of the soil surface was wetted in the surrounding field. The increased surface wetting inside the lysimeter would cause the total ET measurement and estimation of evaporation from soil to be overstated, especially during periods of partial surface cover by vegetation.

Some seriously flawed lysimeter results have been produced by a so-called "bloom effect" where the area of exposed plant canopy has exceeded the assumed effective area of the lysimeter. Tanner (1967) provides an



Fig. 7-3. A sweet corn crop growing on a 2-m weighing lysimeter system near Kimberly, Idaho

Source: Photo courtesy of J. L. Wright (USDA-ARS), personal communication, 1999

excellent discussion of lysimeters and, along with Penman (1963), was probably one of the earliest to recognize how serious this problem can be. Coverage of this and other aspects of lysimetry was detailed by King et al. (1956), Pruitt and Lourence (1985), Meyer and Mateos (1990), and Allen et al. (1991a). Examples are frequent in the literature of reported crop or pan coefficients ranging from 1.3 to 1.8 or even higher. Penman (1963) provided a simple formula for estimating increased capture of solar radiation from lysimeter vegetation when taller than its surroundings and the resulting increase in measured ET. The physical law of conservation of energy should be applied to all measurements of ET, especially those representing ET from extensive surfaces. In those situations, any crop coefficient greater than 1.1 for use with the alfalfa reference ET or greater than 1.3 for use with the grass reference ET should lead to a strong suspicion that the ET determinations (whether by lysimetry or meteorological techniques) may be in error, or that they represent conditions other than continuous expanses of vegetative surfaces. This point is discussed further in Chapter 10 on cover and crop coefficients.

Incorrect estimation of the effective evaporating area of a lysimeter is probably the most common error made in computing lysimeter ET. Equivalent, one-dimensional ET is computed from weighing lysimeters as the change in mass of the lysimeter divided by the evaporating area of lysimeter vegetation. Often, in practice, the dimension of the inside

lysimeter tank is mistakenly used as the divisor, rather than using the true vegetative area, causing significant error. Because the area of net radiation absorption and aerodynamic exchange by lysimeter vegetation generally exceeds that of the inner lysimeter tank, measured ET will be overestimated if the inner tank area is used to represent the evaporative and vegetative area. This error seems subtle and insignificant at first glance. However, in reality, its effect can be quite significant. For example, if a lysimeter is constructed with inside tank dimensions of 1 m<sup>2</sup> and has an undesirable 10-cm gap between the inner tank and outer enclosure (including both inner and outer enclosure rims), the average vegetation and evaporating area should be approximated as having a dimension of 1.1 m × 1.1 m. This dimension is the average of the dimensions of the inner tank and of the outer enclosure and is a reasonable approximation, assuming that vegetation from inside and outside the lysimeter reaches across the lysimeter rim and meets near the center. The ratio of effective vegetation area to inside area in this example is 1.1<sup>2</sup>/1.0<sup>2</sup> or 1.21. In other words, lysimeter measurements of ET will be overstated by 21% if the inner tank dimension is used to calculate the effective evaporating area. This type of bias in measuring ET is intolerable and greatly harms the compilation of representative and dependable ET measurement and associated crop coefficients. The effect is amplified if lysimeter vegetation is allowed to extend outside the lysimeter boundaries, replacing outside vegetation. The increased absorption of solar radiation and aerodynamic vapor exchange surface can be substantial. This problem frequently occurs when conditions immediately outside the lysimeter are impaired, as described in the next paragraphs.

A serious problem with lysimeters relates to foot and farm machinery traffic in and around lysimeters as they are serviced. This can be especially serious with grain crops, alfalfa, or other similar, closely spaced tall crops. Similarly, compaction of soil surrounding lysimeters during construction or installation has disqualified (or should have disqualified) many lysimeter data sets due to subsequent stunted growth of crops outside of lysimeters and therefore opportunity for exhibition of the bloom effect and overmeasurement of ET by the lysimeter systems.

Crop height differences inside and outside a lysimeter as produced by differing degrees of lodging and growth rates can be a problem, as discussed by Penman (1963). Again, the possible error in estimating actual field ET is greater with smaller lysimeters. Pruitt and Lourence (1985) provide an example that illustrates this problem, although in this case, with large 29-m<sup>2</sup> lysimeters, errors of only 5 to 10% were noted for a barley crop in spite of extreme differences between lodging inside and outside the lysimeter. Another example of the effect of expanded lysimeter vegetative area described by Pruitt and Lourence (1985) and Allen et al. (1991a) was with beans grown on the 6.1-m diameter floating lysimeter at Davis,

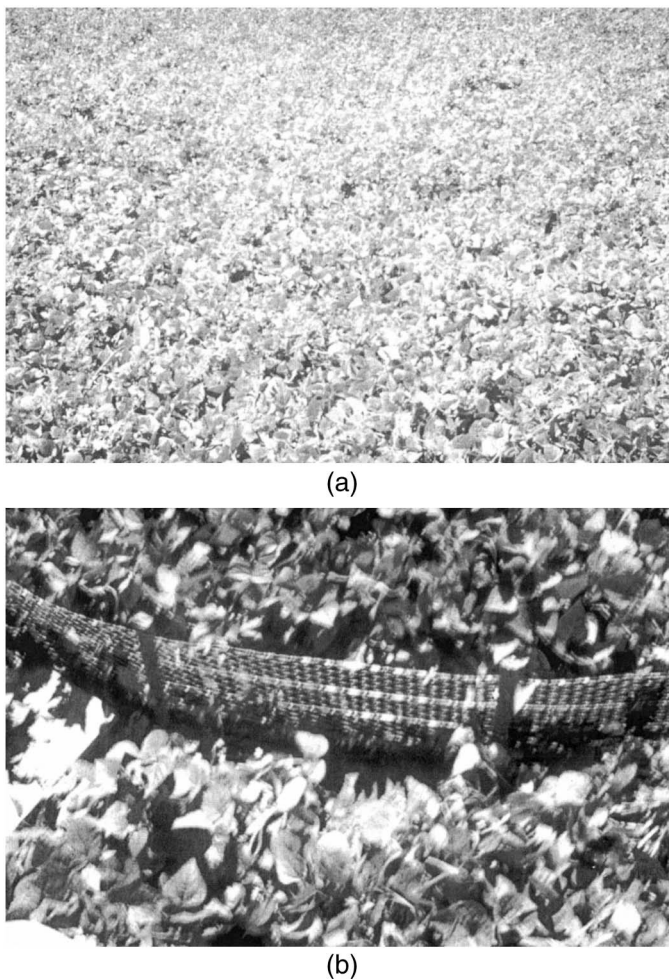


*Fig. 7-4. Example of bean plant growth surrounding a lysimeter in the center of the picture (a) before a fence was installed to contain the plants within the lysimeter area and (b) closeup of a retaining fence surrounding the lysimeter to constrain inner vegetation*

Source: Pruitt and Lourence (1985); reproduced with permission from ASABE

California. In this case, the stand of beans inside and outside the lysimeter appeared, at first glance, to be uniform and of excellent quality (Figure 7-4a). However, inspection revealed that a poor stand just to the north of the lysimeter's edge had resulted in excess bean vine growth from inside the lysimeter out into areas in the field as far as 0.9 m, taking up space where plants were sparse. When crowded back into the lysimeter and retained

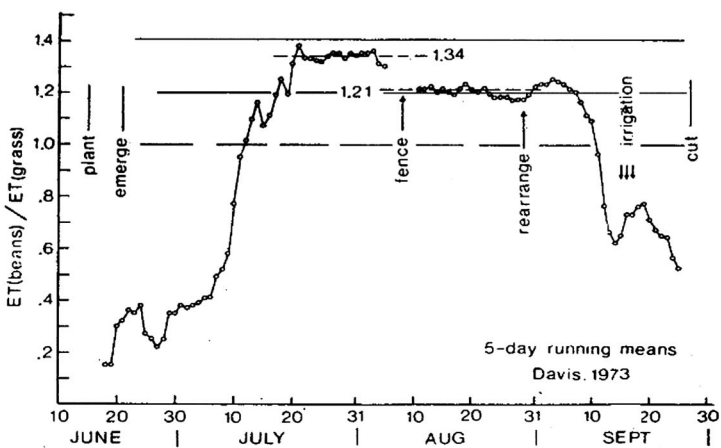


*Fig. 7-5. Effect of constraining bean plant growth to the lysimeter area on measured ET before and after the fence was installed*

Source: Pruitt and Lourence (1985); reproduced with permission from ASABE

there by a short, wire fence (Figure 7-4b), average values of computed  $K_c$  dropped from 1.34 to 1.21 as shown in Figure 7-5. Even lower  $K_c$ s may have occurred if adequate plant material were in place in the partially bare areas outside the lysimeter.

Several sensitive lysimeters capable of hourly determination of ET have been installed in forests (Fritsch et al. 1973; Reyenga et al. 1988; Dunin et al. 1985). In spite of the problems noted, at least in some cases the results with lysimeters about  $10 \text{ m}^2$  in area have been shown to provide ET measurements for forest trees in good agreement with Bowen ratio ET determination (Dunin et al. 1985, 1991).

In general, weighing lysimeters are necessary to accurately determine ET. Nonweighing lysimeter types, where ET is determined by observing changes in the water table level, are difficult to interpret, due to changes in soil water above the water table caused by water extraction by plant roots and changes in the capillary fringe above the water table with changing temperature (Hill and Allen 1991). Hydraulic weighing lysimeters have often been plagued by hysteresis of the hydraulic measurement systems and thermal problems (Kruse and Neale 1988), although such problems are likely less significant for weekly or longer determinations.

With improvements in electronic load cells, low-cost electronic weighing lysimeters that are suitable for daily measurements of ET have been developed for remote operation (McFarland et al. 1983; Kirkham et al. 1984; Allen and Fisher 1990). Some nonweighing lysimeters have been developed where the lysimeter acts merely as a hydraulic barrier to water

movement into or out of the lysimeter and the change in soil water with time is measured by keeping records of all water added to the lysimeter (irrigation and precipitation) and any drainage or runoff. A few examples of the hundreds of such lysimeters around the world are described by Harrold and Dreibelbis (1958), Van Hylckama (1968), Sarraf and Bovée (1973), Boman (1991), and Evans et al. (1991).

Another difficulty with lysimeters is in applications with non-well-watered vegetation (e.g., in natural rainfall areas where precipitation is less than maximum ET for the vegetation). In these applications, differences in soil structure and soil profile (due to disruption during construction), fertility, salinity, and thermal conditions inside lysimeters can make it difficult to control soil water conditions and consequently ET inside lysimeters to match conditions outside the lysimeter. In most cases, undisturbed, natural monolith soil profiles are required in lysimeters to accurately measure natural ET in semiarid and arid regions (Armijo et al. 1972; Dugas et al. 1985; Marek et al. 1988; Schneider and Howell 1991). The latter two publications describe a useful tank “pull-down” technique for obtaining an undisturbed, monolithic soil column inside the lysimeter.

Black et al. (1968) and Dugas and Bland (1991) caution against negative effects of thermal conduction of heat along metal lysimeter container walls that significantly warms the lysimeter soil, especially over long time periods. This unnatural heat source can cause drying of the soil profile under bare soil conditions that exceeds that under natural conditions. It can also promote earlier and more extensive root growth and respiration within the lysimeter tank. Black et al. (1968) recommend insulation of the lysimeter soil tank.

In spite of all these important precautions and opportunities for error and bias, weighing lysimeters continue to be a valuable method for determining ET and crop coefficients (Wright 1982; Howell et al. 2004, 2006). Lysimeters provide the ability to inspect the vegetation and to test calibration of weighing mechanisms. The larger the surface area and the greater the depth, the more likely the attainment of a representative, one-dimensional ET sample.

#### 7.4 ENERGY BALANCE METHODS—BOWEN RATIO

The Bowen ratio energy balance (BREB) method rearranges the energy balance equation [Eq. (4-1) and Eq. (7-14), which is presented later] to cancel aerodynamic transport terms. This permits determination of  $\lambda E$  by measuring air temperature and vapor pressure at two elevations above the surface in addition to  $R_n$  and  $G$ . Because the Bowen ratio  $\beta$  (Bowen 1926) represents the ratio of  $H$  to  $\lambda E$ , the energy balance equation [for example,

Eq. (7-14)] can be rearranged to obtain the BREB equation for application to ET from vegetation:

$$\lambda E = \frac{R_n - G - S_{cb} - P_{syn}}{1 + \beta} \quad (7-7a)$$

where  $S_{cb}$  represents any increase in energy storage in the canopy or boundary layer between the ground surface and height of the air temperature and vapor pressure measurement, and  $P_{syn}$  is energy consumed by photosynthesis.  $S_{cb}$  and  $P_{syn}$  are generally assumed to be zero, but  $S_{cb}$  can be large in forests and during early morning when the boundary layer is warming and increasing.  $P_{syn}$  can consume a few percent of total energy for dense vegetation during daylight. The aerodynamic transport equations for  $\lambda E$  were described in Chapter 6, and equations for both  $H$  and  $\lambda E$  can be found in Brutsaert (1982) and Chapter 4 of the *Hydrology Handbook* (Allen et al. 1996). When  $S_{cb}$  and  $P_{syn}$  are assumed to be zero, the BREB equation for application to vegetation becomes

$$\lambda E = \frac{R_n - G}{1 + \beta} \quad (7-7b)$$

Eq. (7-7b) will overestimate  $\lambda E$  if  $S_{cb}$  and  $P_{syn}$  are positive, but assumed to be zero. When applied to water, the  $G$  term in Eq. 7-7b is replaced with  $Q_t$ , the energy absorbed into the water body.

Under most measurement conditions, the transport coefficients (inverse of aerodynamic resistances) for  $H$  and  $\lambda E$  can be considered to be equivalent between the two measurement heights (Sellers 1965; Tanner 1968; Dyer 1974). However, for sparse vegetation, heat sources can be lower or higher in vegetation than vapor sources (see Chapter 11), which may affect the transport coefficients differently. Given equivalent transport coefficients, the Bowen ratio  $\beta$  can be expressed in a finite difference form as

$$\beta = \frac{H}{\lambda E} = \frac{c_p P}{\lambda \varepsilon} \frac{(\Delta T + \Gamma \Delta z)}{\Delta e} = \gamma \frac{[T_2 - T_1 + \Gamma(z_2 - z_1)]}{e_2 - e_1} \quad (7-8)$$

where  $T_2$  and  $e_2$  are air temperature and vapor pressure at height  $z_2$ , and  $T_1$  and  $e_1$  are air temperature and vapor pressure at height  $z_1$ .  $\gamma$  is the psychrometric constant [Eq. (3-11)], and  $\Gamma$  is the adiabatic lapse rate, generally taken as  $0.01^\circ\text{C m}^{-1}$  for nonsaturated air. Units of  $c_p, P$ , and  $\lambda$  in Eq. (7-8) should provide units for  $\gamma$  of  $\text{kPa}^\circ\text{C}^{-1}$  so that, for  $T$  in  $^\circ\text{C}$  and  $e$  in kPa,  $\beta$  is dimensionless.

Generally the  $z_1$  height should be at least 0.3 m above the crop canopy for a smooth, dense canopy and be farther above the canopy for tall, sparse crops where microscale turbulence among individual plants and

differences among source locations for heat and evaporation can disturb exponentially shaped temperature and vapor profiles. Generally, the  $z_2$  height is 1 to 2 m above  $z_1$ .

Bowen ratio systems are available commercially and are in widespread use for measuring  $\lambda E$  above both agricultural and natural vegetation. An example of a commercial system is shown in Figure 7-6. Generally  $T_2 - T_1$  is measured with differentially wired fine-wire thermocouples that may be naturally or artificially aspirated or with precision resistance thermometers that are shielded from the sun and require artificial aspiration. Vapor pressure is generally measured at each height using aspirated wet and dry bulb psychrometers or electronic hygrometers, or by suctioning air samples from each height through a common chilled-mirror hygrometer or a closed-path gas analyzer. On some systems, the  $z_2$  and  $z_1$  sensors are automatically exchanged with one another each 10 minutes or so to remove instrumentation biases. Generally,  $\lambda E$  is computed every 20 to 30 minutes and is summed over a daylight or 24-hour period to provide daily estimates of ET. Problems with naturally aspirated (exposed) thermocouples include contamination by dust and spiderwebs, which increase radiation loading and thermal bias between  $T_1$  and  $T_2$  ([Allen et al. 1994a](#)). Other types of errors associated with BREB measurements were described by Sinclair et al. ([1975](#)), Ohmura ([1982](#)), and Payero et al. ([2003](#)).



*Fig. 7-6. Systems, Inc. Bowen ratio system at American Falls Reservoir  
Source: Photo courtesy of R. Allen, Radiation Energy Balance*

The net radiation measurement in the BREB calculation should be made from an elevation high enough to measure an average representative surface condition similar to that upwind of the  $T$  and  $e$  measurements. Because of the direct role that  $R_n$  plays in the  $\lambda E$  measurement, multiple  $R_n$  sensors are recommended for improved spatial sampling and quality control. In heterogeneous vegetation cover with variation in vegetation type, size, or density on the scale of fives of meters or more, multiple net radiation systems should always be employed. Idso and Cooley (1971, 1972) and Idso (1974) provide guidance on net radiometer positioning and error analysis.

Soil heat flux density is generally measured 0.08- to 0.15-m below the surface using soil heat flux plates (Campbell Scientific 2003; Ham 2001). The 0.08- to 0.15-m depth range is recommended to ensure that the soil flux density is measured below the zone of soil water vaporization (Ham 2001) and to reduce the influence of the plate on impeding vertical conduction of heat and water flow near the soil heat flux plate. Heat flux plates tend to behave like umbrellas during vertical flow of water, for example, after a wetting event, and can create dry areas below plates during infiltration and above plates during evaporation. Because water content substantially influences thermal conductivity of soil near a plate, the spatial disruption of continuity in water content can cause substantial error in  $G$  and consequently the ET derived from BREB.

Sensible heat absorption and release above soil heat flux plates is estimated by measuring soil temperature change over the plate at multiple depths and at multiple locations. Generally, two or more installations of soil heat flux systems are recommended per BREB site to reduce effects of spatial heterogeneity and to improve representation for the area. The corrected soil heat flux density,  $G$ , is computed using Eq. (4-47).

Important advantages of the BREB method are the ability to measure  $\lambda E$  even from nonpotential surfaces, the elimination of wind or turbulent transfer coefficients, and the absence of surface measurements. The disadvantages are the sophistication and fragility of sensors and data-logging equipment, the numerical instability of Eqs. (7-7) and (7-8) during periods of  $\beta$  near  $-1$ , and the substantial reliance on accurate and representative measurements of  $R_n$  and  $G$ . The requirement for adequate upwind fetch also limits the method.

Most evidence suggests that correction for air stability conditions in the use of the Bowen ratio energy balance measurements is not needed, due to nearly equal impact on both  $\lambda E$  and  $H$ , so that the usual assumption of the near-equality of transfer coefficients for heat and water vapor throughout a wide range of stability conditions is realistic (Cellier and Brunet 1992). However, the major source elevations for  $\lambda E$  and  $H$  in the canopy should be similar for the transfer coefficients of the two processes to be nearly the same (Tanner 1967).

The Bowen ratio method is recognized as one of the most accurate ET measurement methods if  $R_n$ ,  $G$ , and the gradients of temperature and humidity can be accurately measured and are spatially representative and  $\beta$  is small. For tree crops and forest canopies, accurate measurement of the gradients at a height far enough above the canopy to avoid effects of individual trees is difficult due to the very small gradients involved. Nevertheless, the Bowen ratio method has served and continues to serve as one of the major methods employed for forest research ([McNaughton and Black 1973](#); [Thom et al. 1975](#); [McIlroy and Dunin 1982](#); [Denmead and Bradley 1985](#); [Fritsch and Simpson 1985](#); [Dunin et al. 1985, 1991](#)). Accuracies of well-designed and operated BREB systems have been estimated to be approximately 10% ([Sinclair et al. 1975](#); [Ohmura 1982](#); [Payero et al. 2003](#); [Allen et al. 2011c](#)). A disadvantage is the need to measure  $R_n$  and  $G$ , which can be problematic under some conditions such as with sparse or heterogeneous vegetation and over water surfaces.

### Typical Problems with Bowen Ratio Systems

Table 7-2 summarizes advantages, disadvantages, and requirements of Bowen ratio systems. Because of the numerical instability of the BREB approach, which develops as  $\beta$  approaches  $-1$  (when sensible heat transport toward the surface is in near equilibrium with latent heat transport away from the surface), special procedures are required during such periods. Fortunately  $\beta \rightarrow -1$  generally occurs during periods of low  $R_n$  (at dawn and dusk) when ET is normally low. Angus and Watts ([1984](#)), in comprehensive analyses of sensor-produced errors, show the potential for error in calculation of  $\lambda E$  increases rapidly as  $\beta$  drops below  $-0.2$ , with accuracy requirements for all sensors increasing. Ohmura ([1982](#)) and Payero et al. ([2003](#)) describe relative errors associated with the BREB method and techniques for data quality analysis.

The problem with  $\beta$  close to  $-1$  is illustrated in Figure 7-7. Part (a) shows the excellent capabilities of the BREB method in estimating actual ET during most hours of the day. However the problem of  $\beta \rightarrow -1$  is also clearly shown. Although errors are small in magnitude for the 1700–1800 h, 50–100% errors clearly occur even prior to  $\beta$  reaching  $-0.5$ , confirming Angus and Watts ([1984](#)). The data from eight days of an early micrometeorological study by Pruitt ([1963](#)) at Davis (March to October) are shown in Figure 7-7b, with 12 half-hour periods when  $-1.5 < \beta < -0.5$  separated from the other 142 periods. The results also show the excellent response of the BREB method with tests conducted under a wide range of conditions from cool and humid to hot and dry and to a cold and dry day in March having strong wind. Periods of rather drastic errors in estimating ET occurred when  $\beta \rightarrow -1$ .

Pruitt et al. ([1987](#)) utilize an hourly Penman equation to derive ET for periods affected by the problem when  $\beta \rightarrow -1$ . To obtain crop ET estimates

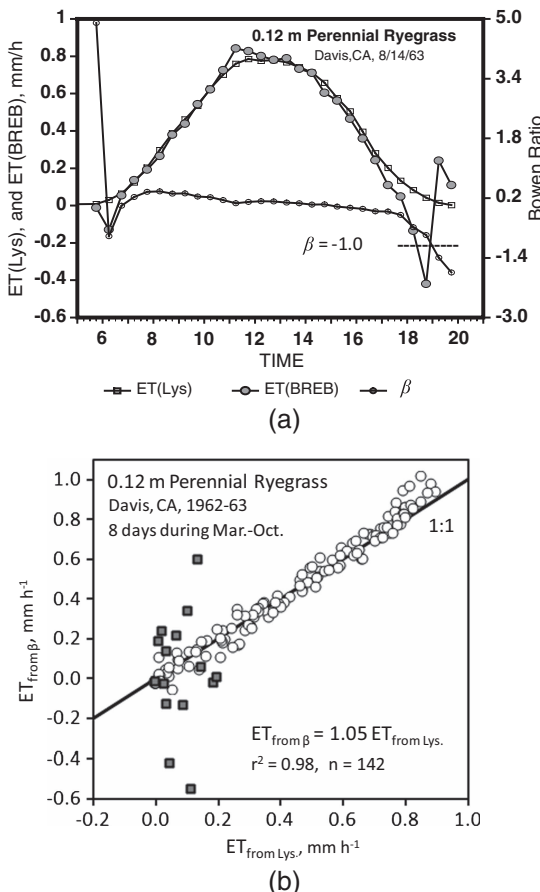


Fig. 7-7. Examples of early tests of the BREB method: (a) Comparison of ET from perennial ryegrass measured by lysimeter with BREB calculations for August 14, 1963, at Davis, California, including reference to  $\beta$ . (b) Regression of ET from Bowen ratio against ET by precision-weighing lysimeter for half-hour time intervals spanning eight days of data collected in 1962–1963 at Davis. Twelve half-hour periods are plotted as square symbols when  $-1.5 < \beta < -0.5$  and the estimation of ET became numerically unstable. The 12 periods were not included with the other 142 periods (round symbols) during regression

Source: Data from Pruitt (1963)

for those problem periods, the  $ET_{ref}$  from the Penman equation is multiplied with a reference ET fraction,  $ET_{ref,F}$ , determined during daylight periods prior to or following the periods of unstable BREB estimates by dividing measured ET by  $ET_{ref}$ . Tanner (1967) suggests that simple

combination equations be substituted for BREB estimates during problem periods. This requires instrumentation for measuring wind speed. More details on BREB computations can be found in Chapter 4 of the ASCE *Hydrology Handbook* (Allen et al. 1996) and in Allen et al. (2011c).

ET determined from BREB is often used to test or "confirm" other energy balance-based models including the combination equation, for example, the PM equation. However, an often-overlooked requirement for testing or confirming models is the need for independency between the tested method and the measured data. In comparisons of models against ET from the BREB, the same  $R_n$  measurements are often used in both the combination equation and in the determination of ET from BREB. Because the  $R_n$  parameter can dominate both the combination equation and BREB-based ET, the ET estimated from the combination equation cannot be confirmed using BREB-derived data, unless an independent measurement or estimation of  $R_n$  is used.

The BREB method is often superior to the direct use of turbulent transfer equations for estimating transfers of water vapor above a surface. This is primarily due to constraints on estimates made using the BREB method due to inclusion of the radiation balance in the method. Errors in estimating gradients of temperature or humidity are not directly related to the estimates of  $\lambda E$  or  $H$  as is the case for strictly aerodynamic methods. In some situations, however, net radiation or heat transfer below the surface is not readily measurable. For forests, brushlands, or orchards, accounting for changes in heat storage of the canopy can be important for periods shorter than 24 hours. For water bodies, accurate measurement of  $R_n - Q_t$  is difficult. For these situations, one should consider using aerodynamic methods, described later in this chapter, that avoid these problems.

### Example Applications for Bowen Ratio Systems

Applications of the BREB system began in the 1960s (Tanner 1960; Fritschen 1965, 1966; Pruitt and Lourence 1966). Allen et al. (1996) present a summary of numerous applications of the system over land surfaces. The BREB approach is difficult to apply to evaporation measurements from water bodies due to the difficulty in measuring the energy ( $Q_t$ ) absorbed into or liberated from the water, as described in Chapter 6. Anderson (1954), Keijman (1974), Hoy and Stephens (1979), Amayreh (1995), Allen and Tasumi (2005), and Chapter 6 discuss applications of the BREB approach to water.

## 7.5 MASS TRANSFER METHOD USING EDDY COVARIANCE

ET can be measured directly using eddy covariance (EC) sampling of the boundary layer (Swinbank 1951) according to the relationship:

$$\lambda E = \rho \overline{w'q'} = \frac{0.622}{P} \rho \overline{w'e'} \quad (7-9)$$

where  $E$  is vapor flux in  $\text{kg m}^{-2}\text{s}^{-1}$ , equivalent to  $\text{mm s}^{-1}$ ;  $q'$  is the instantaneous deviation of specific humidity from mean specific humidity ( $q$ ) in  $\text{kg kg}^{-1}$ ;  $e'$  is the instantaneous deviation of vapor pressure from mean vapor pressure ( $e$ ) in kPa;  $w'$  is the instantaneous deviation of vertical wind velocity from mean vertical wind velocity ( $w$ ) in  $\text{m s}^{-1}$ ;  $P$  is atmospheric pressure, kPa; and  $\rho_a$  is air density,  $\text{kg m}^{-3}$ , assumed to be constant. The overbar indicates means of the products of the instantaneous deviations over 15–30 min periods.

Webb et al. (1980) recommend water vapor and air density corrections to the calculation of  $E$  (Fuehrer and Friehe 2002; Leuning 2007) that can be expressed as

$$E = \rho_a \overline{w'q'} \left( 1 + \frac{q}{1-q} \right) + \frac{q^2}{(1-q)} \frac{H}{c_p T} \quad (7-10)$$

where  $c_p$  is specific heat of moist air in  $\text{J kg}^{-1}\text{K}^{-1}$ , and  $q$  and  $T$  are mean specific humidity and temperature over the averaging period in  $\text{kg kg}^{-1}$  and K. Units for sensible heat flux,  $H$ , are  $\text{W m}^{-2}$ .

Residual  $\lambda E$  can also be computed from the energy balance equation as  $\lambda E = R_n - G - H$  [Eq. (4-2)], where sensible heat flux density is measured by eddy covariance as

$$H = \rho C_p \overline{w'T'} \quad (7-11)$$

where  $T'$  is the instantaneous deviation of air temperature from mean temperature ( $T$ ) in K, and  $H$  has units of  $\text{W m}^{-2}$ .

The concept of eddy covariance (also referred to as eddy correlation) draws on the statistical covariance (correlation) between vertical fluxes of vapor or sensible heat within upward and downward legs of turbulent eddies. This requires high-speed measurement of  $T$ ,  $w$ , and  $e$  or  $q$ , usually at frequencies of 5 Hz (five times per second) or faster using quick-response sensors. Ten Hz is common. The vertical component of wind,  $w$ , is generally measured using a sonic anemometer, and  $T$  is measured using ultrafine wire thermocouples (on the order of 13  $\mu\text{m}$  diameter) or using sonically determined temperature corrected for humidity effects. Specific humidity is measured using quick-response hygrometers such as Lyman-alpha, Krypton, or other open-path hygrometers, or using closed-path gas analyzers (Buck 1976; Campbell and Tanner 1985; Tanner 1988). All measurements must be made at nearly the same point to measure characteristics of the same eddy. Corrections are required for instrument separation, frequency response, and coordinate rotation, and to account

for the type of hygrometer (Baldocchi et al. 1988; Tanner et al. 1993; Moncrieff et al. 1996; Villalobos 1997; Twine et al. 2000; Aubinet et al. 2000, Paw et al. 2000; Massman 2000, 2001; Sakai et al. 2001; Rannik 2001; Wilson et al. 2002). Systems employing three-dimensional (3-D) sonic anemometers allow coordinate (planar) rotation to force mean vertical wind speed  $w$  toward zero (Baldocchi et al. 1988; Wilczak et al. 2001). Eddy covariance systems are commercially available. Figure 7-8 shows an example of an eddy covariance installation with two sonic anemometers employed for data redundancy and independent assessment of measurements.

Software programs for correction of EC data include ECPack from Wageningen University, TK2 software from the University of Bayreuth (Mauder and Foken 2004), EddySoft from the Max Planck Institute for Biogeochemistry in Jena (Kolle and Rebmann 2007), EdiRE software from the University of Edinburgh, APAK from Oregon State University (Vickers and Mahrt 1997, 2003), and Eddy-Pro by LI-COR, Inc. (2012). These software packages include mixtures of the corrections listed.

In addition to these corrections are issues related to flux divergence in the equilibrium boundary layer; nonuniform vegetation or moisture conditions in the source area (i.e., footprint); improper averaging times; and effects of very large episodic eddies and heat plumes with large vertical components that are very efficient in heat and vapor transport, but are



Fig. 7-8. Two three-dimensional sonic anemometers and an open-path infrared water vapor and  $\text{CO}_2$  sensor used to measure  $H$ ,  $\lambda E$ , and  $\text{CO}_2$  fluxes. The use of two sonic anenometers provides data redundancy, the ability for error checking and comparison, and the ability to assess error in  $\lambda E$  and  $\text{CO}_2$  fluxes caused by separation distances between anemometer and open-path infrared sensor  
Source: Photo courtesy of R. G. Allen

largely missed by the sonic sensor or covariance algorithm ([Foken 2008a](#)). Burba and Anderson ([2008](#)) give a good overview of corrections and precautions for eddy covariance.

Computing  $\lambda E$  as a residual of the energy balance by measuring  $H$  as in Eq. (7-11) has the advantage of eliminating the requirement for the quick-response hygrometer, which can be expensive or may require frequent maintenance. The disadvantage of this method is the need to measure  $R_n$  and  $G$ , which can be problematic under some conditions such as with sparse or heterogeneous vegetation and over water surfaces. Eq. (7-11) can be used in an energy balance closure check on Eq. (7-10) using Eq. (7-14). Allen and Tasumi ([2005](#)) combine  $H$  determined from eddy covariance with Bowen ratio from a BREB system to determine  $\lambda E$  from open water as described in Chapter 6.

Table 7-2 summarizes advantages, disadvantages, and requirements of the eddy covariance method. Advantages of the eddy covariance method include direct sampling of the turbulent boundary layer and measurement of ET over both potential and nonpotential surfaces. Eddy covariance has disadvantages similar to other boundary layer sampling techniques, including complex instrumentation and fetch requirements. The sonic anemometer must be set parallel to the surface so that no component of wind speed parallel to the surface biases measurements. If not set parallel to the surface, coordinate rotation must be applied. When positioned over rough vegetation such as trees, the eddy covariance system must be far enough above individual limbs that impacts of limbs on air streamlines are minimized. Otherwise, the zero plane of vertical velocities of streamlines past the anemometer will change with small changes in wind direction during the averaging period and will cause false flux readings that cannot be corrected with coordinate rotation. In general, the eddy correlation method requires personnel who are well trained in electronics, turbulent theory, and biophysics. Instrumentation is somewhat fragile and expensive.

Lack of energy balance closure is common with eddy covariance measurements, where the sum of measured  $\lambda E + H$  does not equal measured  $R_n - G$  ([Balocchi et al. 1988; Twine et al. 2000; Wilson et al. 2002; Foken et al. 2006; Foken 2008a](#)). Possible reasons for the lack of closure are storage of heat in canopies, horizontal advection, change in storage of heat in the developing boundary layer below the instrumentation (causing flux divergence), and frequency response of the sonic and water vapor sensors that does not span the entire spectrum of eddy frequencies. In addition, regional-scale heterogeneity of vegetation and ET fluxes can cause large-scale eddies that are effective in transport of  $\lambda E$  and  $H$  but are not readily sensed by eddy covariance systems typically placed within 20 m of the surface ([Foken 2008a](#)). Many users “close” the energy balance by scaling  $H$  and  $\lambda E$  in the same proportion ([Twine et al. 2000](#)) until the sum equals

$R_n - G$ . However, this places all source of lack of closure on  $H$  and  $\lambda E$  and none on  $R_n - G$ . Allen (2008) suggests using multiple linear regression, where the most dependable component of  $R_n, G, H$ , and  $\lambda E$  is set as the dependent variable, and all others are set as independent variables for data collected during daytime conditions to indicate systematic biases in components. Allen (2008) illustrates where regression indicated that measurements of  $G$  had been undermeasured by as much as 100 to 200%. The multiple regression approach does not explain why a component is biased and can only identify consistent, systematic biases in components. Additional detail on the eddy correlation method can be found in articles by Dyer (1961), Businger et al. (1967), McBean (1972), Brutsaert (1982), Weaver et al. (1986), Kizer et al. (1990), Kizer and Elliot (1991), Twine et al. (2000), Wilson et al. (2002), Shaw and Snyder (2003), Baldocchi (2003), and Foken (2008b).

## 7.6 FETCH REQUIREMENTS FOR BOUNDARY LAYER MEASUREMENT

Upwind fetch for boundary layer instrumentation generally should be on the order of 100 m for each meter  $z_2$  is above the top of the zero plane displacement height of the surface (Brutsaert 1982) to ensure establishment of an internal equilibrium boundary layer that represents the surface energy exchange being measured. Monteith and Unsworth (1990) recommend that a fetch of 50 to 1 is often adequate for micrometeorological measurement of sensible and latent heat flux. Brutsaert (1982) provides theoretical considerations of boundary layer development that can be used to estimate minimum fetch requirements as a function of surface roughness. If one assumes that the lower 10% of an internal boundary layer downwind of a surface discontinuity has reached full adjustment to a new equilibrium with the surface (Petersen 1969; Brutsaert 1982), then Brutsaert's Eq. (7-39) can be expressed for minimum required fetch as

$$x_f = \left[ \frac{30(z - d)}{(z_{om})^{0.125}} \right]^{1.14} \quad (7-12)$$

where  $x_f$  is the minimum fetch distance required for complete boundary layer development in m,  $z$  is the maximum sensor height above the ground in m,  $d$  is zero plane displacement in m, and  $z_{om}$  is momentum roughness height of the surface in m. Eq. (7-12) estimates  $x_f$  for near-neutral conditions ( $H$  near 0). The exponent (1.14) should be increased for increasingly stable situations and can be reduced somewhat where conditions are increasingly unstable (Brutsaert 1982). Eq. (7-12) indicates that as surface roughness increases, the fetch requirement (distance required for the new equilibrium

Table 7-3. Minimum Recommended Upwind Fetch Distances, m, for Various Types of Surface Cover [from Eq. (7-12)] and Assumed Values for  $z_{om}$  and  $d$

Height and Type of Surface Cover	Height of the Upper Measurement above the Ground			
	$z = 1 \text{ m}$	$z = 2 \text{ m}$	$z = 3 \text{ m}$	$z = 12 \text{ m}$
Water ( $d = 0, z_{om} = 0.0001 \text{ m}$ )	180	400	630	3,000
0.12 m Grass ( $d = 0.08 \text{ m}, z_{om} = 0.014 \text{ m}$ )	80	190	300	1,500
0.5 m Alfalfa ( $d = 0.34 \text{ m}, z_{om} = 0.06 \text{ m}$ )	45	130	220	1,200
1.5 m Cattails ( $d = 1.0 \text{ m}, z_{om} = 0.18 \text{ m}$ )	n/a	60	140	950
10 m Dense Trees ( $d = 6 \text{ m}, z_{om} = 1.2 \text{ m}$ )	n/a	n/a	n/a	320

to occur) decreases, as shown in Table 7-3 where  $z_{om}$  and  $d$  for vegetation are estimated as 0.12 and 0.67 times canopy height, respectively. Eq. (7-12) estimates  $x_f$  for discontinuities between surfaces of similar roughness and may not predict well for large changes in vegetation height, such as transitioning from forest to grass or vice versa.

The values for minimum fetch in Table 7-3, computed using Eq. (7-12), indicate that Eq. (7-12) follows the 100:1 rule for a relatively wide range of vegetation and equipment heights. According to the equation, the 100:1 rule represents most closely 0.12-m tall vegetation. Eq. (7-12) becomes sensitive to the lack of roughness as  $z_{om} \rightarrow 0$  so that fetch requirements become large (e.g., for open water).

As an example of application, for a Bowen ratio installation with the  $z_2$  height at 2 m above a ground surface with 0.1-m tall vegetation, the minimum fetch requirement under neutral conditions according to Eq. (7-12) would be approximately 190 m. The 100:1 ratio (relative to equipment height above zero plane displacement) would suggest a fetch of 200 m. A fetch distance of 190 m in all directions would require a minimum vegetation stand size of 4 ha (10 acres) with the BREB system placed at the center. This requirement (which increases as vegetation height increases) makes it difficult to use the BREB or any other boundary layer sampling system to measure  $\lambda E$  from small, isolated stands of vegetation. Confirming these estimates, Pruitt (1963) finds no difference in BREB calculations of ET for 0.1- to 0.15-m tall grass using  $z_1$  and  $z_2$  heights of

0.25 and 0.5 m, respectively, and  $z_1$  and  $z_2$  heights of 0.5 and 1.0 m, when upwind fetch of grass was 180–200 m. However, Dyer and Pruitt (1962), in tests on the same field with sensors of an eddy correlation system placed at 4.0 m height, reported the fetch of grass to be inadequate for sensors at that height. Eq. (7-12) suggests a fetch length of 430 m for  $z_2 = 4$  m over a 0.1-m tall crop.

Heilman et al. (1989) give additional guidelines on fetch requirements for BREB measurement, and several publications describe various models for estimating footprints for both scalar and flux measurement. The “footprint” of a flux or scalar measurement represents the upwind surface area that is statistically responsible for the conditioning of the measurement (Hsieh et al. 2000). Schmid (2002) presents a good review of various models and their mechanics and limitations. Gash (1986), Schuepp et al. (1990), and Shuttleworth (1992) present an expression for estimating the fraction of  $\lambda E$  sensed at a specific instrument height generated from a specific distance of upwind fetch:

$$F = \exp\left(\frac{\left[(z-d)\left(1 - \ln\left(\frac{(z-d)}{z_{om}}\right)\right) - z_{om}\right] - \psi_{sm(z/L)}}{k^2 x_f \left(1 - \frac{z_{om}}{(z-d)}\right)}\right) \quad (7-13)$$

where  $F$  is the fraction of vapor and sensible heat flux densities at the  $z$  height, which is contributed by fetch with an upwind length of  $x_f$  m (i.e.,  $F$  fraction of the flux is contributed by the surface lying along 0 to  $x_f$ ); variable  $k$  (dimensionless) is the von Kármán constant (0.41); and  $\psi_{sm(z/L)}$  (dimensionless) is the integrated stability correction function for momentum transfer, defined later in Eq. (7-26). The subtraction of  $\psi_{sm(z/L)}$  in the numerator of Eq. (7-13) was added by Allen (2006) to account for effects of stability or instability of the equilibrium boundary layer. When  $\psi_{sm(z/L)}$  is set equal to 0, Eq. (7-13) represents  $F$  for conditions having neutral stability. Eq. (7-13) estimates lower  $F$  for stable conditions and greater  $F$  for unstable (buoyant) conditions.

Eq. (7-13) and the method of Hsieh et al. (2000) are useful for assessing quality of measurements by BREB and eddy correlation sensors, where  $F$  represents the fraction of  $\lambda E$  or  $H$  measured that is generated by the fetch of vegetation or surface over which the sensors are located. Clearly, for measurements to be completely representative of the measurement surface,  $F$  should be close to 1.0. Eq. (7-13) estimates  $F \approx 0.8$  for values of  $x_f$  calculated using Eq. (7-12), indicating that it recommends slightly greater fetch requirements than does Eq. (7-12). When applied to BREB systems with  $z = z_2$ , Eq. (7-13) estimates on the conservative side, because the lower BREB measurement would suggest a higher  $F$  if based on  $z = z_1$ . Eq. (7-13) estimates  $F = 0.91$  and  $F = 0.57$  for  $z = 1$  m and  $z = 4$  m, respectively, over

0.1 m grass for  $x_f = 200$  m. These calculations agree with observations by Pruitt (1963) and Dyer and Pruitt (1962) described in an earlier paragraph concerning adequacy of fetch.

Horst and Weil (1992), Hsieh et al. (1997), Leclerc et al. (1997), Schmid (2002), and Hsieh et al. (2000) apply Lagrangian stochastic and large-eddy simulation (LES) strategies along with Gaussian or non-Gaussian diffusion assumptions to estimate three-dimensional distribution of point source or line source fluxes. These complex models are applied over various stability conditions to demonstrate sensitivities of flux and scalar measurements over a range of footprint conditions and discontinuities in fetch at several distances from the sensors.

### Fetch Requirements for Weather Stations

Eqs. (7-12) and (7-13) can be applied to assess the adequacy of green fetch around weather stations for use in estimating reference ET representing well-watered agriculture (Schmid 2002; Allen 2006). Allen (2006) applies results from Horst and Weil (1992) and Hsieh et al. (2000) to various fetch lengths of clipped grass and dry soil to demonstrate the impact that fetch at various lengths of distance has on air temperature and humidity measurements at weather stations. Allen showed the impact to increase more or less logarithmically with distance upwind and then to decrease after some distance even farther upwind. Results indicate that the 100:1 fetch distance:measurement height rule of thumb and Eq. (7-13) appear to apply well to unstable conditions (positive Bowen ratio) for measurement of temperature and humidity at weather stations and may underestimate the fetch requirement for neutral and stable conditions. Appendix H contains tables showing the relative influence of various distances of bare soil or well-watered grass on air temperature and humidity measurements, based on Eq. (7-13). These tables are useful in judging the representativeness of weather station measurements of  $T$  and  $e_a$  to reference ET conditions (i.e.,  $T$  and  $e_a$  occurring over a large expanse of well-watered, transpiring vegetation).

## 7.7 ADVANTAGES AND DISADVANTAGES OF ET MEASUREMENT METHODS

Table 7-2 summarizes advantages, disadvantages, and requirements associated with estimating ET using soil-water balance, lysimetry, Bowen ratio, and eddy covariance methods following Allen et al. (2011c). These four methods tend to be the primary methods in current practice. In addition, when ET measurements or crop coefficients are reported, a thorough description of measurement conditions and methods should be

included to help users understand the context of the data: the condition, type and character of the vegetation measured, and means to judge the likely accuracy of the data (Allen et al. 2011d). Multiple systems should be employed as part of quality control, and the systems should be colocated periodically for bias assessment and adjustment. Independent measurements using different types of methods or equipment from different vendors can be valuable for discovering measurement problems.

## 7.8 COMBINED ENERGY BALANCE AND MASS TRANSFER METHODS

This section describes the combined use of aerodynamic expressions for sensible heat transfer and energy balance methods to estimate ET as a residual of the surface energy balance. Brutsaert (1982), Cellier and Brunet (1992), Chapter 4 of the ASCE *Hydrology Handbook* (Allen et al. 1996), Hatfield et al. (2005), Chapter 6 on open water, and Chapter 11, where the aerodynamic fluxes using iterative energy balance (AFIB) method is described, provide more details on direct use of aerodynamic expressions.

### Mass Transfer with Direct Use of Aerodynamic Expressions

**Calculating ET Using  $(R_n - G - H)$**  For cases where  $\lambda E$  exceeds  $H$  so that measurement or estimation errors of  $H$  are small relative to  $\lambda E$ , the use of energy balance determination of  $\lambda E$ , where  $H$  is calculated aerodynamically, avoids the measurement of humidity gradients or fluxes, which is still one of the more uncertain of micrometeorological measurements. If data for  $R_n$  and  $G$  are available (measured or calculated), the equation for  $ET$  for this approach can be expressed as

$$ET = \frac{R_n - G - H - S_{cb} - P_{syn}}{\lambda \rho_w} \quad (7-14)$$

where  $ET$  is in  $\text{mm s}^{-1}$ ;  $R_n$ ,  $G$ , and  $H$  are in  $\text{W m}^{-2}$  ( $\text{J m}^{-2} \text{s}^{-1}$ );  $\lambda$  [Eq. (3-17)] is in  $\text{KJ kg}^{-1}$ ;  $\rho_w$  is water density in  $\text{kg m}^{-3}$ ,  $S_{cb}$  represents any changes in energy storage in the canopy or boundary layer between the ground surface and height of the  $H$  determination; and  $P_{syn}$  is energy consumed by photosynthesis.  $S_{cb}$  and  $P_{syn}$  are generally assumed to be zero, but  $S_{cb}$  can be large in forests and during early morning when the boundary layer is warming and increasing in depth.  $P_{syn}$  can consume a few percent of total energy during daylight. Eq. (7-14) is commonly used in remote sensing applications using satellite imagery (Bastiaanssen et al. 1998a, b; Allen et al. 2005d, 2007; Tasumi et al. 2005a, b; Anderson et al. 2005, 2012).

**Correcting for Boundary Layer Stability** In calculating ET for short time periods (hourly or less) using aerodynamic approaches, the inclusion of stability-correction expressions in the log-law or other wind profile equations becomes vital as evidenced by Rossby and Montgomery (1935), Monin and Obukhov (1954), Swinbank (1955), Panofsky (1963), Businger (1966), Dyer (1967), Dyer and Hicks (1970), Webb (1970), Pruitt et al. (1973), and Oke (1978). Aerodynamic estimation of water vapor or sensible heat flux typically involves use of the Monin-Obukhov universal wind profile expression involving the modification of the log-law wind profile to provide applicability under nonadiabatic conditions. It can be expressed as

$$\frac{\partial u}{\partial z} = \frac{u_*}{k(z-d)} \phi_M \quad (7-15)$$

where  $\partial u / \partial z$  is the gradient of the horizontal component of wind speed at height  $z$ ,  $u_*$  is the friction velocity in  $\text{ms}^{-1}$ ,  $k$  is the von Kármán constant (taken as 0.41), and  $d$  is the zero plane displacement of the wind profile by the canopy. The Monin-Obukhov (1954)  $\phi_M$  is a gradient function calculated at height  $z$  that is equal to 1.0 for neutral buoyancy conditions in the equilibrium boundary layer, less than 1.0 for unstable conditions, and greater than 1.0 for stable conditions. Monin and Obukhov relate  $\phi_M$  to their dimensionless height ratio,  $z/L$ , in a Taylor series expression. Only the first two terms have found wide usage, where

$$\phi_M = 1 + \alpha_{mo}(z/L) \quad (7-16)$$

where  $z/L$  is a stability-related function (Obukhov 1946), and  $\alpha_{mo}$  is a constant determined experimentally by Monin-Obukhov (1954). The Obukhov scale length  $L$  in meters, as defined by Businger and Yaglom (1971) and Brutsaert (1982), is

$$L = \frac{-u_*^3 \rho}{kg \left( \frac{H}{T_a c_p} + 0.61 ET \right)} \quad (7-17)$$

where  $u_*$  is in  $\text{m s}^{-1}$ ,  $\rho_a$  is air density in  $\text{kg m}^{-3}$  [Eq. (3-15)],  $g$  is acceleration of gravity ( $9.807 \text{ ms}^{-2}$ ),  $H$  is the sensible heat flux density in  $\text{W m}^{-2}$  (negative if to the surface),  $T_a$  is mean air temperature at the  $z$  height in  $K$ , and  $c_p$  is specific heat of moist air in  $\text{J kg}^{-1} \text{K}^{-1}$ .  $ET$  is evaporation flux density in  $\text{kg m}^{-2} \text{s}^{-1}$  (this is equivalent to  $\text{mm s}^{-1}$  when the ET flux is divided by the water density,  $\rho_w$ , in  $\text{Mg m}^{-3}$ ). Generally,  $\rho_w = 1.0 \text{ Mg m}^{-3}$ . Eq. (7-17) is often expressed without the 0.61  $ET$  term, as the computation of  $L$  has only about 1/7 the sensitivity to  $\lambda E$  as it does to  $H$  (both in  $\text{W m}^{-2}$ ). The inclusion of  $ET$  in Eq. (7-17) accounts for buoyancy caused by water

vapor with less density than dry air. ET in  $\text{mm s}^{-1}$  is obtained by dividing  $\lambda E$  in  $\text{W m}^{-2}$  by  $\lambda$  in  $\text{J kg}^{-1}$ .

Generally,  $\phi_M$  is not used in energy balance calculations because it is a gradient function and changes with elevation above the surface. Instead, an integration of  $\phi_M$  (i.e.,  $\psi_{sm(z/L)}$ ) is used, as defined in the next section.

### Sensible Heat from Temperature Differences

As indicated with the eddy correlation and aerodynamic methods,  $\lambda E$  can be determined indirectly by solving the energy balance for  $\lambda E$ , having computed  $H$  by other means. A promising method for determining  $H$  is the use of a near-surface temperature gradient estimated using air temperature at some height  $z$  and surface temperature measured using an infrared thermometer. Hatfield et al. (1984) and Katul and Parlange (1992) describe examples. Hatfield et al. (1984) provide results of testing the method at several U.S. locations and with several crops.

Sensible heat flux is commonly estimated by expressing the sensible heat equation in a difference form and by using an aerodynamic resistance term,  $r_a$  ( $\text{sm}^{-1}$ ), leading to

$$H = -\frac{\rho c_p}{r_a} (\theta_{T_z} - \theta_{T_o}) \quad (7-18)$$

where  $\theta_{T_z}$  and  $\theta_{T_o}$  are mean values for potential temperature at the  $z$  height and at the surface (K) calculated from  $T_z$  (air temperature at height  $z$ ) and  $T_o$  (surface temperature) using Eq. (7-19). Potential temperature,  $\theta_T$  for micrometeorological studies is defined as

$$\theta_T = T + \Gamma z \quad (7-19)$$

where  $\theta_T$  and  $T$  are in K.  $\Gamma$  is the lapse correction ( $^{\circ}\text{C m}^{-1}$ ), and  $z$  is the elevation of the  $T$  measurement relative to a specified datum. The potential temperature is the temperature that would result if air were brought adiabatically to the surface pressure level (Brutsaert 1982) and provides for inclusion of the effect of lapse rate in stability and  $H$  calculations. The use of  $\theta_T$  in place of  $T$  has little effect on the calculation of sensible heat where sensors are within a few meters of one another. The aerodynamic resistance,  $r_a$ , between the surface and height  $z$  can be estimated by

$$r_a = \frac{[\ln(\frac{z-d}{z_{om}}) - \psi_{sm(z/L)}] [\ln(\frac{z-d}{z_{oh}}) - \psi_{sh(z/L)}]}{k^2 u_z} \quad (7-20)$$

where  $d$  is the zero plane displacement,  $z_{om}$  is the surface roughness length for momentum transfer (see Chapter 8 for estimation of these terms),  $z_{oh}$  is

the surface roughness length for sensible heat transfer (approximated for most vegetative surfaces as 1/10 of  $z_{om}$ ), "ln" is the natural logarithmic function, and  $\psi_{sm(z/L)}$  and  $\psi_{sh(z/L)}$  are integrated stability functions for describing effects of buoyancy or stability between the surface and height  $z$  on sensible heat and momentum transfer. Massman (1999) and Su et al. (2001) describe more complicated approximations for  $z_{oh}$ . For water surfaces,  $z_{oh}$  is characteristically three to five times the value of  $z_{om}$  based on relationships by Brutsaert (1982). A similar equation for  $r_a$ , but for where wind, temperature, and humidity measurements are at different heights, is presented as Eq. (8-3) in Chapter 8.

### Integrated Stability Functions

The bulk integrated stability-correction expressions  $\psi_{sm(z/L)}$  and  $\psi_{sh(z/L)}$  are recommended for all surface-to-air determinations of heat, vapor, and momentum fluxes in place of the gradient  $\Phi$  functions. They are certain to be required for studying tall crops such as tree crops and forests and where strong stability (advection) or instability (low  $\lambda E/R_n$  ratios) exists. As with the purely aerodynamic estimates of  $H$  or  $E$ , measurements of  $u$  and  $T$  should be based on 30-minute mean data or less. Stability corrections should not be applied with 24-hour means due to errors in averaging  $T_z$  and  $T_o$  over long periods and large change in  $\psi_{sm(z/L)}$  and  $\psi_{sh(z/L)}$  during the day. Another factor requiring attention in applying surface-to-air models for such applications is that the adiabatic lapse rate  $\Gamma$  (approx.  $0.01^{\circ}\text{C m}^{-1}$ ) must be taken into account, e.g., in the calculation of  $H$  where use of virtual air temperature,  $T_v$ , and potential virtual temperature  $\theta_{T_v}$ , may be important.

Brutsaert (1982) provides a comprehensive discussion on the subject of stability correction in which his formulas relate to the use of the Monin-Obukhov (1954)  $z/L$  stability parameter. The use of  $z/L$  requires an iterative solution to solve for several unknown parameters, with closure on the energy balance. Because most of the commonly used stability correction expressions were developed in relation to  $z/L$ , its use is recommended. A study by Katul and Parlange (1992) illustrates the use of iterative solution for  $z/L$ .

With some simplifying assumptions, the following presents the calculation of sensible heat flux  $H$  using integrated forms of stability correction for the aerodynamic method of exchange between the surface and some height, or between two heights, along with the use of  $z/L$ .

**Surface-to-Air Temperature Differences** When surface temperature is used, the profile expression involving sensible heat flux density, including correction for stability, is

$$H = -a_h k u_* \rho_a c_p \frac{(\theta_{T_z} - \theta_{T_o})}{[\ln\left(\frac{z-d}{z_{oh}}\right) - \psi_{sh(z/L)}]} \quad (7-21)$$

where  $a_h$ , the ratio of  $k$  for heat to  $k$  for momentum, is generally assumed to be equal to or close to 1.0, and  $\theta_{T_o}$  and  $\theta_{T_z}$  are mean values for potential temperature at the surface and  $z$  heights, computed using Eq. (7-19). Units for the  $z$ ,  $d$ , and  $z_{oh}$  terms in Eq. (7-21) must cancel, and other terms must combine to provide  $H$  with units normally of  $\text{Jm}^{-2}\text{s}^{-1}$  (i.e.,  $\text{Wm}^{-2}$ ). The term  $\psi_{sh(z/L)}$  (dimensionless) is the integrated stability function for heat transfer between the surface and  $z$ . Eqs. (7-20) and (7-21) sometimes include a second  $\psi_{sm(z_{om}/L)}$  and/or  $\psi_{sh(z_{oh}/L)}$  term (Su et al. 2001). However, that term affects the estimation of  $r_a$  or  $H$  by less than 1% for essentially all conditions except for very rough surfaces such as forest with low wind speed and large sensible heat fluxes and can therefore generally be ignored.

With the assumptions that roughness lengths are normally much smaller than  $L$  and that the Businger-Dyer expressions are valid,  $\psi_{sh(z/L)}$  for unstable conditions ( $z/L < 0$ ) can be expressed as (Paulson 1970)

$$\psi_{sh(z/L)} = 2 \ln \left[ \frac{(1+x^2)}{2} \right] \quad (7-22)$$

with

$$x = \left( 1 - 16 \frac{z-d}{L} \right)^{1/4} \quad (7-23)$$

Normally,  $(z-d)/L$  is used in Eq. (7-23) in place of  $z/L$  following Brutsaert (1982), where  $d$  is the zero plane displacement length and  $L$  is the Monin-Obukhov stability length [Eq. (7-17)]. In the case of surface-to-air differences,  $z$  in Eq. (7-23) is the height of the air temperature and wind measurements.

The other unknown in Eq. (7-21) is  $u_*$ , which can be obtained for surface-to-air applications from

$$u_* = \frac{k u_z}{\ln\left(\frac{z-d}{z_{om}}\right) - \psi_{sm(s/L)}} \quad (7-24)$$

where  $\psi_{sm(z/L)}$  (dimensionless) is the integrated stability correction function for momentum transfer, again, assuming that the roughness lengths are normally much smaller than  $L$  (Paulson 1970). The integral form of the expression for  $\psi_{sm(z/L)}$  for unstable conditions for use with  $T_o - T_z$  is

$$\psi_{sm(z/L)} = 2 \ln[(1+x)/2] + \ln[(1+x^2)/2] - 2 \arctan(x) + \pi/2 \quad (7-25)$$

with  $x$  obtained from Eq. (7-23) and where the arctan function is in radians.

For stable conditions, agreement as to appropriate stability functions is less certain. Fortunately, the method being considered, i.e., the estimation first of  $H$  using temperature differences and then solving for  $ET$ , allows for some uncertainty. Also, except for hot, arid, or desert climates, stable conditions primarily relate to late afternoon to early morning periods when  $ET$  is small.

Assuming that the gradient stability functions for stable conditions ( $z/L > 0$ ) are equal and the functions of Webb (1970) are accepted, the recommended relationships for integrated stability forms are

$$\psi_{sm(z/L)} = \psi_{sh(z/L)} = -5.2(z/L) \quad (7-26)$$

for  $0 < (z - d)/L < 1.0$  and where the Monin-Obukhov  $z/L$  parameter is computed as  $(z - d)/L$ . For  $(z - d)/L > 1$ , Brutsaert (1982) recommends limiting  $\psi_{sm(z/L)}$  and  $\psi_{sh(z/L)}$  to about  $> -5$  or  $-6$ .

**Calculation Steps** To calculate  $H$  and subsequently  $ET$  from the energy balance using the integrated stability functions and  $z/L$ , one should follow an iterative procedure, where one first uses Eqs. (7-21) and (7-24) to solve for  $H$  and then Eq. (7-14) to solve for  $ET$ , assuming neutral stability conditions ( $\psi_{sh(z/L)}$  and  $\psi_{sm(z/L)}$  are initially set equal to 0). Variable  $L$  is then calculated using Eq. (7-17) using the initial estimates of  $H$  and  $ET$ .  $\psi_{sh(z/L)}$  and  $\psi_{sm(z/L)}$  are then solved using Eq. (7-22), (7-25), or (7-26), depending on the sign of  $z/L$ , and Eqs. (7-24) and (7-21) are then resolved for  $u_*$  and  $H$ .  $ET$  for use in Eq. (7-17) is recalculated using the energy balance equation, Eq. (7-14), and the process is repeated until the values  $(z - d)/L$ ,  $u_*$ , and  $H$  become numerically stable. Generally only three to four iterations are required.

**$H$  from Air-to-Air Temperature Differences** When air temperature and wind are measured at two heights in the profile (rather than measuring  $T_o$ ), the integrated forms of stability correction between  $z_1$  and  $z_2$  are employed, where the following variations on Eqs. (7-21) and (7-24) are used. The profile expression involved for sensible heat flux density, including correction for stability, is

$$H = -a_h k u_* \rho c_p \frac{(\theta_{T_2} - \theta_{T_1})}{[\ln\left(\frac{z_2-d}{z_1-d}\right) - \psi_{sh(z_2/L)} + \psi_{sh(z_1/L)}]} \quad (7-27)$$

where  $\theta_{T_2}$  and  $\theta_{T_1}$  are potential temperatures at  $z_2$  and  $z_1$  heights, computed from  $T_2$  and  $T_1$  using Eq. (7-19). Units for the  $z$ ,  $d$ , and  $z_{oh}$  terms in Eq. (7-27) must cancel, and other terms must combine to provide  $H$  with units normally of  $\text{Wm}^{-2}$ . The terms  $\psi_{sh(z_2/L)}$  and  $\psi_{sh(z_1/L)}$  (dimensionless) are

integrated stability functions between the surface and  $z_2$  and between the surface and  $z_1$ . Thus, the integrated stability adjustment for the distance between  $z_1$  and  $z_2$  is determined by differencing the two terms. The terms are calculated for sensible heat transfer using Eq. (7-22) or (7-26), where  $(z - d)/L$  is equal to  $(z_2 - d)/L$  and  $(z_1 - d)/L$  for  $\psi_{sh(z_2/L)}$  and  $\psi_{sh(z_1/L)}$ , respectively.

Friction velocity,  $u_*$ , can be obtained from wind speed measurements at two heights as

$$u_* = \frac{k(u_2 - u_1)}{[\ln\left(\frac{z_2-d}{z_1-d}\right) - \psi_{sm(z_2/L)} + \psi_{sm(z_1/L)}]} \quad (7-28)$$

where terms  $\psi_{sm(z_2/L)}$  and  $\psi_{sm(z_1/L)}$  (dimensionless) are integrated stability functions for momentum transfer and are calculated using Eq. (7-25) or (7-26) with  $z/L$  equal to  $(z_2 - d)/L$  and  $(z_1 - d)/L$ , respectively. Variables  $u_2$  and  $u_1$  are mean horizontal wind speed measurements at the  $z_2$  and  $z_1$  heights. Units for  $u_*, u_2$ , and  $u_1$  are equivalent. In situations where  $T_1$  and  $T_2$  are measured at the  $z_1$  and  $z_2$  heights, but where only one measurement for  $u_z$  is made, then  $u_*$  can be calculated with Eq. (7-24) using an estimation of surface roughness,  $z_{om}$ . This assumes constant  $u_*$  with height, which is a valid assumption because of conservation of momentum flux. The same iterative procedure for calculating  $H, u_*$ , and  $z/L$  is followed as for surface-to-air measurements described previously.

**Estimating ET from Air-to-Air Humidity Differences** As in the estimation of  $H$  from Eq. (7-27), ET can be estimated from humidity gradients:

$$E = -a_v k u_* \rho \frac{(q_2 - q_1)}{[\ln\left(\frac{z_2-d}{z_1-d}\right) - \psi_{sv(z_2/L)} + \psi_{sv(z_1/L)}]} \quad (7-29)$$

where  $a_v$  is the ratio of  $k$  for water vapor to  $k$  for momentum, commonly assumed to be 1.0, and the same steps used in solving for  $H$  in Eq. (7-27) are used in solving for ET, assuming equality of the  $\psi_{sh}$  and  $\psi_{sv}$  functions. Parameters  $q_2$  and  $q_1$  are specific humidities at  $z_2$  and  $z_1$ , in  $\text{kg kg}^{-1}$ , defined in Eq. (3-5). Units for ET will be  $\text{kg m}^{-2} \text{s}^{-1}$ , which is equivalent to  $\text{mm s}^{-1}$  when the ET flux is divided by the water density,  $\rho_w$ , in  $\text{Mg m}^{-3}$ .

Chapter 11 describes an alternative application method for use when air temperature, humidity, and wind speed are measured at a single height, and iterative application of equations for  $H, \lambda E, u_*, \psi_{sh}, \psi_{sm}, T_o, R_n$ , and  $G$  is made. The iteration is pursued until the estimate for  $T_o$  is numerically stable. As discussed in Chapter 11, the dependence of  $R_n, G, H$ , and  $\lambda E$  on

the estimate for  $T_o$  makes it important to determine  $T_o$ . That method can be more accurate than the Penman-Monteith method. Its application does require an estimate for bulk surface resistance, which can be uncertain.

**Advantages, Disadvantages, and Precautions** The energy balance equation with  $H$  estimated using Eq. (7-18), Eq. (7-21), or Eq. (7-27) has the advantage of ET estimation in areas where precipitation is less than ET and therefore where plant water stress occurs, because neither knowledge of surface resistance ( $r_s$ ) nor measurement of humidity profiles is required. The estimation of  $r_a$  or use of surface temperature does require measurement of wind speed and perhaps surface roughness. Estimation of equivalent surface roughness,  $z_{om}$  and  $z_{oh}$ , along with measurement of a representative average  $T_o$  in Eqs. (7-20) and (7-21) can be problematic in tall, sparse canopies such as are found in forest and natural settings. Even in short agricultural crops, sensing the effective surface temperature can be a problem, where  $T_o$  at night may be influenced by leaf layers closest to the warm soil surface and where differences exist between radiometric  $T$  (as measured by an infrared thermometer) and aerodynamic temperature (the heat source temperature used in the aerodynamic equations for  $H$ ) (Kustas et al. 1994; Qualls and Brutsaert 1996). For crops with sparse canopies, proper integration of soil and vegetation temperatures is especially difficult (Qualls and Brutsaert 1996).

An additional disadvantage of the energy balance approach is that  $T_1$  and  $T_2$  or  $T_o$  and  $T_z$  measurements need to be specific to the surface in question. Therefore, historic measurements of air temperature over standard weather surfaces are not useful with this method.

As with the Bowen ratio and eddy correlation methods, and all boundary layer sampling techniques for that matter, it is critical that a large fetch of like vegetation occurs upwind of all sensors. This is necessary because the surface temperature-energy balance method, as with all boundary layer methods, assumes that equilibrium (one-dimensional vapor, wind, and temperature profiles) has developed. Divergence from equilibrium energy exchange conditions may cause substantial estimation errors due to decoupling of the energy exchange surface from the boundary layer profile and resulting divergence of flux densities within the boundary layer. Fetch requirements for each sensor should be adhered to as discussed previously.

Estimating  $ET$  as  $R_n - G - H$  generally requires the use of stability correction factors discussed previously, especially over dry surfaces. Pruitt and Lourence (1966) present an example illustrating the seriousness of ignoring air profile stability conditions when using  $ET = R_n - G - H$ , showing up to an order of magnitude of underestimation of actual  $ET$  of grass during calm, midmorning periods and an overestimation of  $ET$  by a factor of 2 to 3 during late-afternoon stable periods with colder, heavier air near the surface. During periods with winds  $>4$  to  $5 \text{ ms}^{-1}$  stability correction

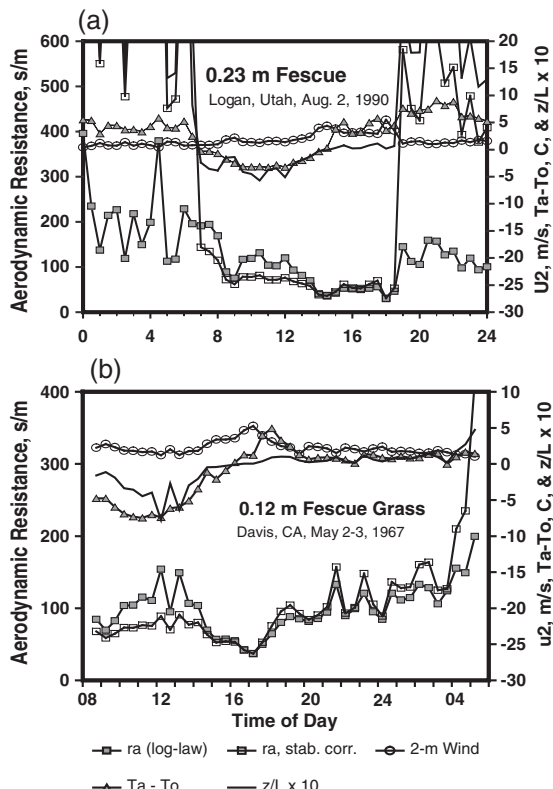


Fig. 7-9. Aerodynamic resistance ( $r_a$ ) over grass computed with and without stability correction for studies at a) Logan, Utah, and b) Davis, California. Included are measurements of  $T_z - T_o$  (expressed as  $T_a - T_o$ ), 2-m wind speed, and  $z/L$

Source: From R. G. Allen and W. O. Pruitt, personal communications, 1994, for data from Morgan et al. (1971)

was no longer needed over the transpiring crop due to the strong mechanical mixing and creation of turbulence, making the near-surface boundary layer nearly neutral.

Examples showing effects of stability correction on estimation of  $r_a$  using surface and air temperature measurements are given in Figure 7-9 for 0.23-m- and 0.12-m-high fescue grass at Logan, Utah, and at Davis, California, respectively. Both installations had full vegetation ground cover under fully watered conditions and with large fetch. Surface temperatures at both sites were made using infrared (IR) thermometers. However, at Davis,  $T_o$  was based on averages of 5-cm and 10-cm leaf thermocouples for

$R_n$  less than 0 because the warm nighttime soil surface appeared to dominate the IR readings. At both locations surface temperature was lower than air temperature during nighttime and late afternoon periods, causing moderately strong stability of the boundary layer. Correction for this stability using Eq. (7-24) with  $H$  calculated using Eq. (7-21), using an iterative solution for  $z/L$ , increased calculations of  $r_a$  dramatically, especially at Logan during nighttime periods where  $z/L$  became quite large due to low wind speeds ( $u_2 < 1 \text{ ms}^{-1}$ ). With the calm and cooler and more humid morning conditions during daytime between 0800 and 1400 hours at both sites, which normally produce ratios of  $\lambda E/(R_n - G) < 1.0$ ,  $T_o$  exceeded  $T_z$  and unstable conditions resulted. These unstable conditions lasted until midafternoon, when  $z/L$  became positive. The corrected values of  $r_a$  during some morning periods [made using Eqs. (7-20), (7-22), (7-25), and (7-28)] ranged from 50 to 80  $\text{sm}^{-1}$  lower than the uncorrected values for both locations.

The effects of stability and instability on estimation of  $r_a$  shown in Figure 7-9 appear to be quite significant. However, Figure 7-10 clearly shows that where ET was estimated using the energy balance Eq. (7-14) with  $H$  calculated using Eq. (7-21), that only for the Davis study did a large need exist for stability correction due to 15–20% overestimation of ET, e.g., at midday, by the uncorrected log-law values. The corrections applied to calculate  $H$  for stability agreed very well for Davis with independent estimates of  $H$  made by subtracting lysimeter measurements of ET from  $R_n - G$ . Use of the calculated  $H$  in the energy balance resulted in underestimation of ET (more negative values) at Davis during nighttime hours, although dewfall had occurred in this case. This underestimation may have been caused by errors in the measurements for  $R_n$  or  $G$ .

For the Logan results, differences only occurred at night in corrected and noncorrected estimates of ET of more than a few percent, because the grass forage was transpiring during the daytime at near maximum rates, so that little instability occurred and  $H$  was small. The magnitude of  $H$  at Davis was more than double that at Logan, no doubt due to cooler and more humid conditions of early May leading to greater instability at Davis. In applications over water-stressed natural vegetation,  $H$  may become large relative to  $\lambda E$  and  $T_o - T_z$  will increase. Such effects will increase the importance of applying stability corrections. The primary benefit of applying stability corrections at Logan was evident during the nighttime hours when the uncorrected  $H$  resulted in estimation of ET of about  $0.05 \text{ mmh}^{-1}$ , whereas ET estimated using corrected  $H$  and ET measured by lysimeter indicated negative ET during this period. These errors are small, but would cause an error in the 24-hour sum for ET of almost  $1 \text{ mm d}^{-1}$  if the errors occurred over an 8-hour night.

Allen and Tasumi (2005) present a second example of applying Eq. (7-27) and (7-29) for  $H$  and ET using temperature and humidity gradients over

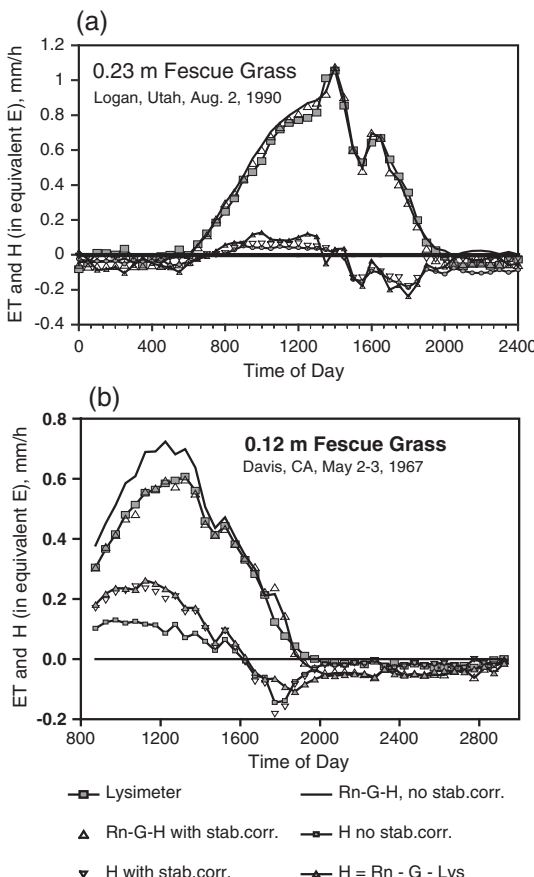


Fig. 7-10. Comparison of measured  $ET$  (lysimeter) with  $ET$  calculated from  $R_n - G - H$  with  $H$  calculated using the log-law and log-law corrected with integrated stability expressions at (a) Logan, Utah, and (b) Davis, California  
Source: Data from Allen and Fisher (1990) and W. O. Pruitt, personal communication, 1994, with Davis data from Morgan et al. (1971)

American Falls Reservoir, Idaho, as illustrated in Figure 6-21, where estimates for  $E$  by these equations (labeled “aerodynamic estimate”) were compared with  $E$  determined by a combination of eddy covariance and Bowen ratio.

Many satellite-based energy balance models for determining  $ET$  utilize Eq. (7-14) with  $H$  from Eq. (7-27). For example, the SEBAL (Bastiaanssen et al. 1998a, 2005) and METRIC (Allen et al. 2007b) remote sensing-based models apply Eq. (7-27), where the difference  $\theta_{T_2} - \theta_{T_1}$  is estimated by

indexing to surface temperature:  $\theta_{T_2} - \theta_{T_1} = a + bT_s$ , where  $a$  and  $b$  are empirical coefficients fitted specifically to each satellite image and  $T_s$  is surface temperature of each pixel in the satellite image. The relationship between  $\theta_{T_2} - \theta_{T_1}$  and  $T_s$  is determined in SEBAL and METRIC by inverse calibration at extreme (wet and dry) conditions to reduce impacts of biases in estimates for net radiation, soil heat flux, and other parameters ([Allen et al. 2007b](#)).

This page intentionally left blank

# CHAPTER 8

## REFERENCE CROP ET

### 8.1 INTRODUCTION

The combination of the sensible [Eq. (7-18)] and latent heat transfer equations [Eq. (6-7)] with the energy balance equation [Eq. (7-14)], following simplifying assumptions by Penman (1948, 1956a, 1963) results in the well-known Penman equation, here expressed generically, to produce ET for a defined reference crop (generally clipped, cool-season grass or full cover alfalfa):

$$ET_{ref} = \left( \frac{\Delta}{\Delta + \gamma} \frac{(R_n - G)}{\rho_w \lambda} + \frac{\gamma}{\Delta + \gamma} \frac{E_a}{\rho_w \lambda} \right) 1,000 \quad (8-1a)$$

and

$$E_a = K_u (a_w + b_w u_2) (e_s - e_a) \quad (8-1b)$$

where  $R_n$  is net radiation and  $G$  is soil heat flux density into the ground in  $\text{J m}^{-2} \text{ t}^{-1}$ ,  $\Delta$  is the slope of the saturation vapor pressure curve in  $\text{kPa}^\circ\text{C}^{-1}$ ,  $\gamma$  is the psychrometric constant in  $\text{kPa}^\circ\text{C}^{-1}$ ,  $E_a$  is the aerodynamic evaporation rate in  $\text{J m}^{-2} \text{ t}^{-1}$ ,  $K_u$  is a unit conversion factor typically in  $\text{J m}^{-2} \text{ t}^{-1} \text{ kPa}^{-1}$ ,  $e_s$  is mean saturation vapor pressure at air temperature in  $\text{kPa}$ ,  $e_a$  is actual vapor pressure of the air in  $\text{kPa}$  at height  $z$ ,  $u_2$  is wind speed in  $\text{m s}^{-1}$  at the 2-m height,  $\lambda$  is the latent heat of vaporization in  $\text{J kg}^{-1}$ ,  $\rho_w$  is density of water in  $\text{g m}^{-3}$ , and  $a_w$  and  $b_w$  [ $\text{s m}^{-1}$ ] are empirical wind function coefficients. These units produce  $ET_{ref}$  with units of  $\text{mm t}^{-1}$ , with the 1,000 term having units of  $\text{mm m}^{-1}$ . Penman's wind coefficients for grass were based on his original study, and those for water were based on the Lake

Hefner equation. Values for  $a_w$  and  $b_w$  are presented in Chapter 6 for open water, following Eq. (6-22) and in Appendix K for clipped grass and alfalfa references. Eq. (8-1) follows Eqs. (6-3) and (6-18).

## 8.2 THE PENMAN-MONTEITH EQUATION

To better simulate the effects of behavior of vegetation with regard to energy balance, Monteith (1965) and Rijtema (1965) independently introduced a surface resistance parameter into the Penman equation and replaced the linear wind function term with an aerodynamic resistance parameter. The result is what is now commonly called the Penman-Monteith (PM) equation. Written in terms of evaporation or ET expressed as latent heat flux ( $\lambda E$ ),

$$\lambda E = \frac{\Delta(R_n - G) + \rho_a c_p(e_s - e_a)/r_a}{\Delta + \gamma \left(1 + \frac{r_s}{r_a}\right)} \quad (8-2)$$

where units of  $\lambda E$ ,  $R_n$ , and  $G$  are in  $\text{J m}^{-2} \text{s}^{-1}$  (or  $\text{W m}^{-2}$ );  $\rho_a$  is air density,  $\text{kg m}^{-3}$ , computed using Eq. (3-15),  $c_p$  is specific heat of dry air,  $\text{J kg}^{-1} \text{C}^{-1}$ , generally taken as  $1,010 \text{ J kg}^{-1} \text{C}^{-1}$ ; variables  $e_s$  and  $e_a$  are in kPa;  $r_a$  is aerodynamic resistance in  $\text{s m}^{-1}$ ;  $r_s$  is the bulk surface resistance in  $\text{s m}^{-1}$ ; and units for  $\Delta$  and  $\gamma$  are in  $\text{kPa}^\circ\text{C}^{-1}$ . Equations for calculating  $e_s$  and  $e_a$  for use with 24-hour calculations in  $\text{kPa}^\circ\text{C}^{-1}$  are given later in this chapter. For convenience,  $\Delta$  is generally computed using Eq. (3-2) at mean air temperature, which is a valid assumption when estimating  $\lambda E$  for the reference crop, which generally has near-neutral stability conditions. Aerodynamic resistance to vapor and heat transfer,  $r_a$ , in Eq. (8-2) is computed using Eq. (7-20) re-expressed as Eq. (8-3). Bulk surface resistance,  $r_s$ , is defined in the following paragraphs. Appendix J includes a derivation of the PM equation that combines aerodynamic and energy balance equations utilizing the Bowen ratio.  $\lambda E$  from Eq. (8-2) is converted to  $ET_{ref}$  (if the  $r_a$  and  $r_s$  parameters are defined for a reference crop) by dividing the numerator by  $\lambda$  ( $2.45 \times 10^6 \text{ J kg}^{-1}$ ) and  $\rho_w$  ( $1,000 \text{ kg m}^{-3}$ ) and multiplying by  $1,000 \text{ mm m}^{-1}$ , so that  $\lambda E \text{ W m}^{-2}$  and  $\text{J m}^{-2} \text{s}^{-1}$  yields  $ET_{ref}$  in  $\text{mm s}^{-1}$ . Further multiplication by  $3,600 \text{ s h}^{-1}$  yields  $\text{mm h}^{-1}$ , and multiplication by  $86,400 \text{ s d}^{-1}$  yields  $\text{mm d}^{-1}$ . Eq. (8-15) later in this chapter is a simplified, standardized form of the PM equation with the conversion units to  $\text{mm h}^{-1}$  and  $\text{mm d}^{-1}$  embedded in the equation.

Aerodynamic resistance between the surface and height  $z$  for use in Eq. (8-2) that uses the integrated stability correction forms is calculated as

$$r_a = \frac{\left[ \ln\left(\frac{z_u-d}{z_{om}}\right) - \Psi_{sm}(z_u/L) \right] \left[ \ln\left(\frac{z_{T,e}-d}{z_{oh}}\right) - \Psi_{sh}(z_{T,e}/L) \right]}{k^2 u_z} \quad (8-3)$$

where "ln" is the natural logarithm;  $k$  is the von Kármán constant (0.41); and measurement heights for wind speed,  $u_z$ , (at height  $z_u$ ) and temperature and vapor pressure (at height  $z_{T,e}$ ) may differ. The integrated stability functions in Eq. (8-3) must be solved using  $z/L = z_u/L$  [or  $(z_u - d)/L$ ] for  $\Psi_m$  and  $z/L = z_{T,e}/L$  [or  $(z_{T,e} - d)/L$ ] for  $\Psi_h$  using procedures from Chapter 7. These stability parameters can be set equal to zero for calculating  $\lambda E$  for reference surfaces where near-neutral conditions typically exist (Allen et al. 2006a) and for calculation with 24-h time steps. Variables  $z_{om}$  and  $z_{oh}$  are roughness parameters defined in Eqs. (8-7) and (8-8). Units for all  $z$  and  $d$  are in m.

For mean air temperature  $T = 21.5^\circ\text{C}$ ,  $\lambda$  has the commonly used value  $2.45 \times 10^6 \text{ J kg}^{-1}$ . When applied to 24-hour periods,  $R_n$ ,  $G$ ,  $r_a$ , and  $r_s$  in Eq. (8-2) should represent 24-hour totals or averages for these parameters (Jensen et al. 1990; Allen et al. 1996, 1998; ASCE 2005).

The combination equations that adhere to the form of Eq. (8-1) (Penman 1948, 1963; Doorenbos and Pruitt 1977; Wright and Jensen 1972; Wright 1982) produce straight-line relationships for ET as a function of wind speed at given values of  $R_n - G$ . However, some findings indicate that a curvilinear relationship might be more appropriate, e.g. Rijtema (1965), Pruitt and Doorenbos (1977, pp. 112–114), and Penman (1948, p. 129). The Wright (1982) wind function coefficients, redefined in Jensen et al. (1990), have values for  $a_w$  and  $b_w$  that vary with time of year. With the inclusion of the surface resistance term in the PM equation, the equation projects a curvilinear wind function, where the rate of increase in ET decreases with increasing wind speed. The traditional Penman form with linear wind function may overestimate ET under moderate to strong winds if the winds continue through the night and  $RH_{max}$  remains low. However, in the PM method, aerodynamic resistance decreases with higher wind speeds, resulting in an increase in  $\gamma(1 + r_s/r_a)$  and, in turn, a decrease in  $\{\Delta/[\Delta + \gamma(1 + r_s/r_a)]\}$  ( $R_n - G$ ). This has the effect of reducing the influence of the aerodynamic term of the PM equation on ET estimates for a given surface resistance,  $r_s$ . The PM method is thus less susceptible to overestimation under high wind conditions than are the traditional Penman models. The PM equation has the further advantage of flexibility in assigning roughness and surface resistance values to fit various types and heights of vegetation. This extends its direct application to a wide variety of surfaces and soil moisture conditions. A disadvantage of the logarithmic function for  $r_a$  in the PM equation as opposed to the linear wind function of the Penman equation with a constant offset,  $a_w$ , is the calculation of nearly

infinite aerodynamic resistance as  $u_2$  approaches 0. In reality, as  $u_2$  approaches 0 under positive  $R_n - G$ , sensible heat flux caused by warming of the surface will create buoyancy forces and consequent instability that will cause  $r_a$  to be substantially lower than infinity. To account for this compensatory process, Allen et al. (1998) and ASCE (2005) propose limiting  $u_2 \geq 0.5 \text{ ms}^{-1}$  during calculations.

The PM equation has been widely used to represent reference  $ET_o$  for use in irrigation management (Allen et al. 1989; Jensen et al. 1990; Martin et al. 1993; Allen et al. 1994b, 1994d, 1996, 1998, 2006a). When used with algorithms to increase surface resistance  $r_s$  (bulk stomatal resistance) under conditions of low soil water, the PM equation can be used to estimate actual ET,  $ET_a$ , for a wide variety of natural vegetation under nonpotential soil water conditions, as addressed in Chapter 11.

Saturation vapor pressure,  $e_s$ , for hourly periods is calculated as

$$e_s = e^o(T_{avg}) \quad (8-4a)$$

where  $T_{avg}$  is the average hourly temperature and  $e^o()$  is the saturation vapor pressure function given as Eq. (3-1). For daily or longer calculation time steps,  $e_s$  in the PM equation is computed using Eq. (8-4b) (Allen et al. 1989, 1996; ASCE 2005):

$$e_s = \frac{e^o(T_{max}) + e^o(T_{min})}{2} \quad (8-4b)$$

where  $T_{max}$  and  $T_{min}$  are maximum and minimum daily air temperature for the 24-hour period at  $z$  height, and  $e_s$  is the estimated average saturation vapor pressure during the period. Actual 24-hour vapor pressure of the air,  $e_z$ , or  $e_a$ , is generally computed as

$$e_z = e^o(T_d) \quad (8-5)$$

where  $T_d$  is daily average or early morning dew point temperature. Parameter  $e_a$  can also be calculated as average  $e_a$  during the 24-hour period. ASCE (2005) presents prioritized methods for estimating  $e_a$  from various humidity parameters and summarizes all calculation steps for the standardized  $ET_o$  and  $ET_r$  equations. Appendix H, Table H-4, summarizes this list.

### 8.3 AERODYNAMIC AND SURFACE PARAMETERS FOR THE PM EQUATION

When used to estimate ET from a dense grass or alfalfa reference, aerodynamic resistance in the PM equation can be calculated using the following parameter estimations (Allen et al. 1989, 1996; Jensen et al. 1990; Walter et al. 2000; ASCE 2005):

$$d = 0.67h \quad (8-6)$$

$$z_{om} = 0.12h \quad (8-7)$$

$$z_{oh} = 0.1z_{om} \quad (8-8)$$

where  $d$  is the zero plane displacement height,  $z_{om}$  is roughness length affecting momentum transfer, and  $z_{oh}$  is roughness length affecting sensible heat and vapor transfer.  $z_{om}$ ,  $z_{oh}$ ,  $d$ , and mean plant height,  $h$ , are in m. Aerodynamic resistance,  $r_a$ , is computed using Eq. (8-3). Additional equations for estimating  $z_{om}$  and  $d$  and general values for  $z_{om}$  for various types of vegetation are listed in Chapter 11.

Surface resistance,  $r_s$ , for densely growing vegetation is generally computed as

$$r_s = \frac{r_l}{LAI_{eff}} \quad (8-9)$$

where  $r_l$  is the bulk stomatal (or surface) resistance of the vegetation per unit  $LAI$  ( $\text{m}^{-1}$ ), and  $LAI_{eff}$  is the effective leaf-area index contributing to ET and energy exchange. Parameter  $r_l$  is the inverse of  $g_l$ , the stomatal conductance per unit leaf area, which is also discussed in Chapter 11. The value for  $r_l$  has been generally taken as  $100 \text{ s m}^{-1}$  for many well-watered agricultural crops (Monteith 1965; Szeicz and Long 1969; Allen et al. 1989, 1996; Jensen et al. 1990) when calculations are made on a 24-hour basis. When ET calculations are made on an hourly or shorter basis,  $r_l$  should be reduced to about  $70\text{--}80 \text{ s m}^{-1}$  for the well-watered and reference conditions. When deficient soil water reduces ET to less than maximum levels,  $r_l$  must be increased following procedures outlined in Chapter 11.

A "minimum" or "unconstrained" surface resistance,  $r_{s_{min}}$ , is defined and listed in Table 11-2 in Chapter 11 as the surface resistance when all environmental parameters (notably  $R_s$ ,  $T$ , VPD, and soil water) are at optimum levels. Under these conditions, values for a "minimum"  $r_l$ ,  $r_{l_{min}}$ , may be about  $40 \text{ s m}^{-1}$  for many agricultural crops. However, values for  $r_{l_{min}}$  should only be used in Eq. (8-9) in combination with stomatal conductance reducing functions [ $g()$ ; see Chapter 11], because the environmental parameters are rarely all at optimum levels necessary to sustain the  $40 \text{ s m}^{-1}$  value (Allen et al. 1996, 2006a). For purposes of standardization of the definition and calculation of reference ET, the values for  $r_s$  in Eq. (8-2) and consequently the value for  $r_l$  has been kept constant (ASCE 2005).

### Effective Leaf-Area Index

A standardized  $LAI_{eff}$  has been established for grass and alfalfa reference crops (Allen et al. 1989, 1994b, 1996; Jensen et al. 1990) as

$$LAI_{eff} = 0.5 LAI \quad (8-10)$$

The 0.5 multiplier suggests that generally only the upper half of a dense canopy such as dense stands of grass and alfalfa is active in heat and vapor transport and is the zone of major net radiation absorption (Szeicz and Long 1969). Field research on wheat by Choudhury and Idso (1985) supports the 0.5 multiplier. Ben-Mehrez et al. (1992) present an expression for  $LAI_{eff}$  that accounts for larger ratios of  $LAI_{eff}/LAI$  at small  $LAI$  and smaller ratios of  $LAI_{eff}/LAI$  when  $LAI$  is large:

$$LAI_{eff} = \frac{LAI}{0.3 LAI + 1.2} \quad (8-11)$$

Eq. (8-11) is based on data from Shuttleworth (1991) and Rochette et al. (1991) for semidense agricultural crops and estimates  $LAI_{eff} = 0.67 LAI$  at  $LAI = 1$  and  $LAI_{eff} = 0.24 LAI$  at  $LAI = 10$ . The equation estimates  $LAI_{eff} = (0.4 \text{ to } 0.5) LAI$  at  $LAI_s$  between 3 and 4, which are common for grass and alfalfa references, so that it is in general agreement with Eq. (8-10) when used with standard reference vegetation heights. Eq. (8-11) is intuitively attractive for practical use, because it automatically reduces effective  $LAI$  as  $LAI$  becomes large and as shading of interior leaves increases and air exchange inside canopies decreases. The equation may not apply to sparse vegetation such as in forests.

The  $LAI$  for dense, clipped grass can be computed following Allen et al. (1989) as

$$LAI = 24 h \quad (8-12)$$

where  $LAI$  is defined as the total leaf area (one side) per unit land area,  $\text{m}^2 \text{ m}^{-2}$ , and  $h$  is mean crop height, m, limited in Eq. (8-12) to  $\leq 0.4$  m. The  $LAI$  for an alfalfa reference crop was estimated by Allen et al. (1989) as

$$LAI = 5.5 + 1.5 \ln(h) \quad (8-13)$$

where  $h$  is in m, and  $h > 0.03$  m. Additional relationships for estimating  $LAI$  are given in Chapter 11.

## Stability Correction

The combination energy balance–aerodynamic methods (combination equations) used to estimate surface-to-air transfers are far less affected by stability conditions than are the purely aerodynamic equations [for example, Eq. (7-29)], especially for near-potential evaporation conditions and when estimating reference crop ET. However, for watersheds and other nonirrigated environments where inadequate precipitation reduces evaporation or transpiration to levels much lower than reference ET, hourly calculations with combination equations that include stability correction expressions are recommended. Chapter 11 describes these sorts of applications. Under inadequate water conditions, reduction in surface conductance functions (increases in surface resistance) may be an even more important consideration. Under reference conditions, the surface and air temperatures are generally within a few degrees of one another because  $\lambda E \rightarrow R_n - G$  so that  $H \rightarrow 0$  and  $T_s \rightarrow T_a$ . Therefore, stability correction is usually small and is ignored during calculation of reference ET (Allen et al. 2006a).

Chapter 11 includes examples of applying the PM equation to grass cover. The first of these examples (shown in Figure 11-12), showing half-hourly calculations with and without stability correction at Logan, Utah, and Davis, California, for the same days as in Figure 7-9 and 7-10, indicates that correction for stability over the well-watered grass surfaces is not nearly as important and critical for the PM equation as it is in estimating ET as  $\lambda E = R_n - G - H$ . The presence of  $1/r_a$  in both the numerator and denominator of the Penman-Monteith equation (PM) dampens the effect of aerodynamic stability or instability (and wind speed) on the ET estimate.

## 8.4 REFERENCE $ET_{ref}K_c$ APPROACH

The most common application of the Penman or PM equations to date for estimating evapotranspiration involves a two-step process. The two steps are (1) determining a reference  $ET_{ref}$ , which has generally been for either clipped grass (Doorenbos and Pruitt 1977; Allen et al. 1998, 2006a; ASCE 2005) or alfalfa (Wright and Jensen 1972; Wright 1982; Allen et al. 1989, 1996; ASCE 2005) and (2) multiplying  $ET_{ref}$  by a crop coefficient,  $K_c$ , to obtain an estimate of actual ET for a particular crop or surface condition, where

$$ET_c = K_c ET_{ref} \quad (8-14)$$

The  $K_c$  used in Eq. (8-14) must be the  $K_c$  associated with the specific reference type used (grass or alfalfa).

The two-step  $K_c ET_{ref}$  approach has been successful and widely applied for several reasons. One reason is the ready “visualization” of the crop coefficient,  $K_c$ , which generally has fixed limits governed by potential energy availability. Another reason for the widespread use of the  $K_c ET_{ref}$  approach has been the standardization of the  $ET_{ref}$  estimate (Smith et al. 1991; Allen et al. 1998; ASCE 2005) and the general consistency of  $K_c$ . Relating  $ET_{ref}$  to a specific reference and utilizing  $K_c$ s in a two-step process that separates processes between energy/aerodynamics and crop has the additional major advantage of giving the individual making calculations a mental representation of the process. In addition, selecting consistent crop coefficients and validating reference equations in new areas are somewhat straightforward.

The alternative to using the  $K_c ET_{ref}$  approach is the direct application of the Penman-Monteith or other multilayer combination equation to estimate actual ET directly (Monteith 1965; Shuttleworth and Wallace 1985). This approach, with the potential for more accurate estimates through more direct and graphic description of surface characteristics, is generally harder to apply and usually includes uncertainty in the exact nature of surface parameters and uncertainties that occur when using weather data collected above a surface that differs from that for which ET is estimated (Allen et al. 2005b). Also difficult is the incorporation of evaporation from underlying soil that varies with time and fraction of ground covered by vegetation. As discussed in Chapter 11, accurate application of the PM method to partial cover vegetation or to stressed vegetation requires the iterative determination of surface temperature to accurately incorporate the impacts of surface temperature on the calculation of  $\Delta$ , boundary layer stability, and emitted long-wave radiation from the surface. The impacts of surface temperature on all three terms can be substantial, as shown in Chapter 11.

When surface temperature is iteratively determined for the PM by solving the aerodynamic expressions for  $H$  and  $\lambda E$ , the need for the PM equation diminishes. In fact, the PM equation, when the relations for  $H$  and for  $\Delta$  as functions of surface temperature are inserted, reverts to the original energy balance equation that employs aerodynamic equations for  $H$  and  $\lambda E$ . Therefore, one can conclude that the PM method is only applicable to—and should be reserved for—well-watered conditions only, such as those represented by the reference ET definition. In fact, a well-watered surface, where surface temperature and air temperature can be assumed to be nearly equal because  $H$  is small, is a basic tenet and requirement of the Penman (1948) paper, where  $\Delta$  is computed using air temperature only.

### Reference ET Types and Definitions

For grass reference ET,  $ET_o$ , the reference crop is generally accepted to be a “cool-season” C-3 type of grass with roughness, density, leaf area, and bulk surface resistance characteristics similar to clipped perennial ryegrass

(*Lolium perenne* L.) or clipped tall fescue (*Festuca arundinacea*). Wright and Jensen (1972, p. 194) define alfalfa reference ET,  $ET_r$ , as, "... ET from well watered, actively growing alfalfa with 8 in. (20 cm) or more of growth . . .," and Wright (1982, p. 60) defines it as "... when the alfalfa crop was well watered, actively growing, and at least 30 cm tall; so that measured ET was essentially at the maximum expected level for the existing climatic conditions." The height of alfalfa (*Medicago sativa* L. v. ranger) in the data set used to develop surface resistance algorithms for the ASCE PM application to  $ET_r$  (Jensen et al. 1990) ranged from about 0.15 to 0.80 m in height and averaged 0.47 m (Allen et al. 1989).

Generally, reference ET for a tall crop like alfalfa is about 1.1 to 1.4 times that of a short crop like grass,  $ET_o$ , during summer months due to the greater roughness, higher leaf area, lower  $G$ , and lower  $r_s$  of alfalfa. The higher value (1.4) represents the ratio of  $ET_r$  to  $ET_o$  under arid and windy conditions [minimum daytime relative humidity ( $RH$ ) < 20%, and wind speed  $>5 \text{ m s}^{-1}$  (11 mph)] and the lower value (1.1) represents the ratio of  $ET_r$  to  $ET_o$  under humid, calm conditions (Pereira et al. 1999a; Wright et al. 2000).  $ET_r$  is sometimes preferred over  $ET_o$  because its larger roughness and leafiness cause it to better approximate the upper limit of ET expected from all types of vegetation (Pereira et al. 1999a). Wright and Jensen (1972) provide the following reasons for using alfalfa as a reference to represent maximum expected rates of ET. These reasons are still valid: (1) alfalfa has an extensive root system that minimizes the effects of decreasing soil water on ET; (2) it provides dense ground cover; (3) it has a low leaf resistance to the diffusion of water vapor; and (4) it is an aerodynamically rough crop. However, alfalfa as a reference has a few limitations. It does not grow well under some tropical conditions and at elevations above about 2,000 m, and it can be difficult to manage within reference conditions of full water supply, free of disease, and, in the case of lysimeters, constrained to the area of the lysimeter. Therefore it is not universally available to evaluate  $ET_r$  estimates using local measurements, and a virtual reference must be calculated using a standardized equation. This is generally not an issue, however, due to the international acceptance of the standardization. Cool-season grasses can be cultivated over a wide range of climates, seasons, and elevations, for example, at 4,000 m in Bolivia (Garcia et al. 2004), with the primary exceptions being lower elevations in hot tropical environments. However, the shallower root zone of grass can cause midday stress and reduced  $ET$  measurements under  $ET$  demands greater than about  $7 \text{ mm d}^{-1}$  (Wright et al. 2000).

Because of the challenges in growing and maintaining living reference vegetation, where the  $LAI$  and thus the value for  $r_s$  can vary between clippings for grass or cuttings for alfalfa by nearly a factor of two, a calibrated  $ET_{ref}$  equation is now generally used to represent the "hypothetical" and "fixed" reference. The Food and Agriculture Organization (FAO)

of the United Nations ([Smith et al. 1991, 1996; Allen et al. 1998](#)) has adopted the PM equation as a standardized definition for  $ET_o$  where values for  $r_s$ , surface albedo, and aerodynamic roughness are fixed (FAO-56). FAO Irrigation and Drainage Paper No. 56 ([Allen et al. 1998](#), p. 23) defines  $ET_o$  in terms of the PM equation as the rate of evapotranspiration from “a hypothetical reference crop with an assumed crop height of 0.12 m, a fixed surface resistance of  $70 \text{ s m}^{-1}$ , and an albedo of 0.23,” and where the reference surface “closely resembles an extensive surface of green grass of uniform height, actively growing, completely shading the ground and with adequate water.”

### Penman-Monteith as a Definition for Reference ET

Eq. (8-2) introduces the PM equation in its full form. The PM formulation of the combination equation incorporates aerodynamic and surface resistance terms that represent physical characteristics of the particular reference crop. Aerodynamic resistance in Eq. (8-2) is generally calculated using Eq. (8-3). Normally  $\Psi_m$  and  $\Psi_h$  are assumed to be zero because the reference surface is well watered so that boundary layer stability is close to neutral, or only mildly unstable, or stable and values for  $\Psi_m$  and  $\Psi_h$  are small ([Allen et al. 2006a](#)). This simplifies the calculation process and allows for the use of standard weather data of air temperature, vapor content, wind speed, and solar radiation.

### Reference ET Calculations

A range in height in the reference crop definitions (both for grass and alfalfa) has been necessary to allow the use of field ET measurements in calibrating and validating  $ET_{ref}$  equations. However, standardizing reference crop heights is necessary when applying  $ET_o$  and  $ET_r$  equations such as the PM equation to specifically characterize the surface parameters (roughness and bulk stomatal resistance) and to produce standardized climatic references. [Allen et al. \(1989\)](#), [Jensen et al. \(1990\)](#), [Smith et al. \(1991\)](#), [Allen et al. \(1994b; 1994d; 1996\)](#) and [ASCE \(2005\)](#) suggest adopting a fixed height of 0.12 m for the grass reference and 0.5 m for the alfalfa reference in the PM equation and associated fixed values for  $r_s$ .

### Standardization of the PM Equation for $ET_{ref}$

Standardized parameterizations of Eqs. (8-2) and (8-3) have been proposed by [ASCE \(2005\)](#) for both a short crop,  $ET_o$ , and a tall crop,  $ET_r$ , following the format adopted by FAO-56 ([Smith et al. 1991; Allen et al. 1998](#)). When the supporting parameter equations for  $r_a$ ,  $\rho_a$ , and  $\lambda$  are reduced and combined into Eq. (8-2), the FAO styled and reduced [ASCE \(2005\)](#) equation results:

$$ET_{ref} = \frac{0.408\Delta(R_n - G) + \gamma \frac{C_n}{(T+273)} u_2(e_s - e_a)}{\Delta + \gamma(1 + C_d u_2)} \quad (8-15)$$

where  $ET_{ref}$  applies to both clipped grass and alfalfa reference surfaces.  $ET_{ref}$  has units of  $\text{mm d}^{-1}$  for 24-hour time steps and  $\text{mm h}^{-1}$  for hourly time steps;  $R_n$  and  $G$  are in  $\text{MJ m}^{-2} \text{d}^{-1}$  or  $\text{MJ m}^{-2} \text{h}^{-1}$ ;  $T$  is mean daily or hourly air temperature ( $^{\circ}\text{C}$ );  $u_2$  is mean daily or hourly wind speed at 2-m height ( $\text{m s}^{-1}$ );  $e_s$  and  $e_a$  are in kPa;  $\Delta$  and  $\gamma$  are in  $\text{kPa}^{\circ}\text{C}^{-1}$ ; and  $C_n$  and  $C_d$  are coefficients that change with calculation time step, reference type (grass  $ET_o$  or alfalfa  $ET_r$ ), and, in some cases, with time of day, as shown in Table 8-1. Table 8-2 summarizes standardized terms for 24-hour and hourly versions. The values for hourly  $C_d$  for  $ET_o$  are based on the use of  $r_s = 50 \text{ sm}^{-1}$  during daytime and  $r_s = 200 \text{ sm}^{-1}$  during nighttime, and the 24-hour time step value for  $C_d$  is based on  $r_s = 70 \text{ sm}^{-1}$ . ASCE (2005) and Allen et al. (2006a) provide additional background on  $r_s$  for  $ET_o$ . For  $ET_r$ , the values for hourly  $C_d$  are based on the use of  $r_s = 30 \text{ sm}^{-1}$  during daytime and  $r_s = 200 \text{ sm}^{-1}$  during nighttime, and the 24-hour time step value for  $C_d$  is based on  $r_s = 45 \text{ sm}^{-1}$ . The standardized definitions imply vegetation heights for the  $ET_o$  and  $ET_r$  surfaces of 0.12 and 0.5 m, respectively.

Table 8-3 lists parameter equations recommended for use with the ASCE (2005) standardized  $ET_{ref}$ . Wind measured at heights other than 2 m above the ground surface can be adjusted to 2 m using Eq. (6-5) if the wind measurement is made over clipped grass and using Eq. (11-60) for wind measurement made over a surface other than clipped grass. Net radiation,  $R_n$ , in Eq. (8-15) can be measured, but is usually estimated due to challenges and expenses associated with accurate and unbiased measurement. When estimated, ASCE (2005) recommends standardized estimation procedures that use a fixed albedo of 0.23.

When Eq. (8-15) is used with daily values for  $C_n$  and  $C_d$  of 900 and 0.34, respectively, it is equivalent to the FAO-56 PM equation (Allen et al. 1998). However, when applied hourly, the values for  $C_n$ ,  $C_d$ , and  $G/R_n$  vary from Allen et al. (1998), although they are the same as a more recent recommendation on application of the FAO-56 equation on an hourly or shorter basis, where the coefficients of ASCE (2005) were recommended (Allen et al. 2006a).

The use of the standardized definitions for  $ET_o$  and  $ET_r$  provide for a consistent index of evapotranspiration that is readily compared between climates, locations, and time periods. The definition, although standardized, is tied to measurable surfaces, so that the full predictive equation (8-2) can be compared with local measurements when desired or necessary. When calculation of  $ET_o$  and  $ET_r$  follows that of ASCE (2005), the products are referred to as for  $ET_{os}$  and  $ET_{rs}$  where the "s" subscript refers to "standardization."

Table 8-1. Values for  $C_n$  and  $C_d$  in Eq. (8-15) and Ratios of  $G/R_n$  Used to Estimate Soil Heat Flux Density

Calculation Time Step	Short Reference, $ET_o$			Tall Reference, $ET_r$			Units for $ET_o$ , $ET_r$	Units for $R_n$ , $G$
	$C_n$	$C_d$	$G/R_n$	$C_n$	$C_d$	$G/R_n$		
Daily	900	0.34	0.00	1,600	0.38	0.00	$\text{mm d}^{-1}$	$\text{MJ m}^{-2} \text{d}^{-1}$
Hourly during daytime	37	0.24	0.10	66	0.25	0.04	$\text{mm h}^{-1}$	$\text{MJ m}^{-2} \text{h}^{-1}$
Hourly during nighttime	37	0.96	0.50	66	1.7	0.20	$\text{mm h}^{-1}$	$\text{MJ m}^{-2} \text{h}^{-1}$

Source: Data from ASCE (2005).

Table 8-2. ASCE Penman-Monteith Terms Standardized for Application of the Standardized Reference Evapotranspiration Equation

Term	$ET_{os}$	$ET_{rs}$
Reference vegetation height, $h$	0.12 m	0.50 m
Height of air temperature and humidity measurements, $z_h$	1.5–2.5 m	1.5–2.5 m
Height corresponding to wind speed, $z_w$	2.0 m	2.0 m
Zero plane displacement height, $d$	0.08 m	0.08 m <sup>a</sup>
Latent heat of vaporization, $\lambda$	2.45 MJ kg <sup>-1</sup>	2.45 MJ kg <sup>-1</sup>
Surface resistance, $r_s$ , daily	70 s m <sup>-1</sup>	45 s m <sup>-1</sup>
Surface resistance, $r_s$ , daytime	50 s m <sup>-1</sup>	30 s m <sup>-1</sup>
Surface resistance, $r_s$ , nighttime	200 s m <sup>-1</sup>	200 s m <sup>-1</sup>
Value of $R_n$ for estimating daytime	>0	>0
Value of $R_n$ for estimating nighttime	$\leq 0$	$\leq 0$

<sup>a</sup>The zero plane displacement height for  $ET_{rs}$  assumes that the wind speed measurement is over clipped grass, even though the reference type is tall. This is done to accommodate a majority of weather stations that are located over grass or other smooth surface. When wind speed is measured over a surface with vegetation taller than about 0.3 m, the wind speed measurement should be adjusted using Eq. (11-60).

Source: Parameters from ASCE (2005)

The wind height for Eq. (8-15) is fixed in the standardization at 2 m above the surface for consistency with prior usage (Pruitt and Doorenbos 1977; Wright 1982; Allen et al. 1998). However, the ASCE (2005) report on standardization encourages wind measurement at 3 to 4 m height, with subsequent adjustment to the 2-m standardized height using Eq. (6-5) or Eq. (11-60). The higher measurement height reduces impacts of tall agricultural crops, such as corn, and local obstacles, such as trees, buildings, and fences, on the wind measurement. Field corn is often taller than 2 m and can substantially reduce wind speed measured by nearby anemometers placed at 2 m (ASCE 2005). Wind speed measured over vegetation that is taller than about 0.3 m should be adjusted to that expected over clipped grass using Eq. (11-60).

### Preferred Time Steps for Reference ET Calculation

The ASCE (2005) standardization supports both 24-h and hourly (or shorter) calculation time steps. The 24-h calculation time step has proven to be generally consistent and accurate for estimating reference ET (Doorenbos and Pruitt 1977; Jensen et al. 1990; ASCE 2005), and many

Table 8-3. Equation Numbers for Recommended Parameter Estimation in the ASCE (2005) Standardized Penman-Monteith  $ET_{os}$  and  $ET_{rs}$  Equations

Parameter	Daily Calculation Time Steps		Hourly Calculation Time Steps	
	$ET_{os}$	$ET_{rs}$	$ET_{os}$	$ET_{rs}$
$\Delta$	Eq. (3-2)			
$\gamma$	Eq. (3-11b)			
$\lambda$	2.45 $\text{MJ kg}^{-1}$			
$P$	Eq. (3-14)			
$\alpha$	0.23			
$R_n$	Eqs. (4-31), (4-39) with $(T_{max}^4 + T_{min}^4)/2$ , 4.40a	Eqs. (4-31), (4-39) with $(T_{max}^4 + T_{min}^4)/2$ , 4.40a	Eqs. (4-31), (4-39), (4-40)	Eqs. (4-31), (4-39), (4-40)
$G$	0	0	0.1 $R_n$ daytime 0.5 $R_n$ nighttime	0.04 $R_n$ daytime 0.2 $R_n$ nighttime
$R_{so}$	Eqs. (4-3), (4-5)			
$u_2$	Eq. (6-5) or (11-60) with $d = 0.08 \text{ m}$ and $z_{om} = 0.015 \text{ m}$			
$e_s$	Eq. (8-4b)	Eq. (8-4b)	Eq. (8-4a)	Eq. (8-4a)
$r_a$	Eq. (8-3) <sup>a</sup>	Eq. (8-3) <sup>a</sup>	Eq. (8-3) <sup>a</sup>	Eq. (8-3) <sup>a</sup>

Note: Equation numbers in cells refer to equations in the main text and appendixes  
<sup>a</sup> $r_a$  is embedded into the standardized PM form, with integrated stability terms set to zero

lysimeter-based studies have used the 24-h time step as a basis for calibration or verification of reference ET methods. ASCE (2005) uses the ASCE-PM equation and associated component equations on a 24-h calculation time step as the basis for the development of standardization of reference ET calculation in the United States (Itenfisu et al. 2003). The general consistency and accuracy of the PM method for 24-h time steps speaks to the combination equation's robustness in estimating evaporative behavior given a particular set of meteorological conditions.

ASCE (2005) presents a comprehensive comparison of major reference ET equations using weather data from 49 sites across the United States. The 16 states contributing data ranged from New York to California and from Florida to Washington and represented diverse climates, ranging from humid to arid (Itenfisu et al. 2003). Site elevations ranged from 2 to 2,895 m, and mean annual precipitation ranged from 150 to 2,030 mm. ASCE (2005) shows the ASCE-PM, when applied hourly to the 49 locations and then summed daily, to closely match estimates made on 24-hour calculation time steps. The yearly ratio of summed hourly to daily estimates for the alfalfa reference averaged 0.98 and ranged from 0.90 to 1.07 over the 49 locations, and the growing season ratios averaged 0.995 and ranged from 0.90 to 1.08. The yearly ratio of summed hourly to daily estimates for the grass reference (defined by the standardized ASCE-PM equation) averaged 1.01 over all locations and ranged from 0.94 to 1.08 with a standard deviation in ratios of 0.029 (ASCE 2005; Allen et al. 2006a).

The standardized PM method applied daily is considered to be accurate and dependable during growing periods. It was, in fact, used during the ASCE standardization work to confirm the selection of surface resistance values for hourly time step applications. The daily time step, however, may not accurately estimate reference ET during freezing winter and other nongrowing season periods, where conditions represented by the reference crop do not physically exist (surface resistance of  $45 \text{ s m}^{-1}$  for  $ET_{rs}$  and  $70 \text{ s m}^{-1}$  for  $ET_{os}$  over a 24-h period). The hourly calculation time step, because it keeps radiation and aerodynamic parameters synchronized in time, is considered to be more dependable and accurate in simulating the ET conditions represented by the standardized definitions, especially under conditions where wind speed, solar radiation, and vapor pressure deficit are not in proximate time synchronization during the day. The use of hourly time steps enables a more accurate energy balance process calculation than 24-h time steps during times of the year when day length is relatively short. During these times, some of the compensating assumptions in the procedures for applying the combination method on a 24-h time step may break down.

Application of ET equations over only daytime periods (i.e., ignoring calculations during nighttime) is discouraged. This practice ignores any ET

that may occur during nighttime, which can be as much as 15% of 24-h ET in arid and semiarid climates (Tolk et al. 2006). In addition, application of the combination or energy balance equation solely for a daytime period requires estimation of soil heat flux,  $G$ , which cannot be assumed to be zero as it generally can for 24-h calculation time steps.

Values calculated for reference ET for nighttime hours occasionally take on negative values. The user may feel compelled to set negative values to zero before summing over the 24-hour period. However, in some situations, negative hourly computed  $ET_{os}$  or  $ET_{rs}$  may indicate some condensation of vapor during periods of early morning dew and should therefore be registered as negative during the summing of 24-hour ET. In other situations, negative hourly  $ET_{os}$  or  $ET_{rs}$  during nighttime reflects the uncertainties in some parameter estimates, including  $R_n$  and assumptions implicit to the combination equation, and represent some of the random variation of ET estimates about a mean value that may be zero during some nighttime periods. These random negative ET estimates should be retained in the 24-h sum to counterbalance random positive ET estimates during the same nighttime period. In general, the impact of negative hourly values on ET summed over daily periods is usually less than a few percent.

### 1985 Hargreaves-Samani Equation

The Hargreaves-Samani equation (Hargreaves and Samani 1982, 1985) is suggested as a means for estimating  $ET_o$  in situations where data are limited and contain only maximum and minimum air temperatures along with location latitude. The Hargreaves-Samani (H-S) equation is not recommended in regions with consistently windy conditions (daily mean  $u_2 > \sim 3.0 \text{ m s}^{-1}$ ) and/or low  $RH_{min}$  ( $RH_{min} < \sim 20\%$ ) without calibration or confirmation using the ASCE-PM method. The equation may tend to overestimate in humid climates (Hargreaves and Allen 2003, 2004) and should be verified using the ASCE-PM method. The form of the 1985 H-S equation is

$$ET_o = 0.0023(T_{max} - T_{min})^{0.5}(T_{mean} + 17.8)\left(\frac{R_a}{\lambda\rho_w}\right) \quad (8-16)$$

where  $T_{max}$  and  $T_{min}$  are maximum and minimum daily air temperature in °C,  $T_{mean}$  is mean daily air temperature  $[(T_{max} + T_{min})/2]$ , and  $R_a$  is average daily exoatmospheric radiation [Eq. (4-11)] with units of  $\text{MJ m}^{-2} \text{ d}^{-1}$ .  $\rho_w$  is the density of liquid water ( $1.0 \text{ Mg m}^{-3}$ ) and  $\lambda$  has units of  $\text{MJ Rg}^{-1}$ .  $ET_o$  in Eq. (8-16) has the same units as  $R_a/(\lambda\rho_w)$ , typically  $\text{mm d}^{-1}$ .

The 1985 H-S equation was the highest ranked temperature-related method for calculating  $ET_o$  reported in the ASCE 70 analysis (Jensen et al.

1990). Allen (1992) finds Eq. (8-16) to estimate well in a wide range of latitudes and climates for periods of five days or longer without significant error.

The principal feature of the H-S equation is the inclusion of the difference between maximum and minimum daily air temperature. The temperature difference indicates general humidity and cloudiness. This occurs due to the fact that when humidity levels are high, differences between  $T_{max}$  and  $T_{min}$  are somewhat low and ET rates are somewhat low. The lower temperature differences occur because higher dew point temperatures under conditions of high humidity hold  $T_{min}$  to relatively higher levels. When cloud cover occurs, maximum temperatures are lower due to decreased solar radiation, and minimum temperatures are usually higher due to increased long-wave emittance and reflection by nighttime cloud cover.

One advantage of an equation such as the 1985 H-S equation over more complex equations is the reduced data requirement. For the 1985 H-S equation, only maximum and minimum air temperatures are required in addition to exoatmospheric solar radiation, which can be calculated for any latitude. This is advantageous in regions where solar radiation, humidity, and wind data are unavailable or of poor quality. Generally, air temperature can be measured with less error and by less trained individuals than can the other three parameters required by combination equations. Eq. (8-16) can be calibrated against the PM equation [Eq. (8-15)] where data are available to produce a "regionally" calibrated temperature equation.

An alternative to using a temperature-based equation such as Eq. (8-16) when data are lacking is to employ the PM equation using estimates for missing variables. Generally, applying Eq. (8-15) on a daily or monthly basis with  $R_s$  estimated using Eq. (4-26) or Eq. (4-27) with Eq. (4-28) or (4-29);  $T_d = T_{min} - K_o$ , where  $K_o$  varies from 0 for humid regions to as much as 5°C for arid regions (ASCE 2005); and  $u_2 = 2 \text{ ms}^{-1}$  provides estimates similar to Eq. (8-16) for agricultural weather sites (Droogers and Allen 2002; Hargreaves and Allen 2003; Allen and Robison 2007). Appendix E of ASCE (2005) contains recommendations for estimating missing weather parameters. Selected material from that appendix is presented in the following section.

### ***ET<sub>o</sub>* Software Programs**

Allen (2012) and Snyder (2004) present software programs for computing  $ET_{ref}$  by various common and popular  $ET_{ref}$  equations. These personal computer-based programs are useful for calculating  $ET_{ref}$  and comparing estimates among various reference equations and for validating  $ET_{ref}$  computations.

## 8.5 MISSING OR BAD WEATHER DATA

The calculation of reference ET with the standardized ASCE-PM reference ET equation requires air temperature, vapor pressure, solar radiation, and wind speed data. The climate data should reflect the environment within the area for which an estimate of ET is required. If some of the required weather data are missing or do not accurately represent an irrigated site/region or are erroneous, then data may be estimated to apply the equation. The quality of calculated reference ET values depends on the quality and completeness of weather data. If the estimated data for missing periods are reasonably representative of a site within a well-watered area, then the reference ET values from the standardized equation calculated with these data are likely to be more reliable than reference ET estimates made using other more empirical ET methods such as Eq. (8-16). This section provides procedures for estimating solar radiation, vapor pressure, and wind speed data when they are missing or of questionable quality. Users should employ some type of “flagging” procedure to clearly identify data that have been estimated.

### Minimum Data Requirements

Many of the suggested procedures for estimating missing data are based on measured maximum and minimum air temperatures. Daily maximum and minimum air temperature, or at the very least daily mean air temperatures, are considered to be the absolute minimum data requirements necessary to apply the standardized PM method. In situations where solar radiation, humidity, and wind speed data are available, but air temperature data are missing, temperature may be estimated from a nearby weather station site using some form of regression or interpolation-extrapolation procedures. Estimated temperature data should not be used at a site if the temperature data are subsequently used to estimate humidity and solar radiation data, as the resulting  $ET_{ref}$  would essentially have been calculated using no local data.

### Estimates of Missing Humidity Data

Where daily humidity data are missing or of questionable quality, vapor pressure,  $e_a$ , can be estimated for the reference environment by assuming that dew point temperature ( $T_{dew}$ ) is near the daily minimum air temperature ( $T_{min}$ ):

$$T_{dew} = T_{min} - K_o \quad (8-17)$$

where  $K_o$  is approximately 2 to 5°C in dry (semiarid and arid) climates and  $K_o$  is approximately 0°C in humid to subhumid climates. Allen and Robison (2007) develop values for  $K_o$  that vary monthly for application throughout

Idaho. The values were based on observations of  $K_o$  at automated weather stations located in agricultural environments. Under extremely dry conditions, such as in the American southwest, where daytime  $RH$  can drop near to 10% even under reference conditions,  $K_o$  may take on values of 5 to 10°C. An alternative to applying Eq. (8-17) is to assume that relative humidity,  $RH$ , approaches 90 to 100% during early morning hours (before sunrise) over well-watered (i.e., reference) settings so that the assumption that  $RH_{max} \sim 90\%$  or  $RH_{max} \sim 100\%$  can be employed. Daily vapor pressure is then calculated using the estimated  $RH_{max}$  and measured  $T_{min}$ :

$$e_a = e^o(T_{min}) \frac{RH_{max}}{100} \quad (8-18)$$

where  $e_a$  is estimated vapor pressure, kPa;  $e^o(T_{min})$  is saturation vapor pressure at daily minimum temperature, kPa; and  $RH_{max}$  is daily maximum relative humidity. However, use of  $RH_{max} \sim 100\%$  is equivalent to using  $K_o \sim 0^\circ\text{C}$  in Eq. (8-17), which may overestimate  $T_{dew}$ .

When humidity data are available from a nearby station, for example, within 100 km, the user can estimate  $T_{dew}$  for a site having no humidity data or having faulty data using Eq. (8-19):

$$T_{dew} = T_{min} - (T_{min} - T_{dew})_{stn2} \quad (8-19)$$

where  $(T_{min} - T_{dew})_{stn2}$  is the measured difference at the nearby weather station. This relationship presumes that differences between  $T_{dew}$  and  $T_{min}$  are similar between stations. Similar results and estimates of humidity can be obtained by transferring  $RH$  measurements between locations and calculating  $e_a$  using the transferred  $RH$  data and local air temperature. The similarity in relationships between  $T_{dew}$  and  $T_{min}$  or in  $RH$  should be confirmed using temporary measurement of humidity or analysis of data from adjacent stations having overlapping periods.

By definition, reference  $ET_{os}$ , or  $ET_{rs}$ , is ET from an extensive surface of well-watered vegetation. Therefore, when humidity data are available only from a site that is known to deviate substantially from a reference environment, then use of "adjusted" dew point temperature in the standardized PM equation may produce more reliable and representative reference ET than those obtained using the original humidity data from the nonreference site. The user should "flag" any estimated humidity data and describe the procedures that were used.

### Estimates of Missing Solar Radiation Data

**Solar Radiation Data Derived from Observed Sunshine Hours** If observed hours of sunshine are measured, solar radiation for 24-hour and longer time periods can be estimated using the Angstrom formula, which

relates solar radiation to exoatmospheric radiation and relative sunshine duration ([Doorenbos and Pruitt 1977](#)):

$$R_s = \left( a_s + b_s \frac{n}{N} \right) R_a \quad (8-20)$$

where  $R_s$  is solar or shortwave radiation,  $\text{MJ m}^{-2} \text{d}^{-1}$ ;  $n$  is actual duration of sunshine, hours;  $N$  is the maximum possible duration of sunshine or daylight hours;  $n/N$  is relative sunshine duration, dimensionless;  $R_a$  is exoatmospheric radiation,  $\text{MJ m}^{-2} \text{day}^{-1}$  ([Chapter 4](#));  $a_s$  is a constant expressing the fraction of exoatmospheric radiation reaching the earth's surface on overcast days (when  $n=0$ );  $b_s$  is a constant expressing the additional fraction of exoatmospheric radiation reaching the earth's surface on a clear day; and  $a_s + b_s =$  fraction of exoatmospheric radiation reaching the earth's surface on a clear day (when  $n=N$ ).

$R_s$  in Eq. (8-20) is in  $\text{MJ m}^{-2} \text{d}^{-1}$  for  $R_a$  in  $\text{MJ m}^{-2} \text{d}^{-1}$ . Depending on atmospheric conditions (humidity, dust), solar declination (latitude and month), and typical cloud type and density, the Angstrom values  $a_s$  and  $b_s$  will vary. Where no actual solar radiation data are available and no calibration has been carried out for improved  $a_s$  and  $b_s$  parameters, the values  $a_s = 0.25$  and  $b_s = 0.50$  from FAO 24 ([Doorenbos and Pruitt 1977](#)) and FAO-56 ([Allen et al. 1998](#)) are recommended. Accuracy of Eq. (8-20) and values for coefficients  $a_s$  and  $b_s$  should be assessed at a location in the region where measured  $R_s$  and  $n$  data are available.

The potential daylight hours,  $N$ , are given by

$$N = \frac{24}{\pi} \omega_s \quad (8-21)$$

where  $\omega_s$  is the sunset hour angle in radians and is calculated using Eq. (4-14).

**Solar Radiation Data from a Nearby Weather Station** For 24-hour and longer time periods, solar radiation can be relatively similar over large areas. Similarity in solar radiation depends on (1) the size of the region, (2) the air masses governing rainfall and cloudiness being similar across the region, and (3) the physiographic characteristics being similar. Differences in relief can strongly influence the movement of air masses and development of cloud systems, so that these should be small if radiation data are to be transferred between locations. Generally, calculations of daily reference ET using estimated radiation data are justified when utilized as a sum or as an average over a multiple-day period so that differences due to frontal activity or individual convective cloud systems tend to average out. This is the case for the computation of total ET demand between successive irrigations or when planning irrigation schedules. Under these conditions,

the relative error for one day may be compensated by an error for another day within the time period.

**Solar Radiation Data Derived from Air Temperature** Solar radiation can be estimated using an empirical equation derived using the difference between maximum and minimum air temperature and exoatmospheric solar radiation. The difference between the maximum and minimum air temperature relates to the degree of cloud cover at a location. Clear sky conditions result in higher air temperatures during the day (i.e.,  $T_{max}$ ) than under cloudy conditions because the atmosphere is transparent to incoming solar radiation. Clear sky conditions result in relatively lower air temperatures during nighttime (i.e.,  $T_{min}$ ) than under cloudy conditions because less outgoing long-wave radiation is absorbed and re-emitted by the atmosphere. In contrast, under overcast conditions,  $T_{max}$  is often lower than on clear days because a significant portion of the incoming solar radiation never reaches the earth's surface and is absorbed and reflected by the clouds. Similarly,  $T_{min}$  will be relatively higher because cloud cover acts as an absorbing and re-emitting blanket and therefore decreases the net outgoing long-wave radiation. Therefore, the difference between the maximum and minimum air temperature ( $T_{max} - T_{min}$ ) can be used as an indicator of the fraction of extraterrestrial radiation that reaches the earth's surface. This principle was used by Hargreaves and Samani (1982) to develop estimates of  $ET_o$  using only air temperature data. The Hargreaves-Samani style of radiation prediction formula [also introduced as Eq. (4-26)] has the form:

$$R_s = k_{R_s} \sqrt{(T_{max} - T_{min})} R_a \quad (8-22)$$

where  $R_a$  is exoatmospheric radiation,  $\text{MJ m}^{-2} \text{d}^{-1}$ ;  $T_{max}$  is maximum air temperature,  $^{\circ}\text{C}$ ;  $T_{min}$  is minimum air temperature,  $^{\circ}\text{C}$ ; and  $k_{R_s}$  is an adjustment coefficient,  $^{\circ}\text{C}^{-0.5}$ . The adjustment coefficient  $k_{R_s}$  is empirical and differs for "interior" and "coastal" regions. The values presented here for  $k_{R_s}$  are from Allen et al. (1998):

- For interior locations, defined as where the local land mass dominates and air masses are not strongly influenced by a large water body,  $k_{R_s} \approx 0.16$ ; and
- For coastal locations, situated on or adjacent to the coast of a large land mass and where air masses are influenced by a nearby water body,  $k_{R_s} \approx 0.19$ .

$R_s$  estimated by Eq. (8-22) should be limited to  $\leq R_{so}$ , which is the  $R_s$  for a cloud-free day. The temperature difference method is recommended for locations where importing radiation data from a regional station is not appropriate, either because homogeneous climate conditions do not occur,

or because data for the region are lacking. For island conditions, the methodology is not appropriate due to the moderating effects of the surrounding water body. Bristow and Campbell (1984) present an equation similar to Eq. (8-22). However, their formulation is more complex to apply and is of similar accuracy (Ball et al. 2004). Allen (1997) demonstrates the application of Eq. (8-22) with means to autocalibrate  $k_{R_s}$  using the  $R_{s0}$  clear sky envelope for seven locations in the western United States. Amatya et al. (2000) find the Allen autocalibration technique to provide good estimates of daily solar radiation at three locations in North Carolina. The Thornton and Running (1999) equation for estimating  $R_s$  from air temperature builds on Bristow and Campbell (1984) and was introduced as Eqs. (4-27) and (4-28). The Thornton-Running method has advantages over Eq. (8-22) in that it is self-limiting to  $R_{s0}$  as an upper bound and tends to estimate more representative ranges in  $R_s$  under cloudy conditions, as illustrated by Allen and Robison (2007).

### Missing Wind Speed Data

**Wind Speed Data from a Nearby Weather Station** Extrapolating wind speed data from a nearby agricultural weather station, as for radiation data, relies on the assumption that the airflow is similar within the region. Large variation in wind speed can occur through the course of a day, which can translate into substantial differences in concurrent measurements of wind speed at two locations. However, when averaged over time periods of one day or longer, differences between locations become smaller. Data from a weather station may be extrapolated to a nearby location where  $ET_{ref}$  is to be estimated if the governing air masses are of the same origin and location where the same weather frontal systems govern the regional airflow. The surrounding relief of the two locations should be similar. In areas having large differences in relief, density-induced "drainage" of air and shielding and direction of air movement by relief can cause substantial differences in observed wind speed over relatively short distances. Where short periods of wind data are available for the location, ratios of wind speed between two locations can be established and used to estimate wind data for the data-short location.

Wind speed data from airports in the United States typically are measured at a height of 10 m. In arid and semiarid areas, the airport anemometer is often surrounded by nonirrigated, short grass. Wind speed from airports measured at 10 m height, when adjusted to 2 m height using the logarithmic wind profile, may exceed wind speed that is measured at 2 m height in an agricultural area during the growing season. This can occur because of greater vegetation roughness of agricultural crops, as compared with airport environments, and more entrainment of higher velocity air from aloft over an airport because of increased air buoyancy caused by larger  $H$ .

When extrapolating wind speed data from another station, trends in other meteorological parameters and relief should be compared. Strong winds are often associated with low relative humidity, and light winds are common with high relative humidity. Thus, trends in variation of daily maximum and minimum relative humidity should be similar in both locations. In mountainous areas, data should not be extrapolated from the nearest station but from nearby stations having similar elevation, similar vegetation surrounding the sensors, and similar exposure to the dominant winds. The pairing of stations may vary from one season to another, depending on the dominant winds.

**Empirical Estimates of Monthly Wind Speed** The variation in average wind speed between monthly periods is often relatively small and fluctuates around average values. Therefore, in situations of no, or faulty, wind speed data, monthly values of wind speed may be estimated based on general information available for the regional climate, taking seasonal changes into account. Or, if regional information is unavailable, general values for wind speed suggested in Table 8-4 can be employed with caution.

A preliminary value of  $2 \text{ m s}^{-1}$  can be used as a first estimate of 2-m wind speed for an agricultural setting. This value is based on an average computed from more than 2,000 weather stations around the globe (Allen et al. 1998). In general, estimated wind speed at 2 m should be limited to about  $u_2 \geq 0.5 \text{ ms}^{-1}$  when used to calculate standardized reference ET. This lower limit accounts for the influence of boundary layer instability caused by buoyancy of air in promoting exchange of heat and vapor at the surface when air is calm. This effect occurs when the wind speed is small and buoyancy of warm air induces air exchange at the surface. As with humidity and solar radiation data, estimated wind speed data should be flagged in the data set, and the user should describe the procedures used to make the estimates.

Table 8-4. General Classes of Wind Speed Data

Description	Mean Wind Speed at 2 m
Light wind	$\leq 1.0 \text{ m s}^{-1}$
Light to moderate wind	$1\text{--}3 \text{ m s}^{-1}$
Moderate to strong wind	$3\text{--}5 \text{ m s}^{-1}$
Strong wind	$\geq 5.0 \text{ m s}^{-1}$

Source: Data from FAO-56 (Allen et al. 1998)

A growing source of wind data is the use of “gridded” weather data, which is becoming more readily available from the North American Land Data Assimilation System (NLDAS) and Global Land Data Assimilation System (GLDAS). These data sets are described in a following section. The “reanalysis” data sets provide some gridded data going back to the 1950s that are available via the Internet. Certain precautions regarding ‘dryness’ of the data sets are needed in using these data sets for agricultural areas, as described in the section titled “Gridded Weather Data from Climate and Land Process Models” near the end of this chapter.

### Missing Maximum or Minimum Air Temperature Data

Some weather data sets contain daily mean air temperature summaries but do not contain values for maximum and minimum air temperature. Daily maximum and minimum air temperatures are used in the standardized reference ET procedure for calculating net radiation and the saturation vapor pressure. During the process of calculating daily  $ET_{ref}$  using data sets where  $T_{max}$  and  $T_{min}$  are not available, but where daily mean air temperature and solar radiation data are available, accuracy of calculations for net radiation and saturation vapor pressure can be improved by estimating values for  $T_{max}$  and/or  $T_{min}$  by inverting Eq. (8-22) and solving for  $T_{max} - T_{min}$ :

$$(T_{max} - T_{min})_{est} = \left( \frac{R_s}{k_{R_s} R_a} \right)^2 \quad (8-23)$$

where  $R_s$  is measured solar radiation,  $\text{MJ m}^{-2} \text{d}^{-1}$ ;  $R_a$  is exoatmospheric radiation,  $\text{MJ m}^{-2} \text{d}^{-1}$ ;  $T_{max}$  is maximum air temperature,  $^{\circ}\text{C}$ ;  $T_{min}$  is minimum air temperature,  $^{\circ}\text{C}$ ; and  $k_{R_s}$  is an adjustment coefficient, defined previously,  $^{\circ}\text{C}^{-0.5}$ .

Values for  $T_{max}$  and/or  $T_{min}$  can be estimated using  $(T_{max} - T_{min})_{est}$  from Eq. (8-23) as follows:

$$T_{max} = T_{mean} + \frac{(T_{max} - T_{min})_{est}}{2} \quad (8-24a)$$

$$T_{min} = T_{mean} - \frac{(T_{max} - T_{min})_{est}}{2} \quad (8-24b)$$

The estimated values for  $T_{max}$  and  $T_{min}$  should be clearly identified in the data set as estimated values.

## Gridded Weather Data from Climate and Land Process Models

Until recently, the modeling of reference ET was solely based on important weather variables collected from weather stations that are generally located on selected agro climatic locations. Since 2000, the North American Land Data Assimilation System (NLDAS) and Global Land Data Assimilation System (GLDAS), operated by the National Oceanic and Atmospheric Administration (NOAA), National Centers for Environmental Prediction (NCEP), and National Center for Atmospheric Research (NCAR) have produced climate parameter data sets for each three and six hours that include the meteorological variables required to calculate daily reference ET. These data sets are produced for the whole globe at 1-degree spatial resolution and for North America at 12- and 32-km resolution. The data are produced by somewhat complex land process models operated for weather forecasting and climate change modeling. The models are “forced” using available weather measurements from selected sites around the globe. Results are generally available from NOAA and other websites.

The USGS at the Center for Earth Resources Observation and Science (EROS) has been producing daily reference ET since 2000 ([Senay and Verdin 2003](#)), and the results have been used for various models for drought and streamflow monitoring on an operational basis. Senay et al. ([2005, 2007](#)) evaluated GLDAS-based reference ET estimates using data from the California Irrigation Management Information System (CIMIS). Daily CIMIS  $ET_o$  estimates from more than 120 stations were compared with GLDAS-based  $ET_o$  at different spatial and temporal scales using 2004 data. Despite large differences in spatial scale (point measurements for CIMIS vs. approximately 100-km gridded data for GLDAS), correlations between station-based ET and GLDAS ET were high, exceeding 0.90 on a daily basis to more than 0.98 on time scales of more than 10 days ([Senay et al. 2005](#)).

A second gridded data set is the International Water Management Institute (IWMI) World Water and Climate Atlas (<http://www.iwmi.cgiar.org/WAtlas/>), which includes monthly and annual summaries for weather data on a 10-minute arc (one-sixth of a degree) grid. The data include precipitation, air temperature, humidity, hours of sunshine, wind speed, total number of days with and without rainfall, days without frost, and reference  $ET_o$  based on the FAO Penman-Monteith equation. The atlas grid was assembled from 30,000 weather stations around the globe from the period 1961–1990. The atlas data are intended to support irrigation and agricultural planning.

When used to calculate  $ET_{ref}$ , the GLDAS, NLDAS, and other data sets should be reviewed to determine whether the gridded data contain substantial “artifacts” of dryness of the original weather data used to drive the models and assumptions in the GLDAS models. These artifacts

may produce weather data that are characteristic of regional weather systems, which in semiarid and arid climates reflect general aridity of the region and may not exhibit the conditioning effects of irrigation where air temperature is reduced and humidity content is increased by ET supplied by irrigation. Generally, the models creating the gridded data sets do not include irrigation in the daily soil water balances used to partition available energy into  $H$  and ET. Lewis et al. (2014) and McEvoy et al. (2014) represent first attempts at comparing NLDAS gridded weather data to agricultural ground-based weather data in the western United States. The user can review solar radiation daily  $RH_{max}$  or dew point and daily minimum air temperature data in the gridded data sets following recommendations by ASCE (2005) to assess general aridity of the data sets.  $ET_o$  from the IWMI Climate Atlas was evaluated for aridity effects by Droogers and Allen (2002).

## 8.6 REFERENCE ET BY ANALOGY OR ASSOCIATION

Reference ET has been associated with measured evaporation from atmometers and from evaporation pans to produce estimates of reference ET. These measurement systems can represent conditions within a local environment, which may be useful for some applications.

### Evaporimeters and Atmometers

The use of evaporation pans to estimate evaporation from water bodies was introduced earlier, along with some of the factors that can produce a wide range of results as related to the local environment, placement, size of pan, etc. Pans and atmometers have been used more widely in estimating crop water use than in lake evaporation estimation. Pruitt and Doorenbos (1977) list 15 references that involved some eight different countries where the pan evaporation method was used significantly in irrigation scheduling schemes. In terms of the percentage of irrigable land within a country, where evaporation pans have played an important part, the country of Israel probably leads the list. An early reference for Israel is Stanhill (1962b), which summarizes  $ET/E_p$  relationships for many crops reported later by Shalhev et al. (1981). Chapter 6 describes various types of evaporation pans.

**Reference ET from Pan Evaporation** Pan evaporation data can be used to estimate  $ET_{ref}$  from the simple proportional relationship of

$$ET_{ref} = k_p E_p \quad (8-25)$$

where  $ET_{ref}$  is reference crop ET,  $k_p$  is a pan coefficient that is dependent on the pan type involved and several other factors as discussed earlier,

and  $E_p$  is measured pan evaporation. When the reference crop is short, well-watered grass, the reference ET is referred to as  $ET_o$ . Pruitt and Doorenbos (1977) describe the development of the FAO 24 pan evaporation method, which was first published in Jensen (1973) and subsequently by Doorenbos and Pruitt (1975, 1977), Burman et al. (1980), Jensen et al. (1990), Shuttleworth (1992), Woottton et al. (1996), and Allen et al. (1998). The method is based primarily on studies of the effect of pan type, local environment, and general weather conditions on  $k_p$  by Ramdas (1957), Pruitt (1960, 1966), and Stanhill (1962a).

The FAO 24 pan method provides tables of recommended  $k_p$ s for the Class A pan, upwind fetch of both dry- and wet-surface environments, mean relative humidity, and daily wind run. Table 8-5 reproduces the original tables for the Class A pan as developed by Pruitt in the FAO analysis, rounded off to the nearest 0.01 rather than to 0.05. Figure 8-1 presents a sketch explaining an idealized situation for both dry (Case A) and wet (Case B) upwind fetches.

Many weather stations do not easily fit into the simplified classifications suggested in Figure 8-1. One exception is illustrated by a weather station planted to Bermuda grass that was dormant during several months of the year (Case B) and was a green, growing crop during other months (Case A). The Case B classification might apply well for weather stations with bare soil environments during dry seasons of the year, but Case A may be more appropriate during consistently rainy periods. Doorenbos and Pruitt (1977) envision another complicated situation, suggesting that when pans are placed in a small enclosure surrounded by tall crops, the coefficients for dry, windy climates should be increased by up to 30% to account for shielding of wind over the pan, but for calm, humid conditions, a 5 to 10% increase should be sufficient to compensate for wind shielding of the pan by the tall crop, because evaporation is dominated by solar radiation under humid conditions.

In addition to the variation of  $k_p$  with wind and humidity, an interaction also occurs with radiation intensity. Because smaller coefficients under drier and windier conditions are largely the result of greater response of pans to sensible heat advection as compared with crops (short, smooth crops), the relative effect (and hence, coefficients) will be greater under the lower radiation conditions of fall, winter, and spring than under the higher radiation of midsummer (Jensen et al. 1990).

### Pan Coefficients

The coefficients in Table 8-5 apply to National Weather Service (NWS) Class A pans mounted on a standard wooden platform such that the top of the pan is about 0.4 m above the surrounding ground level. For the Case A siting, the grass should be irrigated during dry periods, frequently enough

Table 8-5. Suggested Values of  $k_p$  for Relating Evaporation from a U.S. Class A Pan to ET from 0.08–0.15 m Tall, Well-Watered Grass Turf ( $ET_o$ ), Based on Original FAO Analysis Leading to FAO 24 Pan Method

2-m Wind km/day	Case A: Pan Surrounded by Short, Green, Growing Crop, Preferably Grass, or a Wet Soil Surface						Case B: Pan Surrounded by Dry, Bare Soil or Dry, Dormant Grass							
	$(RH_{\max} + RH_{\min})/2$			$(RH_{\max} + RH_{\min})/2$			Dry			Low			Med	High
	Wet	Low	Med	High	Upwind Fetch, m	<40%	40–70%	>70%	Upwind Fetch, m	<40%	40–70%	>70%		
Light <175 km/d(< 2 m/s)	0	0.55	0.64	0.73	0	0	0	0	10	0.7	0.8	0.85		
	10	0.66	0.75	0.82	0.82	0.82	0.82	0.82	100	0.6	0.7	0.8		
	100	0.74	0.81	0.85	0.85	0.85	0.85	0.85	1,000	0.55	0.65	0.75		
Moderate 175–425 km/d(2–5 m/s)	0	0.50	0.58	0.65	0	0	0	0	1,000	0.5	0.6	0.7		
	10	0.60	0.68	0.75	0.75	0.75	0.75	0.75	10	0.55	0.65	0.7		
	100	0.66	0.73	0.78	0.78	0.78	0.78	0.78	100	0.5	0.6	0.65		
Strong 425–700 km/d(5–8 m/s)	0	0.45	0.52	0.59	0	0	0	0	1,000	0.45	0.55	0.6		
	10	0.52	0.60	0.67	0.67	0.67	0.67	0.67	10	0.5	0.55	0.65		
	100	0.58	0.66	0.71	0.71	0.71	0.71	0.71	100	0.45	0.5	0.6		
Very Strong >700 km/d(> 8 m/s)	0	0.40	0.46	0.52	0	0	0	0	1,000	0.4	0.45	0.55		
	10	0.45	0.53	0.61	0.61	0.61	0.61	0.61	10	0.45	0.5	0.55		
	100	0.50	0.59	0.65	0.65	0.65	0.65	0.65	100	0.4	0.45	0.5		
	1,000	0.55	0.63	0.68	0.68	0.68	0.68	0.68	1,000	0.35	0.4	0.45		

Source: Data from Doorenbos and Pruitt (1975, 1977)

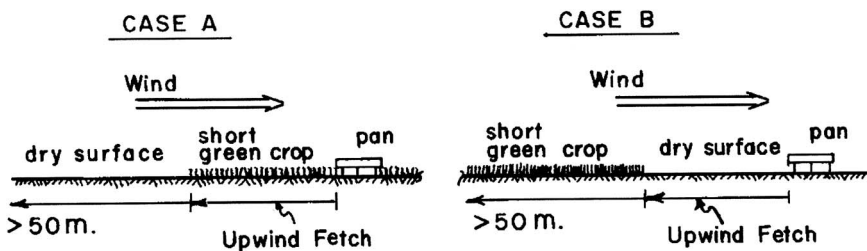


Fig. 8-1. Example environments surrounding evaporation pans for FAO 24 method

Source: Doorenbos and Pruitt (1975, 1977); reproduced with permission from U.N. Food and Agriculture Organization

to ensure low leaf resistances at all times, and the extent of the grass surface should be 50 m in all directions. Also presumed is the maintenance of a water level within a zone ranging from 0.05 to 0.075 m below the top of the pan. If the pan is protected from birds, e.g., with 12.5-mm (0.5-in.) mesh screen, coefficients should be increased 5 to 10% (Stanhill 1962a). Pans made of monel metal, or older galvanized metal pans that have lost their original reflectance characteristics, may need a reduction of  $k_p$  of up to 5%. In general the water should be kept clean, although turbidity differences appear to produce little difference in evaporation from Class A pans. The need to avoid contamination by oil-related products should be evident.

For those using computer programs in estimating  $ET_o$  from the FAO 24 pan method, polynomial equations based on the data in Table 8-5 were developed by Allen and Pruitt (1991) and published in Jensen et al. (1990), App. E, and Allen et al. (1998). The equation for situations where the pan is located downwind of a green or wet surface that has an evaporation rate close to that of reference ET (Case A), the estimation of  $k_p$  is

$$k_p = 0.108 - 0.0286 u_2 + 0.0422 \ln(Fetch) + 0.1434 \ln(RH_{\text{mean}}) - 0.000631 [\ln(Fetch)]^2 \ln(RH_{\text{mean}}) \quad (8-26)$$

where  $u_2$  is wind run at 2-m height in  $\text{m s}^{-1}$ ,  $Fetch$  is the upwind fetch in m, and  $RH_{\text{mean}}$  is the average of daily maximum and daily minimum relative humidity in percent. For Case B situations (dry fetch upwind), the suggested equation is

$$k_p = 0.61 + 0.00341 RH_{\text{mean}} - 0.000162 u_2 RH_{\text{mean}} - 0.00000959 u_2 Fetch + 0.00327 u_2 \ln(Fetch) - 0.00289 u_2 \ln(86.4 u_2) - 0.0106 \ln(86.4 u_2) \ln(Fetch) + 0.00063 [\ln(Fetch)]^2 \ln(86.4 u_2) \quad (8-27)$$

Limits should be imposed on Eqs. (8-26) and (8-27) to avoid unreasonable estimates. They are

$$30 \leq RH_{\text{mean}} \leq 84\%, \quad 1 \leq u_2 \leq 8 \text{ ms}^{-1}, \quad \text{and} \quad 1 \leq Fetch \leq 1,000 \text{ m}$$

Thom et al. (1981) developed a “reasonably physically-based” approach to using Class A pan evaporation, although their paper did not deal specifically with upwind fetch conditions and distances, an important factor in semiarid to arid conditions. Therefore, users must be cautious in applying this methodology.

More recently, Snyder et al. (2005) reviewed equations used to estimate grass reference ET from  $E_p$  and provided a simple method to convert pan evaporation to  $ET_o$  for conditions like those in California. The method accounts for fetch differences by first adjusting  $E_p$  rates to expected values for 100 m of grass fetch. Then, an empirical relationship between  $ET_o$  and adjusted  $E_p$  is used to determine  $ET_o$  values. The method eliminates the need for relative humidity and wind speed data that are often not available. The resulting equation was developed to estimate the fetch adjustment factor equivalent to 100 m of grass fetch ( $F_{100}$ ) based on actual fetch distances:

$$F_{100} = -0.0035 [\ln (Fetch)]^2 + 0.622 [\ln (Fetch)] + 0.79 \quad (8-28)$$

where  $Fetch$  is the actual amount of (well-watered) green fetch in m. Then  $E_{pa} = F_{100} \times E_p$  provides an estimate of pan evaporation adjusted to represent evaporation from a pan surrounded by 100 m of fetch, with the restriction that  $E_{pa} \leq 19.2 \text{ mm d}^{-1}$ . Then  $ET_o$  is estimated using the following equation:

$$ET_o = 10 \sin \left[ \left( \frac{E_{pa}}{19.2} \right) \frac{\pi}{2} \right] \quad (8-29)$$

where  $ET_o$  and  $E_{pa}$  are in  $\text{mm d}^{-1}$ .

## Atmometers

Atmometers are a class of small evaporimeters that generally consist of a wet, porous surface that is fed by a connected water reservoir. In some cases, the surface is covered with a fabric to simulate solar radiation characteristics of vegetation and to increase resistance to evaporation to mimic ET from vegetation. The water reservoir is filled with distilled water that evaporates out of the surface via a suction tube. Some atmometers have a special membrane to keep rainwater from seeping into the porous surface. Atmometers are typically mounted on a post near or within

agricultural fields and are finding use in irrigation scheduling (Broner 1993; Irmak et al. 2005). Manually read and electronically monitored atmometers are commercially available.

Phene et al. (1990) review the use of several types of atmometers to estimate reference  $ET_o$ . Because of their low cost and ease of use, atmometers or evaporimeters are acceptable where weather station data or pan evaporation data are not available. Brutsaert (1982) describes three types of atmometers that are in limited use today: the Piche evaporimeter developed in France, the Wild evaporimeter developed in Russia, and the Bellani-Livingston evaporimeter developed in Italy as a flat porous disk (Bellani) and now available commercially in the United States.

The Piche atmometer is constructed with a transparent glass tube sealed at the top that is about 0.2 to 0.3 m long and 10 to 30 mm in diameter with a disk of moist blotting paper that is 800 to 1,300  $\text{mm}^2$  exposed on the bottom. A small hole on the side of the tube serves as an air vent. The tube is filled with water, and as water evaporates from the paper, which is held in place with a steel wire spring, the water level will sink in the tube. The instrument is installed about 1.2 m above the ground in an instrument shelter. Stanhill (1962b) related the evaporation from the Piche atmometer to the drying power of the atmosphere, and Brochet and Gerbier (1972) and Thom et al. (1981) empirically inserted the Piche evaporation into the aerodynamic term of the Penman equation. Brochet and Gerbier developed procedures to estimate constants for the aerodynamic Piche term for any latitude or time of year in France.

The Wild evaporimeter has a shallow cylindrical dish about 25 mm deep and 178 mm in diameter that is filled with water and placed on a counterbalanced scale. The instrument is deployed similarly to the Piche atmometer at about 1.2 m above the ground in a shelter.

The Bellani-Livingston evaporimeter is a porous surface with a flat disk used for the Bellani type and a spherical surface used for the Livingston type (Livingston 1935). This instrument, unlike the Piche and Wild evaporimeters, can be directly exposed to the environment. Altenhofen (1985) modified the Bellani atmometer by placing various types and thicknesses of green canvas cover over the ceramic top to simulate the resistance and albedo of a green leaf. Evaporation from this instrument has been shown to correlate well with reference ET equations using meteorological data (Broner and Law 1991; Altenhofen 1985; Irmak et al. 2004, 2005). An electronic readout version of the instrument is available for automatic recording or irrigation control (Parchomchuk et al. 1996) and canvas covers that simulate the surface resistances for either grass or alfalfa.

Precautions to be exercised with atmometers include the placement of the instruments and the dryness of the local environment. Similar to weather stations used to provide data for calculating reference ET, atmometers should be placed in local environments that are similar to those of

the vegetation for which they are to provide ET indication, in terms of amount of relative wetness of the surrounding surface or vegetation. Manufacturers of the systems generally provide advice on standardized mounting heights for the instruments to produce desired aerodynamic exchange. However, the height of surrounding vegetation should be considered, especially with tall vegetation such as corn. Because of the "artificial" surface of the atmometer system, the evaporation measurements should not be expected to reproduce calculated reference ET exactly. Because atmometers respond to the dryness of the surrounding environment, using atmometers to evaluate the impact of weather station dryness on the  $ET_{ref}$  calculation might be possible by locating one atmometer in the weather station environment and a second atmometer within a few km from the station, but in a more well-watered "reference setting." The ratio of evaporation from the two atmometers may indicate the "aridity effect" of the weather station on calculated  $ET_{ref}$ . Research is needed on this application.

# CHAPTER 9

## EVAPORATION FROM SOIL

### 9.1 INTRODUCTION

This chapter focuses mainly on evaporation from bare or nearly bare soils and includes procedures for adjusting estimated evaporation for partial plant cover. Estimates for evaporation from bare soil are important early and late in crop-growing periods and during nongrowing periods and for estimating effects of wet soil within vegetation on total ET. Evaporation losses from soil can comprise a substantial part of the total water balance under rain-fed conditions in dry climates. A review of literature by Burt et al. (2005) describes some general models for estimating evaporation from soil and plant canopies and some experimental findings. Additional material on soil properties, including evaporation and hydraulics, was introduced in Chapter 3.

### 9.2 THE EVAPORATION PROCESS

When noncracking soils dry, observations of soil water profiles show the soil water content initially decreases exponentially toward the surface. For example, Rose (1968a) measured soil water profiles during drying and found that the soil water content in a sandy soil after four days was near air-dry at the surface and increased to near field capacity at a depth of 0.12 to 0.15 m. Hanks et al. (1967) measured soil water profiles in the laboratory when drying occurred under either wind or radiation conditions and reported similar profiles. Jackson (1973) conducted a comprehensive study of evaporation on a loam soil near Phoenix, Arizona. He measured soil water profiles by 0.01-m increments to a depth of 0.09 m for 16 days after irrigation in July 1970 and for 37 days after irrigation during a relatively

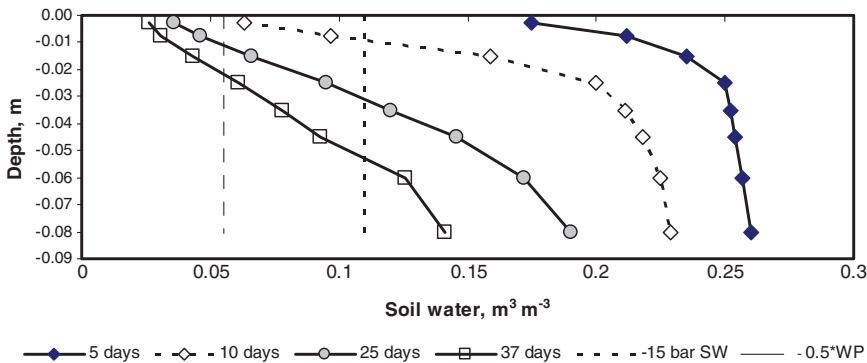


Fig. 9-1. Soil water distribution in a loam soil on days 5, 10, 25, and 37 after wetting near Phoenix, Arizona, during March–April 1971  
Source: Data from Jackson (1973)

humid and cool period during March–April 1971 (Figure 9-1). The distribution of soil water for the first 10 days after irrigating showed an exponential distribution with depth similar to that reported by Rose (1968a). Profiles at 25 and 37 days tended to become less exponential in this upper layer.

Evaporation from bare soil has often been divided, time-wise, into two or three stages that characterize the form or nature of control on the evaporation process and rate. Ritchie (1972) and others define stage 1 evaporation as the rate of evaporation following wetting when the evaporation rate is limited only by energy availability. During stage 1, the soil is sufficiently wet so that water is transported to the surface at a rate at least equal to the evaporation potential. The duration of stage 1 and the amount evaporated are related to the hydraulic conductivity and water-holding capacity of the soil and evaporative conditions. In stage 2, the surface soil water content has decreased to where the hydraulic capacity of the soil is unable to supply the potential, energy-limited rate. The evaporation rate during stage 2 progressively decreases with time, often in proportion to the square root of time, as described later. Figure 9-2 shows a typical evaporation trend line with stages 1 and 2. Occasionally, for example, with deep-cracking soils, a third evaporation stage is added, where a low, long-term evaporation rate is supplied by water exposed by deep cracks or by substantial upward flow (Idso et al. 1974; Ritchie and Adams 1974; Allen et al. 2005a; Burt et al. 2005).

### 9.3 DIURNAL EFFECTS AND REDISTRIBUTION OF SOIL WATER

Jackson (1973) measured the 0–0.09 m surface layer at hourly intervals for seven days in 1970 and at half-hour intervals for 19 days in 1971. These

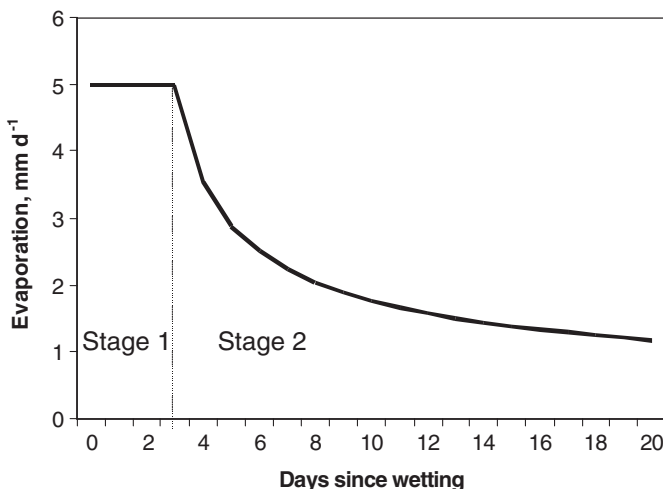


Fig. 9-2. Idealized evaporation rate curve from bare soil showing sharp transition between stage 1 and stage 2 evaporation where the potential evaporation rate is  $5 \text{ mm} \text{d}^{-1}$

data show that large diurnal changes occur in the surface layer during the evaporation process, which is similar to the results from Rose (1968a). At the end of the seven days in July 1970, 69% of the total water evaporated came from the 0–0.09 m depth. At the end of the 16 days in March 1971, 66% of the total water evaporated came from the 0–0.09 m depth, indicating an upward flux of about 1/3 of the evaporated water from below the top 0.09-m layer.

As the surface of the soil dries, the rate of evaporation decreases as the resistance to evaporation increases. In a field study on bare soil, van de Griend and Owe (1994) used an air circulation chamber to measure surface resistance to vapor diffusion in drying of the topsoil in central Spain. Measurements were made on a fine sandy loam during a 13-day dry down period after wetting. Surface resistance began to increase at a water content of 15% by volume in the 0.01-m top layer, which was 50% of field capacity. The measurements showed a very pronounced diurnal pattern due to drying of the very top layer during the day and recovery of the soil water profile during nighttime hours similar to that reported by Rose (1968a) and Jackson (1973).

#### 9.4 STAGE 1 EVAPORATION

Stage 1 evaporation is defined as the rate of evaporation following wetting when the evaporation rate is limited only by energy availability.

The evaporation rate during stage 1 drying is a function of evaporative drying power of the atmospheric boundary layer and is generally estimated as a coefficient  $K_{e\max}$  times reference  $ET_{ref}$ , as described in Eq. (9-1) where  $ET_{ref}$  is reference ET for clipped grass,  $ET_o$ , or alfalfa,  $ET_r$ . The duration of stage 1 and the start of stage 2 may range from one to several days after rainfall or irrigation depending on the amount of water applied, the soil, and evaporative conditions.

The total depth of cumulative evaporation during stage 1, referred to as readily evaporable water ( $REW$ ) in the FAO-56 procedure, varies with soil type.  $REW$  can be estimated using  $REW$  values from Table 9-1 based on recommendations by Ritchie et al. (1989), or using Eq. (9-23a-c) presented later. Ritchie (1972) presents cumulative amounts of stage 1 evaporation for four soils ranging from 6 mm for sand to 12 mm for a clay loam. Stage 2 evaporation is often said to begin when the soil surface becomes visibly dry for most of the day. Local observation of  $REW$  is recommended. During stage 2, the evaporation rate ( $E_2$ ) is governed by the flux of water through the upper layer of soil to or near the evaporation site and is limited by  $K_{e\max}ET_{ref}$ .

The rate of  $E$  for stage 1 drying can be estimated using reference ET to represent potential evaporation energy as

$$E_1 = K_{e\max} ET_{ref} \quad (9-1)$$

where  $E_1$  is the evaporation rate during stage 1, which can change daily, depending on the value for  $ET_{ref}$ . When the total  $E_1$  summed over the stage 1 period, termed  $\sum E_1$ , exceeds  $REW$ , stage 1 is assumed to end and stage 2 begins. The parameter  $K_{e\max}$  generally ranges from 1.05 to 1.2 for use with  $ET_o$  and 0.8 to 1.0 for use with  $ET_r$ , depending on ambient temperature of

Table 9-1. Typical Values of  $REW$  by Soil Type

Soil Type (U.S. Soil Texture Classification)	Evaporation Parameter ( $REW$ ) mm
Sand	2–7
Loamy sand	4–8
Sandy loam	6–10
Loam	8–10
Silt loam	8–11
Silt	8–11
Silty clay loam	8–11
Silty clay	8–12
Clay	8–12

Source: Data from Allen et al. (1998)

the soil prior to wetting, where heat stored in hot, dry soil prior to wetting contributes to the evaporation rate. The parameter  $K_{emax}$  is similar to parameter  $K_{cmax}$  described in Eq. (10-3) of Chapter 10, except that no adjustment is made for height of vegetation, as is done for  $K_{cmax}$ . Recommended "standardized" values for  $K_{emax}$  are 1.2 for use with  $ET_o$  and 1.0 for use with  $ET_r$ .

The duration of stage 1 evaporation beginning the day after irrigation or rain, designated  $t_1$ , is estimated as

$$t_1 = \frac{REW}{\bar{E}_1} \quad (9-2)$$

where  $REW$  is in mm and  $\bar{E}_1$  is mean  $\bar{E}_1$  in mm over the  $t_1$  period in  $\text{mm d}^{-1}$ . An iterative solution or daily calculation of depletion from the evaporation layer, as presented in Eq. (9-28), is required. Setting the calculation time step to determine when  $\sum E_1$  exceeds  $REW$  to less than one day in length simplifies identifying the specific transition time. When using daily  $ET_{ref}$  one can, for example, divide the 24-hour period into tenths of a day and divide the daily  $ET_{ref}$  value by 10 to approximate shorter time steps. Alternatively, hourly  $ET_{ref}$  and calculation time steps can be used. The duration of  $t_1$  determined in this manner assumes that no redistribution of soil water occurs during the following night, as observed by Rose (1968a), Jackson (1973), and van de Griend and Owe (1994). Redistribution of soil water can reinstate stage 1 evaporation the following morning for part of a day.

$REW$  can be measured in the field or laboratory by conducting soil water balances and calculating the evaporation rate. When laboratory cores are used to determine  $REW$ , values can be much higher than field-determined values (Ritchie and Johnson 1990). By definition, stage 1 ends when the measured  $E$  begins to decrease below  $K_{emax}ET_{ref}$ .  $REW$  equals the cumulative evaporation depth,  $\sum E_1$ , when this occurs. The soil must have been sufficiently wetted to at least a 0.3-m depth. Account can be made in Eq. (9-2) for effects of slow drainage from the top 100 to 150 mm of soil that can hold water content of that layer above field capacity for some time duration and thereby increase the effective  $REW$ .

## 9.5 STAGE 2 EVAPORATION

Estimating evaporation from the soil becomes more complex as the surface soil dries and stage 2 evaporation begins. Stage 2 evaporation begins when evaporation proceeds at less than potential rates due to hydraulic constraints. During stage 2, the evaporation rate is governed by the rate of water movement in the liquid phase and vapor phase to or

near the surface when not limited by environmental conditions (Rose 1968a). Some soil water in the “evaporation” layer may also be extracted by plant roots when plants are present. Villalobos and Fereres (1990) measured evaporation from soil using special small lysimeters of 0.3 m depth into which root growth was not restricted. Early in the morning, the roots were cut, and the microlysimeters were cleaned, sealed, weighed, and replaced in their respective positions. The next day, they were weighed again to measure evaporation. Comparison of the soil water content in the microlysimeters without extraction by cotton roots with soil water content in microlysimeters with extraction by cotton roots showed similar values, indicating that cotton roots extracted little water from the top 0.3-m layer at the time the roots were cut. With corn, the water content inside the microlysimeters without root extraction was higher than for adjacent soil with root extraction, indicating some extraction by corn roots from the top 0.3-m layer. Shawcroft and Gardner (1983), Klocke et al. (1985, 1996), Villalobos and Fereres (1990), Daamen et al. (1993), Evett et al. (1995), Jara et al. (1998), and Todd et al. (2000) report similar microlysimeter studies. Evett et al. (1995) also describe desirable characteristics in microlysimeter design.

Soil characteristics and the change in soil water content govern the rate of stage 2 evaporation as described by the equation of Richards (1931). In terms of soil water pressure, and with no water extraction by roots, the combined Darcy's law and continuity equation for one-dimensional vertical flow (Jensen and Hanks 1967) can be written as

$$\frac{\partial \theta}{\partial t} = \frac{\partial}{\partial z} \left\{ K(h) \frac{\partial H}{\partial z} \right\} \quad (9-3)$$

where  $\theta$  is the volumetric soil water content,  $t$  is time,  $z$  is vertical distance,  $K(h)$  is the hydraulic conductivity,  $H$  is the total hydraulic head ( $H = P_w/\gamma_f + z = h + z$ ),  $z$  is the vertical coordinate,  $P_w$  is the pressure of the wetting fluid,  $h$  is the fluid pressure head, and  $\gamma_f$  is the weight of fluid per unit volume.

Entekhabi and Eagleson (1989) combine the diffusivity equation of Gardner (1959) and conservation of mass equations for porous media to describe the soil water desorption process as

$$\frac{\partial \theta}{\partial t} = \frac{\partial}{\partial z} \left[ D(\theta) \frac{\partial \theta}{\partial z} \right] + \frac{\partial K}{\partial z} \quad (9-4)$$

where  $\partial K/\partial z$  is the rate of drainage due to gravity, and  $D(\theta)$  is the soil water diffusivity defined as

$$D(\theta) = K(s) \frac{\partial \psi}{\partial \theta} \quad (9-5)$$

where  $K(s)$  is the unsaturated hydraulic conductivity,  $s$  is relative saturation, and  $\psi$  is matric potential. Black et al. (1969) describe the flow equation and boundary conditions without the gravity component as

$$\frac{\partial \theta}{\partial t} = \frac{\partial}{\partial z} \left[ D(\theta) \frac{\partial \theta}{\partial z} \right] \quad (9-6)$$

$$\theta = \theta_i, \quad z \geq 0, \quad t = 0$$

$$\theta = \theta_o, \quad z = 0, \quad t > 0$$

where  $\theta_i$  is the initial water content for  $t = 0$  and  $z \geq 0$ ;  $\theta_o$  is the water content at the boundary ( $z = 0$ ), assumed constant for  $t > 0$ ; and  $z$  is defined as elevation above some depth in the soil profile where water content is considered to be constant.

Black et al. (1969) solved Eq. (9-6) analytically (Crank 1956) for a semi-infinite slab with constant diffusivity,  $D$ , to yield flux at the surface,  $q$ , as

$$q = (\theta_i - \theta_o)(D/\pi t)^{1/2} \quad (9-7)$$

Integration of Eq. (9-7) with respect to time gives the cumulative flux,  $E$ :

$$E = 2(\theta_i - \theta_o)(Dt/\pi)^{1/2} \quad (9-8)$$

When  $D$  can be expressed as a function of  $\theta$ ,  $D$  can be replaced by weighted-mean diffusivity  $\bar{D}$ . Crank (1956) gives expressions relating weighted-mean diffusivity to the true diffusivity. For the desorption process this relation is given by the following integral:

$$\bar{D} = \frac{1.85}{(\theta_i - \theta_o)^{1.85}} \int_{\theta_o}^{\theta_i} D(\theta)(\theta_i - \theta)^{0.85} d\theta \quad (9-9)$$

For convenience a factor  $C$  was defined such that  $E = Ct^{1/2}$  so that

$$C = 2(\theta_i - \theta_o)(\bar{D}/\pi)^{1/2} \quad (9-10)$$

## 9.6 EVAPORATION MODELS

There are a number models used to estimate evaporation from soils. When used in conjunction with total estimates of ET and on an operational basis, simplified models are often applied that do not require extensive data on soil hydraulic data. These models are described in this section.

### Square Root of Time (SRT) Model

Philip (1957) and Black et al. (1969) express the theoretical cumulative evaporation during stage 2 evaporation of an initially wet, deep soil as

$$\sum E_2 = \alpha_r \sqrt{t_2} \quad (9-11)$$

where  $\sum E_2$  is the cumulative evaporation during stage 2;  $\alpha_r$  is soil water desorptivity, which depends on the hydraulic properties of the soil; and  $t_2$  is time in days since the start of stage 2 evaporation. Philip (1957) developed Eq. (9-11), which is used extensively in early evaporation and crop ET models (Ritchie 1972, 1974).

Ritchie (1972) presents values for  $\alpha_r$  ranging from  $3.34 \text{ mm} d^{-0.5}$  for sand to  $5.08 \text{ mm} d^{-0.5}$  for a clay loam. Ritchie and Johnson (1990) report several direct measurements of  $\alpha_r$  in a diversity of soils resulting in values of about  $3.5 \text{ mm} d^{-0.5}$ . Ventura et al. (2001) report values of  $\alpha_r$  of about  $4.0 \text{ mm} d^{-0.5}$  for a flood-irrigated field in the Imperial Valley of California.

Eq. (9-11) is differentiated to provide the evaporation rate at the end of day  $t_2$  during stage 2 drying:

$$E_2 = \frac{\alpha_r}{2\sqrt{t_2}} \quad (9-12)$$

where  $E_2$  is the evaporation rate during stage 2. Because Eq. (9-12) estimates the evaporation rate at the end of day  $t_2$  of the stage 2 process, the evaporation rate averaged over day  $t_2 > 1$  must be calculated as the difference between  $E_2$  for  $t_2$  and  $E_2$  for  $(t_2 - 1)$  based on Eq. (9-11):

$$\begin{aligned} E_2 &= \alpha_r (\sqrt{t_2} - \sqrt{t_2 - 1}) && \text{for } t_2 > 1 \\ E_2 &= \alpha_r && \text{for } t_2 = 1 \end{aligned} \quad (9-13)$$

Estimating cumulative evaporation using Eqs. (9-8)–(9-11) requires knowledge of weighted-mean diffusivity  $D$  for the soil in question. Suleiman and Ritchie (2003) replace the terms in Eq. (9-8) to obtain an estimate of  $\alpha_r$ :

$$\alpha_r = 2(\theta_{dul} - \theta_{ad})(\bar{D}/\pi)^{1/2} \quad (9-14)$$

where  $\theta_{dul}$  is the drained upper limit (field capacity), and  $\theta_{ad}$  is the air-dry water content. Suleiman and Ritchie (2003) calculate the soil water diffusivity for each of 12 theoretical soils ranging in texture from sand to clay using the van Genuchten et al. (1991) soil water diffusivity function equations. Some properties were obtained from soil properties described by Rose (1968b). A comparison of calculated  $\alpha_r$  vs.  $\theta_{dul}$  indicates a linear relationship of the form:

$$\alpha_r = K_\alpha \theta_{dul} \quad (9-15)$$

where  $\alpha_r$  is in  $\text{mm} d^{-1/2}$ ,  $\theta_{dul}$  is water content at the drained upper limit (field capacity) in  $\text{m}^3 \text{ m}^{-3}$ , and  $K_\alpha$  is the slope of the relationship that was found to

equal  $13.9 \text{ mm d}^{-1/2}$  for the 12 theoretical soils (Suleiman and Ritchie 2003). Entekhabi and Eagleson (1989) propose a more complicated function for  $\alpha_r$ , based on the Brooks and Corey (1966) soil pore-size distribution index, porosity, and saturated conductivity.

Because weighted-mean diffusivity values are not generally available for most soils, estimates of cumulative evaporation in mm can be obtained using the approximate relation between  $\alpha_r$  and  $\theta_{dul}$  when  $\alpha_r$  is not measured, as

$$\sum E_2 = 13.9 \theta_{dul} t_2^{1/2} \quad (9-16)$$

where  $t_2$  is the time in days since stage 2 evaporation began, and  $\sum E$  is the cumulative stage 2 evaporation in mm at the end of the time period in days. The rate of evaporation can be estimated using Eq. (9-13).

The SRT evaporation estimates are based on the assumption that potential evaporation rate ( $K_{e\max} ET_{ref}$ ) is always greater than the estimated stage 2 evaporation rate. Furthermore, no provision is made for modifying evaporation estimates to account for intervening small amounts of rainfall or irrigation that may occur. The procedures for estimating stage 2 evaporation by Ritchie (1972) and Suleiman and Ritchie (2003) are intended for use in other models that require estimates of evaporation from the soil and that separately account for intervening small amounts of rainfall. Comparison of several methods for estimating evaporation during stage 2 are made later in this chapter.

The SRT function approaches but never reaches a zero evaporation rate, due to its theoretical form. In practice, the hydraulic conduction of water toward the surface, and thus evaporation, may be disrupted by soil layering, incomplete wetting, plant root extraction, and tillage impacts, so that when applied to long time periods between wetting events, for example, longer than a month, a time limit should be considered, after which  $E_2$  is set to zero or to a very small value. In addition, the SRT model assumes that the soil begins the drying event with a fully wetted profile near field capacity. This assumption is required to support the continuous upward flow implicit in the method. Wetting events that do not fully rehydrate at least the upper 1 to 2 m of the soil profile will have drying events that do not reach the evaporation rates estimated by the SRT model, especially after long periods of time.

When wetting events occur that do not fully rehydrate the surface evaporation layer of the soil, some means is needed to set back the clock for the SRT method, i.e., parameter  $t_2$  in Eq. (9-11). This can be done by inverting the equation to solve for an adjustment to  $t_2$ :

$$t_2 = \left[ \frac{[(\sum E_2)_j - (P_j - RO_j + I_j)]^2}{\alpha_r} \right]^{1/2} \quad (9-17)$$

where  $(\sum E_2)_j$  is the cumulative stage 2 evaporation (mm) estimated for day  $j$  before any correction to  $t_2$ .  $P_j$  and  $RO_j$  are precipitation and precipitation runoff from the soil surface on day  $j$  (mm), and  $I_j$  is the irrigation depth on day  $j$  that infiltrates the soil (mm). The adjusted value for  $t_2$  is used to replace the unadjusted value for the end of day (or time step)  $j$ . If the sum of  $P_j - RO_j$  and  $I_j$  exceeds  $(\sum E_2)_j$  then the evaporation process should be set back to stage 1 and Eq. (9-17) is not utilized. Small depths of precipitation during stage 2 will wet the surface and may shift the stage back to stage 1 for a brief period of time depending on the precipitation amount, with a subsequent resumption of stage 2 drying. This is shown later for the FAO-56 model using the skin evaporation enhancement.

### Crop Coefficient-Based Evaporation Model

Various procedures have been proposed for adjusting or increasing the crop coefficient  $K_c$ , or calculating an evaporation coefficient,  $K_e$ , to account for evaporation following rainfall or irrigation.

**Wright (1982) Procedure** Wright (1982) suggests the following time-based expression for  $K_e$  applicable for limited times after rainfall or irrigation:

$$K_e = (K_{c \max} - K_s K_{cb}) \left[ 1 - \left( \frac{t}{t_d} \right)^{1/2} \right] f_w \quad (9-18)$$

where  $K_{c \max}$  is the maximum value for  $K_c$  normally occurring after rain or irrigation.  $K_{c \max}$  is generally 0.8 to 1.0 for an alfalfa-based  $K_c$  and 1.0 to 1.2 for a grass-based  $K_c$ .  $K_{cb}$  is the basal crop coefficient, and  $K_s$  is the fraction of available soil water in the root zone. Variable  $t$  in Eq. (9-18) represents the days after major rain or irrigation, and  $t_d$  is the usual number of days required for the soil surface layer to dry. Variable  $f_w$  is the relative fraction of the soil surface wetted by rainfall or irrigation. Normally, for precipitation and sprinkler and surface irrigations that wet the entire soil surface,  $f_w = 1.0$ . For very small fractions of soil wetted, the effective area may be larger. Recent studies of evaporation from wet soil in drip-irrigated olive orchards indicate that the effective value of  $f_w$  for accurate estimation of evaporation may be greater than the actual fraction of area wetted due to microscale advection from surrounding dry soil (Bonachela et al. 2001).

Eq. (9-18) simulates the time-based reduction in evaporation as the soil dries. General values for  $t_d$  are three days for sandy soils, five days for silty soils, and seven days for clayey soils (Wright 1982). However, the value for  $t_d$  will be longer during cool or humid periods and shorter in hot or dry periods. Variable  $t$  must be limited to  $0 \leq t \leq t_d$ . If soil wetting occurs in the morning, then  $t$  is generally set equal to 0 for that day. Most evaporation

occurs in the first few days after the soil is wetted. Hill et al. (1983) and Martin and Gilley (1993) caution that  $t$  must be limited for each wetting event so that total evaporation estimated over the  $t_d$  period is constrained by the depth of precipitation or irrigation. Daily precipitation totals that are less than about 0.3  $ET_o$  can be ignored.

**General Model for  $K_e$**  A general model for  $K_e$  for estimating the evaporation from the surface layer of soil after rain or irrigation was introduced in FAO-56 (Allen et al. 1998) for use with the basal crop coefficient:

$$K_e = K_r(K_{c\ max} - K_s K_{cb}) \quad \text{such that} \quad K_e \leq f_{ew} K_{c\ max} \quad (9-19)$$

where  $K_e$  is the soil evaporation coefficient,  $K_{cb}$  is the basal crop coefficient,  $K_{c\ max}$  is the maximum value of  $K_c$  following rain or irrigation,  $K_s$  is a reduction coefficient to account for reduced transpiration under soil water shortage,  $K_r$  is a dimensionless evaporation reduction coefficient (0–1), and  $K_s$  is a dimensionless soil water stress factor (0–1).  $K_r$  can be expressed as a function of time [i.e., Eq. (9-18)] or in the FAO-56 dual  $K_c$  approach as a function of the cumulative depth of water depleted by evaporation from the soil. Parameter  $f_{ew}$  is the fraction of soil surface from which most of the evaporation occurs, which is generally taken as the fraction of soil surface that is both exposed to drying and is wetted during the wetting event. The FAO-56 application of Eq. (9-19) is intended to overcome problems that occur with Eq. (9-18) regarding the value for  $t$  during small wetting events. Its use of cumulative depth of evaporation to estimate  $K_r$  tends to stretch out drying periods when  $ET_{ref}$  is low and shorten them when  $ET_{ref}$  is high. A daily water balance of the effective surface evaporation layer is required. In Eq. (9-19), transpiration is preferred over evaporation from soil (i.e.,  $K_s K_{cb}$  is subtracted from  $K_{c\ max}$  before calculating  $K_e$ ). In some ET models, such as that by Ritchie (1972), evaporation from soil has priority over transpiration.  $K_s K_{cb}$  is set to 0 when Eq. (9-19) is applied to completely bare soil.

In contrast to the SRT model where cumulative evaporation from bare soil is proportional to the increase in  $\sqrt{t}$  after stage 2 evaporation begins (Philip 1957; Black et al. 1969; Ritchie 1971, 1972), the FAO-56 method uses a water balance of an effective evaporation layer to estimate the decreasing evaporation rate. The effective layer is typically the upper 0.1 to 0.15 m during the first three to four weeks of evaporation, potentially increasing to 0.20 to 0.25 m depth for longer time periods. For maximum accuracy, estimates of the upward flux of water into this layer from below may be required, especially for medium and fine-textured soils (Ventura et al. 2001). However, estimation of upward flux may require relatively complicated models and specific parameterization or soil hydraulic and thermal characteristics. Cahill and Parlange (1998, 2000) and Grifoll et al. (2005) apply

sophisticated evaporation models that account for convective transport in both the gas and liquid water phases in addition to vapor dispersion and liquid sensible heat dispersion. Cahill and Parlange (1998, 2000) conclude that models and approaches for describing coupled heat and moisture transport in soils are able to explain most, but not all, measured changes in soil water profiles and flux rates. As demonstrated in the next subsection, for practical applications, a fixed potential depth of water depletion per drying event can generally be determined from field observation for specific soils and the decreasing evaporation rate estimated using the relatively simplified FAO-56 procedure. In the absence of field data, the total evaporable water can be estimated using an effective depth of the evaporation layer. Comparisons against simulations by the HYDRUS-1D one-dimensional finite element model shown in a later section tend to confirm this.

### The FAO-56 Evaporation Model

The FAO-56 (Allen et al. 1998) evaporation procedure calculates a water balance for the effective evaporation layer of soil that tends to be approximately 0.1 to 0.15 m in depth. The method represents a compromise between complexity and general application by assuming that upward flux of water or vapor to the layer from below is considered negligible or that its effects are incorporated into the effective depth of the evaporating layer that dries to a threshold dryness point. In the case of the FAO procedure, the threshold point is taken as the mean soil water content halfway between air-dry and wilting point. This is an arbitrary dry point, but one that is relatively straightforward for field application and is reproducible. The maximum depletion depth for the layer provides a consistent stopping point for the evaporation cycle to ensure conservation of mass and can be customized for each application to fit observations.

The FAO procedure assumes that evaporation takes place in two stages following Ritchie (1971): the energy limiting stage 1 and the falling rate stage 2. When the soil is wet (in stage 1), the evaporation reduction coefficient,  $K_r$ , in Eq. (9-19) is assumed to be 1.0. When the water content in the effective evaporation layer begins to limit evaporation (in stage 2),  $K_r$  decreases to below 1.0. The value for  $K_r$  is set to zero when the total amount of water in the effective evaporation layer is depleted during the drying cycle. Assuming that the soil is at field capacity ( $\theta_{fc}$ ) shortly after rainfall or irrigation and that it can dry to halfway between 0 and the wilting point ( $\theta_{wp}$ ), the total amount of water that can be depleted by evaporation ( $TEW$ ) from the effective evaporation layer during a drying cycle is estimated as

$$TEW = 1,000(\theta_{fc} - 0.5\theta_{wp})z_e \quad (9-20a)$$

where  $TEW$  is the total evaporable water in mm,  $\theta_{fc}$  and  $\theta_{wp}$  are in  $m^3 m^{-3}$ , and  $z_e$  is the effective depth of the surface layer that is dried by evaporation in m. The value for  $\theta_{fc}$  in Eq. (9-20a) may be set a few percentage points above normal values listed in Table 3-6 to compensate for extra soil water retained in the evaporation layer above  $\theta_{fc}$  for one or two days after wetting. The cumulative depth of evaporation,  $D_e$ , at the end of stage 1 is the readily evaporable water ( $REW$ ) that normally ranges from 5 to 12 mm depending on soil texture (Ritchie 1972).

Allen et al. (1998, 2005a) recommend downward adjustment of  $TEW$  during extended periods of low  $ET_{ref}$  (i.e.,  $ET_o < 5 \text{ mm d}^{-1}$ ) commonly experienced during nongrowing periods. During cool conditions, for example, during winter or other cool periods, less radiation energy is available for heating the soil surface layer and evaporating water, and total effective  $TEW$  representing a drying event will typically be smaller than during a warm period. Allen et al. (1998) suggest using  $ET_o$  as a surrogate for temperature and radiation conditions to reduce the value for  $TEW$ . When  $ET_o < 5 \text{ mm d}^{-1}$ ,  $TEW$  is estimated as

$$TEW = 1,000(\theta_{fc} - 0.5\theta_{wp})z_e \sqrt{\frac{ET_o}{5}} \quad (9-20b)$$

where  $ET_o$  is an average representing the general estimation period in  $\text{mm d}^{-1}$ . A monthly average for  $ET_o$  is recommended. Varying  $ET_o$  in Eq. (9-20b) on a daily basis is not recommended because doing so will cause  $TEW$  to vary daily, which can cause numerical inconsistencies.

During the falling rate stage, where  $D_e > REW$ , the evaporation rate is estimated in proportion to the amount of water remaining in the surface soil layer, and  $K_r$  of Eq. (9-19) is calculated as

$$K_r = F_{\text{stage1}} + (1 - F_{\text{stage1}}) \max \left[ \min \left( \frac{TEW - D_{e(i-1)}}{TEW - REW}, 1.0 \right), 0.0 \right] \quad (9-21)$$

where  $D_{e(i-1)}$  is the cumulative depth of evaporation at the end of time step  $(i-1)$ , representing the previous time step, and  $F_{\text{stage1}}$  is the fraction of the time step (day or hour) that resides in stage 1 evaporation.  $1 - F_{\text{stage1}}$  of the time step resides in stage 2. The use of  $F_{\text{stage1}}$  is an extension to the original FAO-56 model made by Allen et al. (2011a) to provide better definition of the transition from stage 1 to stage 2 drying during a time step and provide a more accurate, averaged value for  $K_r$  during that transition time step. The improved definition can be important when using daily calculation time steps, especially for coarse soils having small  $REW$ . The max function determines the greater of the two values in the brackets that are separated by the comma, and the min

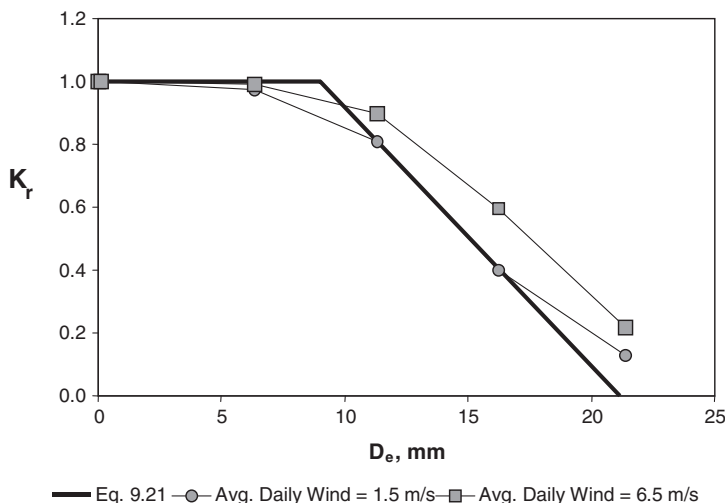


Fig. 9-3. Measured  $K_r$  reported by Chanzy and Bruckler (1993) for a loam soil near Avignon, France, under two wind speed conditions, and  $K_r$  modeled by Burt et al. (2005) using Eq. (9-21) with  $REW = 9 \text{ mm}$  and  $TEW = 21 \text{ mm}$  based on  $z_e = 0.1 \text{ m}$ ,  $F_{stage1} = 0$ , and average  $\theta_{fc}$  and  $\theta_{wp}$  values for loam from Table 3-6

function determines the lesser of the two values in the parentheses that are separated by the comma. These functions effectively limit the value for  $K_r$  to  $0 \leq K_r \leq 1.0$ . Setting  $F_{stage1}$  to 0 causes Eq. (9-21) to revert to the original FAO-56 form. Burt et al. (2005) find the linear proportionality of  $K_r$  to the depth of remaining evaporable water, as expressed by Eq. (9-21), to follow experimental data by Chanzy and Bruckler (1993) well for three soil types spanning clay, silty clay loam, and loam, as shown in Figure 9-3 for loam.

FAO-56 (example 31) presents a set of sample calculations for applying the FAO-56  $K_e$  method (Allen et al. 1998). Setting the effective depth of evaporation,  $z_e$ , can be subjective, because the entire  $z_e$  layer will not uniformly approach air-dry conditions during a drying period, and an upward flux to this layer from below is not considered. The selection of  $z_e$  should be set to a value that causes the FAO-56 procedure to reproduce observed average total evaporation depth for the same or a similar soil after a long drying period and therefore include the effects of depletion of water from below the  $z_e$  layer (Allen et al. 2005a). Usually a value for  $z_e$  of 0.1 or 0.15 m is used. For evaporation periods extending beyond three or four weeks, a transition in  $z_e$  to a depth of 0.2 to 0.25 m may be required to better represent the soil depth contributing to total evaporation (Raes et al. 2009).

The fraction of calculation time step  $i$  that resides in stage 1,  $F_{\text{stage}1}$ , is approximated following Allen (2011) as

$$F_{\text{stage}1} = \frac{REW - D_{REW_{i-1}}}{K_e \max ET_{ref}}, \quad 0 \leq F_{\text{stage}1} \leq 1.0 \quad (9-22)$$

where time step length can be one day, a tenth of a day, or one hour;  $D_{REW_{i-1}}$  is the depletion of the upper “skin” soil surface layer that directly contributes to stage 1 drying, mm, at the end of time step  $i - 1$ ; and  $K_e \max$  is the value for  $K_e$  expected during stage 1 drying. The value for  $K_e \ max$  is tied to the reference ET type, where  $K_e \ max \sim 1.0$  is recommended when using the alfalfa reference,  $ET_r$ , and  $K_e \ max \sim 1.2$  is recommended when using the clipped grass reference,  $ET_o$ . Typically,  $K_e \ max$  can be set equal to  $K_c \ max$ , defined earlier.  $F_{\text{stage}1}$  is limited to the range  $0 \leq F_{\text{stage}1} \leq 1.0$ . The water balance equation for determining  $REW$  is given later as Eq. (9-29). Figure 9-4 illustrates the three depths describing contributing portions of the soil profile, referred to as the skin layer; the total evaporation layer,  $z_e$ ; and the root zone depth,  $z_r$ , in the case of presence of plants. Each depth is contained within the domain of the next deeper depth in the FAO-56 model, which is different from most layered soil water models. In other words, each layer is a subset of the next deeper layer.

Ritchie et al. (1989) suggest empirical equations to estimate potential values of  $REW$  based on soil texture:

$$REW = 20 - 0.15(Sa) \quad \text{for } Sa > 80 \quad (9-23a)$$

$$REW = 11 - 0.06(Cl) \quad \text{for } Cl > 50 \quad (9-23b)$$

$$REW = 8 + 0.08(Cl) \quad \text{for } Sa < 80 \quad \text{and} \quad Cl < 50 \quad (9-23c)$$

where  $Sa$  and  $Cl$  are percentage fractions of sand and clay in the soil. Units for  $REW$  are mm. Typical values of  $REW$  suggested by FAO-56 are summarized in Table 9-1. Limiting values for  $REW$  to less than  $TEW$  is important.

**Experimental Values for  $z_e$ ,  $TEW$ , and  $REW$**  Because the typical soil water distribution after evaporation follows an exponential relationship as illustrated in Figure 9-2, the surface 0–0.05 m layer can be expected to approach air-dry approximated as  $0.5 \theta_{wp}$ . Below 0.05 to 0.1 m, the soil likely will not dry to less than  $\theta_{wp}$  between irrigation or rainfall events. After 37 days of evaporation from a loam soil near Phoenix, Arizona, the soil water content below 0.04 m did not decrease to air-dry conditions and below 0.05 m was only approaching  $\theta_{wp}$  (Jackson 1973). An alternate estimate of  $TEW$  assumes that only the 0–0.05 m layer would dry to  $0.5 \theta_{wp}$ , and below this depth the soil would dry only to  $\theta_{wp}$ , or

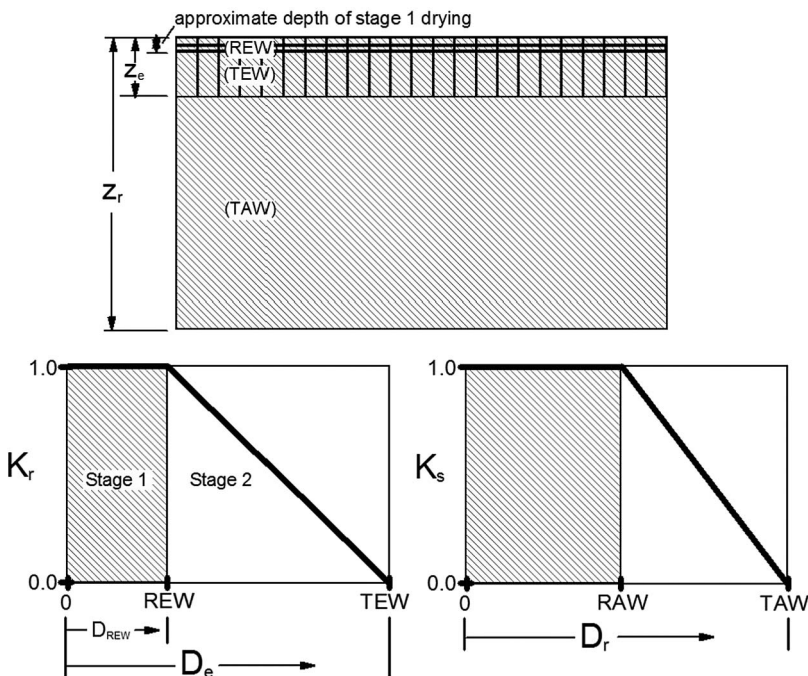


Fig. 9-4. Top: relative depths for the upper soil surface layer, referred to as the skin layer, contributing to stage 1 drying; the total evaporation layer,  $z_e$ ; and the root zone depth,  $z_r$ , in the case of presence of plants. Lower left: the shape of the  $K_r$  function vs.  $D_e$  and placement of REW and TEW defining stage 1 and stage 2 drying. Lower right: the shape of the  $K_s$  function vs.  $D_r$  and placement of readily available water, RAW, and total available water, TAW

$TEW = 1,000 \ [(0.05 - 0)(\theta_{fc} - 0.5\theta_{wp}) + (z_e - 0.05)(\theta_{fc} - \theta_{wp})]$ . However, this adjustment is typically implicit in the establishment of the value for  $z_e$  and is generally not made.

The selection of the value of  $z_e$  to use in the calculation of  $TEW$  should be based on experimental data, when possible. Hunsaker et al. (2003) find good accuracy in application of the FAO-56 approach for  $K_r$  using  $z_e = 0.125$  m in Eq. (9-20) and  $REW = 10$  mm for cotton on a clay loam soil in Arizona. Hunsaker et al. (2002) use  $z_e = 0.15$  m,  $TEW = 34$  mm, and  $REW = 10$  mm for a loam soil under alfalfa based on lysimeter observations. Tolk and Howell (2001) and Howell et al. (2004) use  $z_e = 0.15$  m,  $TEW = 33\text{--}38$  mm, and  $REW = 10$  mm for a clay loam soil and  $z_e = 0.10$  m,  $TEW = 20$  mm, and  $REW = 9$  mm for a fine sandy loam near Amarillo, Texas. Allen et al. (2005c) use  $z_e = 0.10$  m,  $TEW = 25$  mm, and  $REW = 10$  mm to fit lysimeter data on evaporation for a silt loam soil near Kimberly,

Idaho. Allen et al. (2005a) find  $z_e = 0.15$  m to fit observed evaporation data in Imperial Valley, California, for silty clay and silty clay loam and  $z_e = 0.35$  m for sand. The larger value for  $z_e$  for sand accounts for upward flow of water to the surface. Mutziger et al. (2005) use  $z_e = 0.10$  m for a sandy clay loam and 0.15 m for silt loam soils to fit experimental data using the two-stage FAO-56 model. They apply the extended three-stage model of Allen et al. (2005a, b) for three cracking soils to account for low-level diffusive evaporation from crack faces over long time periods. Burt et al. (2005) use  $z_e = 0.10$  m and mean values from Table 3-6 for  $\theta_{fc}$  and  $\theta_{wp}$  in Eq. (9-20a) to model evaporation data reported by Chanzy and Bruckler (1993) for loam, silty clay loam, and clay soils. The average absolute value of percent differences between measured and FAO-56 modeled cumulative evaporation was 5%. The  $\theta_{fc} = 0.35$  and  $\theta_{wp} = 0.13 \text{ m}^3 \text{m}^{-3}$  presented by Jackson (1973) for the loam soil near Phoenix in Figure 9-1 and a value of  $z_e = 0.1$  m produces  $TEW = 30$  mm. Jackson (1973) observed maximum cumulative evaporation of 29 to 31 mm from the soil profile during his two test periods, which is in close agreement.

**Stage 3 Evaporation for Cracking Soils** Drying to depths as deep as 0.5 m or more is possible for severely cracking soils containing large amounts of montmorillonite clay where cracks can extend as deep as 0.6 m (Ritchie and Adams 1974) and 1 m (Petry and Switzer 1996). An extension to the FAO evaporation model (Allen et al. 2005a) created a stage 3 where evaporation progresses in soils that crack substantially upon drying, thereby exposing progressively deeper depths to the drying process. The progressive drying tends to continue at low rates over extended periods of time and prolongs the time for  $K_r$  to decrease to zero, thereby creating a prolonged baseline evaporation rate.

In the extension for stage 3 drying, stage 2 transitions to stage 3 when  $K_r$  reduces to a threshold value labeled  $K_{r2}$ , as shown in Figure 9-5. For a three-stage drying system with the skin evaporation extension, Eq. (9-21) for  $K_r$  is replaced with Eq. (9-24) for the second stage when  $REW < D_{e,i-1} < TEW_2$ :

$$K_r = K_{r2} + (1 - K_{r2}) \times \left\{ F_{\text{stage } 1} + (1 - F_{\text{stage } 1}) \max \left[ \min \left( \frac{TEW_2 - D_{e,i-1}}{TEW_2 - REW}, 1.0 \right), 0.0 \right] \right\} \quad (9-24)$$

and  $K_r$  during stage 3 when  $TEW_2 \leq D_{e,i-1} \leq TEW_3$  is

$$K_r = F_{\text{stage } 1} + (1 - F_{\text{stage } 1}) K_{r2} \max \left[ \min \left( \frac{TEW_3 - D_{e,i-1}}{TEW_3 - TEW_2}, 1.0 \right), 0.0 \right] \quad (9-25)$$

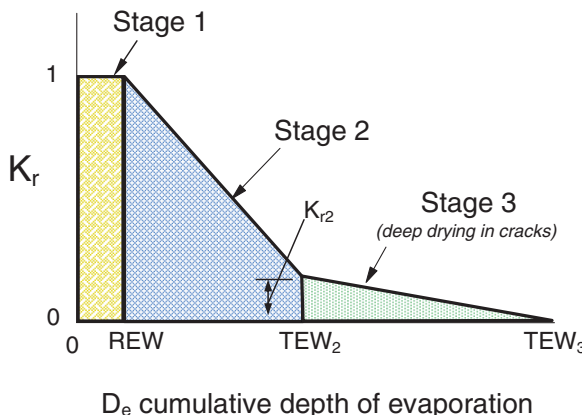


*Fig. 9-5. General schematic showing the transition of the  $K_r$  function [Eqs. (9-24) and (9-25)] for a cracking soil having stage 3 evaporation as a function of cumulative depth of evaporation depletion,  $D_e$*

Source: Allen et al. (2005a); copyright ASCE

where  $TEW_2$  is the  $D_e$  when  $K_r = K_{r2}$  (point at which evaporation transitions from stage 2 to stage 3 drying, mm), and  $K_{r2}$  is the value for  $K_r$  at the junction of stage 2 and stage 3 drying.  $TEW_3$  is maximum cumulative depth of evaporation (depletion) from the soil surface layer when the soil is dry and no further evaporation occurs ( $K_r = 0$ ), mm. The value  $TEW_3$  includes  $REW$  and  $TEW_2$ .  $K_r$  is 0 when  $D_{e,i-1} \geq TEW_3$ . In all cases, for Eq. (9-24) and (9-25),  $K_r$  is limited to  $0 \leq K_r \leq 1.0$ .  $TEW_2$  is typically set to  $TEW$  computed from Eq. (9-20a, b) using  $z_e = 0.1$  or  $0.15$  m, and  $TEW_3$  is estimated from Eq. (9-20a, b) using a value for  $z_e$  greater than the  $z_e$  used to estimate  $TEW_2$ . Comparisons against observed data are recommended to determine best parameter values.

Generally, the value for  $K_{r2}$  ranges between about 0.05 and 0.4, depending on the nature and degree of cracking as the soil dries. Allen et al. (1998, 2005a) recommend  $K_{r2} \sim 0.2$  for cracking soils. Mutziger et al. (2005) find best fit values for  $K_{r2}$  for two cracking soils in Texas to be 0.3 and 0.2 when comparing against lysimeter measurements of evaporation for a black clay and clay loam. Stage 3 drying in the FAO-style model has been applied to cracking heavy clay soils in the Imperial Irrigation District of California (Allen et al. 2005a) and to two cracking or partially cracking soils in Texas (Mutziger et al. 2005). Values for the Imperial soils were  $REW = 8$  mm,  $TEW_2 = 50$  mm,  $TEW_3 = 100$  mm, and  $K_{r2} = 0.2$ . Best fit values to lysimeter evaporation measurements for the Houston black clay and Pullman clay loam soils of Mutziger et al. (2005) were  $REW = 7$  mm,  $TEW_2 = 30$  and 22 mm, and  $TEW_3 = 50$  and 45 mm. The stage 3 option for the FAO-56

method can also be used to simulate effects of upward flow from deeper soil layers for noncracking soils as illustrated later in comparisons against the HYDRUS model.

**Application within the Dual  $K_c$  Context** In the FAO-56 dual  $K_c$  model, described in Chapter 10,  $f_w$ , the fraction of the surface wetted by irrigation and/or precipitation, is used to limit the potential spatial extent of evaporation. Common values for  $f_w$  are listed in Table 9-2. When the soil surface is completely wetted, as by precipitation or sprinkler, the fraction of exposed wetted soil,  $f_{ew}$ , is set equal to  $(1 - f_c)$ , where  $f_c$  is the fraction of soil surface effectively covered by vegetation. For irrigation systems where only a fraction of the ground surface ( $f_w$ ) is wetted,  $f_{ew}$  is limited to  $f_w$ :

$$f_{ew} = \min(1 - f_c, f_w) \quad (9-26)$$

Both  $(1 - f_c)$  and  $f_w$ , for numerical stability, have limits of 0.01–1. In the case of drip irrigation, Allen et al. (1998) suggest that where most soil wetted by irrigation is beneath the crop canopy and is shaded  $f_w$  be reduced to about one-half to one-third of that given in Table 9-2. Their general recommendation for drip irrigation is to multiply  $f_w$  by  $[1 - (2/3) f_c]$ . Pruitt et al. (1984) and Bonachela et al. (2001) describe evaporation patterns and extent under drip irrigation.

Using a three-dimensional crop energy balance model, Luquet et al. (2005) suggest that plant transpiration in a cotton canopy can increase by 10% when shifting from furrow irrigation to drip irrigation due to transfer of heat from dry soil to adjacent vegetation. This implies that the  $K_{cb}$  might increase by a small amount when irrigated by drip or other irrigation

Table 9-2. Common Values for the Fraction of Soil Surface Wetted by Irrigation or Precipitation

Wetting Event	$f_w$
Precipitation	1.0
Sprinkler irrigation, field crops	1.0
Sprinkler irrigation, orchards	0.7 ... 1.0
Basin irrigation	1.0
Border irrigation	1.0
Furrow irrigation (every furrow), narrow bed	0.6 ... 1.0
Furrow irrigation (every furrow), wide bed	0.4 ... 0.6
Furrow irrigation (alternate furrows)	0.3 ... 0.5
Microspray irrigation, orchards	0.3 ... 0.8
Trickle (drip) irrigation	0.3 ... 0.4

Source: Data from FAO-56, Allen et al. (1998)

method where only a small fraction of the surface is wetted. However, the increase is a function of the fraction of time that the soil surface is wet. Typically drip irrigation wets the surface more frequently than a surface irrigation method so that some of the reduced evaporation from smaller  $f_w$  and perhaps increased transpiration by heat transfer is compensated by more frequent wetting events as opposed to surface or sprinkle irrigation (Burt et al. 2005). A schematic illustrating common extent and location of  $f_w$  and  $1 - f_c$  is shown in Figure 9-6.

Visual observation generally determines the value for  $f_c$ . For purposes of estimating  $f_{ew}$ ,  $f_c$  can be estimated using a general relationship between  $f_c$  and  $K_{cb}$  from FAO-56:

$$f_c = \left( \frac{K_{cb} - K_{c \min}}{K_{c \max} - K_{c \min}} \right)^{(1+0.5h)} \quad (9-27)$$

where  $K_{c \min}$  is the minimum (basal)  $K_c$  for dry bare soil with no ground cover, and  $h$  is the height of the crop in m. The differences  $K_{cb} - K_{c \min}$  and  $K_{c \max} - K_{c \min}$  are limited to  $\geq 0.01$  for numerical stability. The value for  $f_c$  will change daily as  $K_{cb}$  changes.  $K_{c \min}$  ordinarily has the same value as  $K_{cb}$  during the initial growth period for annual crops,  $K_{cb \text{ini}}$ , which represents nearly bare soil conditions (i.e.,  $K_{c \min} \sim 0.10$  to  $0.15$ ). However,  $K_{c \min}$  is set to 0 or nearly zero under conditions with long time periods between wetting events, for example, in applications with natural vegetation in deserts. The value for  $f_c$  decreases during the late season period in proportion to  $K_{cb}$  to account for local transport of sensible heat from senescing leaves to the soil surface.  $K_{cb}$ ,  $K_{c \min}$ , and estimation of  $K_{c \max}$  are discussed in more detail in Chapter 10. The FAO-56 dual  $K_c$  model can be applied using  $ET_o$  and  $ET_r$  references, provided the  $K_{cb}$  values used in the procedure are associated with the specific reference.

## 9.7 RELATIONSHIPS BETWEEN EVAPORATION AND TRANSPERSION

For partial or full plant cover, the rate of stage 1 evaporation under a crop canopy relative to reference ET is strongly linked to the LAI, or plant cover, that affects net radiation at the soil surface. Allen et al. (1964) illustrate how crop canopies intercept radiation, thus reducing energy for evaporation at the surface. Measurements of evaporation under corn, cotton, and maize canopies in Spain by Villalobos and Fereres (1990) indicate that  $E/ET_o$  decreases as LAI increases (Figure 9-7) in a manner similar to the decrease in the ratio reported by Ritchie (1972). Ritchie and Burnett (1971) show the ratio of net radiation at the soil surface ( $R_{ns}$ ) to total

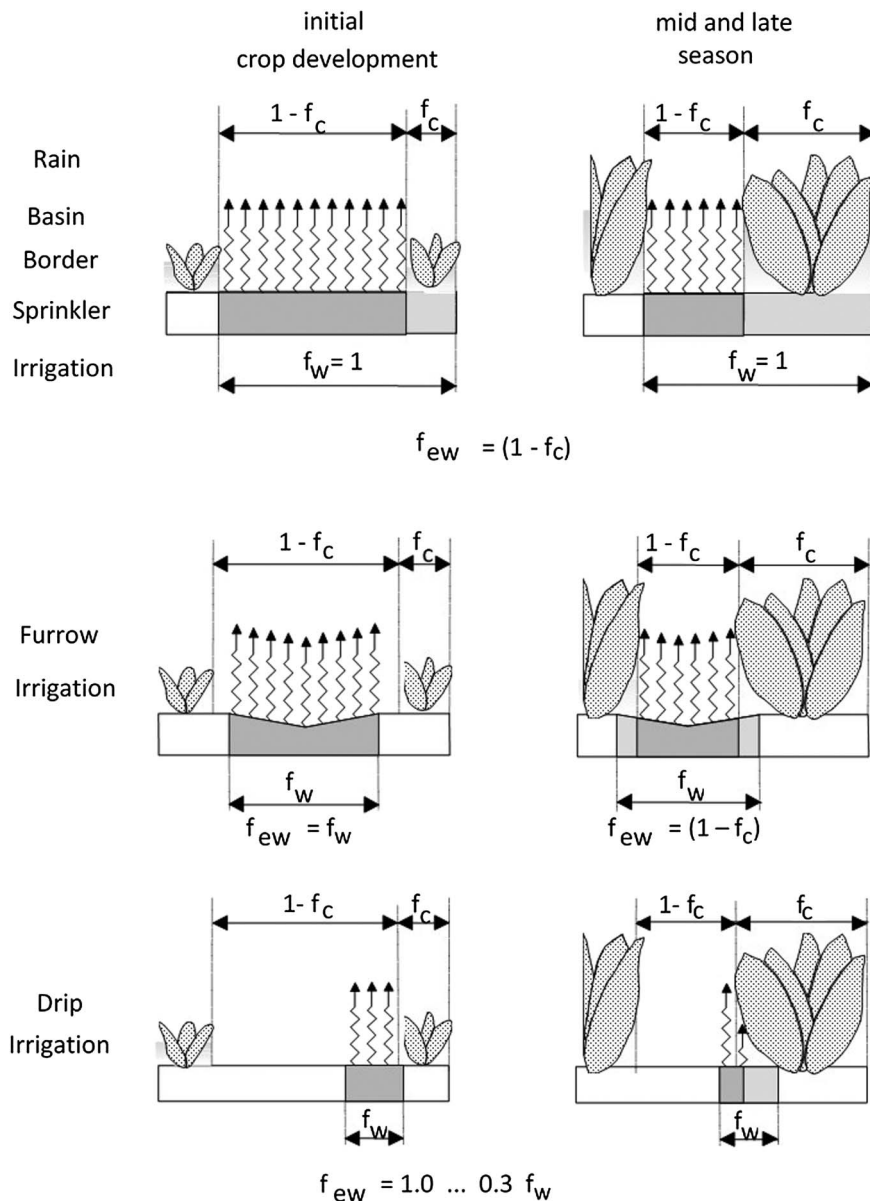


Fig. 9-6. Determination of  $f_{ew}$  (gray areas) as a function of the fraction of ground surface coverage ( $f_c$ ) and the fraction of the surface wetted ( $f_w$ )  
 Source: Allen et al. (1998); reprinted with permission from the U.N. Food and Agriculture Organization

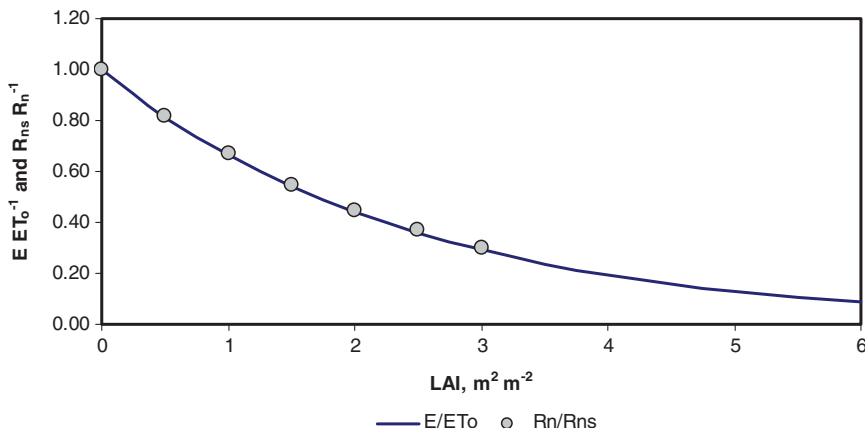


Fig. 9-7. Decrease in the ratios of  $E/ET_o$  during stage 1 evaporation in relation to LAI, which is nearly identical to the calculated decrease in  $R_{ns}/R_n$  using the relationship presented by Ritchie and Burnett (1971) as LAI increases  
Source: Data from Villalobos and Fereres (1990)

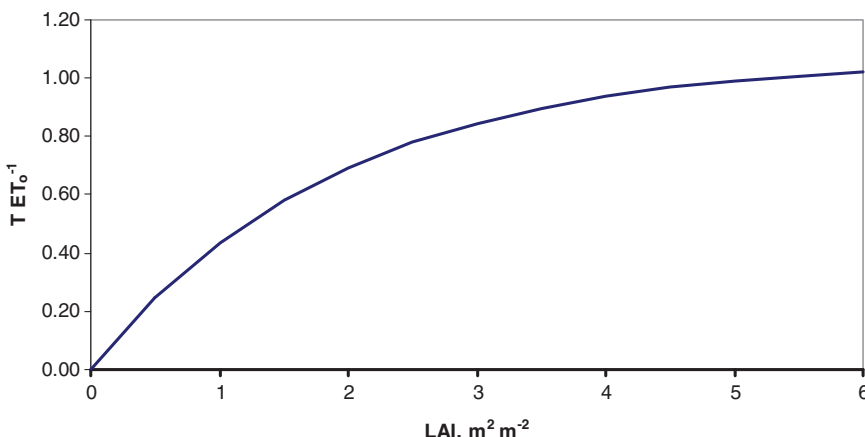


Fig. 9-8. Increase in the ratio of  $T/ET_o$  as LAI increases  
Source: Data from Villalobos and Fereres (1990)

net radiation above the canopy to decrease in a nearly identical proportion to the increase in LAI (Figure 9-7). These data indicate that variation in stage 1 evaporation for given weather conditions as LAI increases is largely due to the effect of LAI, or plant cover, reducing net radiation at the soil surface. In a similar manner, Villalobos and Fereres (1990) show that the ratio of transpiration ( $T$ ) to  $ET_o$  increases as LAI increases (Figure 9-8).

The ratio  $T/ET_o$  at a given level of LAI varies depending on the wetness of the soil surface.

Villalobos and Fereres (1990) show the interdependence of E and T processes. As evaporation from the soil decreases as the soil dries, an increase in transpiration occurs at a given level of reference ET and LAI. They report  $T/ET_o$  in cotton that was 1.1 at LAI = 3 when the soil surface was dry and E was low. When the soil was wetted by rain or irrigation, the calculated  $T/ET_o$  ratio dropped to 0.6 the first day after wetting. In the FAO-56 procedure, fraction of cover,  $f_c$ , is used as a surrogate for LAI, to proportion potential T and E.

## 9.8 WATER BALANCE OF THE EVAPORATION LAYER

Estimation of  $K_e$  using the FAO evaporation model via Eqs. (9-17) and (9-19) requires a water balance conducted for the  $f_{ew}$  fraction of the surface soil layer on a daily or shorter time step:

$$D_{e,i} = D_{e,i-1} - \left[ (1-f_b) \left( P_i - RO_i + \frac{I_i}{f_w} \right) + f_b \left( P_{i+1} - RO_{i+1} + \frac{I_{i+1}}{f_w} \right) \right] + \frac{E_i}{f_{ew}} + T_{e,i} \quad (9-28)$$

where  $D_{e,i-1}$  and  $D_{e,i}$  are cumulative depletion depth at the ends of days  $i-1$  and  $i$  in mm;  $P_i$  and  $RO_i$  are precipitation and precipitation runoff from the soil surface on day  $i$  in mm;  $I_i$  is the irrigation depth on day  $i$  that infiltrates the soil in mm;  $E_i$  is evaporation on day  $i$  (i.e.,  $E_i = K_e ET_{ref}$ ) in mm;  $T_{e,i}$  is the depth of transpiration from the exposed and wetted fraction of the soil surface layer on day  $i$  in mm; and  $f_b$  is the fraction of the precipitation and irrigation during a calculation time step (hour or day) that is assumed to contribute immediately to evaporation during that same time step, with  $1-f_b$  of the precipitation and irrigation not contributing to evaporation until the following time step, on average. If unknown,  $f_b$  can be set to 0.5.  $f_b$  has limits of 0 and 1.0.  $f_b$  effectively controls the immediacy of evaporation from a wetting event that may occur at an unknown time within the calculation time step, for example, nighttime irrigations during a daily time step. Eq. (9-28) is a form for  $D_{e,i}$  proposed by Allen et al. (2011a) to distribute  $P$  and  $I$  between adjacent time steps to account for their influence on the timing of the increase in E stemming from the wetting event. This may be important for daily time steps, but generally is not important for hourly or shorter time steps. Variables having subscripts " $i+1$ " indicate values for the time step following current time step  $i$ . Assuming that the surface layer is at field capacity following heavy rain or irrigation, the minimum value for  $D_{e,i}$  is zero. The deep percolation term of the original FAO-56 formulation for Eq. (9-28) is omitted in the new equation forms for Eqs. (9-28) and (9-29) as it is not needed.

Instead,  $D_{e,i}$  and  $D_{e,i-1}$  are constrained to limits of  $0 \leq D_{e,i} \leq TEW$ . Any  $P$  or  $I$  additions in excess of  $D_{e,i}$  [and  $D_{REW,i}$  in Eq. (9-29)] are assumed to infiltrate to depths in the soil below  $z_e$  (or below the skin in the case of  $D_{REW,i}$ ).

The irrigation depth  $I_i$  is divided by  $f_w$  to approximate the infiltration depth to the  $f_w$  portion of the soil surface. Similarly,  $E_i$  is divided by  $f_{ew}$  because all  $E_i$  (other than residual evaporation implicit to the  $K_{cb}$  coefficient) is assumed to be taken from the  $f_{ew}$  fraction of the surface layer. Soil water content can exceed field capacity for a few days following a large wetting event, and some drainage in soil occurs at very small rates at water contents below field capacity. To some extent, effects of these simplifying assumptions can be compensated for in setting the value for  $z_e$  or  $TEW$ .

The parameter  $D_{REW,i-1}$  in Eq. (9-22) is the depletion of water from the  $REW$  layer, referred to as the skin layer, at the end of the prior  $i - 1$  time step. Eq. (9-22) estimates the  $F_{\text{stage1}}$  parameter used in Eqs. (9-19) and (9-21) to simulate any stage 1 evaporation that may occur from light or heavy wetting events. Allen (2011) provides background. For light wetting events, stage 1 evaporation may last for only part of a single time step. The calculation of  $D_{REW,i}$  is designed, similar to Eq. (9-28), to be forward looking with regard to the wetting event to consider soil surface wetting and corresponding evaporation from a wetting event occurring during the current time step  $i$ :

$$D_{REW,i} = D_{REW,i-1} - \left[ (1-f_b) \left( P_i - RO_i + \frac{I_i}{f_w} \right) + f_b \left( P_{i+1} - RO_{i+1} + \frac{I_{i+1}}{f_w} \right) \right] + \frac{E_i}{f_{ew}} \quad (9-29)$$

where  $D_{REW,i-1}$  and  $D_{REW,i}$  are cumulative depletion depth at the ends of days  $i - 1$  and  $i$  in mm, and all other terms are the same as for Eq. (9-28).  $D_{REW,i}$  and  $D_{REW,i-1}$  are constrained to limits of  $0 \leq D_{REW,i} \leq REW$ .

The amount of transpiration extracted from the  $f_{ew}$  fraction of the evaporating soil layer is generally a small fraction of total transpiration. When the surface 0.01 m of soil dries, the resistance to evaporation increases greatly (van de Griend and Owe 1994; Aluwihare and Watanabe 2003). Healthy plant roots are not likely to be in the surface 0–0.05 m of soil that, depending on the rate of evaporation, may become air-dry within a few days following irrigation due solely to evaporation. Although some roots and soil water extraction may be present between 0.05 m and 0.10 m, under normal irrigation practices the decrease in soil water content of this layer due to transpiration will not significantly affect the evaporation rate that is controlled by the dry upper layer and the rate of water movement by liquid and vapor flow from lower depths. An exception to this is for shallow-rooted crops like vegetables that may extract some water from this evaporation layer, which is hydrated more frequently.

For shallow-rooted annual crops with rooting depth less than about 0.5 m and where deep cultivation is not practiced,  $T_e$  may have significant effect on the water balance of the surface layer and therefore on estimation of the evaporation component during the development period. The following extension to FAO-56 from Allen et al. (2005b) estimates  $T_e$  from the  $f_{ew}$  fraction of the evaporation layer in proportion to the water content of that layer:

$$T_e = K_t K_s K_{cb} ET_{ref} \quad (9-30)$$

where  $K_t$ , (0–1) is the proportion of basal ET ( $= K_{cb} ET_{ref}$ ) extracted as transpiration from the  $f_{ew}$  fraction of the surface soil layer.  $K_s$  is the soil water stress factor computed for the root zone (0–1). ( $K_s$  is discussed in Chapter 10.)  $K_t$  is determined by comparing relative water availability in the  $z_e$  and root zone ( $z_r$ ) layers (where the  $z_e$  layer is a subset of the  $z_r$  layer) along with the presumed rooting distribution. For the  $f_{ew}$  fraction,

$$K_t = \left( \frac{1 - \frac{D_e}{TEW}}{1 - \frac{D_r}{TAW}} \right) \left( \frac{z_e}{z_r} \right)^{0.6} \quad (9-31)$$

where the numerator and denominator of the first expression are limited to  $\geq 0.001$ , and the value for  $K_t$  is limited to  $\leq 1.0$ .  $z_e$  and  $z_r$  have the same units.  $D_r$  is depletion of the total effective root zone, estimated from Eq. (10-9) of Chapter 10. In the simple water balance procedure of FAO-56, the soil water content is assumed to be limited to  $\leq \theta_{fc}$  on the day of a complete wetting event. This is a reasonable assumption considering the shallowness of the surface layer.

## 9.9 EXAMPLE ESTIMATES OF EVAPORATION

The following examples show how performances of the simple SRT and FAO-56 models compare with absolute measurements of evaporation taken by a precision-weighing lysimeter system. The examples also show comparisons against the more complex model HYDRUS-1D. These examples illustrate how evaporation models can be intercompared and tested.

### Comparisons of Models with a Weighing Lysimeter

The following figures show example applications of the SRT model and various levels of the FAO-56 model for a bare silt loam soil near Kimberly, Idaho. Comparisons are made against evaporation measured by a large weighing lysimeter system. The first example compares evaporation measurements during stage 1 and stage 2 with estimates from the FAO-56 (Allen et al. 1998) method and with stage 2 evaporation estimates from the

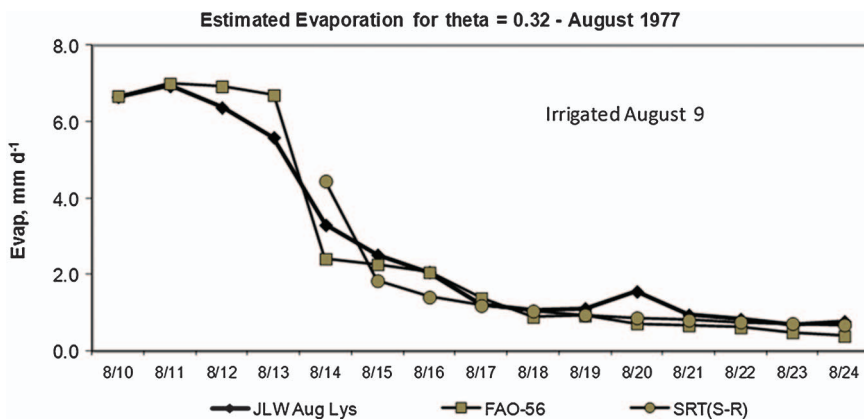


Fig. 9-9. Comparison of measured evaporation (JLW Aug Lys) with estimated evaporation during August 10–24, 1977, near Kimberly, Idaho, using the FAO-56 procedure [Eq. (9-19), (9-20a), and (9-21) with  $F_{\text{stage}1}$  set to 0] and using the SRT model [Eq. (9-11)] with  $\alpha_r$  estimated using Eq. (9-15) with  $K_a = 13.9 \text{ mm d}^{-1}$ . "JLW" = James L. Wright. "S-R" = Suleiman and Ritchie (2003)

Source: Data from Dr. J. L. Wright, USDA-ARS (retired)

SRT model [Eqs. (9-1), (9-11)] where  $\alpha_r$  is estimated from the drained upper limit (field capacity) using Eq. (9-15). Variable  $K_\alpha$  for the SRT model was set =  $13.9 \text{ mm d}^{-1}$ , based on the weighted-mean diffusivity from  $\theta_{dul}$  to  $\theta_r$  (Suleiman and Ritchie 2003). Comparisons are shown for two drying series, one in mid-August 1977 (Figure 9-9) and one in early September 1977 (Figure 9-10). In the first example, the original form and application of the FAO-56 method is used where Eqs. (9-19), (9-20a), and (9-21) were applied with the  $F_{\text{stage}1}$  parameter of Allen et al. (2011a) set to 0. The second example applied the same equations and settings for  $z_e$ , REW, and TEW as used for example 1, but with the water balance of the 0 to 0.15 m  $z_e$  evaporation layer experimentally modified to include an estimate of upward flux into the evaporation layer, based on the SRT model. This second example illustrates the relative sensitivity of the FAO-56 model to replacing the implicit assumption that deep upward flux to the  $z_e$  layer is reflected in the value for  $z_e$  with an explicit estimation of upward flux.

In the first two examples, the length of stage 1 evaporation and start of stage 2 evaporation for the SRT application was based on observing when the ratio of measured  $E$  to  $ET_o$  began to decay below 1.1 to 1.2. This occurred after the fourth day after irrigation for both time series. This type of observation is not typically available in practice, and the start of stage 2 evaporation generally needs to be estimated using a water balance of the skin evaporation layer, such as is done with Eq. (9-29). In the experimental application of example 2, the upward flow into the evaporation layer

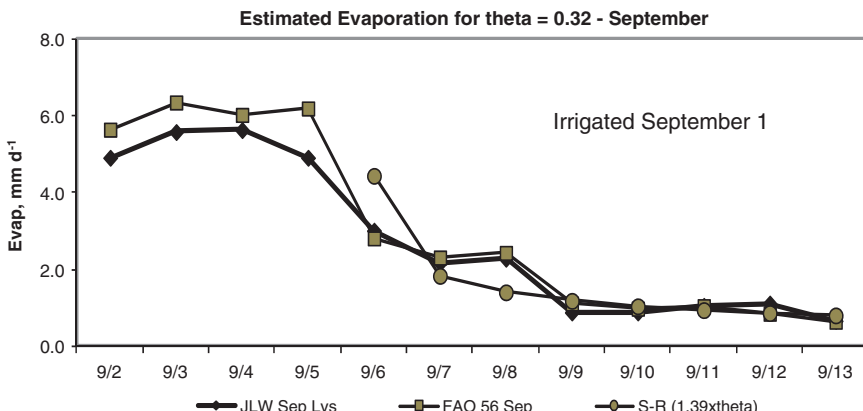


Fig. 9-10. Comparison of estimated evaporation with measured evaporation during September 2–13, 1977, near Kimberly, Idaho, using the FAO-56 procedure [Eqs. (9-19), (9-20a), and (9-21) with  $F_{stage1}$  set to 0] and using the SRT model [Eq. (9-11)] with  $\alpha_r$  estimated using Eq. (9-15) with  $K_a = 13.9 \text{ mm d}^{-1}$ . Source: Data from Dr. J. L. Wright, USDA-ARS (retired).

during stage 2 is estimated as 0.2 of the stage 2 evaporation rate using the SRT model with Eq. 9-15 of Suleiman and Ritchie (2003) (S-R). Day 1 occurred at the beginning of stage 2 evaporation. Impact of the inclusion of estimated upward flow is minor, as illustrated by comparing Figure 9-9 with Figure 9-11 and Figure 9-10 with Figure 9-12.

Dr. J. L. Wright, USDA-ARS (retired), Kimberly, Idaho, collected the lysimeter data in 1977, which were described in Mutziger et al. (2005). The Kimberly lysimeter system was a precision-weighing lysimeter 1.83 m on a side and 1.2 m deep and filled with Portneuf silt loam soil. Evaporation measurements were made hourly, but only 24-hour totals were commonly evaluated from the system (Wright 1982). Two time series of evaporation were available during August and September 1977 from a bare surface following harvest of a crop of peas. Irrigation of the lysimeter and surrounding field was by furrow. The relatively large irrigation doses to the lysimeter were spread over parts of a day to avoid overtopping the lysimeter during surface ponding. The irrigation amount for the August series was 103 mm on August 9. Irrigation amounts for the late August–early September series were 60, 19, and 34 mm on August 25, August 29, and September 1. The August 10–24 series represents an evaporation event following a single large wetting event, and the extended August 25–September 24 series represents a series with multiple irrigations in succession at the beginning and a series of small precipitation events near the end. In examples 1 and 2, shown in Figures 9-9 and 9-10, the starting date for the evaporation series was assumed to be September 2. For

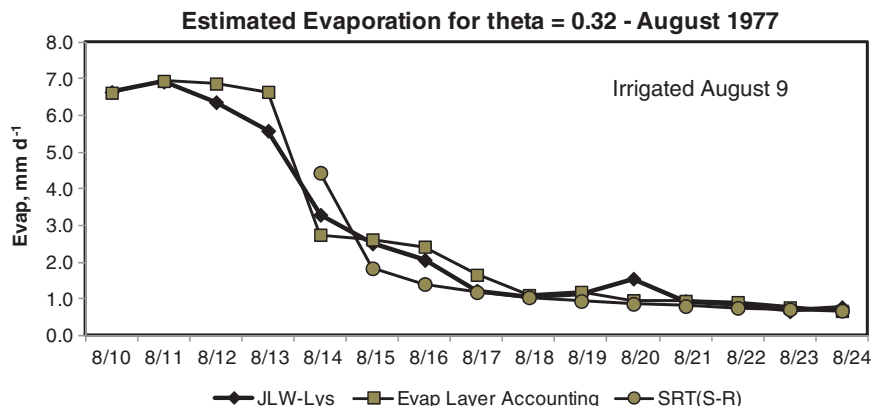


Fig. 9-11. Comparison of calculated evaporation with measured evaporation during August 10–24, 1977, near Kimberly, Idaho, using the FAO-56 procedure [Eqs. (9-19), (9-20a), and (9-21) with  $F_{\text{stage}1}$  set to 0], using a water balance model that considers upward flux into the evaporation layer, and using the SRT model [Eq. (9-11), with  $\alpha_r$  estimated using Eq. (9-15) with  $K_a = 13.9 \text{ mm d}^{-1}$ . "JLW" = James L. Wright. "S-R" = Suleiman and Ritchie (2003)  
Source: Data from Dr. J. L. Wright, USDA-ARS (retired)

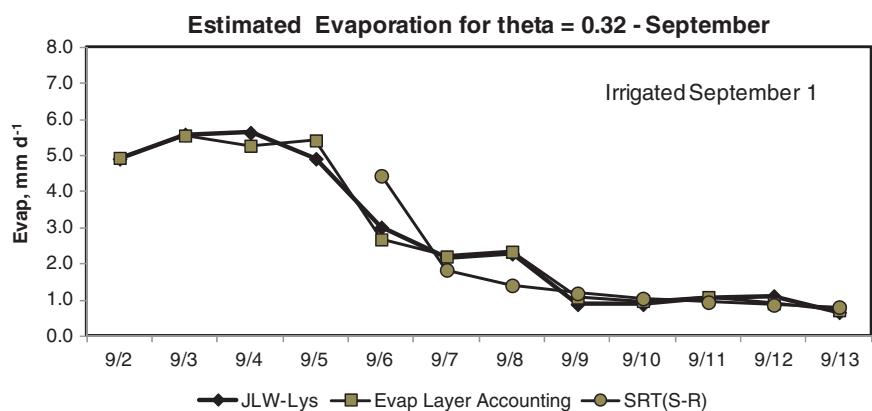


Fig. 9-12. Comparison of calculated evaporation with measured evaporation during September 2–13, 1977, near Kimberly, Idaho, using the FAO-56 procedure [Eqs. (9-19), (9-20a), and (9-21) with  $F_{\text{stage}1}$  set to 0], using a water balance model that considers upward flux into the evaporation layer, and using the SRT model [Eq. (9-11)] with  $\alpha_r$  estimated using Eq. (9-15) with  $K_a = 13.9 \text{ mm d}^{-1}$ . "JLW" = James L. Wright. "S-R" = Suleiman and Ritchie (2003)  
Source: Data from Dr. J. L. Wright, USDA-ARS (retired)

the third example, shown in Figure 9-11, the full series with all three irrigation days and four precipitation events was evaluated. The large doses of irrigation on the Kimberly lysimeter and delayed drainage required delaying the transition out of stage 1 drying in examples 1 and 2 by delaying the final start of stage 1. This was done by setting  $D_e$  to 0 at the beginning of both August 10 and 11 in Eq. (9-21) in the first series and at the beginning of September 2 and 3 for the second series. The need for the override was negated in example 3 by implementing a delay function for infiltration following the large irrigation doses. Parameter  $f_b$  in Eq. (9-28) was set to 0 in all three examples.

For Figures 9-9 through 9-12, the REW for the FAO-56 model application was estimated to be 11 mm based on Table 9-1. The TEW was estimated to be 39 mm based on  $z_e = 0.15$  m and reported soil water values of  $\theta_{fc} = 0.32$ ,  $\theta_{wp} = 0.12$ , and the assumption  $\theta_{ad} = \theta_{wp}/2 = 0.06 \text{ m}^3 \text{ m}^{-3}$ . The value for  $K_{e\max}$  was set to 1.2 for stage 1 evaporation estimates because grass reference  $ET_o$  was used. A summary of daily evaporation estimates for the first time series is presented in Figure 9-9 and estimates for the second drying series are presented in Figure 9-10. Use of  $K_{e\max} = 1.2$  for September resulted in about 10% overestimation of evaporation during stage 1.

The estimated start of stage 2 evaporation for the two series in Figs. 9-9–9-12 was August 14 (day 5 after irrigation) and September 6 (day 5 after irrigation). Table 9-3 summarizes measured and estimated stage 2 evaporation values for August 14–24 and September 6–13 using the FAO-56 and SRT(S-R) models.

Table 9-3. Summary of Measured and Estimated Stage 2 Evaporation Values for August 14–24 and September 6–13 Using the FAO-56 and SRT (Suleiman and Ritchie 2003) (S-R) Models

	RMSD*
August lysimeter measured stage 2 evaporation =	16.1 mm —
FAO-56 estimated stage 2 evaporation =	12.8 mm (80%) $0.42 \text{ mm d}^{-1}$
SRT(S-R) estimated stage 2 evaporation =	14.8 mm (92%) $0.50 \text{ mm d}^{-1}$
September lysimeter measured evaporation =	12.1 mm —
FAO-56 estimated stage 2 evaporation =	11.5 mm (95%) $0.18 \text{ mm d}^{-1}$
SRT(S-R) estimated stage 2 evaporation =	11.6 mm (96%) $0.75 \text{ mm d}^{-1}$

\*RMSD = Root mean square difference

Table 9-4. Summary of Measured and Calculated Stage 2 Evaporation from Eqs. (9-19) and (9-21) Based on Evaporation Layer Water Balance for August 14–24 and September 6–13 Using an Experimental Estimate of Upward Flux into the Evaporation Layer

		RMSD*
August lysimeter measured stage 2 evaporation =	16.1 mm	—
Water balance calculation of stage 2 evaporation =	15.6 mm (97%)	0.33 $\text{mm d}^{-1}$
September lysimeter measured evaporation =	12.1 mm	—
Water balance calculation of stage 2 evaporation =	11.9 mm (98%)	0.18 $\text{mm d}^{-1}$

\*RMSD = Root mean square difference

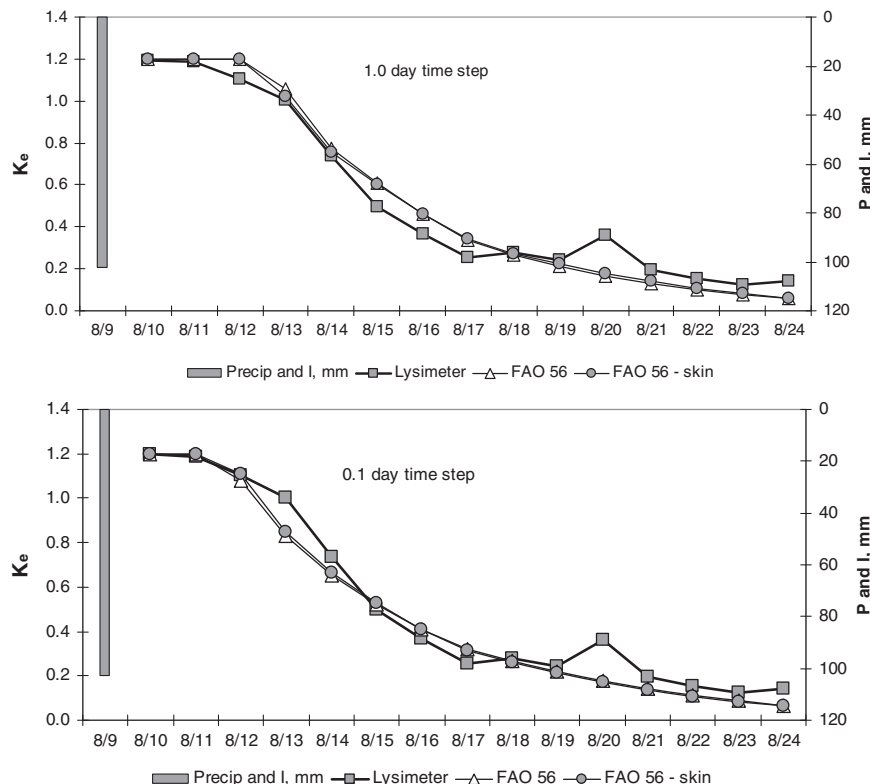
Table 9-4 summarizes measured and calculated stage 2 evaporation based on evaporation layer water balance for August 14–24 and September 6–13 using an experimental estimate of upward flux into the evaporation layer of the FAO-56 model during stage 2 evaporation based on the SRT(S-R) model.

The FAO-56 method provides reasonable estimates with a root-mean square of the daily difference (RMSD) of  $0.42 \text{ mm d}^{-1}$  in August and  $0.16 \text{ mm d}^{-1}$  in September. The RMSDs for the SRT(S-R) estimates were 0.50 and  $0.71 \text{ mm d}^{-1}$  for the August and September time series, respectively. When assuming that upward flux into the evaporation layer equals one-half of the SRT(S-R) stage 2 evaporation, the RMSD of water balance calculated evaporation in August was reduced to  $0.30 \text{ mm d}^{-1}$ . For this example, day 1 of stage 2 for calculating the SRT(S-R) upward flux was August 10 and September 2. The estimated upward flux was about 25% of the calculated stage 2 evaporation. The upward flux resulted in higher calculated stage 2 evaporation, which was closer to lysimeter-measured evaporation in August than when upward flux was not considered. No reduction occurred in the RMSD when considering upward flux for September.

A third example application for the FAO-56 model includes Eqs. (9-19), (9-20a), and (9-21) with the  $F_{\text{stage}1}$  parameter estimated using Eq. (9-22) and Eq. (9-29) to provide better definition of transition from stage 1 to stage 2 drying for 24-hour calculation time steps and to improve estimation of evaporation following small wetting events. This example also illustrates the effect of using shorter 0.1-day calculation time steps as compared with using 24-hour calculation time steps. The example implemented a maximum drainage rate of  $75 \text{ mm d}^{-1}$  from the  $z_e$  evaporation layer following irrigation at the beginning of the mid-August series to account for delayed

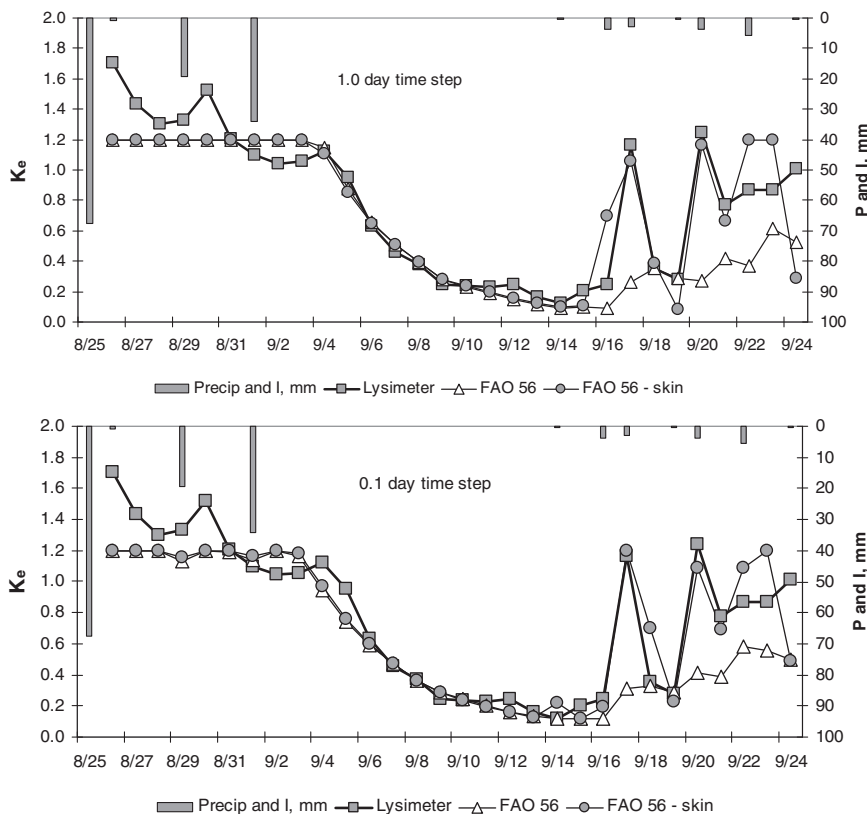
infiltration of surface ponded irrigation water when the large 103-mm dose was applied. The delayed infiltration in the lysimeter may have been caused by effects of entrapped air. The use of the drainage rate eliminated the need to reset depletion depth  $D_e$  to zero for one day following irrigation as was done with examples 1 and 2.

Figure 9-13 shows results for the third example for the August 10–24 evaporation series, and Figure 9-14 shows the August 25–September 24 series.  $K_e$  is presented in the form  $E/ET_o$ . Delayed drainage ( $Inf$ ) from the



*Fig. 9-13. Evaporation coefficient,  $K_e$ , during stage 1 and stage 2 drying for 12 days during August 10–24, 1977, near Kimberly, Idaho, using a 1-day calculation time step (top) and 0.1-day calculation time step (bottom) for the FAO-56 procedure [Eqs. (9-19), (9-20a), and (9-21)] with  $F_{stage1}$  set to 0 to represent the original FAO-56 method (triangles) and with  $F_{stage1}$  calculated with Eqs. (9-22) and (9-29) to consider skin evaporation (circles), compared against evaporation measured by weighing lysimeter. Irrigation of 103 mm occurred on August 9, with infiltration of 28 mm delayed to August 10*

*Source: Data from Dr. J. L. Wright, USDA-ARS (retired)*



*Fig. 9-14. Evaporation coefficient,  $K_e$ , during stage 1 and stage 2 drying for 30 days during August 25–September 24, 1977, near Kimberly, Idaho, where three frequent irrigations occurred early in the period and four light precipitation events occurred late in the period, using a 1-day calculation time step (top) and 0.1-day calculation time step (bottom) for the FAO-56 procedure [Eqs. (9-19), (9-20a), and (9-21)] with  $F_{stage1}$  set to 0 to represent the original FAO-56 method (triangles) and with  $F_{stage1}$  calculated with Eqs. (9-22) and (9-29) to consider skin evaporation (circles), compared against evaporation measured by weighing lysimeter*

Source: Data from Dr. J. L. Wright, USDA-ARS (retired)

evaporation layer during the August 10–24 series, following the large irrigation dose, prolonged the length of stage 1 by about one day. The three irrigations over the first seven days of the second evaporation series (August 25–September 24) were close enough together in time to create an essentially single, extended stage 1 period having a length of 9 days and cumulative evaporation depth of more than 40 mm before the start of stage

2 drying. The end of stage 1 was determined when  $D_{e,j}$  exceeded the value for  $REW$ , which was 11 mm in all cases. The measured total cumulative evaporation during the two series was 43 and 87 mm. Both of these values were greater than the estimated  $TEW$  of 39 mm due to the extended lengths of stage 1 drying caused by delayed drainage in the first series and multiple wetting events in the second series.

The performance of the FAO-56 model was similar between the original application where skin evaporation was not considered and the second application when using the skin evaporation for the first time series for which only one large irrigation at the beginning of the period and no light events occurred (Figure 9-13). Differences did occur between the original formulation, where  $F_{stage1}$  was set to 0, and the newer skin evaporation formulation near the end of the second time series when small precipitation events of less than 8 mm occurred. Under that situation, the original model mixed the small additions of water into the water balance for the  $z_e$  layer. The reduction in the value for  $D_e$  was not enough to transition the evaporation process, via  $K_r$ , into stage 1. The use of the  $F_{stage1}$  parameter via Eqs. (9-22) and (9-29) did transition the process into stage 1 until the new additions of water evaporated. That process simulated the "flash" evaporation events by operating the separate water balance for the top "REW" layer. The skin evaporation enhancement followed the measurements by the lysimeter relatively well during the light precipitation events, as Figure 9-14 shows for both calculation time steps. The impact of calculation time step length was not large for either time series. The 0.1-day time step estimated an earlier transition from stage 1 to stage 2 than did the 1-day calculation time step, but impacts were minor. The performance of the skin evaporation enhancement was similar for the two time step lengths.

Lysimeter-measured  $K_e$  exceeded 1.3 for the first five days of the evaporation cycle, using the grass reference  $ET_o$  as the basis. These values exceed the maximum values for  $K_e$  expected and may have stemmed from stored heat in the soil from the dry period prior to the wetting event.

Figure 9-15 shows cumulative evaporation during stage 1 and stage 2 drying for the 30-day period from August 25 to September 24, 1977, based on  $K_e$  calculations from Figure 9-14. Results are for the 1-day calculation time step and resemble those from the 0.1-day calculation time step. Figure 9-15 also shows cumulative evaporation for the SRT model using the same settings as for examples 1 and 2. Stage 1 evaporation for the SRT application was estimated using the FAO-56 procedure [Eq. (9-19)]. Therefore the cumulative evaporation is similar for the FAO-56 and SRT models until stage 2. During stage 2, the SRT model estimates less evaporation than the FAO-56 model and as measured by the lysimeter. The long estimated time for stage 1 was caused by the multiple irrigation events, which delayed the reduction in  $E$  by the SRT model for stage 2.

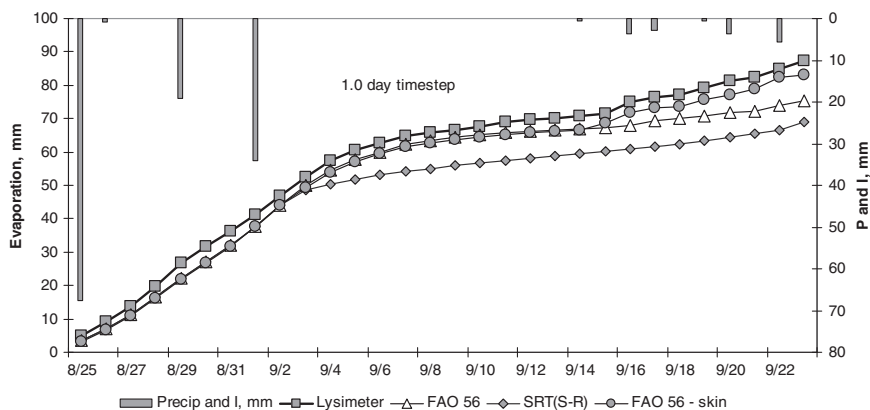


*Fig. 9-15. Cumulative evaporation during stage 1 and stage 2 drying for the 30-day period from August 25 to September 24, 1977, based on  $K_e$  calculations from Fig. 9-14 using a 1-day calculation time step plus application of the SRT model with the same settings as for examples 1 and 2 with stage 1 evaporation estimated using the FAO-56 procedure*

Source: Measured data from Dr. J. L. Wright, USDA-ARS (retired)

### Comparison of the FAO-56 Model with HYDRUS-1D

HYDRUS-1D ([Šimůnek et al. 1998, 2005](#)) is a widely used, one-dimensional, gridded finite-difference model that employs the theoretical Richards equation for unsaturated flow ([Richards 1931](#)), including flow to the surface for evaporation. The evaporation rate in HYDRUS-1D is governed by potential evaporative demand, soil water content, and soil potential gradients near the surface and hydraulic properties of the soil. A finite element numerical solution technique is used to solve gridded equations. Estimation of evaporation by HYDRUS-1D is sensitive to the grid density near the surface, where a fine grid is required to cope with potentially large hydraulic gradients and finite changes in soil water content and hydraulic conductivity. The advantage of HYDRUS-1D is its use of a hydraulic basis for evaporation and the ability to consider effects of soil water storage at various depths below the surface on the surface evaporation estimate. Disadvantages are the requirement for unsaturated hydraulic characteristics for the soil. However, standardized soil types residing within HYDRUS-1D can be utilized ([Šimůnek et al. 2005](#)).

Figs. 9-16 and 9-17 illustrate the performance of the somewhat simple FAO-56 model compared against the HYDRUS-1D model for a full calendar year of weather data collected near Kimberly, Idaho, during 2002. The HYDRUS-1D model was applied using standardized van Genuchten soil

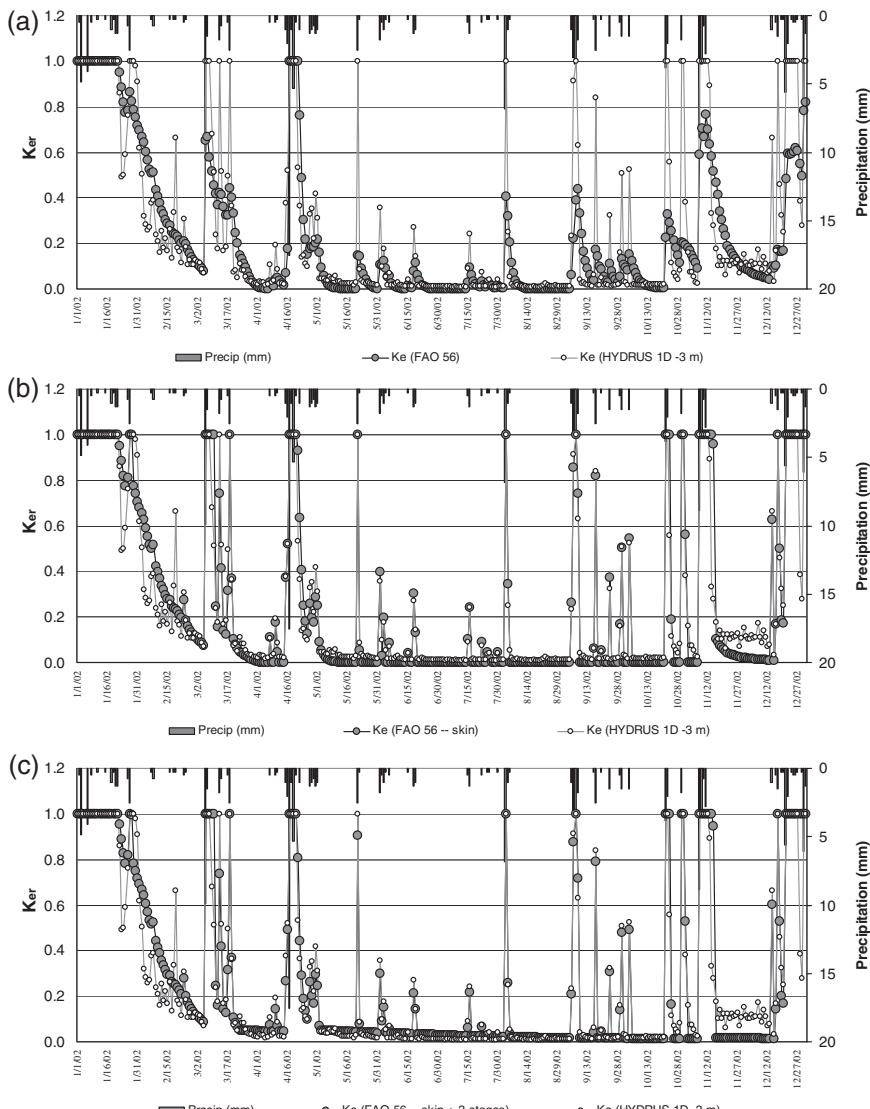
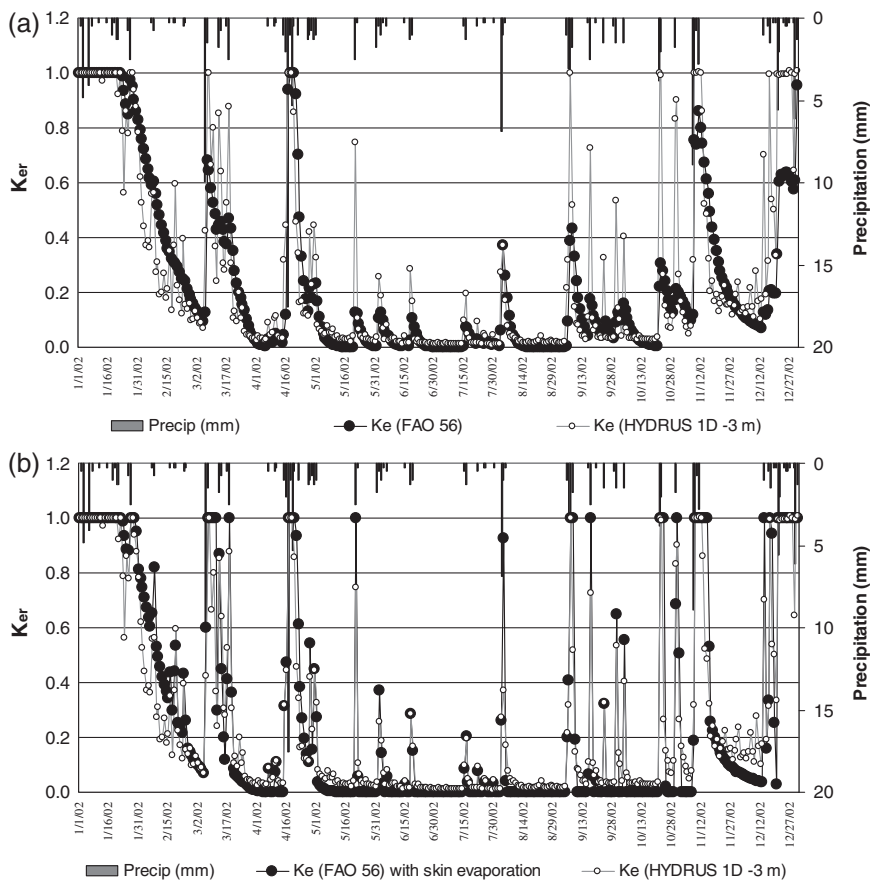


Fig. 9-16. Daily  $K_e$  (alfalfa reference basis) for FAO-56 calculations on a 24-hour time step for (a) the original FAO model without the skin evaporation enhancement with  $F_{stage1}$  set to 0.0; (b) with the skin evaporation enhancement; and (c) with the skin evaporation enhancement and with three stages of drying compared against  $K_e$  from HYDRUS-1D

Source: HYDRUS calculations by R. Dhungel and R. G. Allen, Univ. Idaho, Kimberly, personal communication



*Fig. 9-17. Daily  $K_e$  (alfalfa reference basis) for FAO-56 calculations on an hourly time step for (a) the original FAO model without the skin evaporation enhancement with  $F_{stage1}$  set to 0.0 and (b) with the skin evaporation enhancement compared against  $K_e$  from HYDRUS-1D*

Source: HYDRUS calculations by R. Dhungel and R. G. Allen, Univ. Idaho, Kimberly, personal communication

water potential and hydraulic conductivity parameters for the standard silt loam soil of HYDRUS-1D (Šimůnek et al. 1999, 2005). The initial 2-m soil profile was assumed to be moist, with initial soil water potential set at  $-3\text{ m}$ , representing conditions near field capacity, to illustrate effects of upward flow from depth for a moist soil condition. The HYDRUS-1D grid was designed using 5-mm soil layers to a depth of 2 m to provide high resolution in solutions for evaporation. The soil surface was assumed to be bare, with no transpiration extraction and using  $f_{ew} = 1.0$  in the

FAO-56 equations. The FAO-56 application was applied using typical values for a silt loam soil,  $TEW = 25$  mm and  $REW = 8$  mm. These values are not the same values as used for the specific Portneuf silt loam soil in previous examples. Weather data recorded at Kimberly, Idaho, during a full year (2002) were used for the simulations, with  $ET_{ref}$  estimated using the tall ASCE standardized Penman-Monteith (alfalfa) reference method (ASCE 2005) and  $K_{e\max}$  set to 1.0 to reflect the tall reference. Potential evaporation in the HYDRUS-1D application was estimated as  $K_{e\max} ET_{ref}$ .

Figure 9-16 shows daily comparisons of  $K_e$  (denoted  $K_{er}$  to indicate the alfalfa reference basis) for the FAO-56 model where calculations were made on a 24-hour time step (a) without the skin evaporation enhancement [Eqs. (9-19), (9-20a), and (9-21) with  $F_{stage1}$  set to 0.0], (b) with the skin evaporation enhancement [ $F_{stage1}$  calculated with Eqs. (9-22) and (9-29)], and (c) with the skin evaporation enhancement and three stages of drying [Eqs. (9-24) and (9-25)]. The HYDRUS-1D calculations for  $K_e$  were determined by dividing 24-hour  $E_s$  by 24-hour  $ET_{ref}$ , where 24-hour  $E_s$  was summed in HYDRUS-1D from internally determined time steps that are dynamically varied in HYDRUS-1D according to rates of change in state variables of potentials and water contents.

$K_e$  estimated by the FAO-56 model compared well with that by HYDRUS-1D for all three variations of the FAO-56 model following substantial wetting events that rehydrated  $D_e$  of the  $z_e$  layer. For light wetting events, the FAO-56 model with the skin evaporation enhancement best estimated  $K_e$ , where short-lived  $K_e$  spikes extended toward  $K_{e\max} = 1.0$ . The basic FAO-56 model without the skin evaporation enhancement underestimated the evaporation spikes because the slab model assumes complete mixing of small additions of water into the  $z_e$  layer, thus only reducing the total depletion of the slab by a relatively small amount. In contrast, the HYDRUS-1D model tended to capture small water additions near the soil surface and allowed them to evaporate somewhat rapidly. The result was a larger spike in  $K_e$ , often reaching 1.0, and a short duration of decay. The use of the skin evaporation enhancement simulated the flash evaporation events relatively well and reduced the RMSD between the FAO-56 model and HYDRUS-1D runs for the 365-day period from  $0.51 \text{ mm d}^{-1}$  for the FAO-56 model with no skin evaporation enhancement to  $0.27 \text{ mm d}^{-1}$  with skin evaporation enhancement. The RMSD decreased further to  $0.23 \text{ mm d}^{-1}$  with both skin evaporation and three-stage drying enhancements.

The differences in annual evaporation estimation were somewhat small among applications, with total estimated annual evaporation of 159, 169, and 190 mm for the three applications of FAO-56 compared with 175 mm estimated by HYDRUS-1D and 154 mm of precipitation. The annual evaporation estimates exceeded precipitation because of assumed water stored in the soil prior to January 1. The use of skin evaporation only increased the annual evaporation estimate by 10 mm, or less than 7%,

due to the conservation of mass exercised by the FAO-56 model. Addition of stage 3 drying to simulate upward flow increased estimated evaporation by an additional 20 mm over the calendar year. Best agreement between low levels of  $K_e$  by the FAO-56 model and by HYDRUS over extended periods of drying during summer months were obtained with the stage 3 implementation using  $TEW_3 = 60$  mm, with  $TEW_2 = TEW = 25$  mm and with  $K_{r2} = 0.05$ . With the stage 3 drying option, the very low values for  $K_e$  during long drying periods ranged from 0.05 during May to near 0.0 in August. These values contrasted with the essentially 0.0 values estimated by the standard two-stage FAO-56 model. The 0.05 values for  $K_e$  over the extended drying period tend to follow estimates by HYDRUS-1D and are responsible for adding the additional 20 mm of evaporation to the annual total.

Figure 9-17 compares the same data set and HYDRUS-1D simulations, but where the FAO-56 model was operated using hourly calculation time steps and hourly reference ET and precipitation data, the HYDRUS-1D model was populated with hourly potential evaporation and precipitation data. In both applications, hourly evaporation estimates were summed to daily time steps prior to calculating  $K_e$ . The impact of using hourly time steps as compared with daily time steps was relatively minor, with results nearly indistinguishable from those with the daily calculation time step. The RMSD between FAO-56 and HYDRUS-1D evaporation estimates was 0.39 and 0.38  $\text{mm d}^{-1}$ , with and without the skin enhancement in the FAO model. The similarity of the two RMSDs was due to some overestimation by the skin evaporation option over some extended drying periods that was partly counterbalanced by underestimation of flash evaporation spikes by the original (nonskin evaporation) model. For both applications (with and without the skin evaporation enhancement), total evaporation over the year was similar between the two FAO model runs (147 and 153 mm) and in comparison with the HYDRUS-1D run (169 mm). The RMSD was poorer for the FAO-56 model using the skin evaporation enhancement for the hourly time step as compared with the 24-hour calculation time step due to more variability in the transition from stage 1 to stage 2 evaporation.

## 9.10 SUMMARY

Estimating evaporation from soil is important when conducting soil water balances over extended periods. Evaporation can be a major component of ET for bare soil and for conditions of partial vegetation cover. The FAO-56  $K_e$  model and SRT model are both relatively simple models that adequately simulate evaporation from the soil surface when parameterized for the general soil type. The SRT model has the advantage of implicitly estimating upward flow from a wet soil profile, whereas the

model has the disadvantages of overestimating upward flow when the lower soil profile is dry and requiring a separate water balance technique to estimate the start of stage 2 drying. Parameterization for some soil types may be uncertain. The FAO-56 model has the advantage of simplicity in calculation procedures and parameterization and disadvantages of not implicitly incorporating upward flow from below the slab layer. However, comparisons shown against lysimeter measurements and against HYDRUS-1D simulations indicate that the setting of the  $z_e$  depth can compensate for that simplification. The skin evaporation layer enhancement may be important for improving accuracy of the FAO-56 method when accuracy on a day-to-day basis is important. When evaporation estimates are aggregated over a period of one week or longer, the standard model without skin evaporation has similar accuracy as compared with use of the skin evaporation enhancement.

This page intentionally left blank

# CHAPTER 10

## CROP COEFFICIENT METHOD

### 10.1 INTRODUCTION

Chapter 8 describes the combination of equations for sensible and latent heat transfer, following simplifying assumptions, to produce the well-known Penman combination equation (Penman 1948). Monteith (1965) and Rijtema (1965) independently introduced a surface resistance parameter to the Penman equation and replaced the linear wind function term with an aerodynamic resistance parameter. That resulting combination equation, known as the Penman-Monteith (PM) equation, is now the most widely used basis for estimating evapotranspiration (ET) in engineering, agriculture, and landscape applications, where the equation serves as the reference ET basis in the two-step crop coefficient ( $K_c$ )–reference ET ( $ET_{ref}$ ) approach. The first step in the two-step approach is to estimate reference ET representing potential weather or climate impacts on the ET process. Chapter 8 describes the calculation of  $ET_{ref}$ . The second step is to apply a crop or vegetation coefficient to estimate actual ET,  $ET_c$ , according to growth stage, plant type, and cover and wetness of the soil surface and soil profile. The same general two-step approach has also been applied in hydrologic studies. This chapter focuses on the use of the two-step approach for estimating ET for farm crops, landscapes, and some natural vegetation. Applications to forests can be found in Chapter 4 of the ASCE *Hydrology Handbook* (Allen et al. 1996).

### 10.2 THE CROP COEFFICIENT

The crop coefficient ( $K_c$ ) having a basis of reference crop  $ET_{ref}$  was clarified in 1968 (Jensen 1968) and first used in a computerized irrigation scheduling program (Jensen 1969; Jensen et al. 1970, 1971). The two-step

procedures for estimating ET for well-watered agricultural crops can be applied to various types of natural vegetation and to crops under rain-fed conditions and in general hydrologic studies. For these reasons, the  $K_c$  term might be more appropriately referred to as a "vegetation cover coefficient" rather than as a "crop" coefficient. Usage and application would be the same. However, to be consistent with past literature and applications, this manual adheres to the use of the term "crop coefficient" with the understanding that this term can be applied to nonagricultural vegetation and to bare soil.

Early  $K_c$  curves had nonreference bases, with values determined by measuring depletion of soil water between two or more sampling dates (Hargreaves 1948; Veihmeyer and Hendrickson 1955; Erie et al. 1965, 1982). Later, more refined curves were developed based on daily ET measured in lysimeters that were then related to a grass or alfalfa reference ET. Some curves were refined for conditions of dry surface soil, or when the soil visually appeared dry, and were called *basal crop* coefficients (Wright 1982). More accurate ET estimates could be obtained using basal coefficients and then adjusted for the wetness of the surface soil for several days following rains or irrigation using the dual  $K_c$  approach (Wright 1982; Allen et al. 1998).

Numerous publications over the past decades have focused on measuring ET and calculating associated crop coefficients. Various ET measurement methods have been used, including eddy covariance, Bowen ratio, lysimeters, and remote sensing. Many data sets have been based on lysimeter data. Publications have included information on cereal crops; fiber crops such as cotton, forage crops, fruit tree crops like olives, apricots, peaches, and pecans; grapes; cool- and warm-season grasses; turfgrasses; legume crops like beans and peas; oil crops like safflower; root crops like potatoes; tropical fruits like banana, cassava, and coffee; and various vegetable crops. In addition, there have been coefficients for natural vegetation such as grasslands and wet vegetation such as cattails, grasses, and reeds. Some of these publications have included models and systems for calculating the crop coefficient. Most of these publications have been from Australia, Brazil, China, India, Spain, England, Italy, and the United States. Appendix G describes recommended documentation for crop coefficient and ET data reporting that can improve the quality and consistency of published crop coefficients.

The primary factor causing an increase in the crop coefficient is an increase in plant cover or leaf-area per unit area (LAI) as the crop develops, resulting in a decrease in bulk surface resistance. Most publications on crop coefficient curves have presented  $K_c$  as a function of some form of absolute or scaled time basis. However, some studies relate the rate of increase in LAI and therefore  $K_c$  for various crops as a function of daily weather such as cumulative degree days.

## Crop Coefficient Variables

By expressing  $ET_c$  and  $ET_{ref}$  in terms of the PM equation following the form presented in Eq. (8-15), where the additional “*c*” subscripts represent characteristic values for the actual vegetation and the additional “*r*” subscripts represent the same for the reference crop, one can visualize that the value of  $K_c$  depends on the relative roughness, leaf area, and albedo (in the net radiation calculation) of the actual vegetative surface in relation to the same characteristics for the grass or alfalfa reference surface.

$$K_c = \frac{ET_c}{ET_{ref}} = \frac{\frac{\Delta(R_{nc} - G_c) + \rho c_p(e_z^o - e_z)/r_{ac}}{\Delta + \gamma(1 + r_{sc}/r_{ac})}}{\frac{\Delta(R_{nr} - G_r) + \rho c_p(e_z^o - e_z)/r_{ar}}{\Delta + \gamma(1 + r_{sr}/r_{ar})}} \quad (10-1)$$

The relative proportions of net radiation, wind, temperature, and vapor pressure deficit all affect the value of  $K_c$  to some degree. Clearly, the more similar the vegetative cover is to the reference condition, especially at full cover, the closer the value of  $K_c$  will be to 1.0 and the less varying the value of  $K_c$  will be with changing weather conditions. One precaution in applying Eq. (10-1) is that the equation does not consider the effects of differences between  $ET_c$  and  $ET_{ref}$  on conditioning the near-surface equilibrium boundary layer above the vegetation. This conditioning can modify levels of  $T$ ,  $e_z^o$ ,  $e_z$ ,  $\Delta$ , and wind speed to some degree, due to differences in partitioning available energy at the surface into  $H$  and  $\lambda E$  when  $ET_c$  is different from  $ET_{ref}$ . These generally negative feedback effects can affect the value determined for  $K_c$  and are described in more detail in Chapter 11.

## Field-Scale Applications

When applying the standardized reference ET equation [Eq. (8-15)] under humid conditions, where a majority of energy for the ET process is from net radiation, the  $K_c$  for large expanses of similar vegetation does not exceed about 1.0 to 1.1 relative to the alfalfa reference and about 1.2 relative to the grass reference. In dry climates, where additional advection of warm dry air can occur to increase ET from irrigated surfaces, the  $K_c$  still does not exceed about 1.0 to 1.1 relative to the alfalfa reference but can reach maximum values of about 1.3 to 1.4 relative to the grass reference. The reason for the near-constant 1.0 to 1.1 crop coefficients for the alfalfa reference is that the alfalfa reference crop has about the same albedo, LAI, and roughness as most agricultural crops at full cover and therefore converts similar amounts of radiant energy and sensible heat to vapor transfer. An expanse of reference crop (especially alfalfa) will approach the maximum conversion of available energy into  $\lambda E$ , so that the ratio of  $\lambda E$  for any other tall, leafy crop to alfalfa  $\lambda E$  will be near 1.0. This observation is

borne out in viewing the maximum values for  $K_c$  reported by Wright (1982), reproduced for the standardized PM alfalfa reference in Appendixes E and F, where none of Wright's  $K_c$ s, based on the alfalfa reference, exceed 1.03 when averaged over weekly or longer periods. In the case of the grass reference, where the vegetation is shorter and LAI may be less, values for  $K_c$  may approach 1.3 for tall, dense crops under arid and semiarid conditions (Doorenbos and Pruitt 1977; Allen et al. 1998).

Limiting  $K_c$  to approximately 1.0 for an alfalfa reference base or to 1.3 for a grass reference base applies to large expanses of vegetation ( $>200$  m diameter) and is significant and important when evaluating field measurements of ET. Higher values for  $K_c$  may very likely indicate problems with field measurements. Measurement problems include (1) improper computation of vegetation area in lysimeter studies (Allen et al. 1991a, 2011c), (2) violation of necessary fetch requirements in boundary layer (energy balance) measurements, and (3) weather data collection difficulties and errors. The first two problems are discussed in Chapter 7. All are discussed in detail in Allen et al. (2011c).

### Small Expanses of Vegetation

When ET is measured from small expanses of vegetation, the internal boundary layer above the vegetation may not be in equilibrium with the new surface and may not have developed up to the height of instrumentation. In addition, small expanses of tall vegetation surrounded by shorter cover can result in a "clothesline effect," where the interchange between air and vegetation is much more efficient than with the logarithmic type of equilibrium boundary layer established over large fields. In these cases, ET from the isolated stands, on a per unit area basis, may be significantly greater than the corresponding  $ET_r$ , or  $ET_o$  computed for an alfalfa or grass reference, assuming an infinitely large fetch of similar reference vegetation. An example of these situations would be ET from a single row of trees surrounded by short vegetation, ET from a narrow strip of cattails along a stream channel, or a vegetated lysimeter surrounded by shorter vegetation. Allen et al. (1994a) report  $K_c$  values for small (6-m wide) stands of cattails and bulrushes surrounded by grass pasture equal to 1.6 to 1.8 during midseason, relative to an alfalfa reference. These measurements indicate a strong clothesline effect. Coefficients were only 1.15 for a cattail wetland that was 200 m in diameter (Allen et al. 1994a). In an extreme illustration, van Bavel et al. (1963) measured ET from 1-m tall Sudan grass in Arizona following cutting of the grass around the lysimeter, so that the vegetation inside the lysimeter functioned as a clothesline. After cutting, 14.7 mm of ET during a 24-h period was measured compared with 9.8 mm three days before the cutting—a 50% increase. The weather data were similar for both clear days. In a similar situation, Allen et al. (1991a) report measured ET

from 0.6-m fescue grass to increase by 1.6 times relative to the PM equation when the surrounding grass was clipped to 0.1 m, but the vegetation inside the lysimeter remained at 0.6 m. The ET rate from the lysimeter under the clothesline condition reached  $16 \text{ mm d}^{-1}$ , whereas the PM equation estimated  $11 \text{ mm d}^{-1}$  for 0.6-m grass having extensive fetch of other 0.6-m grass.

Pruitt (personal communication, 1976) reported  $K_c$  values for a nearly isolated 4.2-m tall Monterey pine tree (*Pinus radiata*) varying from 1.4 in February–March to 2.0 during spring and summer and approaching 3.0 during late fall and dry, early-winter months relative to  $ET_o$ . The tree grew on a 1.83-m by 2.44-m hydraulic-pillow lysimeter located within a 1-ha dry, noncropped field. It was near the middle of a 10-tree windrow oriented normal to prevailing winds near Davis, California, thereby creating a clothesline effect.

The preceding discussion indicates the importance of knowing the type of setting for which ET estimates are needed and the conditions from which measurements are collected. If ET estimates are needed for small, isolated stands of vegetation, then  $K_c$  may be allowed to exceed the 1.0 value for an alfalfa reference and the 1.3 value for a grass reference by up to 50%. However, if ET estimates are to represent large expanses of vegetation or small stands of vegetation surrounded by mixtures of other vegetation having similar roughness and soil water conditions, then  $K_c$ s will generally be less than or equal to 1.0 for alfalfa and 1.3 for grass references. Allen et al. (1998) propose procedures for estimating  $K_c$  and ET for isolated stands of wetlands and tall wind breaks such as single rows of trees that are presented later in the section on natural vegetation. They caution that an upper limit on  $K_c$  exists for isolated vegetation that is governed by root uptake ability and stomatal behavior.

### 10.3 CROP (VEGETATION COVER) COEFFICIENTS

Two families of  $K_c$  curves for agricultural crops have been developed for the two commonly used reference crops (tall and short). These are the grass-based curves by Pruitt (Doorenbos and Pruitt 1977; Jensen et al. 1990; Allen et al. 1998) and others and alfalfa-based  $K_c$  curves by Wright (1981, 1982) and others (Tolk and Howell 2001; Howell et al. 2004, 2006). The user must exercise caution to avoid mixing grass-reference-based  $K_c$ s with an alfalfa reference and vice versa. Usually  $K_c$ s based on an alfalfa reference can be “converted” for use with a grass reference during summer months by multiplying by a factor ranging from 1.1 to 1.3, depending on climate (1.1 for humid, calm conditions and 1.3 for arid, moderately windy conditions). The conversion ratio can be estimated by ratioing  $ET_{rs}$  and  $ET_{os}$  from the standardized PM estimates from Chapter 8. Grass-based  $K_c$ s

are presented and discussed first in this manual (Section 10.4) due to the large number of  $K_c$ s that have been presented in FAO-24, FAO-56, the ASABE publication *Design and Operation of Farm Irrigation Systems* (Allen et al. 2007c) and elsewhere (Snyder et al. 1989a, b) for agricultural crops. Alfalfa-based  $K_c$ s for eight irrigated crops in southern Idaho developed by Wright (1981, 1982) and presented in Manual 70, 1st edition (Jensen et al. 1990) have been updated in this edition of Manual 70 for use with standardized  $ET_{rs}$  and are presented in Appendix E.

Generalized crop coefficient curves for estimating crop  $ET_c$  for crops or other vegetation are shown in Figure 10-1. The  $K_{cb}$  curve represents "basal" crop coefficients for conditions where the soil surface is visually dry, so that evaporation from soil is minimal, but where the availability of soil water does not limit plant growth or transpiration. This curve represents a minimum  $ET_c$  situation for adequate soil water. The "spikes" in Figure 10-1 indicate occurrences of precipitation or irrigation that wet the soil surface and temporarily increase total  $ET_c$  for one to five days. These spikes decay to the  $K_{cb}$  curve as the soil surface dries. The spikes generally approach a maximum value of 0.8 to 1.0 for an alfalfa  $ET_r$  base (Wright 1982) and

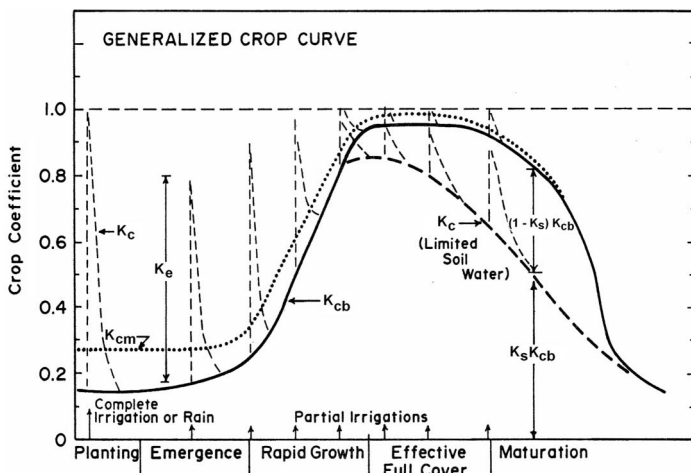


Fig. 10-1. Generalized cover coefficient curves showing the effects of growth stage, wet surface soil, and limited available soil water on crop coefficient values. The solid line represents the basal  $K_{cb}$  curve, the short-dashed line represents the soil evaporation coefficient,  $K_e$ , addition to  $K_{cb}$  when the soil surface is wet, the dotted curve represents a time-averaged 'mean'  $K_c$  curve that averages the effects of the  $K_e$  spikes and the  $K_{cb}$  curve, and the long-dashed line represents a departure from the potential  $K_c = K_{cb} + K_e$  curve under limiting soil water conditions  
Source: Data from Wright (1982); Jensen et al. (1990)

1.0 to 1.2 for a grass  $ET_o$  base (Allen et al. 1998). The  $K_{cm}$  curve in Figure 10-1 represents a so-called “mean” crop coefficient that includes averaged effects of wet soil (spikes) under specific rainfall or irrigation frequencies. Sometimes the  $K_{cm}$  is referred to as the “single”  $K_c$ . The final, “limited soil water” curve in the figure represents the decrease in  $ET_c$  when plant water uptake is limited by available soil water.

### **$K_c$ and ET Terminology**

Actual ET, denoted here as  $ET_{cact}$  or  $ET_a$ , is the ET rate that occurs under actual field conditions.  $ET_{cact}$  is often used interchangeably with the term crop ET,  $ET_c$ . The value for  $ET_{cact}$  may be less than the value for potential  $ET_c$ , sometimes denoted as  $ET_{cpot}$ , when water stress occurs in the vegetation.  $ET_{cact}$  or  $ET_c$  is calculated using Eq. (8-14) as  $ET_{cact} = ET_c = K_c ET_{ref}$ . Both  $ET_{cact}$  and  $ET_c$  (and  $ET_{cpot}$ ) terms can include varying degrees of direct evaporation from soil as represented by  $K_e$ .

In FAO and European literature,  $ET_{cact}$  is often presented as “ $ET_{adj}$ ” representing adjusted ET and based on an adjusted  $K_{cadj}$  as determined from Eq. (10-2) (Pereira et al. 1999a, b). That same literature generally reserves the use of the term crop ET, denoted as  $ET_c$ , and the term  $K_c$  to represent only the potential, or upper limit on ET for a particular crop, in other words, representing a pristine, well-watered condition. In the European tradition, any reduction in  $K_c$  due to water stress or other factors such as reduced density, disease, or salinity are encapsulated into a second expression referred to as “actual”  $K_{cact}$  or  $K_{caact}$  (Allen et al. 1998).

The traditional American usage of the terms  $ET_c$  and  $K_c$  have tended to be more relaxed in their usage of the  $ET_c$  and  $K_c$  terms and allows these terms to represent both potential and actual conditions. The European usage is less ambiguous, but the American usage is more encompassing. The less formal American usage is defensible because when using the mean  $K_{cm}$  of the following section, the value for  $K_{cm}$  changes substantially with wetting frequency and therefore is not a well-defined, consistent coefficient. The differences between the two systems are largely semantic, but can cause confusion and some degree of frustration within the user community unless carefully defined. This manual follows the American tradition.

### **Basal Crop Coefficients**

Basal crop coefficients represent primarily the transpiration component of ET and a small evaporation component from soil that is visually dry at the surface. Their use requires adjustment for wet soil effects after rain or irrigation. This results in more accurate estimates of  $ET_c$  on a daily basis for use in soil water modeling and irrigation scheduling than using mean

coefficients in which the effects of local rainfall or irrigation frequencies are included. The total crop coefficient,  $K_c$ , is computed from  $K_{cb}$  as

$$K_c = K_s K_{cb} + K_e \quad (10-2)$$

where  $K_s$  is a dimensionless coefficient dependent on available soil water, and  $K_e$  is a coefficient to adjust for increased evaporation from wet soil immediately after rain or irrigation. The value for  $K_s$  is 1 unless available soil water limits transpiration, in which case it has a value less than 1. Potential  $ET_c$  is estimated as  $ET_c = K_c ET_{ref}$  when  $K_s$  in Eq. (10-2) equals 1. Actual  $ET_a$  is estimated as  $ET_a = K_c ET_{ref}$  when  $K_s$  in Eq. (10-2) is less than 1. The values for  $K_e$  represent the "spikes" shown in Figure 10-1. Estimation of  $K_e$  for bare soil conditions is described in detail in Chapter 9, which presents and illustrates the square root of time (SRT) model and the FAO-56  $K_e$  model [Eqs. (9-19)–(9-31)].

$K_{cmax}$  is used in Eq. (9-19) to estimate the evaporation coefficient  $K_e$  and represents the maximum value for  $K_c$  following rain or irrigation, under conditions of both bare soil and some degree of vegetation cover. The value for  $K_{cmax}$  is governed by the amount of energy available for evaporation of water, which is largely encapsulated by reference  $ET_{ref}$ . Because  $K_c$  is the ratio of  $ET$  to  $ET_{ref}$ , the value for  $K_{cmax}$  is not expected to exceed 1.0 to 1.3. Because of the lower value for the grass reference ( $ET_o$ ) as compared with the alfalfa reference,  $K_{cmax}$  for use with  $ET_o$  ranges from about 1.05 to 1.3 and varies with general climate (Allen et al. 1998, 2005b):

$$K_{cmax_o} = \max \left( \left\{ 1.2 + [0.04(u_2 - 2) - 0.004(RH_{min} - 45)] \left(\frac{h}{3}\right)^{0.3} \right\}, \{K_{cbo} + 0.05\} \right) \quad (10-3a)$$

where  $u_2$  is average wind speed at 2 m during the growth stage or period,  $RH_{min}$  is average daily minimum relative humidity during the growth state or period,  $h$  is the mean plant height (m) during the period of calculation (initial, development, midseason, or late season), and the max () function indicates the selection of the maximum of the values separated by the comma.  $K_{cmax_o}$  denotes the use of  $K_{cmax}$  with  $ET_o$  and with  $K_{cb}$  based on  $ET_o$ , denoted as  $K_{cbo}$ . Parameters  $u_2$  and  $RH_{min}$  are discussed later with Eqs. (10-15)–(10-17).

$K_{cmax}$  for the tall reference  $ET_r$ , denoted as  $K_{cmax_r}$ , does not require adjustment for climate, due to the greater roughness of the reference basis:

$$K_{cmax_r} = \max[1.0, (K_{cbr} + 0.05)] \quad (10-3b)$$

where  $K_{cbr}$  denotes a basal  $K_{cb}$  used with  $ET_r$ . Eqs. (10-3a) and (10-3b) require that  $K_{cmax}$  be greater than or equal to the sum  $K_{cb} + 0.05$ , suggesting that wet

soil increases the  $K_c$  value over  $K_{cb}$  by about 0.05 following complete wetting of the soil surface, even during periods of full ground cover. Eqs. (10-3a) and (10-3b), and the FAO-56 evaporation Eqs. (9-19)–(9-31), can be applied with both the straight-line  $K_{cb}$  curve style of FAO and with the curvilinear  $K_{cb}$  curves such as by Wright (1982), as illustrated later in this section.

### Water Stress Adjustment

Several linear and curvilinear functions have been proposed to adjust for the effects of decreasing available water on ET or for the  $K_s$  used in Eq. (10-2). The simple linear model for estimating  $K_s$  as described in FAO-33 (Doorenbos and Kassam 1979) is commonly used:

$$K_s = \frac{\theta - \theta_{wp}}{\theta_t - \theta_{wp}} \quad \text{for } \theta < \theta_t \quad (10-4)$$

where  $\theta$  is mean volumetric soil water in the root zone in  $\text{m}^3\text{m}^{-3}$ , and  $\theta_t$  is the threshold  $\theta$  below which transpiration is decreased linearly due to water stress.  $K_s = 1.0$  for  $\theta \geq \theta_t$ . The wilting point,  $\theta_{wp}$ , is the soil water at the lower limit of soil water extraction by plant roots in  $\text{m}^3\text{m}^{-3}$ . Typical values of  $\theta_{wp}$  for various soil texture classes are listed in Table 3-6. The threshold soil water,  $\theta_t$ , can be estimated from the relationship:

$$\theta_t = (1 - p)(\theta_{fc} - \theta_{wp}) + \theta_{wp} \quad (10-5)$$

where  $p$  is the average fraction of available soil water that can be depleted before water stress and ET reduction occur. Variable  $\theta_{fc}$  is the soil water content at field capacity or the drained limit of the soil in  $\text{m}^3\text{m}^{-3}$ . Values for all  $\theta$  parameters should represent averages over the effective root zone. Values for  $\theta_{fc}$  are listed in Table 7-1, and values for  $p$  for agricultural crops are listed in Appendix B.

Parameter  $p$  normally ranges from 0.30 depletion of available soil water ( $\theta_{fc} - \theta_{wp}$ ) for shallow-rooted plants at high rates of  $ET_c (> 8 \text{ mm d}^{-1})$  to 0.70 for deep-rooted plants at low rates of  $ET_c (< 3 \text{ mm d}^{-1})$  (Raes et al. 2009; Appendix B). A value of 0.50 is commonly used for many agricultural crops. After computation of  $K_c$ ,  $ET_c$  is computed using Eq. (8-14).

An equivalent expression to Eq. (10-4), but in terms of depletion,  $D_r$ , of available water in the root zone is, for  $D_r > RAW$ :

$$K_s = \frac{TAW - D_{r,i-1}}{TAW - RAW} = \frac{TAW - D_{r,i-1}}{(1 - p) TAW} \quad \text{for } D_{r,i-1} > RAW \quad (10-6)$$

where  $TAW$  is the total depth of available soil water in the root zone in mm,  $RAW$  is the depth of readily available water in the root zone in mm, and  $p$  is the fraction of  $TAW$  that a crop can extract from the root zone without suffering water stress. When  $D_r \leq RAW$ ,  $K_s = 1.0$ . The total available water in the root zone is estimated as the difference between the water content at field capacity and wilting point:

$$TAW = 1,000 (\theta_{fc} - \theta_{wp}) z_r \quad (10-7)$$

where  $z_r$  is the effective rooting depth in m, and  $z_r$  contains  $z_e$ , the effective depth of the evaporation layer described in Chapter 9 and illustrated in Figure 9-4. The 1,000 factor converts from m to mm.  $RAW$  is estimated as

$$RAW = p TAW \quad (10-8)$$

where  $RAW$  has the same units as  $TAW$  (mm). Appendix B contains typical maximum effective values for  $z_r$ .

The mean soil water balance for the root zone in terms of  $\theta$  can be computed on a daily basis using Eqs. (7-3) and (7-4). Computations are made for the complete  $z_r$  root depth, including the evaporation layer.

The soil water balance for the root zone in terms of depletion is

$$D_{r,i} = D_{r,i-1} - (P - RO)_i - I_i - CR_i + ET_{cact,i} + DP_i \quad (10-9)$$

where  $D_{r,i}$  is root zone depletion at the end of day  $i$  in mm;  $D_{r,i-1}$  is root zone depletion at the end of the previous day,  $i - 1$ , in mm;  $P_i$  is precipitation on day  $i$  in mm;  $RO_i$  is runoff from the soil surface on day  $i$  in mm;  $I_i$  is net irrigation depth on day  $i$  that infiltrates the soil in mm;  $CR_i$  is capillary rise from the groundwater table on day  $i$  in mm;  $ET_{cact,i}$  is actual crop evapotranspiration on day  $i$  in mm; and  $DP_i$  is water loss out of the root zone by deep percolation on day  $i$  in mm.

Although soil water content might temporally exceed field capacity following heavy rain or irrigation, in the previous equation, the total amount of water exceeding field capacity is assumed to be lost the same day via deep percolation, following any ET for that day. This permits the extraction of one day's ET from this excess before percolation. That assumption can be modified by delaying  $DP$  as in Eq. (10-12b). The root zone depletion will gradually increase as a result of ET and percolation. In the absence of a wetting event, the root zone depletion will ultimately reach the value  $TAW$  that is defined from rooting depth,  $\theta_{fc}$  and  $\theta_{wp}$  from Eq. (10-7). At that moment no water is left for ET, and  $K_s$  becomes zero, from Eq. (10-6). Limits imposed on  $D_{r,i}$  are consequently

$$0 \leq D_{r,i} \leq TAW \quad (10-10)$$

The lower limit 0 can be relaxed if some delayed drainage from the root zone is allowed as discussed later with Eq. (10-12b).

To initiate the water balance for the root zone, the initial depletion  $D_{r,i-1}$  can be derived from measured soil water content by

$$D_{r,i-1} = 1,000(\theta_{fc} - \theta_{i-1})z_r \quad (10-11)$$

where  $\theta_{i-1}$  is the average soil water content at the end of day  $i-1$  for the effective root zone. The 1,000 factor converts from m to mm. Following heavy rain or irrigation, the user can assume that the root zone is near field capacity, i.e.,  $D_{r,i-1} \approx 0$ . Daily precipitation in amounts less than about  $0.2 ET_{ref}$  is normally entirely evaporated and can generally be ignored in depletion calculations (in both the computation of  $D_{r,i}$  and computation of  $ET_{cact}$ ). In the case of using the dual  $K_c$  method of Eq. (10-2), light precipitation events will generally be evaporated using  $K_e$  and should be included in the  $P$  estimate.  $I_i$  is equivalent to the mean infiltrated irrigation depth expressed for the entire field surface. Runoff from the surface during precipitation can be estimated using standard procedures from hydrologic texts.

**Capillary Rise (CR)** The amount of water transported upward by capillary rise from the water table to the root zone or soil surface depends on the soil type, the depth of the water table, and the wetness of the root zone. CR can normally be assumed to be zero when the water table is more than a few meters below the bottom of the root zone. Figure 10-2 shows estimated flux of water from a shallow water table to a bare soil surface under dry conditions. Data in the figure were based on simulations by the UPFLOW model (Raes and deProost 2003; Raes 2004). Similar figures for wet soil conditions and for flux into a 1-m root zone are presented in Appendix I along with regression equations that reproduce the figures. Appendix I also describes an analytical technique for estimating capillary rise by Brutsaert (1982). Medium textured soils tend to have higher upward fluxes than fine and coarse textured soils due to a favorable combination of capillarity and hydraulic conductivity.

**Deep Percolation from the Root Zone (DP)** Following heavy rain or irrigation, the soil water content in the root zone may exceed field capacity. In application of Eq. (10-9), DP is assumed to occur at the end of the same day of a wetting event, so that the depletion  $D_{r,i}$  becomes zero. Therefore,

$$DP_i = (P_i - RO_i) + I_i - ET_{cact,i} - D_{r,i-1} \quad (10-12a)$$

where  $DP_i$  is limited to  $DP_i \geq 0$ . As long as the soil water content in the root zone is below field capacity (i.e.,  $D_{r,i} > 0$ ), the soil is assumed to not drain

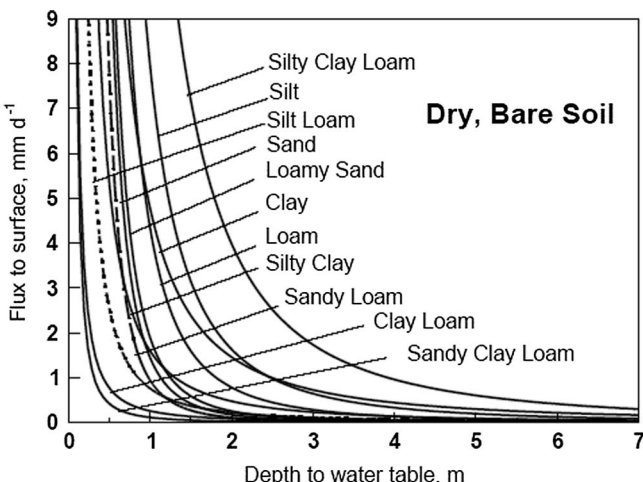


*Fig. 10-2. Estimated flux of water to the ground surface for evaporation as a function of depth to the water table for various soil textures, based on numerical simulations using the UPFLOW (Raes 2004) model*

and  $DP_i = 0$ . If drainage from the root zone is expected to be delayed by a day or more following a large infiltration event, then daily  $DP_i$  in Eq. (10-9) can be estimated as

$$DP_i = \max\{\min[(P_i - RO_i) + I_i - ET_{cact, i} - D_{r, i-1}, DR_i], 0\} \quad (10-12b)$$

where  $DR_i$  is an expected maximum rate of drainage from the root zone on day  $i$ , with units for  $DR_i$  the same as  $P$  and  $I$ . Limiting  $DP_{r,i}$  to  $DR_i$  has the effect of causing  $D_{r,i}$  in Eq. (10-9) to be negative for one or more days. Values for  $DR_i$  can be estimated from hydraulic conductivity characteristics for the root zone soil layer.

The recommended order of calculation of parameters in the dual  $K_c$  procedure and associated equation numbers are as follow:  $K_{cb}$ ,  $K_{cmax}$  (10-3),  $K_s$  (10-6),  $f_c$  (9-27),  $f_{ew}$  (9-26),  $F_{stage1}$  (9-22),  $K_r$  (9-21 or 9-24, 9-25),  $K_e$  (9-19),  $K_I$  (9-31),  $T_e$  (9-30),  $K_c$  (10-2),  $ET_c$  (8-14),  $RO_i$ ,  $E_i = K_e ET_{ref}$ ,  $D_{e,i}$  (9-28),  $D_{REW,i}$  (9-29),  $DP_i$  (10-12a,b), and  $D_{r,i}$  (10-9). Examples of application of the FAO-56 dual  $K_c$  procedure include Hunsaker (1999), Tolk and Howell (2001), de Medeiros (2001), Hunsaker et al. (2002, 2003, 2005), Howell et al. (2004), Mutziger et al. (2005), and Allen et al. (2005c).

### Mean Crop Coefficients

In basin-wide water balance studies or irrigation system planning, use of mean, or single, crop coefficients may be more useful and convenient than computing a daily  $K_c$  based on a combination of  $K_{cb}$ ,  $K_s$ , and  $K_e$  as used in the dual  $K_c$  method of Eq. (10-2). The mean crop curve,  $K_{cm}$ , shown in

Figure 10-1, lies above the basal curve by an amount that depends on the frequency of soil wetting. When a mean coefficient is used, usually no additional adjustment is made for the effects of surface soil wetness. Adjustments can be made for the effects of limited soil water as

$$K_c = K_s K_{cm} \quad (10-13)$$

where  $K_s$  is defined in Eqs. (10-4) and (10-6). Values for  $K_{cm}$  during partial crop cover are dependent on precipitation frequency and irrigation practices that wet all or part of the soil surface.  $K_{cm}$  curves can be generated from  $K_{cb}$  curves for known or simulated precipitation or irrigation frequencies using the dual  $K_{cb}$  approach.

#### 10.4 FAO GRASS-BASED CROP COEFFICIENTS

Although several crop coefficient models use a curvilinear curve shape, the linear segment model proposed by the FAO is widely used and easy to formulate (Figure 10-3). The procedure for constructing crop (cover) coefficients was presented in FAO-24 (Doorenbos and Pruitt 1977) and FAO-56 (Allen et al. 1998). In the FAO procedure, a  $K_c$  curve such as that shown in Figure 10-3 is constructed by

1. Dividing the growing season into four parts that describe crop phenology or growth stages:
  - a. Initial period (1),
  - b. Crop development period (2),
  - c. Midseason period (3), and
  - d. Late season period (4);

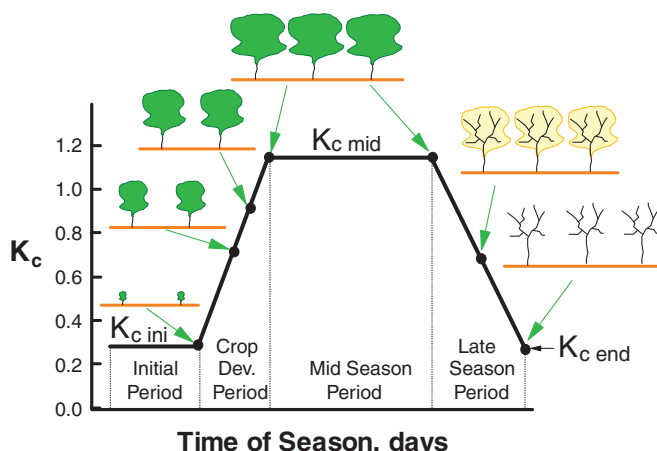


Fig. 10-3. FAO crop coefficient curve and stage definitions  
Source: Allen et al. (2005b); copyright ASCE

2. Selecting three  $K_c$  values that represent
  - a. Average  $K_c$  during the initial period ( $K_{cini}$ ),
  - b. Average  $K_c$  during the midseason period ( $K_{cmid}$ ), and
  - c. Average  $K_c$  at the end of the late season (i.e., at the time of harvest or leaf-fall) ( $K_{cend}$ ); and
3. Placing straight line segments through each of the four periods, with the lines through the initial and midseason periods placed horizontally.

Only three tabularized values for  $K_c$  are required to describe and construct the FAO-style  $K_c$  curve.  $K_{cmid}$  represents the average value for  $K_c$  expected during the total midseason period, rather than the absolute peak daily  $K_c$  reached by the crop.

The four crop growth stages are generally characterized in terms of benchmark crop growth stages or cultivation practices. Definitions of these stages are given in Table 10-1 and are closely tied to crop phenology.

Values for  $K_{cini}$ ,  $K_{cmid}$ , and  $K_{cend}$  are listed in Appendix B for mean  $K_{cm}$  for various agricultural crops. Most information in Appendix B was taken from FAO-24 (Doorenbos and Pruitt 1977) and FAO-56 (Allen et al. 1998) with additional information from Wright (1982), Snyder et al. (1989a, b), Jensen et al. (1990), Allen and Pereira (2009), and Allen et al. (2011a). Lengths of growth stages common to crops are listed in Appendix C. Values for  $K_{cb}$  are listed in Appendix D. Lengths of growth stages are strongly influenced by air temperature, time of year, and crop variety. Therefore the values for lengths in Appendix C are useful for general estimates only and should be verified or varied using local information and observation, including remote sensing (Bausch and Neale 1987; Neale et al. 1989; Tasumi et al. 2005a; Singh and Irmak 2009).

Table 10-1. General Benchmark Growth Stages for Defining FAO Crop Stages

Period	Growth Stages
Initial	<i>planting to 10% ground cover</i> (length is strongly dependent on crop and time of year)
Crop development	<i>10% ground cover to effective cover</i> (effective cover = initiation of flowering for many crops)
Midseason	<i>effective cover to start of maturity</i> (start of maturity is often indicated by the beginning of aging, yellowing or senescence of leaves, browning of fruit, etc.)
Late season	<i>start of maturity to harvest</i>

## Adjustment of $K_c$ for Climate

The ratio of  $ET_c$  to grass reference  $ET_o$  for many crops increases as wind speed increases and as minimum daily relative humidity,  $RH_{min}$ , decreases (Doorenbos and Pruitt 1977). This is due primarily to differences in roughness between tall agricultural crops and the clipped grass reference. The result is a high  $K_c$  value caused by increased roughness and perhaps leaf area for a tall crop, making the aerodynamic aspects of vapor transport more important and significant. The adjustment to  $K_c$  is generally required only for coefficients based on the grass  $ET_o$  reference. No adjustment for climate is necessary for coefficients based on the alfalfa  $ET_r$  reference because of the greater height, roughness, and leaf area of alfalfa (Wright 1982; Pereira et al. 1999a). The FAO procedure for adjusting the  $ET_o$ -based  $K_c$  values uses mean  $RH_{min}$  and wind speed, where  $K_{c mid}$  and  $K_{cb mid}$  values are adjusted for climates having  $RH_{min}$  greater than or less than 45%, or having mean wind speed at 2 m( $u_2$ ) that is greater than or less than  $2.0 \text{ ms}^{-1}$ , as

$$K_{c mid} = K_{c mid(table)} + [0.04(u_2 - 2) - 0.004(RH_{min} - 45)] \left(\frac{h}{3}\right)^{0.3} \quad (10-14)$$

where  $K_{c mid(table)}$  is the value for  $K_{c mid}$  or  $K_{cb mid}$  taken from Appendix B or D, and  $h$  is the mean maximum plant height in m during the midseason period, or full cover period. Eq. (10-14) is valid for  $h$  to 20 m. Mean values for  $h$  are listed in Appendix B for the crops and vegetation listed. For local applications,  $h$  should be based on field observations. Eq. (10-14) will increase  $K_{cb mid}$  by about 0.1 for mean wind speed of  $5 \text{ ms}^{-1}$  or  $RH_{min}$  of 15% when crop height is about 1–2 m.

The  $K_{c end}$  or  $K_{cb end}$  at the time the growing period ends is adjusted for climate with  $RH_{min}$  less than or greater than 45% or with wind speed at 2 m( $u_2$ ) less than or greater than  $2 \text{ ms}^{-1}$  as

$$K_{c end} = K_{c end(table)} + [0.04(u_2 - 2) - 0.004(RH_{min} - 45)] \left(\frac{h}{3}\right)^{0.3}, \quad (10-15a)$$

for  $K_{c end(table)} \geq 0.4$

$$K_{c end} = K_{c end(table)} + 0.001(RH_{min} - 45), \quad \text{for } K_{c end(table)} < 0.4 \quad (10-15b)$$

where  $K_{c end(table)}$  is the value taken from Appendix B or D.

Minimum daily relative humidity,  $RH_{min}$ , is defined as the average daily minimum relative humidity during a growth stage. It can be calculated as

$$RH_{min} = \frac{e^o(T_d)}{e^o(T_{max})} \quad (10-16)$$

When dew point temperature or other hygrometric data are not available, then  $RH_{\min}$  can be estimated by substituting  $T_{\min}$  for  $T_d$ . Then

$$RH_{\min} \cong \frac{e^o(T_{\min} - K_o)}{e^o(T_{\max})} \quad (10-17)$$

where  $K_o$  is a dew point offset coefficient introduced with Eq. (8-17) and has values of approximately 2 to 5°C in semiarid and arid climates and approximately 0°C in humid to subhumid climates. The values for  $u_2$  and  $RH_{\min}$  in Eqs. (10-14) and (10-15) need only be approximate, averaged values representing the midseason or late season periods. Application of these equations can be made on a daily basis, but may not improve accuracy over using averaged values.

### Estimation of Initial $K_{cini}$ with the FAO Mean $K_c$ Procedure

Values for mean  $K_{cini}$  in Appendix B represent mean soil wetting conditions expected for each type of crop during the initial period. These  $K_{cini}$ s can be used for making approximate estimates of ET during planning studies. More accurate estimates of  $K_{cini}$  consider local characteristics including the frequency that the soil surface is wetted and soil type, as this significantly affects the ET rate during the initial and development periods, when ET predominantly comprises evaporation. Values for  $K_{cmid}$  and  $K_{cend}$  are less affected by wetting frequency because vegetation during these periods is generally near full ground cover so that effects of surface evaporation are generally small.

When the ground surface is bare or nearly bare, then  $K_{cini}$  is dominated by the evaporation from bare soil, denoted here for time-averaged periods as  $K_{soil}$ . Figures 10-4a–10-4c from FAO-56 present  $K_{soil}$  as a function of  $ET_o$ , soil type, and wetting frequency. Figure 10-4a is used for all soil types when wetting events (precipitation and irrigation) are light (i.e., infiltrated depths average about 10 mm per wetting event); Figure 10-7b is used for “heavy” wetting events, where infiltrated depths are greater than 30–40 mm, on coarse textured soils; and Figure 10-4c is used for heavy wetting events on fine and medium textured soils. In general, the mean time interval is estimated by counting all rainfall and irrigation events occurring during the initial period that are greater than a few mm. Wetting events occurring on adjacent days are typically counted as one event. When average infiltration depths are between 10 and 40 mm, the value for  $K_{soil}$  can be interpolated between Figure 10-4a and Figure 10-4b or Figure 10-4c. Besides the use of  $K_{soil}$  for  $K_{cini}$  when the ground is nearly bare during the initial period (so that  $K_{cini} = K_{soil}$ ), estimates for  $K_{soil}$  are used later in Eq. (10-26) to estimate the effect of soil evaporation on the value for  $K_{cm}$  estimated from fraction of ground covered by vegetation.  $K_{soil}$  is also used to estimate landscape water use in Eq. (10-33b).

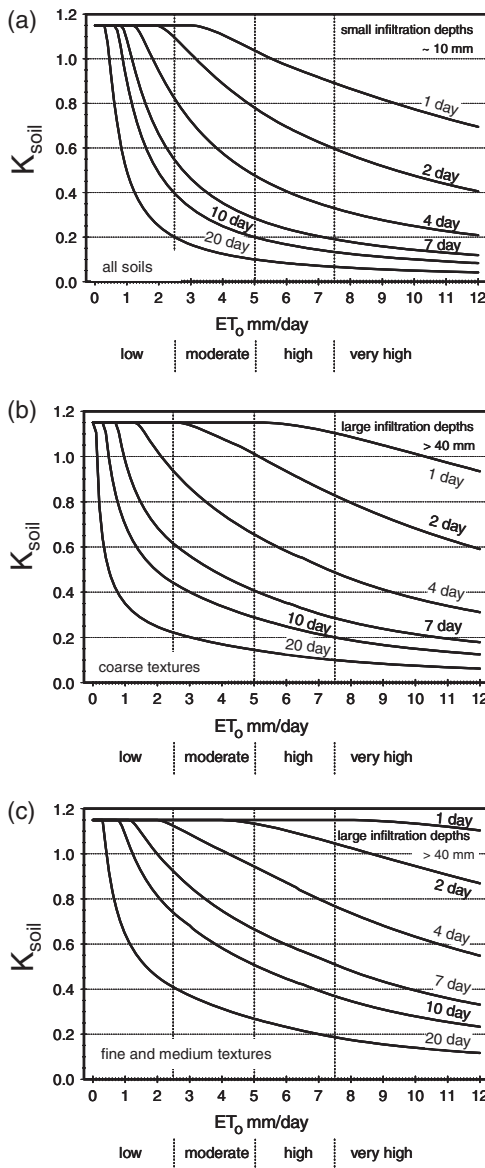


Fig. 10-4. Average  $K_{soil}$  for the initial crop development stage as related to the level of grass reference  $ET_0$  and the interval between irrigations and/or significant rain during the initial period for (a) all soil types when wetting events are light (about 10 mm per event), (b) coarse-textured soils when wetting events are greater than about 40 mm, and (c) medium and fine-textured soils when wetting events are greater than about 40 mm.  $K_{soil}$  is equivalent to  $K_{cini}$  when the soil surface is primarily bare  
Source: Data from FAO-56, Allen et al. (1998)

In equation form,  $K_{soil}$ , following Allen et al. (1998, 2005c), is

$$K_{soil} = \frac{TEW - (TEW - REW)e^{\left[ \frac{-(t_w E_{so} - REW)}{TEW - REW} \right]}}{t_w ET_{ref}} \quad \text{for } t_w > t_1 \quad (10-18)$$

where  $TEW$  is total evaporable water,  $REW$  is readily evaporable water,  $t_w$  is the average time interval between wetting events in days, and  $E_{so}$  is the potential evaporation rate during stage 1 drying in  $\text{mm d}^{-1}$ . The symbol  $e$  in Eq. (10-18) is the base of the natural logarithm. Eq. (10-18) is valid when  $t_w > t_1$  where  $t_1$  is the length of stage 1 evaporation in days. The length of stage 1,  $t_1$ , is calculated as

$$t_1 = \frac{REW}{E_{so}} \quad (10-19)$$

and parameter  $E_{so}$  is potential evaporation calculated as

$$E_{so} = (K_{cmax} - K_{cb}) ET_{ref} \quad (10-20)$$

where, during the initial period, when  $K_{cb}$  mostly represents residual, basal evaporation,  $K_{cb}$  can be set equal to 0.0 in Eq. (10-20) to combine all evaporation, so that  $E_{so} = K_{cmax} ET_{ref}$ . Under frequent wetting, where  $t_w \leq t_1$ , the entire evaporation process resides within stage 1 and  $K_{soil}$  is calculated as

$$K_{soil} = \frac{E_{so}}{ET_{ref}} = \frac{(K_{cmax} - K_{cb})}{ET_{ref}} \quad (10-21)$$

Figures 10-4a–10-4c are reproduced from Eqs. (10-18) and (10-21) using the values for  $TEW$  and  $REW$  summarized in Table 10-2. The max () and min() functions in Table 10-2 indicate the selection of the maximum or minimum value of parameters separated by the comma.  $K_{soil}$  values from Figure 10-4 are for use with the grass reference  $ET_o$ . For use with the alfalfa reference  $ET_r$ , the  $K_{soil}$  from Figure 10-4 can be divided by 1.2. Eqs. (10-13)–(10-21) can be applied directly with alfalfa reference  $ET_r$  using  $K_{cmax} = 1.0$ .

Allen et al. (1998, 2005a) describe the calculation of  $t_w$  from precipitation and irrigation information. Allen et al. (2005a) provide calculation of a weighted  $f_w$  used in Eq. (9-26) when  $f_w$  for irrigation is less than the  $f_w = 1$  for precipitation.

A second and more accurate procedure for estimating mean  $K_{cini}$  is to apply the dual  $K_{cb} + K_e$  approach using actual sequences of precipitation and irrigation during the initial period for one or more years, assuming that the basal  $K_{cb}$  is 0.10 to 0.15 when the initial condition is nearly bare soil. A time-averaged value for  $K_{cb} + K_e$  can then be determined.

Table 10-2. Values for  $TEW$  and  $REW$  in mm to Recreate Fig. 10-4a–c in Allen et al. (2005a) where  $ET_o$  is Grass Reference ET in  $\text{mm d}^{-1}$

Figure	Parameter in Eqs. (10-18), (10-19)
Fig. 10-4a	$TEW = 10 \text{ mm}$ $REW = \max[2.5, 6/(ET_o)^{0.5}]$
Fig. 10-4b	$TEW = \min[15, 7(ET_o)^{0.5}]$ $REW = \min(6, TEW - 0.01)$
Fig. 10-4c	$TEW = \min[28, 13(ET_o)^{0.5}]$ $REW = \min(9, TEW - 0.01)$

### Lengths of Growth Stages

FAO-24 (Doorenbos and Pruitt 1977) and FAO-56 (Allen et al. 1998) provide general lengths for growth (development) stages for various types of climates and locations. Appendix C summarizes this information. The rate of vegetative development and attainment of effective full cover is affected by weather conditions, especially by mean daily air temperature (Ritchie and NeSmith 1991). Therefore, the length in time between planting or plant emergence and effective full cover for various crops or other vegetation will vary with climate, latitude, elevation, and planting date (if cultivated) and with species and cultivar (variety). Generally, once effective full cover for a plant canopy has been reached, the rate of phenological development (flowering, seed development, ripening, and senescence or death of leaf tissue) often proceeds at a rate that depends on plant genotype rather than weather (Wright 1982). In some situations, the emergence of vegetation, greenup, and attainment of effective full cover can be estimated using cumulative degree-based regression equations or plant growth models (Sinclair 1984; Sammis 1985; Snyder 1985; Flesch and Dale 1987; Ritchie and NeSmith 1991; Ritchie 1991; Slack et al. 1996; Snyder et al. 1999; Ceseraccio et al. 2001; Sammis et al. 2004; Allen and Robison 2007). The use of cumulative growing degree days provides a quantitative stretching or shrinkage of the generated  $K_c$  curves for years or growing seasons that run cooler or warmer than average. Appendix F provides  $K_c$  curves traceable to those of Wright (1981, 1982) for Kimberly, Idaho, that are converted to a cumulative growing degree day basis.

Local observations of plant stage development should be used when possible, with values in Appendix C used as a guide and for comparison. Local information can be obtained from farmers, ranchers, agricultural extension agents, local researchers, or remote sensing. When determining stage dates from local observations, the following guidelines may be helpful.

Effective full cover for row crops such as beans, sugar beets, potatoes, and corn is generally considered to occur when leaves of plants in adjacent rows intermingle so that soil shading becomes nearly complete near solar noon, or when plants reach nearly full size, if no intermingling occurs and plant cover >75% (Wright 1982). If, for some reason, shading of the soil does not become complete for crops that generally do nearly completely shade the soil, then the value for  $K_{cmid}$  should be scaled down accordingly (perhaps 0.5% decrease in the standardized  $K_{cmid}$  for each 1% of unshaded soil; Allen et al. 1998). Incomplete ground cover may occur from reduction in plant growth due to disease, grazing, pests, soil water stress, or cultural practices calling for vegetation-free strips between crop rows.

Because visually determining when densely sown vegetation such as winter and spring cereals and grasses reach effective full cover is difficult, the more easily detectable stage of heading has been used (Wright 1982). For dense grasses, effective full cover will occur at about 0.10–0.15 m height. For thin stands of grass (dry rangeland), grass height may approach 0.3 to 0.5 m before effective full cover is reached. Densely planted forage such as alfalfa and clover reaches effective full cover at about 0.3 to 0.4 m height.

For many agricultural plants, effective full cover is considered to occur when the leaf-area index, LAI, approaches 3.0 (Ritchie 1972; Wright 1982; Ritchie and NeSmith 1991). Kang et al. (2003) and Duchemin et al. (2006) report similar results. LAI is defined as the average total area of leaves (one side) per unit area of ground surface.

The length of the initial and development periods may be relatively short for deciduous trees and shrubs that develop leaves in spring at relatively fast rates. Under some conditions, the initial period may include the time period from flowering until leaf bloom. The  $K_{cini}$  selected for trees and shrubs should reflect the ground condition prior to leaf bloom (the amount of grass or weed cover, wetness, mulch density, etc., affect  $K_{cini}$ ). For example, the  $K_{cini}$  for a deciduous orchard having grass ground cover may be as high as 0.8 to 0.9 prior to and during leaf initiation in frost-free climates, whereas the  $K_{cini}$  for a deciduous orchard having a bare soil surface may be as low as 0.3 to 0.4 prior to leaf initiation if wetting of the soil by irrigation or by precipitation is infrequent.

The end of the midseason and beginning of the late season are usually marked by senescence (browning or dying) of leaves, often beginning with the lower leaves of plants. This, along with less efficient stomates in aging leaf surfaces, causes the reduction in  $K_c$ . The length of the late season may be relatively short (on the order of 5 to 10 days) for vegetation killed by frost or for agricultural crops that are harvested fresh. The value of  $K_{cend}$  used after the termination of plant growth or following harvest should reflect the condition of soil (surface soil water, mulch cover) and condition of the vegetation following plant death or harvest. Often  $K_c$  after harvest can be estimated using  $K_{csoil}$  from Eq. (10-18) or Figure 10-4.

### An FAO $K_c$ Example

An example for constructing an FAO  $K_c$  curve under mean soil wetness conditions is presented in Figure 10-5 for spring barley planted at Logan, Utah (latitude of about  $42^\circ$ ). The initial, development, midseason, and late season stages were taken from Appendix C to have lengths equal to 20, 25, 60, and 30 days for March/April planting at a high latitude site ( $35\text{--}45^\circ$ ). Values for  $K_{cini}$ ,  $K_{cmid}$ , and  $K_{cend}$  were selected from Appendix B as 0.3, 1.15, and 0.25. Mean wind speed at Logan during the mid and late seasons is about  $2 \text{ ms}^{-1}$  and average  $RH_{min}$  is about 30%. Therefore,  $K_{cmid}$  is adjusted using Eq. (10-14) as  $K_{cmid} = 1.15 + [0.04(2-2)-0.004(30-45)](1/3)^{0.3} = 1.19$ .  $K_{cend}$  was adjusted using Eq. (10-15b) as  $K_{cend} = 0.25 + 0.001(30-45) = 0.23$ .  $K_{cend}$  is slightly lower than the value in Appendix B ( $RH_{min} = 45\%$ ), because the adjustment considers that the soil surface and crop during the late season would be slightly drier under the more arid conditions (Doorenbos and Pruitt 1977).

$ET_o$  during the initial and development periods (April) averaged  $4 \text{ mm d}^{-1}$ , and the irrigation and precipitation wetting interval during April was about 12 days. Therefore, from Figure 10-4c,  $K_{csoil}$  is approximately 0.5. This is an improved estimate for  $K_{cini}$  for Logan over that listed in Appendix B (0.3). An FAO mean  $K_c$  curve can now be constructed based on the three  $K_{cm}$  values of 0.5, 1.19, and 0.23 and the four lengths of growth stages (20, 25, 60, and 30 days) as shown in Figure 10-5.

Crops that are harvested several times during the growing season, such as forage crops, are typically modeled as a series of individually constructed curves, one for each growing cycle, as shown in Figure 10-6. Lengths of growth stages may vary from cycle to cycle as weather conditions change.

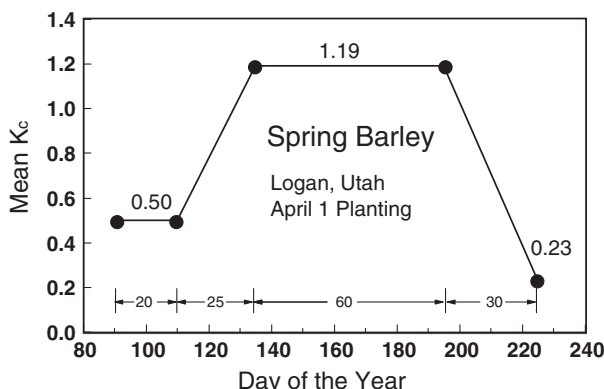


Fig. 10-5. Example construction of an FAO-24 crop coefficient curve

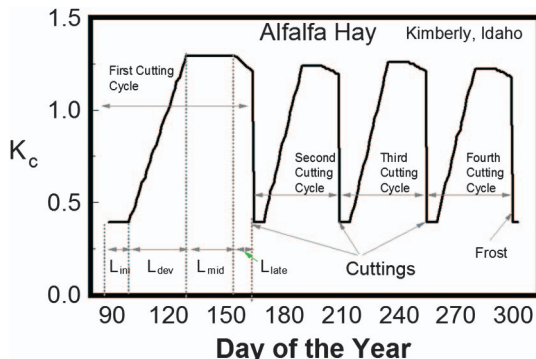


Fig. 10-6. Example mean  $K_c$  curve constructed for four growing cycles of alfalfa hay near Kimberly, Idaho, using  $K_c$  values from Appendix B for grass reference  $ET_o$  following adjustment for climate using Eqs. (10-14)–(10-15)

### Use of the FAO Basal Crop Coefficient Procedure in Calculations

Estimates of  $K_c$  and  $ET_c$  made using the basal  $K_{cb}$  approach with calculations of soil evaporation made on daily time steps can be up to 10 to 20% more accurate than mean  $K_c$  estimates that are based on values in Appendices B and E, especially for the first few days following soil wetting. This is especially true during the initial and development periods.

The FAO crop coefficients can be used in basal calculations by selecting  $K_{cbmid}$  and  $K_{cbend}$  from Appendix D and by setting  $K_{cbini} = K_{cmin}$  during the initial period to represent conditions of a nearly bare soil surface. Appropriate adjustment to  $K_{cbmid}$  and  $K_{cbend}$  for the  $ET_o$  basis is made using Eqs. (10-14) and (10-15) to reflect general humidity and wind speed conditions. The *basal* curve is then drawn using the values for  $K_{cbini}$ ,  $K_{cbmid}$ , and  $K_{cbend}$  following the same procedures described previously for the general FAO  $K_c$  curve.  $K_{cmin}$  represents residual evaporation from a nearly dry bare soil. A typical value for  $K_{cmin}$  for a nearly dry, bare agricultural soil is generally taken as 0.10 to 0.15, recognizing that periodic tillage, precipitation, and irrigation tend to support this residual rate. Over extended fallow periods having no tillage, irrigation, or precipitation, the value for  $K_{cmin}$  tends toward zero. For grasses, brush, and trees, the  $K_{cmin}$  at the start of greenup or leaf development may be on the order of 0.3.

The first step in applying the FAO  $K_c$  in basal computations is to construct the basal  $K_{cb}$  curve using  $K_{cbini}$ ,  $K_{cbmid}$ , and  $K_{cbend}$  as described previously. Eq. (10-2), repeated here,

$$K_c = K_s K_{cb} + K_e \quad (10-22)$$

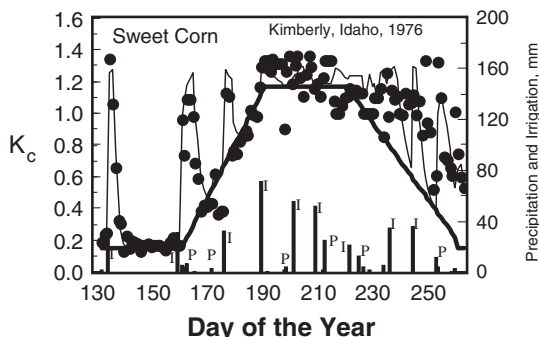


Fig. 10-7. Measured and estimated daily crop coefficients for a sweet corn crop near Kimberly, Idaho, for grass reference  $ET_o$ . The basal crop curve ( $K_{cb}$ ) was derived setting  $K_{cbini} = K_{cmin} = 0.15$  and using data from J. L. Wright (1990, personal communication to R. G. Allen)

is used to calculate  $K_c$  using the  $K_{cb}$  curve, where  $K_e$  and  $K_s$  are calculated on a daily time step using Eqs. (9-19) and (10-4) or (10-6).  $K_{cmax}$  in Eqs. (9-19) and (10-21) ranges from 1.2 to 1.25 for use with the grass-based FAO coefficients [Eq. (10-3a)] and generally equals 1.0 when used with alfalfa-based basal coefficients [Eq. (10-3b)].

An example of applying the FAO  $K_c$  procedure in a basal fashion is shown in Figure 10-7 for a sweet corn crop that was harvested as dry seed. The data in the figure were measured using a precision lysimeter system near Kimberly, Idaho (J. L. Wright, personal communication, 1990). The 24-hour  $K_c$  measurements (symbols) were calculated by dividing daily measured  $ET_c$  by daily calculated  $ET_o$ . The agreement between the estimated daily  $K_c$ s from Eq. (10-2) (shown as a thin, continuous line) and measured  $K_c$ s is relatively good. Measured and calculated  $K_c$ s increased following wetting by rainfall or irrigation. The measured  $K_c$  tended to be well above the  $K_{cb}$  line between days 230 and 250 due to effects of soil wetting on evaporation and thus total  $ET$ . This was reflected in the estimated  $K_c$  as well. A small amount of moisture stress may have occurred around day 220, where measured  $K_c$  fell below the  $K_{cb}$  curve that was not picked up by the  $K_c$  simulation. Some of the day-to-day variation in measured  $K_c$ s shown in Figure 10-7 was due to measurement variation in the lysimeter (about 0 to 5%). However, much of the variation is likely caused by random error in the  $ET_o$  estimate caused by timescale effects in the daily  $ET_o$  equation and fixed aerodynamic, reflectance, and surface conductance characteristics implicit to the  $ET_o$  definition that vary from the day-to-day characteristics of the sweet corn vegetation and by error in weather measurements. Other error is caused by error in the  $K_c$  estimation and by the assumption of a relatively constant ratio of  $ET_c$  to

$ET_o$  (constant  $K_{cb}$ ) from one day to the next. Total root mean square error (RMSE) calculated on a daily basis over the time period shown in Figure 10-7 is 0.17 on a  $K_c$  basis and 0.83 mm d<sup>-1</sup> on an ET basis. The measured  $K_{cb}$  from the lysimeter for the silt loam soil averaged about 0.15 during the period from day 140 to 155 prior to growth of vegetation. That low background rate was supplied by slow diffusive evaporation from the wet subsoil. Even though the  $K_{cb}$  during late season was well below measured  $K_c$ , the addition of estimated  $K_e$  from irrigation and precipitation events caused the summed  $K_{cb}$  and  $K_e$  to approximate measured  $K_c$  relatively well.

Application of the FAO-56  $K_{cb}$  procedure involving Eqs. (9-19)–(9-31) and (10-2) was made by Hunsaker et al. (2002) over a growing season of alfalfa containing eight cutting cycles at a field site in Phoenix, Arizona. Estimated  $ET_c$  was compared against measurements by three weighing lysimeters with good results, as shown in Figure 10-8. The RMSE for the Hunsaker et al. comparisons was 0.44 mm d<sup>-1</sup>. Custom  $K_{cb}$  values for constructing local climate-adjusted FAO-56 style  $K_{cb}$  curves were determined as 0.30, 1.22, and 1.05 for the initial, middle, and end of late season,

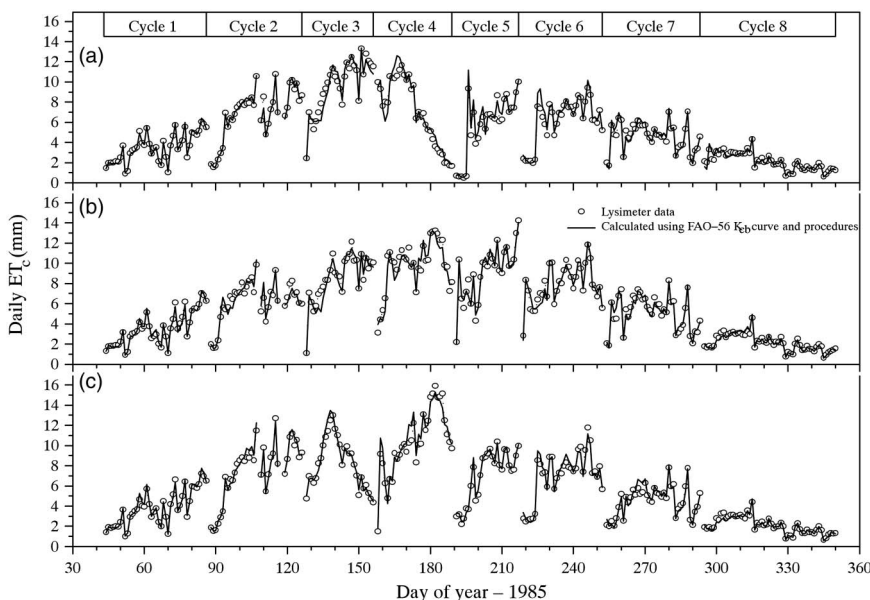


Fig. 10-8. Measured and estimated daily crop evapotranspiration over an entire growing season of alfalfa containing eight cutting cycles at a field site in Phoenix, Arizona. Measurements are shown for three lysimeter systems (a, b, c)  
Source: Hunsaker et al. (2002); reproduced with permission from ASABE

respectively. Lengths of growth stages were varied for each cycle and lysimeter according to visual observation.

## 10.5 ALFALFA-BASED CROP COEFFICIENTS

The primary set of alfalfa-based crop coefficients developed in the United States is traceable to data from Wright (1981, 1982) in southern Idaho. Coefficients developed by Howell et al. (2006) from measurements in northern Texas have recently supplemented these. The Wright  $K_c$  curves are curvilinear, rather than linearly segmented like the FAO-style  $K_c$  curves, and attempt to more closely follow the expected progression of  $K_c$  with crop development. Wright developed  $K_c$  curves for eight crops common to the intermountain west of the United States. Wright's crop coefficients have been widely used in the United States, and many engineers and agronomists are familiar with adjusting the timescale to match local crop conditions. The mean and basal alfalfa-based crop coefficients of Wright (1981, 1982), converted for use with the ASCE Standardized Reference ET equation, are presented in Appendix E. Those same  $K_c$ s are converted to a cumulative growing-season time basis in Appendix F.

### Procedure

Many of the principles and procedures described for using the FAO grass-based crop coefficients are applicable when using alfalfa-based crop coefficients. The main exception is that the alfalfa-based  $K_c$ s do not need to be adjusted for climate [Eqs. (10-14) and (10-15)], because most agricultural crops at full cover have roughness and leaf areas similar to alfalfa. Therefore, alfalfa-based crop coefficients for many agricultural crops have a maximum  $K_c$  near 1.0. The proximity of measured maximum  $K_c$  near 1.0 under full cover conditions serves as a useful reality check for field data and helps users visualize the development and shape of the crop coefficient curve for annual crops and forage crops that are cut periodically. Another advantage of alfalfa-based crop coefficients is that they are more convenient for use with satellite imagery-based energy balance methods for estimating ET over large areas, because maximum  $ET_c$  of many crops corresponds to the alfalfa-based  $ET_r$ . For example, the Landsat satellite imagery program for mapping evapotranspiration at high resolution (METRIC) that Allen et al. (2007b) describe uses alfalfa-based  $ET_r$  for calibration and produces crop coefficients that are alfalfa based. The alfalfa-based  $K_{cb}$  values from Appendixes E and F can be applied in Eq. (10-2) with  $K_c$  derived from Eq. (9-18) from Wright (1982), or the alfalfa-based  $K_{cb}$  values can be applied with the FAO-56  $K_c$  procedure [Eqs. (9-19)–(9-31) and (10-2)], with the  $K_{cmax}$  term in Eq. (9-19) estimated using Eq. (10-3b).

In the Wright  $K_c$  time-based procedure, the time base for  $K_c$  is scaled based on the relative time from planting to effective full cover and, following the time of effective full cover, on days after effective full cover. Wright (1982) defines effective (full) cover as the time when leaves between row crops begin to interlock, at heading of grain, and flowering of peas. The shape of the  $K_c$  curve from planting or greenup to effective full cover is described by expressing values for  $K_c$  for each 10% of the total time length (Appendix E) and values for  $K_c$  for time after effective full cover are expressed for each 10 days following attainment of effective full cover. The  $K_c$  curves are constructed from decadal data (Appendix E) using linear or curvilinear interpolation between adjacent data columns or by fitting regression equations to the first half (planting to effective full cover) and to the second half (days after effective full cover) for each curve. Appendix E summarizes strategic dates of crop development recorded by Wright (1982).

The  $K_{cb}$  curves of Wright (1982) have been re-expressed in Appendix F as functions of cumulative growing degree days (CGDD) to provide automated flexure of the curve basis for varying weather conditions. Wright (2001) and Allen and Wright (2006) converted the Wright (1982)  $K_{cb}$  curves into CGDD-based curves where the  $K_{cb}$  values for the growing season were expressed as a ratio of the CGDD required for the crop to develop from the date of planting or greenup until effective full cover. The winter wheat curve of Allen and Wright (2006) was applied by Allen and Robison (2007) during the Idaho winter by beginning the curve in October, with reductions in CGDD applied when  $T_{min}$  fell below threshold values during cold winter periods.

### An Alfalfa-Based Example

Figure 10-9 is an example comparing  $K_c$  estimated using basal alfalfa-based crop coefficients from Appendix F and the FAO-56  $K_e$  procedure [Eqs. (9-19)–(9-31) and (10-2)–(10-3)] with daily ET measured with a precision lysimeter for a sweet corn crop near Kimberly, Idaho (data by J. L. Wright 1990, in personal communication to R. G. Allen, are the same as shown in Figure 10-7). The lysimeter data are the same data used by Wright (1982) to develop the  $K_{cb}$  curve, so that the  $K_{cb}$  estimates are not statistically independent of the measurements. The maximum  $K_{cb}$  for the sweet corn crop is about 0.9 for the alfalfa reference. The FAO-56 style method for estimating  $K_e$  performed relatively well with the curvilinear  $K_{cb}$  curve. The RMSE calculated on a daily basis over the time period shown in Figure 10-9 is 0.13 on a  $K_c$  basis and  $0.75 \text{ mm d}^{-1}$  on an ET basis. This compares with the RMSE of 0.17 on a  $K_c$  basis and  $0.83 \text{ mm d}^{-1}$  on an ET basis for the linear FAO-56 calculations of Figure 10-7. The magnitude of RMSE is affected by how the  $K_{cb}$  curves were originally constructed and measurement data

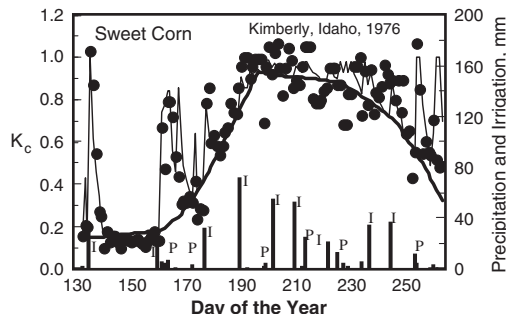


*Fig. 10-9. Measured and estimated daily crop coefficients for a sweet corn crop near Kimberly, Idaho, based on alfalfa reference  $ET_r$ . The basal ( $K_{cb}$ ) crop curve is based on Wright (1982) curvilinear  $K_{cb}$  from Appendix F, and  $K_e$  is based on the FAO-56 procedure [Eqs. (9-19)–(9-31) and (10-1)–(10-12)]*

*Source: Data from J. L. Wright (personal communication to R. G. Allen, 1990)*

interpreted. In this case, the  $K_{cb}$  estimates are not statistically independent of the lysimeter measurements, although the  $K_e$  estimates are independent.

### Expression of $K_c$ Curves and the Time Basis

Because of uncertainty in day-to-day values for  $K_c$  or  $K_{cb}$  due to random error in weather data and  $ET_{ref}$  estimates and in determination of  $K_c$  from field or research measurements, the straight-line  $K_c$  curve method of the FAO method is generally appropriate for most applications. Hunsaker (1999) developed and compared  $K_{cb}$  curves for a cotton crop in Arizona using the straight-line method of FAO and curvilinear curves based on days after planting and based on cumulative growing degree days (Figure 10-10). Hunsaker concludes that any of the three  $K_{cb}$  curve construction methods should result in good estimates of daily  $ET_c$  for the early-maturity cotton measured, when grown under climatic conditions similar to those of the study.

## 10.6 ESTIMATES OF $K_c$ CURVES FOR NATURAL AND AGRICULTURAL VEGETATION

The two-step  $K_c ET_{ref}$  approach provides a simple, convenient way to estimate  $ET_c$  from natural vegetation, where  $K_c$ , if unknown, can be estimated according to the fraction of ground covered by vegetation. The developed cover (crop) coefficient curves represent the ratios of  $ET_c$  to  $ET_{ref}$  during various growth stages. A previous section describes estimation of lengths of growth stages. Often, for unknown  $K_c$  curves, the  $K_c$  during the

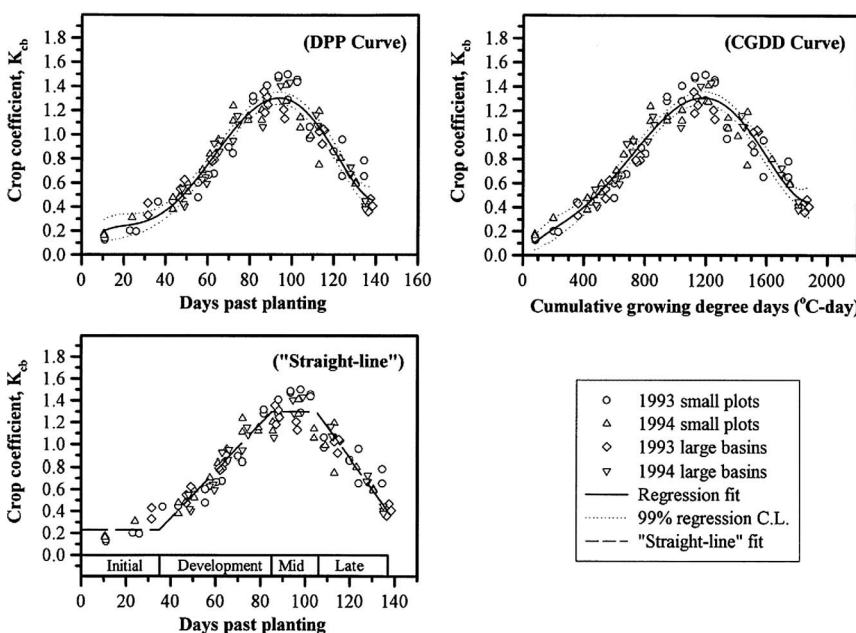
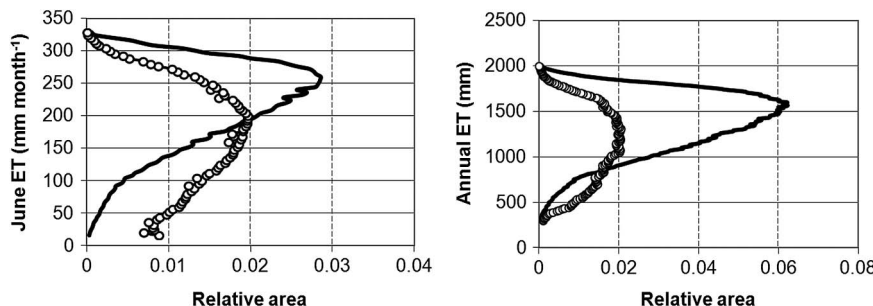


Fig. 10-10. Basal crop coefficient ( $K_{cb}$ ) curves derived as functions of days past planting (DPP) and cumulative growing degree days (CGDD) and using the FAO straight-line method for an early maturing cotton crop in Arizona with comparison to measurements (symbols)

Source: Hunsaker 2003; reproduced with permission from Springer International Publishing

peak growth period ( $K_{cmid}$ ) can be estimated according to the amount of ground shaded by vegetation, the density and height of plants, and the amount of stomatal regulation under moist soil conditions. The value for  $K_c$  for conditions of low soil water availability is generally determined using Eq. (10-4) or (10-6).

The  $K_c$  development process should adhere to upper limits for  $K_c$  of 1.1 for an alfalfa reference and about 1.25 for a grass reference for stands of vegetation larger than 500 to 2,000  $\text{m}^2$ . Energy exchange principles within established equilibrium boundary layers and the principle of conservation of energy as discussed in the previous sections on field-scale applications and small expanses of vegetation govern ET from these stands.  $K_{cs}$  for small stands ( $<500 \text{ m}^2$ ) should also adhere to these limits when the vegetation height and leaf area are less than or equal to those of surrounding vegetation and soil water availability is similar. Only under conditions of "clothesline effects" (where vegetation height is greater than surroundings) or "oasis effects" (where vegetation has higher soil water availability than



*Fig. 10-11. Frequency distributions of ET from 6,000 ha of cottonwood and salt cedar (tamarisk) along the Middle Rio Grande in New Mexico during June and all of 2002*

Source: Allen et al. (2007a); copyright ASCE

surroundings) will peak  $K_c$ s exceed the previously stated limits. The user should exercise caution when extrapolating ET measurements from small vegetation stands or plots to large stands or regions, as overestimation of regional ET may occur.

Derived  $K_c$  values for natural vegetation based on vegetation amount represent the potential  $K_c$  when soil water is available for full ET. Often, however, soil water levels for natural plant communities fall below adequate supplies due to drought or, for riparian vegetation, due to declining water tables. Therefore, the frequency distribution of ET can be broad for a population of vegetation, as shown in Figure 10-11, where a frequency distribution of June and annual ET for cottonwood and salt cedar along the Middle Rio Grande valley is shown as derived from satellite-based energy balance (Allen et al. 2007a). ET from salt cedar (e.g., tamarisk) showed larger variance due to its tendency to grow across a broad range of water availability (water table depth), soil types, and salinity conditions, whereas cottonwoods, which exhibited a smaller variance in the population of ET, are typically found close to stream channels and consistent water supply. Wide variation was also noted for tree population density, which added to variance in the populations of ET.

Allen et al. (1998) propose estimating  $K_c$  and ET for isolated, narrow stands of wetlands and tall wind breaks such as single rows of trees using a description of stand height and width and with dampening for vegetation with a high degree of stomatal control:

$$K_c = \min\left(K_{cmax} + \frac{F_r h_{canopy}}{\text{width}}, 2.5\right) \quad (10-23)$$

where  $K_{cmax}$ , the maximum  $K_c$  expected for large fields, is 1.2 for use with  $ET_o$  and 1.0 for use with  $ET_r$ ;  $F_r$  is a stomatal resistance correction factor;

$h_{\text{canopy}}$  is the mean vertical height of the canopy area in m; and width is the horizontal thickness of the windbreak or patch of wetland vegetation normal to the general wind direction in m. For vegetation such as some desert vegetation and trees with leaf resistance significantly greater than that of most agricultural crops where  $r_l$  is commonly about  $100 \text{ s m}^{-1}$ ,  $F_r$  can be approximated based on the FAO form of the PM equation:

$$F_r = \frac{\Delta + \gamma(1 + 0.34u_2)}{\Delta + \gamma\left(1 + 0.34u_2\frac{r_l}{100}\right)} \quad (10-24)$$

where  $r_l$  is the mean leaf resistance for the vegetation in question in  $\text{sm}^{-1}$ . The mean leaf resistance,  $r_l$  is  $100 \text{ sm}^{-1}$  for the  $ET_o$  and  $ET_r$  references and for many agricultural crops. Values for  $r_l$  for many agricultural and nonagricultural plants can be found in Table 11-2 and Körner et al. (1979).

As discussed earlier, the value for  $K_{c\text{mid}}$  for natural vegetation reduces when plant density or leaf area fall below full ground cover ( $\text{LAI} < 3$ ). Because  $K_c$  tends to increase in proportion to the amount of vegetation,  $K_c$  at midseason,  $K_{c\text{mid}}$ , can be expressed as a function of a density coefficient,  $K_d$  (Allen and Pereira 2009), where

$$K_{cb\text{mid}} = K_{c\text{min}} + K_d(K_{cb\text{full}} - K_{c\text{min}}) \quad (10-25a)$$

where  $K_{cb\text{mid}}$  is the approximation for  $K_{cb}$  during the midseason period,  $K_{cb\text{full}}$  is the estimated basal  $K_c$  during peak plant growth for conditions of nearly full ground cover (or  $\text{LAI} > 3$ ), and  $K_{c\text{min}}$  is the minimum basal  $K_c$  for bare soil ( $K_{cb\text{min}} \sim 0.15$  under typical agricultural conditions and  $K_{cb\text{min}} \sim 0.0$  to  $0.15$  for native vegetation, depending on rainfall frequency). The density coefficient  $K_d$  can be estimated as a function of measured or estimated leaf-area index (LAI) or as a function of fraction of ground covered by vegetation. For tree crops having grass or other ground cover, Eq. (10-25a) can take the form

$$K_{cb\text{mid}} = K_{cb\text{cover}} + K_d \left[ \max \left( K_{cb\text{full}} - K_{cb\text{cover}}, \frac{K_{cb\text{full}} - K_{cb\text{cover}}}{2} \right) \right] \quad (10-25b)$$

where  $K_{cb\text{cover}}$  is the  $K_{cb}$  of the ground cover in the absence of tree foliage. The second term of the max function reduces the estimate for  $K_{cb\text{mid}}$  by half the difference between  $K_{cb\text{full}}$  and  $K_{cb\text{cover}}$  when this difference is negative. This accounts for impacts of shading of the surface by vegetation with  $K_{cb}$  lower than that of the surface cover, due to differences in stomatal conductance. Eq. (10-25) can be applied to estimate  $K_{cb}$  during other periods besides the midseason by estimating  $K_d$  using Eqs. (10-27) and (10-28) with LAI or  $f_{ceff}$  for that period.

Eq. (10-25) can similarly be applied to estimate a mean  $K_{cm}$  for any period with less than full vegetative cover by accounting for the effect of evaporation from predominantly exposed areas of soil among the vegetation, much as is done in the dual  $K_{cb} + K_e$  approach:

$$K_{cm} = K_{soil} + K_d \left[ \max\left(K_{cb\text{full}} - K_{soil}, \frac{K_{cb\text{full}} - K_{soil}}{2}\right) \right] \quad (10-26)$$

where  $K_{soil}$  is obtained from Figure 10-4 or Eq. (10-18) and represents the average  $K_c$  from the nonvegetated (exposed) portion of the surface. The value for  $K_{soil}$  reflects the effect of wetting frequency, soil type, and relative ET rate (i.e.,  $ET_{ref}$ ) during the same period as  $K_d$  and  $K_{cb\text{full}}$ . The  $K_{cm}$  represents an average  $K_c$  value that considers the mean impact of evaporation from soil.  $K_{cm}$  can be used to represent the midseason or other period as defined by  $K_d$ ,  $K_{cm}$ , and  $K_{cb\text{full}}$ .

For large stand size (>about 500 m<sup>2</sup>),  $K_{cb\text{full}}$  for use with  $ET_o$  can be approximated for crops not listed in Appendix D as a function of mean plant height and adjusted for climate similar to the  $K_{cbmid}$  parameter and following Allen et al. (1998):

$$\begin{aligned} (\text{for } ET_o) \dots \dots K_{cb\text{full}} &= \min(1.0 + 0.1h, 1.20) + [0.04(u_2 - 2) \\ &\quad - 0.004(RH_{\min} - 45)] \left(\frac{h}{3}\right)^{0.3} \end{aligned} \quad (10-27a)$$

For use with alfalfa reference  $ET_r$ ,  $K_{cb\text{full}}$  can be approximated for crops not listed in Appendix F as

$$(\text{for } ET_r) \dots \dots K_{cb\text{full}} = \min(0.8 + 0.1h, 1.0) \quad (10-27b)$$

where  $h$  is mean maximum plant height in m,  $u_2$  is the mean value for wind speed at 2-m height during the midseason in m s<sup>-1</sup>, and  $RH_{\min}$  is the mean value for minimum daily relative humidity during the midseason in percent. The climatic correction is not required for  $K_{cb\text{full}}$  when used to derive the  $K_{cb}$  for  $ET_r$  because of the aerodynamic and canopy characteristics of the alfalfa reference crop.

The value  $K_{c\text{full}}$  represents a general upper limit on  $K_{cbmid}$  for tall vegetation with full ground cover and LAI > 3 under full water supply. The min function in Eq. (10-27b) selects the minimum expression in the parentheses. Eqs. (10-27a) and (10-27b) produce general approximations for the increase in  $K_{cb\text{full}}$  with plant height and climate. The estimate from Eq. (10-27) may need adjustment downward if the vegetation exhibits more stomatal control on transpiration than is typical for agricultural crops, for example, for some types of trees or natural vegetation.

Where LAI can be measured or approximated,  $K_d$  can be approximated under normal conditions (Allen et al. 1998) as

$$K_d = (1 - e^{[-0.7 \text{LAI}]}) \quad (10-28)$$

LAI is defined as the area of leaves per area of ground surface averaged over a large area with units of  $\text{m}^2\text{m}^{-2}$ . Only one side of green healthy leaves that are active in vapor transfer is considered. The relationship in Eq. (10-28) is similar to one used by Ritchie (1974).

Where estimates of the fraction of ground surface covered by vegetation are available, the  $K_d$  can be estimated as (Allen and Pereira 2009)

$$K_d = \min \left[ 1, M_L f_{ceff}, f_{ceff}^{\left(\frac{1}{1+h}\right)} \right] \quad (10-29)$$

where  $M_L$  is a multiplier on  $f_{ceff}$  describing the effect of canopy density and conductance on maximum relative ET per fraction of ground shaded (1.5–2.0),  $f_{ceff}$  is the effective fraction of ground covered or shaded by vegetation (0.01–1) near solar noon, and  $h$  is the mean height of the vegetation in m. For canopies such as trees or randomly (nonrow) planted vegetation,  $f_{ceff}$  can be estimated from Allen et al. (1998) as

$$f_{ceff} = \frac{f_c}{\sin(\beta)} \leq 1 \quad (10-30)$$

where  $\beta$  is the mean angle of the sun above the horizon during the period of maximum ET (generally between 11.00 and 15.00). Generally,  $f_{ceff}$  can be assigned to solar noon (12.00), so that  $\beta$  can be calculated as

$$\beta = \arcsin[\sin(\phi) \sin(\delta) + \cos(\phi) \cos(\delta)] \quad (10-31)$$

where parameters  $\phi$  and  $\delta$  are defined in Chapter 4 [see Eq. (4-10) for example]. Figure 10-12 schematically illustrates  $f_c$ ,  $f_{ceff}$ , and  $\beta$ .

The  $M_L$  multiplier on  $f_{ceff}$  in Eq. (10-29) imposes an upper limit on the relative magnitude of transpiration per unit of ground area as represented by  $f_{ceff}$  (Allen et al. 1998) and is expected to range from 1.5 to 2.0, depending on the canopy density, thickness, and maximum conductance. Parameter  $M_L$  is an attempt to simulate the physical limits imposed on water flux through the plant root, stem, and leaf systems (Allen and Pereira 2009). The value for  $M_L$  can be modified to fit the specific vegetation. Values for  $M_L$  used to calculate values for  $K_{cb}$  for orchard crops in Appendix D and that served as the basis for  $K_{cm}$  for orchard crops in Appendix B are listed in Table D-2 of Appendix D. Figure 10-13 shows values for  $K_d$  over a range of  $f_{ceff}$  and a range of  $h$  for  $M_L = 1.5$  and for  $M_L = 2$  when  $h = 5$  m. The estimates by Eq. (10-29) agree with those

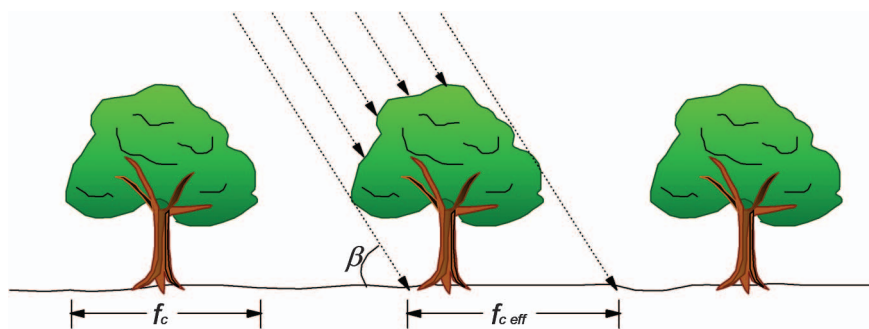


Fig. 10-12. Schematic showing extent of  $f_c$ ,  $f_{c,eff}$ , and  $\beta$  for tree vegetation where  $f_c$  is the fraction of surface covered by vegetation as measured from directly overhead

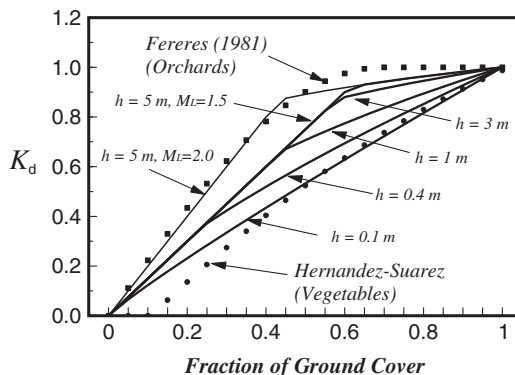


Fig. 10-13. Density coefficient,  $K_d$ , estimated from Eq. (10-29) with  $M_L = 1.5$  over a range of ground cover fractions and various plant heights and compared with estimates by Fereres (1981) for orchards and Hernandez-Suarez (1988) for vegetables

Source: Comparative data from Fereres (1981) and Hernandez-Suarez (1988)

previously suggested by Fereres (1981) and Hernandez-Suarez (1988) for specific types of vegetation.

When the mean stomatal control by the vegetation is greater than for agricultural vegetation, then FAO-56 suggests that the estimate by Eq. (10-29) be reduced by about 10 or 20% for each doubling of  $r_1$  above  $100 \text{ s m}^{-1}$ . The value for  $K_{cb,mid}$  estimated by Eq. (10-25) is applied as a basal coefficient using the dual  $K_{cb} + K_e$  method, where the actual  $K_c$  may increase to 1.0 for  $ET_r$  or 1.2 for  $ET_o$  following precipitation even if the

estimated  $K_{cbmid}$  is small, due to surface evaporation from among sparse vegetation. In addition,  $K_c$  should be reduced via Eq. (10-2) or (10-22) using  $K_s$  from Eq. (10-4) or (10-6) when soil water is low.

Eq. (10-29) suggests that as  $h$  increases, total leaf area and resulting net radiation capture will increase, thereby increasing  $K_c$ . In addition, as  $h$  increases, more opportunity for microadvection of heat from soil to canopy occurs, and turbulent exchange within the canopy increases for the same amount of ground coverage. Both of these conditions increase the relative magnitude of  $K_{cbmid}$ . Values for  $K_{cbend}$  can be scaled from  $K_{cbmid}$  in proportion to the health and leaf condition of the vegetation at termination and the length of the late season period (i.e., whether leaves senesce slowly or are killed by frost). The  $f_c$  parameter and  $h$  are probably the simplest indices to estimate in the field.

Ringersma and Sikking (2001) apply Eqs. (10-25), (10-27a), and (10-29) to estimate ET from Sahelian vegetation barriers. They find Eq. (10-27a) to overestimate  $K_{cbfull}$ , even with adjustment using  $F_r$ , but find Eq. (10-29) to produce representative estimates. Ringersma and Sikking suggest distinction between C3 and C4 photosynthetic behavior for LAI and  $f_c$  based estimation, because C4 vegetation can have limited stomatal control. Descheemaeker et al. (2011) apply Eqs. (10-25), (10-26), and (10-29) to savannah vegetation in Ethiopia and find good agreement between estimated ET and ET measured gravimetrically. Vegetation types ranged from sparse, grazed grasses to full forest canopy.

## 10.7 LANDSCAPE COEFFICIENTS

Water requirements and consumption by residential and urban landscapes have become increasingly important because of the quantity and value of water consumed. Procedures similar to those from agriculture have been adapted to estimate ET from landscapes. However, two distinctions are made between agriculture and landscapes: (1) landscape systems often comprise mixtures of types and species of vegetation, thereby complicating the estimation of ET, and (2) typically, the objective of landscape irrigation is to promote appearance rather than biomass production, whereas biomass production is generally maximized in agriculture. Therefore, target ET for landscapes may include intentional water stress in the baseline estimate for  $ET_c$ , because landscape plants are watered less than they would be if they were irrigated like a crop. Landscape vegetation should generally be watered sufficiently for acceptable appearance and to survive, but the plants can often be stressed to some degree and will not be at maximum productivity. This adjustment can produce significant water conservation. The magnitude of the stress factor depends on physiological and morphological requirements of the plants;

the goal is to sustain health and appearance with minimal irrigation. For example, water conservation studies on turfgrass have demonstrated water savings of 30% for cool-season turfgrasses and 40% for warm-season turfgrasses without significant loss of quality (Meyer and Gibeault 1986; Pittenger and Shaw 2001, 2004). Some shrubs and ground covers can be managed for even more stress-induced reduction in ET (Kjelgren et al. 2000). A third departure of landscape ET from agricultural ET is that few landscape sites meet the “extensive surface” requirement needed to ensure equilibrium between the lower boundary layer of the atmosphere and the vegetation that is implied in the Penman-Monteith equation. Therefore, compensating adjustments are necessary to the landscape coefficient in the form of a microclimate factor to account for effects of local surroundings.

Because of the frequent inclusion of water stress in target ET values for landscape design and management, distinction must be made between these target ET values and actual ET values. Actual ET values may exceed target ET values if the landscape receives more water than required by the target that includes intentional stress. Under these conditions, landscape vegetation may exploit the additional available water, subject to some limit constrained by environmental energy available for evaporation and leaf area. The upper environmental energy limit, which follows behavior and principles used for agricultural crops, may exceed the targeted ET rate for the particular landscape cover. Conversely, actual ET may be less than targeted ET values if actual stress levels to the landscape are more excessive than targeted. Therefore, two ET values for landscape are distinguished here. The first is the *target landscape ET*, referred to as  $ET_L$ , that is based on minimum ET levels, relative to climate, necessary to sustain a healthy, attractive landscape. The second ET value is the actual landscape ET,  $ET_{Lact}$ , that is based on landscape type and on actual water availability. Traditionally, landscape ET estimation is based on the grass reference  $ET_o$  rather than on alfalfa reference  $ET_r$ . The target ET for a landscape is calculated as

$$ET_L = K_L ET_o \quad (10-32)$$

where  $ET_L$  is the target landscape ET (in  $\text{mm d}^{-1}$ ,  $\text{mm month}^{-1}$ , or  $\text{mm year}^{-1}$ ), and  $ET_o$  is the grass reference ET in the same units.  $K_L$  is the target landscape coefficient, similar to the crop coefficient used in agricultural applications.

Somewhat limited experimental research exists on quantifying water needs of the vast and diverse array of landscape plant types (Pittenger and Henry 2005). Some of the leading work on landscape ET from ground covers and shrubs has been done in California, where water applied to landscapes in southern California is estimated to be 25 to 30% of all water used in the region (Pittenger and Shaw 2001). St. Hilaire et al. (2008)

produced a table of  $K_L$  values for 35 landscape ground covers and shrubs that are targeted to provide acceptable landscape performance after initial establishment and that induce a managed amount of moisture stress via limited water application. Costello et al. (2000) and Irrigation Association (2003) describe a procedure from California termed WUCOLS (water use classification of landscape species), where the  $K_L$  was decoupled into reproducible and visually apparent components representing the effects of three or four factors that control the value for  $K_L$ . The decoupling was done to facilitate application to the wide diversity of vegetation types and environments of landscape systems. Snyder and Eching (2004, 2005) propose a similar decoupled procedure for estimating a formulated  $K_L$  that uses different ranges for the components:

$$K_L = K_v K_d K_{sm} K_{mc} \quad (10-33a)$$

where  $K_v$  is a vegetation species factor,  $K_d$  is a vegetation density factor,  $K_{mc}$  is a microclimate factor, and  $K_{sm}$  is a managed stress factor.  $K_v$  can be considered to be the ratio of  $ET_v$  to  $ET_o$  for a specific single or mixture of plant species under full or nearly full ground cover and full soil water supply, where  $ET_v$  is the vegetation  $ET$  assuming no water deficits and greater than 70 to 80% ground cover. Factors  $K_d$ ,  $K_{mc}$ , and  $K_{sm}$  modify  $K_v$  for less than effective full ground cover ( $K_d$ ), for effects of shading or for exposure to advective or reflective sources ( $K_{mc}$ ), and for intentional water stress ( $K_{sm}$ ). Each of these factors can be estimated separately from the other based on visual observation of the landscape (for  $K_d$  and  $K_{mc}$ ) and based on grower experience (for  $K_{sm}$ ). Following the estimation of the individual factors,  $K_L$  is calculated using Eq. (10-33) and represents a generally accurate and reproducible estimate of relative landscape  $ET$ . The procedure of Snyder and Eching (2004, 2005), used in the University of California-Davis's LIMP software, differs from that of WUCOLS (Costello et al. 2000; Irrigation Association 2003) in the ranges used to define  $K_d$ . The Snyder-Eching definition and range for  $K_d$  are congruent with estimates for  $K_d$  from Eq. (10-29), where  $K_d$  ranges from 0 to 1.

An alternative form of Eq. (10-33a) conforms to the procedure used to derive the agricultural  $K_c$  as a function of vegetation density where account is made for evaporation from exposed bare soil among the vegetation [see Eqs. (10-25a, b)]:

$$K_L = (K_{soil} + K_{vsd} K_d K_{sm}) K_{mc} \quad (10-33b)$$

where  $K_{vsd}$  is a coefficient describing the difference in  $ET$ , per unit of surface, between  $K_v$  and  $K_{soil}$ :

$$K_{vsd} = \max\left(K_v - K_{soil}, \frac{K_v - K_{soil}}{2}\right) \quad (10-34)$$

and  $K_{\text{soil}}$  is the evaporation coefficient representing the evaporation (relative to  $ET_o$ ) from bare soil caused by wetting by precipitation or irrigation.  $K_{\text{soil}}$  is included in Eq. (10-33b) to consider the impact of evaporation occurring between plants, and its inclusion becomes more significant with lower plant density ( $K_d$ ) and with frequency of soil wetting.  $K_{\text{soil}}$  is estimated as a function of soil wetting frequency and magnitude of  $ET_o$  from Figure 10-4 or using Eqs. (10-18)–(10-21). As in Eq. (10-25b) and (10-26), the second term of the max function in Eq. (10-34) reduces the estimate for  $K_L$  by about half the difference between  $K_v$  and  $K_{\text{soil}}$  when this difference is negative. This accounts for effects of shading of the soil surface by vegetation with  $K_v$  lower than that of the evaporating soil, due to high stomatal resistance. As an alternative to Eq. (10-33b), a daily dual  $K_{cb} + K_e$  procedure, described previously, can be applied where  $K_{cb}$  is set equal to  $K_L$  from Eq. (10-33b), using  $K_{\text{soil}} = 0.15$ , and  $K_e$  is estimated daily in accordance with wetting frequency. Eq. (10-33b) reverts to Eq. (10-33a) when  $K_{\text{soil}} = 0$ . Eq. (10-33b) is useful to assess the impact of irrigation frequency on total ET of turf with less than full ground cover. Effects of evaporation of water intercepted by vegetation following irrigation or precipitation are estimated later with Eq. (10-37).

## The Vegetation Coefficient

The  $K_v$  for landscape vegetation represents the near maximum ratio of  $ET_v$  to  $ET_{omc}$  that occurs when generally 70% or more cover (shading) of the ground exists and soil water supply is full.  $ET_{omc}$  is the  $ET_o$  for the microclimate where the vegetation grows.  $ET_{omc}$  can deviate from the standard  $ET_o$ , where  $ET_o$  is a regional estimate of reference evapotranspiration based on measured weather data, whereas  $ET_{omc}$  is a local  $ET_o$  corrected for microclimate differences. The microclimate coefficient,  $K_{mc} = ET_{omc}/ET_o$ , is estimated or determined experimentally and is described in the following section.  $K_v$  establishes the maximum ratio  $K_L = ET_v/ET_{omc}$  for the vegetation under ideal conditions. Based on the definition for  $K_v$ , where  $K_v$  is the fraction of  $ET_{omc}$  when the foliage is at near maximum density ( $K_d = 1$ ) and has full water availability ( $K_{sm} = 1$ ), many types of landscape vegetation tend to exhibit similar values for  $K_v$  due to similarities in total leaf area, stomatal response, and energy absorption. Therefore, condensed tables of typical values for general species types can be used to provide general estimates for  $K_v$ , where  $K_v$  ranges from about 0.8 to 1.2. Because landscape vegetation is usually taller and rougher than grass, the upper limit for  $K_v$  can exceed 1.0 for well-watered landscapes. Table 10-3 contains general values for  $K_v$  for general types of landscape vegetation. Primary sources for values in Table 10-3 are listed in the table footnote.

The typical  $K_v$  values in Table 10-3 represent full effective ground cover ( $f_c > \sim 0.7$ –0.8) and no water stress. The values are general and, under most

Table 10-3. General Vegetation (Species) Factors,  $K_v$ , for General Plant Types for High-Density Cover of the Ground and Full Water Supply

Vegetation Category <sup>a</sup>	$K_v$
Trees	1.15
Shrubs	
desert species	0.7
nondesert	0.8
Ground cover	1.0
Annuals (flowers)	0.9
Mixture of trees, shrubs, and ground cover <sup>b</sup>	1.2
Cool-season turfgrass <sup>c</sup>	0.9
Warm-season turfgrass <sup>d</sup>	0.9

<sup>a</sup>The tree, shrub, and ground cover categories listed are for landscapes composed solely or predominantly of one of these vegetation types with somewhat dense coverage (shading) of the ground.

<sup>b</sup>Mixed plantings are composed of two or three vegetation types (i.e., where a single vegetation type does not dominate).

<sup>c</sup>Cool-season grasses include Kentucky bluegrass, fescues, and perennial ryegrass.

<sup>d</sup>Warm-season grasses include Bermuda grass, St. Augustine grass, buffalo grass, and blue grama.

Source: Data from Irrigation Association (2011). Primary sources of data include cool-season turfgrass (Aronson et al. 1987; Brown et al. 2001); warm-season turfgrass (Brown et al. 2001; Jia et al. 2009); other vegetation (Irrigation Association 2011)

conditions, are not met due to the density factor being less than 1.0 and due to intentional moisture stress (Brown et al. 2001; Jia et al. 2009). The  $K_v$  value for warm-season grass is equal to that for cool-season grass in Table 10-3 because both of these grass types tend to have similar  $ET_v/ET_{omc}$  under conditions of no water stress. Typically, however, warm-season grasses tolerate higher levels of moisture stress than cool-season grasses; so that a lower managed stress factor can be applied to warm-season grasses with less visual effect, as is illustrated in Table 10-5. The  $K_v$  values for both cool-season and warm-season grasses are less than 1.0 in Table 10-3 due to the tendency for their mean height to be less than that of the standardized 0.12-m grass reference. Comparison of  $K_L$  for warm-season grasses from Eq. (10-33a) and Tables 10-3–10-5 and measurements for a Florida application are presented as Figure 10-14.

$K_v$  values for ground cover and annuals or flowers are assumed to be nearly or equal to 1.0, reflecting the likely  $K_v$  when the vegetation completely covers the ground ( $K_d=1.0$ ) and when no stress occurs ( $K_{sm}=1.0$ ). Because of the hundreds, if not thousands, of species of flowers and ground cover types, estimating or establishing  $K_v$  values for each of

Table 10-4. Microclimate Factor,  $K_{mc}$ , for Landscape Plant Types

Vegetation	High (Hostile Environment)	Average (Reference Condition)	Low (Protected or Shaded Environment)
Trees	1.4	1.0	0.5
Shrubs	1.3	1.0	0.5
Ground cover, flowers	1.2	1.0	0.5
Mixture of trees, shrubs, and ground cover	1.4	1.0	0.5
Turfgrass	1.2	1.0	0.8

Source: Data from Irrigation Association (2003, 2011)

Table 10-5. Managed Stress Factors,  $K_{sm}$ , for General Landscape Plant Types and the Depletion Fraction for No Stress

Vegetation Category	High Stress	Average Managed Stress	Low Stress	Depletion Fraction, $p$ , for No Stress
Trees	0.4	0.6	0.8	0.6
Shrubs				
desert species	0.3	0.4	0.6	0.6
nondesert	0.4	0.6	0.8	0.6
Ground cover	0.3	0.5	0.8	0.5
Annuals (flowers)	0.5	0.7	0.8	0.4
Mixture of trees, shrubs, and ground cover <sup>a</sup>	0.4	0.6	0.8	0.6
Cool-season turfgrass	0.7	0.8	0.9	0.4
Warm-season turfgrass	0.6	0.7	0.8	0.5

<sup>a</sup>Mixed plantings are composed of two or three vegetation types where a single vegetation type does not predominate.

Source: Data from Irrigation Association (2011)

these species is difficult. Rather, the upper limit for  $K_v$  is established, which can be reduced when specific information on a species is determined. The  $K_v$  for mixed systems of trees, shrubs, and/or ground cover is discussed in the next section.

Carrow (2004) suggests common target values for  $K_L$  for cool-season grasses to range from about 0.70 to 0.95 in the southeast United States as

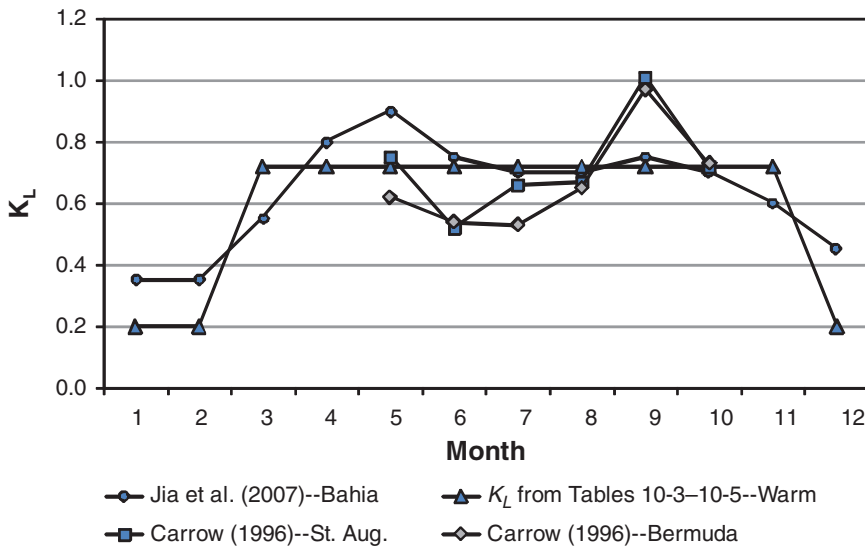


Fig. 10-14. Measured monthly  $K_L$  for Bahia grass in Florida by Jia et al. (2009) and for St. Augustine and Bermuda grasses in Georgia by Carrow (1996) compared with a steady target  $K_L$  from Eq. (10-33b) and Tables 10-3-10-5 for a warm-season grass

Source: Data from Jia et al. (2009) and Carrow (1995, 1996)

compared with  $K_L$  for warm-season turfgrasses of 0.65 to 0.85 when the irrigation regime is 3 to 7+ days between events, which allows mild moisture stress during hot periods. At these  $K_L$  values, turf generally maintains acceptable quality and growth. As  $K_L$  values fall below these general ranges using a similar irrigation schedule but with smaller doses per irrigation, turf performance and appearance may rapidly decline. Carrow (1995) reports turfgrass  $ET_c$  to be 40 to 60% less in a humid environment compared with the same cultivar in an arid environment, but with similar  $K_L$  values for both environments.

### Density Factor

Landscapes can vary considerably in vegetation density, due to wide variation in plant spacing and maturity. The plant density factor,  $K_d$ , can be estimated using Eq. (10-29). Vegetation density refers to the collective leaf area of all plants in the unit landscape area. More densely growing vegetation will have a higher  $K_d$  and will transpire and require more water. Immature and sparsely planted landscapes have less total leaf area per unit landscape area than mature landscapes and have a lower value for  $K_d$ . Often, landscapes have two and three tiers (horizontal levels) of

vegetation including turf or ground cover, shrubs, and trees. Overlapping tiers are capable of more radiative and other energy exchange and tend to increase ET, as shown by the  $K_v$  value of 1.20 in Table 10-3 for the "mixture" class. When two substantial tiers of vegetation are present, for example, trees shading grass or flowers, the value for height,  $h$ , can be approximated in proportion to the  $f_c$  for each tier. The important factor is the fraction of the sunlight intercepted by the plants and the fraction that reaches the ground. By observation at different times of the day, one can estimate the fraction of direct sunlight reaching the ground. The plant light interception is usually slightly more than the percentage of ground cover, so that the observed light interception can be used to estimate the  $K_d$  factor. If more than 80% of the sunlight onto the landscape is intercepted by the plants over the day, then one should expect the  $K_d$  factor to be close to 1.0.

### Microclimate Factor

The microclimate factor,  $K_{mc}$ , accounts for impacts on ET by sun, shading, protected areas, hot and cool areas, reflected and emitted radiation from structures, wind, and transfer of heat energy from low ET surroundings. Structures and paved areas typical of urban landscapes can have pronounced effect on the local energy balance due to the transfer of energy for evaporation from these surfaces to local vegetation. The environmental conditions of a landscape can vary significantly across the landscape, for example, areas on the south side of a building vs. areas on the north side. Vegetation plantings adjacent to paved, open areas may have 50% higher ET demand than similar plantings among other vegetation due to the transfer of energy to the vegetation from the nonevaporating areas. Conversely, plantings in areas shaded from sun and wind may have ET rates that are only one-half as high as those for open settings. Another important factor is wind blockage by buildings and vegetation. Reference evapotranspiration weather stations are typically placed in well-exposed areas with wind speeds that represent the region. If the landscape is exposed to less wind due to shielding by buildings or vegetation, then the  $ET_{omc}$  (see earlier definition) may be less than  $ET_o$ . The LIMP program from Snyder and Eching (2004, 2005) provides a methodology to address these microclimate factors.

Values for  $K_{mc}$  are listed in Table 10-4 for general classes of vegetation. The "high" category ( $K_{mc} > 1$ ) in Table 10-4 reflects harsh microclimate conditions such as planting in direct sunlight near paved or other non-vegetated surfaces, near reflective or heat-absorbing surfaces such as windows or buildings, or in exposed, windy conditions. "Hot" surfaces of buildings can emit substantial amounts of long-wave radiation to nearby vegetation. The "low" category ( $K_{mc} < 1$ ) represents environments where the plantings are located in shade, are shielded from wind, and are away from dry, hot surfaces. The average or medium category ( $K_{mc} = 1$ )

represents reference conditions similar to open settings, such as in parks, where conditions caused by buildings, pavement, shade, and reflection do not influence the ET by the landscape. The values given for  $K_{mc}$  are only approximate, and local measurements can confirm or be used to derive local values. Values for  $K_{mc}$  can be interpolated between the high, average, and low classes and should be selected for each sector of a landscape.

### Managed Stress Factor

Typically, the objective of landscape irrigation is to promote appearance rather than biomass production, unlike agriculture, where biomass is generally maximized. Therefore, target ET for landscapes can include an intentional and managed “stress” factor in the baseline value for  $ET_L$ , where landscape plants are watered less than they would be if they were irrigated like a crop. This management is done by adjusting irrigation water schedules to apply less water than the vegetation will potentially transpire. The magnitude of the stress factor depends on physiological and morphological requirements of the plants.

The managed stress factor,  $K_{sm}$ , represents the fraction of the full ET rate targeted to obtain the functional and visual characteristics of the landscape vegetation. Parameter  $K_{sm}$  has a range of 0 to 1.0, where 1.0 represents conditions of no moisture stress and 0 represents complete lapse of plant transpiration and probable plant death or dormancy. High values for  $K_{sm}$  will sustain predominantly lush, high leaf-area vegetation stands that tend to maximize ET. Low values for  $K_{sm}$  represent substantial managed plant water stress and reduction in ET, generally at the cost of biomass accumulation and potentially loss of pleasant visual effects (Richie and Pittenger 2000). Typical values for  $K_{sm}$  are presented in Table 10-5. Those values, when inserted into Eq. (10-33a) with values for  $K_v$  from Table 10-3, produce values for  $K_L$  that are similar to those reported by Meyer and Gibeault (1986), Smeal et al. (2001), Carrow (2004), and Pittenger and Shaw (2007).

Many landscape species exercise significant stomatal control and can be forced toward relatively lower levels of ET. For instance, the low range for  $K_{sm}$  for ground cover is 0.2, which is appropriate for a select group of drought-tolerant ground cover species. This value may not be appropriate for some ornamental ground covers that require more water (and less water stress) to maintain health and appearance. One should consult local or regional sources to determine appropriate values for  $K_{sm}$ . Pittenger and Shaw (2007) suggest  $K_L$  for more than 30 ground covers and shrubs grown in southern California that contain low  $K_{sm}$  components and thus provide good water conservation. Many of the vegetation types listed by Pittenger and Shaw are native desert vegetation types that tolerate water stress. Other sources of  $K_L$  information for specific species include the WUCOLS publication by Costello and Jones (1999), where the  $K_L$  includes an implied  $K_{sm} < 1$ .

Management of landscape vegetation to implement a particular value for  $K_{sm}$  requires selection of a target depletion fraction prior to irrigation that produces the  $K_{sm}$ , on average. Typically the high stress category for trees, shrubs, and ground cover does not require irrigation, but relies on natural rainfall. In situations where irrigation is practiced, the irrigation interval must be sufficiently long to produce increasingly greater stress as soil water is depleted so that the stress averaged over the entire interval equals the desired value for  $K_{sm}$ . The stress factor  $K_s$  equals 1.0, for no stress, for a period following irrigation (assuming that the irrigation depth was substantial) until the soil water depletion from the root zone exceeds RAW. Following that point in time,  $K_s$  will progressively decrease until the next irrigation. The  $K_s$  prior to the next irrigation will be less than the  $K_{sm}$ , because  $K_{sm}$  represents the average  $K_s$  over the entire interval. Tables 10-6 and 10-7 list target values for management-allowed depletion fraction,  $MAD$ , at the time of irrigation to produce the desired average managed stress factor  $K_{sm}$  to be used in Eq. (10-33). The target values for  $MAD$  (at the initiation of irrigation) are a function of the depletion fraction,  $p$ , when the particular vegetation begins to experience stress. The values for  $p$  in

Table 10-6. Management-Allowed Depletion Fraction,  $MAD$ , to Produce the Stated Managed Stress Factor ( $K_{sm}$ ), Given the Depletion Fraction for No Stress ( $p$ ) and Assuming Complete Refilling of the Root Zone Each Irrigation ( $MAD$  Expressed as a Decimal)

Managed Stress Factor, $K_{sm}$	Depletion Fraction, $p$ , for No Stress				
	0.3	0.4	0.5	0.6	0.7
1.00	0.30	0.40	0.50	0.60	0.70
0.95	0.47	0.57	0.66	0.75	0.86
0.90	0.55	0.65	0.73	0.81	0.88
0.85	0.62	0.71	0.79	0.86	—
0.80	0.68	0.76	0.83	0.89	—
0.75	0.74	0.80	0.87	—	—
0.70	0.78	0.84	0.89	—	—
0.65	0.82	0.88	—	—	—
0.60	0.86	0.90	—	—	—
0.55	0.90	—	—	—	—
0.50	—	—	—	—	—

Note: “—” as an entry indicates that the value for  $MAD$  approaches or exceeds 1 so that the soil water content approaches or exceeds the permanent wilting point and the vegetation is, by definition, in danger of death or dormancy.

Source: Data from Irrigation Association (2003, 2011)

Table 10-7. Average Management-Allowed Depletion Fraction,  $MAD$ , to Produce the Stated Managed Stress Factor ( $K_{sm}$ ), Given the Depletion Fraction for No Stress ( $p$ ) and Assuming Only Partial Refilling of the Root Zone Each Irrigation, Where the Depletion between Wetting Events Is Managed to Range from  $MAD - 0.1$  to  $MAD + 0.1$  ( $MAD$  Expressed as a Decimal)

Managed Stress Factor, $K_{sm}$	Depletion Fraction, $p$ , for No Stress				
	0.3	0.4	0.5	0.6	0.7
1.00	0.20	0.30	0.40	0.50	0.60
0.95	0.30	0.39	0.48	0.57	0.66
0.90	0.35	0.44	0.53	0.61	0.69
0.85	0.39	0.47	0.56	0.64	0.72
0.80	0.43	0.51	0.58	0.66	0.74
0.75	0.46	0.54	0.61	0.68	0.76
0.70	0.50	0.57	0.64	0.70	—
0.65	0.53	0.59	0.66	0.72	—
0.60	0.57	0.62	0.68	0.74	—
0.55	0.60	0.66	0.71	0.76	—
0.50	0.64	0.68	0.73	—	—
0.45	0.67	0.71	0.76	—	—
0.40	0.70	0.74	—	—	—
0.35	0.74	—	—	—	—

Note: “—” indicates that the value for  $MAD$  approaches or exceeds 1 so that the soil water content approaches or exceeds the permanent wilting point and the vegetation is, by definition, in danger of death or dormancy.

Source: Data from Irrigation Association (2003, 2011)

Tables 10-6 and 10-7 should be modified for specific vegetation types or species when information is available. The values for  $MAD$  in the tables exceed the values for  $p$  that produce stress.

As an example of using Table 10-6, for  $p=0.4$ , the  $MAD$  should be 0.76 prior to irrigation to produce a  $K_{sm}$  of 0.8 when the root zone is completely refilled each irrigation. This means that 76% of the total available water (TAW) is depleted prior to irrigation. To produce a  $K_{sm}$  of 0.6,  $MAD$  must be 0.90, and the amount of depletion prior to irrigation is  $0.9 \times TAW$ . The values for  $MAD$  in Tables 10-6 and 10-7 were derived by integrating Eq. (10-6) over a range in depletion,  $D_r$ , from 0 to  $MAD$  that produced an average value for  $K_s$  equal to  $K_{sm}$ .

The values for  $MAD$  in Table 10-6 assume that irrigation, when it occurs, completely replenishes soil water to field capacity so that depletion of the root zone  $D_r=0$  and the equivalent depth of water added equals

$MAD \times TAW$ . Note that for a typical  $p$  of 0.5, drying the soil 90% of the way to wilting point will only reduce the  $K_{sm}$  to 0.7 for an irrigation cycle comprising large irrigations spaced relatively far apart in time. The reduced ET will still average 70% during the total period. This is due to the complete recharging of the root zone to field capacity after large irrigation events and a substantial period of no stress.

An alternative strategy to implementing soil water stress is to add less than  $MAD \times TAW$  depth at a higher frequency, where irrigation additions are low enough to create some degree of moisture stress over a greater portion of the irrigation interval. This strategy can provide less stress at the time of the more frequent, but reduced depth, irrigations and thus reduce the risk of plant death or dormancy. This can be done in an automated, soil-moisture-sensor-based irrigation system by applying relatively frequent, small doses of water but with the trigger soil moisture level setting at a "dry" level. The drawback to this strategy is that the percentage of water lost from evaporation from the soil surface increases as the irrigation frequency increases, especially when the irrigation doses are small. Evaporation of water from the soil surface is not nearly as effective in sustaining vegetation health and appearance as is transpiration through the plant system.

Table 10-7 lists  $MAD$  values required to produce the managed  $K_{sm}$  values listed, given the  $p$  value for the vegetation and given that soil water depletion will be managed in the interval of  $MAD - 0.1$  to  $MAD + 0.1$ . For the same example, given  $p = 0.4$  for a specific plant variety and a target  $K_{sm}$  of 0.8, the value of  $MAD$  from Table 10-7 is 0.51, so that soil water depletion would be maintained between 0.41 and 0.61. In other words, the soil would be watered when 61% of available water is depleted, and enough water would be added by irrigation to reduce the depletion to 41% depletion of available water. Therefore, 20% of the water between field capacity and wilting point would be added back to the soil each irrigation. The percentage of water lost from evaporation from the soil surface increases as the irrigation frequency increases, especially when the irrigation doses are small.

The values for  $MAD$  in Table 10-6 were derived by integrating Eq. (10-6) over a range in depletion,  $D_r$ , from 0 to  $MAD$  that produced an average value for  $K_s$  equal to  $K_{sm}$ . Values in Table 10-7 were derived by integrating Eq. (10-6) over a range of  $MAD - 0.1$  to  $MAD + 0.1$  that produced an average value for  $K_s$  equal to  $K_{sm}$ . Depleting soil water to 0.9 of available water, as in the first example of Table 10-6, is risky in that, by definition, a depletion of 1.0 will result in permanent wilting and generally plant death or dormancy. Following the second strategy of Table 10-7, where smaller doses of water maintain stress at a more level value, would suggest recharging the root zone to  $MAD = 0.41$  following

irrigation and allowing the root zone to dry to  $MAD = 0.61$  prior to irrigation, so that  $MAD$  averages 0.51 over the irrigation and drying cycle. Both management strategies will produce a  $K_{sm} = 0.8$ . For more reduction in  $K_{sm}$ , managing for  $MAD$  ranging from 0.52 to 0.72 and averaging 0.62 will produce an average  $K_{sm} = 0.6$ . This latter range in  $MAD$  is less risky and likely easier to manage than the value of 0.9 required by the strategy of Table 10-6.

### Actual ET from Landscapes

The vegetation coefficient  $K_v$  described in previous sections represents the landscape  $K_c$  under a water supply that is sufficient to support full ET from somewhat dense vegetation with near maximum ground cover and open environmental exposure. However, the  $K_L$  coefficient may contain an implicit amount of managed stress for purposes of water conservation. The degree of implied managed stress is quantified in Eq. (10-33) by the  $K_{sm}$  term. However, the  $K_L$  derived from Eq. (10-33a) or (10-33b) using a targeted  $K_{sm}$  term may not represent actual conditions where actual stress may be higher or lower than the target managed stress. Under these conditions, for purposes of water balance and determination of consumptive use from landscaped or larger areas, the managed stress coefficient in Eq. (10-33a, b) is replaced by an actual stress coefficient,  $K_s$ , where  $K_s$  is computed using Eq. (10-4) or (10-6) based on soil water depletion determined from a daily balance of root zone soil water. Eq. (10-33a) therefore takes the form

$$K_{Lact} = K_v K_d K_s K_{mc} \quad (10-35a)$$

where  $K_{sm}$  in Eq. (10-33a) is replaced by an actual stress coefficient  $K_s$  and where  $K_{Lact}$  is the actual  $K_L$  anticipated from the landscape under actual water availability. Eq. (10-33b), which includes effects of evaporation from soil, becomes

$$K_{Lact} = (K_{soil} + K_{vsd} K_d K_s) K_{mc} \quad (10-35b)$$

where  $K_{vsd}$  is a coefficient describing the difference between  $K_v$  and  $K_{soil}$ , defined in Eq. (10-34).  $K_{soil}$  is from Eq. (10-18) or Figure 10-4. Actual ET from the landscape under actual watering conditions is

$$ET_{Lact} = K_{Lact} ET_o \quad (10-36)$$

When  $K_s$  is estimated from Eq. (10-4) or (10-6), the depletion fraction  $p$  parameter, used to estimate  $RAW$ , should be set to specific values determined for the species if these are available. The effective depth of the root

zone used to estimate TAW is species or variety specific and therefore obtaining information specific to the variety is important.

### Impact of Canopy Wetting and Irrigation Frequency on $K_L$

Wetting of landscape vegetation by irrigation or rainfall can substantially increase the potential ET from the landscape due to the combined influence of evaporation from exposed, wet soil and evaporation from water intercepted by vegetation during the wetting event, if by rainfall or sprinkler. The more frequent the wetting events, the greater the potential ET rate. Often, landscape irrigation is accomplished with automatic controllers that are easily set to irrigate frequently, even daily. The water intercepted and retained on the vegetation surfaces is freely evaporated during and following a wetting event, even if the underlying vegetation is experiencing some level of water stress and the soil is dry. Evaporation of intercepted water can occur even with nighttime irrigation where the primary evaporation may occur the following day.

The impact of evaporation from exposed soil among vegetation when the density coefficient,  $K_d$ , is less than 1 is accounted for using Eq. (10-33b), coupled with estimates for  $K_{soil}$  from Figure 10-4 or Eqs. (10-18)–(10-21). The process of evaporation of intercepted water from vegetation is described in the form of the direct Penman-Monteith ET method in Chapter 11. Here, a simpler general method is used to estimate the impact of evaporation of intercepted water stored on the vegetation canopy on increasing the value for  $K_L$ , as

$$K_L = K_{Lb} + \frac{S}{t_w ET_o} \left( 1 - \frac{K_{Lb}}{K_{c\ max}} \right) \quad (10-37)$$

where

$$K_{Lb} = K_v K_d K_{sm} K_{mc} \quad (10-38)$$

and  $K_{Lb}$  represents the  $K_L$  estimated by Eq. (10-33a) under conditions where any exposed soil surface is assumed to be dry (when  $K_d$  is less than 1.0).  $K_{Lb}$  is, in effect, a “basal” landscape coefficient. The value for  $K_{Lb}$  is the same as that produced by Eq. (10-33a) when effects of intercepted rain or wet exposed soil are not considered. Parameter  $S$  is the depth of intercepted water on vegetation leaves from precipitation or irrigation in mm, and  $t_w$  is the time between wetting events in days.  $K_{c\ max}$  is the maximum limit on  $K_L$ , estimated from Eq. (10-3a).  $ET_o$  has units of  $\text{mm d}^{-1}$ . Values for  $S$  are typically about 1 mm for trees (Tables 11-5 and 11-6) and about 0.5 to 1 mm for turf (Hoffman et al. 1992; Breuer et al. 2003). The derivation of Eq. (10-37) assumes that evaporation of intercepted water on leaves

dominates the ET process until the vegetation surface is dry, so that transpiration is depressed by the energy consumed by E. This observation was noted by Tolk et al. (1995). In the application of Eq. (10-37), the limits  $K_{Lo} = K_v K_d K_{mc} K_{sm} \leq K_{c\ max}$  and  $K_L \leq K_{c\ max}$  are applied.

For applications where ground cover is less than full ( $K_d < 1$ ) and the exposed soil is occasionally wetted by rain or irrigation, Eq. (10-37) can be combined with a form of Eq. (10-34b) to yield

$$K_L = K_{Lb} + (1 - K_d)(K_{soil} - K_{c\ min}) + \frac{S}{t_w ET_o} \max\left(K_d - \frac{K_{Lb}}{K_{c\ max}}, 0\right) \quad (10-39)$$

where  $K_{Lb}$  is calculated in Eq. (10-38) and  $K_{soil}$  is taken from Figure 10-4 or Eqs. (10-18)–(10-21) and is a function of wetting frequency and  $ET_o$  rate.  $K_{c\ min}$  is the minimum basal  $K_c$  for a “dry” bare soil. Under typical landscape conditions,  $K_{cb\ min} \sim 0.10$  to 0.15. The effect of Eq. (10-39) is to increase the value for  $K_L$  over that estimated by Eq. (10-33a) or (10-33b) alone so that  $K_L$  includes effects of both wet soil surface and wet canopy surface following rainfall of irrigation.

The effect on  $K_L$  by evaporation of intercepted water from vegetation is illustrated in Table 10-8 where Eq. (10-37) is applied to a range of  $K_{Lb} = K_v K_d K_{sm} K_{mc}$  under three levels of  $ET_o$  and for three irrigation intervals (1, 2, and 7 days). Interception depth,  $S$ , was assumed to be 1 mm and  $K_{c\ max} = 1.2$ . The effect of evaporation of intercepted water on  $K_L$  is most pronounced for daily watering intervals and at lower values for  $K_{Lb}$ . For turfgrass under typical conditions where when  $ET_o = 4 \text{ mm d}^{-1}$ ,  $K_d$  and  $K_{mc} = 1$  and  $K_{sm} = 0.9$  (mild imposed stress),  $K_{Lb} = K_v K_d K_{mc} K_{sm} \sim 0.8$ , and daily watering is estimated to increase  $K_L$  to 0.88 as compared with  $K_L = 0.81$  for weekly watering. The  $K_L$  under daily watering increases to only 0.84 under  $ET_o = 8 \text{ mm d}^{-1}$  because the amount of interception (1 mm) becomes relatively small compared with the higher total daily ET rate.

Application of Eq. (10-39), where evaporation of intercepted water on vegetation from sprinklers and evaporation from wet soil in between plants are both considered, is illustrated in Table 10-9 over a range of  $K_{Lb}$  under two levels of  $ET_o$  and for irrigation intervals of 1, 2, 3, and 7 days. Two entries are shown for  $K_{Lb} = K_v K_d K_{sm} K_{mc} = 0.8$ , where  $K_d = 1.0$  and 0.8. These two values for  $K_d$  represent (1) full surface cover, as for turfgrass, and (2) a landscape with approximately 20% exposed soil, for dense ornamentals, for example. The effect of wet soil among vegetation without complete ground cover is pronounced. The  $K_L$  under daily watering approaches 1.0 under moderate  $ET_o = 4 \text{ mm d}^{-1}$ , even when the “dry”  $K_{Lb}$ , based on Eq. (10-38), is only 0.4 to 0.6. The contribution of evaporation from exposed soil among plants causes this increase. The effect of daily watering is lower under high  $ET_o$  conditions because the water intercepted

Table 10-8.  $K_L$  Estimated from Eq. (10-37) for Various Levels of  $K_v K_d K_{mc} K_{sm}$  and  $ET_o$  and for Irrigation Intervals,  $t_w$ , of 1, 2, and 7 days for Conditions of a Surface Fully Covered by Vegetation

$K_{lb} = K_v K_d K_{sm} K_{mc}$	$ET_o = 4 \text{ mm d}^{-1}$						$ET_o = 6 \text{ mm d}^{-1}$						$ET_o = 8 \text{ mm d}^{-1}$					
	$t_w = 1$			$t_w = 2$			$t_w = 7$			$t_w = 1$			$t_w = 2$			$t_w = 7$		
	$K_L$	$K_L$	$K_L$	$K_L$	$K_L$	$K_L$	$K_L$	$K_L$	$K_L$	$K_L$	$K_L$	$K_L$	$K_L$	$K_L$	$K_L$	$K_L$	$K_L$	
1.2	1.20	1.20	1.20	1.20	1.20	1.20	1.20	1.20	1.20	1.20	1.20	1.20	1.20	1.20	1.20	1.20	1.20	
1	1.04	1.02	1.01	1.03	1.01	1.03	1.01	1.03	1.01	1.00	1.00	1.02	1.01	1.01	1.02	1.01	1.00	
0.8	0.88	0.84	0.81	0.86	0.81	0.86	0.83	0.83	0.81	0.81	0.81	0.84	0.82	0.82	0.84	0.82	0.81	
0.6	0.73	0.66	0.62	0.68	0.62	0.68	0.64	0.64	0.61	0.61	0.61	0.66	0.63	0.63	0.66	0.63	0.61	
0.4	0.57	0.48	0.42	0.51	0.42	0.51	0.46	0.46	0.42	0.42	0.42	0.48	0.44	0.44	0.48	0.44	0.41	

Note: For interception depth  $S = 1 \text{ mm}$  and  $K_{c,max} = 1.2$ . Units of  $t_w$  are in days.

Table 10-9.  $K_L$  Estimated from Eq. (10-39) for Various Levels of  $K_{Lb} = K_v K_d K_{sm} K_{mc}$  and Density Factor; Two Levels of  $ET_o$ ; and for Irrigation Intervals,  $t_w$ , of 1, 2, 3, and 7 Days

$K_{Lb} = K_v K_d K_{sm} K_{mc}$	$K_d$	$ET_o = 4 \text{ mm d}^{-1}$				$ET_o = 8 \text{ mm d}^{-1}$			
		$t_w = 1$		$t_w = 2$	$t_w = 3$	$t_w = 7$	$t_w = 1$		$t_w = 2$
		$K_{soil} = 1.1$		$K_L$	$K_L$	$K_L$	$K_{soil} = 1.1$		$K_L$
		$K_{soil} = 1.1$	$K_{soil} = 1.1$	$K_L$	$K_L$	$K_L$	$K_{soil} = 1.1$	$K_{soil} = 1.1$	$K_L$
1.2	1.00	1.20	1.20	1.20	1.20	1.20	1.20	1.20	1.20
1	1.00	1.04	1.02	1.01	1.01	1.02	1.01	1.01	1.00
0.8	1.00	0.88	0.84	0.83	0.81	0.84	0.82	0.81	0.81
0.8	0.80	1.02	0.97	0.92	0.86	0.96	0.92	0.89	0.83
0.6	0.60	1.01	0.91	0.83	0.72	0.89	0.83	0.76	0.66
0.4	0.50	0.92	0.80	0.69	0.56	0.77	0.69	0.61	0.48

Note: For interception depth  $S = 1 \text{ mm}$  and  $K_c \text{ max} = 1.2$ .  $K_{soil}$  was selected from Fig. 10-4 using  $ET_o$  and  $t_w$  and interpolation among charts.  $t_w$  has units of days.

by vegetation surfaces evaporates quickly and evaporation becomes a smaller component of total ET.

The example values in Table 10-9 strongly support increasing intervals between watering events to conserve water. However, one needs to recognize constraints on long time intervals between watering events imposed by maximum water dosage rates to limit surface runoff on low intake soils and by water availability to shallow-rooted vegetation on coarse soils.

In the case of cool-season turf with mild imposed stress ( $K_{sm} = 0.9$ ) so that  $K_{Lb} = K_v K_d K_{sm} K_{mc} \sim 0.8$ , under  $ET_o = 4 \text{ mm d}^{-1}$ , increasing the watering interval from daily to 7 days could potentially reduce water consumption by  $(0.88 - 0.81) / 0.88 = 8\%$ . In the case of ornamentals where some soil is exposed among plants so that  $K_d = 0.8$ , the reduction in water consumption for the same  $K_{Lb} \sim 0.8$  would be  $(1.02 - 0.86) / 1.02 = 16\%$ . At an  $ET_o$  of  $4 \text{ mm d}^{-1}$ , about 5 mm out of a total irrigation dose of 23 mm would be conserved per irrigation.

### Comparisons against Recent Measurements of $K_L$

Brown et al. (2001) report  $K_L$  for Tiffany bermudagrass, a warm-season grass, in Tucson, Arizona, with daily watering ranging from  $K_L = 0.78$  during high  $ET_o$  periods (June and July) to  $K_L = 0.83$  during low  $ET_o$  periods (September). Using a  $K_v = 0.9$  for warm-season grass from Table 10-3,  $K_d = 1$  and  $K_{mc} = 1$  and mild stress  $K_{sm} = 0.9$ , the estimated  $K_{Lb} = K_v K_d K_{sm} K_{mc}$  from Eq. (10-38) is  $\sim 0.8$ . From Eq. (10-39) or Table 10-9, the  $K_L$  associated with these values is 0.84 during high  $ET_o$  periods ( $ET_o = 8 \text{ mm d}^{-1}$ ) and 0.88 under low  $ET_o$  periods ( $ET_o = 4 \text{ mm d}^{-1}$ ). These values are about 10% higher than reported by Brown et al. The twice-weekly mowing height reported by Brown et al. (2001) was 2.2 to 2.5 cm, which is somewhat short and may explain the differences between  $K_L$  estimated by Eq. (10-39) and reported  $K_L$ . If no moisture stress is assumed in the Brown study due to the daily watering, then  $K_{sm} = 1.0$  and  $K_{Lb} = K_v K_d K_{sm} K_{mc} \sim 0.9$ , and, from Eq. (10-39) or Table 10-9 (interpolated),  $K_L = 0.96$  under  $ET_o = 4 \text{ mm d}^{-1}$  and  $K_L = 0.93$  under  $ET_o = 8 \text{ mm d}^{-1}$ . These values are about 15% higher than reported by Brown et al. (2001) and again may be due to the short and frequent cutting heights in the study. Brown et al. (2001) report  $K_L$  values for bermudagrass from the literature ranging from 0.57 to 0.83. These values include some amount of managed water stress.

Brown et al. (2001) report  $K_L$  for Froghair intermediate ryegrass, a cool-season grass, overseeded into bermudagrass in Tucson, Arizona, with daily watering ranging from  $K_L = 0.85$  to 0.90 during high  $ET_o$  periods (May and June) to 0.78 to 0.82 during low  $ET_o$  periods with relatively short day lengths (December to February). Using a  $K_v = 0.9$  for cool-season grass from Table 10-3,  $K_d = 1$  and  $K_{mc} = 1$  and mild stress  $K_{sm} = 0.9$ , the estimated

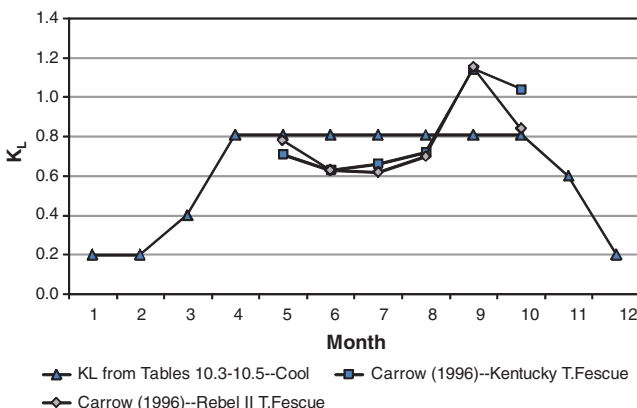


Fig. 10-15. Measured monthly  $K_L$  for two types of tall fescue grass in Georgia by Carrow (1996) compared with a steady target  $K_L$  from Eq. (10-33b) and Tables 10-3–10-5 for a cool-season grass  
Source: Data from Carrow (1995, 1996)

$K_{L0}$  is  $\sim 0.8$ . From Eq. (10-39) or Table 10-9, the  $K_L$  associated with these values is estimated to be 0.84 during high  $ET_o$  periods ( $ET_o = 8 \text{ mm d}^{-1}$ ) and 0.88 under low  $ET_o$  periods ( $ET_o = 4 \text{ mm d}^{-1}$ ). These values are about 5% lower than reported by Brown et al for the high  $ET_o$  periods and about 10% higher than by Brown et al. for the low  $ET_o$  periods. Brown et al. (2001) report  $K_L$  values for cool-season turfgrasses from the literature ranging from 0.60 to 1.04.

Figure 10-15 compares monthly  $K_L$  for warm-season grasses and cool-season grasses as derived using Eq. (10-33b) and Tables 10-3–10-5 with measurements by eddy covariance from Florida (Jia et al. 2007) and by time domain reflectometry in Georgia (Carrow 1995). The  $K_L$  values reported for the warm-season bahiagrass measured by Jia include some moisture-stressed time periods, as do those by Carrow, where both wet and stressed periods are included in the two-year data sets. The  $K_L$  from Eq. (10-33b) uses  $K_v = 0.9$  for both warm- and cool-season grasses during the growing season,  $K_d = 1.0$ ,  $K_{mc} = 1.0$ , and  $K_{sm} = 0.8$  for warm-season and  $K_{sm} = 0.9$  for cool-season curves. The latter two values reflect influences of low amounts of stress, on average. A value of  $K_{soil} = 0.2$  is used during the off-season to reflect background evaporation from dormant turf. It was assumed that no overseeding of cool-season grass occurred during winter.

The  $K_L$  curve measured for bahiagrass in central Florida is higher than the straight-line “target” curve during April and May when the climate was generally wet and then relatively steadily followed the target curve

during June–September when some stress occurred due to longer times between wetting events (Jia et al. 2007). The data of Carrow (1995) fall below the target curve during June–August when substantial stress occurred and rise above the target curve during the wetter period of September. The trends observed by Carrow (1995) for cool-season tall fescue grasses are similar for the same reasons. On average, the observed data followed the steady target  $K_L$  values within uncertainties common to water measurement and management.

## 10.8 ESTIMATES OF $K_c$ DURING WINTERTIME AND NONGROWING SEASONS

Nongrowing periods are defined as periods during which no agricultural crop has been planted. In temperate climates, nongrowing periods may include periods of frost and continuously frozen conditions. Estimation of ET during these periods can be important for annual water balances used in hydrologic studies and for estimation of accruals to soil water from precipitation during nongrowing seasons.

### Types of Surface Conditions

The type and condition of the ground surface during nongrowing periods dictate the range for  $ET_c$ . When the surface is bare soil, then  $K_c$  will be similar to the  $K_{soil}$  estimated by Eq. (10-18). When dead or dormant vegetation or some type of organic mulch or crop residue covers the surface, then  $K_c$  will be similar to that for agriculture with a surface mulch. When weed growth or “volunteer” plants cover the surface, then  $K_c$  will vary according to the leaf area or fraction of ground covered by the vegetation, as estimated by Eq. (10-25) using  $K_d$  from Eq. (10-28) or (10-29), and by the availability of soil water. When the surface is snow covered or frozen, then  $K_c$  is difficult to estimate and a low, constant value for  $ET_c$  may have to be assumed.

**Bare Soil** Where the ground is mostly bare following harvest or other removal of vegetation, then the frequency and amount of precipitation will strongly influence  $K_c$ .  $K_{cm}$  for bare soil can be calculated as  $K_{cm} = K_{soil}$ , where  $K_{soil}$  is estimated using Eq. (10-18) or Figure 10-4, and varies with frequency of wetting events and magnitude of reference ET. Martin and Gilley (1993) and Allen et al. (1998) recommend this approach, and Snyder and Eching (2005) use a similar approach in the LIMP software to estimate a  $K_{cm}$  during winter that is then melded with a  $K_{cm}$  curve for the growing season. Where a daily soil water balance can be applied, the user may elect to apply the dual or basal  $K_{cb}$  approach [Eq. (10-2)]. During long dormant periods with little or no precipitation, the topsoil layer may dry to very low

water contents. Under these conditions, the value for  $K_{cb}$  in Eq. (10-2) and the value for  $K_{cmin}$  in other equations should be set to nearly zero. This provides the opportunity for  $ET_c = 0$  during long periods of no rainfall and may be necessary to preserve the water balance of the evaporation layer and of the root zone in total.

**Surface Covered with Dead Vegetation** Stubbles and mulches reduce soil evaporation by providing a mechanical barrier to aerodynamic forces and shielding the soil surface from solar radiation. Mulches also reduce the connection between liquid or vapor in the soil and the air above (Burt et al. 2005). Burt et al. (2005) describe studies of evaporation experiments from organically mulched soil covers and report a 20% reduction in E from a no-till standing wheat stubble as compared with conventional tillage in North Dakota, 40% reduction in E from standing wheat stubble in cotton in Texas, and nearly 50% reduction in E from soil covered with spread straw relative to bare soil in Nebraska. They note that soil surface mulches are less effective at reducing soil evaporation under dryland conditions where longer periods for drying occur between wetting events as compared with conditions under irrigation.

When the ground surface has a plant residue or other dead organic mulch cover, or where part of the unharvested crop remains suspended above the surface in a dead or senesced condition, then the surface will respond similarly to a surface covered by mulch. In this case,  $K_c$  can be set equal to  $K_{soil}$  as estimated from Figure 10-4 or Eq. (10-18), with the value for  $K_{soil}$  reduced by about 5% for each 10% of soil surface that is effectively covered by organic mulch (Allen et al. 1998). In applications using Eqs. (10-2) and (9-19)–(9-31), evaporation from dead, wet vegetation can be substantial for a few days following a precipitation event. Therefore, in the FAO  $K_{cb}$  approach, the value for  $f_c$  during dormant periods should be set equal to zero to reflect the lack of green cover, and  $f_w$  should be set equal to 1.0 to reflect the wetting of both soil and mulch cover by precipitation. The dead mulch or vegetation will dry more quickly than would the underlying soil if it were exposed. In addition, the soil will be protected somewhat from evaporation by the dead mulch or vegetation cover, and total evaporation losses will be less than the TEW estimated from Eq. (9-20). This can be accounted for by reducing the value for TEW by about 5% for each 10% of soil surface that is effectively covered by organic mulch (Allen et al. 1998). The value for REW may need to be reduced to account for quicker drying of the mulch fraction and should be limited to less than or equal to that for TEW.

**Surface Covered with Live Vegetation** During frost-free periods following harvest, weeds may germinate and grow. This vegetation extracts water from storage within the soil profile and from any rainfall. In addition, crop seed lost during harvest may germinate following rainfall

events and add to the ground cover. The amount of ground surface covered by vegetation will depend on the severity of weed infestation, the density of the volunteer crop, the frequency and extent of soil tillage, the availability of soil water or rain, and any damage by frost. The value for  $K_{cb}$  during the nongrowing period can be estimated over time according to the amount of vegetation covering the surface using Eqs. (10-25)–(10-29) or from remote sensing images by way of a vegetation index. In the  $K_{cm}$  approach, the value for  $K_{cb}$  determined using Eq. (10-25) and (10-27)–(10-29) can be converted into an equivalent  $K_{cm}$  by adding 0.05 to 0.15 according to the frequency of rainfall and surface wetting or using Eq. (10-26).

The  $K_c$  for vegetation during the nongrowing period must be limited by the amount of soil water available to supply evapotranspiration to satisfy the law of conservation of mass. Under all conditions, the integration of  $K_c ET_{ref}$  over the course of the nongrowing period cannot exceed the sum of precipitation occurring during the period plus any residual soil water in the root zone after harvest that can be subsequently depleted by the vegetation plus any upward flow from a shallow saturated system. The root zone in this case is the root zone for the weeds or volunteer crop. A daily soil water balance may provide the best estimate of soil water-induced stress and associated reductions in  $K_c$  and  $ET_c$ .

If using the dual crop coefficient approach [Eq. (10-2)],  $K_{cb}$  can be estimated according to the amount of surface that is covered by vegetation using Eqs. (10-25) and (10.27)–(10-29). A daily soil water balance of the topsoil together with a full daily soil water balance of the root zone can be employed including estimation of  $K_s$  to account for any stress. The soil water balance will automatically adhere to the law of conservation of mass, so that total  $ET_c$  from the weed or volunteer vegetation will not be overestimated. Because the topsoil layer may dry to below wilting point under conditions of sparse rainfall, the values for  $K_{cb}$  and  $K_{cmin}$  for bare soil conditions should be set equal to zero or nearly zero for these conditions (Allen et al. 2005b).

Tasumi et al. (2005a) and Allen et al. (2007a) sampled populations of  $K_c$  in south-central Idaho for major crop types using a Landsat satellite-based surface energy balance. Figure 10-16 shows distributions of the  $K_c$  populations for winter wheat crops on 12 satellite overpass dates between March 15 and October 20. The large variances in distributions of  $K_c$  during March and April reflect large variation in development of winter wheat fields coming out of winter. Values for  $K_c$  following harvest of the wheat crops averaged about 0.20 based on an alfalfa reference and varied according to amount of vegetation present in the form of weeds, nursed alfalfa, or volunteer wheat and variation in irrigation of fields following harvest, coupled with cultivation. Variances of distributions of  $K_c$  during the period of peak  $K_c$  were relatively small because nearly all fields were at or near effective full cover so that  $K_c$  values clustered closely about 1.0.

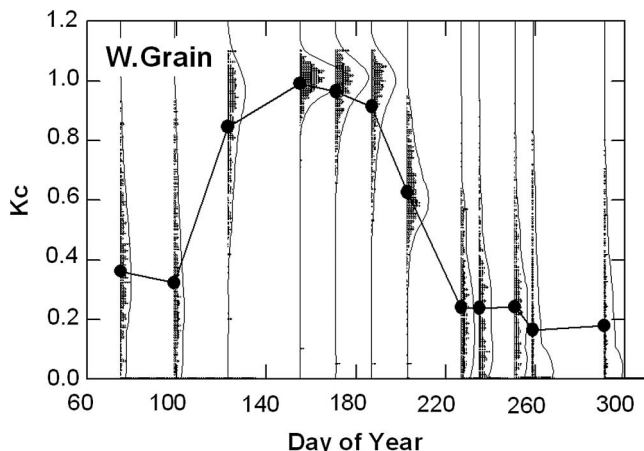


Fig. 10-16. Populations of  $K_c$  in south-central Idaho for winter wheat fields using a Landsat satellite-based surface energy balance on 12 satellite overpass dates (vertical lines) between March 15 and October 20, 2000, where small symbols represent samples from individual fields and the large symbols are averages over all fields

Source: Data from Tasumi et al. (2005) and Allen et al. (2007a)

**Frozen or Snow-Covered Surfaces** When the ground surface is snow covered or frozen, any vegetation will be largely nonresponsive and will not contribute directly to  $ET_c$ . In these situations  $ET_c$  will be closely related to the availability of free water at the surface and to the albedo of the surface. The albedo of snow-covered surfaces can range from 0.40 for old, dirty snow cover to 0.90 for fresh, dry snow as described in Table 4-1. Therefore, the  $ET_c$  for snow cover will be less than  $ET_{ref}$ , as 25–85% less shortwave energy is available. In addition, some energy must be used to melt the snow before evaporation, besides energy consumed in melting snow that seeps into the snowpack. Under conditions of snow cover where the surface of the snow does not have a liquid film, the saturation vapor pressure at air temperature used in the vapor pressure deficit calculation in the Penman-Monteith reference equation should be computed over ice rather than water. Eq. (3-1) for saturation vapor pressure over ice becomes (Murray 1967)

$$e_{ice}^o = 0.6108 \exp\left(\frac{21.87T}{T + 265.5}\right) \quad (10-40)$$

for  $T$  in  $^{\circ}\text{C}$  and  $e^o$  in kPa.

The use of  $ET_{ref}$  under such conditions is of limited value, as the assumption of conditions sustaining a green grass or alfalfa cover is

violated. It is even possible to obtain negative values for  $ET_{ref}$  on some winter days where the long-wave radiation from the surface is large and the vapor pressure deficit is small. Under these conditions, net condensation of water from the atmosphere is possible, which corresponds to negative evaporation. Some negative values for  $ET_{ref}$  during winter occur from normal error in the  $ET_{ref}$  estimates and weather data. Given the limited utility of using  $ET_{ref}$  under snow-covered or frozen conditions, use of a single average value may be justified to estimate  $ET_c$ . Wright (1993) measured  $ET_c$  averaging 1 mm d<sup>-1</sup> over nongrowing season periods at Kimberly, Idaho, that were six months long (1 October to 30 March). The latitude of Kimberly is 42° N, and the elevation is about 1,200 m. Over the six-year study period, the ground was at least 50% covered by snow for 25% of the time from 1 October to 30 March. The ground, when exposed, was frozen about 50% of the time. The  $K_c$  averaged 0.25 during periods when the soil was not frozen but where frosts occurred (October and early November). When the ground had 50% or greater snow cover,  $ET_c$  averaged only 0.4 mm d<sup>-1</sup>. Wright found that over the six-month non-growing period, total cumulative  $ET_c$  exceeded precipitation by about 50 mm, indicating a drying soil.

Figure 10-17 shows averaged measurements of  $ET_c$  by Wright (1993) during the 1985–1991 winter periods. The measurements have high correspondence to the total shortwave radiation energy available on a clear day,  $R_{so}$ , estimated as 0.75  $R_a$ . Some lag occurs between  $ET_c$  and  $R_{so}$  and  $R_s$  caused by cooler temperatures in January–March as compared with the

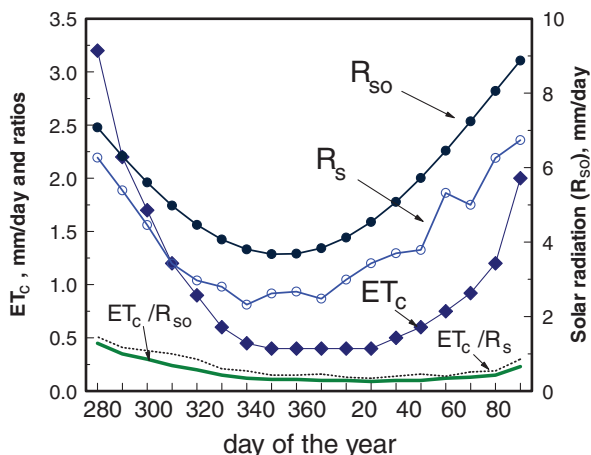


*Fig. 10-17. Mean evapotranspiration measured during nongrowing winter periods at Kimberly, Idaho, by Wright (1993)*  
Source: Data from Allen et al. (1998)

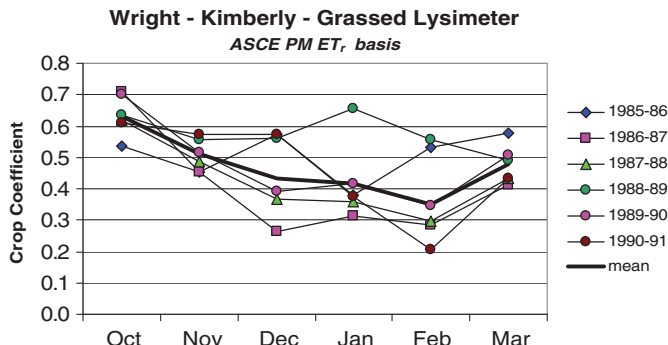


Fig. 10-18. Mean monthly  $K_c$  measured by Wright (1993) from dormant grass using a weighing lysimeter during nongrowing periods at Kimberly, Idaho, based on the ASCE PM alfalfa reference  $ET_r$  equation

Source: Data from Allen and Robison (2007)

October–December period. The  $ET_c/R_{so}$  ratio averaged only 0.17 over the six-month period and averaged 0.11 from 1 December to 10 March. The  $ET_c/R_s$  ratio averaged 0.23 over the six-month period and averaged 0.15 from 1 December to 10 March. The  $K_{cm}$  measured by Wright (1993) and converted to the standardized Penman-Monteith  $ET_r$  basis averaged about 0.45 during the October–December period over years 1985–1991 for dormant fescue grass cover (Figure 10-18) and for nongrass covers including tilled soil (Figure 10-19). Even though these values for  $K_{cm}$  are relatively high due to relative wetness of the surface during the nongrowing periods, the total ET rates were relatively low due to low values for  $ET_r$  during these periods.

A similar study conducted in Logan, Utah (latitude 41.6° N, elevation 1,350 m) (Allen 1996b), shows  $ET_c$  to vary widely with soil surface wetness and air temperature during winter months. The “average”  $K_c$  from November to March was 0.5 for days having no snow cover. For days with snow cover,  $ET_c$  ranged from 0 to 1.5 mm d<sup>-1</sup>.

A daily soil water balance using the dual crop coefficient approach may improve accuracy in estimating  $ET_c$  under freezing and snow-covered conditions. In the dual crop coefficient method, a daily water balance is conducted for the topsoil, and the estimate for  $K_c$  can be reduced according to available water. However, in addition to the limited validity of the concept of  $ET_{ref}$  under frozen or snow-covered conditions, the evaporation coefficient,  $K_e$ , may have low values when the ground surface is frozen, as the water in a frozen state is less available.

Somewhat complex models for estimating  $ET_c$  under nongrowing season conditions, snow cover, and freezing are available in the literature

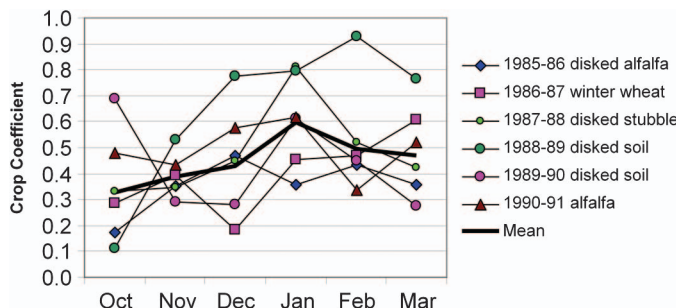


*Fig. 10-19. Mean monthly  $K_c$  measured by Wright (1993) during nongrowing periods at Kimberly, Idaho, using a weighing lysimeter for various types of nongrass cover based on the ASCE PM alfalfa reference  $ET_r$  equation*  
Source: Data from Allen and Robison (2007)

and should be consulted and perhaps applied when precise estimates for  $ET_c$  are required, for example, Flerchinger (1991), Flerchinger et al. (1996), and Saxton and Willey (2005).

The basis for the mean  $K_c$  values in Figures 10-18 and 10-19 is the ASCE standardized Penman-Monteith method. The ASCE PM alfalfa reference  $ET_r$  standard represents 0.5-m tall green alfalfa, even during winter, where the crop is a hypothetical potential reference. Therefore, under even wet conditions, the  $K_c$  during wintertime is not expected to reach 1.0 because much vegetation may be frozen, cold stressed, or dormant. Mean  $K_c$  ( $K_{cm}$ ) did approach or exceed 0.8 during December 1988–March 1989 for the disked soil, a period with a nearly continuous distribution of precipitation and wet surface condition.

### Estimated Wintertime Evaporation

Allen and Robison (2007) estimate wintertime evaporation across the state of Idaho using daily calculation of Eq. (10-2) (dual  $K_c$  approach) requiring a daily soil water balance. The wintertime calculations are combined with calculations for growing periods to produce daily  $ET$  estimates for entire annual periods. Allen and Robison (2007) define the nongrowing season (winter) period as the period beginning when a  $K_{cb}$  curve representing the growing cycle for a specific crop ends or when a killing frost occurs and ending at greenup or planting of the same crop the following year (or October 1 in the case of winter wheat). A basal  $K_{cb}=0.1$  is used for bare soil conditions during nongrowing season periods, for surfaces covered with some amount of mulch, and for dormant turf/sod systems.  $K_{cb}$  represents conditions when these surfaces had a dry soil surface, but had sufficient moisture at depth to supply

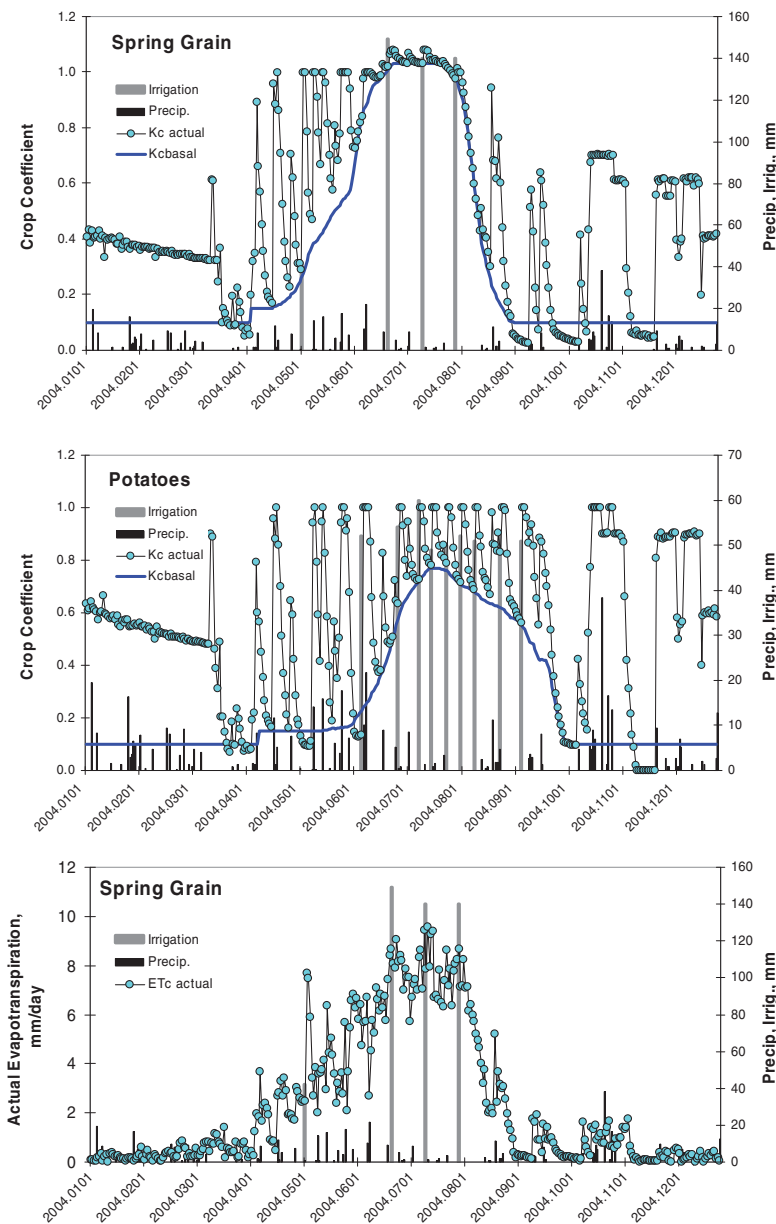


Fig. 10-20. Example  $K_{cb}$  ( $K_{cbasal}$ ) and resulting  $K_c$  ( $K_{cactual}$ ) curves for spring wheat and potato crops near Ashton, Idaho, during 2004. Simulated irrigation events are shown as vertical bars. The  $K_{cactual}$  traces include the evaporation ( $K_e$ ) components that appear as spikes above the  $K_{cb}$  curves following precipitation and irrigation events. Also shown in the bottom figure is daily actual  $ET_c$  for the spring grain

some diffusive evaporation. The evaporation ( $K_e$ ) component is estimated separately in the daily soil water balance, where  $K_{cmax}$  during the nongrowing period was 0.9 for bare soil, 0.85 for mulched surfaces, and 0.8 for dormant grass cover. The lower value for grass accounted for the insulative effects of grass and its higher albedo. The use of a low value for  $K_{cb}$  permits the  $K_e$  function in the daily calculations to increase the value for total  $K_c$  according to wetting frequencies by rain and snow. An effective “rooting zone” of 0.10 m is used during the nongrowing season for the fraction of surface under the cover. For all surfaces, a daily soil water balance was conducted and a stress coefficient based on Eq. (10-6) was applied when soil water content of the upper 0.10 m dropped below a critical value. This caused actual  $K_c$  to fall below  $K_{cb}$  when both the ground surface and subsurface soil were dry. All land use types, including agricultural, landscape, horticultural, and natural vegetation, are assigned one of the three winter cover conditions (dormant grass, bare soil, or mulch classes) for estimating evaporation losses during winter. Allen and Robison (2007) describe functions for estimating sublimation from snow.

Typical  $K_{cb}$  and  $K_c$  curves for spring wheat and potato crops for a full calendar year are shown for a location near Ashton, Idaho, during 2004 in Figure 10-20. Simulated irrigation events, necessary to estimate evaporation from soil following unknown irrigation events, are shown as vertical bars. The  $K_c$  curves resulting from application of Eq. (10-2) (dual  $K_c$  procedure using alfalfa  $ET_r$ ) include the evaporation ( $K_e$ ) components that appear as spikes above the  $K_{cb}$  curves following precipitation and irrigation events. Actual  $K_c$  fell below  $K_{cb}$  curves during fall for the wheat and potato crops whenever the water content of the soil evaporation layer fell below levels required to support the  $K_{cb}=0.10$  values assumed for harvested surfaces that were mostly bare. Although values for  $K_c$  during wintertime were somewhat high due to wet soil surfaces and frequent snow cover (January–March 2004, for example), the total  $ET_c$  rates during wintertime were somewhat low due to low values for  $ET_r$  during the Idaho winters. This is illustrated in the bottom figure of Figure 10-20, which shows daily actual  $ET_c$  for the spring grain.

## 10.9 SUMMARY

In summary, the  $K_c ET_{ref}$  approach is a convenient and robust method for estimating actual and potential ET from agricultural crops, landscapes, and natural vegetation. The method adheres to energy conservation principles and implicitly incorporates environmental, boundary layer, and physiological factors affecting the  $ET_c$  from the particular vegetation. Many of these factors must be explicitly estimated when using a direct estimation equation such as the Penman-Monteith equation discussed in the next

chapter. The dual  $K_c$  method provides means to estimate effects of wetting frequency on total water consumption and to estimate ET year round. Crop coefficients can be estimated for new or understudied vegetation types via visual description of the vegetation density and general vegetation type. Publications will continue to present or update crop coefficients for new crops and for local areas. Some agencies and private entities post crop coefficients for their respective areas on the Internet.

# CHAPTER 11

## DIRECT PENMAN-MONTEITH AND AERODYNAMIC ENERGY BALANCE EQUATIONS

### 11.1 INTRODUCTION

Application of the Penman-Monteith (PM) and other resistance-based methods enables the user to adjust the physically based parameters of surface roughness and bulk surface resistance to represent characteristics of the surface or vegetation type in question. This provides the means to produce estimates of ET without the need for empirical multipliers, as in the case of the two-stage crop coefficient  $\times$  reference ET method. The flexibility and power of producing direct estimates does come at the cost of more complexity in determining and applying functions to estimate resistance-based parameters and in applying the technique to sparse canopies containing mixtures of vegetation and exposed soil. Typically, the user objectively characterizes a surface based on visual observations and measurements, remote sensing, or photography and then estimates the corresponding roughness and bulk surface resistance parameters using approaches discussed in subsequent sections.

#### Advantages

The main advantage of the PM equation and other combination equations over direct aerodynamic approaches is that air temperature and humidity measurements are required at only one reference height, rather than measurement of air and humidity gradients or measurement of temperature and humidity at the surface. The PM equation is less sensitive to omission of stability correction adjustments as compared with gradient methods because the available energy component reduces weighting on the aerodynamic component, plus the aerodynamic resistance appears in both the numerator and denominator. The PM equation can be used to estimate ET

on hourly, daily, and even monthly calculation time steps (Allen et al. 1994c, 1996). The PM and direct aerodynamic approaches have advantage over the crop coefficient–reference ET ( $K_c ET_{ref}$ ) method in that surface parameters affecting evaporation and transpiration, such as bulk surface resistance, aerodynamic roughness, and water content of the surface soil layer affecting evaporation, can be specified for the specific surface and temporal conditions. However, specifying these parameters over time, especially for sparse vegetation cover, can be challenging, as described in the following section.

### Disadvantages and Challenges

For applications in hydrology, and depending on equations being compared, a disadvantage of the PM equation includes the problem of characterizing average relationships between leaf stomatal resistance and solar radiation for sparse or multilayered vegetation such as forests in semiarid regions (Stewart 1983; Denmead 1984) and developing crops. In these situations, mean heights and locations of sinks for momentum and radiation are different from mean heights and locations of sources of  $\lambda E$  and  $H$ . These variations create differences in eddy diffusivities (aerodynamic resistances) within and directly above canopies and also create problems in characterizing average relationships between leaf stomatal resistance and solar radiation.

Other challenges with the PM and other combination equations include difficulties in quantifying bulk surface resistance for complex canopies, especially when soil water is limiting. In addition, significant errors may be introduced when weather data used in the PM equation are measured above surfaces that may be significantly different from air properties occurring over a complex canopy. For example, applications may require using weather measurements taken over clipped grass to estimate ET from forest vegetation where conditioning of the air (temperature, vapor content, wind speed) is different. Because of nonlinear interactions among weather parameters, ET flux rates, and buoyancy effects, direct Penman-Monteith and aerodynamic-energy balance equations are best applied using hourly or shorter time-period data. For many engineering applications, weather data from one or more existing weather stations may be the only data that are available for use. However, gridded weather data sets from land surface models associated with the National Center for Atmospheric Research (NCAR) Weather Research and Forecasting (WRF) model are becoming widely available, and many of these reflect the influence of underlying surface and vegetation conditions on the temperature, vapor, and wind profiles. Many of the land surface models used with WRF employ some form of the Penman-Monteith equation for estimating the ET components of the surface energy balance, and they also assimilate measured weather data as a correction mechanism. In many cases,

however, especially in semiarid to arid environments, the WRF simulations do not consider effects of irrigation in supplying water for ET and consequent conditioning of the local and regional air masses. Therefore, these data sets may require postconditioning.

Furthermore, and as described in more detail in a later section, the PM works best under well-watered conditions of nearly full vegetation cover. Under these conditions, surface temperature,  $T_s$ , is closest to air temperature,  $T_a$ , so that the assumptions explicit in  $\Delta$  and emitted long-wave radiation, which commonly assume that  $T_s = T_a$  and which may neglect buoyancy corrections, are not large. Other challenges include the need for parallel modeling of evaporation from exposed soil that is affected by frequency and amounts of wetting events and amount of vegetation cover. These issues and requirements also affect the  $K_c ET_{ref}$  method; however, that method has more consistent and standardized procedures for estimating evaporation as outlined in Chapters 9 and 10.

## 11.2 COMMON FORMS OF RESISTANCE-BASED EQUATIONS

Many land surfaces have vegetation canopies that do not completely cover the ground surface or understory. These surfaces include forests, cultivated row crops, orchards, vineyards, and natural systems. Sensible heat and vapor fluxes from exposed soil fractions and from canopy can be quite different due to variations in water availability at these surfaces and aerodynamic characteristics. These fluxes can also interact between the two surfaces, with microadvection and radiative emission of heat, for example, from a dry soil surface into the adjacent canopy, or with the humidification of the boundary layer over a soil surface due to evaporation from an adjacent canopy. Various resistance-based networks and methods have been proposed over the past 50 years to describe fluxes of sensible heat and latent heat within both uniform and sparse canopies. Often these resistance networks have been incorporated into a Penman-Monteith type of combination equation to reduce the weather data requirements to only those measured at some reference height above the vegetation, thereby negating the need for surface temperature measurements. As described later, however, knowledge of or iteration for surface temperature may be required for acceptable accuracy.

This section describes three resistance-based methods for estimating ET from sparse canopies. These methods are the standard Penman-Monteith method, also known as the single-layer model; the multilayer method, also referred to as the interactive resistance model (Daamen and McNaughton 2000); and the two-source method, also referred to as the patch model. The interactive model is the most complex model, and the Penman-Monteith the least complex. Following the introduction of these models, their strengths and weaknesses will be discussed. In addition, the PM is reverted

back into its original energy balance and aerodynamic components to show the merits and advantages of using the original components to iteratively determine surface temperature. That method is known as the AFIB method (aerodynamic fluxes using an iterative energy balance).

The general resistance networks used in the three models are illustrated in Figure 11-1 in terms of direct latent heat of vaporization (LE) expressions and in Figure 11-2 in terms of direct sensible heat flux,  $H$ , expressions. The resistance diagrams for  $H$  may be implicitly built into PM models or into multilayer or multisource models. Specific resistance terms in Figures 11-1 and 11-2 are defined in later equations for various model types. Two

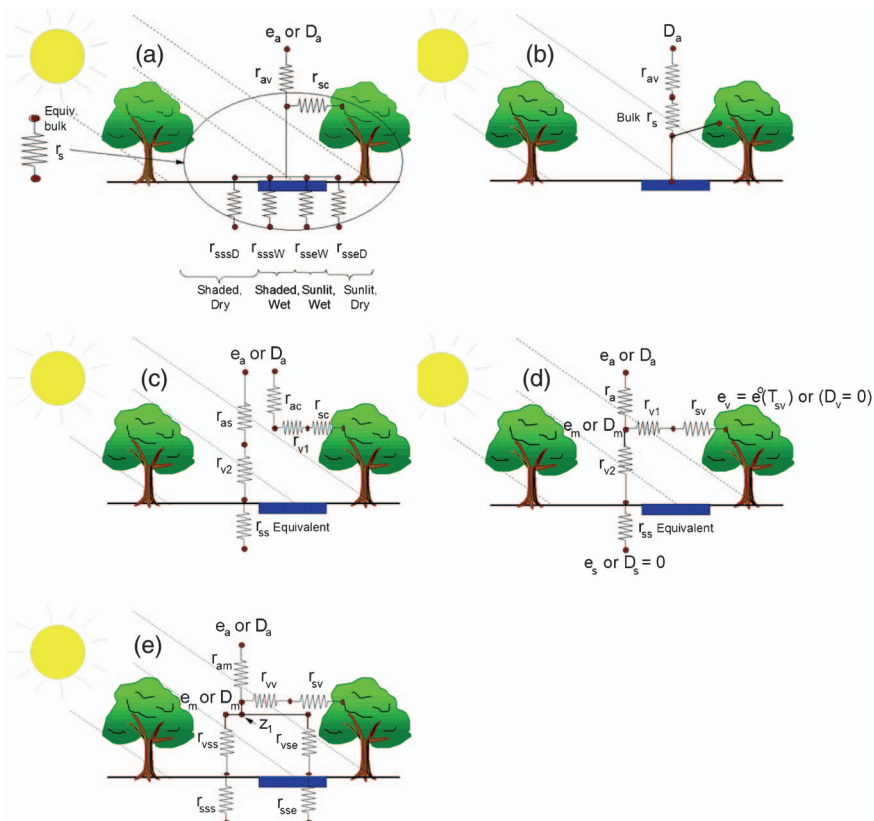


*Fig. 11-1. Example general resistance networks used in three resistance-based ET models: (a) single-layer model represented by integrating a complex of parallel surface resistors, (b) a bulk surface resistance expression for the single-layer model, (c) a two-source (patch) model, (d) a two-layer (interactive) model, and (e) a two-layer (interactive)/three-source model*

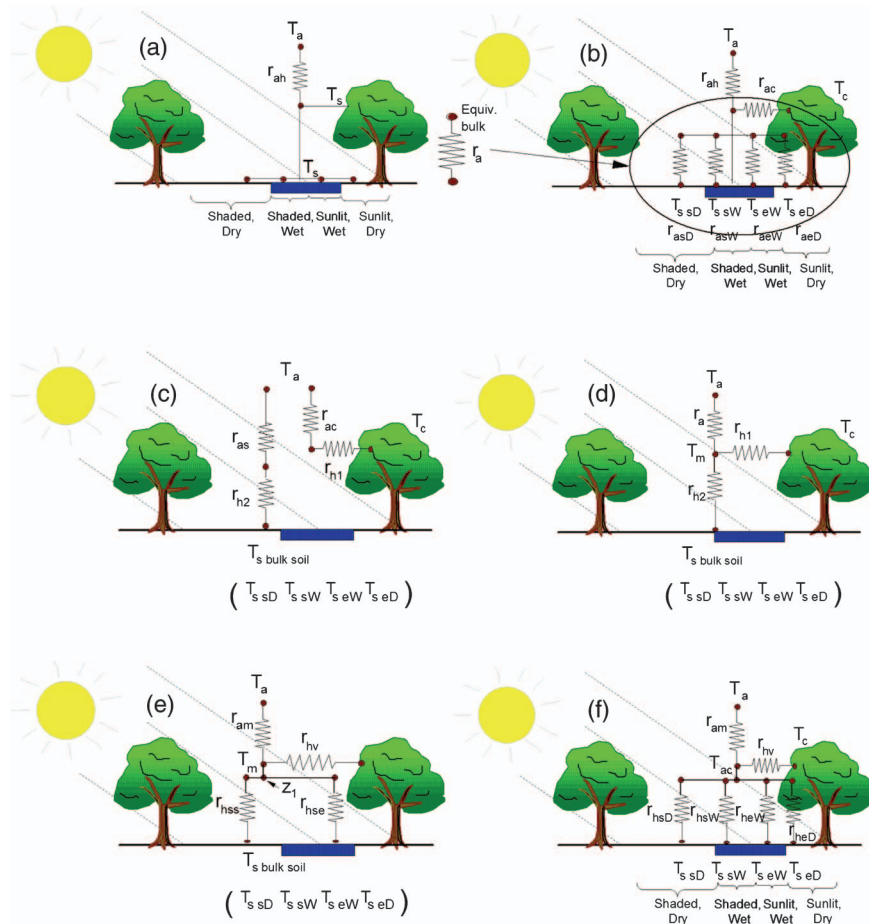


Fig. 11-2. Example general resistance networks used in three resistance-based models for sensible heat flux as counterparts of some ET models: (a) single-layer model, (b) a single-layer model represented by integrating a complex of parallel aerodynamic resistors, (c) a two-source (patch) model, (d) a two-layer (interactive) model, (e) a two-layer (interactive)/three-source model, and (f) a two-layer (interactive)/five-source model

resistance networks are expressed for the single-layer model in Figure 11-1 parts a and b. The two-source (patch) model is represented in both Figures 11-1 and 11-2, as figure part c, and the two-layer (interactive) model is represented by figure part d. Figure 11-1a shows how the soil surface can be partitioned into four conditions in regard to available energy (sunlight) and relative wetness of the soil surface. The partitioning of

relative wetness can be important when simulating irrigated systems where only part of the ground surface is wetted. The combination of the four surface resistances representing these four soil surface conditions into a single equivalent  $r_{ss}$  is described in a later section, including its incorporation into a bulk surface resistance to be used in a single-layer model.

A highly recommended source on these three resistance model types is Daamen and McNaughton (2000), which describes and contrasts common formulations of the three model types and compares their estimated ET rates under several surface conditions. Much of the following material and contrasts follow from Daamen and McNaughton (2000).

### The Single-Layer Penman-Monteith Equation

Appendix J describes the derivation of the Penman-Monteith equation, which is similar to the derivation of the Penman equation except that the wind function of the Penman equation is replaced by an aerodynamic resistance term, and a bulk surface resistance term is explicitly placed between the inner leaf, where air is assumed saturated, and the midlevel of the crop canopy, where the mean source area for both heat and vapor is assumed to exist and where aerodynamic resistance is assumed to begin. The “breakthrough” of the combination (Penman and PM) equations was that by combining the radiation and aerodynamic terms and using  $\Delta$  defined using air temperature only, the need for surface temperature is eliminated from the “combined energy balance” and only more readily measured air parameters  $T$ ,  $e$ , and wind speed are required, in addition to net radiation. This simplified data set has made the single-layer combination equation very successful, especially when applied as a reference method. The PM equation was introduced as Eq. (8-2) and is repeated here:

$$\lambda E = \frac{\Delta(R_n - G) + \rho_a c_p (e_s - e_a) / r_{ah}}{[\Delta + \gamma(1 + \frac{r_s}{r_{ah}})]} \quad (11-1)$$

where units of  $\lambda E$ ,  $R_n$ , and  $G$  are in  $\text{Jm}^{-2} \text{s}^{-1}$  (or  $\text{Wm}^{-2}$ ),  $\rho_a$  is air density in  $\text{kgm}^{-3}$ ;  $c_p$  is specific heat of dry air in  $\text{Jkg}^{-1}\text{C}^{-1}$ , generally taken as  $1,010 \text{ Jkg}^{-1}\text{C}^{-1}$ ; and variables  $e_s$  and  $e_a$  are saturation vapor pressure at air temperature and actual vapor pressure of the air in kPa. Parameter  $r_{ah}$  is bulk aerodynamic resistance to sensible heat transfer and is calculated using a combination of effective roughness for momentum,  $z_{om}$ , and effective roughness for sensible heat transfer,  $z_{oh}$ . Variable  $r_{ah}$  is essentially the equivalent of a combination of  $r_{am}$  and  $r_h$  introduced later with the multilayer models. Parameter  $r_s$  is a bulk surface resistance that incorporates effects of relative water availability and conductance from both vegetation and soil surfaces.

The PM equation was initially developed to describe the energy fluxes from a fully vegetated land surface and may inadequately describe the

combined fluxes from a sparsely vegetated surface at the point(s) where bulk surface resistance, describing resistance to vapor flow from both soil and vegetation, ends and where the bulk aerodynamic resistance, again, describing heat and vapor transfer from both soil and vegetation), begins. The single-layer PM model blends any variations of microclimate within the vegetation and assumes that each leaf surface that contributes to energy exchange is at the same temperature and has the same saturation deficit at its surface. In the PM method, all surface resistance values for both leaf and soil subareas must contribute to the value for bulk  $r_s$ , as can be seen by studying Figures. 11-1 and 11-2, in which more sophisticated and complete resistance expressions shown in Figures. 11-1c–e are simplified into the single-layer, bulk expressions of Figure 11-1b or Figure 11-2a that are used in the PM equation.

An often overlooked requirement with application of the combination equation (Penman or Penman-Monteith) is that surface temperature must be sufficiently similar to air temperature for the calculation of  $\Delta$  to be based on air temperature only. Dry surfaces tend to have substantially higher temperature than air temperature, and under these conditions  $\Delta$  should be calculated using Eq. (11-3) with  $T_s$  solved by iterative application of equations for  $\lambda E$ ,  $H$ ,  $G$ , and  $R_n$  via energy balance. As illustrated in the following, the PM formulation where  $\Delta$  is solved using  $T_a$  only is only completely accurate, in the commonly used form of Eq. (11-1), when bulk surface temperature,  $T_s$ , has nearly the same value as  $T_a$ . Under this condition three important assumptions to the PM method, as generally practiced, hold. These three assumptions are (1) that  $\Delta$  can be estimated using air temperature only, (2) that stability correction to  $r_{ah}$  is not required, and (3) that long-wave radiation emitted from the surface can be estimated using  $T_a$  only. As shown later in Tables 11-5 and 11-6, under conditions of relatively low  $\lambda E$  and relatively high  $H$ , as experienced under low vegetation cover or under conditions of water shortage,  $T_s$ , by physical requirement, exceeds  $T_a$ . Under extreme conditions,  $R_n$  can reduce by as much as  $100 \text{ W m}^{-2}$  with increasing  $T_s$  as compared with the reference condition due to increased thermal radiative emission from the surface. In addition, buoyancy-driven mixing of the boundary layer with increased  $T_s$  compared with  $T_a$  caused by increasing  $H$  can require stability correction to reduce  $r_{ah}$  and provide correct estimation of  $\lambda E$ .

Therefore, when vegetation cover is low or the water supply limits ET, i.e., the system is in a nonreference crop condition,  $T_s$  must be iteratively solved, by for example using the following AFIB procedure. Ironically, when  $T_s$  is iteratively solved for or measured, the reason for the existence for the PM and other combination equations essentially evaporates, because substitution of a  $T_s$ - and  $T_a$ -based computation for  $\Delta$  in the equation causes it to decompose back to the original component equations for  $H$  and  $\lambda E$  (see Appendix J). Effects of employing iteratively determined

$T_s$  for calculating  $\Delta$ ,  $R_{lout}$ ,  $G$ , and stability correction are illustrated later in Tables 11-5 and 11-6.

The required suite of equations and inversion of the sensible heat equation to replace the PM equation includes the following and can be termed the AFIB approach (aerodynamic fluxes via iterative solution of the energy balance):

$$R_n = (1 - \alpha)R_s + R_{L-in}(1 - \varepsilon) - \varepsilon\sigma T_s^4 \quad (11-2a)$$

$$G = [0.05 + K_G \exp(-0.5LAI)](R_n + H) \quad (11-2b)$$

$$\lambda E = \frac{\rho_a c_p [e^0(T_s) - e^0(T_a)]}{r_{av} + r_s} \quad (11-2c)$$

$$T_s = \frac{(R_n - G - \lambda E)r_{ah}}{\rho_a c_p} + T_a \quad (11-2d)$$

$$H = \rho_a c_p \frac{(T_s - T_a)}{r_{ah}} \quad (11-2e)$$

$$r_{ah} = r_{av} = \frac{\left\{ \ln\left(\frac{z_u-d}{z_{om}}\right) - \Psi_m \left[ \frac{z_u}{L(H)} \right] \right\} \left\{ \ln\left(\frac{z_T-d}{z_{oh}}\right) - \Psi_h \left[ \frac{z_T}{L(H)} \right] \right\}}{k^2 u_z} \quad (11-2f)$$

where  $z_u$  is the height above the ground surface for the wind speed measurement,  $d$  is the zero plane displacement of the logarithmic wind profile,  $z_{om}$  is a roughness length governing the transfer of momentum from the surface,  $\Psi_m$  is the correction factor for momentum transfer to account for instability or stability of the boundary layer,  $z_T$  is the height of the air temperature measurement above the ground surface,  $z_{oh}$  is an assumed roughness length governing the transfer of sensible heat from the surface,  $\Psi_h$  is a correction factor for sensible heat transfer to account for instability or stability of the boundary layer,  $k$  is the von Kármán constant (0.41), and  $u_z$  is the wind speed measured at the  $z_u$  height. Equations for estimating  $\Psi_m$  and  $\Psi_h$  are given in Chapter 7. Eq. (11-2b) is from Allen et al. (2013) and represents the likelihood for  $G$  to be influenced by  $H$  due to their codependence on temperature gradients that share a common  $T_s$ .  $K_G$  is a fitting coefficient that is affected by relative thermal conductivity of soil. A value of  $K_G = 0.2$  is recommended for tilled soils, and  $K_G = 0.10$  to  $0.15$  is recommended for soils in a natural state having less bulk particle-to-particle

contact. When  $H$  is low, and most  $R_n$  is converted into  $\lambda E$ ,  $G$  becomes a function of  $R_n$ , which is a traditional means for estimation (Choudhury et al. 1987). The  $L(H)$  in Eq. (11-2f) indicates that the Monin  $L$  is a function of  $H$  and thus  $T_s$ . Eq. (11-2f) is also presented as Eq. (7-20) in Chapter 7 and Eq. (8-3) in Chapter 8. Eqs. (11-2a–f) are iteratively solved until the estimate for  $T_s$  is known. At that point,  $\lambda E$  will be known from Eq. (11-2c).

Once  $T_s$  is known,  $\Delta$  can be estimated from Eq. (11-3) for use in the PM equation; however, the calculation of  $\lambda E$  from the PM equation using  $\Delta$ ,  $R_n$ ,  $G$ , and  $r_{ah}$  from Eqs. (11-2a–f) will be within a few percent of, or even identical to,  $\lambda E$  solved using Eq. (11-2c). In other words, the PM equation ceases to provide any new usefulness as compared with the AFIB method.

$$\Delta = \frac{e^0(T_s) - e^0(T_a)}{(T_s - T_a)} \quad (11-3)$$

The solution of Eqs. (11-2a–f) does not create computational challenges with modern computing systems, and once coded, tends to provide consistent estimates. The iteration can progress through any ordering of the equations and can be initiated with the assumption that  $H=0$  and therefore the initial estimate for  $T_s$  is  $T_s = T_a$ . Numerical stability in the solution can be ensured with dampening calculations by averaging new values for  $T_s$  and, if needed, the Monin  $L$  with their values from the previous iteration step.

One is cautioned not to “improve” the estimate for  $\Delta$  without also improving all factors that affect both the estimate for  $T_s$  and the estimation by the PM itself. These factors include the buoyancy correction and the net thermal radiation component of  $R_n$ , as described by Eqs. (11-2a–f).

When the values for  $r_s$ ,  $z_{om}$ , and  $z_{oh}$  in Eqs. (11-2c) and (11-2f) are set to those for the standardized reference definitions, for example,  $r_s = 30 \text{ sm}^{-1}$ ,  $z_{om} = 0.062 \text{ m}$ , and  $z_{oh} = 0.0062 \text{ m}$ , the AFIB process of Eqs. (11-2a–f) will produce estimates for  $\lambda E$  that are close to those from the standardized ASCE PM equation for the alfalfa reference, Eq. (8-2), (8-15), or (11-1). This is because, under the reference conditions that define a well-watered vegetation condition so that  $r_s = 30 \text{ sm}^{-1}$ ,  $T_s$  becomes similar to  $T_a$ , and all simplifications and assumptions in Eq. (8-15) are fulfilled (computing  $\Delta$  and  $R_n$  using  $T_a$  only and ignoring buoyancy-induced boundary layer stability correction).

The following conclusions regarding the AFIB approach are made: (1) the AFIB method of Eqs. (11-2a–f) is, in essence, a decomposition of the PM equation into its original component equations; (2) the AFIB method of Eqs. (11-2a–f) tends to reproduce estimates by the standardized reference equation for reference conditions when using the standard reference crop settings; and (3) estimates from Eqs. (11-2a–f) confirm the need to incorporate knowledge of  $T_s$  into the  $R_n$ ,  $\Delta$ , and  $r_{ah}$  terms of the PM equation under nonreference conditions. One can additionally conclude

that the PM equation, or any combination equation, is only useful and can only provide correct estimates that are  $T_a$  based under reference or nearly reference conditions. Under all other conditions where  $\lambda E < \lambda ET_{ref}$ , the AFIB method of Eqs. (11-2a-f) is recommended. One limitation with both the direct Penman-Monteith and AFIB methods is that each is best applied using hourly or shorter time-period data when actual ET rates are sufficiently less than reference ET rates to induce sensible heat flux rates that are more than 20 to 40% of available energy ( $R_n - G$ ). This limitation is caused by the somewhat strong nonlinearity in buoyancy or stability corrections that can vary hourly with ratios of  $H$  to  $R_n - G$ . Stability corrections applied using 24-h data will typically underestimate the power of buoyancy effects on surface energy exchange.

### The Multilayer (Interactive) Resistance-Based Model

The saturation vapor deficit,  $D$ , is a principal term in the PM equation and is defined as  $D = e^o(T) - e_{air}$ , or  $e_s - e_a$ , where  $e^o(T)$  is saturation vapor pressure at temperature  $T$  and  $e_{air}$  is actual vapor pressure of the air or surface. In reality, in sparsely vegetated systems, not all parts of the vegetation surfaces and soil surfaces experience the same surface saturation vapor deficit,  $D_s$ , but rather undergo a range of saturation deficits, depending on their position within the canopy structure and their relative water supply. In many multilayer models, a single value for  $D$ ,  $D_m$ , where the  $m$  subscript represents "mixed," is assumed to exist at some point within the mixed canopy air space, as illustrated in Figures 11-1d and e. This  $D_m$  will be smaller than the  $D_a$  of the general airstream that exists at some reference height above the canopy. With the assumption of a common  $D_m$  within the canopy air space, a network of resistances is established in multilayer or multisource models that describe internal surface and boundary layer transfer of heat and vapor, as shown in Figure 11-1d, and these resistances can be used to tie applications of the PM-style equation together for the various layers. Were et al. (2008) assume the mean height of common  $D_m$  within the canopy air space to occur at height  $d + z_{om}$ , which is typically at about 0.8 of canopy height,  $h_c$ .

Some interactive models use the PM model once to describe the flux between the canopy (overstory) surface and the in-canopy air space and a second time for the flux from the understory surface to the in-canopy air space. In addition, the estimates for within-canopy aerodynamic resistances  $r_{vs}$  and  $r_{vv}$  (see Figure 11-1e, for example) are implicitly made for completely bare and completely vegetated conditions and then averaged based on an explicitly applied scheme. Differences in  $D$  at the component surfaces are maintained by boundary layer resistances  $r_{vi}$  as shown in Figure 11-1d. Fluxes from one component surface interact with fluxes from other component surfaces by influencing the in-canopy environment

[ $T_m$ ,  $e_m$ , and thus  $D_m = f(T_m, e_m)$ ], where  $T_m$  and  $e_m$  are temperature and vapor pressures in the mixed in-canopy air space.

Early derivations of multilayer models include Shuttleworth and Wallace (1985), Shuttleworth and Gurney (1990), and Dolman (1993). These models have been widely tested and parameterized in research applications, but have not been widely used operationally due to the difficulty of establishing parameterizations for some of the internal resistances, which can change markedly with vegetation type and density, and due to errors associated with impacts of unknown or unresolved  $T_s$  on  $\Delta$ ,  $R_{L-out}$ , and within- and above-canopy  $\psi$  as described previously for the PM model.

Brenner and Incoll (1997) and Were et al. (2008) suggest the following form of a multilayer/multisource model, and it illustrates how a multiple-PM model can be formulated and how primary parameters and resistances can be estimated. The Brenner-Incoll-Were model is a two-layer/three-source model with vegetation canopy (labeled  $i=1$  or  $v$ ), shaded soil (labeled  $i=2$  or  $ss$ ), and exposed soil (labeled  $i=3$  or  $se$ ) sources. Typically, component within-canopy aerodynamic resistances, labeled  $r_v$  for vapor transport and  $r_h$  for heat transport, are assumed equal, and the  $r_h$  label is often assigned in the PM equation. Part of this assignment stems from the derivation of the PM equation, where a mixture of  $r_v$  for vapor transport and  $r_h$  is used (see Appendix J). The PM equation for each source area can be written as

$$\lambda E_i = \frac{\Delta(R_n - G) + \frac{\rho_a c_p D_a}{r_{h_i} + r_{am}} - \Delta_i(R_{ni} - G_i) \frac{r_{h_i}}{r_{h_i} + r_{am}}}{\left[ \Delta + \gamma \left( 1 + \frac{r_{s_i}}{r_{h_i} + r_{am}} \right) \right]} \quad (11-4a)$$

where  $\lambda E_i$  is the latent heat flux associated with each cover type  $i$ , and  $D_a$  is the averaged, mixed vapor pressure deficit at some reference height above the canopy-surface system (Figure 11-1d). The subscript  $i$  in Eqs. (11-2a–c) signifies the parameter assigned to each specific component surface (vegetation, understory, wet or dry exposed or shaded soil, etc.). In the case of  $R_n$  and  $G$ ,  $R_n - G$  is the total bulk surface net radiation and soil heat flux density averaged over the entire surface, whereas  $R_{ni}$  and  $G_i$  represent values for the  $i$ th surface, where both parameters are influenced by the temperature of the  $i$ th surface. Parameter  $r_{h_i}$  is the boundary layer resistance to the flow of heat and vapor from surface  $i$  to the place of the in-canopy air having deficit  $D_m$ , and  $r_{s_i}$  is the resistance to water vapor flow from inside surface  $i$  to immediately outside the surface. Resistance  $r_{h_i}$  is assumed equal to resistance  $r_{v_i}$  shown in Figure 11-1d. Parameter  $\Delta_i$  is best calculated as the slope of the saturation vapor pressure curve using temperature of the specific  $i$ th surface and air temperature at the reference height. Resistance  $r_{am}$  is the aerodynamic resistance between the in-canopy location of  $D_m$  and the above-canopy reference  $D_a$ . The formulation of Eq. (11-4a) allows for the omission of  $D_m$ . Because no express contact with a surface occurs between

these two locations, the formulation for  $r_{am}$ , as seen later, is for momentum transfer only, and its calculation does not include the parameter  $z_{oh}$ .

Were et al. (2008) express Eq. (11-2a) in a different form (an omitted term is corrected), but where  $\Delta_i$  is assumed to be equal to the general, bulk  $\Delta$ :

$$\lambda E_i = \frac{\Delta(R_n - G)r_{am} + \rho_a c_p D_a + \Delta[(R_n - G) - (R_{ni} - G_i)]r_{h_i}}{[(\Delta + \gamma)(r_{h_i} + r_{am}) + \gamma r_{s_i}]} \quad (11-4b)$$

The equation can be expressed in an even different form, if again,  $\Delta_i$  is assumed to be equal to the general, bulk  $\Delta$ :

$$\lambda E_i = \frac{\Delta(R_n - G) + \rho_a c_p D_a/r_{am} + \Delta[(R_n - G) - (R_{ni} - G_i)]r_{h_i}/r_{am}}{\left[\Delta\left(1 + \frac{r_{h_i}}{r_{am}}\right) + \gamma\left(1 + \frac{r_{h_i}}{r_{am}} + \frac{r_{s_i}}{r_{am}}\right)\right]} \quad (11-4c)$$

The assumption that  $\Delta_i$  equals the value for the general, bulk  $\Delta$  that is computed from bulk surface temperature and bulk air temperature via Eq. (11-3) may cause biases in model estimates. In the same way, the long-wave component for  $R_{ni}$  should be based on an estimate of surface temperature of surface  $i$ . However, knowledge of  $T_s$  for surface  $i$  would require an iterative solution using a system of equations similar to the AFIB Eqs. (11-2a–f) and is generally not done. Note that if surface  $i$  is assumed to be directly coupled to the above-canopy airstream, via  $r_{am}$ , so that within-canopy aerodynamic resistance  $r_{h_i}$  is 0, then Eqs. (11-4a) and (11-4c) reduce to exactly the original PM equation [Eq. (11-1)], but where the typical  $r_{ah}$  is used in place of  $r_{am}$ .

Total ET from the complex surface is summed, in the multilayer, interactive model over the two or more types of surfaces:

$$\lambda E = \sum_i p_i C_i \lambda E_i \quad (11-5)$$

where  $p_i$  represents the fractional surface represented by cover  $i$ , and  $C_i$  is a coefficient derived by combining resistances involved among the various sources, for example,  $v$ ,  $ss$ , and  $se$ , representing the vegetation canopy, shaded soil or understory, and exposed soil or understory. In a multisource model such as the Were model, the sum of  $p_i$  over all surfaces,  $i$ , can total  $>1.0$ , for example, in the case of understory vegetation or understory soil that can take up the same horizontal area as the overlying canopy.  $C_i$  in Eq. (11-5) is expressed in the Were et al. (2007, 2008) model as

$$C_v = \frac{R_{ss} R_{se} (R_v + R_a)}{R_v R_{ss} R_{se} + f R_{ss} R_{se} R_a + f R_v R_{se} R_a + (1-f) R_v R_{ss} R_a} \quad (11-6a)$$

$$C_{ss} = \frac{R_v R_{se} (R_{ss} + R_a)}{R_v R_{ss} R_{se} + f R_{ss} R_{se} R_a + f R_v R_{se} R_a + (1-f) R_v R_{ss} R_a} \quad (11-6b)$$

$$C_{se} = \frac{R_v R_{ss} (R_{se} + R_a)}{R_v R_{ss} R_{se} + f R_{ss} R_{se} R_a + f R_v R_{se} R_a + (1-f) R_v R_{ss} R_a} \quad (11-6c)$$

where variables  $R_v$ ,  $R_{ss}$ , and  $R_{se}$  are defined as

$$R_i = (\Delta + \gamma) r_{h_i} + \gamma r_{s_i} \quad (11-7)$$

where subscript  $i$  is replaced by subscripts  $v$ ,  $ss$ , and  $se$  in Eqs. (11-6a–c) (see Figures 11-1d–e, where  $r_{h_i}$  is replaced by  $r_{v_i}$ , and Figures 11-2d–e), and

$$R_a = (\Delta + \gamma) r_{am} \quad (11-8)$$

Parameters  $f$  and  $(1-f)$  correspond to the fractional covers of vegetation and bare soil (or understory), respectively. Eqs. (11-6a–c) follow Brenner and Incoll (1997) and correct for an error in Eq. (3-5) of Were et al. (2008).

One of the serious challenges in applying the multilayer or patch models to sparse vegetation systems is in the parameterization of  $r_h$ , which is the aerodynamic resistance within and across the canopy or near-surface boundary layers, and in the validity of applying the PM equation over this region. The traditional equations for aerodynamic resistances across  $T$  and  $e$  gradients assume that the  $T$ ,  $e$ , and  $u$  profiles follow semilogarithmic shaped vertical profiles, the shapes of which are governed by surface roughness and density-induced buoyancies. However, within vegetation canopies, turbulent diffusion theory (K theory) has been shown to be inadequate to describe convective transfer where even countergradient fluxes can exist (Raupach 1989; van den Hurk and McNaughton 1995; McNaughton and van den Hurk 1995; Daamen and McNaughton 2000). Therefore, empirical formulations have to be applied. Choudhury and Monteith (1988) and Zhao et al. (2006) provide examples for these, where, for  $r_{hs}$ ,

$$r_{hs} = \frac{h_c \exp(n) \ln\left(\frac{z_a - d}{z_o}\right)}{nk^2 u_a (h_c - d)} \left[ \exp\left(\frac{-nz_{os}}{h_c}\right) - \exp(-0.76n) \right] \quad (11-9)$$

as do Shuttleworth and Wallace (1985) and Brisson et al. (1998):

$$r_{hs} = \frac{\ln\left(\frac{z_a - d}{z_o}\right)}{k^2 u_a} \frac{h_c}{n(h_c - d)} \left\{ \exp(n) - \exp\left[n\left(1 - \frac{d + z_o}{h_c}\right)\right] \right\} \quad (11-10)$$

where  $h_c$  is mean height of the vegetation canopy;  $z_a$  is the measurement height for wind speed and air temperature,  $T$ , and humidity;  $d$  is zero plane displacement height;  $z_o$  is the aerodynamic roughness length for the complete surface;  $u_a$  is wind speed at height  $z_a$ ;  $z_{os}$  is aerodynamic roughness length for the underlying soil or understory; and  $n$  is an empirical eddy diffusion decay constant.  $n = 2.5$  when  $h_c < 1$  m,  $n = 2.31 + 0.194 h_c$  for  $1 < h_c < 10$  m, and  $n = 4.25$  for  $h_c > 10$  m. Daamen and McNaughton (2000) use  $n = 2.0$ . Note that  $r_{hs}$  is applied for both shaded soil, some of which may be beneath a dense vegetation canopy, and exposed soil that may have substantial exposure to the boundary layer, especially with sparse vegetation. The former situation will have a high value for  $r_{hs}$  and the latter a lower value. In addition,  $r_{hs}$  for soil exposed to the sun can have substantial buoyancy boost to convection, lowering the value for  $r_{hs}$  from that estimated from Eqs. (11-9) and (11-10). Under those conditions, a buoyancy term can be added to those equations by replacing the  $\ln(z_a - d)/z_o$  term with  $\{\ln[(z_a - d)/z_o] - \psi_m\}$ , where  $\psi_m$  is an integrated stability correction calculated from  $z_0$  to  $z_a$ .

For the bulk boundary layer resistance between vegetation and in-canopy location  $z_m$ , Brisson et al. (1998) propose treating all single-leaf boundary layers as if in parallel:

$$r_{hv} = \frac{\sigma_b r_b}{LAI} \quad (11-11)$$

where  $\sigma_b$  is a shielding factor taken as 0.5 and with the single-leaf boundary resistance based on an extinction function from Shuttleworth and Gurney (1990):

$$r_b = \frac{100}{n[1 - \exp(-\frac{n}{2})]} \left( \frac{w}{u_h} \right)^{0.5} \quad (11-12)$$

where  $w$  is the characteristic leaf width in mm,  $u_h$  is the wind speed at the top of the canopy in  $\text{ms}^{-1}$ , and  $n$  is the eddy diffusivity decay constant. Units of all resistances are  $\text{sm}^{-1}$ .

The aerodynamic resistance,  $r_{am}$ , between the in-canopy air space and reference height where the mean wind speed measurement is made is assumed to be well mixed and representative of the entire land surface structure. The formulation for  $r_{am}$  is similar to that formulated by Shuttleworth and Wallace (1985), where  $z_{oh}$  is omitted because the resistance does not include boundary layer effects, but where some decay of eddy diffusivity is assumed:

$$r_{am} = \frac{\ln\left(\frac{z_a-d}{z_o}\right)\left(\ln\left(\frac{z_a-d}{h_c-d}\right) + \frac{h_c}{n(h_c-d)}\left\{\exp\left[n\left(1 - \frac{d+z_a}{h_c}\right)\right] - 1\right\}\right)}{k^2 u_a} \quad (11-13)$$

Eqs. (11-9)–(11-13) do not include corrections for density-induced buoyancy impacts on convective transport, which can be large over dry, warm surfaces. The equation for  $r_{am}$  was modified by Shuttleworth and Gurney (1990) to include buoyancy effects as

$$r_{am} = \frac{\ln\left(\frac{z_a-d}{z_o}\right)\left(\ln\left(\frac{z_a-d}{h_c-d}\right)(1+\delta)^e + \frac{h_c}{n(h_c-d)}\{\exp[n(1-\frac{d+z_a}{h_c})] - 1\}\right)}{k^2 u_a} \quad (11-14)$$

Parameter  $(1+\delta)^e$  is a stability correction factor based on the bulk Richardson number (Shuttleworth and Gurney 1990; Choudhury and Monteith 1988) where

$$\delta = \frac{5g(z_a-d)(T_o - T_a)}{T_a u_a} \quad (11-15)$$

where  $T_o$  is air temperature in K at the intermediate height of  $D_m$ , and  $T_a$  is air temperature at reference height  $z_a$ . Parameter  $e$  has a value of  $-2$  for  $\delta < 0$  and a value of  $-0.75$  for  $\delta > 0$  (Choudhury and Monteith 1988). However, the use of  $(1+\delta)^e$  only provides stability correction to the temperature profile in Eq. (11-14) and not to the wind profile as represented by the first logarithmic term. In addition, stability correction formulations built on the Richardson number are not as robust as those based on Monin-Obukhov similarity theory (Brutsaert 1982; Allen et al. 1996). The  $h_c - d$  expression in Eqs. (11-13)–(11-14) represents the beginning height,  $z$ , for the start of  $r_{am}$ . This is point  $z_1$  in Figure 11-1e. Height  $z_a$  represents the endpoint for  $r_{am}$ .

An improved equation for  $r_{am}$  using stability correction based on Monin-Obhukov is

$$r_{am} = \frac{[\ln\left(\frac{z_a-d}{z_o}\right) - \Psi_{mz_a}]([\ln\left(\frac{z_a-d}{h_c-d}\right) - (\Psi_{hz_a} - \Psi_{hh_c})] + \frac{h_c}{n(h_c-d)}\{\exp[n(1-\frac{d+z_a}{h_c})] - 1\})}{k^2 u_a} \quad (11-16)$$

where  $\Psi_{mz_a}$  and  $\Psi_{hz_a}$  are integrated stability correction parameters based on Monin-Obhukov formulations for momentum and heat fluxes, respectively, where the integration is along the vertical between momentum roughness height  $z_o$  and  $z_a - d$  for momentum correction and along the vertical between  $z_1 = h_c - d$  and  $z_2 = z_a - d$  for heat flux profile correction (necessitating the subtraction of  $\Psi_{hh_c}$  from  $\Psi_{hz_a}$ ). Chapter 7 presents equations for the Monin-Obhukov formulations. Similar buoyancy corrections are needed for the  $r_h$  terms in both the multilayer and patch models, especially when one of the surfaces is dry and sensible heat flux is relatively large. However, the nature and structure of buoyancy correction within a

sparse canopy is uncertain, even though it can constitute a very effective mechanism for transport of sensible heat and vapor upward within tall canopies such as trees, where mechanical mixing from wind is low due to sheltering. This increases uncertainty in applying multisource and multi-layer models as formulated here.

Formulations for other parameters are available from the literature. Formulations for aerodynamic roughness and surface resistance are described in following sections. Lagos (2008) and Lagos et al. (2009, 2012) describe application of an interactive model to partial cover vegetation having substantial surface residue.

Large differences in surface resistances of soil and vegetation components or soil and soil components can cause large differences in temperatures and vapor densities at the component surfaces. The resulting gradients between the surfaces may be enough to drive significant fluxes between surfaces. A common example occurs when a sparse overstory canopy well supplied with water has an underlying dry soil surface. In this case a net sensible heat transfer (microadvection) from the understory, having a somewhat high surface temperature, to the overstory occurs. In contrast, when both the overstory and understory are water stressed, a positive sensible heat flux away from both surfaces is likely, and the interaction of fluxes is less important (Daamen and McNaughton 2000). In some situations, using a patch type of model such as shown in Figure 11-1c and applying aerodynamic and energy balance equations directly may be more effective, similar to the AFIB procedure of Eqs. (11-2a–f), rather than applying the Penman-Monteith method, but using formulations for  $r_a$  from Eqs. (11-9)–(11-16). Both approaches may require an iterative solution for surface temperature to adequately calculate emitted long-wave radiation; soil heat flux; and, in the case of the PM method,  $\Delta$ , from the various surfaces.

### The Two-Source (Patch) Resistance-Based Model

The patch model is intermediate in complexity as compared with the simpler single-layer Penman-Monteith and AFIB models and the more complicated interactive layered models. The two-source model applies the PM equation or a full suite of aerodynamic AFIB-style equations for  $H$  and  $\lambda E$  separately to two different component surfaces, assuming no interaction between the surfaces. Evaporation from the soil and “transpiration” from vegetation is calculated separately for assumed homogeneous patches, and the areal average is weighted according to the fractional cover of each patch type. The patch model essentially uses two noninteracting PM or AFIB models side by side. It is justified at the scale where a boundary layer is fully developed over each patch, so that separate temperature, vapor, and wind speed profiles can be assumed to extend to some blended reference

height close to each surface and so that K theory can be assumed to apply, and where edge effects between patches are insignificant. As the size of patches decreases, the model becomes less valid. In some applications, a common  $r_{am}$  is used from a blending point above the two references up to the reference height where  $T$ ,  $e$ , and  $u$  are measured. This is done to account for blending effects of smaller patch size on the airstream near the canopy. Daamen and McNaughton (2000) suggest that patch size should be 10 times vegetation height or larger to satisfy the boundary layer requirements.

Examples of patch models include the Energy-Water-Balance (ENWATBAL) model (Evett and Lascano 1993; Lascano 2000); a three-patch model by Brenner and Incoll (1997); and, using explicit equations for  $LE$  and  $H$  fluxes, the Two-Source-Energy-Balance (TSEB) model of Kustas (1990) and Kustas and Norman (1999) that is applied in a surface energy balance mode using thermal imagery. The TSEB model is often applied to row crops, which violates the 10:1 guideline of Daamen and McNaughton (2000), and uses the Priestley-Taylor equation for estimating transpiration rather than the more complete PM model as in Eq. (11-17). The patch model was developed for simplicity. However, because direct interchange between surface types is ignored, defining appropriate resistance values is often challenging. When patches are extensive in size, such that the microclimate of one does not affect the microclimate of the other, then the aerodynamics and resistances of different surface types can be characterized by different roughness lengths and with quite different  $r_{am}$  values (Daamen and McNaughton 2000). Conversely, when patch sizes are small (<10 times vegetation height), each surface type (i.e., vegetation and bare soil) will tend to affect the aerodynamics of the other to some degree.

When written in the form of the PM equation, the patch model will have the form

$$\lambda E_i = p_i \frac{\Delta(R_{ni} - G_i) + \rho_a c_p (D_a)/(r_{ai} + r_{hi})}{\left[ \Delta + \gamma \left( 1 + \frac{r_{si}}{r_{ai} + r_{hi}} \right) \right]} \quad (11-17)$$

and

$$\lambda E = \sum_i p_i \lambda E_i \quad (11-18)$$

where  $p_i$  represents the fractional surface represented by cover  $i$ .

Often, the effective fraction of surface or fraction of net radiation absorbed by the overstory,  $f$ , is expressed as a function of leaf-area index:

$$f = 1 - \exp(-aLAI) \quad (11-19)$$

where  $a$  is an empirical constant that ranges from 0.5 for short-grass steppe to 2.0 for sparse row crops to 3 for a sheltered kiwifruit orchard (Daamen and McNaughton 2000). Alternately,  $f$  can be estimated from remotely sensed vegetation indices such as the normalized difference vegetation index (NDVI) or soil-adjusted vegetation index (SAVI) indices (Carlson and Ripley 1997).

### 11.3 CHALLENGES WITH TYPES OF RESISTANCE-BASED MODELS

Complexity in models can bring complexity in parameterization of the models. This can definitely be the case with multilayer and patch models where the characterization of heat and vapor transport within a canopy have, as a necessity, a degree of speculation and empiricism. If not formulated properly, these characterizations can induce more inaccuracy than accuracy (Were et al. 2008), especially if key factors such as buoyancy correction or penetration of air into the canopy by random eddy movement are not accounted for. For example, the required form and structure of formulations for internal resistances,  $r_h$ , may change with plant density, leaf area, patch size, wind speed, and buoyancy. K theory, which establishes nearly logarithmic wind speed and  $T$  and  $e$  profiles above some zero plane displacement height, is not strictly applicable within canopies and along patch boundaries. Also difficult to accurately account for is the horizontal transfer of sensible heat (and vapor deficit) from understory into canopy and vice versa.

In addition to uncertainties in estimates for resistances, uncertainties exist in estimating the net radiation,  $R_{ni}$ , associated with specific component surfaces. A dry, warm soil surface exposed to the sun can emit up to  $100 \text{ W m}^{-2}$  more thermal radiation than a cool adjacent canopy. This reduces the available energy at the soil surface and substantially affects the energy balance and boundary layer stability estimation. The calculation of  $R_{ni}$  for soil is further complicated by whether the soil is shaded or exposed and by the estimation of downwelling thermal radiation, which is a mixture of relatively lower rate from exposed sky and relatively higher rate from the relatively warmer canopy that is in view of the soil. Various canopy model formulations have dealt with the estimation of net thermal and net shortwave radiation as described later.

Estimation of soil heat flux densities can be uncertain under complex canopies, as thermal gradients and associated heat fluxes into soil change with solar angle and with surface temperature and water contents, which can be highly variable in a complex canopy. Even accurate measurement of  $G$ , required to parameterize a model, is extremely demanding in complex canopies and can require tens of locations within the canopy structure to

adequately sample all combinations of shading, rainfall capture, plant root extraction, aerodynamic exposure, surface mulching, wetting by irrigation, and plant architecture.

As described for the single-layer PM equation, an often overlooked requirement for any application, including multilayer applications, is error caused by assuming that surface temperature is sufficiently similar to air temperature for the calculation of  $\Delta$ , or that all surfaces have similar  $T_s$  when calculating  $\Delta$ , emitted long-wave radiation, and near-surface air buoyancy. Often, dry surfaces have substantially higher temperatures than air temperature, and  $\Delta$  should be solved by iterative application of AFIB types of equations such as Eqs. (11-2a–f).  $T_s$  for a specific surface is estimated using energy balance and aerodynamic theory:

$$T_{si} = \frac{(R_{ni} - G_i - \lambda E_i)r_{ai}}{\rho c_p} + T_{ai} \quad (11-20)$$

where the  $i$  subscript denotes the  $i$ th component surface.  $T_{si}$  is surface temperature, and  $T_{ai}$  is air temperature at some height, with  $r_{ai}$  the aerodynamic resistance over the vertical distance between  $T_{si}$  and  $T_{ai}$ . Depending on the placement of  $T_{ai}$ ,  $r_{ai}$  will include  $r_h$  and  $r_{am}$ . Once  $T_{si}$  is known,  $\Delta$  can be estimated for use in the PM or  $PM_i$  equation with calculation made using  $T_{si}$  and  $T_{ai}$ . The estimate for  $T_{si}$  can be used to improve the estimation of thermal radiation emitted from the surface and in estimating buoyancy effects.

As noted earlier, one of the drawbacks of the single-layer PM equation, especially for use in sparse canopies, is the implicit assumption that the mean horizontal plane of momentum sink within the canopy is at the same height ( $d + z_{om}$ ) as that for sensible heat (source or sink) and for latent heat (source) so that common expressions for  $r_a$  can be used for  $H$  and  $LE$  components and the Bowen ratio can be used to derive the combined Penman form (see Appendix J). Similarity of source heights for  $H$  and  $LE$  is not generally true for sparse canopies, or for dense canopies having intermittent gaps with exposed lower story vegetation or bare soil. Under these conditions, a significant amount of solar radiation can penetrate to levels below  $d + z_{om}$ , resulting in the generation of sensible heat at lower levels with only the possible conversion to latent heat. The combination of bulk stomatal resistance with soil resistance into a single surface resistance,  $r_s$ , as is done for the PM equation or AFIB method, implies that the soil and canopy surfaces are at nearly the same vertical level. This is generally not the case, and consequently the assumption ignores the aerodynamic resistance between the soil surface and the mean height of heat and vapor exchange in the canopy.

The errors induced by the assumption of a single exchange plane in the PM and AFIB methods are sometimes partially accounted for by varying

the “apparent”  $z_{om}/h$  ratio, “effective” leaf area, single-leaf resistance, or radiation extinction coefficient,  $K_r$ , during analysis of research data (Daamen and McNaughton 2000). However, because the transport resistances within the canopy are dynamically linked to wind speed, canopy structure, radiation levels, and soil water, fitted parameters may not transfer well to other growth stages or locations. Ben-Mehrez et al. (1992), Raupauch (1989), and Raupauch et al. (1996) discuss and estimate wind speed and movement within canopies.

#### **11.4 PARAMETERS FOR THE PENMAN-MONTEITH FOR EQUIVALENCY WITH MORE COMPLICATED MODELS**

Often, operational models that are applied routinely over large types of vegetation and conditions are necessarily reduced in complexity to accommodate reliable parameterization and available data and observations. Many operational systems, including some land simulation (LSM) systems such as those used in the Weather Research and Forecasting (WRF) model have, in the past, been based on a single-layer Penman-Monteith model (Mahrt and Ek 1984; Chen and Dudhia 2001), whereas more recent models use patch types of resistance-based models similar to the AFIB process where surface temperatures for vegetation and soil are estimated separately (Oleson et al. 2004; Niu et al. 2011). Resistance parameters in these models are typically formulated by combining and reducing resistances developed for the multilayer and multisource models.

Often, the uppermost aerodynamic resistors in the patch model, i.e.,  $r_{as}$  and  $r_{ac}$ , are aligned in a network in the form of parallel resistors. In that situation, the equivalent total resistance of those resistors is equivalent to  $r_{am}$  as used in the multilayer model, and the in-series combination of  $r_h$  and  $r_{am}$  is equivalent to the bulk  $r_{ah}$  as used in the single-layer PM model or AFIB models. The resistance values are calculated in simplified models as  $r_{as}/f_s$  and  $r_{ac}/f_c$  where  $f_c$  is the fraction of ground covered by vegetation and  $f_s$  is the fraction of exposed soil, where  $f_s + f_c = 1.0$ . This formulation effectively divides the air space from the canopy to the reference height between the two component surfaces (Daamen and McNaughton 2000).

Were et al. (2008) formulate effective surface and aerodynamic resistances for the single-layer PM model by aggregating various soil and plant resistances as used in a more complicated multilayer-multisource model. They solve for surface temperature using iteration. They compare estimates of ET with flux measurements and conclude that the use of effective surface resistances aggregated in parallel with effective aerodynamic resistances aggregated in series in a single-layer PM model produce similar accuracy as a multilayer model for natural brush vegetation in southeast Spain. In

some cases, they find the single-layer model to outperform the multilayer model in terms of accuracy.

### Net Radiation

As described earlier, both total surface net radiation and net radiation of individual surface components,  $R_{ni}$ , should include surface-specific estimation of emitted long-wave radiation using Eq. (4-32), especially for dry surfaces, where emitted long-wave radiation can be as much as  $100 \text{ W m}^{-2}$  greater, and thus  $R_{ni}$   $100 \text{ W m}^{-2}$  less, than that for the well-watered reference surface represented by Eq. (4-37), where surface temperature is usually within a few degrees of near-surface air temperature. When estimating  $R_{ni}$  for bare, dry soil exposed to the sun, one should avoid estimating  $R_{ni}$  as an exponential function of leaf-area index multiplied by the total bulk surface net radiation, as is sometimes done in many applications of multilayer models ([Shuttleworth and Wallace 1985](#); [Kelliher et al. 1995](#); [Zhao et al. 2006](#)), because of the potential differences in surface temperature between bulk surface and soil. In addition, soil albedo can be substantially greater than the typical vegetation albedo of 0.2 to 0.25, when soils are dry and organic content is low, ranging as high as 0.4 to 0.5. Conversely, high organic, wet soil can have albedos as low as 0.1 to 0.15 ([Fritsch 1967](#)).

## 11.5 COMPARATIVE MODEL PERFORMANCE

Daamen and McNaughton ([2000](#)) compare ET estimates by three evaporation models represented by combinations of Eqs. (11-4)–(11-16) for six different sparsely vegetated land surfaces and a range of conditions of water supply. Vegetation types ranged from short-grass steppe to sparse rangeland to sparse cotton and millet to kiwi and lemon orchards. The three evaporation models (single-layer, multilayer, and patch) based on the PM formulation were parameterized to measurements from the six locations and were then operated over ranges of water availability and combinations of relative resistance.

Estimates by the single-layer PM model application closely resembled those from the iterative (multilayer) model when applied to short-grass steppe over a broad range of surface and relative aerodynamic resistances due to the somewhat dense structure of the grass. The exception was when the surface resistance from soil was set to 0, representing a saturated surface. Differences among models were greater for more sparsely vegetated surfaces, where ratios of  $r_{am}$  to  $r_h$  (Figure 11-1) were relatively small due to greater roughness.

Daamen and McNaughton ([2000](#)) show the patch and interactive models to have best agreement as canopy sparsity and patch size increase, for

example, with the lemon orchard, and agreement decreases with plant density and increasing ratios of  $r_{am}$  to  $r_h$ . They find higher evaporation estimated by the interactive model than patch model under some conditions due to interactions of fluxes between the component surfaces. As expected, the flux interactions are largest when the surface resistances for the soil and vegetation components are most different (for example, dry soil surface and well-watered canopy) and when  $r_{am}$  is larger than  $r_{hv}$  and fractions of exposed soil and canopy are similar. When flux interactions are largest, differences between the single-layer and interactive (multilayer) models are the smallest. This suggests that a land surface as a whole can be well approximated by a single homogeneous surface with appropriately averaged properties when a large interaction (mixing of fluxes and micro-scale advection) occurs between the component surfaces.

Daamen and McNaughton (2000) suggest that the ratio of  $r_{am}$  to  $r_h$  in Figures 11-2e and f can be a good indicator of the best choice in type of simplified model (patch or single-layer). As  $r_{am}$  to  $r_h$  becomes small, the difference between the in-canopy vapor pressure deficit,  $D_m$ , and vapor pressure deficit of the airstream above the canopy becomes small in the interactive model, and the patch and interactive models approach each other. When the  $r_{am}$  to  $r_h$  ratio is large,  $D_m$  is closer to the vapor pressure deficits at the component surfaces and the single-layer model can serve as a good approximation. A relatively small ratio  $r_{am}$  to  $r_h$  can occur under high wind speed or with relatively large vegetation roughness, and a relatively large ratio can occur under lower wind speeds or with relatively small aerodynamic roughness.

Under dry conditions, differences among all three models become less significant. When surface resistances exceed  $300 \text{ sm}^{-1}$ , the patch and single-layer PM models estimate energy fluxes to within  $50 \text{ W m}^{-2}$  of the interactive model for the grass steppe and millet land surfaces (Daamen and McNaughton 2000). At these higher surface resistances, evaporation is largely controlled by surface resistance, and interactions among fluxes become less important. However, under conditions of low available water, accuracy of ET estimates becomes sensitive to the value estimated for the surface resistances for both vegetation and soil surfaces.

Often, the total soil evaporation estimate is not overly sensitive to the parameterization of resistances when precipitation events are separated by periods of five days or more. This is due to the impact of conservation of water in the topsoil layer on values assigned to surface resistance that are updated each calculation time step. Provided that the resistance and evaporation models implement upper limits on total evaporation, and provided a majority of evaporable water is depleted between events, evaporation rates from soil can be over- or underestimated, but the final total evaporation estimate will not be greatly affected. The partitioning between  $E$  and  $T$  is affected, however, and the partitioning between sunlit and shaded and

wetted and shielded areas of soil remains important. Various functions for estimating soil surface resistances are described in Section 11.8.

## 11.6 ROUGHNESS LENGTH AND ZERO PLANE DISPLACEMENT

Aerodynamic roughness length and displacement of the zero plane of the wind profile are common parameters to many of the physically based models. Roughness of the surface affects the convective transfer of heat, vapor, and momentum. General relationships are available to provide estimates of these aerodynamic parameters.

### General Parameters

The direct application of the PM equation uses the basic PM combination equation [Eq. (8-2)] and the aerodynamic resistance,  $r_a$  or  $r_{ah}$ , computed using Eq. (7-20), (8-3), or (11-2f). Bulk stomatal resistance is generally estimated as a function of leaf-area index ( $LAI$ ) and an average stomatal resistance. Alternatively, a minimum stomatal resistance ( $r_{l_{min}}$ ) for well-ventilated, sunlit leaves with no soil water limitation can be divided by multiplicative stomatal conductance reducing functions,  $g()$ , which are based on environmental variables (Stewart 1989) as discussed in Section 11.7.

Roughness length for momentum transfer,  $z_{om}$ , and zero plane displacement,  $d$ , required in Eqs. (7-20), (8-3), and (11-2f), can be estimated for somewhat dense vegetation canopies ( $LAI > 2$ ) using Eqs. (11-21) and (11-22) (Brutsaert 1975; Monteith 1981; Allen et al. 1989; Jensen et al. 1990).

$$d = 0.67h \quad (11-21)$$

$$z_{om} = 0.12h \quad (11-22)$$

where  $h$  is the mean maximum height of the plant canopy. Units for  $z_{om}$ ,  $d$ , and  $h$  are the same. Note that both  $z_{om}$  and  $d$  are essentially "synthetic" parameters that describe a mean, smoothed idealized wind profile as it dissipates to zero within the canopy. By definition, the idealized wind profile dissipates to zero at  $d + z_{om}$ . Both values can be determined by measuring wind at two or more heights above the roughness sublayer (Cellier and Brunet 1992; Raupach et al. 1991) and fitting to an assumed smoothed and continuous profile, as described later in Eqs. (11-33) and (11-35). Alternatively,  $z_{om}$  can be determined from friction velocity data obtained by 3-D sonic anemometers. The profile measurement and fitting is generally done under near-neutral conditions, although Zhao et al. (2008) describe a procedure for estimating the parameters using data collected under unstable conditions.

Generally the value for  $d$  decreases as density of vegetation decreases, as shown later in Eq. (11-29).

For tall or sparse vegetation, more complex and elaborate equations may be required to estimate  $z_{om}$  (Tanner 1968; Lettau 1969; Plate 1971; Brutsaert 1975; Monteith 1981), for example, Eq. (11-23) by Lettau (1969):

$$z_{om} = 0.5h^* \frac{s}{S} \quad (11-23)$$

where  $h^*$  is the effective obstacle height of the vegetation in m,  $s$  is the silhouette area (area "seen" by wind) in  $\text{m}^2$ , and  $S$  is the horizontal plane area (total ground area divided by the number of roughness elements) in  $\text{m}^2$ .

Thom (1971) and Garratt and Hicks (1973) propose the following equation for estimating  $z_{om}$  for forest canopies:

$$z_{om} = \sigma(h - d) \quad (11-24)$$

or, alternatively,

$$\frac{z_{om}}{h} = \sigma \left( 1 - \frac{d}{h} \right) \quad (11-25)$$

where  $\sigma$  was suggested to be equal to 0.36, which is equivalent to the relationship suggested by Brutsaert (1982) for dense, uniform plant stands:

$$z_{om} = \frac{1}{e}(h - d) \quad (11-26)$$

where  $e$  is the natural number (2.718). When  $d$  is estimated as  $0.67 h$ , then Eq. (11-24) with  $\sigma = 0.36$  and Eq. (11-26) both reduce to  $z_{om} = 0.12 h$ , which is equivalent to Eq. (11-22).

Measurements of  $z_{om}/h$  and  $d/h$  by Leuning and Attiwill (1978) for 27-m eucalyptus trees with projected areas of 80% of the ground surface, measurements by Jarvis et al. (1976) for 13 coniferous forest regions with mean tree heights of 10 to 28 m, and measurements by de Bruin and Moore (1985) for 18-m tall Scots pine (*Pinus sylvestris* L.) indicate a value of  $\sigma = 0.22$ . Canopy densities in these studies were not specified. Moore (1974) determined a value of  $\sigma = 0.27 \pm 0.07$  for 105 published estimates of  $d$ ,  $z_{om}$ , and  $h$  for vegetation types ranging from smooth grass to forest. Zhao et al. (2006) varies the coefficient in Eq. (11-22) in proportion to height, with the multiplier (and  $z_{om}/h$  ratio) reducing with increasing  $h$ :

$$\begin{aligned} z_{om} &= 0.13h, & h \leq 1\text{m} \\ z_{om} &= 0.139h - 0.009h^2, & 1 < h < 10\text{m} \\ z_{om} &= 0.05h, & h \geq 10\text{m} \end{aligned} \quad (11-27)$$

The 0.05 multiplier for tall vegetation is in line with the de Bruin and Moore (1985) value for  $\sigma = 0.22$ , which is equivalent to a direct multiplier on  $h$  of 0.07 for  $d \sim 2/3 h$ .

The utility of Eq. (11-24) is that it is applicable to canopies where zero plane displacement varies with plant density and height. Segner (1974) discusses the variation in  $z_{om}/h$  and  $d/h$  with increasing canopy density from a theoretical point of view.  $z_{om}/h$  logically varies with stand density, because as stand density increases the more roughness elements are present to affect momentum transfer to the surface. However, as density increases beyond a particular limit, the logarithmic wind profile begins to become displaced upward in the canopy ( $d$  increases) so that length of roughness elements become less effective in momentum transfer and  $z_{om}/h$  begins to decrease.

Following this logic, Perrier (1982) proposes relationships to estimate  $z_{om}/h$  and  $d/h$  as a function of  $LAI$  for well-defined canopies:

$$\frac{z_{om}}{h} = (1 - e^{\frac{-alAI}{2}}) e^{\frac{-alAI}{2}} \quad (11-28)$$

$$\frac{d}{h} = 1 - [1 - (e^{\frac{-alAI}{2}})] \left( \frac{2}{alAI} \right) \quad (11-29)$$

where  $LAI$  is total leaf-area index ( $m^2 m^{-2}$ ) and  $a$  is an adjustment factor for  $LAI$  distribution within the canopy. Parameter  $a = (2f)$  for  $f \geq 0.5$  and  $a = 1/[2(1-f)]^{-1}$  for  $f < 0.5$ , where  $f$  is the proportion of  $LAI$  lying above  $h/2$ . Estimates by Eqs. (11-28) and (11-29) are shown in Figure 11-3 for  $f = 0.5$  (uniform canopy structure),  $f = 0.7$  (top-heavy canopy), and  $f = 0.3$  (sparsely topped canopy). Also included in Figure 11-3 are  $z_{om}/h$  and  $d/h$  reported by Jarvis (1976) for coniferous forests and  $z_{om}/h$  estimated by Eq. (11-25) using  $\sigma = 0.27$  and  $d$  estimated by Eq. (11-29) with  $f$  set equal to 0.7 to resemble structures of pine trees. The agreement in Figure 11-3 between Eqs. (11-28) and (11-29), and measured values by Jarvis for coniferous forests is poor for  $LAI < 3$ , where  $d$  was underestimated and  $z_{om}$  was overestimated.

Recommending which  $z_{om}/h$  relations will best predict  $z_{om}$  for sparse or tall canopies is difficult. Equations (11-28) and (11-29) may adequately predict  $z_{om}/h$  and  $d/h$  for dense forests and for sparse vegetation where  $LAI$  and  $h$  are large. The Perrier functions are intuitively sound, as they predict small  $d$  for low  $LAI$  and a peak in  $z_{om}$  as stand density thickens with  $d/h < 0.5$ . However, the ratio  $z_{om}/h$  estimated for  $LAI > 5$  may become too low for  $f > 0.3$ . This can be corrected by establishing a lower limit on  $z_{om}/h$  in Eq. (11-28) (for example,  $z_{om}/h = 0.10$ ) for  $LAI > 5$ . The use of Eq. (11-24) or (11-27) in conjunction with  $d$  estimated using Eq. (11-29) may be a useful approach, with  $\sigma$  in the range of 0.20 to 0.40. This equation combination does estimate large  $z_{om}/h$  for small values of  $LAI (< 0.5)$ , which may be

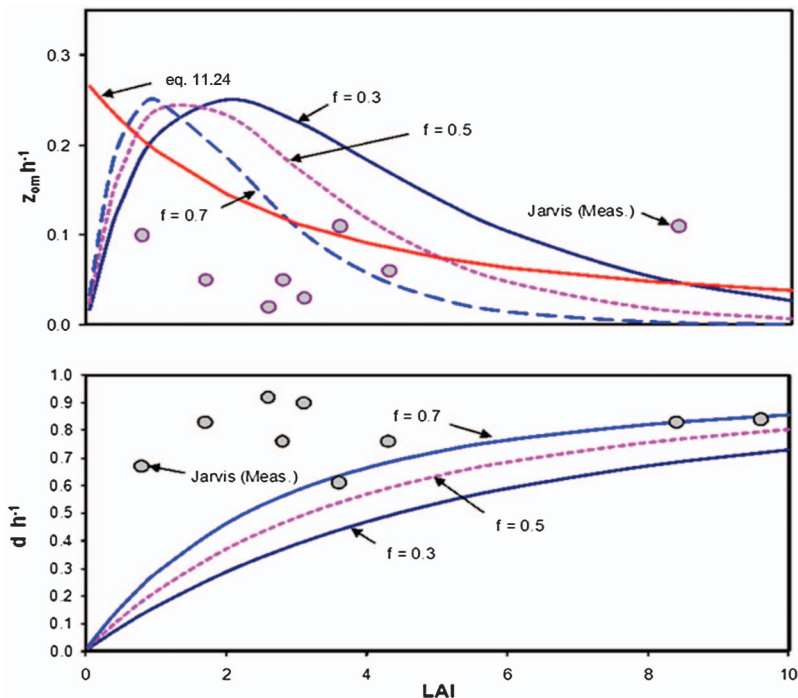


Fig. 11-3. Ratios of  $z_{om} = h$  and  $d = h$  computed using Eqs. (11-28) and (11-29) by Perrier (1982), and  $z_{om} = h$  estimated using Eq. (11-24) with  $\sigma = 0.27$  and with  $d$  estimated using Eq. (11-29) with  $f = 0.7$ . Symbols represent measurements by Jarvis (1976) for coniferous forests

Source: Data from Jarvis (1976)

unreasonable. However, at values of  $LAI < 0.5$ ,  $r_s$  predicted for use in the PM equation should be somewhat high, thereby keeping  $ET$  estimates low. Raupach (1989) and Raupach et al. (1996) report similar approaches for estimating  $z_{om}$ .

As an example of application of Eq. (11-23), Lettau (1969) estimates  $s$  and  $S$  for 0.1-m clipped fescue grass cover as  $4 \text{ cm}^2$  and  $16 \text{ cm}^2$ , so that Eq. (11-23) estimates  $z_{om} = 0.013 \text{ m}$ . Eq. (11-21) estimates  $z_{om} = 0.012 \text{ m}$  for 0.1-m grass cover, which is equivalent. For dense, full cover alfalfa, where  $h* = 0.3 \text{ m}$ , silhouette area  $s$  of the upper portion of a stem may be  $60 \text{ cm}^2$ , and ground area per stem  $S$  may be  $100 \text{ cm}^2$ ,  $z_{om}$  is estimated by Eq. (11-23) to be  $0.09 \text{ m}$ . This indicates that Eq. (11-23) may apply best to sparse vegetation (Lettau 1969).

Example values for  $z_{om}$  and ratios of  $z_{om}/h$  and  $d/h$  reported in the literature from various sources are listed in Table 11-1. These are general values and are typical for various types of vegetation.

Table 11-1. Examples of Roughness Lengths for Various Surfaces and Associated Ratios of  $z_{om}/h$ 

Surface Description	$z_{om}, m$	$z_{om}/h$	$d/h$
Mud flats, ice	0.00001		
Smooth airport runway	0.00002		
Large water surface	0.0001–0.0006		
Grass lawn ( $h = 0.01 \text{ m}$ )	0.01	0.1	
Grass at airport	0.0045		
Prairie grass	0.00665		
0.075 m artificial grass	0.01	0.13	
0.1 m thick grass	0.023	0.23	
0.12 m reference grass standard <sup>a</sup>	0.015	0.12	
0.5 m thin grass	0.05	0.1	
0.18 m wheat stubble	0.024	0.14	
Grass, scattered bushes	0.04		
1–2 m vegetation, Cape Canaveral	0.2	0.13	
10–15 m trees, Cape Canaveral	0.4–0.7		
Deciduous trees <sup>b</sup>	0.015, 0.2, 1.0	0.04	
Orchards <sup>b</sup>	0.015, 0.2, 0.3		
Scots pine <i>Pinus sylvestris</i> ( $h = 18 \text{ m}$ ) <sup>c</sup>		0.069	0.69
Lodgepole pine <i>Pinus contorta</i> ( $h = 15 \text{ m}$ , 4 m tree spacing) <sup>d</sup>	1.0	0.067	
Coniferous forests, general ( $h = 10\text{--}28 \text{ m}$ ) <sup>e</sup>		0.02–0.16 (mean = 0.07)	0.67–0.68
27 m eucalyptus <sup>f</sup>	1.9–4.1	0.07–0.15	
Savannah scrub (25% trees, 65% dry grass, 10% burnt grass, sand)	0.4		

(Continued)

Table 11-1. Examples of Roughness Lengths for Various Surfaces and Associated Ratios of  $z_{om}/h$  (Continued)

Surface Description	$z_{om}, m$	$z_{om}/h$	$d/h$
Wyoming big sagebrush <i>Artemisia tridentata</i> ( $h = 0.8$ m) <sup>d</sup>	0.05 m	0.06	
Cotton (0.4–1.2 m) <sup>e</sup>	0.03–0.13	0.10	
Snap beans (0.1–0.6 m) <sup>f</sup>	0.05–0.2	0.08–0.5 (mean = 0.13)	
Maize (0.2–2 m) <sup>g</sup>	0.01–0.14	0.065	
Impervious urban <sup>h</sup>	1.0		
Bare rock, bare soil <sup>i</sup>	0.005		

<sup>a</sup>FAO-56<sup>b</sup>MORECS values by Hough and Jones (1997) for defoliated trees, trees at leaf emergence, and trees at full leaf, respectively<sup>c</sup>de Bruin and Moore (1985)<sup>d</sup>Zhao, W., and R. Allen, 2013, Univ. Idaho, via sonic anemometer<sup>e</sup>Jarvis et al. (1976)<sup>f</sup>Leuning and Attiwill (1978)<sup>g</sup>Pieri and Fuchs (1990)<sup>h</sup>Allen et al. (1995)<sup>i</sup>Jacobs et al. (1989)<sup>j</sup>MORECS value by Hough and Jones (1997)  
All others are from Brutsaert (1982)

Research shows that for many crops,  $d$  and  $z_{om}$  can vary considerably with wind speed. Szeicz et al. (1973) find  $z_{om}$  to range from under 0.01 m at  $1.5 \text{ m s}^{-1}$  to 0.07 m at  $5 \text{ m s}^{-1}$  for a crop of sorghum. The zero plane displacement,  $d$ , of flexible crops is particularly susceptible to varying wind speeds. In the PM method the estimate of aerodynamic resistance,  $r_a$ , is less sensitive to  $d$  when wind,  $T$ , and  $e$  measurements are taken at elevations greater than twice the crop height.

**Lengths of Scalars** In the single-layer Penman-Monteith application, the “bulk aerodynamic resistance,”  $r_{ah}$ , represents the total resistance between the heat and vapor exchange surfaces and a reference height,  $z$ , some vertical distance above the surface. The integration of  $r_{ah}$  begins at the roughness lengths for sensible heat and vapor transfer,  $z_{oh}$  or  $z_{ov}$ . In multilayer resistance-based applications (Figs. 11-1 and 11-2), additional in-canopy boundary layer resistances are employed that use eddy diffusion decay techniques without the need for  $z_{oh}$  or  $z_{ov}$ . Generally,  $z_{oh}$  and  $z_{ov}$  used in calculating  $r_{ah}$  have values less than  $z_{om}$  due to effects of bluff body transfer (pressure effects) on momentum transfer that affect the value of  $z_{om}$  but do not significantly affect values for  $z_{oh}$  and  $z_{ov}$ , for example Eqs. (11-9)–(11-16). Brutsaert (1982) suggests that  $z_{oh}$  and  $z_{ov}$  can range from values slightly greater than  $z_{om}$  for aerodynamically smooth surfaces, e.g., smooth soil or water, to  $z_{oh}/z_{om}$  and  $z_{ov}/z_{om}$  ratios of 1/7 to 1/12 for permeable rough surfaces, a category into which most vegetated surfaces fall. This manual suggests using

$$z_{oh} = z_{ov} = 0.1z_{om} \quad (11-30)$$

in bulk  $r_{ah}$  calculations for agricultural surfaces having somewhat dense vegetation. The ratios  $z_{oh}/z_{om}$  and  $z_{ov}/z_{om}$  are affected to some degree by the shape of the surface roughness elements and Reynold's number (Garratt and Hicks 1973). Thom (1972), Garratt and Hicks (1973), Brutsaert (1982), and Verma (1989) discuss in depth the relationship between  $z_{oh}$ ,  $z_{ov}$ , and  $z_{om}$ , where the sublayer Stanton number  $B^{-1}$  is used to represent the differences among the roughness lengths. Basically, the ratio  $z_{oh}/z_{om}$  decreases to very small values with increasing wind speed and roughness for nonpermeable rough surfaces such as plowed soil and rigid vegetation with large leaves such as beets, cabbage, or vineyards (Brutsaert 1982; Verma 1989). In those situations, momentum is transferred to the surface much more efficiently than heat and vapor due to pressure forces. In contrast,  $z_{oh}/z_{om}$  is somewhat constant for surfaces or vegetation having more porous or fibrous roughness elements, such as for grass, corn, and forests (Brutsaert 1982). For vegetation with sparse canopy, the ratio  $z_{oh}/z_{om}$  is highly affected by the mean source heights of heat and vapor in the canopy and the mean sink height for momentum (Qualls and Brutsaert 1996).

According to data summarized by Garratt and Hicks (1973), the following mean values can be used for general estimates of  $z_{oh}/z_{om}$  under conditions of neutral stability:

- Short grass and agricultural crops:  $z_{oh}/z_{om} = 0.08$  to  $0.14$  (mean =  $0.10$ );
- Pine forests:  $z_{oh}/z_{om} = 0.35$ ; and
- Lake evaporation:  $z_{oh}/z_{om} = 1$ .

Other observations include heterogeneous forests with 1-m tall grass understory where  $z_{oh}/z_{om} = 0.08$  (Garratt 1978). Ratios of  $z_{ov}/z_{om}$  can be expected to be similar.

Zhao et al. (2008) have conducted additional work on  $z_{oh}/z_{om}$  ratios, and simulation of  $z_{oh}/z_{om}$  ratios was done by Lhomme et al. (1997). The NCAR Weather Research and Forecasting (WRF) model's Noah land process submodel uses a formulation for  $z_{oh}/z_{om}$  that considers the Reynold's number and fractional density of vegetation (Zeng and Wang 2007):

$$z_{oh}/z_{om} = \exp[0.2(1-f)^2 R_e^{0.5}] \quad (11-31)$$

where  $f$  is fraction of green vegetation cover, and the Reynold's number is dimensionless:

$$R_e = \frac{(u^*) z_{om}}{v} \quad (11-32)$$

where  $u_*$  is friction velocity,  $\text{m s}^{-1}$  [Eq. (7-23)], and  $v$  is kinematic viscosity ( $\text{m}^2 \text{s}^{-1}$ ).

## Determinations from Wind Profile Measurements

**Roughness Lengths** Roughness length for momentum transfer,  $z_{om}$ , can generally be determined for unfamiliar surfaces from wind profile measurements. For most measurements, a recommended minimum of four anemometers are placed above the vegetation canopy with increased spacing between instruments with height to better sample the wind profile. Although two anemometers are sufficient to determine  $z_{om}$  using the following Eq. (11-33), measurements with four anemometers are recommended to confirm adherence of the wind profile to a logarithmic relationship during neutral periods and to verify integrity of the anemometers used to solve for  $z_{om}$  (Monteith and Unsworth 1990). Eq. (7-24) of Chapter 7 expresses  $u_*$  from wind speed measured at  $z$  height,  $u_z$ ;  $z_{om}$ ;  $d$ ; and integrated stability correction function  $\psi_{sm(z/L)}$  for momentum transfer:

$$u_* = \frac{k u_z}{\ln\left(\frac{z-d}{z_{om}}\right) - \psi_{sm(z/L)}} \quad (7-24)$$

where  $k$  is the von Kármán constant. By conservation of momentum,  $u_*$  can be assumed to be constant with  $z$ , so that Eq. (7-24) can be expressed as

$$u_* = \frac{ku_{z1}}{\ln\left(\frac{z_1-d}{z_{om}}\right) - \psi_{sm(z_1/L)}} = \frac{ku_{z2}}{\ln\left(\frac{z_2-d}{z_{om}}\right) - \psi_{sm(z_2/L)}}$$

If application of this equation is limited to nearly neutral conditions so that  $\psi_{sm(z/L)}$  can be assumed to be zero, the equation can be solved for  $z_{om}$ :

$$z_{om} = \exp\left[\frac{u_2 \ln(z_1 - d) - u_1 \ln(z_2 - d)}{u_2 - u_1}\right] \quad (11-33)$$

where  $u_2$  and  $u_1$  are wind speeds at  $z_2$  and  $z_1$  elevations above the ground surface and  $d$  is the zero plane displacement height.  $z_{om}$  in Eq. (11-33) has the same units as  $z$  and  $d$ , which is normally m.

Generally,  $z_{om}$  is determined from wind speed profile data for neutral conditions only, as stability or instability of the boundary layer profile will influence the wind profile shape. Neutral conditions can be verified by computing a discrete Richardson number,  $Ri$ , between the two sensor elevations as

$$Ri = \frac{g[T_2 - T_1 + \Gamma(z_2 - z_1)](z_2 - z_1)}{0.5(T_2 + T_1)(u_2 - u_1)^2} \quad (11-34)$$

where  $g$  is in  $\text{m s}^{-2}$ ,  $T_1$  and  $T_2$  are absolute air temperatures in K, at heights  $z_1$  and  $z_2$  (m) above the surface, and  $\Gamma$  is the dry adiabatic lapse rate ( $0.01 \text{ Km}^{-1}$ ). Values of  $T$  and  $u$  should be based on mean profile data, preferably involving periods of 30 min or less.  $\Gamma$  is usually ignored for investigations near the surface where  $(z_2 - z_1)$  is only a distance of a meter or two.

Generally, a range of  $-0.01 < Ri < 0.01$  is used to indicate neutral buoyancy (Monteith and Unsworth 1990). In other words, the temperature profile should be nearly constant with  $z$  so that  $H$  and buoyancy are nearly zero. An alternative to using  $Ri$  is to calculate the Monin-Obukhov stability length,  $L$ , given in Eq. (7-17). Near neutrality can be assumed to exist when  $-0.2 < z_2/L < 0.2$ . Measurements of  $u$  and  $T$  for profile analyses are normally averaged over periods of 30 min or less.

Values for  $z_{om}$  can also be computed by inverting Eq. (7-24) for friction velocity,  $u_*$ , where measurements for  $u_*$  are derived from high-frequency measurements by three-dimensional sonic anemometers. These systems

are becoming relatively commonplace and low cost. The integrated stability correction function  $\psi_{sm(z/L)}$  for momentum transfer can be solved using equations in Chapter 7.

Garratt (1980) and Cellier and Brunet (1992) present conclusive evidence that suggests that wind profile measurements must be made at elevations that are at least two to three times the canopy height or three times individual plant or tree spacing, whichever is greater, to obtain valid results from Eq. (11-33). Jacobs et al. (1989) recommend placing instruments above the  $d + 10z_{om}$  elevation. At elevations below those recommended, wind, temperature, and vapor density profiles deviate from the classic Monin-Obukhov profile shapes and application of Eq. (11-33) may underestimate the value for  $z_{om}$ . The minimum elevation applies to the lowest anemometer setting, so that sensor masts placed over tall vegetation must be quite high. The thickness of the "roughness sublayer" in which this problem occurs is greater for sparse canopies such as rangeland, arid land forests, and sparsely planted orchards so that the potential for having wind profile measurements within the roughness sublayer increases with decreased vegetation density. For more detailed information concerning this precaution, the reader can consult Cellier and Brunet (1992), Thom et al. (1975), Raupach (1979, 1994), Garratt (1980, 1992), Cellier (1986), van de Griend and van Boxel (1989), and Raupach et al. (1991, 1996).

**Zero Plane Displacement** When three or more measurements of wind speed are available, zero plane displacement,  $d$ , can be obtained under neutral stability conditions by combining Eq. (11-33) at two pairs of heights following Monteith and Unsworth (1990):

$$\ln(z_{om}) = \frac{u_2 \ln(z_1 - d) - u_1 \ln(z_2 - d)}{u_2 - u_1} = \frac{u_3 \ln(z_1 - d) - u_1 \ln(z_3 - d)}{u_3 - u_1} \quad (11-35a)$$

so that

$$\frac{(u_2 - u_1)}{(u_3 - u_1)} = \frac{u_2 \ln(z_1 - d) - u_1 \ln(z_2 - d)}{u_3 \ln(z_1 - d) - u_1 \ln(z_3 - d)} \quad (11-35b)$$

where  $u_1$ ,  $u_2$ , and  $u_3$  are wind speeds at  $z_1$ ,  $z_2$ , and  $z_3$  heights, and  $z$  and  $d$  have the same units. Eq. (11-35) is solved implicitly using a Newton secant or other solution method. Zhao et al. (2008) describe an iterative method to solve for both  $z_{om}$  and  $d$ . Again, the same precautions in minimum height of anemometer placement must be exercised for determination of  $d$  as are followed for  $z_{om}$ .

## 11.7 BULK SURFACE (STOMATAL) RESISTANCE

The inclusion of bulk surface resistance into the Penman-Monteith equation was a major advancement in estimating ET from specific crop surfaces. Surface resistance or conductance of vegetation and vegetation-soil complexes is a difficult process to model exactly. However, simplified methods have been developed that provide approximate estimates of bulk surface resistance that are useful in producing operational estimates of ET.

### Resistance and Leaf Area

**Factors Affecting Resistance** Stomatal resistance of leaves is a dynamic parameter that changes with sunlight illumination, vapor pressure deficit, leaf temperature, and soil water potential (Jarvis 1976; Stewart 1989; Price and Black 1989; Stewart and Verma 1992; Kelliher et al. 1995). For a single-layer model as the PM equation, the bulk surface resistance,  $r_s$ , represents the integration of resistance to vapor movement through leaf stomates, vapor diffusion from soil, and vapor transport within the canopy. For sparse crops, an integrated value for  $r_s$  is computed by considering resistances for exposed soil and vegetation in parallel, as is discussed in a later section. The single-layer PM equation should be considered as only an approximate estimate for ET from sparse vegetation or from crops during early development when the leaf-area index is less than 1.0 due to complexities in energy exchange between the soil and canopy. In these situations, the user should consider using multilayered equations (described earlier in Sections 11.2–11.5) or even the simpler, but potentially more robust,  $K_c ET_{ref}$  approach of Chapter 10.

For vegetation where  $LAI > 1$ , the effect of soil evaporation is generally low relative to transpiration and  $r_s$  is dominated by the vegetation. Under these conditions,  $r_s$  can usually be estimated using Eq. (8-9) with effective leaf area,  $LAI_{eff}$ , estimated from Eq. (8-10) or Eq. (8-11). For dense canopies,  $LAI_{eff}$  is the upper sunlit portion of the canopy where most heat and vapor transport activity occurs. Szeicz and Long (1969) and Allen et al. (1989, 1998) have used Eq. (8-10) to estimate  $LAI_{eff}$  for dense pine forest canopies, for wheat, and for grass and alfalfa reference surfaces. Eq. (8-11) may serve as a more universal estimate of  $LAI_{eff}$  for  $LAI$  ranging from sparse to very dense (Ben-Mehrez et al. 1992).

Parameter  $r_l$  in Eq. (8-9) is average stomatal resistance for a single LAI layer ( $LAI = 1$ ) characteristic of ambient soil water and other environmental factors such as  $R_s$ , VPD, and  $T$ . Monteith (1965, 1981) and Sharma (1985) suggest a value of  $r_l = 100 \text{ sm}^{-1}$  for many agricultural crops under mean daytime conditions. Allen et al. (1989) and Jensen et al. (1990) find  $r_l = 100 \text{ sm}^{-1}$  to approximate well for cool-season grass and alfalfa references for 24-hour calculation time steps. Valle et al. (1985) measure average

values of  $r_l = 120 \text{ sm}^{-1}$  for soybeans under ambient conditions. ASCE (2005) and Allen et al. (2005d) suggest  $r_l = 70 \text{ sm}^{-1}$  for hourly and shorter periods for well-watered grass and alfalfa references.

When stomatal conductance reducing functions,  $g(\text{env.})$ , introduced in a later section, are employed, then  $r_l$  can be estimated as  $r_l = r_{l_{\min}}/g(\text{env.})$ , where  $r_{l_{\min}}$  is a minimum or unconstrained  $r_l$  when all environmental parameters are at optimum levels [ $g(\text{env.}) = 1$ ], and where  $g(\text{env.})$  is the composite conductance reducing factor for various environmental parameters. For most vegetation,  $r_l$  is about 1.5 to 3 times the value for  $r_{l_{\min}}$  because  $R_s$ , VPD, and  $T$  are often at lower or higher levels than optimum for full stomatal opening (Kelliher et al. 1995).

Values for  $r_l$  for natural (nonagricultural) vegetation are likely to be substantially higher than those for agricultural crops due to selective breeding of the latter to maximize photosynthesis and biomass production. Some values for  $r_l$  in the literature are greater than the  $100 \text{ sm}^{-1}$  recommended here for agricultural crops because the value for  $r_l$  used here is intended to be congruent with the use of effective  $LAI_{\text{eff}}$  as described in Eq. (8-9). Leaf resistance is generally greater for trees than for agricultural crops. In conifers, stomatal pores are usually located at the bottom of an indentation in the leaf epidermis, which is filled with wax tubes, resulting in higher  $r_l$  relative to nonconifers. The larger  $r_l$  for conifers enables trees to avoid rapid dehydration due to generally large  $LAI$  and small aerodynamic resistance  $r_a$ . Jarvis et al. (1976) summarize reported measurements of  $r_l$  for various types of conifers. Minimum values of  $r_l$  range from 120 to  $300 \text{ sm}^{-1}$  for new needles of most conifer types to 1,100 to  $1,400 \text{ sm}^{-1}$  for 3 and 4 year-old needles (Table 11-2). Jarvis et al. (1976) calculate general ratios of  $r_s/r_a$  between 20 to 40 for Sitka spruce and 20 to 70 for Scots pine. Stewart (1988) reports similar values. These ratios contrast with ratios of  $r_s/r_a$  for field crops, which are much lower, often between 1 and 2 (Monteith 1965).

Irmak et al. (2008) scale measured and simulated  $r_l$  to bulk  $r_s$  using photon flux densities on individual leaves in a maize canopy with somewhat good comparison with  $r_s$  retrieved by inverting the PM equation using ET measured by the Bowen ratio. Stability correction was not utilized in the calculation of aerodynamic resistance, so some bias in retrieved  $r_l$  likely existed. That study did document that effectiveness of total leaf area of a dense canopy changes with leaf area and with sunlight intensity.

**Estimating Leaf Area** Leaf area indices can often be estimated for various vegetation types as a function of mean plant height, shape, and stand density. Due to the wide diversity in canopy structures and leaf design,  $LAI$  vs.  $h$  relationships are unique to specific vegetation types. Allen et al. (1989) and ASCE (2005) suggest Eq. (8-12) for dense stands of clipped grass and Eq. (8-13) for alfalfa. The equation for clipped grass indicates a

Table 11-2. Typical Values for the Stomatal Resistance per Unit Leaf Area,  $r_l$ , and Bulk Stomatal Resistance,  $r_s$ , for Various Canopy Types; Parameters  $r_{l_{min}}$  and  $r_{s_{min}}$  Are Minimum Daytime Values<sup>a</sup> with  $g(\text{env.}) = 1$

Canopy Type	$r_l \text{ sm}^{-1}$	$r_{l_{\min}} \text{ sm}^{-1}$	$r_s \text{ sm}^{-1}$	$r_{s_{\min}} \text{ sm}^{-1}$	Reference
<b>Forest</b>					
Tropical					
<i>Ficus Benjamin</i>	45	100–160	60 (LAI=5)	50	Shuttleworth (1984) Shuttleworth (1989) Dorman and Sellers (1989) Bailey et al. (1993) Verma et al. (1986)
<b>Deciduous</b>					
Amazon broadleaf	150	100–150	90	120	Perrier (1982) Choudhury and Monteith (1986)
Aspen	400	120	90	Dai et al. (2004)	Sikka (1993)
Boreal aspen-hazelnut			65		Blanken and Black (2004)
Aspen overstory			100		Blanken and Black (2004)
Hazelnut understory			200		Blanken and Black (2004)
Eucalyptus	200–400	200–400	250	100	Körner et al. (1979) Körner et al. (1979)
Maple	400–700	400–700	250	60	Bernacchi et al. (2003)
Poplar	100	100	60		

(Continued)

Table 11-2. Typical Values for the Stomatal Resistance per Unit Leaf Area,  $r_l$ , and Bulk Stomatal Resistance,  $r_s'$  for Various Canopy Types; Parameters  $r_{l_{min}}$  and  $r_{s_{min}}$  Are Minimum Daytime Values<sup>a</sup> with  $g(\text{env.}) = 1$  (Continued)

Canopy Type	$r_l \text{ sm}^{-1}$	$r_{l_{min}} \text{ sm}^{-1}$	$r_s \text{ sm}^{-1}$	$r_{s_{min}} \text{ sm}^{-1}$	Reference
<b>Coniferous</b>					
<i>Pinus resinosa</i> (Pine) current year needles <sup>b</sup>	310				Waggoner and Turner (1971), as cited by Jarvis et al. (1976)
1 year old	430				
2 year old	860				
3 year old	890				
4 year old	1,100				
<i>Picea sitchensis</i> (Sitka spruce) current year needles <sup>b</sup>	120				Ludlow and Jarvis (1971) and Neilson et al. (1972) as cited by Jarvis et al. (1976)
1 year old	480				
2 year old	650				
3 year old	1,400				
Mean	300	80	40 (LAI = 12)	Milne (1979)	
<i>Pseudotsuga menziesii</i> (Douglas fir)	120–300				Jarvis et al. (1976)
General conifers	200	160	35	70	Humphreys et al. (2002)
					Dekker et al. (2000)
					Jarvis et al. (1976)
					Shuttleworth (1989)
					Noilhan and Planton (1989)
					Dorman and Sellers (1989)
					Kelliher et al. (1993)
					30–60

<b>Other</b>		200–300	Perrier (1982)
Savannah	100	30	Shuttleworth (1989)
Shrubs	240	100	Garratt (1978)
Sagebrush ( <i>Artemisia tridentata</i> )	1,000		Sikka (1993) Körner et al. (1979)
Mesophytes <sup>c</sup>	100–200		Gates (1980)
Xerophytes <sup>d</sup>		150–500	Cowan and Milthorpe (1968)
Grassland		800–2,000	Cowan and Milthorpe (1968)
	30–50	40	Dorman and Sellers (1989)
		40–50	Kelliher et al. (1993)
		(LAI=1.3)	
Kansas prairie big bluestem ( <i>Andropogon gerardii</i> )		40 (LAI=3)	Stewart and Verma (1992)
Indian grass ( <i>Sorghastrum nutans</i> )		65 (LAI=1.3)	Stewart and Gay (1989)
Purple false brome ( <i>Brachypodium distachyon</i> )			Ryu et al. (2008)
Clover, lesser hop Trefoil ( <i>Trifolium dubium</i> )		90	Perrier (1982)
temperate		100	
Subtropical		200	

*(Continued)*

Table 11-2. Typical Values for the Stomatal Resistance per Unit Leaf Area,  $r_l$ , and Bulk Stomatal Resistance,  $r_s'$  for Various Canopy Types; Parameters  $r_{l_{min}}$  and  $r_{s_{min}}$  Are Minimum Daytime Values<sup>a</sup> with  $g(\text{env.}) = 1$  (Continued)

Canopy Type	$r_l \text{ sm}^{-1}$	$r_{l_{min}} \text{ sm}^{-1}$	$r_s \text{ sm}^{-1}$	$r_{s_{min}} \text{ sm}^{-1}$	Reference
Crops, general	50–320		40–130	20–75	Slatyer (1967) Perrier (1982)
			30–35	20–150 30	Sellers and Dorman (1987) Noilhan and Planton (1989) Dorman and Sellers (1989)
Grain sorghum	100 200	150	100–140 (LAI = 2)		Monteith (1965), Sharma (1985) Szeicz et al. (1973)
Snap beans ( <i>Phaseolus vulgaris</i> )		150 130			Choudhury and Monteith (1986) Choudhury and Monteith (1986)
Soybeans	120			50 (LAI = 3.4) 40 25 (LAI = 3.5)	Valle et al. (1985) Grant and Baldocchi (1992) McGinn and King (1990) Jacobs et al. (1989) Rochette et al. (1991)
Maize	70 70 70	80		40 70	Körner et al. (1979)
Barley	160 150–250 (young to old)	45	40		Szeicz and Long (1969)
Wheat			70 50	30	Perrier (1982) Hatfield (1985)

Alfalfa	80	50	50	60	Perrier (1982)
					Choudhury and Idso (1985)
					Cowan and Milthorpe (1968)
					Perrier (1982)
Cotton					McGinn and King (1990)
					Allen et al. (1989); ASCE (2005)
Sugar beets					Stanhill (1976)
					Cowan and Milthorpe (1968)
					Körner et al. (1979)
					Perrier (1982)
Citrus					Szeicz and Long (1969)
0.15 m clipped grass					Pruitt (personal communication, 1994)
0.10 to 0.12 irrig., clipped grass					Allen et al. (2005); ASCE (2005)

<sup>a</sup> $r_{l_{min}}$  and  $r_{s_{min}}$  represent minimum daytime values of  $r_l$  and  $r_s$ , which occur when all environmental variables are optimum. For example, full levels of irradiance, low vapor pressure deficit, optimum leaf temperature, etc. These levels will occur in dense canopies only for sunlit leaves and only when all other variables are optimum.  $r_{l_{min}}$  and  $r_{s_{min}}$  should only be used in conjunction with the  $g()$  functions.

<sup>b</sup>Current year, 1, 2, 3, and 4 year refer to the age of needles measured.

<sup>c</sup>Mesophytes are tropical and temperate plants that need plentiful water for survival.

<sup>d</sup>Xerophytes are plants structurally adapted for life and growth with a limited water supply.

Source: Data from Garratt (1992) and other sources

proportional increase in leaf area with increasing height of grass due to uniform vertical leaf extension with height. This would probably not be the case with nonclipped range or pasture grass, where much of the mature plant height may be due to stem and seed head extension rather than leaf extension. Eq. (8-13) for alfalfa suggests an exponentially decreasing rate of increase in  $LAI$  with increase in  $h$  as stem extension with less leaf development occurs in maturing plants. Alfalfa is generally grown in densely planted stands so that for  $h$  greater than approximately 0.2 m, leaf and stem development is essentially one-dimensional (vertical).

For row crops where plants are somewhat round and extend similarly in width and height, a quadratic relationship can be employed, such as  $LAI = 10 h^2$  as suggested by Allen et al. (1996) for snap beans (*Phaseolus vulgaris*) planted in 0.6-m rows. Height is limited to  $h \leq 0.75$  m.

The following relationships can be derived for maize, cotton, and grass prairie based on data presented by Jacobs et al. (1989), Pieri and Fuchs (1990), and Verma et al. (1992), respectively: for tall maize,  $LAI = 1.6 h$ ; for cotton,  $LAI = 2.5 h$  for  $h \leq 0.4$  m and  $LAI = 3.4 + 2.4 \ln(h)$  for  $0.4 < h < 1.2$  m; for rain-fed grass prairie in Kansas,  $LAI = 5 h$  before leaf senescence. The utility of basing  $LAI$  on  $h$  is that  $h$  is a relatively easy parameter to observe or to collect and is required for estimating  $z_{om}$ . In rangeland and other situations having sparse plant density, plant density may need to be added to  $LAI - h$  relationships as discussed in the following paragraph. Tasumi (2003), using LAI and  $h$  data from J. L. Wright (USDA-ARS, Kimberly), established a somewhat universal, linear relationship between LAI and  $h$  for potatoes, snap beans, sugar beets, peas, wheat, and alfalfa as  $LAI = 6.7 h$ . Field corn had less LAI for the same  $h$  as other Idaho crops where  $LAI = 3 h$ . Estimated LAI was limited to  $\leq 6$  in all cases for agricultural crops.

Leaf-area indices for rangelands, brushlands, and forests vary widely depending on grass, shrub or tree density, maturity, and type. Rauner (1976) reports total LAI for deciduous forests ranging from 4 to about 7. Jarvis et al. (1976) lists LAI for 10 conifer species based on projected canopy area at midday. The LAI per projected tree area ( $LAI_{pa}$ ) ranges from 2.5 to 4.5 for many pine species and ranges from 8 to 10 for *Picea abies* and *Picea sitchensis* species of spruce. Jarvis et al. (1976) calculate an areal average LAI as

$$LAI = LAI_{pa} A_s S_d \quad (11-36)$$

where  $LAI_{pa}$  is the projected area LAI (LAI based on the shaded ground area during midday),  $A_s$  is the midday shaded area per plant ( $m^2 \text{ plant}^{-1}$ ), and  $S_d$  is stand density ( $\text{plants m}^{-2}$ ).

For annual types of vegetation, the increase in  $LAI$  during the growing season can often be expressed as a function of time or as a function of

thermal units, similar to the approach used for crop coefficients. When  $LAI$  or  $h$  functions are expressed in terms of  $LAI/LAI_{max}$  and  $h/h_{max}$ , respectively, where  $LAI_{max}$  is the maximum  $LAI$  of green leaves during the season and  $h_{max}$  is the maximum obtained plant height, the developed functions are more able to transfer to other cultivar types having different values for  $LAI_{max}$  and  $h_{max}$ .

### General Bulk Surface Resistance Values

**General Daytime Values** Transpiration increases with increasing  $LAI$  until nearly complete closure of the canopy. For agricultural crops, maximum transpiration is often attained after  $LAI = 3$  (Ritchie 1972; Tanner and Jury 1976; Wright 1982; Sharma 1985). Increases in  $LAI$  above 3 generally increase  $ET$  little, depending on canopy structure, as most available energy (radiation and sensible heat) has been converted into  $\lambda E$  within the canopy when  $LAI > 3$ . This provides the rationale behind using Eq. (8-10) or Eq. (8-11) for estimating  $LAI_{eff}$ . In general, the PM equation estimates show little increase in  $ET$  for  $LAI > 3$ .

Table 11-2 lists typical values for  $r_s$  and  $r_l$  reported in the literature. Additional values for  $r_s$  that have been used by the British Meteorological Office rainfall and evaporation calculation system (MORECS) are listed in Table 11-3 and mean "green"  $LAI$  values are listed in Table 11-4 (Hough and Jones 1997). Values for  $r_l$  in column 1 and  $r_s$  in column 3 of Table 11-2 represent constrained surface resistance for a unit  $LAI$  and complete canopies, respectively, and are intended for use in hourly, daily, or monthly  $ET$  calculations where  $g()$  functions are not employed. Values for  $r_{l_{min}}$  and  $r_{s_{min}}$  in Table 11-2 represent minimum  $r_l$  and  $r_s$  where all environmental variables (namely  $R_s$ ,  $T$ ,  $VPD$ , and  $\theta$ ) are at optimum levels and should only be used in conjunction with the  $g()$  functions.

The MORECS  $r_s$  values in Table 11-3 were developed to support direct application of the PM equation across Great Britain on a 6-km grid. Parallel resistance calculations were used to integrate effects of soil evaporation and plant transpiration as discussed in a following section. Calculations in MORECS were made on daily time steps for daylight periods, so that values of  $r_s$  in Table 11-3 represent general daytime values of  $r_s$ . Mean monthly values of  $r_s$  listed for grass and riparian vegetation are low during spring months with leaf development and increase late in the growing season as leaves senesce (die off) or go dormant. Additional values for  $r_l$ , which were summarized from a wide range of literature sources, can be found in Körner et al. (1979) in addition to Table 11-2. Because values for  $r_l$  and  $r_s$  are typically solved by inversion of ET or AFIB models, values in Tables 11-2 and 11-3 can be biased toward the procedure used to determine them.

For hourly or shorter calculation time steps, adjusting  $r_l$  for levels of  $R_s$ ,  $VPD$ ,  $T$ , and  $\theta$  as described in a following section may be useful.

Table 11-3. Generalized Daytime Values of Bulk Surface Resistance for Dense Green Cover in Great Britain Having Adequate Soil Water

Type of Cover	$r_s, \text{ sm}^{-1}$
Grass and riparian vegetation	80, 80, 60, 50, 40, 60, 60, 70, 70, 70, 80, 80 (Jan–Dec)
Cereals	40
Potatoes and sugar beets	40
Deciduous trees	80
Conifers	70 <sup>a</sup>
Upland vegetation	120 (Jan–Mar), 100 (Apr–Sept), 120 (Oct–Dec)
Bare soil	100
Water	0

<sup>a</sup>At zero vapor pressure deficit and 20°C and assumed independent of soil surface resistance

Source: Data from Hough and Jones (1997)

Table 11-4. Maximum Leaf-Area Indices for Dense Green Cover in Great Britain as Used in MORECS

Type of Cover	Green Leaf-Area Index
Grass and riparian vegetation	2.0, 2.0, 3.0, 4.0, 5.0, 5.0 5.0, 5.0, 4.0, 3.0, 2.5, 2.0 (Jan–Dec)
Cereals	5.0
Potatoes	4.0
Sugar beets	4.0
Deciduous trees	6.0
Conifers	6.0

Source: Data from Hough and Jones (1997)

For hydrologic water balance studies, where water balances and  $ET$  are estimated on daily or longer calculation time steps, mean 24-hour or daytime values for  $r_s$  can be used where  $r_s$  is estimated as the quotient of mean values for  $r_l$  and effective leaf area, with additional adjustment for limited soil water and incidence of wet soil among foliage following rain or irrigation events.

**Hourly or Shorter Period Values** For most vegetation, leaf resistance decreases with increasing irradiance (solar radiation) and may increase

with increasing vapor pressure deficit. In addition, leaf resistance increases with decreasing soil water due to partial stomatal closure. Jarvis (1976), Stewart (1988, 1989), Price and Black (1989), Stewart and Verma (1992), Daamen et al. (1998), and Ortega-Farias et al. (2005, 2010) have proposed computing bulk surface resistance for short time periods in terms of meteorological variables and soil water deficit. Boegha et al. (2000) utilized satellite to estimate bulk surface resistance. Generally computations are expressed in terms of bulk surface conductance,  $g_s$ , which is the reciprocal of  $r_s$  ( $g_s = 1/r_s$ ). Monteith (1995) and Mott and Parkhurst (1991) have suggested that stomata and  $g_s$  may respond (decrease) primarily with the transpiration rate itself, rather than vapor pressure deficit. This suggests that plant systems may control maximum water fluxes through the root-stem-leaf systems. However, because potential transpiration is highly controlled by solar radiation, temperature, and vapor pressure deficit, a strong correlation is observed between  $g_s$  and these parameters, and behavior of  $g_s$  may be better explained by them.

A widely used surface conductance model proposed by Jarvis (1976) uses a multiplicative means for incorporating the effects of specific environmental factors and is commonly used with both the single-layer and multilayer Penman-Monteith models (Zhao et al. 2006). Stewart (1989) expresses the Jarvis function as

$$g_s = g_{\max} g(\text{env.}) = g_{\max} [g(LAI), g(R_s), g(VPD), g(T), g(\theta)] \quad (11-37)$$

where  $g_{\max}$  is the maximum bulk surface conductance when all other functions are not limiting. Functions  $g(LAI)$ ,  $g(R_s)$ ,  $g(VPD)$ ,  $g(T)$ , and  $g(\theta)$  represent reducing functions for leaf area, solar radiation, vapor pressure deficit, air temperature, and soil water, respectively. Variable  $g(\text{env.})$  represents the multiplicative effect of the individual functions. All reducing functions in Eq. (11-37) are limited by  $0 \leq g() \leq 1$ , including the cumulative  $g(\text{env.})$ . The form of Eq. (11-37) assumes that each environmental parameter will independently reduce  $g_s$  (increase  $r_s$ ), with the reduction accelerated by changes in other parameters.

Price and Black (1989) present an alternative equation to Eq. (11-37) that finds better agreement with measured data when the reduction in  $g_s$  is based on only the most limiting environmental parameter. The equation suggested by Price and Black is

$$g_s = g_{\max} g(\text{env.}) = g_{\max} \{\min[g(LAI), g(R_s), g(VPD), g(T), g(\theta)]\} \quad (11-38)$$

where the  $g()$  functions are the same as those defined for Eq. (11-37) and are limited to  $0 \leq g() \leq 1$ . In the examples provided near the end of this chapter, the form of Eq. (11-37) is employed.

When  $g_{max}$  is not measured,  $g_{max}$  can be estimated as  $g_l LAI_{max\ eff}$ , where  $LAI_{max\ eff}$  is maximum effective leaf area, estimated using Eq. (8-10) or (8-11) and  $g_l$  is the maximum stomatal conductance per unit leaf area in the same units as  $g_{max}$ . Estimates of  $g_l$  can be made from Table 11-2, where  $g_l = 1/r_{lmin}$ . In addition,  $g_{max}$  can be estimated from Tables 11-2 and 11-3 where  $g_{max} = 1/r_{smin}$ . Values for  $g_l$  and  $g_{max}$  decrease with leaf age (senescence), as noted in Table 11-2 for conifer needles over a multiyear period. Conductances of leaves of annual plants may decrease with time through the growing season (Burrows and Milthorpe 1976), especially if damage from insects, environmental stress (soil water and air temperature), and disease or air pollution occurs.

Forms of reducing functions that have been suggested for use in Eqs. (11-37) and (11-38) include the following series of equations. For example, for  $g(LAI)$  Stewart (1989) proposes

$$g(LAI) = \frac{LAI_{eff}}{LAI_{max\ eff}} \quad (11-39)$$

where  $LAI_{max\ eff}$  is the maximum value of  $LAI$  during the year. The values for  $LAI_{eff}$  and  $LAI_{max\ eff}$  in Eq. (11-39) are "effective"  $LAI$ , as defined in Eq. (8-10) or (8-11), to account for effects of shading on  $r_a$  and  $r_l$  within tall, dense canopies and the potential for nonlinearity of  $LAI_{max}$  relative to total  $LAI$  [Eq. (8-11)].

For a surface conduction based on solar radiation,  $g(R_s)$ , Stewart (1988, 1989) proposes

$$g(R_s) = \frac{R_s(1,000 + K_R)}{1,000(R_s + K_R)} \quad (11-40)$$

where  $R_s$  is global shortwave radiation in  $\text{W m}^{-2}$ , and  $K_R$  is an empirical factor ranging from 40 to 100  $\text{W m}^{-2}$  for Scots pine (*Pinus sylvestris*) (Stewart 1988). Zhao et al. (2006) use  $K_R = 400 \text{ W m}^{-2}$  for agricultural crops. The estimate for  $g(R_s)$  reaches 0.8 at  $R_s = 130, 270$ , and  $530 \text{ W m}^{-2}$  for values of  $K_R = 40, 100$ , and  $400 \text{ W m}^{-2}$ . Therefore, a higher value for  $K_R$  indicates increasingly higher levels of  $R_s$  required to fully open stomates.

Price and Black (1989) propose

$$g(R_s) = 1 - e^{-0.003R_s} \quad (11-41)$$

for a 22-year-old stand of Douglas fir (*Pseudotsuga menziesii*) where  $R_s$  is in  $\text{W m}^{-2}$ .

Stewart (1988, 1989) proposes a function for predicting effects of specific humidity deficit on  $g()$ , which in terms of vapor pressure deficit is expressed as

$$g(VPD) = 1 - K_{VPD} VPD \quad \text{for } 0 < VPD < VPD_c \quad (11-42)$$

$$g(VPD) = 1 - K_{VPD} VPD_c \quad \text{for } VPD \geq VPD_c \quad (11-43)$$

with  $K_{VPD} = 0.50 \text{ kPa}^{-1}$  and  $VPD_c$ , a threshold vapor pressure deficit, = 1.5 kPa for Scots pine. Stewart and Gay (1989) find  $K_{VPD} = 0.12$  to 0.19  $\text{kPa}^{-1}$  for rain-fed grass prairie in Kansas. Zhao et al. (2006) use  $K_{VPD} = 0.41$  for short vegetation and  $K_{VPD} = 0.24 \text{ kPa}^{-1}$  for tall vegetation in applications to the Mekong River basin. Price and Black (1989) propose

$$g(VPD) = 2.24e^{(-1.6VPD^{0.45})} \quad (11-44)$$

for Douglas fir, where  $g(VPD) \leq 1$ . Kelliher et al. (1993) propose a means for computing  $VPD$  at the leaf surface, which eliminates effects of  $r_a$  on the decoupling of the  $g(VPD)$  vs.  $VPD$  relationships that are based on  $VPD$  computed above the canopy. These adjustments can improve the consistency and transferability of the aforementioned  $VPD$  relationships (Blanken and Black 2004).

For air temperature, Stewart (1988, 1989) proposes a relationship after Jarvis (1976):

$$g(T) = \frac{(T - T_L)(T_H - T)^a}{(K_T - T_L)(T_H - K_T)^a} \quad (11-45)$$

where

$$a = \frac{(T_H - K_T)}{(K_T - T_L)} \quad (11-46)$$

and  $T$  is air temperature in  $^{\circ}\text{C}$ ;  $T_L$  and  $T_H$  represent lower and upper limits of stomatal activity, where  $T_L$  is taken as  $0^{\circ}\text{C}$  and  $T_H$  as  $40^{\circ}\text{C}$  by Stewart (1988) for a Scots pine forest; and  $K_T$  is an empirical “optimum” conductance temperature fitted from field data.  $K_T$  ranges from 17 to  $19^{\circ}\text{C}$  for Scots pine. Articles by Ritchie and NeSmith (1991) and Norman and Arkebauer (1991) suggest values of  $T_L$ ,  $K_T$ , and  $T_H$  equal to about 0, 25, and  $40^{\circ}\text{C}$  for wheat; 12, 35, and  $48^{\circ}\text{C}$  for corn; and 5, 28, and  $46^{\circ}\text{C}$  for soybeans. Information in McArthur et al. (1975) suggests values of 16, 27, and  $35^{\circ}\text{C}$  for cotton. Noilhan and Planton (1989) published alternative formulations for  $g(R_s)$ ,  $g(VPD)$ ,  $g(T)$ , and  $g(\theta)$ .

Conductance functions ( $g_s = 1/r_s$ ) based on soil water,  $\theta$ , are generally used in hydrologic studies as surrogates for more direct and perhaps accurate functions based on leaf water potential or soil water potential. The surrogate  $g(\theta)$  functions are used because estimates of  $\theta$  are easily made

available from soil water balance calculations, whereas leaf water and soil water potentials must be measured or inferred from soil characteristic curves and plant models. For operational  $ET$  estimates,  $g(\theta)$  is adequate for predicting the reduction in  $ET$  with reduction in soil water availability.

For the effect of decreasing soil water, three primary functions are recommended. The first is a function similar to that used by Stewart (1988), which is of the form

$$g(\theta) = 1 - e^{-K_\theta \theta} \quad (11-47)$$

where  $K_\theta$  is an empirical factor equal to about 6.7 for Scots pine. A second form of the function is by Stewart and Verma (1992)

$$g(\theta) = \frac{1 - e^{-K_\theta \theta_e}}{1 - e^{-K_\theta}} \quad (11-48)$$

where  $K_\theta$  ranges from 0.25 to 0.12 for grass prairie. Variable  $\theta_e$  in Eqs. (11-47) and (11-48) represents the effective fraction of available soil water, calculated as

$$\theta_e = \frac{\theta - \theta_{wp}}{\theta_{fc} - \theta_{wp}} \quad (11-49)$$

where  $\theta$  is the mean volumetric soil water in the root zone in  $\text{m}^3 \text{m}^{-3}$ ,  $\theta_{wp}$  is the mean volumetric soil water at wilting point or the lower limit of soil water extraction by plant roots in  $\text{m}^3 \text{m}^{-3}$  (Table 7-1), and  $\theta_{fc}$  is the mean volumetric soil water at field capacity or the drained upper limit in  $\text{m}^3 \text{m}^{-3}$  (Table 7-1).

The third  $g(\theta)$  function is a sinusoidal relationship (Allen et al. 1996; Hatfield and Allen 1996):

$$g(\theta) = K_{sf} \theta_e - \frac{\sin(2\pi\theta_e)}{2\pi} \quad (11-50)$$

where  $g(\theta) \leq 1$ , and  $\theta_e$  is defined as in Eq. (11-49).  $K_{sf}$  is an empirical "tenacity" factor ( $K_{sf} \geq 1$ ) that describes the ability of plants to extract soil water before any reduction in  $g(\theta)$ .  $K_{sf}$  ranges from 1 for sensitive plants to 1.5 for moderately sensitive plants to 3 for insensitive (tenacious) plants. The value for  $g(\theta)$  from Eq. (11-50) must be limited to less than or equal to 1 during computations.

Eq. (11-50) predicts values for  $g(\theta)$  that reduce slowly from 1 at high levels of  $\theta_e$ , reaching maximum rates of reduction near  $\theta_e = 0.5$ , and that approach 0 when  $\theta_e$  is approximately 0.2 (Figure 11-4). This type of response is realistic, as most plants leave stomates nearly wide open at

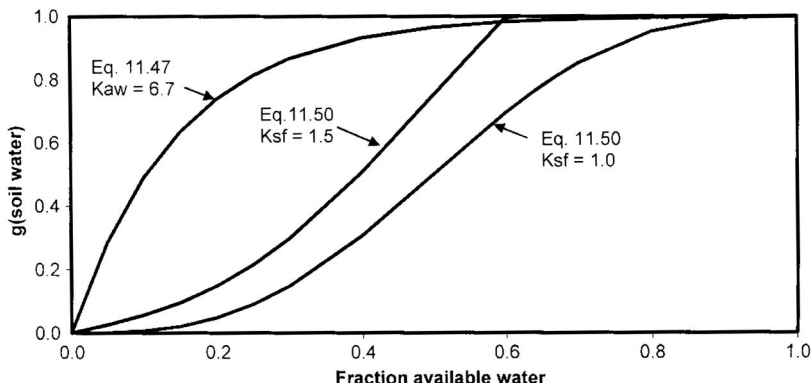


Fig. 11-4. Surface conduction functions for available soil water based on Eqs. (11-47) and (11-50) ( $K_{aw}$  is the same as  $K_\theta$ )

high levels of  $\theta_e$  (all other environmental factors at optimum) to maximize transpiration and photosynthesis, but close stomates almost completely before  $\theta_e$  approaches  $\theta_{wp}$ , and then "hold on" for sometimes long periods of low  $\theta_e$ , transpiring at low subsistence rates controlled by diffusion through nearly closed stomates and through the leaf epiderm (Turner 1979; Jones 1979; Burrows and Milthorpe 1976). In some situations, the user may wish to reduce the value for  $K_{sf}$  to 1.0 during periods having high ET rates to reflect difficulty of low soil hydraulic conductivity in supplying high ET rates. Sene (1996) uses a direct exponential equation for soil surface resistance as  $r_{sse} = 20(\theta/\theta_s)^{-2.3}$ ,  $\text{sm}^{-1}$ , for bare soil under a sparse grape canopy in Spain, where  $\theta$  and  $\theta_s$  are water content and saturation water content of the upper few cm of soil. Calvet et al. (1998) and Ortega-Farias et al. (2010) set  $g(\theta) = \theta_e$ .

The characteristics of Eqs. (11-47) to (11-50) do not conform to those of the  $K_s$  function used in the crop coefficient approach [Eqs. (10-4) and (10-6)], because  $g_s$  can reduce (and  $r_s$  increase) by nearly 40% in many agricultural situations before significant reductions in  $\lambda E$ , as estimated by the PM equation, occur. Effects of applying Eqs. (11-47) to (11-50) in a daily soil water balance are illustrated in a following section.

Applications of both approaches for reducing  $ET$  ( $g_s$  vs.  $\theta$  and  $K_s$  vs.  $\theta$ ) are conservative, in that they are both based on a soil water balance. Therefore, errors in over- or underestimating  $g_s$  or  $K_s$  will generally cause smaller relative error in estimated  $ET_a$  over long periods in low rainfall areas, where generally all precipitation evaporates during the growing season. Therefore, in an arid or semiarid situation, error in  $g_s$  or  $K_s$  may affect the estimated timing in  $ET$  reduction but may not significantly affect the total estimate of cumulative  $ET$ . This may not be the case in subhumid

regions, where soil water deficits occur over short time periods, so that errors in the nature of the  $g(\theta)$  and  $K_r(\theta)$  functions are more critical.

A final environmental characteristic that can affect the value for  $g_s$  is the concentration of carbon dioxide. Some studies conclude that as global concentrations of CO<sub>2</sub> increase, values for  $g_s$  may decrease in partial response to the increasing CO<sub>2</sub> levels (de Bruin and Jacobs 1993; Bernacchi et al. 2007). However, the decreases determined for  $g_s$  have generally been small and variable among experiments. Bernacchi et al. (2003) provide a good review of experimental literature on  $g_s$  vs CO<sub>2</sub> studies. Jacobs and de Bruin (1997) introduce methods based on plant physiology, where a correlation relationship between the leaf stomatal conductance and the net photosynthetic rate at leaf scale is used to upscale conductance from a leaf to canopy. The latter method is able to incorporate effects of CO<sub>2</sub> concentrations on stomatal conductance and thus transpiration and direct effects of photosynthetically active radiation (PAR) on primary productivity rate, leaf surface temperature, and vapor pressure deficit.

**Minimum Stomatal Conductance** Utilization of some of the  $g()$  functions described in this section can result in  $g() = 0$ , notably for Eq. (11-39) (for  $LAI = 0$ ), Eqs. (11-40) and (11-41) (for  $R_s = 0$ ), and Eq. (11-45) (for  $T \leq T_L$  or  $T \geq T_H$ ). However,  $g() = 0$  implies that total surface conductance,  $g_s = 0$  so that  $r_s$  is infinity. This never occurs in nature (except perhaps in the desert), because all vegetation will have some cuticular conductance (about 0.0003 m s<sup>-1</sup> per unit LAI) (Rochette et al. 1991). In addition, a minimum residual  $g_s$  (or maximum residual  $r_s$ ) must be retained to account for evaporation from soil beneath vegetation, for example, by making use of Eq. (11-51) presented in the next section. As indicated in a later section,  $r_s$  is about 50 sm<sup>-1</sup> for moist bare soil and exceeds 2,000 sm<sup>-1</sup> for dry soil. Therefore, depending on the soil surface soil water conditions and the amount of transfer of sensible heat and radiation through the vegetation cover to the soil, some residual  $g_s$  should be specified even for dense vegetation. In analyzing  $ET$  data from Davis for grass irrigated six days earlier, Pruitt (personal communication, 1994) found nighttime values for  $r_s$  averaging almost 200 sm<sup>-1</sup>. This was during a 2-h period around midnight, [ $R_s$  and  $g(R_s) = 0$ ], and yet with a 5-m s<sup>-1</sup> wind at 2 m, 20°C air temperature, an RH of 60%, and a VPD of 0.95 kPa,  $ET$  averaged 0.08 mm h<sup>-1</sup>. A value of  $r_s = 200$  sm<sup>-1</sup> is also recommended in the ASCE (2005) standardization for reference ET during nighttime and is equivalent to a minimum  $g_s$  of 0.005 m s<sup>-1</sup>. Pruitt (personal communication, 1994) used the ASCE standard value during nighttime periods whenever  $g_{max} g(env.)$  fell below this value. When soil surface water is measured or can be predicted by a simulation model (using a soil surface layer balance or time since wetting), then the minimum value for  $g_s$  can be varied to fit the actual soil water conditions.

**Applications** Other surface conductance or surface resistance functions have been proposed such as those by Szeicz and Long (1969), Szeicz et al. (1973), Hatfield (1985), and Choudhury (1983, 1989). In general, unique "K" coefficients should be determined for  $g()$  functions for specific vegetation types. Stewart (1988) demonstrates difficulty in applying some  $g()$  coefficients among different years for the same type of vegetation.

Improvements in application of the  $g(T)$  and  $g(VPD)$  functions can be made when surface temperature and VPD at the leaf surface are used rather than  $T$  and VPD at some reference height (Collatz et al. 1991; Dickinson et al. 1991; Blanken and Black 2004), because the leaf responds most directly to environmental conditions at the leaf surface rather than to conditions in the boundary layer above. However, this increases the difficulty and computational complexity involved in applying the PM equation, because one must conjunctively and iteratively utilize the energy balance equation [Eq. (4-1)] along with the PM equation to solve for  $H$  and then  $T_o$  and  $g(T_o)$ .

Dickinson et al. (1991) describe three regional ET models that employ various forms of the  $g()$  functions described in this section. These models were used as components of general circulation models (GCM) to assess effects of climate change. Misson et al. (2004) provide additional testing for pine forests. The Jarvis algorithm [Eq. (11-37)] has been shown to perform well across many different forest types (Massman and Kaufmann 1991; Bosveld and Bouten 2001), including drought-stressed ecosystems (Running 1994). Allaway and Milthorpe (1976) and Burrows and Milthorpe (1976) provide reviews of mechanics and processes of stomatal conductance and environmental interactions.

All  $g()$  functions that affect the value of  $g_s$  should be utilized in estimating  $g(env.)$ , because the absence of any one of the parameters may bias estimates of  $g_s$  upward and result in overestimation of  $ET$ . Note that in Table 11-2, values for  $r_l$  [that represent average  $g(env.)$  conditions] are generally two to three times the values given for  $r_{l_{min}}$  for the same type of vegetation. Therefore, one should expect, under normal conditions, that  $g_s$  calculated from  $g_{max}$  when averaged over all daylight periods (preferably weighted according to  $ET$  flux density) will be only about one-half the value of  $g_{max}$ , especially in semiarid regions. This should occur when all relevant  $g()$  functions are included in the  $g_s$  calculation.

An example of use of  $g()$  functions is shown in Figure 11-5, where  $g()$  functions for  $R_s$ ,  $T$ , and VPD are plotted during a typical summer day in Logan, Utah, and a spring day in Davis, California, where  $ET$  was near maximum levels and soil water was high. These are the same days and locations used in  $ET$  calculations shown in Figure 7-9. Only data past 0800 hours were available for Davis on the 2nd of May.

The  $g(R_s)$  function [Eq. (11-40)] with  $K_R = 100 \text{ W m}^{-2}$  estimated  $g(R_s)$  near 1 during most daylight periods at both locations, indicating sufficient

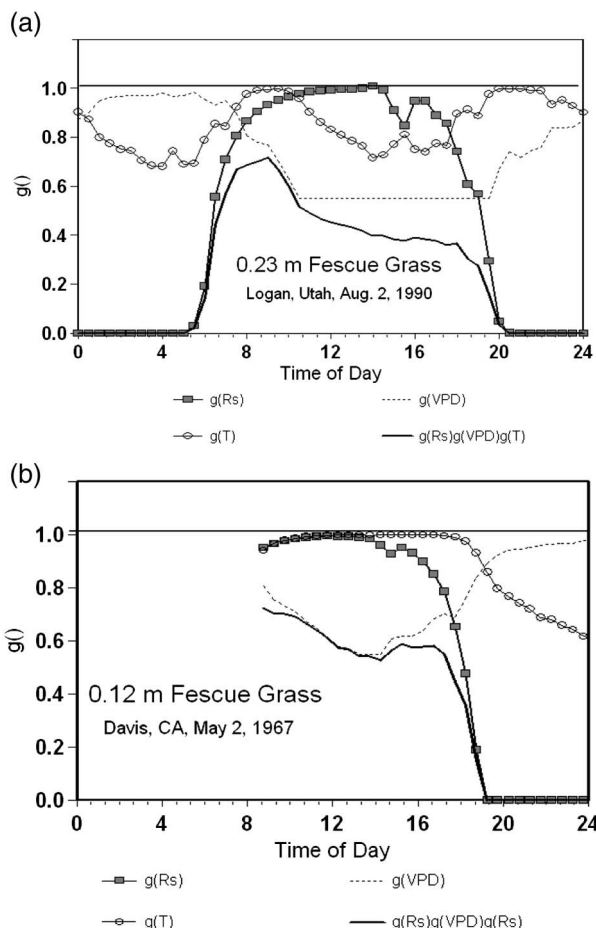


Fig. 11-5. Stomatal conductance functions for (a) August 2, 1990, at Logan, Utah, and (b) May 2, 1967, at Davis, California, computed using Eqs. (11-37)–(11-46)

Source: (a) R. G. Allen, personal communication; (b) W. O. Pruitt, personal communication

sunlight to open stomates. Eq. (11-40) was relatively insensitive to the value used for  $K_R$ . Air temperature was also at near optimum levels [ $g(T) = 1$ ] during daylight hours except at Logan during midafternoon when temperatures exceeded optimum levels and  $g(T)$  decreased to about 0.7 (Figure 11-5a). Values for  $T_L$ ,  $K_T$ , and  $T_H$  in Eq. (11-45) were set at 0, 20, and 40°C for the grass cover at both sites. Low values for  $g(T)$  during early morning hours at Logan occurred when  $T$  was less than  $K_T$ .

The primary reducing function at both Logan and Davis during the days shown in Figure 11-5 was  $g(VPD)$  [using Eq. (11-42)], which reached a minimum level (about 0.55) during afternoon periods at Logan and approached this minimum level during afternoon periods at Davis. Coefficients used in the  $g(VPD)$  equation were  $K_{VPD} = 0.3 \text{ kPa}^{-1}$  and  $VPD_c = 1.5 \text{ kPa}$ . The  $K_{VPD} = 0.3 \text{ kPa}^{-1}$  best fit  $g_s$  values calculated as residuals from the lysimeter data at both locations and is about halfway between the  $K_{VPD} = 0.5 \text{ kPa}^{-1}$  used by Stewart (1988) for Scots pine and the  $K_{VPD} = 0.12$  to  $0.19 \text{ kPa}^{-1}$  used by Stewart and Gay (1989) for natural prairie. The  $VPD_c$  value was the same as that used by Stewart (1988) for Scots pine. The net effect of the conductance reducing functions was to estimate  $g(\text{env.})$ , using Eq. (11-37) with  $g(LAI)$  and  $g(0) = 1$ , equal to about 0.4 to 0.7 during daylight periods at Logan (Figure 11-5a) and  $g(\text{env.})$  equal to about 0.55 to 0.7 during daylight periods at Davis (Figure 11-5b). The  $g_{max}$  at both locations ( $g_{max} = 0.07 \text{ ms}^{-1}$  for 0.23 m grass at Logan and  $g_{max} = 0.036 \text{ ms}^{-1}$  for 0.12 m grass at Davis) was calculated as  $g_l LAI_{eff}$  where  $LAI_{eff} = 0.5 LAI$  [Eq. (8-10)]. The value for  $g_l$  was set equal to the maximum  $g_l$  computed as  $1/r_{l_{min}}$  where  $r_{l_{min}}$  equaled  $40 \text{ sm}^{-1}$  (Table 11-2, second-to-last row). This value for  $r_{l_{min}}$  compares to a value of  $r_l = 75 \text{ sm}^{-1}$  that best fit hourly lysimeter measurements of  $ET$  for cool-season grass at five lysimeter sites in the United States and Spain when no  $g()$  functions were employed (Allen et al. 2005d). A minimum value for  $g_s$  was set equal to  $0.002 \text{ ms}^{-1}$  to account for evaporation from moist soil. Calculations of  $ET$  using the PM equation with  $r_s$  computed with and without  $g()$  functions are presented for these same two days and locations near the end of this chapter.

Values for  $g_{max}$  fitted from  $ET$  measurements range from  $0.018$  to  $0.024 \text{ ms}^{-1}$  for Scots pine (Stewart 1988), equivalent to  $r_{s_{min}} = 40$  to  $55 \text{ sm}^{-1}$ . Price and Black (1989) estimate  $g_{max}$  for the Douglas fir forest as  $0.022 \text{ ms}^{-1}$ , which is equivalent to  $r_{s_{min}} = 45 \text{ sm}^{-1}$ . The  $LAI$  of the Douglas fir was about 3, while the understory had an  $LAI$  of about 2. Eq. (8-9) with  $r_{l_{min}} = 120 \text{ sm}^{-1}$  (Table 11-2) would estimate  $r_{s_{min}} = 48 \text{ sm}^{-1}$  for  $LAI_{eff} = 0.5 LAI$  [Eq. (8-10)], which is in agreement with the measured values.

In application to big bluestem (*Andropogon gerardii*) and Indian grass (*Sorghastrum nutans*) prairie in Kansas, Stewart and Gay (1989) use  $g_{max} = 0.016 \text{ ms}^{-1}$ , which is equivalent to  $r_{s_{min}} = 63 \text{ sm}^{-1}$ . Coefficients used by Stewart and Gay in Eq. (11-40) range from  $K_R = 190$  for  $LAI = 0.5$  to  $K_R = 500$  for  $LAI = 1.3$ .

**Constant vs. Variable Resistance** For 24-hour or longer calculation time steps, use of a constant value for  $r_s$  in the PM equation is generally adequate, with adjustments made only for low soil water. In some situations, increases in daily values for  $r_s$  can be made to account for stomatal closure during periods of low or very high air temperature during early

spring, late fall, and midsummer [using Eq. (11-45) or similar equation]. The value used for  $r_s$  for 24-hour calculations should represent mean effects of  $g(R_s)$  and  $g(VPD)$  during the day. Perrier (1982) concludes that high values of  $r_s$  that occurred during the beginning and end of a day did not substantially affect the cumulative  $ET$  estimates for the whole day due to low energy availability ( $R_n$ ) and low  $VPD$  during early and late day periods and due to the occurrence of dew during morning hours in some locations.

Use of a constant value for  $r_s$  in the PM equation for calculation time steps of less than 24 hours is often acceptable if the calculations are to be summed over daily or longer periods so that errors in specific hourly estimates are not relevant. Allen et al. (2005d) and ASCE (2005) suggest  $r_s = 50 \text{ sm}^{-1}$  for the clipped cool-season grass reference for hourly and shorter time steps, and ASCE (2005) suggests  $r_s = 30 \text{ sm}^{-1}$  for the tall alfalfa reference for hourly and shorter time steps. These values compare to  $r_s = 70$  and  $45 \text{ sm}^{-1}$  for the standardized clipped grass and tall alfalfa references for 24-hour time steps. Where coefficients for Eqs. (11-39)–(11-50) are available or can be fitted to field measurements, then the stomatal conductance functions described in Eqs. (11-39)–(11-50) can be employed along with  $r_{s_{min}}$  for hourly (or shorter) calculation time steps. The impact of using constant  $r_s$  without  $g()$  functions vs.  $r_s$  computed using  $g()$  for half-hourly data is demonstrated in the application examples in a following section.

### Example of Applying the Penman-Monteith to a Dry Surface

Tables 11-5 and 11-6 summarize calculations that illustrate the application of the PM method using weather measurements collected over a dry, rangeland surface where iterative solution of surface temperature,  $T_s$ , is used to calculate various parameters used in the PM equation in successive progression. The location of data collection was 4 km west of Balanced Rock, Idaho, over dry grass rangeland with an estimated LAI of about 0.5. Standard weather parameters  $T_a$ ,  $e_a$ ,  $u_z$ , and  $R_s$  were measured at hourly time steps in addition to measurement of all four components of  $R_n$  [Eq. (11-2a)] using a four-component radiometer. Surface temperature was retrieved from measured  $R_{Lout}$  for comparison with  $T_s$  estimated by inverting Eq. (4-32). The AFIB process of Eqs. (11-2a–f) was applied to the standard measurements over a seven-day period from August 22 to 28, 2008, for the hourly period spanning 1 pm to 2 pm. Antecedent rainfall to the area was less than 15 mm over the prior two months, so a somewhat high value for  $r_s = 1,500 \text{ sm}^{-1}$  was assigned. Aerodynamic roughness was assumed to be 0.005 m for the nearly bare soil condition, and  $z_{oh} = 0.0005 \text{ m}$ . A value for  $K_G = 0.15$  was used in Eq. (11-2b) for  $G$  during the AFIB solution.

Table 11-5 lists weather measurements and  $R_n$ ,  $G$ ,  $T_s$ , and  $H$  calculated using iterative solution of Eqs. (11-2a–f) (the AFIB method). The iteratively determined values for  $T_s$  averaged within  $1.5^\circ\text{C}$  of measured  $T_s$ , indicating

Table 11-5. Calculations from 2 pm Hourly Weather Measurements Collected over Dry Rangeland Near Balanced Rock, Idaho, from August 22 to 28, 2008<sup>a</sup>; Also Shown Are Measured  $T_a$ , Measured  $T_s$  (col. 6), and  $u_z$  at 3 m

DoY	$R_{n,act} \text{ W m}^{-2}$	Est. $G_{act}, \text{ W m}^{-2}$	Est. $R_{n,ref} \text{ W m}^{-2}$	$T_a, ^\circ\text{C}$	Iterative $T_s, ^\circ\text{C}$	Measured $T_s, ^\circ\text{C}$	$u_z, \text{ ms}^{-1}$	$e_a, \text{ kPa}$	$H, \text{ W m}^{-2}$	$\Delta$ from $T_a, T_s, \text{ kPa } ^\circ\text{C}^{-1}$
(1)	(2)	(3)	(4)	(5)	(6)	(7)	(8)	(9)	(10)	(11)
235	444	117	566	24.0	42.1	45.0	3.0	0.55	239	0.179
236	433	113	582	29.1	48.6	42.8	2.3	0.54	196	0.233
237	393	102	541	34.5	50.9	50.6	2.7	0.71	153	0.303
238	411	105	582	34.5	48.6	50.5	3.6	0.69	183	0.303
239	326	87	388	19.6	28.9	32.7	5.8	0.51	198	0.142
240	440	116	555	27.0	38.0	43.0	6.3	0.47	252	0.209
241	433	114	552	27.4	39.0	41.7	5.7	0.61	245	0.213
avg.	411	108	538	28.0	42.0	44.0	4.2	0.58	209	0.226

<sup>a</sup> $R_n$  (col. 1),  $G$  (col. 2),  $T_s$  (col. 5), and  $H$  (col. 9) were solved by iterative solution of Eqs. (11-2a-f) (AFIB method);  $\Delta$  (col. 10) was calculated using  $T_a$  only and  $\Delta$  (col. 11) was calculated using both  $T_a$  and iteratively determined  $T_s$ .  $R_{n,ref}$  was measured over irrigated alfalfa (reference surface).

Table 11-6. Calculations for  $\lambda E$  for 2 pm Hourly Weather Measurements Collected over Dry Rangeland Near Balanced Rock, Idaho, from August 22 to 28, 2008, Using the Penman-Monteith Equation with Progressively More Parameters Calculated Using Iteratively Determined  $T_s$

DoY	Aerodynamic $\lambda E$ , Wm $^{-2}$	AFIB				Penman-Monteith $\lambda E$				% Difference of Penman-Monteith $\lambda E$ from Aerodynamic (AFIB) $\lambda E$			
		(0)	(1)	(2)	(3)	(4)	(5)	(6)	(1a)	(2a)	(3a)	(4a)	(5a)
235	88	108	98	131	107	101	85	23	11	49	22	15	-4
236	124	157	143	188	148	137	111	27	16	51	20	10	-10
237	138	168	155	187	158	138	120	22	12	36	15	0	-13
238	123	151	140	165	148	126	115	23	14	34	20	2	-7
239	40	46	42	48	46	42	40	14	4	18	13	4	0
240	72	83	76	88	84	74	71	15	7	23	17	4	-1

241	74	87	80	93	88	77	73	17	8	26	19	4	-1
avg.	94	114	105	129	111	99	94	20	10	34	18	6	-5

Notes:

- col. (0):  $\lambda E$  using aerodynamic Eq. (11-2c) with  $T_s$  from iterative application of Eqs. (11-2a-f) (AFIB equations)
- col. (1):  $\lambda E$  from the PM equation [Eq. (11-1)] using  $T_{\text{air}}$  only;  $R_n$  and  $G$  calculated for the reference definition using Eqs. (4-31), (4-39), (4-40), and (4-41);  $G$  calculated as  $0.1R_n; \Psi(z/L) = 0$ ; and  $\Delta$  from  $T_a$
- col. (2):  $\lambda E$  from the PM equation [Eq. (11-1)] using  $R_n$  calculated for the reference definition with Eqs. (4-31), (4-39), (4-40), and (4-41);  $G$  calculated from Eq. (11-2b) using  $T_s; \Psi(z/L) = 0$ ; and  $\Delta$  from  $T_a$
- col. (3):  $\lambda E$  from the PM equation [Eq. (11-1)] using  $R_n$  calculated for the reference definition with Eqs. (4-31), (4-39), (4-40), and (4-41);  $G$  calculated from Eq. (11-2b) using  $T_s; \Psi(z/L) = 0$ ; and  $\Delta$  from  $T_a$  and  $T_s$
- col. (4):  $\lambda E$  from the PM equation [Eq. (11-1)] using  $R_n$  calculated for the reference definition with Eqs. (4-31), (4-39), (4-40), and (4-41);  $G$  calculated from Eq. (11-2b) using  $T_s; \Psi(z/L)$  from Eqs. (7-22)–(7-26); and  $\Delta$  from  $T_a$  and  $T_s$
- col. (5):  $\lambda E$  from the PM equation [Eq. (11-1)] using  $R_n$  calculated from Eq. (11-2a) using  $R_{\text{out}}$  based on  $T_s; \Psi(z/L) = 0$ ; and  $\Delta$  from  $T_a$  and  $T_s$
- col. (6):  $\lambda E$  from the PM equation [Eq. (11-1)] using  $R_n$  calculated from Eq. (11-2a) using  $R_{\text{out}}$  based on  $T_s; G$  calculated from Eq. (11-2b) using  $T_s; \Psi(z/L)$  from Eqs. (7-22)–(7-26); and  $\Delta$  from  $T_a$  and  $T_s$

Columns 1a–6a show percent differences from the value for  $\lambda E$  determined using aerodynamic equation (11-2c)

reasonable settings of LAI,  $G$ ,  $r_s$ , and  $z_{om}$  parameters. Iteratively determined  $T_s$  exceeded measured  $T_a$  by an average 14°C, illustrating the large temperature gradients existing between surface and air temperature.

Table 11-6 lists  $\lambda E$  based on aerodynamic Eq. (11-2c) of the AFIB method and using  $T_s$  from iterative application of Eq. (11-2a-f) and a progression of solutions of the PM equation [Eq. (11-1)]. The first PM solution applied 11.1 following the standardized reference crop application (see footnote of Table 11-6) using  $\Delta, R_n$ , and  $G$  calculated using  $T_a$  only, ignoring stability correction. The exception was use of aerodynamic roughness characteristic of the sparse range grass. The estimate for  $\lambda E$  exceeded the  $\lambda E$  calculated by the AFIB method by an average of 20%. The second column summarizes application of the PM with replacement of  $G$  with an estimate from Eq. (11-2b), which is considered to be more realistic for the warm, dry surface than using the  $G = 0.1R_n$  used in the hourly  $ET_o$  method. The replacement  $G$  averaged about 60 W m<sup>-2</sup> greater than the previous value. Deviation of  $\lambda E$  from  $\lambda E$  from Eq. (11-2c) decreased to 10%.

The third column for PM application represents the calculation of  $\lambda E$  where  $T_s$  is solved iteratively by combining  $\lambda E$  from Eq. (11-1) with equations for  $H$ ,  $G$ , and  $R_n$ , and then using  $T_s$  to calculate  $\Delta$  based on both  $T_a$  and  $T_s$  with Eq. (11-3), but where the impact of  $T_s$  on  $G$ ,  $R_{lout}$ , and  $\psi(z/L)$  is ignored. The impact of this approach is to create the greatest error in estimated  $\lambda E$ , where  $\lambda E$  is overestimated by an average of 34%, ranging from 18 to 51% over the seven-day period, as compared with  $\lambda E$  from Eq. (11-2c). These results indicate that using an estimate for  $T_s$  in the calculation for  $\Delta$  only is not sufficient and actually can induce greater error than using strictly  $T_a$  only, due to other compensating factors.

The fourth column for PM application represents the calculation of  $\lambda E$  with the addition of  $\psi(z/L)$  from Eqs. (7-22)–(7-26) and  $\Delta$  from  $T_a$  and  $T_s$ . The addition of  $\psi(z/L)$  to  $r_{ah}$  reduced the overestimation of  $\lambda E$  from 34% to 18%. The fifth column for PM application includes the addition of calculating  $R_n$  from Eq. (11-2a) using  $R_{lout}$  based on  $T_s$ , along with  $G$  calculated from Eq. (11-2b) using  $T_s$ , and  $\Delta$  from  $T_a$  and  $T_s$ , but with  $\psi(z/L) = 0$ . The use of  $T_s$  to calculate  $R_{lout}$  reduced the estimate for  $R_n$  by an average of 120 W m<sup>-2</sup>, which is a substantial change caused by the increased thermal emission from the warm surface that averaged 14°C warmer than measured air temperature. The use of the more correct estimate for  $R_n$  reduced the difference in  $\lambda E$  from the PM equation from  $\lambda E$  from Eq. (11-2b) to about 6%.

Finally, the sixth column in Table 11-6 applies the PM equation [Eq. (11-1)] using all parameters based on iteratively determined  $T_s$ . These included  $R_{lout}$  (and  $R_n$ ),  $G$ , calculated from  $T_s$ ,  $\psi(z/L)$ , and  $\Delta$ . The complete use of  $T_s$  for PM parameters reduced the difference in  $\lambda E$  from the PM equation to about 5% lower than  $\lambda E$  determined by Eq. (11-2b) and the AFIB method. The 5% difference is relatively small and stems from the linearization of the calculation for  $\Delta$ .

In summary, the example calculations in Tables 11-5 and 11-6 illustrate and support why the iterative solution using the AFIB method [Eqs. (11-2a-f)] is preferred when a surface is sufficiently drier than the “reference” condition so that departure of  $T_s$  from  $T_a$  creates the need to utilize  $T_s$  in the estimation of  $R_{lout}$ ,  $G$ ,  $\Delta$ , and  $\psi(z/L)$ . When these latter parameters are calculated using  $T_s$ , especially  $\Delta$ , the need for the PM combination equation is essentially eliminated. The PM can still be applied, however, if with iteratively determined  $R_{lout}$ ,  $G$ ,  $\Delta$ , and  $\psi(z/L)$  parameters, with little departure from  $\lambda E$  estimated using Eq. (11-2c). The example illustrates that all four parameters  $R_{lout}$ ,  $G$ ,  $\Delta$ , and  $\psi(z/L)$  are tied to measured or iteratively determined  $T_s$  and that lack of a  $T_s$  basis for any one of them can introduce error.

## 11.8 EVAPORATION FROM SOIL AND SURFACE RESISTANCE

Evaporation from soil generally dominates the computation of  $ET$  and  $r_s$  for low amounts of leaf area and should be considered in  $ET$  estimates when  $LAI$  is less than 2 to 3 or when a multilayer or multisource application of the PM equation is used. Horton and Wierenga (1983), Novak (1989), Horton and Chung (1991), Šimůnek et al. (1999, 2005), and Saito et al. (2006) have introduced complex models for simulating the flow of heat into and out of soil and evaporation of water from bare and partially vegetated soils, in addition to the multilayer models described earlier in this chapter. Many of these models are generally complex and may be too data intensive for routine application. Often, for purposes of estimating  $ET$  on a daily basis, soil water evaporation can be determined by varying surface resistance with cumulative evaporation.

For a single-layer PM model application, Grant (1975) proposes calculating an integrated surface resistance,  $r_s$ , for uniform vegetation cover that considers vegetative surface resistance and soil resistance in parallel. His equation is of the form

$$\frac{1}{r_s} = \frac{1 - K_r^{LAI}}{r_{sn}} + \frac{K_r^{LAI}}{r_{ss}} \quad (11-51)$$

where  $r_{sn}$  = bulk stomatal (surface) resistance for a fully developed vegetative canopy in  $\text{sm}^{-1}$ , and  $r_{ss}$  = effective soil resistance to evaporation in  $\text{sm}^{-1}$ .  $K_r$  is a “radiation extinction” coefficient, which helps to characterize the net exposure of vegetation and soil. Values for  $K_r$  equal to 0.85 and 0.70 were suggested by Monteith and Unsworth (1990) for beans and wheat, respectively. Eq. (11-51) is conservative in that it incorporates the bulk surface resistance for a fully developed canopy. The radiation extinction constant is used in Eq. (11-51) to simulate the close coupling between

radiation absorption within a canopy and the energy available for evaporation beneath the canopy.  $K_r$  also serves as a surrogate for ease of heat and vapor transport to and from “deep” leaf layers in the canopy to the canopy surface.

Perrier (1982) suggests a relationship similar to Eq. (11-51) for nonuniform vegetation cover of the form:

$$\frac{1}{r_s} = f_c \frac{LAI_{eff}}{r_l} + (1 - f_c) \frac{1}{r_{ss}} \quad (11-52)$$

where  $f_c$  is the fraction of soil covered and/or shaded by vegetation, and  $r_l$  is stomatal resistance,  $\text{sm}^{-1}$ , per unit  $LAI$ .

Soil resistance to evaporation,  $r_{ss}$ , varies significantly with soil water. Minimum values occur when the soil surface is nearly saturated. Values increase nearly exponentially as the surface 1-cm layer dries due to evaporation (van de Griend and Owe 1994). The thickness of the total soil layer that dries by evaporation is a function of soil hydraulic and thermal properties and evaporative demand.

Early in a drying cycle, when bare soil near the surface is moist, water is transported toward the surface by liquid transport according to hydraulic properties of the soil. During this period, evaporation occurs at rates close to potential. This stage is often referred to as the “first stage of evaporation.” After the soil surface has dried to the extent that hydraulic transport to the surface lags evaporative demand, then “second stage” drying begins. As the hydraulic conductivity near the soil surface decreases, evaporation occurs at lower rates and is limited by conduction of sensible heat (soil heat flux density) downward into the soil and by diffusion of vapor and liquid water from below the surface to the surface. Because the hydraulic conductivity and thermal conductivity of soil decrease with decreasing soil water, the rate of evaporation decreases with drying until it reaches a very low rate. At this point,  $r_{ss}$  assumes a maximum value. More description of stage 1 and 2 drying is given in Chapters 9 and 10. Typical water content profiles in the upper 0.10 m of soil are illustrated in Figure 11-6.

Van de Griend and Owe (1994) proposed estimating  $r_{ss}$  from the water content of the top 1 cm of soil:

$$r_{ss} = 10 \exp(\alpha_\theta(\theta_1 - \theta)) \quad (11-53)$$

where  $\theta_1$  is the volumetric water content in percent, at the end of stage 1 drying for the top 1 cm;  $\theta$  is water content of the top 1-cm soil layer in percent; and  $\alpha_\theta$  is an empirical coefficient, set to 0.356 by van de Griend and Owe (1994). Eq. (11-53) suggests  $r_{ss} = 10 \text{ sm}^{-1}$  during stage 1 drying until the beginning of stage 2. Van de Griend and Owe (1994) estimate  $\theta_1$  as  $\theta_{fc}/2$ , where  $\theta_{fc}$  is volumetric water content at field capacity. In contrast to

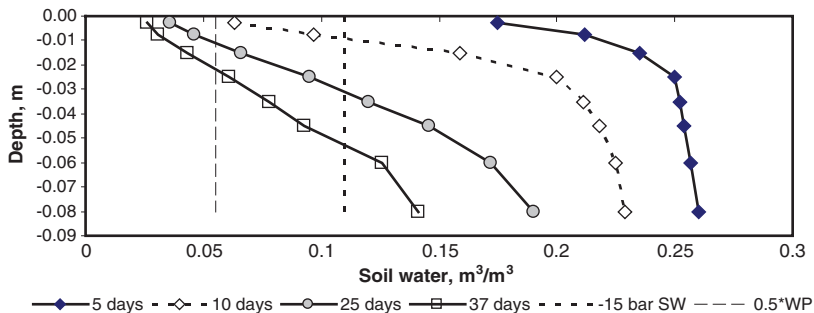


Fig. 11-6. Soil water distribution on day 5, 10, 25, and 37 after wetting  
Source: Data from Jackson (1973)

the use of a shallow 10-mm soil depth to estimate  $r_{ss}$ , Ortega-Farias et al. (2010) used water content of the top 200 mm of soil in a vineyard, where  $r_{ss} = 19 (\theta/\theta_s)^{-3.5}$  and  $\theta_s$  is water content at saturation. A time-based water balance of the upper soil layer is needed to estimate  $\theta$  for each time step of a model. Farahani and Ahuja (1996), Lagos (2008), and Lagos et al. (2012) describe functions to estimate resistance for soil having organic residue cover.

For many soils,  $r_{ss}$  can be expressed as a function of the amount of water evaporated from the soil relative to the maximum amount of water that can be evaporated

$$r_{ss} = r_{ssn} + (r_{ssx} - r_{ssn}) \left[ \frac{\Sigma E_s}{(\Sigma E_s)_x} \right]^{K_{rs}} \quad (11-54)$$

where  $r_{ssn}$  is minimum soil resistance in  $\text{sm}^{-1}$  when the soil surface is wet from rainfall or irrigation, and  $r_{ssx}$  is maximum soil resistance in  $\text{sm}^{-1}$  when the upper soil layer has been depleted of all evaporable water.  $\Sigma E_s$  is the cumulative depth of water evaporated from the soil surface, mm, and  $(\Sigma E_s)_x$  is the maximum cumulative depth of evaporable water, mm. The exponent  $K_{rs}$  in Eq. (11-54) ( $K_{rs} > 1$ ) simulates the length of first-stage drying where  $r_{ss}$  remains close to  $r_{ssn}$  for one to three days while the soil supplies water for evaporation at nearly the potential rate and then begins a rapid increase in  $r_{ss}$  as the water in the soil surface nears depletion. Illustrative values for  $r_{ssn}$ ,  $r_{ssx}$ , and  $K_{rs}$  are  $50 \text{ sm}^{-1}$ ,  $2,000 \text{ sm}^{-1}$ , and 10, respectively, for a bare Portneuf silt loam soil in Idaho (Allen et al. 1996; data from Wright, personal communication, 1991).  $(\Sigma E_s)_x$  is best determined from empirical studies based on soil water depletion measured under bare soil conditions. Alternatively,  $(\Sigma E_s)_x$  is made equivalent to the TEW term representing total evaporable water defined in Chapter 9 and is

estimated using Eq. (9-20) based on estimated field capacity, wilting point, and effective evaporation depth. Eq. (11-55) is similar to Eq. (9-20):

$$\left( \sum E_s \right)_x = 1,000 \left[ \theta_{fc} - \frac{(\theta_{wp} + \theta_{od})}{2} \right] z_e \quad (11-55)$$

where  $z_e$  is the total estimated depth of soil, m, contributing to evaporation and water contents with dimensionless units of  $\text{m}^3 \text{m}^{-3}$ .

For example, if a silt loam soil with  $\theta_{fc} = 0.31 \text{ m}^3 \text{ m}^{-3}$ ,  $\theta_{wp} = 0.14 \text{ m}^3 \text{ m}^{-3}$ , and oven-dry soil water content of less than  $0.005 \text{ m}^3 \text{ m}^{-3}$  were dried by evaporation to a depth of 0.12 m, the total surface evaporable water,  $(\Sigma E_s)_x$ , would be approximately

$$\left( \sum E_s \right)_x = 1,000 \left[ 0.31 - \frac{(0.14 + 0.005)}{2} \right] 0.12 = 29 \text{ mm}$$

The value of  $(\Sigma E_s)_x$  varies with soil texture, structure, and organic cover and period of time. Approximate values for  $(\Sigma E_s)_x$  are about 10 to 20 mm for a bare, sandy soil; 30 mm for a bare silt loam; and 40 mm for a bare, clay-textured soil.  $(\Sigma E_s)_x = 30 \text{ mm}$  for a bare Portneuf silt loam soil, based on data from Wright (1991). Soil covered with organic mulch or other insulative cover tends to reduce the peak evaporation rate and often the total depth of evaporation  $(\Sigma E_s)_x$ , as discussed in Chapters 9 and 10. Denmead (1984) suggests that evaporation from a forest floor covered with litter might be only one-half of what is expected from a bare exposed soil. Gonzalez-Sosa et al. (1999) measured similar reductions for a cornfield covered with organic mulch in France. Allen et al. (1998, 2005b) propose similar reductions in TEW for organic and plastic covers. Li et al. (2005) report field-measured evaporation from plastic-covered soil that ranged from 11 to 70% of rates from an exposed bare soil.

$\Sigma E_s$  can be estimated using a daily calculation time step basis with a soil water balance of the upper 0.10 to 0.20-m soil layer for normal drying cycles. A general equation for  $\Sigma E_s$  for the  $f_{ev}$  fraction of soil that is exposed to drying is

$$\sum E_{s_i} = \sum E_{s_{i-1}} - P_i - I_i + \frac{ET_a - ET_b}{f_{ev}} \quad (11-56)$$

where  $\Sigma E_{s_i}$  is cumulative soil evaporation on day  $i$ ,  $\Sigma E_{s_{i-1}}$  is cumulative soil evaporation on day  $i - 1$ ,  $P_i$  and  $RO_i$  are precipitation and precipitation runoff from the soil surface on day  $i$ ,  $I_i$  is mean irrigation depth on day  $i$ , and  $ET_a$  is actual  $ET$  on day  $i$  computed using the PM equation where  $r_s$  includes the effects of  $r_{ss}$ .  $ET_b$  is a "basal"  $ET$  rate that reflects a visually

dry soil surface and is computed using the PM equation where  $r_s$  is calculated using  $r_{ss} = r_{sx}$  for a dry soil surface. The difference  $ET_a - ET_b$  represents the soil evaporation component, and  $f_{ev}$  is the effective fraction of the total soil surface contributing to evaporation. The presence of  $f_{ev}$  in Eq. (11-56) is intended to concentrate the extraction of evaporation into the  $f_{ev}$  fraction of the ground surface, similar to that done in Eq. (9-27) for the dual  $K_c$  procedure. The value of  $f_{ev}$  may be less than 1 when part of the soil is shaded by dense vegetation;  $f_{ev} < 1$  causes  $\Sigma E_{si}$  to approach  $(\Sigma E_s)_x$  more quickly.  $\Sigma E_{si}$  in Eq. (11-56) has limits of 0 and  $(\Sigma E_s)_x$ .

Figure 11-7 shows an example of estimating surface resistance using resistance data for maize reported by Jacobs et al. (1989).  $K_r$  in Eq. (11-51) was estimated as 0.7. Surface resistance of the canopy at maximum LAI,  $r_{sn}$ , was estimated as  $60 \text{ s m}^{-1}$  based on  $r_l = 100 \text{ s m}^{-1}$  and  $LAI_{eff}$  from Eq. (8-11) for  $LAI = 3.8$ . Calculations were somewhat insensitive to the value of  $K_r$  between 0.6 and 0.8. Eq. (11-52) was applied assuming  $r_l = 100 \text{ s m}^{-1}$  and  $r_{ss} = 200 \text{ s m}^{-1}$ , and  $f_c$  was assumed to range from 0.05 at  $LAI = 0.5$  to 0.95 when  $LAI = 4$ . Jacobs et al. (1989) present no information concerning occurrences of soil wetting. Therefore,  $r_{ss} = 200 \text{ s m}^{-1}$  was used as an approximation for the entire period.

Eqs. (11-51) and (11-52) both replicated measured  $r_s$  somewhat well, using the assigned estimates for  $r_{ss}$  and  $LAI_{eff}$ . Eq. (11-51) agreed more closely with observed measurements of  $r_s$  during periods of significant soil water evaporation ( $LAI < 1$ ) than did Eq. (11-52), indicating the importance of the radiation extinction term. If the occurrences of soil wetting had been

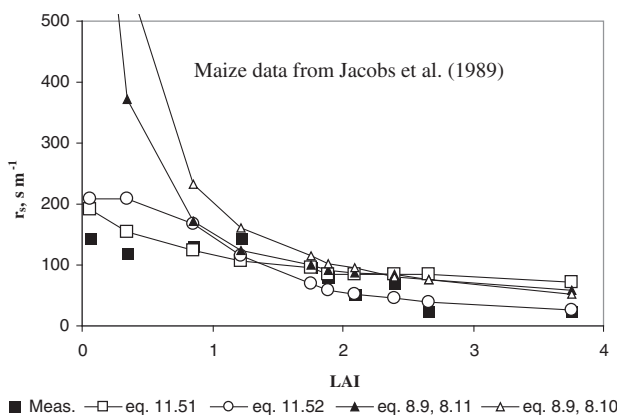


Fig. 11-7. Examples of calculations for total surface resistance using Eqs. (8-9), (11-51), and (11-52) with application to data from Jacobs et al. (1989)  
Source: Data from Jacobs et al. (1989)

known, then Eq. (11-55) could have been applied, where  $\Sigma E_s$  would have been computed on daily time steps using Eq. (11-56).

The effect of ignoring soil evaporation in computing  $r_s$  [e.g., using Eq. (8-9) with Eq. (8-10) or (8-11) only] is significant at  $LAI < 1$  as shown in Figure 11-7. The effect of ignoring soil evaporation was less when  $LAI > 1.5$ .

The Grant (1975) approach in Eq. (11-51) can be extended for sparse or immature crops or vegetation with exposed bare soil between plants or rows to apply to a mixture of shaded and nonshaded soil surfaces and, for incomplete wetting of the soil surface during irrigation, for a mixture of wetted and nonwetted parts of the surface. This is done through combination of surface resistances  $r_{sc}$  and  $r_{ss}$  acting in parallel as expressed by Allen et al. (1996) according to the fractions of surface represented by each parallel resistance component:

$$\frac{1}{r_s} = \frac{f_c(1 - K_r^{LAI/f_c})}{r_{sc}} + K_r^{LAI/f_c} \left( \frac{f_{csW}}{r_{ssW}} + \frac{f_{csD}}{r_{ssD}} \right) + \frac{f_{eW}}{r_{sseW}} + \frac{f_{eD}}{r_{sseD}} \quad (11-57)$$

where  $f_c$  is the effective fraction of ground shaded by vegetation, which is computed as a function of sun angle, row height and width, leaf density, and row orientation. Fractions  $f_{csW}$ ,  $f_{csD}$ ,  $f_{eW}$ , and  $f_{eD}$  are the fractions of the soil surface that are (a) shaded and wet, (b) shaded and dry, (c) sunlit and wet, and (d) sunlit and dry, as illustrated in Figures 11-1a and 11-8. By definition,  $f_{csW} + f_{csD} + f_{eW} + f_{eD} = 1$  and  $f_{csW} + f_{csD} = f_c$ . Resistance  $r_{sc}$  is

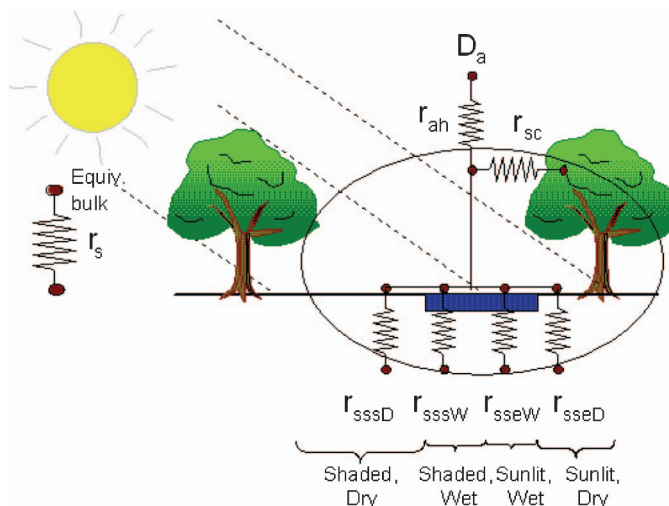


Fig. 11-8. Schematic of soil resistances for evaporation for incomplete vegetation cover and spatially variable wetting of the soil surface

the surface resistance of the canopy,  $r_{ssW}$  is the surface resistance of soil shaded by the canopy that is wetted by irrigation or precipitation,  $r_{ssD}$  is the surface resistance of soil shaded by the canopy that is not wetted by irrigation or precipitation,  $r_{sseW}$  is the surface resistance of soil exposed to sunlight (not shaded by the canopy) and that is wetted by irrigation or precipitation, and  $r_{sseD}$  is the surface resistance of soil exposed to sunlight that is not wetted by irrigation or precipitation. The application of Eq. (11-57) requires a soil water balance for each of the  $f_{cs}$  and  $f_e$  fractions of the surface. Generally,  $r_{ssD}$  and  $r_{sseD}$  can be assumed to equal maximum  $r_{ssx}$ , if those fractions of the soil surface are dry.

The use of the PM equation using  $r_s$  from Eq. (11-57), even though  $r_s$  is well parameterized, uses a single aerodynamic resistance,  $r_a$ , thus assuming that all evaporation and heat transfer originates from a single plane. Thus PM is often referred to as the “big-leaf” model (Monteith 1965). In situations where the vegetation canopy has substantial height, such as for trees, or where vegetation is somewhat sparse, a multilayer ET model, discussed in an earlier section, may produce better estimates. Also, differences in emitted long-wave radiation between dry, sunlit soil and canopy can be as large as  $100 \text{ W m}^{-2}$ , as illustrated in Tables 11-5 and 11-6. This can reduce the accuracy or consistency of applications of single-layer PM equations comprising blended resistances. Leuning et al. (1994) and Brisson (1998) apply separate Penman-Monteith equations for evaporation and transpiration and then recouple them, similar to procedures commonly used for multilayer ET models.

For sun angles other than directly overhead,  $f_c$  can be estimated for a row crop following Allen et al. (1998) as

$$f_c = \frac{W + h |\sin(\eta + \beta)| \tan \theta_z}{S} \quad (11-58)$$

where  $h$  is mean plant height,  $\theta_z$  is the solar zenith angle [ $0^\circ$  = nadir (overhead)],  $\eta$  is the sun azimuth angle ( $0^\circ$ =north), and  $\beta$  is the row orientation relative to north ( $\beta=0^\circ$  for north-south orientation,  $\beta=90^\circ$  for east-west row orientation),  $W$  is row width, and  $S$  is row spacing with the same units as  $h$ . Eq. (11-58) presumes a nearly rectangular continuous row shape of height  $h$  and width  $W$  and has an upper limit of  $f_c=1$ . In some situations,  $W$  may not be measured or available, but an estimate of LAI may be available. In this case,  $f_c$  may be approximated during incomplete row closure as

$$f_c = \frac{LAI}{LAI_c} + \frac{h}{S} |\sin(\eta + \beta)| \tan \theta_z \quad (11-59)$$

where  $LAI_c$  is the LAI at complete row closure and shading of the ground. Variations on Eqs. (11-58) and (11-59) can be made to fit the particular row architecture, for example, when spacings occur between tree canopies. Campbell and Norman (1998) suggest a simple model to estimate effects of tree canopies that do not extend to the ground. The value for  $f_c$  and subsequently for  $r_s$  changes with time of day and interacts with  $R_n$ ,  $G$ , wind speed, and temperature.

For 24-hour computation time steps, an average daily value for  $f_c$  is determined for computing soil moisture balances for shaded and unshaded soil. An average daily value for  $f_c$  for east-west rows can be determined by weighting Eq. (11-59) for sunlight intensity and integrating between the limits of sunrise and sunset or by standardizing on solar noon time. For north-south row orientation, all soil is sunlit and shaded at various times of the day, so one may set  $f_c = W$ .

An example of applying the direct PM equation using  $r_s$  from Eq. (11-57) is shown in Figure 11-9 for a growing season for snap beans near Kimberly, Idaho, in 1974. The daily estimates were divided by alfalfa reference  $ET_r$  to normalize. The dry-soil curve represents estimates from the direct PM using  $r_{ssx}$  for a dry surface. The ratio of the dry-soil estimates to reference  $ET_r$  varied from day to day due to differences between the direct PM, which used net radiation measured over the bean crop, and the standardized PM,

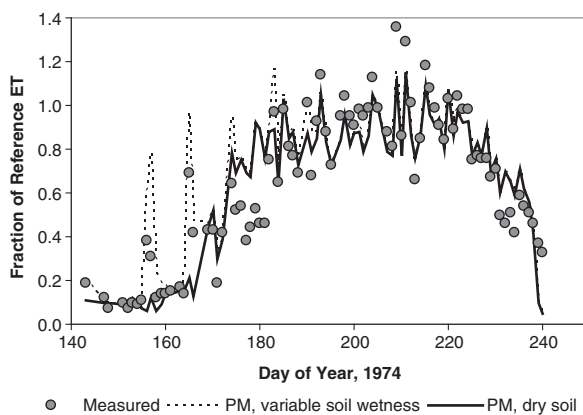


*Fig. 11-9. Daily ET for a bean crop near Kimberly, Idaho, calculated using the direct PM equation using  $r_s$  from Eq. (11-57) where, for the dry soil condition,  $r_{ss}$  was set equal to  $r_{ssx}$ , and where ET is expressed as a fraction of daily alfalfa reference ET<sub>r</sub> calculated using the ASCE standardized PM equation. Calculations are from Allen et al. (2000), lysimeter data compliments of Dr. J. L. Wright, USDA-ARS (retired)*

*Source: Allen et al. (2000); Dr. J. L. Wright, USDA-ARS (retired)*

which used standardized calculated net radiation. In this example,  $r_{sc\ min}$  was set at  $25\text{ sm}^{-1}$ . Agreement between the direct PM and measurement data was relatively good. The RMSE was  $1.1\text{ mm d}^{-1}$  ( $n=86$ ). The method overestimated peak ET on days having wet soil and partial vegetation cover early in the growing period, where  $f_{csW} + f_{eW} = 0.5$  was assumed.

## 11.9 WEATHER MEASUREMENTS FOR DIRECT APPLICATION OF THE PENMAN-MONTEITH AND AFIB METHODS AND REFERENCE ET CALCULATION

### Basic Measurements

When applying the PM or other boundary layer equations, wind, humidity, and temperature should be measured over the surface in question. This is important, as the rates of  $\lambda E$  and  $H$  from a vegetative surface affect the shapes and magnitudes of vapor and air temperature profiles. In the same manner, the roughness of an evaporating surface affects the shape and magnitude of wind velocities above the surface. Vapor and air temperature profiles established above a surface function as feedback mechanisms to  $\lambda E$  and  $H$  and play important roles in dampening differences in  $r_s$  and  $r_a$  among vegetation types.

As the value of  $r_s$  decreases (higher bulk stomatal conductance),  $\lambda E$  increases and consequently  $H$  (if positive) decreases. The result is relatively higher vapor concentration in the equilibrium boundary layer above the surface and cooler temperatures. These two changes work together in reducing the vapor pressure deficit of the boundary layer, thereby dampening the increase in  $\lambda E$  demand (negative feedback). An increase in the value of  $r_s$  works in the opposite direction. With an increase in  $r_s$ , the VPD of the boundary layer increases due to reduced vapor concentration and increased air temperature, resulting in higher  $\lambda E$  demand on the vegetation (positive feedback). The higher  $\lambda E$  demand of the boundary layer partially dampens decreases in  $\lambda E$  caused by increases in surface resistance.

The functioning of boundary layer feedback processes and "conditioning" of the near-surface airstream are important and may present problems when  $RH$  and  $T$  data are measured over surfaces with aerodynamic and surface characteristics and soil water availability that are different from the surface in question. This is an especially common problem in semiarid climates where irrigated agriculture can create oases of relatively wet surfaces with near-surface boundary layers that can be quite different from those of the ambient regional surroundings. Errors introduced to ET calculations based on using weather data reflecting the region or a locally dry condition can be substantial. Errors can also occur in the case of estimating evaporation of intercepted precipitation from tall,

aerodynamically rough forest canopies using weather data from adjacent grassed weather sites. In this situation, the smoother aerodynamics and lower  $\lambda E$  of the grassed site result in higher wind speeds, higher temperatures, and lower vapor pressures. When transposed over a tall-vegetated surface with low  $r_s$ , overestimation of ET occurs. In addition to conditioning of the equilibrium boundary layer, the generally cooler surface temperature associated with an evaporating surface increases  $R_n$  by reducing  $R_{lout}$ . The cooler surface also often reduces  $G$  due to reduced thermal gradients. Both of these effects increase available energy and ET that may counter some of the effects of the conditioning of the airstream.

In situations where ET is estimated for natural rain fed vegetation using a direct equation application such as with the PM equation, then humidity, air temperature, and wind measurements should be made over the same type of vegetation or directly or iteratively adjusted to reflect the conditioning by that surface. In situations where the  $K_c ET_{ref}$  approach is utilized, then humidity, temperature, and wind measurements should be made over a well-watered agricultural surface, preferably clipped grass, because that is what the calibrations of the reference ET equations are "expecting." Most  $ET_{ref}$  equations have been calibrated against weather data gathered over well-watered clipped grass (Doorenbos and Pruitt 1977; Wright 1982; Jensen et al. 1990; ASCE 2005), and  $K_c$ s are usually computed using this standardized  $ET_{ref}$ .

Obtaining humidity, temperature, and wind measurements is generally difficult over unique types of vegetative canopies, especially when estimating ET for historical periods. Often, such data are available only from grassed or even barren weather sites. Often weather measurement sites are located in nonagricultural, nongrassland, or nonforested sites such as in cities or near airport runways and buildings. Under these circumstances the user should make allowances for the uncharacteristic nature of the humidity, temperature, and wind data and perhaps assign some type of uncertainty level to the ET estimates.

All weather station equipment used in estimating ET should conform to accepted standards and specifications regarding equipment type, placement, maintenance, calibration, and reporting frequency. Ley and Elliott (1993) report on proposed standards for agricultural weather stations and discuss recommended standards and specifications. These standards are now available as the ASABE standard EP505 (ASABE 2004, revised 2009) "Measurement and Reporting Practices for Automatic Agricultural Weather Stations."

Measurements of meteorological data should be screened for integrity and accuracy before use as recommended by Allen et al. (1998, 2011d). Calibration and maintenance of sensors should be confirmed and documented. Air temperature and humidity data should be evaluated using procedures discussed in the next section. Daily and hourly solar radiation data should be plotted against clear sky solar radiation ( $R_{so}$ ) to assess

whether maximum measurements of  $R_s$  follow the  $R_{so}$  “envelope.” Occasionally,  $R_s$  can exceed  $R_{so}$  when clouds are present outside of the view angle of the sun and reflect additional radiation toward the sensor.  $R_{so}$  can be estimated from extraterrestrial radiation ( $R_a$ ) using Eq. (4-3). Jensen et al. (1990), Allen et al. (1994c, 2005d), and Appendix H describe methods for computing  $R_a$  and  $R_{so}$  for hourly periods. Monthly values for  $R_s$  can be compared against  $R_s$  estimated using Eqs. (4-24) and (4-26) to assess general data integrity.

### Adjustments of Noncharacteristic Weather Data

**Air Temperature and Humidity** When air temperature and humidity data are required for use in an  $ET_o$  calculation or in a direct application of a single- or multilayer PM equation, they may need to be adjusted to account for dryness of the weather station environment. Allen et al. (1983) and Allen and Pruitt (1986) developed empirical procedures for adjusting air temperature measurements from weather stations located in environments where ET was less than maximum rates due to limited soil water or green vegetation. The objective of the adjustments was to create air temperature data sets reflective of well-watered environments over clipped grass for use in an  $ET_{ref}$  equation. An aridity rating procedure was used to characterize effects of dryness of the local station environment and the region on required air temperature adjustments. In the application to weather stations in Idaho, daily maximum and minimum air temperatures were adjusted downward by as much as 4.5°C for stations with nonirrigated, nontranspiring surfaces surrounded by similar conditions. The magnitude of adjustments by Allen and Pruitt (1986) were based on paired observations of air temperatures by Allen et al. (1983).

Ley and Allen (1994) apply more complex methods for adjusting air temperature and humidity data from nonreference stations using energy balance and water balance relationships. These methods require measurement of  $R_s$ ,  $T$ , humidity, wind, and precipitation on a daily basis. Allen (2012) applies surface energy balance and blending height theory to establish expected  $T$ ,  $e$ , and  $u$  profiles to a 200-m blending height above a weather surface and to then extrapolate back to the surface using ET and energy balance estimated for a well-watered reference surface. The iterative procedure produces near-surface  $T$ ,  $e$ , and  $u$  (at 2-m height) that reflect the conditioning of a well-watered reference surface and that can be used to produce more accurate and representative reference ET calculations. In an application to weather data from an Idaho desert setting (annual  $P = 200$  mm), Allen (2012) shows that conditioning of the desert air mass by localized or regional irrigation (or establishment of a “reference ET” surface) nearly doubled humidity content at 2 m. This is shown in Figure 11-10. The blending height-flux profile procedure can be applied over other types of

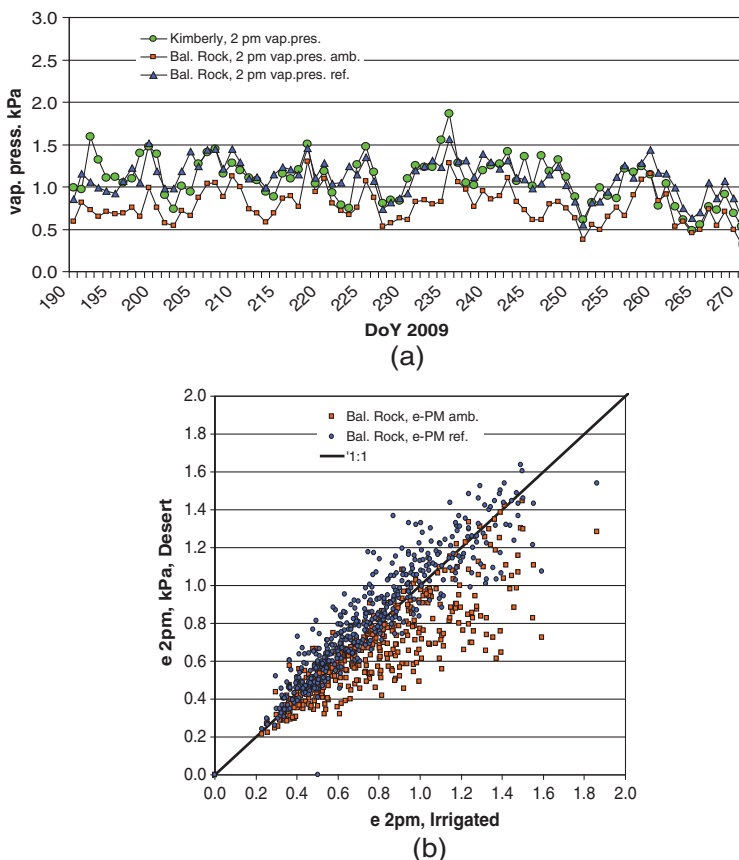


*Fig. 11-10. (a) Daily midafternoon vapor pressure measured over a dry desert location in southern Idaho near Balanced Rock, Castleford ("Bal. Rock, 2 pm vap. pres. amb.") and the same vapor pressure adjusted (i.e., conditioned using blending height and flux profile theory) to reflect vapor pressure expected over a "reference ET" surface ("Bal. Rock, 2 pm vap. pres. ref.") compared with measured midafternoon vapor pressure at an irrigated site 60 km to the east "Kimberly, 2 pm vap. pres."; and (b) the same data from Balanced Rock plotted against measured vapor pressure at the irrigated Kimberly location before ("Bal. Rock, e-PM amb.") and after ("Bal. Rock, e-PM ref.") adjustment by conditioning*

*Source: Data from Allen (2012)*

surfaces where a direct PM application is made to make iterative adjustments to  $T$ ,  $e$ , and  $u$  profiles that incorporate feedback effects from the surface.

Humidity measurements over arid, nonirrigated surfaces are in general lower than those made over well-watered grassed surfaces or over

other well-watered vegetation. If humidity data are to be used to estimate  $ET_{ref}$ , which by definition is ET from a well-watered surface, then humidity measurements should be made in a well-watered environment. In an environment having healthy vegetation and adequate soil water, minimum daily air temperature,  $T_{min}$ , usually approaches dew point temperature,  $T_d$ , especially if the wind dies down by early morning. Air temperatures decrease during nighttime hours due to surface cooling caused by long-wave radiation and evaporation caused by a positive VPD until the dew point is reached, provided that wind speed is relatively calm so that large amounts of warm, dry air (in an arid region) are not transported to the surface. When near-surface air temperature nears  $T_d$ ,  $T$  is prevented from decreasing below  $T_d$  by condensation of vapor from the air and the corresponding heating effect of released latent heat. Under these conditions, the relationship  $T_{min} = T_d$  generally holds and can be used to assess the relative impact of nonrepresentative station environment on humidity and air temperature on  $ET_{ref}$  calculations.

When soil water or vegetation cover limits ET to less than  $ET_{ref}$ ,  $T_{min}$  may remain above  $T_d$ . This occurs due to two factors. The first factor is the large reservoir of sensible heat in the atmosphere that is transferred toward the surface during the night, reducing the effect of cooling by long-wave emission. The large reservoir of heat is created during the daytime due to large flux densities of sensible heat,  $H$ , resulting from low ET. The second factor is the effect of lower soil water availability on limiting evaporative cooling during nighttime hours.

Under most evaporative conditions,  $T_d$  is higher during daytime hours than during nighttime hours due to humidification of the boundary layer by ET. Consequently, daytime measurements of absolute humidity may exceed nighttime values by 5 to 20%. Therefore, the relationship between  $T_{min}$  and  $T_d$  may not be strictly one to one when  $T_d$  is based on 24-hour or daylight averages. In these cases, especially during winter months,  $T_{min}$  measurements can be expected to go a few degrees below 24-hour average  $T_d$  measurements.

An example of the effect of dryness of weather station environment on proximity of  $T_{min}$  to  $T_d$  is shown in Figure 11-11 where mean monthly differences between  $T_{min}$  and  $T_d$  are plotted against ratios of mean monthly precipitation and  $ET_o$  for two data sets (26 Weather Service locations across the United States and two stations in southern Idaho). The ratios of  $P$  to  $ET_o$  indicate the relative wetness of the station during a particular month and the likelihood of healthy, transpiring natural vegetation. Figures 11-11a and b indicate that  $T_d \approx T_{min}$  where vegetation of the weather sites is in a reference (well-watered) condition (monthly  $P/ET_o > 1$ ). This would represent conditions within most large irrigation projects. The average absolute difference between  $T_{min}$  and  $T_d$  is about 2°C when  $P/ET_o > 1$ .

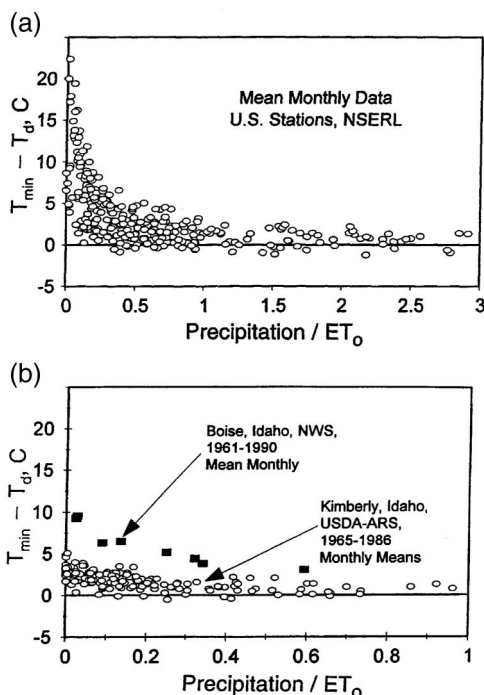


Fig. 11-11. Monthly mean  $T_{min}$  – monthly mean  $T_d$  for (a) 26 U.S. Weather Service stations across the United States and (b) two weather stations in southern Idaho. Boise represents a dry, airport environment, and Kimberly represents an irrigated environment

When measured in a dry environment (monthly  $P/ET_0$  near zero),  $T_d$  can be as much as  $20^{\circ}\text{C}$  less than  $T_{min}$ . Daily differences between  $T_{min}$  and  $T_d$  are similar to the monthly averages shown.

The effect of irrigation on  $T_{min} - T_d$  is shown in Figure 11-11b, where data from Kimberly and Boise, Idaho, represent measurements from a semiarid climate (annual rainfall <250 mm per year), but where the Kimberly location is over irrigated grass surrounded by more than 150,000 ha of patchwork irrigated land in which fields of crops are in various stages of growth. The Boise location is the Boise airport, which is surrounded by predominantly nonirrigated rangeland for a 10-km distance. Irrigated land lies beyond the nonirrigated rangeland in the predominant upwind direction. The effect of surrounding the weather station with well-watered vegetation is obvious. Values for  $T_{min} - T_d$  would increase for both of these locations if they had been surrounded by large expanses of only rangeland.

Graphical comparisons of  $T_{min}$  vs.  $T_d$  can be used as a check on data integrity and how well the data represent well-watered conditions. When data are to represent a well-watered reference setting, then the relationship  $T_d \approx T_{min} - K_o$  can be used as a comparative reference, where  $K_o$  is an offset, generally equal to 0 to 2 K in subhumid and humid climates and 2 to 7 K in semiarid to arid climates during spring, summer, and fall. During wintertime,  $K_o$  can be negative when comparing mean daily  $T_d$  to  $T_{min}$  because daytime evaporation and warming of air can increase humidity levels above saturation at nighttime  $T_{min}$  (Allen and Robison 2007).

When measured  $T_{min}$  substantially exceeds  $T_d$  due to station dryness, and data representing a reference setting are desired, then one method to empirically adjust  $T_{max}$ ,  $T_{min}$ , and  $T_d$  is by subtracting 0.5  $\Delta T$  from  $T_{max}$  and  $T_{min}$  and by adding 0.5  $\Delta T$  to  $T_d$ , where  $\Delta T = T_{min} - T_d - K_o$  (Allen et al. 1998). However, when applying the PM equation directly over dry vegetation, no adjustment of temperature and humidity data should be made. Additional suggestions for adjusting noncharacteristic humidity and temperature data are presented in the ASCE *Hydrology Handbook* (Allen et al. 1996), ASCE (2005) Appendixes D and E, and Appendix H of this manual. One can also employ a more physically based boundary layer conditioning method (Allen 2012).

**Wind Speed** Aerodynamic resistance computed by Eq. (8-3) assumes that the wind speed at some reference height is measured above the surface in question and is therefore governed by exponentially shaped profiles for height above the zero plane displacement that are characteristic of the surface roughness. When wind measurements are made over 0.12-m grass, for instance, wind speed measured at 2 m will generally be significantly higher than that measured at 2 m above tall vegetation, for example, an adjacent forest of 10-m trees.

Rutter et al. (1975) found wind speeds measured at 2 m above the top of a 20-m tall pine forest to be 0.45 of wind speeds measured at 2 m above a nearby grassed area. Allen and Wright (1997) found wind speeds at 1.3 m above the top of 0.7-m tall snap beans (2 m above ground surface) to be 0.7 of speeds measured at 2-m height over 0.12-m grass 0.8 km away. Wind speeds at 1 m above the top of 1-m tall winter and spring wheat (2 m above ground surface) were 0.6 times speed measured at 2-m height over 0.12-m grass. Ley et al. (2013) report similar reduction in wind speed over alfalfa as compared with over clipped grass for the same measurement height relative to the ground surface. These differences were found to significantly affect estimates of ET made with aerodynamic methods. In addition, wind speeds measured over dry, warm surfaces are usually stronger than those measured over wetter, cooler surfaces due to effects of instability (buoyancy-induced turbulence) on mixing of higher velocity air from aloft

to the warmer surface. Adjustments for this effect can be made using the blending height-flux profile method of Allen (2012); however, assumptions of large fetches of both types of surfaces must be made.

Rutter et al. (1975) propose adjusting wind measurements for differences in surface roughness and zero plane displacement by extrapolating upward from the measurement surface to some height of a “regional” internal boundary layer,  $z_{IBL_R}$ , where the mean horizontal wind velocity of the equilibrium boundary layer is an integration of regional effects and is presumed to be generally independent of underlying surface roughness of a specific location. The wind velocity at the  $z_{IBL_R}$  height is then extrapolated downward from the  $z_{IBL_R}$  height to some elevation above the surface in question using aerodynamic parameters characteristic of the new surface.

Allen and Wright (1997) improve this procedure by combining equations for adjusting wind velocities for both roughness and wind sensor elevation differences into one equation, which considers the relative heights of internal boundary layers developed over both the weather station surface and the surface in question. The equation is of the form

$$u_2 = u_{2w} = u_{zw} \frac{\ln\left(\frac{z_{IBL_w} - d_w}{z_{om_w}}\right) \ln\left(\frac{z_{IBL_v} - d_R}{z_{om_R}}\right) \ln\left(\frac{z_v - d_v}{z_{om_v}}\right)}{\ln\left(\frac{z_w - d_w}{z_{om_w}}\right) \ln\left(\frac{z_{IBL_w} - d_R}{z_{om_R}}\right) \ln\left(\frac{z_{IBL_v} - d_v}{z_{om_v}}\right)} \quad (11-60)$$

where  $u_{zw}$  is the wind speed adjusted to represent conditions at the  $z_v$  height over vegetation or water surface  $v$ , and  $u_{zw}$  is the original wind speed measurement at the  $z_w$  height over the weather station surface  $w$ . Variable  $z_{IBL_w}$  is the height of the internal boundary layer developed over surface  $w$ , which is in equilibrium with surface  $w$ . Variable  $z_{IBL_v}$  is the height of the internal boundary layer developed over surface  $v$ , which is in equilibrium with surface  $v$ . These parameters are estimated using Eq. (11-61). Variables  $z_{om_w}$ ,  $z_{om_v}$ , and  $z_{om_R}$  are roughness lengths for momentum transfer characterizing the weather surface, the vegetation  $v$ , and the integrated region. Variables  $d_w$ ,  $d_v$ , and  $d_R$  are zero plane displacement heights for the weather surface, vegetation (or water surface)  $v$ , and the region. Units of all  $z$  and  $d$  variables are the same (m) and units for  $u$  are in  $\text{ms}^{-1}$ . The  $z_{om}$  and  $d$  parameters can be estimated using Eqs. (11-21)–(11-29).

Values for  $z_{IBL_w}$  and  $z_{IBL_v}$  may range from only 1 to 2 meters for small fields of 1 ha size to more than 100 m for very large stands of homogeneous vegetation. On a regional scale, the height of a regional internal boundary layer,  $z_{IBL_R}$ , may vary from tens of meters to perhaps 2,000 m and may average about 100 to 400 m (Brutsaert 1982). Brutsaert (1982) presents an

equation to predict boundary layer growth downwind of a discontinuity between two surfaces of similar but unequal roughness:

$$z_{IBL} = d + 0.33z_{om}^{0.125}x_f^{0.875} \quad (11-61)$$

where  $z_{IBL}$  is the height of the perturbed internal boundary layer above a surface of new roughness ( $z_{om}$ ) and zero plane displacement ( $d$ ). Variable  $x_f$  in Eq. (11-61) is the horizontal distance downwind of the surface discontinuity (horizontal fetch). Variables  $z_{IBL}$ ,  $d$ ,  $z_{om}$ , and  $x_f$  in Eq. (11-61) have units of m. Eq. (11-61) can be applied to estimate both  $z_{IBL_w}$  and  $z_{IBL_v}$ . Eq. (11-61) rearranges Eq. (7-12), except that the difference ( $z - d$ ) in Eq. (7-12) is first multiplied by a factor of 10 to approximate the height of the full  $z_{IBL}$ , which is generally 10 times that of the fully mixed internal sublayer, where flux densities of  $H$  and  $\lambda E$  are in equilibrium with the new surface (Brutsaert 1982).

Limitations in the application of Eq. (11-60) are that  $z_w < z_{IBL_w}$  and  $z_v < z_{IBL_v}$ . If these conditions do not exist, then one should use alternate equations presented in Allen and Wright (1997). Other limitations in Eq. (11-60) are that all  $ds$  must be less than the corresponding elevations ( $z$ ) to prevent negative values and extrapolation of wind speed to below zero plane displacement heights and the assumption of near neutrality of the boundary layers. Ley et al. (2013) apply Eq. (11-60) to adjust wind speed measured at 2 and 3 m over alfalfa in Colorado to an equivalent wind speed measured over clipped grass with good results.

In summary, in application of Eqs. (11-60) and (11-61),  $u_{z_v}$  is wind speed predicted to have occurred at the  $z_v$  elevation if the ground cover was vegetation of type  $v$  rather than type  $w$ . The postulation of Eq. (11-60) is that wind speeds measured over surfaces can be extrapolated upward from  $z_w$  using a logarithmic relationship (assuming near-neutral conditions) to some  $z_{IBL_w}$  height using aerodynamic roughness properties characteristic of the weather measurement surface, then extrapolated further upward or downward using aerodynamic properties of the region, and then extrapolated back downward to near the surface using a logarithmic shape characteristic of roughness properties of the vegetation in question. This approach suggests that wind speeds above  $z_{IBL_w}$  and  $z_{IBL_v}$  are driven by the general speed of an air mass, but that logarithmic profiles in equilibrium with the underlying surfaces tie the regional or local air mass and momentum sink to the ground. This simplifies actuality, especially during periods of boundary layer thermal instability, because wind profiles above intermixed vegetation stands do not remain completely separate of each other. However, the approach does provide an approximate adjustment mechanism, which has some application value. Eq. (11-60) can be modified to incorporate effects of boundary layer instability by adding integrated stability corrections based on the Monin-Obhukov formulations (Chapter 7). However, this requires knowledge or estimation of relative magnitudes of sensible heat fluxes from the various surfaces.

## 11.10 EXAMPLE APPLICATIONS OF THE SINGLE-LAYER PENMAN-MONTEITH

The following section summarizes several example applications of the single-layer PM method for estimating ET directly, without the use of crop coefficients. The first example was calculated using a half-hour data set at Davis, California, and Logan, Utah, for grassed surfaces. The second example is for grass forage at Logan, Utah, under soil water-stress conditions with calculations made on a daily (24-hour) basis.

### Half-Hourly Calculations

The PM method with resistance algorithms for grass [Eqs. (8-3), (8-6)–(8-10), and (8-12)] was applied using half-hourly measurements of micrometeorological data at both Logan, Utah, and Davis, California, with calculations compared with lysimeter measurements. The details of the data sets are the same as those described for the energy-balance method applications shown in Figure 7-7, with aerodynamic resistances computed using the same integrated stability corrections [Eqs. (7-22)–(7-26)] based on infrared measurements of surface temperature. The micrometeorological data in this example were collected over the grass crops. Results of the application are shown in Figure 11-12a for the day of August 2, 1990, at Logan, Utah, and in Figure 11-12b for the days of May 2–3, 1967, at Davis, California.

The grass at Logan was primarily fescue and was grown as forage. The grass height on August 2 was 0.23 m. The LAI at Logan was estimated from Eq. (8-12) as 5.5. The grass at Davis was alta fescue and was clipped as turf. The grass height on May 2–3 was 0.12 m, and the LAI measured on May 2 was 2.94. Bulk surface resistance,  $r_s$ , at both locations was calculated using Eq. (8-9) with  $LAI_{eff}$  calculated using Eq. (8-10). Net radiation was calculated at Logan from measured  $R_s$  using the standard procedures described in Chapter 4, because the grass approximated a well-watered surface and would have similar surface temperature. Net radiation at Davis was an average of measurements by three net radiometers.

Two procedures were used to approximate  $r_l$ . In the first procedure, a constant value of  $r_l = 75 \text{ sm}^{-1}$  was used during all time periods to represent a mean daily value for  $r_l$  for use with half-hourly calculations with stability correction (see last entry of Table 11-2). Calculations of  $r_a$  were made with and without stability correction. Resulting calculations by the PM equation [Eqs. (8-2), (11-1)] with these resistances are labeled “PM, no stab.cor.” and “PM, Int.stab.cor.” In the second procedure, a value of  $r_{l,min} = 40 \text{ sm}^{-1}$  was used in conjunction with the stomatal conductance reducing functions [ $g()$ ] to provide a variable  $r_l$  during the calculation periods. Calculations for  $r_a$  were made using integrated stability correction functions. Resulting

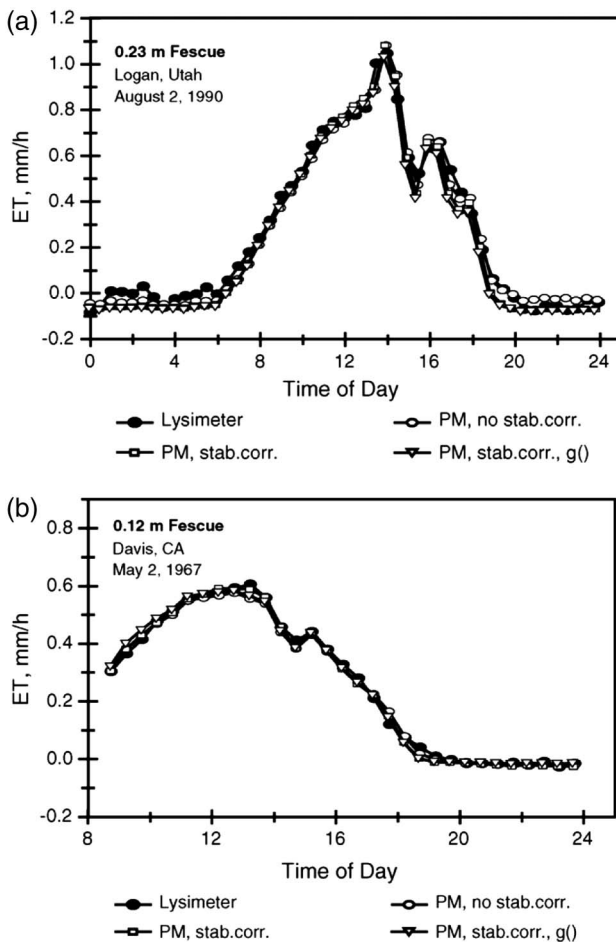


Fig. 11-12. Comparisons of measured ET and ET estimated using the PM equation [Eqs. (8-2), (11-1)] with and without integrated stability correction with  $r_l = 75 \text{ sm}^{-1}$  and with integrated stability correction and  $r_l = r_{l_{\min}}$  of  $40 \text{ sm}^{-1}$  divided by  $g(R_s)g(T)g(\text{VPD})$  for (a) 0.23-m fescue grass at Logan, Utah, and (b) 0.12-m fescue grass at Davis, California

Source: Logan, Utah, data from Allen and Fisher (1990); Davis, California, data from W. O. Pruitt (personal communication, 1994), with data from Morgan et al. (1971)

calculations by the PM equation are labeled "PM, Int.stab.corr,g()" in Figure 11-12.

In the first procedure,  $g(\theta)$  was set equal to 1.0 to reflect high soil water conditions at each site. Data in Figure 11-5 show products of

$g(R_s)g(VPD)g(T)$  calculated for August 2, 1990, at Logan and May 2, 1967, at Davis reached highs of about 0.75 during midmorning hours and then decreased to about 0.4 to 0.6 during afternoon hours when both VPD and  $T$  increased. In the first procedure with constant  $r_l$ , the resulting values for  $r_s$  were  $27 \text{ sm}^{-1}$  at Logan and  $50 \text{ sm}^{-1}$  at Davis, the differences being due to differences in LAI.

In the second procedure,  $r_{s_{min}}$  equaled  $14 \text{ sm}^{-1}$  for  $g_{max} = 0.07 \text{ ms}^{-1}$  at Logan, and  $r_{s_{min}}$  equaled  $27 \text{ sm}^{-1}$  for  $g_{max} = 0.037 \text{ ms}^{-1}$  at Davis. The inclusion of the  $g()$  functions increased the values for  $r_s$  in the second procedure from  $14 \text{ sm}^{-1}$  to  $35 \text{ sm}^{-1}$  during afternoon hours at Logan and from  $27 \text{ sm}^{-1}$  to about  $50 \text{ sm}^{-1}$  at Davis. Surface resistance during nighttime hours ( $R_n < 0$ ) was set equal to  $200 \text{ sm}^{-1}$  to approximate  $r_s$  for moist soil beneath the grass canopies (see discussions in Section 11.8).

The PM calculations fit lysimeter-measured ET well using both procedures for estimating  $r_s$  [constant  $r_l = 75 \text{ sm}^{-1}$  throughout the calculation periods, and  $r_l = r_{l_{min}}$  of  $40 \text{ sm}^{-1}$  divided by  $g(R_s)g(T)g(VPD)$ ]. Calculations were influenced little by inclusion of stability corrections at either location, where values for the Monin-Obukhov  $z/L$  numbers ranged from  $-0.5$  to more than  $2$  at Logan and  $-0.7$  to  $0.1$  at Davis. This is in contrast to the  $ET = R_n - G - H$  calculations presented in Figure 7-10, which were significantly influenced by stability corrections, especially at Davis. The seeming lack of influence of stability correction on the PM estimates stems from the presence of  $1/r_a$  in both the numerator and in the denominator of the PM equation, so that a major amount of change in  $1/r_a$  due to stability correction is self-canceling, depending on the relative magnitudes of  $R_n - G$ ,  $e_z^o - e_z$  and  $r_s$ . This was not the case with the energy balance calculations, which were shown in Figure 7-10. Under strong conditions of instability brought on by water stress, effects of stability correction on PM estimates would become noticeably stronger.

Slight underestimation occurred during the highest half-hour period at Davis at about 1,300 hours, and a slight "lag" in estimates occurred relative to lysimeter measurements during morning hours at Logan. The PM equation predicted slight net condensation of moisture (dew) during portions of nighttime periods at both locations, especially when corrected for stability. The gain in weight due to condensation was also indicated by most of the nighttime lysimeter records, especially at Davis. Under these conditions,  $r_s$  should technically be set to 0. However, without the use of a highly sensitive lysimeter or a leaf wetness sensor, predicting when condensation is occurring is often difficult. In the examples shown in Figure 11-12a and 11-12b, use of  $r_s = 0$  rather than  $r_s = 200 \text{ sm}^{-1}$  made very little difference in the ET predictions at night because aerodynamic resistances were high due to very light wind and stable conditions and VPDs were very small. The dips in calculated and measured ET during mid-afternoon periods at both locations were due to cloud fronts, which passed

overhead, reducing net radiation and air temperatures. Overall, agreement between the PM equation and measurements was very good, with the equation showing very similar sensitivity to changes in solar radiation (overhead clouds) and wind speed as the lysimeter measurements.

### Daily Calculations under Conditions of Soil Water Stress

The PM equation was applied to a three-month data set of micrometeorological and lysimeter data from Logan, Utah, which were collected during a March 20–June 30, 1992, study. The grass cover was tall fescue grown for forage. All irrigation of the lysimeter and surrounding 40-ha field was withheld during 1992 so that the grass crop experienced progressively increasing water stress caused by progressively decreasing soil water. Figure 11-13 exhibits daily (24-hour) calculations of ET made using the PM equation [Eqs. (8-2), (11-1)], where the PM (no stress) calculations were made using  $r_s$  calculated using Eq. (8-9) with  $r_l = 100 \text{ sm}^{-1}$ . This curve represents the upper limit of ET under conditions of limited water stress. The other curves in the figure represent calculations by the PM equation where  $r_s$  was reduced by dividing  $r_s$  by the product  $g(T)g(\theta)$ . The  $g(\theta)$  function was calculated using the three methods described in the section on stomatal conductance functions [Eqs. (11-47), (11-48), and (11-50)]. Because the computation time steps were 24-hour, the  $g(R_s)$  and  $g(VPD)$  functions,

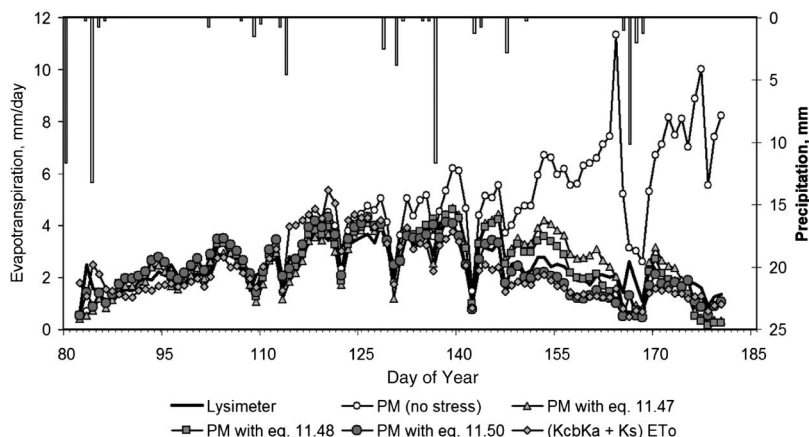


*Fig. 11-13. Comparison between measured ET and ET estimated using the PM equation [Eqs. (8-2), (11-1)] for fescue grass forage at Logan, Utah, March–June, 1992, under conditions of low soil water using 24-hour calculation time steps for three  $g(\theta)$  functions plus the dual crop coefficient method*  
Source: Data from R. G. Allen (personal communication, 1994)

which apply to instantaneous values of  $R_s$  and  $VPD$ , were set equal to 1.0. However, because the first part of the season (late March and April) was cool, the  $g(T)$  function was applied to the daily time steps to adjust for low stomatal conductance caused by low daytime temperatures. Parameters used in Eq. (11-45) were  $T_L = 0^\circ\text{C}$ ,  $K_T = 20^\circ\text{C}$ , and  $T_H = 40^\circ\text{C}$ . Because calculations were made on a 24-hour basis, a mean value of daytime air temperature for use in Eq. (11-45) was approximated for each 24-hour period as  $T = (2T_{\max} + T_{\min})/3$ . In addition, no corrections for boundary layer instability were made because calculations were made on 24-hour time steps.

The grass height for the Logan data set ranged from 0.01 m on March 20 to 0.60 m in June. Leaf-area index for the tall fescue was estimated as  $LAI = 0.20h$ , where  $h$  is mean plant height in m, based on a set of LAI measurements made at  $h = 0.4$  m. LAI was linearly reduced after June 1 to account for leaf senescence and browning of leaves near the bottoms of plants caused by drought conditions. Total LAI was reduced by 1.5 after April 25 due to a hard frost ( $-5^\circ\text{C}$ ) on that date. Because of the tall height of the forage and large LAI,  $LAI_{eff}$  in Eq. (8-9) was computed using Eq. (8-11) by Ben-Mehrez et al. (1992).

Parameters applied in the  $g(\theta)$  functions were  $K_\theta = 1.2$  in Eq. (11-47),  $K_\theta = 0.25$  in Eq. (11-48), and  $K_{sf} = 1.2$  in Eq. (11-50). A value of  $K_\theta = 1.2$  was required in Eq. (11-46) rather than the  $K_\theta = 6.7$  suggested by Stewart (1988) for Scots pine to better follow measured data. The value  $K_\theta = 0.25$  in Eq. (11-48), which was suggested by Stewart and Verma (1992) for Kansas prairie worked well for the fescue at Logan. The values for  $\theta_{fc}$  and  $\theta_{wp}$  for the clay loam soil were 320 and  $140 \text{ mm m}^{-1}$ . The rooting depth for the fescue grass was taken as 1 m.

The  $ET = K_c ET_o$  approach was also applied to this data set, with  $K_c$  estimated using Eq. (10-2) ( $K_c = K_s K_{cb} + K_e$ ). The  $K_{cb}$  curve was constructed using  $K_{c1} = 0.4$  and  $K_{c2} = K_{c3} = 1.1$ . The  $K_s$  values were calculated using Eq. (10-4), and  $K_e$  was calculated using Eqs. (9-19), (9-21), and (9-22) where  $\theta_{fc}$  and  $\theta_{wp}$  had the same values as for the  $g(\theta)$  functions.  $p$  in Eq. (10-5) was set equal to 0.4.  $ET_o$  was calculated using Eq. (8-15).

All three  $g(\theta)$  functions performed relatively well in reducing the estimated ET according to soil water availability. Eq. (11-48) followed lysimeter ET most closely, with Eq. (11-47) overestimating lysimeter measurements during June when soil water was low and Eq. (11-50) estimating well during April and May, but underestimating measurements during June by about 30%. The  $K_c ET_o$  procedure overestimated lysimeter ET by about 20% during late April and early May because no reduction in  $K_c$  occurred until 40% of available soil water was depleted. The procedure underestimated lysimeter measurements during June by about 30%. In general, all four water-stress procedures or functions evaluated show usefulness in estimating effects of decreasing soil water.

### Other Applications of the Single-Layer Penman-Monteith Model

Kustas (1990) applied single- and two-layer PM resistance models to a furrowed cotton field having 20% cover and a dry soil surface in an arid environment. Results were compared with eddy correlation and remotely sensed energy balance methods. The single-layer model generally performed better than the two-layer model, but only when using a bluff-body correction to the aerodynamic resistance made by incorporating heat and water vapor transfer by molecular diffusion into Kolmogorov-scale eddies. However, the empirical adjustment to the surface resistance with the one-layer approach was not applicable over a wide range of conditions. For the two-layer model, large changes in parameters for computing soil evaporation had a small impact on computed fluxes while a significant change in estimated leaf area appeared to amplify deviations between measured and modeled ET values.

Farahani and Bausch (1995) evaluated performance of single-layer PM and S-W ET models over a growing season by comparing against Bowen ratio-based measurements over irrigated maize near Fort Collins, Colorado. When LAI was <2, the PM model, as parameterized for canopy resistance only, did not perform well. When LAI exceeded 2, performance improved. The S-W model performed satisfactorily over the entire range of canopy cover, underestimating ET by 4% over the season. Farahani and Bausch found evaporation from soil estimated by the S-W model to comprise 29% of total ET. This figure was larger than expected for furrow-irrigated maize. Soil evaporation was only about 15% of total ET when LAI was greater than 3. Their study concluded that a generalized and straightforward functional relationship describing soil and canopy resistance is needed and that bulk stomatal resistance should be estimated using a dynamic calculation for effective LAI.

Schaap and Bouteren (1996) compared evaporation from a forest floor beneath a dense Douglas fir stand with weighing lysimeter measurements during 44 days in early spring and summer. The single-layer PM was used to model the evaporation rates. Values of resistance parameters were changed slightly when the Penman-Monteith model was optimized for measured evaporation rates rather than to reproduce measured temperature differences between air and surface. With appropriate parameter sets, the model estimated measured hourly forest floor evaporation rates and surface temperature dynamics relatively well. Schaap and Bouteren showed that in a forest understory, the PM aerodynamic term dominates over the available energy term. As a result, the evaporation flux was matched by an almost equal, downward sensible heat flux to the surface from the canopy above. Forest floor water content dynamics exhibited a strong control on evaporation flux. Spatial variability in forest floor water contents caused the forest floor evaporation to

range from  $0.19 \text{ mm d}^{-1}$  in a dry part of the forest to  $0.3 \text{ mm d}^{-1}$  in a wet part.

Daamen et al. (1998) conducted an interesting study of fluxes from trees and orchard floor in a sheltered lemon orchard where the canopy of the lemon trees covered 39% of the orchard floor and bare understory. Lemon tree transpiration was measured using the stem heat balance method with branch measurements scaled up to canopy level. Those measurements compared well with Penman–Monteith-based transpiration estimates. For the understory, the sum of latent and sensible heat fluxes measured by eddy correlation equaled available energy. Eddy correlation and Bowen ratio methods of flux measurement compared well in the understory.

Ortega-Farias et al. (2005) applied the single-layer PM model to a furrow-irrigated tomato crop having LAI ranging from 1.3 to 3 under different soil water and atmospheric conditions. They used a variable surface canopy resistance model where resistance was computed as a function of environmental variables air temperature, vapor pressure deficit, net radiation and soil heat flux, and normalized soil water availability. Comparisons against ET from a Bowen ratio system indicated errors of 3.6 and 3.9% for 20-minute and daily periods. ET based on the FAO-56  $K_c ET_o$  method underestimated daily ET with an error of 5.2%.

Were et al. (2008) combined internal boundary layer and surface resistances of a multilayer/multisource PM model similar to that described in Figure 11-1e for sparse brush vegetation to create bulk  $r_{ah}$  and  $r_s$  resistances to use in the single-layer PM method. They found the best combination for  $r_s$  to be

$$\frac{1}{r_s} = \frac{f_c}{r_{sv} + r_{sss}} + \frac{1 - f_c}{r_{sse}} \quad (11-62)$$

where  $f_c$  is the effective fraction of ground shaded by vegetation, and  $r_{sv}$ ,  $r_{sss}$ , and  $r_{sse}$  are surface resistances for vegetation, shaded, and exposed soil described in Figure 11-1e. The formulation of Eq. (11-62) follows that of Eq. (11-57) for combination of resistors in parallel. Were et al. (2008) found best agreement between the single-layer PM and multilayer model when the bulk aerodynamic resistance,  $r_{ah}$ , in the single-layer model was formulated from the multilayer resistances as

$$r_{ah} = f_c(r_{hv} + r_{hss}) + (1 - f_c)r_{hse} + r_{am} \quad (11-63)$$

where the boundary layer resistances are defined in Figure 11-2e. Eq. (11-63) performed better than using the classical function for combining the boundary layer resistances in parallel with aerodynamic resistance in series.

Zhang et al. (2008) compared the single-layer, multilayer, and patch models with Bowen ratio measurements of ET for a vineyard in the arid desert region of northwest China. Generally, the variation in estimated ET from all three models was similar to that of measured ET. They found the single-layer model, as parameterized, to overestimate ET significantly, with the multilayer and patch models agreeing better with measurements. Following a frost, the patch model significantly overestimated ET because the canopy resistance of the vines was substantially reduced.

Irmak and Mutiibwa (2009) applied the single-layer PM to maize over a growing season in Nebraska with comparisons to Bowen ratio-derived ET. They found a seasonal average minimum bulk canopy resistance of  $56 \text{ sm}^{-1}$  inversely computed from the Bowen ratio energy balance system (BREBS) data that was somewhat consistent day to day. They also investigated the impact of the source of meteorological data on the PM method, including using weather data from a “near-reference” grassed weather station and using meteorological data from the BREBS system itself, measured over the maize canopy. There was good agreement ( $\text{RMSD} = 0.11 \text{ mm h}^{-1}$ ) between the PM estimates using grassed weather data and ET from BREBS with 9% overestimation. When applied using weather data measured over the maize crop, including measured  $R_n$  and  $G$ , the performance of the PM improved with estimations within 2% of the ET from BREBS and  $\text{RMSD} = 0.08 \text{ mm h}^{-1}$ . A significant amount of this improvement was due to using common  $R_n$  and  $G$  in both the BREB and PM calculations, which compromised the independence of the two methods, and due to the inverse solution of mean values for  $r_s$ . In general, the use of grassed weather station data did not substantially affect the application accuracy of the PM for the maize crop.

Zhao et al. (2010) applied the single-layer PM model to a maize field in an arid region of northwest China and estimated bulk canopy resistance using a Jarvis type of approach (Eq. 11-37) with parameterization by Noilhan and Planton (1989) (N-P) and Jacobs and de Bruin (1997) (J-D) approach based on plant physiology, where a correlation relationship between the leaf stomatal conductance and the net photosynthetic rate at leaf scale is used to upscale conductance from a leaf to the canopy. The latter method is able to incorporate impacts of  $\text{CO}_2$  concentrations on stomatal conductance and thus transpiration and impacts of leaf temperature, radiation levels, and vapor pressure deficit. ET estimates were compared with half-hourly measurements from an eddy covariance system. Results indicated that the N-P approach slightly underestimated bulk canopy resistance, while the J-D approach, as parameterized, overestimated. ET estimates using the N-P approach were more consistent than those with the J-D approach during the full growing season. The PM model with J-D bulk canopy resistance slightly underestimated ET throughout the maize growing season, but overestimated ET during a period of dry soil

surface. The relatively good fit of ET from the P-M model with N-P bulk canopy resistance on a half-hourly time step was concluded to be partially due to the relatively high homogeneity and lack of water stress in the maize field.

### Examples of Applications of Multilayer Penman-Monteith Models

Brenner and Incoll (1997) investigated the importance of clumping of vegetation for modeling evaporation from soil and shrubs in southeast Spain using single-layer, multilayer, and patch models. Stomatal conductances of shrubs were found to decline linearly with increasing in-canopy water vapor saturation deficit ( $D_c$ ). Soil surface resistances were found to increase quadratically with time after wetting of the soil surface. A patch model that included clumping was compared with single- and two-source models. The multilayer model included feedbacks between plant resistances, in-canopy vapor pressure saturation deficits, and total evaporation from the surface. The single-layer and two-source patch models overestimated transpiration by 1% and 8%, respectively, whereas the clumped model underestimated transpiration by 5%. They concluded that overestimation of transpiration by the conventional two-source model resulted primarily from overestimation of radiation absorbed by the canopy. The underestimation by the clumping model may have resulted from underestimation of the long-wave radiation emitted from the soil and absorbed by the canopy.

Sene (1996) applied the two-layer Shuttleworth-Wallace (S-W) model to a sparse vineyard in Spain. The bulk canopy resistance was found to be generally proportional to single leaf resistance divided by total LAI. Diurnal variations in  $r_l$  exhibited a daily minimum value for  $r_l$  of about  $200 \text{ sm}^{-1}$ , increasing to about  $700 \text{ sm}^{-1}$  near dawn and dusk. The diurnal trend was similar from day to day, suggesting that it was primarily linked to variations in solar radiation. A fixed diurnal pattern scaled on the midday value was used with the midday value determined as a function of leaf-area index. Sene used a parameterization for soil heat flux of exposed soil as  $G = G_{dry} [1 - 3(\theta/\theta_s)^2]$  where  $\theta$  is the volumetric water content of the shallow surface soil layer,  $\theta_s$  is the saturation water content, and  $G_{dry}$  is soil heat flux of a dry soil,  $G_{dry} = 0.29R_n - 23$ ,  $\text{W m}^{-2}$ . Undercanopy  $G$  was estimated as 0.7 of  $G$  for exposed soil.

Daamen (1997) applied a two-layer PM style model to sparse millet in Niger where the model was patterned after the S-W model and Choudhury and Monteith (1988). The exception was the use of a heat and mass transfer model for soil heat and vapor fluxes rather than parameterization of a soil surface resistance term. Simulated and measured values of daily evaporation from soil were not significantly different, and simulated soil water content was generally within one standard deviation of the mean measured

value. Using their model, they were able to test several parameterizations of the soil surface resistance term for the S-W model and found that a simple linear resistance model where soil resistance increased with time after rainfall may be adequate in a two-source model when leaf-area index is 2 or higher, but it is inadequate for lower leaf-area indices. Daamen (1997) also simulated microscale transfer of heat from dry soil to the vegetation canopy and found the greatest increase of transpiration above the incident net radiation partitioned to the canopy occurred at LAI between 1.0 and 1.5.

Iritz et al. (1999) tested a modified version of the two-layer S-W model for a mixed 50–100-year-old boreal forest in central Sweden and compared estimates against eddy correlation flux measurements. Their model had modified terms for bulk canopy resistance and aerodynamic resistance. A soil moisture submodel was used to estimate soil-water-induced regulation on canopy resistance. That submodel performed well in estimating ET over a growing season. Their model assumed that canopy stomata and boundary layer resistances acted in parallel at some hypothetical level in the canopy.

Domingo et al. (1999) applied a two-source patch model to *Retama sphaerocarpa* shrubs in eastern Spain and tested model parameters for their importance in controlling evaporation. ET estimates were compared with measurements by a BREB system, and transpiration estimates were compared against measurements by sap flow of shrub stems. Modifications were made to the original two-source clumped model to significantly improve agreement between estimated and measured ET rates. Modifications included improved parameterization of soil surface conductance, a more detailed description of the radiation balance, and improved parameterization of the soil aerodynamic conductance terms. Improvements in the soil surface conductance estimates made the most significant improvement in model estimates, with the other two modifications showing less significant improvement in estimation of evapotranspiration. A sensitivity analysis indicated that somewhat large variations of leaf-area index or albedo caused little variation in ET, whereas variation in soil water content caused large change in estimated ET. Transpiration rates of shrubs (measured and modeled) were largely independent of surface soil moisture (0–25 cm) indicating that the shrubs accessed reserves of water deep in the soil.

Gardiol et al. (2002) compared a simplified patch model with the single-layer PM and Shuttleworth-Wallace (S-W) models and against ET measurements from a corn crop obtained by soil water balance at Balcarce, Argentina. The single-layer model, as parameterized, underestimated ET. The S-W model, with improved simulation of soil evaporation, estimated total ET relatively accurately for LAI < 4 (sparse canopy condition), but overestimated total ET when LAI > 4.

Fisher et al. (2004) applied a single-layer PM and a two-layer S-W model to a ponderosa pine forest ecosystem at an Ameriflux site in northern California. The S-W method performed better than did the Penman-Monteith (1965) model, although a simple Priestley-Taylor model with a defined  $\alpha$  value performed best compared with the other models. This suggests difficulty in adequately describing surface and aerodynamic parameters in the more complex models or uncertainties in the eddy covariance measurements. A constant canopy resistance was used in the S-W and PM models. ET estimates increased by as much as 26% when canopy resistance was set to a minimum value and decreased by as much as 20% when canopy resistance was set to a maximum value.

Mo and Beven (2004) applied two- and three-source multilayer models to a wheat crop and showed that parameter sensitivities were different between the model types, with the three-source model having more constrained uncertainty bounds. They found net radiation on shaded leaves to be about 20% of that on sunlit leaves, whereas latent heat flux around noon from shaded leaves was 50% of that from sunlit leaves. They concluded that shaded leaves acted as sinks for sensible heat, reducing predicted temperature differences between the two groups of leaves.

Villagarcía et al. (2007) compared two methods for obtaining soil boundary layer resistance ( $r_{hs}$  in Figure 11-2) in multilayer models, with one method based on turbulent diffusion (TD) theory [i.e., Eqs. (11-9)–(11-12)] and another based on inverse calculation of boundary layer resistance using an energy balance (EB) between heated and unheated sources/sensors placed in the canopy. They studied how estimates from each method were affected by canopy structure parameters for typical sparse vegetation. They found the EB-based boundary-layer resistances, unlike those from TD, to implicitly consider peculiarities of plant architecture and structure and the presence or absence of substrate under canopies. In contrast, when applying the TD method, quantitative descriptions for vegetation (average vegetation height, leaf-area index, fractional vegetative cover, drag coefficient, and the eddy diffusivity decay constant,  $n$ ) are all necessary, which is not only difficult to obtain in most applications, but also tended to be insufficient in explaining the development of the soil boundary layer in sparse semiarid vegetation. The advantages of using the EB method are both practical and theoretical, although *in situ* measurements are required. Positioning of required heaters and sensors was straightforward and did not require knowledge of the aerodynamic attributes of the vegetated area. Villagarcía et al. (2010) in a following study showed that soil surface resistance,  $r_{ss}$ , was best estimated using shallow simulation or measurements of soil surface water content, preferably at 1 cm depth.

Ortega-Farias et al. (2007) applied the two-layer S-W model to a drip-irrigated Cabernet Sauvignon vineyard in Chile and compared against

half-hourly ET from eddy covariance with relatively good results. RMSE was  $29 \text{ W m}^{-2}$ . The largest disagreement occurred under dry atmospheric conditions. They found the S-W model formulation to be sensitive to error in leaf-area index and mean stomatal resistance where change in ET was as high as  $\pm 20$  and  $\pm 18\%$  when these parameters were varied by  $\pm 30\%$ . ET estimates were not substantially affected by error in estimation of aerodynamic resistance.

Poblete-Escheverria and Ortega-Farias (2009) expanded their application of multilayer models on vines to a three-source clumped (patch) model with application to a drip-irrigated Merlot vineyard trained on a vertical shoot positioned system under semiarid conditions in Chile. The vineyard had an average fractional cover of 30%, and the model was partitioned among canopy transpiration, evaporation from soil under the vine canopy, and evaporation from soil between rows, with weighting according to fractional covers following a formulation by Brenner and Incoll (1997). Most parameterizations of resistances followed those of Shuttleworth and Wallace (1985) or Shuttleworth and Gurney (1990). Results were compared against two years of ET from an eddy covariance system. Accuracy of the clumped model, as parameterized, was good, with RMSE of  $0.33 \text{ mm d}^{-1}$  and RMSE for daytime LE of  $36 \text{ W m}^{-2}$ . They found major underestimation on clear days following rainfall or foggy days and during high-evaporation demand periods when  $\lambda E$  exceeded  $300 \text{ W m}^{-2}$ . Maximum values for both measured and simulated ET occurred about 2 h after the peak values of  $R_n$ , due to lags in temperature and vapor pressure deficit. They concluded that application of a clumped model requires a good characterization of the vineyard architecture.

Ortega-Farias et al. (2010) employed variable canopy resistance functions in a two-layer S-W model over a drip-irrigated Merlot vineyard with  $\text{RMSE} = 34 \text{ W m}^{-2}$ . Canopy resistance followed the Jarvis style of conductance functions [Eq. (11-37)] with parameterization for photosynthetically active radiation, vapor pressure deficit, air temperature, and soil water stress.

Zhongmin et al. (2009) applied the two-layer S-W model to partition ET into evaporation and transpiration (T) for four grassland ecosystems in China. Estimates were compared against ET from the eddy covariance technique. Monte Carlo simulations were used to estimate key parameters in the model and to evaluate the accuracy in model partitioning (i.e., E/ET). Results showed good agreement with measurements at both hourly and seasonal timescales. The model tended to underestimate ET by 3–11% on rainy days, probably due to the lack of model representation of rainfall interception. In general, E accounted for a large proportion of ET from the grasslands, with E/ET ranging from 12% to 56% during the peak growing season and annual E/ET ranging from 50% to 67% across the four ecosystems. Canopy stomatal conductance controlled E/ET at the diurnal

timescale, and the variations and magnitude of leaf-area index (LAI) explained most of the seasonal, annual, and site-to-site variations in E/ET. A simple linear relationship between growing season LAI and E/ET explained 80% of the variation observed over the 10 modeled site-years. Daily E/ET decreased to a minimum value of 10% for values of LAI greater than 3 in a grass system having a dense canopy. The sensitivities of E/ET to changes in LAI increased with the decline in water and vegetation conditions at both the seasonal and the annual time scales.

### 11.11 APPLICATIONS OF EVAPOTRANSPIRATION MODELS USING REMOTE SENSING INPUTS

The advantage of the PM and other models is that they can be applied with routine weather data on hourly or daily time steps. The continuous applications have the strong advantages of incorporating effects of precipitation and changing weather conditions on total aggregated ET. They also have the strong advantage of being coupled with soil water balances to provide feedback on water supply to support the ET process. A disadvantage of soil and weather-based process models is in the parameterization of these models over large areas having wide variation in vegetation and water availability. In these situations, the applications can be substantially assisted, or even made possible, by the use of vegetation information and thermal information provided by remote sensing. Generally the remotely sensed information is via satellite due to the large extents of coverage.

Satellite coverage at moderate resolution (<50 m pixel sizes) is generally only available from polar-orbiting satellites such as Landsat, SPOT, ICONOS, Quickbird, etc., so that imagery for a particular location is relatively infrequent. For example, Landsat revisit time is every 16 days. The infrequent coverage is insufficient for estimating a time-integrated ET in and of itself (Allen et al. 2007b). However, when coupled with an hourly or daily ET process model, the use of the infrequent satellite imagery to improve estimates of surface albedo, surface temperature, surface roughness, and the partitioning of surface energy between latent and sensible heat fluxes can greatly improve the accuracy of the process-based estimates.

Moran et al. (1996) used remotely sensed measurements of surface reflectance and temperature to apply the PM equation to partially vegetated fields with improved estimates of percent vegetation cover and canopy resistance. The Penman-Monteith equation was combined with the energy balance equation to estimate the surface temperature ( $T_s$ ) associated with four states: surfaces characterized by full-cover vegetation and bare soil with evaporation rates at potential and zero.  $T_s$  values from satellite data were linearly interpolated between full cover and bare soil

conditions to provide information for intermediate states. Maps of surface air temperature and wind speed were combined with maps of surface temperature and spectral vegetation index to produce regional estimates of evaporation rates for a grassland biome.

Kustas (1990), Kustas et al. (2004), Anderson et al. (2005), Li et al. (2005), and Kustas and Anderson (2009) have led the development of the two-source energy balance (TSEB) patch model that utilizes radiometric surface temperature inputs from satellites, surface reflectance, and vegetation indices to estimate ET from sparse canopies.

The Mapping Evapotranspiration at High Resolution Using Internalized Calibration or METRIC model (Allen et al. 2007b) applies a full-surface energy balance to Landsat, MODIS, and other thermally equipped satellite image products to develop images of the fraction of alfalfa-reference ET,  $ET_r F$ , that are then interpolated using a spline function and multiplied by daily  $ET_r$  to produce time series of daily and monthly ET. Satellite-based mapping of ET provides valuable spatial information on within-field and field-to-field variation in ET and will become increasingly used in water rights management, water transfers, and streamflow depletion studies.

## 11.12 MEASUREMENT AND ESTIMATION OF ET ON SLOPING LANDS

Many studies of hydrologic processes under natural conditions involve sloping land surfaces. On sloping surfaces, the potential amount of solar energy converted into ET will increase for southward facing slopes (in the Northern Hemisphere) and will decrease for northward facing slopes. The increase or decrease will be related to the change in the angle between the slope and the angle of the sun (Swift 1976; Perez et al. 1986). Under most conditions of small slope (< about 15°), ET calculations can be made on a horizontal basis with little error. However, the user must bear in mind that the ET flux density calculated horizontally (for example, expressed in mm or  $m^3 m^{-2}$ ) is based on a per-unit horizontal land area. To convert to a unit area basis parallel to the land slope, a trigonometric adjustment should be made.

When calculations are made on an along-slope basis, then net radiation measurements or calculations should be made parallel to the slope, or calculations of  $R_n$  must be adjusted for the effect of slope. With slopes greater than about 15%, horizontally measured  $R_n$  adjusted for slope angle can deviate from  $R_n$  measured parallel to the slope, because the upper surface of a horizontally placed radiometer may "see" some long-wave and reflected shortwave radiation from the ground or vegetation surface uphill (Nie and Kanemasu 1989; Fritsch and Qian 1990). When measurements of  $R_n$  are made parallel to slopes, the interpretation of measurements is

more straightforward than if the radiometer is placed horizontally. When parallel to the slope, the upper surface(s) of the radiometer see an unobstructed view of sky (except for obstruction by cross-valley terrain), and the bottom surface(s) see ground and vegetation only. In mountainous areas,  $R_n$  on a slope can be affected by long-wave emissions from cross-valley slopes. In the case of a south-facing slope, the cross-valley emission will be smaller than in the case of a north-facing slope that views a warmer south-facing slope. In all cases, the thermal emission of the cross-valley slope will be greater than that from the atmosphere and should be accounted for. Allen et al. (2006b) developed integrated equations for estimating daily net radiation on slopes assuming infinite slope lengths. Flint and Childs (1987) presented a more complex model for solar radiation on slopes that uses terrain models to account for surrounding ridges and tall trees that may block both direct beam and diffuse sky shortwave radiation.

On slopes, wind speeds used in ET equations that are applied on an along-slope basis should represent wind movement parallel to the slope, and  $z$  heights used in resistance calculations are expressed as perpendicular to the slope. Examples of applications of ET equations for sloped areas include Dozier and Frew (1990) and Neale et al. (1995).

Other problems in calculating or measuring ET in areas having variable land slope include convergence or divergence of wind streamlines, especially downwind of abrupt changes in slope. This can cause severe errors in eddy correlation and Bowen ratio measurements. In addition, density-induced drainage of air in downslope directions during periods of low solar radiation and in upslope directions during periods of high solar radiation, can substantially affect local wind speeds, air temperatures, and vapor gradients, especially during calm periods. In application of ET equations over areas having large changes in elevation, air temperatures can be adjusted during extrapolation over areas with changing elevation using lapse correction (about  $0.01^{\circ}\text{C m}^{-1}$  for nonsaturated air).

### 11.13 EVAPORATION OF INTERCEPTED RAINFALL

When leaves are wet from rain,  $r_l$  effectively becomes zero and evapotranspiration occurs at substantially higher rates than from dry leaves, all other micrometeorological factors being equal. Evaporation of intercepted rainfall can be a significant portion of the water balance, especially in forests with large total leaf area and where single-leaf stomatal resistances are large.

Interception is usually measured as a difference between gross precipitation and that reaching the soil. In forests, the annual interception may be 10–40% of total precipitation (Zinke 1967; Sharma 1985) depending on canopy storage and rainfall amount, intensity, and frequency. Rutter (1975)

and Rutter et al. (1975) estimated canopy storage during individual rainfall events to vary from 0.8 to 1.5 mm for established forests, with no distinct difference between storage capacity of forests and herbaceous species. Dickinson (1984) approximated maximum canopy storage,  $S$ , as

$$S = 0.2LAI \quad (11-64)$$

where  $S$  is in mm and  $LAI$  is total leaf-area index.

The potential increase in total ET due to evaporation of intercepted rainfall can be inferred from the PM equation [Eq. (11-1)], if one ignores feedback effects of evaporation on conditioning of the air boundary layer, as

$$\frac{E_i}{ET_c} = \frac{\Delta + \gamma(1 + \frac{r_s}{r_a})}{\Delta + \gamma} \quad (11-65)$$

where  $E_i$  is potential evaporation (or ET) during evaporation of intercepted rainfall, and  $ET_c$  is total ET during a similar period having a dry canopy, but with the same  $T$ ,  $RH$ , and wind measurements. Because  $r_a$  of forests is generally small and  $r_s$  of forests is generally large relative to agricultural crops, the ratio of  $r_s/r_a$  is large for forests, characteristically ranging between 10 and 70 or more (Jarvis et al. 1976). This is in contrast to agricultural crops, which commonly have ratios close to 1. Therefore, the ratio  $E_i/ET_c$  can be as high as 5/1 for forests as compared with ratios of perhaps 1.6/1 for agricultural crops. These ratios assume that the canopies are exposed to the same weather conditions under wet and dry scenarios. However, this is seldom the case, where the large evaporative flux density from a wet forest canopy will invariably humidify and cool the equilibrium boundary layer above the canopy, thereby reducing the vapor deficit gradient and consequently the ratio of  $E_i/ET_c$ . A previous section on weather measurement discussed modification of the weather of the boundary layer. It should also be understood that the period of  $E_i$  may be quite short, depending on the storage capacity of the canopy.

Rutter et al. (1975) proposed a generalized method for predicting evaporation of rainfall interception in forests. A variation of his proposed method is included here. If variable  $S$  is defined as the surface storage capacity of a canopy (maximum retained interception), expressed as mm depth over the land surface, then when the amount of water on a canopy,  $C$ , equals or exceeds  $S$ , evaporation of intercepted precipitation,  $E_c$ , is set equal to  $E_i$  as computed using the PM equation [Eq. (11-1)] with  $r_s = 0$ . When  $C < S$ , then  $E_c$  is reduced in proportion to the ratio of  $C$  to  $S$  as

$$E_c = E_i \frac{C}{S} \quad (11-66)$$

When  $C \geq S$ , transpiration during interception,  $T_i$ , is assumed to be zero, and all evaporative energy is consumed by evaporation of intercepted water. When  $C < S$ ,  $T_i$  is estimated as

$$T_i = \left(1 - \frac{C}{S}\right) ET_c \quad (11-67)$$

where  $ET_c$  is the ET rate from dry foliage, computed using Eq. (11-1) with  $r_s > 0$ . Total evapotranspiration from the canopy,  $ET_i$ , at any time, is computed as

$$ET_i = E_c + T_i \quad (11-68)$$

When  $C \geq S$ ,  $ET_i = E_c = E_i$  and  $T_i = 0$ . When  $C < S$ ,  $ET_i < E_i$  and  $T_i \leq ET_c$ . When  $C = 0$ ,  $ET_i = T_i = ET_c$  and  $E_c = 0$ . This approach essentially assumes that evaporation from the forest floor during the interception event is zero and that all evaporation occurs within the wetted canopy. If this assumption is not true, for example, in sparse canopies, then the soil evaporation component of the evapotranspiration flux should be included using procedures detailed in the preceding section on soil evaporation.

In the Rutter model, it is assumed that  $(1 - p) P$  rainfall is added to the canopy ( $C$  term) during each computation time step, where  $p$  is the fraction of rain that falls between gaps in the canopy, and  $P$  is rainfall depth during the time step. The drainage rate from the canopy,  $D$ , during a time step is computed as

$$D = e^{(a+bC)} \quad (11-69)$$

where  $D$  has units of  $P$ , and  $a$  and  $b$  are empirical coefficients. Rutter et al. (1975) suggest a value for  $b = 3.7$  for most canopies for  $C$  in mm. Coefficient  $a$  is computed by noting canopy drainage rate when  $C = S$ . Rutter et al. (1975) determined  $D$  for a Corsican pine stand equal to  $0.002 \text{ mm min}^{-1}$  when  $C = S$  and suggested estimating  $D$  for other canopies as  $0.0019 S$  for  $S$  in mm. Table 11-7 lists typical values of  $p$  and  $S$  for forest stands evaluated by Rutter et al. (1975).

Due to the dynamic nature of the Rutter model in accounting for storage of water on the vegetative canopy with new additions of  $P$  and losses of  $D$  with time, using short measurement time steps for  $P$  and short computation time steps in the model is important. Rutter et al. (1975) suggest using hourly measurement and computation time steps, with time steps longer than 3 hours providing poor results.

Generally, when computing ET on daily time steps, the increase in total ET due to evaporation of intercepted precipitation,  $E_{it}$ , can be approximated by the following:

$$E_{it} = (ET_i - ET_c)t_p + S \quad (11-70)$$

Table 11-7. Values of Fractions of Rain Falling between Gaps in the Canopy,  $p$ , and Canopy Storage Capacity,  $S$ , per  $\text{m}^2$  of Land Surface

Stand Type	Mean Tree Height, $m$	$p$	$S \text{ Mm}$
Corsican pine	20	0.25	1.05
Douglas fir	24	0.09	1.2
Norway spruce	10	0.25	1.5
Hornbeam, leafy	17	0.35	1.0
Hornbeam, leafless	17	0.55	0.65
Oak, leafy	15	0.45	0.88
Oak, leafless	15	0.80	0.28
Oak, defoliated	15	0.85	0.18

Source: Data from Rutter et al. (1975)

where  $ET_i$  is the potential rate of ET when leaves are wet, estimated using Eq. (11-1) with  $r_s = 0$ , and  $ET_c$  is the ET rate when leaves are dry ( $r_s > 0$ ).  $ET_i$  and  $ET_c$  should be computed using wind, humidity, and air temperature measured during or surrounding the precipitation event. Parameter  $t_p$  is the duration of the precipitation event, and  $S$  is canopy storage capacity. If  $E_{it}$  and  $S$  have units of mm and  $ET_i$  and  $ET_c$  have units of  $\text{mm h}^{-1}$ , then  $t_p$  must have units of h. If the time of day of the precipitation event is unknown, then 24-hour averages of  $ET_i$  and  $ET_c$  can be used as a general approximation. The total evaporation of intercepted precipitation,  $E_{it}$ , converted to  $\text{mm h}^{-1}$  units, can be added to  $ET_c$  for the period encompassing the precipitation event to obtain total ET for the period. It is important to note that both  $ET_i$  and  $ET_c$  are almost always less during a rainfall event as compared with periods with no rainfall due to reduced net radiation,  $R_n$ , and generally increased humidity and decreased temperature during rainfall.

This page intentionally left blank

## CHAPTER 12

# REGIONAL ESTIMATES OF EVAPOTRANSPIRATION

### 12.1 INTRODUCTION

Estimates of regional evapotranspiration (ET) are necessary inputs to world climate models, to regional water use and supply planning and assessment, to estimation of potential food production capacities and supplies, and for hydrologic studies. Methods for determining ET at specific locations cited in Chapter 11 and this chapter are valid for regional ET estimates when applied with gridded or spatially representative data. The major problem in estimating regional ET has been in extending information from point sources to larger areas. One approach is to aggregate water balance and weather data from watershed studies to produce watershed-averaged estimates. Remote sensing is used more and more to produce spatial information regarding water consumption. Current applications typically involve remote sensing combined with surface energy balance models.

Agricultural cultivars have been selectively developed over the years for maximum agronomic production. Consequently, stomatal resistances of crop cultivars are generally low (unless developed specifically for drought tolerance), and cultivated plants transpire at near potential rates when water is not limiting. In contrast, natural vegetation in semiarid and arid areas has evolved over time to exercise stomatal control for survival under stressed conditions. Thus, its stomatal (or surface) resistances may be an order of magnitude greater than for cultivated vegetation, and its root systems may be more aggressive. For regional ET computations, a logical division is to separate land uses into cultivated and natural vegetation. Regions can also be divided using primary precipitation gradients or humid and arid climate zones.

For cultivated vegetation in semihumid to humid areas, regional ET is generally limited by the available energy ( $R_n - G$ ) at the surface unless under drought. Therefore, a simple measurement or estimation of net radiation in humid areas can yield first-order approximations of ET from cultivated vegetation. Regional ET may be somewhat less than  $R_n$  for natural vegetation in humid areas, ranging from 0.4 of  $R_n$  during cold periods of the year having daytime average temperature of about 0°C and approaching  $1.0 \times R_n$  during hot summer and fall months. In zones well away from the equator, a well-defined cyclic relationship among  $\lambda E$ , the latent heat of E and ET, and  $R_n$  can be expected, with higher ratios in fall than in spring. Regional ET is typically both water and energy limited in semiarid and arid areas. Therefore, a simple measurement or estimation of both net radiation and precipitation in arid areas can yield first-order approximations of ET from nonirrigated cultivated vegetation.

## 12.2 THEORY

Of the methods presented in previous chapters, the most readily used for regional application are the water balance method, lysimeters, energy balance methods, and mass transfer or modeling methods. Application of these methods to regional studies is discussed here.

The Bowen ratio energy balance method (BREB) combines transport and energy balance equations measured locally. This method was presented in Eqs. (7-7) and (7-8), and Chapter 7 discusses operational procedures. The main assumptions in the Bowen ratio method, as described in Chapter 7, are (1) the transport of  $H$  and  $\lambda E$  is one-dimensional (vertical); (2) the surface is homogeneous, dense, and shallow (i.e., heat, water, and momentum sources and sinks are indistinguishable); and (3) steady-state conditions exist. These assumptions are less demanding for BREB than for other meteorological techniques because the gradient measurements for the BREB are usually made close to the surface and wind speed measurements are not required. Recommendations on minimum fetch requirements are also discussed in Chapters 7 and 11.

The other common method for measuring local fluxes is the eddy covariance method described in Chapter 7. That method is somewhat routine to set up, however, equipment maintenance and "correction" of turbulent flux products can require substantial education and training in the physical sciences. Chapter 7 presents various precautions and recommendations for both Bowen ratio and eddy covariance approaches.

Challenges with the BREB, eddy covariance, and other "local" measurements of ET lie in extrapolation over the region, where vegetation and water availability can be spatially variable. The BREB and eddy covariance methods can be used to calibrate or verify methods such as the

Penman-Monteith method that can then be used with gridded weather and vegetation data and satellite-based energy balance and vegetation-based methods.

For large areas of somewhat wet surfaces with minimal advection, evaporation may approach an equilibrium condition. Priestley and Taylor (1972) present an empirical relationship for equilibrium conditions:

$$\lambda E_{eq} = \alpha \frac{\Delta (R_n - G)}{\Delta + \gamma} \quad (12-1)$$

where  $\lambda E_{eq}$  is equilibrium evaporation or evapotranspiration for a large wet area,  $R_n$  is net radiation,  $G$  is soil heat flux,  $\gamma$  is the psychrometric constant, and  $\Delta$  is the slope of the curve of saturation-specific humidity versus temperature. Priestley and Taylor derived a value of  $\alpha = 1.26$  for semihumid to humid areas when the region was wet following general rains. Stewart and Rouse (1977) reproduced the value of 1.26 for a saturated sedge meadow at 58° N latitude during the month of July and for a 2-m deep lake at 46° N latitude between June and September. The value of  $\Delta/(\Delta + \gamma)$  at 25°C is approximately 0.74. Therefore, under these conditions, from Eq. (12.1),  $\lambda E = 1.26(0.74) (R_n - G) = 0.93 (R_n - G)$  or equilibrium latent heat flux is approximately equal to net radiation.

Caution is needed in using Eq. (12-1) during late-fall to late-winter months in zones well away from the equator where the long nights of negative  $R_n$  can to some extent negate the response of  $\lambda ET$  to solar radiation,  $R_s$ , and daytime positive  $R_n$  (Nakayama et al. 1983; Pruitt and Doorenbos 1977). These authors found the use of 24-h  $R_n$  to result in experimentally determined values of  $\alpha$  close to 2.0 in winter months at Davis, California, even under low or nonadvection conditions. For higher latitude locations, e.g., Copenhagen, Denmark, the equation breaks down completely during winter periods when 24-h  $R_n$  becomes negative over extended periods even though some ET is produced by daytime positive net radiation. Under arid or semiarid conditions with advection of heat in air masses, Eq. (12-1) can significantly underestimate ET (Jury and Tanner 1975; Jensen et al. 1990; Jones and Kiniry 1986; Steiner et al. 1991). The recommended alternative is to estimate short crop reference ET for dry climates instead of using only  $R_n$ .

When the water supply is limited, ET will tend to be less than  $\lambda E_{eq}$ . The Penman-Monteith (PM) type of resistance-based combination equation [Eqs. (8-2), (11-1)] is recommended under these conditions. Values for the bulk surface resistance,  $r_s$ , for different canopies are summarized in Table 11-2. Typical values are 100  $s m^{-1}$  for forests, 40  $s m^{-1}$  for grassland, and 30 to 50  $s m^{-1}$  for crops. These are minimum values assuming that sufficient soil water is available. The value of  $r_s$  will increase with decreasing soil water, increasing vapor pressure deficit, and decreasing  $R_s$  or  $R_n$ .

Procedures for increasing  $r_s$  to reflect effects of decreasing soil water when applying the PM equation are described in Chapter 11.

The value for the aerodynamic resistance term,  $r_a$ , of the PM equation is somewhat large for smooth surfaces and somewhat small for rough surfaces such as forests. Consequently the effect of  $r_s$  has the strongest effect over forests. For  $r_s = 40 \text{ s m}^{-1}$ ,  $ET_c/ET_i \approx 0.9$  for grassland and  $\approx 0.5$  for forest, where  $ET_c$  is the PM estimate for the particular cover under well-watered conditions ( $r_s = 40 \text{ s m}^{-1}$ ) and  $ET_i$  is the PM estimate with the same  $r_a$  value but with  $r_s = 0$  (representing evaporation immediately following rain). Section 11.13 discusses increased sensitivity of evaporation from forests to  $r_s$ .

## 12.3 APPLICATIONS

The following section describes applications of the complimentary approach and energy balance models for regional estimates of ET from forests, grasslands, and agricultural areas. The section describes data sources to support regional ET estimates including the use of gridded weather data.

### Complimentary Approach to Estimating ET

Whenever available soil water limits ET, it decreases below the maximum rate for the particular surface, and the component of sensible heat flux density to the air ( $H$ ) increases, following Eq. (4-1). This increases the heating of the boundary layer of air above the surface, which manifests in two ways: (1) air temperatures increase, and (2) vapor pressure deficits increase. These two increases in turn increase the potential evaporative demand by the environment on the vegetation and form a type of feedback process, which further increases water stress in the vegetation. The total increased evaporative demand can be estimated by inserting the elevated temperatures and reduced vapor pressures measured over water-stressed vegetation into a Penman-type equation. This estimate, termed  $ET_{ps}$ , for ET potential over water-stressed vegetation, can be compared with an ET estimate that represents ET under conditions of unlimited soil water under regionally potential conditions, such as represented by the Priestley-Taylor equation ( $E_{eq}$ ). Then the difference  $ET_{ps} - E_{eq}$  can be used to represent the decrease in ET due to deficit soil moisture. In this case, actual ET from the water-short vegetation,  $ET_a$ , can be estimated as

$$ET_a = E_{eq} - (ET_{ps} - E_{eq}) = 2E_{eq} - ET_{ps} \quad (12-2)$$

Eq. (12-2) is known as the complementary approach and was first introduced by Bouchet (1963) and further developed by Brutsaert and

Stricker (1979) and Morton (1983). A difficulty with the complementary method is in estimating  $E_{eq}$ , especially in semiarid areas where  $E_{eq}$  as estimated with the Priestley-Taylor equation is less than the equilibrium, well-watered ET rate approached in semiarid regions even under moist soil conditions over long periods of time. Huntington et al. (2011) recommend estimating  $E_{eq}$  using net radiation,  $R_n$ , which represents conditions expected under well-watered conditions and means a somewhat cool surface. Chapter 11 describes how  $R_n$  can be 100 W m<sup>-2</sup> greater for cool, evaporating surfaces than it is for hot, dry surfaces. Thilini et al. (2013) describe applying the complementary relationship using gridded weather data from the NOAA Noah land surface model and North American regional reanalysis (NARR) data system. Szilagyi (2007) and Venturini et al. (2012) describe combining complementary theory with thermal imagery from the MODIS satellite to estimate ET at the 1-km scale. For further information on the complementary method, the reader is referred to the articles by Brutsaert and Stricker (1979), Morton (1983), Szilagyi (2007), Huntington et al. (2011), and Venturini et al. (2012).

### Application of Energy Balance Models to Forests and Grasslands

Several models have been developed for estimating ET from large catchment areas. These models generally integrate various resistances affecting vapor and heat transfer within complex canopies and may consider the development of multistoried canopies over time. Early models include a forest ET–CO<sub>2</sub> uptake and water balance model by Running and Coughlan (1988), a forest transpiration–photosynthesis–CO<sub>2</sub> uptake model by Price and Black (1989), and a rangeland–snow melt–ET–heat and water flow model by Flerchinger and Pierson (1991). The previous chapter discusses some components of the Price and Black model on surface conductance functions. Energy–balance–crop growth models have been developed for agricultural crops and include the CERES–Maize model (Jones and Kiniry 1986), CERES–Wheat (Ritchie and Otter 1985), ENWATBAL (Lascano et al. 1987), and SOYGRO (Jones et al. 1987). Various crop models for estimating climate risk and optimizing agronomic practices in response to climate risk were discussed at an international symposium in Brisbane, Australia in 1990 (Muchow and Bellamy 1991). Multilayer or patch models described in Chapter 11 that can be applied regionally include those by Brenner and Incoll (1997), Daamen and McNaughton (2000), Gardiol et al. (2002), Mo and Beven (2004), Villagarcía et al. (2007), Were et al. (2008), and Lagos et al. (2009, 2012).

Sikka (1993) and Sikka et al. (1993) modify and apply the Running–Coughlan model to a 210-km<sup>2</sup> catchment area in northern Utah and utilize a fuzzy clustering algorithm along with Landsat thematic mapper data and digital elevation data to predict the variation in leaf-area index (LAI) and

vegetation types for hydrologic units within the watershed. Vegetation comprised a mixture of conifer, aspen, shrubs, and sagebrush, with average LAIs for hydrologic units ranging from 0.6 to 2.5. Sikka et al. (1993) find the modified Running–Coughlan model to provide acceptable results provided computerized calibrations are made on the specific watershed using historical weather and streamflow data.

Mao et al. (2002) estimate ET for three wetland environments in Florida. Input data were based on measurements of climate data, ET, and pan evaporation during 1996–1999. The results suggest that mean monthly ET for open water, cattails, and young and mature sawgrass calculated by the PM, Priestley-Taylor, reference ET, and pan evaporation were all relatively close in the humid climate when monthly varying coefficients were used. The PM method requires reliable values for canopy resistance. Seasonal and annual canopy resistance values for cattails and sawgrass for the region are presented in Tables 3 and 4 of Mao et al. (2002).

In general, ET–vegetation development–energy balance models require rather extensive data describing the phenological development of vegetative canopy cover, photosynthetic–stomate interactions, and penetration of light within canopies. Therefore, these models are usually applied in specialized studies where accurate fluxes are needed during short time periods or in studies examining sensitivity of ET and other fluxes to changes in vegetation, climate, or hydrology. Complex models will be increasingly applied with gridded weather data from the weather forecasting models coupled with land surface models.

### Application of Energy Balance Models to Regional Cultivated Lands

Recently, satellite imagery combined with surface climate measurements has been used for estimating ET from large-scale cultivated lands and the productivity of water in these areas. Moran (2000) describes the use of remote sensing for monitoring evaporation over managed watersheds. Bastiaanssen et al. (1998b, 2005) describe a surface energy balance model (SEBAL), and Allen et al. (2005d, 2007c) and Kilic et al. (2012) describe a similar model (METRIC) that takes into account slope and aspect and measured weather data. Kite and Droogers (2000) compare estimates of ET for a basin in western Turkey using remote sensing, hydrologic models, and field data. They conclude that no single method is ideal. Each has its advantages and disadvantages. A combination of methods may be better than a single method alone. They combined models at three scales, the field scale, the irrigation-scheme scale, and the basin scale in the Turkey study. The three linked models enabled assessing water productivity at three scales and the effects that changing water availability, management practices, and climate might have on the productivity of irrigation and other water uses within the basin (Droogers and Kite 1999). Kite (2000) describes a basin-scale

model used to estimate crop transpiration and evaporation from soil. Allen et al. (2002a, b; 2007a) describe the use of satellite imagery for estimating ET for the southern part of Idaho. Scott et al. (2003) evaluate the use of remotely sensed data for mapping root zone soil water on a river basin scale in Pakistan. Tasumi et al. (2005b) discuss operational aspects of satellite energy-based models for irrigated crops in the semiarid United States.

Singh et al. (2008) assess the operational characteristics and performance of the surface energy balance algorithm for land (SEBAL) for estimating crop ET and other energy balance components and mapping spatial distribution and seasonal variation of  $ET_c$  on a large scale in south-central Nebraska. Cloud-free Landsat Thematic Mapper (TM)/Enhanced Thematic Mapper (ETM) satellite images from May to October were processed to generate  $ET_c$  maps and to estimate surface energy fluxes. Instantaneous and daily predictions from SEBAL were compared with the Bowen ratio energy balance system (BREBS)-measured fluxes over an irrigated cornfield. The  $ET_c$  maps show a progression of  $ET_c$  during the growing season. Overall, a good correlation exists between the BREBS-measured and SEBAL-estimated  $ET_c$  with a root mean square difference of  $1.0 \text{ mm d}^{-1}$ . Estimated  $ET_c$  is within 5% of BREBS-measured values. The model overestimates albedo by 25%, with the greatest difference early in the season before full canopy cover. The model underestimates soil heat flux, and most of the underestimation occurs late in the late growing season. Local calibration improves the agreement between measured and estimated values. Anderson et al. (2011) provide an overview of estimating regional ET using thermally based surface energy balance methods. Cammalleri et al. (2013) explore the fusion of thermal and reflected imagery from the Landsat satellite with spatial resolution of 30–100 m with imagery from the MODIS satellite with spatial resolution of 500–1,000 m to produce time series of ET in central Iowa having field-scale spatial resolution of 30 m and temporal resolution of approximately eight days.

### Approximation of Monthly Streamflow for Ungauged Watersheds

The water balance technique, also referred to as the inflow-outflow or mass balance method, can be applied over large, integrated areas of land and water to develop watershed-scale estimates of ET. These types of estimates are useful for calibration or validation of watershed and remote-sensing based models. Examples of ET by water balance are applications to large areas such as valleys where the inflow and outflow are determined from streamflow and precipitation measurements and where the basin is confined to eliminate other significant sources of inflow or outflow such as groundwater underflow (Lowry and Johnson 1942; Chow et al. 1988; McCabe and Markstrom 2007; Gao et al. 2007; Dingman 2008). Such studies generally provide only gross seasonal estimates of the average water

evaporated and transpired from agricultural and nonagricultural areas within a watershed or project. The results represent ET from a combination of vegetation types and generally apply only to climatic, vegetation, and water availability conditions similar to those existing in the study area. An evaluation of large-scale models of an experimental catchment (watershed) and a river basin in Australia indicates satisfactory agreement in monthly values between the computed and measured ET ([Dunin and Aston 1984](#)). Wilson et al. ([2002](#)) find good agreement between ET derived from an inflow-outflow analysis of a 98-ha forested watershed and eddy covariance methods in Tennessee.

Mass balances require precipitation as the primary input, and consequently the ET estimate can only be as accurate as the precipitation estimate. Fine resolution grids of precipitation on the scale of a km or less may be required in areas having substantial precipitation from convective storms and areas having substantial relief with orographic influence on precipitation amounts. As with soil water balance applications, precipitation data from standard gauges should be corrected for undercatch. Accurate measurement of basin or irrigation project outflow is necessary, as is locating the measurement area boundaries to minimize groundwater inflows and outflows.

Often, ET information is needed to estimate mean streamflow from ungauged watersheds. In locations where streamflows are not gauged, approximate estimates for monthly stream discharges can sometimes be made by employing a general, basic hydrologic balance:

$$Q = P - ET - GW - \Delta \text{Storage} \quad (12-3)$$

where  $Q$  is the monthly stream discharge from a watershed, having the same units as  $P$ ,  $ET$ , and  $GW$ ;  $GW$  is groundwater discharge from the basin; and  $\Delta \text{Storage}$  is the net change in soil water or groundwater storage in the watershed, with the same units as  $Q$ . In simple applications of Eq. (12-3) to watersheds where groundwater flow discharge from the watershed is small, the last two terms of Eq. (12-3) can be ignored, so that  $Q$  can be estimated as the difference between  $P$  and  $ET$ . Hargreaves ([1993](#)) finds good agreement between monthly  $Q$  estimated as  $Q = P - ET_o$  and measured  $Q$  for several watersheds in Central America and in the United States, where  $ET_o$  was calculated grass reference ET.  $ET_o$  provided a general approximation of ET throughout the watershed areas under the assumption that ET will approach  $ET_o$  when  $P > ET_o$  during any month.

### Data Sources in Cultivated Areas

An accurate and online database is required to fully utilize regional ET estimation methods. Since the 1970s, rapid expansion of nonfederal

automated weather stations (AWSs) has occurred across the United States and Canada. Many states have some sort of network of AWSs: these include Alabama, California, Colorado, Florida, Georgia, Idaho, Louisiana, Minnesota, Nebraska, Nevada, New Mexico, New York, North Carolina, Ohio, Oklahoma, Oregon, South Dakota, Texas, Utah, Washington, and Wisconsin. Meyer and Hubbard (1992) review early agricultural networks. Regional systems operated by the U.S. Bureau of Reclamation include the Agrimet system. Most of the AWSs are part of a national network of Regional Climate Centers or part of agricultural weather networks such as those housed at the Agricultural Water Conservation Clearinghouse ([http://agwaterconservation.colostate.edu/ET\\_Network\\_Information.aspx](http://agwaterconservation.colostate.edu/ET_Network_Information.aspx)). Six Regional Climate Centers exist and are located in Nevada, Nebraska, Illinois, Louisiana, North Carolina, and New York (<http://www.ncdc.noaa.gov/oa/climate/regionalclimatecenters.html>). Data and calculations from most of the AWSs are available in real time and for low cost or free. Hubbard et al. (2005) review some data quality control techniques for weather station networks, and ASCE (2005) describes algorithms for supporting visual data quality assessments. Appendix H summarizes the ASCE algorithms.

### Data Sources in Natural Vegetation

In addition to the AWS systems, which can be expected to provide the most representative weather data for agricultural settings and for use in estimating ET from agricultural crops, other national networks typically located over natural vegetation include the U.S. Department of Energy Atmospheric Radiation Measurement program, which contains the Cloud and Radiation Testbed (CART) (Xuebao et al. 2005), which measures evaporative flux by the Bowen ratio energy balance (BREB) and eddy covariance techniques. Other evaporative and energy balance flux collection programs include the Long Term Ecological Research (LTER) program, Fluxnet, Ameriflux, ParkNet, National Atmospheric Deposition Program/National Trends Network, and Multistate Atmospheric Power Production Pollution Study. Weather data systems in wildland settings include the RAWS (remote automated weather system) operated by the U.S. Forest Service and Bureau of Land Management. These data are generally available through the Regional Climate Centers.

### Gridded Weather Data

Gridded weather data sets are becoming increasingly common and more and more complete both nationally and globally. Data sets for the continental United States include the PRISM set (Daly et al. 2008; Daly and Bryant 2013), Daymet (Maurer et al. 2002), NARR (North American

Regional Reanalysis), NLDAS (North American Land Data Assimilation System) (Mitchell et al. 2004), and GridMet (Abatzoglou 2013). Global data sets include GLDAS (Global Land Data Assimilation System). These data sets utilize a wide range of techniques for assimilating measured weather data and making spatial and temporal assimilations. Grid sizes vary, and wind speed and precipitation data have the least certain spatial accuracy (Luo et al. 2003). Precipitation data may originate from NEXRAD (Next-Generation Radar) sources or interpolation from point data. Because assimilated data originate from various weather locations, many of which may not be in well-watered settings such as at regional airports, gridded weather data may have a pronounced aridity, with air temperature higher than and vapor pressure lower than expected over a well-watered vegetated surface. These data may benefit from conditioning prior to use to estimate reference ET.

The 30+ year (1979–present) NLDAS retrospective forcings have 1/8 degree resolution (~12 km × 12 km). NLDAS phase 2 retrospective forcings (NDAS-2) contain daily precipitation, solar radiation, 2-m reference height temperature and humidity, and 10-m reference height wind speed (<http://www.emc.ncep.noaa.gov/mmb/nldas/>). Model-based NLDAS forcings of temperature, humidity, and wind speed are derived from spatially and temporally interpolated NCEP North American Regional Reanalysis (NARR) data.

Several NLDAS validation studies have been conducted with focus in Oklahoma (Luo et al. 2003; Robock et al. 2003), where NLDAS solar radiation, based on GOES satellite, was compared with ground-based observations. While Luo et al. (2003) show fairly good correlation (correlation coefficient ~0.92) of simulated to measured hourly  $R_s$ , bias was often caused by overprediction by NLDAS.

Agricultural data sets have also been organized into gridded systems, for example, in California, CIMIS weather data have been gridded by Hart et al. (2009). These gridded systems generally cover nonmountainous systems and better represent well-watered conditions.

# **PART 3**

## **WATER REQUIREMENT ESTIMATES**

This page intentionally left blank

# CHAPTER 13

## SELECTION OF APPROPRIATE ESTIMATING METHOD

### **13.1 INTRODUCTION**

All methods for calculating evaporation (E) and evapotranspiration (ET) that are based on climatological data produce only estimates of ET. The accuracy of estimates depends substantially on the quality of data and on the completeness and physical basis of the method. The best method to select for a particular application depends on the available time frame for completing the task, the required accuracy, the area of coverage, the length of the calculation time step, and the availability of existing climate data or whether specific new climate data measurements can be made. The intended end use of the ET estimate is also a factor, for example, whether for use in project and system planning; design, operation, and management practices; hydrologic studies; water rights management; water transfers; environment mitigation; or litigation. The method selected and its accuracy in application depends on the resources available to the user, including the capabilities of trained personnel to assess input data quality, apply models that combine remotely sensed data and surface weather data, and calculation of parameters. The computing capacity available to the user should also be considered.

### **13.2 TIME FRAME AND REQUIRED ACCURACY**

Considerations in both method selection and resource allocation include the time required to collect and screen climate data for quality and to process the climate data. Also to be considered is the time required to obtain associated relevant data such as soil type, crops being grown or

landscape vegetation, and characteristics of the weather station sites used. Soils databases for the United States include the STATSGO and SSURGO databases (<http://soils.usda.gov/survey/geography/ssurgo/>).

The required accuracy of ET estimates depends on their intended use. The highest accuracy may require measured field data for development, calibration, or verification. For moderate accuracy, the use of available crop and landscape vegetation coefficients along with calculated reference ET may be adequate. Generally, the longer the time interval for which ET estimates are produced, the higher the accuracy, for example, hourly vs. daily vs. 10-day vs. monthly, vs. growing season time intervals. The increase in accuracy occurs due to the tendency for random errors or bias in weather data or ET parameter settings to cancel over time. The canceling mostly occurs when ET calculated for short time intervals is summed over longer time intervals. Most estimates of E and ET made using the equations and guidelines described in this manual can be considered to be useful for routine water planning and management purposes.

### **13.3 INPUT DATA COLLECTION, SCREENING, AND PROCESSING**

Some archived climate data provided by various service groups may have already been subjected to quality control, with bad or questionable data flagged. Even so, reviewing the available archived climate data for obvious data errors and independently identifying data that may be suspect due to bad sensors, gradual changes in calibration coefficients, or unit errors is always prudent. Likewise, current or real time data that are available via the Internet should be screened. The major weather variables that need to be reviewed are solar radiation, temperature, humidity, and wind speed. ASCE (2005) and Appendix H describe graphics-based procedures for screening weather data.

#### **Solar Radiation**

The primary source of energy for E and ET is solar radiation. The best measured or estimated data should be used. Hourly and daily solar radiation data ( $R_s$ ) should be screened by comparison with calculated cloudless day values ( $R_{so}$ ) using Eqs. (4-11)–(4-15) or the detailed procedures outlined for the ASCE-EWRI standardized reference ET equation (ASCE 2005). Measured  $R_s$  should approach the  $R_{so}$  values on cloudless days. Occasionally, daily or hourly values may slightly exceed  $R_{so}$  due to reflection from nearby clouds.

## Humidity and Air Temperature

Humidity and air temperature data, whether collected specifically for a study or obtained from an agency or private source, should be screened to identify possible erroneous or nonrepresentative values. The user should have a general knowledge of what values are reasonable or unreasonable. Maximum relative humidity (RH) more than about five percentage points above 100% in a natural environment may indicate a problem with the humidity sensor such as a faulty or drifting calibration coefficient. Values greater than 100% should be set to 100% prior to use in calculations. Maximum daily RH should generally approach 100% in humid and subhumid climates, but may be less in arid climates during warm summer periods. Minimum RH should not be less than about 30% in subhumid regions or less than about 10% in arid regions when collected over extensive, well-watered surfaces. Collection over extensive, well-watered surfaces conditions the humidity and temperature data to reflect the well-watered surface and is "anticipated" by the reference ET methods.

Another check of humidity data is to calculate daily average dew point temperature from RH data and compare it with daily minimum air temperature ( $T_{min}$ ). Daily average dew point temperature can be calculated by first calculating average daily vapor pressure using  $RH_{max}$  and  $RH_{min}$  as follows:

$$e_a = \left[ e^o(T_{min}) \frac{RH_{max}}{100} + e^o(T_{max}) \frac{RH_{min}}{100} \right] / 2 \quad (13-1)$$

where  $e_a$  = actual average vapor pressure in kPa, and  $e^o$  = saturation vapor pressure calculated using Eq. (3-1) for  $T_{min}$  and  $T_{max}$ . Dew point is then calculated using Eq. (3-9) and the average vapor pressure. Average calculated daily dew point values should approach  $T_{min}$  most days in humid regions. In arid areas, daily dewpoint values may be 2–5°C lower than  $T_{min}$ , even when measurements are made at a site that meets reference crop requirements. Differences can be as much as 10°C in parts of Arizona and Southern California, where the regional air masses are extremely dry (ASCE-EWRI 2005). Daily dew point temperatures that are much below  $(T_{min} - 5)$ °C indicate that the weather station site likely does not meet reference crop conditions, and some adjustment of humidity data may be required. Additional discussion of humidity data problems is presented in Appendix D of ASCE-EWRI (2005) and in Appendix H.

Air temperature is the simplest and most consistent weather parameter that is commonly measured, especially when measured in a reference-type environment. Extreme air temperature data should be compared with historical record extremes for the site or region. Temperatures that routinely exceed recorded extremes indicate possible problems with the sensor or the radiation shield. Additional discussion of temperature data problems and

the effects of nonreference weather station sites on humidity and temperature are presented in Appendix D of ASCE (2005) and in Appendix H.

### Wind Speed

For reference ET calculations, wind speed should be measured in open, fieldlike areas away from buildings and trees and over a grasslike surface. Accuracy of wind speed measurements is difficult to assess unless duplicate instrumentation is used. A comparison of reported wind speed data with historic means or those of nearby stations may indicate a malfunctioning anemometer, or temporary failure due to ice when temperatures are below 0°C. Consistently low readings may indicate worn out or dirty anemometer bearings or a failed anemometer. An assessment of the gust factor, calculated as the ratio of maximum hourly wind speed to average daily wind speed or as the ratio of a one- to five-minute wind speed to hourly wind speed, is another method for evaluating wind speed data. Consistently high gust factors indicate a failing anemometer that becomes sluggish during low wind speeds and creates nonlinearity in the anemometer response. However, one should recognize that wind speed during nighttime is often a factor of 2 to 3 times lower than wind speed during daytime. Wind speed data can be compared among local weather sites to note common behavior and trends, as illustrated in Appendix H.

## 13.4 CROP COEFFICIENT METHOD VS. DIRECT METHODS

In general, the crop coefficient–reference ET method has proven to be accurate, robust, consistent, and straightforward to apply. The reference crop ET method has been standardized through the FAO-56 and ASCE-EWRI (2005) definitions, which have facilitated establishing standardized sets of crop coefficients that should transfer across a wide range of climates. The crop coefficient method has a long legacy in irrigation water management, scheduling, and water rights proceedings.

The direct ET methods described in Chapter 11 have the potential for more precise measurements, but generally require more detailed parameterization and crop-specific information. Weather data sets may not be available to drive some of these methods, especially those that expect that weather measurements be taken over the surfaces being estimated. Gridded weather data sets described in Chapter 12 may be useful for the direct ET methods when estimating ET for rainfall conditions. These data sets are developed using precipitation-based water balances and reflect the effect of water stress on air mass characteristics. This is especially important when estimating ET for irrigated fields in arid and semiarid climates. Direct ET methods may be useful for extrapolating ET measurements, for

example, from eddy covariance and Bowen ratio systems, where the direct methods are parameterized or calibrated using the measurement data. Those fitted models can then be applied over larger areas and under different weather conditions.

Huntington et al. (2015) applied the  $K_c ET_{ref}$  method to a large number of weather stations in major river basins in the western United States as part of a climate change impacts study. The dual  $K_c$  procedure was used along with extensive quality assurance and control of weather data. Allen and Robinson (2007) and Huntington and Allen (2010) provide examples of producing estimates of  $ET$  and irrigation requirements state wide.

Satellite-based mapping of  $ET$  is increasingly used, with the advent of very low cost or even free satellite imagery beginning around 2000 and development of operational algorithms. Because of the wide variation in vegetation and land-form characteristics, satellite-based  $ET$  systems should utilize the best physically based methods possible, given time and resource constraints and the intended use of the  $ET$  products. When possible, satellite-based approaches should be compared against measurements by ground-based systems and use independent models such as the crop coefficient and/or direct  $ET$  methods. Measurements by ground-based systems need to be subjected to quality assessment and control.

### 13.5 EVAPORATION AND EVAPOTRANSPIRATION CALCULATIONS

In studies of effects of environmental stresses or climate change, energy balance methods using surface temperature measurements and/or the Penman-Monteith (PM) method with hourly or shorter time steps and iterative computation of surface temperature may be most appropriate. In studies where effects of changes in vegetation type, density, height, or water availability are evaluated, the PM equation, AFIB [Eqs.(11-2a-f)], or more complex multilayered energy balance equations should be used, because changes in vegetation characteristics can be more directly and readily incorporated into the calculations for aerodynamic and surface resistances. Where specific documentation of  $ET$  is required for small areas, direct measurements must usually be made using micrometeorological methods including the Bowen ratio and eddy covariance methods or using soil water balance methods including lysimeters and measured changes in soil profile water content between two dates. Chapter 7 discusses various precautions that must be exercised when measuring  $ET$  by the soil water profile.

Generally, when changing from a coefficient-reference  $ET$  approach (either the  $K_{co} ET_o$  or  $K_{cr} ET_r$ ) to a direct  $ET$  approach, the amount of data required increases, the required calculation time step decreases, and the

requirement for accuracy of input data increases. Applying the direct PM equation or AFIB method is difficult using historical data from standard weather stations, because the historical weather data generally reflect ET flux densities of the weather measurement surface. When applied to some other vegetation type, the direct methods may over- or underpredict, because the effect of feedback mechanisms between ET and vapor content and temperature of the boundary layer are not reflected in the data.

Energy balance methods, including the combination equations [Penman, Eq. (8-1), and PM Eq. (8-2)], and energy balance equation [Eqs. (4-1), (11-2a-f)], are generally more dependable and consistent in estimating ET as compared with direct aerodynamic methods because the inclusion of energy availability in the former equations places an upper limit on ET estimates. In addition, instrumentation requirements are often less rigorous and demanding.

The  $K_{co}ET_o$  or  $K_{cr}ET_r$  procedure may be the best overall approach to estimating ET because the use of  $ET_o$  or  $ET_r$  provides a measure of general energy available for ET. The  $K_{co}$  or  $K_{cr}$  coefficient, where the subscript "o" or "r" identifies the coefficient to be used with either  $ET_o$  or  $ET_r$ , can incorporate a wide assortment of physiological and environmental factors affecting ET rate, including plant density, soil evaporation, and effects of sparse plant densities. The implicit incorporation makes the  $K_cET_o$  or  $K_cET_r$  approach robust in application and fairly transferable to other climates, regions, and time periods. Physiological and environmental factors need to be explicitly identified and incorporated during direct application of the PM and other directly applied boundary layer equations, making these approaches usually more data intensive. However, application of the direct PM equation or AFIB method can often serve as a valuable check on validity of  $K_c$  values and can in some instances be used to develop  $K_c$ s for new types or variations of vegetation.

Usually, calculations made using the PM equation on a 24-hour basis are sufficient for hydrologic studies. Under most conditions, 24-hour estimates of  $ET_o$  or  $ET_r$  calculated using the PM equation using 24-hour time steps provide estimates of total 24-hour  $ET_o$  or  $ET_r$  that are within 5 to 10% of 24-hour sums made using hourly time steps for any given day, with differences varying randomly, depending on the general proportions of daytime to nighttime wind speeds and daylengths (Allen et al. 1994c, 2006c). Results are similar for calculations made using the direct PM equation and AFIB method. The exception is for situations where the stomatal conductance functions ( $g()$ ) or stability corrections are to be applied. In these situations, calculations should be made on an hourly or shorter basis. Energy balance methods using hourly or shorter time steps usually involve measurements or estimates of surface temperature, which are highly correlated with solar radiation, and corrections for stability are generally employed, especially under conditions of water stress.

Calculations of  $ET_o$  or  $ET_r$  on a monthly basis are generally equivalent to those made on a 24-hour basis and summed over the month (Jensen et al. 1990; Allen et al. 1994b). Alternative approaches to reviewing data and calculating E and ET are presented in FAO-56 (Allen et al. 1998). During the nongrowing season, when actively growing vegetation does not exist and when daytime hours are less than nighttime hours, calculated  $ET_o$  and  $ET_r$  may serve as an index, but not a realistic estimate of reference ET conditions, because active vegetation is not present. Irmak et al. (2008) evaluate the ratios of calculated  $ET_r$  to  $ET_o(K_r)$  using different equations during the growing season (May–September) and nongrowing season at locations in California, Florida, Missouri, Nebraska, and Texas. The variability of  $K_r$  values among locations is large. Some of methods calculated unrealistically high values during the nongrowing season because hypothetical reference conditions are usually not met during this period in many locations. Of the five locations, only Nebraska had long cold winters. The empirical equation for estimating  $ET_o$  using extraterrestrial solar radiation and mean air temperature by Hargreaves and Samani (1985) and Hargreaves et al. (1985) may also provide a nongrowing season index.

As more experience is gained using various methods of calculating ET, refinements in the methods can be expected. Users should review publications summarizing the results of new studies before selecting a method for a particular study or application.

### 13.6 SUMMARY

The method used to calculate or estimate evapotranspiration (ET) will depend on the type of application and the amount and accuracy of data available. For large-scale applications including basin-scale water balances, application of a crop coefficient-reference ET ( $K_{co}ET_o$  or  $K_{cr}ET_r$ ) approach with monthly calculation time steps may be appropriate.  $ET_o$  for monthly time steps can generally be calculated using the Hargreaves air temperature method [Eq. (8-16)] or using the PM equation with estimated  $R_s$ ,  $T_d$ , and wind (see Section 8.5) when these variables are not measured. For applications to smaller areas, especially those having relatively homogeneous surface cover, the  $K_cET_o$  or  $ET_r$  and direct PM approaches may be equally appropriate. Calculations using the PM method are commonly made on an hourly or 24-hour basis.

This page intentionally left blank

# CHAPTER 14

## ESTIMATES OF IRRIGATION WATER REQUIREMENTS AND STREAMFLOW DEPLETION

### 14.1 INTRODUCTION

The irrigation water requirement includes several components, with the major component being the replacement of soil water depleted by evaporation (E) and crop or landscape evapotranspiration (ET). This component is water that is consumed via conversion from liquid to vapor during the ET process. Other components provide water for leaching, or controlling the soil salinity level, and for various miscellaneous purposes such as ensuring germination of seeds, controlling soil crusting, controlling frost, and conditioning the soil to enable harvesting root crops. Only part of the water for these other components is consumed by E or ET. The part not consumed remains somewhere in the water resources system, but may be degraded in quality.

### 14.2 NET IRRIGATION WATER REQUIREMENT AND EFFECTIVE PRECIPITATION

The net irrigation water requirement,  $NIWR$ , can be referred to as a precipitation deficit,  $P_{def}$ , where  $P_{def}$  is the amount of soil water that must be made up to complete the potential ET requirement,  $ET_{pot}$ , and avoid undesirable water stress.  $P_{def}$  is generally calculated as  $ET_{pot} - P_{rz}$  where  $P_{rz}$  is the precipitation infiltrating into and residing in the root zone.  $P_{def}$  represents the amount of additional water that the soil and crop would evaporate or transpire beyond  $P_{rz}$  if that water were made available at the right time during the growing or nongrowing season to fulfill the necessary ET requirement.

$P_{def}$  can have a negative value when calculated over a short period of time if the depth of precipitation during a period, for example, 3, 7, 15, or 30 days, is greater than the value of  $ET_{pot}$ . This is likely to occur during winter and periods having substantial rain. A negative value indicates precipitation in excess of ET and a net recharge to soil water. When comparing  $P_{def}$  for a nonirrigated condition with  $P_{def}$  for the same irrigated crop, the  $P_{def}$  calculated for the nonirrigated condition is often lower than that for the irrigated condition. This is an artifact of the calculation of  $ET_{pot}$  using a dual  $K_c$  method where  $E$  for the rain-fed crop does not contain  $E$  from soil following irrigation events. When determining the  $IWR$ , one should use the  $P_{def}$  for the irrigated condition to reflect the increased  $E$  for the irrigated condition, which, in essence, burns off part of the added irrigation water.

Defining precipitation that enters the soil in two different ways is useful in terms of its ultimate disposition into  $E$  or into transpiration,  $T$ . The *precipitation residing in the root zone* ( $P_{rz}$ ) is the depth of gross reported precipitation infiltrating the soil (i.e., less any surface runoff) that remains in the root zone and is available for later consumption by  $E$  or  $T$ .  $P_{rz}$  is computed as  $P - RO - DP$  where  $P$  is gross reported precipitation,  $RO$  is estimated surface runoff, and  $DP$  is deep percolation of any precipitation below the maximum root zone for the crop or land-use condition. The difference between  $P_{rz}$  and  $ET_{act}$  during extended periods of no irrigation, including the nongrowing season (where  $ET_{act}$  includes evaporation following precipitation events), represents the amount of recharge to the root zone. During the nongrowing season, the difference  $P_{rz} - ET_{act}$  represents an increase in soil water storage that is available at the start of the growing season to fulfill later plant water requirements. The ratio of  $(P_{rz} - ET_{act})/P$  represents the efficiency or effectiveness of gross precipitation, including snow, in building soil water for use during the growing season.

A second useful term and category for  $P$  that enters the root zone is the *precipitation residing in the root zone that is available for transpiration (rather than for evaporation)*,  $P_{efT}$ .  $P_{efT}$  is the amount of gross reported precipitation that infiltrates into the soil (i.e., less any surface runoff) and that remains in the root zone and is ultimately used to supply  $T$  by the crop or land use cover.  $P_{efT}$  does not include the amount of infiltrated precipitation that evaporates from the surface evaporation layer (for example, the upper 100 mm of soil).  $P_{efT}$  is usually less than  $P_{rz}$  because of the loss of infiltrated  $P$  in the form of evaporation from the soil surface. One reason to separate the contributions of  $P$  into  $E$  and  $T$  is that, in many cases, only the  $T$  component of  $P$  and/or irrigation,  $I$ , is considered to be economically or beneficially used. Conservation programs may promote means to reduce the evaporation components and maximize the transpiration components of both  $P$  and  $I$ .

The  $P_{efT}$  parameter is useful for estimating the amount of  $P$  during the nongrowing season that is stored and later made available for  $T$

requirements during the subsequent growing season.  $P_{efT}$  is also useful to calculate during the growing season to determine how efficient or effective precipitation is in fulfilling the  $T$  requirement of a crop, as opposed to simply burning off as  $E$  from the soil surface.  $P_{efT}$  is calculated as  $P_{efT} = P_{rz} - E = P - RO - DP - E$ , where  $P_{rz}$  is precipitation infiltrating and residing in the maximum root zone for the crop.

Typically, the effectiveness of  $P$  in satisfying  $T$  requirements is low if  $P$  occurs in frequent, small doses. In that situation, most  $P$  is converted into  $E$  and does not appreciably reduce the NIWR. In calculating the effectiveness, using an ET-estimating method with the ability to increase the estimate for  $E$  with increased frequency of  $P$  is important.

The NIWR is estimated similarly to  $P_{def}$ , where

$$\begin{aligned} NIWR &= ET_{pot} - (P - RO - DP) \\ &= E + T_{pot} - (P - RO - DP) \\ &= E + T_{pot} - P_{rz} \\ &= T_{pot} - P_{efT} \end{aligned} \quad (14-1)$$

The alternative component expressions in Eq. (14-1) illustrate the importance of including accurate estimation of  $E$  in the estimation of ET if the depth for  $P$  used in the same equation contains the portion of ET that becomes  $E$ . Otherwise, the NIWR may be underestimated and effectiveness of  $P$  overestimated.

Effective rainfall during historical periods is best estimated by applying a daily soil moisture balance, including estimated surface runoff, soil evaporation, unsaturated drainage, and soil water-ET relationships. Constructing computer software or spreadsheets that make the necessary calculations is straightforward. Chapters 9 and 10 introduce water balance equations for estimating or incorporating  $E$  and ET using the dual  $K_c$  approach, and examples of calculations using daily time steps are shown.

The depth of effective rainfall stored in the soil during a period is dependent upon the frequency of occurrence and characteristics (amount, duration, and intensity) of the precipitation, the soil surface condition, and the soil water storage capacity available at the time of rainfall. The amount lost to surface runoff is that portion of the rainfall in excess of the intake capacity of the soil and leaf interception unless the excess is ponded until intake occurs.

As described later, effective rainfall can also supply leaching requirements. Precipitation lost by runoff from the soil surface and by drainage through the soil is not considered effective in reducing ET water requirements, but the leaching requirement may be reduced by rainfall-induced drainage. Precipitation that only redistributes salt concentrations through the soil within the root zone may not decrease the leaching requirement.

The soil water storage capacity available when rainfall occurs varies with the depth and characteristics of the soil within the root zone; the elapsed time since irrigation or rainfall, which impacts the infiltration rate; the depletion allowed before irrigation; and the rate of depletion by ET. Generally, rainfall effectiveness increases with higher  $T$  rates, greater allowed depletions between irrigations, and larger soil water storage capacities.

In the absence of a daily water balance simulation, effective rainfall stored in the soil can be estimated using a very general relationship presented by USDA (1970), but with reduced accuracy. In the USDA (1970) procedure, average monthly effective rainfall,  $R_e$ , is estimated according to mean monthly rainfall,  $R_t$ ; average monthly ET for the crop; and the normal depth of depletion prior to irrigation,  $D$ , mm:

$$R_e = f(D)(1.25R_t^{0.824} - 2.93)(10^{0.000955 ET}) \quad (14-2)$$

where units for rainfall and ET parameters are mm per month and  $f(D)$  is a factor to adjust for depletion depths other than 75 mm, described by the following equation:

$$f(D) = 0.53 + 0.0116D - 8.94 \times 10^{-5}D^2 + 2.32 \times 10^{-7}D^3 \quad (14-3)$$

Depletion depth,  $D$ , accounts for impacts of soil water-holding characteristics and rooting or soil depth and is similar to the term RAW estimated with Eqs. (10-7) and (10-8). The value of  $R_e$  should be limited to the lesser of the values of  $R_t$ , ET, or the equation estimate. The USDA (1970) relationships are based on a calculated daily accounting of soil water storage, rainfall, and evapotranspiration for a 50-year period at 22 weather stations in the United States, representing climates from humid to arid, and for combinations of crops and soils common to irrigated areas. Irrigation was assumed to occur when soil water storage was depleted to a pre-determined level. Daily rainfall in excess of available soil water storage was assumed lost to surface runoff or deep percolation.

Eq. (14-2) may be used to estimate effectiveness of fall and winter precipitation by substituting the remaining available soil water storage capacity at the beginning of each monthly or seasonal period for the normal depth of depletion,  $D$ , and setting ET to a low value. This relationship will not adequately predict effectiveness of winter precipitation if significant surface runoff occurs due to frozen soil conditions, if snow is removed by wind action, or if wetting events are frequent and light, with large fractions of  $P$  lost as increased  $E$ . As explained in the previous section,  $P_{efT}$  represents the most appropriate definition and expression of the effectiveness of  $P$  in supporting transpiration requirements of vegetation. Other empirical methods for estimating effective rainfall and reviews of the

USDA (1970) method have been presented by Dastane (1974) and Kopec et al. (1984).

### 14.3 LEACHING REQUIREMENT

All irrigation waters contain some dissolved salts. ET removes pure water from the soil, thereby concentrating the salts in the remaining soil water solution. Salts in the soil solution decrease the osmotic potential (greater negative pressure) as compared with pure water. Lower osmotic potential decreases the potential gradient of soil water to plant roots. Concentration of salts can result in conditions unsuitable for crop growth unless controlled. The practical method for controlling concentration of salts in the soil solution is by leaching. Leaching is considered a necessary and beneficial use of water and must be included in determining irrigation water requirements. Leaching is accomplished by having a portion of the infiltrated water percolate through the root zone. The portion that actually passes through the root zone is called the *leaching fraction* (Tanj 1990) calculated as

$$LF = \frac{Q_{dp}}{Q_{iw} + Q_{ep}} \quad (14-4)$$

where  $LF$  is the leaching fraction, dimensionless;  $Q_{dp}$  is the volume of water that percolates through the root zone commonly expressed as volume per unit area (i.e., depth);  $Q_{iw}$  is the infiltrated irrigation water also expressed as depth; and  $Q_{ep}$  is effective precipitation expressed as depth. The leaching fraction can also be expressed in terms of soil salinity as

$$LF = \frac{C_a}{C_d} \quad (14-5)$$

where  $C_a$  is the salt content of infiltrated water (irrigation plus precipitation), and  $C_d$  is the salt content of water draining past the root zone (Hoffman 1990). The salt content of water and the soil solution is commonly expressed in terms of electrical conductivity (EC) in units of decisiemens per m ( $dS\text{ m}^{-1}$ ), where  $1 dS\text{ m}^{-1} = 1 \text{ mmho cm}^{-1}$ . The latter unit was commonly used in the past. When expressed in terms of volume of water infiltrated ( $V_{inf\ w}$ ) and drained ( $V_{dw}$ ) per unit area and the EC of the waters, and assuming no dilution or precipitation of salts in the profile, the  $LF$  becomes

$$LF = \frac{V_{dw}}{V_{inf\ w}} = \frac{EC_{inf\ w}}{EC_{dw}} \quad (14-6)$$

where  $EC_{\text{inf } w}$  is the salinity of the infiltrated water, and  $EC_{dw}$  is the salinity of the drained water,  $\text{dS m}^{-1}$ .

The leaching requirement ( $LR$ ) is the amount of leaching required to maintain a viable irrigated agriculture. It depends on the salt content of the irrigation water, the type of soil, the salt tolerance of the crop grown, the climate, and the irrigation management practices. The  $LR$  was originally defined in USDA Handbook 60 ([U.S. Salinity Laboratory Staff 1954](#)) as the lowest value of the  $LF$  that can be allowed without  $EC_{dw}$  becoming excessive for optimum plant growth. The required amount of water to be infiltrated ( $V_{r \text{ inf}}$ ) to replace soil water depleted by ET and the  $LR$  is

$$V_{r \text{ inf}} = \frac{V_{ET}}{(1 - LR)} \quad (14-7)$$

where  $V_{ET}$  is the volume of soil water depleted by ET that is to be replaced per unit area, and  $LR$  is the estimated leaching requirement. Rhoades ([1974](#)) introduces a procedure for estimating the  $LR$  based on the average soil  $EC$  calculated as the average of the saturated paste at the top and bottom of the root zone and an approximate ratio of the water content of the saturated paste and the water content at field capacity taken as 2. The  $EC$  of the saturated paste is about one-half of the  $EC$  of soil water content at field capacity. The resulting equation is

$$LR_t = \frac{EC_{\text{inf } w}}{(5 EC_e^* - EC_{\text{inf } w})} \quad (14-8)$$

where  $LR_t$  is the traditional estimate of the  $LR$ ,  $EC_{\text{inf } w}$  is the  $EC$  of the infiltrated water, and  $EC_e^*$  is the average  $EC$  of the saturated-paste extracts appropriate for a given crop allowing a tolerable yield depression (usually 10%) or so-called threshold level of salt tolerance ([Maas 1990](#)). The  $LR_t$  model has been used extensively ([Ayers and Westcot 1985](#)).

For soil salinity exceeding the threshold level for a given crop, the resulting relative yield ( $Y_r$ ) is estimated as

$$Y_r = 100 - b(EC_e - a) \quad (14-9)$$

where  $a$  is the salinity threshold level expressed in  $\text{dS m}^{-1}$ ,  $b$  is the slope expressed as % per  $\text{dS m}^{-1}$ , and  $EC_e$  is the mean electrical conductivity of a saturated soil extract taken from the root zone. Salt tolerance values for various crops expressed as the threshold level and slope per  $\text{dS m}^{-1}$  were presented by Maas ([1990](#)), Tables 13.1 and 13.2, and in FAO-56, Table 23 ([Allen et al. 1998](#)). Salt tolerances for selected common crops are summarized in this chapter in Table [14-1](#).

Table 14-1. Salt Tolerance of Selected Crops

Crop		Electrical Conductivity of Saturated Soil Extract		
Common Name	Botanical Name	Threshold, dS m <sup>-1</sup>	Slope, % per dS m <sup>-1</sup>	Rating <sup>a</sup>
<b>Cereals</b>				
Barley	<i>Hordeum vulgare</i>	8.0	5.0	T
Maize	<i>Zea mays</i>	1.7	12.0	MS
Maize (Sw corn)	<i>Zea mays</i>	1.7	12.0	MS
Millet, foxtail	<i>Setaria italica</i>			MS
Rice, paddy	<i>Oryza sativa</i>	3.0	12.0	S
Sorghum	<i>Sorghum bicolor</i>	6.8	16.0	MT
Wheat	<i>Triticum aestivum</i>	6.0	7.1	MT
Wheat, semi-dwarf	<i>Triticum aestivum</i>	8.6	3.0	T
Wheat, durum	<i>Triticum turgidum</i>	5.9	3.8	T
<b>Forages</b>				
Alfalfa	<i>Medicago sativa</i>	2.0	7.3	MS
Bermuda	<i>Cynodon dactylon</i>	6.9	6.4	T
Clover, red	<i>Trifolium pratense</i>	1.2	12.0	MS
Fescue, tall	<i>Festuca elatior</i>	3.9	5.3	MT
Rye-grass, perennial	<i>Lolium perenne</i>	5.6	7.6	MT
Sudan grass	<i>Sorghum sudanense</i>	2.8	4.3	MT
Wheatgrass, standard	<i>Agropyron sibiricum</i>	3.5	4.0	MT
<b>Legumes</b>				
Bean	<i>Phaseolus vulgaris</i>	1.0	19.0	S
Cowpea	<i>Vigna unguiculata</i>	4.9	12.0	MT
Groundnut (peanut)	<i>Arachis hypogaea</i>	3.2	29.0	MS
Pea	<i>Pisum sativum</i>			S
Soybean	<i>Glycine max</i>	5.0	20.0	MT
<b>Miscellaneous</b>				
Apples	<i>Malus sylvestris</i>			S
Citrus (Orange)	<i>Citrus sinensis</i>	1.7	16.0	S
Cotton	<i>Gossypium hirsutum</i>	7.7	5.2	T

(Continued)

Table 14-1. Salt Tolerance of Selected Crops (*Continued*)

Common Name	Botanical Name	Electrical Conductivity of Saturated Soil Extract		
		Threshold, $\text{dS m}^{-1}$	Slope, % per $\text{dS m}^{-1}$	Rating <sup>a</sup>
Grapes	<i>Vitis sp.</i>	1.5	9.6	MS
Olives	<i>Olea europaea</i>			MT
Sugar beet	<i>Beta vulgaris</i>	7.0	5.9	T
Sugar cane	<i>Saccharum officinarum</i>	1.7	5.9	MS
Sunflower	<i>Helianthus annuus</i>			MS
<b>Vegetables</b>				
Broccoli	<i>Brassica oleracea botrytis</i>	2.8	9.2	MS
Cabbage	<i>Brassica oleracea capitata</i>	1.8	9.7	MS
Carrots	<i>Daucus carota</i>	1.0	14.0	S
Cauliflower	<i>Brassica oleracea botrytis</i>			MS
Celery	<i>Apium graveolens</i>	1.8	6.2	MS
Lettuce	<i>Lactuca sativa</i>	1.3	13.0	MS
Melons				
Onions	<i>Allium cepa</i>	1.2	16.0	S
Pepper	<i>Capsicum annuum</i>	1.5	14.0	MS
Potato	<i>Solanum tuberosum</i>	1.7	12.0	MS
Tomato	<i>Lycopersicon lycopersicum L.</i>	2.5	9.9	MS
Watermelon	<i>Citrullus lanatus</i>			MS

<sup>a</sup>Estimates: Tolerant (T), moderately tolerant (MT), moderately sensitive (MS), and sensitive (S)

Source: Tables 13-1, 13-2 of Maas (1990); copyright ASCE

Because of the complex chemical reactions that occur in soil solutions and the dynamics of the leaching process, transient-state solute transport models have been developed for estimating time-varying salinity within the crop root zone and the resulting *LR*. One model that requires limited input is WATSUIT (Rhoades and Merrill 1976). TETRANS is a simplified transient model that predicts changes in solute and soil water in irrigated crop root zones (Corwin et al. 1990). More details on the use of saline

waters for irrigation can be found in several FAO publications ([Rhoades et al. 1992, 1999](#)). Hoffman and Shannon ([2007](#)) present a detailed discussion on controlling salinity and salinity impacts on design and management of irrigation systems. ASCE Manual 71 on "Agricultural Salinity Assessment and Management," updated in 2011 ([Wallender and Tanji 2011](#)), contains substantial information on managing salinity and salt-affected soils and land application of wastes.

## 14.4 MISCELLANEOUS WATER REQUIREMENTS

Several minor but important water requirements must be considered for some crops. These requirements are often based on local practices and needs of specialty crops. Some of these are described below.

### Germination

Many small-seeded crops such as lettuce, carrots, etc., cannot be established unless the surface soil water content is maintained near field capacity for several days after planting to ensure germination and emergence of the seedlings. During midsummer, surface soil temperatures may reach levels fatal to the young plants unless cooled by frequent wetting during the high solar radiation periods. Sprinkler systems usually are more efficient for this purpose because several small intermittent applications per day may be required to maintain the desired soil water and temperature conditions. In the Imperial Valley of California, it has long been common practice to set up a sprinkler system to establish the crop and then to furrow irrigate during the balance of the season, a practice based on research conducted by Robinson ([1969](#)).

### Frost Protection

Application of water, usually by sprinkler irrigation, can be used to prevent or minimize frost damage to crops by utilizing the specific heat of water released in cooling to 0°C and in the latent heat of fusion released as water changes from a liquid to a solid state. The water required for frost control is generally much in excess of daily ET requirements. It varies with the heat lost through convection, radiation, and evaporation. Wolfe et al. ([1972](#)) indicate that sprinklers operated for frost protection when air temperatures range from -4°C to -7°C must apply 2.5 to 4 mm h<sup>-1</sup>. Leaf temperatures will not fall below 0°C in this range of air temperature if a film of unfrozen water is maintained on the ice-coated leaf. One limit to the continuous buildup of ice is the ability of the plant to support the weight of ice without damage to the plant. Water application must continue as long as the wet bulb temperature of the air is near or below the critical

temperature. When the ambient air temperature rises above 0°C, the ice will begin to melt. Heat absorbed in evaporating water from the surface of the ice may lower the temperature of the ice below the danger level unless sprinkling continues. The system capacity must be large enough to permit simultaneous application of water to the entire cropped area to be protected. A web-based publication on frost protection was made available by Snyder and de Melo-Abreu (2000).

### Blossom Delay

Water application from over-tree sprinklers in fruit trees has been used to cool the developing buds on warm days in the early spring. This evaporative cooling can cause a delay in a blossoming of up to 21 days (Griffin et al. 1976), which increases the probability of avoiding the last spring frost. The resultant maturity delay has also been used by growers to schedule harvesting dates. Griffin et al. (1976) recommend that the Christiansen uniformity coefficient be at least 80% and that the system be designed to provide  $3.8 \text{ mm h}^{-1}$  during high temperature periods. Pulsing of the system may be used to reduce the total volume of water as long as the desired cooling is attained.

### Wind Erosion Protection

When establishing crops in high wind areas, especially those with sandy soils, sprinkler irrigation has been used to control wind erosion and reduce damage to seedlings. Applications of 10 to 15 mm per day during high wind periods following planting may be required to protect the soil from eroding. In this case, however, sprinklers are usually operated at night when the wind speeds are low to achieve a more uniform application of water.

### Plant Cooling

Some plant components, such as flowers or seed heads, have a small number of stomata per unit area. With low wind speed, those plant components that are exposed to direct sunlight may reach temperatures that are 10 to 15°C above the ambient temperature due to a lack of evaporative cooling. Periodic misting at 1 to  $1.5 \text{ mm h}^{-1}$  has been used to wet these plant parts, thereby reducing their temperatures substantially below that of air temperature, but not below the wet bulb temperature (Kohl and Wright 1974). The duration of the cooling depends on the amount of water retained on these plant parts. Similarly, periodic misting of some fruit crops and lettuce may provide some economic benefits provided increased disease incidence does not offset gains from plant cooling.

## 14.5 SYSTEM LOSSES

Estimating total irrigation water requirements of irrigation projects and fields includes estimating various system “losses” associated with the delivery of water to the farm or field and associated hydraulics and uniformity of water application to the field.

### Net Irrigation Water Requirements

The net irrigation requirement per unit area is the water that must be supplied by irrigation to satisfy ET, leaching, and miscellaneous water requirements that are not provided by water stored in the soil or by precipitation that enters the soil.

$$W_r = (W_{ET} - R_e + \Delta W_s) + W_L + W_m \quad (14-10)$$

where  $W_r$  is the unit irrigation water requirement for the period being considered,  $W_L$  is the water required for leaching,  $W_m$  is the miscellaneous requirement,  $R_e$  is the effective rainfall,  $W_{ET}$  is the total water used in ET, and  $\Delta W_s$  is the increase in soil water. Units are volume per unit area or depth. A negative value for the quantity or depth of  $\Delta W_s$  represents a decrease in soil water during the period that can be utilized to fulfill  $W_r$ .  $R_e$  is set equal to  $P_{eff}$  if the  $W_{ET}$  does not include increased  $E$  stemming from wetting from  $P$ .  $R_e$  is set equal to  $P_{rz}$  if the  $W_{ET}$  does include the increased  $E$  associated with the  $P$  events.

### Allowances for Nonuniform Distribution

Water can neither be applied with perfect uniformity, nor without some unavoidable losses with most surface irrigation systems. Worldwide, surface irrigation is still the predominant irrigation method. In flat land areas, basin system is the most common method, and nonuniform surface elevation is the main reason for nonuniform water distribution. On sloping lands, surface runoff is inherent with most surface irrigation methods. Surface runoff is often captured and used on lower lying fields, or captured in holding ponds and pumped for reuse onto the same field or on another field, thereby reducing the fraction of loss as the area of focus increases. An illustration of typical flow and intake characteristics for a uniformly graded surface irrigation system is illustrated in Figure 14-1. Fields may be diked at the lower end to enhance infiltration, thereby resulting in little or no runoff. This practice may also reduce deep percolation near the upper end.

If water is applied to furrows with no end dikes until an adequate amount is infiltrated at the lower end of the field, then water application efficiency may be only 65% or less. The surface storage and subsurface

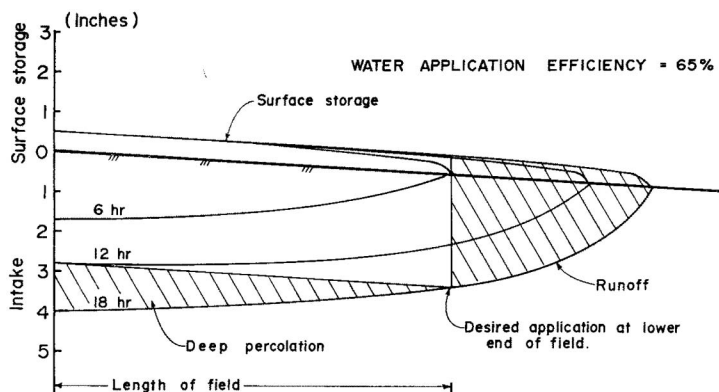


*Fig. 14-1. Sketch of longitudinal water application profile along a furrow*

Source: M. E. Jensen, personal communication

storage illustrated in Figure 14-1 are typical characteristics for an average furrow. Design of surface irrigation systems typically involves a water balance, i.e., accounting for water stored on the surface and that infiltrated. Several computer models are available for computing the complex dynamics of surface irrigation such as those by Clemmens et al. (1995) and Strelkoff (1990). Details on the design of surface irrigation systems, including reviews of earlier publications by USDA (1974, 1984), can be found in publications by Clemmens et al. (2007), Walker (1989), Walker and Skogerboe (1987), and Kay (1986).

The field application uniformity may be estimated as a modification from the average furrow by including the effects of soil variability along the furrow and intake differences between wheel rows and nonwheel rows and from variations in stream size, furrow shape, and other miscellaneous losses. These variations can decrease the distribution uniformity for the field by 25 to 30% from the distribution uniformity calculated for a single furrow.

As with surface systems, sprinkler systems do not apply water with perfect uniformity under calm conditions, and application uniformity is adversely affected as wind speed increases. Sprinkler application patterns typically follow a normal distribution of infiltration depths, i.e., some areas receive more water than the average and other areas receive less. With multiple irrigations under different wind speeds and directions, some compensation may occur in the over- or underirrigated areas. With sprinkler irrigation systems, there is also some evaporation from the spray. Spray evaporation losses seldom exceed 5% except where wind causes spray drift, which allows more time for evaporation to occur. Under some wind conditions evaporation losses from the sprinkler streams

may be as high as 12–14%, however, much of that evaporation reduces ET demands of vegetation downwind of the evaporation through cooling and humidification of the near-surface boundary layer. Therefore, on average, no more than 5% evaporation losses is recommended in estimating water depletion.

Sprinkler systems can have appreciable edge effects without mirrored overlap at field borders. They also may be subject to pressure differences due to elevation and friction head loss in the pipeline if pressure regulation is not part of the system. These differences can reduce the field distribution uniformity by 10 to 20%, depending on nozzle spacing and field size. Hundreds of papers have been written about sprinkler application uniformity and wind effects, spray losses, runoff, erosion, and crop yields since the 1950s. Examples of publications are those of Mateos et al. (1997), Jiusheng and Kawano (1996), Howell et al. (1995), Mantovani et al. (1995), Han et al. (1994), Seginer et al. (1991), Kranz and Eisenhauer (1990), Kohl and DeBoer (1984), Hathoot et al. (1994), and Yazar (1984). A publication on the design of sprinkler systems by Martin et al. (2007) and a center pivot design publication by Allen et al. (2000) contain procedures to estimate distribution uniformities and evaporation losses from these systems.

Use of drip or trickle irrigation systems, now called microirrigation systems, has expanded greatly since the 1960s. Typically, microirrigation systems are used mainly on high-value crops because of system costs. As with sprinkler systems, numerous publications address emitters, tubing, filters, and automatic controls. Design uniformities for microirrigation systems generally include the effects of pressure differences and the effects of plugging of emitters. A comprehensive review of the design and operation of microirrigation systems was presented by Nakayama and Bucks (1986). Edge effects are negligible. A recent publication on the design of microirrigation systems is by Evans et al. (2007).

### Storage and Distribution System Losses

From a project viewpoint, a substantial portion of runoff from surface systems and canal or lateral leakage may be recovered for use within a project or for use on downstream projects, depending on geology and topography. Estimates of evaporation from storage and regulating reservoirs may be required when estimating flow and storage capacities using procedures described in Chapter 6. Leakage from canals, laterals, and reservoirs may result in the growth of nonbeneficial vegetation depending on local subsurface soil and geologic conditions. Estimates of these losses can be made using procedures described in Chapters 9 and 10.

## Expected Occurrences of ET

When using irrigation water requirements for irrigation or water resources systems planning and design, some level of probability is generally utilized to ensure successful attainment of crop water demands for a specified number of years within a multiyear period. The probability level selected for design purposes should be based on an economic analysis considering both the reduction in crop yield and quality expected to occur should soil water availability be reduced below the desired minimum level during the averaging period and the incremental increases in the farm irrigation distribution system cost to provide capacity for higher probability levels. The use of a 50% probability level would result in soil water availability less than the minimum level for full ET in one out of two years. The degree to which soil water is depleted below the minimum should also be considered. Usually a higher probability level (80 to 90%) is selected for high-value, shallow-rooted crops than for common farm crops.

The expected reference ET on which to base the design capacity of farm or project irrigation systems will usually reduce with longer duration of the period, in days, being considered. The value will also vary with the desired probability level for the crop. A typical example of frequency distributions for reference ET is presented in Figure 14-2, where daily alfalfa reference  $ET_r$ , estimated using the ASCE-EWRI standardized Penman-Monteith equation is shown for a 20-year period at Kimberly, Idaho. Comparing the top figure, where daily  $ET_r$ , is plotted, to the bottom figure, where 10-day running average  $ET_r$ , is plotted, shows the substantial decrease in the range in reference ET values when they are averaged over several days. Overlying the  $ET_r$  data are probability lines for various levels of non-exceedence, based on a normal probability distribution. Nonexceedence is defined as the value of ET that is not expected to be exceeded  $p\%$  of the time, where  $p$  is the probability level.

A normal probability distribution presumes that the coefficient of skewness ( $CS$ ) = 0, where  $CS$  is the ratio of skew to the population mean. Generally, with evapotranspiration,  $CS$  approaches 0, so that frequency estimates based on the normal distribution are generally valid (Allen et al. 1983). In the case of the normal distribution, an estimate for ET for a specific probability of nonexceedance is estimated as

$$ET_{Pn} = ET_{\text{mean}} + K_{Pn}s \quad (14-11)$$

where  $ET_{Pn}$  is the ET rate expected to be exceeded only  $100\% - p\%$  of the time,  $K_{Pn}$  is a probability factor, and  $ET_{\text{mean}}$  and  $s$  are the estimates for the mean and standard deviation of the underlying ET population. Generally,  $ET_{\text{mean}}$ ,  $s$ , and  $ET_{Pn}$  are computed for a specific time period

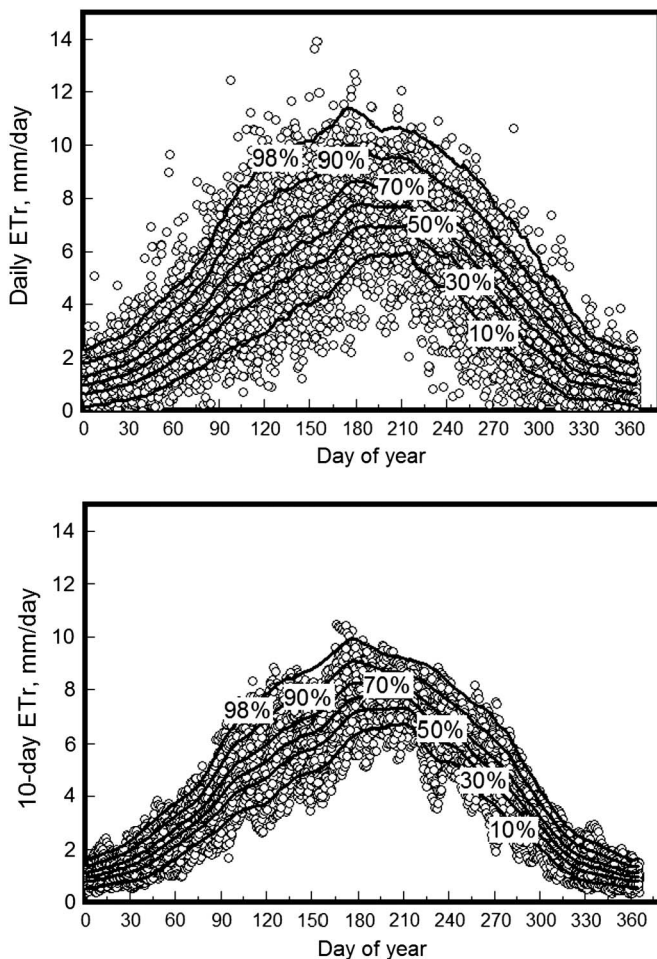


Fig. 14-2. Frequency distribution of alfalfa reference ET for Kimberly, Idaho, vs. time of year for daily time steps (upper figure) and 10-day running averages (lower figure) over a 20-year period

during the growing season, for example, for the peak 10- or 30-day period. Values for  $K_{Pn}$  are listed in Table 14-2 for the normal distribution. Allen et al. (2007c) include procedures for applying the log-Pearson distribution for skewed  $ET$  populations.

#### Available Water and Rainfall Effects

The peak period for ET may not last for more than three weeks for many annual crops. Therefore, the required capacity of the system may

Table 14-2. Probability Factors ( $K_{P_n}$ ) for a Normal Distribution

be affected by the amount of soil water storage that is available for depletion during the peak use period. The minimum or net design capacity may be reduced if leaching can be delayed during the peak use period and water applied for leaching off-season or when reference ET is not at its peak.

## 14.6 PRECIPITATION RUNOFF

Runoff ( $RO$ ) during precipitation events is strongly influenced by precipitation intensity and duration, soil texture, soil structure, vegetation cover, sealing and crusting of the soil surface, land slope, local land forming (tillage and furrowing), and antecedent moisture. As a result, estimates for  $RO$  from precipitation can have considerable uncertainty. For general applications,  $RO$  is often estimated using the USDA-NRCS Curve Number (CN) approach. The CN procedure is simple to apply and is widely used within the hydrologic and water resources communities. Required data are daily precipitation depth and computation of a daily soil water balance by which to select the antecedent soil water condition. Because only daily precipitation data are used, rather than hourly or shorter measurements, the intensity of rainfall is not considered and therefore, the accuracy of estimates is reduced as compared to methods that consider intensity. The CN procedure is generally adequate for purposes of estimating NIWR.

The CN represents the relative imperviousness of the soil-vegetation complex and ranges from 0 for surfaces having infinite infiltration properties to 100 for surfaces having complete imperviousness and consequently total runoff. Generally the value for CN is selected from standard tables based on general crop and soil type and is adjusted for the soil water content prior to the wetting event. Examples of values for CN for various crop and soil combinations are given in Table 14-3.  $RO$  is calculated from a parameter  $S$  representing the maximum depth of water retained as infiltration and canopy interception during a single precipitation event (in mm).  $S$  is calculated as

$$S = 250 \left( \frac{100}{CN} - 1 \right) \quad (14-12)$$

and surface runoff is then calculated for  $P > 0.2S$  as

$$RO = \frac{(P - 0.2S)^2}{P + 0.8S} \quad (14-13)$$

Table 14-3. Typical Curve Numbers for General Crops for Antecedent Soil Water Condition (AWC) II from USDA-SCS (1972) and Allen et al. (1988)

Crop	Soil Texture		
	Coarse	Medium	Fine
Spring wheat	63	75	85
Winter wheal	65	75	85
Field corn	67	75	85
Potatoes	70	76	88
Sugar beets	67	74	86
Peas	63	70	82
Dry edible beans	67	75	85
Sorghum	67	73	82
Cotton	67	75	83
Paddy rice	50	60	70
Sugar cane, virgin	60	69	75
Sugar cane, ratoon	60	68	76
Fruit trees, bare soil	65	72	82
Fruit trees, ground cover	60	68	70
Small garden vegetables	72	80	88
Tomatoes	65	72	82
Alfalfa hay	60	68	77
Suggested defaults	65	72	82

where  $RO$  is the depth of surface runoff during the event (mm) and  $P$  is the depth of rainfall during the event (mm). The  $0.2S$  term is the abstracted precipitation, representing the amount of  $P$  that is intercepted by the vegetation canopy and soil surfaces before any runoff occurs. If  $P \leq 0.2S$ , then  $RO=0.0$ . In addition,  $RO \leq P$  applies.

The CN is affected by the soil water content prior to the rainfall event, since soil water content affects the soil infiltration rate. Therefore, the CN is adjusted according to estimated soil water content prior to the rainfall event. This soil water content is termed the antecedent soil water condition (AWC) Adjustment ranges for CN were defined by USDA-SCS (1972) for dry (AWC I) and wet (AWC III) conditions, SCS defined AWC I as occurring when "watershed soils are dry enough for satisfactory plowing or cultivation to take place" and AWC III as when the "watershed is practically saturated from antecedent rains" (USDA-SCS. 1972.p.4.10). AWC II is defined as the "average condition" and represents values in Table 14-3.

Hawkins et al. (1985) expressed tabular relationships in USDA-SCS (1972) in the form of equations relating  $CN$  for AWC I and AWC III to  $CN$  for AWC II:

$$CN_I = \frac{CN_{II}}{2.281 - 0.01281CN_{II}} \quad (14-14)$$

$$CN_{III} = \frac{CN_{II}}{0.427 + 0.00573CN_{II}} \quad (14-15)$$

where  $CN_I$  is the curve number associated with AWC I (dry) [0–100],  $CN_{II}$  is the curve number associated with AWC II (average condition) [0–1001], and  $CN_{III}$ , the curve number associated with AWC III (wet) [0–100].

The soil surface layer water balance associated with the dual  $K_e$  procedure (Eq. 9-28) can be used to estimate the AWC condition. An approximation for the depletion of the soil surface layer at AWC III (wet) is when  $D_e = 0.5 REW$ , i.e., when the evaporation process is halfway through stage I drying. This point will normally be when approximately 5 mm or less have evaporated from the top 150 mm of soil since the time it was last completely wetted. Thus, the relationship:

$$D_{e-AWCIII} = 0.5 REW \quad (14-16)$$

where  $D_{e-AWCIII}$  is the depletion of the evaporative layer at AWC III. AWC I can be estimated to occur when 15 to 20 mm of water have evaporated from the top 150 mm of soil from the time it was last completely wetted. This is equivalent to when the evaporation layer has dried to the point at which  $D_e$  exceeds 30% of the total evaporable water in the surface layer beyond  $REW$ . This depletion amount is expressed as  $D_e = REW + 0.3(TEW - REW)$ , where  $TEW$  is the total evaporable water in the surface layer. Therefore,

$$D_{e-AWCI} = 0.7 REW + 0.3 TEW \quad (14-17)$$

where  $TEW$  is the cumulative evaporation from the surface soil layer at the end of stage 2 drying. When  $D_e$  is in between these two extremes, i.e.,  $0.5 REW < D_e < 0.7 REW + 0.3 TEW$ , then the AWC is in the AWC II condition and the  $CN$  value is linearly interpolated between  $CN_I$  and  $CN_{III}$ . In equation form:

$$CN = CN_{III} \quad \text{for } D_e \leq 0.5 REW \quad (14-18)$$

$$CN = CN_I \quad \text{for } D_e \geq 0.7 REW + 0.3 TEW \quad (14-19)$$

and, for  $0.5 \text{REW} < D_e < \text{REW} + 0.3(\text{TEW} - \text{REW})$ ;

$$CN = \frac{(D_e - 0.5 \text{REW})CN_I + (0.7 \text{REW} + 0.3 \text{TEW} - D_e)CN_{III}}{0.2 \text{REW} + 0.3 \text{TEW}} \quad (14-20)$$

Eq. 14-20 estimates values similar to  $CN_{II}$  when it is halfway between the endpoints of  $CN_I$  and  $CN_{III}$  due to the symmetry of  $CN_I$  and  $CN_{III}$  relative to  $CN_{II}$ .

Once the surface runoff depth is estimated using the curve number procedure, the depth of rainfall infiltrated is calculated as

$$P_{\text{inf}} = P - RO \quad (14-21)$$

where  $P_{\text{inf}}$  = depth of infiltrated precipitation, mm

$P$  = measured precipitation depth, mm

$RO$  = depth of surface runoff, mm.

If the soil will not hold the amount infiltrated, the remainder goes to deep percolation.

## 14.7 IMPROVEMENTS IN ESTIMATING WATER REQUIREMENTS

Approaches for estimating irrigation water requirements and procedures have changed greatly since the first edition of this manual. Practitioners are usually trained in computer programming and spreadsheet operation and other computerized data handling procedures. Much of our data collection is now electronic and is remotely controlled from a distance, with data transmission made over the Internet. Large amounts of data are available via simple requests to sources via the Internet. Our knowledge of hydrologic impacts of irrigation practices is now more advanced so that practitioners are able to, and are expected to, produce estimates of ET, irrigation water requirements, and impacts of water management practices in the overall context of basin hydrology.

### Impacts of Better Training

The training most engineers now receive includes some background in energy balance, meteorology, soil physics, and plant science. Essentially every new engineer is computer literate, and most have had some experience in solving multidisciplinary problems. Engineers associated with universities generally have immediate access to the latest worldwide literature in digital form. For others, the Internet can provide rapid access information on almost any subject. No longer must the recommended approach to solving a problem be "simple" as has generally been the practice in the past. However, the recommended approach to problem

solving must still be rational and understandable by all engineers and by professionals in other disciplines who are involved in water supply and management issues.

### Irrigation System and Water Consumption Interactions

For decades, policymakers and many engineers have misunderstood the meaning of the classic term *irrigation efficiency*. The frequent misinterpretation of reported low irrigation efficiencies was that if efficiency could be increased, less water would be consumed and new water would be available for other uses. Typically, the opposite is true because the classical efficiency term involves only the water diverted or applied to fields that is consumed. Both the consumed and nonconsumed components of water extractions must be considered as part of a water balance, and the disposition of nonconsumed water must be determined during assessment of impacts of “conservation” programs (Perry 2007; Perry et al. 2009; Fredericksen and Allen 2011). As an example of impacts of improving efficiency, Pfeiffer and Lin (2010) reported that when users in Kansas moved toward higher efficiency water systems, water use tended to increase. With the better systems, farmers were able to meet crop water needs during midsummer and, as a result, they tended to plant higher water use and higher return crops. As people moved to more and more efficient systems, less return flow to the groundwater occurred that in turn eventually entered river systems. Over the last decade, a region in Kansas has seen a shift away from the concept that increased water efficiency equals effective water conservation, finding that producers willingly adopt more efficient systems. However, those producers may either use the same amount of water for a higher water-use crop or put more acres into production, depending on the maximum water extraction limits stipulated by state water law. Many state cost-share practices for upgrading irrigation systems have been reduced or eliminated (Pfeiffer and Lin 2010).

Recent papers review the classic irrigation efficiency term and related terms. More recently the focus has been on the physical or economic productivity of water (Jensen 2007; Perry 2007; Perry et al. 2009; Molden 1997, 2007). Basically, irrigation water requirements involve mainly water consumption, and “efficiency” is not directly involved. Overall, there is a better understanding of irrigation and its effect on water resources and crop production than existed when the first edition of this manual was published in 1990.

## 14.8 DEPLETIONS TO THE WATER RESOURCE

Often quantification of depletions to river discharge are required as part of multistate compact management or for in-state water rights

management, and depletions to groundwater systems are needed for managing long-term sustainability. Depletions to the water resource caused by irrigation are equivalent to the NIWR calculated in Section 14.3 when the ET is at the potential value. This will occur when irrigation water is fully applied. Under water shortage or scarcity, however, crops may not receive a full water supply, and some water stress may occur. In addition, irrigation of some crops may be managed to induce some stress during some stages of growth, even under full water supply, to affect market quality and maximize profits.

When  $ET_{act} < ET_{pot}$ , methods are needed to estimate the amount of reduction in  $ET_{act}$ . When water additions are known, a daily water balance can be made for irrigated fields, with a stress function, such as described in Chapter 10, utilized. Often, however, field-scale water additions are not known on a multifield basis. In those cases, a water balance can be conducted on an irrigation scheme or district basis, or watershed basis, with ET closed upon as a residual. Horizontal flows for groundwater and diffusive forms of returns of surface water to streams can make these calculations uncertain. Satellite-based surface energy balance is becoming more widely used to estimate  $ET_{act}$  for use in scheme or district scale water balance (Allen et al., 2007a, for example), where  $ET_{act}$  from hundreds or thousands of individual fields can be quantified, provided a moderate resolution satellite having thermal imaging capacity, such as Landsat, is available. A fourth means to estimate  $ET_{act}$  is through the employment of crop yield-ET relationships, where reductions in yield are associated with reductions in ET. These relationships generally need to be calibrated locally to account for lower yields caused by other than constrained water supply, such as disease, salinity, or poor fertility.

On a field scale, the depletion to the water resource,  $D_{WR}$ , is estimated similar to NIWR [Eq. (14-1)], except that actual transpiration or actual ET is used rather than potential values:

$$\begin{aligned}
 D_{WR} &= ET_{act} - (P - RO - DP) \\
 &= E + T_{act} - (P - RO - DP) \\
 &= E + T_{act} - P_{rz} \\
 &= T_{act} - P_{aft}
 \end{aligned} \tag{14-22}$$

The comments in Section 14.7 apply to the quantification and characterization of  $D_{WR}$ , where returns of abstracted water back to streams or groundwater via surface runoff or percolation must be accurately measured or estimated and should not be considered to be part of  $D_{WR}$ , unless substantially impaired in quality, or lost directly to a saline sink such as the ocean (Frederiksen and Allen 2011; Molden 1997, 2007; Pfeiffer and Lin 2010).

## **APPENDIX A**

### **CONVERSION AND METEOROLOGICAL TABLES**

Table A-1. Conversion Factors

Length	
1 micrometer ( $\mu\text{m}$ )	$= 10^{-6} \text{ m}$
1 millimeter (mm)	$= 10^{-1} \text{ cm}$
1 centimeter (cm)	$= 10^{-2} \text{ m}$
1 meter (m)	$= 10^2 \text{ cm}$
1 kilometer (km)	$= 10^5 \text{ cm}$
1 degree of latitude <sup>a</sup> (Elat.)	$= 25.4 \text{ mm}$
1 inch (in.)	$= 12 \text{ in.}$
1 foot (ft)	$= 5,280 \text{ ft}$
1 statute mile (stat. mi)	$= 1,609.3 \text{ m}$
	$= 10^{-3} \text{ m}$
	$= 0.3937 \text{ in.}$
	$= 3,2808 \text{ ft}$
	$= 10^3 \text{ m}$
	$= 111.14 \text{ km}$
	$= 2.54 \text{ cm}$
	$= 30.48 \text{ cm}$
	$= 39,370 \text{ in.}$
	$= 3,280.8 \text{ ft}$
	$= 69,057 \text{ stat. mi}$
	$= 0.62137 \text{ stat. mi}$
	$= 3,280.8 \text{ ft}$
	$= 69,057 \text{ stat. mi}$
	$= 0.62137 \text{ stat. mi}$
Area <sup>b</sup>	
1 square meter ( $\text{m}^2$ )	$= 10^4 \text{ cm}^2$
1 square foot ( $\text{ft}^2$ )	$= 144 \text{ in.}^2$
1 acre	$= 43,560 \text{ ft}^2$
1 hectare (ha)	$= 10^4 \text{ m}^2$
	$= 1,550,000 \text{ in.}^2$
	$= 0.092903 \text{ m}^2$
	$= 4,046.856 \text{ m}^2$
	$= 2.471 \text{ acre}$
Volume	
1 cubic meter ( $\text{m}^3$ )	$= 10^6 \text{ cm}^3$
1 liter (L) <sup>c</sup>	$= 1,000 \text{ cm}^3$
1 acre-foot	$= 1,233,480 \text{ m}^3$
1 cubic inch ( $\text{in.}^3$ )	$= 16.387 \text{ cm}^3$
1 cubic foot ( $\text{ft}^3$ )	$= 1,728 \text{ in.}^3$
1 gallon, U.S. (U.S. gal.)	$= 231 \text{ in.}^3$
	$= 35,315 \text{ ft}^3$
	$= 0.26417 \text{ U.S. gal.}$
	$= 43,560 \text{ ft}^3$
	$= 28,3168 \text{ L}$
	$= 0.0283168 \text{ m}^3$
	$= 3,78534 \text{ L}$
	$= 264,172 \text{ U.S. gal.}$
	$= 325,851 \text{ U.S. gal.}$
	$= 219.97 \text{ Brit. gal.}$

Time	
1 mean solar minute (min.)	= 60 s
1 hour (h)	= 3,600 s
1 mean solar day (d)	= 86,400 s
Velocity (speed)	
1 meter per second ( $\text{m s}^{-1}$ )	= 3,600 km $\text{h}^{-1}$
1 kilometer per hour ( $\text{km h}^{-1}$ )	= 0.27778 m $\text{s}^{-1}$
1 knot	= 1 naut. mi $\text{h}^{-1}$
1 mile per hour ( $\text{mi h}^{-1}$ )	= 0.866839 knot
1 foot per second ( $\text{ft s}^{-1}$ )	= 0.68182 mi $\text{h}^{-1}$
Mass	
1 gram (g)	= 0.0022046 lb
1 kilogram (kg)	= $10^3$ g
1 metric ton, tonne (t)	= $10^3$ kg
1 pound avoirdupois (1 lb)	= 453.59 g
1 short ton (U.S. ton)	= 2,000 lb
1 long ton	= 2,240 lb
Density of water ( $4^\circ\text{C}$ )	
$1 \text{ g cm}^{-3}$	= 62.428 lb $\text{ft}^{-3}$ (Specific wt)
$1 \text{ kg m}^{-3}$	= $10^{-3}$ kg $\text{cm}^{-3}$
$1 \text{ Mg m}^{-3}$	= $10^3$ kg $\text{m}^{-3}$

(Continued)

Table A-1. Conversion Factors (*Continued*)

Force	
1 gram force 1 newton (N)	= 980.665 dynes = $10^5$ dynes
Energy, Work	
1 erg 1 joule (J)	= 1 dyne-centimeter = $10^{-7}$ joule(J) = $10^7$ ergs = 251.996 ITcal = 4.1868 joules = 1.35582 joules = $3.6 \times 10^6$ joules
1 British thermal unit (Btu) 1 International Steam Tables calorie (ITcal) 1 foot-pound (ft lb) 1 kilowatt-hour (kW·h)	= 0.23884 ITcal = 1055.07 joules = 3.6 megajoules (MJ)
Pressure <sup>e</sup>	
1 dyne per square centimeter (dyne cm <sup>-2</sup> ) 1 millibar (mb)	= $10^{-3}$ mb = $10^3$ dynes cm <sup>-2</sup> = 0.029530 in. Hg (standard)
	= $10^{-6}$ bar = 0.1 pascal (Pa) = 0.750062 mm Hg (standard) = 100 pascal (Pa)

	Power	Energy per Unit Area		
1 bar (b)				
1 standard millimeter of mercury [mm Hg (standard)]	$= 10^6 \text{ dynes cm}^{-2}$ $= 10^5 \text{ pascal (Pa)}$ $= 133.32 \text{ Pa}$	$= 10^3 \text{ mb}$ $= 10^2 \text{ kPa}$ $= 1.333224 \text{ mb}$	$= 10^5 \text{ N m}^{-2}$	$= 0.039370 \text{ in.}$
1 standard inch of mercury [in. Hg (standard)]	$= 0.49115 \text{ lb in.}^{-2}$ $= 25.4 \text{ mm Hg}$ $= 2.0360 \text{ in. Hg}$ $= 1013.25 \text{ mb}$	$= 33.864 \text{ mb}$ $= 3.3864 \text{ kPa}$ $= 68.9476 \text{ mb}$ $= 760 \text{ mm Hg (standard)}$	$= 6.89476 \text{ kPa}$ $= 29.921 \text{ in. Hg}$	
1 pound per sq. inch (lb in. $^{-2}$ )	$= 14.696 \text{ lb in.}^{-2}$ $= 1 \text{ N m}^{-2}$	$= 101.325 \text{ kPa}$ $= 10^{-3} \text{ kPa}$	$= 10^{-4} \text{ lb in.}^{-2}$	$= 1.4504 \cdot 10^{-4} \text{ lb in.}^{-2}$
1 standard atmosphere (standard)				
1 Pa				

*(Continued)*

Table A-1. Conversion Factors (*Continued*)

Power per Unit Area		
$1 \text{ cal}_{15} \text{ cm}^{-2} \text{ min}^{-1}$	$= 1 \text{ Ly min}^{-1}$	$= 0.6978 \text{ kilowatts m}^{-2}$
$1 \text{ Btu ft}^{-2} \text{ min}^{-1}$	$= 0.18928 \text{ kilowatts m}^{-2}$	

<sup>a</sup>Average value, 1/90 of meridian quadrant.

<sup>b</sup>The unit of land area, hectare, is commonly used in the metric system, but its dimensions,  $10^4 \text{ m}^2$ , do not follow the SI guide of multiples of  $10^3$ . The dunam =  $10^3 \text{ m}^2$  is a more practical land unit, but it is not in common usage and its symbol may conflict with SI recommendations. The hectare with the symbol ha was derived from hecto, a multiple of 100 having the symbol h, and the "are," which is a unit of land area =  $100 \text{ m}^2$  abbreviated "a."

<sup>c</sup>The General Conference on Weights and Measures in 1964 redefined the liter to be exactly  $1,000 \text{ cm}^3$ . Hence, the cubic decimeter, expressed as  $10^{-3} \text{ m}^3$ ,  $\text{dm}^3$ , or  $1,000 \text{ cm}^3$  may be a preferred unit to avoid errors. However, for practical purposes the new and old liters are essentially the same. (1 liter originally was defined as the volume occupied by 1 kilogram of water at its temperature of maximum density, but has been redefined).

<sup>d</sup>The Btu used here is defined by the relationship:  $1 \text{ Btu } ^\circ\text{F}^{-1} \text{ lb}^{-1} = 1 \text{ ITcal } ^\circ\text{C}^{-1} \text{ g}^{-1}$ .

<sup>e</sup>The pressure units one standard inch of mercury, one standard millimeter of mercury, and one standard atmosphere are defined in terms of the conventional standard value of gravitational acceleration of  $980.665 \text{ cm s}^{-2}$ , which was adopted by the International Committee on Weights and Measures. These units have been proposed for general meteorological use.

Source: Data from Table 1, List (1984); ASTM (1976), Wandmacher and Johnson (1995).

Table A-2. Saturation Vapor Pressure over Water in kPa<sup>a</sup>

°C	0	0.1	0.2	0.3	0.4	0.5	0.6	0.7	0.8	0.9
0	0.6108	0.6152	0.6197	0.6242	0.6288	0.6333	0.6379	0.6422	0.6472	0.6519
1	0.6566	0.6614	0.6661	0.6709	0.6758	0.6807	0.6856	0.6895	0.6955	0.7004
2	0.7055	0.7105	0.7156	0.7207	0.7259	0.7311	0.7363	0.7404	0.7469	0.7522
3	0.7575	0.7629	0.7683	0.7738	0.7793	0.7848	0.7904	0.7964	0.8016	0.8072
4	0.8129	0.8187	0.8245	0.8303	0.8361	0.8420	0.8479	0.8479	0.8598	0.8659
5	0.8719	0.8780	0.8842	0.8903	0.8966	0.9028	0.9091	0.9091	0.9218	0.9282
6	0.9346	0.9411	0.9477	0.9542	0.9608	0.9675	0.9742	0.9742	0.9877	0.9945
7	1.001	1.008	1.015	1.022	1.029	1.036	1.043	1.043	1.058	1.065
8	1.072	1.079	1.087	1.094	1.102	1.109	1.117	1.117	1.132	1.140
9	1.147	1.155	1.163	1.171	1.179	1.187	1.195	1.195	1.211	1.219
10	1.227	1.235	1.244	1.252	1.261	1.269	1.277	1.277	1.295	1.303
11	1.312	1.321	1.329	1.338	1.347	1.356	1.365	1.365	1.383	1.393
12	1.402	1.411	1.420	1.430	1.439	1.449	1.458	1.458	1.477	1.487
13	1.497	1.507	1.517	1.527	1.537	1.547	1.557	1.557	1.577	1.587
14	1.598	1.608	1.619	1.629	1.640	1.650	1.661	1.661	1.683	1.693
15	1.704	1.715	1.726	1.738	1.749	1.760	1.771	1.771	1.794	1.806
16	1.817	1.829	1.841	1.852	1.864	1.876	1.888	1.888	1.912	1.924
17	1.937	1.949	1.961	1.974	1.986	1.999	2.012	2.012	2.037	2.050
18	2.063	2.076	2.089	2.102	2.115	2.129	2.142	2.142	2.169	2.183
19	2.196	2.210	2.224	2.238	2.252	2.266	2.280	2.280	2.308	2.323
20	2.337	2.352	2.366	2.381	2.396	2.411	2.426	2.426	2.456	2.471
21	2.486	2.501	2.517	2.532	2.548	2.563	2.579	2.579	2.611	2.627
22	2.643	2.659	2.675	2.692	2.708	2.725	2.741	2.741	2.775	2.792
23	2.809	2.826	2.843	2.860	2.877	2.895	2.912	2.912	2.947	2.965
24	2.983	3.001	3.019	3.037	3.056	3.074	3.092	3.092	3.130	3.148

(Continued)

Table A-2. Saturation Vapor Pressure over Water in kPa<sup>a</sup> (*Continued*)

°C	0	0.1	0.2	0.3	0.4	0.5	0.6	0.7	0.8	0.9
25	3.167	3.186	3.205	3.224	3.243	3.263	3.282	3.282	3.321	3.341
26	3.361	3.381	3.401	3.421	3.441	3.462	3.482	3.482	3.523	3.544
27	3.565	3.586	3.607	3.628	3.649	3.671	3.692	3.692	3.736	3.758
28	3.780	3.802	3.824	3.846	3.869	3.891	3.914	3.914	3.959	3.982
29	4.005	4.029	4.052	4.076	4.099	4.123	4.147	4.147	4.195	4.219
30	4.243	4.267	4.292	4.317	4.341	4.366	4.391	4.391	4.442	4.467
31	4.493	4.518	4.544	4.570	4.596	4.622	4.649	4.649	4.702	4.728
32	4.755	4.782	4.809	4.836	4.864	4.891	4.919	4.919	4.974	5.003
33	5.031	5.059	5.087	5.116	5.145	5.174	5.203	5.203	5.261	5.290
34	5.320	5.350	5.380	5.410	5.440	5.470	5.500	5.500	5.562	5.593
35	5.624	5.655	5.686	5.718	5.749	5.781	5.813	5.813	5.877	5.910
36	5.942	5.975	6.008	6.041	6.074	6.107	6.141	6.141	6.208	6.242
37	6.276	6.311	6.345	6.380	6.414	6.449	6.484	6.484	6.555	6.591
38	6.626	6.662	6.698	6.735	6.771	6.808	6.845	6.845	6.919	6.956
39	6.993	7.031	7.069	7.107	7.145	7.183	7.222	7.222	7.299	7.339
40	7.378	7.417	7.457	7.497	7.537	7.577	7.617	7.617	7.698	7.739
41	7.780	7.821	7.863	7.905	7.946	7.988	8.031	8.031	8.116	8.159
42	8.202	8.245	8.288	8.332	8.375	8.419	8.464	8.464	8.553	8.597
43	8.642	8.687	8.733	8.778	8.824	8.870	8.916	8.916	9.010	9.056
44	9.103	9.151	9.198	9.246	9.294	9.342	9.390	9.390	9.487	9.536
45	9.585	9.635	9.684	9.734	9.784	9.835	9.885	9.885	9.987	10.038
46	10.089	10.141	10.193	10.245	10.297	10.350	10.403	10.403	10.509	10.562
47	10.616	10.670	10.724	10.778	10.833	10.888	10.943	10.943	11.054	11.110
48	11.166	11.222	11.279	11.336	11.393	11.450	11.507	11.507	11.623	11.682
49	11.740	11.799	11.858	11.917	11.977	12.037	12.097	12.097	12.218	12.278
50	12.340	12.401	12.462	12.524	12.587	12.649	12.712	12.712	12.838	12.901

<sup>a</sup>Calculated using Goff-Gratch formulation (List, 1984, p. 350). 1 mb = kPa × 10.

Table A-3. Thermodynamic Constants

Basic constants	
	Recommended values
	Range of actual values
Apparent molecular weight of dry air, $M_a$	$M_a = 28.966 \text{ g mol}^{-1}$ or $\text{kg kmol}^{-1}$
Universal gas constant, $R$	$R = 8.3144 \text{ joule mol}^{-1} \text{ K}^{-1}$ or $\text{kJ kmol}^{-1} \text{ K}^{-1}$
	$= 1.98583 \text{ ITcal mol}^{-1} \text{ K}^{-1}$
Specific gas constant for dry air, $R_a = R/M_a$	$R_a = 8.3144 \text{ joule mol}^{-1} \text{ K}^{-1} / 28.966 \text{ g mol}^{-1}$
	$= 0.28704 \text{ joule g}^{-1} \text{ K}^{-1}$
	$= 0.28704 \text{ kJ kg}^{-1} \text{ K}^{-1}$
	$= 6.8557 \times 10^{-2} \text{ ITcal g}^{-1} \text{ K}^{-1}$
Molecular weight of water vapor, $M_v$	$M_v = 18.0160 \text{ g mol}^{-1}$ or $\text{kg kmol}^{-1}$
Specific gas constant for water vapor, $R_v = R/M_v$	$R_v = \frac{8.3144}{18.0160} = 0.46150 \text{ joule g}^{-1} \text{ K}^{-1}$
	$= 0.46150 \text{ kJ kg}^{-1} \text{ K}^{-1}$
	$= 0.110226 \text{ ITcal g}^{-1} \text{ K}^{-1}$
Absolute temperature of the ice point <sup>a</sup> , $T_o$	$T_o = 273.15 \text{ K}$
Specific heats	
Dry air:	
constant pressure, $c_p = 7R_a/2$	$= 0.240 \text{ ITcal g}^{-1} \text{ K}^{-1}$ $= 1.0046 \text{ kJ kg}^{-1} \text{ K}^{-1}$
constant volume, $c_v = 5R_a/2$	$= 0.171 \text{ ITcal g}^{-1} \text{ K}^{-1}$ $= 0.7176 \text{ kJ kg}^{-1} \text{ K}^{-1}$

(Continued)

Table A-3. Thermodynamic Constants (*Continued*)

	Specific heats	Range of actual values
	Recommended values	
<b>Water:</b>		
liquid, $c_w$	1.000 $\text{ITcal g}^{-1} \text{K}^{-1}$ 4.1868 $\text{kJ kg}^{-1} \text{K}^{-1}$	0.999–1.3 4.180–5.4
ice, $c_i$	0.5 $\text{ITcal g}^{-1} \text{K}^{-1}$ 2.0934 $\text{kJ kg}^{-1} \text{K}^{-1}$	0.5–0.3 2.092–1.26
<b>Water vapor:</b>		
constant pressure, $c_{pv} = 4R_v$	$= 0.441 \text{ ITcal g}^{-1} \text{K}^{-1}$ $= 1.846 \text{ kJ kg}^{-1} \text{K}^{-1}$	0.44–0.46 1.84–1.92
constant volume, $c_{vv} = 3R_v$	$= 0.331 \text{ ITcal g}^{-1} \text{K}^{-1}$ $= 1.3845 \text{ kJ kg}^{-1} \text{K}^{-1}$	0.33–0.34 1.381–1.42
<b>Moist air:</b>		
Brutsaert (1982)	$= c_{pd}(1+0.84q)$ where $q = \text{specific humidity}$	
constant pressure, $c_p$	$= 0.242 \text{ ITcal g}^{-1} \text{K}^{-1}$ $= 1013 \text{ J kg}^{-1} \text{K}^{-1}$	

<sup>a</sup>The International Temperature Scale of 1990 (ITS-90).

Source: Data from Table 70, List (1984).

Table A-4. Density of Air

The density of air in  $\text{g cm}^{-3}$  and  $\text{kg m}^{-3}$  is

$$\rho = 10^{-3} \frac{P}{R_a T_v} \text{ g cm}^{-3}, \quad \text{or} \quad \rho = \frac{P}{R_a T_v} \text{ kg m}^{-3}$$

where  $P$ =total barometric pressure, kPa;  $R_a$  = specific gas constant for dry air =  $0.28704 \text{ kJ kg}^{-1} \text{ K}^{-1}$ ;  $T_v$ =virtual temperature (the temperature dry air would have to be to have the same density as moist air at the same pressure).

$$T_v = T \frac{1+r/0.622}{1+r}$$

where  $r$  = the mixing ratio ( $r = m_v/m_a \approx 0.622e/P$ ) and  $T$ =absolute temperature. For  $P$  in kPa, the density  $\rho$  is

$$\rho = 3.4838 P/T_v \text{ kg m}^{-3} \quad \text{or} \quad \rho = 0.0034838 P/T_v \text{ g cm}^{-3}$$

*Example:* For  $P=101.325 \text{ kPa}$  and  $T_v=273.15 \text{ K}$  ( $0^\circ\text{C}$ )

$$\rho = 3.4838(101.325/273.15) = 1.292 \text{ kg m}^{-3}$$

$$\rho = 0.0034838(101.325/273.15) = 0.001292 \text{ g cm}^{-3}$$

(Continued)

Table A-4. Density of Air (*Continued*)

$T_v$ , (°C)	Pressure (kPa)				
	110	100	90	80	70
0	1.4029	1.2754	1.1478	1.0203	0.8928
5	1.3777	1.2525	1.1272	1.0020	0.8767
10	1.3534	1.2303	1.1073	0.9843	0.8612
15	1.3299	1.2090	1.0881	0.9672	0.8463
20	1.3072	1.1884	1.0695	0.9507	0.8319
25	1.2853	1.1684	1.0516	0.9348	0.8179
30	1.2641	1.1492	1.0343	0.9193	0.8044
35	1.2436	1.1305	1.0175	0.9044	0.7914
40	1.2237	1.1125	1.0012	0.8900	0.7787
45	1.2045	1.0950	0.9855	0.8760	0.7665
50	1.1859	1.0780	0.9702	0.8624	0.7546

Source: Data from Table 71, List (1984).

Table A-5. Day of Year

In the many energy balance equations, the day of the year,  $J$ , is often required. A procedure for calculating  $J$  (ASCE 2005) is

$$J = D_M - 32 + \text{Int}\left(275 \frac{M}{9}\right) + 2\text{Int}\left(\frac{3}{M+1}\right) + \text{Int}\left[\frac{M}{100} - \frac{\text{Mod}(Y, 4)}{4} + 0.975\right] \quad (\text{A5-1})$$

where  $D_M$  is the day of the month (1–31),  $M$  is the number of the month (1–12), and  $Y$  is the number of the year (for example 1996 or 96). The “Int” function in Eq. (A5-1) finds the integer number of the argument in parentheses by rounding downward. The “Mod( $Y, 4$ )” function finds the modulus (remainder) of the quotient  $Y/4$  and corrects for the effect of a leap year.

For monthly periods, the day of the year at the middle of the month ( $J_{\text{month}}$ ) is approximately

$$J_{\text{month}} = \text{Int}(30.4M - 15) \quad (\text{A5-2})$$

The day of the year (DoY) for the 15th of each month is

Month	DoY	Month	DoY
January	15	July	196
February	45	August	227
March	74	September	258
April	105	October	288
May	135	November	319
June	166	December	349

This page intentionally left blank

## APPENDIX B

### MEAN CROP COEFFICIENTS IN SUBHUMID CLIMATES

This appendix presents the mean crop coefficients,  $K_c$ , for well-managed crops in subhumid climates for use with clipped grass reference  $ET_o$ , range of maximum effective rooting depth, and soil water depletion fraction for no stress,  $p$ , based on FAO-56 ([Allen et al. 1998](#)). Guidelines on applying  $K_c$  values in this appendix are given in Chapter 10.

Table B-1. Mean Crop Coefficients<sup>1</sup>

Crop	$K_{cini}$ <sup>a</sup>	$K_{cmid}$ <sup>b</sup>	$K_{cend}$ <sup>b</sup>	Max. ht, m	Max. root depth <sup>c</sup> , M	$p$ <sup>d</sup>
<b>a. Small Vegetables</b>	<b>0.7</b>	<b>1.05</b>	<b>0.95</b>			
Broccoli		1.05	0.95	0.3	0.4–0.6	0.45
Brussels sprouts		1.05	0.95	0.4	0.4–0.6	0.45
Cabbage		1.05	0.95	0.4	0.5–0.8	0.45
Carrots		1.05	0.95	0.3	0.5–1.0	0.35
Cauliflower		1.05	0.95	0.4	0.4–0.7	0.45
Celery		1.05	1.00	0.6	0.3–0.5	0.20
Garlic		1.00	0.70	0.3	0.3–0.5	0.30
Lettuce		1.00	0.95	0.3	0.3–0.5	0.30
Onions						
dry		1.05	0.75	0.4	0.3–0.6	0.30
green		1.00	1.00	0.3	0.3–0.6	0.30
seed		1.05	0.80	0.5	0.3–0.6	0.35
Spinach		1.00	0.95	0.3	0.3–0.5	0.20
Radish		0.90	0.85	0.3	0.3–0.5	0.30
<b>b. Vegetables—Solanum Family (<i>Solanaceae</i>)</b>	<b>0.6</b>	<b>1.15</b>	<b>0.80</b>			
Eggplant		1.05	0.90	0.8	0.7–1.2	0.45
Sweet Peppers (bell)		1.05 <sup>e</sup>	0.90	0.7	0.5–1.0	0.30
Tomato		1.15 <sup>e</sup>	0.70–0.90	0.6	0.7–1.5	0.40
<b>c. Vegetables—Cucumber Family (<i>Cucurbitaceae</i>)</b>	<b>0.5</b>	<b>1.00</b>	<b>0.80</b>			
Cantaloupe	0.5	0.85	0.60	0.3	0.9–1.5	0.45

## MEAN CROP COEFFICIENTS IN SUBHUMID CLIMATES

Cucumber						
fresh market	0.6	1.00 <sup>e</sup>	0.75	0.3	0.7–1.2	0.50
machine harvest	0.5	1.00	0.90	0.3	0.7–1.2	0.50
Pumpkin, winter squash		1.00	0.80	0.4	1.0–1.5	0.35
Squash, zucchini		0.95	0.75	0.3	0.6–1.0	0.50
Sweet melons		1.05	0.75	0.4	0.8–1.5	0.40
Watermelon	0.4	1.00	0.75	0.4	0.8–1.5	0.40
<b>d. Roots and Tubers</b>	<b>0.5</b>	<b>1.10</b>	<b>0.95</b>			
Beets, table		1.05	0.95	0.4	0.6–1.0	0.50
Cassava						
year 1	0.3	0.80 <sup>f</sup>	0.30	1.0	0.5–0.8	0.35
year 2	0.3	1.10	0.50	1.5	0.7–1.0	0.40
Parsnip	0.5	1.05	0.95	0.4	0.5–1.0	0.40
Potato		1.15	0.75 <sup>g</sup>	0.6	0.4–0.6	0.35
Sweet potato		1.15	0.65	0.4	1.0–1.5	0.65
Turnip (and rutabaga)		1.10	0.95	0.6	0.5–1.0	0.50
Sugar beet	0.35	1.20	0.70 <sup>h</sup>	0.5	0.7–1.2	0.55 <sup>i</sup>
<b>e. Legumes (<i>Leguminosae</i>)</b>	<b>0.4</b>	<b>1.15</b>	<b>0.55</b>			
Beans, green	0.5	1.05 <sup>e</sup>	0.90	0.4	0.5–0.7	0.45
Beans, dry, and pulses	0.4	1.15 <sup>e</sup>	0.35	0.4	0.6–0.9	0.45
Chickpea		1.00	0.35	0.4	0.6–1.0	0.50
Fava bean (broad bean)						
fresh	0.5	1.15 <sup>e</sup>	1.10	0.8	0.5–0.7	0.45
dry/seed	0.5	1.15 <sup>e</sup>	0.30	0.8	0.5–0.7	0.45

(Continued)

Table B-1. Mean Crop Coefficients<sup>1</sup> (*Continued*)

Crop	$K_{cini}$ <sup>a</sup>	$K_{cmid}$ <sup>b</sup>	$K_{cend}$ <sup>b</sup>	Max. ht, m	Max. root depth <sup>c</sup> , M	$p$ <sup>d</sup>
Garbanzo	0.4	1.15	0.35	0.8	0.6–1.0	0.45
Green gram and cowpeas		1.05	0.60–0.35 <sup>j</sup>	0.4	0.6–1.0	0.45
Groundnut (peanut)		1.15	0.60	0.4	0.5–1.0	0.50
Lentil		1.10	0.30	0.5	0.6–0.8	0.50
Peas						
fresh	0.5	1.15 <sup>e</sup>	1.10	0.5	0.6–1.0	0.35
dry/seed		1.15	0.30	0.5	0.6–1.0	0.40
Soybeans		1.15	0.50	0.5	0.6–1.3	0.50
f. Perennial Vegetables (with winter dormancy and initially bare or mulched)	0.5	1.00	0.80			
Artichokes	0.5	1.00	0.95	0.7	0.6–0.9	0.45
Asparagus	0.5	0.95 <sup>k</sup>	0.30	0.2–0.8	1.2–1.8	0.45
Mint	0.60	1.15	1.10	0.6–0.8	0.4–0.8	0.40
Strawberries	0.40	0.85	0.75	0.2	0.2–0.3	0.20
g. Fiber Crops	0.35					
Cotton		1.15–1.20	0.70–0.50	1.2–1.5	1.0–1.7	0.65
Flax		1.10	0.25	1.2	1.0–1.5	0.50
Sisal <sup>l</sup>		0.4–0.7	0.4–0.7	1.5	0.5–1.0	0.80
h. Oil Crops	0.35	1.15	0.35			
Castor bean ( <i>Ricinus</i> )		1.15	0.55	0.3	1.0–2.0	0.50
Rapeseed, canola		1.0–1.15 <sup>m</sup>	0.35	0.6	1.0–1.5	0.60

## MEAN CROP COEFFICIENTS IN SUBHUMID CLIMATES

475

Safflower		1.0–1.15 <sup>m</sup>	0.25	0.8	1.0–2.0	0.60
Sesame		1.10	0.25	1.0	1.0–1.5	0.60
Sunflower		1.0–1.15 <sup>m</sup>	0.35	2.0	0.8–1.5	0.45
<b>i. Cereals</b>	<b>0.3</b>	<b>1.15</b>	<b>0.4</b>			
Barley		1.15	0.25	1	1.0–1.5	0.55
Oats		1.15	0.25	1	1.0–1.5	0.55
Spring Wheat		1.15	0.25–0.4 <sup>n</sup>	1	1.0–1.5	0.55
Winter Wheat						
with frozen soils	0.4	1.15	0.25–0.4 <sup>n</sup>	1	1.5–1.8	0.55
with nonfrozen soils	0.7	1.15	0.25–0.4 <sup>n</sup>			
Maize, field (grain) ( <i>field corn</i> )		1.20 <sup>o</sup>	0.60, 0.35 <sup>p</sup>	2	1.0–1.7	0.55
Maize, sweet ( <i>sweet corn</i> )		1.15 <sup>o</sup>	1.05 <sup>q</sup>	1.5	0.8–1.2	0.50
Millet		1.00	0.30	1.5	1.0–2.0	0.55
Sorghum						
grain		1.00–1.10	0.55	1–2	1.0–2.0	0.55
sweet		1.20	1.05	2–4	1.0–2.0	0.50
Rice	1.05	1.05–1.20 <sup>r</sup>	0.90–0.60	1	0.5–1.0	0.20 <sup>s</sup>
<b>j. Forages</b>						
Alfalfa hay						
averaged cutting effects	0.40	0.95 <sup>t</sup>	0.90	0.7	1.0–2.0	0.55
individual cutting periods	0.40 <sup>u</sup>	1.20 <sup>u</sup>	1.15 <sup>u</sup>	0.7	1.0–2.0	0.55
for seed	0.40	0.50	0.50	0.7	1.0–3.0	0.60
Bermuda hay						
averaged cutting effects	0.55	1.00 <sup>t</sup>	0.85	0.35	1.0–1.5	0.55
spring crop for seed	0.35	0.90	0.65	0.4	1.0–1.5	0.60

(Continued)

Table B-1. Mean Crop Coefficients<sup>1</sup> (*Continued*)

Crop	$K_{cini}$ <sup>a</sup>	$K_{cmid}$ <sup>b</sup>	$K_{cend}$ <sup>b</sup>	Max. ht, m	Max. root depth <sup>c</sup> , M	$p$ <sup>d</sup>
Clover hay, berseem						
averaged cutting effects	0.40	0.90 <sup>t</sup>	0.85	0.6	0.6–0.9	0.50
individual cutting periods	0.40 <sup>u</sup>	1.15 <sup>u</sup>	1.10 <sup>u</sup>	0.6	0.6–0.9	0.50
Ryegrass hay						
averaged cutting effects	0.95	1.05	1.00	0.3	0.6–1.0	0.60
Sudan grass hay (annual)						
averaged cutting effects	0.50	0.90 <sup>t</sup>	0.85	1.2	1.0–1.5	0.55
individual cutting periods	0.50 <sup>u</sup>	1.15 <sup>u</sup>	1.10 <sup>u</sup>	1.2	1.0–1.5	0.55
Grazing pasture						
rotated grazing	0.40	0.85–1.05	0.85	0.15–0.30	0.5–1.5	0.60
extensive grazing	0.30	0.75	0.75	0.10	0.5–1.5	0.60
Switchgrass <sup>v</sup>	0.20	1.05	0.20	1.0–2.0	1.5–2.0	0.60
Turfgrass						
cool-season <sup>w</sup>	0.90	0.90	0.90	0.10	0.5–1.0	0.40
warm-season <sup>w</sup>	0.85	0.90	0.90	0.10	0.5–1.0	0.50
<b>k. Sugarcane</b>	0.40	1.25	0.75	3	1.2–2.0	0.65
<b>l. Tropical Fruits and Trees</b>						
Banana						
1st year	0.50	1.10	1.00	3	0.5–0.9	0.35
2nd year	1.00	1.20	1.10	4	0.5–0.9	0.35

## MEAN CROP COEFFICIENTS IN SUBHUMID CLIMATES

Cacao		1.00	1.05	1.05	3	0.7–1.0	0.30
Coffee	bare ground cover	0.90	0.95	0.95	2–3	0.9–1.5	0.40
	with weeds	1.05	1.10	1.10	2–3	0.9–1.5	0.40
Palms (including date palms) <sup>x</sup>				8	0.7–1.1	0.65	
	no ground cover—high density ( $f_{c\text{eff}}=0.7$ ) <sup>z</sup>	0.90	0.95	0.95			
	no ground cover—medium density ( $f_{c\text{eff}}=0.5$ )	0.80	0.80	0.80			
	no ground cover—low density/young ( $f_{c\text{eff}}=0.25$ )	0.50	0.55	0.55			
	no ground cover—very low density/young ( $f_{c\text{eff}}=0.1$ )	0.35	0.35	0.35			
	active ground cover <sup>aa</sup> —high density ( $f_{c\text{eff}}=0.7$ )	0.95	0.95	0.95			
	active ground cover—medium density ( $f_{c\text{eff}}=0.5$ )	0.90	0.90	0.90			
	act. ground cover—low density/young ( $f_{c\text{eff}}=0.25$ )	0.85	0.85	0.85			
	act. ground cover—very low density/young ( $f_{c\text{eff}}=0.1$ )	0.80	0.80	0.80			
Pineapple <sup>bb</sup>	bare soil	0.50	0.30	0.30	0.6–1.2	0.3–0.6	0.50
	with grass cover	0.50	0.50	0.50	0.6–1.2	0.3–0.6	0.50
Rubber trees		0.95	1.00	1.00	10	1.0–1.5	0.40
Tea	non-shaded	0.95	1.00	1.00	1.5	0.9–1.5	0.40
	shaded <sup>cc</sup>	1.10	1.15	1.15	2	0.9–1.5	0.45

(Continued)

Table B-1. Mean Crop Coefficients<sup>1</sup> (*Continued*)

Crop	$K_{cini}$ <sup>a</sup>	$K_{cmid}$ <sup>b</sup>	$K_{cend}$ <sup>b</sup>	Max. ht, m	Max. root depth <sup>c</sup> , M	$p$ <sup>d</sup>
<b>m. Grapes and Berries</b>						
Berries (bushes)	0.30	1.05	0.50	1.5	0.6–1.2	0.50
Grapes, table or raisin <sup>x</sup>				2	1.0–2.0	0.35
no ground cover—high density ( $f_{ceff} = 0.7$ ) <sup>dd</sup>	0.30	1.10	0.90 <sup>ee</sup>			
no ground cover—medium density ( $f_{ceff} = 0.5$ ) <sup>z</sup>	0.30	0.95	0.75 <sup>ee</sup>			
no ground cover—low/young ( $f_{ceff} = 0.25$ )	0.25	0.60	0.50 <sup>ee</sup>			
Grapes, wine				1.5–2	1.0–2.0	0.45
no ground cover—high density ( $f_{ceff} = 0.7$ )	0.30	0.75 <sup>ff</sup>	0.60 <sup>ee, ff</sup>			
no ground cover—medium density ( $f_{ceff} = 0.5$ ) <sup>z</sup>	0.30	0.70 <sup>ff</sup>	0.55 <sup>ee, ff</sup>			
no ground cover—low/young ( $f_{ceff} = 0.25$ )	0.30	0.45 <sup>ff</sup>	0.40 <sup>ee, ff</sup>			
Hops	0.30	1.05	0.85	5	1.0–1.2	0.50
<b>n. Fruit Trees</b>						
Almonds, no ground cover <sup>x</sup>					1.0–2.0	0.40
no ground cover—high density ( $f_{ceff} = 0.7$ )	0.40	1.00	0.70 <sup>ee</sup>	5		
no ground cover—medium density ( $f_{ceff} = 0.5$ ) <sup>z</sup>	0.40	0.85	0.60 <sup>ee</sup>	4		
no ground cover—low density/young ( $f_{ceff} = 0.25$ )	0.35	0.50	0.40 <sup>ee</sup>	3		
active ground cover <sup>aa</sup> —high density ( $f_{ceff} = 0.7$ )	0.85	1.05	0.85 <sup>ee</sup>	5		
active ground cover—medium density ( $f_{ceff} = 0.5$ )	0.85	1.00	0.85 <sup>ee</sup>	4		
active ground cover—low density/young ( $f_{ceff} = 0.25$ )	0.85	0.95	0.85 <sup>ee</sup>	3		
Apples, Cherries, and Pears <sup>x</sup>					1.0–2.0	0.50
no ground cover—high density ( $f_{ceff} = 0.7$ )	0.50	1.15	0.80 <sup>ee</sup>	4		
no ground cover—medium density ( $f_{ceff} = 0.5$ ) <sup>z</sup>	0.45	1.05	0.75 <sup>ee</sup>	3		

no ground cover—low density/young ( $f_{c\text{eff}}=0.25$ )	0.40	0.70	0.55 <sup>ee</sup>	3	
active ground cover <sup>aa</sup> , killing frost—high density ( $f_{c\text{eff}}=0.7$ )	0.50	1.20	0.85 <sup>ee</sup>	4	
active ground cover, killing frost—medium density ( $f_{c\text{eff}}=0.5$ ) <sup>z</sup>	0.50	1.15	0.85 <sup>ee</sup>	3	
active ground cover, killing frost—low density ( $f_{c\text{eff}}=0.25$ )	0.50	1.05	0.85 <sup>ee</sup>	3	
active ground cover, no frosts—high density ( $f_{c\text{eff}}=0.7$ )	0.85	1.20	0.85 <sup>ee</sup>	4	
active ground cover, no frosts—medium density ( $f_{c\text{eff}}=0.5$ ) <sup>z</sup>	0.85	1.15	0.85 <sup>ee</sup>	3	
active ground cover, no frosts—low density ( $f_{c\text{eff}}=0.25$ )	0.85	1.05	0.85 <sup>ee</sup>	3	
Apricots, peaches, and stone fruit <sup>x, gg</sup>				1.0–2.0	0.50
no ground cover—super high density ( $f_{c\text{eff}}=0.9$ ) <sup>dd</sup>	0.50	1.20	0.85 <sup>ee</sup>	3	
no ground cover—high density ( $f_{c\text{eff}}=0.7$ ) <sup>hh</sup>	0.50	1.15	0.80 <sup>ee</sup>	3	
no ground cover—medium density ( $f_{c\text{eff}}=0.5$ ) <sup>z</sup>	0.45	1.0	0.70 <sup>ee</sup>	2.5	
no ground cover—low density/young ( $f_{c\text{eff}}=0.25$ ) <sup>ii</sup>	0.40	0.60	0.45 <sup>ee</sup>	2.5	
active ground cover <sup>aa</sup> , killing frost—super high density ( $f_{c\text{eff}}=0.9$ )	0.50	1.25	0.85 <sup>ee</sup>	3	
active ground cover, killing frost—high density ( $f_{c\text{eff}}=0.7$ ) <sup>z</sup>	0.50	1.20	0.85 <sup>ee</sup>	3	
active ground cover, killing frost—medium density ( $f_{c\text{eff}}=0.5$ )	0.50	1.15	0.85 <sup>ee</sup>	2.5	
active ground cover, killing frost—low density ( $f_{c\text{eff}}=0.25$ )	0.50	1.00	0.85 <sup>ee</sup>	2.5	

(Continued)

Table B-1. Mean Crop Coefficients<sup>1</sup> (*Continued*)

Crop		$K_{cini}$ <sup>a</sup>	$K_{cmid}$ <sup>b</sup>	$K_{cend}$ <sup>b</sup>	Max. ht, m	Max. root depth <sup>c</sup> , M	$p$ <sup>d</sup>
	active ground cover, no frosts—super high density ( $f_{ceff} = 0.9$ )	0.80	1.25	0.85 <sup>ee</sup>	3		
	active ground cover, no frosts—high density ( $f_{ceff} = 0.7$ ) <sup>z</sup>	0.80	1.20	0.85 <sup>ee</sup>	3		
	active ground cover, no frosts—medium density ( $f_{ceff} = 0.5$ )	0.80	1.15	0.85 <sup>ee</sup>	2.5		
	active ground cover, no frosts—low density ( $f_{ceff} = 0.25$ )	0.80	1.00	0.85 <sup>ee</sup>	2.5		
Avocado <sup>x</sup>					0.5–1.0		0.70
	no ground cover—high density ( $f_{ceff} = 0.7$ )	0.50	1.00	0.90	4		
	no ground cover—medium density ( $f_{ceff} = 0.5$ ) <sup>z</sup>	0.50	0.90	0.80	3		
	no ground cover—low density/young ( $f_{ceff} = 0.25$ )	0.40	0.65	0.60	3		
	active ground cover—high <sup>aa</sup> density ( $f_{ceff} = 0.7$ )	0.85	1.05	0.95	4		
	active ground cover—medium density ( $f_{ceff} = 0.5$ )	0.85	1.00	0.95	3		
	active ground cover—low density/young ( $f_{ceff} = 0.25$ )	0.85	0.95	0.90	3		
Citrus <sup>x</sup>					1.2–1.5		0.50
	no ground cover—high density ( $f_{ceff} = 0.7$ ) <sup>jj</sup>	0.95	0.90	0.90	4	1.2–1.5	0.50
	no ground cover—medium density ( $f_{ceff} = 0.5$ )	0.80	0.75	0.75	3	1.1–1.5	0.50
	no ground cover—low density/young ( $f_{ceff} = 0.25$ )	0.55	0.50	0.50	2	0.8–1.1	0.50
	active ground cover—high <sup>aa</sup> density ( $f_{ceff} = 0.7$ ) <sup>kk</sup>	1.00	0.95	0.95	4	1.2–1.5	0.50
	active ground cover—medium density ( $f_{ceff} = 0.5$ )	0.95	0.95	0.95	3	1.1–1.5	0.50
	active ground cover—low density/young ( $f_{ceff} = 0.25$ )	0.90	0.90	0.90	2	0.8–1.1	0.50

## MEAN CROP COEFFICIENTS IN SUBHUMID CLIMATES

Conifer trees <sup>ll</sup>	1.00	1.00	1.00	10	1.0–1.5	0.70
Kiwi	0.40	1.05	1.05	3	0.7–1.3	0.35
Mango <sup>x</sup>				5–15	1.5	0.50
no ground cover—high density ( $f_{\text{eff}} = 0.7$ ) <sup>mm</sup>	0.35	0.90	0.75	5		
no ground cover—medium density ( $f_{\text{eff}} = 0.5$ )	0.35	0.75	0.60	4		
no ground cover—low density/young ( $f_{\text{eff}} = 0.25$ )	0.30	0.45	0.40	4		
Olives <sup>x</sup>				3–5	1.2–1.7	0.65
no ground cover—high density ( $f_{\text{eff}} = 0.7$ ) <sup>z, nn</sup>	0.65	0.70	0.60	4		
no ground cover—medium density ( $f_{\text{eff}} = 0.5$ ) <sup>oo</sup>	0.60	0.60	0.55	4		
no grnd covry—low density/young ( $f_{\text{eff}} = 0.25$ ) <sup>oo, pp</sup>	0.40	0.40	0.35	3		
no grnd covry—very low density/young ( $f_{\text{eff}} = 0.05$ ) <sup>pp</sup>	0.30	0.25	0.25	2		
active ground cover <sup>aa</sup> —high density ( $f_{\text{eff}} = 0.7$ )	0.80	0.75	0.75	4		
active ground cover—medium density ( $f_{\text{eff}} = 0.5$ )	0.80	0.75	0.75	4		
act. ground cover—low density/young ( $f_{\text{eff}} = 0.25$ )	0.80	0.75	0.75	3		
act. ground cover—very low density/young ( $f_{\text{eff}} = 0.05$ )	0.80	0.75	0.75	2		
Pistachios <sup>x</sup>	0.80	0.75	0.75	3–5	1.0–1.5	0.40
no ground cover—high density ( $f_{\text{eff}} = 0.7$ )	0.40	1.00	0.70	3		
no ground cover—medium density ( $f_{\text{eff}} = 0.5$ )	0.35	0.85	0.60	2.5		
no ground cover—low density/young ( $f_{\text{eff}} = 0.25$ )	0.30	0.50	0.40	2		
active ground cover—high <sup>aa</sup> density ( $f_{\text{eff}} = 0.7$ )	0.80	1.00	0.75	3		
active ground cover—medium density ( $f_{\text{eff}} = 0.5$ )	0.80	1.00	0.75	2.5		
act. grnd cover—low density/young ( $f_{\text{eff}} = 0.25$ )	0.80	0.85	0.75	2		

(Continued)

Table B-1. Mean Crop Coefficients<sup>1</sup> (*Continued*)

Crop	$K_{cini}$ <sup>a</sup>	$K_{cmid}$ <sup>b</sup>	$K_{cend}$ <sup>b</sup>	Max. ht, m	Max. root depth <sup>c</sup> , M	$p$ <sup>d</sup>
Walnut orchard <sup>x</sup>					1.7–2.4	0.50
no ground cover—high density ( $f_{ceff} = 0.7$ ) <sup>z</sup>	0.50	1.10	0.65 <sup>ee</sup>	5		
no ground cover—medium density ( $f_{ceff} = 0.5$ )	0.45	0.90	0.60 <sup>ee</sup>	4		
no ground cover—low density/young ( $f_{ceff} = 0.25$ )	0.35	0.55	0.40 <sup>ee</sup>	4		
active ground cover <sup>aa</sup> —high density ( $f_{ceff} = 0.7$ )	0.85	1.15	0.85 <sup>ee</sup>	5		
active ground cover—medium density ( $f_{ceff} = 0.5$ )	0.85	1.10	0.85 <sup>ee</sup>	4		
active ground cover—low density/young ( $f_{ceff} = 0.25$ )	0.85	0.95	0.85 <sup>ee</sup>	4		
<b>o. Wetlands, temperate climate</b>						
Cattails, bulrushes, killing frost	0.30	1.20	0.30	2		
Cattails, bulrushes, no frost	0.60	1.20	0.60	2		
Short veg., no frost	1.05	1.10	1.10	0.3		
Reed swamp, standing water	1.00	1.20	1.00	1		
Reed swamp, moist soil	0.90	1.20	0.70	1		
<b>p. Special</b>						
Open water, <2 m depth or in subhumid climates or tropics	1.05	1.05				
Open water, >5 m depth, clear of turbidity, temperate climate	0.50– 0.70 <sup>qq</sup>	0.80– 1.30 <sup>qq</sup>				

<sup>a</sup>These are general values for  $K_{cini}$  under typical irrigation management and soil wetting. For frequent wettings such as with high-frequency sprinkle irrigation or daily rainfall, these values may increase substantially and may approach 1.0 to 1.2.

$K_{cini}$  is a function of wetting interval and potential evaporation rate during the initial and development periods and is more accurately estimated using Fig. 10-4, or using the dual  $K_{cbini} + K_e$ .

<sup>b</sup>The values for  $K_{cmid}$  and  $K_{cend}$  are values expected in subhumid climates, where daily minimum relative humidity ( $RH_{min}$ )  $\sim 45\%$  and daily mean wind speed at 2 m height ( $u_2$ )  $\sim 2 \text{ m s}^{-1}$ . For different climatic conditions, the values given can be adjusted using Eqs. (10-14) and (10-15).

<sup>c</sup>The larger values for maximum root zone  $z_r$  are for soils having no significant layering or other characteristics that can restrict rooting depth. The smaller values for  $z_r$  may be used for irrigation scheduling and the larger values for modeling soil water stress or for rain-fed conditions.

<sup>d</sup>The values for  $p$  apply for  $ET_c \approx 5 \text{ mm/day}$ . The value for  $p$  can be adjusted for different  $ET_c$  according to  $p = p_{AppB} + 0.04(5 - ET_c)$  where  $p$  is expressed as a fraction and  $ET_c$  as mm/day.

<sup>e</sup>Beans, peas, legumes, tomatoes, peppers, and cucumbers are sometimes grown on stalks reaching 1.5 to 2 m in height. In such cases, increased  $K_c$  values need to be taken. For green beans, peppers, and cucumbers, 1.15 can be taken, and for tomatoes, dry beans, and peas, 1.20. Under these conditions height  $h$  should be increased also.

<sup>f</sup>The midseason values for cassava assume nonstressed conditions during or following the rainy season. The  $K_{cend}$  and  $K_{cbend}$  values account for dormancy during the dry season.

<sup>g</sup>The  $K_{cend}$  value for potatoes is about 0.40 and 0.35 for long season potatoes with vine kill.

<sup>h</sup>This  $K_{cend}$  value is for no irrigation during the last month of the growing season. The  $K_{cend}$  value for sugar beets is higher, up to 1.0 and 0.9, when irrigation or significant rain occurs during the last month.

<sup>i</sup>Sugar beets often experience late afternoon wilting in arid climates even at  $p < 0.55$ , with usually only minor impact on sugar yield.

<sup>j</sup>The first  $K_{cend}$  is for harvested fresh. The second value is for harvested dry.

<sup>k</sup>The  $K_c$  for asparagus usually remains at  $K_{cini}$  during harvest of the spears, due to sparse ground cover. The  $K_{cmid}$  value is for following regrowth of plant vegetation following termination of harvest of spears.

<sup>l</sup> $K_c$  for sisal depends on the planting density and water management (e.g., intentional moisture stress).

<sup>m</sup>The lower values are for rain-fed crops having less dense plant populations.

<sup>n</sup>The higher value is for hand-harvested crops.

<sup>o</sup>These  $K_{cmid}$  values for maize are for robust, pristine crops having plant populations of 50,000 plants per ha or higher. For less dense populations or uniform growth,  $K_{cmid}$  can be reduced by 0.10 to 0.2.

<sup>p</sup>The first  $K_{cend}$  value is for harvest at high grain moisture. The second  $K_{cend}$  value is for harvest after complete field drying of the grain (to about 18% moisture, wet mass basis).

<sup>q</sup>If harvested fresh for human consumption. Use  $K_{cend}$  for field maize if the sweet maize is allowed to mature and dry in the field.

<sup>r</sup>The lower value for rice is for dense, uniform stands having low aerodynamic roughness (smooth canopy surface) and low to moderate wind conditions ( $< 2 \text{ m s}^{-1}$ ). The higher value is for somewhat sparser, but inundated (flooded) conditions having greater roughness and lower albedo caused by shadowing, due to the sparseness.

<sup>s</sup>The value for  $p$  for rice is 0.20 of saturation.

<sup>t</sup>This  $K_{c\text{mid}}$  coefficient for hay crops is an overall average  $K_{c\text{mid}}$  coefficient that averages  $K_c$  for both before and following cuttings. It is applied to the period following the first development period until the beginning of the last late season period of the growing season.

<sup>u</sup>These  $K_c$  coefficients for hay crops represent immediately following cutting; at full cover; and immediately before cutting, respectively. The growing season is described as a series of individual cutting periods.

<sup>v</sup>These  $K_c$  values are based on measurements of ET from prairie in Kansas by Verma et al. (1989, 1992) comprised of switchgrass (*Panicum virgatum*), big bluestem (*Andropogon gerardii*), and Indian grass (*Sorghastrum nutans*). Values for height and rooting depth are from Elbersen et al. (2004).

<sup>w</sup>Cool-season grass varieties include dense stands of bluegrass, ryegrass, and fescue. Warm-season varieties include Bermuda grass and St. Augustine grass. The values given here are for potential conditions representing a 0.06 to 0.08 m mowing height. Turf, especially warm-season varieties, can be stressed at moderate levels and still maintain appearance (see section "Evapotranspiration Coefficients for Landscapes" in Chapter 10). Generally a value for the stress coefficient  $K_s$  of 0.9 for cool-season and 0.7 for warm-season varieties can be employed where careful water management is practiced and rapid growth is not required. Incorporation of these values for  $K_s$  into an "actual  $K_c$ " using potential values in this table will yield  $K_{c\text{act}}$  values of about 0.8 for cool season turf and 0.65 for warm-season turf.

<sup>x</sup>These values for  $K_{c\text{ini}}$ ,  $K_{c\text{mid}}$ , and  $K_{c\text{end}}$  were modeled using  $K_{cb\text{ini}}$ ,  $K_{cb\text{mid}}$  and  $K_{cb\text{end}}$  modeled using Eqs. (10-24), (10-26), (10-27a), and (10-29) with parameters listed in Table D-3 of Appendix D, along with  $h$  from Table D-2 for various  $f_{c\text{eff}}$ , where values listed in the last three columns of Table D-3 were added to the values modeled for  $K_{cb}$  to derive  $K_c$  that include average, expected amounts of evaporation from soil.  $f_{c\text{eff}}$  is the effective fraction of ground covered or shaded by vegetation (0 to 1.0) near solar noon, and  $h$  is the mean height of the vegetation, m.

<sup>y</sup>The values in parentheses apply to date palms.

<sup>z</sup>The values in this row are similar to the entry in FAO-56 (Allen et al. 1998).

<sup>aa</sup>For nonactive or only moderately active ground cover (active indicates green and growing ground cover with LAI > about 2),  $K_c$  should be weighted between  $K_c$  for no ground cover and  $K_c$  for active ground cover, with the weighting based on the "greenness" and approximate leaf area of the ground cover.

<sup>bb</sup>The pineapple plant has very low transpiration because it closes its stomates during the day and opens them during the night. Therefore, the majority of  $ET_c$  from pineapple is evaporation from the soil. The  $K_{c\text{mid}} < K_{c\text{ini}}$  because  $K_{c\text{mid}}$  occurs during full ground cover so that soil evaporation is less. Values assume that 50% of the ground surface is covered by black plastic mulch and that irrigation is by sprinkler. For drip irrigation beneath the plastic mulch,  $K_c$ s given can be reduced by 0.10.

<sup>cc</sup>Includes the water requirements of the shade trees.

<sup>dd</sup>The values in this row are similar to those by Johnson et al. (2005).

<sup>ee</sup>These  $K_{cend}$  values represent  $K_c$  prior to leaf drop. After leaf drop,  $K_{cend} \approx 0.20$  for bare, dry soil, or dead ground cover and  $K_{cend} \approx 0.50$  to 0.80 for actively growing ground cover.

<sup>ff</sup>These  $K_{cmid}$  and  $K_{cend}$  values include an implicit  $K_s$  (stress) factor of about 0.7 [see Eq. (10-13)], which is common for wine production. In practice, a  $K_s$  model and estimate should be applied where  $K_s$  can range from 0.5 to 1.0. Under no stress, the  $K_{cmid}$  and  $K_{cend}$  for wine grapes may equal that for table grapes, depending on plant density, age, and pruning structure.

<sup>gg</sup>Stone fruit category applies to peaches, apricots, pears, plums, and pecans.

<sup>hh</sup>The values in this row are derived from Girona et al. (2005) and Ayars et al. (2003) with  $f_{ceff} = 0.7$  and  $M_L = 1.5$ .

<sup>ii</sup>The values in this row are similar to those by Paço et al. (2006) and Ayars et al. (2003) with  $f_{ceff} = 0.25$  and  $M_L = 1.5$ .

<sup>jj</sup>The values for citrus are about 20% higher than those reported in FAO-56.

<sup>kk</sup>The values in this row are similar to those by Rogers et al. (1983) for citrus in Florida having Bahia grass cover.

<sup>ll</sup>Conifers exhibit substantial stomatal control due to soil water deficit. The  $K_c$  can easily reduce below the values presented, which represent well-watered conditions for large forests.

<sup>mm</sup>The values in this row are derived from de Azevedo et al. (2003).

<sup>nn</sup>Pastor and Orgaz (1994) found monthly  $K_c$  for olive orchards having  $f_c \sim 60\%$  similar to the values shown, except that  $K_{cmid} = 0.45$ , with stage lengths = 30, 90, 60, and 90 days, respectively for initial, development, midseason, and late season periods (see Appendix C), and using  $K_c$  during the winter ("off season") in December to February = 0.50.

<sup>oo</sup>The values in this row are similar to those by Villalobos et al. (2000) when  $f_{ceff}$  of ~0.3 to 0.4 are applied.

<sup>pp</sup>The values in this row are derived from Testi et al. (2004).

<sup>qq</sup>These  $K_c$ s are for deep water in temperate latitudes where large temperature changes in the water body occur during the year, and initial and peak period evaporation is low as radiation energy is absorbed into the deepwater body. During fall and winter periods ( $K_{cend}$ ), heat is released from the water body that increases the evaporation above that for grass. Therefore,  $K_{cmid}$  corresponds to the period when the water body is gaining thermal energy and  $K_{cend}$  when releasing thermal energy. The higher values for  $K_{cend}$  represent climates having freezing winter conditions and where  $ET_o$  is low and therefore  $K_{cend}$  is high. These  $K_c$ s should be used with caution.

Sources: FAO-56 (Allen et al. 1998), with information from Doorenbos and Kassam (1979), Doorenbos and Pruitt (1977); Pruitt (1986); Wright (1981, 1982), Snyder et al. (1989a, b) and Allen et al. (2011a).

This page intentionally left blank

## **APPENDIX C**

### **LENGTHS OF CROP DEVELOPMENT STAGES**

Table C-1. Lengths of Crop Development Stages<sup>a</sup> in Days for Various Planting Periods and Climatic Regions Based on FAO-24 ([Doorenbos and Pruitt 1977](#)) and FAO-56 ([Allen et al. 1998](#))

Crop	Init. ( $L_{ini}$ )	Dev. ( $L_{dev}$ )	Mid ( $L_{mid}$ )	Late ( $L_{late}$ )	Total	Plant Date	Region
<b>a. Small Vegetables</b>							
Broccoli	35	45	40	15	135	Sep	Calif. Desert, USA
Cabbage	40	60	50	15	165	Sep	Calif. Desert, USA
Carrots	20	30	50/30	20	100	Oct/Jan	Arid Climate
	30	40	60	20	150	Feb/Mar	Mediterranean
	30	50	90	30	200	Oct	Calif. Desert, USA
Cauliflower	35	50	40	15	140	Sep	Calif. Desert, USA
Celery	25	40	95	20	180	Oct	(Semi) Arid
	25	40	45	15	125	Apr	Mediterranean
	30	55	105	20	210	Jan	(Semi) Arid
Crucifers <sup>a</sup>	20	30	20	10	80	Apr	Mediterranean
	25	35	25	10	95	Feb	Mediterranean
	30	35	90	40	195	Oct/Nov	Mediterranean
Lettuce	20	30	15	10	75	Apr	Mediterranean
	30	40	25	10	105	Nov/Jan	Mediterranean
	25	35	30	10	100	Oct/Nov	Arid Region
	35	50	45	10	140	Feb	Mediterranean
Onion (dry)	15	25	70	40	150	Apr	Mediterranean
	20	35	110	45	210	Oct, Jan	Arid Region; Calif., USA

Onion (green)	25	30	10	5	70	Apr/May	Mediterranean
	20	45	20	10	95	Oct	Arid Region
	30	55	55	40	180	Mar	Calif., USA
Onion (seed)	20	45	165	45	275	Sep	Calif. Desert, USA
Spinach	20	20	15/25	5	60/70	Apr	Mediterranean
	20	30	40	10	100	Sep/Oct/ Nov	Arid Region
Radish	5	10	15	5	35	Mar/Apr	Mediterranean; Europe
	10	10	15	5	40	Winter	Arid Region
<b>b. Vegetables—Solanum Family (<i>Solanaceae</i>)</b>							
Eggplant	30	40	40	20	130	Oct	Arid Region
	30	45	40	25	140	May/Jun	Mediterranean
Sweet peppers (bell)	25/30	35	40	20	125	Apr/Jun	Europe and Mediterranean
	30	40	110	30	210	Oct	Mediterranean Arid Region
Tomato	30	40	40	25	135	Jan	Arid Region
	35	40	50	30	155	Apr/May	Calif., USA
	25	40	60	30	155	Jan	Calif. Desert, USA
	35	45	70	30	180	Oct/Nov	Arid Region
	30	40	45	30	145	Apr/May	Mediterranean
<b>c. Vegetables—Cucumber Family (<i>Cucurbitaceae</i>)</b>							
Cantaloupe	30	45	35	10	120	Jan	Calif., USA
	10	60	25	25	120	Aug	Calif., USA

(Continued)

Table C-1. Lengths of Crop Development Stages<sup>a</sup> in Days for Various Planting Periods and Climatic Regions Based on FAO-24 (Doorenbos and Pruitt 1977) and FAO-56 (Allen et al. 1998) (*Continued*)

Crop	Init. ( $L_{ini}$ )	Dev. ( $L_{dev}$ )	Mid ( $L_{mid}$ )	Late ( $L_{late}$ )	Total	Plant Date	Region
Cucumber	20	30	40	15	105	Jun/Aug	Arid Region
	25	35	50	20	130	Nov/Feb	Arid Region
Pumpkin, winter squash	20	30	30	20	100	Mar/Aug	Mediterranean
	25	35	35	25	120	Jun	Europe
Squash, zucchini	25	35	25	15	100	Apr/Dec	Mediterranean; Arid Region
	20	30	25	15	90	May/Jun	Mediterranean; Europe
Sweet melons	25	35	40	20	120	May	Mediterranean
	30	30	50	30	140	Mar	Calif., USA
	15	40	65	15	135	Aug	Calif. Desert, USA
	30	45	65	20	160	Dec/Jan	Arid Region
Watermelons	20	30	30	30	110	Apr	Italy
	10	20	20	30	80	Mar/Aug	Near East (desert)
<b>d. Roots and Tubers</b>							
Beets, table	15	25	20	10	70	Apr/May	Mediterranean
	25	30	25	10	90	Feb/Mar	Mediterranean; Arid
Cassava	year 1	20	40	90	60	210	Tropical Regions
	year 2	150	40	110	60	360	Rainy season

Potato	25	30	30/45	30	115/130	Jan/Nov	(Semi) Arid Climate
	25	30	45	30	130	May	Continental Climate
	30	35	50	30	145	Apr	Europe
	45	30	70	20	165	Apr/May	Idaho, USA
	30	35	50	25	140	Dec	Calif. Desert, USA
Sweet potato	20	30	60	40	150	Apr	Mediterranean
	15	30	50	30	125	Rainy seas.	Tropical Regions
Sugar beet	30	45	90	15	180	Mar	Calif., USA
	25	30	90	10	155	Jun	Calif., USA
	25	65	100	65	255	Sep	Calif. Desert, USA
	50	40	50	40	180	Apr	Idaho, USA
	25	35	50	50	160	May	Mediterranean
	45	75	80	30	230	Nov	Mediterranean
	35	60	70	40	205	Nov	Arid Regions
e. Legumes ( <i>Leguminosae</i> )							
Beans (green)	20	30	30	10	90	Feb/Mar	Calif., Mediterranean
	15	25	25	10	75	Aug/Sep	Calif., Egypt, Lebanon
Beans (dry)	20	30	40	20	110	May/Jun	Continental Climates
	15	25	35	20	95	Jun	Pakistan, Calif.
	25	25	30	20	100	Jun	Idaho, USA
Fava bean	15	25	35	15	90	May	Europe
Broad bean	20	30	35	15	100	Mar/Apr	Mediterranean
Dry bean	90	45	40	60	235	Nov	Europe
Green bean	90	45	40	0	175	Nov	Europe
Green gram, cowpeas	20	30	30	20	110	Mar	Mediterranean

*(Continued)*

Table C-1. Lengths of Crop Development Stages in Days for Various Planting Periods and Climatic Regions Based on FAO-24 (Doorenbos and Pruitt 1977) and FAO-56 (Allen et al. 1998) (*Continued*)

Crop	Init. ( $L_{ini}$ )	Dev. ( $L_{dev}$ )	Mid ( $L_{mid}$ )	Late ( $L_{late}$ )	Total	Plant Date	Region
Groundnut	25	35	45	25	130	Dry season	West Africa
	35	35	35	35	140	May	High Latitudes
	35	45	35	25	140	May/Jun	Mediterranean
Lentil	20	30	60	40	150	Apr	Europe
	25	35	70	40	170	Oct/Nov	Arid Region
Peas	15	25	35	15	90	May	Europe
	20	30	35	15	100	Mar/Apr	Mediterranean
Soybeans	35	25	30	20	110	Apr	Idaho, USA
	15	15	40	15	85	Dec	Tropics
	20	30/35	60	25	140	May	Central USA
	20	25	75	30	150	Jun	Japan
<b>f. Perennial Vegetables (with winter dormancy and initially bare or mulched soil)</b>							
Artichoke	40	40	250	30	360	Apr (1st yr)	California
	20	25	250	30	325	May (2nd yr)	(cut in May)
Asparagus	50	30	100	50	230	Feb	Warm Winter
	90	30	200	45	365	Feb	Mediterranean
<b>g. Fiber Crops</b>							
Cotton	30	50	60	55	195	Mar-May	Egypt; Pakistan; Calif., USA
	45	60	45-75	45	195-225	Mar	Calif. Desert, USA
	30	50	60	55	195	Sep	Yemen
	30	50	55	45	180	Apr	Texas

Flax	25	35	50	40	150	Apr	Europe
	30	40	100	50	220	Oct	Arizona
<b>h. Oil Crops</b>							
Castor beans	25	40	65	50	180	Mar	(Semi) Arid Climates
	20	40	50	25	135	Nov	Indonesia
Safflower	20	35	45	25	125	Apr	California, USA
	25	35	55	30	145	Mar	High Latitudes
Sesame	35	55	60	40	190	Oct/Nov	Arid Region
	20	30	40	20	100	Jun	China
Sunflower	25	35	45	25	130	Apr/May	Mediterranean; Calif., USA
<b>i. Cereals</b>							
Barley/oats/wheat	15	25	50	30	120	Nov	Central India
	20	25	60	30	135	Mar/Apr	35–45° L
	15	30	65	40	150	July	East Africa
	40	30	40	20	130	Apr <sup>c</sup>	
	40	60	60	40	200	Nov	
	20	50	60	30	160	Dec	Calif. Desert, USA
	20 <sup>b</sup>	60 <sup>b</sup>	70	30	180	Dec	California, USA
Winter wheat	30	140	40	30	240	Nov	Mediterranean
	160	75	75	25	335	Oct <sup>c</sup>	Idaho, USA
Grains (small)	20	30	60	40	150	Apr	Mediterranean
	25	35	65	40	165	Oct/Nov	Pakistan; Arid Region

(Continued)

Table C-1. Lengths of Crop Development Stages in Days for Various Planting Periods and Climatic Regions Based on FAO-24 (Doorenbos and Pruitt 1977) and FAO-56 (Allen et al. 1998) (*Continued*)

Crop	Init. ( $L_{ini}$ )	Dev. ( $L_{dev}$ )	Mid ( $L_{mid}$ )	Late ( $L_{late}$ )	Total	Plant Date	Region
Maize (grain)	30	50	60	40	180	Apr	East Africa (alt.)
	25	40	45	30	140	Dec/Jan	Arid Climate
	20	35	40	30	125	Jun	Nigeria (humid)
	20	35	40	30	125	Oct	India (dry, cool)
	30	40	50	30	150	Apr	Spain (spr, sum.); Calif., USA
							Idaho, USA
Maize (sweet)	30	40	50	50	170	Apr <sup>c</sup>	Philippines
	20	20	30	10	80	Mar	Mediterranean
	20	25	25	10	80	May/Jun	Arid Climate
	20	30	50/30	10	90	Oct/Dec	Idaho, USA
	30	30	30	10 <sup>d</sup>	110	Apr	Calif. Desert, USA
	20	40	70	10	140	Jan	Pakistan
Millet	15	25	40	25	105	Jun	Central USA
	20	30	55	35	140	Apr	USA; Pakistan;
Sorghum	20	35	40	30	130	May/Jun	Mediterranean
Rice	20	35	45	30	140	Mar/Apr	Arid Region
	30	30	60	30	150	Dec/May	Tropics;
	30	30	80	40	180	May	Mediterranean Tropics

<b>j. Forages</b>									
Alfalfa, total season <sup>e</sup>	10	30	var.	var.	60	Jan			
Alfalfa <sup>e</sup> 1st cutting cycle	10	20	20	10	75	Apr (last -4° deg)			
	10	30	25	10		Mar			
Alfalfa <sup>e</sup> , other cutting cycles	5	10	10	5	30	Calif., USA			
	5	20	10	10	45	Idaho, USA			
Bermuda for seed	10	25	35	35	105	Calif. Desert, USA			
Bermuda for hay (several cuttings)	10	15	75	35	135	Calif. Desert, USA			
Grass pasture <sup>e</sup>	10	20	—	—	—	—			
Sudan, 1st cutting cycle	25	25	15	10	75	Apr			
Sudan, other cutting cycles	3	15	12	7	37	Jun			
Switchgrass <sup>f</sup>	20	45	40	60	165	Apr	Kansas, USA		
<b>k. Sugarcane</b>									
Sugarcane, virgin	35	60	190	120	405	Low Latitudes			
	50	70	220	140	480	Tropics			
	75	105	330	210	720	Hawaii, USA			
Sugarcane, ratoon	25	70	135	50	280	Low Latitudes			
	30	50	180	60	320	Tropics			
	35	105	210	70	420	Hawaii, USA			
<b>l. Tropical Fruits and Trees</b>									
Banana, 1st yr	120	90	120	60	390	Mediterranean			
Banana, 2nd yr	120	60	180	5	365	Mediterranean			
Pineapple	60	120	600	10	790	Hawaii, USA			

*(Continued)*

Table C-1. Lengths of Crop Development Stages in Days for Various Planting Periods and Climatic Regions Based on FAO-24 (Doorenbos and Pruitt 1977) and FAO-56 (Allen et al. 1998) (Continued)

Crop	Init. ( $L_{ini}$ )	Dev. ( $L_{dev}$ )	Mid ( $L_{mid}$ )	Late ( $L_{late}$ )	Total	Plant Date	Region
<b>m. Grapes and Berries</b>							
Grapes	20	100	90	30	240	Apr	Low Latitudes
	20	100	90	30	240	Mar	Calif., USA
	20	90	50	20	180	May	High Latitudes
	20	90	80	20	210	Apr	Mid Latitudes (wine)
Hops	25	40	80	10	155	Apr	Idaho, USA
<b>n. Fruit Trees</b>							
Citrus	90	30	150	95	365	Jan	Mediterranean
Deciduous orchard, light pruning	10	10	160	30	210	Mar	High Latitudes
	10	10	190	60	270	Mar	Low Latitudes
	10	10	190	30	240	Mar	Calif., USA
Deciduous orchard, heavy pruning	10	80	90	30	210	Mar	High Latitudes
	10	80	120	60	270	Mar	Low Latitudes
	10	60	140	30	240	Mar	Calif., USA
Mango	20	40	50	50	160	July	Brazil
Olives	10	20	150	90	270 <sup>b</sup>	Mar	Mediterranean
Pistachios	10	20	80	40	150	Feb	Mediterranean
Walnuts	10	10	140	30	190	Apr	Utah, USA
<b>o. Wetlands—Temperate Climate</b>							
Wetlands (cattails, bulrushes)	10	30	80	20	140	May	Utah, USA; killing frost
Wetlands (short veg.)	180	60	90	35	365	Nov	Florida, USA
	180	60	90	35	365	Nov	Frost-free climate

<sup>a</sup>Lengths of crop development stages provided in this table are indicative of general conditions, but may vary substantially from region to region, with climate and cropping conditions, and with crop variety. The user is strongly encouraged to obtain appropriate local information.

<sup>b</sup>Crucifers include cabbage, cauliflower, broccoli, and Brussels sprouts. The wide range in lengths of seasons is due to varietal and species differences.

These periods for winter wheat will lengthen in frozen climates according to days having zero growth potential and wheat dormancy. Under general conditions and in the absence of local data, fall planting of winter wheat can be presumed to occur in northern temperate climates when the 30-day running average of mean daily air temperature decreases to 11°C or December 1, whichever comes first. Allen and Robison (2007) reduced canopy development of winter wheat (and amount of  $K_c$  above  $K_{c,int}$ ) whenever  $T_{min}$  was  $<-25^{\circ}\text{C}$  and no snow cover was present. They further reduced development by a lesser amount whenever  $T_{min}$  was  $<-10^{\circ}\text{C}$  as a retardation penalty after a cold freeze. Planting of spring wheat can be assumed to occur when the 30-day running average of mean daily air temperature ending on the planting date increases to 4°C. Spring planting of maize-grain can be assumed to occur when the 30-day running average of mean daily air temperature increases to 10°C.

The late season for sweet maize will be about 35 days if the grain is allowed to mature and dry.

<sup>c</sup>In climates having killing frosts, growing seasons can be estimated using specific temperature or cumulative growing degree days or running average air temperature to begin and killing frosts to terminate. For example, for alfalfa and grass:

*alfalfa*: last  $-4^{\circ}\text{C}$  in spring until first  $-4^{\circ}\text{C}$  in fall (Everson et al. 1978) or accumulation of 240 degree days since January 1 using 0° base for greenup and first occurrence of  $-7^{\circ}\text{C}$  frost in fall (Allen and Robison 2007).

*grass*: 7 days before last  $-4^{\circ}\text{C}$  in spring and 7 days after last  $-4^{\circ}\text{C}$  in fall (Kruse and Haise 1974) or 30 day running average mean air temperature for period ending on day of greenup =  $4^{\circ}\text{C}$  and first occurrence of  $-5^{\circ}\text{C}$  frost in fall (Allen and Robison 2007).

<sup>d</sup>Based on measurements of ET from prairie in Kansas by Verma et al. (1989, 1992) comprising switchgrass (*Panicum virgatum*), big bluestem (*Andropogon gerardii*), and Indian grass (*Sorghastrum nutans*).

<sup>e</sup>Olive trees gain new leaves in March and often have transpiration during winter, where the  $K_c$  continues outside of the "growing period" and total season length may be set to 365 days.

Source: Values in this appendix are primarily from FAO-56 (Allen et al. 1998) with modification to period lengths for some tree crops.

This page intentionally left blank

## APPENDIX D

# BASAL CROP COEFFICIENTS IN SUBHUMID CLIMATES

This appendix presents basal crop coefficients,  $K_{cb}$ , for well-managed crops in subhumid climates for use with clipped grass reference  $ET_o$ , based on FAO-56 ([Allen et al. 1998](#)). Guidelines on applying  $K_{cb}$  values in this appendix are given in Chapter 10.

Table D-1. Basal Crop Coefficients for Well-Managed Crops in Subhumid Climates

Crop	$K_{cb\ ini}^a$	$K_{cb\ mid}$	$K_{cb\ end}$
<b>a. Small Vegetables</b>	<b>0.15</b>	<b>0.95</b>	<b>0.85</b>
Broccoli	0.95	0.85	
Brussels sprouts	0.95	0.85	
Cabbage	0.95	0.85	
Carrots	0.95	0.85	
Cauliflower	0.95	0.85	
Celery	0.95	0.90	
Garlic	0.90	0.60	
Lettuce	0.90	0.90	
Onions			
dry	0.95	0.65	
green	0.90	0.90	
seed	1.05	0.70	
Spinach	0.90	0.85	
Radish	0.85	0.75	

*(Continued)*

Table D-1. Basal Crop Coefficients for Well-Managed Crops in Subhumid Climates (*Continued*)

Crop	$K_{cb\ ini}$ <sup>a</sup>	$K_{cb\ mid}$	$K_{cb\ end}$
<b>b. Vegetables—Solanum Family (<i>Solanaceae</i>)</b>	<b>0.15</b>	<b>1.10</b>	<b>0.70</b>
Eggplant		1.00	0.80
Sweet peppers (bell)		1.00 <sup>b</sup>	0.80
Tomato		1.10 <sup>b</sup>	0.60–0.80
<b>c. Vegetables—Cucumber Family (<i>Cucurbitaceae</i>)</b>	<b>0.15</b>	<b>0.95</b>	<b>0.70</b>
Cantaloupe		0.75	0.50
Cucumber			
fresh market		0.95 <sup>b</sup>	0.70
machine harvest		0.95	0.80
Pumpkin, winter squash		0.95	0.70
Squash, zucchini		0.90	0.70
Sweet melons		1.00	0.70
Watermelon		0.95	0.70
<b>d. Roots and Tubers</b>	<b>0.15</b>	<b>1.00</b>	<b>0.85</b>
Beets, table		0.95	0.85
Cassava			
year 1		0.70 <sup>c</sup>	0.20
year 2		1.00	0.45
Parsnip		0.95	0.85
Potato		1.10	0.65 <sup>d</sup>
Sweet potato		1.10	0.55
Turnip (and rutabaga)		1.00	0.85
Sugar beet		1.15	0.50 <sup>e</sup>
<b>e. Legumes (<i>Leguminosae</i>)</b>	<b>0.15</b>	<b>1.10</b>	<b>0.50</b>
Beans, green		1.00 <sup>b</sup>	0.80
Beans, dry, and pulses		1.10 <sup>b</sup>	0.25
Chickpea		0.95	0.25
Fava bean (broad bean)			
fresh		1.10 <sup>b</sup>	1.05
dry/seed		1.10 <sup>b</sup>	0.20
Garbanzo		1.05	0.25
Green gram and cowpeas		1.00	0.55–0.25 <sup>f</sup>
Groundnut (peanut)		1.10	0.50
Lentil		1.05	0.20
Peas			
fresh		1.10 <sup>a</sup>	1.05
dry/seed		1.10	0.20
Soybeans		1.10	0.30

Table D-1. Basal Crop Coefficients for Well-Managed Crops in Subhumid Climates (*Continued*)

Crop	$K_{cbini}^a$	$K_{cbmid}$	$K_{cbend}$
<b>f. Perennial Vegetables (with winter dormancy and initially bare or mulched)</b>			
Artichokes	0.15	0.95	0.90
Asparagus	0.15	0.90 <sup>g</sup>	0.20
Mint	0.40	1.10	1.05
Strawberries	0.30	0.80	0.70
<b>g. Fiber Crops</b>			
Cotton		1.10–1.15	0.50–0.40
Flax		1.05	0.20
Sisal <sup>h</sup>		0.4–0.7	0.4–0.7
<b>h. Oil Crops</b>			
Castor bean ( <i>Ricinus</i> )		1.10	0.45
Rapeseed, canola		0.95–1.10 <sup>i</sup>	0.25
Safflower		0.95–1.10 <sup>i</sup>	0.20
Sesame		1.05	0.20
Sunflower		0.95–1.10 <sup>i</sup>	0.25
<b>i. Cereals</b>			
Barley	0.15	1.10	0.25
Oats		1.10	0.15
Spring wheat		1.10	0.15–0.3 <sup>j</sup>
Winter wheat			
with frozen soils	0.15	1.10	0.15–0.3 <sup>j</sup>
with nonfrozen soils	0.15–0.5 <sup>k</sup>	1.10	0.15–0.3 <sup>j</sup>
Maize, field (grain) ( <i>field corn</i> )	0.15	1.15 <sup>l</sup>	0.50, 0.15 <sup>m</sup>
Maize, sweet ( <i>sweet corn</i> )		1.10 <sup>l</sup>	1.00 <sup>n</sup>
Millet		0.95	0.20
Sorghum			
grain		0.95–1.05	0.35
sweet		1.15	1.00
Rice	1.00	1.00–1.15 <sup>o</sup>	0.70–0.45 <sup>o</sup>
<b>j. Forages</b>			
Alfalfa hay			
individual cutting effects	0.30 <sup>p</sup>	1.15 <sup>p</sup>	1.10 <sup>p</sup>
for seed	0.30	0.45	0.45
Bermuda hay			
averaged cutting effects	0.50	0.95 <sup>q</sup>	0.80
spring crop for seed	0.15	0.85	0.60

(Continued)

Table D-1. Basal Crop Coefficients for Well-Managed Crops in Subhumid Climates (*Continued*)

Crop	$K_{cbini}^a$	$K_{cbmid}$	$K_{cbend}$
Clover hay, berseem individual cutting periods	0.30 <sup>p</sup>	1.10 <sup>p</sup>	1.05 <sup>p</sup>
Ryegrass hay averaged cutting effects	0.85	1.00 <sup>q</sup>	0.95
Sudan grass hay (annual) individual cutting periods	0.30 <sup>p</sup>	1.10 <sup>p</sup>	1.05 <sup>p</sup>
Grazing pasture rotated grazing	0.30	0.80–1.00	0.80
extensive grazing	0.30	0.70	0.70
Switchgrass <sup>r</sup>	0.15 <sup>r</sup>	1.00 <sup>r</sup>	0.10 <sup>r</sup>
Turfgrass cool-season <sup>s</sup>	0.80	0.85	0.85
warm-season <sup>s</sup>	0.75	0.80	0.80
<b>k. Sugarcane</b>	0.15	1.20	0.70
<b>I. Tropical Fruits and Trees</b>			
Banana			
1st year	0.15	1.05	0.90
2nd year	0.60	1.10	1.05
Cacao	0.90	1.00	1.00
Coffee			
bare ground cover	0.80	0.90	0.90
with weeds	1.00	1.05	1.05
Palms (including date palms) <sup>t</sup>			
no ground cover—high density ( $f=0.7$ ) <sup>u</sup>	0.80	0.85	0.85
no ground cover—medium density ( $f=0.5$ )	0.70	0.70	0.70
no ground cover—low density/young ( $f=0.25$ )	0.40	0.45	0.45
no ground cover—very low density/young ( $f=0.1$ )	0.25	0.25	0.25
active ground cover—high density ( $f=0.7$ )	0.85	0.90	0.90
active ground cover—medium density ( $f=0.5$ )	0.80	0.85	0.85

Table D-1. Basal Crop Coefficients for Well-Managed Crops in Subhumid Climates (Continued)

Crop	$K_{cbini}^a$	$K_{cbmid}$	$K_{cbend}$
active ground cover—low density/young ( $f=0.25$ )	0.75	0.80	0.80
active ground cover—very low density/young ( $f=0.1$ )	0.70	0.75	0.75
Pineapple <sup>w</sup>			
bare soil	0.15	0.25	0.25
with unirrigated grass cover	0.30	0.45	0.45
Rubber trees	0.85	0.90	0.90
Tea			
nonshaded	0.90	0.95	0.90
shaded <sup>x</sup>	1.00	1.10	1.05
<b>m. Grapes and Berries</b>			
Berries (bushes)	0.20	1.00	0.40
Grapes—table or raisin			
no ground cover—high density ( $f=0.7$ ) <sup>y</sup>	0.20	1.05	0.80
no ground cover—medium density ( $f=0.5$ ) <sup>u</sup>	0.20	0.90	0.70
no ground cover—low/young ( $f=0.25$ )	0.15	0.55	0.45
Grapes—wine			
no ground cover—high density ( $f=0.7$ )	0.20	0.70	0.55 <sup>z, aa</sup>
no ground cover—medium density ( $f=0.5$ ) <sup>u</sup>	0.20	0.65	0.50 <sup>z, aa</sup>
no ground cover—low/young ( $f=0.25$ )	0.25	0.40	0.30 <sup>z, aa</sup>
Hops	0.15	1.00	0.80
<b>n. Fruit Trees<sup>t</sup></b>			
Almonds, no ground cover			
no ground cover—high density ( $f=0.7$ )	0.20	0.95	0.65 <sup>z</sup>
no ground cover—medium density ( $f=0.5$ ) <sup>u</sup>	0.20	0.80	0.55 <sup>z</sup>
no ground cover—low density/young ( $f=0.25$ )	0.15	0.45	0.35 <sup>z</sup>

(Continued)

Table D-1. Basal Crop Coefficients for Well-Managed Crops in Subhumid Climates (Continued)

Crop	$K_{cb\ ini}^{\text{a}}$	$K_{cb\ mid}$	$K_{cb\ end}$
active ground cover—high density ( $f=0.7$ )	0.75	1.00	0.80 <sup>z</sup>
active ground cover—medium density ( $f=0.5$ )	0.75	0.95	0.80 <sup>z</sup>
active ground cover—low density/young ( $f=0.25$ )	0.75	0.90	0.80 <sup>z</sup>
Apples, cherries, pears <sup>t</sup>			
no ground cover—high density ( $f=0.7$ )	0.30	1.10	0.75 <sup>z</sup>
no ground cover—medium density ( $f=0.5$ ) <sup>u</sup>	0.30	1.00 <sup>bb</sup>	0.70 <sup>z</sup>
no ground cover—low density/young ( $f=0.25$ )	0.25	0.65	0.50 <sup>z</sup>
active ground cover, killing frost—high density ( $f=0.7$ )	0.40	1.15	0.80 <sup>z</sup>
active ground cover, killing frost—medium density ( $f=0.5$ ) <sup>u</sup>	0.40	1.10	0.80 <sup>z</sup>
active ground cover, killing frost—low density ( $f=0.25$ )	0.40	1.00	0.80 <sup>z</sup>
active ground cover, no frosts—high density ( $f=0.7$ )	0.75	1.15	0.80 <sup>z</sup>
active ground cover, no frosts—medium density ( $f=0.5$ ) <sup>u</sup>	0.75	1.10	0.80 <sup>z</sup>
active ground cover, no frosts—low density ( $f=0.25$ )	0.75	1.00	0.80 <sup>z</sup>
Apricots, peaches, stone fruit <sup>t, cc</sup>			
no ground cover—super density ( $f=0.9$ )	0.30	1.15	0.80 <sup>z</sup>
no ground cover—high density ( $f=0.7$ ) <sup>dd</sup>	0.30	1.10	0.75 <sup>z</sup>
no ground cover—medium density ( $f=0.5$ ) <sup>u</sup>	0.25	0.95	0.65 <sup>z</sup>
no ground cover—low density/young ( $f=0.25$ ) <sup>ee</sup>	0.20	0.55	0.40 <sup>z</sup>
active ground cover, killing frost—super density ( $f=0.9$ )	0.40	1.20	0.80 <sup>z</sup>
active ground cover, killing frost—high density ( $f=0.7$ ) <sup>u</sup>	0.40	1.15	0.80 <sup>z</sup>

Table D-1. Basal Crop Coefficients for Well-Managed Crops in Subhumid Climates (Continued)

Crop	$K_{cbini}^a$	$K_{cbmid}$	$K_{cbend}$
active ground cover, killing frost—medium density ( $f=0.5$ )	0.40	1.10	0.80 <sup>z</sup>
active ground cover, killing frost—low density ( $f=0.25$ )	0.40	0.95	0.80 <sup>z</sup>
active ground cover, no frosts —super density ( $f=0.9$ )	0.70	1.20	0.80 <sup>z</sup>
active ground cover, no frosts —high density ( $f=0.7$ ) <sup>u</sup>	0.70	1.15	0.80 <sup>z</sup>
active ground cover, no frosts —medium density ( $f=0.5$ )	0.70	1.10	0.80 <sup>z</sup>
active ground cover, no frosts —low density ( $f=0.25$ )	0.70	0.95	0.80 <sup>z</sup>
Avocado <sup>t</sup>			
no ground cover—high density ( $f=0.7$ )	0.30	0.95	0.85
no ground cover—medium density ( $f=0.5$ ) <sup>u</sup>	0.30	0.85	0.80
no ground cover—low density/young ( $f=0.25$ )	0.25	0.60	0.50
active ground cover—high density ( $f=0.7$ )	0.75	1.00	0.90
active ground cover—medium density ( $f=0.5$ )	0.75	0.95	0.90
active ground cover—low density/young ( $f=0.25$ )	0.75	0.90	0.85
Citrus <sup>t</sup>			
no ground cover—high density ( $f=0.7$ ) <sup>ff</sup>	0.85	0.85	0.85
no ground cover—medium density ( $f=0.5$ )	0.70	0.70	0.70
no ground cover—low density/young ( $f=0.25$ )	0.45	0.45	0.45
active ground cover <sup>ff</sup> —high density ( $f=0.7$ ) <sup>gg</sup>	0.90	0.90	0.90
active ground cover—medium density ( $f=0.5$ )	0.85	0.90	0.90
active ground cover—low density/young ( $f=0.25$ )	0.80	0.85	0.85

(Continued)

Table D-1. Basal Crop Coefficients for Well-Managed Crops in Subhumid Climates (Continued)

Crop	$K_{cbini}^a$	$K_{cbmid}$	$K_{cbend}$
Conifer trees <sup>hh</sup>	0.95	0.95	0.95
Kiwi	0.20	1.00	1.00
Mango <sup>t</sup>			
no ground cover—high density ( $f=0.7$ ) <sup>ii</sup>	0.25	0.85	0.70
no ground cover—medium density ( $f=0.5$ )	0.25	0.70	0.55
no ground cover—low density/young ( $f=0.25$ )	0.20	0.40	0.35
Olives <sup>t</sup>			
no ground cover—high density ( $f=0.7$ ) <sup>ujj</sup>	0.55	0.65	0.55
no ground cover—medium density ( $f=0.5$ ) <sup>kk</sup>	0.50	0.55	0.50
no ground cover—low density/young ( $f=0.25$ ) <sup>ll</sup>	0.30	0.35	0.30
no ground cover—very low density/young ( $f=0.05$ ) <sup>ll</sup>	0.20	0.20	0.20
active ground cover <sup>v</sup> —high density ( $f=0.7$ )	0.70	0.70	0.70
active ground cover—medium density ( $f=0.5$ )	0.70	0.70	0.70
active ground cover—low density/young ( $f=0.25$ )	0.70	0.70	0.70
active ground cover—very low density/young ( $f=0.05$ )	0.70	0.70	0.70
Pistachios <sup>t</sup>			
no ground cover—high density ( $f=0.7$ )	0.30	0.95	0.65
no ground cover—medium density ( $f=0.5$ )	0.25	0.80	0.55
no ground cover—low density/young ( $f=0.25$ )	0.20	0.45	0.35
active ground cover <sup>v</sup> —high density ( $f=0.7$ )	0.70	0.95	0.70
active ground cover—medium density ( $f=0.5$ )	0.70	0.95	0.70
active ground cover—low density/young ( $f=0.25$ )	0.70	0.80	0.70

Table D-1. Basal Crop Coefficients for Well-Managed Crops in Subhumid Climates (Continued)

Crop	$K_{cbini}$ <sup>a</sup>	$K_{cbmid}$	$K_{cbend}$
<b>Walnut orchard<sup>b</sup></b>			
no ground cover—high density ( $f=0.7$ )	0.40	1.05	0.60 <sup>c</sup>
no ground cover—medium density ( $f=0.5$ )	0.35	0.85	0.55 <sup>c</sup>
no ground cover—low density/young ( $f=0.25$ )	0.25	0.50	0.35 <sup>c</sup>
active ground cover <sup>v</sup> —high density ( $f=0.7$ )	0.75	1.10	0.80 <sup>c</sup>
active ground cover—medium density ( $f=0.5$ )	0.75	1.05	0.80 <sup>c</sup>
active ground cover—low density/young ( $f=0.25$ )	0.75	0.90	0.80 <sup>c</sup>

Note: The values for  $K_{cbmid}$  and  $K_{cbend}$  are values expected in semiarid climates, where daily minimum relative humidity ( $RH_{min}$ )  $\sim 45\%$  and daily mean wind speed at 2-m height ( $u_2$ )  $\sim 2 \text{ ms}^{-1}$ . For different climatic conditions, the values given can be adjusted using Eqs. (10-14) and (10-15).

<sup>a</sup>The values for  $K_{cbini}$  (and  $K_{cbmid}$  and  $K_{cbend}$ ) represent conditions having a dry soil surface. These values must be adjusted using the dual K+K procedure described in Chapter 10.

<sup>b</sup>Beans, peas, legumes, tomatoes, peppers, and cucumbers are sometimes grown on stalks reaching 1.5 to 2 m in height. In such cases, increased  $K_c$  values need to be taken. For green beans, peppers, and cucumbers, 1.15 can be taken, and for tomatoes, dry beans, and peas, 1.20. Under these conditions height  $h$  should be increased also.

<sup>c</sup>The midseason values for cassava assume nonstressed conditions during or following the rainy season. The  $K_{cend}$  and  $K_{cbend}$  values account for dormancy during the dry season.

<sup>d</sup>The  $K_{cbend}$  values for potatoes are about 0.40 and 0.35 for long season potatoes with vine kill.

<sup>e</sup>This  $K_{cbend}$  value is for no irrigation during the last month of the growing season. The  $K_{cbend}$  value for sugar beets is higher, up to 1.0 and 0.9, when irrigation or significant rain occurs during the last month.

<sup>f</sup>The first  $K_{cbend}$  is for harvested fresh. The second value is for harvested dry.

<sup>g</sup>The  $K_{cb}$  for asparagus usually remains at  $K_{cbini}$  during harvest of the spears, due to sparse ground cover. The  $K_{cbmid}$  value is for following regrowth of plant vegetation following termination of harvest of spears.

<sup>h</sup> $K_c$  for sisal depends on the planting density and water management (e.g., intentional moisture stress).

<sup>i</sup>The lower values are for rain fed crops having less dense plant populations.

<sup>j</sup>The higher value is for hand-harvested crops.

<sup>k</sup>The two  $K$  values for winter wheat are (1) for less than 10% ground cover and (2) for during the dormant, winter period, if the vegetation fully covers the ground, and conditions are nonfrozen.

<sup>l</sup>These  $K_{cbmid}$  values for maize are for robust, pristine crops having plant populations of 50,000 plants per ha or higher. For less dense populations or uniform growth,  $K_{cbmid}$  can be reduced by 0.10 to 0.2.

<sup>m</sup>The first  $K_{cbend}$  value is for harvest at high grain moisture. The second  $K_{cbend}$  value is for harvest after complete field drying of the grain (to about 18% moisture, wet mass basis).

<sup>n</sup>If harvested fresh for human consumption. Use  $K_{cbend}$  for field maize if the sweet maize is allowed to mature and dry in the field.

<sup>o</sup>The lower value for rice is for dense, uniform stands having low aerodynamic roughness (smooth canopy surface) and low to moderate wind conditions (<2 ms). The higher value is for somewhat sparser, but inundated (flooded) conditions having greater roughness and lower albedo caused by shadowing, due to the sparseness.

<sup>p</sup>These  $K_{cb}$  coefficients for hay crops represent immediately following cutting; at full cover; and immediately before cutting, respectively. The growing season is described as a series of individual cutting periods.

<sup>q</sup>This  $K_{cbmid}$  coefficient for Bermuda and ryegrass hay crops is an overall average  $K_{cbmid}$  coefficient that averages  $K_{cb}$  for both before and following cuttings. It is applied to the period following the first development period until the beginning of the last late season period of the growing season.

<sup>r</sup>These  $K_c$  values are based on measurements of ET from prairie in Kansas by Verma et al. (1989, 1992) comprising switchgrass (*Panicum virgatum*), big bluestem (*Andropogon gerardii*), and indiangrass (*Sorghastrum nutans*).

<sup>s</sup>Cool-season grass varieties include dense stands of bluegrass, ryegrass, and fescue. Warm-season varieties include bermuda grass and St. Augustine grass. The values given here are for potential conditions representing a 0.06 to 0.08 m mowing height. Turf, especially warm-season varieties, can be stressed at moderate levels and still maintain appearance (see section “Evapotranspiration Coefficients for Landscapes” in Chapter 10). Generally a value for the stress coefficient  $K_s$  of 0.9 for cool-season and 0.7 for warm-season varieties can be employed where careful water management is practiced and rapid growth is not required. Incorporation of these values for  $K_s$  into an “actual  $K_c$ ” using potential values in this table will yield  $K_{cbact}$  values of about 0.75 for cool-season turf and 0.55 for warm-season turf.

<sup>t</sup>These values for  $K_{cbini}$ ,  $K_{cbmid}$ , and  $K_{cbend}$  were modeled using Eqs. (10-25a), (10-27a), and (10-29) with parameters listed in Table D-3 of Appendix D, along with  $h$  from Table D-2 for various  $f_{ceff}$ , where  $f_{ceff}$  is the effective fraction of ground covered or shaded by vegetation (0 to 1.0) near solar noon and  $h$  is the mean height of the vegetation, m.

<sup>u</sup>The values in this row are similar to the entry in FAO-56 (Allen et al. 1998).

<sup>v</sup>For nonactive or only moderately active ground cover (active indicates green and growing ground cover with LAI > about 2),  $K_c$  should be weighted between  $K_c$  for no ground cover and  $K_c$  for active ground cover, with the weighting based on the “greenness” and approximate leaf area of the ground cover.

<sup>w</sup>The pineapple plant has low transpiration because it closes its stomates during the day and opens them during the night. Therefore, the majority of  $ET_c$  from pineapple is evaporation from the soil.

<sup>x</sup>Includes the water requirements of the shade trees.

<sup>y</sup>The values in this row are similar to those by Johnson et al. (2005).

<sup>z</sup>These  $K_{cbend}$  values represent  $K_{cb}$  prior to leaf drop. After leaf drop,  $K_{cbend} \approx 0.10$  to 0.20 for bare, dry soil or dead ground cover and  $K_{cbend} \approx 0.50$  to 0.80 for actively growing ground cover.

<sup>aa</sup>These  $K_{cbmid}$  and  $K_{cbend}$  values include an implicit  $K_s$  (stress) factor of about 0.7 (see Eq. 10-2), which is common for wine production. In practice, a  $K_s$  model and estimate should be applied where  $K_s$  can range from 0.5 to 1.0. Under no stress, the  $K_{cbmid}$  and  $K_{cbend}$  for wine grapes may equal that for table grapes, depending on plant density, age, and pruning structure.

<sup>bb</sup>For pears having  $f = 0.5$ , Girona et al. (2003) measured  $K_{cbmid} = 0.85$ , which is estimated using Eqs. (10-24), (10-25a), and (10-29) using  $K_{cbfull} = 1.1$  and  $M_L = 1.5$ .

<sup>cc</sup>Stone fruit category applies to peaches, apricots, pears, plums, and pecans.

<sup>dd</sup>The values in this row are derived from Girona et al. (2005) and Ayars et al. (2003) with  $f = 0.7$  and  $M_L = 1.5$ .

<sup>ee</sup>The values in this row are similar to those by Paço et al. (2006) and Ayars et al. (2003) with  $f = 0.25$  and  $M_L = 1.5$ .

<sup>ff</sup>The values for citrus are about 20% higher than those reported in FAO-56.

<sup>gg</sup>The values in this row are similar to those by Rogers et al. (1983) for citrus in Florida having Bahia grass cover.

<sup>hh</sup>Conifers exhibit substantial stomatal control due to soil water deficit. The  $K_c$  can easily reduce below the values presented, which represent well-watered conditions for large forests.

<sup>ii</sup>The values in this row are derived from de Azevedo et al. (2003).

<sup>jj</sup>Pastor and Orgaz (1994) found monthly  $K_c$  for olive orchards having  $f \sim 60\%$  similar to the values shown, except that  $K_{cmid} = 0.45$ , with stage lengths = 30, 90, 60, and 90 days, respectively, for initial, development, midseason, and late-season periods (see Table 5-6), and using  $K_c$  during the winter ("off season") in December to February = 0.50.

<sup>kk</sup>The values in this row are similar to those by Villalobos et al. (2000) when  $f$  of  $\sim 0.3$  to 0.4 are applied.

<sup>ll</sup>The values in this row are derived from Testi et al. (2004).

Sources: FAO-56 (Allen et al. 1998), with information from Doorenbos and Kassam (1979), Doorenbos and Pruitt (1977); Pruitt (1986); Wright (1981, 1982); Snyder et al. (1989a, b); and Allen et al. (2011a).

Table D-2. Mean Plant Height,  $h$ , m, Used in Eqs. (10-27a,b) and (10-29) for Estimating  $K_{cbini}$ ,  $K_{cbmid}$ , and  $K_{cbend}$  in Table D-1 and Parameter  $M_L$  Used in Eq. (10-29).

Category	$f = 0.05\text{--}0.1$	$f = 0.25$	$f = 0.5$	$f = 0.7$	$f = 0.9$	$M_L$
Almonds	3	4	5			1.5
Apples, cherries, pears	3	3	4			2.0
Apricots, peaches, stone fruit	2.5	3	3	3	1.5	
Avocado	3	3	4			2.0
Citrus	2	2.5	3			1.5
Mango	4	4	5			1.5
Olives	2	3	4	4		1.5
Pistachios	2	2.5	3			1.5
Walnut	4	4	5			1.5
Palms	8	8	8	8		1.5
Grapes—table or raisin	2	2	2			1.5
Grapes—wine	1.5	1.5	1.5			1.5

Table D-3. Parameters Used in Eqs. (10-25a,b) and (10-26) for Estimating  $K_{cbini}$ ,  $K_{cbmid}$ , and  $K_{cbend}$  in Table D-1 and Using  $f$  in Table D-2

Category	$K_{cbfull}$ -initial	$K_{cbfull}$ -mid	$K_{cbfull}$ -end	$K_{cmin}$	$K_{cbcover}$ -initial	$K_{cbcover}$ -mid, end	Add <sup>a</sup> to $K_{cb}$ for $K_{cm}$	Add <sup>a</sup> to $K_{cb}$ for $K_{cm}$	Add <sup>a</sup> to $K_{cb}$ for $K_{cm}$
Almonds									
- no ground cover	0.20	1.00	0.70 <sup>a</sup>	0.15	—	—	0.20	0.05	0.05
- ground cover	0.20	1.00	0.70 <sup>a</sup>	0.15	0.75	0.80	0.10	0.05	0.05
Apples, cherries, pears									
- killing frost	0.30	1.15	0.80 <sup>a</sup>	0.15	0.40	0.80	0.20	0.05	0.05
- no killing frost	0.30	1.15	0.80 <sup>a</sup>	0.15	0.75	0.80	0.10	0.05	0.05
Apricots, peaches, pears, plums, pecans									
- killing frost	0.30	1.20	0.80 <sup>a</sup>	0.15	0.40	0.80	0.20	0.05	0.05
- no killing frost	0.30	1.20	0.80 <sup>a</sup>	0.15	0.70	0.80	0.10	0.05	0.05
Avocado									
- no ground cover	0.30	1.00	0.90	0.15	—	—	0.20	0.05	0.05
- ground cover	0.30	1.00	0.90	0.15	0.75	0.80	0.10	0.05	0.05
Citrus									
Mango									
- no ground cover	0.25	0.85	0.70	0.15	—	—	0.10	0.05	0.05
Olives									
Pistachios									
Walnut									

(Continued)

Table D-3. Parameters Used in Eqs. (10-25a,b) and (10-26) for Estimating  $K_{cbini}$ ,  $K_{cbmid}$ , and  $K_{cbe}$  in Table D-1 and Using  $f$  in Table D-2 (Continued)

Category	$K_{cbfull}$ -initial	$K_{cbfull}$ -mid	$K_{cbfull}$ -end	$K_{cmin}$	$K_{cbcover}$ -initial	$K_{cbcover}$ -mid, end	Add <sup>a</sup> to $K_{cb}$ for $K_{cm}$	Add <sup>a</sup> to $K_{cb}$ for $K_{cm}$	Add <sup>a</sup> to $K_{cb}$ for $K_{cm}$
Palms									
– no ground cover	0.85	0.90	0.90	0.15			0.10	0.10	0.10
– ground cover	0.85	0.90	0.90	0.15	0.70	0.70	0.10	0.05	0.05
Grapes									
– table or raisin	0.20	1.15	0.90 <sup>b</sup>	0.15			0.10	0.05	0.05
– wine	0.20	0.80	0.60	0.15			0.10	0.05	0.05

Note: The  $K_{cbfull}$ -initial and  $K_{cbfull}$ -mid, end values were used in Eq. (10-25b) to represent  $K_{cbfull}$  for ground cover during the initial and for the midseason and late-season periods during estimation of  $K_{cbini}$ ,  $K_{cbmid}$  and  $K_{cbe}$  in Table D-1 for tree crops having typical ground cover vegetation between or under trees. For nonactive or only moderately active ground cover (active indicates green and growing ground cover with LAI > about 2),  $K_{cb}$  can be weighted between  $K_{cb}$  for no ground cover and  $K_{cb}$  for active ground cover, with the weighting based on the "greenness" and approximate leaf area of the ground cover.

<sup>a</sup>The last three columns are values added to  $K_{cb}$  values estimated for the initial, midseason, and late-season periods during application of Eqs. (10-25a, b), (10-26) and (10-27a) to obtain mean  $K_{cm}$  values.

<sup>b</sup>These  $K_{cbfull}$  values for end of season represent  $K_c$  for full cover conditions prior to leaf drop. After leaf drop,  $K_{cend} \approx 0.20$  for bare, dry soil or dead ground cover and  $K_{cend} \approx 0.50$  to 0.80 for actively growing ground cover.

## APPENDIX E

### MEAN AND BASAL CROP COEFFICIENTS FOR CROPS COMMON TO TEMPERATE AND CONTINENTAL CLIMATES

This appendix presents mean and basal crop coefficients,  $K_c$  and  $K_{cb}$ , for crops common to temperate and continental climates for use with alfalfa reference  $ET_r$ , as computed by the ASCE standardized Penman-Monteith reference method.

The crop coefficient curves developed by Wright (1981, 1982) for nine crops common to southern Idaho have been widely accepted in the western United States for use in irrigation water management, irrigation water rights, irrigation water transfers, and related legal applications. This section describes the conversion of the mean and basal crop coefficients of Wright (1981, 1982), as reported in Jensen et al. (1990), for application with the ASCE standardized reference evapotranspiration equation (ASCE 2005) for the alfalfa reference ( $ET_{rs}$ ). The Wright coefficients were originally derived for use with the 1982 Kimberly Penman equation, and small differences exist between the two reference calculations. The  $K_c$  and  $K_{cb}$  curves are traceable to time-based curves based on weighing lysimeter measurements at Kimberly, Idaho.

The ASCE standardized Penman-Monteith  $ET_r$  method, which is standardized for a 0.5-m tall vegetation reference for all times of the year, tends to estimate higher than the 1982 Kimberly Penman equation during early spring and fall months (Wright et al. 2000) and to estimate slightly below the 1982 Kimberly Penman method during the peak summer period. Conversion of the Wright (1981, 1982) coefficients to the standardized  $ET_r$  basis provides for equivalent calculation of crop  $ET_c$  for a southern Idaho type of climate using the ASCE standardized Penman-Monteith method.

The conversion was performed by Allen and Wright (2006, 2007) and used weather data sets collected at Kimberly (latitude = 42.5° N,

longitude = 114.4° W, elevation = 1,195 m) for the same year as was used for the original coefficient determination. The specific years are summarized in Table E-4. The same original weather data sets were used so that target  $ET_c$  values produced from smoothed  $K_c$  curves of Wright (1981, 1982) are identical to those produced originally by Wright. The converted  $K_c$  curves for use with  $ET_{rs}$  reproduce cumulative  $ET_c$  vs. time series for the Kimberly crops, which is the same as that obtained using the original coefficients and the 1982 Kimberly Penman method. This procedure retains all decision-making and original curve-shaping decisions made by Wright (1981, 1982). It is expected that the converted  $K_c$  curves will produce applicable and representative  $ET_c$  for other temperate and continental climates similar to Kimberly, Idaho, that have cold winters with defined dormant periods.

During the conversion work, standardized  $ET_r$ , denoted as  $ET_{rs}$ , was computed daily using Kimberly weather data for air temperature, humidity, and wind speed collected by the National Weather Service at the USDA-ARS Center at Kimberly and using solar radiation data collected by the USDA-ARS at Kimberly. The weather data were quality checked and controlled using procedures from ASCE (2005) Standardized Report Appendix D, including comparison of measured solar radiation data with theoretical clear sky curves and comparison of daily dew point temperature with daily minimum air temperature. Solar radiation for portions of some years required adjustment.

The same crop coefficient tabular format as used by Wright (1982) was used to summarize the converted crop coefficient curves:

- $K_c$  from planting to effective full cover expressed as a function of percent time from planting to effective full cover, in multiples of 10%; and
- $K_c$  after effective full cover expressed as a function of days after full cover in multiples of 10 days.

For the conversion, target crop  $ET_c$  was computed daily as  $ET_{cKP} = K_{cWright} \times ET_{rKP}$  where  $ET_{cKP}$  represented  $ET_c$  based on the original crop coefficient data set ( $K_{cWright}$ ) of Wright (1981, 1982), as reported in Jensen et al. (1990), Tables 6.6 and 6.9, and where some adjustment had been made by Wright (1995).  $ET_{rKP}$  represented alfalfa reference ET calculated using the 1982 Kimberly Penman equation and associated equations (Wright 1982).  $ET_c$  for the standardized Penman-Monteith was computed as  $ET_{cs} = K_{cs} \times ET_{rs}$  where  $ET_{cs}$  represents crop ET computed with the standardized ASCE procedure, and  $K_{cs}$  represents the crop coefficients converted for use with  $ET_{rs}$ .

During the conversion work, tabularized values for  $K_{cs}$  were adjusted so that cumulative  $ET_{cs}$  vs. time was identical to cumulative  $ET_{cKP}$  vs. time. The adjustments forced the two cumulative  $ET_c$  curves to graphically

coincide, and the use of cumulative  $ET_c$  curves created a somewhat smooth and continuous evolution in  $K_c$  vs. time and minimized the total root mean square error (RMSE) for the standardized mean  $K_c$ , denoted as  $K_{cms}$ , or the standardized basal  $K_c$ , denoted as  $K_{cbs}$ . Results of the conversion are listed in Table E-1 for mean crop coefficients and in Table E-2 for basal crop coefficients. The planting, effective full cover, and harvest dates reported by Wright (1981, 1982) are summarized in Table E-3. RMSE between cumulative  $ET_c$  by the original and converted curves were generally less than 1 mm per decadal period, as summarized in Table E-4. This translates into less than about 0.2  $\text{mm d}^{-1}$  RMSE in most cases. Graphical illustrations of the cumulative  $ET_c$  were given by Allen and Wright (2006).

The  $K_c$  curves for winter wheat were generated from the date of planting in fall until estimated dormancy in early winter and then again from greenup in spring until harvest following Wright (1982). Alfalfa  $K_c$  curves were converted for each of the four growth cycles as done by Wright (1981, 1982). In addition, a growing-season long curve that smooths the impacts of reduced  $K_c$  following cuttings was converted for use with  $ET_{rs}$ . Three years of weather and lysimeter data from 1969, 1970, 1971 had been used by Wright to construct the alfalfa curves. Therefore, a combined daily series for  $ET_r$  was created by averaging the daily  $ET_r$  from these three years. Similarly, two years, 1973 and 1974, were averaged to construct the daily  $ET_r$  curve for the snap bean crop, where those two years were used in defining the original  $K_c$  curves (Wright 1982).

The second and third growth cycles for alfalfa at Kimberly use the same  $K_c$  and  $K_{cb}$  curves in Tables E-1 and E-2. That middle growth cycle curve was converted so that each of the two growth cycles shared any "error" created by the curve conversion. The clipped ryegrass crop was not reported by Wright (1981) nor Wright (1982), but was included in Jensen et al. (1990) and traces to the Kimberly lysimeters operated by Wright, and was therefore converted and reported by Allen and Wright (2007). That crop was grown at Kimberly during years 1983 and 1984, so that the  $ET_r$  for those two years was averaged to produce a single daily time series.

Table E-1. Mean Crop Coefficients,  $K_c$ , for Crops Common to Temperate and Continental Climates for Use with Alfalfa Reference  $ET_r$  Computed by the ASCE Standardized Penman-Monteith Reference Method

Crop	Mean ET Crop Coefficients, $K_c$ Pct, time from planting to effective cover										
	0	10	20	30	40	50	60	70	80	90	100
Spring grain <sup>a</sup>	0.20 <sup>b</sup>	0.20	0.20	0.25	0.37	0.50	0.63	0.76	1.00	1.03	1.03
Peas	0.15	0.17	0.19	0.21	0.32	0.42	0.52	0.63	0.73	0.83	0.93
Sugar beets	0.26	0.26	0.26	0.26	0.26	0.28	0.30	0.38	0.55	0.74	1.03
Potatoes	0.20	0.20	0.20	0.22	0.30	0.41	0.53	0.67	0.73	0.77	0.80
Corn	0.20	0.20	0.20	0.20	0.24	0.34	0.44	0.58	0.72	0.90	1.00
Beans	0.20	0.20	0.22	0.26	0.35	0.45	0.55	0.68	0.83	0.95	0.97
Winter wheat	0.25	0.25	0.27	0.38	0.60	0.80	0.90	0.96	1.00	1.03	1.03

Crop	DT, days after effective cover										
	0	10	20	30	40	50	60	70	80	90	100
Spring grain <sup>a</sup>	1.03	1.03	1.03	1.03	0.94	0.50	0.30	0.15	0.10		
Peas	0.93	0.93	0.70	0.54	0.38	0.22	0.12	0.10			
Sugar beets	1.03	1.03	1.03	1.00	0.97	0.92	0.82	0.74	0.65	0.61	0.56
Potatoes	0.80	0.80	0.76	0.72	0.68	0.63	0.58	0.50	0.38	0.20	0.15
Field corn	1.00	0.99	0.98	0.95	0.88	0.80	0.72	0.63	0.35	0.18	
Sweet corn	1.00	0.97	0.94	0.90	0.84	0.70	0.55	0.35	0.20	0.10	
Beans	0.97	0.97	0.94	0.64	0.32	0.15	0.10	0.05			
Winter wheat	1.03	1.03	1.03	1.03	1.00	0.55	0.25	0.15	0.10		

Crop	Time from new growth or harvest to harvest (%)										
	0	10	20	30	40	50	60	70	80	90	100
Alfalfa (1st cycle) <sup>c</sup>	0.50	0.62	0.73	0.83	0.88	0.94	1.00	1.00	1.00	0.98	0.95
(Intermediate cycles)	0.30	0.40	0.55	0.80	0.94	0.97	1.00	1.00	1.00	0.97	0.94
(Last cycle)	0.30	0.35	0.45	0.53	0.58	0.58	0.54	0.48	0.46	0.44	0.44
<i>Total season (days from beginning of spring growth)</i>											
Crop	0	20	40	60	80	100	120	140	160	180	200
Alfalfa											
20-day average	0.45	0.69	0.87	0.88	0.7	0.75	0.88	0.81	0.88	0.71	0.65
60-day average	0.44	0.77	0.82	0.86	0.9	0.88	0.85	0.82	0.78	0.66	0.5
seasonal curve											
single seasonal											
mean											
Perennial ryegrass (8–15 cm)	0.55	0.66	0.77	0.80	0.80	0.80	0.78	0.76	0.72	0.68	0.55

Note: Converted from original crop coefficients of Wright (1981), Manual 70 Table 6-6, and updates by Wright (1995) and Allen and Wright (2007).

<sup>a</sup>Spring grain includes wheat and barley.

<sup>b</sup>The values 0.15–0.26 for all crops are appropriate for somewhat dry surface soil conditions from planting until significant crop development. For moderately wet surface soil, as with preemergence irrigation(s) or some precipitation, use 0.35, and for very wet conditions use 0.50 for the first part of the growing season until that value is exceeded by a table value.

<sup>c</sup>1st denotes first harvest, intermediate harvests may be one or more depending on length of season. The last harvest is when crop becomes dormant in cool weather. Cultivar used was Ranger.

Table E-2. Basal Crop Coefficients,  $K_{cb}$ , for Crops Common to Temperate and Continental Climates for Use with Alfalfa Reference  $ET_r$  as Computed by the ASCE Standardized Penman-Monteith Reference Method

Crop	Basal ET Crop Coefficients, $K_{cb}$ Pct, time from planting to effective cover										
	0	10	20	30	40	50	60	70	80	90	100
Spring grain <sup>a</sup>	0.15	0.15	0.15	0.19	0.24	0.36	0.48	0.62	0.92	0.98	1.03
Peas	0.12	0.13	0.14	0.15	0.18	0.27	0.36	0.50	0.65	0.78	0.92
Sugar beets	0.15	0.15	0.15	0.15	0.15	0.16	0.17	0.21	0.40	0.66	1.03
Potatoes	0.15	0.15	0.15	0.15	0.15	0.20	0.34	0.49	0.64	0.72	0.77
Corn	0.15	0.15	0.15	0.16	0.17	0.20	0.27	0.41	0.55	0.80	0.96
Beans	0.15	0.15	0.17	0.19	0.23	0.35	0.46	0.60	0.78	0.93	0.95
Winter wheat	0.12	0.12	0.14	0.22	0.45	0.70	0.84	0.96	1.00	1.03	1.03
DT, days after effective cover											
Crop	DT, days after effective cover										
	0	10	20	30	40	50	60	70	80	90	100
Spring grain <sup>a</sup>	1.03	1.03	1.03	1.03	0.94	0.40	0.15	0.07	0.05	0.05	0.05
Peas	0.92	0.92	0.72	0.52	0.32	0.16	0.07	0.05	0.05	0.05	0.05
Sugar beets	1.03	1.03	1.02	0.98	0.93	0.86	0.78	0.72	0.66	0.60	0.54
Potatoes	0.77	0.77	0.73	0.68	0.64	0.59	0.54	0.47	0.20	0.08	0.08
Field corn	0.96	0.96	0.96	0.92	0.85	0.79	0.72	0.62	0.28	0.16	0.12
Sweet corn	0.96	0.95	0.93	0.88	0.80	0.65	0.47	0.23	0.12	0.12	0.12
Beans	0.95	0.95	0.88	0.64	0.30	0.09	0.05	0.20	0.10	0.05	0.05
Winter wheat	1.03	1.03	1.03	1.00	0.50	0.20	0.10	0.05	0.05	0.05	0.05

Crop	Time from new growth or harvest to harvest (%)										
	0	10	20	30	40	50	60	70	80	90	100
Alfalfa (1st cycle) <sup>b</sup>	0.35	0.45	0.56	0.72	0.82	0.90	1.00	1.00	1.00	0.98	0.96
(Intermediate cycles)	0.25	0.30	0.42	0.72	0.90	0.95	1.00	1.00	0.98	0.96	0.94
(Last cycle)	0.25	0.27	0.36	0.42	0.50	0.45	0.35	0.3	0.25	0.22	0.22
Total season (days from beginning of spring growth)											
Crop	0	20	40	60	80	100	120	140	160	180	200
Alfalfa											
20-day average	0.45	0.69	0.87	0.88	0.70	0.75	0.88	0.81	0.88	0.71	0.65
60-day average	0.50	0.74	0.82	0.86	0.88	0.88	0.86	0.84	0.78	0.70	0.50
seasonal mean											
Perennial ryegrass (8–15 cm)	0.60	0.68	0.76	0.78	0.80	0.80	0.79	0.76	0.73	0.68	0.60

Note: Converted from original crop coefficients of Wright (1982), Manual 70 Table 6-6, and updates by Wright (1995) and Allen and Wright (2007).

<sup>a</sup>Spring grain includes wheat and barley.

<sup>b</sup>1st denotes first harvest, intermediate harvests may be one or more depending on length of season. The last harvest is when crop becomes dormant in cool weather. Cultivar used was Ranger.

Table E-3. Dates of Various Crop Growth Stages for Crops Studied at Kimberly, Idaho, 1968-1979

Crop	Date of Occurrence (Month/Day)					Planting to Full Cover Days	Planting to Full Cover to Harvest Days
	Planting	Emergence	Rapid Growth	Full Cover or Bloom	Ripening	Harvest	
Spring grain <sup>a</sup>	04/01	04/15	05/10	06/10	07/20	08/10	70
Peas	04/05	04/25	05/10	06/05	07/05	07/25	61
Sugar beets	04/15	05/10	06/01	07/10	10/15	86	97
Potatoes	04/25	05/25	06/10	07/10	09/20	10/10	76
Field corn	05/05	05/25	06/10	07/15	09/10	09/20	71
Sweet corn	05/05	05/25	06/10	07/15	07/20	08/15	71
Beans	05/22	06/05	06/15	07/15	08/15	08/30	54
Winter wheat <sup>b</sup>	(2/15)	(3/1)	03/20	06/05	07/15	08/10	66
Alfalfa (1st) <sup>c</sup>	04/01		04/20			06/15	
Alfalfa (2nd) <sup>c</sup>	06/15		06/25			07/31	
Alfalfa (3rd) <sup>c</sup>	07/31		08/10			09/15	
Alfalfa (4th) <sup>c</sup>	09/15		10/01			10/30	

<sup>a</sup>Spring grain includes barley and wheat.<sup>b</sup>Effective dates are in parentheses. Crop was planted on 10/10 and emerged 10/25 the previous season.<sup>c</sup>Effective planting date for established alfalfa is the date growth begins in spring or harvest of preceding crop. Dates for cuttings are indicated. Final harvest is the date crop became dormant.

Sources: Data from Wright (1982), and Table 6.7 of Jensen et al. (1990). Minor changes from Wright (1982) reflect additional data for some crops (Wright, personal communication, 1984).

Table E-4. Years of Original Lysimeter and Weather Data Collection Reported by Wright (1981, 1982) and RMSE for Crop Coefficient Conversion

Crop	Year of Data	RMSE of $ET_c$ Produced during the Conversion of $K_{cm}$ from the Kimberly Penman Basis to the ASCE Standardized Penman-Monteith Reference ET basis, mm per Decadal <sup>a</sup> Period
Spring grain ( <i>Triticum aestivum</i> )	1979	1.1
Peas ( <i>Pisum sativum</i> )	1977	1.0
Sugar beets ( <i>Beta vulgaris</i> )	1975	0.9
Potatoes ( <i>Solanum tuberosum</i> )	1972	0.7
Field corn ( <i>Zea mays</i> )	1976	0.9
Sweet corn ( <i>Zea mays</i> convar. <i>saccharata</i> )	1976	0.9
Snap beans ( <i>Phaseolus vulgaris</i> , cv. Slimgreen)	1973, 1974 (ave.)	0.3
Winter wheat ( <i>Triticum aestivum</i> )	1977–78	1.4
Alfalfa ( <i>Medicago sativa</i> , cv. Ranger)	1969, 1970, 1971 (ave.)	0.7 (season) 0.4, 1.3, 1.3, 0.4 for cuttings 1, 2, 3, 4
Ryegrass ( <i>Lolium perenne</i> )	1983, 1984	0.7

<sup>a</sup>A decadal period represents 10% of the planting to effective full cover period or each 10 days following effective full cover until harvest.

This page intentionally left blank

## APPENDIX F

# BASAL CROP COEFFICIENTS FOR CROPS COMMON TO TEMPERATE AND CONTINENTAL CLIMATES WITH THERMAL BASIS

This appendix presents the basal crop coefficients,  $K_{cb}$ , for crops common to temperate and continental climates for use with alfalfa reference  $ET_r$ , as computed by the ASCE standardized Penman-Monteith reference method and using a growing degree day basis.

### F.1 INTRODUCTION

The  $K_{cb}$  curves of Wright (1982) for nine crops common to southern Idaho are traceable to weighing lysimeter measurements at Kimberly, Idaho, and have been widely accepted in the western United States for use in irrigation water management, irrigation water rights, irrigation water transfers, and related legal applications. The  $K_{cb}$  curves of Wright (1982) presented in Appendix E for the original time basis are reformulated in this appendix as functions of cumulative growing degree days (CGDD). The use of CGDD provides automated flexure, expansion, or compression of the  $K_c$  curve basis under varying weather conditions and eliminates the need to specify the time of effective full cover. Wright (1998) originally made the conversion of Wright (1982)  $K_{cb}$  curves to CGDD that was repeated by Allen and Wright (2006) following the conversion to the ASCE standardized reference evapotranspiration equation (ASCE 2005) for the alfalfa reference ( $ET_{rs}$ ) basis, as outlined in Appendix E. The conversion and basis for applying CGDD is described here. In addition,  $K_{cb}$  curves for other crops common to temperate and continental climates are presented in this appendix. These additional crops are not traceable to lysimeter measurements, but are helpful in estimating crop ET for a broad range

of crops. A description of statewide application of the estimation procedures by Allen and Robison (2007) is given for Idaho.

## F.2 GROWING DEGREE BASIS FOR $K_c$

Plant functions of evapotranspiration, photosynthesis, water and nutrient absorption and transport, enzyme activity, and other biological and chemical activities are regulated by temperature. For this reason, the development of the crop is generally more closely related to the amount of heat the crop is exposed to than to calendar days. In many applications, the emergence of vegetation, greenup, and attainment of effective full cover have been estimated using cumulative degree-based regression equations or plant growth models (Sinclair 1984; Sammis 1985; Ritchie and NeSmith 1991; Slack et al. 1996; Snyder et al. 1999; Cesaraccio et al. 2001; Ojeda-Bustamante et al. 2004; Allen and Robison 2007; Martínez-Cob 2008; Ceglar et al. 2011; Gharnaria et al. 2013; Payero and Irmak 2013). The use of cumulative growing degree days provides a quantitative stretching or shrinkage of the generated  $K_c$  curves for years or growing seasons that run cooler or warmer than average and reduces the need for manual estimation of these dates and intervention to the  $K_c$  estimation process. This approach is required for prospective studies of climate change impacts on crop water and irrigation requirements, for example, by Saadi et al. (2014) and Huntington et al. (2015) as a means to facilitate transfer of crop coefficients among regions. Cumulative growing degree days (CGDD) since planting have commonly been used as a basis for crop coefficient development, as a means for automatically adjusting lengths of development and growth periods to account for variation in temperature among years (Sammis et al. 1985; Slack et al. 1996; Howell et al. 1997; Mitchell 1997; Snyder et al. 1999; Wright 2001; deTar 2004; Marek et al. 2006; Nebraska-HPCC 2006).

A wide range of computation methods for growing degree days (GDD) have been utilized. These include the standard method that has long been used for corn (Van den Brink et al. 1971):

$$GDD_{\text{corn}} = \frac{\max[\min(T_{\max}, 30), 10] + \max[\min(T_{\min}, 30), 10]}{2} - 10 \quad (\text{F-1})$$

where  $T_{\max}$  is daily maximum air temperature in °C, and  $T_{\min}$  is daily minimum air temperature in °C. The standard corn equation is often referred to as a heat unit equation and is also known as the 86/50 method, referring to the maximum threshold of 30°C and minimum threshold of 10°C, which are 86 and 50°F. The GDD equation for corn assumes no growth at air temperatures above 30°C and no retardation or negative penalty to growth rate if the minimum temperature goes below 10°C.

A common, basic formula for computing daily growing degree days (GDD) for crops other than corn is to average daily maximum and daily minimum air temperatures for each day and to subtract a minimum average daily temperature (base temperature) required for growth to proceed (Mitchell 1997; Wright 2001). There is no penalty applied when  $T_{max}$  exceeds a threshold, as is done with corn, and no numerical boost is given to  $T_{min}$  when it is lower than the minimum threshold, as is the case for corn. The basic equation for the general GDD is

$$GDD = \max\left(\frac{T_{max} + T_{min}}{2} - T_{base}, 0\right) \quad (\text{F-2})$$

where  $T_{base}$  is a base temperature representing when average daily air temperature is sufficient for plant growth to proceed. When  $T_{min}$  is far enough below  $T_{base}$  to cause the average daily temperature  $(T_{max} + T_{min})/2$  to dip below  $T_{base}$ , then GDD is set to 0°C-days. Days having high  $T_{max}$ , but with  $T_{min}$  below  $T_{base}$  are estimated by Eq. (F-2) to have lower growth rates than by Eq. (F-1), where  $T_{min}$  is boosted. Wright (2001) suggests that Eq. (F-2) is realistic for most crops grown in semiarid climates such as Idaho, where cold nighttime temperatures can retard growth during daytime even when midday temperatures are high.

### F.3 CONVERSION OF WRIGHT (1982) $K_{cb}$ CURVES TO THE CGDD BASIS

The conversion of the  $K_{cb}$  curves of Wright (1982) from a time base to a normalized GDD base was produced by Allen and Wright (2006) to follow that originally developed by Wright (2001), but for use with the standardized ASCE-PM  $ET_r$  method. Weather data for the specific year of curve development was used to compute CGDD as described in Appendix E.  $T_{base}$  values used for crops were based on selections by Wright (2001) and ranged from 0°C for early spring crops such as spring grain to 5°C for crops such as potatoes and dry beans, as shown in Table 3-1. All crops used Eq. (F-2) for GDD with the exception of corn, where the standard corn GDD method was used ( $T_{base} = 10^\circ\text{C}$  and Tupper threshold =  $30^\circ\text{C}$ ) for consistency with standardized usage within the United States.

The approach of Wright (2001) was followed, where the CGDD basis was normalized in terms of the quantity of CGDD required to advance from planting or greenup to effective full cover. This normalized CGDD (termed NCGDD) ranged from 0 to 1.0 over the period from planting or greenup until effective full cover. Normalization of CGDD provides the means to change only one number (NCGDD at full cover) when fitting curves to a new variety or region. NCGDD ranges from 1.0 to typically

more than 2.0 for the period from effective full cover to harvest or die-down. NCGDD was computed each day by dividing by the CGDD for that day by the CGDD at effective full cover. Effective full cover dates were taken from Table E-3, following Wright (1982).

Translation of curves was similar to the time-based conversion of the  $K_{cb}$  curves to the ASCE-PM  $ET_r$  basis, as described in Appendix E, where cumulative ET was computed vs. time using the 1982 Kimberly Penman  $ET_r$  applied using the weather data for the specific year of lysimeter measurement and multiplied by the crop coefficient curve of Wright (1982). The crop coefficient curve of Wright (1982) was constructed using the dates for planting, effective full cover, and harvest given in that paper and the crop coefficients reported there or updated by Wright (1995) and listed in Table E-2. The result was a reconstructed lysimeter ET data set that reflected the smoothing by the  $K_c$  curves and filtering and decision making by Wright (1981, 1982, 2001). The cumulative ET vs. time curves were then paired against equivalent normalized CGDD calculated for the same year and weather data set, and the value for CGDD at the time of reported effective full cover was determined. NCGDD was computed each day by dividing the CGDD for that day by the CGDD at effective full cover. Finally, percentile values for  $K_{cb}$  were selected from the plots, numerically in increments of 10% for NCGDD.

The snap bean crop, which also represents dry, edible beans, was grown at Kimberly in 1973 and 1974. The NCGDD curves for the beans were developed using data from 1973. For alfalfa hay,  $K_c$  vs. NCGDD curves were established for individual cuttings using data from Wright (1981, 1982) and lysimeter records for the 1969–1971 period at Kimberly. Unique  $K_c$  vs. NCGDD were developed for the first growth period, for intermediate growth periods, and for the final growth period prior to frost. The unique  $K_c$  vs. NCGDD shapes were established to account for differences in regrowth rates for the three periods. The NCGDD values for the first growing cycle are accumulated beginning at greenup of the crop in spring, assuming a dormant or near-dormant period during winter. NCGDD for the other growth cycles are accumulated from the time of cutting. Greenup was estimated for alfalfa using CGDD from January 1 and a temperature base of 0°C. The month of January in Idaho usually represents a period of no significant CGDD accumulation, where the alfalfa crop is dormant. Therefore, this is a good starting point to begin the CGDD accumulation for alfalfa. A CGDD of 240°C-days from January 1 was used to signal greenup, based on Kimberly data and observations across southern Idaho. No penalties were applied to CGDD of alfalfa during winter or early spring as was the case for winter wheat, when subfreezing temperatures occurred.

During the conversion, the  $K_c$  v. NCGDD curve for winter wheat was begun October 1 and run through the winter, which deviates from

Wright (2001), where his NCGDD curve began at an artificial greenup date in late winter or early spring. The October 1 date is a typical planting date in many parts of Idaho and agrees with the October 10 date reported by Wright (1982) for the winter wheat crop of 1977–78. The CGDD-based  $K_{cb}$  curve for winter wheat extends back to October 1 and provides  $K_{cb}$  information during winter. The  $K_{cb}$  curve has a shape following the heading of the wheat crop that agrees closely with the Wright (1982)  $K_{cb}$  curve.

$K_{cb}$  is expressed for potato crops for two classes of potatoes: long season, late-harvested varieties representing baking potatoes and other varieties that are harvested in September and October in southern Idaho, and short season varieties representing processing potatoes that begin to be harvested as early as August. Planting and development dates for both varieties are generally similar, and therefore a single curve is used for the period between planting and effective full cover. Separate curves are used for the period from effective full cover to harvest, both based on a normalized cumulative growing degree day scale. The  $K_{cb}$  vs. NCGDD relationship for the long season class is that developed from Wright (1982) and listed in Table F-1 as curve no. 6. The  $K_{cb}$  vs. NCGDD relationship for the short season class (curve 7) was developed from that for the long season variety by shortening the relative time required for maturity and reducing values for  $K_{cb}$  beginning at about 1.75 times NCGDD<sub>Planting to Effective Cover</sub>. The recommended CGDD at harvest for the long season variety is about 1,800°C-days and that for the short season variety is about 1,600°C-days.

The grass hay  $K_{cb}$  curve was constructed to follow the shape of the  $K_{cb}$  curve for first cycle alfalfa, but with peak  $K_{cb}$  of 0.95 rather than 1.0 and with 50% longer CGDD required until cutting (1,300°C-days at base 0°C). Following a first cutting (at NCGDD = 1.0), the  $K_{cb}$  is presumed to stay near 0.70 and then decline toward fall, when grazing may occur. The curve ends at killing frost. The shape is similar to the  $K_{cb}$  curve developed and reported by the U.S. Bureau of Reclamation Agrimet system (P. Palmer, USBR, personal communication, 1999).

Figure F-1 shows  $K_{cb}$  vs. NCGDD for the nine Kimberly crops plotted together. The NCGDD value at the attainment of effective full cover equals 1.0 in the figure. The shapes of the  $K_{cb}$  curves are similar to one another during the development period because all crops except alfalfa are annuals and because of the use of normalized CGDD as the basis for the  $K_{cb}$  vs. NCGDD curve. All of the  $K_{cb}$  curves run between 0.9 and 1.0 after effective full cover due to the attainment of nearly full ground cover. The exception is the curve for potatoes, which peaked at about 0.80, due, perhaps to varietal effects for the russet Burbank crop. Figure F-2 shows the first, intermediate, and final  $K_{cb}$  vs. NCGDD curves derived for the Ranger variety alfalfa crop at Kimberly, and Figure F-3 shows the  $K_{cb}$  vs. NCGDD curve developed for grass hay.

Table F-1A.  $K_{cb}$  for Use with the Standardized ASCE-EWRI Penman-Monteith  $ET_r$ , Based on Normalized Cumulative Growing Degree Day from Planting to Effective Full Cover, Traceable to Wright (1982) and the USDA-ARS Kimberly Lysimeter Systems

Curve No.:	1	2	3	4	5	6	7	8	9	10	
Normalized Cumulative GDD from Planting (or Greenup) to Effective Full Cover, %	Spring Wheat	Winter Wheat	Peas, Seed	Peas, Fresh	Sugar Beets	Harvest Potato	Late Harvest Potato	Early Harvest Potato	Grain Corn	Silage Corn	Sweet Corn
0	0.15	0.12	0.12	0.12	0.15	0.15	0.15	0.15	0.15	0.15	0.15
10	0.15	0.12	0.14	0.14	0.15	0.15	0.15	0.15	0.15	0.15	0.15
20	0.20	0.15	0.15	0.15	0.16	0.15	0.15	0.15	0.15	0.15	0.15
30	0.28	0.20	0.16	0.16	0.17	0.17	0.17	0.17	0.17	0.17	0.17
40	0.40	0.27	0.20	0.20	0.18	0.23	0.23	0.23	0.19	0.19	0.19
50	0.50	0.40	0.32	0.32	0.21	0.35	0.35	0.35	0.28	0.28	0.28
60	0.59	0.72	0.46	0.46	0.40	0.48	0.48	0.48	0.42	0.42	0.42
70	0.82	0.93	0.63	0.63	0.57	0.62	0.62	0.62	0.54	0.54	0.54
80	0.95	0.99	0.77	0.77	0.73	0.69	0.69	0.69	0.73	0.73	0.73
90	0.99	1.03	0.85	0.85	0.88	0.74	0.74	0.74	0.86	0.86	0.86
100 (Eff. Full Cov.)	1.03	1.03	0.92	0.92	1.03	0.77	0.77	0.77	0.96	0.96	0.96
110	1.03	1.03	0.92	0.92	1.03	0.77	0.77	0.77	0.96	0.96	0.96
120	1.03	1.03	0.92	0.92	1.03	0.77	0.77	0.76	0.96	0.96	0.95
130	1.03	1.03	0.91	0.91	1.03	0.75	0.75	0.72	0.96	0.96	0.94
140	1.03	1.02	0.84	0.84	1.02	0.72	0.70	0.70	0.96	0.96	0.93
150	1.03	1.00	0.78	0.78	1.01	0.70	0.68	0.68	0.94	0.94	0.90

160	1.03	0.72	0.71	0.71	0.99	0.68	0.65	0.90	0.90	0.86
170	1.01	0.43	0.65	0.65	0.97	0.66	0.63	0.86	0.86	0.82
180	0.97	0.25	0.58	0.58	0.95	0.64	0.59	0.82	0.82	0.78
190	0.88	0.15	0.52	0.52	0.91	0.61	0.54	0.78	0.78	0.73
200	0.64	0.10	0.45	0.45	0.87	0.58	0.40	0.73	0.73	0.65
210	0.41	0.05	0.38	0.38	0.82	0.54	0.10	0.65	0.65	0.20
220		0.28	0.31	0.31	0.77	0.48		0.44	0.44	0.10
230		0.16	0.27	0.27	0.73	0.16		0.22	0.22	0.10
240		0.10	0.22	0.22	0.69	0.10		0.13	0.13	0.10
250		0.05	0.18	0.18	0.63					
260			0.14	0.14	0.57					
270			0.10	0.10	0.10					
280										
290										
300										
	GDD Base, °C <sup>a</sup>	0	0	0	5	5	5	10-corn	10-corn	10-corn
	CGDD <sub>Planting to EFC</sub> <sup>b</sup>	935 <sup>c</sup>	1,350 <sup>c</sup>	635	710 <sup>c</sup>	780 <sup>c</sup>	780	510 <sup>c</sup>	510	510
	CGDD <sub>Planting to Terminate</sub> <sup>c</sup>	2,160	2,608	1,616	1,000	1,843 <sup>e</sup>	1,850 <sup>e</sup>	1,600 <sup>e</sup>	1,200 <sup>e</sup>	800 <sup>e</sup>

<sup>a</sup>The GDD Base, °C is base or minimum threshold used when computing the growing degree day.

<sup>b</sup>The CGDD<sub>Planting to EFC</sub> is the cumulative growing degree days from planting (or greenup) until effective full cover is set differently for each crop (Wright 1982).

<sup>c</sup>The 935 value for spring wheat was changed to 840, the 1,350 value for winter grain was changed to 1,080, the 780 for baking potatoes was reduced to 700, the 710 for sugar beets was increased to 970, and the 510 value for corn was changed to 540 by Allen and Robison (2007) to fit recent observations of crop development since 2000.

<sup>d</sup>The CGDD<sub>Planting to Terminate</sub> is the total cumulative growing degree days from planting (or greenup) until termination (harvest) of the crop. This parameter signals the end of the  $K_{cb}$  curve construction.

<sup>e</sup>The 1,843 value for sugar beets was changed to 2,600, the 1,850 and 1,600 for potatoes were changed to 1,780 and 1,550, and the 1,200 value for field corn was changed to 1,400 and the 800 value for sweet corn was changed to 1,000 to fit recent observations by Allen and Robison (2007).

Table F-1B.  $K_{cb}$  for Use with the Standardized ASCE-EWRI Penman-Monteith  $ET_r$ , Based on Normalized Cumulative Growing Degree Day from Planting to Effective Full Cover, Traceable to Wright (1982) and the USDA-ARS Kimberly Lysimeter Systems, plus Grass Hay

Curve No.:	11	12	13	14	15	16
% PL-EC or PL-TM (type 1-2-4)	Snap Beans, Dry	Snap Beans, Fresh	Alfalfa 1st Cycle	Alfalfa Int Cycle	Alfalfa Last Cycle	Grass Hay
0	0.15	0.15	0.25	0.25	0.25	0.20
10	0.16	0.16	0.51	0.33	0.29	0.46
20	0.19	0.19	0.73	0.45	0.38	0.68
30	0.23	0.23	0.84	0.80	0.56	0.79
40	0.38	0.38	0.90	0.93	0.79	0.85
50	0.49	0.49	0.98	0.99	0.91	0.93
60	0.60	0.60	1.00	1.00	0.96	0.95
70	0.74	0.74	1.00	0.99	1.00	0.95
80	0.86	0.86	0.99	0.97	0.99	0.94
90	0.94	0.94	0.97	0.96	0.96	0.92
100 (Eff. Full Cov.)	0.95	0.95	0.96	0.94	0.94	0.91
110	0.95	0.95				0.50
120	0.95	0.95				0.55
130	0.93	0.93				0.70
140	0.90	0.90				0.75
150	0.85	0.85				0.75
160	0.75	0.75				0.75
170	0.64					0.75
180	0.49					0.75
190	0.34					0.70
200	0.19					0.70
210	0.08					0.70
220						0.65
230						0.65
240						0.65
250						0.60
260						0.55
270						0.50
280						0.45
290						0.45

Table F-1B.  $K_{cb}$  for Use with the Standardized ASCE-EWRI Penman-Monteith  $ET_r$ , Based on Normalized Cumulative Growing Degree Day from Planting to Effective Full Cover, Traceable to Wright (1982) and the USDA-ARS Kimberly Lysimeter Systems, plus Grass Hay (Continued)

Curve No.:	11	12	13	14	15	16
% PL-EC or PL-TM (type 1-2-4)	Snap Beans, Dry	Snap Beans, Fresh	Alfalfa 1st Cycle	Alfalfa Int Cycle	Alfalfa Last Cycle	Grass Hay
GDD Base, °C <sup>a</sup>	5	5	0	0	0	0
CGDD <sub>Planting to EFC</sub> <sup>b</sup>	670	670	—	—	—	1,300
CGDD <sub>Planting to Terminate</sub> <sup>c</sup>	1,350	950	850	1,050 <sup>d</sup>	1,050 <sup>d</sup>	4,000
CGDD <sub>Planting to Terminate-alt</sub> <sup>e</sup>			700	850 <sup>d</sup>	850 <sup>d</sup>	

<sup>a</sup>The GDD Base, °C is base or minimum threshold used when computing the growing degree day.

<sup>b</sup>The CGDD<sub>Planting to EFC</sub> is the cumulative growing degree days from planting (or greenup) until effective full cover. Effective full cover is set differently for each crop (Wright 1982).

<sup>c</sup>The CGDD<sub>Planting to Terminate</sub> is the total cumulative growing degree days from planting (or greenup) until termination (harvest) of the crop. This parameter signals the end of the  $K_{cb}$  curve construction.

<sup>d</sup>The value of 1,050 (for “beef style” alfalfa hay) was reduced to 900, and the 850 value (for “dairy style” hay) was set to 650 by Allen and Robison (2007) during more recent processing to better match recent, local observations.

<sup>e</sup>For alfalfa hay, the value of CGDD<sub>Planting to Terminate</sub> for “dairy hay” having relatively frequent cuttings.

#### F.4 APPLICATION OF $K_{cb}$ CURVES WITH THE CGDD BASIS

To apply the  $K_{cb}$  vs. NCGDD curves, one needs to determine the planting or greenup date to begin the season. No other information other than daily calculated CGDD is required. To construct the curve, CGDD from the estimated day of planting or greenup is accumulated using the base temperature for the crop using Eq. (F-2) for all crops except corn, where Eq. (F-1) is used. NCGDD is calculated as the ratio of CGDD to the CGDD entered in Table F-1 for the “CGDD<sub>Planting to EFC</sub>” entry in the table. For example, for spring wheat, the CGDD<sub>Planting to EFC</sub> value is 935° C-days. The ratio NCGDD is used as the entry point in column 1 of Table F-1 and the value for  $K_{cb}$  is selected by interpolation. The ratio NCGDD is calculated by dividing CGDD accumulated since planting

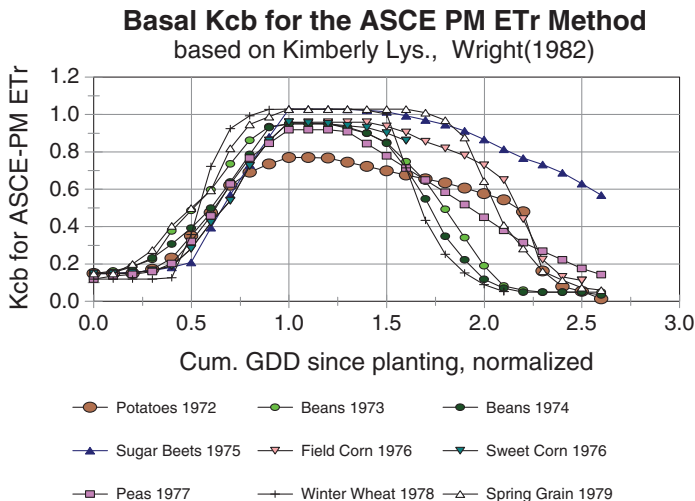


Fig. F-1.  $K_{cb}$  vs. NCGDD for the crops grown on Kimberly lysimeters  
Source: Data from Wright (1982 and personal communication)

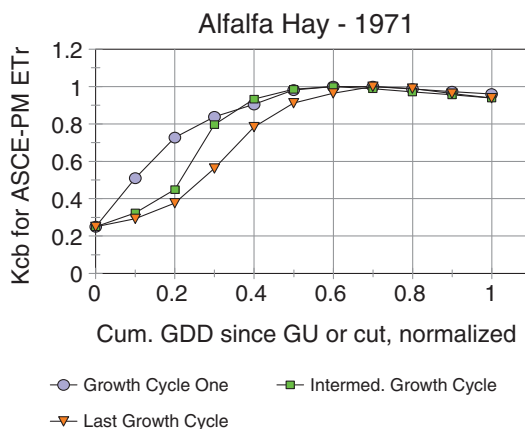


Fig. F-2.  $K_{cb}$  vs. NCGDD for the Ranger variety alfalfa crop grown on Kimberly lysimeters  
Source: Data from Wright (1982 and personal communication)

(or greenup of alfalfa) by the CGDD<sub>Planting to EFC</sub> value. This ratio is applied to the entire season or cutting cycle until either CGDD exceeds the value for CGDD<sub>Planting to Terminate</sub> that is in the table or when a killing frost occurs.

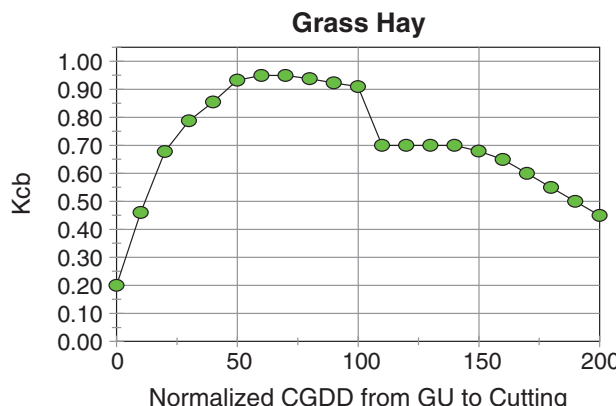


Fig. F-3.  $K_{cb}$  vs. NCGDD for a grass hay crop grown in high elevation, mid-latitude climates having a single midsummer cutting and limited regrowth following the cutting

#### Adjustments in NCGDD-Based $K_{cb}$ Applications

The cumulative growing degree day values at the time of effective full cover ( $CGDD_{Planting\ to\ EFC}$ ) values in Table F-1 are based on observed times of effective full cover or timing of plateauing of the  $K_{cb}$  curve. Modern crop varieties may require the establishment of different values for  $CGDD_{Planting\ to\ EFC}$  to account for more rapid or less rapid development rates for the same thermal conditions. For example, the following adjustments were made to the CGDD-based  $K_{cb}$  curves during application to 123 weather station locations in Idaho by Allen and Robison (2007) and as noted in footnotes c and e of Table F-1. The adjustments were made to account for differences between Kimberly data derived from lysimeter measurements in the 1970s and 1980s and observations for more current crops and growing practices.

$CGDD_{Planting\ to\ EFC}$  values were increased for corn by 5%, and  $CGDD_{Planting\ to\ Terminate}$  was increased by about 20% relative to values that occurred during the specific year of lysimeter measurements. This was done to produce seasonal curves that reflected behavior of current corn cultivars.  $CGDD_{Planting\ to\ EFC}$  values were reduced for potatoes by 5% relative to values that occurred during the specific year of lysimeter measurements. This was done to produce seasonal curves that terminated naturally before killing frosts for more years across major potato growing locations in southern Idaho.  $CGDD_{Planting\ to\ EFC}$  values were reduced for spring grain by 10% and for winter grain by approximately 25% to shorten estimated season lengths to better match those currently observed across southern Idaho relative to that in the 1970s. The  $CGDD_{Planting\ to\ EFC}$

value for sugar beets was increased from 710 to 970°C-days to reflect current observation of growth rates for south-central Idaho. The CGDD<sub>Planting to Terminate</sub> value was increased from 1,843 to 2,600°C-days. Similar adjustments to CGDD<sub>Planting to Terminate</sub> were made by Huntington and Allen (2010).

$K_{cb}$  vs. NCGDD curves for crops harvested fresh are derived from the full  $K_{cb}$  curves in Table F-1 by specifying a smaller value for NCGDD<sub>Planting to Termination</sub>. For example, for fresh-harvested peas, snap beans, and sweet corn, Allen and Robison (2007) applied the  $K_{cb}$  curves for peas, dry beans, and sweet corn using NCGDD<sub>Planting to Termination</sub> values set to 1.6, 1.6, and 2.2, respectively. The  $K_{cb}$  value during postharvest periods for fresh-harvested crops was set to 0.1 for bare, dry soil surface conditions or to a higher value if some residual green vegetation was present following harvest.

Additional adjustment was made to the computed  $K_{cb}$  during fall periods for alfalfa, to account for effects of cold nighttime temperatures and occasional light, but nonkilling frosts. The adjustment reduced the value for  $K_{cb}$  following the first occurrence of a  $-3^{\circ}\text{C}$  in the fall by 0.005 each day following the  $-3^{\circ}\text{C}$  temperature. This reduced the value for  $K_{cb}$ , for example, by 0.10 by the 20th day in succession of having light frost. The killing frost temperature for alfalfa was  $-7^{\circ}\text{C}$ .

### Adjustments during Application of the Winter Wheat $K_{cb}$ Curve

The CGDD clock for winter wheat is assumed to begin on October 1. When applying the winter wheat crop during winter, some periodic adjustments to the cumulative CGDD may be needed to account for impacts of extremely cold weather that tend to retard growth for several days or may even burn the existing vegetation. These adjustments are based on observations of vegetation appearance during winter in southern Idaho and follow the following rules. In computing CGDD for fall, winter, and early spring periods for winter wheat, the following adjustments can be made. These apply to winter wheat only:

- If  $T_{min}$  is  $< -4^{\circ}\text{C}$  on a day, then GDD is set to zero for that day, regardless of the value for  $T_{max}$  or  $T_{mean}$ . This is done as a delay penalty to the growth rate of winter wheat on the day of the cold temperature. The occurrence of little or no growth on days where  $T_{min} < -4^{\circ}\text{C}$  is based on observations by Wright (personal communication, 2002).
- Whenever  $T_{min}$  is  $< -10^{\circ}\text{C}$  then the GDD for the following day, if greater than 0, is reduced by 5 GDD units. This reduction is enforced as a retardation penalty to the growth rate of winter wheat following a cold freeze. GDD on all days was limited to 0 or greater.

- Whenever  $T_{min}$  is  $< -25^{\circ}\text{C}$  and there is no documented snow cover present, 10% of the current crop canopy is assumed to suffer from frost burn and is no longer effective in facilitating growth or transpiration. This impact is enacted by reducing the CGDD that has been accumulated since October 1 by 10% for the day following the occurrence of  $-25^{\circ}\text{C}$ .

### Impact of Weather Station Aridity

Chapter 8 discusses the impact of local and regional dryness on increasing measured values for  $T_{max}$  and  $T_{min}$  in the absence of irrigation. In applications to Idaho National Weather Service Coop stations, Allen and Robison (2007) reduced values for  $T_{max}$  and  $T_{min}$  for some stations according to perceived station aridity effects using aridity ratings described by Allen et al. (1983). This adjustment was done prior to calculating CGDD, because the CGDD thresholds “expect” to have input from weather stations having relatively well-watered surroundings. The adjusted  $T_{max}$  and  $T_{min}$  were not used in computation of  $ET_r$ , but only for calculation of NCGDD and  $K_{cb}$  values.

## F.5 BEGINNINGS AND ENDS OF GROWING SEASONS

Automation of the estimation of planting dates and greenup dates for crops is required to enable the  $K_c$  computation process to operate for multiyear periods without manual intervention or specification of starting and ending dates for  $K_c$  curves. The greening (greenup) of perennial vegetation in spring can be strongly affected by short-term weather conditions, primarily by air temperature and to some degree by wetting events and general amounts of solar radiation. Strong correlation exists among air temperature, wetness, and cloudiness. In general, air temperature can be used as a predictor of when perennial vegetation begins to green up in spring. Planting of annual crops is strongly influenced by soil temperature at seed depth, and relationships have been established for limited crops. However, soil temperature is not commonly measured at cooperative NWS weather stations and is generally available at regional stations only. Therefore, 30-day average mean daily air temperature is often used as a surrogate for soil temperature, based on correlation between soil temperature and air temperature over an extended period.

A 30-day running average mean air temperature ( $T_{30}$ ) to estimate planting of annual crops was utilized by Allen and Robison (2007) for statewide estimation of  $ET_c$  for agricultural crops. Their development was based on lysimeter and cropping records at Kimberly, Idaho. The use of 30-day average temperature follows the SCS TR-21 (USDA 1967) where that publication listed typical mean monthly values for air temperature for planting and greenup of crops. However, some of those dates, for example,

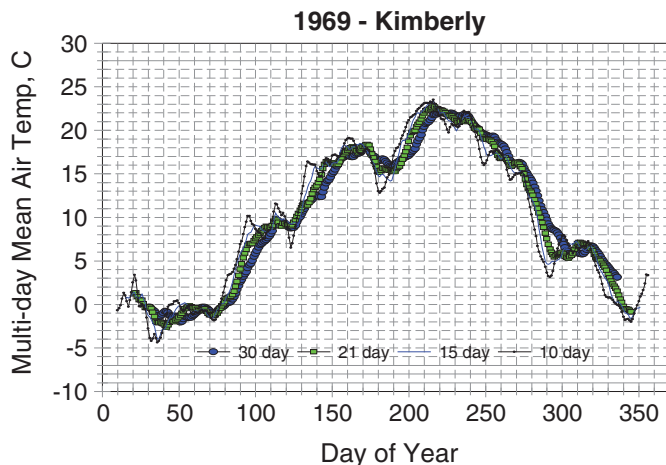


*Fig. F-4. 30-, 21-, 15-, and 10-day running average air temperature at Kimberly, Idaho, during 1969. The values are plotted on the last day within each average. Thirty-day running average temperature is plotted as the thick line*

for alfalfa greenup, do not estimate well for Idaho (Allen and Robison 2007). In addition, SCS TR-21  $T_{30}$  values are centered on the midpoint of the 30-day period, whereas the more logical method is to associate the  $T_{30}$  values with the date of the end of the 30-day period, because the  $T_{30}$  temperature during the previous 30 days is the temperature affecting the current soil temperature.

Figure F-4 shows variation in 30-day, 21-day, 15-day, and 10-day running average air temperature for year 1969 at Kimberly. The 30-day running averages are required to produce a generally monotonically increasing average temperature during the first half of the year in a temperate climate such as in southern Idaho. Temperature averages for shorter than 30-day periods that increase during warm periods but then decrease after that during cold periods can produce unrealistically large swings in planting or greenup estimates. Figure F-5 shows running temperature averages at Kimberly for a long-term period for the same four averaging periods. The  $T_{30}$  exhibited better monotonicism than the 21-day average, with shorter periods having more episodic decreases in average temperature.

Table F-2 shows values for  $T_{30}$  at Kimberly that are equivalent to the planting dates noted by Wright (1982) for the Kimberly lysimeter crops. The values for  $T_{30}$  were selected from the year each crop was planted. These dates were used as a general basis for  $T_{30}$  dates used around the state for estimating startups for growing seasons. Some adjustments were made based on field observations by Allen and Robison (2007) across southern Idaho. These temperatures are for dates at the end of the 30-day periods.

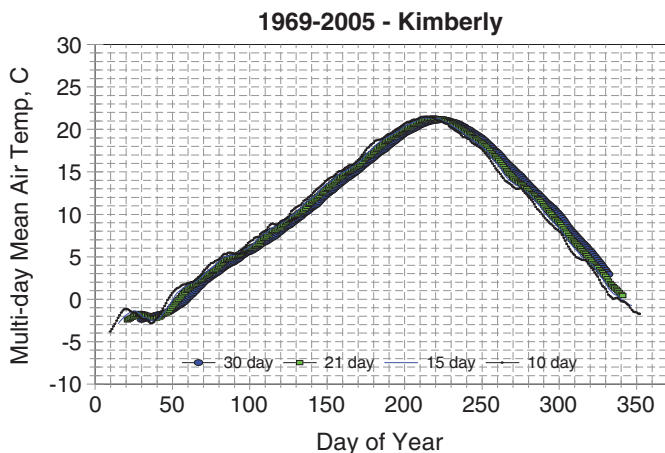


Fig. F-5. 30-, 21-, 15-, and 10-day running average air temperature at Kimberly, Idaho, averaged over the 1969–2005 period. Thirty-day running average temperature is plotted as the thick line

In computing  $T_{30}$  for various NWS stations, local aridity of the station can elevate air temperature measurements above that expected within an agricultural field. Therefore, the computed values for  $T_{30}$  at NWS stations were adjusted downward in cases where the weather station was considered to be arid using aridity ratings and adjustments used by Allen et al. (1983) in a previous consumptive use study. Examples of aridity ratings are listed in that publication. The amount of maximum adjustment by month is listed in Table H-6.

During the estimation of planting or greenup dates for crops and natural vegetation, a “no earlier than” and “no later than” date can be used to constrain estimated planting or greenup dates to realistic ranges based on expected behavior of farmers or requirements of the vegetation itself. For many crops this may be  $+/-40$  days from the mean date based on a long-term average temperature.

For alfalfa, better consistency in estimation of greenup in spring was found by Allen and Robison (2007) using cumulative growing degree days (CGDD) since January 1 rather than using  $T_{30}$ . This finding was based on observed greenup for lysimeter crops during 1969–1971 and on field observations by Allen and Robison (2007) between 1998 and 2005. CGDD =  $240^{\circ}\text{C}$ -days using a  $0^{\circ}\text{C}$  GDD basis was selected by Allen and Robison (2007) to estimate greenup based on a CGDD analysis of daily ET and leaf area and height development data for alfalfa for years 1969–1971 by Wright at Kimberly. No penalty was applied for cold weather during the winter period. CGDD =  $240^{\circ}\text{C}$ -days estimates an average greenup date

Table F-2. 30-Day Mean Air Temperature for the 30-Day Period Prior to the Observed Planting Dates for Kimberly, Idaho, Crops Associated with Wright (1982) Dates for Lysimeter Crops and Recommended  $T_{30}$  Values Based on the Lysimeter Data and Field Observations by Allen (Personal Communication) between 1999 and 2005

Crop	Year	Planting Date	30-day $T$ ( $^{\circ}\text{C}$ ) Ending on Date	Recomm. $T_{30}$ to Use, $^{\circ}\text{C}$
Barley or spring wheat	1979	4/1/79	4.8	4.7
Peas	1977	4/10/77	4.4	5
Sugar beets	1975	4/15/75	2.1	5 (8) <sup>a</sup>
Potatoes	1972	4/25/72	6.0	7
Corn	1976	5/5/76	7.9	8 (10) <sup>a</sup>
Beans	1973	5/22	12.5	12 (14) <sup>a</sup>
	1974			

<sup>a</sup>The value in parentheses was used in Allen and Robison (2007) calculations based on comparisons with satellite-based  $K_c$  determination using the METRIC energy balance model over the Kimberly, Idaho, area and based on other local observations of planting dates across southern Idaho.

of March 30 for alfalfa at Kimberly, Idaho, on average, over the 1969–2005 period, with a standard deviation of 11 days. Huntington and Allen (2010) used 300° C-days since January 1 and 880° C-days from greenup to first cutting for alfalfa in Nevada with good accuracy.

## F.6 ESTIMATION OF KILLING FROSTS

Killing frosts can terminate growing seasons prematurely for crops that grow late into fall or for crops that are sensitive to light frost. Temperatures for killing frosts can be assigned to crops based on literature and Internet searches and personal field observation. The following lists killing frost temperatures for various crops and land-use types applied by Allen and Robison (2007) in Idaho:

- $-7^{\circ}\text{C}$  for alfalfa.
- $-4^{\circ}\text{C}$  for field corn and silage corn and  $-5^{\circ}\text{C}$  for early sweet corn. No early frost death was estimated for late sweet corn, which was assumed to grow during a frost-free period until mechanical harvest. The  $-4$  and  $-5^{\circ}\text{C}$  temperatures are lower than commonly used for some corn varieties, but account for differences between temperatures recorded inside radiation shelters at observation height at

weather stations and actual temperature at the surface of a fully vegetated field of corn. The lower values may prevent unreasonably truncated growing seasons.

- $-2^{\circ}\text{C}$  for wetland vegetation (cattails commonly freeze at 0 or  $-1^{\circ}\text{C}$ ), however,  $-2^{\circ}\text{C}$  was used to account for differences between weather station environments and wetland environments that benefit from heat transfer from water surfaces.
- $-4^{\circ}\text{C}$  for sugar beets.
- $-2^{\circ}\text{C}$  for potatoes.
- $-2^{\circ}\text{C}$  for melons.
- $-3^{\circ}\text{C}$  for grapes.
- $-3^{\circ}\text{C}$  for asparagus.
- $-5^{\circ}\text{C}$  for turf and pasture.
- $-5^{\circ}\text{C}$  for leaf fall on fruit trees and poplars.
- $-4^{\circ}\text{C}$  for cottonwoods and  $-6^{\circ}\text{C}$  for willows.

## F.7 EXAMPLE OF LENGTHS OF GROWING SEASONS ESTIMATED ACROSS IDAHO

Figures F-6–F-9 show growing-season lengths averaged over multiyear periods estimated by Allen and Robison (2007) for 123 weather station locations throughout Idaho. Estimates were based on the  $T_{30}$  method for all

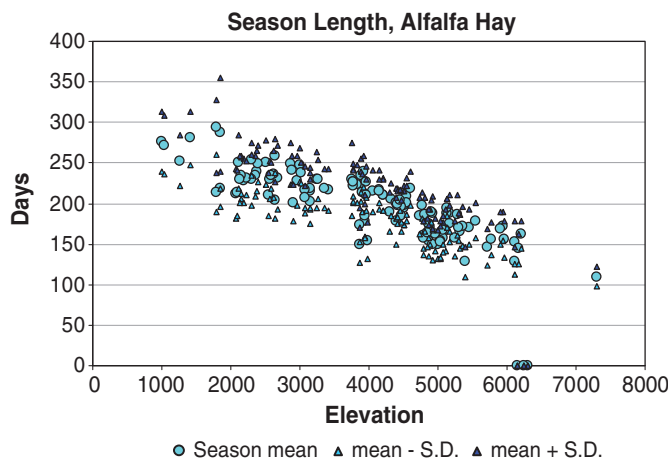


*Fig. F-6. Growing season lengths estimated for alfalfa hay plotted against location elevation in ft above mean sea level using CGDD for alfalfa for 123 locations in Idaho*

*Source: Data from Allen and Robison (2007)*

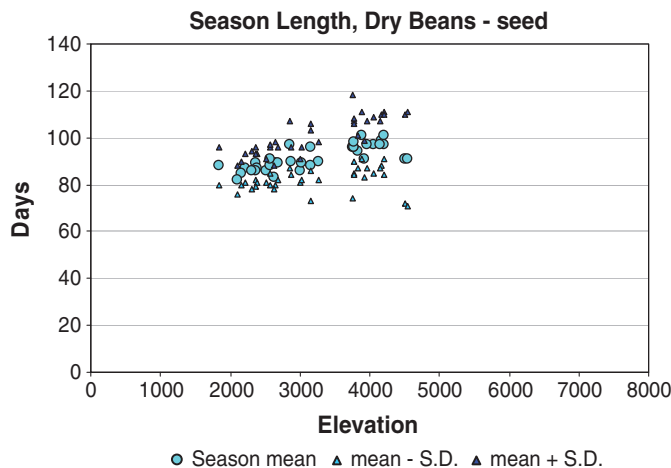


*Fig. F-7. Growing season lengths estimated for dry beans plotted against location elevation in ft above mean sea level using  $T_{30}$  for 50 locations in Idaho that cultivate dry beans*

Source: Data from Allen and Robison (2007)

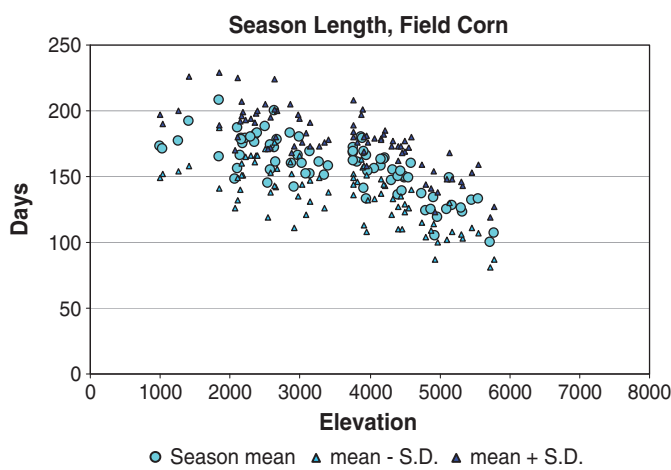


*Fig. F-8. Growing season lengths estimated for field corn plotted against location elevation in ft above mean sea level using  $T_{30}$  for 123 locations in Idaho*

Source: Data from Allen and Robison (2007)

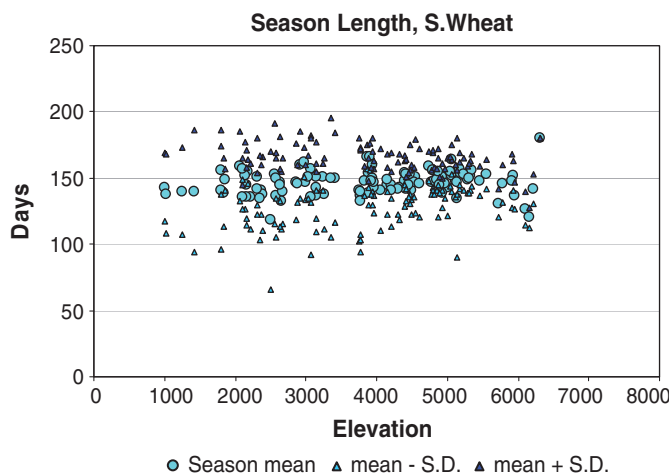


*Fig. F-9. Growing season lengths estimated for spring grain plotted against location elevation in ft above mean sea level using  $T_{30}$  for 123 locations in Idaho*  
Source: Data from Allen and Robison (2007)

crops, except alfalfa, which used 240 CGDD since January 1 with a  $T_{base} = 0^{\circ}\text{C}$ . Mean and mean plus/minus one standard deviation (over the period of record) are plotted vs. the elevation of the location. For alfalfa and field corn, season length has strong negative correlation with elevation due to the impact of elevation on air temperature. This affects both the start of the growing season and the duration. The growing season increased with elevation for dry beans, due to their somewhat late planting date in late May and the longer duration required at higher elevation due to cooler air temperature. Season duration was somewhat constant for spring wheat. The figures illustrate the outcome of basing growing season start and growing season duration on air temperature.

This page intentionally left blank

## APPENDIX G

# DOCUMENTATION FOR CROP COEFFICIENT AND ET DATA REPORTING AND DETERMINATION OF ET FROM REMOTE SENSING

### G.1 INTRODUCTION

ET information is frequently used as a foundation for court determinations of injury among water users, for parameterization of important hydrologic and water resources planning and operations models, for operating weather and climate change forecasting models, and for water management and allocation in water-scarce regions, including the partitioning of water resources among states and nations. All too frequently the documentation of ET information used in these processes is deficient or uncertain, with too little descriptive information in the reporting to facilitate judgment of its quality.

Over the past decades increasing numbers of publications have reported measured evapotranspiration (ET) and crop coefficients ( $K_c$ ). Publications include information on cereal crops; fiber crops such as cotton; forage crops like alfalfa; fruit tree crops like olives, apricots, peaches, and pecans; grapes; cool- and warm-season grasses; turfgrasses; legume crops like beans; oil crops like sunflower; tropical fruit crops like banana, cassava, and coffee; and various vegetable crops. In addition, there have been coefficients for natural vegetation such as grasslands and wet vegetation such as cattails, grasses, and reeds. Some of these publications have described the calibration of models and systems for calculating crop coefficients. Many publications include coefficients for multiple crops as a function of ground cover, for example, Grattan et al. (1998), Parkes et al. (2005), Wang et al. (2007), and Allen and Pereira (2009).

The crop coefficient literature will continue to grow. Adherence to physics, careful measurement, quality control of data, and reporting of details will be important. In general, future  $K_c$  values are not expected to

change substantially, because ET relative to reference ET is strongly tied to vegetation amount. However, some variation in new  $K_c$  values is expected as a result of changes in crop varieties, agronomic practices, planting densities, and genetic modification to leaf structure to reduce vapor loss and ET.

ET data and ET models or model calibrations reported in the literature for even “well-behaved” agricultural systems can contain serious biases caused by flaws in experimental design, measurement equipment, vegetation management, data reduction, model parameterization, and interpretation of results. Therefore, it is essential that reporting of ET measurements and related products such as crop coefficients or parameterized models contain sufficient description of the procedures used to measure and derive ET information so that readers can be aware of potential flaws or shortcomings in data measurement and can be alerted to the need to question representativeness of ET presentations.

Because of the wide range of complexities in making ET and associated weather measurements and the abundance of opportunities for biases to enter ET and weather data sets, users of ET literature need sufficient information reported in articles on ET to assess the likelihood for opportunities of bias or error to enter reported data and sufficient information to examine or recreate the reported data using some type of ET model. This is currently often not the case, and many journal articles do not contain sufficient information to enable readers to gauge accuracies and representativeness of information.

This appendix discusses upper limits to be expected for crop coefficients that supplements Chapter 10; contains a summary of precautions, recommendations, and literature associated with sap flow and remote sensing-based determination of ET and  $K_c$  to supplement Chapter 7; and ends with a section listing detailed types of documentation that should accompany publication of ET and  $K_c$  data that are useful when applying or interpreting reported values.

## G.2 UPPER LIMITS ON ET AND CROP COEFFICIENTS

Chapters 7 and 10 discuss maximum expected limits on ET and crop coefficients. That discussion is expanded here. Evaporation constitutes the conversion of liquid water to vapor and as a result requires substantial amounts of energy. The availability of energy incident to vegetation places a constraint on the potential evaporation rate and forces adherence to the law of conservation of energy. ET rates that exceed available radiation energy ( $R_n$ ) at the surface less the energy conducted as sensible heat to the ground ( $G$ ), i.e.,  $R_n - G$ , must essentially extract that additional energy from the atmosphere via downward (negative) sensible heat flux ( $H$ ) via convective transfer through the equilibrium boundary layer of air above

the surface. Because increasingly negative  $H$  creates increasingly stronger density-induced stability to the equilibrium boundary layer, it becomes increasingly difficult to transport the required  $H$  to the surface to support the conversion to ET, especially without strong mechanical mixing brought about by high wind speed (Brutsaert 1982; de Bruin et al. 2005). As a result there is an upper limit on ET, even under extreme advection, caused by limitations on aerodynamic transport and on equilibrium forces above a vegetation canopy coupled with surface resistance. That upper limit on ET is relatively well represented by the tall (alfalfa) reference that has been defined by ASCE (2005) using a parameterized Penman-Monteith equation (Allen et al. 1989, 2007c).

The upper limit on potential crop evapotranspiration ( $ET_c$ ) is readily approximated by comparing against the widely used reference ET ( $ET_{ref}$ ) through a crop coefficient ( $K_c$ ).  $ET_{ref}$  may refer to two types of reference crops, clipped, cool-season grass or tall alfalfa (whose common symbols are  $ET_o$  and  $ET_r$ , respectively), thus crop coefficients may be expressed in relation to clipped, cool-season grass as more often used (Allen et al. 1998, 2007c) or to alfalfa, for which the symbol  $K_{cr}$  is adopted (ASCE 2005; Allen et al. 2007c). An alternative and synonymous expression for  $K_{cr}$  can be used, which is the term alfalfa reference ET fraction,  $ET_r F$  (ASCE 2005; Allen et al. 2007b).

The terms  $K_c$  and  $ET_r F$  are defined as the ratio of ET for a specific surface,  $ET_c$ , to the ET of the standard reference surface,  $ET_{ref}$ , and are discussed in detail in Chapter 10. An expression for  $K_c$  in terms of ratios of the Penman-Monteith equation (Monteith 1965) applied to the crop and to the reference crop is given as Eq. (10-1). That equation illustrates that the value for  $K_c$  (or  $ET_r F$ ) depends on the relative roughness, leaf area, and albedo (affecting  $R_n$ ) of the actual vegetative surface in relation to the same characteristics for the grass or alfalfa reference surface. Clearly, the more similar a vegetative cover is to the reference condition, especially at full cover, the closer the value of  $K_c$  (or  $ET_r F$ ) will be to 1.0 and the less variation in the value of  $K_c$  (or  $ET_r F$ ) with changing weather conditions (see discussions in Pereira et al. 1999a and ASCE-EWRI 2005).

Implicit to Eq. (10-1) is the consideration of impacts that differences between  $ET_c$  and  $ET_{ref}$  have on conditioning of the equilibrium boundary layer above the surfaces and on conditioning of the surfaces themselves. This conditioning modifies levels of  $e_z^o$ ,  $e_z$ ,  $\Delta$ , and wind speed caused by differences in cooling and humidification brought about by rates of  $ET_c$  being different from  $ET_{ref}$ . This conditioning generally creates a negative feedback effect on the value for  $K_c$  (or  $ET_r F$ ).

The tall (alfalfa) reference and its parameterizations in the PM equation tend to represent sufficiently low surface resistance and sufficiently high aerodynamic roughness to approximate near maximum rates of ET expected from large expanses of well-watered vegetation cover, even

under conditions of strong regional advection (Allen et al. 1989; Pereira et al. 1999a). Therefore, alfalfa reference-based crop coefficients tend toward a maximum of 1.0, and an expanse of tall, well-watered vegetation that fully covers the ground will approach the maximum conversion of available energy into latent heat flux ( $\lambda E$ ), and the maximum ratio of  $\lambda E$  for any tall vegetation to alfalfa  $\lambda E$  will be near 1.0. This observation is borne out in viewing the maximum values for  $K_c$  reported by Wright (1982) for nine annual crops in southern Idaho, where none of Wright's  $K_c$ s, when based on the standardized alfalfa reference (Allen and Wright 2006), exceeded 1.03 (see Table E-1 and Figure F-1). In the case of grass reference  $ET_o$ , values for  $K_c$  may approach 1.3 for tall, dense crops under windy arid and semiarid conditions because of the smoother roughness and small leaf-area index of the grass reference as compared with the alfalfa reference.

In humid climates, ET is dominated more by net radiation availability and less by aerodynamics and vapor deficit. Because the grass and alfalfa reference crops have about the same albedo as many crops at full cover, their energy, heat, and vapor transfer rates and thus ET and  $K_c$  rates are more similar in humid and semihumid climates than under arid conditions. Based on total energy constraints, under humid conditions, where a majority of energy for the ET process is from net radiation and regional advection is usually minor, the  $K_c$  generally cannot exceed about 1.0 to 1.05 relative to the alfalfa reference for large expanses of similar vegetation and about 1.2 to 1.3 relative to the grass reference. In arid and semiarid climates, the constraint of  $K_c \sim 1.0$  to 1.1 for the alfalfa reference holds because of the tendency toward similarity in aerodynamic exchange and leaf area between even tall vegetation and the alfalfa reference. In the case of the grass reference, however, differences in aerodynamic and surface conductances, coupled with potentially strong regional advection, may cause  $K_c$  based on the grass reference in arid and semiarid climates to be as high as 1.3 to exceptionally high values of 1.4 for tall, well-watered vegetation.

H. L. Penman's comment (Penman 1948) that crop evaporation should never exceed evaporation from an open water surface may be somewhat extreme; however, the exceedance of measured or reported  $K_c$  above about 1.0 for alfalfa reference or 1.2 for grass reference in subhumid regions or above about 1.0 for alfalfa reference or about 1.3 to 1.4 for grass reference in arid regions should give cause for intense scrutiny of the ET measurements, the weather data used to calculate  $ET_{ref}$ , and the data-processing procedure. Exceeding those values should also give cause for rejecting the data.

Limiting  $K_c$  to approximately 1.0 for an alfalfa reference base or 1.2 for a grass reference base in humid climates and to approximately 1.0 for an alfalfa reference base or 1.2 to 1.4 for a grass reference base in arid climates applies to large expanses of vegetation (>200 m diameter) and is significant and important when evaluating field measurements of ET. Measuring ET from small expanses of vegetation should be avoided when the objective of

the ET measurement is to represent general conditions of crop ET for medium to large (say  $> 200$  m) fields or clusters of small fields. When ET is measured from small expanses of vegetation, the internal boundary layer above the vegetation may not be in equilibrium with the surface and may not have developed up to the height of any meteorological or flux instrumentation. In addition, small expanses of tall vegetation surrounded by shorter cover cause a “clothesline effect” where the interchange between air and vegetation is much more efficient than with the logarithmic type of boundary layer established over large fields and that is assumed in essentially all aerodynamically based ET equations. In these cases, ET from the isolated stands, on a per unit area basis, may be significantly greater than the corresponding  $ET_{ref}$  computation and will not represent large expanses. These situations are discussed in more detail in Chapter 10.

When calculating reference ET, the global standardizations of ASCE and FAO are highly recommended for consistency and transferability of results and derived coefficients (Allen et al. 1998, 2006; ASCE 2005).

### G.3 MORE ON ET MEASUREMENT

In many agricultural systems, plant density, height, vigor, and water availability are generally uniform, and the application of estimation algorithms and the measurement of ET can be straightforward, although they are still not without substantial challenge. In the case of nonagricultural systems such as forest, desert, and riparian systems, the heterogeneous nature of vegetation, terrain, soils, and water availability make surface energy and aerodynamic processes highly variable and poorly defined. This is especially true, for example, for riparian systems such as cottonwood, tamarisk, and Russian olive in semiarid regions that can have widely varying vegetation density, tree height, stand extent, and availability of water. Most information and estimates of water consumption by forest and riparian systems come from in-place measurements that have a strong empirical and local character.

Chapter 7 describes requirements and considerations for technique, equipment, and data handling when determining ET or  $K_c$  from soil water balance, lysimeters, Bowen ratio, and eddy covariance methods. Besides those four common and important methods, other means to estimate  $K_c$  include use of sap flow methods and remote sensing. The following sections briefly describe the merits and challenges of those additional methods and complement the information in Chapters 7 and 10. Additional general information on sap flow systems and expected error is given in Shackel et al. (1992), Ewers and Oren (2000), Nadezhina et al. (2002), Green et al. (2003), Steppe et al. (2010), and Allen et al. (2011c). Some material in the following section was contributed by E. Glenn (2010, personal communication).

## Sap Flow Methods

Sap flow methods generally introduce a source of low-grade heat into the trunk or branch of a plant and measure the flow of water in the xylem by either the velocity of a heat pulse carried away from the heat source in the transpiration stream or by the dissipation of heat energy in the stem due to convection in the transpiration stream. These methods do not measure the direct evaporation component of ET, but only the plant transpiration component. This can be an advantage if the goal is to measure plant water use, but a disadvantage if the goal is to project total evaporation over a heterogeneous surface. Three main methods are employed: the heat pulse-sap velocity method (Green and Clothier 1988; Green et al. 2003); the Granier heat dissipation method (Granier 1985, 1987); and the tissue heat balance method (Sakuratani 1981; Valancogne and Nasr 1989, 1993; Kjelgaard et al. 1997). Swanson (1994) suggested that no one set of theory and instrumentation is applicable to all sizes or species of trees. As outlined below, each method has important scaling limitations that need to be considered when interpreting ET rates based on sap flow methods.

Sap flow methods may require scaling from branches or whole plants to stands of plants to provide wide area estimates of ET. Granier sensor studies typically use a stem census method for scaling, in which the cross-sectional area of gauged trunks is related to the density and cross-sectional area of trees in the area of interest (Hultine et al. 2010). Stem census methods can be difficult to apply to natural stands of plants, especially when the plants present myriad branches of different sizes (Hultine et al. 2010), as in the case of riparian systems such as tamarisk and deciduous forests. Tissue heat balance methods require a further scaling step, to scale from branches to whole plants and then to stands of plants. Leaves or leaf areas on gauged branches can be harvested and measured, and scaling can then be accomplished by measuring LAI in plant stands of interest (e.g., Nagler et al. 2009). However, optical methods for estimating LAI must be calibrated by leaf harvesting, because many plant stands violate the geometric assumptions built into the optical measurement devices. For example, the commonly used LI-COR LAI 2000 measurements are based on the amount of light transmitted through the canopy at five different angles as measured by a fish-eye type lens system. Assuming a uniform overhead canopy in thickness and leaf density, LAI can be calculated from Beer's law, by calculating a relative path length of light through the canopy at each view angle and combining the estimates to get a single estimate of LAI. Multiple view angles are needed to account for leaf and branch angle effects on LAI. Unfortunately, individual tree canopies, or irregular canopies with gaps between plants, seriously violate the assumption of a uniform canopy, and there is no simple way to correct the instrument readings except by combining them with leaf harvest methods, a step that

is often omitted. Nagler et al. (2004) found that LI-COR LAI 2000 measurements of LAI on individual cottonwood and willow canopies were low by a factor of three when compared with leaf-harvesting methods.

Scaling ET from individual limbs to full plants and from full plants to large areas is uncertain due to differences among tree structure, radiation interception per tree, and water availability. Shaded limbs tend to have lower rates of transpiration than sunlit limbs, and limbs lower in a canopy tend to have less aerodynamic exchange of energy and vapor. Besides scaling of transpiration from specific species of trees, additional uncertainty in areal ET is caused by stands of multiple species, presence of understory vegetation, and evaporation from bare soil. Mackay et al. (2002) used a two-source evaporation model with sap flow data to produce total ET. Users should consider that large uncertainties can exist when determining transpiration using sap flow methods and determining accurate, quantitative ET estimates.

### Remote Sensing Energy Balance to Determine Crop Coefficients

New techniques using satellite imagery have been developed since about 1990 to estimate E and ET from large areas using energy balance (Bastiaanssen et al. 1998a, b, 2005; Kustas and Norman 1999; Moran 2000; Kustas et al. 2003; Allen et al. 2007a, b; Kilic et al. 2011, 2012). The emerging technology of energy balance by satellite shows promise for application over large areas and over a wide range of vegetation types and water availability. The approach has been used to quantify and illustrate population variance in ET from the same vegetation type and to refine  $K_c$  or  $ET_F$  curves (Tasumi et al. 2005a; Anderson et al. 1997, 2005; Kustas et al. 2003; Kustas and Norman 1999; Li et al. 2005; Norman et al. 1995, 2000, 2003; Allen et al. 2007a, b; Tasumi and Allen 2007; Singh and Irmak 2009). Remotely sensed energy balance techniques are useful for identifying areas experiencing water stress and corresponding reductions in ET and to populate hydrologic models (Irmak and Kamble 2009; Kamble and Irmak 2009). Users of this information must bear in mind, however, that satellite-based ET data are simply retrievals and rely on best estimates of aerodynamic and radiative processes as viewed from space, and cannot be considered to be "measurements." Estimation by remotely sensed energy balance should be expected to adhere to the same limitations and physics as other measurement methods. Nevertheless, remotely sensed energy balance is increasing in use to estimate  $K_c$  and ET over large areas.

Some "operational" satellite-based energy balance models such as SEBAL (Bastiaanssen et al. 1998a, b, 2005) and METRIC (Allen et al. 2007a, b; Kilic et al. 2011) employ an internal calibration technique referred to as CIMEC (calibration using inverse modeling at extreme conditions)

([Allen et al. 2008](#)). The CIMEC technique involves the inverse calibration of the energy balance process via the sensible heat flux,  $H$ , computed by specifying ET, and thus the energy balance equation, at two extreme conditions (dry and wet) in the satellite image. ET is estimated at the two conditions based on knowledge of available energy and surface conditions, usually with ties to ground-based weather data. The outcome of the CIMEC calibration is to imbed all systematic estimation biases in  $R_n$ ,  $G$ , and other intermediate components that are endemic to nearly all satellite-based calculations into the estimate and calibration of  $H$ . These biases are in turn removed when ET is computed for the millions of pixels in a typical image as  $ET = \lambda E / (\lambda \rho_w) = (R_n - G - H) / (\lambda \rho_w)$ , where the calculation of  $H$  is a function of surface temperature. Other more regional-scale models such as the ALEXI model ([Anderson et al. 2005](#)) use inversion based on radiosonde profilings over time to estimate large-scale heat flux and evaporation. Ordinarily, surface energy balance models that do not apply endpoint calibration will be affected by the various biases that can plague satellite-based component estimation.

Advantages of remote sensing-based energy balance (RSEB) models for determining  $K_c$  and ET include

- The energy balance yields actual ET that may be lower than potential ET due to water and other stresses;
- The process covers large areas, enabling sampling and integration over diverse areas;
- RSEB procedures are generally more economic than point measurements;
- RSEB procedures can be used to extend or extrapolate high-intensity point measurements of ET to large areas;
- Products can have high spatial resolution (30 m for satellite, 2 to 5 m for aerial); and
- RSEB procedures are valuable for determining spatial variation in ET for highly variable systems such as riparian or forest.

Disadvantages of remote sensing-based energy balance models include

- Time gaps exist between estimates of ET for many satellite systems, especially those having high spatial resolution, where images are obtained only periodically for a specific location, for example, every 16 days for a Landsat satellite; therefore, effects of evaporation from precipitation events occurring in between satellite overpasses may be missed, or processing of “wet” images from recent precipitation events may bias seasonal estimates and must be mitigated ([Allen et al. 2007b](#));
- Data collection using aerial platforms including unmanned aerial vehicles can be expensive;

- Satellite pixels over narrow vegetation systems such as riparian systems and small agricultural fields may overlay broad mixtures of vegetation types and densities so that surface temperature signals are mixed and the ET retrievals are difficult to interpret;
- Uncertainty in estimating aerodynamic components and surface temperature retrievals may require “inversion” techniques to calibrate;
- Most remote sensing energy balance processes assume 1-D aerodynamics:
  - This may not hold true for narrow, tall systems such as riparian:
    - Aerodynamic exchanges in narrow vegetation systems may be three-dimensional and therefore flow lines are poorly behaved;
    - Klaassen et al. (2002) found that horizontal penetration of flow lines and heat transfer into the leading edge of a forest canopy increased available energy by 15% over the first 400 m of canopy;
    - Klaassen and Sogachev (2006) concluded that flux measurements over riparian systems should be corrected for impacts of horizontal variations in turbulence downwind of the edge; and
    - The problem of narrowness of stands and edge effects affects nearly all measurement systems that use aerodynamics or energy balance (EC, scintillometry, remote sensing based EB), even sap flow due to change in transpiration with distance into the system;
  - Satellite view angles can affect reflectance (albedo) and surface temperature estimates:
    - The Landsat satellites have a view angle that is nearly nadir (directly overhead);
    - The MODIS satellites have a large scan angle, with the view angle varying from -55 to +55 degrees; this viewing angle variation affects reflectance measurements and requires correction;
    - The satellite (and aerial) measurement of reflectance is “bidirectional,” whereas the reflectance needed in energy balance (for  $R_n$ ) is directional-hemispherical;
    - Bidirectional reflectance may be lower than directional-hemispherical reflectance for tall canopies containing shadows, especially at lower sun angles and for nadir looking satellites;
    - Potential bias in nadir-derived albedo and surface temperature for tall canopies may cause overstatement of ET by 5 to 10% due to shadows and nadir views deep into canopies (this impact needs further investigation);

- Potential biases exist in retrieved albedo and surface temperature ( $T_s$ ) from satellite and airborne systems, making CIMEC or other bias-correcting calibration methods necessary.

### Satellite-Based ET Using Vegetation Indices

Satellite-based or ground-based energy balance methods generally require extensive time investment and require learned skill sets. The energy balance products can be used, however, to calibrate more simple methods that utilize general vegetation indices (VI) to estimate crop coefficients (i.e.,  $K_c$  or  $ET_rF$ ) (Tasumi et al. 2005a; Tasumi and Allen 2007; Singh and Irmak 2009). The estimate of  $K_c$  from VI is possible because of the generally close correspondence between vegetation amount and transpiration, where, as vegetation cover increases, leaf area increases and transpiration increases (reviewed in Glenn et al. 2007). Challenges with VI-based methods are estimating evaporation from bare soil following precipitation events and estimating reduced ET associated with soil water shortage, because these processes are not adequately reflected in the VI.

A common VI is the normalized difference vegetation index (NDVI) that is estimated from two shortwave bands typically measured by satellites: the red band ( $\sim 0.6\text{--}0.7 \mu\text{m}$ ) and the near infrared band ( $\sim 0.7\text{--}1.3 \mu\text{m}$ ). A linear relationship between the NDVI and the crop coefficient  $K_c$  was introduced by Heilman et al. (1982) and theoretically established by Choudhury et al. (1994). The resulting equation is

$$K_{co} = 1.25NDVI + 0.2 \quad (\text{G-1})$$

where  $K_{co}$  represents the grass-based crop coefficient. Tasumi et al. (2005b) and Tasumi and Allen (2007) found a similar relationship for eight major irrigated crops in Idaho, as did Singh and Irmak (2009) for irrigated corn and soybeans in Nebraska, which, when expressed for the alfalfa reference is approximately

$$K_{cr} = ET_rF = 1.25NDVI \quad (\text{G-2})$$

Generally, NDVI values from different satellites show close correlation (Calera-Belmonte et al. 2005). However, some differences occur due to differences in bandwidths. The degree and type of atmospheric correction of the image can also have an impact.

It is important to establish, with  $K_c$  vs. NDVI or other VI relationships, whether the relationships are to represent the average ET that includes averaged amounts of evaporation from the soil surface caused by precipitation and irrigation or are to represent a basal  $K_{cb}$  condition where the VI-based relationship is established to represent conditions

where the soil surface is dry enough to reduce evaporation from the soil surface to relatively low levels, when compared to transpiration, but transpiration still occurs (Allen et al. 2005b). The basal  $K_{cb}$  vs. NDVI relationship is more consistent because transpiration has a much closer association with vegetation amount than does evaporation from soil. When the  $K_{cb}$  vs. NDVI relationship is used, then estimates for soil evaporation are determined separately and added to produce total evaporation (Burnett et al. 2008). Allen et al. (2011b) showed that NDVI was a better basis for the  $K_c$  vs. VI relationship than was the soil-adjusted vegetation index (SAVI) because NDVI tends to reach a maximum value (e.g., "saturate") at about the same time as does  $K_c$ , which is at about LAI of 3.0, whereas SAVI tends to continue to increase with increasing LAI beyond 3.0.

Advantages of VI-based crop coefficient ( $K_c$  and  $K_{cb}$ ) estimation are

- Quick analyses can be made by midlevel technicians;
- Large areas can be covered;
- Relationships can be calibrated using satellite-based energy balance; and
- Spatial resolution can be high, especially if aerial imagery is used.

Disadvantages of VI-based  $K_c$  and  $K_{cb}$  estimation are

- Relationships may vary with type of vegetation:
  - Stomatal control, and thus  $K_c$  or  $K_{cb}$  vs. VI relationships, can vary among types of vegetation. Therefore, single  $K_c$  and  $K_{cb}$  vs. VI or ET vs. greenness indices can vary and have large uncertainty; and
  - Trees, when short of water can exhibit more stomatal control than agricultural crops and therefore cause a shift in the  $K_c$  vs. VI relationship;
- Relationships tend to overestimate ET during conditions of acute water shortage because of time lag in adjustment in vegetation amount (NDVI) by the vegetation following reduced stomatal conductance and water use;
- Estimation of the evaporation (from soil) component is less certain than the transpiration component because of the lack of a direct relationship with vegetation amount;
- Quality estimates of reference ET are required to transform  $K_c$  into ET where the reference ET calculation requires quality weather data; and
- VIs may not identify or quantify multistoried canopies and their effects on total ET, especially for more dense vegetation.

Nagler et al. (2009) found a reasonable correspondence between saltcedar ET estimated by sap flow sensors and satellite estimates based on a VI at the Cibola National Wildlife Refuge on the lower Colorado River.

However, at any given measurement station, ground measurements showed high variability of ET due in part to differences in stomatal conductance due to stress effects, which were not captured in the remote sensing estimates.

#### G.4 CROP COEFFICIENT AND ET DATA REPORTING

ET information available in the literature is often deficient in regard to documentation necessary to judge its quality and representativeness. Allen et al. (2011b) describe desired documentation of published evapotranspiration (ET) information, including description of field procedures, instrumentation, data filtering, model parameterization, and site review. This information is important to readers to assist with discerning the accuracy and representativeness of reported data and ET parameters, including derived crop coefficients. Documentation should include a description of the vegetation, its aerodynamic fetch, water management and background soil moisture, types of equipment and calibration checks, photographs of the measured vegetation/equipment combinations, and independent assessments of measured ET using models or other means. Documentation and assessment should include a description of, or reference to, all weather-recording equipment and parameters, including the vegetation and water management environment of the weather station. Suggestions are given for documentation describing the primary types of ET measuring systems including recommended independent testing.

In addition to documentation on ET measurements and associated weather data that may be used in models, documentation should describe the nature of the vegetation measured, including type, variety, density, age, health, water availability, timing of development and senescence, height, fraction of ground cover or leaf-area index, type of irrigation, if practiced, and other features useful to users of the data or users of derived crop coefficients and other ET parameters. Sufficient description of canopy architecture is needed to assist modelers in setting model parameters and, more simply, to compare against findings from similar studies. In the case of crop coefficients, the documentation should describe whether the reported crop coefficient(s) represent potential (i.e., well-watered and nonstressed) conditions and whether they are intended to represent the basal (ET from vegetation having a mostly dry soil surface condition) or an average crop coefficient condition (Allen et al. 1998, 2005d, 2007c).

Authors of ET data and model results are encouraged to apply careful study and critique of the measurement method and application procedures prior to publication and to compare ET data or derived  $K_c$ s against ET estimates derived from more or less standard models and/or prior

Table G-1. Recommendations on Essential and Desired Information Reporting with Measured Evapotranspiration and Water Consumption Data, Crop Coefficients, or Resistance-Based ET Methods

Essential	Desired
All Systems	
Vegetation	<ul style="list-style-type: none"> <li>• Vegetation variety(s)</li> <li>• Dates of crop stages or phenological stages           <ul style="list-style-type: none"> <li>◦ planting or greenup</li> <li>◦ full cover or effective cover or maximum cover</li> <li>◦ flowering</li> <li>◦ start of senescence</li> <li>◦ harvest, or maturation, or end of season</li> </ul> </li> <li>• Plant density</li> <li>• Plant spacing along row (if agricultural)</li> <li>• Spacing between plant rows</li> <li>• Measured or estimated vegetation height vs. time</li> <li>• Measured or estimated fraction of ground cover vs. time</li> <li>• Size of field (or stand of trees) containing the measurement system</li> <li>• Location of measurement system relative to the field, system, or expanse of vegetation measured</li> <li>• Size of general agricultural area (or other vegetation system) surrounding the measurement field</li> <li>• Mulch type, density, and coverage (if present)</li> </ul>

(Continued)

Table G-1. Recommendations on Essential and Desired Information Reporting with Measured Evapotranspiration and Water Consumption Data, Crop Coefficients, or Resistance-Based ET Methods (*Continued*)

Essential	Desired
<p><i>If an orchard, tree crop, or forest, additional information includes</i></p> <ul style="list-style-type: none"> <li>• Age of trees</li> <li>• Size of trees, height, and crown diameter</li> <li>• Tree spacing along rows and between rows</li> <li>• Ground covered by mulch:           <ul style="list-style-type: none"> <li>◦ type of mulch</li> <li>◦ density</li> <li>◦ coverage</li> </ul> </li> <li>• Ground covered by active substory vegetation           <ul style="list-style-type: none"> <li>◦ understory vegetation height</li> <li>◦ density</li> <li>◦ tillage and ground cover management</li> <li>◦ soil moisture management</li> </ul> </li> </ul> <p><i>Supporting Meteorological Data</i></p> <ul style="list-style-type: none"> <li>• Reference ET method, if used, and procedures for calculation (can be a citation of published work)</li> <li>• Description of supporting meteorological data for calculating ET, including solar radiation, net radiation, soil heat flux, air temperature, surface temperature, soil temperature, vapor pressure, wind speed</li> <li>• Summary of primary weather data relative to the experimental period</li> </ul>	<ul style="list-style-type: none"> <li>• Photos of           <ul style="list-style-type: none"> <li>◦ individual trees</li> <li>◦ community of trees (can be placed with metadata)</li> </ul> </li> <li>• Pruning</li> <li>• Description of uniformity of trees</li> <li>• Dates for treatments that may change ground cover by the trees           <ul style="list-style-type: none"> <li>◦ leaf out</li> <li>◦ leaf fall</li> </ul> </li> </ul> <ul style="list-style-type: none"> <li>• Description of other weather or micrometeorological equipment</li> <li>• Description of local climate for a period of several years</li> <li>• Description of weather data source (and URL if from or on a public website)</li> </ul>

- Location(s) of meteorological system/sensors
- Size of weather station area and vegetation type and maintenance of station
- Soil moisture management of the weather station
- Degree and type of QA/QC applied, including calibration adjustment and procedures for filling missing data

*Soil and Irrigation Description*

- Soil type and layering or National Resources Conservation Service (NRCS) soil taxonomy ([USDA 1999](#))
- Irrigation type (method and system)
- Irrigation frequency and duration
- Irrigation application depth per irrigation and total irrigation treatments (if applied) with description of
  - nonstressed treatments
  - stressed treatments in relation to non-stressed
  - relative adequacy of soil water in stressed or nonstressed treatments
- Whether incidental water stress occurred
- Method for measuring irrigation input (depth)
- Fraction of surface wetted by irrigation
- Description of treatment of rain events (measurement of rain, inclusion of the rainy day)
- Method for soil water measurement

Conservation Service (NRCS) soil taxonomy ([USDA 1999](#))

- Soil information (by layer)
  - textural characteristics
  - Field capacity and wilting point
  - Soil bulk density
  - Soil permeability (or NRCS soil taxonomy) ([USDA 1999](#))
- Irrigation
  - equipment
  - factors affecting performance
  - application uniformity
  - system for delivery of water to the fields
- Fertility
  - what fertilizers were applied
  - rates and timing of applications
  - how fertilizer rates were determined

(Continued)

Table G-1. Recommendations on Essential and Desired Information Reporting with Measured Evapotranspiration and Water Consumption Data, Crop Coefficients, or Resistance-Based ET Methods (*Continued*)

Essential	Desired
	<ul style="list-style-type: none"> <li>• Drainage management</li> <li>• Tillage system type</li> <li>• Salinity levels and management (if impacting ET)</li> </ul> <p><i>Crop Coefficient Information</i></p> <ul style="list-style-type: none"> <li>• If <math>K_c</math> is reported, provide basal and/or averaged <math>K_c</math>s based on the standardized reference ET</li> <li>• If <math>K_c</math> is reported, indicate whether it should represent well-watered conditions</li> <li>• Refer to reported <math>K_c</math> as <math>K_{c,adj}</math> when some type of environmental stress had reduced the reported value</li> <li>• Comparison of derived <math>K_c</math> to literature values with comments on <ul style="list-style-type: none"> <li>◦ if grass-reference based, the agreement or lack of agreement for <math>K_c</math> for full cover conditions to the expected range of 1.1–1.3</li> <li>◦ if alfalfa-reference based, the agreement or lack of agreement for <math>K_c</math> for nearly full cover conditions to the expected range of 0.95–1.0</li> </ul> </li> </ul>

- specific explanations of values exceeding the above ranges, especially if  $K_c$  values are to represent agricultural field settings
  - If grass-reference based, co-reporting of midseason  $K_c$  values based on the standard FAO climate of  $RH_{min} = 45\%$  and wind speed at 2-m height =  $2 \text{ ms}^{-1}$ . (see [Allen et al. 1998](#), Eq. 62, [Allen et al. 2005b](#), Eq. 5, or [Allen et al. 2007c](#), Eq. 8.59 for transformation equations)
  - Average daily minimum relative humidity and average wind speed during the four growth stages

---

Source: Data from [Allen et al. \(2011d\)](#)

Table G-2. Recommended Essential and Desired Descriptive Information for ET Measurement Systems Eddy Covariance, Bowen Ratio, Lysimeters, Soil Water Differencing, and Sap Flow in Addition to All Factors Listed in Table G-1

Essential	Desired
<b>Eddy Covariance</b> <ul style="list-style-type: none"> <li>Measurement frequency</li> <li>Averaging period</li> <li>Height of sonic anemometer and hygrometer relative to (a) ground, (b) mean vegetation height, and (c) maximum vegetation height or limb height</li> <li>Anemometer and hygrometer instrument separation distances and orientation; a photo is desirable</li> <li>Types of corrections to the flux measurements and specific software used for corrections</li> <li>Type of coordinate rotation employed</li> <li>Fetch length in predominant wind directions and direction thresholds for data filtering</li> <li>Description of measurement of <math>R_n</math> and <math>G</math> for energy balance (EB) closure assessment</li> <li>Description of (a) closure error amount and (b) method of closure</li> <li>Brands and maintenance procedures for <math>R_n</math> and <math>G</math> sensors, sonic anemometer, and hygrometer, including purchase and last rebuild dates</li> <li>Description on numbers of and placement of <math>R_n</math> and <math>G</math> sensors relative to vegetation and individual plants</li> </ul>	<ul style="list-style-type: none"> <li>Description of multiple <math>R_n</math> and <math>G</math> sensors, especially when the fraction of ground cover is <math>&lt; 0.8</math> or when mean vegetation height is <math>&gt; 2\text{ m}</math></li> <li>Footprint analysis</li> <li>Indication of adequacy of soil water supply to support transpiration</li> <li>Description of soil water content monitoring in the vegetation root zone</li> <li>Soil type, field capacity, wilting point, and how these values were determined</li> <li>Estimated rooting depth</li> <li>Summary of QC analysis on <math>R_n</math> measurements using measured <math>R_s</math> and estimated or measured albedo and net long-wave radiation (if there is no <math>R_s</math> measured, use calculated <math>R_{so}</math> for comparing on clear days)</li> <li>Collocation with a Bowen ratio system to confirm values for ratios of <math>H/LE</math> and to provide independent "looks" at <math>LE</math> from EC and BR methods and aerodynamic estimates of <math>H</math> and <math>LE</math> based on <math>T_1 - T_2</math> and <math>e_1 - e_2</math>. See Chapter 6 for an example.</li> <li>Age of all sensors and loggers and information on annual maintenance and storage</li> <li>Data logger type and model</li> </ul>

- Height of  $R_n$  sensor to (a) ground, (b) mean vegetation height, and (c) maximum vegetation height (or limb)
  - For  $G$ , method for measuring soil water content and soil temperature
  - For vegetation, a description of
    - distribution of height
    - fraction of ground cover by vegetation
    - LAI (measured or estimated)
- Description of vegetation type, extent and soil water status upwind of the vegetation being monitored

#### Bowen Ratio

- Brands and maintenance procedures for vapor and temperature sensors,  $R_n$  and  $G$  sensors, including purchase and last rebuild dates
- Procedures to determine the instrument psychrometric constant
- Description on numbers of and placement of  $R_n$  and  $G$  sensors relative to plants
- For  $G$ , method for measuring soil water content and soil temperature
- Separation of the  $T$  and  $e$  sensors and placement relative to (a) ground and (b) vegetation
- Timing of exchange of sensors, if applicable
- If sensors are not exchanged, indication of system for bias reduction between  $T$  and  $e$  measurements at the two elevations

- Description of multiple  $R_n$  and  $G$  sensors, especially when the fraction of ground cover is  $<0.8$  or when mean vegetation height is  $>2$  m
- Footprint analysis
- Indication of adequacy of soil water supply to support transpiration
- Description of soil water content monitoring in the vegetation root zone
- Soil type, field capacity, wilting point (and how these values were determined) or NRCS taxonomy (USDA 1999)
- Estimated rooting depth
- Summary of QC analysis on  $R_n$  measurements using measured  $R_s$  and estimated or measured albedo and

---

(Continued)

Table G-2. Recommended Essential and Desired Descriptive Information for ET Measurement Systems Eddy Covariance, Bowen Ratio, Lysimeters, Soil Water Differencing, and Sap Flow in Addition to All Factors Listed in Table G-1 (*Continued*)

Essential	Desired
<ul style="list-style-type: none"> <li>● Values of typical <math>dT</math> and <math>de</math> measured</li> <li>● For vegetation, a description of           <ul style="list-style-type: none"> <li>○ distribution of height</li> <li>○ fraction of ground cover by vegetation</li> <li>○ LAI (measured or estimated)</li> </ul> </li> <li>● Fetch length in predominant wind directions and direction thresholds</li> <li>● Description of vegetation type, extent and soil water status upwind of the vegetation being monitored.</li> </ul>	<ul style="list-style-type: none"> <li>● net long-wave radiation (if there is no <math>R_s</math> measured, use calculated <math>R_{s0}</math> for comparison on clear sky days)</li> <li>● Collocation with an eddy covariance system to confirm values for ratios of <math>H/LE</math> and to provide independent looks at <math>LE</math> from EC and BR methods and to provide wind speed or friction velocity, <math>u^*</math>, estimates for aerodynamic estimation of <math>H</math> and <math>LE</math> based on <math>T_1 - T_2</math> and <math>e_1 - e_2</math>. See Chapter 6 for an example</li> <li>● Data logger type and model</li> </ul>
<p><b>Lysimeter<sup>a</sup></b></p> <ul style="list-style-type: none"> <li>● Dimensions (width, length, and depth):           <ul style="list-style-type: none"> <li>○ inner tank</li> <li>○ outer tank</li> </ul> </li> <li>● Tank material and thickness</li> <li>● Insulation of inner tank walls</li> <li>● Gap between inner and outer tank</li> <li>● Photos of lysimeter without vegetation</li> <li>● Photos of lysimeter with vegetation including immediate area outside lysimeter</li> <li>● Crop yields for the lysimeter and from the field</li> <li>● Photo of landscape surrounding the lysimeter</li> <li>● How the representative effective areas of the lysimeter are calculated for evaporation and transpiration determination</li> </ul>	<ul style="list-style-type: none"> <li>● Report on two or more lysimeters with the same vegetation and water treatments with error analysis between/among them</li> <li>● Salinity measurements of lysimeter drainage water</li> <li>● Confirmation of adequacy of soil water supply to support transpiration</li> <li>● Soil water content monitoring in the vegetation root zone</li> <li>● Soil type, field capacity, wilting point (and how these values were determined)</li> <li>● Estimated rooting depth</li> </ul>

- Scale type and specifications
- No. scans of load cell(s) per reporting period
- Calibration checks and estimated precision and accuracy
- Method of lysimeter soil construction (monolithic vs. reconstructed)
- Comments and notes on any differences between lysimeter vegetation and that of surrounding field or expanse including relative vegetation amount, fraction of ground cover, height, LAI, soil water availability
  - plant density of field or expanse and that inside lysimeter
    - fraction of soil visible inside and outside lysimeter
    - plant height inside and outside lysimeter
  - Irrigation process for lysimeter and surrounding field and method for measurement
  - Drainage process for lysimeter
  - Soil layering inside and outside of the lysimeter
  - If lysimeter area is not an integer multiplier of average area per plant, including space between plant rows (if applicable), describe how evaporation from nonsampled areas is estimated
  - Description of supporting vegetation data including height (vs. time), LAI
- **Soil Water Differencing**
  - Soil water holding properties by layer to depths greater than the rooting depth
  - Errors in observations

(Continued)

Table G-2. Recommended Essential and Desired Descriptive Information for ET Measurement Systems Eddy Covariance, Bowen Ratio, Lysimeters, Soil Water Differencing, and Sap Flow in Addition to All Factors Listed in Table G-1 (*Continued*)

Essential	Desired
<ul style="list-style-type: none"> <li>● Description of equipment</li> <li>● Maximum depth of measurement</li> <li>● No. of locations measured</li> <li>● Locations of measurement sites</li> <li>● No. of depths observed and respective intervals</li> <li>● Time intervals for measurements</li> <li>● Comments on monitoring locations vs. areas wetted by irrigation, shadows cast by trees, etc.</li> <li>● Special treatment of surface layer</li> <li>● Estimation procedure for drainage and upward flow, including evidence that fluxes were small or negligible</li> <li>● Treatment of rainfall and irrigation events in the water balance</li> <li>● Sampling procedures when observations are performed for tree and vine crops</li> </ul>	<ul style="list-style-type: none"> <li>● Validation of pedotransfer functions when used to characterize soil water holding capacity</li> <li>● Description of the model when one is used, with particular attention to procedures for estimation of deep percolation and groundwater contribution</li> <li>● Procedures used when the crop season includes wintertime with frozen soil</li> </ul>
	<p><b>Sap Flow</b></p> <ul style="list-style-type: none"> <li>● Clear reference to the method used</li> <li>● Information about sampling, concerning the number of plants equipped with sap flow sensors and the</li> </ul>

selection criteria for different dimensions/species in a stand

- Description of scaling-up method to the stand level
- Number of sensors per plant and sensor technical characteristics (e.g., probe length, number of measurement points in a probe)
- Data treatment procedures, including corrections
- Information about calibration procedures, if performed
- For vegetation, a description of
  - distribution of height
  - fraction of ground cover by vegetation
  - LAI (measured or estimated)
- Description of ground cover types and amounts and relative wetness of soil surface layer over time

---

<sup>a</sup>Some of the details listed for lysimeter specifications can be referenced to previously published information on the specific lysimeter installation, provided the reference material is accessible via the Internet or journal articles.  
Source: Data from Allen et al. (2011d).

published  $K_c$ s. Dependable models, when parameterized based on description of the vegetation, weather, and soil and water conditions, can be expected to reproduce general magnitudes of calibrated data within some error tolerance, for example,  $\pm 20\%$ , and preferably even closer, on average. The model estimates should include estimation of both soil evaporation and vegetation transpiration and should consider all weather parameters affecting evaporation (air temperature, humidity, solar radiation, and wind speed).

### Recommended Documentation

Tables G-1 and G-2 list descriptive items that are recommended when reporting studies and measurements of ET. These items provide reviewers and users of data means by which to scrutinize integrity of data and with means to place reported results in their environmental and physiological contexts. The lists illustrate the types of information that can be asked by potential users of the data prior to the data usage.

Table G-1 lists general documentation and information that is useful to accompany ET data sets or the findings that are based on a data set. Table G-2 describes additional documentation or tests that are useful to accompany data collected from eddy covariance, Bowen ratio, lysimeter, soil water differencing, and sap flow systems to improve descriptions of the implementation of these systems and the handling of data. Those systems are described in Chapter 7 and in this appendix. The left-hand columns of Tables G-1 and G-2 list what are considered to be essential information to supply, and the right-hand columns list desirable, but less essential, information that can assist in data assessment for integrity, bias, accuracy, and representativeness.

In many cases, prior publications containing descriptive information can be cited, especially when measurement procedures are relatively standard. In the case of lysimeters, for example, the lysimeter system installation may have been previously described and can be cited. Cited material should be readily accessible to the public via journals or maintained web pages. Journals that publish articles that report findings or models based on ET data should encourage this type of information in submitted and accepted manuscripts.

### G.5 SUMMARY

Substantial measurement biases or incorrect data extrapolations can easily occur in ET data sets, many of which may not be recognized or identified and rectified prior to refereed publication. Precautions need to be exercised to produce accurate and defensible ET data and to recognize

quality data. Data collection systems need to be combined with rigorous quality assessment and quality control procedures. For example, sap flow systems need to include sufficient numbers of trees to reduce statistical error and to sample a representative population of trees. While remote sensing systems do not "measure" ET but rather deduce it via energy balance or vegetation indices, these methods are quite powerful in spatial coverage and quantification of spatial variation in ET, especially those based on thermally driven energy balance. However, they benefit from testing against ground-truth data and comparison against independent data sets. Accuracy of ET measurement requires well-calibrated and well-maintained systems, and, in many cases, a foundational knowledge of the underlying physics of turbulence and heat and radiation transfer that govern the particular measurement. Knowledge of underlying physics is necessary to reduce the impacts of neglect of important biasing factors. In addition, an attitude of thoughtful approach to measurement and critical assessment of data are essential.

Recommendations are provided on the types of documentation that should accompany ET data sets and associated products when published and that should be referred to in journal publications. This documentation describes data measurement and handling by the data collectors and can provide insight to readers of articles and users of data as to data representativeness, context, and quality.

This page intentionally left blank

## APPENDIX H

### WEATHER DATA INTEGRITY

#### H.1 INTRODUCTION

Accurate estimation of evapotranspiration (ET) requires accurate and representative weather data. Combination equations such as the Penman-Monteith (PM) equation can be relatively sensitive to error in weather data. The degree of sensitivity changes with time of year and climate. During summer, solar radiation can dominate the ET estimate. Therefore, especially in humid and subhumid climates, where the relative power of the vapor pressure deficit/wind term of the PM is small relative to the radiation term, error in solar radiation can be the most impacting on the ET estimate. During wintertime, if solar radiation is low, wind speed and vapor pressure deficit can be strong drivers of the ET calculation. Error in wind speed and vapor pressure deficit can also dominate in arid and semiarid climates. Gong et al. (2006) evaluated a 41-year record of daily weather data at 150 national meteorological observatory stations in China. Reference ET ( $ET_{ref}$ ) estimated by the FAO-56 Penman-Monteith method was most sensitive to relative humidity, followed by shortwave radiation, air temperature, and wind speed. The rank of the four climatic variables varied with season and region. Values for sensitivity coefficients were impacted by regional wind-speed patterns. Ley et al. (1994a) analyzed sensitivity of the 1982 Kimberly Penman model at 20 weather stations in central Washington State where 24-hour estimates were most sensitive to combined error in daily maximum and minimum air temperatures, followed by error in daily maximum air temperature, solar radiation, dew point temperature, wind speed, and daily minimum air temperature, when the weather parameters were varied up to an amount equal to the standard deviation of the measured values for specific time periods of the

growing season. Ley et al (1994b) showed that when realistic levels of weather measurement variability (estimated either as the manufacturer's specification of sensor accuracy or as actual measurement variability) are analyzed, 24-hour estimates of  $ET_{ref}$  are most sensitive to solar radiation measurement error, followed by dew point temperature, maximum temperature, and wind speed measurement errors, respectively, for the central Washington climate. In general, sensitivity coefficients for  $ET_{ref}$ , defined as the percentage change in  $ET_{ref}$  per percentage change in the variable, were less than 1.0 (Ley et al. 1994a), which suggests that  $ET_{ref}$  estimates are somewhat robust to error in weather data. However, the relative sensitivity of any one variable is affected by the strength of the other weather variables, for example, in the case of the essentially multiplicative influences of vapor pressure deficit and wind speed in the PM aerodynamic term.

One note made here is that it is often awkward or irrational to express error in some weather parameters in terms of percent error, for example, with air temperature, which, when using a Celsius basis, a 1°C error at a temperature of 1°C constitutes a 100% error, whereas, if expressed on the basis of absolute scale (K), the 1°C error constitutes less than 0.4% error, which is at the other extreme. Because of the impact of the basis for expression of percent error, some recent sensitivity analyses have expressed sensitivity of  $ET_{ref}$  in terms of mm of error in  $ET_{ref}$  per unit error in temperature, wind speed, radiation, or vapor pressure, expressed as °C,  $m\ s^{-1}$ ,  $W\ m^{-2}$ , or kPa (Irmak et al. 2006). All analyses demonstrate the need to exercise care in measuring and handling weather data.

Weather data should be screened before use in an  $ET_{ref}$  equation to ensure that the data are of good quality and are representative of well-watered conditions. This is especially important with electronically collected data, because human oversight and maintenance may be limited. When weather measurements are determined to be faulty, they can be adjusted or corrected using a justifiable and defensible procedure, or the user may elect to replace perceived faulty data with estimates. This appendix reviews some general procedures that may prove useful when assessing the integrity and representativeness of weather data used for  $ET_{ref}$  calculation. Procedures are provided for estimating data in situations where data are shown to be of poor quality or are missing.

## H.2 IMPORTANCE OF THE WEATHER STATION LOCATION

Most modern automated weather stations (AWS) measure the primary variables affecting ET: solar radiation, air temperature, wind speed, and humidity, and therefore provide relatively complete data for estimating ET as compared with the older manually operated weather stations that measured only air temperature and that were routinely used in the past.

An AWS should measure temperature, humidity, and wind speed within the dynamic boundary overlying the ground surface. Properties of this boundary layer characterize the energy balance at the surface and are used to estimate the ET rate. As studies in southern Idaho by Burman et al. (1975) and modern blending height/profile theory models (Chen and Dudhia 2001) have shown, the humidity, temperature, and wind speed levels in the lower level of the atmosphere change when going from desert to a patchwork of irrigated and nonirrigated fields. When making calculations of  $ET_{ref}$ , weather measurements should reflect the environment that is defined by the reference surface. This is important because most reference ET equations were developed for use with meteorological data collected primarily over and downwind of dense, fully transpiring grass or similar vegetation exhibiting behavior similar to the definition of the reference surface condition. Feedback exists between the boundary layer above the surface and the surface, so that the energy balance and evaporation at the surface affect temperature, humidity, and wind speed of the air layer above.

Ideally, weather stations should be centered within large, nearly level expanses of uniform vegetation that are supplied with sufficient water through precipitation and/or irrigation to support ET near maximum levels. The preferred vegetation for the site is clipped grass. However, alfalfa or a grass-legume pasture maintained at a height of less than about 0.5 m may also serve as effective vegetation for the site. Vegetation height should be shorter than about 0.5 m not to affect the wind speed measurement. Meteorological measurements made over other short, green, actively transpiring crops will approach reference measurements, provided canopy cover exceeds approximately 70%. A station may be located on the periphery of a vegetated field, but over a surface having low vegetation cover, provided that the station is downwind of the vegetated field during daytime hours so that the sampled airstream is conditioned to reflect a reference environment. In an ideal setting, the well-watered vegetation extends at least 100 m in all directions from the weather station. However, it is recognized that frequently such a weather station site is not available, and that often some nonvegetated areas or roadways will be present near the station. Allen (2006) summarized a source-area footprint approach to estimate the impact on weather measurements of a local area of dryness in the immediate vicinity of a weather station having transpiring vegetation further upwind, and vice versa. The method is summarized in Section 7.6. That approach can be used to assess whether the size of a patch of bare or dry ground surrounding a weather station, for example, in the corner of a center pivot irrigated field, is large enough to affect the temperature and humidity measurements by more than some fixed percentage. It can also be used to indicate whether a small patch of well-watered vegetation surrounding a weather station is sufficiently large to condition the near-surface boundary layer measured by the weather station so that it represents

reference conditions. Some guidelines based on the method are presented in the next section.

Meteorological data sets obtained from true reference settings are generally difficult to come by. Often, weather stations are located over or adjacent to (1) annual row crops that proceed through a distinct annual growth (and cover) cycle, or (2) range and/or pastureland that is subject to seasonal deficits in soil moisture or is within the vicinity of small buildings and roadways. Many urban weather stations fail both the underlying surface requirement and the recommended separation distance from obstacles. Such failure of a weather station site to meet the definition of a reference condition does not preclude use of the data for estimation of  $ET_{ref}$ . However, data from such a station should be examined carefully before use and may, in some cases, require adjustment to make the data more representative of reference conditions. New weather stations installed for the express purpose of estimating  $ET_{ref}$  should be located in sites that closely approximate the reference conditions outlined above.

It is the intent of this appendix to encourage the use of weather data and to locate weather stations that adhere to the preferred guidelines. When weather data are not from an agricultural or reference environment and are shown to be substantially affected by the lack of local ET, the user should be willing to adjust the data using procedures of this appendix and other publications, for example, ASCE (2005), or to abandon the use of the data.

Weather stations should be isolated from nearby obstacles and obstructions that can impede airflow and/or shade the site. The recommended horizontal separation distance from such obstacles should exceed 10 times the height of the obstacle (ASABE 2004). Fences used to protect the station from unwanted intrusions by animals should be made of a porous fencing material (e.g., woven wire or chain link); fence height should not extend above the height of the anemometer.

### H.3 THE IMPACT OF LOCAL ENVIRONMENT ON TEMPERATURE AND HUMIDITY MEASUREMENTS

The contribution of surface conditions at various distances upwind of temperature ( $T$ ) and humidity ( $e$ ) measurements and associated vapor and sensible heat flux measurements has been extensively studied by the micrometeorological and air quality modeling communities (Horst and Weil 1992; Hsieh et al. 2000; Schmid 2002). The total spatial area that influences the value of a scalar ( $T$  and  $e$ ) or flux ( $H$  and  $LE$ ) is known as the source area footprint. Models developed from footprint studies are useful for assessing the influence of fetch of evaporating cover upwind of an agricultural weather station on conditioning of  $T$  and  $e$  measurements and consequently estimates of  $ET_{ref}$ . The models can also be used to estimate

impacts of nonevaporating surfaces in the vicinity of a weather station, for example, a station sited in the bare corner of a field or near a road, on negative conditioning of the  $T$  and  $e$  measurement.

The following tables are summarized from Allen (2006) to show the relative influence of local ground surface condition, evaporationwise, on  $T$  and  $e$  measurements. The tables were computed using a footprint model by Hsieh et al. (2000) (see Eq. 7-13), which was applied over a range of fetch distances for two surface conditions common to weather stations: well-watered grassed fetch that is recommended for the ideal weather station setting and a nearly dry, bare soil fetch that represents a nonideal weather station setting. The information in the tables can be used to recommend minimum distances of grassed or other vegetation required to promote measurement of  $T$  and  $e$  representing well-watered conditions at a weather site and the negative impact of dry surfaces in the immediate vicinity of a weather station.

During model application, the well-watered grass fetch condition was assumed to be of 0.12 m height in the analyses, and net radiation loading was set at  $500 \text{ W m}^{-2}$  for each surface.  $LE$  was set at  $350 \text{ W m}^{-2}$  for the grass and  $50 \text{ W m}^{-2}$  for the dry soil. A residual amount of  $LE$  is specified for the bare soil surface to represent residual evaporation common to bare soil in an agricultural area. The results were not very sensitive to  $LE = 50 \text{ W m}^{-2}$  vs.  $LE = 0$ . The resulting estimates for soil heat flux,  $G$ , and  $H$  were 47 and  $103 \text{ W m}^{-2}$  for the grass and 250 and  $200 \text{ W m}^{-2}$  for the dry, bare soil. The station elevation was set at 500 m, but results were insensitive to elevation. The Bowen ratios ( $H/LE$ ) for the grassed and bare soil conditions were 0.5 and 5. The values for  $R_n$ ,  $LE$ , and  $H$  are typical of midsummer during midday and when buoyancy effects are large. The values for  $LE$  for the two surfaces are approximately equivalent to daily ET rates of 7 and  $1 \text{ mm d}^{-1}$ , depending on the day length.

The data presented in Table H-1 suggest the influence of a weather station surface having  $x_f$  dimension of one of the vegetation conditions (grassed or bare) in the upwind direction on the measurement of  $T$  or  $e$  at 2-m height. The influences are expressed as a fraction ( $F$ ) of total influence (0 to 1.0) for a range of upwind fetch lengths ( $x_f$ ) of 5 to 200 m and over a range of wind speeds of 0.5 to  $5 \text{ m s}^{-1}$ . The influences, in essence, represent the fraction of the  $T$  and  $e$  "concentrations" (i.e., measurements) that are traceable to the  $x_f$  distance of fetch. One way that the table can be used is to indicate, for example, that a weather station that is placed over bare, dry soil with 20 m to the edge, and having well-watered vegetation beyond that, will "feel" the influence of the bare soil in the form of only a 14% impact on the  $T$  and  $e$  measurements if the wind speed is a typical  $2 \text{ m s}^{-1}$  (Table H-1, row 3, second-to-last column). The  $T$  and  $e$  measurements will therefore be 86% similar to that measured by an equivalent weather station placed over and surrounded completely by transpiring vegetation and only

Table H-1. The Fraction (0 to 1.0) of Total Contribution by a Weather Station Surface, Having  $x_f$  Dimension in the Upwind Direction, on the Temperature and Vapor "Concentrations" (i.e., Measurements) Taken at a 2-m Height, as Influenced by Wind Speed at 2 m

Distance to Upwind Boundary, m ( $x_f$ )	Clipped Grass				Bare, Dry Soil			
	Wind Speed at 2 m, $\text{m s}^{-1}$				Wind Speed at 2 m, $\text{m s}^{-1}$			
	0.5	1	2	5	0.5	1	2	5
5	0.03	0.00	0.00	0.00	0.07	0.01	0.00	0.00
10	0.18	0.05	0.00	0.00	0.27	0.11	0.02	0.00
20	0.42	0.23	0.07	0.00	0.52	0.33	0.14	0.01
50	0.71	0.56	0.34	0.06	0.77	0.65	0.45	0.13
100	0.84	0.75	0.58	0.24	0.88	0.80	0.67	0.37
200	0.92	0.86	0.76	0.49	0.94	0.90	0.82	0.61

Source: Data from Allen (2006)

14% like  $T$  and  $e$  measured over a very large expanse of dry surface. In contrast, for very calm wind conditions of  $0.5 \text{ m s}^{-1}$ , the influence of the underlying dry soil surface, although only 20 m in length in an upwind direction, is 52% on the  $T$  and  $e$  measurement. This occurs due to the relative strength of the buoyancy mechanism of the heated air at the dry surface in transporting warm, dry air parcels upward toward the  $T$  and  $e$  sensors, when horizontal wind movement and mechanical turbulence is low. As wind speed increases, the heated parcels, in essence, move past and below the sensors to a greater degree. Table H-2 shows similar values for  $F$  as for Table H-1, but for a sensor height of 1.5 m that is typical of many weather stations. Differences between the two tables are greatest for smaller values of fetch length, as expected.

The presence of bare soil or other dry surface beneath or nearby a weather station can be cause for concern for reference weather stations due to the perception of aridity impacts and negative conditioning of the air-stream by the dry vicinity. However, Tables H-1 and H-2 suggest that dry fetch of up to 20 m has relatively small impact on  $T$  and  $e$  measurements for wind speeds greater than  $2 \text{ m s}^{-1}$ . Impact of local dry fetch increases, however, with calm wind speed. Table H-2 suggests that 38% of the sensor signal at 1.5-m height will be conditioned by a 10-m fetch of bare soil when wind speed at 2 m height is only  $0.5 \text{ m s}^{-1}$ . Given typical average wind speed at 2 m of about  $2 \text{ m s}^{-1}$ , dry fetch distances of 20 m or less upwind of a weather station are generally tolerable for production of reference

Table H-2. The Fraction (0 to 1.0) of Total Contribution by a Weather Station Surface, Having  $x_f$  Dimension in the Upwind Direction, on the Temperature and Vapor "Concentrations" (i.e., Measurement) Taken at a 1.5-m Height, as Influenced by Wind Speed at 2 m

Distance to Upwind Boundary, m ( $x_f$ )	Clipped Grass				Bare, Dry Soil			
	Wind Speed at 2 m, $\text{m s}^{-1}$				Wind Speed at 2 m, $\text{m s}^{-1}$			
	0.5	1	2	5	0.5	1	2	5
5	0.08	0.01	0.00	0.00	0.14	0.04	0.00	0.00
10	0.28	0.11	0.02	0.00	0.38	0.19	0.05	0.00
20	0.53	0.34	0.13	0.00	0.61	0.43	0.22	0.02
50	0.77	0.65	0.44	0.11	0.82	0.72	0.54	0.21
100	0.88	0.80	0.66	0.34	0.91	0.85	0.74	0.46
200	0.94	0.90	0.82	0.58	0.95	0.92	0.86	0.68

Source: Data from Allen (2006)

weather data sets, provided surfaces beyond 20 m exhibit well-watered characteristics for some extended distance.

Table H-1 is also useful to gauge the adequacy of the relative size of a patch of transpiring vegetation in influencing the  $T$  and  $e$  measurements. For a patch of grass that is 40 m in diameter so that 20 m of transpiring grass extends upwind of a weather station having  $T$  and  $e$  sensors at 2-m height, with a dry surface beyond, the grass has only 7% influence on the  $T$  and  $e$  measurements when wind speed is 2  $\text{m s}^{-1}$ , and 93% of the  $T$  and  $e$  signals will stem from the energy partitioning conditions over the dry soil further upwind. Therefore, the weather data can be expected to exhibit aridity of the region if the region is dry, even though the weather station is technically located over irrigated, clipped grass. Clearly, the 20 m radius of clipped grass is inadequate if surrounded by dry soil beyond.

This example suggests that operators of agricultural weather stations should not be lulled into assuming that  $T$  and  $e$  measurements collected over small patches of grass fulfill needed environmental conditions for a reference weather station and will produce weather data that exhibit the conditioning that is anticipated by an  $ET_{ref}$  method that has been calibrated to reference weather data.

Table H-1 shows  $F$  to increase somewhat logarithmically with fetch distance for both surface conditions and shows  $F$  to decrease somewhat exponentially with increasing wind speed. Influences of both fetch distance and wind speed are large for both conditions. The impact of larger

instability of the near-surface boundary layer over the dry soil did not substantially influence the value for  $F$ , as compared to transpiring grass, for any particular fetch length. However, the table may underestimate the impact of a hot, dry surface because wind speed is held constant. Wind speed may accelerate significantly over extensive hot, dry surfaces due to more efficient entrainment and transfer of higher velocity air from high above the surface toward the surface.

Tables H-1 and H-2 illustrate the influence of surface dryness and subsequent partitioning of surface energy into sensible heat and latent heat fluxes on the  $T$  and  $e$  measurements. One other important influence of surface temperature on the  $T$  measurement at some sensor height is not expressed in the tables, however. That influence is the thermal radiation emitted from a warm surface close to the sensor or sensor enclosure on the sensor reading. A dry surface under full sun conditions can be 30°C warmer than an evaporating or transpiring surface that is cooled by the evaporation. Because thermal emission is proportional to absolute temperature to the fourth power, the thermal emission from a dry surface can be as much as 100 W m<sup>-2</sup> greater than from an evaporating surface. Consequently, the radiation loading of a temperature sensor enclosure can increase substantially, especially under low wind speed, where convective cooling of the enclosure is low. The effect is much like the heat felt by a human when approaching a large fire. That sensation is caused by the thermal radiation from the hot fire. This additional warming factor may tend to cause values in Tables H-1 and H-2 to underestimate the impact of the dry surface. The total amount of impact is unknown and is influenced by the sensor enclosure design (i.e., the design of the radiation shield, use of aspirated vs. nonaspirated airflow, etc.).

Even though the data in Tables H-1 and H-2 show the fallacy of locating a weather station over a small area of grass or other vegetation (of 10 or 20 m diameter), but surrounded by dry, poorly vegetated further upwind, positive effects of a small area of grass that are not expressed by the tables would be the cooling effect caused by the lower thermal radiation emission by the grass as compared to dry soil and the consequent reduced radiation loading of sensor shields. This benefit may be small relative to impacts of lack of upwind fetch.

### Impacts of Fetch Length for Short Vegetation

The results in Tables H-1 and H-2 suggest that a 100:1 fetch to height ratio for instruments placed over well-watered grassed or other vegetated surface will produce  $T$  and  $e$  measurements that are within 75% of reference or conditioned values (as would occur if downwind of a very large expanse of well-watered vegetation having dimensions of km) when wind speed is 2 m s<sup>-1</sup> or less. The other 25% of the  $T$  and  $e$  measurement will have

characteristics of the ground surface beyond  $x_f$ . If this beyond surface is also well-watered or semi-well-watered, then the  $T$  and  $e$  values measured at the weather site will be expected to exhibit representative values for  $T$  and  $e$  under all wind speeds. The contribution of surfaces upwind of  $x_f$  increase beyond the 25% value expected for the 100:1 ratio when wind speed exceeds  $2 \text{ m s}^{-1}$  due to the increased horizontal air movement relative to the buoyancy influenced movement.

Leclerc and Thurtell (1990) applied a Lagrangian particle trajectory model and found that the 100:1 fetch to height rule of thumb underestimated fetch requirements for flux measurements over smooth surfaces under stable conditions. This finding was also evidenced in Hsieh et al. (2000), who found fetch:height ratios of 100:1 for unstable, 250:1 for neutral, and 300:1 for stable conditions needed to condition fluxes over a surface having roughness of 0.04 m.

### Location of Maximum Influence

Hsieh et al. (2000) differentiated the equation for  $x_f$  to solve for the location,  $x$ , of the distance upwind of sensors having largest influence on a flux measurement. Allen (2006) added an approximate adjustment for scaling differences between flux and scalar footprints based on findings of Schmid (1994). Estimates of locations of maximum influence on  $T$  and  $e$  measurements are shown in Table H-3 for 1.5- and 2-m measurement heights for the same conditions used to create Tables H-1 and H-2. The value for  $x$  has a relatively low value at low wind speeds and increases substantially with wind speed. Distance  $x$  is relatively close to the sensor location under nearly all conditions, even though the fraction of impact at the distance may be relatively low. This phenomenon is due partially to the fan shape of the footprint source area, where a narrowing horizontal dimension of the function in the direction of the sensor results in a smaller horizontal area contributing to the sensor location. This narrowing causes

Table H-3. Locations of the Distance Having the Most Relative Influence on  $T$  and  $e$  Measurements (m) at  $z$  Height

Height of Measurement, $z$ (m)	Clipped Grass				Bare, Dry Soil				
	Wind Speed at 2 m, m/s	0.5	1	2	Wind Speed at 2 m, m/s	0.5	1	2	5
1.5	8	13	25	65	6	10	18	47	
2	10	17	32	85	8	13	24	60	

Source: Data from Allen (2006)

locations further from the sensors to have relatively larger impact. The centroid of the  $F$  area is at significantly greater distance than  $x$ .

### Variation of Fetch Influences over Time

Wind speed and direction vary naturally during the course of a day, month, and season. The impact estimates from Tables H-1 or H-2 can be applied to a series of wind speed and direction data to derive a frequency distribution of  $F$  for a range of wind directions, provided a two-dimensional map of fetch for the weather station is available. Such a distribution can be used to rate a site in terms of fetch impact and to make estimates on the impact of local conditioning by fetch on sensor measurements. Conditioning of  $T$  or  $e$  by fetch can be estimated as  $T_{meas} = FT_{fetch} + (1 - F)T_{beyond}$  and  $e_{meas} = Fe_{fetch} + (1 - F)e_{beyond}$  where  $T_{meas}$  is the expected value for the temperature measurement given value  $F$ ,  $T_{fetch}$  is the temperature measured over an extensive area having the same surface as the fetch and  $T_{beyond}$  is the temperature measured over an extensive area having the same surface as that beyond the fetch distance.

Tables H-1 and H-2 may serve as a first approximation of the amount of impact that upwind fetch of distance  $x_f$  has on conditioning or negatively influencing measured air temperature or humidity at height  $z$  above the surface. This information is useful for judging adequacy of green fetch upwind of a weather station and for judging the amount of impact that a dry surface in the vicinity of a weather station has on the  $T$  and  $e$  measurements.

## H.4 WEATHER DATA QUALITY ASSESSMENT AND QUALITY CONTROL

Meteorological data acquired for the purposes of estimating  $ET_{ref}$  should be subjected to a number of quality control checks prior to use. The first and most important quality control check involves gathering information describing the origin of the weather data and conditions impacting measurements. These data should include

1. Local siting of the weather station including the “greenness” of vegetation in the vicinity of the station and beyond,
2. Type and exposure of meteorological sensors employed at the station,
3. Procedures used to maintain and calibrate sensors,
4. Quality control procedures performed and/or data adjustments already performed on the data,
5. Availability of shorter interval data sets (e.g., hourly) to aid the overall QC process, and
6. The station operator’s experience and/or recommendations pertaining to use of the data for  $ET_{ref}$  assessment.

Recommendations pertaining to station siting were discussed in the opening section of this appendix. Where precise location of the station is known, Internet tools such as Google Earth provide excellent opportunities to visually note the nature and extent of vegetation and wetness conditions for the station. The types of sensors employed and their exposure (e.g., height of installation or type of radiation shelter) provide insight into expected error levels for specific measurements and may identify measurements requiring some form of adjustment (e.g., height adjustment for wind speed).

Procedures used to maintain and calibrate meteorological sensors are of extreme importance. Maintenance can be divided into nontechnical and technical categories. Nontechnical maintenance activities include site maintenance (e.g., mowing, irrigation, and fence repair); cleaning sensors; and leveling radiation sensors and rain gauges. Technical maintenance involves repair and replacement of sensors and equipment and represents an important component of the overall calibration process. Technical maintenance should be based on the concept of preventive maintenance, that is, replacement of sensors and equipment before their performance degrades. On-site calibration can be performed at regular intervals by comparing sensors with calibrated sensors that are taken to the site for intercomparison purposes. The operator of the station should provide both the technical and nontechnical maintenance protocols and schedule logs either on a request basis or on a public website. This information should be reported with ET estimates following recommendations, for example, by Allen et al. (2011d) on relevant information to include in publications on crop coefficients and ET estimates and measurements. The ASAE Engineering Practice 505, "Measurement and Reporting Practices for Automatic Agricultural Weather Stations" (ASABE 2004), provides specifications for sensor accuracy, resolution, placement and monitoring, and intervals and procedures for sensor maintenance and calibration.

Data from weather stations operated as part of a weather network are generally subjected to some form of QA/QC (e.g., Stanhill 1992; Meek and Hatfield 1994; Snyder et al. 1996; Shafer et al. 2000). It is useful to investigate the rule structure and guidelines used in the various quality control (QC) routines employed to determine if they are sufficient to provide complete adjustment needed to data. Common quality assessments include comparing incoming parameters against relevant physical extremes (e.g., relative humidity >100%); using statistical techniques to identify extreme or anomalous values; and comparing data with neighboring stations. Some networks flag questionable data while other networks may replace questionable data with estimated values. The user should be aware, however, that QA procedures of some networks contain rather broad or coarse data range assessments, so that application of a QA procedure does not necessarily provide valid data. Furthermore, the QA

system may only identify and flag questionable data. Adjustment to the data via a subsequent QC process may or may not incorporate complete or reliable procedures. Seeking the advice of the data facilitator regarding the fitness of a given meteorological data set for  $ET_{ref}$  assessment is advisable. The facilitator may have insight into whether station sites approach reference conditions, and if not, suggestions on how to correct or adjust the raw meteorological data.

Subsequent sections of this appendix describe procedures recommended by ASCE (2005) for assessing the integrity of meteorological data sets used in the computation of  $ET_{ref}$ . Procedures are described to adjust data to better represent reference conditions. While these procedures are applicable in many circumstances, they are by no means a universal solution to all potential problems with meteorological data. Users of the standardized ASCE Penman-Monteith reference ET equation are encouraged to seek local input regarding the subject of assessment and correction of meteorological data for use in computation of  $ET_{ref}$ .

## Solar Radiation

Solar radiation data can be screened by plotting measurements against clear sky  $R_{so}$  envelopes for hourly or daily time steps. Generally, the best estimates for  $R_{so}$  should be used, which may require applying equations that include the influence of sun angle, turbidity, atmospheric thickness, and precipitable water, for example, Eqs. (4-5)–(4-10) presented in Chapter 4. For daily data sets, one can plot measured  $R_s$  and computed  $R_{so}$  against the day of the year (see Figure H-1). For hourly data, one can plot measured  $R_s$  and computed  $R_{so}$  against time of day, one day at a time, for perhaps five to ten selected “clear sky” days (Figure H-3).

The overlays of plotted  $R_s$  and  $R_{so}$  allow one to observe whether measured  $R_s$  “bumps” up against the clear sky envelope some of the time (i.e., on cloud-free days for daily data or during cloud-free hours for hourly data).  $R_s$  will fall below the clear sky curve on cloudy or hazy days and during times when the atmosphere is more turbid than under conditions of clean air. Conditions of relatively clean air occur following cleansing rain or snow showers and routinely in many areas of the western United States. The transmissivity of the atmosphere and  $R_{so}$  can shift by several percent from day to day due to changes in water vapor, particulate matter, and aerosols, which are all net absorbers and scatterers of solar radiation. If the “upper” values of measured  $R_s$  lie routinely above or below the computed  $R_{so}$  curve by more than 3 to 5%, then the user should scrutinize the maintenance and calibration of the  $R_s$  sensor. Improper calibration, leveling errors, the presence of contaminants on the sensor (e.g., dust, salt, or bird droppings), or electrical problems can cause  $R_s$  to deviate from  $R_{so}$  on clear days. “Abrupt” changes in the clear-day relationship between  $R_s$  and

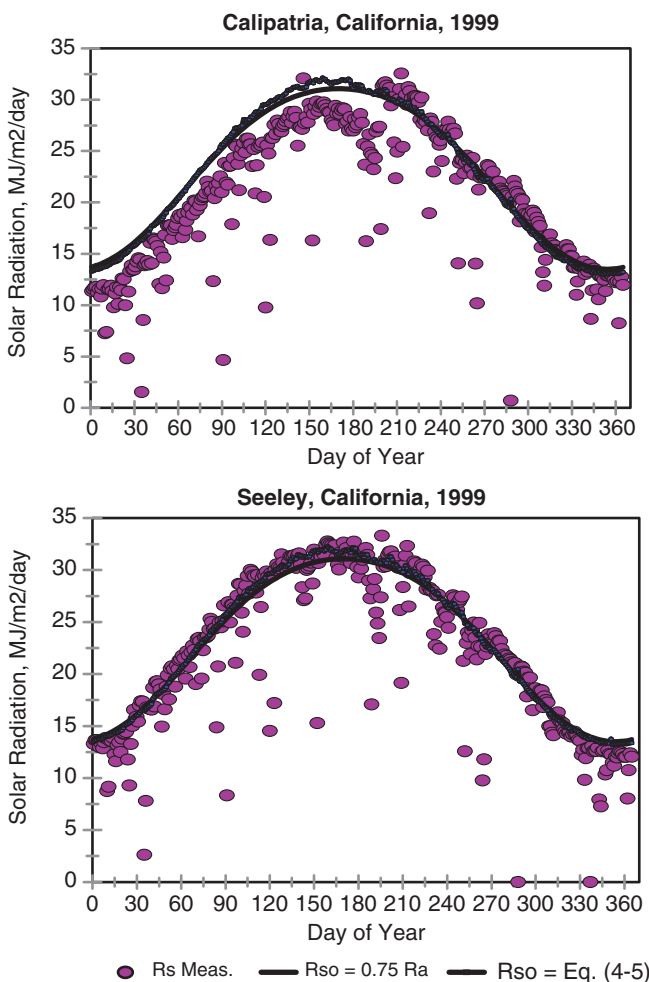


*Fig. H-1. Daily measured  $R_s$  and calculated  $R_{so}$  using Eqs. (4-3)–(4-4) (resulting in  $R_{so} = 0.75 R_a$ ) and using Eqs. (4-5)–(4-10) for Calipatria (top) and Seeley (bottom), California, CIMIS stations in the Imperial Valley during 1999*

$R_{so}$  generally indicate (1) accumulation or removal of contaminants from the sensor; (2) change in sensor level; (3) change in sensor calibration; (4) sensor replacement; (5) problems with wiring or data-acquisition system; or (6) improper programming. Pyranometer maintenance records, if available, may help explain changes in the relationship between  $R_s$  and  $R_{so}$  and aid decisions related to data adjustment. Occasionally,  $R_s$  during hourly periods may exceed  $R_{so}$  due to reflection of sunlight from nearby clouds.

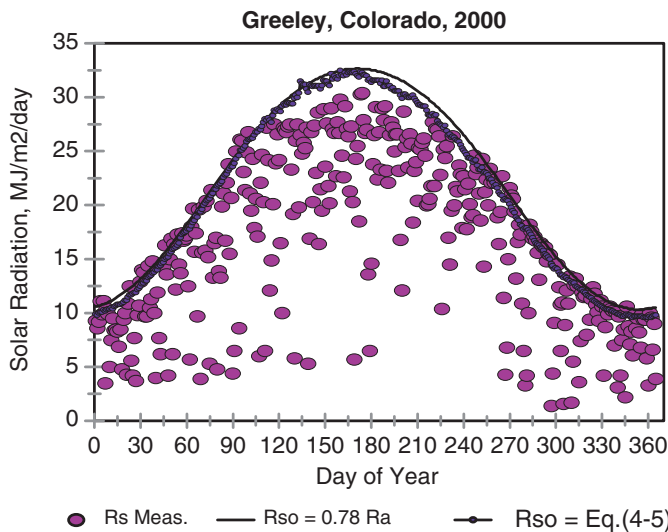


*Fig. H-2. Daily measured  $R_s$  and calculated  $R_{so}$  using Eqs. (4-3)–(4-4) (resulting in  $R_{so} = 0.78R_a$ ) and using Eqs. (4-5)–(4-10) for Greeley, Colorado*

Values for  $R_s$  that are consistently above or below  $R_{so}$  on clear days can be adjusted by dividing  $R_s$  by the average value of  $R_s/R_{so}$  on clear days. This adjustment should be used with appropriate caution as the procedure assumes (1) computed values for  $R_{so}$  are correct; (2) clear days can be effectively identified (for example, during midseason at Greeley in Figure H-2, there is a substantial period having no completely cloud-free days); and (3) the factor causing  $R_s$  to deviate from  $R_{so}$  is static over time. The  $R_{so}$  curves computed by Eqs. (4-5)–(4-10) or by the simpler Eqs. (4-3)–(4-4) are not “perfect.” They assume clean air and common relationships between the diffuse and beam components of shortwave radiation along with typical spectral densities within the shortwave band. Identification of clear days can be difficult in cloud-prone areas, especially if hourly  $R_s$  data are not available to aid in the assessment process. Finally, many of the factors causing  $R_s$  to deviate from  $R_{so}$ , including leveling errors and contaminant accumulation (Stanhill 1992), may not be static over time.

Daily measured  $R_s$  is plotted in Figure H-1 for a full year at two CIMIS weather stations in the Imperial Valley of California.  $R_{so}$  has been calculated using both methods of Chapter 4: Eqs. (4-3)–(4-4) and Eqs. (4-5)–(4-10). Eqs. (4-3)–(4-4) is a simplified procedure, where  $R_{so}$  is computed as a constant fraction of  $R_a$ , with the constant estimated from site elevation. In the case of Imperial Valley, which is at or below sea level, the coefficient in Eq. (4-3) is about 0.75 for both stations. Comparison of the  $R_{so}$  curves with measured  $R_s$  from Calipatria, California, in Figure H-1a indicates that the

pyranometer was measuring about 12% low on clear sky days through about day 200. At around day 200, the sensor was replaced, and readings for clear sky days increased to about 5 to 10% higher than the  $R_{so}$  curves.  $R_s$  data from the nearby Seeley weather station (about 40 km to the SW) during the same year did not exhibit this shift in data. Therefore, for the Calipatria data for year 1999, the data user would be encouraged to contact the data collector and provider for information concerning pyranometer calibration and the user may wish to pursue options for applying some sort of correction to the data, for example, by multiplying  $R_s$  by about 1.12 for days prior to day 200 and by about 0.95 for days following day 200. The user could also consider substituting data from the nearby Seeley station. The more theoretical  $R_{so}$  estimation by Eqs. (4-5)–(4-10) exceeded the simpler  $R_{so}$  curve from Eqs. (4-3)–(4-4) by a few percent during midsummer at Seeley and Calipatria and fit the measured  $R_s$  on clear sky days more closely at Seeley during midsummer (Figure H-1b).  $R_s$  measured at Seeley on some of the clear sky days during spring and fall routinely plotted a few percent above the  $R_{so}$  curves. This indicates that the pyranometer calibration may have been a few percent high or that the theoretical  $R_{so}$  curve is a few percent low for this location due to the very dry atmosphere and potential overestimation of absorption by atmospheric water vapor. The data user may wish to investigate the pyranometer calibration at this site and perhaps conduct an independent assessment of clear sky  $R_s$  using an accurate pyranometer having calibration traceable to the National Standard housed with the Solar Radiation Research Laboratory (<http://srrl.nrel.gov/bms/>) located in the National Renewable Energy Laboratory (NREL) at Golden, Colorado (<http://www.nrel.gov/>). However, agreement between measured  $R_s$  and  $R_{so}$  at Seeley appears to be close enough (within 3–5%) for application for estimating reference ET without any adjustment or correction.

A few unreasonably low values of  $R_s$  are shown in Figures H-1a and b, where measured  $R_s$  was reported as less than  $0.1R_a$ . Generally, the lower bound for 24-hour  $R_s$  is about  $0.2R_a$ . The very low values probably occurred due to sensor or data logger malfunction or missing data occurring during site maintenance. Users can investigate whether a precipitation event, especially snow, may have blocked light transmission or that very dense stratus cloud decks occurred, for example, during winter. Missing or faulty data can be substituted by data from surrounding stations.

Figure H-2 is a plot of daily measured  $R_s$  for a full year at Greeley, Colorado, where both  $R_{so}$  curves [Eqs. (4-3)–(4-4) and (4-5)–(4-10)] follow the upper bound of measured  $R_s$  quite well. Agreement is good throughout the year, except for the late spring–early summer period, when there were no days having completely clear conditions. The relatively long 120-day period with  $R_s < R_{so}$  could be interpreted as a period during which time the pyranometer was dirty, out of level, partially blocked from the sun or sky,

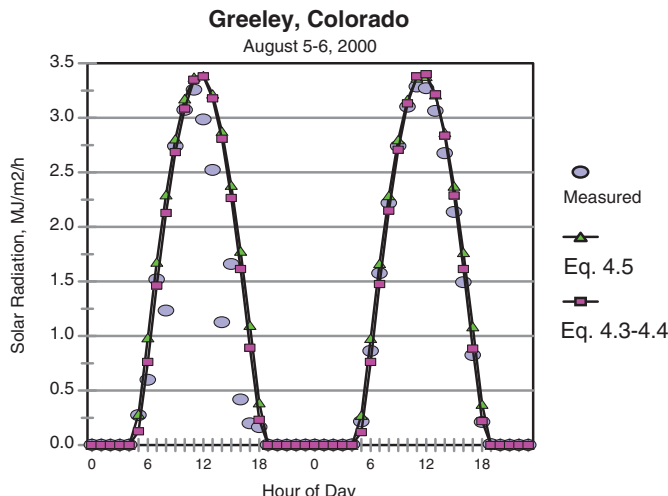


*Fig. H-3. Hourly measured solar radiation and clear sky envelopes for two days in August, 2000, near Greeley, Colorado*

or where a calibration error or program error (saturation of the analog signal) occurred, rather than due to a lack of completely cloud-free days. However, the lack of completely cloud-free days was confirmed by plotting records of hourly  $R_s$  against  $R_{so}$ , for example, as a series of plots similar to Figure H-3, which showed that essentially all days at Greeley during late spring–early summer were subject to afternoon clouding during year 2000. Therefore, no correction to the  $R_s$  data was made to this period. This example is included to caution the data user that sometimes deviation of measured  $R_s$  from the  $R_{so}$  curve for extended periods may be real and valid. The good agreement between measured  $R_s$  for cloud-free days and the computed  $R_{so}$  curve for winter, early spring, and fall periods supports using the solar radiation data from this weather station for the year shown. The  $R_{so}$  curve computed using Eqs. (4-5)–(4-10) dropped a small amount below the  $R_{so}$  curve from Eqs. (4-3)–(4-4) during summer (day 180 on) due to increased absorption by relatively higher humidity levels of the atmosphere during this period.

Figure H-3 illustrates a comparison of hourly measured solar radiation with  $R_{so}$  computed using the simple method of Eqs. (4-3)–(4-4) and using the more complicated method of Eqs. (4-5)–(4-10). The data are from the agricultural weather station near Greeley, Colorado, and data from only two days in August are shown. August 5 had a brief period of cloudiness at around 0800 and then some cloudiness during the afternoon. August 6 was essentially a cloud-free day. The  $R_s$  data from August 6 compared well with both  $R_{so}$  methods throughout the day. The measured data plotted

slightly higher than the simpler  $R_{so}$  estimate from Eq. (4-7) during the morning hours and slightly below the  $R_{so}$  estimate during the afternoon. This may hint of a slight error in the level of the instrument or an incorrect time setting for the data logger clock. In general, the solar radiation data appear to be of excellent quality and calibration.

Plotting hourly measured  $R_s$  against the theoretical  $R_{so}$  can be helpful in detecting errors or shifts in the reported times associated with the data set (i.e., errors in data logger time clocks). Plotting of data can also provide an indication of a lack of level of the instrument. Shifts in time and lack of instrument level can both cause measured  $R_s$  to plot out of phase with the theoretical  $R_{so}$  curve.

## Net Radiation

Where net radiation data are measured, values can be compared with  $R_n$  estimated from equations that use solar radiation as an input as a means of integrity assessment, for example, using Eqs. (4-31)–(4-44) from Chapter 4. One should not expect measured  $R_n$  to exactly agree with estimated  $R_n$ . However, significant variation between the two should be cause for a closer investigation of the measured data. Some net radiometers do not accurately measure the long-wave component of net radiation, and in general, net radiometers are more sensitive to dust and salt stains on the sensor surface than are pyranometers. In addition, net radiometers include the additional input of radiation reflected and emitted from the vegetation surface below. Therefore, the total measurement has less certainty and more opportunity for error. For use in estimating reference ET, the  $R_n$  measurement must be made over a well-watered surface of clipped grass or full cover alfalfa so that albedo is similar to that defined for  $ET_{sz}$ , and, as, or even more importantly, so that the emitted long-wave radiation from the surface, which is proportional to surface temperature to the fourth power, represents that from a surface that is cooled by active transpiring vegetation. As noted previously and discussed in detail in Chapter 11, a hot, dry surface can emit 100 W m<sup>-2</sup> more thermal radiation than cool, transpiring vegetation. This difference can lower the  $R_n$  measurement by 100 W m<sup>-2</sup>, which is substantial.

A shift in the relationship between measured and estimated  $R_n$  may reflect a change in the quality or condition of the surface at the measurement site. Other measurement-related factors that can shift the relationship between measured and estimated  $R_n$  include scratched or dirty radiometer domes, an off-level sensor, or condensation of moisture inside domes of the  $R_n$  sensor. When financially possible, and where, for research or other reasons, it is desirable to measure  $R_n$  rather than to calculate it, it is recommended that the user utilize a four-component net radiometer system that has separate sensors and signals for the four major components of incoming and outgoing shortwave and long-wave radiation, as

described in Eq. (4-31). Using four-component systems has important advantages: (1) it is possible to test and verify the functioning, accuracy, and level of each component using independent sensors such as pyranometers and infrared transducers or using theoretical means such as  $R_{so}$  for incoming shortwave; and (2) one can use the separate data to test or improve upon components of the radiation balance, for example,  $R_{nl}$  and  $R_L$ . All  $R_n$  sensors, whether single, two-, or four-component systems, should be verified for accuracy before deployment. It is much too common for even expensive sensors costing more than \$5,000 to suffer from calibration error or manufacturing quality (Allen et al. 2011c, d). Zhao and Allen (2014) described extensive side-by-side intercomparisons of four-component radiometers, means to discern calibration error of new instruments, and means for correcting them.

Figure H-4 shows hourly measured net radiation and net radiation calculated using the standardized net radiation procedure for one day at Kimberly, Idaho. Agreement between measured and calculated  $R_n$  is judged to be very good, even during nighttime periods, suggesting that good accuracy both from measured  $R_n$  and from calculated  $R_n$  can be obtained when quality of sensors and quality of operation and placement are high and when conditions factored into equations are fulfilled, for example, placement over vegetation having albedo near 0.23 and surface temperature similar to air temperature at 2 m during daytime.

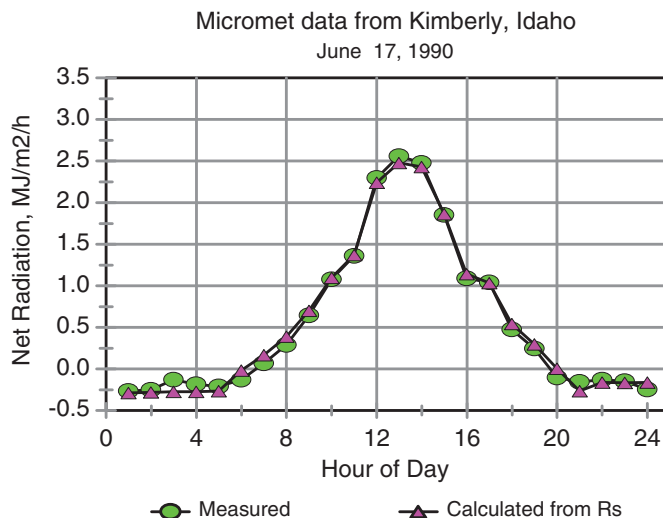


Fig. H-4. Measured and calculated hourly net radiation for one day at Kimberly, Idaho, over clipped grass ( $R_n$  was calculated using Eqs. (4-31) and (4-36)–(4-40))  
Source: Data courtesy of Dr. J. L. Wright, USDA-ARS, Kimberly (retired)

## Humidity and Air Temperature

**Relative Humidity** Humidity and air temperature data should be screened to identify questionable or erroneous data. A portion of the screening process requires the user to have a sense of what are reasonable and unreasonable values. For example, relative humidity ( $RH$ ) values chronically lower than 5 to 10% in arid regions and lower than 30% in subhumid regions are uncommon and may indicate problems with the sensor. Similarly,  $RH$  values in excess of 100% do not occur in the natural environment and may indicate that the sensor is out of calibration. The accuracy of most modern-day electronic  $RH$  sensors is generally within  $+/- 5\%RH$  (ASABE 2004); thus, recorded  $RH$  values in excess of 105% may suggest that the sensor is out of calibration. One should use  $RH$  data sets containing values in excess of 100% with caution. Furthermore,  $RH$  values in excess of 100%, if not accompanied by a QC flag, may indicate that the data set has not been subjected to rigorous QC. All  $RH$  values in excess of 100% should be set equal to 100% prior to use in the  $ET_{sz}$  computation process. Use of this simple adjustment procedure, however, does not mitigate sensor calibration errors for recorded  $RH$  data that lie below 100%. Some type of proportional adjustment to all data may be warranted.

If hourly data are available, it is useful to examine the diurnal variation of  $RH$  over a series of days to ensure that  $RH$  approaches maximum and minimum levels during the coolest and warmest portions of the day, respectively. Hourly time series of  $RH$  should be examined for the presence of spikes and spurious values of  $RH$  that may indicate sensor malfunction. Finally, one should check  $RH$  data on several days having heavy and/or sustained precipitation events or when dew or fog events are known to have occurred. Relative humidity should approach 90–100% during a sustained precipitation, fog, or dew event, and should approach 100% in the evening hours following a heavy rain event. In the case of dew formation, some allowance should be made for the likelihood of higher temperature at a 1.5 or 2 m measurement height as compared to the surface where dew is formed, plus any residual heat storage of the temperature enclosure. Both of these factors may keep  $RH$  at reference height from reaching 100% during radiatively caused dew formation.

**Dew Point Temperature** Dew point temperature ( $T_d$ ), as calculated from  $RH$ , may be reported in lieu of  $RH$  in some data sets.  $T_d$  is the temperature at which air becomes saturated with water vapor, and therefore,  $e^o(T_d) = e_a$ .  $T_d$  is a useful and singular representation of the vapor content of the air at the measurement height. Any error in  $RH$  will cause error in  $e_a$ , because  $e_a = RH * e^o(T)/100$  and thus the computed  $T_d$ . Values for daily average or early morning  $T_d$  should be compared to daily minimum temperatures ( $T_{min}$ ). In humid regions, the  $T_d$  measurement will

approach  $T_{min}$  on many days. Exceptions occur on days that feature a change in air mass (e.g., frontal passage), or that have high winds and/or cloudiness at night. Average daily  $T_d$  may exceed  $T_{min}$  in humid and subhumid climates and during winter in nearly all cold climates because of reduction of near-surface vapor content during dew formation near the time of  $T_{min}$  and subsequent evaporation of the dew and increase in vapor content after sunrise. In addition, evaporation during daytime will generally increase the 24-hour average for  $T_d$  over that occurring during the time of  $T_{min}$  in humid climates and during winter in nearly all climates by a few degrees C.  $T_d$  may approach  $T_{min}$  in arid and semiarid environments if nighttime winds are light and measurements are made over a surface exhibiting behavior similar to the reference definition (i.e., sufficient evaporation to cause evaporative cooling). It is not uncommon in arid and semiarid regions to have  $T_d$  2 to 5°C lower than  $T_{min}$  under reference conditions (see following discussion) but well below  $T_{min}$  if the measurement site is subjected to local aridity. If daily average  $T_d$  routinely exceeds  $T_{min}$  by a substantial amount (for example, more than 3 or 4°C), then the humidity sensor may be out of calibration. Exceptions include the very dry regions of Southern California, Arizona, and New Mexico, where differences between  $T_{min}$  and  $T_d$  can be as much as 10°C, even over irrigated fields (ASCE 2005). Such data should be examined closely and possibly adjusted prior to use. When it is not observed,  $T_d$  can be computed from  $e_a$  using Eq. (3-9).

Figure H-5 illustrates the use of comparisons between  $T_{min}$  and  $T_d$  and use of plots of daily  $RH_{max}$  and  $RH_{min}$  to detect errors in hygrometer data from an AWS in southeast Colorado. The large shifts in mean daily  $T_d$  relative to  $T_{min}$  at days 15 and 200 are obvious. Following day 200, the data began to follow an expected pattern and relationship with  $T_{min}$ , with  $T_d$  in close proximity to  $T_{min}$ . Similar obvious shifts in  $RH_{max}$  and  $RH_{min}$  are apparent also (bottom plot of Figure H-5). During the last half of the year, values for  $RH_{max}$  exceeded 100% by a small amount. However, these errors in RH are considered to be small relative to those occurring during the first part of the year, where the  $T_d$  data required substantial correction. Daily  $RH_{min}$  after day 200 regularly fell below 10%, which is considered to be a very low reading for a reference site. This reflects a relatively "harsh" evaporative environment. The proximity of  $T_d$  to  $T_{min}$  during the same period indicated the general presence of an evaporative surface.

Figure H-6 shows  $T_d$  and  $T_{min}$  for the same station and year as in Figure H-5, but following correction of  $T_d$  using the relationship of Eq. (8-19) in Chapter 8 where data from a second station are used following adjustment for local air temperature. The use of Eq. (8-19) preserved the difference observed between  $T_{min}$  and  $T_d$  observed at the second station and, therefore the relative dryness of the air mass, but adjusted for differences in minimum daily air temperature between the two sites. The resulting plots

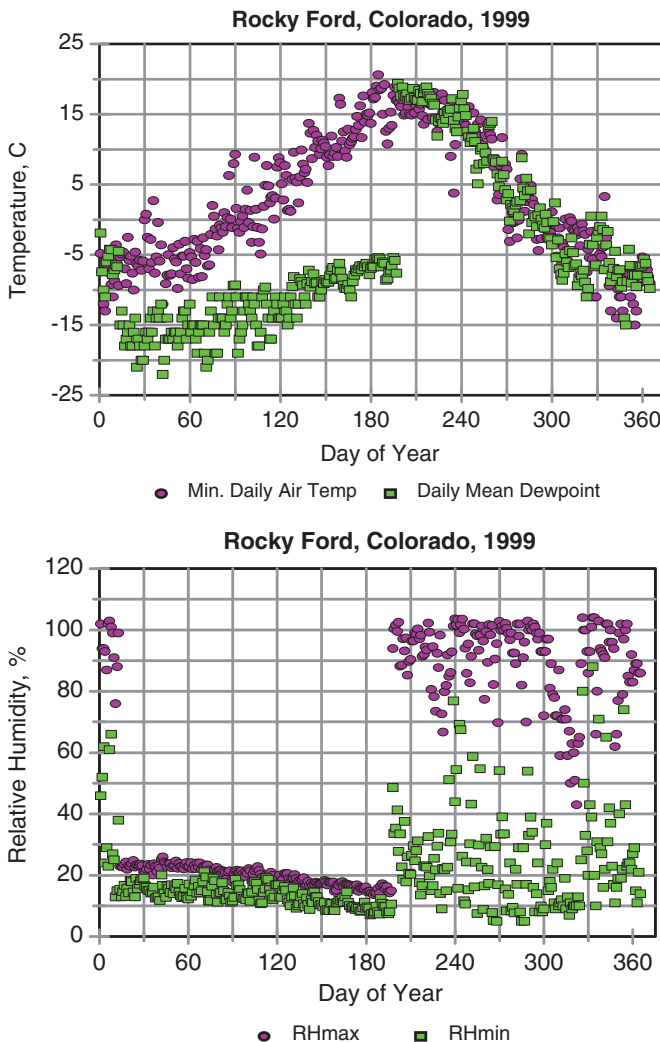
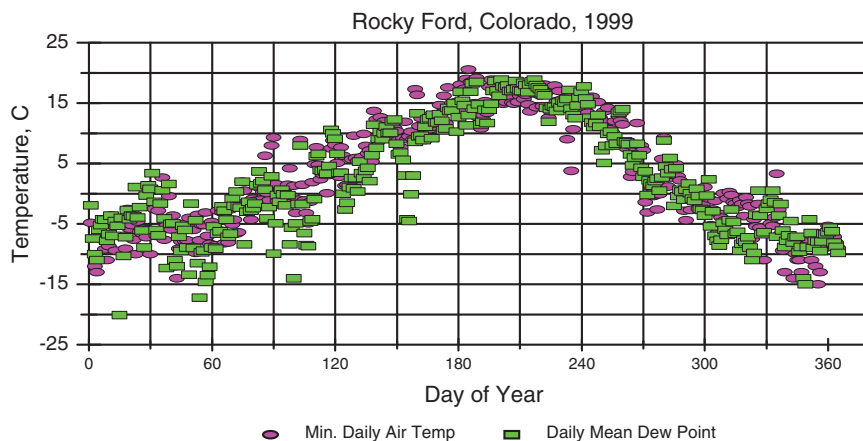


Fig. H-5. Measured daily minimum air temperature and mean daily dew point temperature (top) and daily maximum and minimum relative humidity (bottom) recorded for Rocky Ford, Colorado, during 1999

of  $T_{min}$  and  $T_d$  in Figure H-6 illustrate good continuity of the relationship between  $T_{min}$  and  $T_d$  for the corrected period (days 15–200) and original observations following day 200. The occasionally low values for  $T_d$  during days 15–200 were present in the data set for station 2.

Plots of hourly or shorter period  $T_d$  data may assist in identifying problems in  $T_d$  data. Dew point and vapor pressure are relatively



*Fig. H-6. Measured daily minimum air temperature and mean daily dew point temperature for Rocky Ford, Colorado, during 1999, where  $T_d$  for days 15 to 200 was replaced by estimates using Eq. (8-19)*

conservative parameters and often exhibit little change over a day, especially in humid regions. Often,  $T_d$  will increase somewhat during mid-morning due to evaporation of water and increased capacity for the air to contain vapor (see, for example, Figures H-7 and H-10). Dew point will then stabilize or decline slightly during the midday hours as the vapor near the surface gets mixed into a progressively deeper boundary layer. Hourly variation in  $T_d$  is greater in semiarid and arid settings, especially in areas prone to strong regional advection, where  $T_d$  can drop substantially during afternoon as warm, dry air from outside an irrigated area "breaks into" the boundary layer established over the irrigated area. However, large changes in  $T_d$  during the day, except under circumstances such as a change in air mass (e.g., frontal activity or sea/land breeze) or large change in wind direction, could signal an error or bias in the  $T_d$  measurement. It is common in the western Great Plains of the United States to have distinct dry lines, which extend either N-S or NE-SW. A dry line, which is an atmospheric transition zone having large gradients in vapor content, may move during the day, with larger  $T_d$  values in front of the dry line (typically the eastern side) and with substantially smaller  $T_d$  values behind the dry line (typically the western side). Allen (1996) provided illustrative plots of hourly  $T_d$  data and expected trends over time. Comparison of hourly  $T_d$  to T over a 24-hour period is illustrated in Figure H-7.

ASCE (2005) presented prioritized methods for estimating  $e_a$  from a variety of humidity parameters and summarized all calculation steps for the standardized  $ET_o$  and  $ET_r$  equations. These are listed in Table H-4. The recommendations are based on the likelihood that the data will have integrity

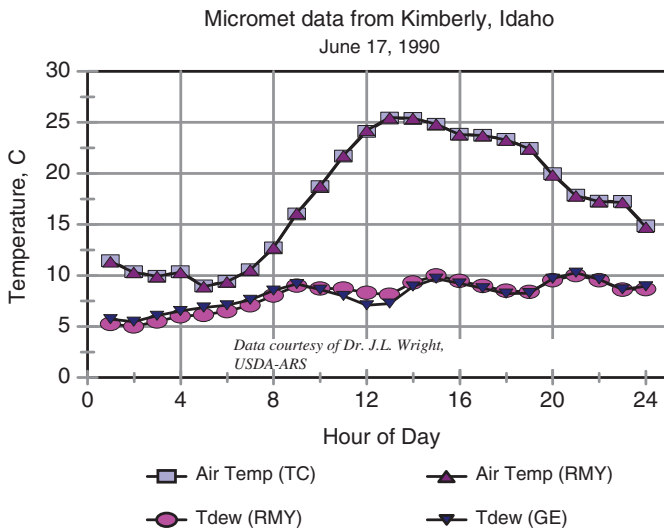


*Fig. H-7. Hourly air temperature and measured dew point temperature from dual sensor systems near Kimberly, Idaho, July 17, 1990*

*Source: Data courtesy of Dr. J. L. Wright, USDA-ARS, Kimberly, Idaho*

and that estimates for  $e_a$  will be representative. The availability and quality of local data, and site conditions, may justify a different order of preference.

When using RH data, it is essential that the RH and air temperature data are "paired," i.e., that they represent the same time of day or time period and that they are taken at the weather measurement site. For daily data, daily maximum relative humidity ( $RH_{max}$ ) can be paired with  $T_{min}$ , which will both occur, generally, during early morning. Daily minimum relative humidity ( $RH_{min}$ ) is paired with  $T_{max}$ .

Depending on the availability of the RH data, the following equations apply, with preference of method listed in Table H-4:

#### Daily $e_a$ from $RH_{max}$ and $RH_{min}$

$$e_a = \frac{e^o(T_{min}) \frac{RH_{max}}{100} + e^o(T_{max}) \frac{RH_{min}}{100}}{2} \quad (H-1)$$

where

$e_a$  = actual vapor pressure [kPa],

$e^o(T_{min})$  = saturation vapor pressure at daily minimum temperature [kPa],

$e^o(T_{max})$  = saturation vapor pressure at daily maximum temperature [kPa],

Table H-4. Recommended Method by ASCE (2005) for Calculating  $e_a$  for Use in Calculating Daily  $ET_{sz}$

Method No.	Method	Preference Ranking	Equation(s)
1	$e_a$ averaged over the daily period (based on hourly or more frequent measurements of humidity) <sup>a,b</sup>	1	—
2	Measured or computed dew point temperature (based on hourly or more frequent) averaged over the daily period	1	—
3	Wet-bulb and dry-bulb temperature averaged over the daily period	2	3-10
4	Measured or computed dew point or measured wet-bulb and dry-bulb temperature at 7 or 8 a.m.	2	3-10
5	Daily maximum and minimum relative humidity	2	H-1
6	Daily maximum relative humidity	3	H-2, 8-18
7	Daily minimum relative humidity	3	H-3
8	Daily minimum air temperature	4	8-17, 8-19
9	Daily mean relative humidity	4	H-4

<sup>a</sup>In many data sets,  $e_a$  may be expressed in terms of an equivalent dew point temperature.

<sup>b</sup>Some data-logging systems may measure  $RH$  and  $T$ , but calculate  $e_a$  or  $T_d$  internally for output as averaged values over some time interval. See ASABE (2004) for further detail.

$RH_{max}$  = daily maximum relative humidity [%], and

$RH_{min}$  = daily minimum relative humidity [%].

### Daily $e_a$ from $RH_{max}$

Older styles of electronic relative humidity sensors, for example, those manufactured before about 1990, often experienced difficulty in accurately measuring  $RH$  when at low levels. When using equipment where errors in estimating  $RH_{min}$  may be large, or when integrity of the  $RH$  data is doubtful, the actual vapor pressure can be computed from  $RH_{max}$ :

$$e_a = e^o(T_{min}) \frac{RH_{max}}{100} \quad (H-2)$$

When accuracy of  $RH$  data is in doubt, error in  $RH_{max}$  causes smaller error in  $e_a$  than error in  $RH_{min}$ , due to the smaller value for the multiplier  $e^o(T_{min})$  as compared with  $e^o(T_{max})$ . In addition,  $RH_{max}$  data are generally easier to assess for accuracy than is  $RH_{min}$ . The value of  $RH_{max}$  generally exceeds 90% and approaches 100% in well-watered settings such as within irrigation projects and in subhumid and humid climates. This proximity to 100% serves as a first check on reasonableness, representativeness, and integrity of the data. Exceptions to this trend are where substantial advection of dry or warm air from dry regions outside the area occurs during nighttime, including, but not limited to some desert areas of New Mexico, Arizona, and California.

#### Daily $e_a$ from $RH_{min}$

Sometimes, only high-quality estimates of daily  $RH_{min}$  are available and must be used to predict  $e_a$

$$e_a = e^o(T_{max}) \frac{RH_{min}}{100} \quad (H-3)$$

However, estimates using Eq. (H-3) may be less desirable than estimates using Eq. (H-1) or (H-2), due to greater impact of error in  $RH_{min}$  on  $e_a$ , as discussed previously. In addition, it is more difficult to assess the integrity of  $RH_{min}$  data.

#### Daily $e_a$ from $RH_{mean}$

In the absence of  $RH_{max}$  and  $RH_{min}$  data, but where daily  $RH_{mean}$  data are available, the actual vapor pressure may be estimated as

$$e_a = \frac{RH_{mean}}{100} e^o(T_{mean}) \quad (H-4)$$

where  $RH_{mean}$  is the mean daily relative humidity, generally defined as the average between  $RH_{max}$  and  $RH_{min}$  and  $T_{mean}$  is mean daily air temperature, generally estimated by averaging  $T_{max}$  and  $T_{min}$ . Eq. (H-4) is less desirable than Eqs. (H-2) or (H-3) because the  $e^o(T)$  relationship is nonlinear. Eq. (H-4) produces estimates of  $e_a$  that are closer to those by Eq. (H-1) and to daily average  $e_a$  computed from hourly values than is the use of alternative forms of Eq. (H-4), such as  $e_a = RH_{mean}/100[e^o(T_{max}) + e^o(T_{min})]/2$  as described in Allen et al. (1998) or as  $e_a = RH_{mean}/100[1/(50/e^o(T_{max}) + 50/e^o(T_{min}))]$  as described in Smith et al. (1991). These latter two methods are not recommended in the standardized procedure.

Table H-5. Recommended Method by ASCE (2005) for Calculating  $e_a$  for Use in Calculating  $ET_{sz}$  for Hourly or Shorter Time Periods

Method No.	Method	Preference Ranking	Equation(s)
1	$e_a$ averaged over period <sup>a,b</sup>	1	—
2	Measured or calculated dew point temperature averaged over period	1	—
3	Average RH and $T$ for the hour	1	H-5
4	Wet-bulb and dry-bulb temperature	2	3-10
5	Daily minimum air temperature (see Chapter 8)	3	8-17, 8-19

<sup>a</sup>In many data sets,  $e_a$  may be expressed in terms of an equivalent dew point temperature.

<sup>b</sup>Some data-logging systems may measure RH and  $T$ , but calculate  $e_a$  or  $T_d$  internally for output as averaged values over some time interval.

In the case of hourly or shorter time periods, ASCE-EWRI (2005) recommended the preference ranking shown in Table H-5 for calculating actual vapor pressure.

The actual vapor pressure of air for hourly periods can be calculated from relative humidity (RH) and saturation vapor pressure at the corresponding air temperature [ $e^o(T)$  from Eq. (3-1)]:

$$e_a = \frac{RH}{100} e^o(T) \quad (\text{H-5})$$

where

RH = mean relative humidity for the hourly period, %, and

$T$  = mean air temperature for the hourly period, °C.

**Air Temperature** In general, air temperature is the simplest and most consistent weather parameter to measure and the parameter most likely to be of highest quality, provided it is measured in a reference type of environment. Air temperature extremes in a data set should be compared to historical record extremes, if such data are available for locations near the site. Temperatures that routinely exceed the recorded extremes for a region indicate a problem either with the sensor or with the radiation shield used to house the sensor. Sensors mounted in non-aspirated radiation shields may produce erroneously high temperatures on days having light winds due to solar heating of the shield (Gill 1983; Tanner et al. 1996). Consistently hot temperatures from a sensor

mounted in an aspirated radiation shield may indicate problems with the ventilation system. An effective check for spuriously high or low temperature extremes is to compare the average of the daily extremes ( $T_{max}$  and  $T_{min}$ ) with the mean daily temperature as averaged by the data logger for the day. Many automated weather stations now generate a recorded average temperature for the 24-hr period that can be used in this comparison. Differences between the average computed from the daily temperature extremes and the recorded 24-hr average for the day will generally run within 2°C. Data should be subjected to closer scrutiny on days when the two averages deviate by more than 3°C. Precipitation events, air mass changes, and unusual wind conditions can cause deviations in excess of 3°C.

When hourly temperature data are available, it is advisable to plot the trend of temperature during the day for selected dates to confirm that temperatures attain maximum and minimum values at the appropriate times of the day. For most locations, minimum temperatures occur shortly before sunrise, and maximum temperatures occur in midafternoon (1400–1600). It is also important to examine hourly time series of temperature for spikes or spurious temperatures that could indicate a malfunctioning sensor. Comparison of mean 24-hour air temperature calculated from  $T_{max}$  and  $T_{min}$  against the mean computed by averaging hourly (or shorter) temperature is a straightforward way to indicate the potential occurrence of spikes or missing values in the hourly set or some type of problem with the  $T_{max}$  and  $T_{min}$ .

Figure H-7 illustrates hourly measurements of both air temperature and dew point temperature during a single day over a grassed surface near Kimberly, Idaho, which has a semiarid climate. Measurements were made using electronic instrumentation, and dual measurements using independent systems from different manufacturers were used for purposes of data backup and redundancy. The two air temperature sensors (TC = thermocouple and RMY=RM Young chilled mirror system) tracked each other consistently throughout the 24-hour period. The two dew point temperature measurements (RMY = RM Young chilled mirror system and GE = General Eastern chilled mirror system) tracked each other closely throughout the period. The closeness of the data measurements from two independent, colocated systems is useful in confirming the accuracy of the data and the proper functioning of both instrument systems. In addition to validation of the air temperature and measured dew point temperatures, the data in Figure H-7 show that minimum daily air temperature, recorded as 9.0°C at about 5 a.m. was about 3°C above the dew point temperature (6.2°C) measured at the same time. This difference is in line with that expected from a well-watered reference environment as discussed previously and in the following section.

## Impact of Nonreference Weather Station Site on Temperature and Humidity

Temperature and humidity data that pass QA/QC checks still may not be advisable for use in estimating  $ET_{ref}$ . The moisture status of the underlying surface affects both temperature and humidity due to the energy balance and impacts of evaporative cooling. Therefore, data collected away from well-watered vegetation (e.g., at airports or over dry, paved, and fallow surfaces) can be negatively influenced by the local aridity, especially in arid and semiarid climates. Data from dry or urban settings may cause overestimation in  $ET_{os}$  or  $ET_{rs}$  because of air temperature measurements that are too high and humidity measurements that are too low, relative to the reference condition. Under these "arid" measurement conditions, the  $ET_{os}$  and  $ET_{rs}$  calculations may reflect ET demand of the "ambient," "nonreference" environment, for instance, where average net rainfall plus irrigation is substantially less than  $ET_o$  or  $ET_r$ , so that air temperature is elevated. These estimates of  $ET_{os}$  and  $ET_{rs}$  tend to overestimate the  $ET_{os}$  and  $ET_{rs}$  that would occur for a well-watered setting. An extreme example of the impact of local aridity on  $ET_{os}$  was observed in a study near Parker, Arizona (Brown, personal communication, 2001) where weather stations were installed in adjacent 15-ha fields containing irrigated alfalfa and fallow ground. Data from each station were used to estimate  $ET_{os}$  using the  $ET_{sz}$  equation. Monthly totals of  $ET_{os}$  computed using the fallow station data set exceeded similar  $ET_{os}$  totals computed using the alfalfa data set by 18–26% during months of June through September (Figure H-8).

Often, an assessment of  $RH$ ,  $T_d$ , and  $e_a$  can indicate whether meteorological data were collected in a reference type of environment. Under reference conditions, daily  $RH_{max}$  generally exceeds 90% and may approach 100% during early morning hours, provided skies are clear and winds are light (Allen 1996). Minimum temperatures under these circumstances will approach  $T_d$ . One can therefore plot and then visually scan plots of  $RH_{max}$  or average (or early morning)  $T_d$  and  $T_{min}$  as a function of time to determine if humidity data reflect the reference condition.

For example, Figure H-9a shows daily  $T_{min}$  and  $T_d$  for the year 2000 for the agricultural weather station near Greeley, Colorado. Mean daily  $T_d$  (calculated from daily average measured vapor pressure) follows  $T_{min}$  relatively closely throughout the year and is generally within a few degrees Celsius of  $T_{min}$ . Figure H-9b shows daily maximum and minimum  $RH$  for 2000 at Greeley. The  $RH_{max}$  tends toward 90 to 100% during many days. Minimum relative humidity ( $RH_{min}$ ) runs a little below the expected 25 to 35% range for a reference setting in a semiarid environment (Allen et al. 1983, Allen 1996). Overall, the humidity and air temperature data at

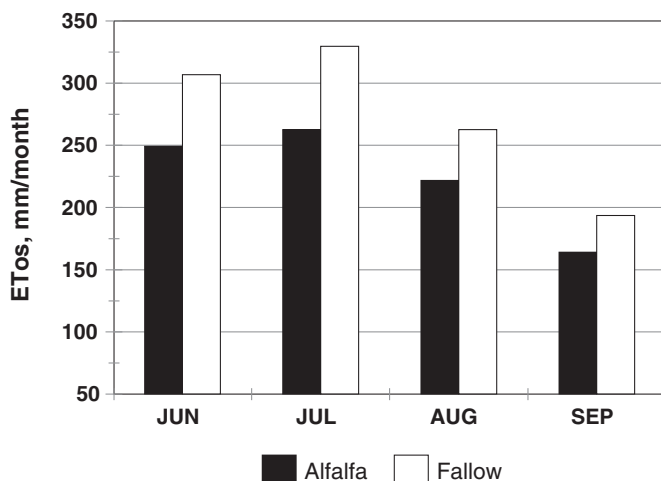


*Fig. H-8. ET<sub>os</sub> by month for the summer of 2000 at Parker, Arizona, computed using meteorological data collected under reference (alfalfa) and nonreference (fallow) conditions*

Source: ASCE (2005); copyright ASCE

Greeley during 2000 are judged to be relatively accurate and reflective of a "reference" condition.

If  $RH_{max}$  is consistently below 80% for a substantial portion of the growing season record, or if  $T_d$  tends to run more than 3–4°C lower than  $T_{min}$  for a substantial portion of the growing season record, then the humidity data should be subjected to further scrutiny. Among the factors to investigate are (1) type, maintenance, and calibration of the  $RH$  or  $T_d$  equipment; (2) presence of cloudiness or wind flow at night, which tend to reduce  $RH_{max}$ ; (3) that the site may not be representative of well-watered conditions; and (4) that the region has characteristically very dry air so that irrigated areas are subject to substantial advection of hot, dry air, for example, in Imperial Valley, California, and portions of Arizona and New Mexico. Historically, humidity has been among the most difficult routine meteorological parameters to measure accurately. The quality of  $RH$  measurements has improved in recent years due to improvements in sensor technology. Prior to 1990, many agricultural weather networks used polystyrene humidity sensors. These sensors degraded rather quickly in agricultural environments (Howell et al. 1984; Brown et al. 1988), and  $RH$  measurement errors in excess of 5%  $RH$  were common under the best of circumstances (Brown et al. 1988). Most networks now utilize thin-film capacitance  $RH$  sensors that are stable for periods in excess of one year and are generally accurate to within 2–3%  $RH$ .

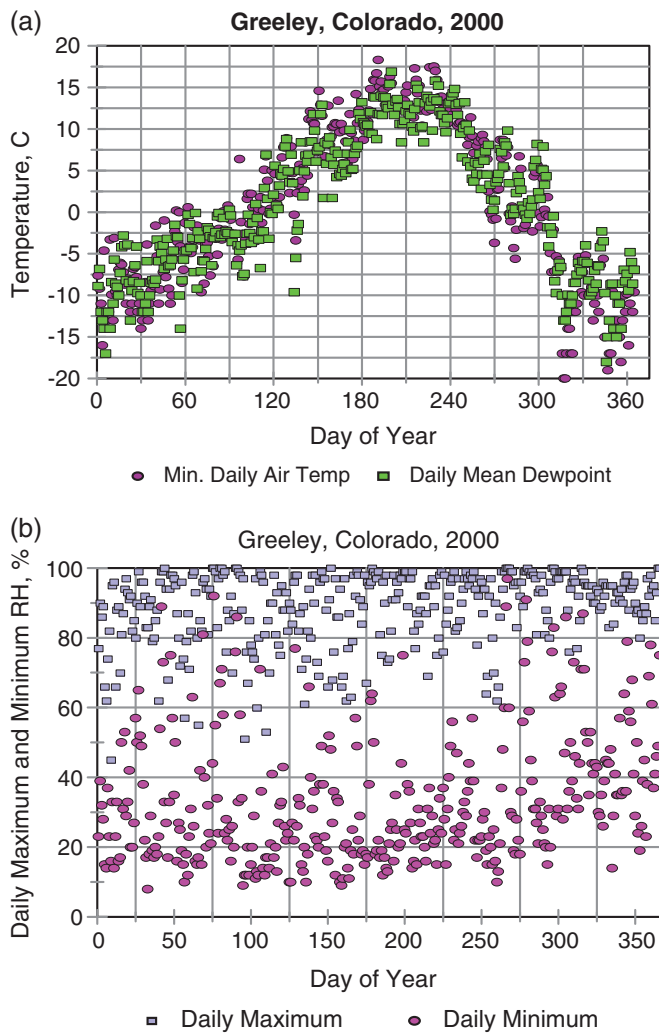


*Fig. H-9. (a) Daily minimum air temperature and daily mean dew point temperature vs. day of the year and (b) daily maximum and daily minimum relative humidity vs. day of the year for Greeley, Colorado, during 2000*

Psychrometers, dew cells, and chilled mirror hygrometers can provide high-quality humidity data, as shown in Figure H-7, provided the sensors receive proper maintenance and are operated within the design range. These sensors are not in widespread use for general climate monitoring in remote, automated weather stations due to cost and maintenance factors. The  $RH$  and  $T_d$  assessments described here may not be effective for

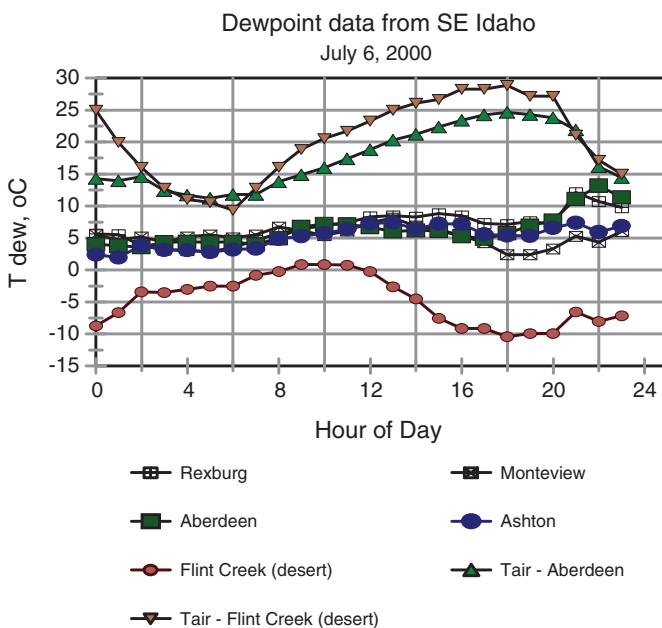


*Fig. H-10. Hourly dew point from four irrigated regions of southeast Idaho and from a desert weather station (Flint Creek) on July 6, 2000. Also shown are air temperatures at Aberdeen and Flint Creek*

identifying data representative of a suitable reference environment in regions prone to cloudiness and large nighttime winds. Cloudiness lowers net loss of long-wave radiation at night, which inhibits cooling and may prevent  $T_{min}$  from approaching  $T_d$  at night. High nighttime wind speed enhances the transfer of sensible heat and dry air to the surface, slowing the rate of cooling by evaporation, and preventing full humidification of the atmospheric boundary layer above well-watered surfaces.

Often, dew point temperature is consistent between locations having similar surface conditions. For example, Figure H-10 shows hourly dew point temperatures for four Agrimet weather stations (data from U.S. Bureau of Reclamation) in southern Idaho that are up to 140 km apart. The recorded dew point temperatures and their trend during the day are largely consistent. The four stations (Rexburg, Montevieu, Ashton, and Aberdeen) are situated in irrigated agricultural settings. Dew point data taken from a desert weather station operated by the Idaho Department of Transportation (Flint Creek, Idaho, lat. 42.08°, long. 112.18°) is substantially lower, averaging 11°C below the average for the four Agrimet stations. Air temperature at Flint Creek averaged 4°C above the Agrimet stations over the 24-hour period. The impact of aridity on both dew point

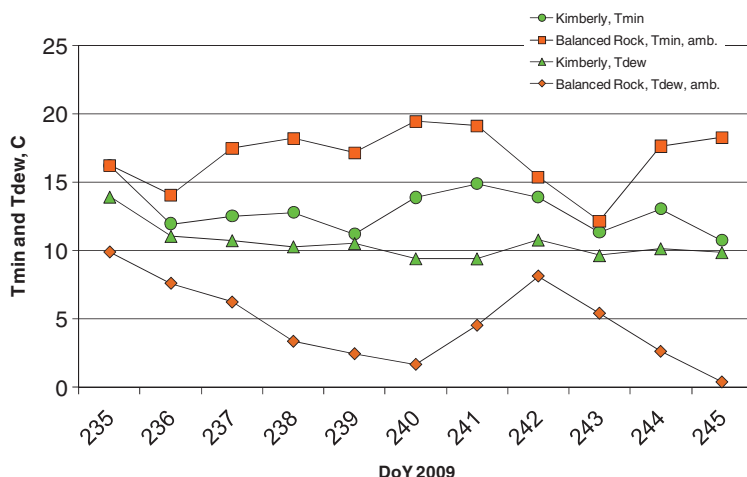
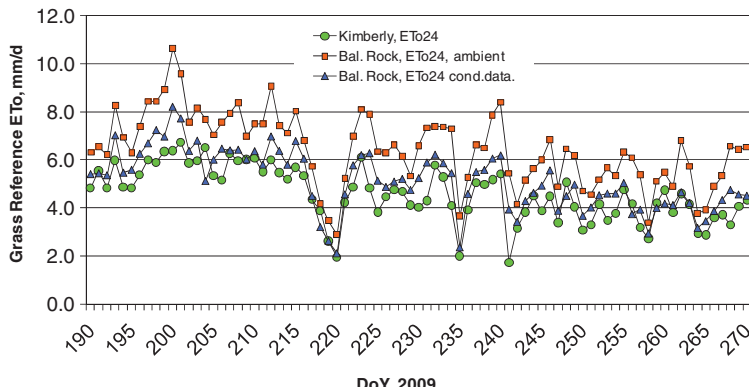


Fig. H-11.  $T_{\min}$  and daily average  $T_d$  at an irrigated alfalfa site near Kimberly, Idaho, and at a desert grass site near Balanced Rock, 50 km west of Kimberly for an 11-day period in August of 2009. The data from Balanced Rock are the unadjusted, or "ambient" data

temperature and air temperature at Flint Creek is obvious and is manifested in erroneously high  $ET_{ref}$  estimates if applied without adjustment.

One final example of the impact of local and regional transpiration from irrigated crops on the conditioning of air temperature and humidity of air is shown in Figures H-11–H-13, where temperature and humidity data from two locations in southern Idaho, Kimberly, and Balanced Rock, are contrasted. The Kimberly site was irrigated alfalfa in the center of a nearly 200,000 ha irrigated region of desert. The Balanced Rock site is approximately 50 km west of Kimberly and is over sparse desert grass surrounded by desert, with mostly desert for more than 200 km in the typical upwind direction. Average annual rainfall is 200 mm.

The daily  $T_{\min}$  over the desert ran 5 to 6°C higher than that over the irrigated site, and the dew point temperature over the desert ranged 3 to 7°C lower than that over the irrigated site. These data illustrate the cooling and humidifying effect that irrigation had on desert air masses as they passed over the substantial irrigated region. The difference between  $T_{\min}$  and  $T_d$  was reduced to a range of 1 to 5°C at Kimberly by the conditioning effect of ET. As shown in Figure 11-10 of Chapter 11, but for a longer period, the vapor content of the near-surface boundary layer, expressed in terms of vapor pressure, nearly doubled at Kimberly due to ET from the irrigation. The "Bal. Rock Cond. 2pm vap.pres. ref." series is the vapor pressure measured at the desert site, but following the application of a



*Fig. H-12. Grass reference  $ET_0$  from the standardized ASCE (2005) Penman-Monteith equation using air temperature, vapor pressure, wind speed, and radiation data collected over an irrigated alfalfa site near Kimberly, Idaho, and over a desert grass site near Balanced Rock, 50 km west of Kimberly over an 80-day period in 2009. The “ambient” data from Balanced Rock used the unadjusted, or “ambient” data, and the “cond.” data used Balanced Rock ambient data following conditioning to simulate reference conditions*

Source: [Allen 2015](#)

“conditioning” routine based on profile and flux theory as introduced in Chapter 11. The conditioning routine adjusted the desert data so that values agreed more closely with the humidity measured over the irrigated site, which better approximates a reference environment for calculating reference ET.

The impact of using weather data collected from dry weather sites surrounded by dry conditions without any conditioning of the data is shown in Figure H-12, where the data from the Kimberly and Balance Rock sites were used to calculate the grass reference  $ET_0$  using the standardized ASCE (2005) Penman-Monteith equation. The result of using the data from the Balanced Rock desert site was to increase calculated  $ET_0$  by up to 20 to 30%.

### Wind Speed

Accuracy of wind speed measurements is difficult to assess unless duplicate instruments are used. Nevertheless, one should visually inspect wind records for the presence of consistently low wind speed values that may indicate a malfunctioning or failed anemometer or the presence of ice if air temperatures are near or below 0°C. Consistent and low wind speeds can indicate dirty anemometer bearings that will increase the anemometer

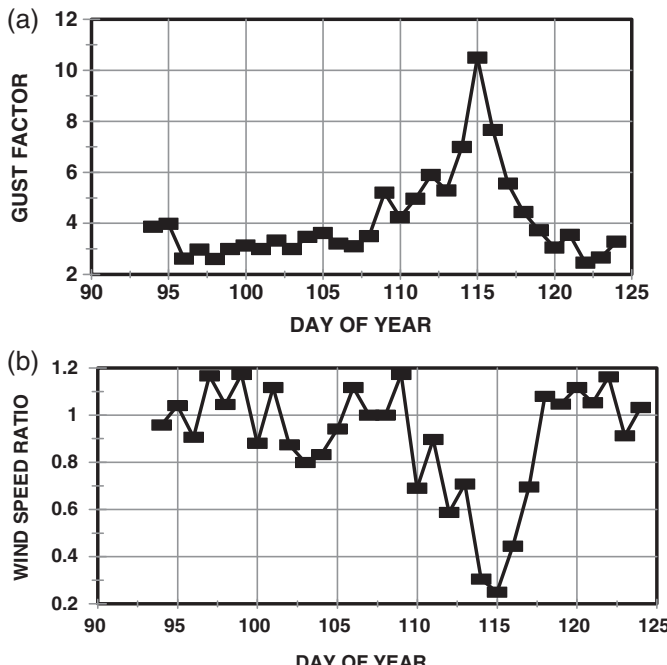


Fig. H-13. (a) Plot showing the increase in the gust factor at Eloy, Arizona, during a period when an anemometer was failing due to bearing contamination; (b) Ratio of daily mean wind speeds at Eloy, Arizona, to those at Maricopa, Arizona, during the period of anemometer failure described in (a)

Source: ASCE (2005); copyright ASCE

wind speed threshold and might eventually seize and stop the anemometer altogether. Wind speeds from failed anemometers will usually appear as small, constant values (less than  $0.5 \text{ m s}^{-1}$  or the wind speed threshold for a new anemometer) if the anemometer is monitored with a data logger. With a failed anemometer, recorded maximum and mean wind speeds will often have the same values and be equal to any numerical offset in the calibration equation.

Maximum wind speed data, if available, can assist in the assessment of low wind speed data by calculating a gust factor, computed as the ratio of maximum wind speed ( $\text{m s}^{-1}$ ) to mean daily wind speed ( $\text{m s}^{-1}$ ). If a plot of gust factors over time indicates a period of excessively large values, then the anemometer may be malfunctioning. For example, Figure H-13a shows data from an anemometer that was malfunctioning between Day 109 to 117 due to bearing contamination. Gust factors often increase as contamination increases the friction in the bearings. The increasing bearing friction has a

greater impact on cup rotation at small as opposed to large wind speeds and thus causes an increase in the ratio of maximum to mean wind speed. The gust factor will exhibit a sudden drop to 1.0 when the anemometer seizes or fails electronically. The data analyst must be cautious, however, in interpretation of a gust factor, because some weather periods can have more gusty, turbulent airflow than others.

Any appreciable period having daily mean wind speeds of less than  $1.0 \text{ m s}^{-1}$  should be viewed with caution. Aside from exceptionally calm periods or anemometer problems, other possible reasons for daily wind speeds of less than  $1.0 \text{ m s}^{-1}$  would include excessive vegetation height at the station or the presence of blocking structures in the nearby landscape (e.g., solid fences or buildings).

Data from a nearby station may also assist in the assessment of wind speeds at a particular site. In some cases, winds at two nearby locations are related, which indicates the ratio of the wind speeds at the two locations will remain nearly constant. By plotting this ratio over time, one can identify a problem anemometer. A sudden and consistent change in the ratio often indicates a failed anemometer; a gradual change in ratio may indicate growing contamination in the bearings (Figure H-13b).

As an illustration of comparing wind speed data from two or more locations, daily wind speed data from three neighboring CoAgMet AWS stations located in the Arkansas River Valley of Colorado are plotted in Figure H-14a. The Vineland and Avondale stations are within 15 km (10 miles) of one another and the Rocky Ford station is about 60 km (40 miles) further east. All stations are located in agricultural environments, and wind was measured at 2 m above the ground. The similarity in wind speed records is apparent. The Vineland station had some fields of corn planted near the weather station during 1995 (Allen, personal communication, 2001) that impeded wind speed measurements during late summer. This is evident in viewing the daily wind plot in Figure H-14a, where daily wind speeds for Vineland fell below those at Avondale and Rocky Ford from day 190 through day 270. Ratios of wind speed for Vineland to wind speed at Rocky Ford show a similar pattern (Figure H-14b), with ratios routinely falling below 0.7 during the period from day 210 through day 270 when the corn crop was tallest. Ratios of wind speed for Avondale to Rocky Ford followed a consistent average of 1.0 all year, as is expected, with some inconsistencies during winter months. This example illustrates the use of data from neighboring stations to discern shifts or anomalies in a data set.

A good preventive maintenance program is required to keep anemometers functioning at peak performance levels. Weather station anemometers should be replaced with newly reconditioned (new bearings) and calibrated anemometers at regular intervals. An annual replacement in light to normal wind regions or semiannual replacement in windy regions

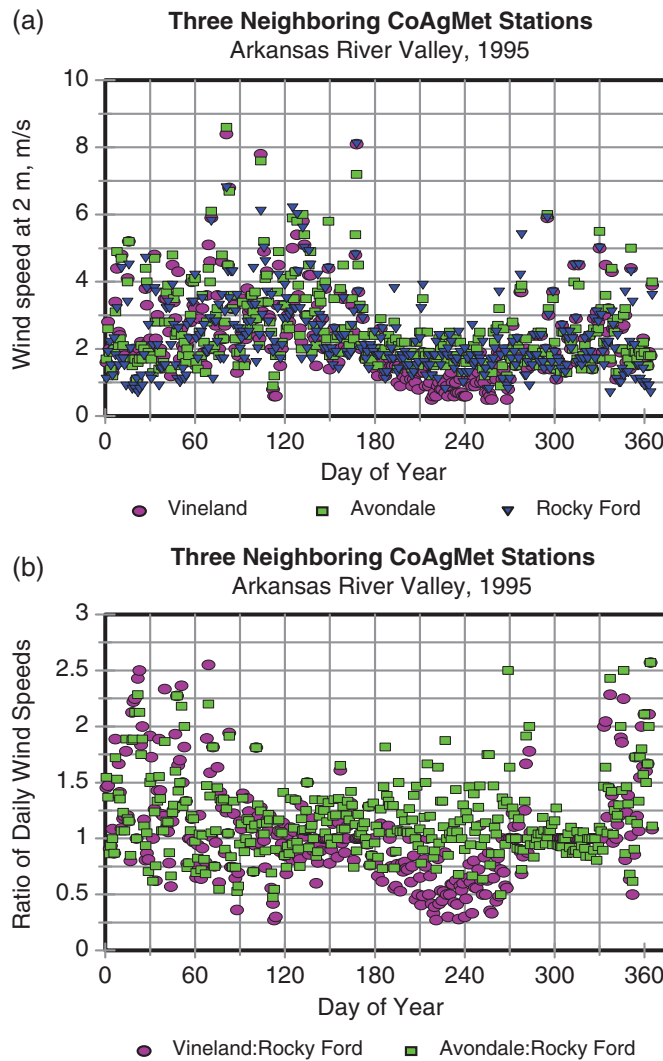


Fig. H-14. Daily mean wind speeds recorded at three neighboring AWS stations in SE Colorado during 1995 (a) and ratios of wind speeds to those at Rocky Ford for the same stations (b).

should be considered for anemometers located in agricultural settings. Some providers of weather data employ a standard practice of replacing anemometers on a regularly scheduled basis. The replacement schedule is typically based on local experience or recommendations of the manufacturer and may be as short as six months. ASABE (2004) provides detailed

recommendations on periodic sensor maintenance. An alternative technique for evaluating anemometers involves redundancy in instrumentation and requires placement of a second anemometer of the same design, but with fresh bearings, at the weather station for a three- or four-day period at least once each year, and comparing recorded values. (If a second data logger is used to record the temporary anemometer, one should be careful to synchronize data logger clocks. Also, one should be careful that adjacent anemometers do not interfere with one another's wind stream.) Variations between recordings can signal a need to replace bearings, switches, or other parts. Two- and three-dimensional sonic anenometers use speed-of-sound-based measurements so that the systems have no moving parts. These systems are capable of measuring very low wind velocities.

Wind speeds over nonreference surfaces may exhibit a systematic upward bias relative to wind speeds measured over reference surfaces. Vegetation in excess of the recommended reference-surface height will impose a greater frictional drag on the near-surface atmosphere and reduce wind speed relative to the reference condition. Smooth, dry surfaces will generate an opposite bias; wind speeds over these surfaces will generally be higher than those measured over reference surfaces. In addition, substantial sensible heat flux from surfaces having low ET due to dryness have greater amounts of buoyancy-induced mixing of the lower atmosphere and tend to entrain higher velocity air toward the surface, thereby increasing near-surface wind speed. Allen and Wright (1997) have suggested procedures for adjusting nonreference wind speed data to better represent reference conditions; however, these procedures assumed neutral buoyancy conditions. Ley et al. (2013) have conducted recent tests of these procedures with good results over irrigated alfalfa in Colorado.

## H.5 ADJUSTMENT OF WEATHER DATA

Adjustment of temperature and/or humidity data may be warranted when the weather station site is known to be in a local environment that substantially departs from a reference condition and assessment of humidity data indicates that the aridity is impacting the weather data. Allen and Pruitt (1986) and Allen (1996) suggested simple, empirical adjustment procedures to make "nonreference" weather data more representative of well-watered reference conditions by subtracting month-specific adjustments from the nonreference data in proportion to the "aridity rating" of the particular station. An example of these adjustments is given in Table H-6. The adjustments will generally vary with climate and precipitation patterns. Annex 6 of FAO-56 includes procedures for evaluating and adjusting humidity and air temperature data for aridity of the

Table H-6. Average Monthly Observed Departures (Elevation) of Daily Maximum, Minimum, and Mean Air Temperature for a Desert Location in Southern Idaho during 1981 from that Measured at an Irrigated Reference Site (Allen et al. 1983; Allen and Pruitt 1986) and the Smoothed Standardized Monthly Departure Used by Allen and Brockway (1983) for Estimating Reference ET in Idaho

Month	$T_{max}$ , °C	$T_{min}$ , °C	$T_{mean}$ , °C	Standard Departure, °C	30-Year Desert Precipitation, mm
April	2.7	2.4	2.5	1	23
May	1.3	0.6	0.9	1.5	28
June	2.4	1.8	2.1	2	22
July	4.8	2.9	3.8	3.5	3
August	5.2	4.3	4.7	4.5	8
September	3.3	2.7	3	3	11
October	0.3	1.6	0.9	0	13

weather station site. Allen and Gichuki (1989) and Ley et al. (1996) suggested more sophisticated, but still empirical approaches that adjusted both air temperature and humidity data. Allen and Robison (2007) and ASCE (2005) recommended adjusting only humidity data, rather than air temperature data, or replacing arid humidity data completely by tying estimates for dew point temperature to minimum daily air temperature. The intended result was for both air temperature and dew point temperature to carry similarly signed biases that in turn tend to compensate during calculation of vapor pressure deficit in the Penman or Penman-Monteith equations. All of these methods have an empirical basis and require at least regional calibration or confirmation of adjustment coefficients. Allen (2015) introduced a more theoretically based boundary layer development-blending height approach to adjust air temperature, humidity, and wind speed data for aridity effects. However, this approach requires a full complement of daily or hourly weather data (solar radiation, air temperature, humidity, wind speed, and precipitation).

### Estimates of $T_d$ Using $T_{min}$

Often, substituting  $T_d = T_{min} - K_o$  for measured  $T_d$  can improve estimates of daily  $ET_{os}$  and  $ET_{rs}$  when data are from a nonreference, arid setting. In arid and semiarid regions, it is best to check with the source of weather data to determine if  $K_o$  values have been developed for the area. For example, in Arizona the value of  $K_o$  was found to vary from 2 to 5°C

and even higher over the course of a year depending on the regional aridity (Brown 2001, personal communication). When local information on  $K_o$  is not available, a  $K_o$  in the range of 2 to 4°C is recommended for semiarid and arid regions (Allen 1996). In humid regions where  $T_d$  approaches  $T_{min}$  on most nights,  $K_o$  is set equal to 0°C. Some irrigated areas in very dry, advective climates can have extended periods during which  $T_{min}$  is more than 5°C above  $T_d$ . These areas include portions of SE California, southern Arizona, and New Mexico. Caution should be exercised in the specification of  $K_o$ .

Using minimum air temperature measurements from a nonreference setting to estimate dew point temperature using  $K_o$  with Eq. (8-17) may tend to overestimate the true  $T_d$  and  $e_a$  that would have occurred under reference conditions. This occurs because measured  $T_{min}$  is higher in the dry setting than in a reference setting and thus  $T_d$  based on  $T_{min} - K_o$  where  $T_{min}$  is elevated due to aridity may be somewhat overestimated. However, because  $e_s$  in the Penman-Monteith equation will be estimated using the same  $T_{min}$  values used to estimate  $T_d$ ,  $e_s$  and  $e_a$  will be essentially equally "inflated." Therefore, the  $e_s - e_a$  difference in the standardized  $ET_{ref}$  equation in general will approximate the  $e_s - e_a$  difference anticipated for the reference condition. As a consequence, a more accurate estimate for  $ET_{os}$  or  $ET_{rs}$  may result than if the actual measurement of  $T_d$  from the arid setting had been used. When humidity is adjusted using  $T_d = T_{min} - K_o$ , no further adjustment is generally needed to the air temperature data set to account for effects of aridity of the weather measurement site (Allen and Robison 2007).

Use of the  $T_d = T_{min} - K_o$  adjustment may produce a slight upward bias in computed net radiation ( $R_n$ ). The adjustment when  $T_{min}$  is impacted by station aridity inflates  $e_a$  above levels expected for reference conditions. This error in  $e_a$  causes atmospheric long-wave radiation to be overestimated, which in turn causes a 1 to 3% overestimation in  $R_n$ . This impact is considered to be relatively minor.

This page intentionally left blank

# APPENDIX I

## CONTRIBUTION OF CAPILLARY FLOW FROM A SHALLOW WATER TABLE TO EVAPORATION AND EVAPOTRANSPIRATION

The contribution of water to evaporation and evapotranspiration from shallow groundwater can be an important part of water balances and determination of irrigation water requirements. Quantification of capillary flow is also important for managing water logging and soil salinization. This appendix contains a description of an analytical procedure and employment of software simulations to estimate the contribution of water from a shallow water table to the ground surface for direct evaporation or into a root zone for extraction by plant roots. The analytical procedure follows Brutsaert (1982) and provides a relatively simple approximation of potential upward flux of water from a water table. In reality, the actual flow and evaporation process can be complicated by soil layering, soil disturbance, soil cracking, soil temperature, and tillage. Therefore, the simplified analytical approach provides only an approximation of upward flow. Detailed field studies and modeling are recommended where high accuracy is needed. The software model, UPFLOW by Raes and deProost (2003) and Raes (2004), considers effects of soil layering, root density, soil moisture distribution, and anaerobiosis effects on upward flux. This model was used here to develop general curves of upward flux vs. depth to groundwater and associated regression equations. Detailed studies of upward flow of water from shallow groundwater, especially under transient conditions, may warrant use of more sophisticated models than are considered here.

### I.1 THE BRUTSAERT-GARDNER ANALYTICAL PROCEDURE

Several simplified methods and computer models have been developed for estimating upward flux from shallow groundwater systems. Analytical models include Milly (1988), Miyazaki (1993), Yuana and Zhiming (2005),

and numerical models include SWAP (Kroes and van Dam 2003), HYDRUS (Šimunek et al. 2005), and UPFLOW (Raes 2004). Many of these methods use specific algorithms to describe the shapes of soil water potential-soil water content and soil water potential-hydraulic conductivity curves for unsaturated soil. A general method of Gardner (1958) and Brutsaert (1982) is presented here that employs traditional, general shape factors to describe hydraulic characteristics for the particular soil. Only saturated hydraulic conductivity and a single pair of hydraulic conductivity – soil water potential data, along with a general shape parameter are required.

The upward flux rate to the surface, termed capillary rise,  $CR$ , was derived by Brutsaert (1982), based on Gardner (1958) and Cisler (1969) as

$$CR = a \left[ \frac{\pi}{n \sin\left(\frac{\pi}{n}\right)} \right]^n d_w^{-n} \quad (I-1)$$

where  $CR$  is the potential steady upward flux rate to the surface,  $\text{md}^{-1}$ , given a depth,  $d_w$ , to the water table where  $CR$  is less than the evaporative demand of the atmosphere. Depth  $d_w$  is in m. Parameter  $n$  is a shape parameter describing the relationship between hydraulic conductivity,  $k$ , and soil water potential, and  $a$  is an empirical coefficient defined by Gardner (1958) that describes the hydraulic conductivity vs. soil water potential relationship:

$$k = \frac{a}{\left( \frac{-p_w}{\gamma_w} \right)^n + b} \quad (I-2)$$

where  $k$  is hydraulic conductivity,  $\text{md}^{-1}$ ,  $a$  and  $b$  are constants where  $a/b = k_s$  at saturation (i.e.,  $a/b = \text{saturated hydraulic conductivity, } k_s$ ,  $\text{md}^{-1}$ , and  $p_w/\gamma_w$  is the soil water potential expressed in m of water ( $p_w/\gamma_w$  is negative above the water table). The value for  $b$  equals the value  $(-p_w/\gamma_w)^n$  associated with  $k$  when  $k = 0.5 k_s$ . This value is selected from a plot of  $k$  vs.  $p_w/\gamma_w$ . Typical values for  $n$  range from 2 for clayey soils to 4 or more for sandy soils (Gardner 1958; Brutsaert 1982). Other functions for describing  $k$  vs.  $p_w/\gamma_w$  can be converted into Eq. (I-2) by plotting the function, noting values for  $k_s$  and  $p_w/\gamma_w$  at  $0.5 k_s$ , and iteratively testing values for  $n$  to obtain a fit between the functions.

$CR$  represents a potential flux to the soil surface under evaporation demands that equal or exceed  $CR$ . When potential evaporation, as estimated from the Penman-Monteith method, for example, is less than  $CR$ , then the actual evaporation flux must be limited to the potential evaporation amount that is governed by weather demands.

### Capillary Rise into the Root Zone

In conditions having vegetation and active root systems, the depth to the water table,  $d_w$ , is expressed as the distance from the water table to a point

in the root zone where sufficient roots are present to extract the upward flux of water. This point may be some distance above the  $z_r$  depth that represents the effective depth of the root zone, due to insufficient root density at  $z_r$ . A reasonable estimate for  $d_w$ , assuming the central extraction point to be 1/4  $z_r$  distance from the bottom of the effective root zone, is  $d_w = z_w - 0.75z_r$  where  $z_w$  is the depth of the water table below the ground surface and  $z_r$  is the effective depth of the root zone. All depths are in m. The UPFLOW simulation model described in the following section employs root density functions to estimate the net sink depth for groundwater extraction by roots.

Under conditions where a water table is chronically near the effective root zone so that lower portions of the root zone are saturated or nearly saturated, hypoxia of roots may develop due to limited oxygen and the effective root depth may be less than potential depths. Adjustments should be made to  $z_r$  under these conditions. In addition, salinity of groundwater will reduce the rate of extraction by plant roots and adjustments are needed under those conditions. The UPFLOW and HYDRUS models employ functions to make these adjustments.

### Example of Application of Eq. (I-1)

An example of applying Eqs. (I-1) and (I-2) is shown here for the example  $k$  vs.  $p_w/\gamma_w$  data of Brutsaert (1982), expressed in his Figure 11.5, which was in turn based on data by Gardner and Fireman (1958) for a Chino clay. The equation for  $k$  vs.  $p_w/\gamma_w$  for the Chino clay according to Brutsaert (1982) is  $k = 0.00108 / [(-p_w/\gamma_w)^2 + 0.05541]$  where  $k$  has units of  $\text{m d}^{-1}$ , and  $p_w/\gamma_w$  has units of m of water. The plot of this function is given in Figure I-1.

Using the values  $a = 0.00108 \text{ m d}^{-1} \text{ m}^n$ ,  $b = 0.05541 \text{ m d}^{-1} \text{ m}^n$ , and  $n = 2$ , the solution of Eq. (I-2) provides estimates for  $CR$  shown in Figure I-2, which reproduce Brutsaert's Figure 11.5. The estimates by Eqs. (I-1) and (I-2) in Figure I-2 are accompanied by estimates of  $CR$  by the UPFLOW model described in the next section. Estimates by UPFLOW for the general clay and silty clay textures in UPFLOW for wet and dry conditions tend to bracket the estimates by the Brutsaert-Gardner functions for the Chino clay. The estimates by UPFLOW for a wet clay soil follow the Brutsaert-Gardner function closely.

## I.2 THE UPFLOW SIMULATION MODEL

UPFLOW (Raes and deProost 2003; Raes 2004) is a software tool that estimates upward water movement from a shallow water table to the root zone during a specific period (typically 10 days) under specific

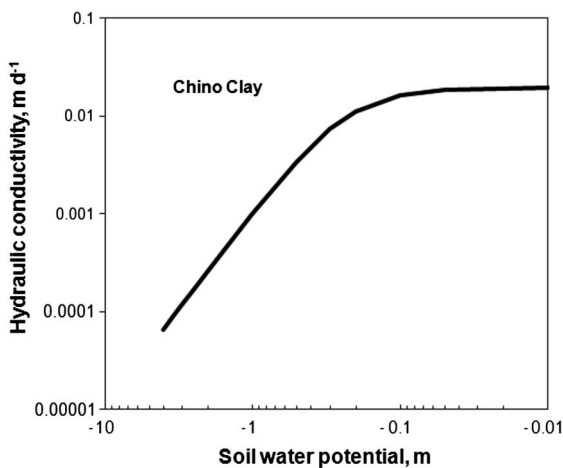


*Fig. I-1. Plot of hydraulic conductivity vs. soil water potential for the Chino clay data of Brutsaert (1982)*

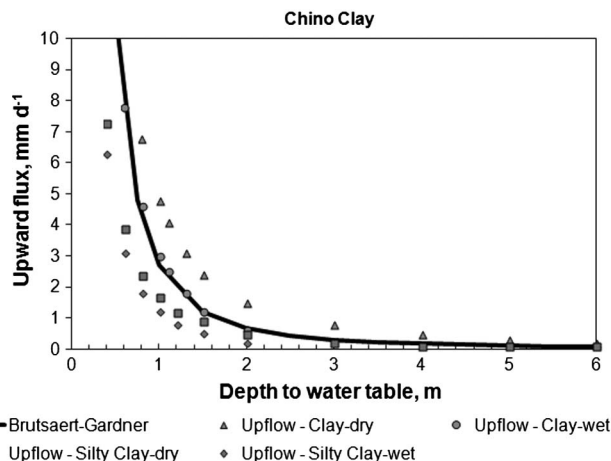
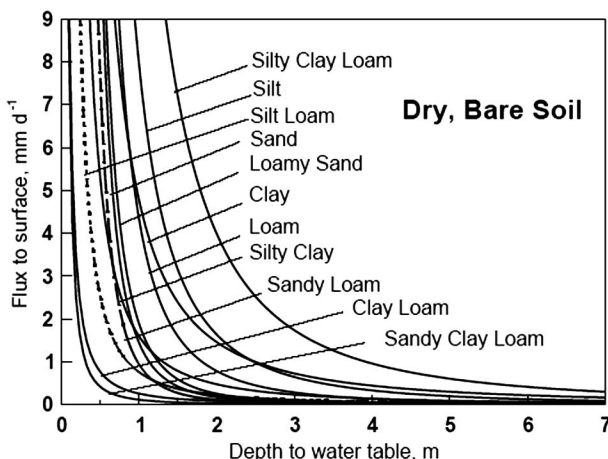


*Fig. I-2. Estimated capillary rise for a bare soil surface condition vs. depth to water table (m) based on the Brutsaert-Gardner function [Eqs. (I-1) and (I-2)] and based on simulations by the UPFLOW model of Raes (2004) for general clay and silty clay soil textures having dry and wet conditions*

environmental conditions. The one-dimensional, steady-state program is designed to work with limited data and contains various sets of soil water retention curves described by Schaap et al. (1999) using van Genuchten et al. (1991) functions or specific soil curves defined in terms of discrete

values. The general soil textures in UPFLOW represent a broad range of typical soil types. UPFLOW considers the influence of evaporative or evapotranspirative demand, the relative soil wetness in the upper soil profile, the depth to groundwater, the water extraction pattern of the plant roots, the thickness and characteristics of successive soil layers, and salinity of the water table. Hydraulic flow computations are made using an integrated Darcy equation. The software estimates aeration conditions in the root zone when the water table is close to the soil surface and the associated effect on reduced root extraction and crop evapotranspiration. Field measurements from loamy sand and sandy loam soils in Belgium were used to confirm UPFLOW simulations (Raes 2004). UPFLOW is public domain software, and an installation disk and manual can be downloaded from the web.

UPFLOW simulations for the clay and silty clay soil textures and default parameters are compared against results from Eqs. (I-1) and (I-2) in Figure I-2 and agreed relatively well. UPFLOW was applied to a range of soil textures and default Schaap et al. (1999) and van Genuchten parameters for bare soil and cropped conditions to create general figures for  $CR$  and to develop some simple regression functions as shown in Figures I-3 through I-6 and summarized in Tables I-1 and I-2. The UPFLOW software was run for the two surface conditions of bare soil and a cereal (small grain) crop having a 1-m root zone. Two soil water contents in the upper soil profile were established, where a wet condition represented conditions similar to field capacity and a dry condition



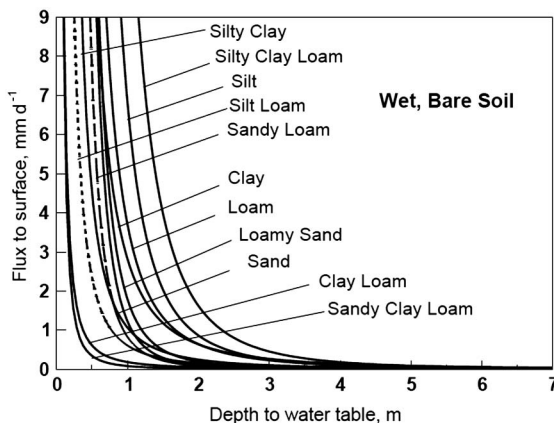
*Fig. I-3. Estimated flux of water to the ground surface for evaporation as a function of depth to the water table for a variety of soil textures for a dry, bare soil condition, based on numerical simulations by the UPFLOW (Raes 2004) model*

Table I-1. Regression Parameters for the Soil Textures Simulated in UPFLOW for a Bare Soil Surface for Dry and Wet Conditions along with Assumed Saturated Hydraulic Conductivities and Soil Water Contents of the Upper Soil Profile

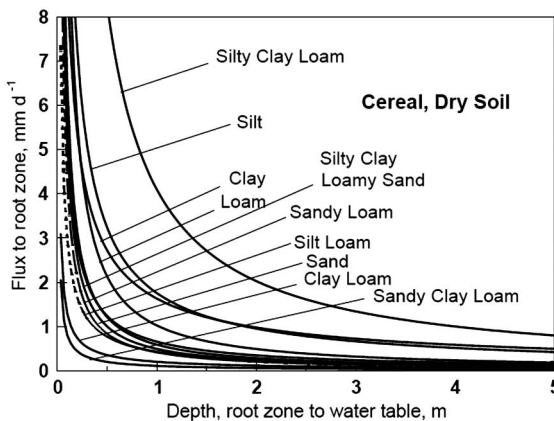
$k_s$ , $\text{md}^{-1}$	$\theta_v$	Dry, Bare Soil			Wet, Bare Soil			$r^2$
		$a_f$	$b_f$	$r^2$	$\theta_v$	$a_f$	$b_f$	
Clay	0.05	44	4.77	-1.70	1.00	54	2.82	-2.13
Silty clay	0.10	37	1.60	-1.73	0.99	49	1.07	-2.08
Clay loam	0.08	28	0.27	-1.54	0.99	40	0.19	-1.70
Silty clay loam	0.11	30	16.50	-2.05	1.00	44	14.20	-3.12
Sandy clay loam	0.13	24	0.12	-1.81	0.99	33	0.09	-1.99
Silt	0.44	17	7.92	-2.27	0.99	32	6.80	-2.97
Silt loam	0.18	19	0.76	-1.73	0.99	32	0.61	-1.94
Loam	0.25	20	4.32	-2.45	0.99	31	3.69	-2.52
Sandy loam	0.38	14	0.94	-3.02	0.99	22	0.83	-3.19
Loamy sand	1.05	10	1.89	-2.85	0.99	16	1.79	-3.16
Sand	1.20	8	1.44	-2.98	1.00	13	1.22	-3.48

Table I-2. Regression Parameters for the Soil Textures Simulated in UPFLOW for a Cereal Crop Having 1-m Root Zone for Dry and Wet Conditions along with Assumed Saturated Hydraulic Conductivities and Soil Water Contents of the Upper Soil Profile

	$k_s$ , md <sup>-1</sup>	$\theta_v$	$a_f$	$b_f$	Dry Soil		Wet Soil	
					$r^2$	$\theta_v$	$a_f$	$b_f$
Clay	0.05	44	1.63	-0.74	0.89	54	0.53	-1.47
Silty clay	0.10	37	0.66	-0.91	0.88	49	0.32	-1.38
Clay loam	0.08	28	0.21	-0.80	0.92	40	0.10	-1.32
Silty clay loam	0.11	30	4.10	-1.02	0.95	44	1.75	-2.04
Sandy clay loam	0.13	24	0.11	-0.86	0.90	33	0.04	-1.55
Silt	0.44	17	1.76	-0.88	0.85	32	0.76	-1.54
Silt loam	0.18	19	0.43	-0.84	0.89	32	0.24	-1.33
Loam	0.25	20	1.03	-1.06	0.86	31	0.57	-1.53
Sandy loam	0.38	14	0.42	-1.01	0.84	22	0.22	-1.55
Loamy sand	1.05	10	0.59	-1.04	0.89	16	0.29	-1.63
Sand	1.20	8	0.50	-1.02	0.84	13	0.25	-1.62



*Fig. I-4. Estimated flux of water to the ground surface for evaporation as a function of depth to the water table for a variety of soil textures for a wet, bare soil condition, based on numerical simulations by the UPFLOW ([Raes 2004](#)) model*



*Fig. I-5. Estimated flux of water into the root zone as a function of depth from bottom of the root zone to the water table for a variety of soil textures for a cereal crop having relatively dry soil condition, based on numerical simulations by the UPFLOW ([Raes 2004](#)) model*

represented about 60% depletion of available soil water content. The two soil water content conditions bracket conditions expected under irrigated agriculture. Simulations were run for a series of depths to groundwater and estimated rates of capillary rise under steady-state conditions were noted. Collected pairs of depths to water table,  $d_w$ , and CR were processed

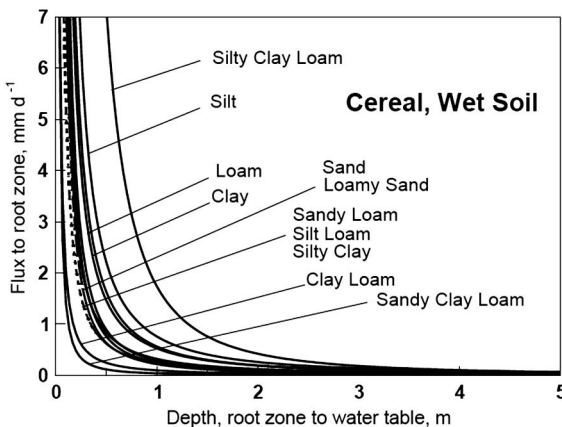


*Fig. I-6. Estimated flux of water into the root zone as a function of depth from bottom of the root zone to the water table for a variety of soil textures for a cereal crop having relatively wet soil condition, based on numerical simulations by the UPFLOW ([Raes 2004](#)) model*

using a regression analysis where a simple power relationship was used to describe the relationship between  $CR$  and  $d_w$ :

$$CR = a_f d_w^{b_f} \quad (I-3)$$

where, in Eq. (I-3),  $d_w$  is depth of water table below the surface (m) for the bare soil condition and depth below the bottom of the effective root zone for the vegetated condition,  $CR$  is capillary rise in  $\text{mm d}^{-1}$ , and  $a_f$  and  $b_f$  are regression coefficients.

Figures I-3 through I-6 show the relationships estimated using the regression functions derived from UPFLOW results for the two surface conditions and two soil water content conditions for the collection of soil textures evaluated. Tables I-1 and I-2 summarize the regression coefficients for each condition and soil texture, the  $r^2$ , and assumed saturated hydraulic conductivity,  $k_s$ , and volumetric water contents for the wet and dry conditions.

The agreement between the simple power function and simulated data was very high for the bare soil conditions, but agreement was poorer for cropped conditions, especially for a wet upper soil profile. A more complex function than Eq. (I-3) may be needed to characterize simulated data points when a crop is present.

This page intentionally left blank

## APPENDIX J

# DERIVATION OF THE PENMAN-MONTEITH EQUATION

### J.1 INTRODUCTION

It is useful to review the derivation of the PM equation to understand how it functions and some of the assumptions made in its development. There are two fundamental approaches to estimate evaporation ( $E$ ) and evapotranspiration ( $ET$ ). These are the surface energy balance equation and the aerodynamic equation. Each equation uses a different approach and each has difficulties for solution when using general weather data comprised of solar radiation, air temperature, vapor pressure, and wind speed. Penman (1948) combined these two approaches into the so-called combination or Penman equation that can be solved using standard weather data only. Monteith (1965) later improved on the Penman (1948) equation by including a surface resistance term and a more rigorous term for aerodynamic transfer. It is useful to review the combination of the two approaches.

### J.2 SURFACE ENERGY BALANCE

The surface energy balance equation relates to the various ways in which net radiation energy from the sun and atmosphere is balanced at the surface by inputs or outputs of energy from nonradiative parameters. The vertical energy balance at the surface is the sum of sensible heat flux to or from the air and to or from the soil, along with latent heat flux, net radiation, and other miscellaneous fluxes. The major components of the vertical energy balance are expressed as

$$R_n = G + \lambda E + H \quad (\text{J-1})$$

where  $\lambda E$  is the latent heat flux (positive during evaporation),  $G$  is conductive heat transfer into the soil (positive when heat is transferred downward in the soil), and  $H$  is the sensible heat exchange from the surface to air (positive if the air is warming). In Eq. (J-1),  $E$  (or  $ET$ ) is expressed in terms of the energy required to convert the amount of liquid evaporated into vapor by multiplying by  $\lambda$ . The miscellaneous terms involved in the surface energy balance, such as heat storage within foliage, photosynthesis, and respiration are generally insignificant relative to magnitudes of  $R_n$ ,  $\lambda E$ ,  $H$ , and  $G$  and are commonly neglected. Under some conditions, change in heat storage in a canopy may need attention, especially in forest canopies. If  $R_n$  and sensible heat flux densities  $H$  and  $G$  can be measured or estimated reliably, then the latent heat flux density,  $\lambda E$ , can be computed from Eq. (J-1) as follows

$$\lambda E = R_n - G - H \quad (\text{J-2})$$

Eq. (J-2) is listed as Eq. (4-2) in Chapter 4. The challenge to the solution of Eq. (J-2) using standard weather data is in solving for  $H$  using commonly available weather data. The traditional aerodynamic expression for  $H$  is given as

$$H = \frac{\rho_a c_p (T_o - T_a)}{r_{ah}} \quad (\text{J-3})$$

where  $T_o$  is surface temperature,  $T_a$  is air temperature, and  $r_{ah}$  is the aerodynamic resistance to heat transfer between some mean height within the surface to some height a few m above the surface. Eq. (J-3) is listed as Eq. 7-20 in Chapter 7.

Eq. (J-3) is analogous to Ohm's law for electrical current flow, where  $T_o$  and  $T_a$  are equivalent to voltages or potentials,  $r_{ah}$  is equivalent to an electrical resistor, and  $H$  is analogous to current. Thus, Eq. (J-3) behaves as a linear electrical circuit, so that if the difference between  $T_o$  and  $T_a$  is doubled,  $H$  will double. If resistance  $r_{ah}$  is halved (through a doubling of wind speed), then  $H$  will double.

The challenge of Eq. (J-3) and thus Eq. (J-2) is in the parameter  $T_o$ , which is surface temperature.  $T_o$  can be measured using infrared thermometers if surface emissivity is known or it can be measured using a fine-thermocouple or other temperature sensor placed just beneath the surface skin. However, these measurements are not common due to the high operational and maintenance requirements of the instruments and difficulty in transfer of measured values to other locations and surface conditions, even those nearby.

The traditional equation for  $r_{ah}$  [reported earlier as Eq. (7-20) in Chapter 7 and Eq. (8-3) in Chapter 8] is given as

$$r_{ah} = \frac{\left[ \ln\left(\frac{z_u-d}{z_{om}}\right) - \psi_m \right] \left[ \ln\left(\frac{z_T-d}{z_{oh}}\right) - \psi_h \right]}{k^2 u_z} \quad (\text{J-4})$$

where  $z_u$  is the height above the ground surface for the wind speed measurement,  $d$  is the zero plane displacement of the logarithmic wind profile,  $z_{om}$  is a roughness length governing the transfer of momentum from the surface,  $\psi_m$  is a correction factor for momentum transfer to account for instability or stability of the boundary layer,  $z_T$  is the height of the air temperature measurement above the ground surface,  $z_{oh}$  is an assumed roughness length governing the transfer of sensible heat from the surface,  $\psi_h$  is a correction factor for sensible heat transfer to account for instability or stability of the boundary layer,  $k$  is the von Kármán constant (0.41), and  $u_z$  is the wind speed measured at the  $z_u$  height. Equations for estimating  $\psi_m$  and  $\psi_h$  are given in Chapter 7. Eq. (J-4) is sometimes criticized for its use of  $z_{oh}$ , commonly expressed as some fraction of  $z_{om}$ , whereas in reality the ratio of  $z_{oh}/z_{om}$  can vary substantially, especially for dry, sparse vegetation (Qualls and Brutsaert 1996). Other forms of Eq. (J-4) can be written that rely on differences in  $T_a$  at two different heights above the surface. These forms eliminate the need for  $z_{oh}$ , however, measurement of  $T_a$  at two heights is not common, and it is challenging to produce an unbiased pair of measurements.

The aerodynamic-based expression for  $\lambda E$  based on the surface to air vapor pressure gradient is given as

$$\lambda E = \frac{\lambda \rho_a \varepsilon (e_o - e_a)}{P(r_{av} + r_s)} = \frac{\rho_a c_p (e_o - e_a)}{\gamma (r_{av} + r_s)} \quad (\text{J-5})$$

where  $\varepsilon$  is the mole ratio of water vapor to air (0.622);  $P$  is barometric pressure;  $e_o$  is vapor pressure “inside” the surface, for example inside a leaf stomatal cavity or beneath the soil skin;  $e_a$  is vapor pressure of the air at some  $z$  height above the ground surface;  $\gamma$  is the psychrometric constant [Eq. (3-11a)];  $r_{av}$  is aerodynamic resistance to turbulent vapor transfer from the surface to some  $z$  height above the surface; and  $r_s$  represents any surface resistance to flow of vapor. Aerodynamic resistance  $r_{av}$  is computed exactly as for  $r_{ah}$ , i.e., using Eq. (J-4), except that  $z_T$  becomes  $z_v$  (height of vapor pressure measurement above the ground);  $z_{oh}$  becomes  $z_{ov}$ , which is an assumed roughness length governing the transfer of vapor from the

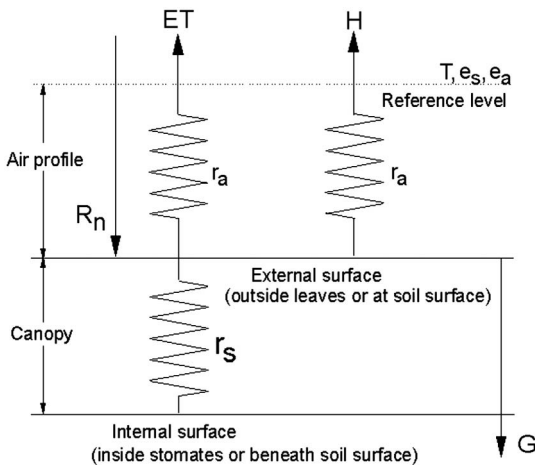


*Fig. J-1. Schematic showing linkage between resistance terms in the PM equation relative to the surface and elevation of temperature and humidity measurements. One common shortcoming of this physical analogy is that the sources of heat and vapor must be at  $d + z_{oh}$  (or  $d + z_{ov}$ ), which might be explicitly invalid, particularly with taller vegetation like forests. A multilayer PM approach can be written ([Choudhury and Monteith 1988](#)), but the single-layer PM may still be more functional ([Raupach and Finnigan 1988](#))*

surface; and  $\psi_h$  becomes  $\psi_v$ , a correction factor to account for effect of instability or stability of the boundary layer on vapor flow. Generally,  $z_T = z_v$  (air temperature and humidity sensors are typically colocated at the same height), and  $z_{ov}$  is assumed equal to  $z_{oh}$  and  $\psi_v$  is assumed equal to  $\psi_h$ , so that  $r_{av}$  can be assumed equal to  $r_{ah}$ . As discussed in Chapter 7, stability parameters  $\psi_v$ ,  $\psi_h$ , and  $\psi_m$  can generally be assumed to be close to zero when estimating ET from well-watered (moist) surfaces such as the grass- and alfalfa-covered reference surfaces.

As with Eq. (J-3), the aerodynamic vapor transfer equation is analogous to Ohm's law, where  $e_o$  and  $e_a$  are equivalent to voltages or potentials,  $r_{av}$  and  $r_s$  are equivalent to electrical resistors in series, and  $\lambda E$  (vapor flux) is analogous to electrical current. Fig. J-1 is a schematic showing the relative locations of resistances  $r_a$  (or  $r_{ah}$  and  $r_{av}$ ) and  $r_s$ , where  $r_s$  represents the internal resistance of the soil (if no vegetation) or of the soil, leaves, and canopy in parallel.

Vapor pressure of air can be determined from coincident measurements of relative humidity and air temperature, which are commonly available, or from measurement of dew point temperature, also commonly available. Vapor pressure inside the soil or plant surface, on the other hand, is rarely

measured, however, so that as with Eq. (J-2), Eq. (J-5) is challenging to apply in routine practice. Hence, the need for the Penman or Penman-Monteith combination equation.

To create the PM equation, one utilizes the Bowen ratio, which is simply the ratio between  $H$  and  $\lambda E$ . Expanded into the equations for  $H$  and  $\lambda E$  and written for transfer from inside the surface to the air above, one obtains

$$\beta = \frac{H}{\lambda E} = \frac{\rho_a c_p (T_o - T_a) \gamma (r_{av} + r_s)}{\rho_a c_p (e_o - e_a) (r_{ah})} \quad (\text{J-6})$$

By canceling similar terms and defining  $\gamma$  as in Eq. (3-11a), one obtains

$$\beta = \frac{H}{\lambda E} = \gamma \frac{(T_o - T_a)(r_{av} + r_s)}{(e_o - e_a)(r_{ah})} \quad (\text{J-7})$$

The energy balance equation can be written as

$$\lambda E = \frac{R_n - G}{1 + \beta} = \frac{R_n - G}{1 + \gamma \frac{(T_o - T_a)(r_{av} + r_s)}{(e_o - e_a)(r_{ah})}} \quad (\text{J-8})$$

The next step in the derivation of the PM equation is to define the term  $\Delta$ , which is defined as the slope of the saturation vapor pressure vs. temperature relation. The  $e^o(T_a)$  function is based on  $T_a$  and describes the ability of air to hold more vapor as temperature increases. The slope  $\Delta$  of the  $e^o(T_a)$  vs.  $T_a$  psychrometric curve that can be expressed as a linear approximation for a segment of the saturation curve between the two temperatures  $T_o$  and  $T_a$ :

$$\Delta = \frac{e_o - e_s}{T_o - T_a} \quad (\text{J-9})$$

where  $e_o$ ,  $e_s$ ,  $T_o$ , and  $T_a$  were defined previously. Vapor pressure inside the surface,  $e_o$ , is assumed to be saturated and is therefore equivalent to  $e^o(T_o)$ . The  $e_s$  term is the saturation vapor pressure associated with  $T_a$ , so that  $e_s = e^o(T_a)$ . Using the relationship from Eq. (J-9) to define  $(e_o - e_s)/\Delta = T_o - T_a$  and parsing  $(e_o - e_s)$  into an equivalent expression of  $(e_o - e_s) = (e_o - e_a) - (e_s - e_a)$  so that  $T_o - T_a = [(e_o - e_a) - (e_s - e_a)]/\Delta$ , this expression is substituted into Eq. (J-8) so that one obtains

$$\lambda E = \frac{R_n - G}{1 + \beta} = \frac{R_n - G}{1 + \frac{\gamma \frac{[(e_o - e_a) - (e_s - e_a)](r_{av} + r_s)}{(e_o - e_a)(r_{ah})}}{\Delta}} = \frac{R_n - G}{1 + \frac{\gamma}{\Delta} \left[ 1 - \frac{(e_s - e_a)}{(e_o - e_a)} \right] \frac{(r_{av} + r_s)}{r_{ah}}} \quad (\text{J-10})$$

We define one more temporary term,  $\lambda E_a$ , following Penman (1948), as

$$\lambda E_a = \frac{\rho_a c_p (e_s - e_a)}{\gamma r_{ah}} \quad (\text{J-11})$$

where  $\lambda E_a$  is similar to Eq. (J-5), the aerodynamic expression for  $\lambda E$ , except that  $r_s$  is omitted and  $(e_o - e_a)$  is replaced with  $(e_s - e_a)$ . Term  $(e_s - e_a)$  is known as the vapor pressure deficit (VPD) of the air, because it represents the difference between the saturation vapor pressure at air temperature [ $e_s = e^o(T_a)$ ] and actual vapor pressure of the air ( $e_a$ ). Both  $e_s$  and  $e_a$  can be determined from commonly available humidity and air temperature data measured at some height above the surface, generally 1.5 to 2 m. It is important to note that  $\lambda E_a$  is not a real vapor flux, but only a convenient temporary parameter. Dividing Eq. (J-11) by Eq. (J-5), and rearranging, one obtains

$$\frac{e_s - e_a}{e_o - e_a} = \frac{\lambda E_a}{\lambda E} \frac{r_{ah}}{r_{av} + r_s} \quad (\text{J-12})$$

Eq. (J-10) then becomes the following upon substitution of Eq. (J-12):

$$\lambda E = \frac{R_n - G}{1 + \frac{\gamma}{\Delta} \left[ 1 - \frac{\lambda E_a}{\lambda E} \frac{r_{ah}}{r_{av} + r_s} \right] \frac{r_{av} + r_s}{r_{ah}}} \quad (\text{J-13})$$

Rearranging Eq. (J-13) and setting  $r_{av} = r_{ah}$ , one obtains the resulting Penman-Monteith equation expressed as

$$\lambda E = \frac{\Delta(R_n - G) + \gamma \lambda E_a}{\Delta + \gamma \left( 1 + \frac{r_s}{r_{ah}} \right)} \quad (\text{J-14})$$

or, in its common form containing the vapor pressure deficit term as

$$\lambda E = \frac{\Delta(R_n - G) + \rho_a c_p (e_s - e_a) / r_{ah}}{\Delta + \gamma \left( 1 + \frac{r_s}{r_{ah}} \right)} \quad (\text{J-15})$$

The evaporation ( $E$  in  $\text{mm s}^{-1}$ ) or evapotranspiration ( $ET$  in  $\text{mm s}^{-1}$ ) rate is given as

$$E \text{ or } ET = \frac{\lambda E}{(\lambda \rho_w)} \text{ or } \frac{\lambda ET}{(\lambda \rho_w)} \quad (\text{J-16})$$

where  $\rho_w$  is the water density ( $1.0 \text{ Mg m}^{-3}$ ), and  $\lambda$  is the latent heat of vaporization ( $\sim 2.45 \times 10^6 \text{ J kg}^{-1}$  at  $20^\circ\text{C}$ ), and where  $\lambda E$  or  $\lambda ET$  are expressed in  $\text{W m}^{-2}$ .

The PM equation has the valuable advantage of requiring only commonly available weather data, namely solar radiation (used to calculate  $R_n$ ), air temperature (used to calculate  $\rho_a$ ,  $e_s$ , and  $\Delta$ ), humidity data (used to calculate  $e_a$  and assist with  $R_n$ ), and wind speed (for  $r_{ah}$ ).  $G$  is generally estimated as a function of  $R_n$ . The surface resistance  $r_s$  is generally estimated as a function of amount of vegetation or amount of surface wetness, if the soil is wet. The PM equation (and historically the Penman equation where  $r_s$  is assumed zero and  $1/r_{ah}$  is replaced by a simpler empirical “wind function”) is widely used around the world as a standard means to estimate evaporation and evapotranspiration.

In practice,  $\Delta$  is often calculated as the slope of  $e^o(T)$  vs.  $T\{\partial[e^o(T)]/\partial T\}$  at  $T_a$  only, because  $T_o$  is usually not known. This is generally acceptable for applying the PM equation to reference vegetation, because  $T_o$  is typically within a few degrees of  $T_a$  and thus little computational error occurs. However, in applications of the PM equation to sparse or water-stressed vegetation,  $T_o$  can exceed  $T_a$  by more than  $10^\circ\text{C}$  and therefore should be included in the computation for  $\Delta$ . This can be accomplished using  $T_a$  only by iteratively (Budyko 1956) estimating  $\lambda E$  using Eq. (J-15) (the PM equation) using  $T_o = T_a$  for  $\Delta$  the first iteration, but then estimating  $H$  from Eq. (J-1) and  $T_o$  from an inversion of Eq. (J-3). Parameters  $\Delta$  and  $\lambda E$  are then recomputed using Eqs. (J-9) and (J-15), and the process is repeated until estimates for  $T_o$ ,  $\Delta$ , and  $\lambda E$  are stable. This type of iterative process [using Eq. (J-15) or alternatively using Eq. (J-5) for  $\lambda E$ ] was described by Brown and Rosenberg (1971) and Paw and Gao (1988). However, as illustrated in Chapter 11, under conditions where values for  $T_o$  and  $T_a$  are substantially different, the user should also apply stability correction as described in Chapter 7 and calculate outgoing long-wave radiation using  $T_o$ . With modern computing systems, the AFIB method of Eqs. (11-2a–f) can, in principle, replace the need for iteration using the PM when values for  $T_o$  and  $T_a$  are substantially different. Other parameters in the PM equation are described in the main text.

This page intentionally left blank

## APPENDIX K

# REGIONAL ESTIMATING METHODS AND METHODS NOT COMMONLY USED IN THE UNITED STATES

### K.1 INTRODUCTION

Several methods for estimating evapotranspiration (ET) that have been used in the past were discussed in the first edition but are not covered in detail in the second edition because they are no longer commonly used. However, because some studies and litigations may involve historical ET data calculated with methods not commonly used, the methods are briefly summarized in this appendix to preserve this information and to point to general references. Other methods, such as the 1982 Kimberly Penman method ([Wright 1982](#)) and CIMIS Penman method, have been used in specific regions of the United States.

### K.2 COMBINATION METHODS

The classical form of the Penman equation ([Penman 1948, 1956a, b, 1963](#)) is

$$ET = \left[ \frac{\Delta}{\Delta + \gamma} (R_n - G) + K_u \frac{\gamma}{\Delta + \gamma} (a_w + b_w u_2) (e_s - e_a) \right] / (\lambda \rho_w) \quad (K-1)$$

where  $R_n$  is net radiation and  $G$  is soil heat flux density into the ground in  $\text{MJ m}^{-2} \text{t}^{-1}$ ,  $\Delta$  is the slope of the curve relating saturation vapor pressure to temperature in  $\text{kPa } ^\circ\text{C}^{-1}$ ,  $\gamma$  is the psychrometric constant in  $\text{kPa } ^\circ\text{C}^{-1}$ ,  $K_u$  is a unit conversion factor typically in  $\text{MJ m}^{-2} \text{t}^{-1} \text{kPa}^{-1}$ ,  $a_w$  and  $b_w$  are wind function coefficients,  $u_2$  is wind speed in  $\text{m s}^{-1}$  at the 2-m height,  $e_s$  is mean saturation vapor pressure at air temperature in  $\text{kPa}$ ,  $e_a$  is actual vapor pressure of the air in  $\text{kPa}$  at height  $z$ ,  $\lambda$  is the latent heat of vaporization in

$\text{MJ kg}^{-1}$ , and  $\rho_w$  is density of water in  $\text{Mg m}^{-3}$  (taken as  $1.0 \text{ Mg m}^{-3}$ ). These units produce  $ET_{ref}$  with units of  $\text{mm t}^{-1}$ . Eq. (K-1) can be applied to 24-hour data or to hourly (or shorter) data. Parameter  $K_u = 6.43$  for ET in  $\text{mm d}^{-1}$  and  $K_u = 0.268$  for ET in  $\text{mm hour}^{-1}$ . The  $a_w$  and  $b_w$  terms are empirical wind coefficients that have often received local or regional calibration and apply to a specific reference type of crop or surface.

### 1963 Penman Method

The values for  $a_w$  and  $b_w$  for the original Penman equation, first applied by Penman (1948) to open water and implicitly to grass, and later by Penman (1963) to clipped grass were  $a_w = 1.0$  and  $b_w = 0.537$ , respectively, for wind speed in  $\text{m s}^{-1}$ ,  $e_s - e_a$  in kPa and grass  $ET_o$  in  $\text{mm d}^{-1}$ . The equations were intended for use with daily computations. In application of the 1963 Penman, saturation vapor pressure is traditionally based on mean daily air temperature rather than on  $T_{max}$  and  $T_{min}$ .

### Penman FAO-24

The FAO-24 publication by Doorenbos and Pruitt (1975, 1977) presented a modified Penman equation for estimating reference ET for grass,  $ET_o$ . The major modifications involved a more sensitive wind function than that used by Penman, and an adjustment factor "c" that is based on local climatic conditions. The assumption that  $G = 0$  for daily periods was the same as Penman used. The vapor pressure deficit is calculated using saturated vapor pressure at mean air temperature minus saturation vapor pressure at dew point temperature when dew point temperature data are available or otherwise using saturation vapor pressure at mean air temperature times one minus mean relative humidity in percent [ $e_s - e_a = e^o(T_{mean})(1 - RH_{mean})/100$ ].

The main differences between the original Penman equation and the 1977 FAO-24 combination method is that the FAO-24 Penman equation is multiplied by a factor,  $c$ , to adjust for the effect of differences in day and night weather conditions. In the format used in the FAO-24 manual, the FAO-24 equation is

$$ET_o = c \left[ \frac{\Delta}{\Delta + \gamma} (R_n - G) + \frac{\gamma}{\Delta + \gamma} 2.7 W_f (e_z^o - e_z) \right] \quad (\text{K-2})$$

in which the wind function  $W_f$  was defined as  $W_f = (1 + 0.01u_2)$  for wind run in  $\text{km d}^{-1}$  and vapor pressure in kPa. In Eq. (K-2),  $R_n$  and  $G$  are in  $\text{mm d}^{-1}$  and  $(e^o - e_z)$  in kPa is based on mean air and dew point temperatures. The factor  $c$  is based on daytime/nighttime wind ratio,  $U_d/U_n$ , maximum relative humidity,  $RH_{max}$ , solar radiation,  $R_s$ , and daytime wind speed (FAO-24, Table 16).

Frevert et al. (1983) expressed the adjustment factor ( $c$ ) in FAO-24, Table 16 as a polynomial. Later, Cuenca (1987, personal communication) rounded the coefficients and terms while maintaining comparable accuracy.

$$c = 0.68 + 0.0028RH_{\max} + 0.018R_s - 0.068U_d + 0.013(U_d/U_n) \\ + 0.0097U_d(U_d/U_n) + 0.43 \times 10^{-4}RH_{\max}R_sU_d \quad (K-3)$$

where  $RH_{\max}$  is in percent,  $R_s$  is in  $\text{mm d}^{-1}$ , and  $U_d$  and  $U_n$  are in  $\text{m s}^{-1}$ . The term  $(U_d/U_n)$  is the day/night wind ratio defined as the mean ratio of daytime (7 a.m.–7 p.m.) to nighttime (7 p.m.–7 a.m.) wind speed.

Evaluations of the FAO Penman method have indicated a tendency to overestimate grass reference ET in semiarid and arid areas. Doorenbos and Pruitt (1977, p. 117) indicated a 15 to 20% overestimation at Davis, California. Batchelor (1984) also indicated that the method may overestimate ET in semiarid and arid areas. Pruitt (1984) and Pruitt et al. (1987a) indicated a need to adjust the  $ET_o$  estimates downward for most regions of California except in the hot, low-desert region.

### 1982 Kimberly Penman Method

The 1982 Kimberly Penman equation was developed from intensive studies of evapotranspiration at Kimberly, Idaho using measurements of full cover alfalfa ET from precision-weighing lysimeters (Wright and Jensen 1972; Wright 1981, 1982, 1988). The 1982 version of the method uses Eq. (K-1) with wind coefficients that vary with time of year. In addition, the coefficients used for computation of net radiation and the method to estimate 24-hour soil heat flux are unique to the Kimberly method.

The Kimberly Penman and associated wind functions are intended for application with 24-hour time steps ( $K_u = 6.43$ ). The form and all units and definitions are the same as those in Eq. (K-1). The Kimberly wind function coefficients  $a_w$  and  $b_w$  for alfalfa vary with time of year and are computed for  $ET$ , as (Wright, personal communication, 1987; Jensen et al. 1990)

$$a_w = 0.4 + 1.4 \exp \left\{ - \left[ \left( \frac{J - 173}{58} \right)^2 \right] \right\} \quad (K-4)$$

$$b_w = 0.605 + 0.345 \exp \left\{ - \left[ \left( \frac{J - 243}{80} \right)^2 \right] \right\} \quad (K-5)$$

where  $J$  is the day of the year. For latitudes south of the equator, one should use  $J'$  in place of  $J$ , where  $J' = (J - 182)$  for  $J \geq 182$  and  $J' = (J + 182)$  for  $J < 182$ . The  $(e_s - e_a)$  term in the 1982 and 1996 Kimberly Penman equations is computed the same as for the standardized Penman-Monteith equation

( $e_s$  is computed at both daily maximum and daily minimum temperatures and averaged).

In the 1982 Kimberly Penman equation, net long-wave radiation is estimated using Eq. (4-39) and (4-40), which is similar to the ASCE (2005) standardization, except that coefficients  $a_1$ ,  $a$ , and  $b$  are calculated using the following equations. Parameter  $a_1$  for alfalfa at Kimberly (42° N) was defined by Wright (1982) as

$$a_1 = 0.26 + 0.1 \exp\{-[0.0154(J - 180)]^2\} \quad (\text{K-6})$$

where  $J$  is the day of the year, and where  $J$  for the Southern Hemisphere is replaced with  $J'$  as described for Eqs. (K-4) and (K-5). Parameter  $b_1 = -0.139$  in Wright (1982). Wright (1982) estimated  $a$  and  $b$  in Eq. (4-40) as

$$\begin{aligned} a &= 1.126 \quad \text{and} \quad b = -0.07 \quad \text{for } R_s/R_{so} > 0.7 \\ a &= 1.017 \quad \text{and} \quad b = -0.06 \quad \text{for } R_s/R_{so} \leq 0.7 \end{aligned} \quad (\text{K-7})$$

Wright (1982) estimated albedo as

$$\alpha = 0.29 + 0.06 \sin[(J + 96)/57.3] \quad (\text{K-8})$$

where  $J$  is the day of the year, and where  $J$  for the Southern Hemisphere is replaced with  $J'$  as described for Eqs. (K-4) and (K-5).

Soil heat flux for 24-hour periods is estimated for the alfalfa reference of Wright (1982) using the difference between mean air temperature of the current day and the mean air temperature of the previous three days

$$G_{24} = 0.38 \left( T_{\text{mean}} - \sum_{i=1}^3 T_{\text{mean},i}/3 \right) \quad (\text{K-9})$$

where  $G_{24}$  is 24-hour soil heat flux in  $\text{MJ m}^{-2} \text{d}^{-1}$ ,  $T_{\text{mean}}$  is mean air temperature on the current day, and  $T_{\text{mean},i}$  is the mean air temperatures of the previous three days. Equation (K-9) may not estimate well under all conditions. In a study on 24-hour heat flux at Kimberly and Logan, Utah, Allen and Wright (unpublished research, 1996) found that using  $G=0$  for 24-hour periods under alfalfa and grass produced less error relative to measured  $G$  than using Eq. (K-9).

### The CIMIS Penman Method

Pruitt (Pruitt and Doorenbos 1977a) developed  $a_w$  and  $b_w$  for estimating grass  $ET_o$  for hourly periods for a clipped-grass reference. These coefficients were adopted for standard  $ET_o$  estimation in the California Irrigation

Management Information Service (CIMIS) by Snyder and Pruitt (1985) and Snyder and Pruitt (1992). The result is the “CIMIS” Penman  $ET_o$  equation, where  $a_w = 0.29$  and  $b_w = 0.53$  for  $R_n > 0$  and  $a_w = 1.14$  and  $b_w = 0.40$  for  $R_n \leq 0$ . These coefficients are applied hourly using Eq. (K-1) where  $ET_o = \text{mm hour}^{-1}$ ,  $R_n = \text{MJ m}^{-2} \text{hour}^{-1}$ , and  $K_u = 0.268$ . The net radiation calculation as applied by CIMIS is similar to that by Dong et al. (1992) and is different than that of the standardized Penman-Monteith method described in Chapter 4. Standard CIMIS calculations assume  $G = 0$ , even for hourly applications.

### K.3 RADIATION METHODS

A number of solar radiation-based reference ET methods were developed in the 1960s to reduce the need for humidity and wind speed data. These methods were common to humid regions of the globe where humidity levels are high and vapor pressure deficits are low. Consequently, reference ET is a strong function of solar radiation and air temperature so that humidity and wind influences can be more readily ignored.

#### Turc Method

Turc (1961) simplified earlier versions of an equation for potential evapotranspiration (assumed to be  $ET_o$ ) for 10-day periods under general climatic conditions of Western Europe. When expressed on a daily basis in  $\text{mm d}^{-1}$ , the equations are

**For  $RH > 50\%$**

$$ET_o = 0.013 \frac{T}{T + 15} (R_s + 50) \quad (\text{K-10})$$

**For  $RH < 50\%$**

$$ET_o = 0.013 \frac{T}{T + 15} (R_s + 50) \left[ 1 + \frac{(50 - RH)}{70} \right] \quad (\text{K-11})$$

where  $T$  is the average temperature in  $^{\circ}\text{C}$ ,  $RH$  is daily mean relative humidity, %, and  $R_s$  is in  $\text{cal cm}^{-2} \text{d}^{-1}$ .

#### Makkink Method

The Makkink (1957) method is similar to the Turc method and is commonly used in Western Europe:

$$ET_o = 0.61 \frac{\Delta}{\Delta + \gamma} \frac{R_s}{2.45} - 0.12 \quad (\text{K-12})$$

where  $ET_o$  is in  $\text{mm d}^{-1}$ ,  $R_s$  is in  $\text{MJ m}^{-2} \text{d}^{-1}$ , and  $\Delta$  and  $\gamma$  are as defined for the Penman equations ( $\text{kPa } ^\circ\text{C}^{-1}$ ). Constant 2.45 is latent heat of vaporization at approximately  $20^\circ\text{C}$ .

The FAO-24 publication of Doorenbos and Pruitt (1977) included a radiation-based method similar to the Makkink equation:

$$ET_o = c \frac{\Delta}{\Delta + \gamma} \frac{R_s}{2.45} - 0.3 \quad (\text{K-13})$$

where  $ET_o$  is in  $\text{mm d}^{-1}$ ,  $R_s$  is in  $\text{MJ m}^{-2} \text{d}^{-1}$ , and  $\Delta$  and  $\gamma$  are as defined for the Penman equations ( $\text{kPa } ^\circ\text{C}^{-1}$ ). Constant  $c$  was a calibration factor that was a function of mean daily relative humidity ( $RH_{\text{mean}}$ ) and daytime wind speed ( $u_d$ ). Doorenbos and Pruitt (1977) presented values for  $c$  in the form of tables. Allen and Pruitt (1991) developed a regression equation for  $c$  having the form

$$\begin{aligned} c = & 1.066 - 0.00128RH_{\text{mean}} + 0.045u_d - 0.0002RH_{\text{mean}}u_d \\ & - 0.0000315(RH_{\text{mean}})^2 - 0.001103(u_d)^2 \end{aligned} \quad (\text{K-14})$$

where  $RH_{\text{mean}}$  has limits  $0 \leq RH_{\text{mean}} \leq 100\%$  and  $u_d$  has limits  $0 \leq u_d \leq 10 \text{ m s}^{-1}$ .

### Jensen-Haise Alfalfa-Reference Radiation Method

Jensen and Haise (1963) evaluated 3,000 observations of ET as determined by soil sampling procedures over a 35-year period. From about 100 values for well-watered crops with full cover in the western United States, a linear relationship of a solar radiation coefficient and mean air temperature was apparent. From these data, the constants for the following linear equation were  $C_T = 0.014$  and  $T_x = 26.4$  for temperature in  $^\circ\text{F}$ , and 0.025 and  $-3$  for temperature in  $^\circ\text{C}$ .  $R_s$  has the same units as  $\lambda ET_r$ .

$$\lambda ET_r = C_r(T - T_x)R_s \quad (\text{K-15})$$

where  $ET_r$  is alfalfa reference ET as defined,  $C_r$  is a temperature coefficient, and  $T_x$  is the intercept of the temperature axis. These coefficients were considered to be constants for a given area. Jensen (1966b) later defined  $C_r$  as

$$C_r = \frac{1}{C_1 + C_2 C_H} \quad (\text{K-16})$$

$$C_H = \frac{5.0}{(e_2 - e_1)} \quad (\text{K-17})$$

where  $e_2$  and  $e_1$  are the saturation vapor pressures in kPa at the mean daily maximum and mean daily minimum temperatures, respectively, for the average warmest month of the year in an area, and  $C_1$  and  $C_2$  are constants ( $C_2 = 13^\circ \text{ F}$  or  $7.3^\circ \text{ C}$ ). Jensen et al. (1970) defined the coefficients in Eqs. (K-16) and (K-17) as follows for temperature in  $^\circ\text{C}$ , elevation in m, vapor pressure in kPa, and  $C_2 = 7.3^\circ\text{C}$ .

$$C_1 = 38 - (2Elev/305) \quad (\text{K-18})$$

$$T_x = -2.5 - 1.4(e_2 - e_1) - Elev/550 \quad (\text{K-19})$$

The long-term air temperatures for July, generally the warmest month, are used to determine the constants  $T_x$ ,  $C_H$ ,  $C_1$ , and  $C_T$  (Burman et al. 1983).

### Priestley-Taylor Method

Priestley and Taylor (1972) proposed a simplified version of the combination equation for use when surface areas generally are wet, which is a condition required for potential evaporation,  $E_p$ . The aerodynamic component was deleted and the energy component was multiplied by a coefficient,  $\alpha = 1.26$ , when the general surrounding areas were wet or under humid conditions. The Priestley-Taylor equation provides estimates for no or low advective conditions. Therefore, if used without calibration ( $\alpha = 1.26$ ), the resulting estimates would be low for wet surfaces under arid conditions where the advection component of energy balance is significant. Basically, this equation is not valid without calibration in semiarid and arid areas. However, the method is still used for approximate comparisons under wet surface conditions and estimates of evaporation from water surfaces.

$$\lambda E = 1.26 \frac{\Delta}{\Delta + \gamma} (R_n - G) \quad (\text{K-20})$$

The Priestley-Taylor method is described in more detail in Chapter 5 [Eq. (5-2)] and Chapter 12 on regional ET estimation [Eq. (12-1)]. Steiner et al. (1991) reviewed values for  $\alpha$  under arid environments.

## K.4 TEMPERATURE METHODS

A number of early American ET methods relied on air temperature measurements because of the widespread availability of air temperature and precipitation data collected at National Weather Service Cooperative weather sites. Relationships between reference ET and air temperature or

between some other form of ET and air temperature are usually empirical and developed using some form of statistical correlation.

### SCS Blaney-Criddle Method

The Blaney-Criddle procedure for estimating ET is well known in the western United States and has been used extensively throughout the world. The basic procedures were based on measurements of ET in the 1920s and 1930s, using primarily soil sampling techniques. Blaney and Morin (1942) first developed an empirical relationship between ET and mean air temperature, average relative humidity, and mean percentage of daytime hours. This relationship was later modified by Blaney and Criddle (1945, 1950, 1962) and Blaney et al. (1952) by excluding the humidity term. The original relationship was developed and intended for seasonal estimates. The basic assumption was that ET varies directly with the sum of the products of mean monthly air temperature and monthly percentage of annual daytime hours for an actively growing crop with adequate soil moisture.

$$U = KF = \sum kf \quad (\text{K-21})$$

As originally defined,  $U$  = estimated evapotranspiration (consumptive use) in in. for the growing period or season;  $K$  is an empirical consumptive use coefficient (irrigation season or growing period);  $F$  is the sum of monthly consumptive use factors,  $f$ , for the season or growing period ( $f = tp/100$  where  $t$  = mean monthly air temperature in °F, and  $p$  = mean monthly percentage of annual daytime hours); and  $k$  = monthly consumptive use coefficient. The monthly percentages of daytime hours by latitudes as used by the USDA Soil Conservation Service were updated Martin and Gilley (1993, Table 2.18) for daily percent of annual daytime hours, and in their Table 2A-1 for monthly percent of annual daytime hours for northern latitudes.

The monthly crop coefficients originally proposed for the Blaney-Criddle equation apparently represent both meteorological and crop effects. For Ladino clover, which would be similar to alfalfa, Pruitt (1960) determined that for conditions near Prosser, Washington, short period estimates could be improved by using  $k = 0.04 + 5.52(tp/100)$  where  $p$  = daily percent of annual daytime hours and  $t$  is in °F.

The Soil Conservation Service (USDA 1970) proposed a composite climatic and crop coefficient,  $k = k_f k_c$  where  $k_f = 0.0173t - 0.314$ . However,  $k_c$  is not constant for a crop like alfalfa in midsummer, indicating that these modified  $k_c$  values also are not independent of climate (Pelton et al. 1960). For example, in a discussion of a paper by Quackenbush and Phelan (1965), Jensen (1966a) showed that after introducing the temperature coefficient,

$k_t$ , ( $u = k_t k_c f = k_t k_c tp / 100$ ) and separating the temperature and crop components ( $k_t t / 10$  and  $k_c p / 10$ ), the product  $k_c p / 10$  decreased from a maximum ratio in proportion to  $R_s / R_{s(max)}$ . This decrease was substantially greater than could be accounted for by the percent of daytime hours,  $p$ . Because in this case the crop coefficient represented grass, it indicated that the SCS  $k_c$  values still contained a meteorological component and that day length did not adequately compensate for radiation changes. The relative change in monthly  $p/100$  at midlatitudes is not as great as the relative change in monthly potential solar radiation during spring and fall months.

### FAO Blaney-Criddle Method

Doorenbos and Pruitt (1977) presented the most fundamental revision of the Blaney-Criddle method since its introduction. The FAO-24 Blaney-Criddle method requires the intermediate step of estimating a grass-related reference crop evapotranspiration,  $ET_o$ , prior to applying grass-related crop coefficients,  $K_{c,grass}$  to obtain crop ET. Earlier versions of the Blaney-Criddle method were not related to the use of reference crop ET.

After calculating  $ET_o$ , grass-related crop coefficients from FAO-24 or another source should be used to estimate crop ET. The FAO-24 Blaney-Criddle method is based on the general linear relationship found between measured reference ET and the Blaney-Criddle "f" factor for many worldwide sites that were investigated. By placing the data from these sites in various classifications based on ranges of daytime wind speed, minimum RH, and sunshine expressed as  $n/N$ , an expression for  $a$  was developed and a table of values for  $b$  was presented for use as follows:

$$ET_o = a + bf \quad (K-22)$$

$$f = p(0.46T + 8.13) \quad (K-23)$$

$$a = 0.0043RH_{min} - n/N - 1.41 \quad (K-24)$$

where  $ET_o$  = grass reference ET in  $\text{mm d}^{-1}$ ,  $p$  = mean daily percent of annual daytime hours,  $T$  = daily mean air temperature in  $^{\circ}\text{C}$ ,  $n/N$  is the ratio of possible to actual sunshine hours,  $RH_{min}$  is the minimum daily relative humidity in percent, and  $U_d$  is daytime wind at 2-m height ( $\text{m s}^{-1}$ ). [Note: FAO-24, pp. 3 and 110, gives  $f = p(0.46 T + 8)$ , but the computer program listed uses  $f = p(0.46 T + 8.13)$ , which is a more exact conversion from in. to mm.] Doorenbos and Pruitt (1977) provided tables for  $b$ . Frevert et al. (1983), Allen and Pruitt (1991), Jensen et al. (1990), and Allen et al. (1998) provided an equation for calculating  $b$  as a function of  $RH_{min}$ ,  $n/N$ , and  $U_d$ , where  $U_d$  is the mean daytime (7 a.m. to 7 p.m.) wind speed at 2-m height. The FAO-24 Blaney-Criddle method was used as the basis for

several statewide irrigation water requirements publications in the 1980s and 1990s, for example, [Allen et al. 1983](#) and [Cuenca et al. 1992](#). However, the use of the method has been superceded by the ASCE standardized Penman-Monteith equation ([ASCE 2005](#)).

## K.5 PAN EVAPORATION METHODS

Pan evaporation data can be used to estimate reference ET using the following simple proportional relationship.

$$ET_o = k_p E_{\text{pan}} \quad (\text{K-25})$$

where  $k_p$  is dependent on the type of pan involved and other factors. Several special methods described in the first edition of this manual such as that of Christiansen ([1968](#)) and Christiansen and Hargreaves ([1969](#)) are no longer commonly used. Pan evaporation data are still used to estimate evaporation from shallow lakes and some reservoirs, as described in Chapter [6](#). Use of  $E_{\text{pan}}$  as a reference is described in Chapter [8](#).

## K.6 OTHER METHODS OF ESTIMATING ET

Many methods for estimating ET were compared in Chapter [7](#) of the first edition of this manual. Comparisons of several of the better known methods of estimating ET are presented in Appendix [L](#). Appendix [L](#) includes tables summarizing the statistics and ranking for monthly estimates of ET at arid and humid locations for the methods compared.

## APPENDIX L

# COMPARISON AND RANKING OF METHODS FOR ESTIMATING ET

### L.1 METHODS SELECTED FOR EVALUATION

Some of the methods for estimating ET not commonly used in the United States (Appendix K) that were compared and ranked in Chapter 7 of the first edition may still be of interest when comparing estimates made with modern methods for special studies or when comparing estimates still being made for litigation purposes. Therefore, most of the methods compared in Chapter 7 of the first edition are summarized in this appendix for documentation purposes (Table L-1). Several methods that were compared have not been used extensively in the United States and are not repeated in this appendix. These methods are the FAO-PPP-17 Penman, the Businger-van Bavel, Thornthwaite, and the Christiansen pan evaporation methods.

All of the methods evaluated, with the exception of the SCS Blaney-Criddle, were defined by the originators to provide either an estimation of "potential evapotranspiration," which was not always defined, or ET for a specific well-watered reference crop whose leaf surfaces are typically not wet. A summary of the type of estimate intended by authors or originators of each method is presented in Table L-2.

The length of period for which the methods are applicable is not always stated in the references. Applicable periods should be about the same as the data from which the various empirical coefficients in the methods were derived. Applications of the methods for shorter time periods may reduce their accuracy. A summary of applicable time periods recommended for each method is presented in Table L-3. Those recommendations are based on the time periods used in deriving coefficients and the recommendations of the authors of this manual.

Table L-1. Classification of Estimating Methods and Principal References

Classification	Method	References
Combination	Penman (1963)	Penman (1963), VPD-1 and VPD-3 <sup>a</sup>
	1972 Kimberly-Penman	Wright and Jensen (1972)
	1982 Kimberly-Penman	Wright (1982)
	FAO-24 Penman ( $c=1$ )	Doorenbos and Pruitt (1975, 1977)
	FAO-24 Corrected Penman	Doorenbos and Pruitt (1977)
	Penman-Monteith	Monteith (1965); Allen (1986); Allen et al. (1989)
	Jensen-Haise	Jensen and Haise (1963); Jensen et al. (1971)
	FAO-24 Radiation	Doorenbos and Pruitt (1977)
	Priestley-Taylor	Priestley and Taylor (1972)
	Turc	Turc (1961); Jensen (1966b)
Temperature	SCS Blaney-Criddle	USDA (1970)
	FAO-24 Blaney-Criddle <sup>b</sup>	Doorenbos and Pruitt (1977); Allen and Pruitt (1986)
	Hargreaves-Samani	Hargreaves et al. (1985); Hargreaves and Samani (1985)
Evaporation	FAO-24 Pan <sup>b</sup> pan	Doorenbos and Pruitt (1977)

<sup>a</sup>VPD-1 is based on saturation vapor pressure at mean air temperature minus saturation vapor pressure at dew point temperature. VPD-3 uses the mean saturation pressure at maximum and minimum air temperatures minus saturation pressure at mean dew point temperature determined early in the day.

<sup>b</sup>Regression equations by Frevert et al. (1983) were used to calculate the coefficients used in these equations.

Methods that were evaluated and considered as typical were selected because they were in use at the time. Regression equations developed by Frevert et al. (1983) were used to estimate the adjustment factor “ $c$ ” in the FAO-24 Corrected Penman method, “ $b$ ” in the FAO-24 radiation method, “ $b$ ” in the FAO-24 Blaney-Criddle method, and  $k_p$  in the FAO-24 Pan method. Since completing these evaluations, Allen and Pruitt (1991) found the Frevert et al. (1983) regression equations to overestimate these coefficients by as much as 10–14% for some climatic conditions where maximum relative humidity is above 80%, solar radiation is above  $10 \text{ mm d}^{-1}$ , and  $U_d/U_n$  ratios are less than 2. The coefficient equations developed by Allen and Pruitt (1991) are recommended for computer calculations, or interpolations made from the FAO-24 tables and figures.

Table L-2. Classification of Estimating Methods and Principal References

Method	Type of Estimate	Remarks
<b>Combination:</b>		
Penman (1963)	Potential ET	Short green crop completely shading the ground and never short of water
1972 Kimberly-Penman	Alfalfa reference, $ET_r$	Full cover alfalfa at Kimberly, Idaho
1982 Kimberly-Penman	Alfalfa reference, $ET_r$	Full cover alfalfa at Kimberly, Idaho
FAO-24 Penman ( $c = 1$ )	Grass reference, $ET_o$	8–15 cm grass reference at various international locations
FAO-24 Corrected	Grass reference, $ET_o$	8–15 cm grass reference at (variable $c$ ) various international locations
Penman	Reference evapotranspiration $ET_r$ and $ET_o$	Reference type is dependent on surface roughness and canopy or bulk stomatal resistances used
<b>Radiation:</b>		
Jensen-Haise	Alfalfa reference, $ET_r$	Reference crop is alfalfa (lucerne), well-watered, with 30–50 cm of growth. Coefficients derived from U.S. data
FAO-24 Radiation	Grass reference, $ET_o$	8–15 cm grass reference at various international locations
Priestley-Taylor	Large rain-fed land areas following regional rains	Australia and United States
Turc	Potential ET	Crop factor = 70, derived from western Europe data
<b>Temperature:</b>		
Hargreaves-Samani	Grass reference, $ET_o$	8–15 cm clipped rye grass at Davis, California
SCS Blaney-Criddle	Evapotranspiration	Evaluated for alfalfa and from specific crop grass references using SCS crop coefficients and adjustment to negate effects of cuttings
FAO-24 Blaney-Criddle	Grass reference, $ET_o$	8–15 cm grass reference from various international locations
Pan:	Grass reference, $ET_o$	
FAO-24 Pan	Grass reference, $ET_o$	8–15 cm grass reference from various international locations

Table L-3. Recommended Minimum Time Periods for Various Estimating Methods

Method	Recommended Minimum Time Period	Remarks
<b>Combination:</b>		
Penman (1963)	Daily	
1972 Kimberly-Penman	Daily	
1982 Kimberly-Penman	Daily	
FAO-24 Penman ( $c = 1$ )	Daily	
FAO-24 Corrected Penman	Daily	
Penman-Monteith	Hourly or daily	Daily when using equations for approximate canopy resistance
<b>Radiation:</b>		
Jensen-Haise	5 days	
FAO-radiation	5 days	
Priestley-Taylor	5 days	Regional evapotranspiration under wet surface conditions
Turc	10 days	
<b>Temperature:</b>		
SCS Blaney-Criddle	Seasonal	Recommended by USDA-SCS
FAO-Blaney-Criddle	Monthly 5 days	If locally calibrated If only long-term estimates of humidity, wind speed, and sunshine data are available, the time period should be limited to monthly
Hargreaves-Samani	10 days	
<b>Pan:</b>		
FAO-Pan	5 days	

## L.2 LOCATIONS AND DATA SELECTED FOR EVALUATION

Data used to evaluate the various methods in Jensen et al. (1990) were selected from publications or obtained by personal communications with investigators working at locations where lysimeter data for well-watered grass or alfalfa were available along with adequate supporting climatic

data. The evaluations were based on mean monthly and daily measured ET and all relevant climatic data. The sites selected ranged in elevation from 30 m below sea level to 2,774 m above sea level. Latitudes ranged from 38° S at Aspendale, Australia, to 56° N at Copenhagen, Denmark, and near the equator in Yangambi, Zaire. A description of the lysimeter sites, climates, and locations is presented in Table L-4. A description of the lysimeter vegetation types and general irrigation practices is presented in Table L-5. The years of available data and principal references for each site are summarized in Table L-6. In many cases it was necessary to estimate some climatic parameters or to obtain them from indirect sources such as the ESSA Climatological Atlas of the United States ([U.S. Dept. Commerce 1968](#)). The origin of data used in estimating ET for each site is summarized in Table L-7.

Evaporation pans at all sites were assumed to be Class A pans with at least 1,000 m of green upwind fetch. Deviations from expected pan values were observed at several sites. The pan at Scottsbluff, Nebraska, was located less than 4 m from adjacent fields of corn in the predominant wind direction during the period of measurement. This exposure likely reduced wind speed at the pan level and reduced evaporation from what would have occurred with an open setting recommended for common practice. The type of pan and exposure at Seabrook was unknown.

### L.3 CALCULATION OF CLIMATIC PARAMETERS

Most methods of estimating evapotranspiration require the computation of parameters such as saturation vapor pressure, latent heat of vaporization, and the psychrometric constant from climatic data. The methods used in the first edition ([Jensen et al. 1990](#)) generally followed those described in Chapters 3 and 4 and are not repeated here.

A summary of conversion factors for specific equations is presented in Table L-8. No adjustments were made to equations for which no specific reference crop was specified in the literature (i.e., the Priestley-Taylor and Turc equations). Heights of lysimeter vegetation and heights for vegetation for weather station surfaces at each lysimeter site that were used in calculation of parameters for the ASCE Penman-Monteith equation are given in Table L-9. These heights were based on ranges published with the original data or by personal communication, when available. Where no information concerning vegetation height was available, heights were estimated based on general cultural practices and climate in the area. The lysimeter locations where specific ranges of vegetation heights were unavailable and therefore required estimates were Scottsbluff, South Park, and Yangambi. General ranges of heights and/or cutting dates were available for Brawley, Coshocton, and Kimberly.

Table L-4. Lysimeter Sites, Climate, and Location Information  
Used in Comparisons

Site	Lat.	Elev., m	<i>M</i> <sup>a</sup>	<i>T</i> <sup>b</sup>	<i>e</i> <sup>c</sup>	<i>R<sub>s</sub></i> <sup>d</sup>	<i>R<sub>n</sub></i> <sup>e</sup>	Wind <sup>f</sup>
Aspendale (Victoria, Australia)	38° S	3	N	18	1.3	22.4	12.9	3.0
			J	23	1.7	28.6	18.5	3.0
			M	19	1.5	17.8	10.3	2.8
Brawley (Imperial Valley, CA)	34° N	-30	M	23	1.1	28.5	16.7*	1.7
			J	32	2.0	26.9	15.7*	1.5
			S	29	1.7	21.2	11.2*	1.9
Copenhagen (Denmark)	56° N	28	M	11	0.9	17.6	8.9	4.2
			J	15	1.4	17.4	9.3	3.2
			S	14	1.2	10.8	3.7	3.9
Coshocton (Ohio)	40° N	360	M	17	1.3	16.2	9.7*	2.0
			J	22	2.0	17.7	11.2*	1.8
			S	19	1.7	13.6	7.7*	1.8
Davis (California)	39° N	16	M	17	1.1	27.4	14.6	2.7
			J	23	1.4	30.2	16.4	2.0
			S	20	1.2	21.1	9.8	2.2
Kimberly (Idaho)	42° N	1,195	M	12	0.7	23.9	12.5*	3.2
			J	21	1.2	27.0	13.9*	2.2
			S	15	0.8	18.4	8.7*	2.4
Lompoc (California)	35° N	26	M	14	1.1	26.8	15.6*	2.0
			J	16	1.3	28.4	17.0*	2.0
			S	17	1.3	21.7	11.9*	1.7
Scottsbluff (Nebraska)	42° N	1,280	M	—	—	—	—	—
			J	22	1.3	26.0	15.0*	2.3
			S	21	1.2	21.4	10.5*	1.9
Seabrook (New Jersey)	39° N	37	M	17	1.2	20.2	9.5*	3.2
			J	25	2.1	21.3	11.6*	3.2
			S	20	1.7	16.1	8.0*	3.6
South Park (Colorado)	39° N	2,774	M	6	0.6	22.9	12.8*	2.7
			J	14	1.4	20.3	11.9*	1.6
			S	7	0.8	16.7	8.5*	1.9
Yangambi (Zaire)	0° N	474	N	25	2.3	17.3*	9.3*	1.0
			J	25	2.3	16.6*	8.0*	0.8
			M	26	2.4	17.8*	9.6*	0.9

\*Calculated.

<sup>a</sup>Months represent May, July, and September for N latitudes and November, January, and March for S latitudes.

<sup>b</sup>Mean air temperature, °C.

<sup>c</sup>Mean vapor pressure, kPa.

<sup>d</sup>Solar radiation, MJ m<sup>-2</sup> d<sup>-1</sup>.

<sup>e</sup>Net radiation, MJ m<sup>-2</sup> d<sup>-1</sup>.

<sup>f</sup>Extrapolated to a standard height of 2 m.

Table L-5. Lysimeter Vegetation and Management

Site	Vegetative Description	Irrigation
Aspendale	Clover and perennial ryegrass maintained at 6 to 10 cm	Often daily
Brawley	Afalfa, harvested as hay. Weather measured over 12-cm grass	Normal commercial irrigation <sup>a</sup>
Copenhagen	Dense clover-grass maintained at 12 to 14 cm height	Watered on 30 mm soil water deficit
Coshcohton	Grass-legume, harvested as hay. Weather measured over 15 cm grass	Natural rainfall only <sup>a,b</sup>
Davis	Perennial ryegrass, 1959-1963 Alta fescue grass, 1964-1969 Mowed weekly to 10 cm	Watered on 50% depletion
Kimberly	Alfalfa, harvested as hay. Weather measured over 12 cm grass	Normal commercial irrigation
Lompoc	Perennial ryegrass, maintained at 6 to 15 cm	Weekly and sometimes longer
Scottsbluff	Alfalfa, harvested as hay	Normal commercial irrigation <sup>a</sup>
Seabrook	Clipped ryegrass	Daily by sprinkling
South Park	Native meadow, harvested as hay	Very shallow water table <sup>a,b</sup>
Yangambi	<i>Bracharia mutica</i> grass	Drainage lysimeter

<sup>a</sup>Periods of regrowth after cutting were not used in developing the mean reference evapotranspiration curves for these sites. Irrigation of alfalfa was generally once per cutting cycle.

<sup>b</sup>Periods of significant plant water stress were not used in developing the mean reference evapotranspiration curve for the site.

Table L-6. Years of Data, Months per Year, and Principal Reference for Each Site

Site	Years	Period	Mo/Year	Principal Reference
Aspendale	3	1959-1961	12	McIlroy and Angus ( <a href="#">1963, 1964</a> )
Brawley	1	1971	8	LeMert ( <a href="#">1972</a> ; personal communication, 1973), Allen and Pruitt ( <a href="#">1986</a> )
Copenhagen	11	1955-1966	8	Jensen and Aslyng ( <a href="#">1967</a> , personal communication)
Coshocton	3	1977-1979	9	Harlukowicz (1984, personal communication)
Davis	4	1959-1963 <sup>a</sup>	12	Pruitt ( <a href="#">1971</a> , personal communication)
	3	1967-1969 <sup>b</sup>		
Kimberly	3	1969-1971	7	Wright (1985, personal communication; 1988)
Lompoc	4	—	12	Nixon (1971, personal communication)
Scottsbluff	1	1977	4	Weiss (1981, personal communication)
Seabrook	10	1949-1959	12	Yoshioka and Mather ( <a href="#">1967</a> )
South Park	1	1969	4	Kruse and Haise ( <a href="#">1974</a> )
Yangambi	1	1959	12	Bernard ( <a href="#">1954</a> ), and Pruitt ( <a href="#">1986</a> , personal communication)

<sup>a</sup>Period of record used in monthly analysis.<sup>b</sup>Period of record used in daily analysis.

Table L-7. Origin of Data Used in Evaluating Estimating Methods

Location	<i>T</i>	<i>T<sub>d</sub></i> <sup>a</sup>	<i>u<sub>z</sub></i>	<i>R<sub>a</sub></i>	<i>R<sub>so</sub></i>	<i>R<sub>s</sub></i>	<i>R<sub>n</sub></i>	<i>G</i>	<i>d<sub>a</sub></i>	<i>n/N</i>	<i>L<sub>d</sub></i>	<i>P</i>	<i>El</i>
Aspendale	P	P	P	E	C	P	E	E	E	P	E	P	P
Brawley	P	P	P	E	C	P	E	E	E	C	E	P	P
Copenhagen	P	P	P	E	C	P	P	P	P	P	E	P	P
Coshocton	P	P	P	E	C	P	E	E	E	P	E	P	P
Davis	P	P	P	E	P	P	P	E	E	P	E	P	P
Kimberly	P	P	P	E	P	P	E	E	E	C	E	P	P
Lompoc	P	P	P	E	C	P	E	E	E	C	E	P	P
Scottsbluff	P	P	P	E	E	P	E	E	E	E	E	C	C
Seabrook	C	C	C	E	C	C	E	E	E	C	E	P	P
South Park	P	P	P	E	C	P	E	E	E	C	E	P	P
Yangambi	P	P	P	E	E	P	E	E	E	E	E	—	P

Note: P indicates parameter found in principal publication for location; E indicates parameter estimated using procedures outlined in chapter 7 of the first edition ([Jensen et al. 1990](#)); and C indicates parameter taken from a climatological source such as the ESSA Climatological Atlas of the United States ([U.S. Dept. of commerce 1968](#)).

<sup>a</sup>Dew point temperatures were often calculated from relative humidity data.

#### L.4 ALFALFA AND GRASS REFERENCE ET MEASUREMENTS AND ESTIMATES

Measurements of ET from both alfalfa and grass were commonly used to approximate the evaporative demand as represented by reference crop ET. Typically, ET from grass,  $ET_o$ , was expected to be only 80 to 87% of that from alfalfa,  $ET_r$ , under arid conditions. Grass is often adaptable to more diverse climates and locations than alfalfa, although there can be significant differences in grass ET due to differences in variety, season, and height. Hargreaves ([1983](#)) and Marsh et al. ([1980](#)) have noted differences in ET rates between warm- and cool-season grasses and between clipped and nonclipped surfaces. Wright ([1988](#)) noted differences in water use between alfalfa varieties at Kimberly, Idaho.

The lysimeter data sets included measurements of either grass or alfalfa ET. Therefore, the ET estimates provided by alfalfa reference equations needed to be adjusted to provide estimates for grass ET at the grass lysimeter sites, and ET estimates provided by grass reference equations needed to be adjusted to provide estimates for alfalfa at alfalfa sites to enable comparisons of all equations at all lysimeter sites. An approximate alfalfa to grass ET ratio of 1.15 was used in the first edition ([Jensen et al. 1990](#)) to adjust  $ET_o$  estimates to  $ET_r$  values and vice versa at all lysimeter locations evaluated. This constant does not fully reflect differences in

Table L-8. Coefficients Used to Adjust Estimates of ET Obtained with Various Equations to Approximate the Reference Crop Grown in the Lysimeter

Site	Alfalfa Lysimeter	Grass Lysimeter
Penman (1963) (original VPD method)	1.15	1.0
Penman (1963) (v. p. def. Meth. #3)	1.15	1.0
Kimberly Penman 1972	1.0	0.87
Kimberly Penman 1982	1.0	0.87
FAO-24 Penman	1.15	1.0
FAO-24 Corrected Penman	1.15	1.0
Penman-Monteith	1.0 <sup>a</sup>	1.0 <sup>a</sup>
Jensen-Haise	1.0	0.87
FAO-24 Radiation	1.15	1.0
Priestley-Taylor	1.15	1.0
Hargreaves-Samani	1.15	1.0
Turc	1.15	1.0
SCS Blaney-Criddle	1.22 <sup>b</sup>	1.1 <sup>c</sup>
FAO-24 Blaney-Criddle	1.15	1.0
FAO-24 Pan	1.15	1.0

Note: Values of 1.15 were used in the 1990 edition of Manual 70 to convert grass ET to alfalfa equivalent, and  $1/1.15 = 0.87$  was used to convert alfalfa ET to grass equivalent. More recent study and analyses suggest that 1.2 to 1.3 is a more appropriate ratio of alfalfa ET to grass ET (Allen et al. 1989; ASCE-EWRI 2005).

<sup>a</sup>Vegetation heights and corresponding surface roughness and leaf-area indices were set to specific values for each site (Table L-9).

<sup>b</sup>Monthly values from the SCS Blaney-Criddle coefficient curve for alfalfa hay were multiplied by 1.22 to convert to an alfalfa reference.

<sup>c</sup>Monthly values from the SCS Blaney-Criddle coefficient curve for grass pasture were multiplied by 1.1 to convert to a grass reference (Doorenbos and Pruitt 1977).

cultivars and crop heights or climatic parameters between locations, but the authors felt that the advantages of using this approximation outweighed the disadvantages.

A postanalysis of the same data sets by Allen et al. (1989) indicated that average ratios of  $ET_r$  to  $ET_o$  during the growing season months at the 11 lysimeter sites, computed with the Penman-Monteith equation with Eq. (8-9) for  $r_s$ , ranged from 1.12 for humid, low-wind conditions at Yangambi, Zaire, to 1.39 for windy conditions at Seabrook, New Jersey, and averaged 1.32. The postanalysis indicates that an average  $ET_r/ET_o$  ratio of 1.2 to 1.25 may have been more representative of the 11 lysimeter sites evaluated. These adjustments have not been made in this second edition to preserve the original results from the first edition.

Table L-9. Vegetation Heights Used in Reference Estimates with the ASCE Penman-Monteith Method

Lysimeter Location	Month	Vegetation Height, cm	Height of Weather Surface Vegetation, cm
Aspendale	All	10	10
Brawley	4	25	12
	5	40	12
	6	45	12
	7	50	12
	8	50	12
	9	30	12
	10	25	12
	11	25	12
	All	12	12
	3	7	7
	4	10	10
Copenhagen	5	25	15
Coshocton	6	25	15
	7	25	15
	8	20	15
	9	20	15
	10	15	15
	11	10	10
Davis	All	12	7
Kimberly	4	25	12
	5	40	12
	6	60	12
	7	50	12
	8	40	12
	9	40	12
	10	20	12
Lompoc	All	9	9
Seabrook	All	12	12
Scottsbluff	6	50	50
	7	50	50
	8	45	45
	9	50	50
	All	12	12
South Park	5	35	35
Yangambi	6	35	35
	All	25	25

The SCS Blaney-Criddle method estimates were converted to an approximate, equivalent grass or alfalfa reference by multiplying the equation estimates by the appropriate SCS  $k_c$  value for either grass pasture or alfalfa hay (USDA 1970). This product was then divided by a reference-based coefficient to convert the pasture or hay ET value to the equivalent grass or alfalfa reference. In the case of a grass lysimeter reference, the SCS Blaney-Criddle grass pasture ET estimate was divided by the ratio of the FAO-24 coefficients for mean and peak pasture which is 0.91 (Table 23 of FAO-24, Doorenbos and Pruitt 1977). In the case of an alfalfa lysimeter reference, the SCS Blaney-Criddle alfalfa hay ET estimate was divided by the mean alfalfa hay coefficient given in Table 6.9 (1st edition) as 0.82. This coefficient is roughly equivalent to the ratios of FAO-24 coefficients for mean and peak alfalfa hay, which are both 0.83 (Table 23 of FAO-24).

The SCS  $k_c$  curves for grass pasture and alfalfa hay were approximated using the following polynomials where  $J_r$  is a relative ratio of time within the calendar year, calculated for the Northern Hemisphere as

$$J_r = \frac{(M + D/30.5 - 1)}{12} \quad (\text{L-1})$$

where  $M$  is the month of the year (1–12) and  $D$  is the day of the month (1–31). The polynomial equation used for the SCS  $k_c$  for alfalfa was

$$k_c = 0.606 + 0.0552J_r + 10.29J_r^2 - 26.7J_r^3 + 24.0J_r^4 - 7.6J_r^5 \quad (\text{L-2})$$

and the polynomial equation used for the SCS  $k_c$  for grass pasture was

$$k_c = 0.472 + 0.273J_r + 8.53J_r^2 - 24.4J_r^3 + 24.3J_r^4 - 8.8J_r^5 \quad (\text{L.3})$$

## L.5 COMPARATIVE ANALYSES OF MONTHLY AND SEASONAL ET ESTIMATES

Comparisons of monthly ET estimates vs. lysimeter measured ET for all 11 lysimeter locations for each of the 19 ET estimating methods and for measured pan evaporation were presented in Figs. 7.56 through 7.75 of the first edition. The estimates were adjusted to represent the type of crop grown in the lysimeter (alfalfa or grass) using the factors listed in Table L-8. Separate tables and statistics were presented for the peak months because the accuracy of these estimates is important in the design and operation of irrigation systems, in water rights determinations and regulation, and in allocating limited water supplies.

In this appendix, only ET estimates for each of the 16 methods expressed as percentages of the corresponding lysimeter-measured ET for peak ET months are presented (Table L-10) for each of the 11 lysimeter locations.

The average relative values for peak ET months for arid locations and humid locations are presented near the bottom of Table L-10 along with the overall average. A value of 100 indicates perfect agreement between the ET estimate and lysimeter ET, but one must bear in mind the impact of uncertainties in converting between the two reference types. The relative consistency of ET estimates by a method from location to location indicates the robustness of an estimating method in performance over a variety of climates. The ASCE Penman-Monteith method is the “full form” version (Eq. 8-2) with surface resistance from Eq. (8-9), (8-10), (8-12), or (8-13) and aerodynamic resistance from Eq. (8-3), with stability corrections set to 0 and zero-plane displacement and aerodynamic roughness from Eqs. (8-6)–(8-8). The full-form procedure was used in the first edition prior to development of the standardized PM equation by ASCE (2005).

The average of the peak ET estimates for the arid and humid locations in Table L-10 indicates that most of the methods underestimated ET during peak months at the six arid locations and overestimated ET at the five humid locations. Underestimation by some  $ET_o$ -based methods would have been reduced had a reference conversion ratio of 1.2 or 1.25 been used rather than 1.15.

Ratios of seasonal ET to seasonal lysimeter-measured expressed as percentages are presented in Table L-11 for the 11 lysimeter locations and for the arid and humid locations. The average of the seasonal ET estimates for the arid and humid locations in Table L-11 indicates that most of the methods also underestimated seasonal ET at the six arid locations and overestimated ET at the five humid locations.

## L.6 STATISTICAL ANALYSES OF MONTHLY ESTIMATES

Standard errors of estimate (SEEs) were calculated between ET estimates and lysimeter measurements according to the equation

$$\text{SEE} = \left[ \frac{\sum_{i=1}^n (Y_i - Y_{ei})^2}{n - 1} \right]^{0.5} \quad (\text{L-4})$$

where  $Y_i$  is the average  $i$ th month lysimeter ET,  $Y_{ei}$  is the corresponding ET estimate, and  $n$  is the total number of observations. The SEE is a measure of the differences between the measured and estimated values and indicates how well each method estimated lysimeter ET measurements over all months of record at each location and over all locations. The SEE, as calculated with Eq. (L-4) has units of  $\text{mm d}^{-1}$  and  $n - 1$  degrees of freedom.

SEEs calculated for monthly ET estimates at each lysimeter location for all months and for peak months are presented in Table L-12 (former Table 7-14). These SEE values indicate the goodness of fit of ET estimates and lysimeter-measured ET without any adjustment or calibration. SEE values also indicate the performances to be expected by methods when

Table L-10. Average Peak Monthly ET Estimates Expressed as Percentage of Lysimeter-Measured ET

Location	Combination												Radiation				Temperature				Pan
	Penman (1963)		1972		1982		FAO-24		FAO-24		ASCE		SCS		FAO-24		Hargr. et al.		FAO-		Pan
	Penman	VPD3	Kimberly	Kimberly	Penman	Penman	Corrected (c=1)	Penman	Monteith	Haise	Jensen- Haise	FAO-24	Priestley- Taylor	Tunc	Blaney- Criddle	Criddle	(1985)	24 Pan	evap	All Methods <sup>a</sup>	
Aspendale	93	98	98	98	103	105	122	82	71	98	81	74	75	82	89	111	92				
Brawley	88	96	94	104	100	107	99	92	97	61	64	96	101	89	110	123	95				
Copenhagen	123	126	127	129	149	158	100	61	143	104	116	139	160	133	92	115	123				
Coshocton	107	111	104	112	116	127	107	79	107	114	87	88	86	86	115	102	101	124			
Davis	99	110	106	116	110	130	97	105	105	114	114	114	114	114	117	118	141	111			
Kimberly	88	95	93	101	100	111	98	95	95	109	64	67	93	104	90	101	110	95			
Lompoc	130	134	124	131	133	160	103	79	146	133	118	89	116	100	137	165	125				
Scottsbluff	83	87	88	92	94	96	98	73	98	57	59	79	94	66	64	74	81				
Seabrook	99	104	106	111	118	126	93	74	103	81	83	121	116	98	61	76	98				
South Park	89	96	90	98	98	106	102	101	96	86	71	84	82	119	105	125	97				
Yangambi	93	97	86	79	97	106	90	99	105	95	100	132	87	132	86	100	99				
Arid locations	89	96	95	102	101	111	96	87	102	70	69	86	97	88	94	109	93				
Humid loc.	109	113	109	111	121	134	98	79	119	102	100	120	115	114	97	117	110				
All locations	99	105	102	107	111	122	97	83	110	86	85	103	106	101	95	113	102				

Note: Equation estimates have been adjusted for the reference crop of the lysimeter.

<sup>a</sup>Average of all equation estimates (excluding FAO-PPP-17, Businger-van Bavel, Thornthwaite, and Christiansen pan methods in former Table 7.12).

Table L-11. Seasonal ET Estimates Expressed as Percentage of Lysimeter-Measured ET

Location	Combination										Radiation				Temperature				Pan	
	Pennman (1963)	Pennman			1982			FAO-24		ASCE		Jensen- Haise	FAO-24 Radiation	Priestley- Taylor	SCS	FAO-24 Hargr. Blaney- Criddle	et al. (1985) 24 Pan evap	FAO- Pan	All Methods <sup>a</sup>	
		VPD3	Kimberly	Pennman	Pennman	(c = 1)	Pennman	Corrected	Pennman	Monteith	Penman									
Aspendale	104	110	111	104	121	128	90	74	105	84	87	85	93	90	96	119	100			
Brawley	96	104	102	100	108	112	100	95	99	66	65	98	102	90	118	129	99			
Copenhagen	127	127	134	127	161	156	102	58	138	95	119	148	157	146	92	115	125			
Coshocton	110	115	113	108	122	123	106	69	97	93	87	120	100	121	101	121	105			
Davis	108	120	121	113	124	135	106	102	118	82	93	81	118	105	107	131	110			
Kimberly	94	103	105	102	109	114	101	83	107	63	62	72	95	84	106	116	95			
Lompoc	130	137	130	121	134	152	107	77	142	118	119	85	121	110	135	162	124			
Scottsbluff	90	95	93	96	99	104	102	81	105	65	65	87	100	76	79	87	89			
Seabrook	115	124	135	121	149	148	111	71	115	74	88	104	124	112	49	61	106			
South Park	92	100	96	99	102	105	97	91	96	82	65	70	79	114	120	148	97			
Yangambi	98	102	90	88	102	111	94	112	118	103	115	142	100	143	96	110	108			
Arid locations	98	106	106	103	112	118	99	88	106	73	74	84	100	91	105	121	99			
Humid locations	114	120	118	110	129	135	104	82	122	97	105	117	116	125	95	114	113			
All locations	106	113	112	107	121	127	101	85	114	85	90	101	108	108	100	118	105			

Note: Equation estimates have been adjusted for the reference crop of the lysimeter.

<sup>a</sup>Average of all equation estimates (excluding FAO-PPP-17, Businger-van Bavel, Thornthwaite, and Christiansen pan methods in former Table 7.13).

Table L-12. Standard Errors of Estimates of Monthly ET vs. Lysimeter-Measured ET in mm d<sup>-1</sup>

Location	Combination		Radiation						Temperature			Pan					
	Penman (1963)	VPD3	1972	1982	FAO-24 Pennman (c=1)	ASCE Pennman	Jensen- Monteith	FAO-24 Haise Radiation	Priestley- Taylor	SCS	FAO-24 Blaney- Criddle	Hargr. et al. (1985)	FAO- Pan evap	All Methods <sup>a</sup>			
Aspendale	0.33	0.45	0.49	0.45	0.86	1.25	0.65	1.24	0.37	0.73	0.91	0.86	0.65	0.41	0.83	0.69	
Brawley	0.97	0.94	1.11	0.57	1.14	1.47	0.44	0.72	0.97	3.23	1.96	0.64	1.08	1.65	2.62	1.43	
Copenhagen	0.64	0.67	0.76	0.67	1.31	1.28	0.11	0.92	0.94	0.26	0.45	1.14	1.34	1.02	0.21	0.33	0.75
Coshocton	0.40	0.54	0.58	0.33	0.78	0.79	0.26	0.96	0.24	0.39	0.43	1.04	0.22	0.68	0.67	1.32	0.60
Davis	0.39	0.83	0.88	0.68	1.02	1.57	0.36	0.22	0.83	0.77	0.45	0.89	0.89	0.28	0.32	1.36	0.73
Kimberly	0.69	0.62	0.91	0.24	0.90	1.17	0.25	1.27	0.69	2.69	2.75	2.20	0.49	1.18	0.69	1.35	1.13
Lompoc	0.97	1.20	0.95	0.79	1.11	1.75	0.33	0.80	1.41	0.83	0.64	0.65	0.76	0.49	1.23	2.06	1.00
Scottsbluff	1.34	0.96	0.94	0.66	0.48	0.73	0.53	2.30	0.69	4.00	3.99	1.66	0.83	2.90	3.08	2.43	1.72
Seabrook	0.54	0.78	1.11	0.73	1.50	1.52	0.48	0.93	0.60	0.82	0.44	0.68	0.90	0.47	1.91	1.12	0.91
South Park	0.67	0.61	0.64	0.44	0.47	0.53	0.27	1.06	0.74	1.16	2.05	1.82	1.29	1.00	1.30	2.81	1.05
Yatgambi	0.24	0.23	0.41	0.52	0.24	0.44	0.32	0.52	0.67	0.26	0.60	1.79	0.33	1.54	0.34	0.45	0.56
Arid loc.	0.58	0.65	0.73	0.48	0.83	1.17	0.41	0.94	0.64	1.79	1.84	1.29	0.66	0.92	0.99	1.52	0.97
Humid loc.	0.57	0.71	0.75	0.59	0.99	1.17	0.31	0.76	0.81	0.55	0.49	1.05	0.71	0.86	0.88	1.17	0.77
All locations	0.57	0.67	0.74	0.53	0.91	1.16	0.36	0.84	0.73	1.29	1.30	1.16	0.68	0.88	0.92	1.34	1.01
Peak month arid	1.22	0.80	0.81	0.72	0.50	1.47	0.72	1.85	0.64	3.40	3.32	1.58	0.99	2.02	1.93	2.12	1.51
Peak month humid	0.84	0.96	0.83	1.09	1.34	2.02	0.37	1.27	1.33	0.99	0.75	1.35	1.26	1.02	1.60	1.98	1.19
Peak month all	0.95	0.77	0.72	0.79	0.84	1.53	0.52	1.44	0.88	2.34	2.26	1.31	0.98	1.47	1.58	1.82	1.26

Notes: Values are standard errors of estimate for ET estimates that have not been adjusted by regression. Unless noted, all statistics are for monthly values over the entire season of record.

<sup>a</sup>Equation estimates have been adjusted for the reference type of lysimeter. Average of all equation estimates (excluding FAO-PPP-17, Businger-van Bavel, Thornthwaite, and Christiansen pan methods in former Table 7.14).

used directly “off the shelf,” i.e., directly from the principal publications listed in Table L-1.

If the distribution of errors or differences between ET estimates and lysimeter measurements follow a normal distribution, then the SEE represents the maximum error in  $\text{mm d}^{-1}$  for 68% of all estimates by that method. Average SEEs for the various methods for all months over all locations ranged from  $0.36 \text{ mm d}^{-1}$  for the Penman-Monteith method to  $1.34 \text{ mm day}^{-1}$  for the pan evaporation method.

## L.7 METHOD PERFORMANCE

The analyses and intercomparisons of methods from the first edition were made over a broad range of climates and geographic locations. Consistency in performance of a method over the range of locations provides confidence in its performance under other conditions.

### Combination Methods

Estimates of ET using combination equation methods correlated well with lysimeter measurements at 10 of the 11 sites. The exception was at South Park because of limited data. In general, the combination methods tended to overestimate reference ET at humid locations. For the arid locations, the average percentage for seasonal estimates was 99 (Table L-11). For the humid climates, the average percentage was 113 (Table L-11). Some of this overestimation occurred during months of low ET because the average percentages for peak months were 93 and 110, respectively, for the arid and humid locations (Table L-10).

All combination methods with the exception of the 1963 Penman method, which underestimated ET, and the FAO Corrected Penman, which overestimated ET, performed well in estimating peak monthly ET in the arid locations. All combination methods with the exception of the ASCE Penman-Monteith equation generally overestimated ET during all months in the humid locations.

### Methods Based Primarily upon Solar Radiation

The Priestley-Taylor method is a simplification of the combination equation. It is the product of  $\Delta/(\Delta + c)$ , net radiation, and a coefficient. The other radiation methods are based on the relationship between air temperature and ratio of  $ET/R_s$ . The radiation methods were nearly always in phase with the monthly measured ET. They produced reasonably good estimates of lysimeter ET in the humid locations with the exception of the Jensen-Haise method, which tended to underestimate, and the FAO-24 Radiation method, which tended to overestimate ET. The Priestley-Taylor and Turc methods typically provided good estimates of both peak and seasonal ET in the humid climates. All radiation methods with the

exception of the FAO-24 Radiation method substantially underestimated both peak and seasonal ET in the arid climates. The advection of sensible heat energy is taken into account by the aerodynamic term of the Penman equation, but is absent in the Priestley-Taylor and Turc equations.

### Methods Using Primarily Air Temperature

Of the temperature methods, the SCS Blaney-Criddle method and Thornthwaite method (not included in the tables), were generally the poorest in estimating lysimeter ET of all methods evaluated. The SCS Blaney-Criddle typically underestimated reference ET in the arid climates and overestimated both peak and seasonal ET in humid climates.

The addition of other parameters to the FAO Blaney-Criddle temperature method improved its performance at the majority of locations. Both the Hargreaves-Samani and FAO Blaney-Criddle methods tended to overestimate ET by 15 to 25% in humid climates. The Hargreaves-Samani method tended to underestimate ET by about 10% in arid climates. The FAO Blaney-Criddle method provided good estimates of both peak and seasonal ET at the arid lysimeter locations. The temperature difference term,  $T_d$ , in the Hargreaves-Samani method incorporates some additional effects of humidity and cloud cover. The Hargreaves-Samani method greatly overestimated ET in the humid, low-radiation climate of Yangambi, Zaire.

### Pan Evaporation Methods

The Christiansen (not included in the tables) and the FAO-24 pan evaporation methods were severely affected by apparently poor or non-representative measurements of pan evaporation. Some of the variation between pan evaporation ET estimates and lysimeter ET measurements is due to unavoidable differences in heat retention, surface roughness of the surrounding area, and variation in exposure of pans with time of season. It appears that poor performance of pan evaporation may have been due to problems in data collection and pan and site maintenance. For example, the evaporation pan at Scottsbluff, Nebraska, was partially surrounded by tall field corn during much of the 1977 growing season. The tall crop would have reduced the wind speed over the pan and reduced the evaporation rate relative to the ET rate from alfalfa lysimeter. This is one of the disadvantages of the pan method, in that its performance is tightly controlled and affected by the consistency and care (or lack thereof) in pan operation and maintenance, including site conditions.

## L.8 EVAPOTRANSPIRATION ESTIMATES BY LOCATION

Most of the empirical ET estimating methods evaluated were developed from data collected in temperate midlatitudes and usually at relatively low elevations. Some of the methods behaved differently at the high-elevation

site of South Park, at the equatorial latitude of Yangambi, at the northern latitude of Copenhagen, and under the coastal climate found at Lompoc than they did in the low- to mid-elevation, temperate sites in which they were developed. The consistency of any ET estimating method over a wide range of latitudes, elevations, and humidity indicates the "robustness" of that method and its ability to represent the physical processes controlling ET.

A complicating factor when comparing methods at various sites is the effect of differences in data quality among locations. Data used in this study were not equally available for all locations and were not all of equal quality. Considerable effort was made to include only data sets from lysimeter and weather station locations for which information was available to indicate a high level of professional care and integrity in operation and maintenance of the site and in data reduction. The resulting data sets in the first edition of this manual were of improved quality as compared to data sets used in the original ASCE report (Jensen 1973).

Poor data quality tends to more heavily penalize the physically based methods, such as the Penman equation, which require more parameters (solar radiation, wind speed, air temperature, and dew point temperature) as compared to single weather parameter methods, such as air temperature used in the Hargreaves-Samani method. Air temperature data tend to be of higher quality more of the time than the radiation or humidity data. Measuring mechanisms for air temperature are simpler and are standardized. Extra effort was made during the first edition study to include only those locations with good data integrity in all parameter measurements. However, the quality and accuracy of weather and lysimeter ET measurements are never known with complete confidence. As a result, some of the differences between locations in this comparison that appear to be associated with climate may actually be due to differences in data quality. Detailed discussion of estimates by location can be found in the first edition of this manual.

## L.9 RANKING OF ET METHODS USING MONTHLY ESTIMATES

Desirable characteristics sought in an evapotranspiration equation are accuracy in estimating peak ET requirements, accuracy in estimating seasonal ET requirements, and ability to accurately estimate ET in a variety of climates and locations. In addition, if methods overestimate or underestimate ET within a specific climate, then an additional attribute would be that the estimation errors be systematic and correctable using simple linear adjustments.

The standard error of estimate, (SEE) as defined in Eq. (L-4), was used to gauge method accuracy and consistency in providing monthly reference ET estimates at the 11 lysimeter locations. Two SEE values were calculated: (1) the SEE of monthly method estimates vs. lysimeter measurements and (2) the SEE of method estimates adjusted using a coefficient based on a linear regression through the origin vs. lysimeter measurements, ASEE.

The use of these two SEEs provided information on both accuracy of unadjusted ET estimates and ease with which the methods can be adjusted or “corrected” with a simple coefficient to fit location ET. The SEE values were calculated for all months and for peak months.

Consistency in low SEE for all locations indicates consistent accuracy in method estimation across a broad range of climate and geography. The maximum SEE for the ASCE PM was  $0.65 \text{ mm d}^{-1}$  at Aspendale, Australia (Table L-12). All other methods—except the 1982 Kimberly Penman, with maximum SEE of  $0.79 \text{ mm d}^{-1}$  at Lompoc, California—had SEE exceeding  $1.0 \text{ mm d}^{-1}$  at at least one location, with some methods exceeding  $2.0 \text{ mm d}^{-1}$ . Weighted SEEs were calculated by weighting season-long values 70% and peak monthly values 30%. Within each of these two groupings, two-thirds (67%) weight was placed on the unadjusted SEE and one-third (33%) weight was placed on the SEE of regression-adjusted estimates. The resulting values of the weighted SEE indicate the ability of methods to accurately estimate ET during all months (47% weight), the ability to accurately estimate peak reference ET (20% weight), and the ability to be corrected using a linear multiplier (33% weight).

Summary statistics and ranking of ET methods over all 11 lysimeter locations are presented in Table L-13. The ASCE Penman–Monteith equation with aerodynamic and canopy resistances estimated according to Eqs. (8-2), (8-3), (8-6)–(8-10), (8-12), and (8-13) following Allen (1986) and Allen et al. (1989) had the lowest SEE and highest correlation coefficients of all methods. Average standard errors of estimate for the ASCE Penman–Monteith method were  $0.52$  and  $0.36 \text{ mm d}^{-1}$  for peak months and all months, respectively, over all 11 lysimeter locations.

The top five methods were forms of the combination equation, with the FAO-24 Radiation and FAO-24 Blaney–Criddle methods, placing sixth and seventh. The 1982 Kimberly Penman (Wright 1982) was ranked second overall, with a standard error of estimate for peak months of  $0.79 \text{ mm d}^{-1}$  and standard error of estimate for all months of  $0.53 \text{ mm d}^{-1}$ . Use of the 1963 Penman equation with the vapor pressure deficit calculated as the average of deficits at maximum and minimum daily air temperatures (VPD #3) did not generally improve the performance of the original Penman equation and is therefore not recommended. The 1972 Kimberly Penman ranked fifth overall and produced relatively good estimates of peak monthly ET but overestimated reference ET over all months by about 12%.

Weighted SEEs were similar for the third through seventh place methods, indicating fairly equal performances by these five methods in estimating both peak month and seasonal ET in all types of climates evaluated. The FAO-24 Radiation method was the best performing radiation method, having a ranking of sixth place overall. This method overestimated ET by an average of 14% over all months, which reduced its ranking. The SEE by the FAO-24 Radiation method was much improved after adjustment by regression. The FAO-24 Blaney–Criddle method was the best performing

Table L-13. Summary of Statistics and Ranking of Methods for Monthly Estimates of ET at All Locations

Rank (1)	Method (2)	All Months						Peak Month			Weighted SEE <sup>f</sup> (13)
		% <sup>a</sup> (3)	SEE <sup>b</sup> (4)	b <sup>c</sup> (5)	r <sup>d</sup> (6)	ASEE <sup>e</sup> (7)	% SEE (8)	b (9)	r (10)	ASEE <sup>e</sup> (11)	
1	Penman-Monteith	101	0.36	1.00	0.99	0.36	97	0.52	1.03	0.99	0.47
2	1982 Kimberly-Penman	107	0.53	0.95	0.98	0.49	107	0.79	0.96	0.96	0.73
3	Penman (1963)	106	0.57	0.99	0.97	0.57	99	0.95	1.07	0.96	0.81
4	Penman (1963), VPD #3	113	0.67	0.93	0.97	0.57	105	0.77	1.00	0.96	0.77
5	1972 Kimberly Penman	112	0.74	0.93	0.96	0.67	102	0.72	1.03	0.97	0.70
6	FAO Radiation	114	0.73	0.91	0.97	0.59	110	0.88	0.95	0.95	0.78
7	FAO-24 Blaney-Criddle	108	0.68	0.95	0.96	0.64	106	0.98	0.98	0.94	0.97
8	FAO-24 Penman ( $c=1$ )	121	0.91	0.88	0.96	0.65	111	0.84	0.95	0.95	0.76
9	Jensen-Haise	85	0.84	1.11	0.95	0.71	83	1.44	1.15	0.92	1.06
10	Hargreaves et al. (1985)	108	0.88	1.00	0.93	0.88	101	1.47	1.07	0.87	1.39
11	FAO-24 Corrected Penman	127	1.16	0.82	0.96	0.65	122	1.53	0.86	0.93	1.00
12	FAO-24 Pan	100	0.92	0.94	0.92	0.88	95	1.58	1.03	0.82	1.57
13	SCS Blaney-Criddle	101	1.16	0.99	0.87	1.15	103	1.31	1.05	0.89	1.26
13	Pan Evaporation	118	1.34	0.82	0.92	0.87	113	1.82	0.88	0.83	1.56
14	Turc	90	1.30	1.20	0.89	1.07	85	2.26	1.31	0.84	1.49
15	Priestley-Taylor	85	1.29	1.22	0.90	1.02	86	2.34	1.28	0.78	1.72

Note: All equations were adjusted for the reference crop of the lysimeter (excluding FAO-PPP-17, Businger-van Bavel, Thornthwaite, and Christiansen pan methods in former Table 720).

<sup>a</sup>Average percentage of lysimeter measurements.

<sup>b</sup>Standard error of the estimate or ET estimates in mm d<sup>-1</sup> that have not been adjusted by regression.

<sup>c</sup>Regression coefficient (slope) for regression through the origin of lysimeter versus equation estimate.

<sup>d</sup>Correlation coefficient for regression through the origin of lysimeter versus equation estimate.

<sup>e</sup>Standard error of estimate for ET estimates in mm d<sup>-1</sup> that have been adjusted by regression through the origin.

<sup>f</sup>Weighted standard error of estimate calculated as  $0.7[0.67(\text{Col. 4}) + 0.33(\text{Col. 7})] + 0.3[0.67(\text{Col. 9}) + 0.33(\text{Col. 12})]$ .

Table L-14. Summary of Statistics and Ranking of Methods for Daily Estimates of ET at Kimberly, Idaho; Coshocton, Ohio; and Davis, California

Rank (1)	Method (2)	All Months				Peak Month			Weighted SEE <sup>e</sup> (11)
		SEE <sup>a</sup> (3)	b <sup>b</sup> (4)	r <sup>c</sup> (5)	A SEE <sup>d</sup> (6)	SEE (7)	b (8)	r (9)	
1	Penman-Monteith	0.77	0.98	0.92	0.75	0.70	1.04	0.80	0.66
2	1982 Kimberly-Penman	0.88	0.94	0.92	0.73	1.03	0.96	0.80	0.64
3	FAO-24 Blaney-Criddle	0.91	0.94	0.92	0.77	0.99	0.93	0.68	0.69
4	Penman (1963)	0.95	0.99	0.90	0.83	0.88	1.07	0.81	0.63
5	1972 Kimberly Penman	1.09	0.92	0.88	0.92	0.92	1.04	0.81	0.62
6	FAO-24 Penman (c=1)	1.18	0.86	0.89	0.88	0.91	0.93	0.81	0.62
7	FAO-Radiation	1.10	0.89	0.89	0.89	1.23	0.91	0.70	0.77
8	FAO-24 Corrected Penman	1.22	0.84	0.91	0.79	1.34	0.87	0.80	0.65
9	Jensen-Haise	1.22	1.21	0.87	0.97	1.06	1.16	0.63	0.79
10	Hargreaves et al. (1985)	1.25	0.99	0.79	1.14	1.23	0.99	0.39	1.11
11	FAO-Pan	1.27	0.87	0.77	1.10	1.42	0.86	0.62	1.09
12	Priestley-Taylor	1.63	1.26	0.82	1.12	1.69	1.26	0.53	0.90

Note: All equations were adjusted for the reference crop of the lysimeter.

<sup>a</sup>Standard error of the estimate for ET estimates in mm d<sup>-1</sup> that have not been adjusted by regression.

<sup>b</sup>Regression coefficient (slope) for regression through the origin of lysimeter versus equation estimates.

<sup>c</sup>Regression coefficient for regression through the origin of lysimeter versus equation estimates.

<sup>d</sup>Standard error of estimate for ET estimates in mm d<sup>-1</sup> that have been adjusted by regression through the origin.

<sup>e</sup>Weighted standard error of estimated calculated as  $0.7[0.67(\text{Col. 3}) + 0.33(\text{Col. 6})] + 0.3[0.67(\text{Col. 7}) + 0.33(\text{Col. 10})]$ .

temperature method over all locations, producing SEEs for peak months that were more than 30% lower than those for the Hargreaves-Samani method. It should be noted, however, that the FAO-24 Blaney-Criddle method required estimates of solar radiation, wind speed, and relative humidity, whereas the Hargreaves-Samani equation required only measurements of minimum and maximum daily air temperature.

The correction term,  $c$ , in the FAO-24 Penman method tended to increase the overestimates with this method. The correction also increased the SEEs after adjustment by regression for peak months. About 3–5% of the overestimation would have been avoided by using the FAO-24 “ $c$ ” table rather than the Frevert et al. (1983) equation. The FAO-24 Corrected Penman was ranked below the “uncorrected” FAO-24 Penman with  $c$  set equal to 1.0. The Jensen-Haise method, ranked ninth overall, had fairly high values of SEE for peak months, even after adjustment by regression (Table L-13). The Jensen-Haise method averaged about 15% low over all locations.

The SCS Blaney-Criddle method, adjusted to approximate a reference ET estimate, produced SEEs that were 70% greater than those for the FAO-24 Blaney-Criddle method.

The two radiation methods (Turc and Priestley-Taylor) ranked second and fourth when only humid locations were considered and ranked within the last two places when all locations were evaluated together. This result is due to the extreme underestimation by these two methods in areas with large daily vapor pressure deficits.

Table L-14 summarizes statistics and ranking of methods for daily estimates of ET at three locations having multiyear data sets of daily lysimeter and weather data. Rankings were similar to those for monthly calculation time steps.

## L.10 SUMMARY

The comparisons that were made and reported in the first edition of Manual 70 were based on data available during the period of about 1959 through 1979. When considering the quality of lysimeter ET measurements and the associated climatic data, the analyses clearly showed that the better estimates of ET were made with methods that incorporated energy balance components. The best ET estimates were obtained when methods incorporated both energy balance and aerodynamic components (combination methods).

Since publication of the first edition in 1990, many studies have been made comparing methods of estimating ET. Those studies have provided more detail on the theoretical basis of the Penman-Monteith combination equation and its applications. Those studies also resulted in the development of a comprehensive publication prepared by an ASCE task committee entitled *The ASCE Standardized Reference Evapotranspiration Equation* (ASCE 2005).

This page intentionally left blank

## APPENDIX M

### GLOSSARY

Glossary terms with an asterisk (\*) are copyright American Meteorological Society (2015) and used with permission.

**absolute humidity\***—Mass of water vapor per cubic meter of air.

**adiabatic process\***—A reversible thermodynamic change of state of a system without the addition or removal of heat or mass.

**advection\***—Horizontal transfer of heat energy by large-scale motions of the atmosphere.

**aerodynamic\***—Refers to forces acting upon the soil or crop surface by moving air.

**aerodynamically rough surface\***—A surface whose roughness elements are sufficiently large that the turbulent boundary layer reaches the surface.

**aerodynamically smooth surface\***—A surface whose roughness elements are sufficiently small to be entirely embedded in the laminar sublayer.

**albedo\***—The ratio of electromagnetic radiation reflected from a soil and crop surface to the amount incident upon it. In practice, the value is applied primarily to solar radiation.

**anemometer level\***—The height above ground at which an anemometer is exposed.

**arid climate\***—Generally any extremely dry climate.

**arithmetic mean\***—1. (Also called mean, average, simple average.) Usually denoted by the symbol  $\bar{x}$  is the sum of  $x_1 + x_2 + \dots + x_n$  divided by  $n$ . 2. Pertaining to a *random variable*, same as *expected value*.

**bar\***—A unit of pressure equal to  $10^6$  dynes per  $\text{cm}^2$ , 100 kilopascals, 29.53 in. of mercury.

**black body\***—A hypothetical “body” that absorbs all electromagnetic radiation striking it; a body that neither reflects nor transmits any of the incident radiation.

**Bowen ratio\***—The ratio of energy flux upward as sensible heat to latent energy flux in the same direction (negative when the fluxes are in opposite directions).

**BPI pan\***—A circular evaporation pan, 6 ft in diameter and 2 ft deep, made of unpainted galvanized iron. The pan is buried in the ground so that about 4 in. of the rim extends above the surrounding ground and the water surface is maintained at about ground level. (BPI stands for Bureau of Plant Industry, USDA, which introduced this instrument.)

**calorie\***—(Abbreviated cal) A unit of heat required to raise the temperature of 1 gram of water from 14.5°C to 15.5°C. The International Steam Table calorie equals 1.00032 cal ([List 1984](#)).

**capillary fringe\***—A shallow zone of soil above a water table that is nearly saturated by capillary action in the smaller pore spaces.

**Celsius\***—Same units as centigrade temperature scale.

**class A pan\***—The U.S. Weather Bureau evaporation pan is a cylindrical container fabricated of galvanized iron or monel metal with a depth of 10 in. and a diameter of 48 in. The pan is placed on an open 2 × 4-in. wooden platform with the top of the pan about 41 cm (16 in.) above the soil surface. It is accurately leveled at a site that is nearly flat, well sodded, and free from obstructions. The pan is filled with water to a depth of 8 in., and periodic measurements are made of the changes of the water level with the aid of a hook gauge set in the still well. When the water level drops to 7 in., the pan is refilled. Its average pan coefficient is about 0.7 for lake evaporation.

**consumed fraction**—The fraction of water withdrawn from a surface or groundwater source that is evaporated, transpired, incorporated into products or crops, consumed by humans or livestock, or otherwise removed from the immediate water environment.

**consumptive use\***—That part of water withdrawn that is evaporated, transpired, incorporated into products or crops, consumed by humans or livestock, or otherwise removed from the immediate water environment (also referred to as water consumed). Water consumed may be defined as beneficial if there are economic or environmental benefits or nonbeneficial if there are no direct economic or environmental benefits.

**crop coefficient\***—The ratio of evapotranspiration occurring with a specific crop at a specific stage of growth to reference crop evapotranspiration at that time usually denoted by the symbol  $K_c$  (not the same as  $K$  used in the Blaney-Criddle method).

**crop water requirement\***—The depth of water needed to meet evapotranspiration of a disease-free crop, growing in large fields under nonrestricting soil conditions and achieving full production potential in a given growing environment.

**Darcy's law\***—The law stating that the velocity of a fluid in permeable media is directly proportional to the hydraulic gradient.

**day length**—The length of day from sunrise to sunset expressed in hours.

**deep percolation\***—The drainage of soil water by gravity below the maximum effective depth of the root zone.

**depletion**—Net rate of water use from a stream or groundwater aquifer for beneficial and nonbeneficial uses. For irrigation or municipal uses, the depletion is the headgate or wellhead diversion less return flow to the same stream or groundwater aquifer.

**dewpoint\***—The temperature to which a given parcel of air must be cooled at constant pressure and at constant water vapor content until saturation occurs, or the temperature at which saturation vapor pressure of the parcel is equal to the actual vapor pressure of the contained water vapor.

**diffusion\***—Turbulent diffusion results from atmospheric motions diffusing water vapor, heat, and other gaseous components by exchanging parcels called eddies between regions in space in apparent random fashion.

**duty of water\***—The total volume of irrigation water required to mature a particular type of crop. It includes consumptive use, evaporation, and seepage from ditches and canals, and water eventually returned to streams by percolation and surface runoff (no longer in common use).

**effective precipitation\***—Precipitation that remains on the foliage or in the soil that is available for evapotranspiration and reduces the withdrawal of soil water by a like amount.

**emissivity\***—The ratio of the emittance of a given surface at a specified wavelength and emitting temperature to the emittance of an ideal black body at the same wavelength and temperature. For energy balance computations under natural conditions, the emissivity is commonly taken as the ratio of the total emittance of a surface to the total emittance of an ideal black body.

**enthalpy\***—In meteorology, enthalpy is sensible heat. In thermodynamics, it is the internal energy plus the product of pressure and volume.

**evaporation\***—The physical process by which a liquid or solid is transformed to the gaseous state which in irrigation usually is restricted to the change of water from liquid to gas.

**evapotranspiration\***—The combined processes by which water is transferred from the earth's surface to the atmosphere; evaporation of liquid or solid water plus transpiration from plants (also see consumptive use).

**extraterrestrial radiation\***—Solar radiation received "on top of" the earth's atmosphere (also known as exoatmospheric radiation).

**Fahrenheit temperature scale\***—(Abbreviated F) A temperature scale with the ice point at 32° and the boiling point of water at 212°. Conversion of the temperature in Celsius (C) to temperature in °F =  $1.8^{\circ}\text{C} + 32$ .

**fetch\***—(Also generating area) The length of fetch area, measured in the direction of the wind from the site in question.

**flux density\***—The rate of flow of any quantity through a unit area of specified surface.

**gas constant\***—The constant factor in the equation of state for perfect gases. The universal gas constant is  $R = 8.3144 \text{ joules mol}^{-1} \text{ K}^{-1}$ .

**global radiation\***—The total of direct solar radiation and diffuse sky radiation received by a unit horizontal surface (essentially less than about 3  $\mu\text{m}$ ).

**hydraulic conductivity\***—The proportionality factor in the Darcy flow law, which states that the effective flow velocity is proportional to the hydraulic gradient.

**hydraulic head\***—The total of fluid pressure head and elevation with respect to a specified datum.

**hydrostatic pressure\***—The pressure in a fluid in equilibrium that is due solely to the weight of fluid above.

**insolation\***—(Contracted from incoming solar radiation) Solar radiation received at the earth's surface.

**irrigation efficiency**—The ratio of the volume of water required for a specific beneficial use as compared with the volume of water delivered for this purpose. It is commonly interpreted as the volume of water stored in the soil for evapotranspiration compared with the volume of water delivered for this purpose, but may be defined and used in different ways.

**irrigation water requirements\***—The quantity of water exclusive of precipitation that is required for various beneficial uses, particularly evapotranspiration.

**joule\***—The unit of energy or work done when the point of application of 1 newton is displaced a distance of 1 meter in the direction of force, 1 joule = 1 watt second.

**laminar flow\***—A flow in which fluid moves smoothly in streamlines in parallel layers or sheets (nonturbulent flow).

**langley\***—A unit of energy per unit area that was commonly used in radiation measurements that is equal to 1 gram calorie per square centimeter.

**latent heat\***—The heat released or absorbed per unit mass of water in a reversible, isobaric-isothermal change of phase.

**leaching requirement**—The fraction of water entering the soil that must pass through the root zone to prevent soil salinity from exceeding a specific value.

**leaf-area index\***—The area of one side of leaves per unit area of soil surface, commonly abbreviated LAI.

**logarithmic velocity profile\***—The variation of wind speed with height in the surface boundary layer. For rough surfaces the profile is  $u/u_* = 1/k \ln(z/z_0)^2$ ,  $z > z_0$  where  $z_0$  is the constant related to the average height of the surface irregularities and is called the roughness length;  $u_*$  is

the friction velocity;  $k$  is the von Kármán constant, and  $z$  is the elevation above the surface.

**long-wave radiation\***—Electromagnetic radiation with a wavelength greater than 0.8  $\mu\text{m}$ . (For convenience, long-wave radiation is normally considered to include all wavelengths greater than solar radiation or essentially 3  $\mu\text{m}$ .)

**micrometer\***—(Abbreviated  $\mu\text{m}$ ) A unit of length equal to one-millionth of a meter, or one-thousandth of a millimeter.

**millibar\***—(Abbreviated mb) A pressure unit of 0.1 kPa, and equal to one-thousandth of a bar. Atmospheric pressures are commonly reported in millibars, or in kilopascals.

**mixing ratio\***—The ratio of the mass  $m_v$  of water vapor to the mass  $m_a$  of dry air with which the water is associated,  $r = m_v/m_a$ .

**mole**—A unit of mass numerically equal to the molecular weight of the substance.

**net radiation\***—The difference of the downward and upward solar and long-wave radiation flux passing through a horizontal plane just above the ground surface.

**neutral stability\***—The state of an unsaturated or saturated column of air in the atmosphere when its environmental lapse rate of temperature is equal to the dry-adiabatic lapse rate or the saturation adiabatic lapse rate, respectively. Under such conditions, a parcel of air displaced vertically will experience no buoyant acceleration.

**newton\***—The unit of force in the  $\text{m kg s}$  system of units; the force that gives to a mass of 1 kg an acceleration of  $1 \text{ ms}^{-2}$ .

**nonconsumptive use**—That part of water withdrawn that is not evaporated, transpired, incorporated into products or crops, consumed by humans or livestock, or otherwise removed from the immediate water environment. Water withdrawn that is not consumed may be recoverable for further use or nonrecoverable or lost to further use such as flows to saline sinks or flows to the sea.

**pascal\***—The unit of pressure in the SI system; 1 pascal equals 1 newton per square meter.

**potential evapotranspiration\***—The rate at which water if available would be removed from wet soil and plant surfaces expressed as the rate of latent heat transfer per unit area or an equivalent depth of water.

**power-law profile\***—An alternative to the logarithmic velocity profile.

**psychrometric chart\***—A nomograph for graphically obtaining relative humidity and dew point from wet and dry bulb thermometer readings.

**pyranometer\***—A general name for actinometers that measure the combined intensity of incoming direct solar radiation and diffuse sky radiation.

**radiation\***—The process by which electromagnetic energy is propagated through free space as distinguished from conduction and

convection (also see global, long-wave, net, shortwave, solar, and thermal radiation).

**random variable\***—A variable characterized by random behavior in assuming its different possible values. Mathematically it is described by its probability distribution, which specifies the possible values of a random variable together with the probability associated with each value.

**relative humidity\***—The dimensionless ratio of actual vapor pressure of the air to saturation vapor pressure, commonly expressed in percent.

**Richardson number\***—A nondimensional number associated with the shearing flows of a stratified fluid.  $Ri = (g/T)(\partial T/\partial z)(\partial u/\partial z)^{-2}$ .

**saline soil**—A nonalkali soil containing soluble salts in such quantities that they interfere with the growth of most plants.

**saturated air\***—Moist air in a state of equilibrium with a plane surface of pure water or ice at the same temperature and pressure, i.e., air whose vapor pressure is the saturation vapor pressure and whose relative humidity is 100%.

**saturation deficit\***—(Also called vapor pressure deficit) The difference between the actual vapor pressure and the saturation vapor pressure at the existing temperature.

**sensible heat\***—Same as enthalpy and is used in meteorology in contrast to latent heat.

**shortwave radiation**—A term used loosely to distinguish solar and diffuse sky radiation from long-wave radiation.

**soil water**—Water present in the soil pores (also called soil moisture, which would include water vapor).

**soil water tension\***—(Also called matric or capillary potential) The work that must be done per unit quantity of pure water to transport it from free water at the same elevation to soil water.

**solar constant\***—The rate at which solar radiation is received outside the earth's atmosphere on a surface normal to the incident radiation. [0.0820 MJ m<sup>-2</sup> per minute or 1.959 calories per cm<sup>2</sup> per minute ([London and Fröhlich 1982](#)); 1,367.5 W m<sup>-2</sup> = 0.08205 MJ m<sup>-2</sup> per min (*Science* 1997), 1923–1924, or 1.957 calories per cm<sup>2</sup> per minute ([Wilson 1997](#)).

**solar radiation\***—The total electromagnetic radiation emitted by the sun (see insolation).

**specific heat\***—The heat capacity of a system per unit mass.

**Stefan-Boltzmann constant**,  $\sigma = 5.673 \times 10^{-8} \text{ J m}^{-2} \text{ K}^{-4} \text{ s}^{-1}$ ;  $\sigma = 5.673 \times 10^{-8} \text{ W m}^{-2} \text{ K}^{-4}$ ;  $\sigma = 4.901 \times 10^{-9} \text{ MJ m}^{-2} \text{ K}^{-4} \text{ d}^{-1}$ .

**Stefan-Boltzmann law\***—One of the radiation laws that states that the amount of energy radiated per unit time from a unit surface area of an ideal black body is proportional to the 4th power of the absolute temperature of the black body  $R = \sigma T^4$ .

**stream depletion**—See depletion.

**surface tension\***—A phenomenon caused by a strong attraction toward the interior of the liquid action on liquid molecules in or near the surface in such a way as to reduce the surface area. The tension that results is usually expressed in N per m.

**thermal radiation\***—See long-wave radiation.

**transpiration\***—The process by which water in plants is transferred as water vapor to the atmosphere.

**triple point\***—The temperature and pressure at which a substance can exist in the liquid, solid, and gaseous state.

**triple point of water\***—The triple point of pure water is at 0.01°C and 4.56 mm Hg (0.611 kPa) and is used to calibrate thermometers.

**turbulence\***—A state of fluid flow in which instantaneous velocities exhibit irregular and apparently random fluctuations.

**vapor pressure\***—The partial pressure of water vapor in the atmosphere.

**water potential\***—The capability of soil water to do work compared with free water.

**water storage changes**—Changes in water storage include the effect of any flows of the same quality to or from soil water, groundwater aquifers, or surface reservoirs.

**water use**—Water that is used for a specific purpose such as domestic use, irrigation, or industrial processing.

**watt\***—Rate of doing work or expending power, which gives rise to the production of energy at a rate of 1 joule per second.

**wet bulb depression\***—The difference in degrees between the dry bulb temperature and the wet bulb temperature.

**wet bulb temperature\***—The temperature an air parcel would have if cooled adiabatically to saturation at constant pressure by evaporation of water into it with all latent heat being supplied by the parcel.

**withdrawal**—Water abstracted from surface- or groundwater sources for any use.

**zero plane displacement\***—An empirically determined constant introduced into the logarithmic velocity profile to extend its applicability to very rough surfaces or to take into account the displacement of a profile above a dense crop.

This page intentionally left blank

## REFERENCES

- Abatzoglou, J. T. (2013). "Development of gridded surface meteorological data for ecological applications and modeling." *Int. J. Climatol.*, 33(1), 121–131.
- Aboukhaled, A., Alfaro, A., and Smith, H. (1982). "Lysimeters." FAO, Rome.
- Adams, E. E., Cosler, D. J., and Helfrich, K. R. (1990). "Evaporation from heated water bodies: Predicting combined forced plus free convection." *Water Resour. Res.*, 26(3), 425–435.
- Allander, K. K., Smith, J. L., and Johnson, M. J. (2009). "Evapotranspiration in the lower Walker River basin, west-central Nevada, water years 2005–07." Rep. 2009-5079, U.S. Geological Survey, Carson City, NV.
- Allaway, W. G., and Milthorpe, F. L. (1976). "Structure and functioning of stomata." *Water deficits and plant growth*, T. T. Kozlowski, ed., Vol. 4, Academic Press, New York, 57–102.
- Allen, L. H., Yocom, C. S., and Lemon, E. R. (1964). "Photosynthesis under field conditions. VII. Radiant energy exchanges within a corn crop canopy and implications in water use efficiency." *Agron. J.*, 56(3), 253–259.
- Allen, R. G. (1986). "A Penman for all seasons." *J. Irrig. Drain Eng.*, 10.1061/(ASCE)0733-9437(1986)112:4(348), 348–368.
- Allen, R. G. (1992). "Evaluation of a temperature difference method for computing grass reference evapotranspiration." Water Resources Development and Management Service Land and Water Development Division, UN-FAO, Rome.
- Allen, R. G., ed. (1993). *Management of irrigation and drainage systems: Integrated perspectives*, ASCE, New York.
- Allen, R. G. (1996a). "Assessing integrity of weather data for reference evapotranspiration estimation." *J. Irrig. Drain Eng.*, 10.1061/(ASCE)0733-9437(1996)122:2(97), 97–106.
- Allen, R. G. (1996b). "Nongrowing season evaporation in northern Utah." *North American Water and Environment Congress & Destructive Water*, C. Bathala, ed., ASCE, New York, 225–230.
- Allen, R. G. (1997). "Self-calibrating method for estimating solar radiation from air temperature." *J. Hydrol. Eng.*, 10.1061/(ASCE)1084-0699(1997)2:2(56), 56–67.

- Allen, R. G. (1998). "Predicting evapotranspiration demands for wetlands." ASCE Wetlands Engineering and River Restoration Conf., Denver, CO.
- Allen, R. G. (2004). "Penman-Monteith equation." *Encyclopedia of soils in the environment*, Vol. 3, Elsevier, Oxford, 180–188.
- Allen, R. G. (2005). "Potential evaporation." *Encyclopedia of hydrological science*, Wiley, London.
- Allen, R. G. (2006). "Footprint analysis to assess the conditioning of temperature and humidity measurements in a weather station vicinity." *World environmental and water resource congress 2006: Examining the confluence of environmental and water concerns*, R. Graham, ed., ASCE, Reston, VA, 1–12.
- Allen, R. G. (2008). "Quality assessment of weather data and micrometeorological flux—Impacts on evapotranspiration calculation." *J. Agric. Meteorol.*, 64(4), 191–204.
- Allen, R. G. (2011). "Skin layer evaporation to account for small precipitation events—An enhancement to the FAO-56 evaporation model." *Agric. Water Manage.*, 99(1), 8–18.
- Allen, R. G. (2012). "REF-ET: Reference evapotranspiration calculation software for FAO and ASCE standardized equations." (<http://extension.uidaho.edu/kimberly/files/2015/06/Ref-ET-reference-evapotranspiration-calculator>), accessed Oct. 15, 2015.
- Allen, R. G. (2015). "Algorithm to conditioning weather data collected in dry settings prior to calculation of reference crop evapotranspiration." Research Rep., Univ. of Idaho, ID.
- Allen, R. G., et al. (1996). "Evaporation and transpiration." *Hydrology handbook*, 2nd Ed., ASCE, New York, 125–252.
- Allen, R. G., et al. (2000). "Issues, requirements, and challenges in selecting and specifying a standardized ET equation." Proc., 4th National Irrigation Symp., ASABE, St. Joseph, MI.
- Allen, R. G., et al. (2002b). "Evapotranspiration from a satellite-based surface energy balance for the Snake River plain aquifer in Idaho." Proc., Conf. on Irrigation and Drainage, C. M. Burt and S. S. Anderson, eds., USCID, Denver, CO, 167–178.
- Allen, R. G., et al. (2006a). "A recommendation on standardized surface resistance for hourly calculation of reference  $ET_o$  by FAO56 Penman-Monteith method." *Agric. Water Manage.*, 81, 1–22.
- Allen, R. G., et al. (2007a). "Satellite-based energy balance for mapping evapotranspiration with internalized calibration (METRIC)—Applications." *J. Irrig. Drain Eng.*, 10.1061/(ASCE)0733-9437(2007)133:4(395), 395–406.
- Allen, R. G., Bastiaanssen, W., Wright, J. L., Morse, A., Tasumi, M., and Trezza, R. (2002a). "Evapotranspiration from satellite images for water management and hydrological balances." 18th Int. Commission on Irrigation and Drainage, ICID, New Delhi, India.

- Allen, R. G., Brockway, C. E., and Wright, J. L. (1983). "Weather station siting and consumptive use estimates." *J. Water Resour. Plann. Manage.*, [10.1061/\(ASCE\)0733-9496\(1983\)109:2\(134\)](https://doi.org/10.1061/(ASCE)0733-9496(1983)109:2(134)), 134–136.
- Allen, R. G., Clemmens, A. J., Burt, C. M., Solomon, K., and O'Halloran, T. (2005a). "Prediction accuracy for projectwide evapotranspiration using crop coefficients and reference evapotranspiration." *J. Irrig. Drain Eng.*, [10.1061/\(ASCE\)0733-9437\(2005\)131:1\(24\)](https://doi.org/10.1061/(ASCE)0733-9437(2005)131:1(24)), 24–36.
- Allen, R. G., and DeBruin, H. A. R. (2008). "Estimating net outgoing long-wave radiation from vegetation in the Idaho RAPID study." Research Rep., Univ. of Idaho, ID.
- Allen, R. G., and Fisher, D. K. (1990). "Low-cost electronic weighing lysimeters." *Trans. ASAE*, [33\(6\)](https://doi.org/10.13031/2130-0544_331823), 1823–1833.
- Allen, R. G., and Gichuki, F. N. (1989). "Effects of projected CO<sub>2</sub>-induced climatic changes on irrigation water requirements in the Great Plain states (Texas, Oklahoma, Kansas, and Nebraska)." EPA-230-05-89-053, U.S. EPA, Office of Policy, Planning and Evaluation, Washington, DC.
- Allen, R. G., Howell, T. A., Pruitt, W. O., Walter, I. A., and Jensen, M. E., eds. (1991a). *Lysimeters for evapotranspiration and environmental measurements*, ASCE, New York.
- Allen, R. G., Howell, T. A., and Snyder, R. L. (2011a). "Irrigation water requirements." *Irrigation*, 6th Ed., L. E. Stetson and B. Q. Mecham, eds., Irrigation Association, Falls Church, VA, 93–172.
- Allen, R. G., Irmak, A., Trezza, R., Hendrickx, J. M. H., Bastiaanssen, W., and Kjaersgaard, J. (2011b). "Satellite-based ET estimation in agriculture using SEBAL and METRIC." *Hydrol. Processes*, [25\(26\)](https://doi.org/10.1002/hyp.24027), 4011–4027.
- Allen, R. G., Jensen, M. E., Wright, J. L., and Burman, R. D. (1989). "Operational estimates of evapotranspiration." *Agron. J.*, [81\(4\)](https://doi.org/10.2134/agronj1989.00021962008100040001x), 650–662.
- Allen, R. G., Kjaersgaard, J., Garcia, M., Tasumi, M., and Trezza, R. (2008). "Fine-tuning components of inverse-calibrated, thermal-based remote sensing models for evapotranspiration." Proc., 17th Pecora Conf. on the Future of Land Imaging, American Society for Photogrammetry and Remote Sensing, Bethesda, MD, 12–23.
- Allen, R. G., and Pereira, L. S. (2009). "Estimating crop coefficients from fraction of ground cover and height." *Irrig. Sci.*, [28\(1\)](https://doi.org/10.1007/s00485-009-9174-2), 17–34.
- Allen, R. G., Pereira, L. S., Howell, T. A., and Jensen, M. E. (2011d). "Evapotranspiration information reporting: I requirements for accuracy in measurement." *Agric. Water Manage.*, [98\(6\)](https://doi.org/10.1016/j.agwat.2011.06.011), 899–920.
- Allen, R. G., Pereira, L. S., Howell, T. A., and Jensen, M. E. (2011e). "Evapotranspiration information reporting: II recommended documentation." *Agric. Water Manage.*, [98\(6\)](https://doi.org/10.1016/j.agwat.2011.06.012), 921–929.
- Allen, R. G., Pereira, L. S., Raes, D., and Smith, M. (1998). "Crop evapotranspiration: Guidelines for computing crop water requirements." FAO-56, United Nations Food and Agriculture Organization, Rome.

- Allen, R. G., Pereira, L. S., Smith, M., Raes, D., and Wright, J. L. (2005b). "FAO-56 dual crop coefficient method for estimating evaporation from soil and application extensions." *J. Irrig. Drain Eng.*, 10.1061/(ASCE)0733-9437(2005)131:1(2), 2–13.
- Allen, R. G., and Pruitt, W. O. (1986). "Rational use of the FAO Blaney-Criddle formula." *J. Irrig. Drain Eng.*, 10.1061/(ASCE)0733-9437(1986)112:2(139), 139–155.
- Allen, R. G., and Pruitt, W. O. (1991). "FAO-24 reference evapotranspiration factors." *J. Irrig. Drain Eng.*, 10.1061/(ASCE)0733-9437(1991)117:5 (758), 758–773.
- Allen, R. G., Pruitt, W. O., and Jensen, M. E. (1991g). "Environmental requirements of lysimeters." *Lysimeters for evapotranspiration and environmental measurements*, R. G. Allen et al., eds., ASCE, New York, 170–181.
- Allen, R. G., Pruitt, W. O., Raes, D., Smith, M., and Pereira, L. S. (2005c). "Estimating evaporation from bare soil and the crop coefficient for the initial period using common soils information." *J. Irrig. Drain Eng.*, 10.1061/(ASCE)0733-9437(2005)131:1(14), 14–23.
- Allen, R. G., and Robison, C. W. (2007). "Evapotranspiration and consumptive irrigation water requirements for Idaho." Idaho Dept. Water Resources, Univ. of Idaho, Kimberly, ID.
- Allen, R. G., Smith, M., Pereira, L. S., and Perrier, A. (1994a). "An update for the calculation of reference evapotranspiration." *ICID Bull.*, 43(2), 35–92.
- Allen, R. G., Smith, M., Perrier, A., and Pereira, L. S. (1994b). "An update for the definition of reference evapotranspiration." *ICID Bull.*, 43(2), 1–34.
- Allen, R. G., and Tasumi, M. (2005). "Evaporation from American Falls Reservoir in Idaho via a combination of Bowen ratio and eddy covariance." Proc., EWRI World Water Conf. (CD-ROM), ASCE, Reston, VA.
- Allen, R. G., Tasumi, M., and Trezza, R. (2005h). "METRIC mapping evapotranspiration at high resolution." *Application manual for Landsat imagery*, Univ. of Idaho, Kimberly, ID.
- Allen, R. G., Tasumi, M., and Trezza, R. (2007b). "Satellite-based energy balance for mapping evapotranspiration with internalized calibration (METRIC)—Model." *J. Irrig. Drain. Eng.*, 10.1061/(ASCE)0733-9437(2007)133:4(380), 380–394.
- Allen, R. G., Trezza, R., and Tasumi, M. (2006b). "Analytical integrated functions for daily solar radiation on slopes." *Agric. For. Meteorol.*, 139(1–2), 55–73.
- Allen, R. G., Trezza, R., and Tasumi, M. (2006c). "Analytical integrated functions for daily solar radiation on slopes for use in energy balance and evapotranspiration studies." *Agric. For. Meteorol.*, 139(1), 55–73.

- Allen, R. G., Trezza, R., Tasumi, T., and Kjaersgaard, J. (2013). "METRIC mapping evapotranspiration at high resolution using internalized calibration applications manual for Landsat satellite imagery, Ver. 2.0.8." Univ. of Idaho, Kimberly, ID.
- Allen, R. G., Vanderkimen, P. J., and Wright, J. L. (1995). "Development of resistance parameters for operational application of the Penman-Monteith equation." Dept. of Biological and Irrigation Engineering, Utah State Univ., Logan, UT.
- Allen, R. G., and Wright, J. L. (1997). "Translating wind measurements from weather stations to agricultural crops." *J. Hydrol. Eng.*, 10.1061/(ASCE)1084-0699(1997)2:1(26), 26–35.
- Allen, R. G., and Wright, J. L. (2006). "Conversion of Wright (1981) and Wright (1982) alfalfa-based crop coefficients for use with the ASCE Standardized Penman-Monteith reference evapotranspiration equation." ([http://extension.uidaho.edu/kimberly/files/2013/Conversion\\_of\\_Wright\\_Kcs\\_2c.pdf](http://extension.uidaho.edu/kimberly/files/2013/Conversion_of_Wright_Kcs_2c.pdf)).
- Allen, R. G., Wright, J. L., Pruitt, W. O., Pereira, L. S., and Jensen, M. E. (2007i). "Water requirements." *Design and operation of farm irrigation systems*, G. J. Hoffman, R. G. Evans, and M. E. Jensen, eds., American Society of Agricultural and Biological Engineers, St. Joseph, MI, 208–288.
- Altenhofen, J. (1985). "A modified atmometer for on-farm evapotranspiration determination." Proc., National Conf. Advances in Evapotranspiration, ASAE, St. Joseph, MI, 177–184.
- Aluwihare, S., and Watanabe, K. (2003). "Measurement of evaporation on bare soil and estimating surface resistance." *J. Environ. Eng.*, 10.1061/(ASCE)0733-9372(2003)129:12(1157), 1157–1168.
- Amatya, D. M., Skaggs, R. W., Cheschier, G. M., and Fernandez, G. P. (2000). "Solar and net radiation for estimating potential evaporation from three vegetation canopies." 2000 ASABE Annual Int. Meeting, ASABE, St. Joseph, MI, 1–20.
- Amayreh, J. A. (1995). "Lake evaporation: A model study." Ph.D. thesis, Utah State Univ., Logan, UT.
- American Meteorological Society. (2015). Meteorology Glossary. ([http://glossary.ametsoc.org/wiki/Main\\_Page](http://glossary.ametsoc.org/wiki/Main_Page)), accessed Oct. 15, 2015.
- Anderson, E. R. (1954). "Energy-budget studies." Technical Rep., ASCE, Reston, VA, 71–119.
- Anderson, M. C., Allen, R. G., Morse, A., and Kustas, W. P. (2012). "Use of Landsat thermal imagery in monitoring evapotranspiration and managing water resources." *Remote Sens. Environ.*, 122(1), 50–65.
- Anderson, M. C., Hain, C., Wardlow, B., Pimstein, A., Mecikalski, J. R., and Kustas, W. P. (2011). "Evaluation of drought indices based on thermal remote sensing of evapotranspiration over the continental United States." *J. Clim.*, 24(8), 2025–2044.

- Anderson, M. C., Norman, J. M., Diak, G. R., Kustas, W. P., and Mecikalski, J. R. (1997). "A time-integrated model for estimating surface fluxes using thermal infrared remote sensing." *Remote Sens. Environ.*, **60**, 195–216.
- Anderson, M. C., Norman, J. M., Kustas, W. P., Li, F., Prueger, J. H., and Mecikalski, J. R. (2005). "Effects of vegetation clumping on two-source model estimates of surface energy fluxes from an agricultural landscape during SMACEX." *J. Hydrometeorol.*, **6**(6), 892–909.
- Angus, D. E., and Watts, P. J. (1984). "Evapotranspiration—How good is the Bowen ratio method?" *Agric. Water Manage.*, **8**, 133–150.
- Arkin, G. F., and Taylor, H. M., eds. (1981). "Modifying the root environment to reduce crop stress." Monograph No. 4, ASAE, St. Joseph, MI.
- Armijo, J. D., Twitchell, G. A., Burman, R. D., and Nunn, J. R. (1972). "A large undisturbed weighing lysimeter for grassland studies." *Trans. ASAE*, **15**(5), 827–830.
- Aronson, L. J., Gold, A., and Hull, R. J. (1987). "Cool-season turfgrass responses to drought stress." *Crop Sci.*, **27**(6), 1261–1266.
- ASABE. (2004). "Measurement and reporting practices for automatic agricultural weather stations." St. Joseph, MI.
- ASAE (American Society of Agricultural Engineers). (1985). "Advances in evapotranspiration." Proc. National Conf. on Advances in Evapotranspiration, St. Joseph, MI, 462.
- ASCE. (1930). "Consumptive use of water in irrigation." *Trans. ASCE*, **94**(9), 1349–1399.
- ASCE. (1949). "Evaporation and transpiration." Chapter 4, *Hydrology handbook*, Reston, VA.
- ASCE. (2005). "The ASCE standardized reference evapotranspiration equation." Task Committee on Standardization of Reference Evapotranspiration, EWRI, Reston, VA.
- ASTM. (1976). "Standards for metric practice." ANSI/ASTM E380-76, West Conshohocken, PA.
- Aubert, E. J., and Richards, T. L. (1981). "IFYGL: The international field year for the great lakes." Great Lakes Environmental Research Laboratory, Ann Arbor, MI.
- Aubinet, M., et al. (2000). "Estimates of the annual net carbon and water exchange of forests: The EUROFLUX methodology." *Adv. Ecol. Res.*, **30**(1), 113–175.
- Ayars, J. E., Johnson, R. S., Phene, C. J., Trout, T. J., Clark, D. A., and Mead, R. M. (2003). "Water use by drip-irrigated late-season peaches." *Irrig. Sci.*, **22**(3–4), 187–194.
- Ayers, R. S., and Westcot, D. W. (1985). "Water quality for agriculture." United Nations Food and Agriculture Organization, Rome.
- Bailey, B. J., Montero, J. I., Biel, C., Wilkinson, D. J., Anton, A., and Jolliet, O. (1993). "Transpiration of *Ficus benjamina*: Comparison of measurements

- with predictions of the Penman-Monteith model and a simplified version." *Agric. For. Meteorol.*, 65(3), 229–243.
- Baldocchi, D. D. (2003). "Assessing the eddy covariance technique for evaluating carbon dioxide exchange rates of ecosystems: Past, present and future." *Global Change Biol.*, 9(4), 479–492.
- Baldocchi, D. D., Hicks, B. B., and Meyers, T. P. (1988). "Measuring biosphere-atmosphere exchanges of biologically related gases with micrometeorological methods." *Ecology*, 69(5), 1331–1340.
- Ball, R. A., Purcell, L. C., and Casey, S. K. (2004). "Evaluation of solar radiation prediction models in North America." *Agron. J.*, 96(2), 391–397.
- Bastiaanssen, W. G. M., Menenti, M., Feddes, R. A., and Holtslag, A. A. M. (1998a). "The surface energy balance algorithm for land (SEBAL): Part 1 formulation." *J. Hydrol.*, 212–213(1), 198–212.
- Bastiaanssen, W. G. M., Noordman, E. J. M., Pelgrum, H., Davids, G., Thoreson, B. P., and Allen, R. G. (2005). "SEBAL model with remotely sensed data to improve water-resources management under actual field conditions." *J. Irrig. Drain. Eng.*, 10.1061/(ASCE)0733-9437(2005)131:1(85), 85–93.
- Bastiaanssen, W. G. M., Pelgrum, H., Wang, J., Ma, Y., Moreno, J., Roerink, G. J., and van der Wal, T. (1998b). "The surface energy balance algorithm for land (SEBAL): Part 2 validation." *J. Hydrol.*, 212–213(1), 213–229.
- Batchelor, J. F. (1984). "The accuracy of evapotranspiration estimated with the modified Penman equation." *Irrig. Sci.*, 5, 223–233.
- Bausch, W. C., and Neale, C. M. U. (1987). "Crop coefficients derived from reflected canopy radiation: A concept." *Trans. ASABE*, 30(3), 703–709.
- Ben-Mehrez, M., Taconet, O., Vidal-Madjar, D., and Valencogne, C. (1992). "Estimation of stomatal resistance and canopy evaporation during the HAPEX-MOBILHY experiment." *Agric. For. Meteorol.*, 58(3), 285–313.
- Bernacchi, C. J., et al. (2003). "Photosynthesis and stomatal conductance responses of poplars to free-air CO<sub>2</sub> enrichment (POPFACE) during the first growth cycle and immediately following coppice." *New Phytol.*, 159 (3), 609–621.
- Bernacchi, C. J., Kimball, B. A., Quarles, D. R., Long, S. P., and Ort, D. R. (2006). "Decreases in stomatal conductance of soybean under open-air elevation of [CO<sub>2</sub>] are closely coupled with decreases in ecosystem evapotranspiration." *Plant Physiol.*, 143(1), 134–144.
- Bernard, E. A. (1954). "Sur diverses consequences de la methode du bilan d'énergie pour l'evapotranspiration des cultures ou des couvertures vegetales naturelles." *Ass. Int. d'Hydrologie Sci. Rome-Assembly*, 8(161), 2.
- Bertuzzi, P., Bruckler, L., Bay, D., and Chanzy, A. (1994). "Sampling strategies for soil water content to estimate evapotranspiration." *Irrig. Sci.*, 14(3), 105–115.
- Black, J. N., Bonython, C. W., and Prescott, J. A. (1954). "Solar radiation and duration of sunshine." *Q. J. R. Meteorolog. Soc.*, 80(344), 231–235.

- Black, T. A., Gardner, W. R., and Thurtell, G. W. (1969). "The prediction of evaporation, drainage, and soil water storage for a bare soil." *Soil Sci. Soc. Am. J.*, 33(5), 655–660.
- Black, T. A., Thurtell, G. W., and Tanner, C. B. (1968). "Hydraulic load cell lysimeter, construction, calibration, and tests." *Soil Sci. Soc. Am. J.*, 32(5), 623–629.
- Blaney, H. F., et al. (1938). "Field methods of determining consumptive use of water." Proc., 4th National Congress Cuban Engineering, Association of Cuban Engineers, Havana, Cuba.
- Blaney, H. F. (1952). "Consumptive use of water: A Symposium: Definition, methods, and research data." *Trans. ASCE*, 117(1), 948–967.
- Blaney, H. F., and Criddle, W. D. (1945a). "Consumptive use of water in the irrigated areas of the upper Colorado River basin." Research Rep., U.S. Dept. of Agriculture Soil Conservation Service, Mimeo, Washington, DC.
- Blaney, H. F., and Criddle, W. D. (1945b). "Determining water requirements in irrigated areas from climatological and irrigation data." Research Rep., U.S. Dept. of Agriculture Soil Conservation Service, Mimeo, Washington, DC.
- Blaney, H. F., and Criddle, W. D. (1950). "Determining water requirements in irrigated areas from climatological and irrigation data." SCS-TP-96, USDA, Washington, DC.
- Blaney, H. F., and Criddle, W. D. (1962). "Determining consumptive use and irrigation water requirements." Technical Bull. 1275, USDA, Washington, DC.
- Blaney, H. F., and Morin, K. V. (1942). "Evaporation and consumptive use of water formulas." *Am. Geophys. Union Trans.*, 23(1), 76–82.
- Blaney, H. F., and Muckel, D. C. (1959). "Evaporation from water surfaces in California." Bull. 73, California Dept. of Water Resources, Sacramento, CA.
- Blanken, P. D., and Black, T. A. (2004). "The canopy conductance of a boreal aspen forest, Prince Albert National Park, Canada." *Hydro. Processes*, 18(9), 1561–1578.
- Boegha, E., Soegaarda, H., and Thomsen, A. (2000). "Evaluating evapotranspiration rates and surface conditions using Landsat TM to estimate atmospheric resistance and surface resistance." *Remote Sens. Environ.*, 79 (2–3), 329–343.
- Bolsenga, S. J., and Vanderploeg, H. A. (1992). "Estimating photosynthetically available radiation into open and ice-covered freshwater lakes from surface characteristics; a high transmittance case study." *Hydrobiologia*, 243(1), 95–104.
- Boman, B. J. (1991). "Alfalfa ET measurements with drainage lysimeters." *Lysimeters for evapotranspiration and environmental measurements*, R. G. Allen, T. A. Howell, W. O. Pruitt, I. A. Walter, and M. E. Jensen, eds., ASCE, New York, 264–271.

- Bonachela, S., Orgaz, F., Villalobos, F. J., and Fereres, E. (1999). "Measurement and simulation of evaporation from soil in olive orchards." *Irrig. Sci.*, 18(4), 205–211.
- Bonachela, S., Orgaz, F., Villalobos, F. J., and Fereres, E. (2001). "Soil evaporation from drip-irrigated olive orchards." *Irrig. Sci.*, 20(2), 65–71.
- Bond, J. J., and Willis, W. O. (1970). "Soil water evaporation: First stage drying as influenced by surface residue and evaporation potential." *Soil Sci. Soc. Am. Proc.*, 34(6), 924–928.
- Boote, K. J., and Loomis, R. S., eds. (1991). "Modeling crop photosynthesis —From biochemistry to canopy." Proc., 1988 Symp. Crop Science Society of America and American Society of Agronomy, Crop Science Society of America, Madison, WI, 140.
- Borg, H., and Grimes, D. W. (1986). "Depth development of roots with time: An empirical description." *Trans. ASAE*, 29(1), 194–197.
- Borrelli, J., Fedler, C. B., and Gregory, J. M. (1998). "Mean crop consumptive use and free-water evaporation for Texas." Dept. of Civil Engineering, Texas Tech Univ., Lubbock, TX.
- Bosveld, F. C., and Bouter, W. (2001). "Evaluation of transpiration models with observations over a Douglas-fir forest." *Agric. Forest Meteorol.*, 108(4), 247–264.
- Bouchet, R. J. (1963). "Evapotranspiration réelle et potentielle, signification climatique." General Assembly Berkeley, International Association of Science Hydrology, Gentbrugge, Belgium, 134–142.
- Bowen, I. S. (1926). "The ratio of heat losses by conduction and by evaporation from any water surface." *Phys. Rev.*, 27(6), 779–787.
- Brenner, A. J., and Incoll, L. D. (1997). "The effect of clumping and stomatal response on evaporation from sparsely vegetated shrublands." *Agric. For. Meteorol.*, 84(3–4), 187–205.
- Breuer, L., Eckhardt, K., and Frede, H. G. (2003). "Plant parameter values for models in temperate climates." *Ecol. Modell.*, 169(2–3), 237–293.
- Briggs, L. J., and Shantz, H. L. (1916). "Hourly transpiration rate on clear days as determined by cyclic environmental factors." *J. Agric. Res.*, 5(14), 583–648.
- Brisson, N. (1998). "An analytical solution for the estimation of the critical available soil water fraction for a single layer water balance model under growing crops." *Hydrol. Earth Syst. Sci.*, 2(2–3), 221–231.
- Brisson, N., Itier, B., L'Hotel, J. C., and Lorendeau, J. V. (1998). "Parameterisation of the Shuttleworth-Wallace model to estimate daily maximum transpiration for use in crop models." *Ecol. Modell.*, 107(2–3), 159–169.
- Bristow, K. L., and Campbell, G. S. (1984). "On the relationship between incoming solar radiation and daily maximum and minimum temperature." *Agric. For. Meteorol.*, 31(2), 159–166.

- Brochet, P., and Gerbier, N. (1972). "Une méthode pratique de calcul de l'évapotranspiration potentielle." *Ann. Agron.*, 23(1), 31–49.
- Broner, I. (1993). "Irrigation scheduling with atmometers." Colorado State Univ., Fort Collins, CO.
- Broner, I., and Law, R. A. P. (1991). "Evaluation of a modified atmometer for estimating reference ET." *Irrig. Sci.*, 12(1), 21–26.
- Brooks, R. H., and Corey, A. T. (1966). "Properties of porous media affecting fluid flow." *J. Irrig. Drain. Div.*, 92(2), 61–90.
- Brown, K. W., and Rosenberg, N. J. (1971). "Turbulent transport and energy balance as affected by a windbreak in an irrigated sugar beet (*Beta vulgaris*) field." *Agron. J.*, 63(3), 351–355.
- Brown, P. W., Kopec, D., and Mancino, C. (1988). "Estimating turfgrass water use with AZMET." *Turfgrass and ornamentals research summary*, Arizona Agricultural Experiment Station, Tucson, AZ, 25–33.
- Brown, P. W., Mancino, C. F., Young, M. H., Thompson, T. L., Wierenga, P. J., and Kopec, D. M. (2001). "Penman Monteith crop coefficients for use with desert turf systems." *Crop Sci.*, 41(4), 1197–1206.
- Brunt, D. (1932). "Notes on radiation in the atmosphere: I." *Q. J. R. Meteorolog. Soc.*, 58(247), 389–420.
- Brunt, D. (1952). *Physical and dynamical meteorology*, 2nd Ed., Cambridge University Press, Cambridge, U.K.
- Brutsaert, W. (1975). "The roughness length for water vapor, sensible heat and other scalars." *J. Atom. Sci.*, 32(10), 2028–2031.
- Brutsaert, W. (1982). *Evaporation into the atmosphere*, D. Reidel, Dordrecht, Netherlands.
- Brutsaert, W., and Stricker, H. (1979). "An advection-aridity approach to estimate actual regional evapotranspiration." *Water Resour. Res.*, 15(2), 443–450.
- Buck, A. (1976). "The variable path Lyman-alpha hygrometer and its operating characteristics." *Bull. Am. Meteorol. Soc.*, 57(9), 1113–1118.
- Budyko, M. I. (1948). "Evaporation under natural conditions." U.S. Dept. of Commerce, Israel Program Science Translation, Washington DC, 751.
- Budyko, M. I. (1956). "The heat balance of the Earth's surface." Weather Bureau PB 131692, U.S. Dept. of Commerce, Washington, DC.
- Burba, G., and Anderson, D. (2008). "Introduction to the eddy covariance method: General guidelines and conventional workflow." ([www.licor.com/env/PDF\\_Files/EddyCovariance\\_READONLY.pdf](http://www.licor.com/env/PDF_Files/EddyCovariance_READONLY.pdf)) (Dec. 26, 2010).
- Burman, R. D., Cuenca, R. H., and Weiss, A. (1983). "Techniques for estimating irrigation requirements." *Advances in irrigation*, D. Hillel, ed., Vol. 2, Academic Press, New York, 335–394.
- Burman, R. D., Jensen, M. E., and Allen, R. G. (1987). "Thermodynamic factors in evapotranspiration." *Irrigation Systems for the 21st century*, L. G. James and M. J. English, eds., ASCE, New York, 140–148.

- Burman, R. D., Nixon, P. R., Wright, J. L., and Pruitt, W. O. (1980). "Water requirements." *Design and operation of farm irrigation systems*, M. E. Jensen, ed., ASAE, St. Joseph, MI, 189–232.
- Burman, R. D., Wright, J. L., and Jensen, M. E. (1975). "Changes in climate and estimated evaporation across a large irrigated area in Idaho." *Trans. Am. Soc. Agric. Eng.*, 18(6), 1089–1093.
- Burnett, B., Allen, R. G., Robison, C. W., Tasumi, M., and Lorite, I. (2008). "Estimating the soil surface evaporation and transpiration components from satellite images in the absence of a thermal band." *World environmental and water resources congress 2008: Ahupua'A*, ASCE, Reston, VA, 1–18.
- Burrows, F. J., and Milthorpe, F. L. (1976). "Stomatal conductance in the control of gas exchange." *Water deficits and plant growth*, T. T. Kozlowski, ed., Vol. 4, Academic Press, New York, 103–152.
- Burt, C. M., Mutziger, A. J., Howes, D. J., and Solomon, K. H. (2005). "Evaporation from irrigated agricultural land in California." Rep. No. 02-001, Irrigation Research Training Center, San Luis Obispo, CA.
- Businger, J. A. (1966). "Transfer of heat and momentum in the atmospheric boundary layer." Proc., Arctic Heat Budget and Atmospheric Circulation, RAND, Santa Monica, CA, 305–332.
- Businger, J. A., Miyake, M., Dyer, A. J., and Bradley, E. F. (1967). "On direct determination of turbulent heat flux near the ground." *J. Appl. Meteorol.*, 6(6), 1025–1032.
- Businger, J. A., and Yaglom, A. M. (1971). "Introduction to Obukhov's paper on 'Turbulence in an atmosphere with a non-uniform temperature.'" *Boundary Layer Meteorol.*, 2(1), 3–6.
- Cahill, A. T., and Parlange, M. B. (1998). "On water vapor transport in field soils." *Water Resour. Res.*, 34(4), 731–739.
- Cahill, A. T., and Parlange, M. B. (2000). "Reply to 'On water vapor transport in field soils.'" *Water Resour. Res.*, 36(10), 3107–3110.
- Calera-Belmonte, A., Jochum, A. M., Cuesta-Garcia, A., Montoro-Rodriguez, A., and Lopez-Fuster, P. (2005). "Irrigation management from space: Towards user-friendly products." *Irrig. Drain. Syst.*, 19(3), 337–353.
- Calvet, J. C., Noilhan, J., and Besseouulin, P. (1998). "Retrieving the root zone soil moisture from surface soil moisture or temperature estimates: A feasibility study on field measurements." *J. Appl. Meteorol.*, 37(4), 371–386.
- Cammalleri, M., Anderson, M. C., Gao, F., Hain, C. R., and Kustas, W. P. (2013). "A data fusion approach for mapping daily evapotranspiration at field scale." *Water Resour. Res.*, 49(8), 1–15.
- Camp, C. R., Sadler, E. J., and Yoder, R. E., eds. (1996). "Evapotranspiration and irrigation scheduling." ASAE, St. Joseph, MI.

- Campbell, G. S., and Campbell, M. D. (1982). "Irrigation scheduling using soil moisture." *Advances in irrigation*, D. Hillel, ed., Academic Press, New York, 25–42.
- Campbell, G. S., and Norman, J. M. (1998). *An introduction to environmental biophysics*, Springer, Berlin.
- Campbell, G. S., and Tanner, B. D. (1985). "A krypton hygrometer for measurement of atmospheric water vapor concentration." *Moisture and humidity*, ISA, Research Triangle Park, NC, 609–612.
- Campbell Scientific. (2003). "HFT3 soil heat flux plate." *Instruction manual*, Logan, UT.
- Carlson, T. N., and Ripley, D. A. (1997). "On the relation between NDVI, fractional vegetation cover, and leaf area index." *Remote Sens. Environ.*, 62(3), 241–252.
- Carpenter, L. G. (1898). "The loss of water from reservoirs by seepage and evaporation." Bull. No. 45, Colorado State Agricultural College, Arizona Agricultural Experiment Station, Fort Collins, CO.
- Carrow, R. N. (1995). "Drought resistance aspects of turfgrasses in the Southeast: Evapotranspiration and crop coefficients." *Crop Sci.*, 35(6), 1685–1690.
- Carrow, R. N. (1996). "Drought resistance aspects of turfgrasses in the southeast: Root-shoot responses." *Crop Sci.*, 36(3), 687–694.
- Carrow, R. N. (2004). "Can we maintain turf to 'customers' satisfaction with less water?" Proc., 4th Int. Crop Science Congress (CD-ROM), International Crop Science Society, Gosford, NSW, Australia.
- Ceglar, A., Črepinský, Z., Kajfež-Bogataj, L., and Pogačar, T. (2011). "The simulation of phenological development in dynamic crop model: The Bayesian comparison of different methods." *Agric. For. Meteorol.*, 151(1), 101–115.
- Cellier, P. (1986). "On the validity of flux-gradient relationships above very rough surfaces." *Boundary Layer Meteorol.*, 36(4), 417–419.
- Cellier, P., and Brunet, Y. (1992). "Flux-gradient relationships above tall plant canopies." *Agric. For. Meteorol.*, 58(1), 93–117.
- Cesaraccio, C., Spano, D., Duce, P., and Snyder, R. L. (2001). "An improved model for degree-days from temperature data." *Int. J. Biometeorol.*, 45(4), 161–169.
- Chanzy, A., and Bruckler, L. (1993). "Significance of soil surface moisture with respect to daily bare soil evaporation." *Water Resour. Res.*, 29(4), 1113–1125.
- Charnock, H. (1955). "Wind stress on a water surface." *Q. J. R. Meteorolog. Soc.*, 81(350), 6.
- Chen, F., and Dudhia, J. (2001). "Coupling an advanced land surface-hydrology model with the Penn State-NCAR MM5 Modeling System. Part I: Model implementation and sensitivity." *Mon. Weather Rev.*, 129(4), 569–585.

- Choudhury, B. J. (1983). "Simulating the effects of weather variables and soil water potential on a corn canopy temperature." *Agric. Meteorol.*, 29(3), 169–182.
- Choudhury, B. J. (1989). "Estimating evaporation and carbon assimilation using infrared temperature data: Vistas in modeling." *Theory and applications of optical remote sensing*, A. Ghassem, ed., Wiley, New York, 628–690.
- Choudhury, B. J., Ahmed, N. U., Idaho, S. B., Reginato, R. J., and Daughtry, C. S. T. (1994). "Relations between evaporation coefficients and vegetation indices: Studies by model simulation." *Remote Sens. Environ.*, 50(1), 1–17.
- Choudhury, B. J., and Idso, S. B. (1985). "Evaluating plant and canopy resistances of field-grown wheat from concurrent diurnal observations of leaf water potential, stomatal resistance, canopy temperature, and evapotranspiration flux." *Agric. For. Meteorol.*, 34(1), 67–76.
- Choudhury, B. J., Idso, S. B., and Reginato, R. J. (1987). "Analysis of an empirical model for soil heat flux under a growing wheat crop for estimating evaporation by an infrared temperature based energy balance equation." *Agric. For. Meteorol.*, 39(4), 283–297.
- Choudhury, B. J., and Monteith, J. L. (1986). "Implications of stomatal response to saturation deficit for the heat balance of vegetation." *Agric. For. Meteorol.*, 36(3), 215–225.
- Choudhury, B. J., and Monteith, J. L. (1988). "A four-layer model for the heat budget of homogeneous land surfaces." *Q. J. R. Meteorolog. Soc.*, 114 (480), 373–398.
- Chow, V., Maidment, D., and Mays, L. (1988). *Applied hydrology*, 2nd Ed., McGraw-Hill, New York.
- Christiansen, J. E. (1968). "Pan evaporation and evapotranspiration from climatic data." *J. Irrig. Drain. Div.*, 94(2), 243–266.
- Christiansen, J. E., and Hargreaves, G. H. (1969). "Irrigation requirements from evaporation." *Trans. Int. Comm. Irrig. Drain.*, 3(23), 569–23.
- Císlér, J. (1969). "The solution for maximum velocity of isothermal steady flow of water upward from water table to soil surface." *Soil Sci.*, 108(2), 148.
- Clemmens, A. J., Dedrick, A. R., and Strand, R. J. (1995). "BASIN: A computer program for the design of level-basin irrigation systems." WCL Rep. No. 19, U.S. Water Conservation Laboratory, USDA/ARS, Phoenix, AZ.
- Clemmens, A. J., Walker, W. R., Fangmeier, D. D., and Hardy, L. A. (2007). "Design of surface systems." *Design and operation of farm irrigation systems*, G. J. Hoffman, R. G. Evans, and M. E. Jensen, eds., American Society of Agricultural and Biological Engineers, St Joseph, MI, 499–531.

- Coats, R. N., Perez-Losada, J., Schladow, G., Richards, R., and Goldman, C. (2006). "The warming of Lake Tahoe." *Clim. Change*, 76(1–2), 121–148.
- Cogley, J. G. (1979). "The albedo of water as a function of latitude." *Mon. Weather Rev.*, 107(6), 775–781.
- Collatz, C. J., Ball, J. T., Grivet, C., and Berry, J. A. (1991). "Physiological and environmental regulation of stomatal conductance, photosynthesis and transpiration: A model that includes a laminar boundary layer." *Agric. For. Meteorol.*, 54(2), 107–136.
- Corwin, D. L., Waggoner, B. L., and Rhoades, J. D. (1991). "A functional model of solute transport that accounts for bypass." *J. Environ. Qual.*, 20(3), 647–658.
- Costello, L. R., and Jones, K. S. (1999). "A guide to estimating irrigation water needs of landscape plantings in California." Univ. of California Extension, Berkeley, CA, 45–144.
- Costello, L. R., Matheny, N. P., and Clark, J. R. (2000). "Estimating the irrigation water needs of landscape plantings in California: Part 1: The landscape coefficient method." California Dept. of Water Resources, Univ. of California Cooperative Extension, Sacramento, CA.
- Cowan, I. R., and Milthorpe, F. L. (1968). "Plant factors influencing the water status of plant tissues." *Water deficits and plant growth*, T. T. Kozlowski, ed., Vol. 1, Academic Press, New York, 137–193.
- Crank, J. (1956). *The mathematics of diffusion*, Oxford Press, London.
- Croley, T. E., II. (1989). "Verifiable evaporation modeling on Laurentian Great Lakes." *Water Resour. Res.*, 25(5), 781–792.
- Croley, T. E., Quinn, F. H., Kunkel, K. E., and Changnon, S. A. (1996). "Climate transposition effects on the Great Lakes hydrologic cycle." NOAA Technical Memo. ERIGLERL-89, NOAA, Ann Arbor, MI.
- Cuenca, R. H., and Nicholson, M. T. (1982). "Application of Penman equation wind function." *J. Irrig. Drain. Div.*, 108(1), 13–23.
- Cuenca, R. H., Nuss, J. L., Martinez-Cob, A., Katul, G. G., and Gonzalez, J. M. (1992). "Oregon crop water use and irrigation requirements." Oregon State Univ., Corvallis, OR, 189.
- Cummings, N. W., and Richardson, B. (1927). "Evaporation from lakes." *Phys. Rev.*, 30(4), 527–534.
- Daamen, C. C. (1997). "Two source model of surface fluxes for millet fields in Niger." *Agric. For. Meteorol.*, 83(3–4), 205–230.
- Daamen, C. C., Dugas, W. A., Prendergast, P. T., Judd, M. J., and McNaughton, K. G. (1999). "Energy flux measurements in a sheltered lemon orchard." *Agric. For. Meteorol.*, 93(3), 171–183.
- Daamen, C. C., and McNaughton, K. G. (2000). "Modeling energy fluxes from sparse canopies and understoreys." *Agron. J.*, 92(5), 837–847.
- Daamen, C. C., Simmonds, L. P., Wallace, J. S., Laryea, K. B., and Sivakumar, M. V. K. (1993). "Use of microlysimeters to measure evaporation from sandy soils." *Agric. For. Meteorol.*, 65(3), 159–173.

- Dai, Y., Dickinson, R. E., and Wang, Y.-P. (2004). "A two-big-leaf model for canopy temperature, photosynthesis, and stomatal conductance." *J. Climate*, 17(12), 2281–2299.
- Dalton, J. (1802). "Experimental essays on the constitution of mixed gasses; on the force of steam or vapour from water and other liquids in different temperatures, both in Torricellian vacuum and in air; on evaporation; and on the expansion of gasses by heat." *Memoirs, Manchester Literary and Philosophical Society*, U.K. Vol. 5, 535–602.
- Daly, C., et al. (2008). "Physiographically sensitive mapping of climatological temperature and precipitation across the conterminous United States." *Int. J. Climatol.*, 28(15), 2031–2064.
- Daly, C., and Bryant, K. (2013). "The PRISM climate and weather system—An introduction." ([www.prism.oregonstate.edu/documents/PRISM\\_history\\_jun2013.pdf](http://www.prism.oregonstate.edu/documents/PRISM_history_jun2013.pdf)), accessed Oct. 15, 2015.
- Dastane, N. G. (1974). "Effective rainfall in irrigated agriculture." United Nations Food and Agriculture Organization, Rome.
- Davies, J. A., and Idso, S. B. (1979). "Estimating surface radiation balance and its components." *Modification of the aerial environment of plants*, B. J. Barfield and J. F. Gerbes, eds., ASABE, St. Joseph, MI, 183–210.
- de Azevedo, P. V., da Silva, B. B., and da Silva, V. P. (2003). "Water requirements of irrigated mango orchards in northeast Brazil." *Agric. Water Manage.*, 58(3), 241–254.
- de Bruin, H. A. R. (1982). "Temperature and energy balance of a water reservoir determined from weather data of a land station." *J. Hydrol.*, 59(3), 261–274.
- de Bruin, H. A. R., Hartogensis, O. K., Allen, R. G., and Kramer, J. W. J. L. (2005). "Note on the regional advection perturbations in an irrigated desert (RAPID) experiment." *Theor. Appl. Climatol.*, 80(2–4), 143–152.
- de Bruin, H. A. R., and Jacobs, C. M. J. (1993). "Impact of CO<sub>2</sub> enrichment on the regional evapotranspiration of agro-ecosystems, a theoretical and numerical modeling study." *Vegetation*, 104–105(1), 307–318.
- de Bruin, H. A. R., and Moore, C. J. (1985). "Zero-plane displacement and roughness length for tall vegetation, derived from a simple mass conservation hypothesis." *Boundary Layer Meteorol.*, 31(1), 39–49.
- de Medeiros, G. A., Arruda, F. B., Sakai, E., and Fujiwara, M. (2001). "The influence of crop canopy on evapotranspiration and crop coefficient of beans (*Phaseolus vulgaris* L.)." *Agric. Water Manage.*, 49(3), 211–224.
- de Vries, D. A. (1963). "Thermal properties of soils." *Physics of plant environment*, W. R. van Wijk, ed., North Holland, Amsterdam, 210–235.
- Dekker, S. C., Bouten, W., and Verstraten, J. M. (2000). "Modeling forest transpiration from different perspectives." *Hydrol. Processes*, 14(2), 251–260.

- Denmead, O. T. (1984). "Plant physiological methods for studying evapotranspiration: Problems of telling the forest from the trees." *Agric. Water Manage.*, 8(1), 167–189.
- Denmead, O. T., and Bradley, E. F. (1985). "Flux-gradient relationships in a forest canopy." *The forest-atmosphere interaction*, B. A. Hutchison and B. B. Hicks, eds., D. Reidel, Netherlands, 421–442.
- Derecki, J. A. (1976). "Multiple estimates of Lake Erie evaporation." *J. Great Lakes Res.*, 2(1), 124–149.
- Descheemaeker, K., et al. (2011). "Two rapid appraisals of FAO-56 crop coefficients for semiarid natural vegetation of the northern Ethiopian highlands." *J. Arid Environ.*, 75(4), 353–359.
- DeTar, W. R. (2004). "Using a subsurface drip irrigation system to measure crop water use." *Irrig. Sci.*, 23(3), 111–122.
- Devitt, D. A., Sala, A., Smith, S. D., Cleverly, J., Shaulis, L. K., and Hammett, R. (1998). "Bowen ratio estimates of evapotranspiration for *Tamarix ramosissima* stands on the Virgin River in southern Nevada." *Water Resour. Res.*, 34(9), 2407–2414.
- Dickinson, R. E. (1984). "Modeling evapotranspiration for three-dimensional global climate models." *Climate processes and climate sensitivity*, J. E. Hansen and T. Takahashi, eds., Wiley, Washington, DC, 58–72.
- Dickinson, R. E., Henderson-Sellers, A., Rosenzweig, C., and Sellers, P. J. (1991). "Evapotranspiration models with canopy resistance for use in climate models, a review." *Agric. For. Meteorol.*, 54(2-4), 373–388.
- Dingman, S. L. (2008). *Physical hydrology*, 2nd Ed., Waveland Press, Long Grove, IL.
- Dolman, A. J. (1993). "A multiple-source land surface energy balance model for use in general circulation models." *Agric. For. Meteorol.*, 65 (1-2), 21–45.
- Domingo, F., Villagarcía, L., Brenner, A. J., and Puigdefábregas, J. (1999). "Evapotranspiration model for semi-arid shrub-lands tested against data from SE Spain." *Agric. For. Meteorol.*, 95(2), 67–84.
- Donelan, M. R., Elder, F. C., and Hamblin, P. F. (1974). "Determination of the aerodynamic drag coefficient from wind set-up (IFYGL)." Proc., 17th Int. Conf. on Association for Great Lakes Research, Ann Arbor, MI, 778–788.
- Dong, A., Grattan, S. R., Carroll, J. J., and Prashar, C. R. K. (1992). "Estimation of net radiation over well-watered grass." *J. Irrig. Drain. Eng.*, 10.1061/(ASCE)0733-9437(1992)118:3(466), 466–479.
- Doorenbos, J., and Kassam, A. H. (1979). *Yield response to water*, 2nd Ed., FAO-33, Food and Agriculture Organization, Rome.
- Doorenbos, J., and Pruitt, W. O. (1975). "Guidelines for prediction of crop water requirements." FAO-24, Food and Agriculture Organization, Rome.
- Doorenbos, J., and Pruitt, W. O. (1977). "Guidelines for predicting crop water requirements." FAO-24, Food and Agriculture Organization, Rome.

- Dorman, J. L., and Sellers, P. J. (1989). "A global climatology of albedo, roughness length and stomatal resistance for atmospheric general circulation models as represented by the simple biosphere model (SIB)." *J. Appl. Meteorol.*, 28(9), 833–855.
- Dozier, J., and Frew, J. (1990). "Rapid calculation of terrain parameters for radiation modeling from digital elevation data." *IEEE Trans. Geosci. Remote Sens.*, 28(5), 963–969.
- Droogers, P., and Allen, R. G. (2002). "Estimating reference evapotranspiration under inaccurate data conditions." *Irrig. Drain. Syst.*, 16(1), 33–45.
- Droogers, P., and Kite, G. (1999). "Water productivity from integrated basin modeling." *Irrig. Drain. Syst.*, 13(3), 249–273.
- Duchemin, B., et al. (2006). "Monitoring wheat phenology and irrigation in central Morocco: On the use of relationships between evapotranspiration, crop coefficients, leaf area index, and remotely-sensed vegetation indices." *Agric. Water Manage.*, 79(1), 1–27.
- Duffie, J. A., and Beckman, W. A. (1991). *Solar engineering of thermal processes*, Wiley, New York.
- Dugas, W. A., and Bland, W. L. (1991). "Springtime soil temperatures in lysimeters in Central Texas." *Soil Sci.*, 152(2), 87–91.
- Dugas, W. A., Upchurch, D. R., and Ritchie, J. T. (1985). "A weighing lysimeter for evapotranspiration and root measurements." *Agron. J.*, 77 (5), 821–825.
- Dunin, F. X., and Aston, A. R. (1984). "The development and proving of models of large scale evapotranspiration. An Australian study." *Agric. Water Manage.*, 8(1–3), 305–323.
- Dunin, F. X., McIlroy, I. C., and O'Loughlin, E. M. (1985). "A lysimeter characterization of evaporation by eucalypt forest and its representativeness for the local environment." Proc., Forest Environmental Measure Conf., B. A. Hutchison and B. B. Hicks, eds., Springer, Netherlands, 271–291.
- Dunin, F. X., Reyenga, W., and McIlroy, I. C. (1991). "Australian lysimeter studies of field evaporation." *Lysimeters for evapotranspiration and environmental measurements*, R. G. Allen, T. A. Howell, W. O. Pruitt, I. A. Walter, and M. E. Jensen, eds., ASCE, New York, 237–245.
- Duty of Water Committee. (1930). "Consumptive use of water in irrigation." *Trans. ASCE*, 94, 1349–1399.
- Dyer, A. J. (1961). "Measurements of evaporation and heat transfer in the lower atmosphere by an automatic eddy-convection technique." *Q. J. R. Meteorolog. Soc.*, 87(373), 401–412.
- Dyer, A. J. (1967). "The turbulent transport of heat and water vapour in an unstable atmosphere." *Q. J. R. Meteorolog. Soc.*, 93(398), 501–508.
- Dyer, A. J. (1974). "A review of flux-profile relationships." *Boundary Layer Meterol.*, 7(3), 363–372.

- Dyer, A. J., and Hicks, B. B. (1970). "Flux-gradient relationships in the constant flux layer." *Q. J. R. Meteorol. Soc.*, 96(410), 715–721.
- Dyer, A. J., and Pruitt, W. O. (1962). "Eddy flux measurements over a small irrigated area." *J. Appl. Meteorol.*, 1(4), 471–473.
- Elbersen, H. W., et al. (2004). "A management guide for planting and production of switchgrass as a biomass crop in Europe." 2nd World Conf. on Biomass for Energy, Industry and Climate Protection, Wageningen, Netherlands, 12.
- Encyclopedia of Hydrological Sciences*. (2002). Wiley, Hoboken, NJ.
- Encyclopedia of Soils in the Environment*. (2004). Elsevier, Amsterdam, Netherlands.
- Entekhabi, D., and Eagleson, P. S. (1989). "Land surface hydrology parameterization for atmospheric general circulation models including subgrid scale spatial variability." *J. Climate*, 2(8), 816–831.
- Erie, L. J., French, O. F., Bucks, D. A., and Harris, K. (1982). "Consumptive use of water by major crops in the southwestern United States." Rep. No. 29, USDA, Washington, DC.
- Erie, L. J., French, O. F., and Harris, K. (1965). "Consumptive use of water by crops in Arizona." Technical Bull. 169, Univ. of Arizona, Tucson, AZ.
- Evans, R. G. (1980). "Irrigation scheduling guide." No. 4.708, Colorado State Univ., Fort Collins, CO.
- Evans, R. G., Benham, B. L., and Trooien, T. P., eds. (2000). "National irrigation symposium." Proc., 4th Decennial Symp., ASCE, Reston, VA.
- Evans, R. G., Kroeger, M. W., and Mahan, M. O. (1991). "Installation and operation of large drainage lysimeters on grapes." *Lysimeters for evapotranspiration and environmental measurements*, R. G. Allen, T. A. Howell, W. O. Pruitt, I. A. Walter, and M. E. Jensen, eds., ASCE, New York, 388–396.
- Evans, R. G., Wu, I.-P., and Smajstrala, A. G. (2007). "Microirrigation systems." *Design and operation of farm irrigation systems*, G. J. Hoffman, R. G. Evans, D. L. Martin, and M. E. Jensen, eds., American Society of Agricultural and Biological Engineers, St Joseph, MI, 632–683.
- Everson, D. O., Faubion, M., and Amos, D. E. (1978). "Freezing temperatures and growing seasons in Idaho." Bull. No. 494, Univ. of Idaho, Moscow, ID.
- Evett, S. R., Howell, T. A., and Schneider, A. D. (1995). "Energy and water balances for surface and subsurface drip irrigated corn." Proc., 5th Int. Microirrigation Congress, ASAE, St. Joseph, MI, 135–140.
- Evett, S. R., and Lascano, R. J. (1993). "ENWATBAL.BAS: A mechanistic evapotranspiration model written in compiled basic." *Agron. J.*, 85(3), 763–772.
- Evett, S. R., and Parkin, G. W. (2005). "Advances in soil water content sensing." *Vadose Zone J.*, 4(4), 986–991.

- Evett, S. R., and Steiner, J. L. (1995). "Precision of neutron scattering and capacitance type soil water content gauges from field calibration." *Soil Sci. Soc. Am. J.*, 59(4), 961–968.
- Evett, S. R., Tolk, J. A., and Howell, T. A. (2003). "A depth control stand for improved accuracy with the neutron probe." *Vadose Zone J.*, 2(4), 642–649.
- Evett, S. R., Tolk, J. A., and Howell, T. A. (2005). "TDR laboratory calibration in travel time, bulk electrical conductivity, and effective frequency." *Vadose Zone J.*, 4(4), 1020–1029.
- Evett, S. R., Tolk, J. A., and Howell, T. A. (2006). "Soil profile water content determination." *Vadose Zone J.*, 5(3), 894–907.
- Ewers, B. E., and Oren, R. (2000). "Analyses of assumptions and errors in the calculation of stomatal conductance from sap flux measurements." *Tree Physiol.*, 20(9), 579–589.
- Farahani, H. J., and Ahuja, L. R. (1996). "Evapotranspiration modeling of partial canopy/residue covered fields." *Trans. ASAE*, 39(6), 2051–2064.
- Farahani, H. J., and Bausch, W. C. (1995). "Performance of evapotranspiration models for maize-bare soil to closed canopy." *Trans. ASABE*, 38(4), 1049–1059.
- Farnsworth, R. K., and Thompson, E. S. (1982). "Mean monthly, seasonal, and annual pan evaporation for the United States." NOAA Technical Rep. NWS 34, NOAA, Silver Spring, MD.
- Farnsworth, R. K., Thompson, E. S., and Peck, E. L. (1982). "Evaporation atlas for the contiguous 48 United States." NOAA Technical Rep. NWS 33, Silver Spring, MD.
- Fereres, E. (1981). "Drip irrigation management." Leaflet No. 21259, Univ. of California, Berkeley, CA.
- Ficke, J. F. (1972). "Comparison of evaporation computation methods, Pretty Lake, LaGrange County, Northeastern Indiana." U.S. Government Printing Office, Washington, DC.
- Fisher, J. B., DeBiase, T. A., Qi, Y., Xu, M., and Goldstein, A. H. (2005). "Evapotranspiration models compared on a Sierra Nevada forest ecosystem." *Environ. Modell. Software*, 20(6), 783–796.
- Fitzpatrick, E. A., and Stern, W. R. (1965). "Components of the radiative balance of irrigated plots in a dry monsoonal environment." *J. Appl. Meteorol.*, 4(6), 649–660.
- Flerchinger, G. N. (1991). "Sensitivity of soil freezing simulated by the SHAW model." *Trans. ASAE*, 34(6), 2381–2389.
- Flerchinger, G. N., Hanson, C. L., and Wight, J. R. (1996). "Modelling of evapotranspiration and surface energy budgets across a watershed." *Water Resour. Res.*, 32(8), 2539–2548.
- Flerchinger, G. N., and Pierson, F. B. (1991). "Modeling plant canopy effects on variability of soil temperature and water." *Agric. For. Meteorol.*, 56(3), 227–246.

- Flesch, T. K., and Dale, R. F. (1987). "A leaf area index model for corn with moisture stress reductions." *Agron. J.*, 79(6), 1008–1014.
- Flint, A. L., and Childs, S. W. (1987). "Calculation of solar radiation in mountainous terrain." *Agric. For. Meteorol.*, 40(3), 233–249.
- Foken, T. (2008a). "The energy balance closure problem: An overview." *Ecol. Appl.*, 18(6), 1351–1367.
- Foken, T. (2008b). *Micrometeorology*, Springer, Berlin.
- Foken, T., Wimmer, F., Mauder, M., Thomas, C., and Liebethal, C. (2006). "Some aspects of the energy balance closure problem." *Atmos. Chem. Phys.*, 6(12), 4395–4402.
- Frederiksen, H. D., and Allen, R. G. (2011). "A common basis for analysis, evaluation and comparison of offstream water uses." *Water Int.*, 36(3), 266–282.
- Frevert, D. K., Hill, R. W., and Braaten, B. C. (1983). "Estimation of FAO evapotranspiration coefficients." *J. Irrig. Drain. Eng.*, 109(2), 265–270.
- Fritschen, L., and Qian, P. (1990). "Net radiation, sensible and latent heat flux densities on slopes computed by the energy balance method." *Boundary Layer Meteorol.*, 53(1–2), 163–171.
- Fritschen, L. J. (1965). "Accuracy of evapotranspiration determinations by the Bowen ratio method." *Bull. Int. Soc. Sci. Hydrol.*, 10(2), 38–48.
- Fritschen, L. J. (1966). "Evapotranspiration rates of field crops determined by the Bowen ratio method." *Agron. J.*, 58(3), 339–342.
- Fritschen, L. J. (1967). "Net and solar radiation relations over irrigated field crops." *Agric. Meteorol.*, 4(1), 55–62.
- Fritschen, L. J., Cox, L., and Kinerson, R. (1973). "A 28-meter Douglas fir in a weighing lysimeter." *For. Sci.*, 19(4), 256–261.
- Fritschen, L. J., and Simpson, J. R. (1985). "Evapotranspiration from forests: Measurement and modeling." *Advances in evapotranspiration*, ASAE, St. Joseph, MI, 393–404.
- Fritz, S., and MacDonald, J. H. (1949). "Average solar radiation in the United States." *Heat. Ventilat.*, 46(7), 61–64.
- Fuehrer, P. L., and Friehe, C. A. (2002). "Flux corrections revisited." *Boundary Layer Meteorol.*, 102(3), 415–458.
- Gao, G., Chen, D., Xu, C., and Simelton, E. (2007). "Trend of estimated actual evapotranspiration over China during 1960–2002." *J. Geophys. Res.*, 112, D11120.
- Garatuza-Payan, J., Pinker, R. T., and Shuttleworth, W. J. (2001a). "High resolution day-time cloud observations for northwestern Mexico from GOES-7 satellite data." *J. Atmos. Oceanic Technol.*, 105(1), 39–56.
- Garatuza-Payan, J., Pinker, R. T., Shuttleworth, W. J., and Watts, C. (2001b). "Solar radiation and evapotranspiration in northern Mexico estimated from remotely sensed measurements of cloudiness." *J. Hydrol. Sci.*, 46(3), 465–478.

- Garcia, M., Raes, D., Allen, R., and Herbas, C. (2004). "Dynamics of reference evapotranspiration in the Bolivian highlands (Altiplano)." *Agric. For. Meteorol.*, 125(1–2), 67–82.
- Gardiol, J. M., Serio, L. A., and Maggiora, A. I. D. (2002). "Modeling evapotranspiration of corn (*Zea mays*) under different plant densities." *J. Hydrol.*, 271(1–4), 188–196.
- Gardner, W. R. (1958). "Some steady state solutions of the unsaturated moisture flow equation with application to evaporation from a water table." *Soil Sci.*, 85(4), 228–232.
- Gardner, W. R. (1959). "Solutions of the flow equation for the drying of soils and other porous media." *Soil Sci. Soc. Am. J.*, 23(3), 183–187.
- Gardner, W. R., and Fireman, M. (1958). "Laboratory studies of evaporation from soil columns in the presence of a water table." *Soil Sci.*, 85(5), 244–249.
- Gardner, W. R., and Hillel, D. I. (1962). "The relation of external evaporative conditions to the drying of soils." *J. Geophys. Res.*, 67(11), 4319–4325.
- Garratt, J. R. (1978). "Transfer characteristics for a heterogeneous surface of large aerodynamic roughness." *Q. J. R. Meteorolog. Soc.*, 104(440), 491–502.
- Garratt, J. R. (1980). "Surface influence upon vertical profiles in the atmospheric near-surface layer." *Q. J. R. Meteorolog. Soc.*, 106(450), 803–819.
- Garratt, J. R. (1992). *The atmospheric boundary layer*, Cambridge University Press, U.K.
- Garratt, J. R., and Hicks, B. B. (1973). "Momentum, heat and vapor transfer to and from natural and artificial surfaces." *Q. J. R. Meteorolog. Soc.*, 99(422), 680–687.
- Garrison, J. D., and Adler, G. P. (1990). "Estimation of precipitable water over the United States for application to the division of solar radiation into its direct and diffuse components." *Solar Energy*, 44(4), 225–241.
- Gash, J. H. C. (1986). "A note on estimating the effect of a limited fetch on micrometeorological evaporation measurements." *Boundary Layer Meteorol.*, 35(4), 409–413.
- Gates, D. M. (1963). "The energy environment in which we live." *Am. Sci.*, 51, 327–348.
- Gates, D. M. (1980). *Biophysical ecology*, Springer, New York.
- Ghamarnia, H., Jafarizade, M., Meri, E., and Gobadei, M. A. (2013). "Lysimetric determination of *Coriandrum sativum* L. water requirement and single and dual crop coefficients in a semiarid climate." *J. Irrig. Drain. Eng.*, 10.1061/(ASCE)IR.1943-4774.0000561, 447–455.
- Gill, G. C. (1983). "Comparison testing of selected naturally ventilated solar radiation shields." NOAA Rep. Contract NA-82-0A-A-266, Stennis Space Center, MS.

- Girona, J., Gelly, M., Mata, M., Arbones, A., Rufat, J., and Marsal, J. (2005). "Peach tree response to single and combined deficit irrigation regimes in deep soils." *Agric. Water Manage.*, 72(2), 97–108.
- Girona, J., Marsal, J., Mata, M., and Del Campo, J. (2003). "Pear crop coefficients obtained in a large weighing lysimeter." 4th Int. Symp. on Irrigation of Horticultural Crops, ACTA Horticulturae, Leuven, Belgium, 277–281.
- Glenn, E. P., Huete, A., Nagler, P., Hirschoock, K., and Brown, P. (2007). "Integrating remote sensing and ground methods to estimate evapotranspiration." *Crit. Rev. Plant Sci.*, 26(3), 139–168.
- Gong, L., Xu, C. Y., Chen, D., Halldin, S., and Chen, Y. D. (2006). "Sensitivity of the Penman-Monteith reference evapotranspiration to key climatic variables in the Changjiang (Yangtze River) basin." *J. Hydrol.*, 329(3), 620–629.
- Gonzalez-Sosa, E., Braud, I., Thony, J. L., Vauclin, M., and Bessemoulin, P. (1999). "Modeling heat and water exchanges of fallow land covered with plant residue mulch." *Agric. For. Meteorol.*, 97(3), 151–169.
- Goss, J. R., and Brooks, F. A. (1956). "Constants for empirical expressions for downcoming atmospheric radiation under cloudless skies." *J. Meteorol.*, 13(5), 482–488.
- Granier, A. (1985). "Une nouvelle méthode pour la mesure du flux de sève brute dans le tronc des arbres." *Annales des Sciences Forestières*, 42(2), 193–200.
- Granier, A. (1987). "Evaluation of transpiration in a Douglas-fir stand by means of sap flow measurements." *Tree Physiol.*, 3(4), 309–320.
- Grant, D. R. (1975). "Comparison of evaporation from barley with Penman estimates." *Agric. Meteorol.*, 15(1), 49–60.
- Grant, R. F., and Baldocchi, D. D. (1992). "Energy transfer over crop canopies: Simulation and experimental verification." *Agric. For. Meteorol.*, 61(1), 129–149.
- Grattan, S. R., Bowers, W., Dong, A., Snyder, R. L., Carroll, J. J., and George, W. (1998). "New crop coefficients estimate water use of vegetables, row crops." *Calif. Agric.*, 52(1), 16–21.
- Gray, D. M. (1970). *Handbook on the principles of hydrology*, Canadian National Committee for the International Hydrological Decade, Ottawa.
- Green, S., Clothier, B., and Jardine, B. (2003). "Theory and practical application of heat pulse to measure sap flow." *Agron. J.*, 95(6), 1371–1379.
- Green, S. R., and Clothier, B. E. (1988). "Water use of kiwifruit vines and apple trees." *J. Exp. Botany*, 39(1), 115–123.
- Griffin, R. E., et al. (1976). "Reducing fruit losses caused by low spring temperatures." Final Rep. Project 562-366-084, Utah State Univ., Logan, UT.

- Grifoll, J., Gasto, J. M., and Cohen, Y. (2005). "Non-isothermal soil water transport and evaporation." *Adv. Water Resour.*, 28(11), 1254–1266.
- Grishchenko, D. L. (1959). "The dependence of albedo of the sea on the altitude of the sun and disturbance of the sea surface." *Tr. Glav. Geofis. Observ.*, 80, 32–38.
- Ham, J. M. (2001). "On the measurement of soil heat flux to improve estimates of energy balance closure." ([http://www.oznet.ksu.edu/envphys/Research/Poster%20PDFs/DPHP\\_and\\_Soil\\_Heat\\_Flux\\_AGU01.pdf](http://www.oznet.ksu.edu/envphys/Research/Poster%20PDFs/DPHP_and_Soil_Heat_Flux_AGU01.pdf)) (Nov. 24, 2006).
- Han, S., Evans, R. G., and Kroeger, M. W. (1994). "Sprinkler distribution patterns in windy conditions." *Trans. ASAE*, 37(5), 1481–1490.
- Hanks, R. J., Gardner, H. R., and Fairbourn, M. L. (1967). "Evaporation of water from soils as influenced by drying with wind or radiation." *Soil Sci. Soc. Am. Proc.*, 31(5), 593–598.
- Hansen, V. E., Israelsen, O. W., and Stringham, G. E. (1979). *Irrigation principles and practices*, Wiley, New York.
- Harbeck, G. E., Jr. (1962). "A practical field technique for measuring reservoir evaporation using mass transfer theory." U.S. Geological Survey, Reston, VA, 101–105.
- Harbeck, G. E., Kohler, M. A., and Koberg, G. E. (1958). "Water-loss investigations: Lake Mead studies." U.S. Geological Survey, Reston, VA.
- Harding, S. T. (1962). "Evaporation from Pyramid and Winnemucca Lakes, Nevada." *J. Irrig. Drain. Div.*, 88(1), 1–14.
- Hardy, E. L., Overpeck, J. C., and Wilson, C. P. (1939). "Precipitation and evaporation in New Mexico." Bull. 269, New Mexico Agricultural Experiment Station, Las Cruces, NM.
- Hargreaves, G. H. (1948). "Irrigation requirement data for central valley crops." U.S. Bureau of Reclamation, Sacramento, CA.
- Hargreaves, G. H. (1983). "Discussion of 'Application of Penman equation wind function.'" *J. Irrig. Drain. Eng.*, 10.1061/(ASCE)0733-9437(1983)109:2(277), 277–278.
- Hargreaves, G. H. (1993). "Estimating runoff from precipitation and temperature." *Management of irrigation and drainage systems: Integrated perspectives*, R. G. Allen, ed., ASCE, New York, 402–408.
- Hargreaves, G. H., and Allen, R. G. (2003). "History and evaluation of Hargreaves evapotranspiration equation." *J. Irrig. Drain. Eng.*, 10.1061/(ASCE)0733-9437(2003)129:1(53), 53–63.
- Hargreaves, G. H., and Allen, R. G. (2004). "Closure of 'History and evaluation of Hargreaves evapotranspiration equation.'" *J. Irrig. Drain. Eng.*, 10.1061/(ASCE)0733-9437(2004)130:5(448), 448–449.
- Hargreaves, G. H., and Samani, Z. A. (1982). "Estimating potential evapotranspiration." *J. Irrig. Drain. Div.*, 108(3), 225–230.
- Hargreaves, G. H., and Samani, Z. A. (1985). "Reference crop evapotranspiration from temperature." *Appl. Eng. Agric.*, 1(2), 96–99.

- Hargreaves, G. L., Hargreaves, G. H., and Riley, J. P. (1985). "Agricultural benefits for Senegal River basin." *J. Irrig. Drain. Eng.*, 10.1061/(ASCE)0733-9437(1985)111:2(113), 113–124.
- Harrison, L. P. (1963). "Fundamental concepts and definitions relating to humidity." *Humidity and moisture*, A. Wexler, ed., Vol. 3, Reinhold, New York.
- Harrold, L. L. (1966). "Measuring evapotranspiration by lysimetry." Proc., Conf. on Evapotranspiration, ASAE, St. Joseph, MI, 28–33.
- Harrold, L. L., and Dreibelbis, F. R. (1958). "Evaluation of agricultural hydrology by monolith lysimeters." Technical Bull. No. 1179, USDA, Washington, DC.
- Hart, Q. J., Brugnach, M., Temesgen, B., Rueda, C., Ustin, S. L., and Frame, K. (2009). "Daily reference evapotranspiration for California using satellite imagery and weather station measurement interpolation." *Civ. Eng. Environ. Syst.*, 26(1), 19–33.
- Hatfield, J. L. (1985). "Wheat canopy resistance determined by energy balance techniques." *Agron. J.*, 77(2), 279–283.
- Hatfield, J. L., and Allen, R. G. (1996). "Evapotranspiration estimates under deficient water supplies." *J. Irrig. Drain Eng.*, 10.1061/(ASCE)0733-9437(1996)122:5(301), 301–308.
- Hatfield, J. L., Baker, J. M., and Viney, M. K. (2005). "Micrometeorology in agricultural systems." American Society of Agronomy, Madison, WI.
- Hatfield, J. L., Reginato, R. J., and Idso, S. B. (1983). "Comparison of longwave radiation calculation methods over the United States." *Water Resour. Res.*, 19(1), 285–288.
- Hatfield, J. L., Reginato, R. J., and Idso, S. B. (1984). "Evaluation of canopy temperature-evapotranspiration over various crops." *Agric. Meteorol.*, 32(1), 41–53.
- Hathoot, H. M., Abo-Ghobar, H. M., Al-Amoud, A. I., and Mohammad, F. S. (1994). "Analysis and design of sprinkler irrigation laterals." *J. Irrig. Drain. Eng.*, 10.1061/(ASCE)0733-9437(1994)120:3(534), 534–549.
- Hedke, C. R. (1924). *Consumptive use of water by crops*, New Mexico State Engineering Office, Santa Fe, NM.
- Heilman, J. L., Brittin, C. L., and Neale, C. M. U. (1989). "Fetch requirements for Bowen ratio measurements of latent and sensible heat fluxes." *Agric. For. Meteorol.*, 44(3), 261–273.
- Heilman, J. L., Heilman, W. E., and Moore, D. G. (1982). "Evaluating the crop coefficient using spectral reflectance." *Agric. J.*, 74(6), 967–971.
- Henderson-Sellers, B. (1986). "Calculating the surface energy balance for a lake and reservoir modeling: A review." *Rev. Geophys.*, 24(3), 625–649.
- Henderson-Sellers, B., and Davis, A. M. (1989). "Thermal stratification modeling for oceans and lakes." *Annual review of numerical fluid mechanics and heat transfer*, C. L. Tien and T. H. Chaula, eds., Vol. 2, Hemisphere, New York, 86–156.

- Hernandez-Suarez, M. (1988). "Modeling irrigation scheduling and its components and optimization of water delivery scheduling with dynamic programming and stochastic  $ET_o$  data." Ph.D. dissertation, Univ. of California, Davis, CA.
- Hickox, G. H. (1946). "Evaporation from a free water surface." *ASCE Trans.*, 111(1), 1–33.
- Hignett, C., and Evett, S. R. (2002). "Neutron thermalization." *Methods of soil analysis*, H. Dane and G. C. Topp, eds., Soil Science Society of America, Madison, WI, 501–521.
- Hill, R. W., and Allen, L. N. (1991). "Water table lysimeter data interpretation." *Lysimeters for evapotranspiration and environmental measurements*, R. G. Allen, T. A. Howell, W. O. Pruitt, I. A. Walter, and M. E. Jensen, eds., ASCE, New York, 254–263.
- Hill, R. W., Johns, E. L., and Frevert, D. K. (1983). "Comparison of equations used for estimating agricultural crop evapotranspiration with field research." USDI, Denver, CO.
- Hoffman, G. J. (1990). "Leaching fraction and root zone salinity control." *Agricultural salinity assessment and management*, K. K. Tanji, ed., ASCE, New York, 236–261.
- Hoffman, G. J., and Shannon, M. C. (2007). "Salinity." *Dev. Agric. Eng.*, 13(1), 131–160.
- Hoffman, O. F., Thiessen, K. M., Frank, M. L., and Blaylock, G. B. (1992). "Quantification of the interception and initial retention of radioactive contaminants deposited on pasture grass by simulated rain." *Atmos. Environ.*, 26(18), 3313–3321.
- Holmes, J. W. (1984). "Measuring evapotranspiration by hydrological methods." *Agric. Water Manage.*, 8(1), 29–40.
- Hooghart, J. C., ed. (1987). "Evaporation and weather." Proc., Information ITNO Committee on Hydrological Research, Netherlands Organization for Applied Scientific Research, Ede, The Hague, Netherlands.
- Horst, T. W., and Weil, J. C. (1992). "Footprint estimation for scalar flux measurements in the atmospheric surface-layer." *Boundary Layer Meteorol.*, 59(3), 279–296.
- Horton, R., and Chung, S. O. (1991). "Soil heat flow." *Modeling plant and soil systems*, R. J. Hanks and J. T. Ritchie, eds., American Society of Agronomy, Madison, WI, 397–438.
- Horton, R., and Wierenga, P. J. (1983). "Estimating the soil heat flux from observations of soil temperature near the surface." *Soil Sci. Soc. Am. J.*, 47(1), 14–20.
- Hostetler, S. W., and Bartlein, P. J. (1990). "Simulation of lake evaporation with application to modeling lake level variations of Harney-Malheur Lake, Oregon." *Water Resour. Res.*, 26(10), 2603–2612.
- Hough, M. N., and Jones, R. J. A. (1997). "The United Kingdom Meteorological Office rainfall and evaporation calculation system: MORECS

- version 2.0—An overview." *Hydrol. and Earth System Sciences Discussion*, 1(2), 227–239.
- Houk, I. E. (1927). "Evaporation on United States reclamation projects." *Trans. ASCE*, 90(1), 266–286.
- Hounam, C. E. (1958). "Evaporation pan coefficients in Australia." *Climatology and microclimatology*, UNESCO, Paris, 52–60.
- Hounam, C. E. (1973). "Comparison between pan and lake evaporation." *Rapport of Rapporteur on Lake Evaporation of the Commission for Hydrology*, WMO, Geneva.
- Howell, T. A. (1990). "Relationship between crop production and transpiration, evapo-transpiration, and irrigation." *Irrigation of agricultural crops*, B. A. Stewart and D. R. Nielsen, eds., American Society of Agronomy, Madison, WI, 391–434.
- Howell, T. A., Dusek, D. A., Tolk, J. A., Copeland, K. S., Colaizzi, P. D., and Evett, S. R. (2006). "Crop coefficients developed at Bushland, Texas for corn, wheat, sorghum, soybean, cotton, and alfalfa." Proc., 2006 World Environmental and Water Resources Congress (CD-ROM), ASCE, Reston, VA.
- Howell, T. A., Evett, S. R., Tolk, J. A., and Schneider, A. D. (2004). "Evapotranspiration of full-, deficit-irrigated, and dryland cotton on the northern Texas high plains." *J. Irrig. Drain. Eng.*, 10.1061/(ASCE)0733-9437(2004)130:4(277), 277–285.
- Howell, T. A., McCormick, R. L., and Phene, C. J. (1985). "Design and installation of large weighing lysimeters." *Trans. Am. Soc. Agric. Eng.*, 28(1), 106–112.
- Howell, T. A., Steiner, J. L., Schneider, A. D., Evett, S. R., and Tolk, J. A. (1997). "Seasonal and maximum daily evapotranspiration of irrigated winter wheat, sorghum, and corn—Southern high plains." *Trans. ASAE*, 40(3), 623–634.
- Howell, T. A., Yazar, A., Schneider, A. D., Dusek, D. A., and Copeland, K. S. (1995). "Yield and water use efficiency of corn in response to LEPA irrigation." *Trans. ASAE*, 38(6), 1737–1747.
- Hoy, R. D., and Stephens, S. K. (1979). "Field study of lake evaporation: Analysis of data from phase 2 storages and summary of phase 1 and phase 2." Dept. of National Development, Australian Water Resources Council, Canberra, Australia.
- Hsieh, C. I., Katul, G., and Chi, T. (2000). "An approximate analytical model for footprint estimation of scalar fluxes in thermally stratified atmospheric flows." *Adv. Water Resour.*, 23(7), 765–772.
- Hsieh, C. I., Katul, G. G., Schieldge, J., Sigmon, J. T., and Knoerr, K. K. (1997). "The Lagrangian stochastic model for fetch and latent heat flux estimation above uniform and non-uniform terrain." *Water Resour. Res.*, 33(3), 427–438.
- Hubbard, K. G., Goddard, S., Sorensen, W. D., Wells, S. N., and Osugi, T. T. (2005). "Performance of quality assurance procedures for an

- applied climate information system." *J. Atmos. Oceanic Technol.*, 22(1), 105–112.
- Hughes, G. H. (1967). "Analysis of techniques used to measure evaporation from Salton Sea, California." U.S. Geologic Survey, Reston, VA, 151–176.
- Hultine, K. R., et al. (2010). "Sap flux-scaled transpiration by tamarisk (*Tamarix* spp.) before, during and after episodic defoliation by the saltcedar leaf beetle (*Diorhabda carinulata*)."*Agric. For. Meteorol.*, 150(11), 1467–1475.
- Humphreys, E. R., et al. (2003). "Annual and seasonal variability of sensible and latent heat fluxes above a coastal Douglas-fir forest, British Columbia, Canada." *Agric. For. Meteorol.*, 115(1–2), 109–125.
- Hunsaker, D. J. (1999). "Basal crop coefficients and water use for early maturity cotton." *Trans. ASAE*, 42(4), 927–936.
- Hunsaker, D. J., Barnes, E. M., Clarke, T. R., Fitzgerald, G. J., and Pinter, P. J., Jr. (2005). "Cotton irrigation scheduling using remotely-sensed and FAO-56 basal crop coefficients." *Trans. ASAE*, 48(4), 1395–1407.
- Hunsaker, D. J., Pinter, P. J., Jr., Barnes, E. M., and Kimball, B. A. (2003). "Estimating cotton evapotranspiration crop coefficients with a multi-spectral vegetation index." *Irrig. Sci.*, 22(2), 95–104.
- Hunsaker, D. J., Pinter, P. J., and Cai, H. (2002). "Alfalfa basal crop coefficients for FAO-56 procedures in the desert regions of the southwestern U.S." *Trans. ASAE*, 45(6), 1799–1815.
- Huntington, J. L., and Allen, R. G. (2010). "Evapotranspiration and net irrigation water requirements for Nevada." State of Nevada, Div. of Water Resources, Carson City, NV.
- Huntington, J. L., et al. (2015). "West-wide climate risk assessments: Irrigation demand and reservoir evaporation projections." Rep. No. 86-68210-2014-01, U.S. Bureau of Reclamation Technical Memorandum, Denver, CO, 242.
- Huntington, J. L., Szilagyi, J., Tyler, S., and Pohll, G. (2011). "Evaluating the complementary relationship for estimating evapotranspiration from arid shrublands." *Water Resour. Res.*, 47, W05533.
- Huschke, R. E., ed. (1959). *Glossary of meteorology*, American Meteorological Society, Boston.
- ICID (International Commission on Irrigation and Drainage). (1985). "On updated evapotranspiration and crop water requirement terms for the ICID multilingual technical dictionary on irrigation and drainage, 1967." *ICID Bull.*, 34(1), 1–5.
- Idso, S. B. (1974). "The calibration and use of net radiometers." *Adv. Agron.*, 26(2), 261–275.
- Idso, S. B. (1981). "A set of equations for full spectrum and 8–14  $\mu\text{m}$  and 10.5–12.5  $\mu\text{m}$  thermal radiation from cloudless skies." *Water Resour. Res.*, 17(2), 295–304.

- Idso, S. B., and Cooley, K. R. (1971). "The vertical location of net radiometers. I. The effects of the underlying air layer." *J. Meteorol. Soc. Jpn.*, 49(5), 343–349.
- Idso, S. B., and Cooley, K. R. (1972). "The vertical location of net radiometers. II. The effects of the net radiometer's shadow." *J. Meteorol. Soc. Jpn.*, 50(1), 49–58.
- Idso, S. B., Reginato, R. J., Jackson, R. D., Kimball, B. A., and Nakayama, F. S. (1974). "The three stages of drying of a field soil." *Soil Sci. Soc. Am.*, 38(5), 831–837.
- Iritz, Z., Lindroth, A., Heikinheimo, M., Grelle, A., and Kellner, E. (1999). "Test of a modified Shuttleworth-Wallace estimate of boreal forest evaporation." *Agric. For. Meteorol.*, 98(3), 605–619.
- Irmak, A., and Kamble, B. (2009). "Evapotranspiration data assimilation with genetic algorithms and SWAP model for on-demand irrigation." *Irrig. Sci.*, 28(1), 101–112.
- Irmak, S., and Mutiibwa, D. (2009). "On the dynamics of evaporative losses from Penman-Monteith with fixed and variable canopy resistance during partial and complete maize canopy." *Trans. ASABE*, 52(4), 1139–1153.
- Irmak, S., et al. (2008). "On the scaling up leaf stomatal resistance to canopy resistance using photosynthetic photon flux density." *Agric. For. Meteorol.*, 148(6-7), 1034–1044.
- Irmak, S., Dukes, M. D., and Jacobs, J. M. (2005). "Using modified Bellani plate evaporation gauges to estimate short canopy reference evapotranspiration." *J. Irrig. Drain. Eng.*, 10.1061/(ASCE)0733-9437(2005)131:2(164), 164–175.
- Irmak, S., Payero, J. O., and Martin, D. L. (2004). "Using modified atmometers (ETgage®) for irrigation management." NebGuide G1579, Univ. of Nebraska–Lincoln, Lincoln, NE.
- Irmak, S., Payero, J. O., Martin, D. L., Irmak, A., and Howell, T. A. (2006). "Sensitivity analyses and sensitivity coefficients of standardized daily ASCE-Penman-Monteith equation." *J. Irrig. Drain. Eng.*, 10.1061/(ASCE)0733-9437(2006)132:6(564), 564–578.
- Irrigation Association. (2003). "Landscape irrigation scheduling and water management: Practices guidelines." Water Management Committee, Falls Church, VA.
- Irrigation Association. (2011). *Irrigation*, 6th Ed., Falls Church, VA.
- Itenfisu, D., Elliott, R. L., Allen, R. G., and Walter, I. A. (2000). "Comparison of reference evapotranspiration calculations across a range of climates." Proc., 4th Decennial Symp. National Irrigation, R. G. Evans, B. L. Benham, and T. P. Trooien, eds., ASAE, St. Joseph, MI, 217–227.
- Itenfisu, D., Elliott, R. L., Allen, R. G., and Walter, I. A. (2003). "Comparison of reference evapotranspiration calculations as part of ASCE standardization effort." *J. Irrig. Drain. Eng.*, 10.1061/(ASCE)0733-9437(2003)129:6(440), 440–448.

- Jackson, R. D. (1973). "Diurnal changes in soil water content during drying." *Field soil water regime*, R. R. Bruce, K. W. Flach, and H. M. Taylor, eds., Soil Science Society of America, Madison, WI, 37–55.
- Jackson, R. D., Idso, S. B., and Reginato, R. J. (1976). "Calculation of evaporation rates during the transition from energy-limiting to soil-limiting phases using albedo data." *Water Resour. Res.*, 12(1), 23–26.
- Jacobs, A. F. G., Halbersma, J., and Przybyla, C. (1989). "Behaviour of the crop resistance of maize during a growing season." *Estimation of areal evapotranspiration*, T. A. Black, D. L. Spittlehouse, M. D. Novak, and D. T. Price, eds., IAHS, London, 165–173.
- Jacobs, C. M. J., and de Bruin, H. A. R. (1997). "Predicting regional transpiration at elevated atmospheric CO<sub>2</sub>: Influence of the PBL vegetation interaction." *J. Appl. Meteorol. Clim.*, 36(12), 1663–1675.
- Jacobs, J., Anderson, M. C., Freiss, L. C., and Diak, G. R. (2004). "Solar radiation, longwave radiation and emergent wetland satellite evapotranspiration estimates from Florida (USA)." *Hydrol. Sci. J.*, 49(3), 461–476.
- James, D. W., Hanks, R. J., and Jurinak, J. J. (1982). *Modern irrigated soils*, Wiley, New York.
- Jara, J., Stockle, C. O., and Kjelgaard, J. (1998). "Measurement of evapotranspiration and its components in a corn (*Zea mays L.*) field." *Agric. For. Meteorol.*, 92(2), 131–145.
- Jarvis, P. G. (1976). "The interpretation of the variations in leaf water potential and stomatal conductance found in canopies in the field." *Phil. Trans. R. Soc.*, B273(927), 593–610.
- Jarvis, P. G., James, G. B., and Landsberg, J. J. (1976). "Coniferous forest." *Vegetation and the atmosphere*, J. L. Monteith, ed., Vol. 2, Academic Press, London, 171–240.
- Jensen, M. E. (1966a). "Discussion of 'Irrigation water requirements of lawns.'" *J. Irrig. Drain. Div.*, 92(1), 95–100.
- Jensen, M. E. (1966b). "Empirical methods of estimating or predicting evapotranspiration using solar radiation." Proc., Conf. on Evapotranspiration, ASAE, Chicago, 57–61.
- Jensen, M. E., ed. (1966c). "Evapotranspiration and its role in water resources management." Proc., Conf. on Evapotration, ASAE, Chicago.
- Jensen, M. E. (1967). "Evaluating irrigation efficiency." *J. Irrig. Drain. Div.*, 93(1), 83–98.
- Jensen, M. E. (1968). "Water consumption by agricultural plants." *Water deficits and plant growth*, T. T. Kozlowski, ed., Vol. 2, Academic Press, New York, 1–22.
- Jensen, M. E. (1969). "Scheduling irrigations with computers." *J. Soil Water Conserv.*, 24(5), 193–195.
- Jensen, M. E., ed. (1973). "Consumptive use of water and irrigation water requirements." Technical Committee on Irrigation Water Requirements of the Irrigation and Drainage Division, ASCE, New York.

- Jensen, M. E. (2003). "Vegetative and open water coefficients for the lower Colorado River accounting system." U.S. Bureau of Reclamation, Boulder City, NV.
- Jensen, M. E. (2007). "Beyond irrigation efficiency." *Irrig. Sci.*, 25(3), 233–245.
- Jensen, M. E., and Allen, R. G. (2000). "Evolution of practical ET estimating methods." National Irrigation Symp., Proc., 4th Decennial Symp., ASAE, St. Joseph, MI, 52–65.
- Jensen, M. E., Burman, R. D., and Allen, R. G. (1990). "Evapotranspiration and irrigation water requirements." *Manual of Practice 70*, ASCE, New York.
- Jensen, M. E., Dotan, A., and Sanford, R. (2005). "Penman-Monteith estimates of reservoir evaporation." *Impacts of global climate change*, Raymond Walton, ed., ASCE, Reston, VA, 1–24.
- Jensen, M. E., and Haise, H. R. (1963). "Estimating evapotranspiration from solar radiation." *J. Irrig. Drain. Div.*, 89(4), 15–44.
- Jensen, M. E., and Hanks, R. J. (1967). "Nonsteady-state drainage from porous media." *J. Irrig. Drain. Div.*, 93(3), 209–242.
- Jensen, M. E., Robb, D. C. N., and Franzoy, C. E. (1970). "Scheduling irrigations using climate-crop-soil data." *J. Irrig. Drain. Div.*, 96(1), 25–38.
- Jensen, M. E., and Wright, J. L. (1978). "The role of evapotranspiration models in irrigation scheduling." *Trans. ASAE*, 21(1), 82–87.
- Jensen, M. E., Wright, J. L., and Pratt, B. J. (1971). "Estimating soil moisture depletion from climate, crop and soil data." *Trans. ASAE*, 14(5), 954–959.
- Jensen, S. (1994). "Genetic improvement of maize for drought tolerance." NRC Water Science and Technology Board Workshop on Future of Irrigation, National Research Council, Washington, DC.
- Jia, X., Dukes, M. D., and Jacobs, J. M. (2007). "Development of bahiagrass crop coefficient in a humid climate." ASABE, St. Joseph, MI.
- Jia, X., Dukes, M. D., and Jacobs, J. M. (2009). "Bahiagrass crop coefficients from eddy correlation measurements in central Florida." *Irrig. Sci.*, 28(1), 5–15.
- Jiusheng, L., and Kawano, H. (1996). "The areal distribution of soil moisture under sprinkler irrigation." *Agric. Water Manage.*, 32(1), 29–36.
- Johnson, M., Saito, L., Anderson, M. A., Weiss, P., Andre, M., and Fontaine, D. G. (2004). "Effects of climate and reservoir and dam operations on reservoir thermal structure." *J. Water Resour. Plann. Manage.*, 10.1061/(ASCE)0733-9496(2004)130:2(112), 112–122.
- Johnson, R. S., Williams, L. E., Ayars, J. E., and Trout, T. J. (2005). "Weighing lysimeters aid study of water relations in tree and vine crops." *Calif. Agric.*, 59(2), 133–136.
- Jones, C. A., Bland, W. L., Ritchie, J. T., and Williams, J. R. (1991). "Simulation of root growth." *Modeling plant and soil systems*, J. R. Hanks and J. T. Ritchie, eds., American Society of Agronomy, Madison, WI, 91–123.

- Jones, C. A., and Kiniry, J. R., eds. (1986). *CERES-maize: A simulation model of maize growth and development*, Texas A&M Univ. Press, College Station, TX.
- Jones, F. E. (1992). *Evaporation of water: With emphasis on applications and measurement*, Lewis, Chelsea, MI.
- Jones, H. G. (1979). "Stomatal behaviour and breeding for drought resistance." *Stress physiology in crop plants*, H. Mussell and R. C. Staples, eds., Wiley, New York, 406–428.
- Jones, J. W., Boote, K. J., Jagtap, S. S., Wilkerson, G. G., Hoogenboom, G., and Mishoe, J. W. (1987). "SOYGRO V5.4 technical documentation." Research Rep., Univ. of Florida, Gainesville, FL.
- Jury, W. A., Gardner, W. R., and Gardner, W. H., eds. (1991). *Soil physics*, Wiley, New York.
- Jury, W. A., and Tanner, C. B. (1975). "Advection modification of the Priestley and Taylor evapotranspiration formula." *Agron. J.*, **67**(6), 569–572.
- Kamble, B., and Irmak, A. (2009). "Combining remote sensing measurements and model estimates through hybrid data assimilation scheme to predict hydrological fluxes." Proc., IEEE Int. Geoscience and Remote Sensing Symp., IEEE, New York.
- Kamgar, A., Hopmans, J. W., Wallender, W. W., and Wendroth, O. (1993). "Plotsize and sample number for neutron probe measurements in small field trials." *Soil Sci.*, **156**(4), 213–224.
- Kang, S., Gu, B., Du, T., and Zhang, J. (2003). "Crop coefficient and ratio of transpiration to evapotranspiration of winter wheat and maize in a semi-humid region." *Agric. Water Manage.*, **59**(3), 239–254.
- Katul, G. G., and Parlange, M. B. (1992). "Estimation of bare soil evaporation using skin temperature measurements." *J. Hydrol.*, **132**(1), 91–106.
- Kay, M. (1986). *Surface irrigation systems and practice*, Cranfield Press, Cranfield, U.K.
- Keijman, J. Q. (1974). "The estimation of the energy balance of a lake from simple weather data." *Boundary Layer Meteorol.*, **7**(3), 399–407.
- Keller, J. (1986). *Sprinkler and trickle irrigation*, Utah State Univ., Logan, UT.
- Kelliher, F. M., Leuning, R., Raupach, M. R., and Schulz, E. D. (1995). "Maximum conductances for evaporation from global vegetation types." *Agric. For. Meteorol.*, **73**(1), 1–16.
- Kilic (Irmak), A., et al. (2011). "Estimation of land surface evapotranspiration: A satellite remote sensing procedure." *Great Plains Res.*, **21**(1), 37–45.
- Kilic (Irmak), A., et al. (2012). "Operational remote sensing of ET and challenges." Chapter 21, *Evapotranspiration—Remote sensing and modeling*, A. Irmak, ed., InTech, Rijeka, Croatia.
- Kimball, B. A., Idso, S. B., and Aase, J. K. (1982). "A model of thermal radiation from partly cloudy and overcast skies." *Water Resour. Res.*, **18**(4), 931–936.

- King, K. M., Tanner, C. B., and Suomi, V. E. (1956). "A floating lysimeter and its evaporation recorder." *Trans. Am. Geophys. Union*, 37(6), 738–742.
- Kirkham, R. R., Gee, G. W., and Jones, T. L. (1984). "Weighing lysimeters for long-term water balance investigations at remote sites." *Soil Sci. Soc. Am. J.*, 48(5), 1203–1205.
- Kite, G. (2000). "Using a basin-scale model to estimate crop transpiration and soil evaporation." *J. Hydrol.*, 229(1–2), 59–69.
- Kite, G., and Droogers, P. (2000). "Comparing evapotranspiration estimates from satellites, hydrological models, and field data." *J. Hydrol.*, 229(1–2), 3–18.
- Kizer, M. A., and Elliott, R. L. (1991). "Eddy correlation systems for measuring evapotranspiration." *Trans. ASAE*, 34(2), 387–392.
- Kizer, M. A., Elliott, R. L., and Stone, J. F. (1990). "Hourly ET model calibration with eddy flux and energy balance data." *J. Irrig. Drain. Eng.*, 10.1061/(ASCE)0733-9437(1990)116:2(172), 172–181.
- Kjaersgaard, J. H., Cuenca, R. H., Plauborg, F. L., and Hansen, F. L. (2007). "Long-term comparisons of net radiation calculation schemes." *Boundary Layer Meteorol.*, 123(3), 417–431.
- Kjelgaard, J. F., Stockle, C. O., Black, R. A., and Campbell, G. S. (1997). "Measuring sap flow with the heat balance approach using constant and variable heat inputs." *Agric. For. Meteorol.*, 85(3–4), 239–250.
- Kjelgren, R., Rupp, L., and Kilgren, R. (2000). "Water conservation in urban landscapes." *HortScience*, 35(6), 1037–1040.
- Klaassen, W., and Sogachev, A. (2006). "Flux footprint simulation downwind of a forest edge." *Boundary Layer Meteorol.*, 121(3), 459–473.
- Klaassen, W., van Breugel, P. B., Moors, E. J., and Nievene, J. P. (2002). "Increased heat fluxes near a forest edge." *Theor. Appl. Climatol.*, 72(3–4), 231–243.
- Klepper, B. (1990). "Root growth and water uptake." *Irrigation of agricultural crops*, B. A. Stewart and D. R. Nielsen, eds., American Society of Agronomy, Madison, WI, 281–322.
- Klocke, N. L., Heermann, D. F., and Duke, H. R. (1985). "Measurement of evaporation and transpiration with lysimeters." *Trans. ASABE*, 28(1), 183–189.
- Klocke, N. L., Todd, R. W., and Schneekloth, J. P. (1996). "Soil water evaporation in irrigated corn." *Appl. Eng. Agric.*, 12(3), 301–306.
- Kohl, R. A., and DeBoer, D. W. (1984). "Drop size distributions for low pressure spray type agricultural sprinkler." *Trans. ASAE*, 27(6), 1836–1840.
- Kohl, R. A., and Wright, J. L. (1974). "Air temperature and vapor pressure changes caused by sprinkler irrigation." *Agron. J.*, 66(1), 85–88.
- Kohler, M. A. (1954). "Lake and pan evaporation." *Water-loss investigations: Lake Hefner studies*, U.S. Geological Survey, Reston, VA, 127–148.

- Kohler, M. A., Nordenson, T. J., and Fox, W. E. (1955). "Evaporation from pans and lakes." U.S. Dept. of Commerce, Silver Spring, MD.
- Kohler, M. A., Nordenson, T. J., and Fox, W. E. (1958). "Pan and lake evaporation." *Water loss investigations: Lake Mead studies*, USGS, Reston, VA, 38–60.
- Kohler, M. A., Nordenson, T. J., and Fox, W. E. (1959). "Evaporation maps for the United States." Weather Bureau, U.S. Dept. of Commerce, Washington, DC.
- Kolle, O., and Rebmann, C. (2007). "EddySoft: Documentation of a software package to acquire and process eddy covariance data." Technical Rep. 10, Max-Planck-Institut f. Biogeochemie, Jena, Germany.
- Kondo, J. (1975). "Air-sea bulk transfer coefficients in diabatic conditions." *Boundary Layer Meteorol.*, 9(1), 91–112.
- Kondo, J. (1994). *Meteorology of the water environment*, Asakura Shoten Press, Tokyo (in Japanese).
- Kopec, A. R., Langley, M. N., and Bos, M. G. (1984). "Major variables which influence effective precipitation." *Int. Comm. Irrig. Drain. Bull.*, 33(2), 65–70.
- Körner, C., Scheel, J. A., and Bauer, H. (1979). "Maximum leaf conductance in vascular plants." *Photosynthetica*, 13(1), 45–82.
- Kozlowski, T. T., ed. (1968a). "Water deficits and plant growth." *Development, control, and measurement*, Vol. 1, Academic Press, New York.
- Kozlowski, T. T., ed. (1968b). "Water deficits and plant growth." *Plant water consumption and response*, Vol. 2, Academic Press, New York.
- Kozlowski, T. T., ed. (1972). "Water deficits and plant growth." *Plant responses and control of water balance*, Vol. 3, Academic Press, New York.
- Kozlowski, T. T., ed. (1976). "Water deficits and plant growth." *Soil water measurement, plant responses, and breeding for drought resistance*, Vol. 4, Academic Press, New York.
- Kranz, W. L., and Eisenhauer, D. E. (1990). "Sprinkler irrigation runoff and erosion control using interrow tillage techniques." *Appl. Eng. Agric.*, 6(6), 739–744.
- Kroes, J. G., and van Dam, J. C., eds. (2003). *Reference manual SWAP version 3.0.3*, Alterra Wageningen UR, Wageningen, Netherlands.
- Kruse, E. G., and Haise, H. R. (1974). "Water use by native grasses in high altitude Colorado meadows." Rep. No. ARS-W-6-1974, USDA-ARS, Washington, DC.
- Kruse, E. G., and Neale, C. M. U. (1989). "Sources of error in hydraulic weighing lysimeter measurements." *Trans. ASAE*, 32(1), 81–88.
- Kustas, W., and Anderson, M. (2009). "Advances in thermal infrared remote sensing for land surface modeling." *Agric. For. Meteorol.*, 149(12), 2071–2081.
- Kustas, W. P. (1990). "Estimates of evapo-transpiration with a one and two layer model of heat transfer over partial canopy cover." *J. Appl. Meteorol.*, 29(8), 704–715.

- Kustas, W. P., et al. (1994). "Surface energy balance estimates at local and regional scales using optical remote sensing from an aircraft platform and atmospheric data collected over semiarid rangelands." *Water Resour. Res.*, 30(5), 1241–1259.
- Kustas, W. P., and Daughtry, C. S. T. (1990). "Estimation of the soil heat flux/net radiation ratio from spectral data." *Agric. For. Meteorol.*, 49(3), 205–223.
- Kustas, W. P., and Norman, J. M. (1999). "Evaluation of soil and vegetation heat flux predictions using a simple two-source model with radiometric temperatures for partial canopy cover." *Agric. For. Meteorol.*, 94(1), 13–29.
- Kustas, W. P., Norman, J. M., Anderson, M. C., and French, A. N. (2003). "Estimating subpixel surface temperatures and energy fluxes from the vegetation index-radiometric temperature relationship." *Remote Sens. Environ.*, 85(4), 429–440.
- Kustas, W. P., Norman, J. M., Schmugge, T. J., and Anderson, M. C. (2004). "Mapping surface energy fluxes with radiometric temperature." *Thermal remote sensing in land surface processes*, D. A. Quattrochi and J. C. Luval, eds., CRC Press, Boca Raton, FL, 205–253.
- Lagos, L. O. (2008). "A modified surface energy balance to model evapotranspiration and surface canopy resistance." Ph.D. dissertation, Univ. of Nebraska–Lincoln, Lincoln, NE.
- Lagos, L. O., Martin, D. L., Verma, S., Suyker, A., and Irmak, S. (2009). "Surface energy balance model of transpiration from variable canopy cover and evaporation from residue covered or bare soil systems." *Irrig. Sci.*, 28(1), 51–64.
- Lagos, L. O., Merino, G., Martin, D., Verma, S., and Suyker, A. (2012). "Evapotranspiration of partially vegetated surfaces." Chapter 13, *Evapotranspiration—Remote sensing and modeling*, A. Irmak, ed., Intech, Rijeka, Croatia.
- Lascano, R. J. (2000). "A general system to measure and calculate daily water use." *Agron. J.*, 92(5), 821–832.
- Lascano, R. J., van Bavel, C. H. M., Hatfield, J. L., and Upchurch, D. R. (1987). "Energy and water balance of a sparse crop: Simulated and measured soil and crop evaporation." *Soil Sci. Soc. Am. J.*, 51(5), 1113–1121.
- Lean, J. (1989). "Contribution of ultraviolet irradiance variations to changes in the sun's total irradiance." *Science*, 244(4901), 197–200.
- Leclerc, M. Y., Shen, S. H., and Lamb, B. (1997). "Observations and large-eddy simulation modeling of footprints in the lower convective boundary layer." *J. Geophys. Res. Atmos.*, 102(D8), 9323–9334.
- Leclerc, M. Y., and Thurtell, G. W. (1990). "Footprint prediction of scalar fluxes using a Markovian analysis." *Boundary Layer Meteorol.*, 52(3), 247–258.

- Lee, X., Massman, W., and Law, B., eds. (2004). *Handbook of micro-meteorology: A guide for surface flux measurement and analysis*, Kluwer, Amsterdam, Netherlands.
- LeMert, R. D. (1972). "Water use of alfalfa in the Imperial Valley." *Imp. Agric. Briefs*, 13, 16.
- Lettau, H. H. (1969). "Note on aerodynamic roughness-parameter estimation on the basis of roughness-element description." *J. Appl. Meteorol.*, 8(5), 828–832.
- Leuning, R. (2007). "The correct form of the Webb, Pearman, and Leuning equation for eddy fluxes of trace gases in steady and non-steady state, horizontally homogeneous flows." *Boundary Layer Meteorol.*, 123(2), 263–267.
- Leuning, R., and Attiwill, P. M. (1978). "Mass, heat and momentum exchange between a mature eucalyptus forest and the atmosphere." *Agric. Meteorol.*, 19(2), 215–241.
- Leuning, R., Condon, A. G., Dunin, F. X., Zegelin, S., and Denmead, O. T. (1994). "Rainfall interception and evaporation from below a wheat canopy." *Agric. For. Meteorol.*, 115(1–2), 109–125.
- Ley, T. W., Allen, R. G., and Jensen, M. E. (2013). "Translating wind-speed measurements over alfalfa having varying height for use in the ASCE standardized reference ET equation." *J. Irrig. Drain Eng.*, 10.1061/(ASCE)IR.1943-4774.0000570, 463–465.
- Ley, T. W., and Allen, R. G. (1994). "Energy and soil water balance analyses of arid weather sites." 1994 Summer Meeting of the American Society of Agricultural Engineers, ASAE, St. Joseph, MI.
- Ley, T. W., Allen, R. G., and Hill, R. W. (1996). "Weather station siting effects on reference evapotranspiration." Proc., Int. Conf. on Evapotranspiration and Irrigation Scheduling, ASAE, St. Joseph, MI, 727–734.
- Ley, T. W., and Elliott, R. L. (1993). "Standards for automated agricultural weather stations." *Management of irrigation and drainage systems: Integrated perspectives*, R. G. Allen, ed., ASCE, New York, 977–984.
- Ley, T. W., Hill, R. W., and Jensen, D. T. (1994a). "Errors in Penman-Wright alfalfa reference evapotranspiration estimates. I Model sensitivity analyses." *Trans. ASAE*, 37(6), 1853–1861.
- Ley, T. W., Hill, R. W., and Jensen, D. T. (1994b). "Errors in Penman-Wright alfalfa reference evapotranspiration estimates. II Effects of weather sensory measurement variability." *Trans. ASAE*, 37(6), 1863–1870.
- Lhomme, J. P., Troufleau, D., Monteny, B., Chehbouni, A., and Bauduin, S. (1997). "Sensible heat flux and radiometric surface temperature over sparse Sahelian vegetation II. A model for the kB -I parameter." *J. Hydrol.*, 188–189(4), 839–854.

- Licor. (2012). "EddyPro users manual." ([http://www.licor.com/env/products/eddy\\_covariance/software.html?](http://www.licor.com/env/products/eddy_covariance/software.html?)), accessed Oct. 15, 2015.
- Li, F., Kustas, W. P., Prueger, J. H., Neale, C. M. U., and Jackson, T. J. (2005). "Utility of remote sensing-based two-source energy balance model under low- and high-vegetation cover conditions." *J. Hydrometeorol.*, **6**(6), 878–891.
- Li, Y., Shao, M., Wang, W., Wang, Q., and Horton, R. (2003). "Open-hole effects of perforated plastic mulches on soil water evaporation." *Soil Sci.*, **168**(11), 751–758.
- Lin, J. D. (1980). "On the force-restore method for prediction of ground surface temperature." *J. Geophys. Res.*, **85**(C6), 3251–3254.
- List, R. J. (1963). *Smithsonian meteorological tables*, Vol. 114, Smithsonian Institution, Washington, DC.
- List, R. J. (1984). *Smithsonian meteorological tables*, 6th Ed., Smithsonian Institution, Washington, DC.
- Liu, P. C., and Schwab, D. J. (1987). "A comparison of methods for estimating  $u^*$  and for given  $u_z$  and air-sea temperature differences." *J. Geophys. Res.*, **92**(C6), 6488–6494.
- Livingston, B. E. (1935). "Atmometers of porous porcelain and paper, their use in physiology ecology." *Ecology*, **16**(3), 438–472.
- Livingston, G. J. (1908). "An annotated bibliography of evaporation." *Mon. Weather Rev.*, **36**, 371–375.
- Livingston, G. J. (1909). "An annotated bibliography of evaporation." *Mon. Weather Rev.*, **37**, 248–242.
- Lofgren, B. M. (2004). "A model for simulation of the climate and hydrology of the Great Lakes basin." *J. Geophys. Res.*, **109**, D18108.
- London, J., and Fröhlich, C., eds. (1982). "A collection of extended abstracts presented at the symposium on the solar constant and the spectral distribution of solar irradiance." IAMAP Third Scientific Assembly, Federal Republic of Germany, Oberpfaffenhofen, Germany, 41.
- Lowry, R. L., Jr., and Johnson, A. F. (1942). "Consumptive use of water for agriculture." *Trans. ASCE*, **107**(1), 1243–1266.
- Ludlow, M. M., and Jarvis, P. G. (1971). "Photosynthesis in Sitka spruce (*Picea sitchensis* (Bong.) Carr.). I. General characteristics." *J. Appl. Ecol.*, **8**(3), 925–953.
- Luo, L., et al. (2003). "Validation of the North American land data assimilation system (NLDAS) retrospective forcing over the southern Great Plains." *J. Geophys. Res.*, **108**(D22), 8843.
- Luquet, D., Vidal, A., Smith, M., and Dauzat, J. (2005). "More crop per drop: How to make it acceptable for farmers?" *Agric. Water Manage.*, **76**(2), 108–119.
- Maas, E. V. (1990). "Crop salt tolerance." *Agricultural salinity assessment and management*, K. K. Tanji, ed., ASCE, New York, 262–304.

- Mackay, D. S., et al. (2002). "Effects of aggregated classifications of forest composition on estimates of evapotranspiration in a northern Wisconsin forest." *Global Change Biol.*, 8(12), 1253–1265.
- Mahrt, L., and Ek, M. (1984). "The influence of atmospheric stability on potential evaporation." *J. Clim. Appl. Meteorol.*, 23(2), 222–234.
- Majumdar, N. C., Mathur, B. L., and Kaushik, S. B. (1972). "Prediction of direct solar radiation for low atmospheric turbidity." *Solar Energy*, 13(4), 383–394.
- Makkink, G. F. (1957). "Testing the Penman formula by means of lysimeters." *J. Inst. Water Eng.*, 11(3), 277–288.
- Mantovani, E. C., Villalobos, F. J., Orgaz, F., and Fereres, E. (1995). "Modelling the effects of sprinkler irrigation uniformity on crop yield." *Agric. Water Manage.*, 27(3), 243–257.
- Mao, L. M., Bergman, M. J., and Tai, C. C. (2002). "Evapotranspiration measurement and estimation of three wetland environments in the upper St. Johns River basin, Florida." *J. Am. Water Resour. Assoc.*, 38(5), 1271–1285.
- Marek, T., Colaizzi, P., Howell, T. A., Dusek, D., and Porter, D. (2006). "Estimating seasonal crop ET using calendar and heat unit based crop coefficients in the Texas High Plains Evapotranspiration Network." 2006 ASABE Annual Int. Meeting, ASABE, St. Joseph, MI.
- Marek, T. H., Schmeider, A. D., Howell, T. A., and Ebeling, L. L. (1988). "Design and construction of large weighing monolithic lysimeters." *Trans. ASAE*, 31(2), 477–484.
- Marsh, A. W., Strohman, R. A., Spaulding, S., Youngner, V., and Gibeault, V. (1980). "Turf grass irrigation research at the University of California: Warm and cool season grasses tested for water needs." *California Turfgrass Culture*, 30(1), 32–33.
- Martin, D. L., and Gilley, J. (1993). "Irrigation water requirements." Chapter 2, *National engineering handbook*, Soil Conservation Service, USDA, Bethesda, MD.
- Martin, D. L., Gilley, J. R., Carmack, W. J., and Hardy, L. A. (1993). "SCS methods for determining irrigation water requirements." *Management of irrigation and drainage systems: Integrated perspectives*, R. G. Allen, ed., ASCE, New York, 1031–1038.
- Martin, D. L., Kincaid, D. C., and Lyle, W. M. (2007). "Design of sprinkler systems." *Design and operation of farm irrigation systems*, G. J. Hoffman, R. G. Evans, and M. E. Jensen, eds., American Society of Agricultural and Biological Engineers, St Joseph, MI, 557–631.
- Martin, E. C., Shayya, W. H., Bralts, V. F., Loudon, T. L., and Johnson, J. A. (1990). "Irrigation scheduling: A statewide program in Michigan." *Visions of the Future: Proc., 3rd National Irrigation Symp.*, ASAE, St. Joseph, MI, 700–707.

- Martínez-Cob, A. (2008). "Use of thermal units to estimate corn crop coefficients under semiarid climatic conditions." *Irrig. Sci.*, 26(4), 335–345.
- Massman, W. J. (1999). "A model study of  $kB_u^{-1}$  for vegetated surfaces using 'localized near-field' Lagrangian theory." *J. Hydrol.*, 223(1), 27–43.
- Massman, W. J. (2000). "A simple method for estimating frequency response corrections for eddy covariance systems." *Agric. For. Meteorol.*, 104(3), 185–198.
- Massman, W. J. (2001). "Reply to comment by Rannik on: A simple method for estimating frequency response corrections for eddy covariance systems." *Agric. For. Meteorol.*, 107(3), 247–251.
- Massman, W. J., and Kaufmann, M. R. (1991). "Stomatal response to certain environmental factors: A comparison of models for subalpine trees in the Rocky Mountains." *Agric. For. Meteorol.*, 54(2–4), 155–167.
- Mateos, L., Mantovani, E. C., and Villalobos, F. J. (1997). "Cotton response to non-uniformity of conventional sprinkler irrigation." *Irrig. Sci.*, 17(2), 47–52.
- Mauder, M., and Foken, T. (2004). "Documentation and instruction manual of the eddy covariance software package TK2." Universitaet Bayreuth, Abt. Mikrometeorologie, Bayreuth, Germany.
- Maurer, E. P., Wood, A. W., Adam, J. C., Lettenmaier, D. P., and Nijssen, B. (2002). "A long-term hydrologically-based data set of land surface fluxes and states for the conterminous United States." *J. Clim.*, 15(22), 3237–3251.
- McArthur, J. A., Hesketh, J. D., and Baker, D. N. (1975). "Cotton." *Crop physiology*, L. T. Evans, ed., Univ. of Cambridge, Cambridge, U.K., 297–325.
- McBean, G. A. (1972). "Instrument requirements for eddy correlation measurements." *J. Appl. Meteorol.*, 11(7), 1078–1084.
- McCabe, G. J., and Markstrom, S. L. (2007). "A monthly water-balance model driven by a graphical user interface." Open-File Rep. 2007–1088, USGS, Washington, DC.
- McDole, R. E., McMaster, G. M., and Larson, D. C. (1974). "Available water-holding capacities of soils in southern Idaho." Univ. of Idaho, Moscow, ID.
- McEwen, G. F. (1930). "Results of evaporation studies conducted at the Scripps Institute of Oceanography and the California Institute of Technology." *Bull. Scripps Inst. Oceanogr. Techn.*, 2(11), 401–415.
- McFarland, M. J., Worthington, J. W., and Newman, J. S. (1983). "Design, installation, and operation of a twin weighing lysimeter for fruit trees." *Trans. ASAE*, 26(6), 1717–1721.
- McGinn, S. M., and King, K. M. (1990). "Simultaneous measurements of heat, water vapor and CO<sub>2</sub> fluxes above alfalfa and maize." *Agric. For. Meteorol.*, 49(4), 331–349.

- McIlroy, I. C., and Angus, D. E. (1963). "The Aspendale multiple weighed lysimeter installation." CSIRO, Melbourne, Australia, 27.
- McIlroy, I. C., and Angus, D. E. (1964). "Grass, water and soil evaporation at Aspendale." *Agric. Meteorol.*, 1(3), 201–224.
- McIlroy, I. C., and Dunin, F. X. (1982). "A forest evaporation technique comparison experiment." 1st National Symp. on Forest Hydrology, Institute of Engineers, Melbourne, Australia, 12–17.
- McNaughton, K. G., and Black, T. A. (1973). "A study of evapotranspiration from a Douglas fir forest using the energy balance approach." *Water Resour. Res.*, 9(6), 1579–1590.
- McNaughton, K. G., and van den Hurk, B. J. J. M. (1995). "A 'Lagrangian' revision of the resistors in the two-layer model for calculating the energy budget of a plant canopy." *Boundary Layer Meteorol.*, 74(3), 261–288.
- Meek, D. W. (1997). "Estimation of maximum possible daily global solar radiation." *Agric. For. Meteorol.*, 87(2), 223–241.
- Meek, D. W., and Hatfield, J. L. (1994). "Data quality checking for single station meteorological databases." *Agric. For. Meteorol.*, 69, 85–109.
- Merriam, J. L., and Keller, J. (1978). *Farm irrigation system evaluation: A guide for management*, Utah State Univ., Logan, UT.
- Meyer, A. F. (1942). "Evaporation from lakes and reservoirs." Minnesota Resources Commission, St. Paul, MN.
- Meyer, J. L., and Gibeault, V. A. (1986). "Turfgrass performance under reduced irrigation." *Calif. Agric.*, 40(7), 8.
- Meyer, S. J., and Hubbard, K. G. (1992). "Nonfederal automated weather stations and networks in the United States and Canada: A preliminary survey." *Bull. Am. Meteorol. Soc.*, 73(4), 449–457.
- Meyer, W. S., and Mateos, L. (1990). "Soil type effects on soybean crop water use in weighing lysimeters III. Effect of lysimeter canopy height discontinuity on evaporation." *Irrig. Sci.*, 11(4), 233–237.
- Milly, P. C. D. (1988). "Advances in modeling of water in the unsaturated zone." *Transp. Porous Media*, 3(5), 491–514.
- Milne, R. (1979). "Water loss and canopy resistance of a young Sitka spruce plantation." *Boundary Layer Meteorol.*, 16(1), 67–81.
- Misson, L., Panek, J. A., and Goldstein, A. H. (2004). "A comparison of three approaches to modeling leaf gas exchange in annually drought stressed Ponderosa pine forests." *Tree Physiol.*, 24(5), 529.
- Mitchell, A. R. (1997). "Irrigating peppermint." EM 8662, Oregon State University Extension Service, Corvallis, OR, 12.
- Mitchell, K. E., et al. (2004). "The multi-institution North American Land Data Assimilation System (NLDAS): Utilizing multiple GCIP products and partners in a continental distributed hydrological modeling system." *J. Geophys. Res.*, 109, D07S90.
- Miyazaki, T. (1993). *Water flow in soils*, Marcel-Decker, New York.

- Mo, X., and Beven, K. (2004). "Multi-objective parameter conditioning a three-source wheat canopy model." *Agric. For. Meteorol.*, 122(1), 39–63.
- Molden, D. (1997). "Accounting for water use and productivity." International Water Management Institute, Colombo, Sri Lanka.
- Molden, D. (2007). "Water for food, water for life: A comprehensive assessment of water management in agriculture." International Water Management Institute, Colombo, Sri Lanka.
- Moncrieff, J. B., Malhi, Y., and Leuning, R. (1996). "The propagation of errors in long-term measurements of land-atmosphere fluxes of carbon and water." *Global Change Biol.*, 2(3), 231–240.
- Monin, A. S., and Obukhov, A. M. (1954). "The basic laws of turbulent mixing in the surface layer of the atmosphere." *Akad. Nauk. SSSR Trud. Geofiz. Inst.*, 24(151), 163–187.
- Monteith, J. L. (1965). "The state and movement of water in living organisms." XIXth Symp. Society for Experimental Biology, Cambridge University Press, Cambridge, U.K., 205–234.
- Monteith, J. L. (1973). *Principles of environmental physics*, Elsevier, New York.
- Monteith, J. L. (1981). "Evaporation and surface temperature." *Q. J. R. Meteorolog. Soc.*, 107(451), 1–27.
- Monteith, J. L. (1987). "In memoriam Howard Latimer Penman (1909–1984)." *Irrig. Sci.*, 8(2), 77–79.
- Monteith, J. L. (1995). "Accommodation between transpiring vegetation and convective boundary layer." *J. Hydrol.*, 166(3–4), 251–263.
- Monteith, J. L., and Szeicz, G. (1962). "Radiative temperature in the heat balance of natural surfaces." *Q. J. R. Meteorolog. Soc.*, 88(378), 496–507.
- Monteith, J. L., and Unsworth, M. H. (1990). *Principles of environmental physics*, 2nd Ed., Edward Arnold, London and New York.
- Moore, C. J. (1974). "A comparative study of forest and grassland micro-meteorology." Ph.D. thesis, The Flinders, Univ. of South Australia, Adelaide, Australia.
- Moran, M. S., Rahman, A. F., Washburne, J. C., Goodrich, D. C., Weltz, M. A., and Kustas, W. P. (1996). "Combining the Penman-Monteith equation with measurements of surface temperature and reflectance to estimate evaporation rates of semiarid grassland." *Agric. For. Meteorol.*, 80(2–4), 87–109.
- Moran, M. S. (2000). "Use of remote sensing for monitoring evaporation over managed watersheds." In *Watershed Management and Operations Management 2000*, ASCE, Reston, VA, 1–12.
- Morgan, D. L., Pruitt, W. O., and Lourence, F. J. (1971). "Analyses of momentum, energy, and mass transfers above vegetative surfaces." Technical Rep. ECOM 68-G10-F, Univ. of California, Davis, CA.

- Morton, F. I. (1971). "Catchment evaporation and potential evaporation—Further development of a climatologic relationship." *J. Hydrol.*, 12(2), 81–99.
- Morton, F. I. (1983). "Operational estimates of areal evapotranspiration and their significance to the science and practice of hydrology." *J. Hydrol.*, 66 (1), 1–76.
- Mott, K. A., and Parkhurst, D. F. (1991). "Stomatal responses to humidity in air and helox." *Plant Cell Environ.*, 14(5), 509–515.
- Muchow, R. C., and Bellamy, J. A. (1991). "Climate risk in crop production: Models and management for the semiarid tropics and subtropics." Proc., Int. Symp. on Climate Risk in Crop Production: Models and Management for the Semiarid Tropics and Subtropics, CAB International, Wallingford, U.K., 548.
- Murray, F. W. (1967). "On the computation of saturation vapor pressure." *J. Appl. Meteorol.*, 6(1), 203–204.
- Musick, J. T., Dusek, D. A., and Mathews, A. C. (1984). "Irrigation water management of winter wheat." ASAE, St. Joseph, MI.
- Mutziger, A. J., Burt, C. M., Howell, T. A., and Allen, R. G. (2005). "Comparison of measured and FAO-56 modeled evaporation from bare soil." *J. Irrig. Drain. Eng.*, 10.1061/(ASCE)0733-9437(2005)131:1(59), 59–72.
- Nadezhina, N, Eermák, J., and Ceulemans, R. (2002). "Radial patterns of sap flow in woody stems of dominant and understory species: Scaling errors associated with positioning of sensors." *Tree Physiol.*, 22(13), 907–918.
- Nagler, P. L., et al. (2009). "Wide-area estimates of saltcedar (*Tamarix* spp.) evapotranspiration on the Lower Colorado River measured by heat balance and remote sensing methods." *Ecohydrology*, 2(1), 18–33.
- Nagler, P. L., Glenn, E. P., Thompson, T. L., and Huete, A. (2004). "Leaf area index and normalized difference vegetation index as predictors of canopy characteristics and light interception by riparian species on the Lower Colorado River." *Agric. For. Meteorol.*, 125(1–2), 1–17.
- Nakayama, F. S., and Bucks, D. A. (1986). *Trickle irrigation for crop production: Design, operation, and management*, Elsevier, Amsterdam, Netherlands.
- Nakayama, K., Pruitt, W. O., and Chandio, B. (1983). "Some aspects of the Priestley and Taylor model to estimate evapotranspiration." Chiba Univ., Japan, 25–30.
- Neale, C. M. U., Artan, G. A., Tarboton, D. G., and Hanson, C. H. (1995). "A spatially distributed energy balance model: Development, validation and application." Proc., 25th Conf. Agricultural and Forest Meteorology, American Meteorological Society, Boston, MA.
- Neale, C. M. U., Bausch, W. C., and Heermann, D. F. (1990). "Development of reflectance-based crop coefficients for corn." *Trans. ASABE*, 32(6), 1891–1899.

- Nebraska-HPCC (Nebraska High Plains Climate Center). (2006). "Crop coefficients, phenology, and growing degree day accumulation." (<http://www.hprcc.unl.edu/awdn.php/>), accessed Oct. 15, 2015.
- Neilson, R. E., Ludlow, M. M., and Jarvis, P. G. (1972). "Photosynthesis in Sitka spruce (*Picea sitchensis* (Bong.) Carr.) II. Response to temperature." *J. Appl. Ecol.*, 9(3), 721–745.
- Nie, D., and Kanemasu, E. T. (1989). "A comparison of net radiation on slopes." Proc., 19th Conf. Agricultural and Forest Meteorology, American Meteorological Society, Charleston, SC, 142–143.
- Niu, G.-Y., et al. (2011). "The community Noah land surface model with multiparameterization options (Noah-MP): 1. Model description and evaluation with local-scale measurements." *J. Geophys. Res.*, 116(D12).
- Noilhan, J., and Planton, S. (1989). "A simple parameterization of land surface processes for meteorological models." *Mon. Weather Rev.*, 117(3), 536–549.
- Norman, J. M., et al. (2003). "Remote sensing of surface energy fluxes at 10<sup>1</sup>-m pixel resolutions." *Water Resour. Res.*, 39(8), 1221.
- Norman, J. M., and Arkebauer, T. J. (1991). "Predicting canopy light-use efficiency from leaf characteristics." *Modeling plant and soil systems*, R. J. Hanks and J. T. Ritchie, eds., American Society of Agronomy, Madison, WI, 125–143.
- Norman, J. M., Kustas, W. P., and Humes, K. S. (1995). "A two-source approach for estimating soil and vegetation energy fluxes from observations of directional radiometric surface temperature." *Agric. For. Meteorol.*, 77(3-4), 263–293.
- Norman, J. M., Kustas, W. P., Prueger, J. H., and Diak, G. R. (2000). "Surface flux estimation using radiometric temperature: A dual-temperature-difference method to minimize measurement errors." *Water Resour. Res.*, 36(8), 2263–2274.
- Novak, M. D. (1989). "The use of analytical solutions to determine the evapotranspiration from bare and vegetated surfaces." *Estimation of areal evapotranspiration*, T. A. Black, D. L. Spittlehouse, M. D. Novak, and D. T. Price, eds., IAHS, London, 133–152.
- NREL (National Renewable Energy Laboratory). (1992). "Interim solar radiation data manual." NREL/TP-463-5176, Boulder, CO.
- Obukhov, A. M. (1946). "Turbulence in an atmosphere with non-uniform temperature." *Boundary Layer Meteorol.*, 2(1), 7–29.
- Ohmura, A. (1982). "Objective criteria for rejecting data for Bowen ratio flux calculations." *J. Appl. Meteorol.*, 21(4), 595–598.
- Ojeda-Bustamante, W., Sifuentes-Ibarra, E., Slack, D. C., and Carrillo, M. (2004). "Generalization of irrigation scheduling parameters using the growing degree days concept: Application to a potato crop." *Irrig. Drain.*, 53(3), 251–261.

- Oke, T. R. (1978). *Boundary layer climates*, Wiley, New York.
- Oleson, K. W., et al. (2004). "Technical description of the community land model (CLM)." [www.cgd.ucar.edu/tss/clm/distribution/clm3.0/](http://www.cgd.ucar.edu/tss/clm/distribution/clm3.0/), accessed Oct. 15, 2015.
- Olivier, H. (1961). *Irrigation and climate*, Edward Arnold, London.
- Ortega-Farias, S., Carrasco, M., Olioso, A., Acevedo, C., and Problete, C. (2006). "Latent heat flux over Cabernet Sauvignon vineyard using the Shuttleworth and Wallace model." *Irrig. Sci.*, 25(2), 161–170.
- Ortega-Farias, S. O., Olioso, A., Fuentes, S., and Valdes, H. (2006). "Latent heat flux over a furrow-irrigated tomato crop using Penman-Monteith equation with a variable surface canopy resistance." *Agric. Water Manage.*, 82(3), 421–432.
- Ortega-Farias, S. O., Poblete-Echeverría, C., and Brisson, N. (2010). "Parameterization of a two-layer model for estimating vineyard evapotranspiration using meteorological measurements." *Agric. For. Meteorol.*, 150(2), 276–286.
- Oster, J. D., Meyer, J. L., Hermsmeier, L., and Kaddah, M. (1984). "Imperial Valley: Irrigation, drainage and runoff." Univ. of California, Oakland, CA.
- Paço, T. A., Ferreira, M. I., and Conceição, N. (2006). "Peach orchard evapotranspiration in a sandy soil: Comparison between eddy covariance measurements and estimates by the FAO 56 approach." *Agric. Water Manage.*, 85(3), 305–313.
- Panofsky, H. A. (1963). "Determination of stress from wind and temperature measurements." *Q. J. R. Meteorolog. Soc.*, 89(379), 85–94.
- Parchomchuk, P., Bernard, R. C., and Van der Gulik, T. W. (1996). "Automated irrigation scheduling using an electronic atmometer." Proc., Int. Conf. Evapotranspiration and Irrigation Scheduling, C. R. Camp, E. J. Sadler, and R. E. Yoder, eds., ASAE, St. Joseph, MI, 1099–1104.
- Parkes, M., Jian, W., and Knowles, R. (2005). "Peak crop coefficient values for Shaanxi, North-west China." *Agric. Water Manage.*, 73(2), 149–168.
- Pastor, M., and Orgaz, F. (1994). "Los programas de recorte de riego en olivar." *Agricultura*, 746(7), 768–776.
- Paulson, C. A. (1970). "The mathematical representation of wind speed and temperature profiles in the unstable atmospheric surface layer." *J. Appl. Meteorol.*, 9(6), 857–861.
- Paw, U. K. T., Baldocchi, D. D., Meyers, T. P., and Wilson, K. B. (2000). "Correction of eddy covariance measurements incorporating both advective effects and density fluxes." *Boundary Layer Meteorol.*, 97(3), 487–511.
- Paw, U. K. T., and Gao, W. (1988). "Applications of solutions to non-linear energy budget equations." *Agric. For. Meteorol.*, 43(2), 121–145.

- Payero, J. O., and Irmak, S. (2013). "Daily energy fluxes, evapotranspiration and crop coefficient of soybean." *Agric. Water Manage.*, 129, 31–43.
- Payero, J. O., Neale, C. M. U., Wright, J. L., and Allen, R. G. (2003). "Guidelines for validating Bowen ratio data." *Trans. ASAE*, 46(4), 1051–1060.
- Pelton, W. L., King, K. M., and Tanner, C. B. (1960). "An evaluation of the Thornthwaite and mean temperature methods for determining potential evapotranspiration." *Agron. J.*, 52(7), 387–395.
- Penman, H. L. (1948). "Natural evaporation from open water, bare soil and grass." *Proc. R. Soc. London*, A193(1032), 120–146.
- Penman, H. L. (1956a). "Estimating evaporation." *Am. Geophys. Union Trans.*, 37(1), 43–50.
- Penman, H. L. (1956b). "Evaporation: An introductory survey." *Neth. J. Agric. Res.*, 4(1), 9–29.
- Penman, H. L. (1963). "Vegetation and hydrology." Commonwealth Bureau of Soils, Harpenden, U.K.
- Penman, H. L., and Schofield, R. K. (1951). "Some physical aspects of assimilation and transpiration." *N. R. Proc. Soc. Exp. Biol.*, 5, 115–129.
- Pereira, L. S. (1995). "Crop-water-simulation models in practice: Selected papers of the 2nd Workshop on crop-water-models." Proc., 15th Congress Int. Commission on Irrigation and Drainage (ICID), ICID, New Delhi, India.
- Pereira, L. S., Perrier, A., Allen, R. G., and Alves, I. (1999a). "Evapotranspiration: Concepts and future trends." *J. Irrig. Drain. Eng.*, 10.1061/(ASCE)0733-9437(1999)125:2(45), 45–51.
- Pereira, L. S., Smith, M., and Allen, R. G. (1999b). "Crop water requirements." *Handbook of agricultural engineering*, Vol. 1, ASAE, St. Joseph, MI, 213–262.
- Perez, R., Stewart, R., Arbogast, C., Seal, R., and Scott, J. (1986). "An isotropic hourly diffuse radiation model for sloping surfaces: Description, performance, validation, site dependency evaluation." *Solar Energy*, 36(6), 481–497.
- Perrier, A. (1982). "Land surface processes: Vegetation." *Land surface processes in atmospheric general circulation models*, P. Eagleson, ed., Cambridge University Press, Cambridge, 395–448.
- Perrier, A., ed. (1985). "Crop water requirements." Proc., Int. Conf., Institut National de la Recherche Agronomique, Cambridge Univ. Press, U.K., 395–448.
- Perrier, A., and Jensen, M. E. (1979). "Question 1—Terminology and question 2—Measurement methods." Int. Round Table Conf. on Evapotranspiration, Int. Commission on Irrigation and Drainage, ICID, New Delhi, India, A-120–A-145.

- Perry, C. (2007). "Efficient irrigation; inefficient communication; flawed recommendations." *Irrig. Drain.*, 56(4), 367–378.
- Perry, C., Steduto, P., Allen, R. G., and Burt, C. M. (2009). "Increasing productivity in irrigated agriculture: Agronomic constraints and hydrological realities." *Agric. Water Manage.*, 96(11), 1517–1524.
- Petersen, E. W. (1969). "On the relation between the shear stress and the velocity profile after a change in surface roughness." *J. Atmos. Sci.*, 26(4), 773–774.
- Pettrey, D. E., and Switzer, R. E. (1996). "Sharkey soils in Mississippi." (<http://msucares.com/pubs/bulletins/b1057.htm>) (Oct. 2015).
- Pfeiffer, L., and Lin, C. (2010). "The effect of irrigation technology on groundwater use." *Choices Mag.*, 25(3), Article 147.
- Phene, C. J., Reginato, R. L., Itier, B., and Tanner, B. R. (1990). "Sensing irrigation needs." *Management of farm irrigation systems*, G. J. Hoffman, T. A. Howell, and K. H. Solomon, eds., ASAE, St. Joseph, MI, 208–261.
- Philip, J. R. (1957). "Evaporation and moisture and heat fields in the soil." *J. Meteorol.*, 14(4), 354–366.
- Phillips, W. D., and Irbe, J. G. (1978). "Land-to-lake comparison of wind temperature and humidity on Lake Ontario during the International Field Year for the Great Lakes (IFYGL)." Rep. CLI-2-77, Environment Canada Atmospheric Environment Service, Downsview, ON, Canada.
- Pieri, P., and Fuchs, M. (1990). "Comparison of Bowen ratio and aerodynamic estimates of evapotranspiration." *Agric. For. Meteorol.*, 49(3), 243–356.
- Pierre, W. H., Kirkham, D., Pesek, D., and Shaw, R. (1966). *Plant environment and efficient water use*, American Society of Agronomy, Madison, WI.
- Pinker, R. T., and Lazlo, I. (1992). "Modeling surface solar irradiance for satellite applications on a global scale." *J. Appl. Meteorol.*, 31(2), 194–211.
- Pittenger, D., and Henry, J. M. (2005). "Refinement of urban landscape water requirements." (<http://groups.ucanr.org/CLUH/files/25773.pdf>) (Mar. 10, 2011).
- Pittenger, D., and Shaw, D. A. (2007). "Review of research on water needs of landscape plants." 2007 Symp. on Efficient Water Use in the Urban Landscape, New Mexico State Univ., Las Cruces, NM.
- Pittenger, D. R., and Shaw, D. (2001). "Applications of recent research in landscape irrigation management." Proc., UCR Turfgrass and Landscape Management Field Day, Univ. of California, Riverside, CA, 17–18.
- Pittenger, D. R., and Shaw, D. (2004). "What we know about landscape water requirements." *CO-Hort*, 6(1), 1–4.
- Plate, E. J. (1971). "Aerodynamic characteristics of atmospheric boundary layers." TID-25465, U.S. Atomic Energy Commission, Germantown, MD.

- Poblete-Escheverria, C., and Ortega-Farias, S. (2009). "Estimation of actual evapotranspiration for a drip-irrigated Merlot vineyard using a three-source model." *Irrig. Sci.*, 28(1), 65–78.
- Pratt, P. F., Warner, J. E., and Nash, P. A. (1976). "Sampling the unsaturated zone in irrigated field plots." *Soil Sci. Soc. Am. J.*, 40(2), 277–279.
- Price, D. T., and Black, T. A. (1989). "Estimation of forest transpiration and CO<sub>2</sub> uptake using the Penman-Monteith equation and a physiological photosynthesis model." *Estimation of areal evapotranspiration*, T. A. Black, D. A. Spittlehouse, M. D. Novak, and D. T. Price, eds., IAHS, London, 213–227.
- Priestley, C. H. B., and Taylor, R. J. (1972). "On the assessment of surface heat flux and evaporation using large scale parameters." *Mon. Weather Rev.*, 100(2), 81–92.
- Pruitt, W. O. (1955). "1955 annual report." Washington State Univ., Pullman, WA.
- Pruitt, W. O. (1960). "Relation of consumptive use of water to climate." *Trans. ASAE*, 3(1), 9–13.
- Pruitt, W. O. (1963). "Application of several energy balance and aerodynamic evaporation equations under a wide range of stability." Final Rep. DA-36-039-SC-80334, Univ. of California, Davis, 107–124.
- Pruitt, W. O. (1964). "Cyclic relations between evapotranspiration and radiation." *Trans. ASAE*, 7(3), 271–275.
- Pruitt, W. O. (1966). "Empirical method of estimating evapotranspiration using primarily evaporation pans." Proc., Conf. on Evapotranspiration and Its Role in Water Resources Management, ASAE, St. Joseph, MI, 57–61.
- Pruitt, W. O. (1971). "Factors affecting potential evapotranspiration." Biological effects in the hydrological cycle, Proc., 3rd Int. Seminar for Hydrology Professors, E. J. Monke, ed., Purdue Univ., West Lafayette, IN, 82–102.
- Pruitt, W. O., et al. (1984). "Microclimate, evapotranspiration, and water-use efficiency for drip- and furrow-irrigated tomatoes." Proc., 12th Congress Int. Commission on Irrigation Drainage, ICID, New Delhi, India, 367–394.
- Pruitt, W. O. (1984). "Procedures for development of  $ET_0$  maps for California." *Irrig. Drain. Bull.*, 32(2), 61–65.
- Pruitt, W. O. (1986). "Traditional methods: Evapotranspiration research priorities for the next decade." ASAE, St. Joseph, MI.
- Pruitt, W. O., and Angus, D. E. (1960). "Large weighing lysimeter for measuring evapotranspiration." *Trans. Am. Soc. Agr. Eng.*, 3(2), 13–15, 18.
- Pruitt, W. O., and Doorenbos, J. (1977). "Empirical calibration, a requisite for evapotranspiration formulae based on daily or longer mean climatic data?" Int. Round Table Conf. on Evapotranspiration, ICID, New Delhi, India.

- Pruitt, W. O., Fereres, E., Kaita, K., and Snyder, R. L. (1987a). "Reference evapotranspiration ( $ET_0$ ) for California." Univ. of California, Davis, CA.
- Pruitt, W. O., and Lourence, F. J. (1966). "Tests of aerodynamic, energy balance and other evaporation equations over a grass surface." Final Rep., USAEPG, Univ. of California, Davis, 37–63.
- Pruitt, W. O., and Lourence, F. J. (1985). "Experiences in lysimetry for ET and surface drag measurements." No. 74-85, ASAE, St. Joseph, MI, 51–69.
- Pruitt, W. O., Morgan, D. L., and Lourence, F. J. (1973). "Momentum and mass transfers in the surface boundary layer." *Q. J. R. Meteorolog. Soc.*, 99 (420), 370–386.
- Pruitt, W. O., Swann, B. D., Held, A., Sutton, B., Matista, A., and Hsiao, T. C. (1987b). "Bowen ratio and Penman: Australian-Californian tests." *Irrigation systems for the 21st century*, L. G. James and M. J. English, eds., ASCE, New York, 149–158.
- Quackenbush, T. H., and Phelan, J. T. (1965). "Irrigation water requirements of lawns." *J. Irrig. Drain. Div.*, 91(2), 11–20.
- Qualls, R., and Brutsaert, W. (1996). "Effect of vegetation density on the parameterization of scalar roughness to estimate spatially distributed sensible heat fluxes." *Water Resour. Res.*, 32(3), 645–652.
- Quinn, F. H. (1979). "An improved aerodynamic evaporation technique for large lakes with application to the International Field Year for the Great Lakes." *Water Resour. Res.*, 15(4), 935–940.
- Raes, D. (2004). "UPFLOW: Water movement in a soil profile from a shallow water table to the topsoil (capillary rise)." K. U. Leuven Univ., Leuven, Belgium.
- Raes, D., and deProost, P. (2003). "Model to assess water movement from a shallow water table to the root zone." *Agric. Water Manage.*, 62(2), 79–91.
- Raes, D., Steduto, P., Hsiao, T. C., and Fereres, E. (2009). "AquaCrop—The FAO crop model to simulate yield response to water: II. Main algorithms and software description." *Agron. J.*, 101(3), 438–447.
- Ramdas, L. A. (1957). "Evaporation and potential evapotranspiration over the Indian sub-continent." *Indian J. Agr. Sci.*, 27(2), 137–149.
- Rannik, U. (2001). "A comment on the paper by W. J. Massman: A simple method for estimating frequency response corrections for eddy covariance systems." *Agric. For. Meteorol.*, 107(3), 241–245.
- Ratliff, L. F., Ritchie, J. T., and Cassel, D. K. (1983). "Field-measured limits of soil water availability as related to laboratory-measured properties." *Soil Sci. Soc. Am. J.*, 47(4), 770–775.
- Rauner, J. L. (1976). "Deciduous forests." *Vegetation and the atmosphere*, J. L. Monteith, ed., Vol. 2, Academic Press, London, 241–264.
- Raupach, M. R. (1979). "Anomalies in flux-gradient relationships over forest." *Boundary Layer Meteorol.*, 16(3), 467–486.

- Raupach, M. R. (1989). "A practical Lagrangian method for relating scalar concentrations to source distributions in vegetation canopies." *Q. J. R. Meteorol. Soc.*, 115(487), 609–632.
- Raupach, M. R. (1994). "Simplified expressions for vegetation roughness length and zero-plane displacement as functions of canopy height and area index." *Boundary Layer Meteorol.*, 71(1–2), 211–216.
- Raupach, M. R., Antonia, R. A., and Rajagopalan, S. (1991). "Rough-wall turbulent boundary layers." *Appl. Mech. Rev.*, 44(1), 1–25.
- Raupach, M. R., and Finnigan, J. J. (1988). "Single-layer models of evaporation from plant canopies are incorrect but useful, whereas multilayer models are correct but useless." *Discuss. Funct. Plant Biol.*, 15(6), 705–716.
- Raupach, M. R., Finnigan, J. J., and Brunet, Y. (1996). "Coherent eddies and turbulence in vegetation canopies: The mixing-layer analogy." *Boundary Layer Meteorol.*, 78(3–4), 351–382.
- Reyenga, W., Dunin, F. X., Bautovich, B. C., Rath, C. R., and Hulse, L. B. (1988). "A weighing lysimeter in a regenerating eucalypt forest: Design, construction, and performance." *Hydrolog. Processes*, 2(4), 301–314.
- Rhoades, J. D. (1974). "Drainage for salinity control." *Drainage for agriculture*, J. van Schilfgaarde, ed., Soil Science Society of America, Madison, WI, 433–461.
- Rhoades, J. D., Chanduvi, F., and Lesch, S. (1999). "Soil salinity assessment: Methods and interpretation of electrical conductivity measurements." United Nations Food and Agriculture Organization, Rome.
- Rhoades, J. D., Kandiah, A., and Mashali, A. M. (1992). "The use of saline waters for crop production." United Nations Food and Agriculture Organization, Rome.
- Rhoades, J. D., and Merrill, S. D. (1976). "Assessing the suitability of water for irrigation: Theoretical and empirical approaches." Soils Bulletin 31, United Nations Food and Agriculture Organization, Rome, 69–109.
- Richards, L. A. (1931). "Capillary conduction of liquids through porous media." *Physics*, 1(5), 318–333.
- Richards, L. A., Gardner, W. R., and Ogata, G. (1956). "Physical processes determining water loss from soil." *Soil Sci. Soc. Am. Proc.*, 20(3), 310–314.
- Richie, W. E., and Pittenger, D. R. (2000). "Mixed landscape irrigation research findings." Proc., UCR Turfgrass and Landscape Management Research Conf., Univ. of California, Riverside, Riverside, CA, 12–13.
- Rijtema, P. E. (1965). "Analysis of actual evapotranspiration." Research Rep. 69, Centre for Agricultural Publication, Wageningen, Netherlands.
- Ringersma, J., and Sikking, A. F. S. (2001). "Determining transpiration coefficients of Sahelian vegetation barriers." *Agroforestry Syst.*, 51(1), 1–9.
- Ritchie, J., and NeSmith, D. S. (1991). *Temperature and crop development*, R. J. Hanks and J. T. Ritchie, eds., American Society of Agronomy, Madison, WI, 5–29.

- Ritchie, J. T. (1971). "Dryland evaporative flux in a subhumid climate: I. Micrometeorological influences." *Agron. J.*, 63(1), 51–55.
- Ritchie, J. T. (1972). "Model for predicting evaporation from a row crop with incomplete cover." *Water Resour. Res.*, 8(5), 1204–1213.
- Ritchie, J. T. (1974). "Evaluating irrigation needs for southeastern U.S.A." *Contribution of Irrigation and Drainage to the World Food Supply*, ASCE, New York, 262–279.
- Ritchie, J. T. (1991). "Wheat phasic development." *Modeling plant and soil systems*, R. J. Hanks and J. T. Ritchie, eds., American Society of Agronomy, Madison, WI, 31–54.
- Ritchie, J. T., and Adams, J. E. (1974). "Field measurement of evaporation from soil shrinkage cracks." *Soil Sci. Soc. Am. Proc.*, 38(1), 131–134.
- Ritchie, J. T., and Burnett, E. (1971). "Dryland evaporative flux in a subhumid climate: II. Plant influences." *Agron. J.*, 63(1), 56–62.
- Ritchie, J. T., Godwin, D. C., and Singh, U. (1989). "Soil and weather inputs for the IBSNAT crop models." Proc., IBSNAT Symp.: Decision Support System for Agrotechnology Transfer: Part 1, IBSNAT, Univ. of Hawaii, Honolulu, HI, 31–45.
- Ritchie, J. T., and Johnson, B. S. (1990). "Soil and plant factors affecting evaporation." *Irrigation of agricultural crops*, B. A. Stewart and D. R. Nielsen, eds., American Society of Agronomy, Madison, WI, 363–390.
- Ritchie, J. T., and Otter, S. (1985). "Description and performance of CERES-Wheat: A user-oriented wheat yield model." ARS Wheat Yield Project. ARS-38, National Technical Information Service, Springfield, VA, 159–175.
- Robins, J. R., Pruitt, W. O., and Gardner, W. H. (1954). "Unsaturated flow of water in field soils and its effect on soil moisture investigations." *Soil Sci. Soc. Am. Proc.*, 18(3), 344–347.
- Robinson, F. E. (1969). "Stands for automation achieved by sprinkling." *J. Irrig. Drain. Div.*, 95(3), 385–390.
- Robock, A., et al. (2003). "Evaluation of the North American Land Data Assimilation System over the southern Great Plains during the warm season." *J. Geophys. Res.*, 108(D22), 8846.
- Rochette, P., Pattey, E., Desjardins, R. L. O., Dwyer, L. W., and Stewart, D. W. (1991). "Estimation of maize canopy conductance by scaling up leaf stomatal conductance." *Agric. For. Meteorol.*, 54(2–4), 241–261.
- Rogers, J. S., Allen, L. H., and Calvert, D. J. (1983). "Evapotranspiration for humid regions: Developing citrus grove, grass cover." *Trans. ASAE*, 26(6), 1778–1783.
- Rohwer, C. (1931). "Evaporation from free water surfaces." USDA Tech. Bull. 271, USDA, Washington, DC.
- Rohwer, C. (1934). "Evaporation from water surfaces." *Trans. ASCE*, 99(1), 673–703.

- Rose, C. W. (1968a). "Evaporation from bare soil under high radiation conditions." *Trans. 9th Int. Cong. of Soil Science*, Vol. 1, International Society of Soil Science, Sydney, Australia, 57–66.
- Rose, C. W. (1968b). "Water movement in porous materials. III. Evaporation of water from soil." *Br. J. Appl. Phys.*, 1(12), 1779–1791.
- Rose, C. W., and Sharma, M. L. (1984). "Summary and recommendations of the workshop on evapotranspiration from plant communities." *Evapotranspiration from plant communities*, M. E. Sharma, ed., Elsevier, New York, 325–342.
- Rosenberg, N. J., Blad, B. L., and Verma, S. B. (1983). *Microclimate: The biological environment*, 2nd Ed., Wiley, New York.
- Rosenberry, D. O., Sturrock, A. M., and Winter, T. C. (1993). "Evaluation of the energy budget method of determining evaporation at Williams Lake, Minnesota, using alternative instrumentation and study approaches." *Water Resour. Res.*, 29(8), 2473–2483.
- Rossby, C. G., and Montgomery, R. B. (1935). "The layer of frictional influence in wind and ocean currents." Woods Hole Oceanographic Institution, MIT, Cambridge, MA.
- Rossow, W. B., and Garder, L. C. (1993). "Cloud detection using satellite measurements of infrared and visible radiances for ISCCP." *J. Clim.*, 6 (12), 2341–2369.
- Running, S. W. (1994). "Testing forest-BGC ecosystem process simulations across a climatic gradient in Oregon." *Ecol. Appl.*, 4(2), 238–247.
- Running, S. W., and Coughlan, J. C. (1988). "A general model of forest ecosystem processes for regional applications: I. Hydrologic balance, canopy gas exchange, and primary production processes." *Ecol. Modell.*, 42(2), 125–154.
- Rutter, A. J. (1975). "The hydrologic cycle in vegetation." *Vegetation and the atmosphere*, J. L. Monteith, ed., Vol. 1, Academic Press, New York, 11–54.
- Rutter, A. J., Morton, A. J., and Robins, P. C. (1975). "A predictive model of rainfall interception in forests: II. Generalization of the model and comparison with observations in some coniferous and hardwood stands." *J. Appl. Ecol.*, 12(1), 367–380.
- Ryan, P. J., Harleman, D. R. F., and Stolzenbach, K. D. (1974). "Surface heat loss from cooling ponds." *Water. Resour. Res.*, 10(5), 930–938.
- Ryu, Y., Baldocchi, D. D., Ma, S., and Hehn, T. (2008). "Interannual variability of evapotranspiration and energy exchanges over an annual grassland in California." *J. Geophys. Res.*, 113(D09), 104.
- Saadi, S., Todorovic, M., Tanasijevic, L., Pereira, L. S., Pizzigalli, C., and Lionello, P. (2014). "Climate change and Mediterranean agriculture: Impacts on winter wheat and tomato crop evapotranspiration, irrigation requirements and yield." *Agric. Water Manage.*, 147(2), 103–115.

- Saito, H., Šimůnek, J., and Mohanty, B. P. (2006). "Numerical analysis of coupled water, vapor, and heat transport in the vadose zone." *Vadose Zone J.*, 5(2), 784–800.
- Sakai, R. K., Fitzjarrald, D. R., and Moore, K. E. (2001). "Importance of low-frequency contributions to eddy fluxes observed over rough surfaces." *J. Appl. Meteorol.*, 40(12), 2178–2192.
- Sakuratani, T. (1981). "A heat balance method for measuring water flux in the stem of intact plants." *Jpn. Agric. Meteorol.*, 37(1), 9–17.
- Sammis, T. W. (1985). "Evapotranspiration crop coefficients predicted using growing-degree-days." *Trans. ASAE*, 28(3), 773–780.
- Sammis, T. W., Mexal, J. G., and Miller, D. (2004). "Evapotranspiration of flood-irrigated pecans." *Agric. Water Manage.*, 69(3), 179–190.
- Sarraf, S., and Bovée, A. C. J. (1973). "Evapotranspiration of bananas." IRA, Lebanon (in French).
- Saxton, K. E., and Willey, P. H. (2005). "The SPAW model for agricultural field and pond hydrologic simulation." *Mathematical modeling of watershed hydrology*, V. P. Singh and D. Frevert, eds., CRC Press, Boca Raton, FL.
- Schaap, M. G., and Bouten, W. (1996). "Forest floor evaporation in a dense Douglas fir stand." *J. Hydrol.*, 193(1–4), 97–113.
- Schaap, M. G., Leij, F. J., and van Genuchten, M. J. (1999). "Estimation of the soil hydraulic properties." *Vadose zone—Science and technology solutions*, B. B. Looney and R. W. Falt, eds., Battelle Press, Richland, WA, 501–509.
- Schmid, H. P. (2002). "Footprint modeling for vegetation atmosphere exchange studies: A review and perspective." *Agric. For. Meteorol.*, 113(1), 159–183.
- Schneider, A. D., and Howell, T. A. (1991). "Large, monolithic, weighing lysimeters." *Lysimeters for evapotranspiration and environmental measurements*, R. G. Allen, T. A. Howell, W. O. Pruitt, I. A. Walter, and M. E. Jensen, eds., ASCE, New York, 37–45.
- Schuepp, P. H., Leclerc, M. Y., MacPherson, J. I., and Desjardins, R. L. (1990). "Footprint prediction of scalar fluxes from analytical solutions of the diffusion equation." *Boundary Layer Meteorol.*, 50(1–4), 355–373.
- Scott, C. A., Bastiaanssen, W. G. M., and Ahmad, M. (2003). "Mapping root zone soil moisture using remotely sensed optical imagery." *J. Irrig. Drain. Eng.*, 10.1061/(ASCE)0733-9437(2003)129:5(326), 326–335.
- Seginer, I. (1974). "Aerodynamic roughness of vegetated surfaces." *Boundary Layer Meteorol.*, 5(4), 383–393.
- Seginer, I., Nir, D., and von Bernuth, R. D. (1991). "Simulation of wind-distorted sprinkler patterns." *J. Irrig. Drain. Eng.*, 10.1061/(ASCE)0733-9437(1991)117:2(285), 285–306.
- Sellers, P. J., and Dorman, J. L. (1987). "Testing the simple biosphere model (SIB) using point micrometeorological and biophysical data." *J. Clim. Appl. Meteorol.*, 26(5), 622–651.

- Sellers, W. D. (1965). *Physical climatology*, Univ. of Chicago Press, Chicago.
- Senay, G., and Verdin, J. (2003). "Characterization of yield reduction in Ethiopia using a GIS-based crop water balance model." *Remote Sens.*, 29(6), 687–692.
- Senay, G., Verdin, J., and Lietzow, R. (2005). "Global daily reference ET modeling and evaluation." Meeting of the American Geophysical Union, Washington, DC.
- Senay, G. B., Budde, M., Verdin, J. P., and Melesse, A. M. (2007). "A coupled remote sensing and simplified surface energy balance approach to estimate actual evapotranspiration from irrigated fields." *Sensors*, 7(6), 979–1000.
- Senay, G. B., Verdin, J. P., Lietzow, R., and Melesse, A. M. (2008). "Global daily reference evapotranspiration modeling and validation." *J. Am. Water Resour. Res.*, 44(4), 969–979.
- Sene, K. J. (1996). "Meteorological estimates for the water balance of a sparse vine crop growing in semiarid conditions." *J. Hydrol.*, 179(1), 259–280.
- Shackel, K. A., Johnson, R. S., Medawar, C. K., and Phene, C. J. (1992). "Substantial errors in estimates of sap flow using the heat balance technique on woody stems under field conditions." *J. Am. Soc. Hort. Sci.*, 117(2), 351–356.
- Shafer, M. A., Fiebrich, C. A., Arndt, D. S., Fredrickson, S. E., and Hughes, T. W. (2000). "Quality assurance procedures in the Oklahoma Mesonet." *J. Atmos. Oceanic Technol.*, 17(4), 474–494.
- Shalheveth, J., Mantell, A., Bielorai, H., and Shimshi, D., eds. (1981). "Irrigation of field and orchard crops under semi-arid conditions." International Irrigation Information Center, Bet Dagan, Israel.
- Sharma, M. L., ed. (1984). "Evapotranspiration from plant communities." *Development in Agricultural and Managed Forest Ecology*, Vol. 13, Elsevier, New York, 344.
- Sharma, M. L. (1985). "Estimating evapotranspiration." *Advances in irrigation*, D. Hillel, ed., Vol. 3, Academic Press, Chicago, 213–281.
- Shaw, R., and Snyder, R. L. (2003). "Evaporation and eddy correlation." *Encyclopedia of water science*, Marcel Dekker, New York, 235–237.
- Shawcroft, R. W., and Gardner, H. R. (1983). "Direct evaporation from soil under a row crop canopy." *Agric. Meteorol.*, 28(3), 229–238.
- Shuttleworth, W. J. (1984). "Eddy correlation of energy partition for Amazonian forest." *Q. J. R. Meteorolog. Soc.*, 110(466), 1143–1162.
- Shuttleworth, W. J. (1989). "Micrometeorology of temperate and tropical forest." *Phil. Trans. R. Soc.*, 324(1223), 299–334.
- Shuttleworth, W. J. (1991). "Evaporation models in hydrology." *Land surface evaporation, measurement, and parameterization*, T. J. Schmugge and J. C. André, eds., Springer, New York, 93–120.

- Shuttleworth, W. J. (1992). "Evaporation." Chapter 4, *Handbook of hydrology*, D. R. Maidment, ed., McGraw-Hill, New York.
- Shuttleworth, W. J., and Gurney, R. J. (1990). "The theoretical relationship between foliage temperature and canopy resistance in sparse crops." *Q. J. R. Meteorolog. Soc.*, 116(492), 497–519.
- Shuttleworth, W. J., and Wallace, J. S. (1985). "Evaporation from sparse crops—An energy combination theory." *Q. J. R. Meteorolog. Soc.*, 111 (469), 839–853.
- Sikka, A. K. (1993). "Modeling the influence of climate change on evapotranspiration and water yield." Ph.D. dissertation, Dept. of Civil Engineering, Utah State Univ., Logan, UT.
- Sikka, A. K., Gunderson, R. W., Limaye, A. S., and Riley, J. P. (1993). "Application of distributed parameter watershed model for determining the effects of climate change on water resources." *Management of irrigation and drainage systems: Integrated perspectives*, R. G. Allen, ed., ASCE, New York, 464–471.
- Šimůnek, J., Šejna, M., and van Genuchten, M. Th. (1998). "The HYDRUS-1D software package for simulating the one-dimensional movement of water, heat, and multiple solutes in variably-saturated media. Vers. 2.0." IGWMC-TPS-70, IGWMC, Golden, CO.
- Šimůnek, J., van Genuchten, M. Th., and Sejna, M. (2005). "The HYDRUS-1D software package for simulating the one-dimensional movement of water, heat, and multiple solutes in variably-saturated media." U.S. Salinity Laboratory, USDA-ARS, Riverside, CA.
- Šimůnek, J., Wendoroth, O., and van Genuchten, M. T. (1999). "Estimating unsaturated soil properties from laboratory tension disc infiltrometer experiments." *Water Resour. Res.*, 35(10), 2965–2979.
- Sinclair, T. R. (1984). "Leaf area development in field-grown soybeans." *Agron. J.*, 76(1), 141–146.
- Sinclair, T. R., Allen, L. H., and Lemon, E. R. (1975). "An analysis of errors in the calculation of energy flux densities above vegetation by a Bowen ratio profile method." *Boundary Layer Meteorol.*, 8(2), 129–139.
- Singh, R. K., and Irmak (Kilic), A. (2009). "Estimation of crop coefficients using satellite remote sensing." *J. Irrig. Drain Eng.*, 10.1061/(ASCE)IR.1943-4774.0000052, 597–608.
- Singh, R. K., Irmak (Kilic), A., Irmak, S., and Martin, D. L. (2008). "Application of SEBAL model for mapping evapotranspiration and estimating surface energy fluxes in south-central Nebraska." *J. Irrig. Drain. Eng.*, 10.1061/(ASCE)0733-9437(2008)134:3(273), 273–285.
- Slack, D. C., Martin, E. C., Sheta, A. E., Fox, F., Jr., Clark, L. J., and Ashley, R. O. (1996). "Crop coefficients normalized for climatic variability with growing-degree-days." Proc., Int. Conf. on Evapotranspiration and Irrigation Scheduling, ASAE, St. Joseph, MI, 892–898.

- Slatyer, R. O. (1967). *Plant water relationships*, Academic Press, New York.
- Slatyer, R. O., and McIlroy, I. C. (1961). *Practical climatology*, CSIRO, Melbourne, Australia.
- Sleight, R. B. (1917). "Evaporation from surfaces of water and riverbed materials." *J. Agric. Res.*, 10(5), 209–262.
- Smeal, D., Owen, C. K., Arnold, R. N., Tomko, J. F., and Gregory, E. J. (2001). "Thirty years of climatological data: 1969 to 1998." Research Rep. 744, New Mexico State Univ., Las Cruces, NM.
- Smith, M., Allen, R., Monteith, J., Perrier, A., Pereira, L., and Segeren, A. (1991). "Report of the expert consultation on procedures for revision of FAO guidelines for prediction of crop water requirements." UN-FAO, Rome.
- Smith, M., Allen, R. G., and Pereira, L. (1996). "Revised FAO methodology for crop water requirements." *Evapotranspiration and irrigation scheduling*, C. R. Camp, E. J. Sadler, and R. E. Yoder, eds., ASABE, St. Joseph, MI, 116–123.
- Snyder, R. L., and Eching, S. O. (2004). "Landscape irrigation management program." Univ. of California, Davis.
- Snyder, R. L. (1985). "Hand calculating degree days." *Agric. For. Meteorol.*, 35(1), 353–358.
- Snyder, R. L. (2004). "Hourly reference evapotranspiration ( $ET_o$ ) calculator user's guide for HRPM.EXE." (<http://biomet.ucdavis.edu/Evapotranspiration.html>) (Oct. 2015).
- Snyder, R. L., Brown, P. W., Hubbard, K. G., and Meyer, S. J. (1996). "A guide to automated weather station networks in North America." *Advances in climatology*, G. Stanhill, ed., Vol. 4, Springer, Berlin.
- Snyder, R. L., and de Melo-Abreu, J. P. (2000). "Frost protection: Fundamentals, practice, and economics." (<http://www.fao.org/3/a-y7223e.pdf>) (Oct. 2015).
- Snyder, R. L., and Eching, S. O. (2005). "Urban landscape evapotranspiration." *Landscape Water Use*, 4(1), 691–693.
- Snyder, R. L., Lanini, B. J., Shaw, D. A., and Pruitt, W. O. (1989a). "Using reference evapo-transpiration ( $ET_o$ ) and crop coefficients to estimate crop evapotranspiration ( $ET_c$ ) for agronomic crops, grasses, and vegetable crops." Univ. of California, Berkeley, CA.
- Snyder, R. L., Lanini, B. J., Shaw, D. A., and Pruitt, W. O. (1989b). "Using reference evapo-transpiration ( $ET_o$ ) and crop coefficients to estimate crop evapotranspiration ( $ET_c$ ) for trees and vines." Univ. of California, Berkeley, CA.
- Snyder, R. L., Orang, M., Matyac, S., and Grismer, M. E. (2005). "Simplified estimation of reference evapotranspiration from pan evaporation data in California." *J. Irrig. Drain. Eng.*, 10.1061/(ASCE)0733-9437(2005)131:3 (249), 249–253.

- Snyder, R. L., Spano, D., Cesaraccio, C., and Duce, P. (1999). "Determining degree-day thresholds from field observations." *Int. J. Biometeorol.*, 42(4), 177–182.
- Stanhill, G. (1962a). "The control of field irrigation practice from measurements of evaporation." *Israel J. Agric. Res.*, 12(2), 51–62.
- Stanhill, G. (1962b). "The use of the Piche evaporimeter in the calculation of evaporation." *Q. J. R. Meteorolog. Soc.*, 88(375), 80–82.
- Stanhill, G. (1976). "Cotton." *Vegetation and the atmosphere*, J. L. Monteith, ed., Vol. 2, Academic Press, London, 121–150.
- Stanhill, G. (1992). "Accuracy of global radiation measurements at unattended, automatic weather stations." *Agric. For. Meteorol.*, 61(1), 151–156.
- Staple, W. L., and Lehane, J. J. (1962). "Variability in soil moisture sampling." *Can. J. Soil Sci.*, 42(1), 157–164.
- State of California. (1975). "Vegetative water use in California, 1974." Sacramento, CA.
- Steiner, J. L., Howell, T. A., and Schneider, A. D. (1991). "Lysimetric evaluation of daily potential evaporation models for grain sorghum." *Agron. J.*, 83(1), 240–247.
- Steppe, K., de Pauw, D. J. W., Doody, T. M., and Teskey, R. O. (2010). "A comparison of sap flux density using thermal dissipation, heat pulse velocity and heat field deformation methods." *Agric. For. Meteorol.*, 150(7–8), 1046–1056.
- Stewart, B. A., and Howell, T. A., eds. (2003). *Encyclopedia of water science*, Marcel-Dekker, New York.
- Stewart, J. B. (1983). "A discussion of the relationships between the principal forms of the combination equation for estimating crop evaporation." *Agric. Meteorol.*, 30(2), 111–127.
- Stewart, J. B. (1988). "Modelling surface conductance of pine forest." *Agric. For. Meteorol.*, 43(1), 19–35.
- Stewart, J. B. (1989). "On the use of the Penman-Monteith equation for determining areal evapotranspiration." *Estimation of areal evapotranspiration*, T. A. Black, D. L. Spittlehouse, M. D. Novak, and D. T. Price, eds., IAHS, London, 3–12.
- Stewart, J. B., and Gay, L. W. (1989). "Preliminary modelling of transpiration from the FIFE site in Kansas." *Agric. For. Meteorol.*, 48(3), 305–315.
- Stewart, J. B., and Verma, S. B. (1992). "Comparison of surface fluxes and conductances at two contrasting sites within the FIFE area." *J. Geophys. Res.*, 97(D17), 628.
- Stewart, J. B., Watts, C. J., Rodriguez, J. C., De Bruin, H. A. R., van den Berg, A. R., and Garatuza-Payan, J. (1999). "Use of satellite data to estimate radiation and evaporation for northwest Mexico." *Agric. Water Manage.*, 38(3), 181–193.

- Stewart, R. B., and Rouse, W. R. (1977). "Substantiation of the Priestley-Taylor parameter  $\alpha = 1.26$  for potential evaporation at high latitudes." *J. Appl. Meteorol.*, 16(6), 649–650.
- St. Hilaire, R., et al. (2008). "Efficient water use in residential urban landscapes." *Hort Sci.*, 43(7), 2081–2092.
- Stone, L. R., Goodrum, D. E., Jaafar, M. N., and Khan, A. H. (2001). "Rooting front and water depletion depths in grain sorghum and sunflower." *Agron. J.*, 93(5), 1105–1110.
- Strelkoff, T. (1990). "SRFR: A computer program for simulating flow in surface irrigation furrows-basins-borders." WCL Rep. No. 17, U.S. Water Conservation Laboratory, USDA/ARS, Phoenix, AZ.
- Stull, R. B. (1988). *An introduction to boundary layer meteorology*, Kluwer, Dordrecht, Netherlands.
- Sturrock, A. M., Winter, T. C., and Rosenberry, D. O. (1992). "Energy budget evaporation from Williams Lake: A closed lake in north central Minnesota." *Water Resour. Res.*, 28(6), 1605–1617.
- Su, Z., Schugge, T., Kustas, W. P., and Massman, W. J. (2001). "An evaluation of two models for estimation of the roughness height for heat transfer between the land surface and the atmosphere." *J. Appl. Meteorol.*, 40(11), 1933–1951.
- Suleiman, A. A., and Ritchie, J. T. (2003). "Modeling soil water redistribution during second-stage evaporation." *Soil Sci. Soc. Am. J.*, 67(2), 377–386.
- Swanson, R. H. (1994). "Significant historical developments in thermal methods for measuring sap flow in trees." *Agric. For. Meteorol.*, 72(1–2), 113–132.
- Swift, L. W. (1976). "Algorithm for solar radiation on mountain slopes." *Water Resour. Res.*, 12(1), 108–112.
- Swinbank, W. C. (1951). "The measurement of vertical transfer of heat and water vapour by eddies in the lower atmosphere." *J. Meteorol.*, 8(3), 135–145.
- Swinbank, W. C. (1955). "An experimental study of eddy transports in the lower atmosphere." CSIRO, Division of Meteorological Physics, Melbourne, Australia.
- Szeicz, G., and Long, I. F. (1969). "Surface resistance of crop canopies." *Water Resour. Res.*, 5(3), 622–633.
- Szeicz, G., van Bavel, C., and Takami, S. (1973). "Stomatal factor in the water use and dry matter production by sorghum." *Agric. Meteorol.*, 12(3), 361–389.
- Szilagyi, J. (2007). "On the inherent asymmetric nature of the complementary relationship of evaporation." *Geophys. Res. Lett.*, 34, L02405.
- Tanji, K. K. (1990). "Conceptual irrigation return flow hydrosalinity model." *Agricultural salinity assessment and management*, K. K. Tanji, ed., ASCE, New York, 504–529.

- Tanner, B. D. (1988). "Use requirements for Bowen ratio and eddy correlation determination of evapotranspiration." *Planning now for irrigation and drainage in the 21st century*, D. R. Hay, ed., ASCE, New York, 605–616.
- Tanner, B. D., Swiatek, E., and Greene, J. P. (1993). "Density fluctuations and use of the krypton hygrometer in surface flux measurements." *Management of irrigation and drainage systems: Integrated perspectives*, R. G. Allen, ed., ASCE, New York, 945–952.
- Tanner, C. B. (1960). "Energy balance approach to evapotranspiration from crops." *Soil Sci. Soc. Am. Proc.*, 24(1), 1–9.
- Tanner, C. B. (1967). "Measurement of evapotranspiration." *Irrigation of agricultural lands*, R. M. Hagan, H. R. Haise, and T. W. Edminster, eds., American Society of Agronomy, Madison, WI, 534–574.
- Tanner, C. B. (1968). "Evaporation of water from plants and soils." *Water deficits and plant growth*, T. T. Kozlowski, ed., Vol. 1, Academic Press, New York, 73–106.
- Tanner, C. B., and Jury, W. A. (1976). "Estimating evaporation and transpiration from a crop during incomplete cover." *Agron. J.*, 68(2), 239–242.
- Tanner, C. B., and Pelton, W. L. (1960). "Potential evapotranspiration estimates by the approximate energy balance method of Penman." *J. Geophys. Res.*, 65(10), 3391–3413.
- Tasumi, M. (2003). "Progress in operational estimation of regional evapotranspiration using satellite imagery." Ph.D. Dissertation, Univ. of Idaho, Moscow, ID.
- Tasumi, M., Allen, R. G., Trezza, R., and Wright, J. L. (2005a). "Satellite-based energy balance to assess within-population variance of crop coefficient curves." *J. Irrig. Drain Eng.*, 10.1061/(ASCE)0733-9437(2005)131:1(94), 94–109.
- Tasumi, M., and Allen, R. G. (2007). "Satellite-based ET mapping to assess variation in ET with timing of crop development." *Agric. Water Manage.*, 88(1–3), 54–62.
- Tasumi, M., Allen, R. G., and Trezza, R. (2008). "At-surface reflectance and albedo from satellite for operational calculation of land surface energy balance." *J. Hydrol. Eng.*, 10.1061/(ASCE)1084-0699(2008)13:2(51), 51–63.
- Tasumi, M., Trezza, R., Allen, R. G., and Wright, J. L. (2005k). "Operational aspects of satellite-based energy balance models for irrigated crops in the semi-arid U.S." *Irrig. Drain. Syst.*, 19(3–4), 355–376.
- Taylor, H. M. (1983). "Managing root systems for efficient water use: An overview." *Limitations to efficient water use in crop production*, H. M. Taylor, W. R. Jordan, and T. R. Sinclair, eds., American Society of Agronomy, Madison, WI, 87–113.
- Taylor, S. A. (1955). "Field determination of soil moisture." *Agric. Eng.*, 36(4), 645–659.

- Testi, L., Villalobos, F. J., and Orgaza, F. (2004). "Evapotranspiration of a young irrigated olive orchard in southern Spain." *Agric. For. Meteorol.*, **121**(1–2), 1–18.
- Tetens, O. (1930). "Über einige meteorologische Begriffe." *Z. Geophys.*, **6**(3), 297–309.
- Thilini, J., Shridhar, V., Huntington, J., and Khanal, M. (2013). "Evaluation of the complementary relationship using Noah land surface model and North American regional reanalysis (NARR) data to estimate evapotranspiration in semiarid ecosystems." *J. Hydrometeorol.*, **14**(1), 345–359.
- Thom, A. S. (1971). "Momentum absorption by vegetation." *Q. J. R. Meteorol. Soc.*, **97**(414), 414–428.
- Thom, A. S. (1972). "Momentum, mass and heat exchange of vegetation." *Q. J. R. Meteorol. Soc.*, **98**(415), 124–134.
- Thom, A. S., Stewart, J. B., Olivier, H. R., and Gash, J. H. C. (1975). "Comparison of aerodynamic and energy budget estimates of fluxes over a pine forest." *Q. J. R. Meteorol. Soc.*, **101**(427), 93–105.
- Thom, A. S., Thony, J. L., and Vauclin, M. (1981). "On the proper employment of evaporation pans and atmometers in estimating potential transpiration." *Q. J. R. Meteorol. Soc.*, **107**(453), 711–736.
- Thorntwaite, C. W. (1948). "An approach toward a rational classification of climate." *Geogr. Rev.*, **38**(1), 55–94.
- Thorntwaite, C. W., and Holzman, B. (1939). "The determination of evaporation from land and water surfaces." *Mon. Rev.*, **67**(1), 4–11.
- Thorntwaite, C. W., and Holzman, B. (1942). "Measurement of evaporation from land and water surfaces." Technical Bull. 817, USDA, Washington, DC.
- Thornton, P. E., and Running, S. W. (1999). "An improved algorithm for estimating incident daily solar radiation from measurements of temperature, humidity and precipitation." *Agric. For. Meteorol.*, **93**(4), 211–228.
- Todd, R. W., Evett, S. R., and Howell, T. A. (1998). "Latent heat flux of irrigated alfalfa measured by weighing lysimeter and Bowen ratio-energy balance." ASAE Summer Meeting, ASAE, St. Joseph, MI.
- Todd, R. W., Evett, S. R., Howell, T. A., and Klocke, N. L. (2000). "Soil temperature and water evaporation of small steel and plastic lysimeters replaced daily." *Soil Sci.*, **165**(11), 890–895.
- Tolk, J. A., and Howell, T. A. (2001). "Measured and simulated evapotranspiration of grain sorghum with full and limited irrigation in three high plains soils." *Trans. ASAE*, **44**(6), 1553–1558.
- Tolk, J. A., Howell, T. A., and Evett, S. R. (2006). "Nighttime evapotranspiration from alfalfa and cotton in a semiarid climate." *Agron. J.*, **98**, 730–736.

- Tolk, J. A., Howell, T. A., Steiner, J. L., Krieg, D. R., and Schneider, A. D. (1995). "Role of transpiration suppression by evaporation of intercepted water in improving irrigation efficiency." *Irrig. Sci.*, **16**(2), 89–95.
- Trask, J. C. (2007). "Resolving hydrologic water balances through novel error analysis with focus on inter-annual and long-term variability in the Tahoe Basin." Ph.D. dissertation, Univ. of California, Davis.
- Turc, L. (1961). "Estimation of irrigation water requirements, potential evapotranspiration: A simple climatic formula evolved up to date." *Ann. Agron.*, **12**(1), 13–49.
- Turner, N. C. (1979). "Drought resistance and adaptation to water deficits in crop." *Stress physiology in crop plants*, H. Mussell and R. C. Staples, eds., Wiley, New York, 343–372.
- Turner, N. C. (1991). "Measurement and influence of environmental and plant factors on stomatal conductance in the field." *Agric. For. Meteorol.*, **54**, 137–154.
- Twine, T. E., et al. (2000). "Correcting eddy-covariance flux underestimates over a grassland." *Agric. For. Meteorol.*, **103**(3), 279–300.
- USACE (U.S. Army Corps of Engineers). (1995). "CE-QUAL-R1: A numerical one-dimensional model of reservoir quality: User's manual." Rep. No. E-82-1, Vicksburg, MS.
- USDA (U.S. Department of Agriculture). (1967). "Irrigation water requirements." Technical Rep. No. 21, Washington, DC.
- USDA (U.S. Department of Agriculture). (1970). "Irrigation water requirements." Technical Rep. No. 21, Washington, DC.
- USDA (U.S. Department of Agriculture). (1974). "Border irrigation." Chapter 4, *National engineering handbook*, Washington, DC.
- USDA (U.S. Department of Agriculture). (1984). "Furrow irrigation." Chapter 5, *National engineering handbook*, Washington, DC.
- USDA (U.S. Department of Agriculture). (1999). *Soil taxonomy: A basic system of soil classification for making and interpreting soil surveys*, 2nd Ed., Washington, DC.
- U.S. Dept. of Commerce. (1968). "Climatic atlas of the United States." Asheville, NC.
- USGS (U.S. Geological Survey). (1954). "Water-loss investigations: Lake Hefner studies." Technical Rep., Reston, VA.
- USGS (U.S. Geological Survey). (1958). "Water-loss investigations: Lake Mead studies." Reston, VA.
- U.S. Salinity Laboratory Staff. (1954). "Diagnosis and improvement of saline and alkali soils." Washington, DC.
- Valancogne, C., and Nasr, Z. (1989). "Une méthode de mesure du débit de sève brute dans de petits arbres par bilan de chaleur." *Agronomie*, **9**(6), 609–617.

- Valancogne, C., and Nasr, Z. (1993). "A heat balance method for measuring sap flow in small trees." *Water transport in plants under climatic stress*, M. Borghetti, J. Grace, and A. Raschi, eds., Cambridge University Press, Cambridge, U.K., 166–173.
- Valle, R., Mishoe, J. W., Jones, J. W., and Allen, L. H. (1985). "Transpiration rate and water use efficiency of soybean leaves adapted to different CO<sub>2</sub> environments." *Crop Sci.*, 25(3), 477–481.
- van Bavel, C. H. M., and Ehrler, W. L. (1968). "Water loss from a sorghum field and stomatal control." *Agron. J.*, 60(1), 84–86.
- van Bavel, C. H. M., Fritsch, L. J., and Reeves, W. E. (1963). "Transpiration by sudangrass as an externally controlled process." *Science*, 141(3577), 269–270.
- van de Griend, A. A., and Owe, M. (1994). "Bare soil surface resistance to evaporation by vapor diffusion under semiarid conditions." *Water Resour. Res.*, 30(2), 181–188.
- van de Griend, A. A., and van Boxel, J. H. (1989). "Water and surface energy balance model with a multilayer canopy representation for remote sensing purposes." *Water Resour. Res.*, 25(5), 949–971.
- Van den Brink, C., Strommen, N. D., and Kenworthy, A. L. (1971). "Growing degree days in Michigan." Research Rep. No. 131, Michigan State Univ., East Lansing, MI.
- van den Hurk, B. J. J. M., and McNaughton, K. G. (1995). "Implementation of near-field dispersion in a simple two-layer surface resistance model." *J. Hydrol.*, 166(3–4), 293–311.
- van Genuchten, M. Th., Leij, F. J., and Yates, S. R. (1991). "The RETC code for quantifying the hydraulic functions of unsaturated soils." EPA Rep. 600/2-91/065, U.S. Salinity Laboratory, USDA, ARS, Riverside, CA.
- Van Hylckama, T. E. A. (1968). "Water level fluctuation in evapotranspirometers." *Water Resour. Res.*, 4(4), 761–768.
- van Wijk, W. R., and de Vries, D. A. (1963). "Periodic temperature variations in a homogeneous soil." *Physics of the plant environment*, W. R. van Wijk, ed., North-Holland, Amsterdam, Netherlands, 102–143.
- Veihmeyer, F. J., and Hendrickson, A. H. (1955). "Does transpiration decrease as the soil moisture decreases?" *Trans. Am. Geophys. Union*, 36(3), 425–448.
- Ventura, F., et al. (2001). "Model for estimating evaporation and transpiration from row crops." *J. Irrig. Drain. Eng.*, 10.1061/(ASCE)0733-9437(2001)127:6(339), 339–345.
- Venturini, V., Krepper, C., and Rodriguez, L. (2012). "Evapotranspiration estimation based on the complementary relationships." Chapter 2, *Evapotranspiration—Remote sensing and modeling*, Ayse Irmak (Kilic), ed., Intech, Rijeka, Croatia.
- Verma, S. B. (1989). "Aerodynamic resistances to transfers of heat, mass and momentum." *Estimation of areal evapotranspiration*, T. A. Black,

- D. L. Spittlehouse, M. D. Novak, and D. T. Price, eds., IAHS, London, 13–20.
- Verma, S. B., Baldocchi, D. D., Anderson, D. E., Matt, D. R., and Clement, R. J. (1986). "Eddy fluxes of CO<sub>2</sub>, water vapour, and sensible heat over a deciduous forest." *Boundary Layer Meteorol.*, 36(1–2), 71–91.
- Verma, S. B., Kim, J., and Clement, R. J. (1989). "Carbon dioxide, water vapor and sensible heat fluxes over a tallgrass prairie." *Boundary Layer Meteorol.*, 46(1–2), 53–67.
- Verma, S. B., Kim, J., and Clement, R. J. (1992). "Momentum, water vapor, and carbon dioxide exchange at a centrally located prairie site during FIFE." *J. Geophys. Res.*, 97(D17), 639.
- Vickers, D., and Mahrt, L. (1997). "Quality control and flux sampling problems for tower and aircraft data." *J. Atmos. Oceanic Technol.*, 14(3), 512–526.
- Vickers, D., and Mahrt, L. (2003). "The cospectral gap and turbulent flux calculations." *J. Atmos. Oceanic Technol.*, 20(5), 660–672.
- Villagarcía, L., Were, A., Domingo, F., García, M., and Alados-Arboledas, L. (2007). "Estimation of soil boundary-layer resistance in sparse semiarid stands for evapotranspiration modeling." *J. Hydrol.*, 342(1–2), 173–183.
- Villagarcía, L., Were, A., García, M., and Domingo, F. (2010). "Sensitivity of a clumped model of evapotranspiration to surface resistance parameterisations: Application in a semi-arid environment." *Agric. For. Meteorol.*, 150(7), 1065–1078.
- Villalobos, F. J. (1997). "Correction of eddy covariance water vapor flux using additional measurements of temperature." *Agric. For. Meteorol.*, 88 (1), 77–83.
- Villalobos, F. J., and Fereres, E. (1990). "Evaporation measurements beneath corn, cotton, and sunflower canopies." *Agron. J.*, 82(6), 1153–1159.
- Villalobos, F. J., Orgaz, F., Testi, L., and Fereres, E. (2000). "Measurement and modeling of evapotranspiration of olive orchards." *Eur. J. Agron.*, 13(2), 155–163.
- Waggoner, P. E., and Turner, N. C. (1971). "Transpiration and its control by stomata in a pine forest." Connecticut Agricultural Experiment Station, Hanford, CT.
- Walker, W. R. (1989). "Guidelines for designing and evaluating surface irrigation systems." FAO of the United Nations, Rome.
- Walker, W. R., and Skogerboe, G. V. (1987). *Surface irrigation: Theory and practice*, Prentice-Hall, Englewood Cliffs, NJ.
- Wallender, W. W., and Tanji, K. K., eds. (2011). *Agricultural salinity assessment and management*, 2nd Ed., ASCE, Reston, VA.
- Walter, I. A., et al. (2000). "ASCE's standardized reference evapotranspiration equation." *Watershed management and operations management 2000*, M. Flug, D. Frevert, and D. W. Watkins, Jr., eds., ASCE, Reston, VA, 1–11.

- Wandmacher, C., and Johnson, A. I. (1995). *Metric units in engineering: Going SI*, ASCE, New York.
- Wang, J., Sammis, T. W., Andales, A. A., Simmons, L. J., Gutschick, V. P., and Miller, D. R. (2007). "Crop coefficients of open-canopy pecan orchards." *Agric. Water Manage.*, 88(1), 253–262.
- Weaver, H. L., Weeks, E. P., Campbell, G. S., Stannard, D. I., and Tanner, B. D. (1986). "Phreatophyte water use estimated by eddy-correlation methods." *Water forum '86: World water issues in evolution*, ASCE, New York, 847–854.
- Webb, E. K. (1970). "Profile relationships: The log-linear range, and extension to strong stability." *Q. J. R. Meteorol. Soc.*, 96(407), 67–90.
- Webb, E. K., Pearman, G. I., and Leuning, R. (1980). "Correction of flux measurements for density effects due to heat and water vapour transfer." *Q. J. R. Meteorol. Soc.*, 106(447), 85–100.
- Were, A., Villagarcía, L., Domingo, F., Alados-Arboledas, L., and Puigdefábregas, J. (2007). "Analysis of effective resistance calculation methods and their effect on modeling evapotranspiration in two different patches of vegetation in semi-arid SE Spain." *Hydrol. Earth Sci. Discuss.*, 4(1), 243–286.
- Were, A., Villagarcía, L., Domingo, F., and Moro, M. J. (2008). "Aggregating spatial heterogeneity in a bush vegetation patch in semi-arid SE Spain: A multi-layer model versus a single-layer model." *J. Hydrol.*, 349 (1–2), 156–167.
- Whitlock, C. H., et al. (1995). "First global WCRP shortwave surface radiation budget data set." *Bull. Am. Meteorol. Soc.*, 76(6), 1–18.
- Wilczak, J. M., Oncley, S. P., and Stage, S. A. (2001). "Sonic anemometer tilt correction algorithms." *Boundary Layer Meteorol.*, 99(1), 127–150.
- Wilson, K. B., et al. (2002). "Energy balance closure at FLUXNET sites." *Agric. For. Meteorol.*, 113(1), 223–243.
- Wolfe, J. W., Brooks, R. H., and Lombard, P. B. (1972). "Measurement of the frost protection capability of a sprinkler irrigation system in an orchard." Rep. 346, Oregon State Univ., Corvallis, OR.
- Wootton, T. P., Cecilio, C. H., Fowler, L. C., and Hui, S. L. (1996). *Hydrology handbook*, 2nd Ed., ASCE, New York.
- World Meteorological Organization. (1966). "Measurement and estimation of evaporation and evapotranspiration." Working Group on Evaporation Measurement, WMO, Geneva.
- World Meteorological Organization. (1970). "Guide to hydrometeorological practices." WMO No. 168.TP.82, Geneva, Switzerland.
- World Meteorological Organization. (1973). "Comparison between pan and lake evaporation." WMO Pub. No. 354, Geneva, Switzerland.
- Wright, J. L. (1981). "Crop coefficients for estimates of daily crop evapotranspiration." ASCE, New York.

- Wright, J. L. (1982). "New evapotranspiration crop coefficients." *J. Irrig. Drain. Div.*, 108(1), 57–74.
- Wright, J. L. (1988). "Daily and seasonal evapotranspiration and yield of irrigated alfalfa in southern Idaho." *Agron. J.*, 80(4), 662–669.
- Wright, J. L. (1993). "Nongrowing season ET from irrigated fields." *Management of irrigation and drainage systems: Integrated perspectives*, ASCE, New York, 1005–1014.
- Wright, J. L. (1995). "Calibrating an ET procedure and deriving ET crop coefficients." Proc., 1995 Specialty Seminar, Water Resources Commission, American Consulting Engineering Council of Colorado, Colorado State Engineers Office, Denver, CO.
- Wright, J. L. (2001). "Growing degree day functions for use with evapotranspiration crop coefficients." Agronomy Abstracts (CD-ROM), American Society of Agronomy, Madison, WI.
- Wright, J. L., Allen, R. G., and Howell, T. A. (2000). "Conversion between evapotranspiration references and methods." Proc., 4th Decennial National Irrigation Symp., ASAE, St. Joseph, MI, 251–259.
- Wright, J. L., and Jensen, M. E. (1972). "Peak water requirements of crops in southern Idaho." *J. Irrig. Drain. Div.*, 96(1), 193–201.
- Xuebao, W., Jun, L., Wenjian, Z., and Fang, W. (2005). "Atmospheric profile retrieval with AIRS data and validation at the ARM CART site." *Adv. Atmos. Sci.*, 22(5), 647–654.
- Yang, D., et al. (1998a). "Accuracy of NWS 80 standard nonrecording precipitation gauge: Results and application of WMO intercomparison." *J. Atmos. Oceanic Technol.*, 15(1), 54–68.
- Yang, D., Goodison, B. E., Ishida, B., and Benson, C. S. (1998b). "Adjustment of daily precipitation data at 10 climate stations in Alaska: Application of World Meteorological Organization intercomparison results." *Water Resour. Res.*, 34(2), 241–256.
- Yang, D., Ishida, S., Goodison, B. E., and Gunther, T. (1999). "Bias correction of daily precipitation measurements for Greenland." *J. Geophys. Res. Atmos.*, 104(D6), 6171–6181.
- Yazar, A. (1984). "Evaporation and drift losses from sprinkler systems under operating conditions." *Agric. Water Manage.*, 8(4), 439–449.
- Yoshioka, G. A., and Mather, J. R. (1967). "Influence of site and exposure evapotranspiration." *Climatology*, 20(2), 253–266.
- Young, A. A. (1947). "Evaporation from water surfaces in California: A summary of pan records and coefficients 1881 to 1946." State of California, Dept. of Public Works, Division of Water Resources, Sacramento, CA.
- Yuana, F., and Zhiming, L. (2005). "Analytical solutions for vertical flow in unsaturated, rooted soils with variable surface fluxes." *Vadose Zone J.*, 4, 1210–1218.

- Zeng, X., and Wang, A. 2007. "Consistent parameterization of roughness length and displacement height for sparse and dense canopies in land models." *J. Hydrometeorol.*, 8(4), 730–737.
- Zhang, B., Kang, S., Li, F., and Zhang, L. (2008). "Comparison of three evapotranspiration models to Bowen ratio-energy balance method for a vineyard in an arid desert region of northwest China." *Agric. For. Meteorol.*, 148(10), 1629–1640.
- Zhao, L., et al. (2006). "Diurnal, seasonal and annual variation in net ecosystem CO<sub>2</sub> exchange of an alpine shrubland on Qinghai-Tibetan plateau." *Global Change Biol.*, 12(10), 1940–1953.
- Zhao, W., and Allen, R. G. (2012). "Placing soil heat flux plates at two depths for ground heat flux integrity assessment." Univ. of Idaho, Kimberly, ID.
- Zhao, W., and Allen, R. G. (2013). "Aerodynamic roughness of lodgepole pine forest near Yellowstone National Park based on sonic anenometer measurements." Univ. of Idaho, Kimberly, ID.
- Zhao, W., and Allen, R. G. (2014). "Rigorous intercomparison of four-component radiometers." Univ. of Idaho, Kimberly, ID.
- Zhao, W., Qualls, R. J., and Berliner, P. J. (2008). "A two-concentric-loop iterative method in estimation of displacement height and roughness length for momentum and sensible heat." *Int. J. Biometeorol.*, 52(8), 849–858.
- Zhao, W. Z., Ji, X. B., Kang, E. S., Zhang, Z. H., and Jin, B. W. (2010). "Evaluation of Penman-Monteith model applied to a maize field in the arid area of northwest China." *Hydrol. Earth Syst. Sci. Discuss.*, 7(1), 461–491.
- Zhongmin, H., et al. (2009). "Partitioning of evapotranspiration and its controls in four grassland ecosystems: Application of a two-source model." *Agric. For. Meteorol.*, 149(9), 1410–1420.
- Zinke, P. J. (1967). "Forest interception studies in the United States." *Forest hydrology*, W. E. Sopper and H. W. Lull, eds., Pergamon, Oxford, U.K., 137–161.

# INDEX

**Page numbers followed by *e*, *f*, and *t*  
indicate equations, figures, and tables.**

- absolute humidity, 36, 38, 38*e*
- actual evapotranspiration, 141
- adiabatic process, 39, 41–42, 163, 178–179
- advection: estimation methods, 87, 90–93, 90*e*, 126, 633, 653–654; lysimetry and, 31; remote sensing and, 545–546; water bodies and, 25, 116, 131–132, 137; weather data integrity and, 590, 593, 597
- aerodynamic and gradient transport theory, evolution of estimation methods, 13
- aerodynamic fluxes using iterative energy balance (AFIB) method, 326, 329–332, 330*e*, 331*e*, 338, 341–342, 374, 375–377*t*, 378–379, 431–432; weather measurement and use of, 387–395, 390*f*, 392*f*, 394*e*, 395*e*
- aerodynamic method (mass transfer): combined energy balance method, 176–178, 176*e*, 177*e*; water surfaces evaporation, 110–113, 110*e*, 111*e*, 112*e*
- aerodynamic parameters, for Penman-Monteith equation, 192–195, 193*e*, 194*e*
- agricultural crops, evaporation rates and, 23
- air: density of, 467–468*t*; physical properties of, 41–42, 41*e*, 42*e*, 42*t*, 43*t*
- air temperature: estimates of missing solar data and, 209–210, 209*e*; evaporation rates and, 22; missing data and reference ET, 212, 212*e*; Penman-Monteith application and, 389–393, 390*f*, 392*f*; water requirement estimates and, 429–430; weather data integrity, 587–601, 589*f*, 590*f*, 591*e*, 591*f*, 592*e*, 592*t*, 593*e*, 594*e*, 594*t*, 597*f*, 598*f*, 599*f*, 600*f*, 601*f*. *See also* temperature estimation methods
- air-entry pressure, 45, 47, 47*f*
- albedo: ASCE standardized estimation process, 96, 119; defined, 25; remote sensing and, 551–552; snow-covered surfaces, 316; soil evaporation and, 28; water bodies and surfaces, 25, 73–74, 74*t*, 113–114, 126; Wright estimation of, 630, 630*e*
- ALEXI model, 550
- alfalfa references, 94–96, 196–197
- alfalfa-based crop coefficients, 265–266, 285–287, 287*f*; estimation methods evaluated, 645–646, 648, 648*e*
- American Society of Agricultural Engineers (ASAE), 10–11
- ASCE Standardized Penman-Monteith Reference Method: basal crop coefficients for temperate and continental climates, 523–541; mean and basal crop coefficients for temperate and continental climates, 513–521
- ASCE standardized references, 96–97
- atmometers, 12, 214, 218–220
- atmosphere. *See air entries*; soil-plant-atmosphere system

- automated weather stations (AWS), 423, 570–571, 588, 603, 604*f*  
 available water, defined, 49*t*, 50
- bare soils: evaporation rates and, 27–28; wintertime and nongrowing seasons estimates of crop coefficient, 313–314
- barometric pressure, 41–42, 42*t*, 43*t*, 91, 112, 621–622, 621*e*
- basal crop coefficients, 262, 267–269, 268*e*; in subhumid climates, 499–509*t*, 510*t*, 511–512*t*; use of FAO in calculations, 282–285, 282*e*, 283*f*, 284*f*
- basal crop coefficients, for temperate and continental climates, 523–541; application of curves with good CGDD basis, 525*e*, 528–531*t*, 531–535; basics of, 523–524; conversion of curves of Wright to normalized GDD base, 525–527, 528–531*t*, 532*f*, 533*f*; growing degrees basis, 524–525, 524*e*, 525*e*; growing season beginning and end, 201*t*, 535–538, 536*f*, 537*f*, 538*t*; growing season estimation, 539, 539*f*, 540*f*, 541, 541*f*; killing frost estimation, 538–539. *See also* mean and basal crop coefficients, for temperate and continental climates
- Bellani-Livingston evaporimeter, 219
- Blaney-Criddle Method: evaluation of, 654, 656; FAO, 635–636, 635*e*; SCS, 634–635, 634*e*, 637, 648, 648*e*, 654, 659
- blossom delay, water requirements, 444
- boundary layer measurement, upwind fetch requirements, 172–175, 172*e*, 173*t*, 174*e*
- boundary layer stability, correcting for, 177–178, 177*e*
- Bowen ratio energy balance (BREB) measurement method: basics of, 32, 99; evolution of estimation methods, 15; example applications, 168; fetch requirements and boundary layer, 171, 173–175, 174*e*; land surfaces, 152–154*t*, 162–168, 163*e*, 164*f*, 167*f*; land surfaces, typical problems, 166–168, 167*f*; Penman-Monteith equation and, 403, 405; regional evapotranspiration and, 416–417
- Brutsaert-Gardner analytical procedure, capillary flow from shallow water table, 372*f*, 609–611, 610*e*, 612*f*
- bulk surface resistance, in soil-plant-atmosphere system, 55
- bulk surface resistance, Penman-Monteith equation and, 355; general surface resistance values, 357–361*t*, 363–374, 364*t*, 365*e*, 366*e*, 367*e*, 368*e*, 369*f*, 372*f*; resistance and leaf area, 193*e*, 194*e*, 355–356, 357–367*t*, 362–363, 362*e*
- California Irrigation Management Information System (CIMIS), 71–72, 213, 424, 582; CIMIS Penman method, 630–631
- canopy wetting, 307–308, 307*e*, 308*e*, 309*t*, 310*t*, 311
- capillary flow, from shallow water table, 609–617; Brutsaert-Gardner analytical procedure, 372*f*, 609–611, 610*e*, 612*f*; UPFLOW simulation model, 609, 610*e*, 611–613, 613*f*, 614*t*, 615*t*, 616*f*, 617*e*, 617*f*
- capillary rise (CR), 270–271, 610–611, 610*e*, 612*f*, 616–617, 617*e*
- CE-THERM model, 126
- CIMEC (calibration using inverse modeling at extreme conditions), 549–550, 552
- climate and land process models, gridded weather data from, 213–214
- climate parameter calculation, estimation methods evaluated, 641, 646*t*, 647*t*
- “clothesline effect,” 264–265, 288–289, 547
- cloudless day solar radiation, 62–66, 63*e*, 63*f*, 64*e*, 65*e*, 66*e*, 66*f*, 69, 69*e*
- combination estimation methods, 627; CIMIS Penman Method, 630–631; evaluation of, 638*t*, 639*t*, 640*t*, 650*t*, 651*t*, 653; 1963 Penman Method, 628;

- 1982 Kimberly Penman Method, 629–630, 629e, 630e; Penman classical equation, 627–628, 627e; Penman FAO 24 method, 628–629, 628e, 629e
- combined energy balance and mass transfer methods, 176; integrated stability functions, 179–187, 180e, 181e, 182e, 184f, 186f; mass transfer with aerodynamic expressions, 176–178, 176e, 177e; sensible heat from temperature differences, 178–179, 178e
- complimentary approach, to estimating regional evaporation, 418–419, 418e
- consumptive use (CU). *See also* evapotranspiration
- conversion factors, 458–462t
- crop coefficient method, 29, 261–322; alfalfa-based crop coefficients, 265–266, 285–287, 287f; American and European terminology, 267; basics, 261–265, 321–322; curves estimates for natural and agricultural vegetation, 287–294, 288f, 289e, 289f, 290e, 291e, 292e, 293f, 510t; documentation for, 543–567; estimates during winter and nongrowing seasons, 74t, 277f, 313–319, 316e, 316f, 317f, 318f, 319f, 320f, 321; FAO grass-based crop coefficients, 273–285, 273f, 274f, 275e, 276e, 277f, 278e, 279f, 281f, 282e, 282f, 283f, 284f; field-scale applications, 263–264; small expanses of vegetation, 264–265; variables, 263, 263e; vegetative cover coefficients, 262, 265–273, 266f, 268e, 269e, 270e, 271e, 272e, 273e; water requirement estimates and, 430–431. *See also* landscape coefficients
- crop coefficient-based evaporation model, 230–232, 230e, 231e
- crop development stages, 488–497t
- cultivated areas: data sources, 422–423; energy balance application to, 420–421
- cumulative growing degree days (CGDD). *See* basal crop coefficients, for temperate and continental climates
- Darcy's law, 47–48, 47e, 48e
- day of year table, 469t
- dead vegetation, wintertime and nongrowing seasons estimates of crop coefficient, 277f, 314
- deep percolation, 243–244, 436, 445; flux density and, 143–146; from root zone, 270–272, 271e, 272e
- deep water bodies, evaporation rates and, 25, 27, 128–131, 129f, 130f
- depletion levels, of soil water, 53–54, 54e
- dew point temperature, 39, 39e
- diffuse radiation, 62–65, 65e
- drained upper limit. *See* field capacity
- dry surface, applying Penman-Monteith to, 374, 375t, 376–377t, 378–379
- "duty of water," 9
- Duty of Water Committee, of ASCE, 9, 12, 13
- eddy covariance measurement method, 32–33; land surfaces and, 154–156t, 168–172, 169e, 170f; regional evapotranspiration and, 416–417; software programs to correct, 170
- effective full cover, 52, 52e, 279–280, 286, 315, 514–515, 523–527, 528t, 533
- energy balance, 10, 59–85; application to forests and grasslands, 419–420; application to regional cultivated lands, 420–421; basics of, 59–61, 60e, 60f; remote sensing and documentation, 549–552; soil heat flux density, 80–81, 82t, 83–85, 83e, 84e, 85e; water requirement estimates and, 431–433. *See also* net radiation, energy balance and
- energy balance, land surfaces, 152–154t, 162–168, 163e, 164f

- energy balance, water surface evaporation estimation and, 113, 113e; factors governing heat storage, 114, 116–117, 116f, 121f; indirect measurements, 120, 121f, 122–123, 122e; meteorological estimates, 119–120, 119e, 120f; net radiation for water, 113–114, 113e, 115t; other components, 123–124, 123e, 124e; thermal profiles, 116f, 117–119, 117f, 118e, 118f, 119f energy budget, 21, 22f energy conservation, law of, 16–17 Enhanced Thematic Mapper (ETM), 421 equilibrium evaporation, 91–93 estimation methods, evaluation of, 11–16, 637–659; alfalfa and grass reference measurements, 645–646, 648, 648e; climate parameter calculation, 344t, 345t, 641; location estimates, 654–655; locations and data selected, 640–641, 642t, 643t, 644t, 645t; method performance, 650t, 651t, 653–654; methods selected, 637–638, 638t, 639t, 640t; monthly and seasonal estimate comparisons, 648–649, 650t, 651t; monthly estimate rankings, 655–656, 657t, 658t, 659; monthly estimate statistical analysis, 649, 649e, 652t; remote sensing and documentation, 547–554 estimation methods, outside U.S.: combination methods, 627–631; pan evaporation methods, 626; radiation methods, 631–634; temperature methods, 633–636 evaporation, generally: controlling factors, 21–27; defined, 19; stages of, 380 evaporation and evapotranspiration processes, 19–34; controlling factors, 21–27; definitions, 19–20; energy budget, 21, 22f; estimating concepts, 27–29; measurement methods, 29–34; water budget, 20, 20e evaporimeters, 214, 218–219 evapotranspiration, generally: American and European terminology, 267; defined, 8, 19; studies in U.S., 9–11 Evapotranspiration in Irrigation and Hydrology Technical Committee, of ASCE, 3, 17, 100 exoatmospheric radiation, energy balance and, 61, 62, 62f, 63f, 66–69, 66e, 67e, 68e, 69e FAO (Food and Agricultural Organization), of UN, 10–11 FAO 56 evaporation model, 232–240, 232e, 233e, 234f, 235e, 236f, 237e, 238f, 239e, 239t; advantages of, 258–259; HYDRUS 1D compared to, 254, 255f, 256–258, 256f; lysimeter compared to, 245–247, 246f, 247f, 248f, 249–253, 249t, 250t, 251f, 252f, 254f FAO Blaney-Criddle Method, 635–636, 635e, 638 FAO grass-based crop coefficients, 273–274, 273f, 274f; adjustment for climate, 275–276, 275e, 276e; estimation of initial with FAO mean procedure, 276, 277f, 278, 278e, 279t; FAO example, 281, 281f, 282f; length of growth stages, 279–280 fetch requirements, boundary layer measurement, 172–175, 172e, 173t, 174e field capacity, 48–49, 49t, 143–144 foliage factors, in soil-plant-atmosphere system, 54–55, 55e forests, energy balance application to, 419–420 frost protection, water requirements, 443–444 frozen or snow-covered surfaces, wintertime and nongrowing seasons estimates of crop coefficient, 74t, 316–319, 316e, 317f, 318f, 319f furrows, nonuniform water distribution, 445–446, 446f Geostationary Operational Environmental Satellite (GOES) system, 71–72, 424

- germination, water requirements, 443  
Global Land Data Assimilation System (GLDAS), 71, 212, 213, 424  
grass reference ET, 94–96, 196–197; estimation methods evaluated, 645–646, 648, 648e  
grass-based curves, 547  
grasslands, energy balance application to, 419–420  
gravimetric sampling, 29–30, 44, 145, 146–148, 147t, 294  
gravitational and pressure potentials, in soil, 45, 45e, 46t  
gridded weather data, 423–424  
GridMet, 424
- Hargreaves-Samani equation, 204–205, 204e; evaluation of, 654, 655, 656, 659  
heat dissipation electronic sensors, 148  
heat storage, energy balance and water surface evaporation, 114, 116–117, 116f, 119–120, 119e, 120f, 121f, 122–123, 122e  
hourly calculations, single-layer Penman-Monteith equation, 167f, 357–361t, 372f, 396–399  
humidity: absolute and specific, 36, 38, 38e; evaporation rates and, 22; Penman-Monteith application and, 389–393, 390f, 392f; reference ET and missing data, 206–207, 206e, 207e; water requirement estimates and, 429, 429e; weather data integrity, 587–601, 589f, 590f, 591e, 591f, 592e, 592t, 593e, 594e, 594t, 597f, 598f, 599f, 600f, 601f  
*Hydrology Handbook* (ASCE), 4  
HYDRUS 1D: advantages of, 259; FAO 56 model compared to, 254, 255f, 256–258, 256f
- integrated stability-correction expressions, 179; advantages, disadvantages, precautions, 135f, 183–187, 184f, 186f; air-to-humidity differences, 182–183, 182e; air-to-temperature differences, 181–182, 181e, 182e; calculation steps, 181; surface-to-air temperature differences, 179–181, 180e, 181e  
intercepted rainfall, evaporation of, 410–413, 411e, 412e, 413t  
International Commission on Irrigation and Drainage (ICID), 10–11  
International Water Management Institute (IWMI) World Water and Climate Atlas, 213  
irradiance. *See* solar radiation  
irrigation, management factor, 26–27  
irrigation efficiency, use of term, 451–452  
irrigation frequency, impact on  $K_L$ , 307–308, 307e, 308e, 309t, 310t, 311  
irrigation water requirements and streamflow depletion, 435–453; depletions to water resource, 452–453, 453e; improvements in estimation of, 451–452; leaching requirement, 439–440, 439e, 440e, 441–442t, 442–443; miscellaneous requirements, 443–444; net irrigation water requirement, 435–439, 437e, 438e; system losses, 445–451, 445e, 446f, 448e, 449f, 450t
- Jensen-Haise Alfalfa-Reference Radiation Method, 632–633, 632e, 633e, 653
- killing frost estimation, 538–539
- land surfaces, measurement and estimation on: advantages and disadvantages of methods, 150–156t, 175–176; basics of, 141–142; Bowen ratio energy balance, 152–154t, 162–168, 163e, 164f, 167f; combined energy balance and mass transfer methods, 176–187, 176e, 177e, 178e, 180e, 181e, 182e, 184f, 186f; information sources, 141; mass balance methods, 151–152t, 156f; mass transfer using Eddy covariance, 154–155t, 168–172, 169e, 170f; upwind fetch for boundary

- layer, 172–175, 172 $e$ , 173 $t$ , 174 $e$ ; volumetric measurements, 49 $t$ , 142–149, 143 $e$ , 144 $e$ , 145 $e$ , 146 $f$ , 147 $t$ , 148 $e$
- Landsat Thematic Mapper (TM), 421
- landscape coefficients, 294–297, 295 $e$ , 296; actual ET from landscapes, 306–307, 306 $e$ ; comparisons against recent measurements of  $K_L$ , 298 $t$ , 300 $f$ , 311–313, 312 $f$ ; density factor, 300–301; impact of canopy wetting and irrigation frequency on  $K_L$ , 307–308, 307 $e$ , 308 $e$ , 309 $t$ , 310 $t$ , 311; managed stress factor, 302–306, 303 $t$ , 304 $t$ ; microclimate factor, 299 $t$ , 301–302; vegetation coefficient, 297–300, 298 $t$ , 299 $f$ , 300 $f$
- landscape vegetation, evaporation rates and, 24
- large lakes, evaporation rates and, 136–137
- latent heat flux density, 21, 22 $f$ , 60, 60 $e$ ; surface-energy and air-mass interactions, 87–93, 90 $e$ , 91 $e$ , 92 $f$
- latent heat of vaporization, 42, 42 $e$
- law of conservation of energy, 16–17
- leaching requirement, irrigation water requirements, 439–440, 439 $e$ , 440 $e$ , 441–442 $t$ , 442–443
- leaf area, bulk surface (stomatal) resistance, 193 $e$ , 194 $e$ , 355–356, 357–367 $t$ , 362–363, 362 $e$
- leaf-area index (LAI), 23, 54, 95; evaporation from soil and, 240, 241 $f$ , 242–243, 242 $f$ ; increase in crop coefficient and, 262; for Penman–Monteith equation and, 194, 194 $e$
- liquid water, physical properties of, 36, 37 $t$
- location, ET estimation methods, evaluation of, 640–641, 642 $t$ , 643 $t$ , 644 $t$ , 645 $t$ , 654–655
- lysimeters: categories of, 31–32; evolution of estimation methods, 12–13, 14; soil evaporation models compared to, 245–247, 246 $f$ , 247 $f$ , 248 $f$ , 249–253, 249 $t$ , 250 $t$ , 251 $f$ , 252 $f$ , 254 $f$ ; tanks and, generally, 149, 156 $f$ , 157; typical problems with, 151–152 $t$ , 157–162, 158 $f$ , 160 $f$ , 161 $f$
- Makkink Method, 14, 631–632, 631 $e$ , 632 $e$
- managed stress factor, for vegetation, 302–306, 303 $t$ , 304 $t$
- management-allowed depletion (MAD), 51 $t$ , 53–54, 54 $e$ , 303–306, 303 $t$ , 304 $t$
- Manuals and Reports on Engineering Practice* No. 70 (ASCE): first edition, 3–4, 9–11, 16; revised edition, 3–7, 16–17
- mass balance methods, land surfaces: lysimeters, typical problems with, 151–152 $t$ , 157–162, 158 $f$ , 160 $f$ , 161 $f$ ; lysimeters and tanks, generally, 149, 156 $f$ , 157
- maximum relative humidity, 207, 429, 591–592, 591 $e$ , 592 $e$ , 628, 638
- mean air temperature, evolution of estimation methods, 11, 13–14, 14
- mean and basal crop coefficients, for temperate and continental climates, 513–515, 516–517 $t$ , 518–519 $t$ , 520 $t$ , 521 $t$
- mean atmospheric air pressure, 41, 41 $e$
- mean crop coefficients, 266 $e$ , 272–273, 273 $e$ ; in subhumid climates, 471, 472–485 $t$
- measurement factors, evaporation rates and, 29–34
- METRIC (Mapping Evapotranspiration at High Resolution Using Internalized Calibration) model, 186–187, 285, 409, 420, 549
- microclimate factor, vegetation, 299 $t$ , 301–302
- microirrigation systems, 447
- minimum daily relative humidity, 275–276, 275 $e$ , 276 $e$
- “minimum” or “unconstrained” surface resistance, 193, 357–361 $t$
- Monin–Obukhov stability parameter, 177, 177 $e$ , 179, 180–181, 181 $e$ , 337, 353–354, 398

- monthly ET estimates, evaluation of, 648–649, 649*e*, 650*t*, 651*t*, 652*t*, 655–656, 657*t*, 658*t*, 659
- multilayer (interactive) Penman-Monteith equation, 325, 326*f*, 327*f*, 332–338, 333*e*, 334*e*, 335*e*, 336*e*, 337*e*; challenges of, 340; comparative model performance, 343–344; equivalency parameters for more complicated models, 326, 342–343; example applications, 404–408
- National Centers for Environmental Prediction (NCEP) of U.S. NWS, 71–72, 213, 424
- natural vegetation: data sources, 423; evaporation rates and, 23–24. *See also vegetation entries*
- net apparent emittance, 77–78, 77*e*
- net irrigation water requirement (NIWR), 435–436, 437*e*, 438*e*, 445, 445*e*
- net radiation, 21, 60, 60*e*, 60*f*, 113–114, 113*e*; measurement and estimation, 72–80, 73*e*, 74*t*, 75*e*, 75*t*, 76*e*, 77*e*, 78*e*, 78*t*, 79*e*, 80*e*; Penman-Monteith model and, 323; solar radiation, 61–69, 62*f*, 63*e*, 63*f*, 64*e*, 65*e*, 66*e*, 66*f*, 67*e*, 68*e*, 69*e*; water surfaces and, 114, 115*t*, 116–117, 116*f*, 121*f*
- neutron moisture meter, 145
- 1963 Penman Method, 628, 653
- 1982 Kimberly Penman Method, 629–630, 629*e*, 630*e*, 656
- nongrowing seasons. *See* wintertime and nongrowing seasons, estimates of crop coefficient during
- nonuniform water distribution, 445–447, 446*f*
- Normalized Difference Vegetation Index (NDVI), 340, 552–553, 552*e*
- North American Land Data Assimilation System (NLDAS), 71–72, 212, 213, 424
- North American Regional Reanalysis (NARR), 71–72, 419, 423–424
- “oasis effects,” 288–289
- pan evaporation, 27; environmental factors, 104–106, 105*f*, 107*f*; evaluation of, 638, 638*t*, 639*t*, 640*t*, 654; land surfaces and, 214–215, 214*e*, 216*t*, 217–218, 217*e*, 217*f*, 218*e*; methods, 626, 626*e*
- pan evaporation, water surfaces and, 99; early U.S. studies, 101–104, 103*f*; environmental factors, 104–106, 105*f*, 107*f*; large lakes, 106, 108–109, 108*f*; traditional methods, 100–101
- Penman combination equation, 10, 13, 15
- Penman equation, 625*e*; background, 10; evolution of estimation methods, 14, 15; reference crop ET and, 189–190, 189*e*
- Penman FAO 24 method, 363, 628–629, 628*e*, 629*e*, 653, 659
- Penman-Monteith (PM) equation, 11, 90, 93, 97, 197–198, 323; advantages of, 323–324; comparative model performance, 343–344; derivation of, 619–625, 619*e*, 620*e*, 621*e*, 622*f*, 623*e*, 624*e*; disadvantages and challenges of, 324–325; equivalency parameters for more complicated models, 326, 342–343; evaporation from soil and surface resistance, 379–387, 379*e*, 380*e*, 381*e*, 381*f*, 382*e*, 383*f*, 384*e*, 384*f*, 385*e*, 386*f*; evolution of estimation methods, 15–16, 17; intercepted rainfall, 410–413, 411*e*, 412*e*, 412*t*; multilayer Penman-Monteith equation, 325, 326*f*, 327*f*, 332–338, 333*e*, 334*e*, 335*e*, 336*e*, 337*e*; multilayer Penman-Monteith equation, example applications of, 404–408; reference crop ET and, 190–192, 190*e*, 191*e*, 192–195, 192*e*, 193*e*, 194*e*; remote sensor use and, 408–409; resistance-based equations, 325–328, 326*f*, 327*f*, 340–342; roughness length and zero plane displacement, 326*f*, 327*f*, 345–354, 345*e*, 346*e*, 347*e*, 348*f*, 349–350*t*,

- 351*e*, 352*e*; single-layer Penman-Monteith equation, 325, 326*f*, 327*f*, 328–332, 328*e*, 330*e*, 331*e*, 375*t*, 375–377*t*; single-layer Penman-Monteith equation, example application of, 167*f*, 357–361*t*, 372*f*, 396–404, 397*f*, 399*f*, 402*e*; sloping lands, 409–410; standardization for reference crop ET, 198–199, 199*e*, 200*t*, 201, 201*t*, 203*t*; two-source (patch) resistance-based model, 325, 326*f*, 327*f*, 338–340, 339*e*; water requirement estimates and, 431–433; weather measurements for direct application of, 387–395, 390*f*, 392*f*, 394*e*, 395*e*
- permanent wilting point, 49–50, 49*t*
- Piche atmometer, 219
- plant cooling, water requirements, 444
- plants. *See* soil-plant-atmosphere (SPA) system
- precipitable water, 64–66, 64*e*
- precipitation deficit, 435–436
- precipitation measurement, 148–149, 148*e*
- precipitation residing in the root zone, 436; available for transpiration, 436–437
- Priestley-Taylor equation, 91–92, 91*e*, 132, 406, 418–420, 633, 633*e*, 638–640*t*, 641, 653–654, 659; evaluation of, 653–654, 659
- pyranometers, 62, 66, 69, 585–586
- radiation balance. *See* net radiation, energy balance and
- radiation estimation methods, 631; evaluation of, 638*t*, 639*t*, 640*t*, 656; Jensen-Haise Alfalfa-Reference Radiation Method, 632–633, 632*e*, 633*e*; Makkink Method, 631–632, 631*e*, 632*e*; Priestley-Taylor Method, 633, 633*e*; Turc method, 631, 631*e*
- rainfall, evaporation of intercepted, 410–413, 411*e*, 412*e*, 413*t*
- readily evaporable water (REW), 224–225, 224*e*, 224*t*, 225*e*, 233–238, 233*e*, 234*f*, 235*e*, 236*f*, 237*e*, 238*f*, 244, 246, 249, 253, 257, 278, 278*e*, 279*f*, 314
- reference crop ET, 189–220; atmometers and, 218–220; defined, 20; pan evaporation and, 214–215, 214*e*, 216*t*, 217–218, 217*e*, 217*f*, 218*e*; Penman equation and, 189–190, 189*e*; Penman-Monteith equation and, 190–195, 191*e*, 192*e*, 193*e*, 194*e*, 290*e*; weather data missing or bad, 206–214; weather measurement and use of, 387–395, 390*f*, 392*f*, 394*e*, 395*e*
- reference  $ET_{ref}K_c$  approach, 195–196, 195*e*; calculations, 198, 201, 203–204; Hargreaves-Samani equation, 204–205, 204*e*; Penman-Monteith equation standardized for, 197–199, 199*e*, 200*t*, 201, 201*t*, 203*t*; software programs for, 205; types and definitions, 196–198
- reference evapotranspiration: ASCE standardized references, 96–97; defined, 20; estimation and, 28; grass and alfalfa references, 94–96; use of term, 93, 94
- regional evapotranspiration, estimation of: basics of, 415–416; complimentary approach, 418–419, 418*e*; cultivated areas, data sources, 422–423; energy balance applied to forests and grasslands, 419–420; energy balance applied to regional cultivated lands, 420–421; gridded weather data, 423–424; natural vegetation, data sources, 423; theory, 357–361*t*, 416–418, 417*e*; ungauged watersheds, streamflow approximation for, 421–422, 422*e*
- relative humidity, 39, 39*e*
- remote sensing, 34, 176, 186–187, 415, 420, 567; crop coefficients and, 549–551; satellite-based surface energy balance, 315, 316*f*, 453; used in model applications, 408–409
- remote sensing, documentation for, 543–567; crop coefficient and ET data reporting, 554, 555–559*t*, 560–565*t*,

- 566; ET measurement and, 547–554; upper limits on ET and crop coefficients, 263e, 544–547
- remote sensing-based energy balance (RSEB) models, 550
- reservoirs, evaporation rates example, 132–135, 134f, 135f
- river-reservoir system, evaporation rates example, 131–132, 132f
- root factors, in soil-plant-atmosphere system, 55–57, 56f
- root zone: capillary rise into, 610–611; deep percolation from, 271–272, 271e, 272e
- rooting depth, of plants, 50, 51t, 52–53, 52e, 53e
- roughness length, Penman-Monteith equation, 326f, 327f, 345–354, 345e, 346e, 347e, 348f, 349–350t, 351e, 352e
- salt tolerance, leaching and, 439–440, 439e, 440e, 441–442t, 442–443
- sap flow methods, ET measurement and, 548–549, 658
- satellites. *See* remote sensing
- saturation vapor pressure, 22, 36, 36e, 68t, 463–464t
- SCS Blaney-Criddle Method, 634–635, 634e; evaluation of, 637, 648, 648e, 654, 659
- seasonal ET estimates, evaluation of, 648–649, 650t, 651t
- SEBAL (surface energy balance model), 186–187, 420–421, 547
- sensible heat flux, 59–60, 60e, 60f; land surfaces, measurement and estimation on, 178–179, 178e; surface-energy and air-mass interactions, 87–89
- shallow water bodies, evaporation rates and, 25, 27, 126–128, 127f, 128f, 128t, 136
- Shuttleworth-Wallace (S-W) model, 401, 404–407
- single-layer (standard) Penman-Monteith equation, 325, 326f, 327f, 328–332, 328e, 330e, 331e, 375t, 375–377t; challenges of, 341; comparative model performance, 343–344; derivation of, 328; equivalency parameters for more complicated models, 326, 342–343; example applications, 167f, 357–361t, 372f, 396–408, 397f, 399f, 402e; other applications, 401–404, 402e
- Slatyer-McIlroy equation, 90–91, 90e
- sloping land: estimation of ET on, 409–410; nonuniform water distribution, 445
- snow. *See* frozen or snow-covered surfaces
- soil, evaporation from, 221–259; basics of, 221–222, 222f; crop coefficient-based evaporation model, 230–232, 230e, 231e; diurnal effects and redistribution of soil water, 222–223; FAO 56 model, 232–240, 232e, 233e, 234f, 235e, 236f, 237e, 238f, 239e, 239t; models compared to lysimeter, 245–247, 246f, 247f, 248f, 249–253, 249t, 250t, 251f, 252f, 254f; Penman-Monteith and, 379–387, 379e, 380e, 381e, 381f, 382e, 383f, 384e, 384f, 385e, 386f; square root of time model, 228–230, 228e, 229e; stage 1, 222, 223–225, 223f, 224e, 224t; stage 2, 222, 223f, 225–227, 226e, 227e; transpiration and, 240, 241f, 242–243, 242f; water balance of evaporation layer, 242–245, 243e, 244e, 245e
- soil factors, evaporation rates and, 25, 26, 27–28
- soil heat flux density, energy balance and, 60, 60e, 60f, 80–81, 82t, 83–85, 83e, 84e, 85e
- soil properties, 44, 44e
- soil water balance, 29–30, 49t, 142–149, 143e, 144e, 145e, 146f, 147t, 148e
- soil water stress, single-layer Penman-Monteith equation, 399–400, 399f
- Soil-Adjusted Vegetation Index (SAVI) indices, 340, 553
- soil-plant-atmosphere (SPA) system, 35–57; components of, 35; physical

- properties of water, water vapor, and air, 35–43; soil properties, 44, 44e; soil-water system, 44–54; vegetative properties, 54–57. *See also* surface-energy and air-mass interactions
- soil-water system, 44–54; energy state of soil water, 45, 45e, 46t; flow of water in soils, 47–48, 47e, 48e; general soil-water properties, 48–50, 49t; soil-plant interactions, 50, 51t, 52–54, 52e, 53e, 54e; soil-water characteristic curve, 45, 47, 47f
- solar constant, 61
- solar radiation, 59, 61, 114, 116f; energy balance and, 61–69, 62f, 63e, 63f, 64e, 65e, 66e, 66f, 67e, 69e; estimation of, 69–72, 69e, 70e, 71e; evaporation rates and, 22; evolution of estimation methods, 12–13, 14, 653–654; GOES estimation and, 71–72; net radiation and energy balance, 68e; reference ET and missing data, 207–210, 208e, 209e; U.S. data base, 71; water requirement estimates and, 428
- specific humidity, 38, 38e
- sprinkler systems, nonuniform water distribution, 446–447
- square root of time (SRT) model, of soil evaporation, 228–230, 228e, 229e; advantages of, 258–259; lysimeter compared to, 245–247, 246f, 247f, 248f, 249–253, 249t, 250t, 251f, 252f, 254f
- standard atmosphere (lower atmosphere), characteristics of, 42, 42t, 43t
- standard error of estimate (SEE), in estimation method evaluation, 649, 649e, 653, 655–656, 659
- stomatal resistance (conductance), 54–55, 55e
- streamflow depletion. *See* irrigation water requirements and streamflow depletion
- subhumid climates: basal crop coefficients in, 499–509t, 510t, 511–512t; mean crop coefficients in, 471, 472–485t
- sublimation, 19, 25, 321
- surface parameters, for Penman-Monteith equation, 192–195, 193e, 194e
- surface resistance, Penman-Monteith equation and, 379–387, 379e, 380e, 381e, 381f, 382e, 383f, 384e, 384f, 385e, 386f
- surface-energy and air-mass interactions, 87–97; basics of, 87–89, 88f, 89f, 90f; energy conversion to latent heat flux, 87–93, 90e, 91e, 92f; reference evapotranspiration and, 93–97
- target landscape ET. *See* landscape coefficients
- temperature estimation methods, 633–634; evaluation of, 638t, 639t, 640t, 654; FAO Blaney-Criddle Method, 635–636, 635e; SCS Blaney-Criddle Method, 634–635, 634e
- tensiometers, 45, 148
- thermal profiles, energy balance and water surface evaporation, 116f, 117–119, 117f, 118e, 118f, 119f
- thermodynamic constants, 465–466t
- thermodynamic wet bulb temperature, 39–40, 40e
- time domain reflectometry (TDR), 145, 148, 312
- time domain transmission (TDT), 148
- time of day, bulk surface (stomatal) resistance, 357–361t, 363–374, 364t, 365e, 366e, 367e, 368e, 369f, 372f
- time steps, in reference ET calculation, 201, 203–204
- timeframe: estimates of missing solar data and, 207–210, 208e, 209e; water requirement estimates and, 427–428
- tissue-heat-balance method, of ET measurement, 548–549
- total evaporable water (TEW), 232–238, 232e, 233e, 235e, 244, 246, 249, 253, 257–258, 278, 278e, 279f, 314, 349, 381–382, 382e

- transpiration: defined, 19; evaporation and, 240, 241*f*, 242–243, 242*f*
- Turc method, 14, 631, 631*e*, 641, 650–652*t*, 653–654, 659
- two-source (patch) resistance-based model, 325, 326*f*, 327*f*, 338–340, 339*e*; challenges of, 340; comparative model performance, 343–344; equivalency parameters for more complicated models, 326, 342–343; example applications, 404–408
- Two-Source-Energy-Balance (TSEB) model, 339, 409
- ungaaged watersheds, streamflow approximation for, 421–422, 422*e*
- UPFLOW simulation model, capillary flow from shallow water table, 609, 610*e*, 611–613, 613*f*, 614*t*, 615*t*, 616*f*, 617*e*, 617*f*
- vapor pressure: defined, 36; gradient and evaporation rates, 22
- vapor pressure deficit (VPD), 39, 39*e*, 203, 316–317, 316*e*, 333, 344, 365–367, 367*e*; estimation methods and, 624, 624*e*, 628, 631, 656, 659; water date integrity and, 569–570, 606
- vapor saturation deficit, 13
- vegetation: curve estimates for natural and agricultural vegetation, 287–294, 288*f*, 289*e*, 289*f*, 290*e*, 291*e*, 292*e*, 293*f*, 508*t*; density factor, 300–301; evaporation rates and, 23–24; small expanses of, 264–265; wintertime and nongrowing seasons estimates of crop coefficient, 314–315, 316*f*
- vegetation coefficient, landscapes, 297–300, 298*t*, 299*f*, 300*f*
- vegetation indices, remote sensing and, 552–554, 552*e*
- vegetative (crop) properties: evaporation rates and, 28; foliage factors, 54–55, 55*e*; root factors, 55–57, 56*f*
- vegetative cover coefficients, 262, 265–273, 266*f*, 268*e*, 269*e*, 270*e*, 271*e*, 272*e*, 272*f*, 273*e*
- water: available, defined, 49*t*, 50; evaporation rates and, 25–26; physical properties of liquid, 36, 37*t*; physical properties of vapor, 36, 38–41, 38*e*, 38*t*, 39*e*, 40*e*; water balance measurement method, 33. *See also* soil-water system
- water budget, 20, 20*e*
- water budget procedure, water surfaces evaporation and, 109–110, 109*e*
- water characteristic curve, 25
- water estimates, method selection: basics of, 133, 427; calculations of evaporation and evapotranspiration, 431–433; crop coefficient and direct methods, 430–431; data collection, screening, procession, 428–430, 429*e*; time frame and required accuracy, 427–428
- water stress adjustments, crop coefficient method, 269–272, 269*e*, 270*e*, 271*e*, 272*e*, 272*f*
- water surfaces, estimation of evaporation from, 27, 99–137; aerodynamic method, 110–113, 110*e*, 111*e*, 112*e*; combination methods, 124–125, 124*e*; deep lake example, 128–131, 129*f*, 130*f*; energy balance method, 113–114, 113*e*, 115*t*, 116–120, 116*f*, 117*f*, 118*e*, 118*f*, 119*e*, 119*f*, 120*f*, 121*f*, 122–124, 122*e*, 123*e*, 124*e*; history of theories of, 99–100; pan evaporation, 99–109, 103*f*, 105*f*, 107*f*, 108*f*; reservoir example, 132–135, 134*f*, 135*f*; river-reservoir system example, 131–132, 132*f*; shallow lake example, 126–128, 127*f*, 128*f*, 128*t*; simulation studies, 125–126; summary of methods, 135–137; water budget procedure, 109–110, 109*e*
- weather, evaporation rates and, 22
- weather data integrity, 569–607; humidity and air temperature, 587–601, 589*f*, 590*f*, 591*e*, 591*f*, 592*e*, 592*t*, 593*e*, 594*e*, 594*t*, 597*f*, 598*f*, 599*f*, 600*f*, 601*f*; location's importance to, 606; net radiation, 585–587, 586*f*; quality

- assessment and quality control, 578–580; solar radiation, 569, 580–585, 581*f*, 582*f*, 584*f*; temperature and humidity's importance to, 572–578, 574*t*, 575*t*, 577*t*
- weather data, missing or bad, 206; air temperature data, 209–210, 209*e*, 212, 212*e*; gridded data from climate and land process models, 213–214; humidity data, 206–207, 206*e*, 207*e*; minimum requirements, 206; solar radiation data, 207–210, 208*e*, 209*e*; wind speed data, 210–212, 211*t*
- weather measurements, for direct P-M, AFIB, and reference ET application, 387–395, 390*f*, 392*f*, 394*e*, 395*e*
- weather stations: aridity, and basal crop coefficients, 535; estimates of missing solar data and, 208–209; estimates of missing wind speed data and, 210–212, 211*t*; fetch requirements, 172*e*, 174*e*, 175
- wet bulb evaporation, 39–40, 40*e*
- Wild evaporimeter, 219
- wind erosion protection, water requirements, 444
- wind speed: evaporation rates and, 22; Penman-Monteith application and, 393–395, 394*e*, 395*e*; reference ET and missing data, 210–212, 211*t*; water requirement estimates and, 430
- wintertime and nongrowing seasons, estimates of crop coefficient during estimated winter evaporation, 319, 320*f*, 321; surface condition types, 74*t*, 277*f*, 313–319, 316*f*, 317*f*, 318*f*, 319*f*
- Wright procedure, crop coefficient-based evaporation and, 230–231, 230*e*
- yield threshold depletion (YTD), water in soil, 53
- zero plane displacement, Penman-Monteith equation and, 326*f*, 327*f*, 345–354, 345*e*, 346*e*, 347*e*, 348*f*, 349–350*t*, 351*e*, 352*e*